United States Department of Agriculture
Forest Service

Forest Products Laboratory

General Technical Report

FPL–GTR–226

Proceedings

18th International Nondestructive Testing and Evaluation of Wood Symposium

Madison, Wisconsin, USA 2013

Abstract

The 18th International Nondestructive Testing and Evaluation of Wood Symposium was hosted by the USDA Forest Service's Forest Products Laboratory (FPL) in Madison, Wisconsin, on September 24–27, 2013. This Symposium was a forum for those involved in nondestructive testing and evaluation (NDT/NDE) of wood and brought together many NDT/NDE users, suppliers, international researchers, representatives from various government agencies, and other groups to share research results, products, and technology for evaluating a wide range of wood products, including standing trees, logs, lumber, and wood structures. Networking among participants encouraged international collaborative efforts and fostered the implementation of NDT/NDE technologies around the world. The technical content of the 18th Symposium is captured in this proceedings.

Keywords: International Nondestructive Testing and Evaluation of Wood Symposium, nondestructive testing, nondestructive evaluation, wood, wood products

September 2013

Ross, Robert J.; Wang, Xiping, eds. 2013. Proceedings: 18th International Nondestructive Testing and Evaluation of Wood Symposium. General Technical Report FPL-GTR-226. Madison, WI: U.S. Department of Agriculture, Forest Service, Forest Products Laboratory. 808 p.

A limited number of free copies of this publication are available to the public from the Forest Products Laboratory, One Gifford Pinchot Drive, Madison, WI 53726–2398. This publication is also available online at www.fpl.fs.fed.us. Laboratory publications are sent to hundreds of libraries in the United States and elsewhere.

The Forest Products Laboratory is maintained in cooperation with the University of Wisconsin.

The use of trade or firm names in this publication is for reader information and does not imply endorsement by the United States Department of Agriculture (USDA) of any product or service.

The USDA prohibits discrimination in all its programs and activities on the basis of race, color, national origin, age, disability, and where applicable, sex, marital status, familial status, parental status, religion, sexual orientation, genetic information, political beliefs, reprisal, or because all or a part of an individual's income is derived from any public assistance program. (Not all prohibited bases apply to all programs.) Persons with disabilities who require alternative means for communication of program information (Braille, large print, audiotape, etc.) should contact USDA's TARGET Center at (202) 720–2600 (voice and TDD). To file a complaint of discrimination, write to USDA, Director, Office of Civil Rights, 1400 Independence Avenue, S.W., Washington, D.C. 20250–9410, or call (800) 795–3272 (voice) or (202) 720–6382 (TDD). USDA is an equal opportunity provider and employer.

Contents

Session 1. Industrial Applications of NDT Technologies

Session 2. Nondestructive Evaluation and Hazard Assessment of Urban Trees

Session 3. Nondestructive Evaluation of Standing Timber

Session 4. Nondestructive Evaluation of Logs

Session 5. Condition Assessment of Historic Wood Structures—Experience from Around the Globe

Session 6. Nondestructive Evaluation of Composite Materials—Nanocellulosic Films to Glued Laminated Timber

Session 7. Nondestructive Evaluation of Structural Materials I— New Techniques and Approaches

Session 8. Nondestructive Evaluation of Structural Materials II— Enhancements to Traditional Methods and New Applications

Session 9. Material Characterization I—Acoustic-Based Techniques

Session 10. Material Characterization II—Near Infrared, Neutron Imaging, and Other Techniques

Session 11. Structural Condition Assessment I—NDT Fundamentals and Assessment Methods

Session 12. Structural Condition Assessment II—New Techniques and Field Experiences

Session 13. Poster Session

Proceedings

18th International Nondestructive Testing and Evaluation of Wood Symposium

Madison, Wisconsin, USA
2013

Edited by
Robert J. Ross, Supervisory Research General Engineer
Xiping Wang, Research Forest Products Technologist
Forest Products Laboratory, Madison, Wisconsin

Preface

The International Nondestructive Testing and Evaluation of Wood Symposium Series started 50 years ago in Madison, Wisconsin, USA. Since its inception, 17 symposia have been held in various countries around the world, including China, Germany, Hungary, Switzerland, and the United States.

The 18th International Nondestructive Testing and Evaluation of Wood Symposium was hosted by the USDA Forest Service's Forest Products Laboratory (FPL) in Madison, Wisconsin, on September 24–27, 2013. This Symposium was a forum for those involved in nondestructive testing and evaluation (NDT/NDE) of wood and brought together many NDT/NDE users, suppliers, international researchers, representatives from various government agencies, and other groups to share research results, products, and technology for evaluating a wide range of wood products, including standing trees, logs, lumber, and wood structures. Networking among participants encouraged international collaborative efforts and fostered the implementation of NDT/NDE technologies around the world.

The 18th Symposium was especially important because in addition to its strong technical content, it was a celebration of 50 years of this symposium series! The opening session, "From Strong Beginnings to an International Research Community," included keynote speakers from around the globe who presented the state-of-the-art in nondestructive testing and evaluation of wood. Of special note was the first presentation of the opening session titled "From Conception to Completion." Individuals who have been key contributors to the success of this symposium series were given special recognition at the symposium's banquet. Engraved plaques were awarded to Helmuth Resch, Bill and Pat Galligan, and Roy and Patti Pellerin in thanks for their outstanding efforts and continuous support. Special events included a Wisconsin style brat fry hosted by the Forest Products Laboratory Employees Association, a 50th anniversary cake, an excellent banquet with outstanding local talent providing entertainment, tours of FPL's Centennial Research Facility, and a post-symposium dinner cruise on Madison's beautiful Lake Monona.

A special publication, *Fifty Years of Nondestructive Testing and Evaluation of Wood Research—International Nondestructive Testing and Evaluation of Wood Symposium Series*, was produced by FPL in commemoration of the 50th anniversary. This publication includes a brief history of the symposium series, summaries of each symposium, and searchable electronic copies of the proceedings from each symposium. Each attendee received a complimentary electronic copy of the publication.

The technical content of the 18th Symposium is captured in the following proceedings. Full length, in-depth technical papers for oral presentations were prepared and are published herein. Abstracts for poster presentations are also included.

The organization of the following proceedings follows that of the sessions at the 18th Symposium. Thirteen technical sessions were held:

1. Industrial Applications of NDT Technologies
2. Nondestructive Evaluation and Hazard Assessment of Urban Trees
3. Nondestructive Evaluation of Standing Timber
4. Nondestructive Evaluation of Logs
5. Condition Assessment of Historic Wood Structures—Experience from Around the Globe
6. Nondestructive Evaluation of Composite Materials—Nanocellulosic Films to Glued Laminated Timber
7. Nondestructive Evaluation of Structural Materials I—New Techniques and Approaches

8. Nondestructive Evaluation of Structural Materials II—Enhancements to Traditional Methods and New Applications
9. Material Characterization I—Acoustic-Based Techniques
10. Material Characterization II—Near Infrared, Neutron Imaging, and Other Techniques
11. Structural Condition Assessment I—NDT Fundamentals and Assessment Methods
12. Structural Condition Assessment II—New Techniques and Field Experiences
13. Poster Session

We express our sincere appreciation and gratitude to members of the Organizing Committee, International Nondestructive Testing and Evaluation of Wood Symposium Series, for their efforts in making this symposium a success:

- Brian K. Brashaw, Program Director, University of Minnesota Duluth, USA
- Francisco Arriaga Martitegui, Professor, Universidad Politécnica de Madrid, Spain
- Ferenc Divos, Professor, University of Western Hungary, Hungary
- Roy F.Pellerin, Professor Emeritus, Washington State University, USA
- Raquel Gonçalves, Associate Professor, University of Campinas, Brazil

We thank the Forest Products Society (FPS) and International Union of Forestry Research Organizations (IUFRO) for their support. Thanks also go to the following organizations for providing financial support in the form of sponsorships or who exhibited equipment and wood products: Natural Resources Research Institute, University of Minnesota Duluth (NRRI UMD); Washington State University (WSU); Forest Products Society—Midwest Section; U.S. Department of Transportation Federal Highway Administration (USDOT FHWA); Beijing Forestry University (BFU); Fakopp Enterprise; Fiber-gen; Agricef; RinnTech; Metriguard, Inc.; Research Institute of Wood Industry, Chinese Academy of Forestry (CAF); Northeast Forestry University; CBS–CBT; IML, Inc.; Whole Trees Architecture and Structures; Forest Products Laboratory Employee Association (FPLEA); Forest Products Society; and Lizz's Food for Thought.

A very special thank you to Ms. Pamela Byrd, FPL, for all her outstanding efforts—from securing arrangements to serving as our main point of contact for speakers and moderators. Thank you, Pam!

A note of thanks to the many individuals who prepared papers for inclusion in the Symposium. Your dedication and efforts make this Symposia Series a success!

We hope that these proceedings provide inspiration to those who read its papers. And welcome to new participants in the global wood NDT/NDE family!

Robert J. Ross, Project Leader, USDA Forest Products Laboratory, USA

Xiping Wang, Research Forest Products Technologist, USDA Forest Products Laboratory, USA

Symposium Co-Chairs

Thank you to this year's sponsors and exhibitors. Your support has helped make this symposium possible!

Session 1

Industrial Applications of NDT Technologies

Field application of processor head acoustic technology in forest harvest operations

Peter Carter
Fibre-gen, Inc. 26 Tiffany Close, Manukau 2016, New Zealand, peter.carter@fibre-gen.com

Xiping Wang
USDA Forest Service, Forest Products Laboratory, Madison, Wisconsin, USA, xwang@fs.fed.us

Robert J Ross
USDA Forest Service, Forest Products Laboratory, Madison, Wisconsin, USA, rjross@fs.fed.us

Abstract

Recent research and development on acoustic technologies has brought the operational assessment of acoustic speed as a measure of stiffness into forest management and log and lumber processing sectors of the industry. Significant values are associated with stiffness in log supply for LVL veneer production as well as structural lumber manufacture. Measurement of acoustic speed allows this value to be captured through better decision-making, allocation of resource to highest value users, and application of best processing methods dependent upon log-by-log measures. This paper reviews recent experience with field application of acoustic technologies to measure the stiffness of logs and trees during harvesting and log-making operations and discusses research challenges which have arisen. It presents results from in-forest and resulting in-mill log-by-log acoustic measurement and associated values.

Key words: Acoustic technology, forest, logs, processor head, mechanised, nondestructive evaluation, stiffness, trees, wood quality

Introduction

Acoustic velocity through wood can be measured using resonance or time-of-flight based equipment. Research has shown both methods to be useful in predicting the stiffness or modulus of elasticity (MOE) of wood and wood products derived from measured logs or tree stems (Wang et al. 2007).

Recent research and development on acoustic technologies has brought the operational assessment of acoustic velocity as a measure of stiffness into forest management and log and lumber processing sectors of the forest and wood processing industry. Fibre-gen has developed a Hitman® (patented) processor head mounted acoustic measurement system and previously reported research and development has involved the integration of Hitman PH330 mechanised acoustic measurement devices into a Ponsse processor head in UK, two Waratah 626 processor heads in New Zealand, and one Waratah 624 processor head in Oregon US. The system measures the time-of-flight of a sound wave in the stem section held by the harvesting processor head, immediately following the previous cross-cut. Depending on the acoustic velocity value, the operator may cut a different log product from the next section of stem, or segregate the next log, based on a user-defined velocity threshold level.

Significant values can be associated with stiffness in log supply for LVL veneer production as well as structural lumber manufacture. Measurement of acoustic velocity allows this value to be captured through better decision-making, allocation of resource to highest value users, and application of best processing methods dependent upon log-by-log measures.

Measurement of acoustic speed on harvest processor heads has been recognised as a means to enable cutting to the correct log lengths and segregating logs for higher value structural markets. This avoids the need to test after logs are cut to length and having to subsequently re-cut those logs which fail to meet the log buyer's acoustic speed specification. Costs can be significant of re-cutting logs to a shorter length expending resources and generating more waste, with the alternative of selling non-structural logs at a discount in non-preferred lengths.

Two alternative objectives have been highlighted by potential users of mechanised acoustic testing on processor heads; increase the average stiffness of a segregated log batch, or meet some specific Hitman HM200 defined minimum log velocity specification. Different approaches may be necessary to meet these two differing objectives.

Previous results from this work have been summarised and presented at a number of meetings including the presentation in September 2011 at the 17th NDT Symposium in Sopron, Hungary. Development and validation undertaken since the 2011 Sopron meeting has involved retro-fit installation into each of a Waratah 624 in West Australia, and a Waratah 626 in Nelson, New Zealand. These two subsequent validation projects have brought together all of the learnings from the previous projects incorporating a number of features bringing improved performance, precision of acoustic measures, and reliability of mechanical and control systems.

The objective of the West Australia project was to validate the segregation capability of Hitman PH330 to generate a higher average sawmill structural lumber grade out-turn and avoid processing lower stiffness logs into structural product.

The objective of the Nelson project was to validate the segregation capability of Hitman PH330 to meet defined Hitman HM200 specifications required by an LVL veneer manufacturing facility.

Performance Validation

West Australia project

The West Australia project involved retro-fit installation of a Hitman PH330 into a Waratah 624 processor head. This Hitman unit incorporated a similar set of improvements which had previously been made and tested on the Waratah 624 project in Oregon, USA. Project results have been reported (Walsh, D 2012) and involved four phases: 1) installation and calibration; 2) productivity study; 3) log-making and segregation in a 34-year-old radiata pine harvest operation; and 4) a mill trial sawing and grading the segregated log batches.

Calibration

Calibration involved precision testing of 25 successive test cycles with the Hitman PH330 in the same position on one log to be compared against 25 successive hit sets in the same probe holes using the hand operated Hitman ST300. Each hit set involves initiation of eight successive hits, the time-of-flight being

ranked from highest to lowest, and the middle four or tightest clustered set of four recordings being averaged to derive and output a mean time-of-flight and acoustic velocity for the set.

Following this initial calibration, further testing was carried out using the Hitman PH330 to measure acoustic velocity on 168 sawlogs from the selected stand. The results were compared with acoustic velocity measurements taken on the same sawlogs using two hand-held acoustic measurement devices, the Hitman ST300 and Hitman HM200.

Productivity study

The productivity trial was conducted in a 34-year-old radiata pine plantation, with uniform stand and site conditions, after three thinnings. Two 100-tree plots (~0.7 ha each) were established within the harvest site. Every tree within the two plots was measured for diameter and height and numbered for identification during harvesting. Both plots were harvested using a Tigercat H860C, fitted with a Waratah HTH624 C super head and a PH330 installed.

The first plot (the control plot) was harvested without using the PH330 while the second plot (the PH330 plot) did use the acoustic assessment system. For ease of identification, in the PH330 plot, sections of stem with acoustic velocity readings above the selected lower quartile threshold level ('structural' sawlogs) were cut into 6.1m or 5.5m sawlogs, while sections of stem with acoustic velocity readings below the threshold level ('non-structural' sawlogs) were cut into 4.9m sawlogs. A detailed time and motion study was completed during the harvesting phase for each plot, and a record taken of the products and volumes cut.

Mill trial

Following the productivity trial, the harvester continued to cut and segregate logs from the PH330 plot using the PH330. The intention was to harvest at least 500 m^3 of sawlogs, classified as structural and 'non-structural', for the mill trial.

At the mill, the sawlogs were segregated in their respective assortments ('structural' 6.1-m or 5.5-m, and 'non-structural' 4.9-m sawlogs). Each assortment was then sawn separately into 100 mm × 38 mm green boards. Following milling, the boards were further segregated into four separate batches, based on their original sawlog acoustic velocity assortment and heart status for drying, i.e. 'free-of-heart' (FOH) or 'heart-in' (HI). FOH and HI boards were separated as a part of the routine sawmill production process using a gamma ray based lumber density sorter which enables separation of heartwood boards from sapwood boards based on their green density.

These batches were then kiln dried and processed through the dry mill where each 90 mm × 35 mm timber board was machine stress-graded.

Nelson, New Zealand project

The Nelson project involved retro-fit installation of a Hitman PH330 into a Waratah 626 processor head. This Hitman unit was redesigned to incorporate the previous 624 improvements with adjustments to suit the different dimensions of the 626 head, along with some further enhancements. A paint marking system was also installed to enable easy identification of logs above and below the acoustic velocity threshold. The study carried out in 2013 involved two phases; installation and calibration, and log-making and segregation in two separate 28-year-old radiata pine harvest operations.

Calibration

Calibration was carried out using the same procedure as outline above for the West Australia project.

Log-making and segregation

Subsequent to calibration, and during the routine harvest and log-making operation, a series of successive log sets were directed to one side of the skid site for further evaluation. Log sets were selected at regular times during the day when it could be accommodated in the production schedule, each comprising 15 - 25 logs in sequence. For each of a total 271 logs, log position within stem, Hitman PH330, and Hitman HM200 acoustic velocities were recorded.

The machine up-time as a proportion of total time available was recorded for a period of 20 operational days. Up-time was considered to be that time when each of the Waratah 626 and the Hitman PH330 were operational without lost time caused by mechanical or other cause of break down.

Results

Calibration and segregation

A series of three independent precision checks from the Hitman PH330 unit installed in West Australia in three separate log positions showed standard deviations of 2.6, 2.6, and 2.7 microseconds respectively on average time-of-flights of 323, 331, and 329. Greater precision was observed in the subsequent Nelson installation (Figure 1) which showed a standard deviation of 1.5 microseconds on an average time-of-flight of 377. Five subsequent precision checks of the Nelson installation showed standard deviations of a 25-test series of the Hitman PH330 time-of-flight of 1.3, 1.0, 1.3, 1.3, and 0.7 microseconds respectively. This compares favorably against the precision of the Hitman ST300 hand tool which showed a standard deviation o

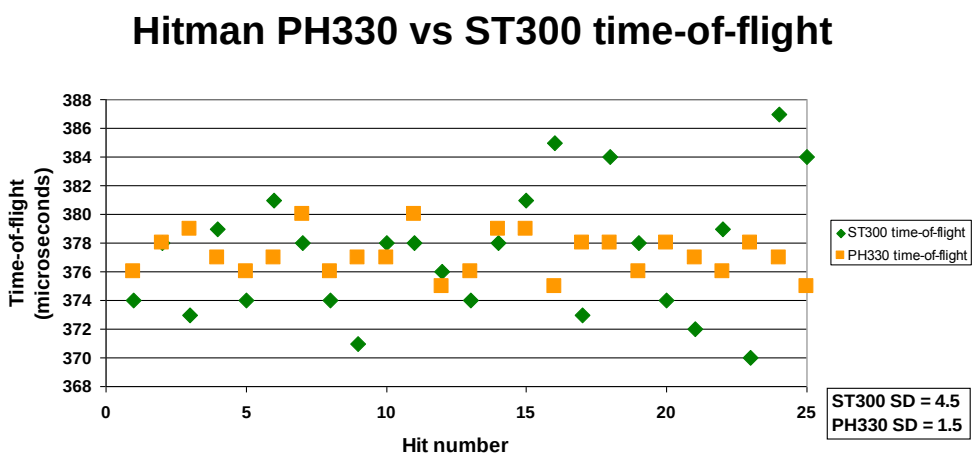

Figure 1—Plot of time-of-flight data showing the relative precision of a 25-test series using the Hitman ST300 and Hitman PH330 devices (Note: standard deviation of the Hitman PH330 is significantly lower than that of the ST300).

Individual Hitman PH330 and HM200 log measurements were taken on 168 logs during the West Australia study. Correlation between individuals showed an r^2 of 0.0.54 and were distributed as shown in Figure 2. Using Hitman PH330 velocity as the basis for log segregation resulted in the selection of the same 5 out of 6 logs which would have been selected if HM200 velocity had been used.

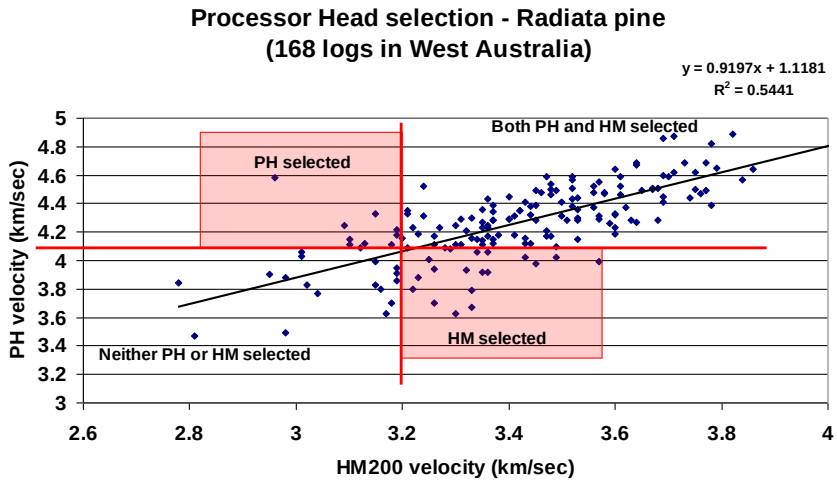

Figure 2—Correlation between Hitman PH330 and HM200 velocity measures on 168 radiata pine logs, highlighting the slightly different selections made using the alternative tools.

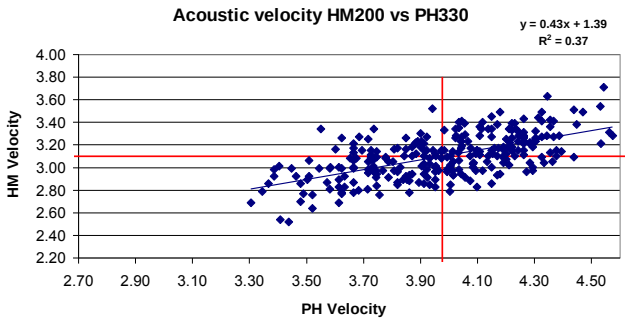

Figure 3—Correlation between Hitman PH330 and HM200 velocity measures on 271 logs in Nelson.

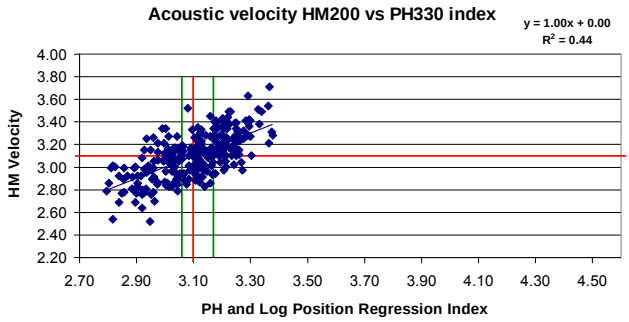

Figure 4—Correlation between Hitman PH330 velocity index including log position and HM200 velocity on 271 logs in Nelson, highlighting the improvement in r^2 using the velocity index.

Individual Hitman PH330 and HM200 log measurements were also taken on 271 logs during the Nelson study. Correlation between individuals showed a lower r^2 of 0.37 as shown in Figure 3. When a PH330 index was generated using a regression including both acoustic velocity and log position within the stem and the index correlated against HM200 velocity, the r^2 improved to 0.44 as shown in Figure 4.

Productivity study

The time study carried out in the two 0.7ha plots with ~100 trees in each as a part of the West Australia project showed no measurable reduction on productivity when using the Hitman PH330. However observation of the PH330 testing process showed a recorded actual average time taken of 1.56 seconds per PH330 test so a theoretical approach was taken to derive a potential productivity impact. At mean 'normal' tree size (1.95m^3) a model based estimated of the impact of operating the Hitman PH330 indicated a 4.2% decrease in productivity (not statistically significant) when using the PH330.

While productivity impact was also considered as a part of the Nelson project, it was a cable hauler operation where production is ~250m^3 per day, constrained by piece size and haul distance. The Waratah

626 processor has a production capacity in excess of 500m^3 per day so operation of the Hitman PH330 had no impact on crew daily productivity.

Hitman PH330 reliability was monitored in the Nelson project during the validation period and over the 20 day period PH330 uptime exceeded 94%. During this same period Waratah uptime was 92% indicating the Hitman PH330 was at least as reliable as the processor head on which it was installed.

Mill study

Structural out-turn from the four batches of boards in the West Australia mill trial are presented in Table 1. Both the Hitman PH330 segregated 'structural' logs and 'non-structural' logs (those from logs tested above and below the lower quartile threshold respectively) generated high levels of structural board recovery from the outer-wood (FOH; free-of-heart) showing little difference in the structural grade recoveries between the two batches of boards.

There was however a significant difference between the structural grade out-turn of the two batches of corewood (HI; heart-in) boards. Sawlogs with Hitman PH330 acoustic velocities above the selected threshold ('structural' sawlogs), had a much higher recovery of HI structural grade boards than those below the selected threshold. A statistical comparison of the mean of the average MOE readings for each board produced in each of the four batches showed they were significantly different ($\alpha = 0.05$).

A cost-benefit analysis indicated that the HI timber boards sawn from the low stiffness ('non-structural') sawlogs identified by the Hitman PH330 would be better sold as green off saw (GOS) product in most market conditions, rather than incurring the extra cost of kiln drying and further processing.

Table 1—Structural grade recovery for the four batches of boards.

	Structural FOH	Non-structural FOH	Structural HI	Non-structural HI
Structural Grade Recovery	91.8%	88.4%	70.7%	56.4%

Table 2—Example potential benefits from using Hitman PH330 to segregate structural logs from within non-structural stands in two regions of New Zealand.

Region	Hitman ST300 mean velocity (km/s)	Hitman HM200 mean velocity (km/s)	Proportion of logs >3.1 km/s	Benefit/crew day
Nelson, NZ	4.25	3.10	50%	$1,775
Northland, NZ	4.43	3.23	72%	$2,574

Table 3—Cost and sensitivity analysis for using Hitman HM200 and PH330 to segregate structural logs from within non-structural stands.

Log segregation	Cost summary [a]		Sensitivity – Hitman PH330 cost/m^3		
	Crew cost/day	Cost/m^3	Sawlog production/day	200 m^3/day	400 m^3/day
Do nothing	$1,500 - $3,000	$15.00	20% Structural	$4.42	$2.21
Hitman HM200	$300 - $1,300	$1.50 - $6.50	35% Structural	$2.53	$1.26
Hitman PH330	$185 - $260	$0.88 - $4.42	50% Structural	$1.77	$0.88

[a] Costs comprise labour associated with using the Hitman HM200 tool; loader to sort the logs marked as structural or non-structural on the skid site; labour and chainsaw to re-cut non-structural logs to a shorter length; wood wasted as non-structural logs are shortened to the next lower value market length; and in the case of PH330, equipment lease and servicing costs

In the Nelson project there was no associated mill study because prior experience and trial results had shown the Hitman HM200 log velocities were effective predictors of subsequent mill out-turn.

Potential financial benefits have been derived for the projects outlined above along with other situations where Hitman PH330 could be applied. Examples of the benefit of operationally extracting structural logs from within what would otherwise be considered non-structural stands are summarised in Table 2 and Table 3.

Conclusions and discussion

Calibration results show the Hitman PH330 to be more precise than the hand-held Hitman ST300 tool. This could be expected due to the more consistent amplitude of hit from the mechanised initiation of the 8 successive hits by the PH300 while the ST300 relies upon the somewhat variable amplitude and angle of hit generated by manual hammer hitting. Further precision improvements of Hitman PH330 velocities relative to those generated using the ST300 could result from the lack of any distance variability in the PH330 vs that of the ST300.

While it is noted that the precision of the Hitman PH330 was higher in the Nelson installation than in West Australia, the correlation of PH330 velocity vs HM200 velocity was lower in Nelson. This cannot be explained by the differing sample size as the Nelson sample was larger than that in West Australia, but the explanation probably lies in the variability of the Nelson log resource having been grown on the side of relatively steep slopes with the presence of lean and resulting compression wood quite common. Because the PH330 uses a time-of-flight velocity measure, and the HM200 uses a resonance-based measure, compression wood on one side and near the base of the stem will have a greater impact on the measured velocity from the PH330 than that from the HM200 tool.

Segregation in the West Australia project resulted in the selection of five out of six sawlogs being the same using both PH330 and HM200 tools. In this case the segregation threshold split the log population at around 80% above and 20% below threshold. In contrast the Nelson project was targeting segregation of a structural log batch comprising close to 50% of the otherwise suitable log population, and the additional client requirements of no more than 10% of logs in the selected structural log batch being below a specified HM200 velocity, and no more than 20% of the available structural logs being mixed in the non-structural batch.

While this rigorous level of selection may have been able to be met in higher average velocity Nelson stands where about 80% of logs were above threshold, in lower velocity stands where about 50% of logs were above threshold it was not possible. This is due to the imperfect relationship between PH330 and HM200 velocities, and the rigorous client requirements specified. The addition of log order with acoustic velocity into an index improved the power of segregation, but still not to the level required.

Using the results from the Nelson project an alternative strategy of deployment was developed involving the use of two threshold levels rather than one. Using a single threshold logs are either included in the structural log batch or not depending upon whether they have a velocity or velocity-based index above or below the threshold. A two threshold strategy includes all logs above the upper threshold in the structural batch, all logs below the lower threshold in the non-structural batch, and those between the thresholds being further tested with the HM200 tool and split above or below based upon the HM200 specification. It was found that typically a mid band comprising 20% - 40% of the log population enables the defined HM200-based specification to be met in the Nelson case.

In the West Australia project where the processor head was typically on the critical path for daily crew productivity, an intense productivity study was carried out. It is interesting to note that the intensive time study was unable to measure any loss of productivity when using the Hitman PH330. This result serves to illustrate that using the PH330 acoustic assessment system results in only a small productivity impact on the harvesting phase, and that there are other factors which were unable to be identified and measured which impacted the processor head's productivity more than the use of the Hitman PH330.

Any potential small impact of using the Hitman PH330 may be further mitigated by testing acoustic velocity while other operations are being carried out such as during the felling operation or while slewing the stem during processing. Further by application of a simple set of testing guidelines the need for testing all logs could be reduced such that only a subset of logs need be tested eg if the first two logs have a high velocity it can be assumed for operational purposes that the third log will also be high.

Mill trial results from the West Australia study demonstrated that the Hitman PH330 was able to identify lower stiffness sawlogs in the forest before any mill processing was undertaken. A cost-benefit analysis suggested the sawmill would gain financially by directing HI (corewood) boards sawn from these sawlogs to GOS (green sawn) product, rather than paying the additional processing cost for drying, planing, and grading them while suffering 43.6% failure rate of the resulting boards.

An example-based analysis of benefits and costs showed positive net benefit from the potential use of Hitman PH330 to segregate structural logs from within stands otherwise considered non-structural in Nelson and Northland Regions in New Zealand. In markets where there is a log sale price premium of $\$15/m^3$, benefits of segregating structural logs from within non-structural stands can range $1,500 - $3,000 per harvest crew day. Segregating these structural logs using the hand held Hitman HM200 tool as an alternative to the Hitman PH330 can only be done following log making, so suffering both the cost of the manual HM200 operation as well as the cost and waste of re-cutting those logs found to be non-structural to shorter client specified lengths.

Hitman PH330 technology has now been demonstrated through a series of research, development, and validation projects over a period of six years and has been confirmed capable of delivering effective segregation strategies to reliably meet a range of market and end user requirements.

Acknowledgements

Developing and introducing new technologies to the sector is a huge task. Many parties have been involved, too many to name individuals, but they have so willingly made significant contributions of their time, ideas, and financial support without which this work could not have been carried out. This huge contribution is gratefully acknowledged.

References

Walsh, D.; Ardille, S.; Carter, P.C.S. 2012 Evaluation of the Hitman PH330 acoustic assessment system for harvesters: CRC for Forestry Bulletin 25.

Wang, X.; P. Carter; R.J. Ross; and B.K. Brashaw. 2007. Acoustic assessment of raw forest materials – A path to increased profitability. Forest Products Journal 57(5):6-14.

Automatic Detection of Resin Pockets in High Speed Industrial CT Images of Norway Spruce

Norvin Laudon
Forest Research Institute Baden-Württemberg, Freiburg, Germany, norvin.laudon@forst.bwl.de

Rafael Baumgartner
Forest Research Institute Baden-Württemberg, Freiburg, Germany, rafael.baumgartner@forst.bwl.de

Diana Carolina Hoyos Montoya
Forest Research Institute Baden-Württemberg, Freiburg, Germany, diana.hoyos@forst.bwl.de

Franka Brüchert
Forest Research Institute Baden-Württemberg, Freiburg, Germany, franka.bruechert@forst.bwl.de

Udo H. Sauter
Forest Research Institute Baden-Württemberg, Freiburg, Germany, udo.sauter@forst.bwl.de

Abstract

Resin pockets in Norway spruce (*Picea abies* (L.) Karst.)) are an internal defect which severely limits potential use of wood. Automatic detection of resin pockets to sort out unsuitable logs prior to sawing would therefore be beneficial.
Microtec, an Italian manufacturer of sawmill scanners, has developed an industrial high speed CT scanner which is running in a log sorting line at 120 m/min. To effectively utilize such a CT scanner to optimize wood quality, algorithms are required for automatic detection of internal defects.
In this study a set of Norway spruce logs was CT-scanned. The logs were sawn into boards; size and location of all resin pockets on the board surfaces were measured. An automatic algorithm was written to detect resin pockets in the CT images. Comparison of the manual measurements with the algorithm shows that it is possible to predict the number of resin pockets with sufficient accuracy for industrial application.

Key words: x-ray, wood features, internal log quality, resin pockets, log sorting, sawing optimization

Introduction

Resin Pockets

Resin pockets, also called pitch pockets, are defined as intercellular circumferentially elongated pockets in the xylem with resin and wound tissue, which are usually occluded the same year as they are formed. (Larson 1994). In softwood species, resin pockets are most commonly formed at the cambium and lie along the annual ring of trees (Temnerud and Oja 1998). When measuring and recording the occurrence of resin pockets, the size and shape typically describe the thickness (measured in radial direction), width (measured tangentially) and length. Both length and width are always greater than the thickness. The size of resin pockets in Norway spruce can vary from a minimum length, width and thickness of 3.0, 2.5, and 0.5 mm to a maximum of 175, 65, and 7.0 mm respectively (Temnerud 1997).

There are three predominant theories about how resin pockets are formed. Firstly, the storm hypothesis argues that the formation of resin pockets is induced by bending stress within the stem caused by heavy wind and blasts (Seifert et al. 2010). Alternatively, the drought hypothesis states that water deficiency induces the formation of resin pockets. This theory is based on quantitative studies that found higher numbers of resin pockets on dry sites (Seifert et al. 2010). The pathogen hypothesis attributes resin pockets appearance to a defense reaction of a tree against insects or fungal attackers that penetrate the bark and cause micro wounds in the cambium and inducing resin pocket formation (Seifert et al. 2010). Other studies refer to the influence of thinning on the formation of resin pockets and reaction wood (Schumacher et al. 1997).

In addition to looking at how resin pockets are formed, previous studies have focused on the frequency and location of resin pockets. Pechman & Lirpemeier (1975) found a high frequency of resin pockets above a height of 18 m in mature trees. Similarily, Temnerud (1999) looked at saw log populations of Norway spruce in Sweden and found that resin pockets were less frequent and smaller in butt logs than in logs from the middle and top of the tree. Seifert (2010) summarized that the increase in the number of resin pockets with the height in the stem is well known for Norway spruce. Clifton (1969) also argued that the number of resin pockets increase with increasing distance from the pith followed by a decrease outwards to the bark, while Gjerdrum (2007) spoke of an increase in number from pith to bark. While there appear to be some common findings, resin pockets frequency also varied between trees and seem to be randomly distributed in all the tree directions: radial angular and axial.

Resin pockets are considered a severe defect in the wood, especially when sawn timber is intended to be used for furniture or other visual applications. The occurrence of resin pockets is a very significant factor in the grading and pricing of spruce lumber (Pechmann and Lippemeier 1975). Resin pouring from cut pockets hampers surface coating in wooden window, door and furniture production. Often, cut resin pockets are considered aesthetically significant enough as to require filling or removal using moulding machinery. Resin pockets have a strong influence in the final use of wood, and as such, detailed rules regarding the occurrence of resin pockets exist in the European standard EN 1927-1. According to these standards, no resin pockets are allowed at the thin end diameter cross-section of the log for the highest quality class and only one resin pocket is allowed for the second best class (Seifert et al. 2010).

Objective

To develop an algorithm that can detect resin pockets in CT images of a saw log, and be used for log quality sorting in sawmill production.

Material and Methods

To evaluate the resin pocket algorithm a total of 11 saw logs of Norway spruce were sampled, at a sawmill in the southern Black Forest in Germany. The logs were chosen by examining the ends of the logs for the presence of resin pockets. After selection, the logs were CT-scanned with a Microtec CT.Log industrial scanner, with a spatial voxel resolution of 1mm by 1mm by 10mm.
The logs were then sawn at the same sawmill using the pattern shown in the figure below. The number of center boards varied with log diameter between 9 and 11 boards. Only the center boards were used for measurement and subsequent analysis, as the automatic algorithm was developed to only detect resin pockets in the heartwood, and the sideboards were predominately sawn from the sapwood.

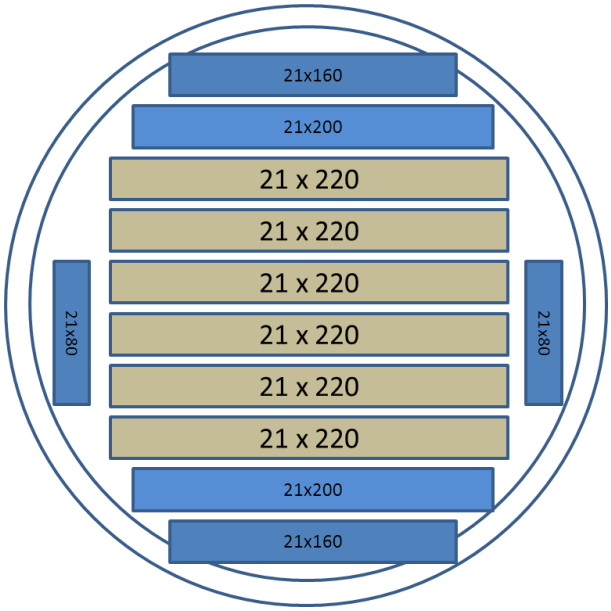

Figure 1 Cutting pattern used for the samples

After sawing the boards were scanned with a Microtec Goldeneye scanner to obtain high resolution color images of the board surfaces.

Procedure for the manual measurement of resin pockets

To validate the automatic algorithm, manual measurements were taken using the color board images. The Microtec Goldeneye scanner produced color images with a resolution of 1.25mm in the lengthwise direction and 0.3mm in the crosswise direction. All images were examined for resin pockets. The recognition of the resin pockets in the image was based on the average shape and size for resin pockets and the fact that resin pockets lie parallel to the annual rings. The length of the resin pockets was measured using a tool which allowed a rectangle to be drawn in the image defining the borders of the resin pocket. Since examination of resin pocket width was not a focus of this study, the rectangles were drawn to ensure the length of the rectangle matched the resin pocket length as closely as possible. Figure 2 shows a color image of a resin pocket on one of the board surfaces, and the corresponding rectangle that was drawn.

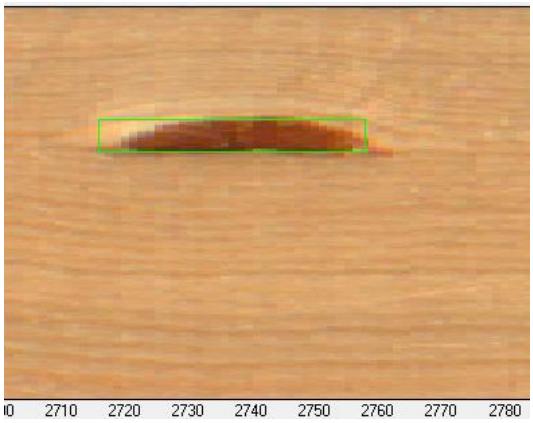

Figure 2 Color picture of a board surface showing a resin pocket and the corresponding manually drawn rectangle in green

Algorithm for automatic detection of resin pockets

An automatic algorithm was developed to detect resin pockets in the three dimensional CT images. In theory, detection of resin pockets in CT images should be relatively simple as their shape is consistent; the typical dimension of a resin pocket is 1 to 2 annual rings in the radial direction, and they are relatively small in angular and longitudinal directions when compared in size to other defects like knots. In practice, however, there are many other features in the log which can be mistaken for resin pockets, the most common being dense annual rings around knots, moisture pockets, compression wood, and annual rings with rapidly changing shape. A significant portion of the algorithm development was therefore devoted to removal of these features to avoid false detections, without removing the real signal of the resin pocket. The algorithm steps are as follows:

1. the raw CT data is convolved with a specially shaped 3 dimensional filter kernel whose dimensions are based on the typical size of resin pockets, which creates a filtered image with increased contrast for items which are of a similar shape to resin pockets.

2. a second image is created using a 3 dimensional low pass filter, whose dimensions were chosen to highlight features with a large length in the longitudinal direction, such as moisture pockets, compression wood, and dense annual rings. The filter produces a floating point image with values between 0 and 1, where lower values indicate the presence of these features.

3. a third image is created using a 3 dimensional low pass filter, whose dimensions were chosen to highlight features with consistent density in the radial direction, such as knots. The filter produces a floating point image with values between 0 and 1, where lower values indicate the presence of these features.

4. the filtered image in step 1 is multiplied by the images in step 2 and 3, to produce a seed image where high values indicate the presence of resin pockets.

5. each potential seed area from step 4 is flood filled into the original filtered image to obtain the actual three dimensional boundary of the resin pocket. If these flood filled regions meet strict size criteria in all three directions, the region is kept as a resin pocket.

Results and Discussion

A total of 11 logs were scanned and used for the manual and for the CT-algorithm comparison. The resin pockets were counted on both of the board's wide surfaces.

For the manual measurements, a total of 694 resin pockets were found; 86% of the resin pockets were found in the heartwood and 14% in the sapwood. For the CT-algorithm measurements, 501 resin pockets were found in heartwood. As mentioned by Skog and Oja (2009), it is not possible to detect resin pockets in sapwood using X ray scanning, as there is very low contrast when the pockets lie adjacent to other high density areas like sapwood or wet wood. Due to the low contrast in sapwood, the algorithm was developed to only detect resin pockets in the heartwood. Table 1 show the total number of resin pockets found for the CT and manual measurements for each log.

Table 1 Resin pockets in heartwood

												Total
Log ID	1	2	3	4	5	8	9	10	12	13	25	
CT	268	30	31	4	23	75	3	5	9	39	14	501
Manual	231	45	49	10	42	91	12	1	31	59	26	597

Number of resin pockets per log

The number of resin pockets detected by the automatic algorithm per log was similar to the number found manually using the color images. In the cases where the algorithm overestimated the amount of resin pockets, the cause was typically false detection in moisture pockets or near knots. These cases were relatively uncommon, as the kernels in the algorithm were generally sized to minimize the number of false detections. There is therefore a general tendency to underestimate the number per log. Additionally, underestimations were caused by resin pockets with little or no contrast in the CT data. The low contrast signal was due to a number of factors, including insufficient spatial resolution to detect very small resin pockets, resin pockets which were located within high density moisture pockets, and resin pockets which were located next to high density annual rings.
The comparison between the two methods is shown in Figure 2. The linear regression shows a good correlation coefficient ($R^2 = 0.97$), which indicates that the algorithm is operating with high precision. As the point with the highest values lies somewhat outside of the normal distribution, it is practical to also calculate the correlation without this point. The correlation coefficient changes to ($R^2 = 0.93$), when the point is removed. The high correlation indicates that the algorithm can accurately predict the real number of resin pockets in the log, and therefore could be used in a log quality sorting application.

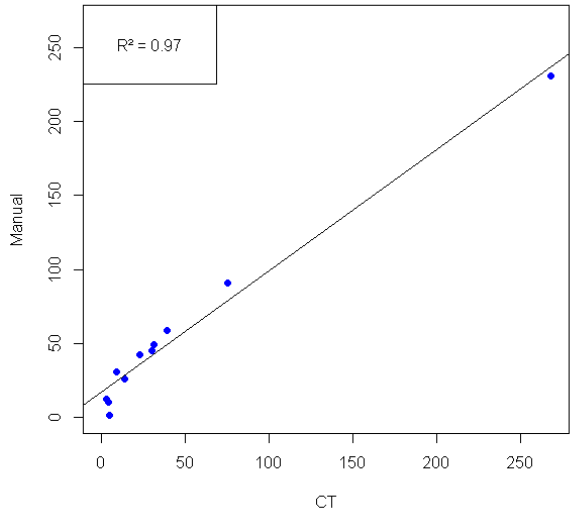

Figure 2 Comparison for the number of resin pockets found per log for the manual and algorithm measurements

Number of resin pockets found in the board surfaces

By comparing the number of resin pockets found on each board surface, it can also be seen that the algorithm tends to underestimate the amount of resin pockets. Despite the previous mentioned difficulties the algorithm can detect the majority of the resin pockets. As can be seen in Figure 4 the coefficient of correlation is $R^2 = 0.64$, indicating a good correlation between the measurements. However, due to the low number of resin pockets allowed per surface by most quality grading rules for visual applications, it is uncertain if this algorithm could be used to predict the number of resin pockets per surface with sufficient precision for use in rotational sawing optimization.

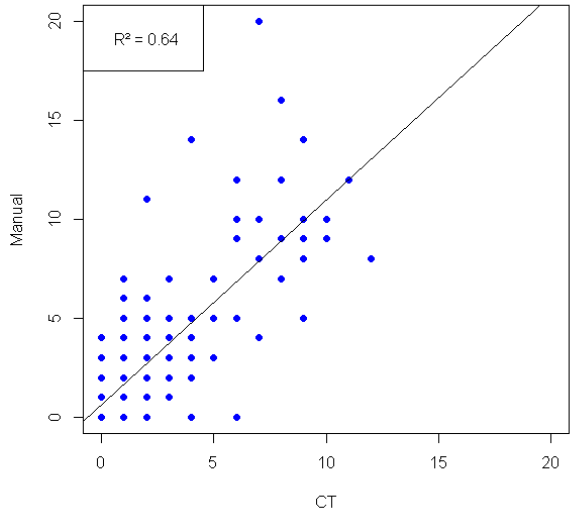

Figure 4 Comparison for the number of resin pockets found per surface for the manual and algorithm measurements

Resin pocket length

The length of each resin pocket found in the colour board surface images was measured. The manually measured lengths varied between 6 and 90 mm. The lengths measured by the algorithm varied between 10 mm 120 mm. The mean for the manual resin pocket length was 28mm and 40mm for the algorithm. The frequency distributions of lengths are shown in the figure below.

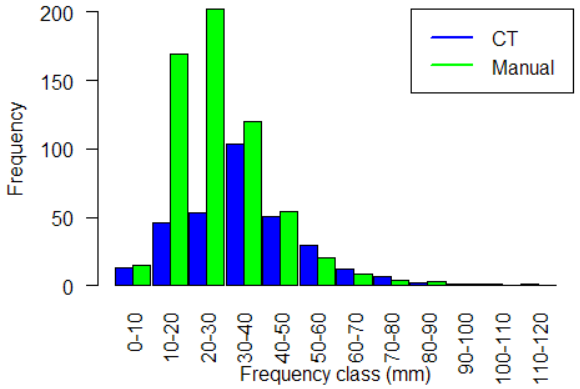

Figure 3 Frequency distribution for the manual and algorithm (CT) measurements of the length

The measured lengths are in agreement with Temnerud (1997), who determined the average length of a resin pocket to be about 30 mm. In this study the peak length class for the algorithm measurements was 30-40 mm and for the manual measurements was 20-30 mm. For the other length classes the amounts of resin pocket were similar. Due to the scanner's spatial resolution of 10mm in the lengthwise direction, it was not possible to detect resin pockets shorter than 10mm.
In the future it would also be interesting to investigate resin pocket detection in other species, particularly Scots pine (*Pinus sylvestris*). This is another commonly sawn species where resin pockets are common, from which visually graded products that limit the amount of resin pockets are produced.

Conclusions

This study shows that using the developed algorithm, it is possible to predict the number and the length of resin pockets in Norway spruce saw logs with sufficient accuracy to be used for the purpose of log quality sorting in a sawmill.
It is also shown that the accuracy of the algorithm is lower when predicting the number of resin pockets on sawn surfaces. In the future, it would be useful to continue improvement of the algorithm to increase the detection accuracy on board surfaces, in order to explore the use of the algorithm in applications such as rotational sawing optimization.
The study also demonstrated that the average resin pocket length as measured both manually and by the algorithm is in agreement with previous studies.

References

Pechmann, H.; Lippemeier, P. (1975): Untersuchungen über die Schnittholzqualität von Tannen und Fichtenholz aus Plenterbeständen. In: Forstw Cbl 94 (1), S. 351-364. Online available under http://dx.doi.org/10.1007/BF02735954.

Schumacher, P.; Tratamiller, M.; Grosser, B. (1997): Beeinträchtigung der Qualität von Fichtenholz durch Harzgallen in Abhängigkeit von der Durchforstungsintensität. In: Holz als Roh-und Werkstoff 55 (2-4), S. 254-254. Online available under http://dx.doi.org/10.1007/BF02990557.

Seifert, Thomas; Breibeck, Julian; Seifert, Stefan; Biber, Peter (2010): Resin pocket occurrence in Norway spruce depending on tree and climate variables. In: Forest Ecology and Management 260 (3), S. 302–312. Online available under http://www.sciencedirect.com/science/article/pii/S0378112710001775.

Skog, J.; Oja, J. (2009): Automatic Detection of Resin Pockets in Norway Spruce by X-ray Scanning. SP Technical Research Institute of Sweden, Wood Technology, Skellefteå, Sweden.

Temnerud, E.; Oja, J. (1998): A preliminary study on unbiased volume estimation of resin pockets using stereology to interpret CT-scanned images from one spruce log. In: Holz als Roh-und Werkstoff 56 (3), S. 193-200 Online available under http://dx.doi.org/10.1007/s001070050298.

Temnerud, Erik (1997): Formation and prediction of resin pockets in Picea abies (L.) Karst. Uppsala, Sweden: Swedish University of Agricultural Sciences (Acta Universitatis Agriculturae Sueciae. Silvestria, 26).

Performance of acoustic tools for pre-sorting of Norway spruce structural timber

Carolin Fischer
Department of Ecology and Natural Resource Management, Norwegian University of Life Science (UMB), Ås, Norway, carolin.fischer@umb.no

Audun Øvrum
Treteknisk (Norwegian Institute of Wood Technology), Oslo, Norway, audun.ovrum@treteknisk.no

Geir I. Vestøl
Department of Ecology and Natural Resource Management, Norwegian University of Life Science (UMB), Ås, Norway, geir.vestol@umb.no

Olav A. Høibø
Department of Ecology and Natural Resource Management, Norwegian University of Life Science (UMB), Ås, Norway, olav.hoibo@umb.no

Abstract

The aim of this study was to assess the feasibility of introducing acoustic measurements early in the conversion chain of structural timber from Norway spruce. Acoustic measurements were performed on trees and logs from 8 different forest sites in Norway using ST300 and HM200 tool from Fibre-gen. The sawn timber was graded with Dynagrade, measuring the frequency, and Precigrader, measuring frequency and density. The classification in sawn timber strength classes was done according to EN 14081 part 4 (Standard Norge 2009).
The results show that the correlation between the IP-value and the velocity measurement in the forest is much better for the HM200 velocity which was used on individual logs than for the ST300 which was used on standing trees. Pre-sorting of logs in the forest with acoustic velocity measurements showed a potential for extracting higher sawn timber strength grades. However, when grading for the low strength class C24 of Dynagrade and C30 of Precigrader only, the sawn timber grade yield was almost 100%, and a presorting of logs was not needed.

Keywords**:** acoustic velocity, strength grading, grade yield, Norway spruce

Introduction

Norway spruce is the most important species for the Norwegian sawmilling industry. The main product is structural timber, which constitutes about one third of the annual output of Norway spruce sawn timber. This timber has to be strength graded according to EN 14081 (Standard Norge 2011). The grading process focuses on the most important physical and mechanical properties: density, modulus of elasticity and bending strength. Based on respective approved setting values given in the standards, the timber is sorted into strength classes. The highest strength class applied in Norway at the moment is C30, while the average bending strength of spruce timber from Norway is more than 40 N/mm^2 (Haartveit and Flæte 2002), although slightly lower strength has been found for spruce grown in Northern Norway (Nagoda 1985), in Western Norway (Eikenes 1991; Lackner and Foslie 1989) and in plantations with large spacing on very fertile sites in Eastern Norway (Høibø 1991). To sort timber into higher strength classes than C30, the strength sorting systems have to be improved.

One option might be to pre-sort the logs prior to sawing, enabling a more precise sorting of the final products.

Using acoustic measurements on logs and trees to predict the stiffness of sawn timber has been investigated in numerous studies, and it has been proven to be a good indicator for the strength properties of Norway spruce sawn timber (Edlund et al. 2006; Kliger et al. 2003; Perstorper 1999). Portable equipments for measuring sound velocity in standing trees and logs are available, and models describing correlations between sound velocity and modulus of elasticity have been developed for several species (Auty and Achim 2008; Grabianowski et al. 2006; Lindström et al. 2009; Moore et al. 2013; Moore et al. 2009).

Wang et al. (2004) found an effect of acoustic red maple log measurements on lumber stiffness. Sorting the logs into four classes according to acoustic velocity showed a significant differentiation. They compared the acoustic classes and E-grades, and showed that logs with a high acoustic velocity contained higher proportions of high-grade lumber. Similar results were shown for radiata pine from New Zealand (Tsehaye et al.1997). Acoustic measurement and a pre-sorting in three acoustic classes showed that the class with the highest acoustic velocity was 90 percent stiffer than that of the lowest velocity. Edlund et al. (2006) measured acoustic velocity and calculated MOE for logs. They found a good effect of avoiding logs with low MOE on the grading result from machine stress grading of sawn wood. Moore et al.(2013) found a good effect of sorting out, with portable acoustic tools, low stiffness individual trees and logs of Sitka spruce.

The aim of this study was to assess the feasibility of introducing acoustic measurements early in the conversion chain of structural timber from Norway spruce. The background for this is the large variation in strength properties in the Norwegian Norway spruce resources. Earlier investigations on acoustics have shown promising results for Norway spruce, and in this study the acoustic approach of the Fibregen tools is extended by taking it into the forest and measuring both on trees with the ST300 and on logs with the HM200.

Material and Methods

Material

The material was sampled from 8 sites in Norway, covering a variation in altitude, latitude and site index. Table 1 shows the geographical and forest inventory data for each site. The material shows a range in altitude from 100 m to 845 m above sea level, which is close to the timberline. The sites had site indices from 10 m to 20 m, according to Tveite (1977).

Table 1—Site data.

Site	Latitude	Longitude	ALT (m)	SI (m)
Begnadalen	N 60.6371	E 9.7993	544	10
Etnedal	N 61.0632	E 9.5403	845	12
Frosta	N 63.6511	E 10.9141	100	13
Stange	N 60.5320	E 11.3701	370	16
Toten	N 60.6618	E 10.8852	220	20
Tretten	N 61.3102	E 10.2391	630	14
Trondheim	N 63.3521	E 10.2455	150	13
Ulsberg	N 62.7471	E 9.9898	470	12

Data collection

At each site 15 trees with DBH above 20 cm were randomly sampled from five strata. Acoustic velocity was recorded on tree and log level. Acoustic velocity on standing trees was detected by using the Director ST300 from Fibre-gen. The device consists of two probes which are hit a couple of centimeters into the wood in a distance of about 1,20 m. By hitting the lower probe with a hammer, an

acoustic wave is sent through the wood and acoustic velocity is calculated. After felling, all trees were cut into logs of 3.6 m, 4.2 m, and 4.6 m. The acoustic velocity of each log was detected by the Director HM200. Since the velocity depends on temperature, the measured values were adjusted according to the calibration equations of Gao et al. (2013). The logs were sawn in either two or four boards, depending on the dimension of the log. The board dimensions were 38x100, 50x100 mm, 50x150 mm, 50x200 mm, and 50x225 mm, respectively. After drying, the boards were machine strength graded with Dynagrade (IP_{DYN}, indicating property value) and Precigrader (IP_{PREC}) according to the requirements of EN 14081 part 1 to 4 (Standard Norge 2011). The values were adjusted to 12% moisture content. Dynagrade is based on frequency measurements, while Precigrader in addition takes density into account.

Results

Relationship between acoustic measurement and machine grading

A linear regression between the acoustic velocity measured on standing trees and the acoustic velocity measured on logs got an r^2-value of 0.45 (Figure 1). An analysis for each log type found a stronger relationship between ST300 velocity and HM200 velocity for butt logs ($r^2 = 0.51$). For middle logs the r^2 decreased to 0.26. For top logs the r^2 was 0.46.

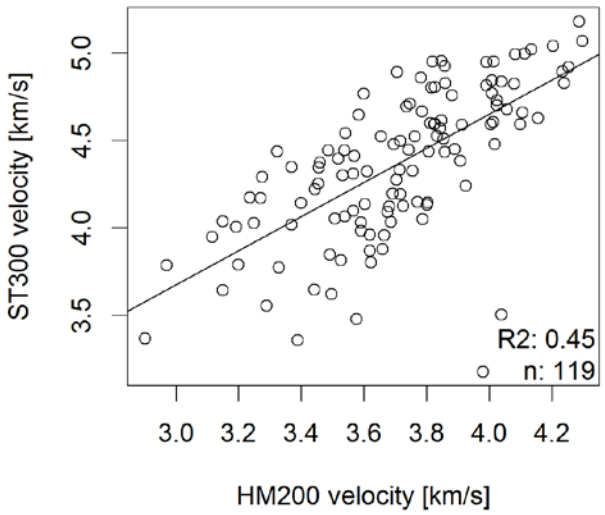

Figure 1—Relationship between ST300 velocity and HM200 velocity [km/s].

The earlier a pre-sorting can be conducted in the conversion chain, the bigger the benefit. Therefore, measurements done on standing trees during harvesting are of great interest. The r^2-values obtained by linear regressions between the velocities measured on standing trees and IP_{DYN} and IP_{PREC} respectively, was 0.27 and 0.28 (Figure 2). With the ST300 tool only one measurement in the lower part of the tree is done. Thus, the relationship between ST300 and the IP_{DYN} or IP_{PREC} should be better for butt logs. A somewhat better correlation for IP_{DYN} ($r^2 = 0.30$) was found when analyzing the butt logs separately. For IP_{PREC} it was somewhat lower. For the butt logs r^2 was 0.23, the best relationship was achieved for the top logs ($r^2 = 0.29$). The correlation was lowest for the intermediate logs.

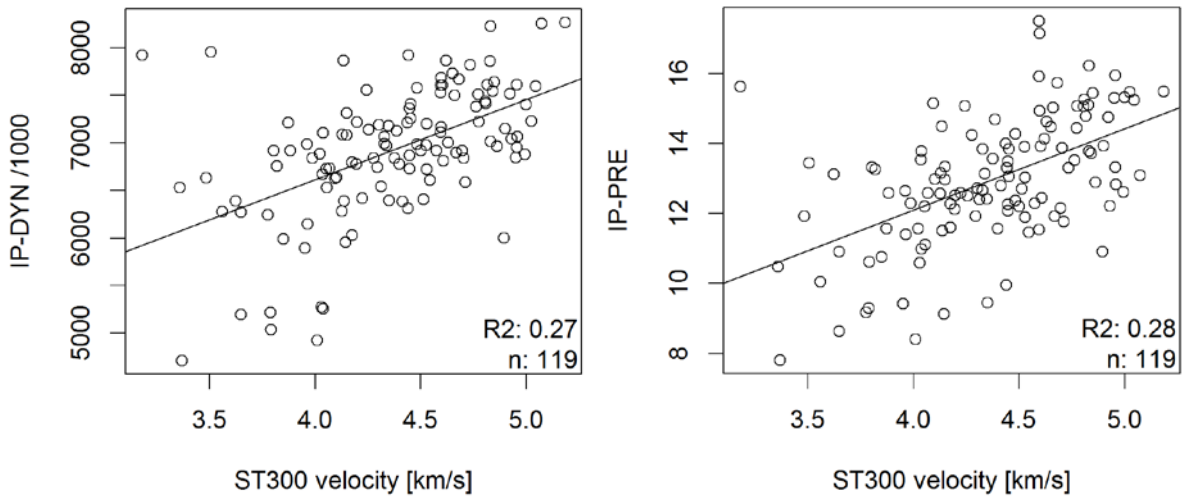

Figure 2—Relationships between machine grading (IP_{DYN} and IP_{PREC}) and ST300 velocity [km/s].

Figure 3 illustrates the relationship between the sound measurements on the logs and the IP-values from the machine grading of the boards.
The r^2-value from a linear regression between the HM200 velocity and the arithmetic mean of IP-values of the boards from the particular log was 0.53 for IP_{DYN} and 0.47 for IP_{PREC}. The results indicate a higher potential for log presorting with HM200 than for tree presorting with ST300.

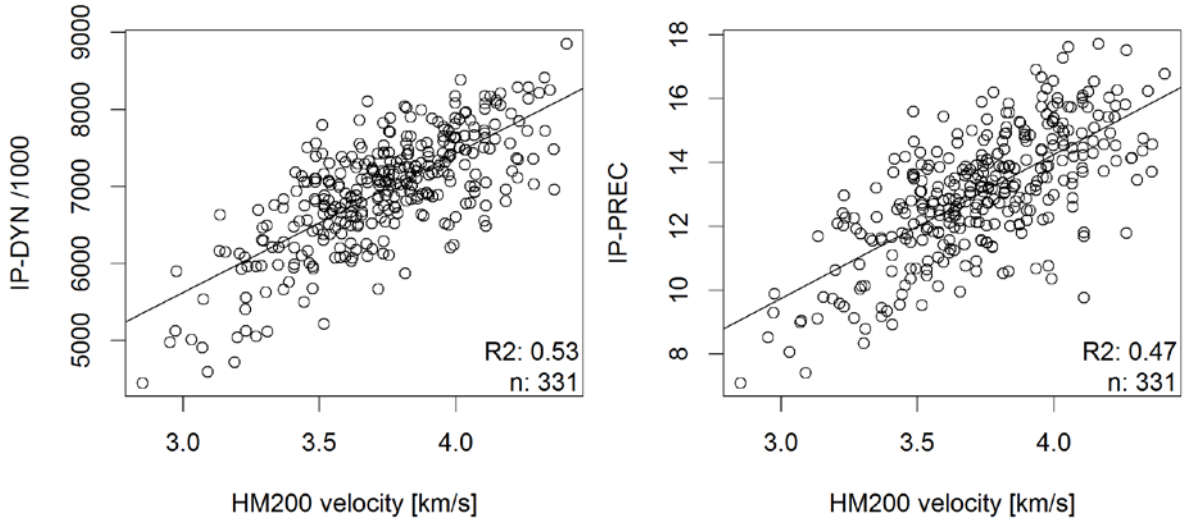

Figure 3—Relationship between machine grading (IP_{DYN} and IP_{PREC}) and HM200 velocity [km/s].

Grade yield

Figure 4 and 5 show the grade yield improvement for the respective strength classes graded as single grades by excluding an increasing portion of trees due to the velocity of the ST300 and HM200. When grading for C24 only, the grade yield was almost 100%. Therefore the C24 results are not presented.

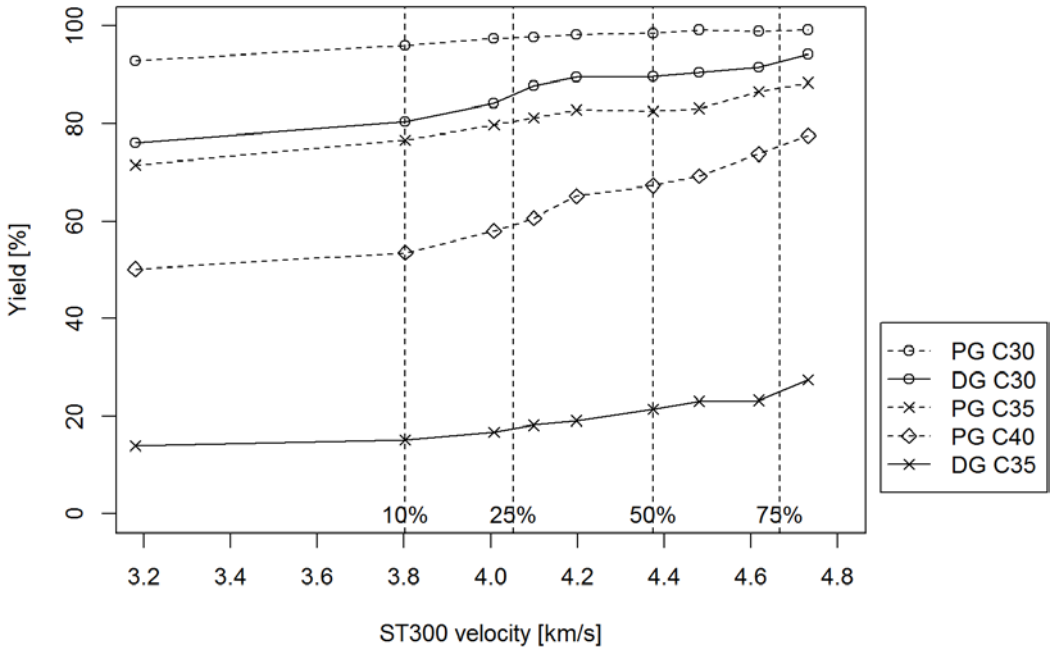

Figure 4—Grade yields from Dynagrade (DG) and Precigrader (PG) and exclusion of boards according to ST300 velocity [km/s].

A considerable part of the trees need to be excluded before the pre-sorting with ST300 velocity shows a substantial effect on the grade yield (Figure 4). For C30 an exclusion of about 50% of the trees increased the grade yield with approximately 15 percent units when the grading was done with Dynagrade and 10 percent units when the grading was done with Precigrader (Figure 4). For C35 graded with Dynagrade, the results show that only 15% of the boards obtained this strength class when considering the whole data set. By excluding about 50% of the trees, the grade yield increased with approximately five percent units.

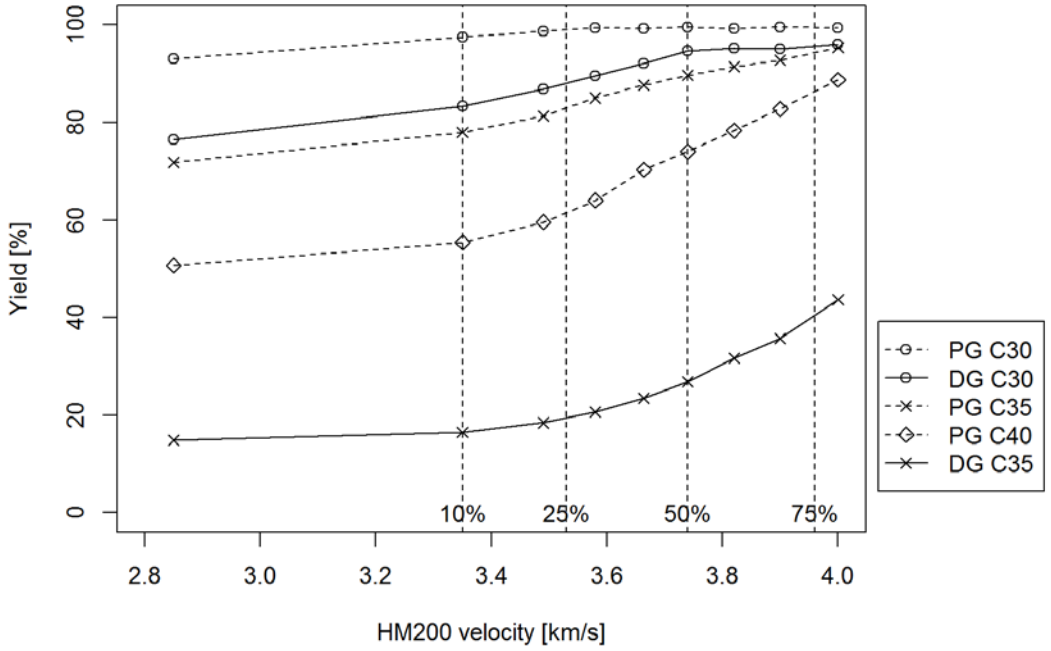

Figure 5—Grade yields from Dynagrade (DG) and Precigrader (PG) and exclusion of boards according to HM200 velocity [km/s].

Figure 5 shows the yield improvements due to acoustic pre-sorting with HM200. When grading with Precigrader for C30 only, the grade yield was almost 90% without any exclusion. However, for the C35 and C40, only a minor percentage of exclusion is required to obtain a considerable increase in grade yield. Excluding the worst 50% of the logs, logs with velocities lower than approximately 3.75 km/s, the yield of boards increased by approximately 20% units for C35 and C40. The effect is somewhat smaller for C30 and C35 when Dynagrade was used. When sawing only the best 50% of the logs, the yield increased with approximately 15% and 10%, respectively (Figure 5).

Discussion

The results of this study show that it is a potential in using acoustic measurements on trees and logs as pre-sorting for structural timber of Norway spruce.
The relationship between the acoustic measurement on the trees and IP-values of the boards is substantially poorer than the relationship between acoustic measurements on the logs and IP values of the boards. This probably is related to the facts that the tree measurements are performed on just a small part of the tree and with one value representing all the boards from the tree, while the log measurement represents only the boards from the particular log. In addition the log measurements were done on the entire log.
For lower grades, like C24 from Dynagrade and C30 from Precigrader, the pre-sorting seems not to be crucial due to already high grade yields. When it comes to the highest grades, especially the upper limit grades of the grading machines, an increased grade yield up to 20% was found, when half of the material was excluded with the HM200 tool.
This is similar to the results of Edlund et al. (2006). They compared MOE classes calculated from sound measurements on logs with the grade yield of machine grading, and found a significant increase for the C30 grade yield in the higher MOE classes. Rais and van de Kuilen (2012) showed for Douglas fir that a threshold value based on acoustic measurement increases the grade yield. Moore et al. (2013) concluded that pre-sorting is not necessary for C16 structural timber of Sitka spruce from UK. Though, when it comes to the production of structural timber with high strength classes, a pre-sorting could be necessary and this could be done by use of acoustic measurements in the forest.

However, the velocity is strongly related to the wood temperature. Searles (2012) found a poor relationship between the velocity of standing trees in summer and winter. Gao et al. (2013) showed that the adjustment for temperature especially around the freezing point is very difficult and uncertain. This fact makes it quite difficult to implement sound measurements in the field in Norway where the winters are long, especially in high altitudes. All the measurements included in this analysis were done well above freezing point.

Conclusion

The study shows that it is possible to improve strength grading with acoustic measurements in the forests. However, the method was only effective for higher strength classes. At the moment the main strength class for structural timber in Norway is C24. If aiming for this grade, presorting in forest seems not to have any substantial effect, but when striving for higher grades like C35 and C40, presorting in forest might be a good option.

Acknowledgement

This study is part of the research project “Tresterk” which is financed by the Research Council of Norway (Grant no. 208085/I10) and the forest and timber industry in Norway.

References

Auty, D.; Achim, A. 2008. The relationship between standing tree acoustic assessment and timber quality in Scots pine and the practical implications for assessing timber quality from naturally regenerated stands. Forestry. 81(4): 475-487.

Edlund, J.; Lindström, H.; Nilsson, F. [and others]. 2006. Modulus of elasticity of Norway spruce saw logs vs. structural lumber grade. Holz als Roh-und Werkstoff. 64(4): 273-279.

Eikenes, B. 1991. Properties of Norway spruce (Picea abies (L.) Karst.) from Western Norway tested on timber in structural sizes. Report. Ås: Agricultural University of Norway, Department of Forestry: 78 p.

Gao, S.; Wang, X.P.; Wang, L.H. [and others]. 2013. Effect of temperature on acoustic evaluation of standing trees and logs: Part 2: Field investigation. Wood Fiber Science. 45(1): 15-25.

Grabianowski, M.; Manley, B.; Walker, J.C.F. 2006. Acoustic measurements on standing trees, logs and green lumber. Wood Science and Technology. 40(3): 205-216.

Haartveit, E.Y.; Flæte, P.O. 2002. Mechanical properties of Norway spruce lumber from monocultures and mixed stands - modelling bending stiffness and strength using stand and tree characteristics [Poster]. In: Connection Between Forest Resources and Wood Quality: Modelling Approaches and Simulation Software. IUFRO WP S5.01-04. Harrison Hot Springs, BC: U.S. Forest Servise, Pacific Northwest Forest and Range Experiment Station, BC Forest Service Research Branch.

Høibø, O.A. 1991. The quality of wood of Norway spruce (Picea abies (L.) Karst) planted with different spacing. Ås: Agricultural University of Norway. PhD thesis.

Kliger, R.; Johansson, M.; Bäckström, M. 2003. Dynamic measuring of modulus of elasticity on logs - a possible way of sorting logs. Report 2003-5. Gothenburg: Chalmers University of Technology, Division of Steel and Timber Structures. 16 p.

Lackner, R.; Foslie, M. 1989. Spruce from Western Norway. Report 487052. Oslo: Norwegian Institute of Wood Technology: 45 p.

Lindström, H.; Reale, M.; Grekin, M. 2009. Using non-destructive testing to assess modulus of elasticity of Pinus sylvestris trees. Scandinavian Journal of Forest Research. 24: 247-257.

Moore, J.; Lyon, A.; Searles, G. [and others]. 2013. Within- and between-stand variation in selected properties of Sitka spruce sawn timber in the UK: implications for segregation and grade recovery. Annals of Forest Science. 70: 403-415.

Moore, J.R.; Lyon, A.J.; Searles, G.J. [and others]. 2009. The Effects of Site and Stand Factors on the Tree and Wood Quality of Sitka Spruce Growing in the United Kingdom. Silva Fennica. 43(3): 383-396.

Nagoda, L. 1985. Strength properties of Norway spruce (Picea abies (L.) Karst.) from Northern Norway tested on timber in structural sizes. Ås: Norwegian Forest Research Institute. 31 p.

Perstorper, M. 1999. Dynamic testing of logs for predicting of timber strength. In: Proceedings of the Pacific Timber Engineering Conference. PTEC'99. Rotorua, NZ: New Zealand Forestry Research Institute: 70-74.

Rais, A.; van de Kuilen, J.W.G. 2012. Pre-grading of Douglas-fir logs for glulam lamella production. In: World Conference on Timber Engineering. Auckland, NZ: New Zealand Timber Design Society: 236-240.

Searles, G. J. 2012. Acoustic Segregation and Structural Timber Production. Edinburgh: Edinburgh Napier University. 206 p. PhD thesis.

Standard Norge. 2009. Timber structures - Strength graded structural timber with rectangular cross section - Part 4: Machine grading - Grading machine settings for machine controlled systems. Norsk Standard NS-EN 14081-4.

Standard Norge. 2011. Timber structures - Strength graded structural timber with rectangular cross section - Part 1: General requirements. Norsk Standard NS-EN 14081-1.

Tsehaye, A.; Buchanan, A.H.; Walker J.C.F. 1997. Log segregation into stiffness classes. In: Proceedings of the Pacific Timber Engineering Conference. PTEC'97. Rotorua, NZ: New Zealand Forestry Research Institute: 7-10.

Tveite, B. 1977. Site-index curves for Norway Spruce (Picea abies (L.) Karst.). In: Meddelelser 33. Ås: Norsk institutt for skogforskning: 1-84.

Wang, X.; Ross, R.J.; Green, D.W. [and others]. 2004. Stress wave sorting of red maple logs for structural quality. Wood Science and Technology. 37(6): 531-537.

Combining acoustic measurements with site-, tree- and log characteristics for pre-sorting of Norway spruce structural timber

Audun Øvrum
Treteknisk (Norwegian Institute of Wood Technology), Oslo, Norway, audun.ovrum@treteknisk.no

Carolin Fischer
Department of Ecology and Natural Resource Management, Norwegian University of Life Science (UMB), Ås, Norway, carolin.fischer@umb.no

Geir I. Vestøl
Department of Ecology and Natural Resource Management, Norwegian University of Life Science (UMB), Ås, Norway, geir.vestol@umb.no

Olav A. Høibø
Department of Ecology and Natural Resource Management, Norwegian University of Life Science (UMB), Ås, Norway, olav.hoibo@umb.no

Abstract

Portable equipment for measuring acoustic velocity in standing trees (ST300) and logs (HM200) has shown its capacity to predict sawn timber strength, but a higher precision for Norway spruce is required to make it economically feasible for this species. In this study logs from 15 trees have been sampled from each of 8 Norway spruce forest sites in south-eastern Norway. Site-, tree and log characteristics were recorded, and the sawn timber was graded with Dynagrade and Precigrader strength grading machines. Combining site-, tree- and log characteristics with acoustic velocity increased the precision of the strength grading. Especially for the ST300 tool, an improvement could be seen. For the models on log level using the HM200 tool, acoustic velocity itself was already such a good predictor that additional information about sites and trees did not improve the precision considerably.

Keywords: acoustic velocity, tree characteristics, log characteristics, strength grading, Norway spruce

Introduction

In the conversion of timber from forest to finished products lot of information about stands, trees, logs and boards are produced. Most of these data usually are dumped and not exploited later in the conversion chain. To use such data to predict the properties of the sawn timber might be of great benefit as the precision might increase, and the amount of waste might decrease. In Norway the main species is Norway spruce, and structural timber is the main product from this specie. As such, an early assessment of timber strength is of great benefit. Øvrum (2013) showed that average tree taper in a stand could be a promising indicator for timber stiffness. Brüchert et al. (2011), showed several models for early assessment of board stiffness for Norway spruce based on various measuring techniques on the different stages of processing along the value chain. Also, new systems for scanning of timber resources, like air-born laser scanning (ALS, LiDAR), could make a stand selection of high strength timber economically feasible and

commercially attractive since this technique is developing towards being able to measure most features of standing trees (Salas et al. 2010).
Acoustics is the most frequent method of early assessement of timber strength, and has been tested succesfully on a number of species (Amishev and Murphy 2008a,b; Auty and Achim 2008; Grabianowski et al. 2006; Ishiguri et al. 2008; Lindström et al. 2002; Lindström et al. 2009; Moore et al. 2009; Tsehaye et al. 2000a; Wang et al. 2001; Amishev and Murphy 2009; Carter et al. 2006; Dickson et al. 2004; Dickson et al. 2003; Jang 2000; Jones and Emms 2010; Tsehaye et al. 2000b). Also for Norway spruce, acoustic measurements to pregrade Norway spruce logs is promising (Edlund et al. 2006; Kliger et al. 2003; Perstorper 1999). These studies were the basis for the study on acoustic tools used for pre-sorting of trees and logs of Norway spruce done by Fischer et al. (2013). They found a significant effect of using acoustic tools on trees and logs, but the reduction of the residual variance was still relatively low, particularly when measuring on standing trees. As such, it would be interesting to see whether other measurable variables in the conversion chain from forest to sawn timber could improve the efficiency of such acoustic pre-sorting of Norway spruce. This has been shown earlier for other species like black spruce (Paradis et al. 2013) and Sitka spruce (Moore et al. 2013). In this study we try to uncover if available data from forest inventories and harvester measurements might be able to improve the efficiency of an acoustic pre-sorting system for Norway spruce.

Material and method

Material

The material used in this study is the same as in Fischer et al. (2013). 15 trees were collected from each of 8 sites in Norway covering a variation in altitude, latitude and site index. Table 1 shows the geographical and forest inventory data for each site.

Table 1—Site data.

Site	Latitude	Longitude	ALT (m)	SI (m)
Begnadalen	N 60.6371	E 9.7993	544	10
Etnedal	N 61.0632	E 9.5403	845	12
Frosta	N 63.6511	E 10.9141	100	13
Stange	N 60.5320	E 11.3701	370	16
Toten	N 60.6618	E 10.8852	220	20
Tretten	N 61.3102	E 10.2391	630	14
Trondheim	N 63.3521	E 10.2455	150	13
Ulsberg	N 62.7471	E 9.9898	470	12

Table 2 shows the different site- tree- and log attributes that have been tested. The response variables were average sawn board IP-values for trees and logs from Dynagrade and Precigrader machines.

Table 2—Tested variables

Variables	Abbreviations	Unit
Site variables		
Site index, dominant height at age 40 years, Tveite (1977)	SI	m
Altitude	Alt.	m.a.s.
Latitude	Lat.	
Tree variables		
Diameter at breast height over bark	DBH	mm
Ratio of DBH of the sample trees to the mean DBH of the stand	DBH_{rel}	
Tree height	H	dm
Tree taper	H/D	mm/m
Height to the whorl where the living crown covered half of the circumference	H_{180}	dm
Height to the whorl where the crown covered the whole circumference	H_{360}	dm
ST300 velocity	ST300	km/s
Log variables		
Relative longitudinal position	LP_{rel}	%
Log taper	LT	mm/m
Log diameter in top end	LD	mm
Log volume	LV	m^3
HM200 velocity	HM200	km/s

Statistical analysis

Stepwise regression analyses were performed to test all the variables of Table 2. Interactions were also tested. The prerequisite for the final models were that all variables should be significant with a p-value below 0.05.

Models for different kind of applications were made, and the different approaches were:

- Harvester models using both ST300 and HM200 technology, with no site information
- Harvester models using both ST300 and HM200 technology with site information
- Log yard models using HM200 technology

Results

In Table 3 the final regression models for the different applications are shown, together with r^2 and RMSE values. For the models including HM200 measurements, the models using a combination of harvester and site information gave the highest r^2 values, but the additional reduction in residual variance was quite small. Also for the models including ST300 measurements, the best models included harvester and site information in combination. For these prediction models the increases in r^2 values were higher than for the HM200 models.

Table 3—Regression models with r^2 and RMSE in percentage of the mean IP-value

Model	Fitted regression equation	Fitted data set	
		R^2	RMSE [%]
acoustic measurements			
IP_{dyn} butt log	2328804,9 + 1034469ST300	0,30	9,8
IP_{prec} butt log	2,416 + 2,357ST300	0,23	14,0
IP_{dyn}	200505,66 + 1808386,3HM200	0,53	7,2
IP_{prec}	-3,757 + 4,504HM200	0,47	10,7
harvester			
IP_{dyn} butt log	-1452948 + 853283,6ST300 + 398054,62H/D + 4997,846DBH - 349182,6ST300*H/D	0,50	8,4
IP_{prec} butt log	-3,741 + 1,826ST300 + 0,829H/D + 0,007DBH - 1,501ST300*H/D	0,45	12,0
IP_{dyn}	1173115,4 + 1622892,1HM200 - 38001,37LT + 42602,111HM200*LT + 412104,56LP_{rel}	0,58	6,9
IP_{prec}	-2,705 + 4,601HM200 - 0,007LD	0,51	10,4
harvester + site			
IP_{dyn} butt log	2144638,2 + 633566,73ST300 + 163732,67H/D - 249858,5ST300*H/D + 71392,095SI - 803,208ALT	0,56	7,9
IP_{prec} butt log	4,621 + 1,211ST300 + 0,518H/D - 1,365ST300*H/D + 0,003ALT	0,50	11,5
IP_{dyn}	848994,91 + 1509542,9HM200 - 25424,94LT + 54629,561HM200*LT + 53216,16SI	0,61	6,6
IP_{prec}	0,399 + 3,964HM200 - 0,007LD + 0,010HM200*LD - 0,002ALT	0,55	9,9
log yard			
IP_{dyn}	1307847,8 + 1614992,5HM200 - 37985,78LT	0,57	6,9
IP_{prec}	-2,848 + 4,601HM200 - 0,006LD + 0,011HM200*LD	0,52	10,3

In the next step the effect of excluding logs and trees on grade yield was investigated. The exclusion was based on the regression models from Table 3. Figure 1 shows the improvement in yield due to increasing exclusion rates for strength class C35 from Dynagrade and strength class C40 from Precigrader (models on tree level). The improvement in yield due to exclusion was greater for Dynagrade IP-values when using combined models than for Precigrader IP-values. A higher increase in yield for models including harvester and harvester+site information was also found. From about 50% exclusion the simple model using only ST300 was best. Most likely this is caused by the large variation within logs and trees in which the models cannot account for since they are predicting average values for logs or trees.

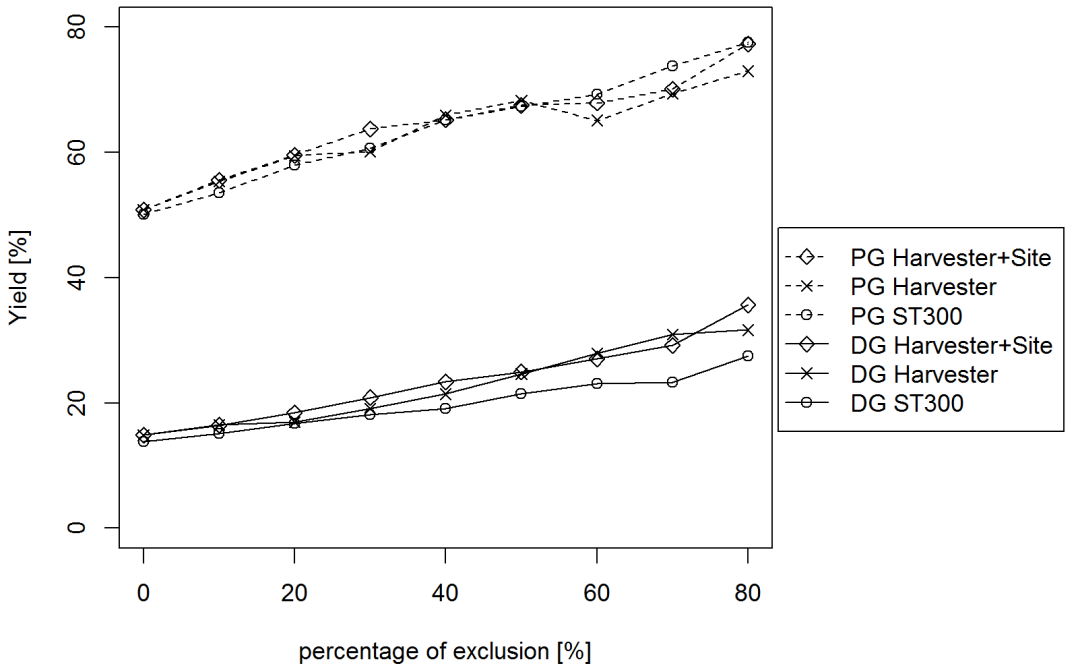

Figure 1—Grade yield improvement of C35 from Dynagrade (DG) and C40 from Precigrader (PG) for the different models including ST300 measurements on tree level.

In Figure 2 the yield improvements for the Dynagrade C35 strength class and the Precigrader C40 strength class for the models on log level including HM200 velocity, are shown. The improvement of adding more information in addition to the HM200 velocity is very low.

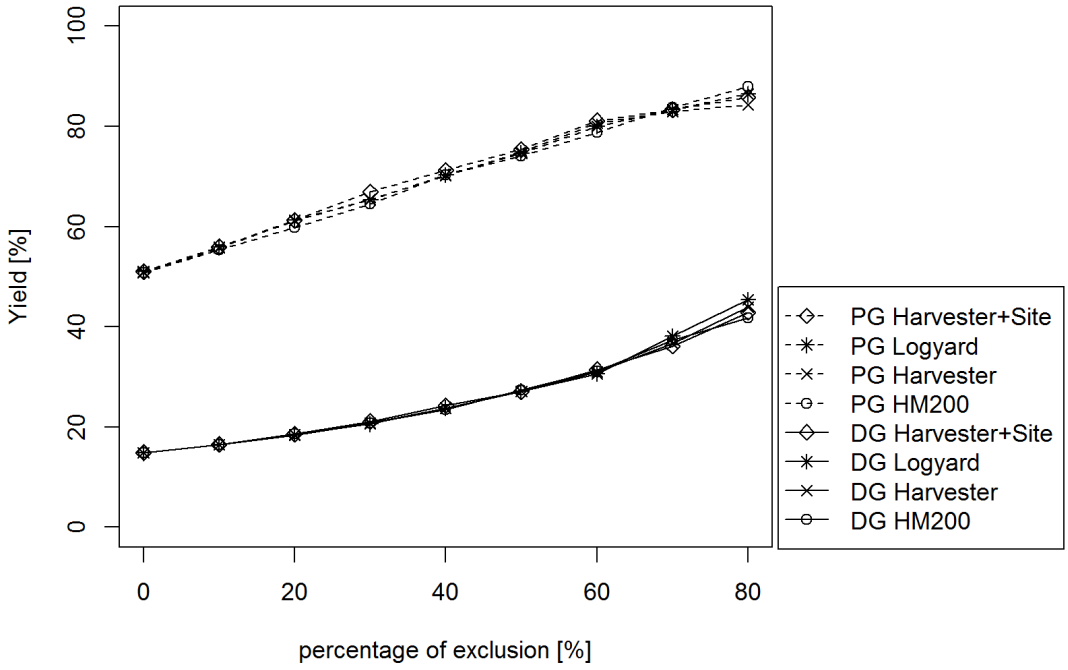

Figure 2—Grade yield improvement of C35 from Dynagrade (DG) and C40 from Precigrader (PG) for the different models including HM200 measurements.

Discussion

In Fischer et al.(2013), the effect of using only ST300 on trees for pre-sorting was quite poor. Adding other tree variables made a substantial additional reduction in the board strength residual variance, especially when the strength grading was done with Precigrader. Adding site information reduced the residual variance even more. These results are reflected in the grade yields.

For the HM200, adding more log characteristics had an effect, but not as for the ST300. Most probably, this is mainly due to a better correlation between the HM200 measurements and mean log IP values, found by Fischer et al. (2013). As such it might be sufficient with just a log yard model for logs measured with the HM200.

For all the models, the r^2 values were lower for Precigrader than for Dynagrade, but the improvement in r^2 was almost similar between the machines when adding more variables to the acoustic measurements. The Precigrader is a more precise grading machine than Dynagrade since it also includes density in the prediction of sawn timber strength. If density measurements had been included in addition to velocity when MOE of the logs and trees were calculated, the difference between the machines might have been smaller. All the boards will be tested in the lab for real strength and stiffness in the near future. This will give more insight to this issue.

What kind of acoustic tool that should be included in a harvester is not straight forward. Alone, the HM200 performs much better than the ST300, but the difference is insubstantial when site-, tree- and log variables are included. Though, Amishev and Murphy (2008a, 2008b) showed in a study on Douglas fir, that the ST300 tool showed very poor results for pre-sorting of veneer quality, while the HM200 tool showed promising results in-forest pre-sorting for green veneer.

Other investigations have shown that including more variables in addition to acoustic tools gives better prediction of board strength. Moore et al. (2013) got similar results to this study. They found significant effects of adding altitude and DBH in models predicting the IP-value of boards of Sitka spruce grown in Scotland. Paradis et al. (2013) found for mean tree static MOE a positive relation to squared velocity and a negative relation to DBH for black spruce.

Conclusion

Site-, tree- and log level variables substantially increased the precision for timber strength predictions from acoustic measurements done on standing trees of Norway spruce by ST300 from Fibregen. For acoustic measurements on logs using the HM200 from Fibregen the improvement was much poorer. The effect on yields reflected this, and suggested that if using the HM200 to predict board strength no additional information is needed, while using the ST300 site and harvester information is necessary to make the implementation of acoustic measurements interesting as a pre-sorting tool.

Acknowledgments

This study is part of the research project “Tresterk” which is financed by the Research Council of Norway (Grant no. 208085/I10) and the forest and timber industry in Norway.

References

Amishev, D.; Murphy, G.E. 2008a. Implementing resonance-based acoustic technology on mechanical harvesters/processors for real-time wood stiffness assessment: opportunities and considerations. International Journal of Forest Engineering. 19(2): 48-56.

Amishev, D.; Murphy, G.E. 2008b. In-forest assessment of veneer grade Douglas-fir logs based on acoustic measurement of wood stiffness. Forest Products Journal. 58(11): 42-47.

Amishev, D.; Murphy, G.E. 2009. Estimating breakeven prices for Douglas-fir veneer quality logs from stiffness graded stands using acoustic tools. Forest Products Journal. 59(4): 45-52.

Auty, D.; Achim, A. 2008. The relationship between standing tree acoustic assessment and timber quality in Scots pine and the practical implications for assessing timber quality from naturally regenerated stands. Forestry. 81(4): 475-487.

Brüchert, F.; Wilhelmsson, L.; Mochan, S.; [and others]. 2011. An integrated approach for wood quality prediction from standing tree to sawn timber. In: Proceedings of the 17th International Nondestructive Testing and Evaluation of Wood Symposium. Sopron, Hungary: University of West Hungary: 40-47.

Carter, P.; Chauhan, S.; Walker J. 2006. Sorting Logs and Lumber for Stiffness Using Director HM200. Wood and Fiber Science. 38(1): 49-54.

Dickson, R.L.; Matheson, A.C.; Joe, B. [and others]. 2004. Acoustic segregation of Pinus radiata logs for sawmilling. New Zealand Journal of Forestry Science. 34(2): 175-189.

Dickson, R.L.; Raymond, C.A.; Joe, W.; Wilkinson, C.A. 2003. Segregation of Eucalyptus dunnii logs using acoustics. Forest Ecology and Management. 179(1-3): 243-251.

Edlund, J.; Lindström, H.; Nilsson, F. [and others]. 2006. Modulus of elasticity of Norway spruce saw logs vs. structural lumber grade. Holz als Roh- und Werkstoff. 64(4): 273-279.

Fischer, C.; Øvrum, A.; Vestøl, G.I. [and others] 2013. Performance of acoustic tools for pre-grading of Norway spruce structural timber. In: 18th International Nondestructive Testing and Evaluation of Wood Symposium. Madison, WI: U.S. Department of Agriculture, Forest Service, Forest Products Laboratory.

Grabianowski, M.; Manley, B.; Walker, J.C.F. 2006. Acoustic measurements on standing trees, logs and green lumber. Wood Science and Technology. 40(3): 205-216.

Ishiguri, F.; Matsui, R.; Iizuka, K. [and others]2008. Prediction of the mechanical properties of lumber by stress-wave velocity and Pilodyn penetration of 36-year-old Japanese larch trees. European Journal of Wood and Wood Products. 66(4): 275-280.

Jang, S.S. 2000. Evaluation of lumber properties by applying stress waves to larch logs grown in Korea. Forest Products Journal. 50(3): 44-48.

Jones, T.G.; Emms, G.W. 2010. Influence of Acoustic Velocity, Density, and Knots on the Stiffness Grade Outturn of Radiata Pine Logs. Wood and Fiber Science. 42(1): 1-9.

Kliger, R.; Johansson, M.; Bäckström, M. 2003. Dynamic measuring of modulus of elasticity on logs - a possible way of sorting logs. Report 2003-5. Gothenburg: Chalmers University of Technology, Division of Steel and Timber Structures. 16 p.

Lindström, H.; Harris, P.; Nakada, R. 2002. Methods for measuring stiffness of young trees. Holz Als Roh-Und Werkstoff. 60(3): 165-174.

Lindström, H.; Reale, M.; Grekin, M. 2009. Using non-destructive testing to assess modulus of elasticity of Pinus sylvestris trees. Scandinavian Journal of Forest Research. 24: 247-257.

Moore, J.; Lyon, A.; Searles, G. [and others]. 2013. Within- and between-stand variation in selected properties of Sitka spruce sawn timber in the UK: implications for segregation and grade recovery. Annals of Forest Science. 70: 403-415.

Moore, J.R.; Lyon, A.J.; Searles, G.J. [and others]. 2009. The Effects of Site and Stand Factors on the Tree and Wood Quality of Sitka Spruce Growing in the United Kingdom. Silva Fennica. 43(3): 383-396.

Paradis, N.; Auty, D.; Carter, P. [and others]. 2013. Using a Standing-Tree Acoustic Tool to Identify Forest Stands for the Production of Mechanically-Graded Lumber. Sensors. 13(3): 3394-3408.

Perstorper, M. 1999. Dynamic testing of logs for predicting of timber strength. In: Proceedings of the Pacific Timber Engineering Conference. PTEC'99. Rotorua, NZ: New Zealand Forestry Research Institute: 70-74.

Salas, C.; Ene, L.; Gregoire, T.G. [and others]. 2010. Modelling tree diameter from airborne laser scanning derived variables: A comparison of spatial statistical models. Remote Sensing of Environment. 114(6): 1277-1285.

Tsehaye, A.; Buchanan, A.H.; Walker, J.C.F. 2000a. Selecting trees for structural timber. Holz als Roh- und Werkstoff. 58(3): 162-167.

Tsehaye, A.; Buchanan, A.H.; Walker, J.C.F. 2000b. Sorting of logs using acoustics. Wood Science and Technology. 34(4): 337-344.

Tveite, B. 1977. Site-index curves for Norway Spruce (Picea abies (L.) Karst.). In: Meddelelser 33. Ås: Norsk institutt for skogforskning: 1-84.

Wang, X.P.; Ross, R.J.; McClellan, M. [and others] 2001. Nondestructive evaluation of standing trees with a stress wave method. Wood and Fiber Science. 33(4): 522-533.

Øvrum, A. 2013. In-forest assessment of timber stiffness in Norway spruce (Picea abies (L.) Karst.). European Journal of Wood and Wood Products. 71(4): 429-435.

Stress Wave E-Rating of Structural Timber—Size and Moisture Content Effects

Xiping Wang
USDA Forest Service, Forest Products Laboratory, Madison, Wisconsin, USA, xwang@fs.fed.us

Abstract

The objectives of this study were to investigate the influence of cross-sectional size and moisture content on stress wave properties of structural timber in various sizes and evaluate the feasibility of using stress wave method to E-rate timber in green conditions. Four different sizes of Douglas-fir (*Pseudotsuga menziesii*) square timbers were tested using both stress wave and static bending methods at different moisture levels, ranging from green to dry conditions. As expected, stress wave velocity increased continuously as moisture content decreased through the whole moisture range studied. Master velocity–moisture relationships were established for Douglas-fir square timbers to convert stress wave velocity values from one moisture condition to any other moisture conditions. It was found that stress wave based dynamic MOE was generally higher than static bending MOE. However, the difference tended to be constant when moisture content was above the fiber saturation point (28%). This implied that green timber could still be sorted effectively based on dynamic MOE values even if there are moisture differences between individual pieces. The results also show that cross-sectional dimension of square timbers has a significant influence on dynamic MOE. As the cross-sectional size of square timbers increased, the MOE deviation increased also. This indicates that different sizes of timbers can not be graded together without making appropriate adjustments on dynamic MOE for size effect.

Keywords: Stress wave, structural timber, modulus of elasticity, moisture content, size

Introduction

Longitudinal stress wave technology has been widely used to evaluate the performance of various wood products in wood industry but more research is needed to enhance its application in timber grading. The fundamental wave theory used to evaluate the modulus of elasticity (MOE) of wood was developed for long slender rods of isotropic and elastic materials. Problems arise for wood with various cross-sectional sizes and high levels of moisture content (above fiber saturation point). Stress wave predicted MOE of wood in the forms of structural lumber (including dimensional lumber and structural timber) were significantly deviated from their static counterpart when the fundamental wave theory was applied. The objectives of this study were to investigate the influence of cross-sectional size and moisture content on stress wave properties of structural timber and evaluate the feasibility of using stress waves to E-rate timbers in green conditions.

Background

Predicting the MOE of structural lumber with longitudinal stress waves has received considerable research effort in recent years in terms of lumber grading or presorting. Typically, the MOE of a lumber is determined from the one-dimensional wave equation:

$$MOE_d = C^2 \rho \quad (1)$$

where MOE_d is dynamic MOE (stress wave MOE), C is wave velocity, and ρ is gross density. This fundamental wave equation was developed for idealized elastic materials in the form of a long slender rod (Meyers 1994). Its application in wood materials can be affected by many factors, such as grain angle, knots, wood moisture content, and wood temperature, as well as dimensional size and geometrical form of a material.

Many investigations have dealt with the effects of moisture content, temperature, grain angle, and knots on stress wave behavior in wood. Stress wave velocity has been shown to decrease as either moisture content or temperature of wood is increased (James 1961; Burmester 1965; Gerhards 1975; Wang 1999; Han et al. 2006). Dynamic MOE calculated from wave velocity and wood density increases as moisture content increases above the fiber saturation point (FSP) (Galligan and Courteau 1965; Gerhards 1975; Sobue 1993). However, no attempt has been made to systematically investigate moisture influence on stress wave properties of structural lumber in different sizes and establish valid moisture adjustment on stress wave measures.

Gerhards (1982) studied the effects of knots on stress waves in lumber and found that wave velocity was slowed through knots and the curved grain around knots. Gerhards also suggested that, in lumber with cross grain and knots, the stress wave does not propagate with a normal wave front as supposed by the long slender rod theory but has a wave front that leads in the direction of the grain and lags across the grain or through knots. This non-normal wave front causes some problems in timing stress waves, particularly in large, short wood members.

The sizes (both cross section and length) and geometrical form of wood have also been recognized as critical factors to the application of the fundamental wave equation for wood property prediction (Wang et al. 2004). Theoretically, the one-dimensional wave Equation (1) is developed based on uniaxial stress. However, in a real case, there is radial inertia and a wave interaction with the external surfaces (free surfaces) of the material (Meyers 1994). Radial inertia is caused by the kinetic energy of the material flowing radially outward as the material is compressed. This effect, controlled by the dimensional size of materials, could have a significant bearing on the interpretation of stress-wave properties. Porter et al. (1972) first noted from experiments that stress-wave velocity could be affected by the dimensional size of the material in lumber testing. As a 51-mm by 305-mm (nominal 2- by 12-in.) lumber was cut down to 51 by 152 mm (nominal 2 by 6 in.) and 51 by 76 mm (nominal 2 by 3 in.), Porter et al. observed a continuous increase in wave velocity. Although the change in wave velocity may not be significant, it may introduce a significant change in dynamic MOE calculated from wave velocity and wood density since dynamic MOE is proportional to C^2. Wang (1999) investigated stress-wave behavior in red pine logs and found that high diameter to length ratio could cause significant changes in the wave propagation path with respect to longitudinal direction. Quantitative analyses of the effect of dimensional size on stress wave E-rating of structural lumber is still lacking.

Materials and Methods

Specimen preparation

The specimens used in this study were green Douglas-fir square timbers that were originally used for a heat sterilization study (Simpson et al 2003). After heat treatment (using steam with low wet-bulb depression), they were immediately stored under water spray for the purpose of this study. The specimens are 2.44-m long and included four size groups: 102 by 102 mm (4 by 4 in.), 152 by 152 mm (6 by 6 in.), 203 by 203 mm (8 by 8 in.), and 254 by 254 (10 by10 in.). Each size group included five specimens, which resulted in a total of 20 square timber specimens.

Experimental procedure

Table 1 shows the experimental matrix for testing square timber specimens. All timber specimens were first nondestructively (stress wave and static bending) tested in their initial green condition (MC_1). They were then stored in a condition room with 23 °C temperature and 65% relative humidity (RH) for air drying. During the drying process, stress wave and static bending tests were performed at four intermediate moisture levels (MC_2, MC_3, MC_4, and MC_5). The dimension, length, and weight of each specimen were also measured each time. At the end, all specimens were stored in a 32 °C and 25% RH condition room for about six months to allow each specimen conditioned to 5% equilibrium moisture content (EMC) (MC_6). Each specimen was then tested using the same procedure.

Table 1. Experimental matrix for examining the size and moisture effects on stress wave properties of structural lumber

Size of specimen	Moisture levels of specimen						Length-depth ratio
	Green	Intermediate moisture condition				5% EMC	
	MC_1	MC_2	MC_3	MC_4	MC_5	MC_6	
	Replicates						
102 by 102	5	5	5	5	5	5	24.0
152 by 152	5	5	5	5	5	5	15.3
203 by 203	5	5	5	5		5	11.2
254 by 254	5	5	5	5		5	8.8

Stress wave measurements

Stress wave measurement was conducted on each timber specimen to obtain the stress wave velocity. A stress wave was initiated by a hammer impact on one end of the timber. Stress wave propagation in the timber was sensed by a piezoelectric transducer mounted on the other end of the timber. Waveforms were displayed and analyzed using a personal computer through a data acquisition system and a software program. The program measured the time (Δt) between adjacent peaks in the waveform, which is the wave propagation time through a timber. Stress wave velocity can be determined by the equation

$$C = \frac{2L}{\Delta t} \tag{2}$$

where C is stress wave velocity in a specimen (m/s), L the length of the specimen (m), and Δt the stress wave propagation time (s). From stress wave velocity (C) and wood density (ρ) of the specimens, the dynamic modulus of elasticity (MOE_d) can be calculated using the fundamental wave Equation (1).

Static bending tests

Following stress wave measurements, all specimens were mechanically tested in bending with an Instron instrument to obtain the modulus of elasticity at various moisture levels. The static bending tests were conducted on each specimen within elastic limit using center-point loading (three replications for each specimen at each moisture condition) (ASTM 2003).

The square timbers were tested with center loading applied to the radial face with a test span of 2.13 m. The load-deflection data was recorded by the machine and the apparent modulus value was calculated using Instron's Merlin software, which is based the equation

$$\mathrm{MOE} = \frac{Pl^3}{48I\delta} \tag{3}$$

where P is the applied load (kgf), l the test span (cm), I moment of inertia (cm^4), and δ the midspan deflection (cm).

Density and moisture content determination

The dimension (cross section size and length) and weight of each specimen were measured at each moisture condition during the experimental process. Density of each specimen was calculated based on the weight and volume at each moisture level. After the stress wave and mechanical tests were completed, a moisture sample was cut from each specimen and its moisture content was determined using the oven dry method (ASTM D 4442-92, ASTM 2003). The size of moisture samples varied for different specimens, but generally was a 38-mm-thick slice cut from the location 152 to 305 mm from one end and contained no defects. The oven-dry determined MC of each moisture sample was then used to estimate the oven-dry weight of the corresponding specimen using the following equation:

$$\hat{W_{OD}} = \frac{W_0}{1 + MC_0} \tag{4}$$

where $\hat{W_{OD}}$ is the estimate of oven-dry weight of the specimen (g),; MC_0, the moisture content of the moisture sample at the equilibrium condition (%), and W_0, the weight of the specimen at equilibrium condition (g).

The moisture content of each specimen at each testing condition was then determined based on the weight measured at the time of testing and the estimated oven-dry weight of the specimen $\hat{W_{OD}}$

$$\mathrm{MC}_i = \frac{W_i - \hat{W_{OD}}}{\hat{W_{OD}}} \times 100\% \tag{5}$$

where MC_i is the moisture content of a specimen at moisture level i (%), and W_i, the weight of the specimen at moisture level i (g).

Results and Discussion

The initial moisture content of the timber specimens ranged from 32% to 63%. The specimens of 102 by 102 mm and 152 by 152 mms were tested at four intermediate moisture levels during drying process as originally planned (Table 1), but 203 by 203 mm and 254 by 264 mm specimens were tested at only three intermediate moisture levels because of limited machine time.

The nominal depth of the timber specimens ranged from 102 to 264 mm, which resulted in span-depth ratios ranging from 24 to 8.8. The small span-depth ratios for square timber specimens, especially for 203- by 203-mm and 264- by 264-mm timbers, could introduce a significant shear deflection to the beam in static bending testing.

The shear deflection, governed by the characteristics of the timber and the loading condition, can be estimated mathematically (Biblis 1965). For a simply supported beam loaded at midspan, the deflection due to shear is given by

$$\delta_s = \frac{0.3Pl}{AG} \tag{6}$$

Where P is the load (kgf), l is the span length (cm), A is the cross section area (cm^2), and G the shear modulus (Pa).

Assume that the ratio of E to G is constant, having a value of 16 for wood, the true modulus of elasticity (E) of the timber specimens can be calculated using the following equation (Bodig and Jayne 1982):

$$E = \left[1 + \frac{K}{(l/h)^2}\right] \mathrm{MOE} \tag{7}$$

Where K is a constant controlled by the loading condition (K = 19.20 for concentrated load at the center), h is the depth of the timber specimens (cm).

The effect of span to depth ratio (l/h) for wood beams with concentrated load at the center is illustrated in Figure 1. As span-to-depth ratio decreases, shear deflection increases, thus the magnitude of error introduced by ignoring shear deflection gets bigger. To correct shear effect, true modulus of elasticity of each timber specimen was determined using Equation (12).

Figure 2 shows the relationship between stress wave velocity and moisture content for all timber specimens. The velocity–moisture relations for timber specimens were found analogous to what observed in dimension lumber specimens (Wang 2008). Stress wave velocity increased continuously as moisture content decreased. Stress wave velocity changed more rapidly in low moisture level (below FSP) than in high moisture level (above FSP). It was noted that all square timber specimens tend to have same type of velocity–moisture relationships. It is therefore possible that a master equation can be built to adjust stress wave velocity for moisture effect.

Table 2 shows the results of regression analysis for the relationships between stress wave velocity and moisture content of Douglas-fir timbers. A nonlinear regression analysis based on a backward selection procedure was performed to establish the empirical relationships. It was found that a second-order polynomial regression model fits the experimental data. By averaging the regression coefficients of individual models, a master velocity–moisture relationship was developed:

$$C = C_0 - 148.706(\mathrm{MC}) + 1.4525(\mathrm{MC}^2) \tag{8}$$

Where C_0 is a constant that depends on the properties of specific timber.

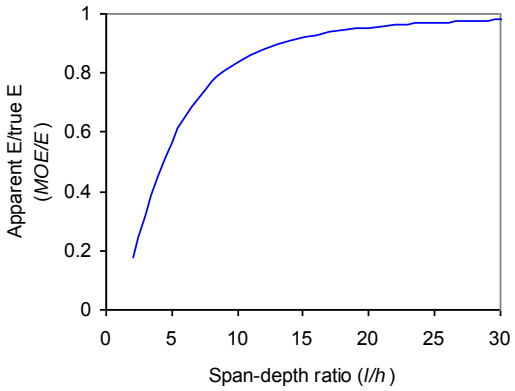

Figure 1. Effect of span to depth ratio (l/h) on the ratio of apparent to true modulus of elasticity for wood beams with concentrated load at the midspan.

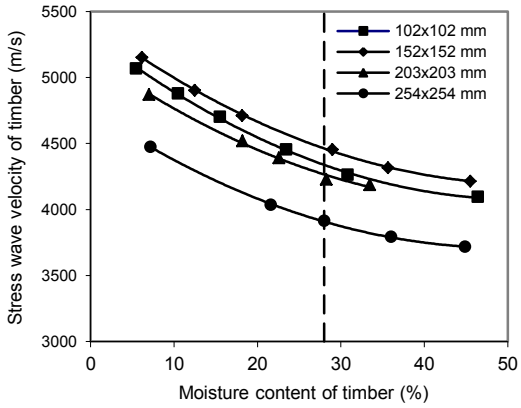

Figure 2. Relationship between stress wave velocity and moisture content of square timbers.

Table 2. Regression analysis of the relationships between stress wave velocity and moisture content of square timbers

Size group	Regression model: $C = a + b(MC) + c(MC^2)$				
	a	*b*	*c*	r^2	S_{xy} *
102 × 102	17472	–158.377	1.5290	0.999	53.3
152 × 152	17780	–152.731	1.4499	0.999	34.4
203 × 203	16949	–145.849	1.4419	0.994	94.8
254 × 254	15594	–137.867	1.3890	1.000	23.7

* S_{xy} - Standard error

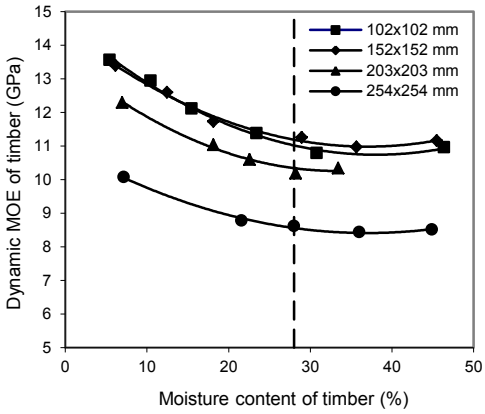

Figure 3. Relationship between dynamic modulus of elasticity and moisture content of Douglas-fir square timbers.

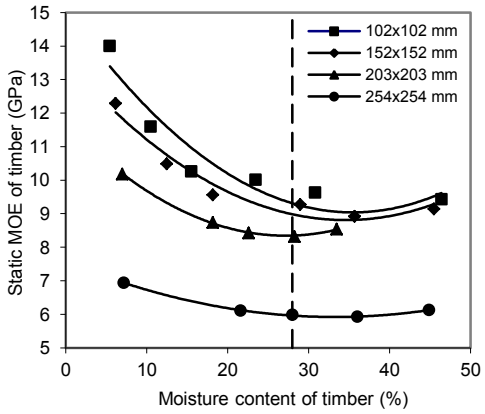

Figure 4. Relationship between static bending modulus of elasticity and moisture content of Douglas-fir square timbers.

For a given timber, if the stress wave velocity (C_1) is measured at moisture condition of MC_1, then the velocity can be converted to a value at any moisture content MC_2 (within the tested moisture range) using the following equation:

$$C_2 = C_1 - 148.706(\mathrm{MC}_2 - \mathrm{MC}_1) + 1.4525(\mathrm{MC}_2^{\,2} - \mathrm{MC}_1^{\,2}) \quad (9)$$

Figure 3 and Figure 4 show the relationships between modulus of elasticity and moisture content for square timber specimens. Note that Figure 4 relates the true modulus of elasticity to MC. The results indicated that both dynamic modulus and static modulus decreased with increasing moisture content when MC was below FSP, but they remained relatively constant when MC was above FSP. This finding is consistent with what we observed in dimension lumber specimens (Wang 2008).

Figure 5 shows the comparison of dynamic MOE and static MOE at various moisture levels for the Douglas-fir timbers. The dynamic MOE of square timber were generally higher than their static counterpart. The deviation of dynamic MOE from static E (true value) was affected by the moisture content for 102- × 102-mm and 152- × 152-mm timbers when MC was below FSP, but the moisture effect on MOE diminished as timber size increased to 203 × 203 mm and 254 × 254 mm.

We also noticed that despite a significant deviation between dynamic and static MOE values, the dynamic MOE generally followed the same trend as static MOE. The MOE deviation in each size group was relatively constant when MC was above FSP. This implied that green timber could still

be sorted effectively on the basis of dynamic MOE value even if there are moisture differences between individual pieces, as long as all timbers are in green condition.

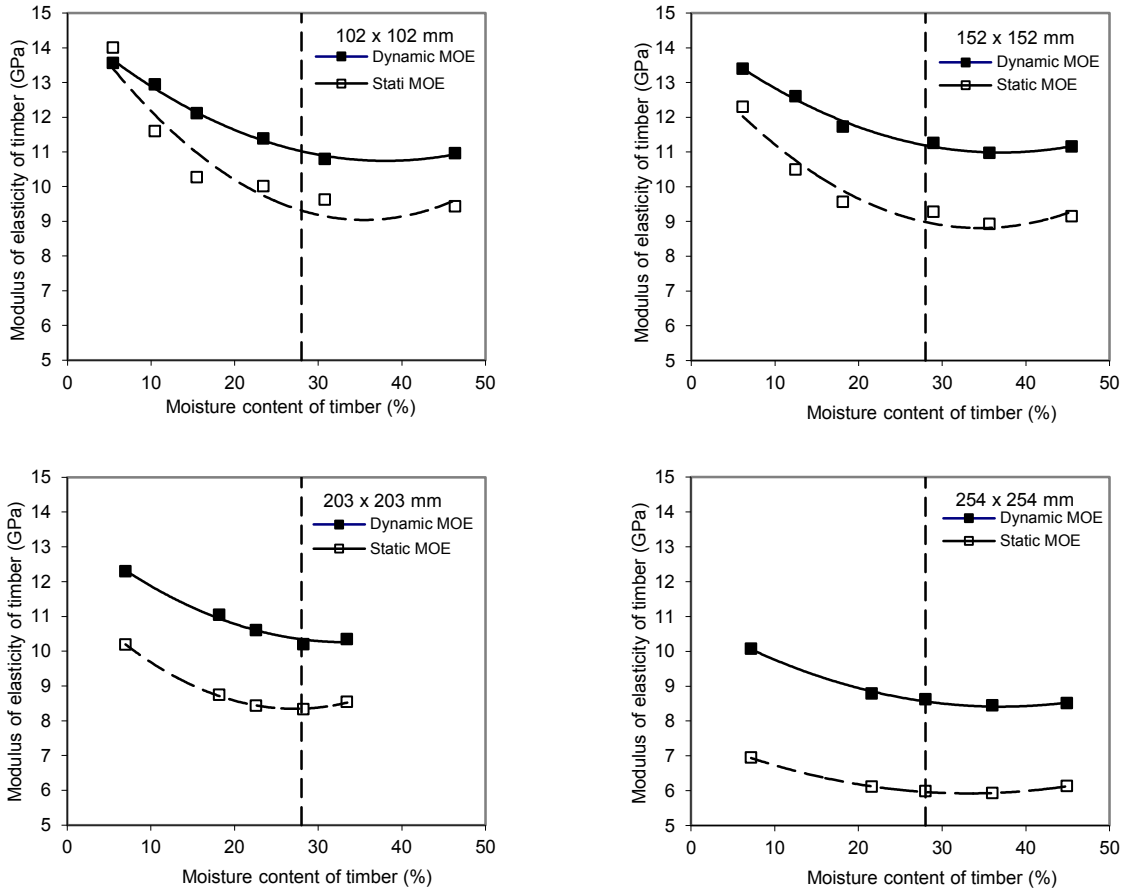

Figure 5. Comparison of dynamic MOE and static MOE at various moisture levels for square timber.

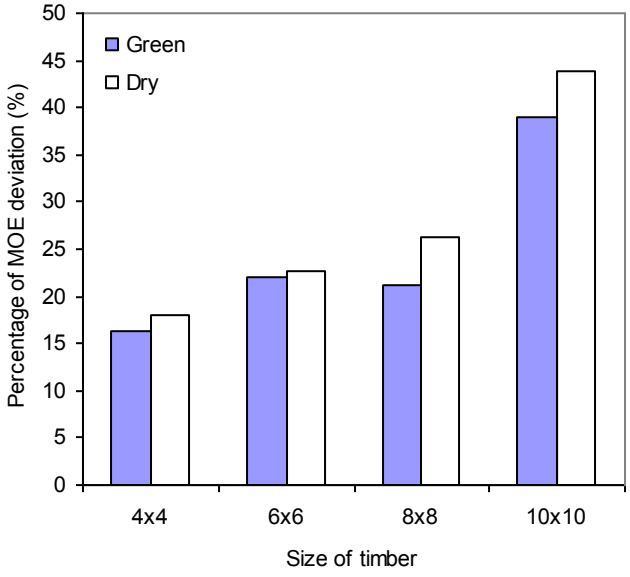

Figure 6. Average percentage of MOE deviation for each size group of square timber specimens at green (34%–46%) and dry (16%–22%) conditions.

Figure 6 is a histogram illustrating the average percentage of MOE deviation for each size group of timber specimens at green (34%–46%) and dry (16%–22%) conditions. Apparently, the size of timber has a significant impact on stress wave-E rating at both green and dry conditions. As the size of timbers increased, the MOE deviation increased. This implies that different sizes of timbers can not be graded together without making appropriate adjustments on dynamic MOE for size effect.

Conclusion

This study explored the effects of moisture content and cross-sectional dimension on stress wave E-rating of Douglas-fir timbers. From the results of the study, we conclude the following:

1. Stress wave velocity of Douglas-fir timbers increased continuously as moisture content decreased through the whole moisture range studied. Stress wave velocity changed at a much slower rate in high moisture levels (above fiber saturation point) than in low moisture levels (below FSP).

2. A master velocity–moisture relationship was formed for different size groups of the square timbers. This empirical model can be used to convert stress wave velocity values measured at one moisture condition to any other moisture conditions.

3. Below the fiber saturation point, dynamic modulus of elasticity increased continuously as moisture content decreased. Above the fiber saturation point, dynamic MOE remained relatively constant.

4. The dynamic modulus of elasticity of the square timbers was generally higher than the static bending modulus of elasticity. The deviation of dynamic MOE from its static counterpart was affected by the moisture content of the specimens when MC was below FSP. The MOE deviation were relatively constant when moisture level was above FSP. This implied that green timber could still be sorted effectively based on dynamic MOE values even if there are moisture differences between individual pieces.

5. We found that the cross-sectional dimension did have a significant influence on MOE deviation for Douglas-fir square timbers. As the cross-sectional size of the timber increased, the MOE deviation increased also. This indicates that different sizes of timbers can not be graded together without making appropriate adjustments on dynamic MOE for size effect.

Reference

ASTM. 2003. Standard test methods of static tests of lumber in structural sizes. ASTM Designation D198-02. Annual Book of ASTM Standards. Vol. 04.10. West Conshohocken, PA: American Society for Testing and Materials.

ASTM. 2003. Standard test methods for direct moisture content measurement of wood and wood-base materials. ASTM Designation D4442-92. Annual Book of ASTM Standards. Vol. 04.10. Wood. West Conshohocken, PA: American Society for Testing and Materials.

Biblis, E.J. 1965. Shear deflection of wood beams. Forest Products Journal. 15(11):492–498.

Bodig, Jozsef, Jayne, B.A. 1982. Mechanics of wood and wood composites. New York: Van Nostrand Reinhold Company. 712 p.

Burmester, A. 1965. Relationship between sound velocity and the morphological, physical, and mechanical properties of wood. Holz als Roh-und Werkstoff. 23(6):227–236.

Galligan, W.L., Courteau, R.W. 1965. Measurement of elasticity of lumber with longitudinal stress waves and the piezoelectric effect of wood. In: Proceedings of the 2nd Symposium on Nondestructive Testing of Wood. April. Washington State University, Pullman, Washington. 223–224.

Gerhards, C.C. 1975. Stress wave velocity and MOE of sweetgum ranging from 150 to 15 percent MC. Forest Products Journal. 25(4):51–57.

Gerhards, C.C. 1982. Effects of knots on stress waves in lumber. Res. Pap. FPL 384. U.S. Department of Agriculture, Forest Service, Forest Products Laboratory, Madison, WI.

Han, G., Wang, X., Wu, Q. 2006. Stress wave velocity of wood-based panels: effect of moisture, products type, and material direction. Forest Products Journal 56(1):28-33.

James, W.L. 1961. Effect of temperature and moisture content on internal friction and velocity of sound in Douglas-fir. Forest Products Journal. 11(9):383–390.

Meyers, Marc A. 1994. Dynamic behavior of materials. New York: John Wiley & Sons, Inc.

Porter, A.W., Kusec, D.J., Olson, S. L. 1972. Digital computer for determining modulus of elasticity of structural lumber. WFPL Info. Rep. VP-X-99. Dept. of Environment, Canadian Forest Service, Vancouver, B.C.

Simpson, W.T., Wang, X., Verrill, S. 2003. Heat sterilization time of ponderosa pine and Douglas-fir boards and square timbers. Res. Pap. FPL-RP-607. Madison, WI: U.S. Department of Agriculture, Forest Service, Forest Products Laboratory. 24 p.

Sobue, Nobuo. 1993. Simulation study on stress wave velocity in wood above fiber saturation point. Mokuzai Gakkaishi. 39(3):271–276.

Wang, X. 1999. Stress wave-based nondestructive evaluation (NDE) methods for wood quality of standing trees. Ph.D. Dissertation, Michigan Technological University, Houghton, MI. 187 pp.

Wang, X. 2008. Influence of size and moisture on stress wave E-rating of structural lumber. In: Proceedings, 10th World Conference on Timber Engineering, June 2-5, 2008, Miyazaki, Japan.

Wang, X., Ross, R.J., Brashaw, B.K., Punches, J., Erickson, J.R., Forsman, J.W., Pellerin, R.F. 2004. Diameter effect on stress-wave evaluation of modulus of elasticity of small-diameter logs. Wood and Fiber Science. 36(3): 368-377.

Whither Machine Graded Lumber

Robert M. Browder
Southern Pine Inspection Bureau, Pensacola, Florida, rmbrowder@spib.org

Abstract

This talk focuses on how the lumber industry in the Southern United States has responded to changes in resource by revisiting the potential of Machine Graded Lumber (MGL). In response to changes in visually graded dimension lumber design values new grades of MGL have been requested and published, mills have examined their product mixes, and engineers have developed solutions for the changes. This presentation discusses why visual design values changed, what products/grades were impacted, and how MGL is part of the Southern Lumber Industries response. Through the course of the presentation a brief history of machine graded lumber (MGL) will be reviewed; the differences between visually graded lumber and MGL will be discussed; the types of machines currently used to produce MGL in the south will be explored; and the range of products produced with MGL technology will be inventoried.

Keywords: machine, stress, grading, softwood, lumber

Introduction

General Information

The Southern Pine Inspection Bureau has been involved with the development of Machine Graded Lumber since the 1970's. During the early development, concerns were raised about the validity of relationships between properties that could be measured non-destructively and strength values that can only be determined by testing a piece to failure. Over time, these issues have been resolved and one might refer to MGL as a mature technology. As a spur to greater use of Machine Graded Lumber the recent revision of visual design values for Southern Pine dimension lumber has been instrumental.

Historical Background

A comprehensive history and practices in the use of machine graded lumber may be found in FPL-GTR-6 (Galligan and McDonald 2000). This paper was originally published in 1977 following approximately fourteen years after the introduction of machine stress rating. At this time the market for MGL (machine graded lumber) was still developing. A description of one manufacturer's involvement in the early years of MGL describes the production of only two grades of MGL at a time, one high and one low (Froome 2004). Concepts for obtaining the best yield from the resource to meet a rather narrow demand were changing. Some of the concepts of applying machine graded lumber to the National Design Specification were addressed by technical representatives of ALSC rules writing agencies (Cheung et al.2002).

The production of MGL is monitored by the various grading agencies under the auspices of the American Lumber Standard Committee (American Lumber Standard Committee 2013). Typically, the rules writing agencies develop procedures suitable for the species under their cognizance (Southern Pine Inspection Bureau 2013). The machines used to mechanically assign stress ratings to lumber must be approved by the ALSC (American Lumber Standard Comittee 2013). Each machine carries restictions and limitations

on use regarding size, moisture content, temperature and other operating characteristics noted by the machine manufacturer.

Changes in Visual Design Values

In 2010 the Southern Pine Inspection Bureau, the rules writing agency for Southern pine, began research to evaluate whether changes had occurred in the resource which would necessitate re-evaluation of visual design values for dimension lumber. An initial assessment of the 2x4 No.2 product indicated that a shift downward in assignable design values had occurred. A full in-grade testing program was conducted with the result that significant reductions in bending and MOE were required. Because of the use of visually graded lumber throughout the building industry, there was concern over the impact of the reductions on existing plans and the availability of material exhibiting the design values that had been in effect for 25 years. Table 1 compares the 1991 referenced design values to the 2013 referenced design values for the unclassified grades.

TABLE 1- Comparison of Some 1991 to 2013 Design Values for Visually Graded Dimension Southern Pine Lumber

		F_b psi		F_t psi		$C_{parallel}$ psi		E psi	
		1991	2013	1991	2013	1991	2013	1991	2013
2x4	SS	2850	2350	1600	1650	2100	1900	1.8	1.8
	No.1	1850	1500	1050	1000	1850	1650	1.7	1.6
	No.2	1500	1100	825	675	1650	1450	1.6	1.4
	No.3	850	650	475	400	975	850	1.4	1.3
2x6	SS	2550	2100	1400	1450	2000	1800	1.8	1.8
	No.1	1650	1350	900	875	1750	1550	1.7	1.6
	No.2	1250	1000	725	600	1600	1400	1.6	1.4
	No.3	750	575	425	350	925	800	1.4	1.3
2x8	SS	2300	1950	1300	1350	1900	1700	1.8	1.8
	No.1	1500	1250	825	800	1650	1500	1.7	1.6
	No.2	1200	925	650	550	1550	1350	1.6	1.4
	No.3	700	525	400	325	875	775	1.4	1.3
2x10	SS	2050	1700	1100	1150	1850	1650	1.8	1.8
	No.1	1300	1050	725	700	1600	1450	1.7	1.6
	No.2	1050	800	575	475	1500	1300	1.6	1.4
	No.3	600	475	325	275	850	750	1.4	1.3
2x12	SS	1900	1600	1050	1100	1800	1650	1.8	1.8
	No.1	1250	1000	675	650	1600	1400	1.7	1.6
	No.2	975	750	550	450	1450	1250	1.6	1.4
	No.3	575	450	325	250	825	725	1.4	1.3

Machine Graded Lumber as a Substitute

While the in-grade testing was being conducted users of visually graded Southern pine began to inquire about the use of MGL in order to preclude having to re-engineer architectural plans on the shelf. In response to these concerns the Southern Pine Inspection Bureau published Machine Stress Rated and Machine Evaluated Lumber grades equivalent to the former visual grades (Southern Pine Inspection Bureau 2012). These replacement combinations are shown in Table 2. Additionally, visual characteristics were published for lower grades of MGL that approximated the No.3 visual grades.

Table 2- Machine Graded Substitutions for 1991 Visual Design Values

Visual Grade	MSR	MEL
2x4 No.1	1850f-1.7E	M-40
2x4 No.2	1500f-1.6E	M-38
2x4 No.3	850f-1.4E	M-33
2x6 No.1	1650f-1.7E	M-39
2x6 No.2	1250f-1.6E	M-37
2x6 No.3	750f-1.4E	M-32
2x8 No.1	1500F-1.7E	M-29*
2x8 N0.2	1200f-1.6E	M-36
2x10 No.2	1050f-1.6E	M-35
2x12 No.2	975f-1.6E	M-34

* Not an exact substitution

An obvious benefit of using MGL is that, compared to visually graded lumber, the assigned design values are static. That is, assigned design values do not shift with changes in the resource. For designers this provides longevity to their engineering drawings.

In June of 2013 the Southern Pine Inspection Bureau published Supplement 13 to the Standard Grading Rules for Southern Pine Lumber 2002 (Southern Pine Inspection Bureau 2013). With publication of this supplement there became a potential for increased demand for MGL grades published in June 2012.

Synthesis of Machine Grading and Visual Grading

While the referenced design values for visually graded dimension lumber were decreasing, technology was still advancing. Computers were introduced to replace humans in determining visual grades. Several companies were able to link the visual grading machines to the stress rating machines. Through this synthesis the repeatability of the machine graded lumber became better, which in due course allowed finer adjustments for the separation of MGL grades.

Several machines now incorporate both visual and strength grading machines. Additional modules are added to the machine along with software upgrades to provide this duel capability.

Demand for Visual Grades of Machine Graded Lumber

Even though specific grades of MGL were published as direct replacements for the 1991 visual grades there has not been a consensus reached by the market on specific optimal grades of MGL as the dominant grade. The trends to date appear inclined to a 1650 Fb as a lower grade produced in combination with a higher grade at or above 2400 Fb. Production of some lower MEL grades is also occurring. The main sector that can drive increased demand for MGL is component manufacturing; however, reports indicate a dramatic shift is not happening (Shields 2013).

The number of MGL producers in the South has almost doubled over the last two years with the total number of mills in excess of 40. The availability of stress evaluating machines that require only a small footprint in the production facilities has enabled the entry of medium size mills into the market. Use of machines to evaluate specialty grades, such as scaffold plank has also increased. Grading of scaffold plank by machine is an especially appropriate use of the non-destructive technologies of MGL. Scaffold plank is not engineered for repetitive use applications and each piece is expected to carry its full design load independently. The fact that each piece is evaluated for strength enhances the perception that MSR Scaffold plank is better suited for the end use.

Conclusion

The publication of revised design values for Southern pine became effective in June of 2013. Production capacity to meet any additional demand for MGL was available. What remains to be seen is to what extent will demand increase and what grades will be actually be produced.

References

American Lumber Standard Committee. 2013. List of Approved Machines. http://www.alsc.org/untreated_machinegraded_mod.htm. Germantown, MD.

American Lumber Standard Committee. 2013. Machine Graded Lumber Policy. http://www.alsc.org/untreated_machinegraded_mod.htm. Germantown, MD.

Cheung, K.; Lockyear S.; DeVissor D.; Johnson L. 2002 Designing with Lumber in the 2001 NDS. Wood Design Focus Winter 2002: 13-17.

Froome, A. 2004. Gulf Lumber: a Tradition of Excellence. Metriguard Technical Note. Pullman, WA.

Galligan, William and McDonald, Kent A. 2002. Machine Grading of Lumber: Practical Concerns of Producers. USDA-FS General Technical Report FPL-GTR-7.

Shields, Sean. 2013. A Light in the Attic. Structural Building Components. August 2013:10-14.

Southern Pine Inspection Bureau 2013. Procedures for Mechanically Graded Lumber. Pensacola, FL.

Southern Pine Inspection Bureau 2012. Supplement 12 of the 2002 Standard Grading Rules for Southern Pine Lumber. Pensacola, FL.

Southern Pine Inspection Bureau 2013. Supplement 13 of the 2002 Standard Grading Rules for Southern Pine Lumber. Pensacola, FL.

Machine Graded Lumber (MSR/MEL) Process in Canada

Richard Desjardins
Engineered Wood Products Manufacturing
FPInnovations

Abstract

This presentation focuses on the machine graded lumber (MGL) industry in Canada. A brief history of MGL will be presented, differences between visually graded lumber and MGL will be discussed, types of machines currently used to produce MGL in Canada will be explored, differences (where they exist) between the U.S. and Canadian systems will be pointed out, and the range of products produced with MGL technology will be inventoried.

Session 2

Nondestructive Evaluation and Hazard Assessment of Urban Trees

Case Study Demonstrating a Protocol for Use of Nondestructive Tree Decay Detection in Combination with Multi-Source Remote Sensing Data to Predict Probability of Property Damage From Tree Failure

Richard Bruce Allison
Forest and Wildlife Ecology, University of Wisconsin, Madison, WI

Huan Gu
Forest and Wildlife Ecology, University of Wisconsin, Madison, WI

Abstract

With a predicted increase in extreme weather events worldwide the probability of tree failure damage to urban buildings, transportation corridors and energy/communication grids increases. Urban forestry managers need to develop improved methods to effectively and economically evaluate standing trees for internal decay. New nondestructive technologies for accurate detection of internal decay detection are expensive and time consuming thus most logically reserved for use on standing trees that due to location, height and health present the greatest risk to adjacent targets. Satellite and aerial imagery reveals physiological information in addition to spatial and height information. This case study demonstrates a protocol for using multi-source remote sensing data in combination with acoustic tomography and microdrill resistance tools to quickly identify trees with high potential for failure in proximity to vulnerable targets.

Keywords: acoustic tomography, multi-source remote sensing data, nondestructive testing, tree stability

Introduction

Standing trees offer many urban amenities and add value to development land but also pose a threat to urban infrastructure and human safety when decay or defect increase failure risk. Nondestructive methods for tree decay detection such as acoustic tomography and microdrill resistance tools offer effective solutions to quantify internal decay but are expensive and time consuming. (Wang, Allison et al 2007) Multi-source remote sensing data can help locate those individual trees that due to proximity to sensitive targets, height and general nutrient and health issues pose the greatest risk. A study was conducted on a wooded land site designated for development of a University of Wisconsin-Madison research park demonstrating how remote sensing data can be used to identify the subset of trees having location and growth characteristics requiring in depth study with nondestructive decay detection tools. This combination of tools allows the land developer or municipal urban forester to make better, more economical and efficient standing tree management decisions.

Materials and Methods

Remote sensing data from airplanes or satellites provide a rich overview of the tree cover including a visual record of change over time, estimates of forest characteristics such as aboveground biomass (carbon stock), mean height, stand density, crown width, crown base height and basal area. Additional

factors such as canopy nutrients and surface temperature can also be identified from remotely sensed data.

Available remote sensing images of the site were:

(a) 2008 1-m resolution NAIP air photo;
(b) 2005 2-m footprint and 2009 2-ft footprint lidar data;
(c) 2010 11.7-m resolution and 2011 7.4-m resolution AVIRIS imaging spectroscopy data;
(d) 2010 and 2011 22-m resolution Master thermal infrared data.

Figure 1—University Research Park Boundary on NAIP air photo

Lidar, (i.e., light detection and ranging) has been widely used in estimating forest structure and productivity over decades (Lefsky et al., 2002). Available lidar data in the study area were collected by City of Madison, WI in 2005 and Ayres Associates, Madison, WI in 2009. Several maps were generated using these lidar data: tree height maps in 2005 and 2009 (Figure 2 (a) and (b)); aboveground biomass maps in 2005 and 2009 (Muss et al., 2011) (Figure 2 (c) and (d)). By differencing the 2009 and 2005 maps, tree height change map and aboveground biomass change map (Figure 2 (e) and (f)) can also be derived.

Changes (either gain or loss) of tree height and aboveground biomass between the years 2005 and 2009 can be observed from these maps. For example, there was a pathway cleared between 2005 and 2009 in the area of red marked circles in figure 2, it shows that more than 25 feet loss in average tree heights, and more than 50 Mg/ha loss in aboveground biomass (roughly 25 Mg/ha carbon stock loss) over the red circled area.

(a) Tree height map in 2005 (b) Tree height map in 2009

(c) Aboveground biomass map in 2005 (d) Aboveground biomass map in 2009

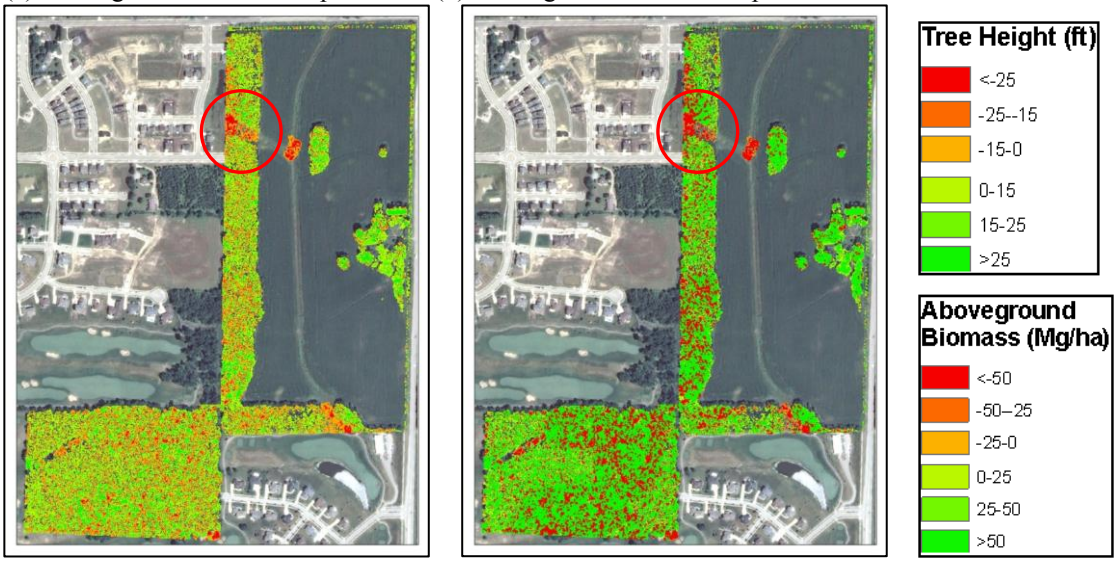

(e) Tree Height Change from 2005 to 2009 (f) Aboveground biomass change from 2005 to 2009

Figure 2—Maps generated using lidar data

Land surface temperature (LST, Voogt et al., 2003) can be estimated from Master thermal infrared data. The Master data used in this project were collected by NASA on Aug 16, 2011; and a surface temperature map was estimated in Figure 3 (b).

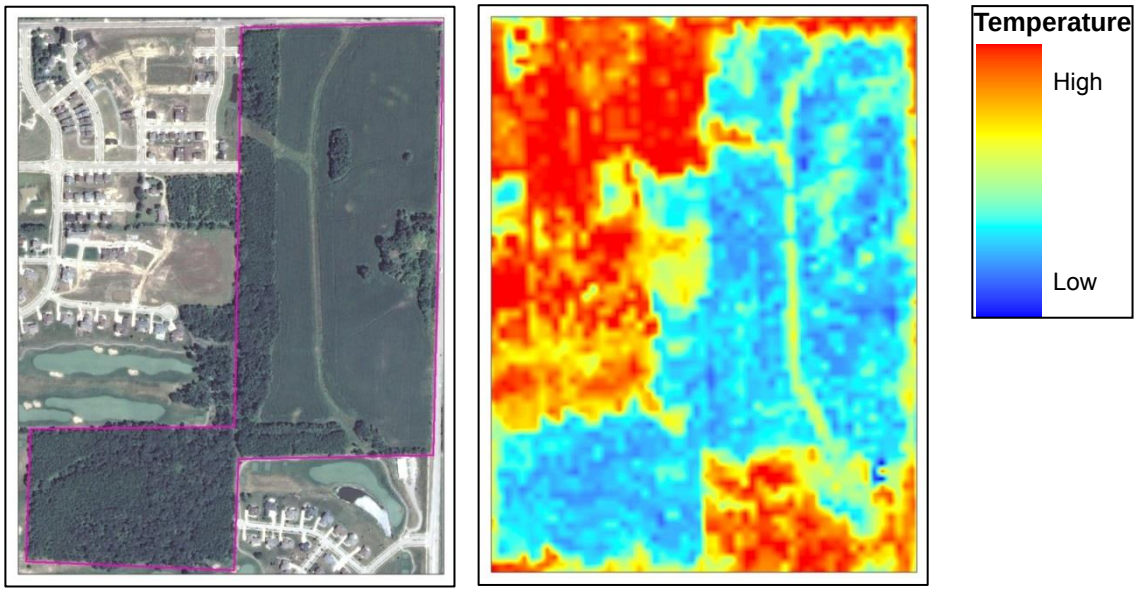

(a) (b)

Figure 3—Temperature map generated using MASTER data

Temperature variations at different land covers can be easily identified. Forest lands have a lowest temperature, while impervious surface has the highest temperature. This provides evidence that trees can help cool down the surface temperature and reduce urban heat island (UHI, Weng et al., 2004) effects.

AVIRIS (Airborne Visible Infrared Imaging Spectrometer) imaging spectroscopy data have been used to quantify biophysical properties to help understand ecosystem processes (Ustin et al., 2004), such as canopy nitrogen concentration (Martin et al., 2008). In this project, AVIRIS imaging spectroscopy data was collected by NASA on Aug 26, 2010; and canopy nitrogen concentration map was estimated in Figure 4 (b).

It is meaningless to compare nitrogen concentrations across different types of land cover, and it is not surprising that fertilized grass lands have a higher nitrogen concentration than forests. However, variations of nitrogen concentration within forest lands is important, since nitrogen is a key factor influencing forest nutrient cycling, tree growth and primary productivity.

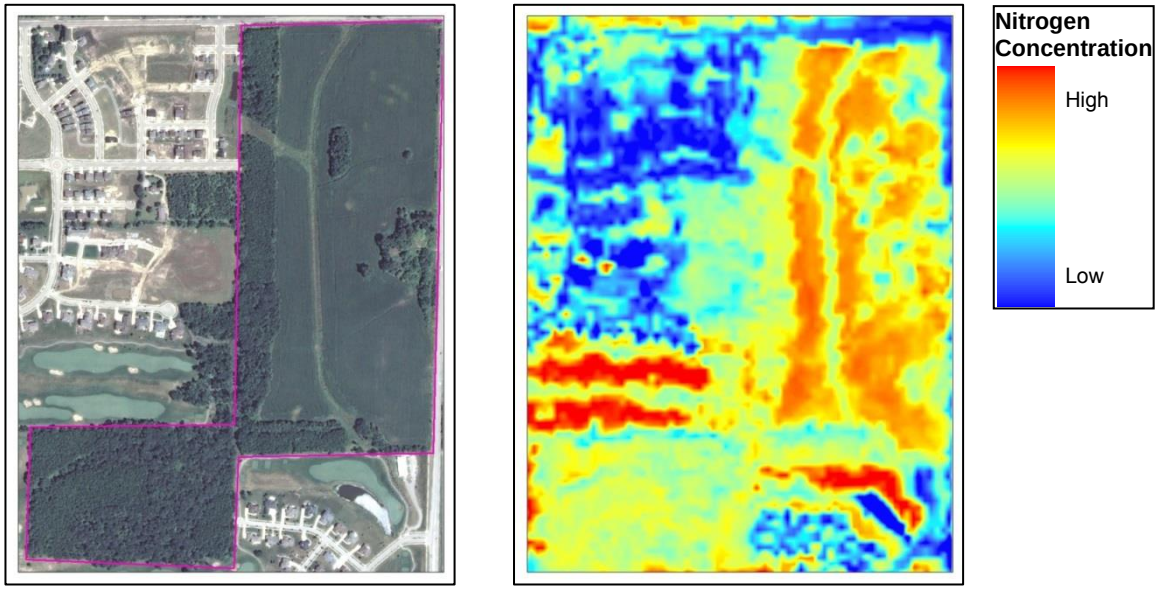

(a) (b)

Figure 4—Nitrogen map generated using AVIRIS imaging spectroscopy data

Verification of forest species mix, stem density, volume and general health was obtained by a ground inventory and random plot sampling. Maps and tables are assembled representing the types of forest cover and the acreage of each. All tree stems greater than 18 inches in diameter were identified in the field and their location and attributes inventoried.

After remote sensing data was assembled and forest characteristics verified by ground truthing a subset of trees was identified requiring visual and nondestructive testing for decay. Trees are often tall, heavy structures subject to failure from decay, defect and extreme weather conditions. Risk from tree structural failure is defined in the International Society of Arboriculture "Tree Risk Assessment," Smiley, Matheny, Lilly (2011) as the probability of failure multiplied by the consequences. Land development introduces tree failure targets including people, vehicles and buildings. Evaluating tree condition, both through visual observation of external characteristics and internal testing with nondestructive tools for decay and defect is required for tree risk management. Remotely sensed data on the existing tree cover on this land development site provided an accurate, efficient means to develop a subset of trees that due to location, height and physiological characteristics could pose a threat to the proposed buildings and infrastructure if they were to fail. Limiting the use of time consuming individual tree examination and nondestructive testing to just those trees in the forest subset with the greatest potential for damage to developed structures and occupants controls costs and labor expenditure.

Tree Risk management starts with a visual inspection by a competent arborist or forester familiar with tree physiology, mycology and tree management literature. A visual inspection of the lower trunks of larger trees was conducted looking for abnormalities in trunk taper, cracks or fissures, and evidence of fungal fruiting bodies. The visual examination sought to identify structural defects or indicators of decay using the "body language" of the trees. A tree's growth is responsive to its environment. It is a self-optimizing biological organism with mechanically influenced structure. To allow a uniform mechanical stress over its entire surface, additional wood is laid down over decayed or damaged areas. Visual indicators of potential decay include the following: old wounds, decayed branch stubs, seams, stem flattening, bulges, included bark, cracks, cankers, abnormally wide taper at trunk base, poor vigor and girdling roots. Positive indicators of decay include: fungal fruiting bodies or mycelia, external cavities, carpenter ant activity, and nesting holes.

Where evidence of problems exist the internal condition of the tree can be explored nondestructively with acoustic tomography and microdrill resistance tools. Those trees, within the subset of interest,

exhibiting any visual signs of internal decay were tested with a Fakopp 3D Arborsonic Acoustic Tomography tool. Tomography uses the velocity variations of impact induced sound waves moving through the wood to create, through projection software, a representation of the tree's internal condition. The use of stress waves to detect tree defects and decay is based on the observations that sound wave movement through wood is directly related to its physical and mechanical properties. Stress waves travel slower in decayed or deteriorated wood than sound wood. In either single path sound wave tools or multipath tomography tools a mechanical impact is used to create a stress wave into the tree. Piezoelectric sensors placed on the trunk detect the time passage of the wave. Significant decreases in the anticipated sound wood velocities indicate decay or defect due to the fact that the wave was required to bypass decay or defect in the area tested. Detailed information on these technologies is available on a technology transfer video http:/vimeo.com/ 5129962 "Tree Decay Detection " (Allison, 2009).

With the Fakopp Arborsonic Tomography, 12 sensors were placed around the trunk circumference at a selected elevation. Distance between sensors is precisely measured with a Picus electronic caliper. Measurements from multiple passes of stress waves create a matrix of sound wave propagation readings that are then interpreted into a computed tomograph using reconstruction and projection software. Using the densest wood measured to establish a scale, areas of reduction in wood density are displayed. It is important to note that the tomogram generated by the test is not a representation of the actual appearance of the cross-section tested, but rather a representation of the acoustic characteristics of the wood. Accurate interpretation based on research and experience is required to effectively translate the tomography data into an understanding of the location and dimensions of the internal defects. To assist in this interpretation, the use of a microdrill resistance test, using an instrument called the Resistograph is conducted in locations suggested by the tomograph.

The Resistograph instrument detects the torsion resistance of a 3 mm drill bit as it passes through the wood to a depth of 40 cm. Changes in wood resistance are displayed on a graph as changes in amplitude with blue fill color below the graph line. Areas of least resistance indicate cavities, decay, cracks or low density. A second meter on the instrument measures feed needle push resistance and is displayed in green on the tomogram. Detailed explanations of the technology and related articles are available online at www.imlusa.com. Microdrill resistance testing was conducted on select trees within the subset of interest that acoustic measurements indicated had some internal decay. The instrument used was the IML PD400 Resistograph microdrill.

From visual and nondestructive testing results trees were rated and color coded on the tree health maps using the following condition criteria of good, fair and poor:

Good: Tree has an extremely low risk of failure over the 10 years. Few external injuries are present, and there are no signs of significant internal decay. Tree appears to be healthy, and growing conditions are suitable for the species.

Fair: Tree has a low to moderate risk of failure over the next 10 years. In addition, there may be a moderate risk for whole-tree mortality during this time period due to low vigor, high stand density, or marginal site conditions. Internal decay may be present but it is not affecting tree stability.

Poor: Tree has a high risk of failure or mortality over the next 10 years. One or more of the following are present: severe internal decay that is affecting tree stability; sizable wounds incapable of being compartmentalized; fruiting bodies of decay fungi throughout the tree; and heavy crown dieback that exceeds 60% of the total canopy cover.

Following are: (1) aerial photos mapping tree cover types and acreage (Figure 5 and 6); (2) maps, both overview and specific location, locating these trees by species and health (Figure 7, 8, 9, 10 and 11).

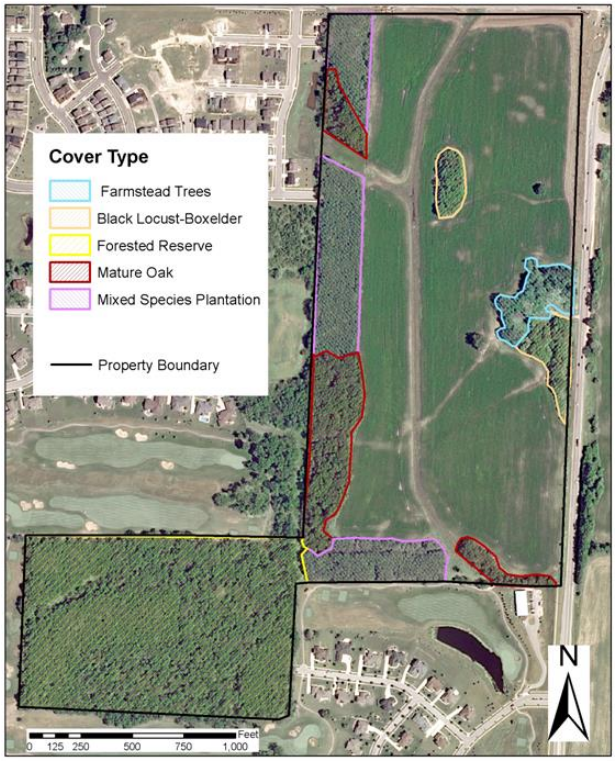

Figure 5—Tree cover types

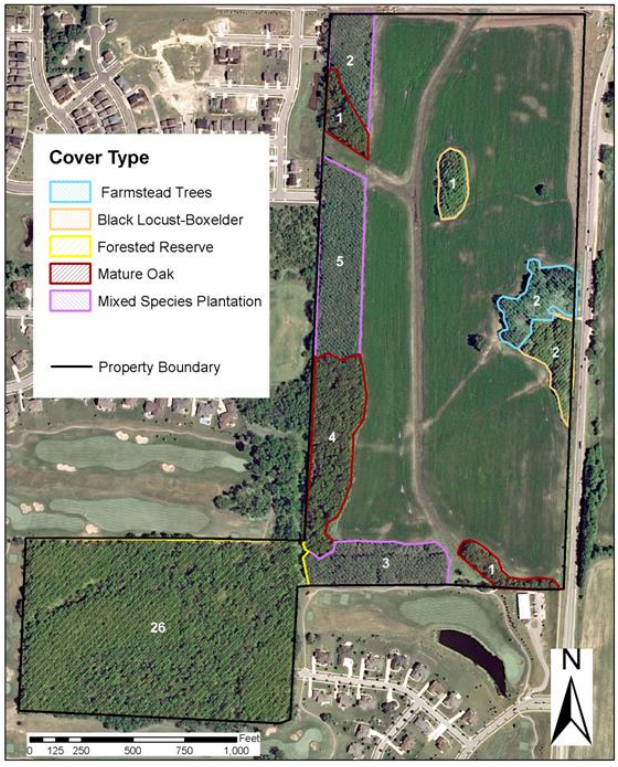

Figure 6—Tree cover types with acreage

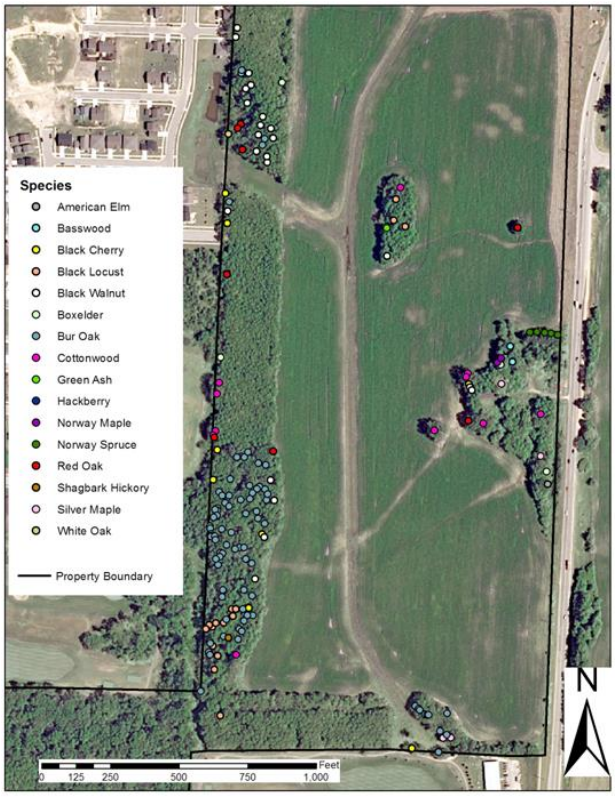

Figure 7—Tree species

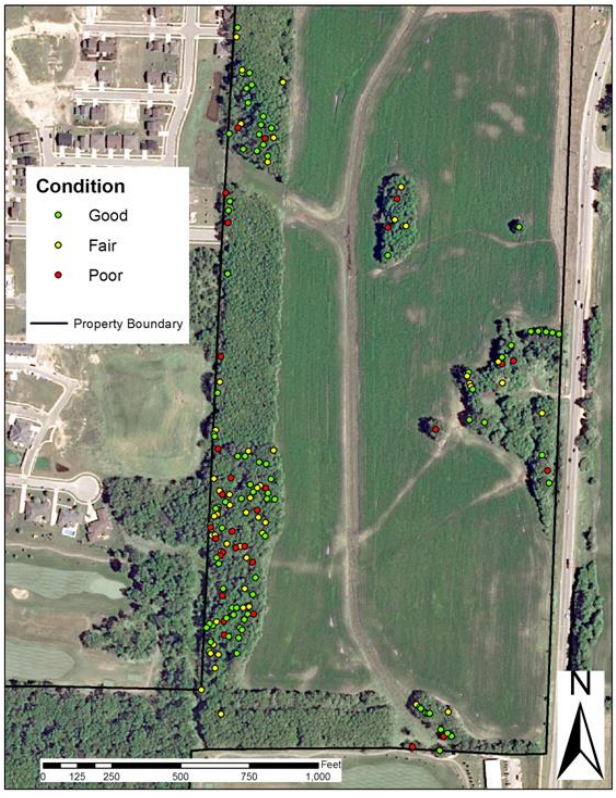

Figure 8—Tree Health Map

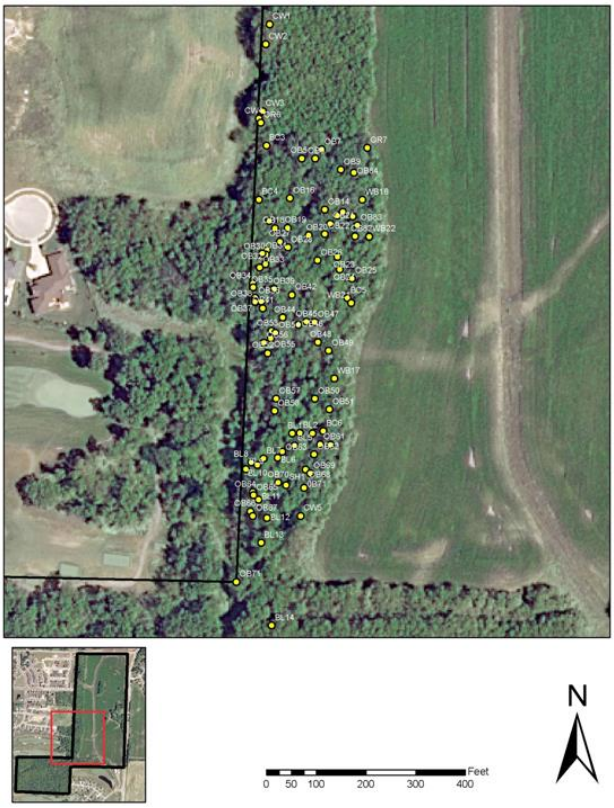

Figure 9—Southwest corner with co-ordinates

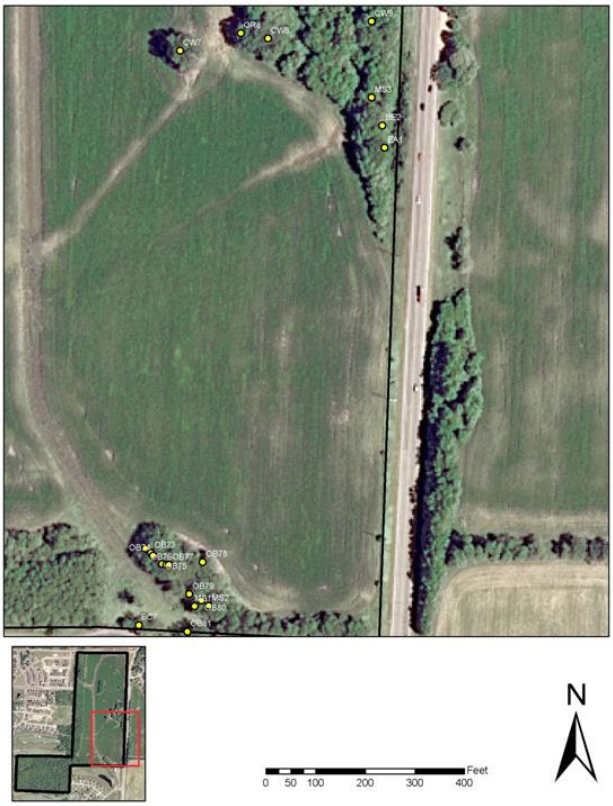

Figure 10—Southeast corner with co-ordinates

Figure 11—East boundary near Hwy M with co-ordinates

Conclusions

Multi-source remote sensing data on the University of Wisconsin-Madison Research Park forested development site allowed for a cost effective method to identify a subset of standing trees whose proximity to proposed buildings and sensitive infrastructure justified further study with nondestructive decay detection tools. Trees selected for nondestructive testing were those whose location and height as determined by aerial imagery could fail into planned roadways, utility corridors, buildings or high occupancy gathering points. The high expense of testing every tree was therefore avoided without compromising the main objective of safety.

Acknowledgements

Professor Phillip A. Townsend and his laboratory, The Forest Ecosystem Remote Sensing Team at the Forest and Wildlife Ecology Department, University of Wisconsin- Madison, provided critical assistance in conducting this case study. The authors also thank the following University of Wisconsin-Madison students for their participation in data collection: Collin Buntrock, Robert Bessert, Kelsey Egelhoff, Ben Spaier and Brian Zweifel.

References

Allison, R. B. 2009. Tree decay detection, a nondestructive procedure using visual inspection in combination with acoustic and microdrill tools. USDA Forest Service Wood Education and Resource Center video.

Lefsky, M.A., Cohen, W.B., Parker, G.G., & Harding, D.J. 2002. Lidar Remote Sensing for Ecosystem Studies. BioScience, v. 52, p. 19-30.

Martin, M.E.; Plourde, L.C.: Ollinger, S.V.; Smith, M.L.; McNeil, B. E. 2008. A generalized method for remote sensing of canopy nitrogen across a wide range of forest ecosystems. Remote Sensing of Environment, v. 112, p. 3511-3519.

Muss, J.D.; Mladenoff, D.J.; Townsend, P.A. 2011. A pseudo-waveform, technique to assess forest structure using discrete lidar data. Remote Sensing of Environment, v. 115, p. 824-835.

Smiley, T. E. ; Matheny, N.; Lilly, S. 2011. Tree Risk Assessment. Internatioal Society of Arboriculture; Champaign, IL.

Ustin, S. L.; Roberts, D. A.; Gamon, J. A. ; Asner, G.P.; Green, R. O. 2004. Using imaging spectroscopy to study ecosystem processes and properties. BioScience, v. 54, p. 523-534.

Voogt, J.A., & Oke, T.R. (2003). Thermal remote sensing of urban climates. Remote Sensing of Environment, 86, 370-384.

Wang, X.; Allison, R.; Wang, L.; Ross, R. 2007. Acoustic tomography for decay detection in red oak trees. Research Paer FPL-RP-642. Madison, WI: U.S. Department of Agriculture, Forest Service, Forest Products Lab. 7p.

Weng, Q., Lu, D., & Schubring, J. (2004). Estimation of land surface temperature-vegetation abundance relationship for urban heat island studies. Remote Sensing of Environment, 89, 467-483.

Determining strength limits for standing tree stems from bending tests

Andreas Detter
Brudi & Partner TreeConsult, Gauting, Germany

Steffen Rust
HAWK University of Applied Science and Arts, Göttingen, Germany

Catharina Rust
HAWK University of Applied Science and Arts, Göttingen, Germany

Georg Maybaum
HAWK University of Applied Science and Arts, Holzminden, Germany

Abstract

Non-destructive tests are essential in urban tree risk assessment. One of the commonly used methods, the pulling test method, relies on wood properties derived from testing small clear samples of green wood. In the past, such data had been suspected to overestimate the strength of intact tree trunks. Here we propose and test a novel method to measure the limit of proportionality directly in large standing trees. Material properties determined in tests on small specimen were not correlated with tree strength derived by testing entire tree stems. Thus, it is important to test strength thresholds on entire tree stems using the new field method described here. Furthermore, we show that stiffness measured during non-destructive pulling tests is a good indicator for yield strength in bending.

Keywords: proportional limit, pulling test method, bending test, *Acer pseudoplatanus, Fraxinus excelsior*

Introduction

The ability of trees to withstand forces exerted by factors like wind, snow and ice is essential in tree risk assessment with regard to public safety (Smiley et al. 2012). The stability of trees must also be addressed when they are used as supports in manmade structures like tree houses or adventure courses (cf. EN 15567-1). Currently, results from material tests on small-scale samples are often used to draw conclusions on the strength of stems and branches (e.g. Petty and Swaine 1985). This procedure was rarely verified (e.g. Brüchert et al. 2000), and when it was, significant discrepancies have been found (e.g. Kane and Clouston 2008). FOREST Gales uses knot factors to estimate stem strength from material properties derived from small samples (Gardiner et al. 2000). Lately, Ruel et al. (2010) examined similar knot factors by testing the actual strength of fresh cut logs of conifers in three-point bending. Yet, any direct proof of a stem's strength will unavoidably involve its destruction.

The non-destructive pulling test method was developed for the assessment of safety against stem rupture and uprooting of urban trees in the late 1980's (Sinn and Wessolly 1989). In order to assess stem strength, the results of bending the stem at low load levels are extrapolated within the elastic

range to a species specific limit of elasticity (Wessolly 1991). The guideline values currently used in the pulling test method were also derived from testing small blocks of green wood (Wessolly and Erb 1998). The number of tree species listed in those tables is limited mainly to Northern European taxa. Material properties for green wood of worldwide occurring species are available from several other sources (Lavers 1973, Jessome 1977, Kretschmann 2010). But those reference values rarely allow for an application in the pulling test method as they usually refer to ultimate strength. Only Jessome (1977) provides data for strength at the limit of proportionality (PL), beyond which plastic deformation occurs (Niklas and Spatz 2012). Wood shows a gradual transition from elastic behavior to plastic deformation when critical loads are exceeded (Bodig 1982). The deviation from the proportional correlation between stress and strain according to Hooke's Law marks the end of any linear extrapolation and is an indicator for the overloading of structure (Gordon 1991).

The pulling test method uses PL as a threshold for strength. This species-dependent property is required to be able to extrapolate from a non-destructive test to stem resistance against fracture. To our knowledge, this property has not been measured in standing trees before. Therefore, we tested a new method for identifying PL by breaking standing trees and deriving strength properties for entire tree stems. We tested the applicability of data on flexural stiffness of tree stems gathered in a non-destructive pulling test as indicators for stem strength. We also tested if estimating the strength at PL may also allow for an assessment of the ultimate strength of tree stems.

A field method to determine the bending moment required for a standing tree stem to exceed the limit of proportionality

The field method was first tested on 10 London Plane trees (*Platanus acerifolia*) in Shalerville, OH, in 2010. The method was replicated on forest trees of two other species (*Acer pseudoplatanus* and *Fraxinus excelsior*) in Göttingen, Germany. Measurements were carried out with two inclinometers and one forcemeter of the TreeQinetic System (argus electronics GmbH, Rostock, Germany). During the test, a lateral force is applied at the stem at roughly half tree height. A forcemeter is positioned in the middle of the rope and the force is applied by a manual winch (e.g. Tirfor 1.6 t). In order to monitor the bending response of the tree, one inclinometer is placed at the base of the stem, the other at a height of 4 to 5 m. Force and inclination are recorded while the tree is pulled to ultimate failure.

The lower inclinometer monitors the inclination of the root plate. The inclinometer higher at the stem records deflection angles due to both root plate tilt and stem bending. The difference between the two inclinometer readings (Δ_N) is a measure for the deflection of the stem due to bending. Within the elastic range, Δ_N will increase proportionally with the applied base bending moment (BBM) according to Hooke's Law. As soon as PL is exceeded, stem deflection will increase at a greater rate than the applied load. A deviation of 2% from the expected linear values for stress or strain was chosen to determine PL in bending (cf. Burgert et al. 2003).

For two species, BBM at PL and at ultimate stem fracture were determined. There was a strong correlation between BBM at PL and at ultimate failure with significant differences between the two species (Figure 1).

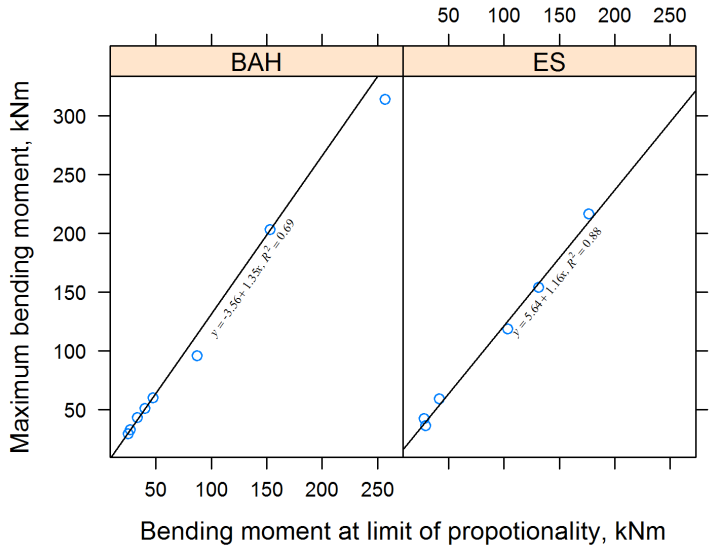

Figure 1-Correlations between bending moments at limit of proportionality and maximum bending stress in *A. pseudoplatanus* (BAH) and *F. excelsior* (ES) were highly significant.

Correlations between critical loads at the proportional limit and flexural stiffness measured in non-destructive pulling tests

In the pulling test method, strains in marginal fibers are measured with strain gauges that record the compression or elongation between two metal probes placed in the wooden body (Elastometer or Dilatiometer). At the same time, the lateral force applied by a mechanical winch is measured with a forcemeter (Brudi and Wassenaer 2002). During this procedure, irreversible damages due to overloading must be prevented. Therefore, tests are aborted well below a typical yield strain. Data gathered is used to assess the load required to exceed PL in bending. The validity of currently used thresholds for the extrapolation has not been scientifically tested for a greater number of trees.

In the present project, all trees were also tested non-destructively before pulling to ultimate failure. In this initial test, compression or extension in marginal fibers was measured with Elastometers (TreeQinetic System, see above) placed on defined positions on the compression or tension side of the tree stems. To measure within the elastic range of green wood, strains beyond 1,250 με were prevented. Simultaneously, the applied force was measured with a Forcemeter (TreeQinetic System, see above) and translated into bending moment at the stem base (BBM), taking into account anchor point height and rope angle.

The slope of a linear regression of BBM on strain is a measure of the flexural stiffness of the stem. This property was tested as an indicator for the BBM at which the PL would de exceeded. According to the statistical analysis, non-destructive strain measurements on standing tree stems are a suitable indicator for BBM at PL (Figure 2).

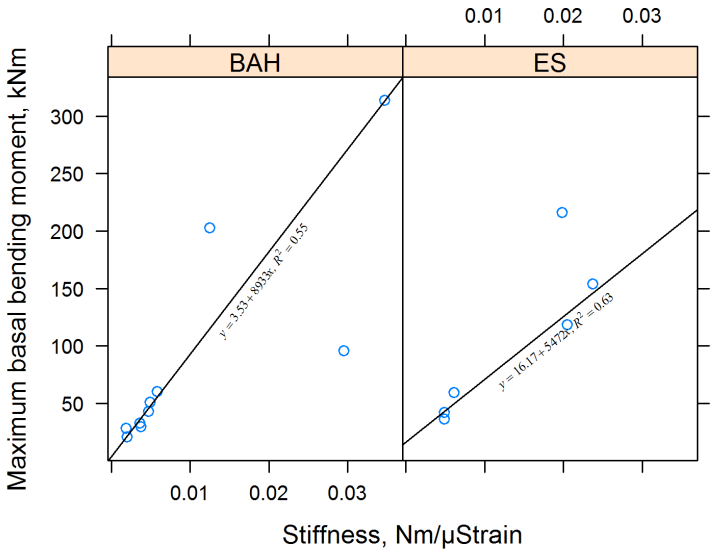

Figure 2-Stiffness of stems in non-destructive bending tests correlated closely with bending moments at failure in *A. pseudoplatanus* (BAH) and *F. excelsior* (ES).

Validating the field test results under lab conditions

The field test method was replicated under lab conditions on 10 almost straight stems of 30 year old *A. pseudoplatanus*. Trees were selected in a forest stand near Göttingen, Germany. They were harvested in January 2013 in a period of continuous subzero temperatures and logs of 6.5 m length were cut from the lowest part of the stem. The logs were immediately brought to the testing facility in Holzminden, stored in cold and moist conditions and tested within 7 days after harvesting. The testing apparatus was modified from standard protocols for four-point-bending (DIN 52186) to accommodate for testing entire logs of 6 m length and mid-diameters between 0.3 and 0.35 m. Two double-T steel beams formed the supports at a distance of 0.9 m around the middle of the stem. At the two ends of the stem low stretch slings were securely attached at a distance of 3 m from the stem center. Each sling was connected to a forcemeter and pulled upwards by two cranes. The speed was kept constant and stems were pulled until ultimate fracture occurred or the cranes reached their maximum capacity (50 kN).

The deformation of the stem was monitored using the TreeQinetic system. Two elastometers recorded compression in the marginal fibers on the top side of the stem. One Inclinometer was positioned at the lateral side of the stem under each support to determine the deflection of the stem from the original curvature. Those four sensors remained on the specimen until the test was terminated. Fiber strain on the tension side, i.e. on the underside of the stem, was recorded prior to the destructive test in the elastic range only and then removed for safety reasons.

PL was determined independently by three methods. For all logs, force was recorded over time as the cranes pulled the ends of the logs up at a constant rate. The force vs. time recordings initially show a proportional trend that turns into an underproportional increase after a specific force is exceeded. Furthermore, the correlation between compressive fiber strains and the mean of the two forces applied consists of a linear range beyond which strains increase overproportionally. A deviation from the proportional response could also be detected from the correlation between the inclination recorded by

the inclinometers and the applied force. For all methods, PL was assumed when forces or deformations exceeded the value expected according to Hooke's law by more than 2%. The bending moments required to reach PL were independent of the three methods applied. The field method to determine PL is measurements. The results confirm that using two inclinometers on standing trees is a suitable procedure to determine BBM at PL.

9 out of 10 stems remained visibly intact while only one fractured before the test was aborted. Each stem was divided in 3 sections in order to differentiate between the parts between the two supports that experienced the greatest bending stresses (section 2) and the lowest and highest part of the stem. The latter were assumed to have been loaded well below the yield point according to the moment curve in four-point bending. From each section, a 0.6 m long disc were cut from all 3 sections and sealed with paraffin. A total of 2132 samples of 20 x 20 x 60 mm were cut and stored directly in a deep freezer. The position of each sample in the section was recorded. Later, samples were thawed and tested in the wet state under axial compression in an INSTRON testing device. MOE was measured in the elastic range over a length of 20 mm. Stress and strain at PL as well as ultimate stress were determined using displacement and force sensors. PL was set at 2% deviation from the theoretical elastic response.

Data published by Jessome (1977) indicates that the ultimate strength of green wood samples in axial compression explains variations of stress at PL measured in a three-point bending test (Figure 3). This could not be confirmed in our study. The ultimate compressive strength of 20x20x60 mm wood blocks was not closely correlated to PL in bending of 20x20x300 mm beams extracted in the direct vicinity (Figure 4). This discrepancy may result from the fact that Jessome (1977) lists mean values derived from several individual trees whereas we only compared wood samples cut from the same log.

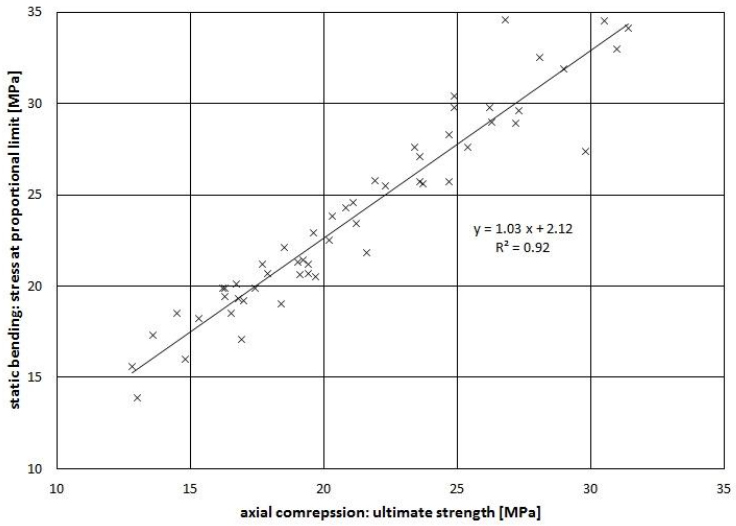

Figure 3-Ultimate strength of green wood samples in axial compression explains variations of stress at PL measured in a three-point bending test in data from Jessome (1977) for 54 species.

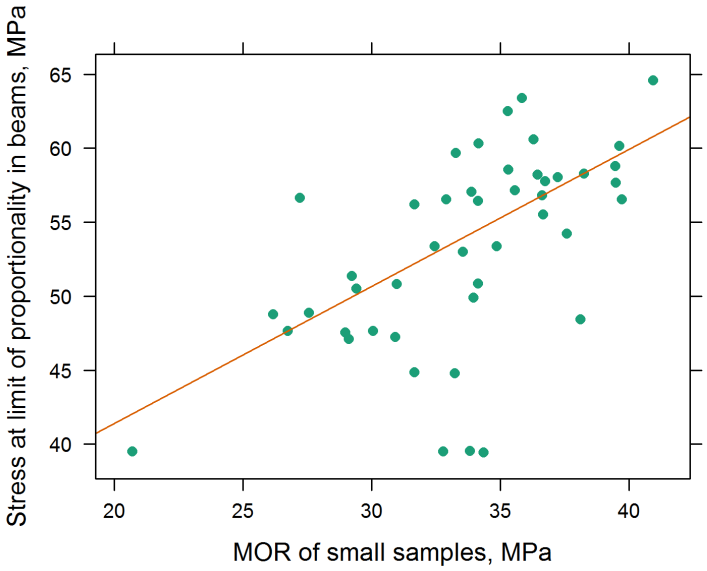

Figure 4-Stress at PL in bending beams of defect free wood of *A. pseudoplatanus* correlated loosely with ultimate strength in axial compression of small samples.

We also found that ultimate stress in compression for small blocks cut from unloaded sections of the stem could not explain variations in stem yield strength at PL (Figure 5). Therefore, it is necessary to investigated how material properties derived from testing small specimen in compression can be used to determine critical loads in entire tree stems (cf. Ruel et al. 2010).

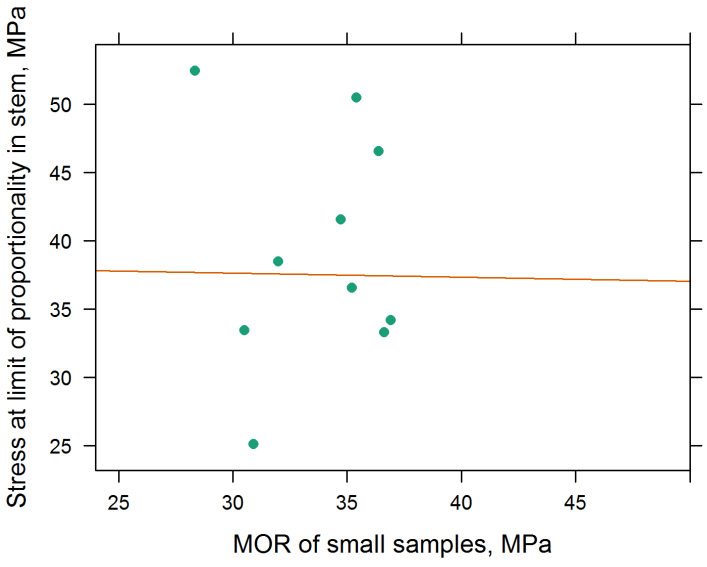

Figure 5-Average strength in axial compression of small clear samples was not correlated with stress at proportional limit of stems in *A. pseudoplatanus*.

Conclusions

It is possible to determine the limit of proportionality in a destructive winching experiment on standing trees by measuring applied forces while monitoring stem deflection with two inclinometers. If strain was previously recorded in marginal fibers during a non-destructive pulling test, critical strains can be derived by this procedure. Stiffness measured during non-destructive tests is a good indicator for yield strength. Material properties determined in tests on small specimen are less relevant for assessments of tree strength than values derived by testing entire tree stems. Thus, it is important to test strength thresholds on entire tree stems using the new field method described here.

Acknowledgements

This work was funded by the German Ministry of Education and Research (research grant 17021X11).

References

Bodig, J. and Jayne, B.A. 1982. Mechanics of wood and wood composites. Van Nostrand Reinhold, New York.

Brüchert, F., Becker, G. and Speck, T. 2000. The mechanics of Norway spruce [Picea abies (L.) Karst.]: mechanical properties of standing trees from different thinning regimes. Forest Ecology and Management 135, 45―62.

Brudi, E. and Wassenaer, P. van, 2002. Trees and statics: nondestructive failure analysis. In: Smiley, E.T., Coder, K. (eds.). Tree structure and mechanics conference proceedings. Champaign Ill. p. 53-69.

Burgert, I., Rohr, C., Frühmann, K. and Stanzl-Tschegg, S.E. 2003. Mechanical Properties of bottom compression side of branches of beech (Fagus sylvatica L.), 4th International Plant Biomechanics Conference. East Lansing MI, USA.

DIN 52186. 1978. Testing of wood; Bending test. Beuth Verlag, Berlin

EN 15567-1. 2007. Sports and recreational facilities - Ropes courses - Construction and safety requirements. Beuth Verlag, Berlin

Gardiner, B., Peltola H., and Kellomaki, S. 2000. “Comparison of Two Models for Predicting the Critical Wind Speeds Required to Damage Coniferous Trees.” Ecological Modelling 129 (1): 1–23.

Gordon, J.E. 1991. The new science of strong materials, Penguin Books. Penguin Books, New York.

Jessome, A.P. 1977. Strength and Related Properties of Woods Grown in Canada, Forestry Technical Report. Eastern Forest Poducts Laboratory, Ottawa.

Kane, B. and Clouston P. 2008. Tree Pulling Tests of Large Shade Trees in the Genus Acer. Urban Forestry and Urban Greening 34 (2), 101–109.

Kretschmann, D. E. 2010. Wood Handbook, Chapter 05: Mechanical Properties of Wood. General Technical Report FPL-GTR-190. Madison, U.S. Department of Agriculture, Forest Service, Forest Products Laboratory: 5-1 - 5-46.

Lavers, G. M. 1983. The strength properties of timber. 3rd edition. Building Research Establishment Report, Watford, UK.

Niklas, K. and Spatz, H.Chr. 2012. Plant Physics. Chicago, USA. 426 p.

Petty, J. A., and Swain, C. 1985. Factors Influencing Stem Breakage of Conifers in High Winds. Forestry 58 (1): 75–84. doi:10.1093/forestry/58.1.75.

Ruel, J.-C., Achim, A., Espinoza Herrera, R. and Cloutier, A. 2010. Relating Mechanical Strength at the Stem Level to Values Obtained from Defect-free Wood Samples. Trees - Structure and Function 24 (6): 1127–1135.

Sinn, G. and Wessolly, L. 1989. A Contribution to the Proper Assessment of the Strength and Stability of. Trees. Arboricultural Journal 13, 45—65.

Smiley, E.T., Matheny, N. and Lilly, S. 2012. ISA Best Management Practices. Tree Risk Assessment, Illinois, USA.

Wessolly, L. and Erb, M. 1998. Handbuch der Baumstatik + Baumkontrolle, Berlin, Patzer.

Wessolly, L. 1991. Verfahren zur Bestimmung der Stand- und Bruchsicherheit von Bäumen. Holz als Roh- und Werkstoff 49, 99–104.

Optical full-field measurement based on DIC: a new tool in urban forestry?

Václav Sebera
Department of Wood Science, Faculty of Forestry and Wood Technology, Mendel University in Brno, Zemědělská 3, 613 00 Brno, Czech Republic, e-mail: seberav@gmail.com

Luděk Praus
Department of Wood Science, Faculty of Forestry and Wood Technology, Mendel University in Brno, Zemědělská 3, 613 00 Brno, Czech Republic, e-mail: ludek.praus@centrum.cz

Jan Tippner
Department of Wood Science, Faculty of Forestry and Wood Technology, Mendel University in Brno, Zemědělská 3, 613 00 Brno, Czech Republic, e-mail: jan.tippner@gmail.com

Jan Čepela
Sobriety Ltd., Náměstí 1. května 63, 664 34 Kuřim, Czech Republic, e-mail: jan.cepela@sobriety.at

Abstract

The goal of the study was to analyze and measure behavior of tree (*Juglans regia* L.) subjected to the mechanical load in terms of its strain response. The analysis addresses issues of urban forestry that calls for a high quality deformation data measured on trees' surfaces in a non-contact and non-invasive way. For these purposes, the 3d digital image correlation (DIC) was proposed and tested against standard extensometers. Measured tree was subjected to a bending by a pulling test to induce the strain in tree stem. DIC successfully provided field strain on a tree bark despite its highly complicated geometry. Vertical averaging of the strain field obtained by the DIC revealed that a tree stem behaves according to the beam theory showing compression and tension parts. The absolute values of strain measured by both techniques agree with each other in order of magnitude, DIC returning lower values (approximately 21.1% and 40.8% for compression and tension part respectively).

Keywords: urban forestry, digital image correlation, pulling test, strain, optical measurement

Introduction

Assessment of mechanical behavior and safety of trees have been paid a big attention in recent years in both ways research and practical. The research – tree biomechanics – mostly focuses on evaluation of tree as it was complicated structure (e.g. "beam") loaded by various mechanical factors (e.g. its own mass, wind, snow etc.) and provide empirical data and models for latter use in more applied fields. Most often, the urban forestry and arboriculture use the most of tree biomechanics' results in way they try to apply its fundamental findings to evaluate safety factors of trees to protect human health and property (Wessolly 1991). To assess the tree safety and health a whole variety of techniques can be used ranging from only qualitative approaches such as visual tree assessment (VTA, Mattheck 1994) to quantitative ones, which enable to determine the probability of failure based on indirect and measured parameters when compared to empirically determined criteria and safety factors (Szorádová *et al*. 2013). The *apriori* knowledge of material properties possibly measured *in situ* (Wessels *et al*. 2011), a stem geometry and potential load often underlies these factors. Based on all these information it is possible to calculate the strength and stiffness of a tree similarly to the structures in civil engineering (Peltola 2006, Brudi and Wassenaer 2001).

A technique that follows this principle and is nowadays often used to assess the tree safety is a pulling test. This test belongs among functional techniques since it examines the mechanical functionality of tree stem (Szorádová et al. 2013). The pulling test is often accompanied by simultaneous measurement with use of inclinometers providing the rotations at stem base and extensometers or strain gauges returning the data about the xylem (wood) deformation – strain (Ennos 1995 and Crook and Ennos 1996). Measured rotations and strains are subsequently compared to the limit values of healthy trees, wood limits respectively,

that were empirically determined by the research community. The pulling test has been used widely for a few last decades (Sinn and Wessolly 1989, Wessolly 1991), the most recently, it is was well explained in Sani et al. 2012, who verified usability of this test on more than 50 trees of mostly Mediterranean species.

One of current trends in tree biomechanics is to enhance quantitative techniques in a way they will be able to predict a tree health, failure eventually, more precise and non-destructively. In terms of the pulling test, one of the ways to enhance it is to get the more continuous and semiglobal strain data on a tree surface – to obtain full-field information. Such data overcome the biggest disadvantage of the standard extensometers and inclinometers – their localness given by their positions within a tree and their discrete character given by a small amount of them installed at the tree. This drawback is even more crucial if we realize the enormous heterogeneity and variability of wood within a single tree – the spiral grain, knots, cracks etc (Bodig and Jayne 1993). Hence, the objective information using standard instruments can be achieved only by repetitive measurement when varying their positions. The other minor disadvantage of these instruments – semi-destructiveness – can be removed by using non-contact techniques. The technique removing these drawbacks would make a big qualitative shift in both tree biomechanics and arboriculture. Available techniques can be found in solid mechanics that is often ahead in instrumental solutions over tree-related disciplines.

Many non-contact full-field techniques such as Moire, Shearography, Holographic interferometry and their mutations (Sharpe 2008) that could possibly provide sufficient information and, hence, replace standard and intrusive extensometers and inclinometers in urban forestry have often enormous demands on equipment (splitting beams, lasers etc.) and testing environment (anti-vibration tables, stable light etc.). Relatively new category of experimental full-field methods dated from Peters and Ranson (1982) that are providing the same physical quantities as those standards ones are based on calculation of pixels' motion and deformation – digital image correlation (DIC) and its 3D mutation volumetric image correlation (VIC) (Sutton et al. 2009, Forsberg 2008). In the field of mechanical assessment of materials and constructions, the DIC-like methods are becoming leading non-destructive method due to its field character returning displacement and strain data equivalent to hundreds of strain gages, relative set-up easiness and sufficient accuracy – 0,01-0,02 subpixel displacement resolution (Muszyński and Launey 2010, Sutton et al. 2009). Therefore, the DIC has the biggest potential to be used also in tree biomechanics, especially its 3D variant that is capable to capture the displacement and strain at curved surfaces.

Therefore, to apply the DIC technique to assess the tree subjected to pulling test is the main goal of this work. This study is, to our knowledge, the first report that shows an application of full-field measurement based on DIC method for an analysis of tree response to pulling test on tree stem. The specific goals of this study are: 1) to carry out tree pulling test and use standard methods using extensometers to measure strain induced in a tree; 2) to apply full-field non-contact measurement based on DIC to measure strain and displacement fields on a tree stem with complexly structured bark; 3) to assess the applicability of DIC measurement in tree assessment as replacement to semi-destructive standard methods.

Material and Methods

Our research consisted of two main phases: a) experimental pulling test of examined tree with use of both the standard and proposed optical equipment based digital image correlation method; b) analysis of obtained data from particular instruments and their mutual comparison with subsequent analysis of usability and applicability of DIC system in tree safety assessment.

Experimental setup

The pulling test was carried out on a 20 years old walnut tree (*Juglans regia* L.) by constantly applying force coming from a manually operated winch. The tree was 14 m high and its diameter at measured height 0.7 was 0.36 m. Because of the exploratory character of the work and in order to avoid damaging the tree, the pulling test was performed only in a range of elastic deformation. This was achieved by a controlling a force, an inclination respectively, up to 12 000 N, 0.1 ° rotation at the stem base respectively. The rope went from the measured tree further to a load cell that was at half-way to the winch. The load-cell was U2b type produced by Hottinger Baldwin Messtechnik GmbH with maximal force 50 kN and accuracy class 0,1.

On a tree stem (0.7 m above the ground) three extensometers in special housings were installed (tagged as EL1, EL2 and EL3) to measure strain in the tree xylem. The extensometers (LVDTs) were halfbridge inductive displacement sensors Mesing T101F produced by Mesing Ltd. with measuring range ± 2 mm and sensitivity 0,01 μm). The extensometers were screwed deeply to wood to avoid measurement of strain on a bark. The data were collected using DEWE43 data-logger manufactured by DEWETRON Elektronische Messgeräte Gesellschaft m.b.H.. The data-logger has 8 fully synchronized channels and maximum frequency 9000 Hz, the acquistion frequency was set up to 10 Hz and was controlled by Dewesoft

7.0 installed at controlling laptop. Next to the tree, an optical stereoscopic video-camera set for obtaining the consecutive images for calculation of the displacement and strain fields at examined area was installed, see Fig. 1a for detail. The set consisted of two mutually calibrated CCD cameras Allied AVT (Stingray) with a resolution of 2452x2056 px^2. The used lenses had a focal length 25 mm.

Before the acquisition of images, the set was calibrated to obtain exsintric and insintric parameters that provide the stereoscopic view on the examined area and. Calibration of the system was carried out with help of a sequence of 20 calibration images that captured a reference ceramic grid at different angles and positions in respect to the cameras, see Fig. 1b and 1c. The calibration grids have chess-board pattern with a single square of 15 mm long, Fig. 1b and 1c. All captured images were black-white with standard grey scaling of 256 levels. The distance of cameras from the measured area was approximately 1.1 m.

There are two crucial requirements on a surface that is being measured and subsequently calculated by the DIC: a) to have a stochastic and unique pattern all over the measured area; b) to have enough light and contrast between the pattern components. To meet the first requirement a two-component pattern was created using a white natural color as a background and black spray color (Fig 1b and 1c). In order to get the best contrast and fast acquisition time the videocameras' shutters were set to the lowest value (10 μs) as possible and at the same time the measured area was lit by a couple of very strong lights that assured good contrast between white and black components on the one hand and suppressed the surrounding sun light that might have changed during the measurement. Variable light during the measurement bring various brightness/shade conditions and, consequently, make the DIC computation from acquired images impossible. For the experiment a couple of very strong LED-based lights was used, each having luminous intensity about 13000 cd (Fig. 1a).

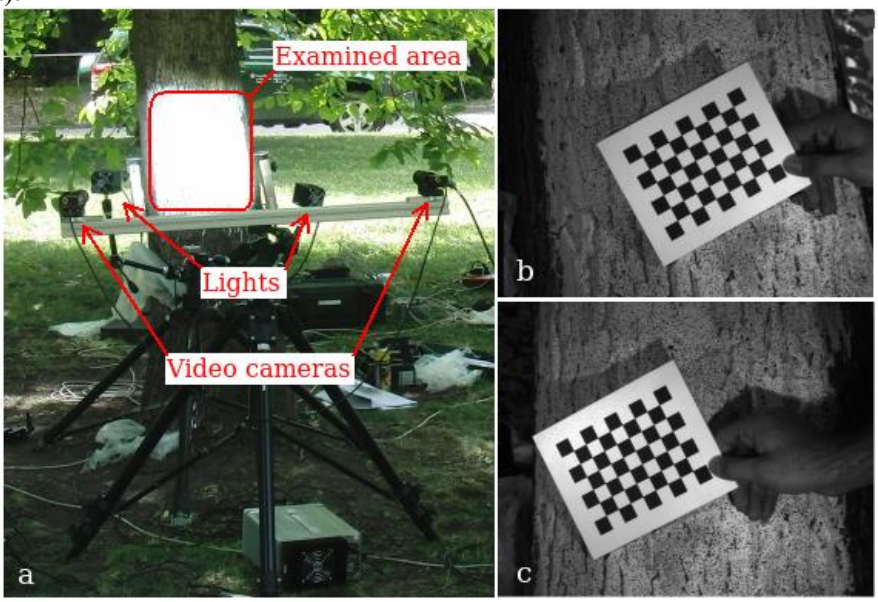

Figure 1: a) stereoscopical measurement setup, b) calibration process using reference grids a) image from left camera, b) image from right camera at the same time

Results

The main goal of this work was to investigate displacement and strain response of a tree (*Juglans Regia* L.) to mechanical load with use of both standard extensometers and full-field measurement based on DIC that provides more detailed information about the tree behavior.

The calibrated stereoscopic system can be also used to obtain 3D coordinates of the surface – the tree bark geometry. The bark geometry can be best viewed in 3D graph where contours express the Z-axis coordinates of the studied object. This is presented in the Fig. 2 with resolution 350x350 calculated values, from which one may see the difficulties that occur when measuring trees using the optical DIC-like methods. The calculated fields are substantially noncontinuous which makes this full-field measurement less informative since huge amount of data were not able to be calculated. This phenomenon is caused by a complexity of a tree bark that contains too deep and steep “hills and valleys” to enable the stereoscopic system – both cameras – to see all points at the same time.

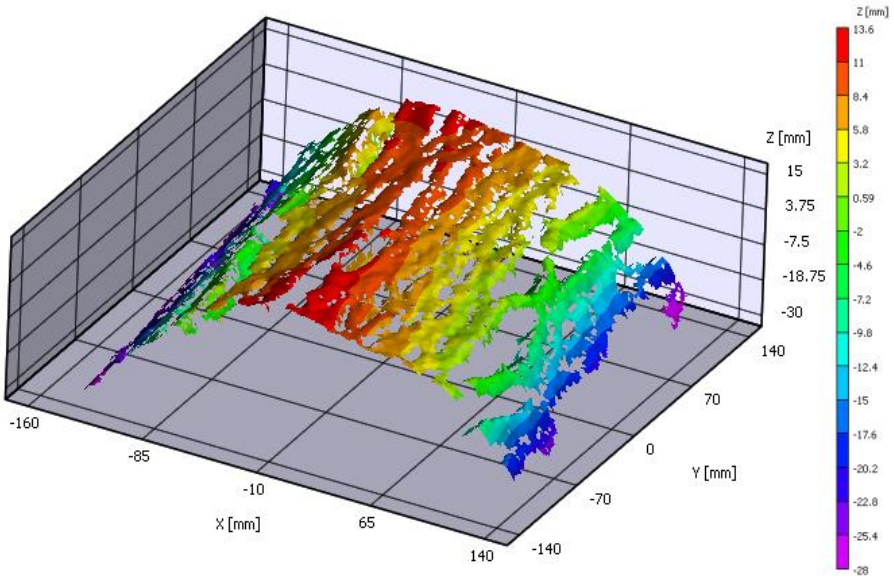

Figure 2 Geometry of the measured stem obtained with use of DIC calculation and expressed as Z-axis coordinate in 3D (subset size 31px)

Therefore, the geometrically complex bark might be, especially for certain species such as pines and oaks, an issue that has to be solved before this method is fully applied in tree biomechanics or arboriculture. This seem even more crucial due to a fact that there is often intention to measure and examine huge and old trees in urban areas that more likely have more complicated bark than the juvenile trees. Nonetheless, from the Fig. 2 we can see that the used optical system had appropriate depth of field, so it could handle examined area roundness (Z axis coordinate) that was maximally ci. 43.6 mm when measured from the lowest to the highest position.

Full-field map of displacement (Fig. 3a to 3d) computed by the DIC for whole process of loading reveal (in Fig. 3 just 2 states are showed) the displacement were successfully computed at the bark surface. Again, all computed quantities include the discontinuities that were mentioned in the Fig. 2. Displacement fields at maximal force of 10360 N (*U* in Fig. 3b and *V* in Fig. 3d) reveal assumed behavior of the tree that is similar to the deflection of cantilever beam with a circular cross-section following beam theory. The highest *U* displacement is 14.6 mm (Fig. 3b) and is located at the top of the examined area and the iso-contours are in horizontal manner. The distribution of the *V* displacement (Fig 3d) has contours organized vertically ranging from negative to positive values, whereas the latter ones are at a convex side of the tree and express the stretching of the bark induced by global stretching of wood fibers in that part of the tree due to its bending. The displacement fields calculated at zero force express the noise of the system (Fig. 3a and 3c).

Analyzing force distribution (Fig. 6), we also see a significant peak that occurred at time of 118 s. This peak is attributed to the rearrangement of the mooring that happened when the force achieved value about 4240 N. It is noteworthy, that this event was recorded by the load cell as well as the optical measurement (*U* displacement, not showed here). Specifically, this physical readjustment of the rope was significantly registered mainly by the *U* displacement component. This knowledge is important since when carrying out the pulling tests of trees, these events often happen and may be important for those who use various instruments without the data acquisition box for synchronizing all inputing signals. Such peaks, then, can be used as a initial footing for the synchronization.

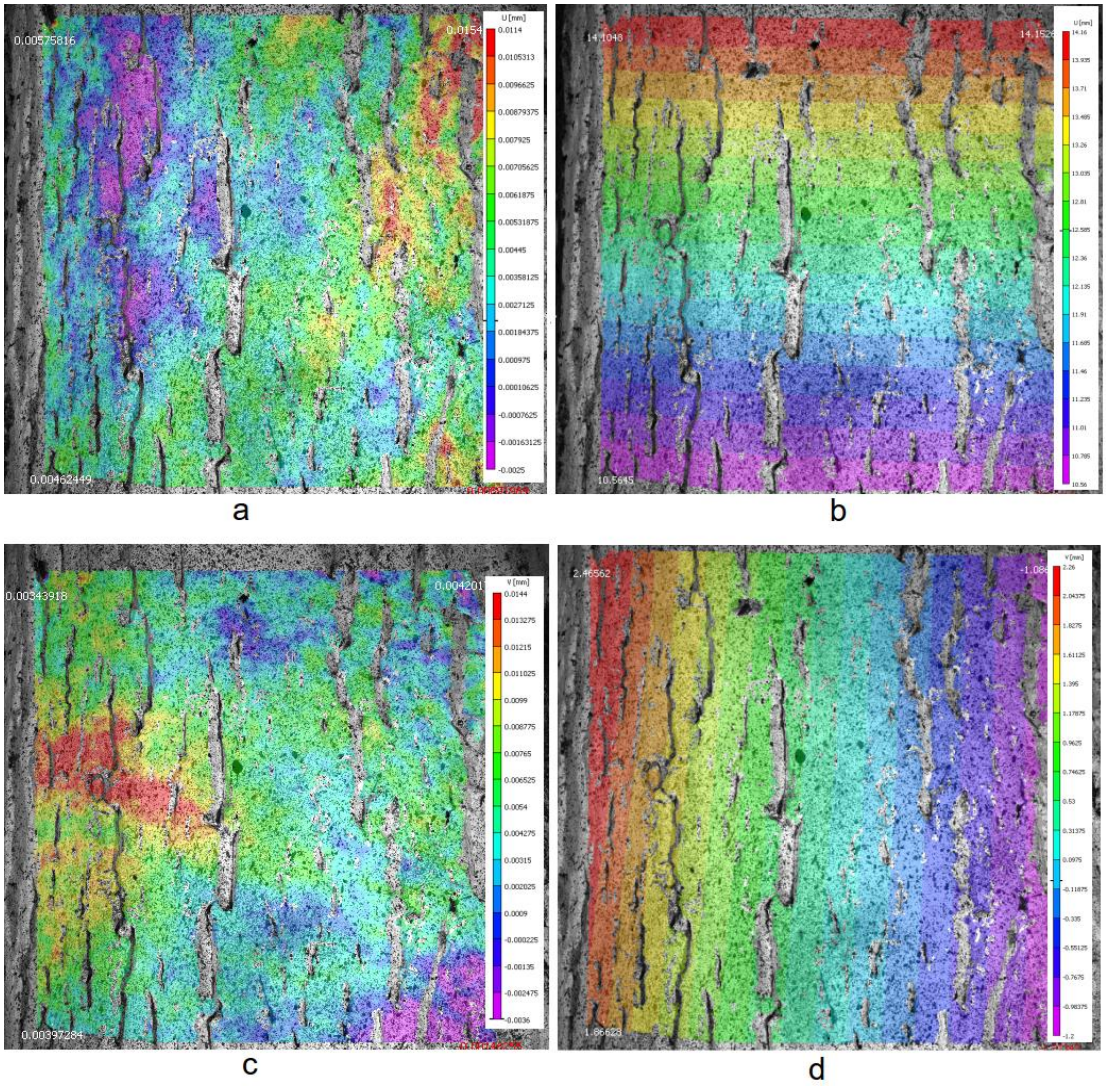

Figure 3 Displacement fields obtained on examined are using DIC computation at subset size 31 px: a) and b) express displacement *U* (~ pulling force direction) for unloaded state and for maximal force; c) and d) express displacement *V* (vertical direction) for unloaded state and maximal force.

The tension and compression parts of the examined are were also reflected in computed strains, see Fig. 4 and Fig. 5, where the standard notation holds truth – compression is of negative values and tension of positive ones. As seen from contours at maximal force (Fig. 4), the strain field is not so predicative when compared to the displacement field (Fig. 3b a 3d) assuming the tree stem behaves similarly to cantilever beams. Nonetheless, there is visible pattern at ε_{yy} (Fig 4b) exhibiting more violet-to-blue shades on right side and yellow-to-red ones on the left.

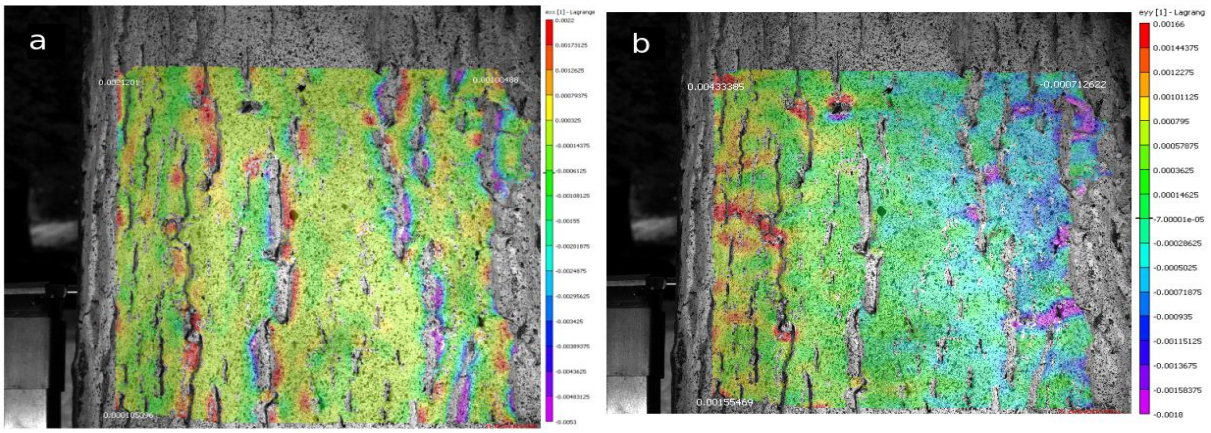

Figure 4 a) strain field in X direction – ε_{xx} (horizontal component); b) strain field in Y direction – ε_{yy} (vertical component). Both strain fields were computed for subset size 31 px and maximal force

To depict strain pattern more clearly, we plotted the ε_{yy} across the stem diameter by dividing measured area into 32 vertical bands. Width of each band ranged from 11 to 12 calculated points, the height of the band ranged from 347 to 355 points, so the minimal amount of ε_{yy} data within the band was 3817 values, the maximal one was 4260. For each band the single mean value of ε_{yy} was subsequently calculated and plotted (Fig. 5). It is important to say that number of calculated points depended on stereo-correlation algorithm and used subset sizes. Therefore, it was necessary to compute strain and displacement fields at different subset sizes. From Fig. 5, we may see that for each subset size, the computed strain field (ε_{yy}) is divided into two halves on negative and positive one (as explained for Fig. 4 above). It is clear that subset size strongly affects computed strains. Based on linear regressions, the highest relative differences between lowest and highest values of strain at both ends of the examined area achieved 200% to 235% (compare solid and dotted lines in Fig. 5).

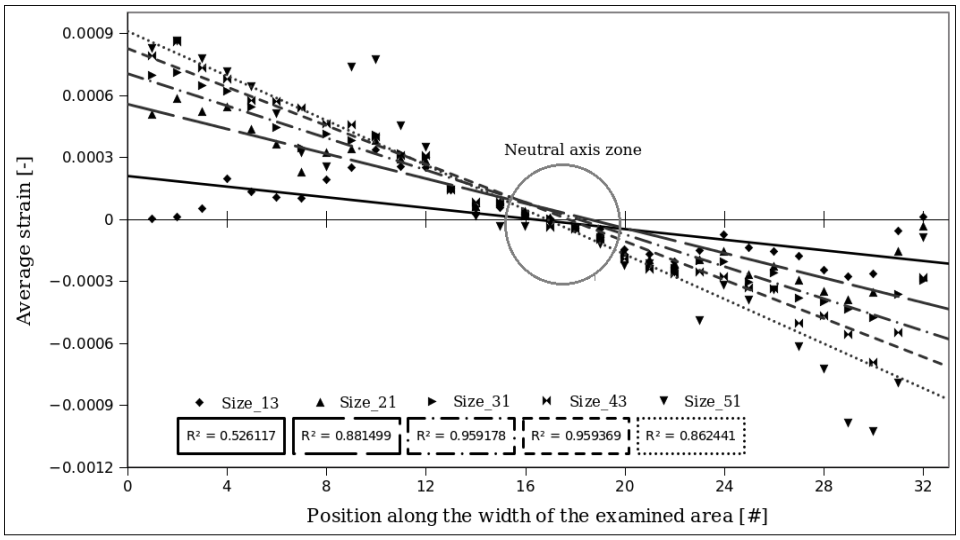

Figure 5 Distribution of vertical strain component ε_{yy} (tree stem axis direction) along the width of examined area computed vertical-wise

Further, we clearly see that nearly in the middle of examined area the ε_{yy} equals zero – the point where each linear regression line crosses the zero line (see the circle in Fig. 5). This corresponds to the standard beam theory, in which such points creates the neutral axis. For ideal cylinders the neutral axis corresponds to a geometric axis, whereas for trees there will always be at different positions due to complicated tree geometry and heterogeneous distribution of properties. Therefore this optical measurement proved to be successful in finding the neutral axis at examined area. This knowledge might be very important for future biomechanical studies since one of the most used arboriculture methods in tree assessment is based on an evaluation of a deflection curve that is often computed at neutral axis. The deflection curve can easily be extracted from full-field data by finding the locations where ε_{yy} equals zero.

As seen from the coefficients of determination (R^2), the highest values (about 0.96) were achieved for subset size 31 px and 43 px and, therefore, they are highly predicative in strain assessment. If the tree was the ideal cylinder with orthotropic material properties in cylindrical coordinate system, the R^2 of such regression would achieve 1. High values of R^2 are desirable in this application, but their use in prediction of optimal subset size must be supported by different analysis that would take into account two phenomena: a) convergence of displacement and strain to hypothetical value as known for mesh-like numerical methods (eg. FEM); b) the projection error that results from breaking the epipolar constraint (Sutton et al. 2009), which is especially for tree the crucial issue since the tree bark has complicated structure and measurement takes place in the environment that brings many factors causing a noise (wind, temperature, vibrations in urban areas etc.).

Comparison of DIC and extensometers

Strains in time measured using both classical extensometers and DIC technique together with the force obtained by load-cell are depicted in Fig. 6. We again see the peaks discussed above are well recognized by the DIC computation. More importantly, the extensometers measured higher absolute values than the DIC technique. The highest relative difference was obtained at maximal force and for compression and tension sides was 21.1% and 40.8% respectively.

The difference can be attributed to the fact that extensometers are directly connected to the wood through screws meanwhile the DIC measures strain on the stem surface (bark). As clear from the beam theory, the strain along the beam length is to be highest at surface layers. From the comparison we see the opposite and, therefore, we can claim the transfer of the strain (stress) from xylem to bark may not be continuous and that effective. The reduced efficiency of strain transfer is most likely caused by a slight independent movement ("floating") of a bark on the xylem part due to various bark layers that rather have transport and insulating functions in a tree than the mechanical ones (Panshin and de Zeeuw 1980).

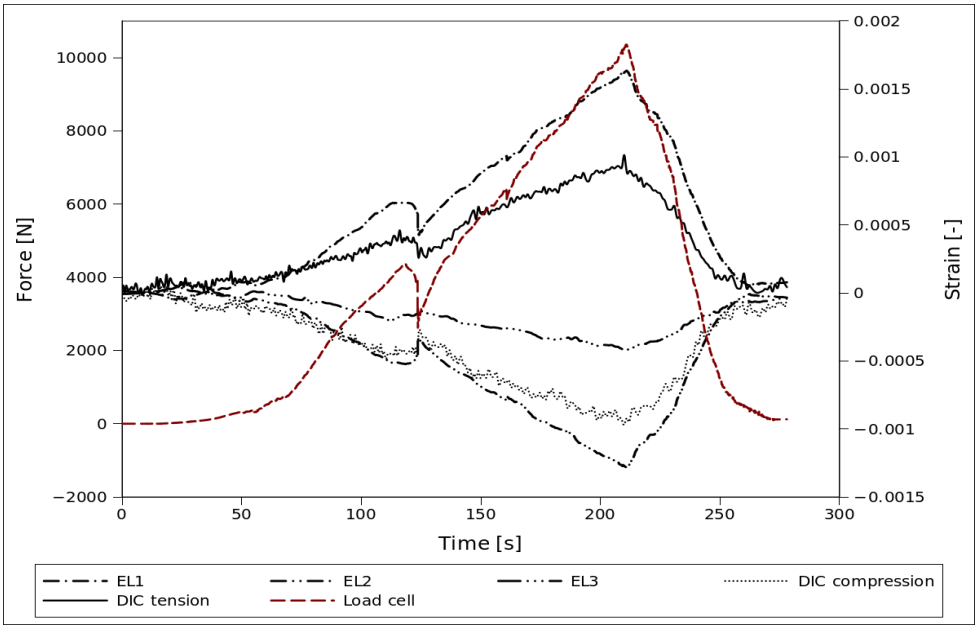

Figure 6 Time-dependent comparison of strain measured with use of standard extensometers (EL1, EL2 and EL3) and DIC technique on compression and tension sides

Conclusions

Both optical and standard strain measurements indicate the proportional limit of wood in tension along the grain (ε_{yy}) was not reached, so we can say the whole test was carried out within the elastic region of deformation. The maximal measured strain obtained with use of EL1 and was ~ 0.16%, whereas wood generally has a proportion limit between 0.6-1% (Bodig and Jayne 1993). This assures the strain measurement is realiable since the fiber failure and buckling most likely did not occur. If we compare strain maximums for tension and compression parts measured either by DIC or extensometers, we see there is higher difference between these parts for extensometers (relative difference is 27%) than for DIC (4.3%). This difference for extensometers may be addressed to their very local positions and discrete character of their measurement. Moreover, unless the repetitive measurements are carried out, one cannot investigate whether the strain is outlying or within a statistical variance. Unlike extensometers, the DIC offered statistically more demonstrative strain results due to its full-field character even despite the fact the examined area was non-continous and vertically averaged.

One of the main problems that arises when evaluation strain is the question to what extent the deformation measured on a tree bark correlates to the deformation in a xylem underneath the bark. Although this is out of scope of this study, future research will have to consider it before full implementation of this method in the tree biomechanics, arboriculture eventually. Moreover, it may be required to investigate this for main kinds of bark morphologies – on an imaginary range starting with smooth bark of beeches and hornbeams up to very rugged bark of oaks and pines. The problem gets more complicated since the bark structure (Panshin and Zeeuw 1980) and consequently the strain transfer efficiency from xylem to bark changes with a tree age differently depending on species. The influence of age on strain distribution was measured also in roots and was attributed to cell maturation process and history of mechanical loading on a tree (Stokes 1999). The research of the strain transfer efficiency will have to measure strain simultaneously on barked and debarked zone to obtain direct comparison. Additionally, such measurement would have to be carried out on both tension and compression parts of the stem because our results show the strain measured by DIC exhibit various differences when compared to the extensometers on those parts. Even though the differences between extensometers and DIC technique were significant, they were of the same order. This gives a positive message for potential use of DIC-like methods in tree and plant biomechanics. Beside the

intention of our study, it is obvious that such optical measurement can be easily applied in mechanics of non-wooden plants too since the technique is universal in terms of the dimensions of studied objects, so the plants' behavior can be studied from seedling to matured plants. The use of DIC in plant biomechanics has one additional demand if the plant is to be preserved. It is using of non-toxic colors in pattern preparation that DIC-like methods require on surfaces of studied objects to perform the correlation calculation. This can be easily obtained using natural colors based on lime and carbon that enable to create required contrast between black and white components. The results also indicate there is a need to watch the subset size since the differences in strains may be high due to the projection error (PE). Our highest obtained difference in strain was ~ 230% when subsets of dimension 13 px and 51 px were compared.

Although the full-field measurement brings higher quality data compared to outputs from extensometers, the processing of data (matrices) is more difficult meaning the computational systems working with matrix algebra are necessary. The authors of the study hope the full-field techniques based on DIC method will find broad applications in plant sciences because of their unquestionable qualities against standard ways to measure strain. Because this work is, to our knowledge, the first to show the application of such technique in plant biomechanics and because current trends in this discipline call for non-contact approaches, we dare to predict its growing use in assessment of plant mechanical behavior.

Acknowledgments

The authors thank to grant no. 39/2012 provided by Mendel University in Brno and the European Social Fund and the state budget of the Czech Republic, project "The Establishment of an International Research Team for the Development of New Wood-based Materials" reg. no. CZ.1.07/2.3.00/20.0269 (EE2.3.20.0269) and Sobriety Ltd. for their advices regarding the DIC.

References

Bodig, J.; Jayne, B.A (1993) Mechanics of wood and wood composites. Krieger Pub Co.
Brudi, E.; Wassenaer, P.V. 2001. Trees and statics: nondestructive failure analysis. In E. T. Smiley, & K.
Crook, M. J., Ennos, A.R. 1996 The anchorage mechanics of deeprooted larch, Larix europea L. japonica. J. Exp. Bot 47, 1509– 1517.
Ennos AR. 1995. Development of buttresses in rainforest trees: the influence of mechanical stress. In: Coutts MP, Grace J, eds. Wind and trees. Cambridge University Press, 293-301.
Forsberg, F., Mooser, R., Arnold, M., Hack, E., Wyss, P. 2008 3D micro-scale deformations of wood in bending: synchrotron radiation mCT data analyzed with digital volume correlation. J. Struct. Biol. 164:255–62.
Mattheck, C. Design in nature. Interdisciplinary Science Reviews (4): 298-314. 1994
Muszynski L., M.E. Launey (2010): Advanced imaging techniques in wood-based panels research. in: Wood-Based Panels - An Introduction for Specialists. State-of-the-Art in Wood-Based Panels Research. COST Action E49: 177-201
Panshin, A.J., de Zeeuw, C. Textbook of wood technology – structure, identification, properties, and uses of the commercial woods of the United States and Canada. McGraw-Hill series in forest resources, 1980. 722 *pp*.
Peltola, H. 2006. Mechanical stability of trees under static loads. American Journal of Botany, 93, 1501-1511.
Peters, W.H., Ranson, W. F. 1982 Digital imaging techniques in experimental stress-analysis. Optical engineering 21(3):427-431
Sani, L., Lisci, R., Moschi, M., Sarri, D., Rimediotti, M., Vieri, M.,Tofanelli, S. 2012 Preliminary experiments and verification of controlled pulling tests for tree stability assessments in Mediterranean urban areas. Biosystems engineering 112:218-226
Sharpe, W.N. (editor) – Springer Handbook of Experimental Solid Mechanics. Springer Science + Bussines Media, LCC, New York, 2008, ISBN: 978-0-387-26883-5
Sinn, G., Wessolly, L. 1989. A contribution to the proper assessment of the strength and stability of trees. Arboricultural Journal, 13, 45e65.
Stokes, A. 1999 Strain distribution during anchorage failure of Pinus pinaster Ait. At different ages and tree growth response to wind-induced root movement. Plant and Soil 217: 17–27.

Sutton, M.A., Orteu, J-J., Schreier, H.W. Digital image correlation for shape and deformation measurements Basic Concepts, Theory and Applications. Springer Springer-Verlag, Heidelberg. 342 p. 2009.
Szorádová, A. Praus, L. Kolařík, J. Evaluation of the root system resistance against failure of urban trees using principal component analysis. Biosystems Engineering 115(3):244-249.
Wessels, C.B., Malan, F.S., Rypstra, T. 2011 A review of measurement methods used on standing trees for the prediction of some mechanical properties of timber. Eur J Forest Res 130:881–893.
Wessolly, L. 1991. 2 new methods to measure the strength and stability of trees. Holz als roh-und werkstoff (3):99-104

Analysis of Wave Velocity Patterns in Black Cherry Trees and Its Effect on Internal Decay Detection

Guanghui Li
School of Information Engineering, Zhejiang Agriculture and Forestry University, Hangzhou, China, lgh@zafu.edu.cn

Xiping Wang
USDA Forest Service Forest Products Laboratory, Madison, WI, USA, xwang@fs.fed.us

Jan Wiedenbeck
USDA Forest Service, Northern Research Station, Princeton, WV, USA, jwiedenbeck@fs.fed.us

Robert J. Ross
USDA Forest Service Forest Products Laboratory, Madison, WI, USA, rjross@fs.fed.us

Abstract

In this study, we examined stress wave velocity patterns in the cross sections of black cherry trees, developed analytical models of stress wave velocity in sound healthy trees, and then tested the effectiveness of the models as a tool for tree decay diagnosis. Acoustic tomography data of the tree cross sections were collected from 12 black cherry trees at a production forest. Trees were subsequently cut, and the disk at each test location was obtained to assess the true physical condition. Stress wave velocity data of different paths across grain, from radial to tangential, were extracted from the acoustic tomography data sets. Our analysis indicated that the ratio of tangential velocity to radial velocity in sound healthy trees approximated a second-order parabolic curve with respect to the symmetric axis $\theta = 0$ (θ is the angle between wave propagation path and radial direction). The analytical model was found in excellent agreement with the real data from healthy trees. Further examination indicated that the analytical model can be used to diagnose internal conditions of trees when a stress wave testing method is used in tree inspection.

Keywords: Stress wave, velocity pattern, trees, internal decay detection, tomography

Introduction

Forests are an extremely valuable resource to human beings. Internal decay of trees endangers the health of forests and decreases the quality and value of timber. Detection of tree decay is important not only to forest management but also to public safety in urban communities. The stress wave method has been well recognized as a robust and low-cost nondestructive technique to test living trees and wood structure for internal conditions. Stress wave transmission time increases dramatically in decayed areas, and internal defects can be detected by the time difference between measured value and the reference value (Pellerin and Ross 2002). Several commercial stress wave testing tools are available to conduct single path stress wave measurements in wood. In addition, some sonic tomography equipment (e.g., ArboSonic 2D, Picus Sonic Tomograph, Arbotom) have been developed to conduct multipath stress wave measurements on trees and construct two-dimensional or three-dimensional tomograms of tree cross sections. An accurate understanding of wave velocity patterns in trees is therefore important to the diagnosis of internal decay, and it is also critical to developing reliable and effective imaging software for internal decay analysis (Bucur 2003).

To improve the precision of decay detection, many researchers studied the relationships between wood mechanical characteristics and stress wave velocity. Dikrallah et al. (2006) presented an experimental analysis of acoustic anisotropy of wood, in particular the dependence of propagation velocities of stress waves on natural

anisotropy axis in the cross section. They found a significant difference in wave velocity between the waves propagating in whole volume and the waves guided on bars. Maurer et al. (2005) studied the anisotropy effects on time-of-flight based tomography, and they assumed elliptic anisotropy, where the angle dependent velocity v can be written as $v = v_{radial}(1- \varepsilon \sin(\phi - \varphi)^2)$, where ϕ is the ray angle. φ represents the azimuth of the v_{radial} direction relative to the axis of the coordinate system, and ε specifies the degree of anisotropy.

Liang et al. (2010) showed that stress waves travel fastest in radial direction and that velocity decreased as the wave propagation path shifted toward to tangential direction. Velocity also increased as the number of annual rings increased. Gao et al. (2012) investigated the effect of environment temperature on acoustic velocity of standing trees and green logs and developed workable models for compensating temperature differences as acoustic measurements are performed in different climates and seasons. Their results indicated that acoustic velocity increased as wood temperature decreased when the temperature was below the freezing point. When the temperature was well above freezing, velocity decreased linearly at a slow rate as wood temperature increased.

The objectives of this study were to investigate the stress wave velocity patterns in cross sections of standing trees and examine the effect of internal tree decay on the velocity pattern. We proposed a theoretical model of stress wave velocity in sound healthy trees and tested the effectiveness of the model as a tool for decay diagnosis.

Theoretical Analysis of Wave Velocity Pattern

With the assumption that the trunk of a tree under test is cylindrical body, and its cross section is in ideal circularity (Fig. 1), we now consider the relationship between stress wave velocity and its propagation direction. In Figure 1, **S** is a source sensor, and **R1** and **R2** are two receiver sensors. Stress wave is transmitted from the source to the receivers. SR0 represents the radial direction ***R***, and SR1 and SR2 represent the tangential direction ***T***. The dynamic modulus of elasticity (***E***, Pa) can be calculated from the stress wave velocity (V, m/s) using the following equation:

$$E = V^2 \rho \tag{1}$$

where ρ is the density of wood (kg/m^3).

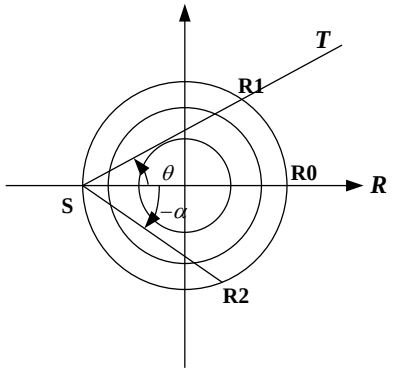

Figure 1. The coordinate system of cross-section plane.

Given the angle θ between radial and tangential directions, let $\boldsymbol{E_R}$, $\boldsymbol{E_T}$, and $\boldsymbol{G_{RT}}$ represent radial modulus of elasticity, tangential modulus of elasticity, and shear modulus, respectively. v_{RT} represents Poisson's ratio of wood material, then we have

$$\overline{E}_R = \frac{1}{\overline{S_R}}, \quad \overline{E}_T = \frac{1}{\overline{S_T}}; \quad \overline{G}_{RT} = \frac{1}{\overline{S_{RT}}} \tag{2}$$

$$\overline{S_R} = \frac{\cos^4\theta}{E_R} + \frac{\sin^4\theta}{E_T} + \left(\frac{1}{G_{RT}} - \frac{2\nu_{RT}}{E_R}\right)\sin^2\theta\cos^2\theta \tag{3}$$

$$\overline{S_T} = \frac{\cos^4\theta}{E_T} + \frac{\sin^4\theta}{E_R} + \left(\frac{1}{G_{RT}} - \frac{2\nu_{RT}}{E_R}\right)\sin^2\theta\cos^2\theta \tag{4}$$

$$\overline{S_{RT}} = 4(\frac{1}{E_R} + \frac{1}{E_T} + \frac{2\nu_{RT}}{E_R})\sin^2\theta\cos^2\theta + \frac{1}{G_{RT}}(\sin^2\theta - \cos^2\theta)^2 \tag{5}$$

From Equations (1) to (5), the relationship between the stress wave velocity V and angle θ can be given as follows (Dikrallah 2006).

$$V_T = V_R\cos^2\theta\sqrt{1 + \frac{E_T}{E_R}\tan^4\theta + 2\frac{G_{RT}}{E_R}\tan^2\theta} \tag{6}$$

where V_T is the tangential velocity and V_R is the radial velocity. Now we can approximate Equation (6) with second order Taylor polynomial. Let $f(\theta)$ represent the ratio of V_T to V_R, then

$$f(\theta) = \cos^2\theta\sqrt{g(\theta)} \tag{7}$$

where
$$g(\theta) = 1 + \frac{E_T}{E_R}\tan^4\theta + 2\frac{G_{RT}}{E_R}\tan^2\theta. \tag{8}$$

From Equations (7) and (8), the derivatives of $f(\theta)$ and $g(\theta)$ can be determined as

$$\begin{aligned} g'(\theta) &= 4\frac{E_T}{E_R}\tan^3\theta(\tan\theta)' + 4\frac{G_{RT}}{E_R}\tan\theta(\tan\theta)' \\ &= 4\frac{E_T}{E_R}\tan^3\theta\sec^2\theta + 4\frac{G_{RT}}{E_R}\tan\theta\sec^2\theta \\ &= \frac{4}{E_R}\tan\theta\sec^2\theta(E_T\tan^2\theta + G_{RT}) \end{aligned} \tag{9}$$

$$\begin{aligned} g''(\theta) &= \frac{4}{E_R}((\tan\theta\sec^2\theta)'(E_T\tan^2\theta + G_{RT}) + \tan\theta\sec^2\theta(E_T\tan^2\theta + G_{RT})') \\ &= \frac{4}{E_R}\sec^2\theta((\sec^2\theta + 2\tan^2\theta)(E_T\tan^2\theta + G_{RT}) + 2E_T\tan^2\theta\sec^2\theta) \end{aligned} \tag{10}$$

$$\begin{aligned} f'(\theta) &= (\cos^2\theta)'\sqrt{g(\theta)} + \cos^2\theta(\sqrt{g(\theta)})' \\ &= -\sin 2\theta\sqrt{g(\theta)} + \frac{1}{2}\cos^2\theta\, g^{-1/2}(\theta)g'(\theta) \end{aligned} \tag{11}$$

$$\begin{aligned} f''(\theta) &= -(\sin 2\theta)'\sqrt{g(\theta)} - \sin 2\theta(\sqrt{g(\theta)})' + \frac{1}{2}(\cos^2\theta)'g^{-1/2}(\theta)g'(\theta) \\ &\quad + \frac{1}{2}\cos^2\theta(g^{-1/2}(\theta)g'(\theta))' \\ &= -2\cos 2\theta\sqrt{g(\theta)} - \frac{1}{2}\sin 2\theta\, g^{-1/2}(\theta)g'(\theta) - \frac{1}{2}\sin 2\theta\, g^{-1/2}(\theta)g'(\theta) \\ &\quad + \frac{1}{2}\cos^2\theta(-\frac{1}{2}g^{-3/2}(\theta)g'(\theta)g'(\theta) + g^{-1/2}(\theta)g''(\theta)) \end{aligned} \tag{12}$$

From Equations (7) to (12), we know

$$g(0) = 1,\ g'(0) = 0,\ g''(0) = 4\frac{G_{RT}}{E_R}$$

$$f(0)=1, f'(0)=0, f''(0)=-2(1-\frac{G_{RT}}{E_R}) \tag{13}$$

So, function $f(\theta)$ can be expanded to Taylor series at $\theta=0$ as follows:

$$\begin{aligned} f(\theta) &= f(0)+\frac{1}{1!}f'(0)\theta+\frac{1}{2!}f''(0)\theta^2+O(\theta^3) \\ &= 1-(1-\frac{G_{RT}}{E_R})\theta^2+O(\theta^3), \end{aligned} \tag{14}$$

$$\approx 1-(1-\frac{G_{RT}}{E_R})\theta^2 \tag{15}$$

where O (θ^3) is the remainder of the Taylor polynomial. For the coordinate system given in Figure 1, we assume the angle $\theta>0$ if θ is counter-clockwise from the radial direction. Otherwise, $\theta<0$ if θ is clockwise from the radial direction. Equation (14) shows that the ratio of V_T to V_R approximates a parabolic curve with the symmetric axis $\theta = 0$. For a real living tree, its cross section may not be in ideal circularity; therefore, the velocity pattern may deviate from the theoretical model shown by Equations (14) and (15).

Materials and Methods

The experimental data used in this study were from an early investigation on tree decay detection (Wang et al. 2009). The field test site was located just south of Kane, Pennsylvania, in McKean County and was part of the Collins Pennsylvania Forest. Twelve black cherry trees were selected as test samples through visual examination and single-pass stress wave test. These selected trees had a wide range of physical conditions in terms of physiological characteristics and stress wave transmission times. For each sample tree, we conducted acoustic tomography tests at three different heights (i.e., 50 cm, 100 cm, and 150 cm) above the ground, and one unique label was used to mark the cross section. For example, "4–50" represents the sample tree No. 4 and the test height is 50 cm. Figure 2 shows the acoustic tomography test on a black cherry tree sample using a Picus Sonic Tomograph tool (Argus Electronic GmbH, Rostock, Germany). The PICUS Sonic Tomograph measurement system consisted of 12 sensors, which were evenly placed around the trunk in a horizontal plane (Fig. 2a). Stress wave transmission times were measured by sequentially tapping each pin of the sensors using a speical steel hammer. For each source sensor, the other 11 sensors receive the stress wave signals, and the wave transmission times were recorded by the system. A complete data matrix was obtained through this measurement process at each test location. Figure 3b shows the sensor arrangement and the paths of stress wave measurements on one cross section.

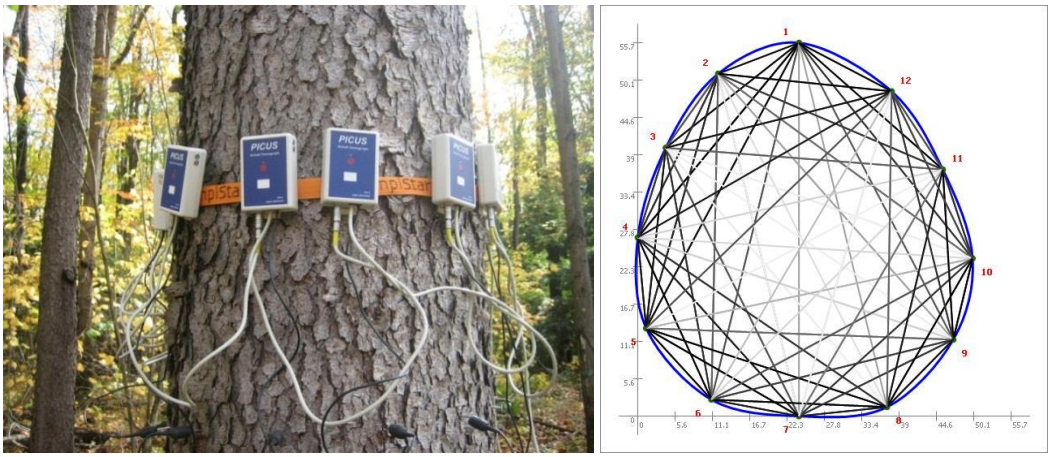

(a) Sensor arrangement (b) Stress wave propagation paths

Figure 2. Sonic tomography test on black cherry trees using a Picus Sonic Tomograph tool.

Experimental Results and Analysis

Trees without decay

Among the selected samples were eight cross sections (No. 4–150, 7–50, 10–50, 11–50, 12–50, 15–50, 16–50, and 17–50) revealed as in sound condition after the trees were cut. As an example, Table 1 shows the velocity measurements of sample No.17–50 with the sequential number 1 to12 representing the source points, and the angle θ representing the position of the receiver points relative to the source point, as defined in Figure 1. For simplicity, the average of the line velocities of the measurement paths with same angle θ from all the 12 source points was calculated. For solid cross section, the velocity in radial direction V_R (with $\theta = 0$) was the highest, and the velocity in tangential direction V_T (with $\theta = \pm 75°$) was the lowest. Consider the tangential velocity at $\theta = \pm 75°$ as a reference velocity, then the ratio of V_T to V_R reflects the wave velocity patterns in a tree cross section.

Figure 3 shows the wave velocity pattern under source point 1. Here, the angle θ was converted into radian unit ($1° = \pi/180$). The relationship between velocity ratio V_T/V_R and angle θ was statistically in a parabolic curve, with a coefficient of determination $R^2 = 0.985$. The coefficients of the second order polynomial regression are $a = -0.1796$, $b = -0.0023$, and $c = 0.9963$. It was noted that the coefficient of the first order term was close to zero and the constant close to 1, which is in good agreement with the Equations (14) and (15). In fact, all the wave velocity pattens under different source points were parabolic curves as shown in Figure 4a. The tomogram of the cross section No. 17–50 taken by the Picus Sonic Tomograph system is shown in Figure 4b, which indicates the cross section in a sound condition.

Ideally, if a tree trunk is considered as transversely isotropic material, the velocity values obtained from the same measurement paths (e.g., 75° and –75° from radial direction) should be same or very close. The average velocity for the same measurement paths under different source points was tabulated in Table 1.

Figure 5 shows the average wave velocity pattern for the cross section No. 17–50. The trend line of ratio V_t/V_r is still a second order parabolic curve ($y = ax^2 + bx + c$) with the coefficients $a = -0.2062$, $b = -0.0096$, $c = 1.0067$, and the coefficient of determination $R^2 = 0.999$. This result is in a good agreement with Equation (15).

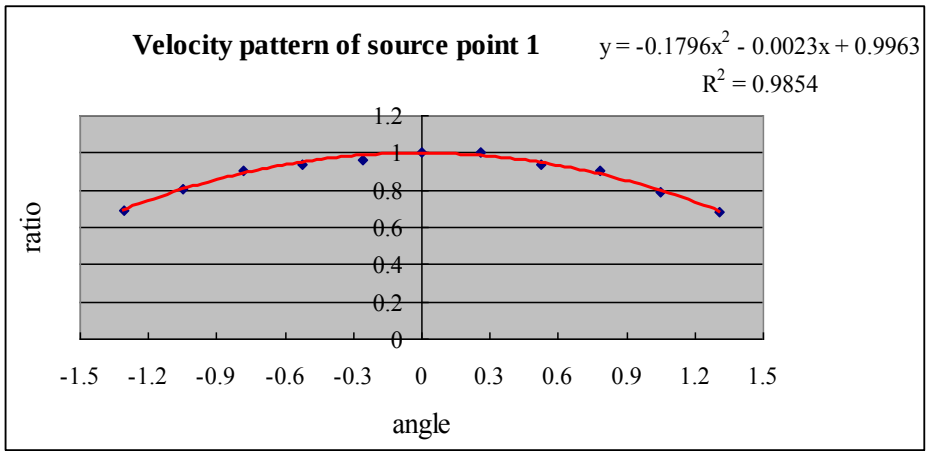

Figure 3. Wave velocity pattern under source point 1 for tree sample 17–50.

Table 1. Acoustic velocity data for tree sample 17–50 (Unit: m/s)

θ (degree)	Source point												Average	V_t / V_r
	1	2	3	4	5	6	7	8	9	10	11	12		
75	1023	888	1013	974	921	875	896	861	874	919	1014	930	932.33	0.636
60	1181	1204	1132	1208	1109	1098	1054	986	1143	1146	1209	1201	1139.25	0.777
45	1354	1280	1293	1339	1243	1161	1249	1161	1309	1332	1394	1311	1285.5	0.877
30	1408	1426	1382	1430	1266	1339	1374	1293	1329	1465	1473	1443	1385.67	0.945
15	1503	1482	1400	1446	1409	1412	1449	1424	1392	1486	1535	1459	1449.75	0.989
0	1500	1447	1360	1541	1434	1456	1462	1469	1397	1505	1528	1500	1466.58	1
-15	1441	1427	1419	1556	1447	1354	1482	1478	1374	1481	1538	1469	1455.5	0.999
-30	1400	1459	1378	1538	1372	1308	1435	1410	1299	1442	1476	1368	1407.08	0.9599
-45	1353	1364	1304	1359	1278	1234	1294	1312	1231	1333	1310	1269	1303.42	0.889
-60	1211	1261	1089	1233	1182	1054	1167	1208	1100	1120	1191	1169	1165.42	0.795
-75	1035	1066	836	1139	927	843	976	993	986	911	1046	909	972.25	0.663

Table 2. Equations for parabolic curves fit to velocity ratio (V_t /V_r) and propagation path (θ) data

Sample No.	*a*	*b*	*c*	R^2
4–150	–0.1957	0.0137	1.0049	0.994
7–50	–0.1992	0.0009	1.0209	0.9919
10–50	–0.2114	0.005	1.0243	0.9885
11–50	–0.2275	0.0026	1.0113	0.9973
12–50	–0.2182	–0.0041	1.0132	0.996
15–50	–0.1855	–0.0103	1.0507	0.9542
16–50	–0.1842	–0.0028	0.9852	0.9916
17–50	–0.2062	–0.0096	1.0067	0.9989
Average	–0.2031	–0.0006	1.0147	0.9891

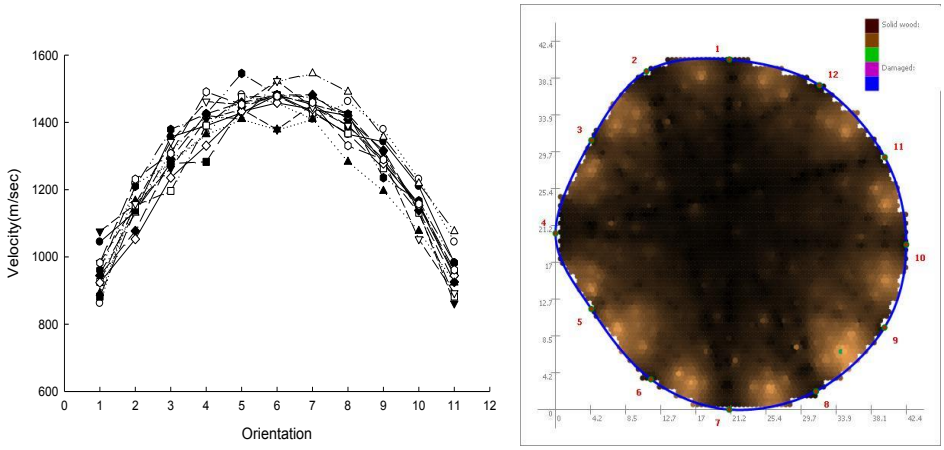

(a) Measured acoustic velocity patterns. (b) Acoustic tomogram

Figure 4. The velocity trend lines and tomogram of sample 17–50.

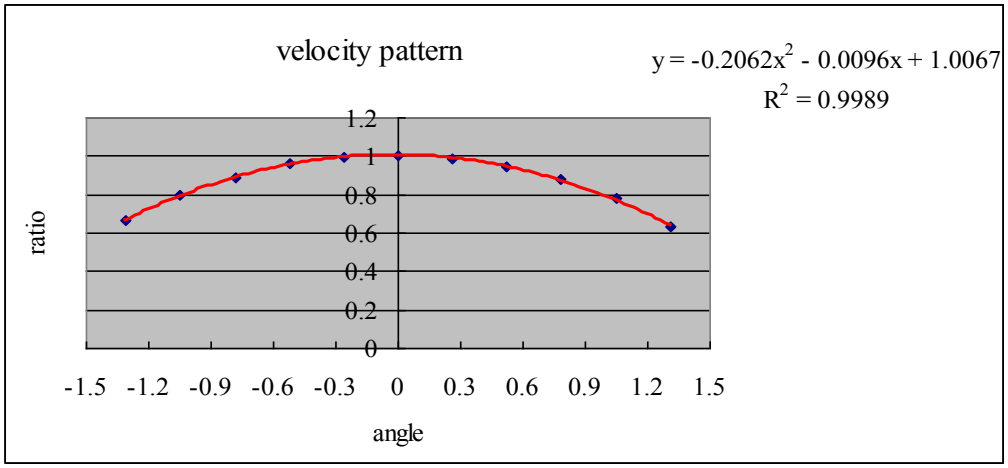

Figure 5. The average acoustic velocity pattern of sample 17–50.

The experimental results indicated that all other sound samples (cross sections) had the similar velocity patterns as sample No. 17–50. The regression relationships between velocity ratio (V_T /V_R) and wave propagation path angle θ are shown in Table 2.

From Table 2, it can be seen that for the sound black cherry trees there exists a second order polynomial relationship ($y = ax^2+bx+c$) between the velocity ratio V_T /V_R and wave propagation path angle θ. A close examination of the correlation coefficients indicated that this relationship can be expressed as the following general form:

$$y = 1 + ax^2 \qquad (16)$$

where the coefficient $a \approx -0.2$. According to Equation (15) we proposed earlier, $a = -(1-G_{RT}/E_R)$ should be determined by the mechanical properties of the tree trunk. The stress wave data obtained from the black cherry tree samples showed that Equation (15) is valid for describing the wave velocity pattens in the cross section of a tree trunk.

Trees with internal decay

The tomography results from the black cherry tree samples showed that twelve cross sections had internal defects. These samples were 1–50, 1–100, 1–150, 2–50, 4–50, 4–100, 18–50, 18–100, 18–150, 19–50, 19–100, 19–150. Figure 6 shows the pictures of the tree samples with internal defects and the corresponding tomograms. Figure 7 displays the corresponding velocity pattern of each tree cross section where the acoustic tomography test was performed.

The structural defects found in tree 1 were the most significant of all tested trees with both tomograms and disk samples confirming heartwood decay at all three heights. Laboratory examination confirmed the presence of brown-rot decay fungus. The tomograms of tree 1 at 50-, 100-, and 150-cm heights showed large acoustic shadows in the central areas of the cross sections. The size of the shadow was the largest at the lower height (50 cm) and decreased progressively as the test height increased. The velocity patterns for tree 1 in Figure 7 show a very different shape compared with that found in sound trees. The stress wave velocity was the lowest in the radial paths at all three heights, as opposed to be the highest in sound trees. This “caved shape” in measured velocity pattern corresponded to the “acoustic shadow” found in the tomogram very well.

In addition, both tomograms and wave velocity pattern figure show that the 2–50 and 4–50 have the same cases as No.1 tree, but 4–100 has only a light internal defect. No.19 tree has a clear crack from its outside, and the tomograms of three cross sections 19–50, 19–100, and 19–150 demonstrate the crack and central decay, so the

velocities decrease in the sixth direction dramatically for all the source points. No. 18 tree also had internal decay and a crack, but the decay area doesn't surround the central point, which resulted in a velocity pattern that is more complex than the No. 19 tree as shown in cross sections 18–50 and 18–100.

Discussion

An acoustic tomography tool typically applies 8 to12 or even more sensors to acquire wave velocity data, and then generate a two-dimensional tomogram for each cross section tested. The measurement process is time consuming because of the delicate procedures for setting up sensors and conducting a series of time-of-flight tests. For practical use in field, it is often desirable to use far fewer sensors and complete tests in a short period of time but still obtain reasonably accurate and sufficient data enabling the detection of internal tree decay.

Based on our theoretical analysis and experimental results, we propose to use the established velocity patterns in healthy trees as a standard model to diagnose the internal tree decay. A reference velocity V_0 can be determined by calculating the average of the line velocities of the neighboring sensors, the wave proagation path angle θ of V_0 is 75° for the case of 12 sensors. This velocity can be used as a reference because typically the sapwood of a tree is intact (Divos and Divos 2005). According to Equations (14) and (15),

$$V_0 / V_r \approx 1 - (1 - \frac{G_{RT}}{E_R})(\frac{75\pi}{180})^2 = 1 - (1 - \frac{G_{RT}}{E_R})(\frac{5\pi}{12})^2 \quad (17)$$

Now, the velocity $V(\theta)$ can be determined by the following equation:

$$V(\theta)/V_0 \approx (1 - (1 - \frac{G_{RT}}{E_R})\theta^2)/(1 - (1 - \frac{G_{RT}}{E_R})(\frac{5\pi}{12})^2) \quad (18)$$

Therefore the trend line of velocity ratio $V(\theta)/V_0$ is also a parabolic curve with the symmetric axis $\theta = 0$. Figure 8 shows the trend line of ratio $V(\theta)/V_0$ for tree cross section 17–50.

When the reference velocity V_0 is determined, the other line velocities can be estimated by Equation (17) and an inference of whether this line is a defect line or not can be made accordingly. If we simplify the measurement to include six test points only, (6 × 5) /2 = 15 velocity measurements can be obtained. Figure 9 shows all possible wave propagation paths in the cross section of a tree trunk with 6 test points. In this case, with respect to each source point, the wave propagation path angles θ are 60°, 30°, 0°, –30°, –60°. The reference velocity can be calculated by the same method as mentioned above, and each line velocity obtained from the measurement can be compared with the velocity calculated from Equation (17). Finally, the decay area within the cross section can be estimated roughly. For example, Figure 9 shows the lines AE, BF, CF and DF as defect lines, and the other lines are sound, thus we can draw an inference that the defect area is located within the polygon AOEF.

Based on the theoretical velocity model and the measured velocity patterns, we can also evaluate the internal decay in a tree trunk without determining a reference velocity V_0. From the theoretical analysis, the velocity pattern of a sound tree trunk exhibits a second-order parabolic curve similiar to the velocity ratio V_T / V_R. As an example, Table 3 shows the measured velocity data for tree sample 1–50. Figure 11 illustrates the theoretical velocity model of the black cherry and the measured velocity data under source point 1, and Figure 12 shows the tomogram of tree sample 1–50.

It can be seen from Table 3 that, from source point 1, the wave velocities were 999 m/s (1–2), 1150 m/s (1–3), 1199 m/s (1–4), 1184 m/s (1–5), 1044 m/s (1–6), 764 m/s (1–7), 826 m/s (1–8), 1048 m/s (1–9), 1110 m/s (1–10), 1064 m/s (1–11), and 996 m/s (1–12). From Figure 10, it can be seen that the line velocities of 1–5, 1–6, 1–7, 1–8, and 1–9 deviated from the theoretical values dramatically. The largest deviation was the line velocity for 1–7, which represents the radial direction. Consequently, we can speculate that internal decay exists in the central area of the cross section, and the decay area is surrounded by the lines 1–5 and 1–9, which matches with the tomogram of sample 1–50 reasonably well as shown in Figure 12.

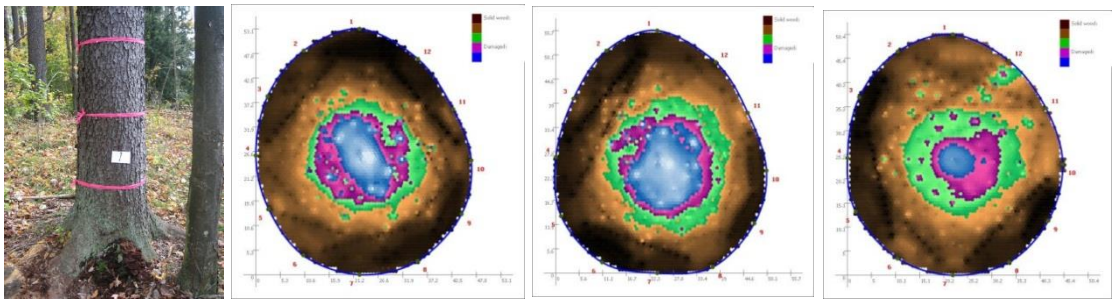

Figure 6. Black cherry trees and their tomograms showing internal defects.

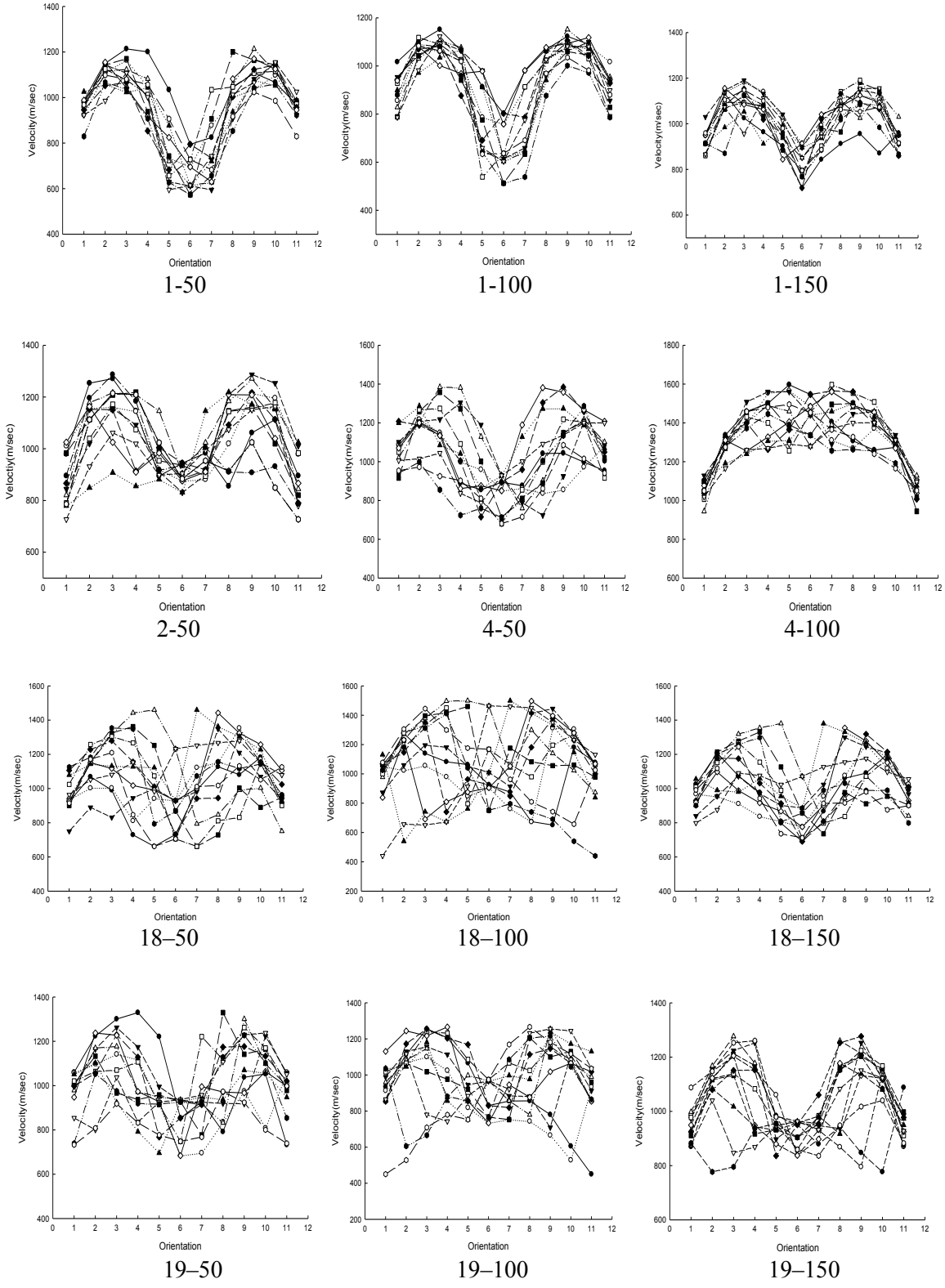

Figure 7. Velocity patterns of the black cherry trees with internal defects.

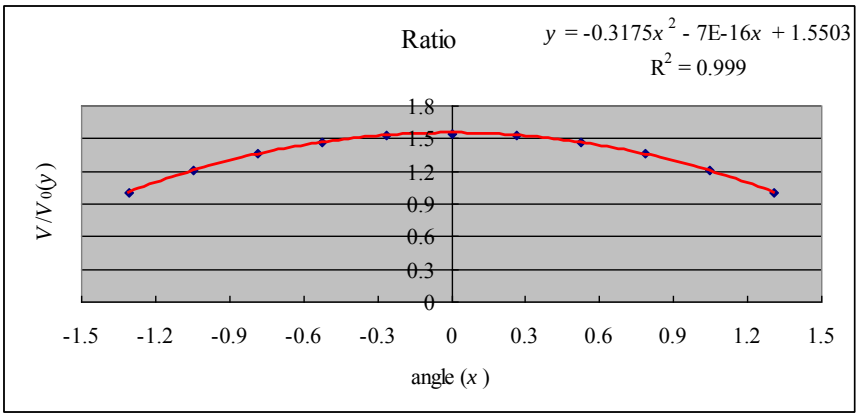

Figure 8. The trend line of ratio $V(\theta)/V_0$ of 17–50.

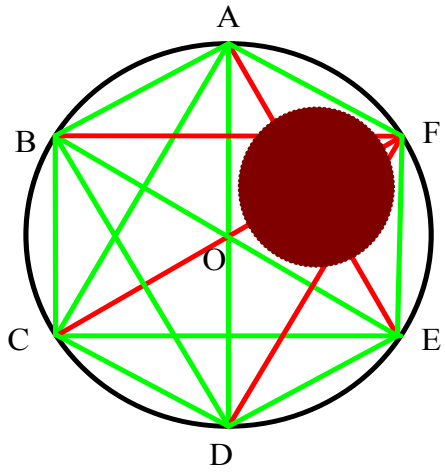

Figure 9. Simplified stress wave measurement in a tree with six test points.

Table 3. Acoustic velocity data of sample 1–50 (unit: m/s)

Test point	1	2	3	4	5	6	7	8	9	10	11	12
1		917	1150	1228	1217	1024	825	823	1040	1106	1069	940
2	999		965	1170	1228	1090	947	730	905	1055	1083	1113
3	1150	881		1025	1190	1111	1035	654	599	651	915	1067
4	1199	1053	923		997	1086	1127	1067	729	616	609	1014
5	1184	1100	1096	972		933	1143	1151	867	766	573	801
6	1044	1003	1103	1145	1019		960	1107	1047	999	679	657
7	764	521	972	1119	1143	953		936	1024	1046	849	677
8	826	661	606	1097	1189	1143	955		936	1125	1028	860
9	1048	849	624	712	1008	1105	1080	1040		1033	1063	999
10	1110	949	539	613	720	1026	1086	1185	1018		969	994
11	1064	991	901	646	574	635	858	1057	1055	877		798
12	996	1083	1094	1100	1012	798	689	973	1048	977	861	

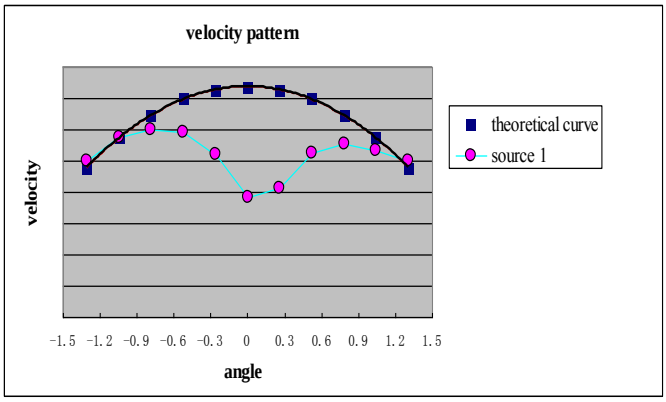

Figure 11. Theoretical velocity pattern and measured velocity data

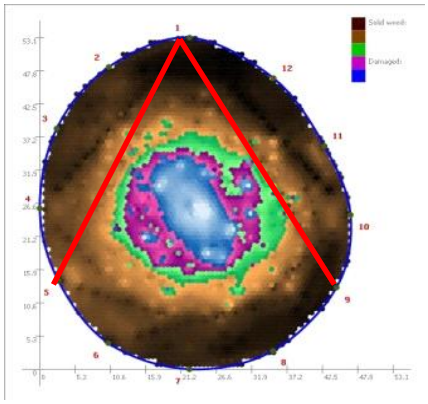

Figure 12. Tomogram of sample 1–50.

Conclusions

With the assumption that the trunk of a tree under test is cylindrical and its cross section is in a round form, we developed a theoretical model of stress wave velocity in sound healthy trees and examined wave velocity patterns in the cross sections of 12 black cherry trees with experimental data. Our theoretical analysis indicated that the ratio of tangential velocity to radial velocity approximated a parabolic curve with symmetric axis $\theta = 0$ (θ is the angle between tangential direction and radial direction). The experimental results of 8 sound cross sections showed that the measured velocity patterns were in a good agreement with the theoretical analysis. The tomograms of 12 cross sections with internal decay reflected the anomaly of velocity pattern. The proposed theoretical velocity model can be used as a diagnostic tool to detect internal decay of live trees.

Acknowledgments

This research was made possible by the collaboration between the USDA Forest Service, Forest Products Laboratory and Zhejiang Agriculture and Forestry University in China. This study was supported in part by the Natural Science Foundation of China (Grant No. 61272313) and Zhejiang Provincial Science and Technology Project (Grant No. 2012C21015). The financial support to Dr. Guanghui Li's visiting study at the USDA Forest Productions Laboratory (FPL) was provided by the China Scholarship Council (CSC).

Reference list

Bucur, V. 2003. Nondestructive characterization and imaging of wood. Berlin Heidelberg, Germany: Springer-Verlag.

Dikrallah, A., Hakam, A., Kabouchi, B., Brancheriau, L., Bailleres, H., Famiri, A., Ziani, M. 2006. Experimental analysis of acoustic anisotropy of green wood by using guided waves. ESWM-COST Action E35. pp. 149–154.

Divos, F., Divos, P. 2005. Resolution of stress wave based acoustic tomography. 14th International Symposium on Nondestructive Testing of Wood. 309–314.

Gao, S., Wang, X., Wang, L., Allison, R.B. 2012. Effect of temperature on acoustic evaluation of standing trees and logs: part 1—laboratory investigation. Wood and Fiber Science. 44(3): 286–297.

Liang, S., Fu, F., Lin, L., Hu, N. 2010. Various factors and propagation trends of stress waves in cross sections of Euphrates poplar. Forest Products Journal. 60(5): 440–446.

Maurer, H.R., Schubert, S.I., Bachle, F., Clauss, S., Gsell, D., Dual, J., Niemz, P. 2005. Application of nonlinear acoustic tomography for nondestructive testing of trees. 14th International Symposium on Nondestructive Testing of Wood. 339–349.

Pellerin, R.F., Ross, R.J. 2002. Nondestructive evaluation of wood. Madison, WI: Forest Products Society.

Wang, X., Wiedenbeck, J., Liang, S. 2009. Acoustic tomography for decay detection in black cherry trees. Wood and Fiber Science. 41(2): 127–137.

Micro-movements of trees

Ferenc Divos
Jozsef Bodig Wood NDT Lab, University of West Hungary, Sopron, Hungary, divos@fmk.nyme.hu

Agnes Kinga Buza
Jozsef Bodig Wood NDT Lab, University of West Hungary, Sopron, Hungary, egyy170@yahoo.com

Abstract

In recreational parks and forests, as well as in urban areas the stability of trees is quite important because of public safety. External loads like wind or snow may exceed the load supporting capacity of individual trees. Severe damage and injuries can occur because of falling trees and break away branches.

This paper describes a new method to access stability of trees exposed to dynamic (wind) loads. The new measurement technique includes an ultrasonic wind speed measurement. The inclination of trees under wind load was assessed by the movement of a laser dot projected to a screen. This micro-movement technique maybe used to establish maximum wind load values for individual trees. Compared to the already developed pulling test, the resolution of this new technique demonstrated significant improvement.

Additionally the stability of larger diameter branches was also investigated. Under simulated wind load the natural frequency decrease was evaluated.

The preliminary results are encouraging demonstrating that the micro-movement measurements of trees and branches may have significant advantages compared to traditional tree stability evaluations.

Keywords: movement, micro-movement, tree stability, stability in wind

Introduction

The long term stability of forest stands and urban trees has been a question since the forest cultivation had started. The changes in wind and snow load resistance of a particular tree were always a challenge because of manifold and unpredictable factors. (James, 2006) Over the years, several methods have been developed to address the question. One of the most successful measuring technique is the so called “pulling test”. The essentials of the methods include a pulling force application at adequate height of the tree. The pulling cable is anchored, tightened and the pulling force is measured by a transducer. At the bottom, near to the soil an inclinometer is measuring the vertical leaning of the trunk. The interested reader can find detailed discussion of this measuring technique in the following publications (Neild, 1999, Petola 2000 and Kamimura 2012)

Not only falling trees can cause injuries but break away branches as well. Some research work has been accomplished during the past decades regarding the load supporting capacity of branches. (van Casteren, 2012) However no modeling of micro-movements of branches was published up today. Nondestructive testing and modeling of the breakaway is another area which might be in interest.

Objectives

The purpose of this preliminary investigation was to develop experiment techniques that are capable of measuring micro-movements of trees and branches. The first segment of the research was devoted to develop trunk inclinations measurement methods with high precision. The new technique should be fast, user friendly and applicable for any environmental conditions that might occur. This new technique should be comparable to any already developed measuring methods.

Because most of the natural failure of trees originates from wind load, a special wind speed measuring device was created to assess the wind velocity at the desired height. To accomplish the goal and adjectives the following materials and methods were used.

The second part of the research included the investigation of micro-movements of branches. Although destructive evaluation method was applied during the development of this technique, our goal is to forecast branch failure on the bases of their micro-movements.

Materials and methods

For comparison purposes the “inclino” type pulling test was used. On the top the inclinometer we fixed a laser light source firmly which projected the laser beam to a detecting screen attached to a web camera. (Fig. 1.) Both the inclinometer and the web camera were connected to a computer and real time load, inclination and pixel movements were recorded. Note, that the laser technique provided data in pixels. Knowing the distance of the screen from the laser beam source, pixel movement can be converted into inclination degrees. The inclinometer resolution was 0.0003 degree. The laser dot movement on the screen as mentioned earlier was in pixels. In every 2 seconds 5 data were collected and recorded.

The rope was fixed on the trees about 5 meters high and anchored to the ground at 18 meters from the center of the trunk. A mechanical cable stretcher applied the pulling load on the trees. The load detection happened through an electronic transducer fixed on the cable and hooked to the computer as well. The web camera and the screen were located 20 meters away from the laser light source.

Special software was developed particularly to this project. Besides the several channels data collecting capability, the movement detection of the laser dot needs some explanation.

Figure 1 — The laser dot on the white surface and the detecting program.

The real time video made by the web camera was directly sent to the program. The video image was turned to black and white using a brightness scale. It means every pixel, having lower brightness than a predetermined brightness value, was turned into black while the other was turned into white. The control value of the brightness can be changed by the user. The black and white video showed the laser dot very

clearly as a big white dot in case of proper level setting. An ellipse was fitted to the dot's image. The movement of the center point was calculated and recorded in pixels.

For comparison purposes the traditional pulling test used the following specifications. The inclinometer resolution was 0.001 degree with 10 Hz. The test was done on three different trees. Thus the cable was fixed at three different locations between 4.75 and 5 meters. The anchor distance from the center of the trunk was between 18 and 20 meters.

To collect data on the wind velocity a special ultrasonic type measuring device was developed. The apparatus is operating on the Doppler-effect. It consists of four combinations of ultrasonic transmitters and receivers which were configured into pairs facing to each other (Fig. 2.).

Figure 2 — The wind measurer on the top of the tower. The perpendicular detector pairs are well seen.

This apparatus was fixed on a pole at 10 meters height and collected wind velocity data from every directions at that particular height. Five data in every two seconds were collected and computerized.

An attempt was made to figurate the natural frequency of heavy branches for certain species. The theoretical consideration behind this investigation is that decayed wood has lower natural frequency. Thus this physical attribute can forecast possible failure. The frequency measurement included marking selected branches and recording the branch movement under one dynamic load. This measuring technique has already been presented in another publication (Buza, 2011).

The recorded movement of branches exposed to dynamic load was the basis of calculations of natural frequencies. Because identification of decayed branches is very hard an accelerated damage were applied during each measurements. Two types of artificial decays were applied. (Fig. 3.)

Figure 3 — Left: a cut from downside with a wide cutting.
Right: a cut from upside just after the breaking, the felling down.

First the branch was cut from the top perpendicular to the centerline of the branch gradually until failure occurred. For other branches the gradual saw kerfs were cut from the bottom side. At each kerf depth, the same load was applied and the branch movement was recorded and compared to the initial (uncut) data. Similar measurement was applied using a homogenous wooden pool to screen at the effect of the possible inhomogeneity of branches.

Measurements were done in the botanical garden of the University of West Hungary and in public space in Sopron. The pulling tests were done on spruces (*Picea abies*) and on a common horse chestnut (*Aesculus hippocastanum*). Branches were cut and measured on oaks (*Quercus*), lime trees (*Tilia*) and walnut trees (*Juglan*).

Results and discussion

Experimental results show that the laser dot inclination measurement is equivalent to the existing pulling test (Fig. 4) demonstrates the similarity of measurements. Note that the new type of determination of trunk inclination is given by pixels; however, these data can be easily converted into micro-degrees. Although the time dependent sensitivity of the inclination measuring device resolution was better than the laser dot method, its inclination sensitivity is higher. This indicates that the newly developed method maybe successfully used in the field further more combined with wind load combinations the cable attachment and tensioning may be avoided.

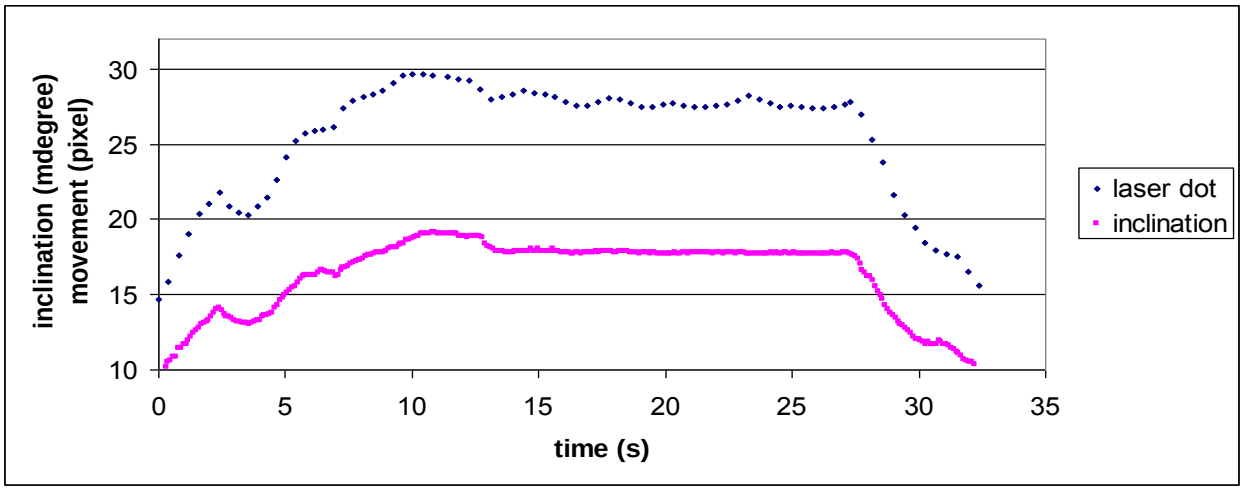

Figure 4 —The movement of the laser dot and the measured inclination. Smaller movements are detectable only with the laser system.

Real dynamic loads as mentioned earlier come from wind gusts our developed measuring technique can access the wind speed with good accuracy. The device was calibrated between 20 and 60 km/h simulated wind speed by 10 km/h increments. Fig 5 demonstrates the measured wind speed and the corresponding inclinations. According to the data there is a strong correlation between wind velocity and inclination of tree as it was expected. This wind speed measuring technique and apparatus may replace cable pulling to access the inclination of trees as a function of wind speed. Furthermore, the standard cup anemometers do not provide enough resolutions to examine the relation between wind velocity and inclinations.

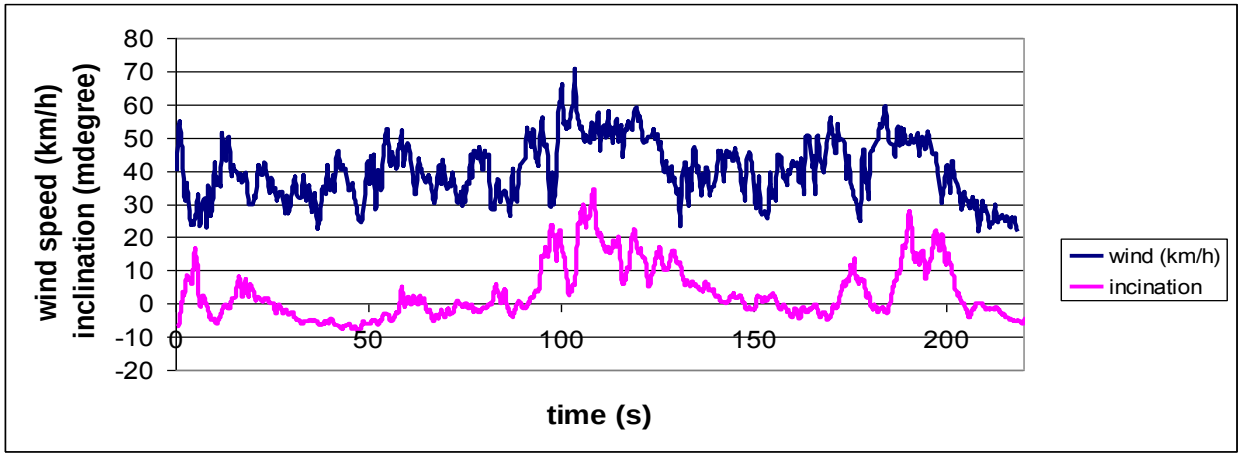

Figure 5 — Wind speed and trunk movements. In this case the movement was measured only by the inclinometer.

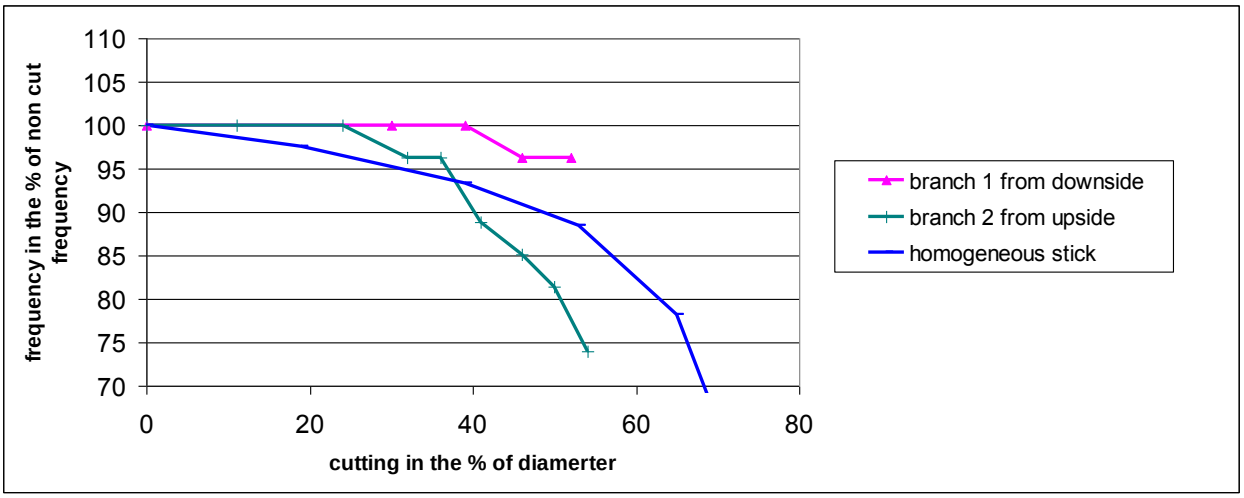

Figure 6 — An example from cutting. One branch was cut from downside (pink line on the top), the frequency changed less than 5%. The other branch was cut from upside (green line on the bottom). Middle line (blue) is from cutting a homogeneous stick for comparing. The difference is noticeable, reaction wood makes downside cutting to make less difference in frequency while more difference during an upside cutting.

Examination of the response of branches to dynamic load resulted significant changes as the branches were cut either from top or bottom sides. Fig. 6 demonstrates the relationship between natural frequency and depth of cut compared to homogenous same diameter pole. Note that the graph shows the changes of natural frequencies of artificially decayed branches. Data clearly indicates the effect of reaction wood. Rapid deterioration can be seen when the upper side is cut while the compressed side can maintain 95% of the frequency up to 60% of the cutting depth. This indicates that the dynamic load and frequency evaluation of branches may work adequately for heavy branches damaged on the top side. However, decays on the bottom side cannot be screen out with certainty because the failure might occur at 95% of the original frequency

Summary and conclusion

This paper describes new measurement for tree inclinations and wind speed and attempted to predict branch failure exposed to dynamic loads. As an overall conclusion it can be stated that the laser dot trunk inclination measurement is equivalent of the traditional inclinometer method. It should be noted however, that care must be exercised using the laser light in urban areas.

The wind speed measuring equipment may be used to access the relationships between the wind speed and the inclination of trees. This is quite important for evaluations of coniferous stands. Spruce, pine and Fear species have shallow root systems and the majority of accidental falling is caused by excessive wind velocity.

For broad leaf species the prediction of branch failure may happen through frequency assessment under dynamic load. Up to date, the limitation of the method is that the prediction of branches damaged at the compression side cannot be forecasted.

This research is still in developments. The preliminary results are encouraging. Due to the limitation of available equipment and resources the wind measurement could be done at only 10 meters height. Results indicate that about 50km/h wind velocity is necessary to evaluate a 12 meters tall tree. The wind measuring technique may not be applied in dense forest because the measuring tower is blocked by the dense canopy of the forest. Further research is needed to address the different wind speed at different height of the tree. Because the wind velocity changes with altitude, multiple wind speed measuring device are necessary to integrate the proper wind load over the entire canopy.

Acknowledgments

This research was supported by the European Union and co-financed by the European Social Fund in frame of the project „Talentum - Development of the complex condition framework for nursing talented students at the University of West Hungary", project ID: TÁMOP 4.2.2.B-10/1-2010-0018.

References

Brudi, E., and P. van Wassenaer. 2002. Trees and statics: Nondestructive failure analysis. In Tree Structure and Mechanics Conference Proceedings. Smiley, T.E., and Coder K. (Eds.). Intern. Soc. Arboriculture, Champaign IL.

Buza A. K., and Divos F. 2011. Dynamic measurements on branches – link with stability. In 7th International Nondestructive Testing and Evaluation of Wood Symposium Proceedings. 207-211. ISBN 978-963-9883-81-9

van Casteren, A., Sellers, W. I., Thorpe, S. K. S., Coward, S., Crompton, R. H. and Ennos, A. R. 2012. Why don't branches snap? The mechanics of bending failure in three temperate angiosperm trees. In Trees, Volume 26, Issue 3, pp 789-797

James, K., R., Haritos, N., and K. Ades P., K. 2006. Mechanical stability of trees under dynamic loads. In American Journal of Botany 93(10): 1522-1530.

Kamimura, K., Kitagawa, K., Saito, S. and Mizunaga, H. 2012. Root anchorage of hinoki (Chamaecyparis obtuse (Sieb. Et Zucc.) Endl.) under the combined loading of wind and rapidly supplied water on soil: analyses based on tree-pulling experiments. In European Journal of Forest Research. Volume 131, Issue 1, pp 219-227

Neild S. A. and Wood C. J. 1999. Estimation stem and root-anchorage flexibility in trees. In Tree Physiology 19. 141-151.

Peltola, H., Kellomaki, S., Hassinen, A., and Granander, M. 2000. Mechanical stability of Scots pine, Norway spruce and birch: an analysis of tree-pulling experiments in Finland In Forest Ecology and Management Volume: 135 Issue: 1-3: 143-153

Nondestructive Assessment of *Schizolobium amazonicum* with Stress Wave Tomography

Frederico França
Department of Forest and Wood Science, Federal University of Espírito Santo, Jerônimo Monteiro, Espírito Santo, Brazil, frederico_franca@hotmail.com

Graziela Vidaurre
Department of Forest and Wood Science, Federal University of Espírito Santo, Jerônimo Monteiro, Espírito Santo, Brazil, grazividaurre@gmail.com

Leif Nutto
Department of Forest Engineering and Technology, Federal University of Paraná, Curitiba, Paraná, Brazil, lnutto.ufpr@gmail.com

Xiping Wang
Forest Product Laboratory, USDA, Madison, Wisconsin, USA, xwang@fs.fed.us

José Tarcísio da Silva Oliveira
Department of Forest and Wood Science, Federal University of Espírito Santo, Jerônimo Monteiro, Espírito Santo, Brazil, jtsilva@npd.ufes.br

Tobias Biechele
Rinntech, Heidelberg, Germany, tobias.biechele@rinntech.com

Abstract

This study aimed to evaluate the potential of stress wave tomography technology for assessing the quality of *Schizolobium amazonicum* standing trees for veneer production. The concept of stress wave tomography operation is based on the measurement of transit time of acoustic pulses that are generated by a hammer knock and move from an initial sensor to many other sensors attached to the tree. Seven 30-year-old *Schizolobium amazonicum* tree were selected and tested in northern Espírito Santo state, Brazil. The measurement data was processed using a specialized equipment software, generating two-dimensional tomogram images of the cross-section of the tree trunk. A yield prediction model was used to estimate the possible yield of veneer that could be produced. The average final yield prediction was 61.2%. Trees with less rotten areas resulted better yield.

Keywords: Yield prediction, Veneer

Introduction

Currently, among the species that are planted in the northern region of Brazil, stands out *Schizolobium amazonicum* (Huber) Ducke, Caelsalpinacea family, known as paricá, which is a pionner specie and provide rapid development, has straight trunk, little amount of branches and is quite cultivated by logging companies for veneer production.

The wood of *Schizolobium* is light and is used for tarticle board, plywood, and furniture (Carvalho, 1994; Iwakiri et al., 2010), althought its mechanical properties are relatively low (Torelli and Gorizek, 1995).

The quality of paricá wood allows better fitness for a particular use, or its ability to fulfill the requirements needed to manufacture a product allowing the generation of differentiated products for supply to specific customers (Vidaurre, 2010).

It has differentiated sapwood heartwood, with a gradual transition zone. The sapwood is creamy and yellowish heartwood is light brown. The wood of this species is susceptible to biological attack and is recommended to be preserved (Carvalho, 2007).

Knowing the optimal age cutoff, depending on the characteristics of the wood and hence the products it originated. In Brazil, the cycles of the stands are short due to climatic conditions favorable to rapid growth (Vidaurre, 2010).

Assuming that at older ages there is a greater chance of finding trees with larger diameters, and thinking that the diameter is the main agent of yield increase, Hoffmann (2009) found that trees with larger diameters obtained higher yield in veneer production due core volume loss got diluted by wood veneer process.

The achievement of NDT requires skilled labor and equipment developed specifically for each type of test. The costs of purchase little influence on the final price of the product and the advantages and profits intangibles brought to its application provide businesses competitiveness and market consolidation. (Cunha Filho, 2002).

A nondestructive method for evaluating the internal quality trees in the inventory pre-cutting would be to use the ARBOTOM®, a product which is based on propagation of stress waves in the wood that are captured by sensors in contact with the tree. Thus, it is possible to measure differences in the properties of wood and detecting the presence or absence of hollow or rotten wood within the tree.

With a tapping carried out on these studs impact waves emitted in a sensor to propagate through all sensors waves impact on the shank, thereby creating links between the various sensors.

Its operation is based on the speed at which a pulse generated by a knock hammer moves a sensor attached to the tree until one or more sensors, connected by fire-wire cables. Woods with greater density usually healthy, without rotting or cracking conduct impulses more quickly from one sensor to another.

This study aimed to evaluate the potential of stress wave tomography technology to detect internal defects nondestructively in individuals trees and predict the potential yield of veneer peeled from *Schizolobium amazonicum* standing trees.

Materials and Methods

The study site was in Vale Nature Reserve, located in the northern of Espírito Santo state, Brazil. 19° 06' and 19° 18' south latitude 39° 45' and 40° 19' west longitude.

The soils are classified as "Yellow dystrophic Oxisol, clayey phase evergreen forest." The climate of this location is tropical humid, with mean annual rainfall of 1202 mm, average temperature 22.2°C, relative humidity of 84.3% and altitude between 28 to 65 m (Jesus, 2001).

It was studied seven representing trees of *Schizolobium amazonicum* (Huber) Ducke, specie known as paricá. The trees were 30 years old when evaluated.

To evaluate the quality of the wood of the tree alive, we used the equipment ARBOTOM®, and the scanner connected to a computer via Bluetooth™ and all speeds are analyzed and stored by ARBOTOM® 2.0 software (Figure 1).

Figure 1 – Tree evaluation and software tomogram image.

Divos and Szalai (2002) proposed possible measurement arrangements with four to eight sensors. They reported that tomography measurements with eight sensors can identify small defects that were 1% of the cross-section area. It were used eight sensors around the stem at the level of dbh.

Impact is generated on each of the eight pins sensors until the variation in the propagation time of the wave be uniform (variation coefficient less than 3%). The equipment was calibrated according to the anatomy and density of the species under study. The range of speeds was found between 880 and 1320 m/s as can be visualized in Figure 2.

Figure 2 - Range of speeds used for the species under study (m/s).

After the data is compiled by ARBOTOM® software, were observed analyzed images that link defects in the wood at different stages. Individuals considered in the experiment were analyzed separately, and characterized individually.

Hoffman (2009) developed equations for trees aged 5 to 7 years to estimate the yield of *Schizolobium amazonicum* in commercial plantations in northern Brazil. The linear equation was used to estimate the yield of wood lamination for the seven trees under study.

$$Y = -0.78178 + 0.26148 * X \quad (R^2 = 79{,}83\%) \qquad (1)$$

where Y is lamination yield (m^3), X is diameter at breast height (cm).

The yield loss of the trees were estimated using the images generated by the tomograph using Equation 2.

$$YL = \frac{\pi * (D-R)^2}{4} * 100 \quad (2)$$

Where YL is yield loss (%), D is diameter at breast height (cm) and R is Rot diameter (cm).

Results and Discussion

The arrangement of sensors, the propagation velocity (m/s) and 2D image illustrating the impact wave velocity for the seven trees analyzed can be seen in Figure 3.

Tree	Arrangement of sensors and wave propagation speeds (m/s)	Tomogram of the cross-section at dbh
Tree no. 1	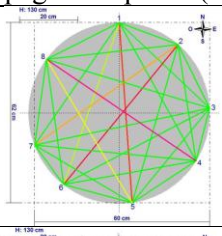	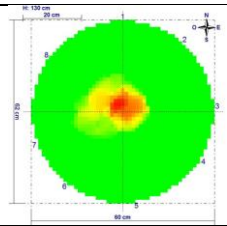
Tree no. 2	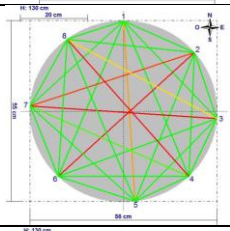	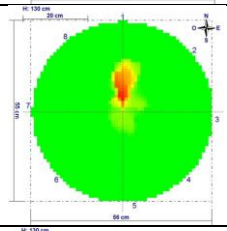
Tree no. 3	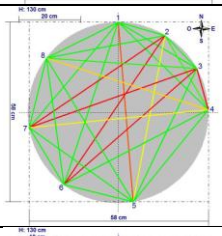	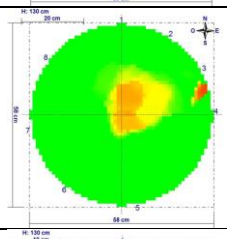
Tree no. 4	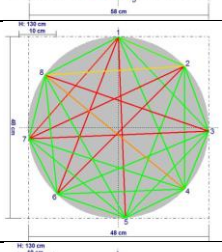	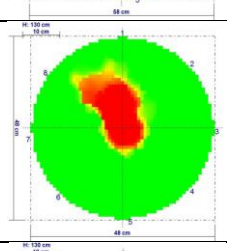
Tree no. 5	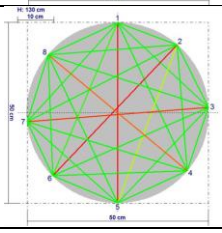	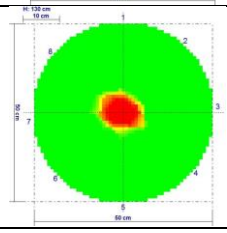

Tree no. 6	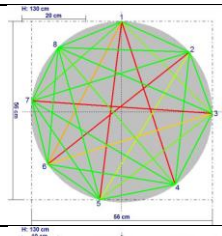	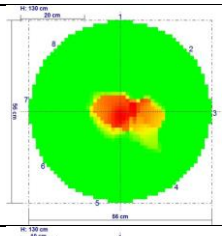
Tree no. 7	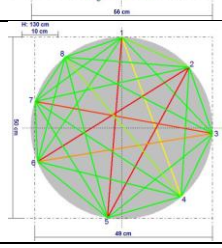	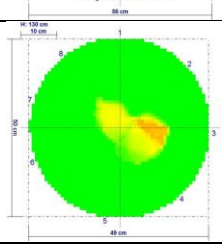

Figure 3 – Arrangement of sensors and the speeds of propagation (m/s) and Illustrative 2D image of the interior of the shaft.

In Tree no. 1 were detected lower stress waves speeds for the inside bole, characterizing possible deterioration in their previous. Was also detected variation in the speed of the wave inside the Tree no. 2, but with different intensity and position of Tree no. 1.

For Tree no. 3, the image shows bigger rot area but with less severity. Also shows a small rot area under the bark on the right side.

The shank of Tree no. 4 showed greater attack surface and greater intensity of degradation among the trees analyzed. Tree no. 5 showed rot close to the pitch. Tree no. 6 shank is partially degraded. The area under attack presented considerable variation in the speed of wave propagation.

The Tree no. 7 showed signs of degradation that can be considered with low intensity degradation, based on the speed of propagation of shock waves.

The DBH, predicted yield using Equation 1, final yield and yield loss are shown on Table 1.

Table 1 – Tree, DBH, predicted yield, final yield and yield loss

	DBH (cm)	Yield estimation from Hoffman`s equation(m^3)	Yield predicted based on tomography results (m^3)	Yield Loss (%)
Tree no. 1	60	14.91	10.85	27.22
Tree no. 2	55	13.60	8.20	39.73
Tree no. 3	58	14.38	5.18	64.00
Tree no. 4	48	11.77	4.56	61.25
Tree no. 5	50	12.29	11.03	10.24
Tree no. 6	56	13.86	10.06	27.44
Tree no. 7	49	12.03	6.90	42.65
AVERAGE	53.7	13.26	8.11	38.93

As shown on Table 1, it was possible to estimate the yield using tomography and prediction yield equation. The average final yield loss prediction was 38.93%.

Conclusions

According to the objective of this study it can be concluded that the ARBOTOM® was able to detect, in a non-destructive damage to the inside of the shaft through the propagation of shock waves in the wood. Thus, the product has potential in selecting trees for sawing or lamination.

Schizolobium amazonicum trees evaluated were in different stages of degradation. It is expected that the monitoring of planting with ARBOTOM® is possible to determine the best age to harvest, higher yielding wood volume without encountering internal degradation of the wood.

Acknowledgments

The company VALE for providing the material under study.

References

Carvalho, P. E. R. Especies florestais brasileiras: Recomendações silviculturais, potencialidades e usos da madeira. Empresa Brasileira de Pesquisa Agropecuária – Centro Nacional de Pesquisas Florestais (EMBRAPA-CNPF), Colombo, Paraná, Brazil. 1994.

Carvalho, P. E. R. Paricá *Schizolobium amazonicum*. Colombo PR: EMBRAPA Florestas, 2007. 12p. (EMBRAPA Florestas. Circular Técnica, 142).

Cunha Filho, J. S. Ensaios não destrutivos: análise de custos versus benefícios. Salvador: VI Conferência sobre Tecnologia de Equipamentos, 2002, 9p.

Devos, F.; Szalai, L. Tree evaluation by acoustic tomography. In: Proceedings of the 13th International symposium on nondestructive testing of wood. Madison, WI: Forest Products Society: 2002. p. 251-256.

Hoffmann, R. G. Caracterização dendrométrica e avaliação do rendimento em laminação de madeira em plantios de paricá (*Schizolobium amazonicum* Huber ex. Ducke) na região de Paragominas, PA. Alegre, 2009. Dissertação (mestrado) – Universidade Federal do Espírito Santo. 97 f.

Iwakiri, S.; Zeller, F.; Pinto, J. A.; Ramirez, M. G. L.; Souza, M. M.; Seixas, R. Avaliação do potencial de utilização da madeira de *Schizolobium amazonicum* "Paricá"e *Cecropia hololeuca* "Embaúba"para produção de painéis aglomerados. 2010. Acta amazônica 40: 303:308.

Jesus, R. M. Manejo florestal: impactos da exploração na estrutura da floresta e sua sustentabilidade econômica. 2001. 244p. Tese (Doutorado) - Universidade de Campinas, 2001.

Torelli, N.; Gorisek, Z. Mexican tropical hardwoods: Mechanical properties in green conditions. European Journal of Wood and Wood Products. 53: 421-423. 1995.

Vidaurre, G. B. Caracterização anatômica, química e físico-mecânica da madeira de paricá (*Schizolobium amazonicum*) para produção de energia e polpa celulósica. Viçosa, 2010. Tese (doutorado) – Universidade Federal de Viçosa. 74f.

Use of Impulse Tomography in Quality Analysis of Maçaranduba Trees, *Manilkara huberi* (Ducke) Chevalier

Lis Rodrigues Uliana
Université Laval, Québec, PQ, Canada

Adriana Maria Nolasco
University of São Paulo, Piracicaba, SP, Brazil

Abstract

This study treated the evaluation of response patterns and effectiveness of impulse tomography method identifying lesions and hollows in the wood of trees of species of *Manilkara huberi* Ducke (Chevalier) (family Sapotaceae). This study was conducted in an area of 3 ha at Paragominas, PA, Brazil. We had evaluated 29 maçaranduba trees with diameter at breast height between 50 and 130 cm. The analysis of the trees occurred by the impulse tomograph. Samples disks from the trees were removed at the height of tomograph analysis and we performed some quality examinations of the discs with the naked eye. These data were compared with the supervised classification of tomographic image in each individual. In addition, we evaluated the correlation between the tomography impulse results with the analysis of the specific gravity mass obtained by two methods: (1) X-ray densitometry and (2) the hydrostatic method. From the 29 trees observed, 18 had hollow spaces. There was a correlation between the image generated by the impulse tomograph with the quality of the stem after cutting; however, in diameters over 90 cm and in trees with very irregular stem form, the tomograph was not able to detect deteriorated wood. No correlation was found between the image generated by the impulse tomograph with the result of X-ray densitometry, and specific gravity mass obtained by the hydrostatic method.

Keywords: Impulse tomography, forest management, *Manilkara huberi*, injuries and hollows, x-ray densitometry

Session 3

Nondestructive Evaluation of Standing Timber

Evaluation of Agarwood (*Aquilaria microcarpa*) Trees Using Ultrasonic Wave Propagation

Lina Karlinasari *
Department Forest Products, Faculty of Forestry, Bogor Agricultural University (IPB), Bogor, West Java, Indonesia, lkarlinasari@gmail.com

Nengsie Indahsuary Uar
Graduate student, Postgraduate Program of Forest Products Science and Technology, Bogor Agricultural University (IPB), Bogor, West Java, Indonesia, khaulaniningsie@yahoo.co.id

Hario Teddy Kusumo
Bachelor student, Department of Forest Products, Faculty of Forestry, Bogor Agricultural University (IPB), Bogor, West Java, Indonesia, harioteddy16@yahoo.com

Erdy Santoso
Forest Research and Development Agency (FORDA), Ministry of Forestry, Republic of Indonesia, Bogor, West Java, Indonesia

Dodi Nandika
Department Forest Products, Faculty of Forestry, Bogor Agricultural University (IPB), Bogor, West Java, Indonesia, dodina@ipb.ac.id

Abstract

Agarwood (eaglewood, aloeswood, or gaharu) has an important role in some commercial industries. This "wood" is produced in certain trees as a result of a fungal infection. World demand for agarwood continues to increase, and over exploitation has caused *Aquilaria microcarpa* to be regarded as an endangered species. Visual assessment and field experience are traditionally used in harvesting agarwood. The aim of this study is to evaluate the presence of agarwood in standing *Aquilaria microcarpa* trees using the nondestructing testing technology of ultrasonic wave propagation. Artificially infected trees were tested by measuring ultrasonic wave velocity at three sections of tree,bottom, breast height, and top. The average value of ultrasonic velocities was 943 m/s. Presence of agarwood at tree was not determined by section of tree altitude as shown by ultrasonic wave velocities.

Keywords: Agarwood, gaharu, endageres species, ultrasonic velocity

Introduction

Agarwood (gaharu, aloeswood, or aloes) is one timber forest products (NTFPs) are produced in certain trees included to the genus Aquilaria, Gryrinops, and Gonystilus from Thymelaeaceae family. Agarwood can be either naturally or artificially formed due to physiological changes in the cells and chemical compounds in wood through the process of infection especially fungal infections, wounds, and non-pathological processes. This process results in a fragrant heartwood resin derived from the infected part of the tree (Tian et al. 2013).

Agarwood or gaharu is an important raw material in the manufacture of industrial soap, perfumes, medicines and the use of versatile, ranging from incense for religious ceremonies and traditional and ornamental functions in many countries (Sitepu et al. 2011). World demand for agarwood continues to

increase (Burfield 2005), and over exploitation has caused one of those species, especially *Aquilaria microcarpa*, to be regarded as an endangered species as cited in CITES Appendix II (Schmidt 2011).

Color, flavor, and aroma are a guide in determining the quality of aloes. Black / dark and strong aroma demonstrates a high quality product as a result of the process of infection is higher. Experts and traders who have experience and have been involved in agarwood trade could distinguish between higher and lower quality.

To determine the presence of agarwood on site, traditional ways through visual assessment combined with field experiences are usually done by agarwood hunter. Harvesting of agarwood depend on the hunter's expertise, this quite often lead to agarwood tree felled giving unexpected result. So that, there are needed technology which help to detect and identify existence of agarwood in tree.

Recently, nondestructive testing/evaluation (NDT/E) technologies in wood science have been intensively evolving and success to evaluate standing trees condition (Yamamoto et al. 1998, Sandoz et al. 2000, Chuang and Wang 2001, Larsson et al. 2003, Ganesan and Hamid 2010). The objective of this study is to investigate and evaluate the existence of agarwood in standing tree using nondestructive testing technology of ultrasonic wave propagation method. This method was chosen because it has been applied to detect internal condition of tree successfully.

Material and Methods

A total 60 trees of *Aquilaria microcarpa* species that were artificially infected by fungi were sampled. Samples were taken from trees located at experimental forest area (Forest with Special Purposes) owned by Ministry of Forestry, Carita, Banten Province. The trees selected were planted at 1998 (about 15 years old) with diameter in a range 13 to 30 cm. The plants are predicted has been producing agarwood as it had undergone the inoculation process once till three times.

A surface-attaching method was used to conduct in situ measurements using ultrasonic wave technique of SylvatestDuo®. Radial measurements were conducted into trunk in two wind direction, north-south and west-east and the testing were done at three sections of heights level i.e. 20 cm, 130 cm, and 200 cm from ground. The ultrasonic wave velocities were calculated using the equation: $V_R = \frac{L}{T}(m/s)$ where L is the distance between the two transducers, and T is the propagation time of the pulse from transmitting transducer to receiving transducers.

An increment core samples were collected to determine bulk density and moisture content of trunk. The green cores were separated into small pieces from the cambium to the pith. Wood density was obtained by dividing weight to volume, while moisture content of specimens was calculated gravimetrically.

Results and Discussion

Results for performance of trees measurement showed that the average value of diameter and height were 18.9 cm and 23.1 m, respectively. Ultrasonic wave velocity for radial measurement varied from the lowest of 153 m/s to about 1400 m/s for the fastest (Table 1). The average velocities of those radial measurements were 943 m/s. The lowest value of radial ultrasonic wave velocity indicated the extremely changes in internal condition of the tree which is presumed of effect from inoculation treatment, and other conditions such as ahollow. The velocity measurements were carried on in two position of two wind direction, north-south (N-S) and west-east (W-E). Figure 1. showed that the distribution of ultrasonic wave velocities were clustered at value of below 1000 m/s . It seemed that

on that value, the agarwood have been developed on the tree. The results of measurement using transducers from two sides were slightly same. It explained that radial-ultrasonic wave propagation passed the same internal condition either N-S or W-S.

Table 1. Radial ultrasonic wave velocity and physical properties of *Aquilaria microcarpa*

Value (n=60)	Diame-ter (cm)	Height (m)	Moisture content (%)	Bulk Density (g/cm^3)	Radial Ultrasonic wave velocity (m/s)							
					North-South				East-West			
					20	130	200	Av. value	20	130	200	Av. value
Av.	**18.9**	**23.1**	**52.78**	**0.75**	**966**	**904**	**963**	***944***	**986**	**931**	**910**	***942***
SD	4.32	4.01	10.04	0.12	156	182	174	-	169	164	176	-
Min	13	9	27.70	0.52	203	161	153	172	187	163	168	173
Max	32	29	70.20	1.12	1439	1174	1366	1326	1368	1222	1258	1283

The average value of bulk density was 0.75 g/cm^3. The density variation from cambium to inner part of pith showed no high variation (Figure 2a). The lower moisture content value was denoted in the outer part of stem at segment 1 and 2 from cambium to inside (Figure 2b). It considered that the outer part was influenced by environment condition. Decreasing value of moisture content at inside of pith led to of juvenile wood.

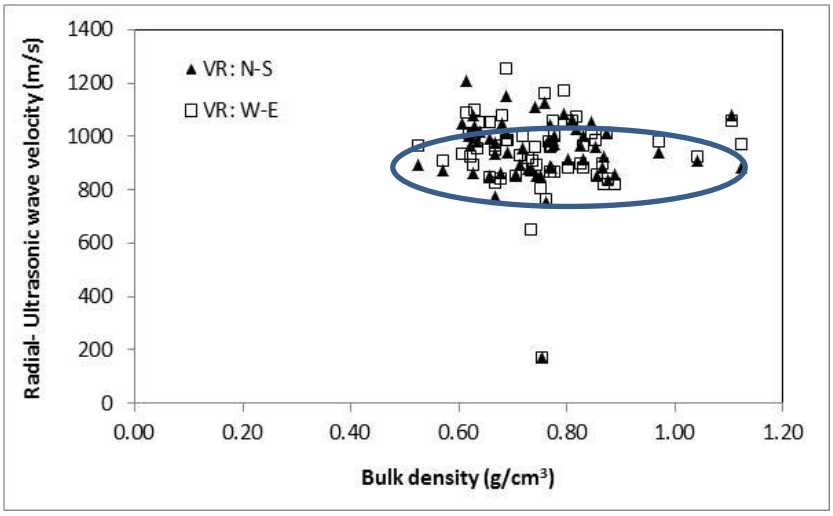

Figure 1. Distribution of radial ultrasonic wave velocity on average bulk density of agarwood

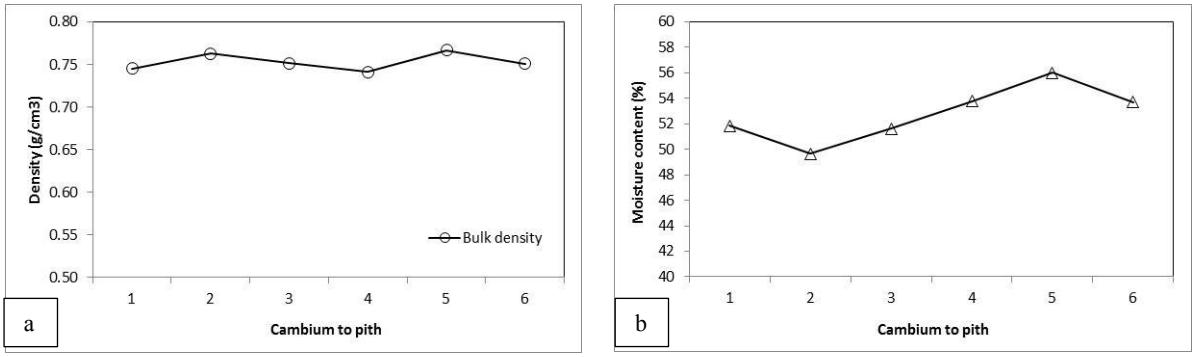

Figure 2. Distribution of density (a) and moisture content (b) from cambium to pith

Based on height of the tree, three level sections from ground (20 cm, 130 cm, and 200 cm) were tested for radial ultrasonic velocity. There was no clear difference in velocity between sections (Figure 3). Statistical analysis showed that there was no significant difference between sections on radial

ultrasonic velocity values. The pattern of artificially infection of inoculation treatment follows zigzag line from bottom to up include the branch. This probably cause that inoculation process is worked at the same condition for the entire stem.

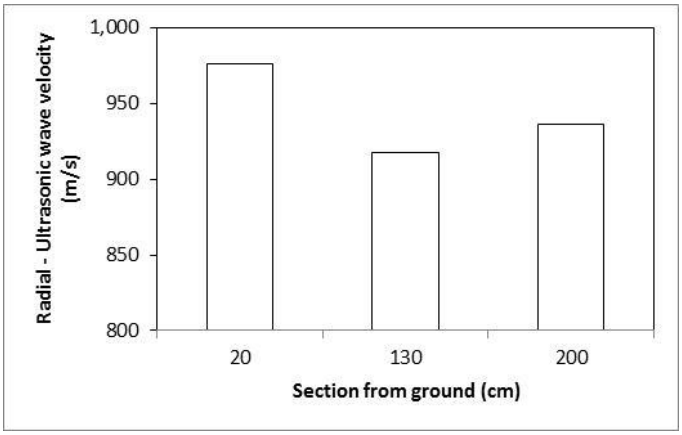

Figure 4. Radial ultrasonic wave velocity in trees with different level section from the ground

Conclusion

The trees are predicted have been producing agarwood had ultrasonic wave velocity value of below 1000 m/s. Presence of agarwood at tree was not determined by section of tree altitude. The variation in wood density in sample trees from cambium to pith was homogen.

Acknowledgement

This research was financially supported by The Osaka Gas Foundation of International Cultural Exchange (OGFICE) Research Grant for fiscal year (FY) 2012-2013 and the Directorate of Higher Education (DIKTI), Ministry of Education and Culture, Republic of Indonesia (Kemendikbud, RI), under "Higher Education Research Grant of IPB" schemes for FY 2013 (Contract No. 265/IT3.41.2/L2/SPK/2013).

References

Azah MAN; Husni, S.S.; Mailina, J. [and others]. 2013. Classification of Agarwood (Gaharu) by Resin Content. Journal of Tropical Forest Science .25(2): 213–219.

Burfield T. 2005. Agarwood Chemistry. http://www.cropwatch.org/agarchem.htm [23 June 2013]

Chuang S.T.; Wang S.Y. 2001. Evaluation of Standing Tree Quality of Japanese Cedar Grown with Different Spacing Using Stress Wave and Ultrasonic-Wave Methods. Journal Wood Science. 47: 245-253.

Ganesan S.K.; Hamid M.A. 2010. Survey of Wood Strength Properties of Urban Trees in Singapore Using The Fractometer II. Journal of Tropical Forest Sciences. 22(1): 97-105.

Larsson B.; Bengtsson B.; Gustafsson M. 2004. Nondestructive Detection of Decay in Living Trees. Tree Physiology. 24: 853-858.

Sandoz J.l.; BenoitY; Demay L. 2000. Standing Tree Assesment Using Acousto Ultrasonic. In Proceeding of International Symposium on Plant Health in Urban Culture. Brauschweig, Germany, 22-25 May 2000.

Schmidt M.S. 2011. Introduction to CITES and Agarwood Overview. Asian Regional Workshop on Agarwood; 22-24 November 2011. Indonesia. http://www.cites.org/common/com/pc/20/inf%20docs/E20-07i-A09.pdf. [27 June 2013]

Sitepu I.R.; Santoso E; Siran S.A; Turjaman M. 2011. Fragrant Wood Gaharu: When The Wild Can No Longer Provide. Proceeding is part of Program ITTO PD425/06 Rev. 1 (I) : Production and Utilization Technology for Sustainable Development of Gaharu (Gaharu) in Indonesia. R&D Centre for Forest Conservation and Rehabilitation. Bogor. Indonesia

Yamamoto K.; Sulaiman O.; Hashim R. 1998. Nondestructive Detection of Heart Rot of *Acacia mangium* Trees in Malaysia. Forest Products Journal. 48(3): 83-86.

First steps in wood density estimation using a conventional drill

Ignacio Bobadilla Maldonado
EUIT Forestal, Universidad Politécnica de Madrid, Madrid; Spain, i.bobadilla@upm.es

Roberto Martínez López
ETSI Montes, Universidad Politécnica de Madrid, Madrid; Spain, roberto.martinez.lopez@upm.es

Javier Calvo López
EUIT Forestal, Universidad Politécnica de Madrid, Madrid; Spain. javier.clv@gmail.com

Francisco Arriaga Martitegui
ETSI Montes, Universidad Politécnica de Madrid, Madrid, Spain. francisco.arriaga@upm.es

Guillermo Íñiguez-González
ETSI Montes, Universidad Politécnica de Madrid, Madrid, Spain. guillermo.iniguez@upm.es

Abstract

The purpose of this work was to develop a simple, reliable and economical method of estimating wood density, based on the use of the residue generated with a conventional drill.
A residue collector coupled to the tool was developed. A total of 42 samples of Spanish sourced *Pinus nigra* Arn were tested by making 3 holes per sample and in the radial and tangential direction.
The weight of the residue, the resulting bore volume and the initial density of the specimen were measured. The density of the wood removed was calculated by its mass / volume ratio, and was slightly lower than the average density of the specimen (4.5%), although there were no statistically significant differences at 95% level of confidence. On the other hand, the weight of the residue was linked directly to the total density of the sample, and a regression model was established with a coefficient of determination r^2 of 0.84.

Keywords: drill, density estimation, probing.

Introduction

Density is one of the most important properties of materials, and it is widely used to characterize them, wood being no exception.
A range of non-destructive methods have been and are used to characterize wood pieces in renovation and restoration work (Ross and Pellerin 1994, Ross et al. 1998; Cai et al. 2002; Brashaw et al. 2005). In this type of material characterization, vibration or acoustic equipment to calculate propagation wave velocity is often combined with probing equipment to estimate local density, in order to obtain the dynamic modulus of elasticity (Bobadilla et al. 2007).
However, the statistical relationships between density and these local measurements are often limited, with slightly lower coefficients of determination at 0.5 to 0.6 for screw withdrawal equipment and penetrometer (Bobadilla et al. 2007, Montón 2012). To achieve more reliable statistical results, more expensive and complex equipment such as a resistograph should be used, obtaining determination coefficients from 0.8 to 0.9 (Marino et al. 2002; Acuña et al. 2011).

Other local evaluation systems for wood consist of extracting a sample using an auger, drill core or a

special deck. Very good statistical relationships in density estimation have been obtained with some of these systems, with determination coefficients of 0.88 (Montón 2012). These sample extraction systems also allow further analysis of factors such as moisture content and wood species, and they even permit testing for some mechanical properties (Bethge et al. 1996). The drawback of these systems is that in some cases they are slightly destructive because of the size of the resulting hole.

Moreover, some researchers and technicians make holes in wooden pieces to determine their condition and possible pathologies, observing the appearance of the sample, evaluating ease of drill penetration and even taking advantage of these drill openings to insert an endoscope to assess the presence and activity of destructive agents (Arriaga et al. 2002). Drills are therefore a standard tool in the rehabilitation and restoration of wooden elements, and they are economical and easy to use.

Given this use of drills, it is now planned to use the residue of the drilling process to estimate the density of the piece tested. This paper therefore aims to demonstrate that it is possible to estimate the density of timber elements in a reliable, simple and inexpensive way, by using a conventional drill with a "collect and store" system for the drilling residue.

Material and methods

44 Laricio pine (*Pinus nigra* Arn) wood specimens from Cuenca (Spain) were tested (see Table 1). As can be seen in figure 1, the dimensions of the specimens were 150 x 90 x 60 mm. Half of the samples were radial and the other half were tangential.

Table 1 - Test material. Laricio pine (*Pinus nigra* Arn.) origin, orientation and number of specimens.

Origin	**Orientation**	**No. of specimens**
Sierra de Cuenca (Spain)	Radial	22
	Tangential	22

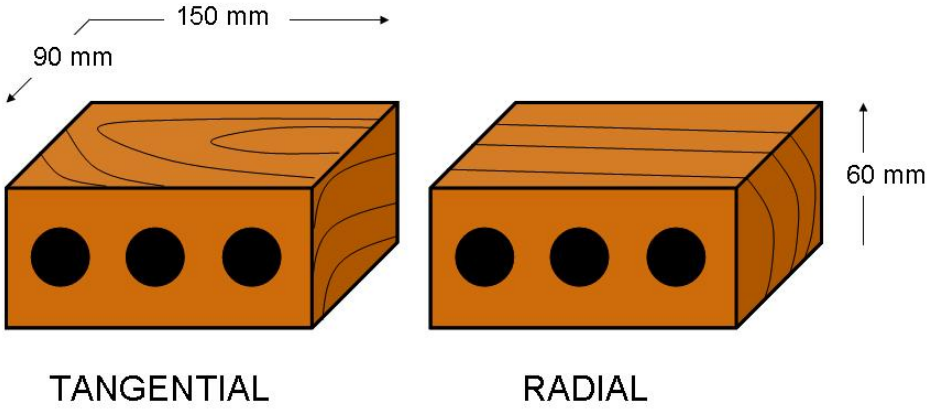

Figure 1 - Detail of wood specimens used. Radial and tangential orientation.

Firstly, all specimen dimensions were measured to an accuracy of 0.01 mm, to calculate their volume. Their mass was also obtained to an accuracy of 0.01 g, and finally density was calculated using equation (1).

$$\rho = \frac{M}{V} \tag{1}$$

Where "ρ" is the density in kg/m^3, "M" is the mass in kg and "V" the volume in m^3.

Three holes were drilled in each specimen (see figure 1). The drilling residue was collected, stored and weighed to an accuracy of 0.01 g. Hole diameter and depth were measured to an accuracy of 0.01 mm. These data give the mass of the extracted material and its volume, so that density can be calculated using equation (1). For each sample, the average density of the three holes was calculated. This method makes it possible to compare the density of the specimens with the average density of the material from the three holes.
The drilling equipment was a conventional Bosch PSB 50 drill, to which a patent pending "residue collection and storage" system was fitted. This device uses the ventilation system of the drill itself to suck sawdust and store it in a paper bag filter located at the intake manifold (Figure 2).

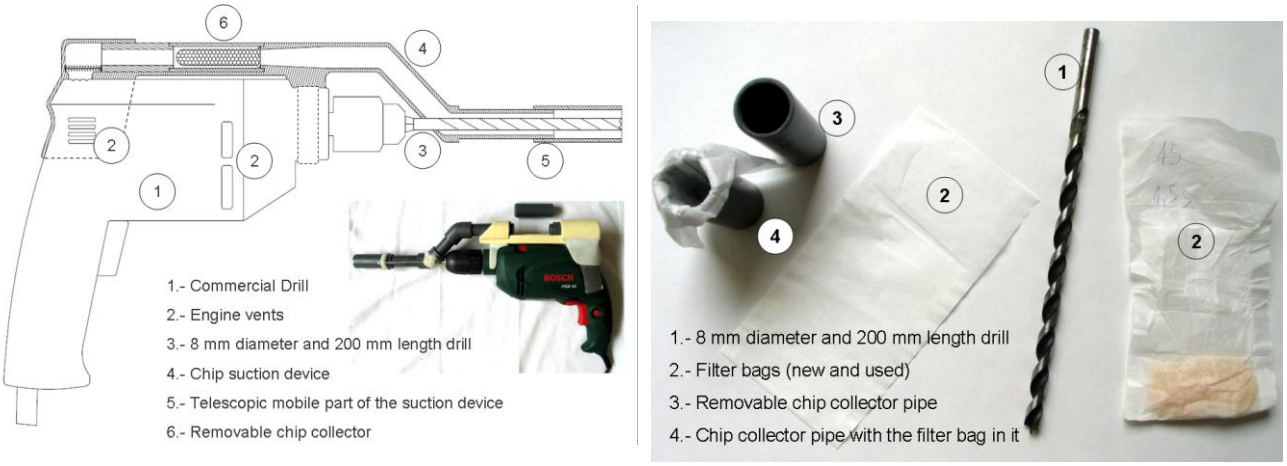

Figure 2 - 2a- Schematic design of drilling equipment with the "residue collection and storage" system fitted. **2b-** Different parts of the sample collector: drill, sawdust collector pipes and new and used filter bags.

Results and discussion

The average calculated densities of the specimens and holes are shown in Table 2.

Table 2 - Mean values for sample and hole density.

Specimen density (kg/m^3)	**CV (%)**	**Residue density** (kg/m^3)	**CV (%)**
618.6	17.6	590.9	19.2

As can be seen in table 2, sample density is slightly higher than that obtained from the material removed by drilling by approximately 4.5% (Figure 3). This may be mainly due to two reasons: firstly there is the possible loss of material (wood dust) during drilling, while secondly moisture is lost from the drilling residue due to heating caused by friction of the tool in the wood. In both cases there is a small loss of mass (water or wood) that makes the density slightly lower.
The average moisture of the samples and residue was 10.54% and 9.35%, respectively, so approximately 1.2% of moisture content is lost.

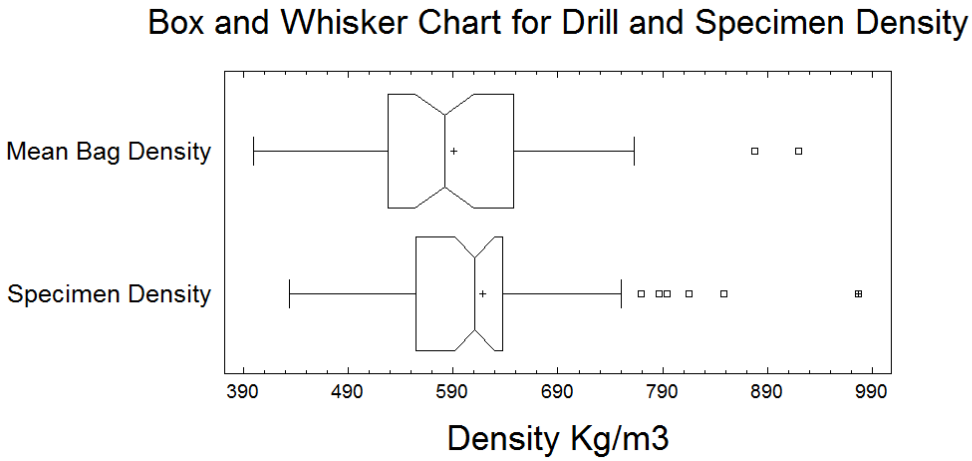

Figure 3 - Box and Whisker chart graph for specimen and hole average densities. Mean bag density refers to the mean value of the densities of the three bags of sawdust.

Despite this small difference between the specimen and residue densities, it was found that there is no statistically significant difference between mean values or data distribution at a confidence level of 95%. Therefore in statistical terms the average density of residue could be used to estimate specimen density without any correction.

However, although there is no statistical difference between specimen and residue densities, a slight default error in measurement occurred, so the authors propose using a regression model to connect sample density with the weight of the material removed by drilling. Firstly, it was found that there are no statistically significant differences between the weights of the residues from three holes drilled in each specimen, with a level of confidence of 95% (Figure 4).

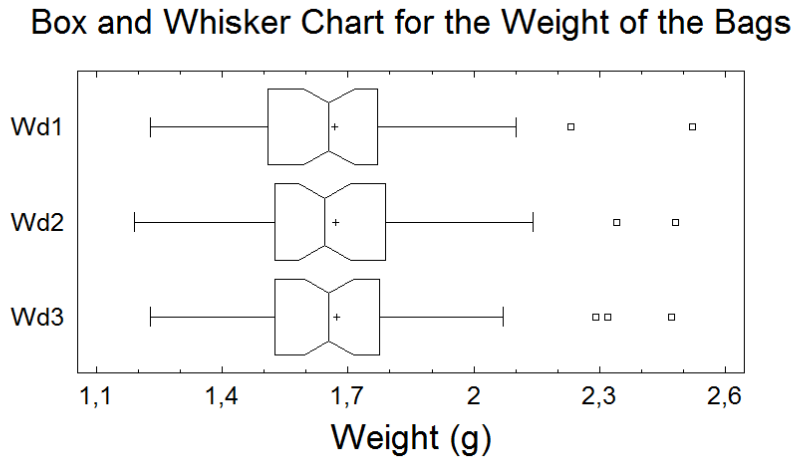

Figure 4 - Box and Whisker Chart for the weights of the drilling residues from all three holes drilled in each specimen.

Likewise, the weights of the residue from the tangential and radial holes show no significant differences at a level of confidence of 95%, although the weight of the residue from tangential holes is slightly higher (Figure 5).

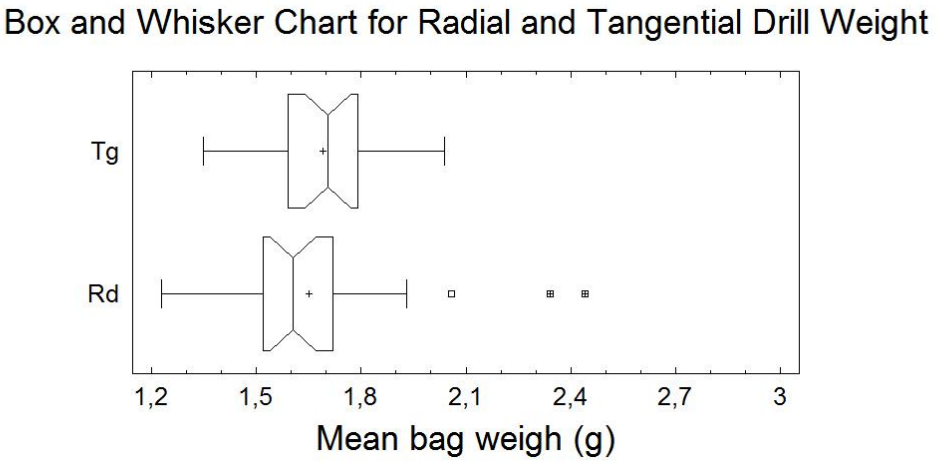

Figure 5 - Box and whisker chart for the weight of residue from tangential and radial holes.

We can therefore conclude that there is no need for multiple holes in any single area of measurement (150 mm), since the result in terms of residue weight is equal. It is also unnecessary to consider drilling direction (radial or tangential), given that the result hardly differs.

If the statistical relationship between the average weight of drilling residue and sample density is analyzed, a strong statistical relationship between the variables (P-value < 0.01) and correlation coefficient "R" of 0.92 is obtained. It therefore seems logical to establish a regression model to estimate density using the weight of the drilling residue as a predictor. The resulting model is shown in equation (2) and Figure 6.

$$\rho = 387.72 \times W - 29.18 \qquad R^2\text{: } 84\% \qquad (2)$$

Where "ρ" is the density (kg/m^3) and "W" the weight (g) of the residue, including the filter bag.

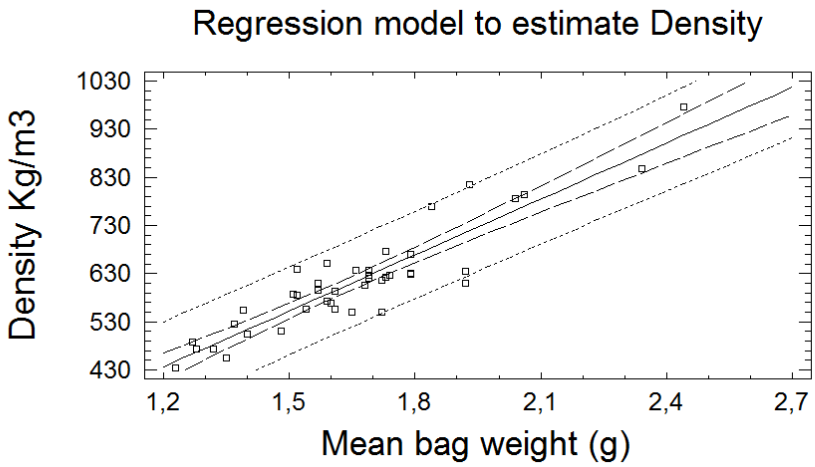

Figure 6 - Regression model graph for density using drilling residue weight. The assumptions of normality, homoscedasticity and linearity were tested.

As can be seen, the R^2 values obtained are significantly higher than those obtained by the same

authors with other probing methods such as the penetrometer (Pilodyn 6J Forest) or screw withdrawal device (Bobadilla et al. 2007; Montón 2012), and they are of the same order, or slightly lower, than those obtained with the resistograph (Marino et al. 2002; Acuña et al. 2011) or sampling methods (Montón 2012).

Conclusions

The equipment and methodology developed in this preliminary study demonstrate the reliability of density estimation using a regression model based on using the weight of the drilling residue as a predictive variable. This regression model has a coefficient of determination R^2 of 84%.

Regarding the methodology, analysis of the results shows that there is no need to repeat measurements (drilled holes) in the same test area (150 mm) because results are statistically equal, and that more interestingly in practical terms, it is also unnecessary to consider drilling direction in timber (radial or tangential) as this does not influence the result. This fact was already evident in measurements using other probing devices such as the Pilodyn 6J Forest or Fakopp Screw Withdrawal Force Meter (Bobadilla et al, 2007).

Due to the variability of the parameter estimated (density) within the same piece of wood, the authors maintain the recommendation to undertake several measurements in different areas to assess large pieces. The number of measurements will depend on the overall dimensions of the piece, for example with 1 measurement per meter, and if possible in different faces (Bobadilla et al. 2007). Additionally, and given the slight damage to pieces caused by 8 mm diameter drilled holes, it is recommended to avoid the mid-span and the tension-side of bending elements, as recommended by other authors (Falk et al. 2003), although the Spanish softwood structural classification standard considers knots of 10 mm or less in diameter to be negligible, and the drilled holes in this method are 8 mm in diameter.

However, the utility of this new device goes beyond the estimation of density, given that residue collection also makes it possible to estimate the moisture content of wood and to identify pathological damage, if present, in test pieces (Bobadilla et al. 2008).

To summarize, this equipment is simple, economic and easy to use, allowing the reliable estimation of density and moisture content, as well as the detection of pathologies. It is a solution that resolves a number of common problems in inspection with a single technique.

Acknowledgments

Ministerio de ciencia e innovación, Plan nacional I+D+i 2008-2011. Proy.: BIA2010-18858. Plan nacional I+D+i 2000-2003. Proy.: AGL 2002-00813 y AGL 2004-01598FOR.
Asociación de Investigación Técnica de la Madera (AiTiM). Proy.: AiTiM-Fucovasa 2012-13.

Bibliography

Acuña, L. Basterra, A. Casado, Mª M. López, G. Ramón-Cueto, G. Relea, E. Martínez, C. González, A. 2011. Application of resistograph to obtain the density and to differentiate wood species. Materiales de Construcción. Vol. 61, 303. Pp 451-464.

Arriaga, F. Peraza, F. Esteban, M. Bobadilla, I. García, F. 2002. Intervención en estructuras de madera. Ed. Aitim. Madrid. 476 pp.

Bethge, K. Mattheck, C. Hunger, E. 1996. Equipment for detection and evaluation of incipient decay in trees. Arboricultural Journal 1996. Vol. 20, pp. 13-37.

Bobadilla I, Arriaga F, Iñiguez-González G, Esteban M, Castro N, 2008. Identificación de Insectos Xilófagos en madera de construcción mediante el análisis morfológico del detrito. Actas de las II Jornadas de Investigación en Construcción del Instituto Eduardo Torroja. May 22-24. Pp 129.

Bobadilla, I. Iñiguez, G. Esteban, M. Arriaga, F. Casas, L. 2007. Density estimation by screw withdrawal resistance and probing in structural sawn coniferous timber. Proceedings of the 15th International Symposium on Nondestructive Testing of Wood. Duluth.

Bobadilla, I. Iñiguez, G. Arriaga, F. Esteban, M. 2009. Técnicas no destructivas en la inspección de estructuras de madera I: El penetrómetro. BIT AiTiM nº 260. Pp 66-70.

Brashaw, B K. Vatalaro, R J. Wacker, J P. Ross, R J. 2005. Condition assessment of timber bridges. Evaluation of a micro-drilling resistance tool. General Technical Report FPL – GTR – 159. Forest Products Laboratory, US Department of Agriculture.

Cai, Z. Hunt, MO. Ross, R J. Soltis, L A. 2002. Screw withdrawal – A means to evaluate densities of in-situ wood members. Proceedings of the 13th International Symposium on Nondestructive Testing of Wood. Berkeley, California.

Falk, R H. DeVisser, D. Plume, G R. Fridley, K J. 2003. Effect of drilled holes on the bending strength of large dimension Douglas-fir lumber. Forest Products Journal. Vol 53, No. 5. Pp 55-60.

Mariño, R. Fernandez, Mª. E. Fernández, C. 2002. Análisis comparativo de la densidad de la madera de Pinus sylvestris L. mediante la utilización del resistógrafo. Revista CIS-Madera nº 9. Pp. 60-70.

Monton, J. 2012. Clasificación estructural de la Madera de *Pinus radiata* D.Don procedente de Cataluña mediante métodos no destructivos y su aplicabilidad en la diagnosis estructural. Tesis Doctoral. UPC. Pp. 102-110.

Ross, RJ. Pellerin, RF. 1994. Non destructive testing for assesing wood members in structures: A review. USDA Forest Service, Forest Products Laboratory, FPL-GTR-70, Madison, WI. pp. 1-40.

Ross, RJ. Soltis, LA. Otton, P. 1998. Assesing wood members in the USS Constitution using non-destructive evaluation methods. APT Bulletin, The Journal of Preservation Technology. 29(2): 21-25.

Use of laser to determine profile of trees

Antonio C. L. Lino
PhD, Center for Engineering and Automation of the Agronomic Institute of Campinas (CEA/IAC), Campinas, São Paulo, Brazil, lino@iac.sp.gov.br

Alex J. Trinca
Postdoctoral Researcher , Laboratory of Nondestructive Testing (LabEND), University of Campinas (UNICAMP), College of Agricultural Engineering (FEAGRI), Campinas, São Paulo, Brazil, ajtrinca@mxb.com.br

Marcos V. G. Silva
PhD student, College of Agricultural Engineering (FEAGRI), University of Campinas (UNICAMP), São Paulo, Brazil, marcos.silva@feagri.unicamp.br

Raquel Gonçalves
Associate Professor, University of Campinas (UNICAMP), College of Agricultural Engineering (FEAGRI) and Coordinator of the Laboratory of Nondestructive Testing (LabEND), Brazil, raquel@agr.unicamp.br

Abstract

Ultrasonic tomography has been largely studied to infer the internal condition of urban and forest trees. Many research groups show interest in developing their own tools adequate to their realities. In function of the measurement and the data processing methodology, knowing the tree's profile perimeter is imperative. This paper presents a tree perimeter digitalization system by means of the laser triangulation technology, in which a laser line is projected onto the steam, and its image, captured through a digital camera, is treated and analyzed to obtain the contour of the tree. The final objective is the generation of more accurate coordinates of the measurement points, which will be transferred into the wave propagation velocity analysis software. A prototype of this system was built to test the concept, and to verify the precision of the proposed method. It was concluded that the technique is adequate, when compared to the real ones.

Keywords: ultrasonic tomography, laser line, log perimeter

Introduction

Based on the research developed by Secco (2011), LabEND (Laboratory of Nondestructive Testing of University of Campinas) has been working on studies to improve image generation by means of ultrasonic tomography, with national technologies that are devoted to both forest and urban Brazilian species. In order to use sensor arrangement proposed by Divos e Szalai (2002) (Figure 1 – in this paper named diffraction arrangement), one must know, precisely, the distance between the transducers (wave path length), that was used to determine the velocities. It is fairly easy to obtain this distance in round stems, such as species proceeding from planted forests. However, tropical forest trees and urban trees usually present much more irregular steams, which make measuring wave path length much more complex.

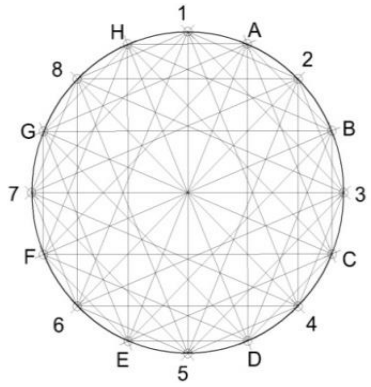

Fig. 1 Transducer arrangement during wave propagation time measurements.

Source: Divos e Szalai (2002)

This distance can be measured by means of instruments that are commonly used in the forest sector. Among them, the-most suitable one for measuring the wave path length would be the caliper, since the remaining ones are more commonly used to determine diameter, and not distance between two specific points. However, this group's proposal is to search for technological solutions that would allow automatized measurements with better results in irregular trunks.

One of the most common methods of obtaining the topographic profile of objects is the laser profilometry, which relies on triangulation techniques. Triangulation is one of the oldest and most common ways of depth measuring points in space (FERNANDES 2007). Usually, one uses a laser beam to enlighten certain points on the surface of the object and, through a camera located at a given angle, the points can be located. Depending on the distance of the object's surface, the points appear on different places in the image. This technique is called triangulation because the laser emitter, the camera and the laser point on the object's surface form a triangle. One must know the length of one of the sides (distance between the camera and the laser emitter) and the emission angle. The vision angle for the camera can be determined by the location of the laser point in the captured image. With these three components, one can determine the triangle dimensions, and the location of the laser point in the object's surface.

In several cases, instead of with points, the sweep can be made with a laser line to improve the data acquisition

rate. The intersection of the plane with the surface defines a line, which is then captured by a visualization system, usually through digital capture camera (DCC) positioned as per the triangulation technique, and with distance and inclination knowledge regarding the enlightened plan (CLARK 2000). Figure 2 presents a diagram using this kind of technique.

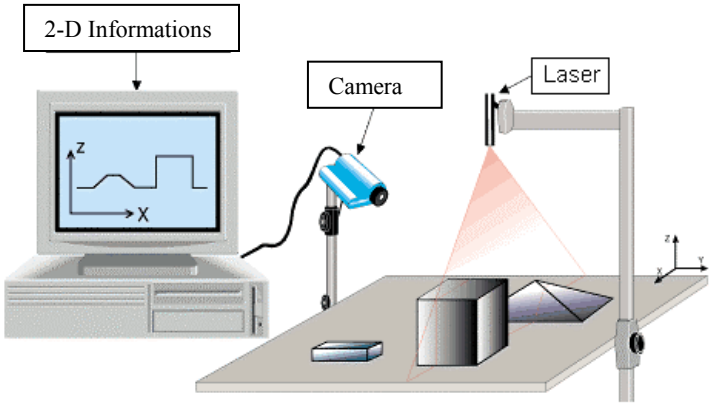

Fig. 2 - Triangulation laser setup
Source: Brückner e Triebel, (1994); Clark, (2000) e Suenaga, (1996)

Methodology

This study was developed at the Image Laboratory (LabImagem), of the Agronomic Institute (IAC)'s Engineering and Automation Center, located in Jundiaí-SP, and at the School of Agricultural Engineering (FEAGRI) of the University of Campinas (UNICAMP), Laboratory of Nondestructive Testing (LabEND).

An experimental arrangement has been built by a 400 mW laser line emitter (LRM-40R, Laser Line) and a digital photographic camera with 8 M*Pixel* (PowerShot Pro1, Cannon), for image capture, in order to reconstruct the entire profile of the object. Three takes of rotated images at 120º (degrees) were needed.

In order to get these images, three tripods were positioned around a trunk, which formed an equilateral triangle with 1500 mm per side (Figure 3). A platform was constructed to help positioning the tripods, on top of which the laser range finder was laid. Another platform - composed by a 400 mW laser line emitter for projection on the analyzed trunk, and a CCD camera (MPX315UC, AOS) with 3 M*Pixel* and USB port for image capture - was constructed in order to position the laser profilometry system.

In order to format the whole profile of the log, three image takes were needed, using the profilometry system positioned on each one of the tripods. The three captured images were then processed by the *ImageJ software* for extraction of profile lines. Afterwards, the lines were used in the *Scilab software* in order to generate the bi-dimensional profile of the log.

Fig. 3 – Profile gathering setup.

Results

On the disc, this technique has been directly applied through the projection of a laser line emitter. (Figure 4a). After detecting the projected line, visualization of the disc's contour was possible (Figure 4b). By means of "Skeletonize" applied on the contour, it was possible to turn the results into one single line, which allowed a bigger precision when reconstructing the profile of the disc.

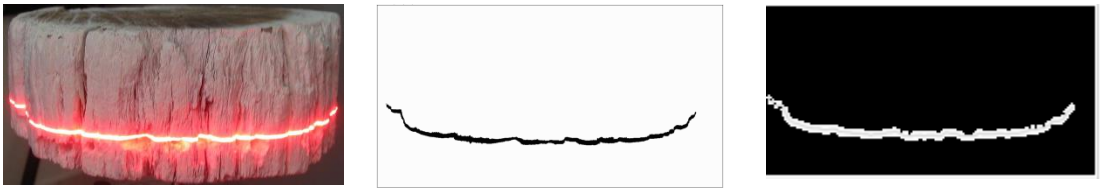

a b c

Fig. 4 - Profile gathering of the log with laser projection on the disc (a), contour isolation (b), and contour line obtention through "Skeletonize"(c)

Regarding the log, all three image takes, with a 120º variation between them, allowed the obtention of a complete profile. Through axis rotation, merging of images for all three surfaces was possible.

To enable the comparison with the log profile obtained by this technique, the log was photographed with a superior view and a black background, which allowed highlighting of the profile (Figure 5).

Fig. 5 - Superior view of the log.

The photo (Figure 5) was processed in the *Imagej* software for profile obtention and quota correction.

The superior view profile, obtained through processing of the photo, was overlapped on the laser profilometry-obtained profile, in order to compare the results. The process' precision is verified by means of the overlapped images (Fig. 6).

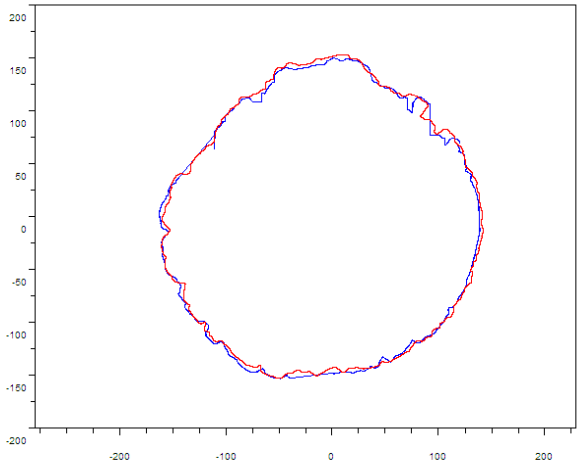

Fig. 6 - Overlapping of the log profiles obtained by means of image capture through the CCD camera with superior view (red line) and laser profilometry (blue line)

CONCLUSION

The profilometry technique has made obtaining log perimeter possible, and has proven to be a viable tool for tree trunks with irregular geometries.

Acknowledgements

We thank the São Paulo Research Foundation (FAPESP) for Postdoctoral scholarship (Proc. 2011/08286-5). We also thank the College of Agricultural Engineering (FEAGRI) for the laboratory infrastructure.

BIBLIOGRAPHY

BRÜCKNER, P.; TRIEBEL, M. – "Berührungslose 3D-Geometriemessung", Carl Hanser Verlag, v. 39, p. 1148-1152, 1994.

CLARK, J. – "Implementing Non-Contact Digitisation Techniques Within the Mechanical Design Process", Sensor Review, v. 20, No. 3, p. 195-201, 2000.

DIVOS, F.; SZALAI, L. 2002. Tree evaluation by acoustic tomography. In: Proceedings of the 13th International symposium on nondestructive testing of wood; 2002 August 19. 21; Berkeley, CA. Madison, WI: Forest Products Society: 251.256. 2002.

FERNANDES, L.A. F.; Estudo de Métodos para Extração de Formas e Realização de Medidas a Partir de Imagens. http://www.inf.ufrgs.br/~laffernandes/fernandes_TI_1159.pdf. April 10th 2007.

SECCO, C.B. Detecção de ocos em toras utilizando métodos de propagação de ondas ultrassonicas. Tese (Mestrado), Engenharia Agrícola, FEAGRI, UNICAMP, 2011. 112p.

SUENAGA, Y. – "3D Measurement Technologies for Computer Animation", Computer Animation' 96, p. 167-174, Geneva, Suisse, June 1996.

Examination of acoustic velocity along veneer value-chain in Douglas-fir trees

Eini C. Lowell
USDA Forest Service, PNW Research Station, Portland, Oregon, USA, elowell@fs.fed.us

Christine L. Todoroki
SCION, Rotorua, New Zealand, Christine.Todoroki@scionresearch.com

David G. Briggs
University of Washington, Seattle, Washington, USA, Dbriggs@uwashington.edu

Dennis P. Dykstra
Blue Ox Forestry, California, USA, Dennisdykstra@blueoxforestry.com

Abstract
A study along the stand-tree-product value chain was conducted on Douglas-fir thinning trial sites to aid understanding of the effects of silvicultural treatments on tree and product modulus of elasticity and to evaluate acoustic testing as an early decision-making tool for land managers. Acoustic velocity was taken with the Fakopp^{TM} TreeSonic on trees from four sites (with an age range of 32 to 51 years, each having five plots with different thinning treatments). Acoustic velocities were stratified at the plot level and a sample of 12 trees per plot randomly selected from the stratifications for further testing. Merchantable length logs from felled and limbed trees were non-destructively tested using the Hitman HM200^{TM}. Disks were cut from the small end of the bottom veneer log and density determined using the water displacement method. Veneer sheets peeled from the trees were tested using the Metrigard 2600^{TM} and stiffness calculated for each sheet. From these data, stiffness was calculated for the two lowermost veneer bolts and the merchantable bole. Relationships among veneer stiffness, tree and merchantable bole acoustic velocity, and wood density were examined.

Keywords: Modulus of elasticity, wood density, Douglas-fir, acoustic velocity, veneer

Introduction
Management of Douglas-fir (*Pseudotsuga menziesii* (Mirb.) Franco) stands, whether natural or planted, impacts the quality of wood harvested from them. Douglas-fir is a commercially important species well known for its stiffness (Modulus of Elasticity, MOE) and strength (Modulus of Rupture, MOR). Concerns regarding negative effects of silvicultural practices (e.g. thinning) on wood quality exist (Kennedy 1995). Visual log grades often do not accurately reflect the quality of the log (Fahey et al. 1991) or guarantee the performance of products manufactured from them. The ability to determine suitability of a tree or log for a designated end use is of great advantage to wood products manufacturers. The earlier in the value chain that a decision can be made as to quality and end product, the more economical the process becomes.

Non-destructive testing (NDT) methods for wood products have been in use for several decades (Pellerin and Ross 2002). Early research focused on using tools for measuring acoustic velocity (AV) of logs and its relationship to quality of products. Log acoustic velocities have good correlations with lumber MOE (Carter et al. 2006, Ross et al. 1997) and are used in production settings for logs (Dickson et al. 2004).

Application to standing trees is more recent. Wessels et al. (2011) provides a review of several non-destructive measurements on standing trees for predicting mechanical properties.

Much research has been conducted on NDT methods for both standing trees and logs and the relationships among these measures (Wang et al. 2007). Wang (2013), in his review on acoustic measurements on trees and logs, discusses why differences exist between standing tree measurements and log measurements. Tree and log velocity deviation are affected by stand age (the ratio increasing as stand age increases), moisture content, wood density, knots, and temperature (Ridoutt et al. 1999, Carter et al. 2005, Wang 2013). Additional measurements, such as log diameter and log order (vertical position within tree) can improve this correlation (Wang et al. 2009).

Mora et al. (2009), working with young (14-19 yr old) loblolly pine (*Pinus taeda*), found standing tree acoustic velocities to be on average 32% higher than butt log velocities. In 8 to 25 yr old radiata pine (*Pinus radiata*) trees, Chauhan et al. (2006) found a strong positive relationship between standing tree AV (Fakopp) and the butt log velocity of the same tree as measured with Fibre-gen's Hitman HM200^{TM} . Auty and Achim (2008) used Fibre-gen's Director ST300 ^{TM} on standing trees from differently managed stands of Scots pine (*Pinus sylvestris* L.) and compared those measures with the MOE and MOR obtained from small clear samples cut from the 1.5 m portion of the stem where measurements were taken. They found acoustic speeds using the time-of-flight (TOF) technique to be reasonable predictors of MOE and MOR and as a tool to discern differences among managed stands. Wang et al. (2001) found stress wave assessment of standing hemlock (*Tsuga heterophylla*) and Sitka spruce (*Picea sitchensis*) trees could differentiate effects of silviculture.

The relationship between standing tree and log acoustic measurements with properties of green lumber from young (8-11 yr old) radiata pine was researched by Grabianowski et al. (2006). They found that in young trees, corewood properties could be predicted from stemwood properties using TOF tools. Briggs et al. (2008) report on the relationship of TOF measures on standing Douglas-fir trees, resonance AV on butt logs, and MOE of lumber sawn from the butt log from four thinning trial test sites reflecting two age classes.

While log acoustic velocities have been used in production settings, the concept of moving the process closer to the beginning of the value chain was studied by Amishev and Murphy (2008a) who bridged tree to log NDT by examining the feasibility of using acoustic technology on harvesting equipment for identification of veneer quality Douglas-fir logs. They also reported on in-woods NDT measurements to determine applicability for in-forest sorting of veneer quality logs in second growth Douglas-fir and found it likely to improve recovery of higher quality logs (Amishev and Murphy 2008b).

In this paper, we examine the relationship of tree and log NDT measures with the stiffness of veneer produced from them. We also analyse whether NDT can be used to detect differences among stands/trees that have experienced various levels of thinning.

Materials and Methods

Sample sites

Figure 1 shows the geographic location of the four sample sites. A description of the original study and sample materials can be found in Briggs et al. (2008) and additional site information is in Todoroki et al. (2012). At harvest, stand ages ranged from 32 to 51 years (51 at 803, 36 at 805, 32 at 805, and 45 at 808).

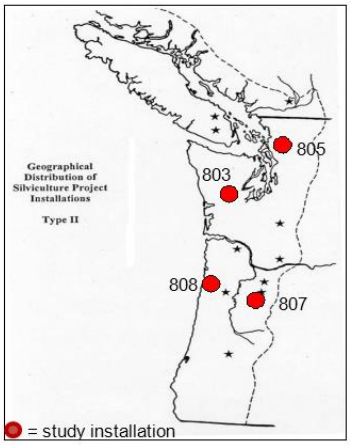

Figure 1 -- Map showing location of Stand Management Cooperative Type II Installations and the four sites sampled for this study.

Five plots were established on each site and each received a thinning treatment. Thinning triggers were based on Curtis' relative density (Curtis 1982) and thinning regimes classified as (A) control, (B) minimal, (C) delayed, (D) light, and (E) heavy. See Todoroki et al. (2012) for a description of treatment regimes and thinning dates. Site 808, plot C, suffered wind damage and could not be included in the study.

Tree level analysis

Three TOF hits with the Fakopp ^{TM} Treesonic at each of 3 locations approximately 120 degrees apart around the base of the tree were recorded on all trees per plot. Measurements on each tree were converted to AV and averaged. Trees were ordered from lowest to highest AV. A stratified random sample of 12 trees was selected from each plot with the following allocation: two trees from the lowest 10%; one to veneer and one to lumber, four trees each from the 11-50% and 51-90% with two trees from each going to veneer and two to lumber, and two trees from the highest 10%; one to veneer and one to lumber.

Trees at each plot were felled and delimbed. Total tree height was measured prior to the tree being bucked. Delimbed trees were bucked to a minimum top diameter of 6-in inside bark for lumber production and 5-in inside bark for veneer production.

Taper was calculated using tree measurements. All four sites are used in tree level analysis. The log level analysis uses only the data recorded for the trees designated for veneer production.

Log level analysis

TheHitman HM200^{TM} was used to obtain resonant AV on the merchantable bole, woods length logs (10.7 m for veneer), and mill length logs (5.1 m for veneer). Each full-length woods log yielded two mill-length logs and each mill-length log yielded two veneer bolts. Disks were sawn from the large end of each woods-length log and measured on site. Disk rings were counted (Nrings), and wood density determined using the water displacement method (Olesen 1971). Bark was removed, disks weighed (Greenkg), then submerged in water and weighed again (Dispkg).

Veneer level analysis

Woods-length logs were hauled to the veneer mill and bucked into mill-length logs that were debarked and bucked into peeler blocks. The identity of each block was maintained throughout the process. Veneer was peeled on a rotary peeler to a 22.6 cm (3.5 in) core and dried. MOE of the veneer was measured using a

Metriguard 2600^{TM} veneer tester. Stiffness was calculated using sheet mass, sheet dimensions, and veneer AV. Average MOE was calculated at the veneer bolt and at the tree level.

Data Analysis

The R statistical software package (R Development Core Team 2008) was used for data analysis. Analysis of variance was used to determine differences among site, treatment, and tree variables. Both linear fixed effects regression models, and mixed effects models (with random effects of the thinning treatments nested within sites) were tested.

Results and Discussion

Tree measurements

Figure 2 illustrates the variation found across sites and treatments for tree dbh, taper, and AV. Diameters at site 807 were considerably lower than at the other sites (as expected due to the younger stand age); but the smaller diameters (and other weather-related logistic constraints) prevented all veneer production from this site. No tree measurements are shown for Plot C, at site 808, as they were lost to the trial through storm damage.

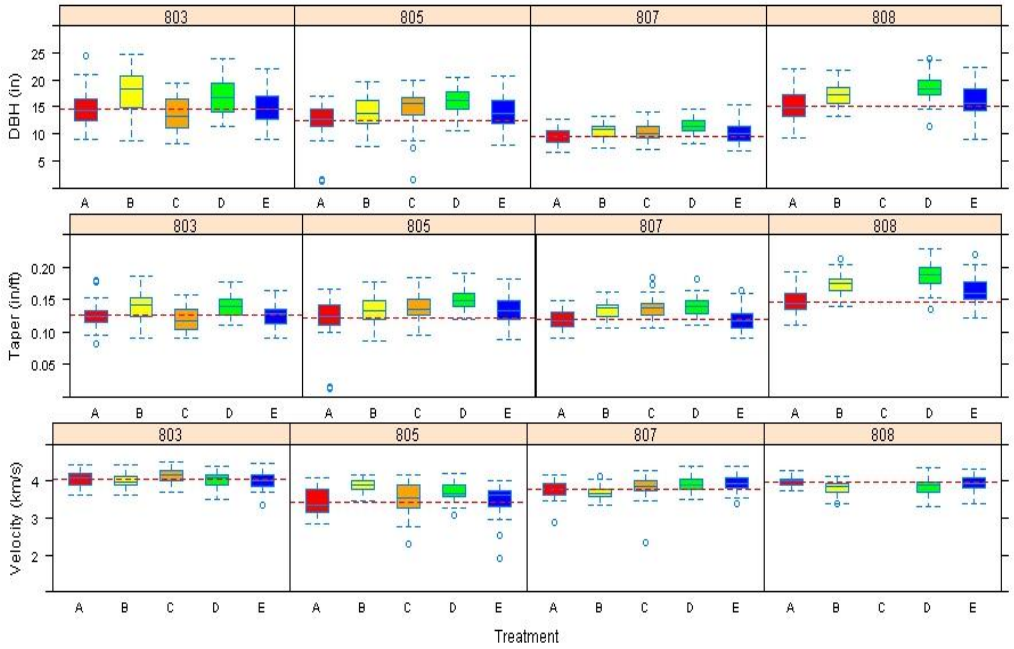

Figure 2 – Box plot summaries of all trees (approximately 50 per thinning treatment on each site) acoustically tested and measured.

An analysis of variance (Table 1) shows that thinning treatment D produced significantly larger trees with greater taper across all sites. The trees on treatment E plots were similar to the control but had more taper on site 808.

Table 1. – Analysis of variance on tree measurements by site and thinning regime.

	dbh (in)				Taper (in/ft)				Velocity (km/s)			
	Site				Site				Site			
Thinning	803	805	807	808	803	805	807	808	803	805	807	808
A	b	c	b	c	b	c	b	d	ab	c	bc	a
B	a	bc	ab	ab	a	abc	a	b	b	a	c	c

C	b	ab	b	-	b	ab	a	-	a	bc	ab	-
D	a	a	a	a	a	a	a	a	b	ab	a	bc
E	b	abc	b	bc	b	bc	b	c	b	bc	a	ab

Relationship of Acoustic Velocity and veneer MOE

Figure 3 shows veneer MOE for individual trees from site 803 by radial and vertical position within the tree. The high velocity class (i.e. low transit time, e.g. A1,B1,..,E1) for the standing trees has a higher representation of stiffer veneer sheets. It can also be noted that those sheets closest to the core and higher in the tree are lower in stiffness as would be expected from juvenile wood.

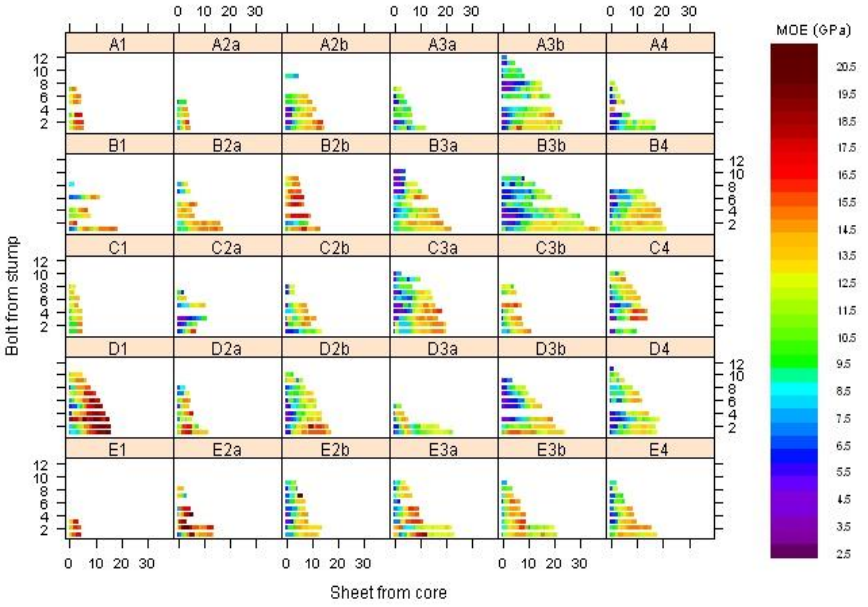

Figure 3 -- Veneer stiffness of individual trees from Site 803, plots A through E. and stratified transit time classes 1 through 4 (1 = low time/high velocity, 4 = high time/low velocity).

When regressing the mean veneer stiffness of sheets from the lower 2 bolts (each 2.6m) against the AV measured at various times during the study, thinning regimes D and E lie predominately above the line, indicating stiffer veneer on average (Figure 4).

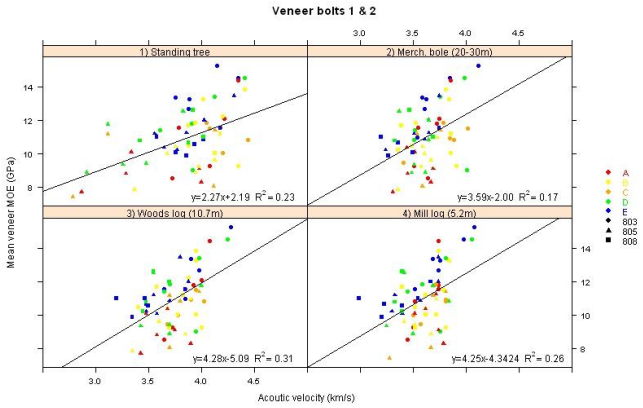

Figure 4 - Relationship between AVs and mean MOE of veneer from the 2 lowermost veneer bolts by site and treatment regime.

When MOE was calculated from the mean of all available veneer within the tree, and regressed against each of the four AV measurements, relationships were weakest for the standing tree AVs (R^2=0.26), and greatest for the woods-length log AVs (R^2=0.45)(Figure 5).

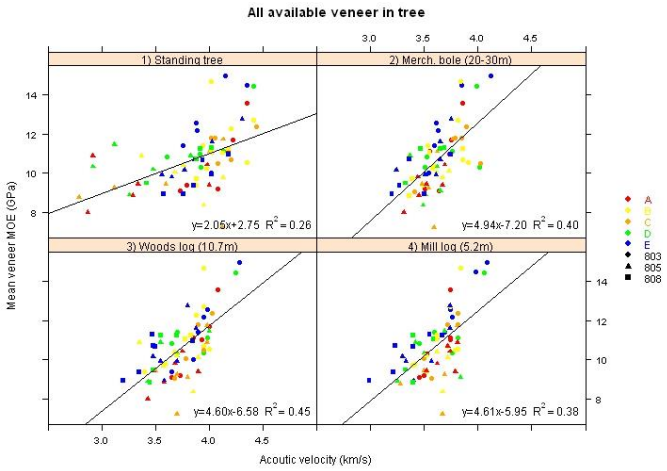

Figure 5 -- Relationship between AVs and mean MOE of all veneer in tree by site and thinning regime.

Considering additional tree variables such as dbh and log order (Wang et al. 2009, Amishev and Murphy 2008b) and age (Chauhan and Walker 206) can improve the predictability of MOE. Auty and Achim (2008) found incorporating density did not improve predictions but accounting for age did. In this study, incorporating additional variables increased the R^2 value of the regression equation (Table 2).

Table 2— Regression model statistics for predicting mean tree veneer MOE. AV in the upper half of the table refers to woods-length AV, while that in the lower part refers to the standing tree AV. Blanks indicate that one or more variables are not significant.

	Fixed Effects Model			Mixed Effects Model				
Variable	R^2	RMSE+	MAPE+	AIC+	BIC+	Loglik+	RMSE*	MAPE*
Wood-length AV								
AV	0.45	1.11	8.05	237	248	-113	0.95	6.89
AV x DBH	0.49	1.06	7.87					
AV x Taper	0.51	1.04	7.74	232	248	-109	0.92	6.79
AV + Nrings	0.52	1.03	7.70	236†	252†	-111†	0.83†	6.33†
AV x Taper+Nrings	0.55	1.00	7.61					
AV x Taper + Nrings + Greenkg	0.58	0.97	7.22	236	256	-109	0.89	6.44
AV x Taper + Nrings + Greenkg + Dispkg	0.61	0.93	6.64	232	254	-106	0.88	6.29
Standing tree AV								
AV	0.26	1.28	8.95	265	277	-128	1.15	8.08
AV x DBH								
AV x Taper								
AV + Nrings	0.32	1.23	8.74	259	275	-122	0.99	7.31
AV + Taper+Nrings	0.36	1.19	8.57	266	282	-126	1.14	8.12
AV x Taper + Nrings + Greenkg								
AV + Taper + Nrings + Greenkg + Dispkg	0.42	1.14	8.41	262	283	-122	1.07	7.84

[+] RMSE = root mean squared error, MAPE = mean absolute percentage error, AIC = Akaike information criterion, BIC = Bayesian information criterion, Loglik = log-likelihood
* Obtained when random effects due to site and treatment are known; when unknown the corresponding values from the fixed effects model apply.
† Model requires interaction between the two variables.
Var1xVar2 is equivalent to Var1 + Var2 + Var1:Var2

Conclusions

A positive correlation was found between mean tree stiffness (as calculated from individual veneer sheets) and AV using TOF tools at the tree level. Correlation is improved when knowledge of additional stand or tree variables is available and included in the prediction models. Further improvement to the models is obtained when tree level AV (i.e. that of the standing tree) is replaced with the woods-length log AV, and when green density, as determined here through the displacement method, augments the model. Silvicultural practices had an effect on the stiffness of trees, logs and veneer. Thinning stands alters crown and branch structure. Knot data are available and will be used in subsequent analyses as branches/knots in the wave propagation path influence measurements.

Acknowledgements

This is a product of the Sustainable Forestry component of Agenda 2020, a joint effort of the USDA Forest Service Research & Development and the American Forest & Paper Association. Research partners include the Stand Management and Precision Forestry Cooperatives and Rural Technology Initiative Program at the University of Washington College of Forest Resources, USFS Pacific Northwest Research Station, and CHH FibreGen. Funds were provided by the Rocky Mountain Research Station, the University of Washington, College of Forest Resources, and the USFS Pacific Northwest Research Station and the USFS Forest Products Laboratory. This project has been further supported through a Joint Venture Agreement between the USDA FS and the New Zealand Forest Research Institute Limited, trading as Scion.

Reference List

Amishev, D. and Murphy, G.E. 2008a. Implementing Resonance-Based Acoustic Technology on Mechanical Harvesters/Processors for Real-Time Wood Stiffness Assessment: Opportunities and Considerations. International Journal of Forest Engineering. 19(2): 48-56.

Amishev, D. and Murphy, G.E. 2008b. In-forest assessment of veneer grade Douglas-fir logs based on acoustic measurement of wood stiffness. Forest Products Journal. 58(11): 42-47.

Auty, D. and Achim, A. 2008. The relationship between standing tree acoustic assessment and timber quality in Scots pine and the practical implications for assessing timber quality from naturally regenerated stands. Forestry. 81(4): 475-487.

Briggs, D.G.; Thienel, G.; Turnblom, E.C. [and others]. 2008. Influence of thinning on acoustic velocity of Douglas-fir trees in western Washington and western Oregon. In: Proceedings of the 15th International Symposium on Nondestructive Testing of Wood, Duluth, Minnesota. Forest Products Society, Madison, WI: 113-123.

Carter, P.; Briggs, D.; Ross, R.J.; and Wang, X. 2005. Acoustic testing to enhance western forest values and meet customer wood quality needs. In: Harrington, C.A.; Schoenholtz, S.H., eds.Proceedings, Productivity of Western Forests: A Forest Products Focus. Gen. Tech. Rep. PNW-GTR-642. Portland, OR: U.S. Department of Agriculture, Forest Service, Pacific Northwest Research Station: 121-129.

Carter, P.; Chauhan, S.; and Walker, J. 2006. Sorting logs and lumber for stiffness using Director HM200^{TM}. Wood and Fiber Science. 38(1): 49-54.

Chauhan, S.S. and Walker, J.C.F. 2006. Variations in acoustic velocity and density with age, and their interrelationships in radiata pine. Forest Ecology and Management. 229(1): 388-394.

Curtis, R.O. 1982. A simple index of stand density for Douglas-fir. Forest Science. 28: 92-94.

Dickson, R.L.; Matheson, A.C.; Joe, B. [and others]. 2004. Acoustic Segregation of Pinus radiata logs for sawmilling. New Zealand Journal of Forestry Science. 34(2): 175-189.

Fahey, T.D.; Cahill, J.M.; Snellgrove, T.A.; and Heath, L.S. 1991. Lumber and veneer recovery from intensively managed young-growth Douglas-fir. Res. Pap. PNW-RP-437. Portland, OR: U.S. Department of Agriculture, Forest Service, Pacific Northwest Research Station. 25 p.

Grabianowski, M.; Manley, B.; and Walker, J.C.F. 2006. Acoustic measurements on standing trees, logs and green lumber. Wood Science and Technology. 40(3): 205-216.

Kennedy, R.W. 1995. Coniferous wood quality in the future: concerns and strategies. Wood Science and Technology. 29:321-338.

Mora, C.R.; Schimleck, L.R.; Isik, F. [and others]. 2009. Relationships between acoustic variables and different measures of stiffness in standing Pinus taeda trees. Canadian Journal of Forest Research. 39(8): 1421-1429.

Olesen P.O. 1971. The water displacement method. Tree Improvement. Arboretet, Horsholrn No. 3. 23 pp.

Pellerin, R. and Ross, R.J. 2002. Nondestructive evaluation of wood. Forest Products Society, Madison, WI. 210 pp.

R Development Core Team. 2008. R: A language and environment for statistical computing. R Foundation for Statistical Computing. Vienna, Austria.

Ridoutt, B.G.; Wealleans, K.R.; Booker, R.E. [and others]. 1999. Comparison of log segregation methods for structural lumber yield improvement. Forest Products Journal. 49(11-12): 63-66.

Ross, R.J.; McDonald, K.A.; Green, D.W.; and Schad, K.C. 1997. Relationship between log and lumber modulus of elasticity. Forest Products Journal. 47(2): 89-92.

Todoroki, C.L.; Lowell, E.C.; Dykstra, D.P.; and Briggs, D.G. 2012. Maps and models of density and stiffness within individual Douglas-fir trees. New Zealand Journal of Forestry Science. 42:1-13.

Wang, X. 2013. Acoustic measurements on trees and logs: a review and analysis. Wood Science and Technology. DOI 10.1007/s00226-013-0552-9

Wang, X.; Carter, P.; Ross, R.J.; and Brashaw, B.K. 2007. Acoustic assessment of wood quality of raw forest materials: a path to increased profitability. Forest Products Journal. 57(5): 6-14.

Wang, X.; Ross, R.J.; McClellan, M. [and others]. 2001. Nondestructive evaluation of standing trees with a stress wave method. Wood and Fiber Science. 33(4): 522-533.

Wang, X.; Verrill, S.; Lowell, E. [and others]. 2009. Acoustic sorting models for log segregation. In: Zhang, H.;Wang, X., eds. Proceedings, 16th international symposium on nondestructive testing and evaluation of wood. 2009 October 12-14. Beijing, China. Beijing Forestry University, Beijing, China: 45-51.

Wessels, C.B.; Malan, F.S.; and Rypstra, T. 2011. A review of measurement methods used on standing trees for the prediction of some mechanical properties of timber. European Journal of Forest Research. 130(6): 881-893.

Comparison of the acoustic velocity of eastern larch grown in Northwestern Ontario measured by the Fibre-gen ST300 and HM200 acoustic tools.

Scott Miller, Faculty of Natural Resources Management, Lakehead University, Thunder Bay, ON., smiller4@lakeheadu.ca

Mathew Leitch, Faculty of Natural Resources Management, Lakehead University, Thunder Bay, ON., mleitch@lakeheadu.ca

Chander Shahi, Faculty of Natural Resources Management, Lakehead University, Thunder Bay, ON., cshahi@lakeheadu.ca

Reino Pulkki, Faculty of Natural Resources Management, Lakehead University, Thunder Bay, ON., reino.pulkki@lakeheadu.ca

ABSTRACT:

Lakehead University Wood Science Testing Facility (LUWSTF) has added acoustic testing to the wood characteristics mapping of eastern larch (*Larix laricina* (Du Roi) K. KOCH) grown in Northwestern Ontario. LUWSTF has collected acoustic velocity of 3,920 trees from 44 sample plots distributed across the 6 EcoRegions of Northwestern Ontario. After the non-destructive acoustic testing using a Fibre-gen ST300 (ST300) acoustic tool, 120 trees were cut down and acoustic velocity was measured from the butt to the base of live crown from 4 bolts representing 25% of the length of the stem. Test bolts were transported to LUWSTF for further acoustic testing from pith to bark.

In the controlled conditions of the laboratory, LUWSTF used moisture, temperature, x-ray densitometry and fibre length to correlate acoustic velocity to MOE from static bending. Validation of the mapping of acoustic velocity of test bolts was completed in two phases; a comparison study between the ST300 and the Fibre-gen HM200 (HM200) acoustic tools, and a comparison study between predicted MOE using acoustic velocity and actual MOE from the test bolts. This article reports the results of the comparison between the acoustic tools.

The acoustic velocity measured by each of the acoustic tools was analyzed using SPSS and it was found that there was no significant difference between the average acoustic velocity of bolts determined by either tool. A Pearson's correlation found that the results from ST300 (time of flight) and the HM200 (resonance-based) acoustic tools were significantly correlated. However, correlations to actual wood properties from pith to bark and butt to the crown were stronger with the ST300 than those from the HM200.

The study suggests that correlating the laboratory results to the standing tree results will allow forest managers to monitor wood properties of standing timber inventories. Thus, forest companies would be better able to understand the potential end uses for their forest resource.

Keywords: Acoustic velocity, acoustic waves, bolts, logs, radial testing, resonance, time-of-flight, trees, wood properties mapping.

Introduction

In the controlled conditions of the laboratory, Lakehead University Wood Science Testing Facility (LUWSTF) used moisture, temperature, x-ray densitometry and fibre length to correlate acoustic velocity of standing trees to MOE determined from static bending. To accommodate this research, LUWSTF first developed an acoustic neutral testing platform to prevent log bounce and loss of acoustic vibration. The platform significantly reduces the variance between standing tree and log acoustic velocity results when using a time of flight acoustic tool. As a means of validating the acoustic velocities obtained using the testing platform a comparison study between the ST300 and HM200 acoustic tools was completed. It is reported that the acoustic velocity measurements of the ST300 (time of flight) and the HM200 (resonance-based) acoustic tools are strongly correlated (Wang 2011; Mochan et al. 2009; Ross and Wang 2005). For example, Ross and Wang (2005) reported that "a species specific empirical model, can be made so that values obtained from the ST300 correspond closely to HM200 values." This article reports the results of the comparison between the acoustic tools.

Background

LUWSTF developed a wood properties mapping system, which identifies the significant differences in axial and radial variability of wood attributes for a target species at the landscape level. This systematic approach will allow forest managers to better define the forest inventory relative to end use and increase the opportunity for value-added wood products. In partnership with the Ontario Ministry of Natural Resources (OMNR) North West Science and Information, LUWSTF has completed intensive stem analysis and destructive wood testing on both under-utilized tree species and species of high economic importance across Northwestern Ontario. In 2010, the joint initiative added acoustic testing to the wood characteristics mapping of eastern larch (*Larix laricina* (Du Roi) K. KOCH) grown in Northwestern Ontario. LUWSTF collected acoustic velocity for 3,920 trees from 44 sample plots distributed across the six EcoRegions of Northwestern Ontario, which included managed and unmanaged natural forests as well as plantation trials.

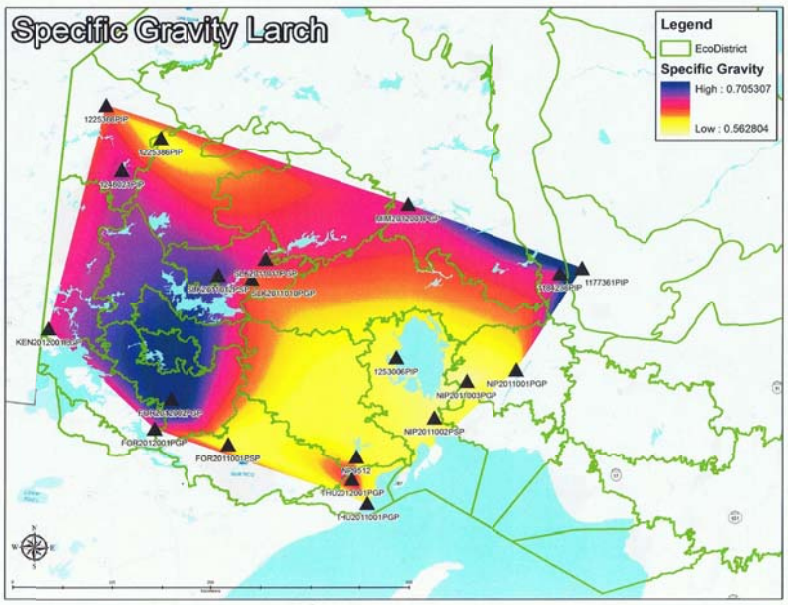

Figure 1-Example of landscape strata for relative density of eastern larch wood for Northwestern Ontario (Corbett, 2012)

Non-destructive acoustic testing was added to LUWSTF's wood testing methodology, using a ST300 acoustic tool, as a cost effective means of increasing the number of sample trees in the study (Ross 2011; Wang 2011; Achim et al. 2010; Ross and Wang 2005; Wang et al. 2005, 2003). The acoustic testing of standing trees effectively merged LUWSTF's destructive sampling of clear wood specimens (OMNR 2012; ASTM D5536-94 2010) with OMNR's stem analysis procedures (OMNR 2011).

Once field testing was completed, 120 trees were randomly selected and cut down and acoustic velocity was measured from the butt to the base of live crown from 4 bolts representing 25% of the length of the stem while lying on the forest floor (OMNR 2011, 2012). Test bolts were transported to LUWSTF for further acoustic testing from pith to bark in the controlled conditions of the lab. Test bolts were processed into test specimens following ASTM standards (ASTM D5536-94 2010). Further, fibre properties, growth ring analysis, water soluble extractives and chemical composition were also determined.

The preliminary findings of the acoustic work completed on eastern larch are consistent with the results reported in the literature. For example, a select group of wood properties, MOE, MOR, wood density and acoustic velocity, were measured at several moisture conditions, green, fibre saturation point (FSP) and 12 percent moisture. The effect of moisture on the selected wood properties above FSP seems to be proportional between the related wood properties, however, this phenomenon reduced the strength of the correlative relationship of these properties between FSP and 12 % moisture content relative to the radial origin of the test specimen; pith, heartwood or sapwood (Goal et al. 2011; Zhang et al. 2009; Wang et al. 2005, 2002). In order to correlate standing non-destructive test trees to the clear test specimens, it was necessary to determine age and diameter for all test trees (Ung et al. 2011; Achim et al. 2010), thus increment cores were collected from full measure non-destructive trees (OMNR 2011).

Materials and Methods

Two dominant mature trees and one co-dominant tree, representing the quadratic mean basil area (QMBA) for the site, were selected from a site in the area surrounding the City of Thunder Bay representing a typical eastern larch site. A 5.62 meter radius temporary sample plot was established and site attributes, stem analysis and destructive wood samples were collected following established methodologies (OMNR 2012, 2011; ASTM D5536-94 2010). Four 2.1 meter long logs were cut above the swell butt of each tree and brought to LUWSTF for processing.

Acoustic velocity was measured for each log using the HM200. Moisture content, temperature and log dimensions were determined for the pith, heart wood and sapwood following ASTM test standards (ASTM D5536-94 2010; ASTM D 4442-07 2008). The logs were then cut into three equal length bolts of 0.7 meters and acoustic velocity measurements were taken every 3 cm from the pith to the bark using the ST300. Figure 2 illustrates the moisture variability between logs, during acoustic testing with both tools.

Acoustic velocity data was analyzed using SPSS statistical software. Hypothesis testing was employed as a means of validating the acoustic velocity measurements derived using LUWSTF's acoustic neutral testing platform. The following two hypotheses were tested:

> H_o 1, No difference in reported outcomes when measuring the variance in acoustic velocity between trees and between logs of trees; and
>
> H_o 2, No significant difference between the grand means of acoustic velocities for each tool.

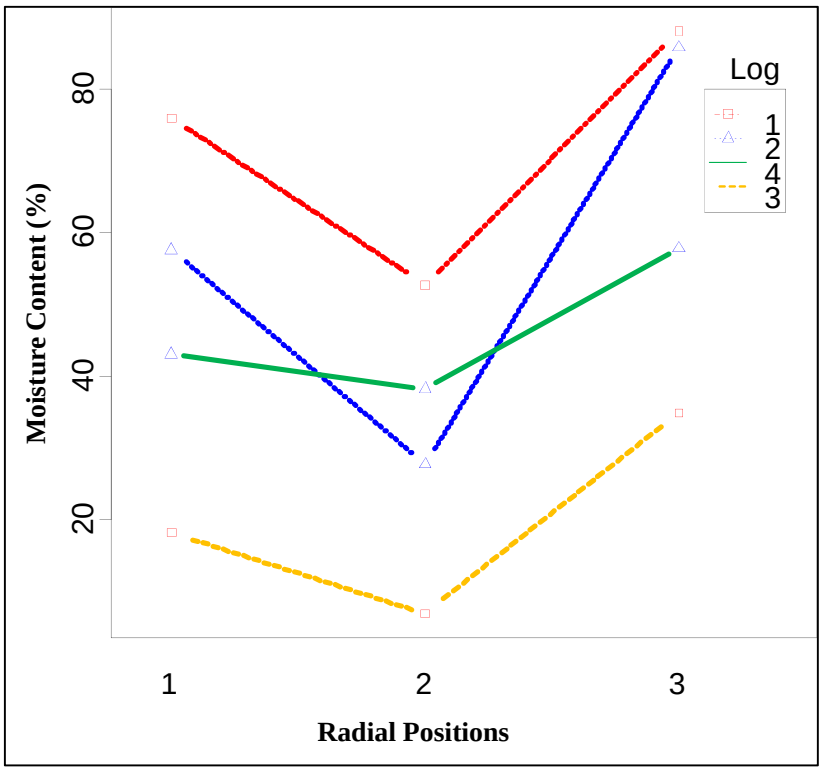

Figure 2- Radial variability of moisture content observed during the acoustic testing of three eastern larch trees.

Results and Discussions

A Shapiro-Wilk normality test and a Bartlett test of homogeneity of variances were performed on the test data, which showed the sample set was normally distributed and homogenous at 99.9% probability; with a:

W = 0.9266, p-value < 2.2e-16, and

Bartlett's K-squared = 6.0753, df = 2, p-value = 0.004795.

To accommodate the comparison of the acoustic tools, the ST300 radial measurements of the 0.7 meter test bolts had to be reduced to a grand mean for the four logs which represent each tree; as illustrated in Figure 3. A weighted average of the acoustic velocity, relative to the percent of the total log volume that each radial test position occupied, was developed for the ST300 measurements. Once this process of averaging was completed, statistical comparison of the acoustic tools was undertaken.

The analysis showed that both tools reported a significant difference in variance of acoustic velocity between trees at 99.9% probability. A TukeyHSD post hoc test denoted that there was significant variance in acoustic velocity between two homogeneous subsets at 99.9% probability. Subset 1 was comprised of the dominant trees (trees 1 and 3) and subset 2 comprised the co-dominant tree representing site QMBA (tree 2). The result were consistent between the ST300 with a standard

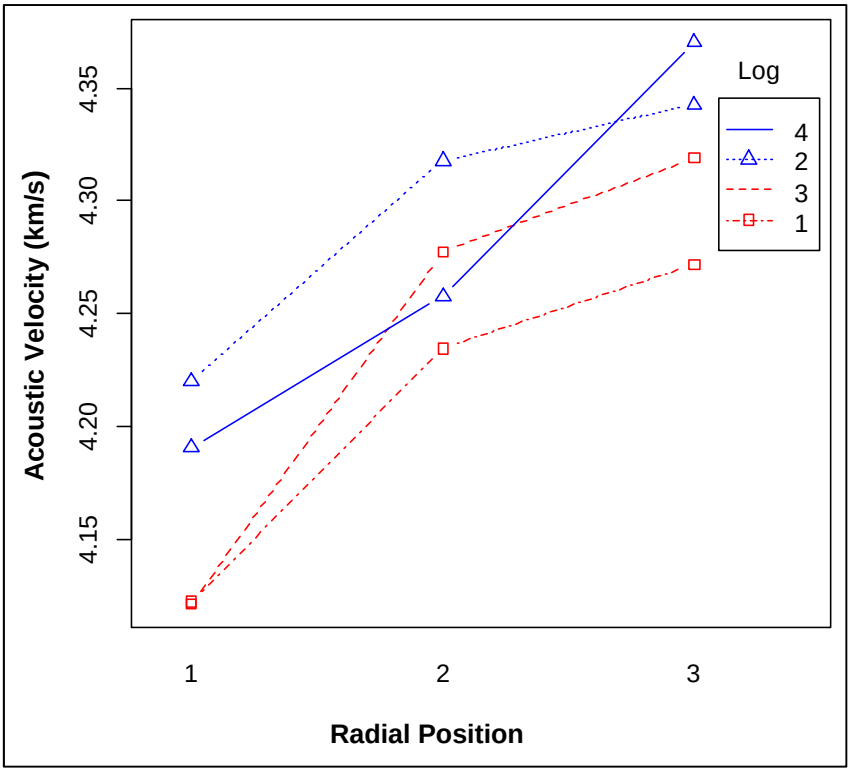

Figure 3- Pith to bark acoustic velocity measurements using the ST300.

deviation of 0.24 and the HM200 with a standard deviation of 0.22; as shown in Table 1. Based on these results, there does not appear to be any significant difference between the reported outcomes of either tool when measuring the variance in acoustic velocity between trees and between logs of trees. Thus, we accepted the H_o that there is no difference in reported variance of acoustic velocity between trees and logs by either tool at 99.9% probability.

Table 1-Comparison of mean acoustic velocity reported by the ST300 and the HM200 acoustic tools.

Tool	Tree 1 (km/s)	Tree 2 (km/s)	Tree 2 (km/s)
ST300	3.980	3.613	4.025
HM200	3.892	3.600	3.970

A Pearson's product correlation between ST300 and HM200 was completed which showed a strong correlation between the results of the two tools with a:

t = 13.9162, df = 46, p-value < 2.2e-16, and sample estimates: cor 0.8989233

as shown in figure 4. Statistical analysis of the results reported by both tools shows no significant difference in the test results at 99.9% probability. The HM200 had a grand mean of 3.821 kilometers per second and the ST300's grand mean was 3.873 kilometers per second; as shown in figure 5. Thus, we accept the H_o that there is no significant difference between the grand means of acoustic velocities for each tool at 99.9% probability.

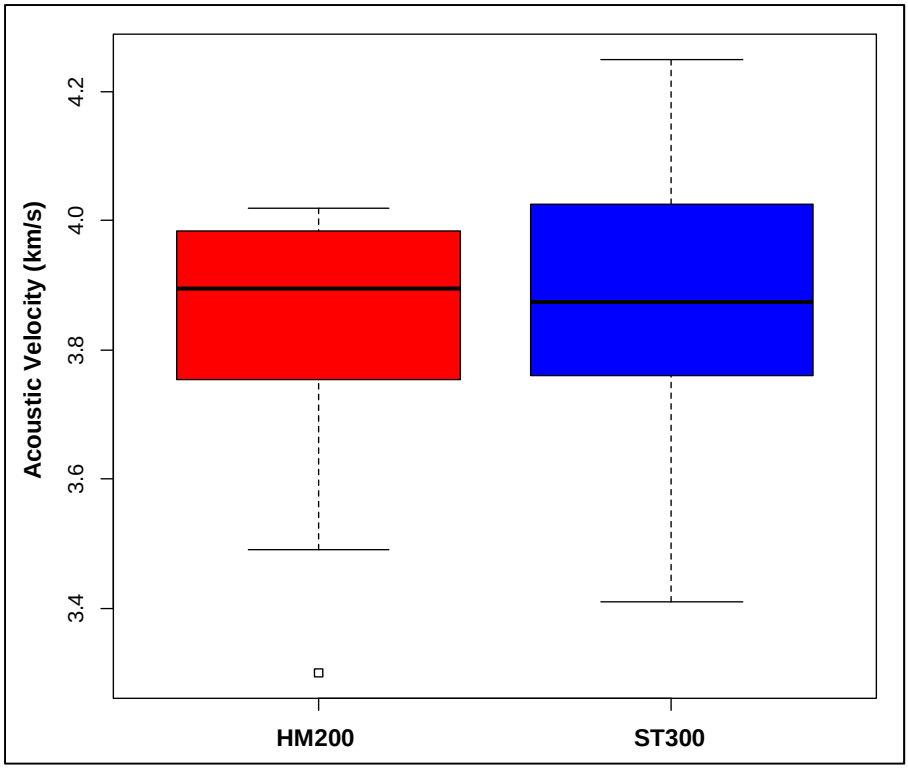

Figure 4-Comparison between ST300 and HM200 variance.

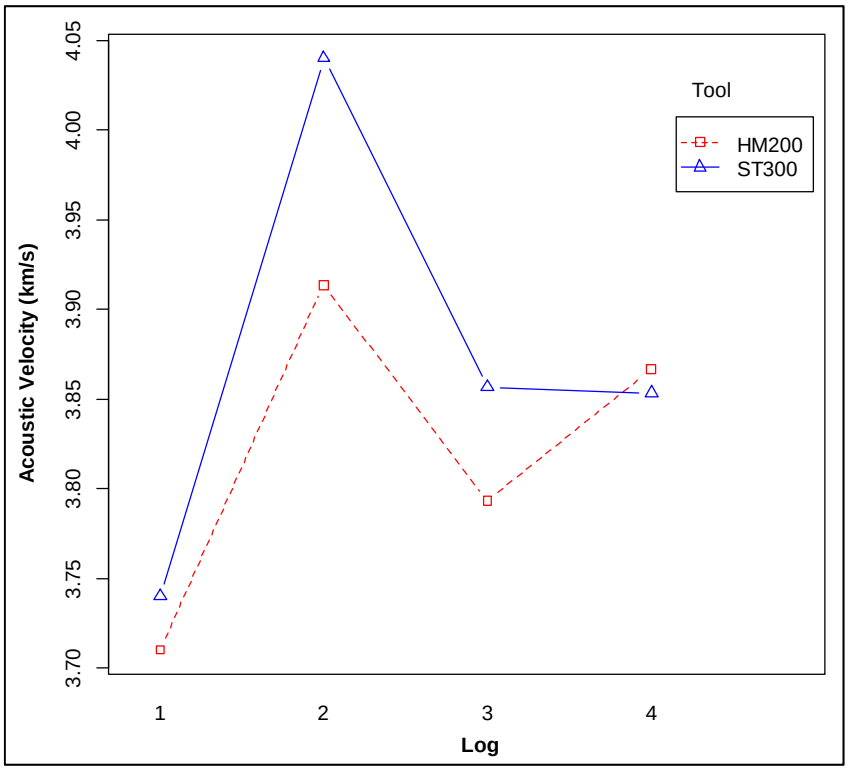

Figure 5-Comparison of acoustic velocity values reported by the ST300 and HM200.

A linear regression was performed using the ST300 as a predictor of the HM200. The regression produced a strong linear model with an adjusted R^2 of 0.8557:

$y = 1.0279x - 0.0546$, adjusted $R^2 = 0.8557$.

This result is consistent with results from similar studies and indicates that the acoustic neutral testing platform allows LUWSTF to produce strong predictive models for eastern larch wood properties without an intermediate correction for standing tree to log.

Conclusions

LUWSTF was able to use the proven fundamental relationship that exists between acoustic velocity measurements, wood moisture, log diameter and age to cost effectively expand the sample size of their wood properties mapping initiative from hundreds to thousands of sample trees. The reliability of the acoustic equipment available today provides wood products professionals and forest managers new opportunities to develop new test procedures, which may improve our understanding of wood properties and wood utilization, which can be verified and validated through both destructive and non-destructive testing methods.

Development of the acoustic neutral testing platform and employing pith to bark testing in all wood attributes sampling seems to have helped to mitigate the increase in acoustic velocity when transitioning from standing tree to test log without the need for mathematical correction.

Based on the strong correlations between the time of flight ST300 and the resonance wave HM200, it seems possible to use the ST300 to develop accurate wood quality grades for the HM200. While the ST300 seems better suited for research and inventory roles, the HM200 is better suited for commercial operations than the ST300.

Acknowledgements

The authors would like to acknowledge the support received from the staff of North West Science and Information, the Ministry of Natural Resources and FedNor. I would like to express my appreciation to Xiping Wang, Peter Carter, and Brian Bradshaw for providing their insight and guidance on this paper; thanks for all your help. Thanks also to Ralph White for the loan of the HM200 acoustic tool; without it we couldn't have completed our study. Funding for this project was provided by NSERC, NOHFC, FedNor, LUWSTF and North West Science and Information.

References

Achim, A. Paradis, A. Salenikovich, A.Power,H. 2010. Using acoustic tools to improve the efficiency of the forestry wood chain in eastern Canada. The Future of Quality Control for Wood & Wood Products. 2010. May 4-7, Edinburgh
The Final Conference of COST Action E53. pp. 9

ASTM D5536-94, 2010. Standard Practice for Sampling Forest Trees for Determination of Clear Wood Properties. ASTM International, Inc. West Conshohocken, PA.

ASTM D 4442-07, 2008. Standard Test Methods for Direct Moisture Content of Wood and Wood-Base Materials. Annual Book of ASTM Standards 2008, 04.10:456-461. ASTM International, Inc. West Conshohocken, PA.

Corbett, D. 2012. Wood specific gravity stratification for eastern larch grown in Northwestern Ontario. North West Science and Information. Ontario Ministry of Natural Resources. Thunder Bay. ON. Canada.

Gaol, S. Wang, X. Wang, L. Allison, R. 2011. Modeling Temperature and Moisture State Effects on Acoustic Velocity in Wood. In. Proceedings 17th International Non-destructive Testing and Evaluation of Wood Symposium. 2011. September 14-16. Sopron. Hungary. University Of West Hungary. Sopron, Hungary. p. 411-418.

Mochan, S. Moore, J. and Connolly, T. 2009. Using acoustic tools in forestry and the wood supply chain. Forestry Commission Research Note (FCRN005). Forest Research. Northern Research Station. Roslin. Midlothian. UK. pp. 6

OMNR, 2012. Scaling Manual. Ontario Ministry of Natural Resources. Toronto. Ontario. pp. 139.

OMNR, 2011. Growth and Yield Program PSP and PGP Reference Manual. Ontario Ministry of Natural Resources. Toronto. Ontario. pp. 524.

Ross, R. 2011. Impact of non-destructive testing and evaluation of wood products. In. Proceedings 17th International Non-destructive Testing and Evaluation of Wood Symposium. 2011. September 14-16. Sopron. Hungary. University Of West Hungary. Sopron, Hungary. p. 3-7.

Ross, R. and Wang, X, 2005. A Review of the Use of Acoustic Speed to Assess Standing Timber Quality. In: Proceedings of the 14th International Symposium on Non-destructive Testing of Wood. 2005 May 2 – 4. Eberswalde , Germany. University of Applied Sciences, Eberswalde. pp. 5.

Ung, C. Duchesne, I. Guo, X. Swift, E. 2011. Testing the impacts of tree and stand attributes on the variability of acoustic velocity in standing trees (ST300) and logs (HM200). Hardwood Initiative –Part 5: Development of new processes and technologies in the hardwood industry (Project 16). Final Report 2010-11. FPInnovations Québec City, Québec. Canada. pp. 11

Wang, X. 2011. Fundamentals of Acoustic Measurements on Trees and Logs and Their Implication to Field Application. In. Proceedings 17th International Non-destructive Testing and Evaluation of Wood Symposium. 2011. September 14-16. Sopron. Hungary. University Of West Hungary. Sopron, Hungary. p. 25-33.

Wang, X. Ross, R. Carter, P. 2005. Acoustic evaluation of standing trees- recent research development. In: Proceedings of the 14th International Symposium on Non-destructive Testing of Wood. 2005 May 2 – 4. Eberswalde , Germany. University of Applied Sciences, Eberswalde. p. 455-466.

Wang, X. Ross, R. Punches, R. Barbour, J. Forsman, J. 2003. Evaluation of small-diameter timber for valued-added manufacturing-A stress wave approach. In: Proceedings, second international precision forestry symposium; 2003 June 15-17; Seattle, WA. Seattle, WA: University of Washington Insitute of Forest Resources; 91-96.

Wang, X. Ross, R. Bradshaw, B. Erickson, J. Forsman, J. Pellerin, R. 2002. Diameter Effect on Stress-Wave Evaluation of Modulus of Elasticity of Logs. In. Proceedings of the 13th International Symposium on Non-destructive Testing of Wood. 2002. August19-21. Berkeley. USA. University of California, Berkeley Campus California, USA. p. 149-156.

Zhang, H. Wang, X. and Ross, R. 2009. Stress wave propagation on standing trees--Part 1. Time-of - flight measurement and 2D stress wave contour maps. In: Proceedings of the 16th non-destructive evaluation of wood symposium. 2009 October 12-14. Beijing, china: Beijing Forestry University, Beijing, China. p. 53--58.

Wood Density Determination of Trees by Microwave Impulse Radar Device

Divos Ferenc
Faculty of Wood Sciences, Jozsef Bodig Wood NDT Laboratory, Univeristy of West Hungary, Sopron, Hungary, divos@fmk.nyme.hu

Dimitrios Tsalagkas
Faculty of Wood Sciences, Institute of Wood and Paper Technology, University of West Hungary, Sopron, Hungary, dtsalag@fmk.nyme.hu

Dimitrios Koutsianitis
Faculty of Forestry and Natural Environment, Laboratory of Forest Utilization, Aristotle University, Thessaloniki, Greece, koutsian@for.auth.gr

Abstract

Density is a major log quality indicator. It is important in carbon balance calculations and in tree breeding as well. This paper describes wood density measurement of standing trees using a microwave radar. We studied the reliability and accuracy of the method. The applied technique was able to penetrate trees ranging from 10 to 20 cm in diameter. Multiple regression analysis has been performed on the measured microwave reflection coefficients and wood material density. The actual density and moisture data were estimated from increment bore samples. Preliminary results from this study suggest that this method is a promising technique to assess the density of standing trees.

Keywords: wood density, tree, microwave radar

Introduction

Wood density is an important index of wood quality because it affects many wood properties (hygroscopicity, shrinkage and swelling, mechanical, electrical etc.) related to the industrial processing of wood. Density is a complex of characteristic and is influenced by moisture, structure (width of growth rings, proportion of latewood), extractives and chemical composition. Even more, there is variation within a tree, between trees of the same species and between species. Wood density has been consistently shown to be under strong genetic control and to have a high heritability (Tsoumis 1991, King et al. 1988). King et al. (1988) estimated genetic parameters for wood density using both cores and Pilodyn methods. Results showed that genetic correlation between the Pilodyn measurements and wood density proved very effective for selecting trees while strong negative correlations existed between wood density and diameter. Thus a suitable selection of trees in the forest during cultivation or prior to harvest could be the optimum process to evaluate timber resource. The cost of any manufacturing process can be eliminated by assessing the raw material quality at the earliest possible stage (Holmes et al. 2013). Timber quality is determined by defects in the log as well as density and moisture content of wood. Current techniques to measure basic density are either time consuming or of limited accuracy (Holmes et al. 2013, Holmes and Cown 2011).

Microwave testing method is a new candidate for determining wood density and moisture content. It has higher wavelength than gamma or X-rays which enables higher penetration depth and the technology is accessible at a moderate price (Divos et al. 2011). Materials such as timber which are lousy and anisotropic causes a linearly polarized electromagnetic wave to be depolarized upon transmission through the material. Microwave nondestructive testing methods (MNDT) are fast,

contact-less, accurate and continuous techniques for evaluation of moisture content, slope of grain, density of knots and specific gravity of timber (Deepak et al. 2000).

Many studies into the application of microwave sensing to the measurement of timber properties have been performed, especially for detecting defects and knots of wood and less to evaluate the density. For instance, Divos et al. (2011) by measuring the amplitude and phase angle were able to determine the density of six different solid wood samples with various densities. According to the co-authors the standard error of this technique was 35 kg/m^3 which is acceptable in most of the industrial applications.

However, these studies have primarily been confined to the examination of timber that has been dried below to the fiber saturation point (FSP) (Holmes and Cown 2011). The objectives of this study were to investigate: a) the influence and relationship of amplitude and time shift with density and moisture content and how microwave sensing performs on unprocessed timber (above FSP), b) the potential use of microwave impulse radar as a portable, accurate and cost effective non destructive testing method for the determination of standing tree wood density and their selection for timber growth quality improvement.

Theoretical considerations

The theoretical background of wooden material interaction with electromagnetic waves is described in detail by Torgovnikov (1993). Electromagnetic sensors essentially measure either the energy transmitted or reflected back from a material and converts it, through the material's physical properties (moisture content and density) to a measurable signal known as permittivity or dielectric constant. Wood as an anisotropic material is the media for the propagation of the electromagnetic waves. Penetration into a media is common concern as the moisture present in the material is seen to absorb the microwave energy. The reflected and transmitted energy, i.e. the dielectric properties of wood are highly influenced on the tree species, heterogeneous structure of wood, density, moisture content, temperature, grain angle and the frequency. It is a quite complicated phenomenon. (Holmes et al. 2013, Divos et al. 2011, Torgovnikov 1993). All the above mentioned factors affect how electromagnetic energy interacts with wood material. Thus, if possible any variations due to the properties which are not of interest must be either eliminated or minimized. (Holmes and Cown 2011). To determine the characteristics of various structural features of living trees a series of experiments was conducted by Holmes et al. 2013.

A dominant factor which will have a direct influence on the microwave measurement is moisture content. Dielectric properties of wood are different in standing trees and logs, since moisture content is different (Holmes et al. 2013). In case of the standing tree, the moisture content can be considered constant and hence basic density will become the dominant factor influencing the measurement. One more critical point is the fiber saturation point (FSP). Below the FSP effects due to basic density are small compared to the dominant moisture content effects, but are still measurable. Permittivity below FSP is constant over the 4 to 8 GHz frequency range. This can be explained, owing to the remaining water within the wood structure is so tightly bound that it no longer contributes significantly to the dielectric losses. This gives wood below FSP a very slow variation in dielectric properties (Holmes et al. 2013, Holmes and Cown 2011).
Considering that the tree acts as a dielectric rod, any incident electromagnetic energy tends to be contained within the tree and little energy radiates externally. In particular the incident wave is focused towards the centre of the tree. In the case of the high moisture content living tree, the electromagnetic waves are focused within the tree and are quickly attenuated within the tree and little is re-radiated. This effect is desirable in this application to standing trees, as distributions external to the tree have little effect on the measured fields (Holmes at al. 2013).

A second factor in extracting the density information requires that the anisotropic nature of the wood due to early wood/ late wood (EW/LW) bands be minimized. Considering the anisotropy of wood the

EW/LW layering has the effect of acting as a conduit of microwave energy in a preferred direction and as a result differences exist in permittivity of EW and LW. In the case of logs applying energy to the side of the log will fix the EW/LW boundaries as orthogonal to the plain of incidence. The permittivity difference between early and latewood is large. A suitable sensing structure to reduce the effects of the non-homogeneity of wood is an open-ended waveguide. To reduce the effects of non-homogeneity of wood material due to the EW/LW bands, an open-ended waveguide sensor structure is required (Holmes et al. 2013, Holmes and Cown 2011).

Both the grain angle and the moisture content of the branch or heartwood are considerably different from the surrounding sapwood. The dielectric constant and loss factor behavior of branches and heartwood are quite similar and exhibit small frequency dependence. However, sapwood samples showed frequency dependence due to the large free amount of water contained in this part of the tree. Measurements have shown that frequencies greater than 4 GHz are required to obtain sufficiently different permittivities to clearly differentiate the variations between sapwood, heartwood and the branches (Holmes et al. 2013, Holmes and Cown 2011). As grain angle will introduce marked effects on the reflected microwave energy, it is preferable to select a measurement site at which the grain angle could be considered to be normal to the plane of incidence. This is important in case of timbers.

Furthermore, the conducted survey by Holmes et al. (2013) showed that the electromagnetic loss factor of the bark material was extremely high. This fact interprets that much of the incident energy would be attenuated in the bark instead of the woody tissue itself. For these reasons, it was proposed from Holmes et al. that for performing microwave measurements of living woody tissue the bark would have to be removed.

Materials and methods

Three tree species of standing trees ranging from 10 to 20 cm with similar densities were chosen for our investigation. In relation with the theory, moisture content of each tree was constant. The selected species were: birch, beech and black locust.

The density of each tree was independently assessed by the use of increment cores taken from each quadrant of the stem at the experimental by the microwave radar area. This area usually was in the breast height point (1.4 m) or close to this in case of knots or any other defects. The collecting steps required to collect the wood samples in the field by using an increment borer is described in Chave (2005). Determination of volume is the crucial factor for settling density values. The volume was calculated by the equation

$$V = \frac{\pi}{4} D_b^2 L_c \qquad (1)$$

where D_b and L_c are the bore diameter and core length of the increment borer respectively (Maeglin 1975).

Moisture content was estimated by the following equation

$$MC\ (\%) = \frac{M_{wet} - M_{dry}}{M_{dry}} \times 100 \qquad (2)$$

where M_{wet} is the initial weight and M_{dry} the oven dry mass of the increment borer samples.
For our investigation we used a wide band Novelda microvave impulse radar. The emitted electromagnetic pulse has a power in the range of nano-Watt, therefore it is below the FCC regulation limit. The applied frequency is in the 1 to 6 GHz range. The antenna is a critical component of the

setup. In our experiment we used a sinus antenna with lenses which were part of the development kit. The experimental set up is given in Image 1.

Image 1 –The applied setup for the measurements of density indication parameters.

Transmission technique has been applied where the antennas were facing each other and the tree was between the antennas. The transmitter antenna emits a short microwave pulse. This pulse travels through the tree and the receiver antenna detects the arrival pulse. The distance between the antennas was 38 cm.

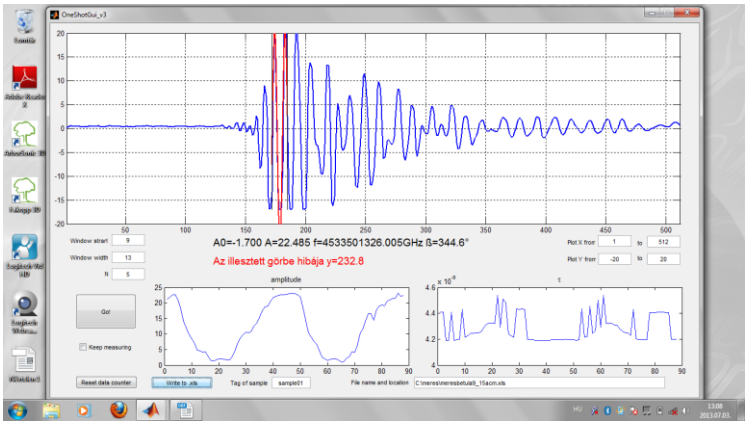

Image 2 -Received signal. The region of interest is the area marked by the red curve. A sine wave is fitted by the evaluation software and converted to the amplitude (left bottom image) and time shift (right bottom image) signal simultaneously. The horizontal axis is time.

The amplitude and the time shift of the received signal were measured as moisture and density indicators. From every tree four measurements were taken (2 repetitions in every tree x 2 measurements in each tree). Then the mean values of amplitude and time shift were determined respectively. Evaluation software has been developed for easy data collection. The view of software is presented in Image 2. The minimum amplitude and maximum time shift values represent the center of the tree (incident wave), while the maximum amplitude and minimum time shift values depict the outer parts, before entering and after passing through totally the standing tree. This phenomenon confirms the fact that tree acts as a dielectric rod.

The measured amplitude (A_{meas}) strongly depends on tree diameter (d), see figure 1. To eliminate the effect of tree diameter, we applied corrected amplitude (A_{cor}) according to the following formula:

$$A_{cor} = A_{meas} e^{0,1638d} \qquad (3)$$

The above formula is a linearization step. Finally, multiple regression linear analysis was performed on the measured microwave parameters (amplitude and time shift) and wood material density and moisture content to examine their correlations.

Results and discussions

The test series were measured under various outside temperatures (15-30^0 C) and wood moisture contents. The results on Figure 1 show the correlation between the measured amplitude and the diameter of trees. Figure 2 presents the correlation between the time shift and trees diameter. The amplitude exhibited a negative correlation, while the time shift in contrast a positive correlation with trees diameter.

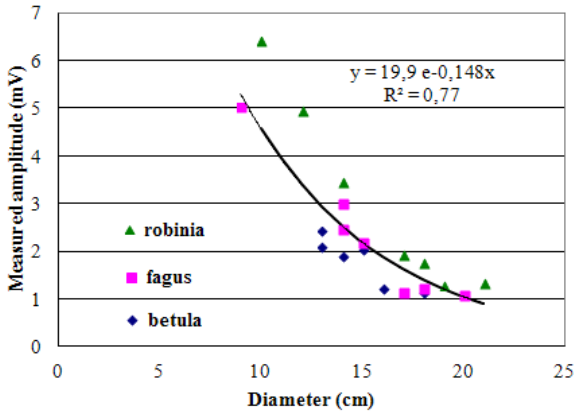

Figure 1- The amplitude as a function of tree diameter.

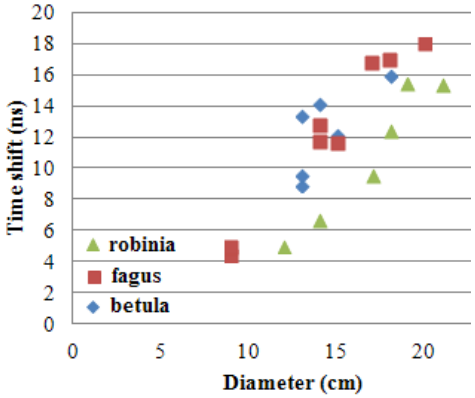

Figure 2- The time shift as a function of tree diameter.

The limited range diameter (10-20cm) is due to the system capabilities. Above the 20 cm diameter the amplifier was not strong enough and the software was not able to distinguish between the arrival pulse and noise. For trees below 10 cm in diameter the measurements could be accomplished without the use of amplifier.

Multiple regression analysis (Statistica software) has been used to reveal any correlations among density and diameter, amplitude and time shift parameters. Using the mentioned method, a significant model emerged for the density and the adjusted R^2 was found to be 88%. Results shown that the most significant variable was tree species ($p<0.0005$). Further density was also statistically correlated with corrected amplitude, defined in equation 3. ($p=0.005$).

Table 1 shows the density and moisture content mean values of the selected trees and the air dry density values in accordance with literature. The comparison of the measured mean values density of the increment cores and the predicted by the investigated radar method is shown in Figure 3.

Table 1-Increment borer mean values of density and moisture content (MC).

Species	Density (kg/m^3)	MC(%)	Air dry density (kg/m^3)$^{(1)}$
Birch	700	42.9	730
Beech	770	56.6	740
Black locust	860	38.5	760
(1) Tsoumis 1991			

Tree density predictor parameters are: corrected amplitude (A_{cor}), time shift (t_{shift}) and species index (SpIn). Birch is marked by 1, beech is marked by 2 and black locust is marked by 3, so tree species is becomes numerical predictor parameter. The best density prediction is provided by the following empirical formula:

$$Predicted\ density = 800{,}8 + 4{,}40\ A_{cor} + 0{,}969\ t_{shif} - 73{,}8\ SpIn$$

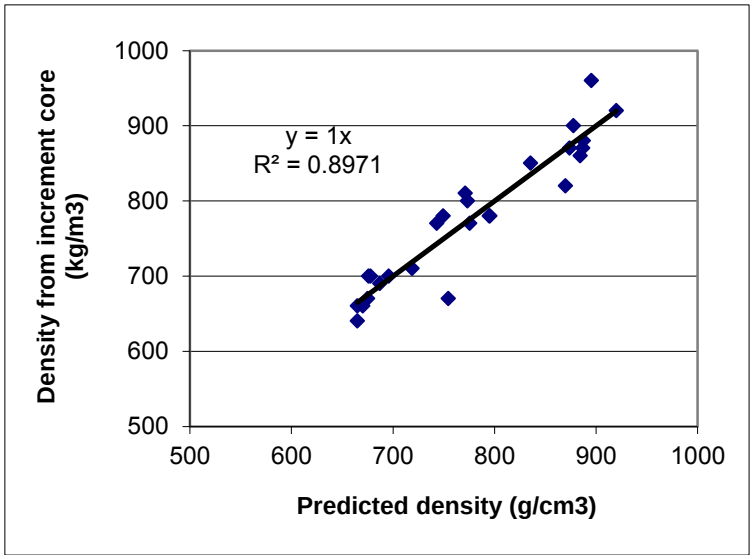

Figure 3- Linear relationship of measured density by the increment sample and predicted density with the microwave impulse radar. Standar error of density determination is 66 kg/m^3.

Similar experiments were made recently by Holmes and Cown. Holmes and Cown (2011) who measured the basic density of standing Radiata pine trees of different years by using microwave reflectometry. Results showed that when trees were segmented into their age groups a marked variation in the sensitivity of the measurement technique to basic density was observed. Additionally, as the age of the trees was increasing the sensitivity to the measurement of the density was decreasing. This effect could be explained by the formation of heartwood within the stem as the tree was growing. The heartwood region of the tree has significantly lower moisture content to that of surrounding sapwood. Further, it was shown that the accuracy of this technique was ±10 kg/m^3 to the measured basic density range.

Conclusions

The measurements obtained by the microwave impulse radar method demonstrated potential to assess the density of standing trees when diameter is less than 20 cm. Additional trials to predict the wood moisture content were not successful, since results exhibited poor correlations. Based on this study

microwave radar needs further investigation to be performed in the determination of standing trees density when diameter is above 20 cm.

Acknowledgements

The authors would like to express their appreciation to Dr. Kiriaki Giagli, Mendel University in Brno, for her assistance.

References

Chave, J. 2005. Measuring wood density for tropical forest trees. A field manual for the CTFS. 7 p.

Deepak, K. Ghodgaonkar.; Wan Mahmood, B W. A.; Majid and Hilmi Bin Husin. 2000 Microwave Nondestructive Testing of Malaysian Timber for Grading Applications. In Proc: 6th World Conference on Timber Engineering, Whistler Resort, British Columbia, Canada, July 31 - August 3, 2000, paper # 7-5-1:1-7.
Divos, F.; Divos, P.; Ther I. 2011. Wood density determination by microwave radar. In Proc: 17th International Nondestructive Testing and Evaluation of Wood Symposium, Sopron, Hungary, September 14-16. : 651-656.

Holmes, S. W.; Mukhopadhyay C. S.; Riley G. S. 2013. Dielectric properties of wood for improved internal imagig. Advancement in Sensing Technology, SSMI 1: 93-104.

Holmes, S. W.; Cown, DJ Dr. 2011. Microwave density measurement of standing trees. In Proc: 9th Conf. on Electromagnetic Wave Interaction with water and Moist Substances, ISEMA: 39-41.

King, N. J.;Yeh, C. F.; Heaman, Ch.; Dancik P. B. 1988. Selection of wood density and diameter in controlled crosses of coastal douglas-fir. Silvae Genetica. 37 (3-4): 152-157.

Maeglin, R. 1975. Increment cores, how to collect, handle and use them. Gen. Tech. Rep. FPL 25: U.S. Department of Agriculture, Forest Products Laboratory: 11.

Torgovnikov, G. I. 1993. Dielectric properties of wood and wood based materials. Spinger Verlag Berlin, Heidelberg, New York.

Tsoumis, G. 1991: Science and Technology of Wood. Structure, Properties, Utilization. New York: Van Nostrand Reinold: 111-127. Chapter 8.

Acoustic Assessment Technologies for Optimal Wood Products and Biomass Utilization

Brian K. Brashaw
Natural Resources Research Institute, University of Minnesota Duluth, Duluth, MN, USA, bbrashaw@nrri.umn.edu

Xiping Wang
USDA Forest Service, Forest Products Laboratory, Madison, WI, USA, xwang@fs.fed.us

Dean Fellman
Center for First Americans Forestlands, College of Menominee Nation, Keshena, WI, USA, dfellman@menominee.edu

Robert J. Ross
USDA Forest Service, Forest Products Laboratory, Madison, WI, USA, rjross@fs.fed.us

Huadong Xu
Northeast Forestry University, Harbin, China, xuhuadong8215@yahoo.com

Abstract

The College of Menominee Nation collaborated with University of Minnesota Duluth and USDA Forest Products Laboratory to advance research on robust nondestructive evaluation technologies capable of predicting the wood properties of trees, stems, and logs, and assessing the value of stands and forests. A comprehensive assessment of the acoustic properties for two important wood species (white pine and sugar maple) was completed. This assessment showed a natural variation in acoustic velocity that could be determined in standing trees using commercial acoustic equipment. The variation in acoustic velocity can be used to sort trees and logs into quality grades than can be used to direct the material into appropriate product classifications. A strong relationship between radial stress wave velocity and cross-section quality was shown for both white pine and sugar maple using the Fakopp microsecond timer. Resistance microdrilling of the radial cross section showed an excellent relationship between the mean resistance and the measured green density of the tree. This could importantly be used to accurately predict weight measures of the stand for use in potential carbon credits or biomass estimation.

Keywords: nondestructive evaluation, trees, logs, acoustic velocity

Introduction

Objective

The objectives of the research project were: 1. Identify implementation strategies and guidelines for use with standing trees, stems and logs for regional application across the varied forest cover types; 2. Develop a nondestructive approach to accurately determine green wood density for individual species within a localized forest stand; and 3. Establish a new partnership between the College of Menominee Nation and the University of Minnesota Duluth, both Land Grant Institutions with a benefit to faculty, staff and students of both Institutions.

General information

Acoustic technologies have been well established as material evaluation tools in the past several decades and their use has become accepted in the forest products industry for on-line quality control and products grading (Pellerin and Ross 2002). Recent research developments on acoustic sensing technology offer further opportunities for wood manufacturers, forest owners, and tribal nations to evaluate raw wood materials (standing trees, stems, and logs) for general wood quality and properties (Wang et al. 2000, 2004, 2007). This strategic information can be used by forest owners and managers to make economic and environmental management decisions on treatments for individual trees and forest stands, improve thinning and harvesting operations, and efficiently allocate timber resources for optimal utilization. For example, the information could be used to sort and grade trees and logs according to their suitability for structural applications and for a range of fiber properties of interest to paper makers. Another example is to determine the relationships between environmental conditions, silvicultural treatments and wood fiber properties so that the most effective forestry treatment can be selected for future plantations for desired fiber quality.

The USDA Forest Product Laboratory (FPL) work on the use of acoustic speed to assess standing timber and log quality began in earnest in 1993. Since that time, the FPL and their cooperators have tested over 1500 trees and logs from various sites in the United States (Alaska, Michigan, Missouri, Oregon, Washington, Louisiana, and Wisconsin), Australia, and New Zealand. Because of the well-known relationship between acoustic speed and wood product quality, FPL focused their research efforts on examining the fundamental relationships between: 1. Standing tree assessment and log quality and 2. Measurements made on logs and resulting product (round wood, veneer, lumber) quality. Numerous publications have been prepared that document our results. Excellent correlations have been observed between acoustic measurements made on trees/logs and resulting product quality. Most recently, members of this project team published a cover story in the Forest Products Journal (Wang et al 2007) noting that the precision of acoustic technology has been improved to the point where tree quality and intrinsic wood properties can be predicted and correlated to structural performance of the final products.

A unique partnership was created for this project with the Menominee Indian Tribe of Wisconsin. Specifically, funds for the project were obtained in a grant application submitted by the College of Menominee Nation (CMN) to the USDA NIFA Tribal Grants Research Program. This research program links 1994 land grant institutions (CMN) with 1862 land grant institutions (UMD).

The Menominee reservation lands are comprised of 235,523 acres (219,000 acres forested), or approximately 357.96 square miles, and include over 407 miles of improved and unimproved roads, 187 rivers and streams, and 53 lakes. The business arm of the tribe is Menominee Tribal Enterprises (MTE), who has demonstrated expert ability to manage, harvest and process timber from the world renowned Menominee Forest - an award winning sustainable forest located on the Menominee Nation Reservation in central Wisconsin. Important species for this mill include white pine (*Pinus strobus*) and sugar maple (*Acer saccharum*), the two focus species assessed in this project.

Research Methods

Literature review of data set relationships between acoustic properties of trees, stems, logs, and products.

A comprehensive literature review of existing acoustic tree data sets was completed by the project team (Gao et al 2012). In addition to this information, a review was completed of previous research where the specific gravity or density was predicted for trees, logs and lumber using a wide variety of NDE

equipment and technologies. This review provided excellent insight on the development of an experimental procedure that could be used for stress wave timing and resistance microdrilling of both harvested discs and standing trees.

Assessment of Menominee Nation species using acoustic-based technologies

Standing trees

In cooperation with CMN, MTE, and USDA Forest Service staff, several stands were identified for evaluation. The target stands included species of importance to the Menominee Nation including white pine and sugar maple. One pine and two hardwood stands were selected. Approximately 35 white pine and 50 sugar maple trees were marked by MTE and CMN staff and identified by a painted number on the bark. Each of these trees were measured using the following methods:

1. Measure diameter at breast height (dbh).
2. Determine stress wave transmission time perpendicular to the grain using a Fakopp Microsecond Timer. Each tree was measured at 90 degrees to each other and taken at dbh.
3. Conduct a microsecond drilling at one of the Fakopp testing locations.
4. Determine longitudinal velocity using a fibre-gen STS 300 standing tree tool. The lower probe was inserted at a 30 degree angle through the tree bark approximately 2 ft above the ground and the upper probe 1.3 meters above the lower probe.

Photographs of the nondestructive testing equipment used to assess standing trees for this project is shown in Figure 1.

Figure 1—Nondestructive equipment used to assess standing trees. Top - stress wave timer; Middle - resistance microdrill; Bottom - standing tree acoustic.

Harvest

Following the experimental testing, each tree was felled by a private sawyer and bucked into typical log lengths. A 3-4 inch thick disc was obtained from most trees, cut from each tree after the first log was cut. It was marked by tree number and species, and then bagged in plastic to minimize drying. Each of the discs collected after felling was taken to UMD NRRI for resistance microdrilling and determination of green density. Figure 2 shows a representative white pine and hard maple tree after felling. Figure 3 shows a disc collected after the tree was sawn into logs. All logs numbered as to tree and log number. For example, 2-1 referred to tree number 2 - log number 1. The logs were then skidded to a log landing.

Figure 2—Harvested trees cut into logs. The left image shows a white pine tree with a 3 inch thick disc cut and the right image shows a sugar maple tree after harvest.

Logs

The logs were transported to MTE and placed into the mill storage yard. Each of the logs was laid out with the number visible on the top of the log. Each log was bar-coded by the MTE staff and visually assessed to determine the diameter, defect amount and volume. The project team completed log assessments approximately two weeks after the trees were harvested. The length and diameter at both ends were measured with a tape measure. The longitudinal stress wave velocity was measured using a fibre-gen HM 200. The HM 200 was firmly placed in contact with one cut end of the log. The log was impacted with a hammer, resulting in the display of the quality of the received signal and the velocity. Photographs were taken for the visual assessment of both ends of each log and along the length. The fibre-gen ST 300 was also used to test the velocity of each log. The probes were inserted into a log in the same manner that was done in the forest. The send and receive probes were approximately 1.3 meters apart and in visual alignment. Figure 3 shows the NDE testing completed for each of the white pine and sugar maple logs.

Figure 3—Assessment of the harvested white pine and sugar maple logs in the MTE log yard using a commercial longitudinal acoustic measuring tool (top) and standing tree tool (bottom).

Disc assessment

Discs were collected from twenty-five trees of the white pine and sugar maple trees harvested during this project. These discs were full size and taken from above the first log, typically 3 m (10 ft) above ground

level. Standard procedures were developed for measuring the discs with a resistance microdrill and a Fakopp Microsecond Timer. The procedure was to:

1. Draw a grid at 90 degrees onto the surface of the sample.
2. Insert Fakopp probes directly across from each other, in the same plane and through the bark and into sound wood. Take 3 measurements with the Fakopp and record the average.
3. Measure each cookie in both directions with the Fakopp.
4. A RINNTECH Resistograph was used conduct drilling at the midpoint of the sample near the location where the Fakopp measurement was taken.
5. Each disc was then cut into a 2-inch wide strip. The strip was measured to determine green density.

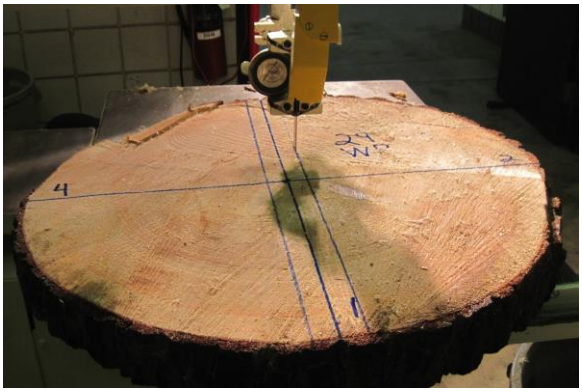

Figure 4—White pine disc being cut into a strip to determine specific gravity after microdrilling.

Figure 4 shows a marked disc being cut to determine green density of a 2 in wide section.

Results and Discussion

Standing trees

Descriptive statistics were used to determine the mean, minimum, maximum, and standard deviation for each species diameter, longitudinal stress wave velocity (ST 300), and transverse stress wave velocity (Fakopp Microsecond Timer - FMT) for each of two measurements taken at 90 degrees to each other. The summary of this data is available in table 1 for the white pine and table 2 for the hard maple. Graphical representation for the species diameter, longitudinal and radial velocities are shown in figures 5-8.

Table 1—Descriptive statistics for white pine trees evaluated during the study.

Stand parameters	Units	Number	Mean	Standard Deviation	Minimum	Maximum
Diameter	in	30	30.7	6.0	18.0	42.5
	cm	30	78.0	15.2	45.7	108.0
Longitudinal Velocity (ST 300)	ft/s	30	12,474	1,317	8,124	15,111
	m/s	30	3,802	402	2,476	4,606
Transverse Velocity 1 (FMT)	ft/s	28	3,438	594	2,394	4,753
	m/s	28	1,048	181	730	1,449
Transverse Velocity 2 (FMT)	ft/s	28	988	160	722	1,261
	m/s	28	3,242	524	2,369	4,136

Table 2—Descriptive statistics for sugar maple trees evaluated during the study.

Stand parameters	Units	Number	Mean	Standard Deviation	Minimum	Maximum
Diameter	in	51	22.2	5.6	11.1	35.4
	cm	51	56.3	14.1	28.2	89.9
Longitudinal Velocity (ST 300)	ft/s	51	13,487	1,249	10,207	15,515
	m/s	51	4,111	381	3,111	4,729
Transverse Velocity 1 (FMT)	ft/s	51	5,187	1,236	1,815	6,806
	m/s	51	1,581	377	553	2,075
Transverse Velocity 2 (FMT)	ft/s	51	5,016	1,201	2,291	7,063
	m/s	51	1,529	366	698	2,153

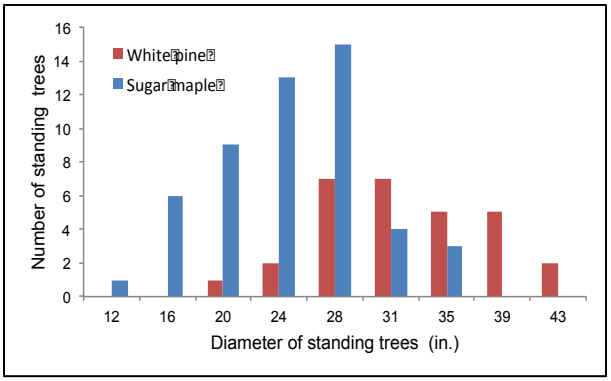

Figure 5—Diameter distribution of the white pine and sugar maple trees measured during this study. Note: 1 in = 2.54 cm.

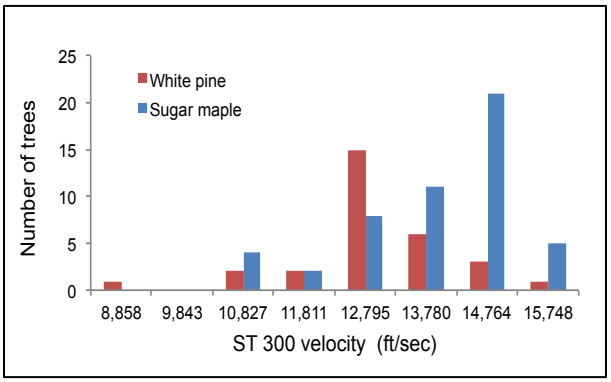

Figure 6—Longitudinal velocity distribution of the white pine and sugar maple trees measured during this study. Note: 1 ft/s = 0.305 m/s.

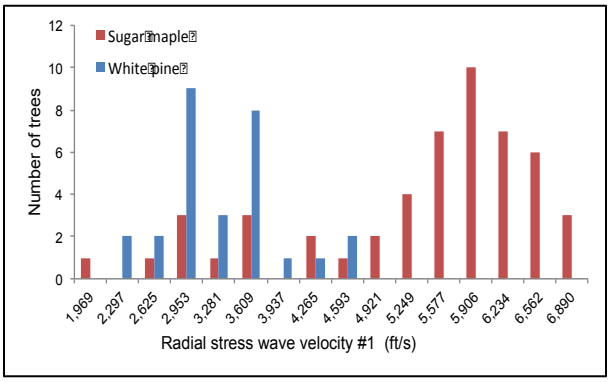

Figure 7—Radial velocity distribution of the white pine and sugar maple trees measured during this study. Note: 1 ft/s = 0.305 m/s.

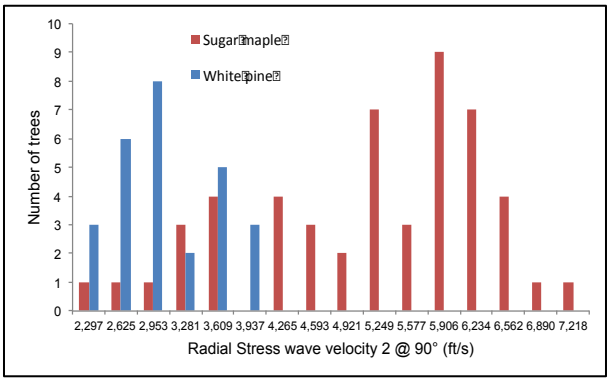

Figure 8—Radial velocity distribution of the white pine and sugar maple trees measured during this study. Note: 1 ft/s = 0.305 m/s.

The diameter of the white pine was larger than the hard maple and the mean longitudinal velocity was greater for the sugar maple. Within each species, there was a range of velocities noted, an important factor needed to create potential log velocity classes. For the transverse velocity, there was also variability in the velocities measured. This was a function of the presence of decay in the cross-section of the wood. The combination of velocities measured in these species can allow forest managers to make

informed decisions on the quality of individual trees or stands during timber cruising or marking for harvest.

Logs

Descriptive statistics were used to determine the mean, minimum, maximum, and standard deviation for each species diameter, longitudinal stress wave velocity (HM 200 and ST 300). The summary of this data is available in table 3 for the white pine and table 4 for the hard maple. Graphical representation for the species diameter and longitudinal velocity are shown in figures 9-11.

Table 3—Descriptive statistics for the white pine logs evaluated during the study.

Parameters	Units	Number	Mean	Standard Deviation	Minimum	Maximum
Diameter	in.	149	23.1	5.9	12.4	40.3
	cm	149	58.6	15.1	31.5	102.2
Length	ft	149	13.9	2.4	8.8	16.9
	m	149	4.2	0.7	2.7	5.2
Longitudinal Velocity (HM200)	ft/s	149	10,914	819	8,497	12,467
	m/s	149	3,326	252	2,5890	3,800
Longitudinal Velocity (ST300)	ft/s	146	13,31	1,429	7,520	17,126
	m/s	146	4,058	436	2,292	5,220

Table 4—Descriptive statistics for the sugar maple logs evaluated during the study.

Parameters	Units	Number	Mean	Standard Deviation	Minimum	Maximum
Diameter	in.	127	18.9	3.9	10.3	29.2
	cm	127	48.0	9.9	26.0	74.0
Length	ft	127	12.3	2.2	7.8	16.8
	m	127	3.8	0.7	2.4	5.1
Longitudinal velocity (HM200)	ft/s	127	11,132	800	7,907	12,697
	m/s	127	3,425	195	3,020	3,870
Longitudinal velocity (ST300)	ft/s	122	14356	1655	10387	18045
	m/s	122	4376	505	3166	5500

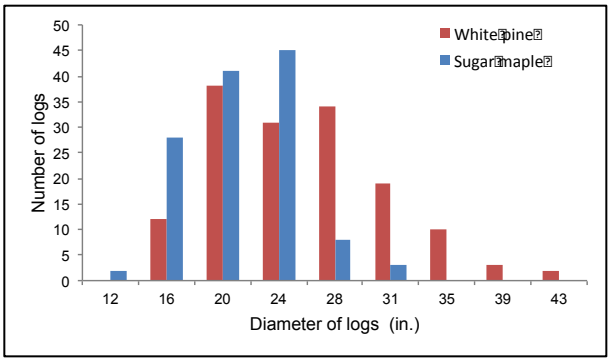

Figure 9—Diameter distribution of the white pine and sugar maple logs measured during this study. Note: 1 in = 2.54 cm.

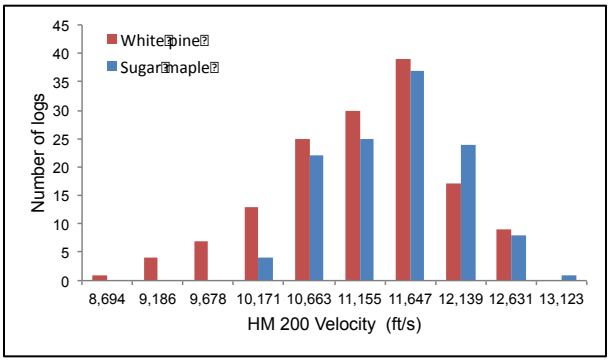

Figure 10— Longitudinal velocity distribution of the white pine and sugar maple trees measured using the HM 200 during this study. Note: 1 ft/s = 0.305 m/s.

This data showed that there was a useful range of velocity measures as determined using the HM 200. The data collection from the ST 300 was to increase the data sets for research purposes, as the ST 300 is not specifically designed for logyard measures. The white pine logs had the greatest variability, as it has the potential for low longitudinal velocity due to poor quality wood containing significant knot whorls in the upper sawlogs or due to internal decay. Additional analyses were completed to assess the relationship between the velocity measurements that were completed on the logs using the ST300 and the HM200. Figures 12 and 13 show the relationship for white pine and sugar maple respectively. The correlation coefficient for the relationship between the velocity as determined from both pieces of equipment was about same for the white pine (0.37) and sugar maple (0.39) logs. It must be noted that the HM measures the full length of the log while the ST only measured 1.3 m.

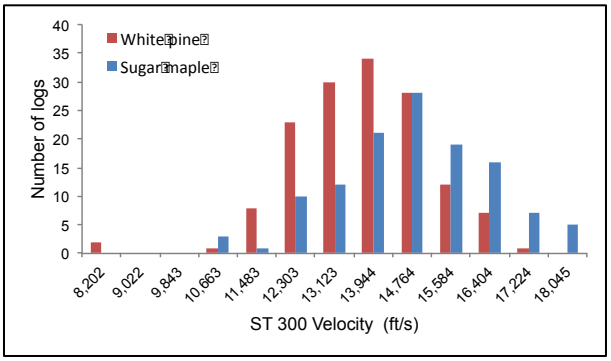

Figure 11— Longitudinal velocity distribution of the white pine and sugar maple trees measured with the ST 300 during this study. Note: 1 ft/s = 0.305 m/s.

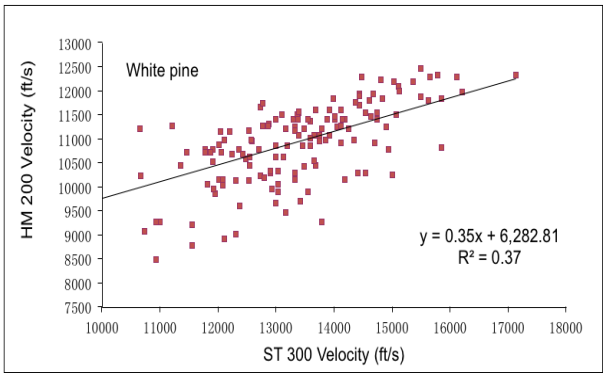

Figure 12—Relationship between the longitudinal velocity measurements obtained for the white pine logs with the HM200 and the ST300 acoustic tools used in this study. Note: 1 ft/s = 0.305 m/s.

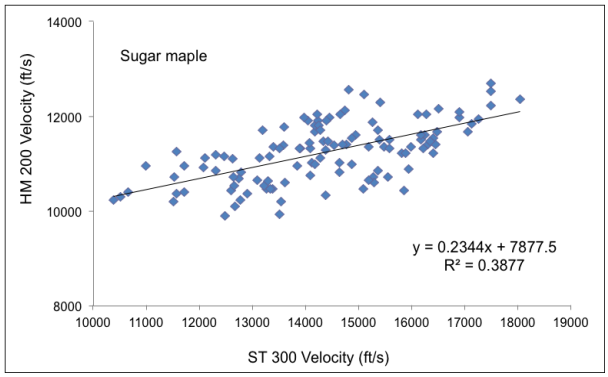

Figure 13—Relationship between the longitudinal velocity measurements obtained for the sugar maple logs with the HM200 and the ST300 acoustic tools used in this study. Note: 1 ft/s = 0.305 m/s.

The data also showed that the velocity was the highest for the second log for each species, then decreasing in the additional logs for each tree. The average for each log number was calculated and plotted for velocities measured using the HM200 and the ST 300. Figures 14 and 15 show the log velocity relationship between log order for both species with each piece of equipment. This is consistent with other reported research results from around the world. The butt log, while may be of high quality, is also affected by issues such as ground level decay that extends into the log, mechanical damage from felling operations, and previous logging damage. In larger and older trees like those measured during this project, the second log is usually of high quality. As the third and following logs are cut, there are more knots, defects, branches and other damage present affecting wood quality.

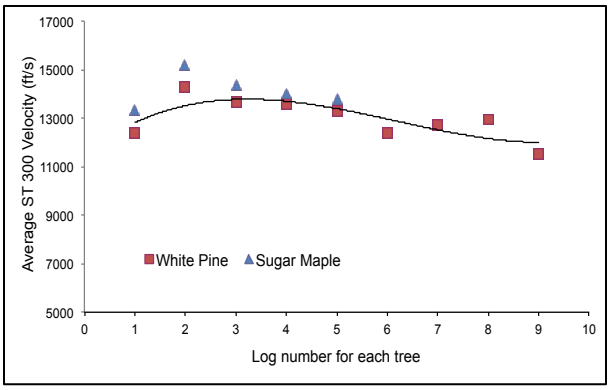

Figure 14—Mean log velocity as determined with the ST300 for each of the log numbers for all white pine and sugar maple trees evaluated in this study. Note: 1 ft/s = 0.305 m/s.

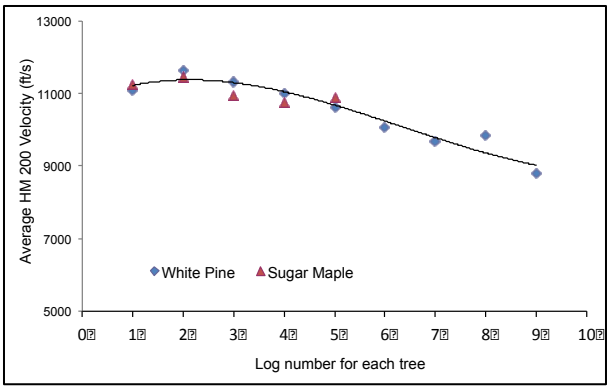

Figure 15—Mean log velocity as determined with the HM200 for each of the log numbers for all white pine and sugar maple trees evaluated in this study. Note: 1 ft/s = 0.305 m/s.

Radial velocity assessment

Further, one goal of the project was to assess the variability in radial or transverse stress wave velocity of standing trees at dbh, and compare that to the visual deterioration and decay present in trees. This tool is extremely effective in determining internal decay and deterioration. In a previous section, Figures 7 and 8 show the radial velocity measurements for all of the white pine and sugar maple trees. This information was converted into the inverse of velocity, as microseconds/ft of travel time is an effective and practical measurement for interpretation for field foresters and staff. Table 10 provides a summary of the mean, maximum, and minimum values for each species. Since two measurements were taken at 90 degrees to each other, the values are an average of those values.

Table 10—Radial stress wave times (microseconds/ft) for each species as determined at diameter breast height using the Fakopp microsecond timer.

Species	Radial Stress Wave Velocity Statistics (microseconds/ft)			
	Number of Trees	Mean	Maximum	Minimum
White Pine	28	307.0	416.3	234.2
Sugar Maple	51	212.4	398.7	150.4

A clear visual difference in wood quality was obvious through inspection of the harvested logs and can be assessed using radial acoustic velocity. This information can be especially valuable for forest management decisions, as the Fakopp can be used while trees are still standing to determine trees with large internal decay pockets that may not be visible from the outside. An assessment of the data showed that the stress wave times greater than 359 microseconds/ft contain deterioration in white pine. An assessment of the data showed that stress wave times greater than 300 microseconds/ft contain significant damage or deterioration for sugar maple.

Green density resistance drill relationship

The resistance microdrilling technique showed potential to predict green density for both species assessed in this project, a meaningful tool for potentially determining estimates of biomass energy

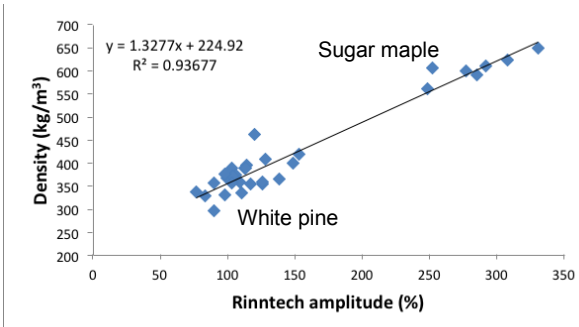

Figure 16—Resistance drilling measures as a function of green density.

mass, or carbon credits. Figure 16 shows the positive relationship between resistance drill amplitude and green density for a RINNTECH resistance microdrill. The figure shows the white pine and the sugar maple combined onto each chart. The lower density numbers are white pine and the higher density numbers are sugar maple. This information could improve the potential of forest managers to understand biomass estimates of their forest growing stock based on green density assessment.

Conclusions

The project activities resulted in a comprehensive assessment of the acoustic properties for two important wood species for the Menominee Nation, white pine and sugar maple. This assessment showed a natural variation in acoustic velocity that could be determined in standing trees using a fibre-gen ST300 and in logs using a fibre-gen HM 200. The variation in acoustic velocity can be used to sort trees and logs into quality grades than can be used to direct the material into appropriate product classifications. High velocity trees and logs showed a higher yield with less defect material (as determined through a visual log scaling) than those with lower velocity. Specifically, those logs with the highest acoustic velocities show the least average defect %. For sugar maple, the defect % was 1.2% for HM 200 velocities over 11,000 ft/s and 1.4% for ST 300 velocities over 14,000 ft/s. For white pine, the defect % was 1.8% for HM 200 velocities over 11,000 ft/s and 1.8% for ST 300 velocities over 14,000 ft/s. However, the use of visual log scaling was determined not to provide enough specific information to sort the logs into more specific grades. While it is not practical to conduct an intensive mill yield study of all sawn lumber, it may be possible to conduct a limited study of 5-10 logs each (high, medium and low velocity,) with the goal of providing improved measures of yield based on acoustic velocity.

A strong relationship between radial stress wave velocity and cross-section quality was shown for both white pine and sugar maple using the Fakopp microsecond timer, which can be used during forest management. It was shown that for a threshold setting for the Fakopp Microsecond Timer of greater than 300 microseconds/ft for sugar maple and 359 microseconds/ft for white pine was effective in identifying significant levels of internal decay in standing trees.

Finally, resistance microdrilling of the radial cross section showed an excellent relationship between the mean resistance and the measured green density of the tree. This could importantly be used to accurately predict weight measures of the stand for use in potential carbon credits or biomass estimation. Two commercial resistance drills were evaluated, with a predictive model of Green Density = (1.3277*Mean Resistance) + 224.92 for the RINNTECH Resistograph and Green Density = (8.6659*Mean Resistance) + 238.59 for the IML F350.

This project created a new partnership between the College of Menominee Nation's Sustainable Development Institute, the University of Minnesota Duluth's Natural Resources Research Institute and Menominee Tribal Enterprises. While the current project focused on acoustic measures at or after harvest, new projects could focus on other important forestry, secondary wood products, new product development or other economic opportunities.

Acknowledgments

The USDA NIFA Tribal Grants Research Program provided support for this project. Menominee Tribal Enterprises provided excellent cooperation. Menominee Tribal Enterprises is committed to excellence in the sustainable management of their forest, and the manufacturing of our lumber and forest products providing a consistently superior product while serving the needs of their forest, employees, wood products customers, tribal community, and future generations.

Reference list

Brashaw, B.K., X. Wang, R. J. Ross, H. Xu, R. Vatalaro and D. Fellman. 2012. Integrated Acoustic Assessment Technologies for Optimal Wood Products and Woody Biomass Utilization. Technical Report NRRI/TR-2012/43. Natural Resources Research Institute. University of Minnesota, Duluth. Duluth, MN.

Gao, S., X. Wang, B.K. Brashaw, R.J. Ross, L. Wang. 2012. Rapid assessment of wood density of standing trees with nondestructive methods – A literature review. In: Proceedings of 2012 the International Conference on Bio-base Material Science and Engineering (IEEE Catalog Number: CFP1240T-ART), Changsha, China, October 21-23, 2012.

Pellerin and Ross. 2002. Nondestructive evaluation of wood. Forest Products Society, Madison, Wisconsin. 210 p.

Wang, X., F. Divos, C. Pilon, B. Brashaw, R.J. Ross, and R.F. Pellerin. 2004. Assessment of decay in standing timber using stress wave timing nondestructive evaluation tools – A guide for use and interpretation. Gen. Tech. Rep. FPL-GTR-147. Madison, WI: U.S. Department of Agriculture, Forest Service, Forest Products Laboratory. 12 p.

Wang, X., P. Carter, R.J. Ross, and B.K. Brashaw. 2007. Acoustic assessment of raw forest materials – A path to increased profitability. *Forest Products Journal* (Invited feature article). 57(5): 6-14.

Wang, X., R.J. Ross, M. McClellan, R.J. Barbour, J.R. Erickson, J.W. Forsman, G.D. McGinnis. 2000. Strength and stiffness assessment of standing trees using a nondestructive stress wave technique. FPL-RP-585. US Department of Agriculture, Forest Service, Forest Products Laboratory, Madison, WI. p. 197-206.

Use of Nondestructive Assessment in Plantation Trials of Tropical Trees

I.Z. Siregar, S. Andini, D. Worabai, P. Pamoengkas, S.W. Budi, L. Karlinasari
Bogor Agricultural University (IPB)
Kampus IPB Darmaga, Bogor 16680, Indonesia

Abstract

The relationship between tree growth and wood quality has not become a main concern of silviculturists in plantation management because of the lack of data and information obtained from well-designed trials, especially in Indonesia. In tree improvement programs, species and progeny trials are often conducted to assess the performance of individuals from a number of species and/or trees. However, the main assessment is usually focused only on tree growth (height, diameter, volume, and health). Two separate plantation trials of commercially and ecologically important tree species were conducted in West Java—(1) a progeny trial of fast-growing *Maesopsis eminii* at 5 years old and (2) a species trial of slow-growing *Shorea* spp. at 9 years old—with the goal of assessing growth and wood quality based on nondestructive testing of standing trees with samples of 48 and 35 trees, respectively. A negative correlation between a wood quality trait (dynamic modulus of elasticity, MOEd) and a growth trait (tree volume) was observed in *M. eminii* (r = –0.246), whereas no correlation at all was observed in *Shorea* spp. Results from the study could be used to improve the selection criteria in the trials.

Keywords: Tree growth, wood quality, nondestructive test, selection criteria, MOEd

Session 4

Nondestructive Evaluation of Logs

Use of a portable near infrared spectrometer for *Populus sp.* log moisture content and basic specific gravity prediction and log sorting

Guillaume Hans
Faculty of Forestry, University of New Brunswick, Fredericton, NB, Canada, guillaume.hans@unb.ca

Brigitte Leblon
Faculty of Forestry, University of New Brunswick, Fredericton, NB, Canada, bleblon@unb.ca

Rod Stirling
FPInnovations, Wood Products, Vancouver, BC, Canada, rod.stirling@fpinnovations.ca

Joseph Nader
FPInnovations, Forest Operations, Pointe-Claire, QC, Canada, josephnader@vif.com

Paul Cooper
Faculty of Forestry, University of Toronto, Toronto, ON, Canada, p.cooper@utoronto.ca

Armand Larocque
Faculty of Forestry, University of New Brunswick, Fredericton, NB, Canada, larocque@unb.ca

Abstract

Portable sensors are required for quick and nondestructive measurement of wood properties in the field in order to sort the raw material prior to processing and ensure optimal use of the fiber. We used a handheld near-infrared (NIR) spectrometer to estimate moisture content (MC) and basic specific gravity (BSG) of quaking aspen (*Populus tremuloides* Michx.) and balsam poplar (*Populus balsamifera* L.) logs. Partial least square (PLS) regression models were developed to estimate MC and BSG. Specific and general PLS models were established by considering the influence of the following factors: log conditions (frozen and unfrozen wood), species and types of wood (sapwood and heartwood). In addition, MC influences were also considered in the BSG estimation. General model performances were compared to the ones of specific models designed for each factor separately. PLS discriminant analysis was applied to NIR spectra and sorting was performed according to MC, BSG, species and wood type, with respective overall accuracies of 79%, 65%, 98% and 79%.

Keywords: basic specific gravity, discriminant analysis, handheld near-infrared spectrometer, log, MEMS, moisture content, near infrared spectroscopy, partial least square regression.

Introduction

Real-time characterization of wood properties is essential at different stages of the forest value chain to optimize the manufacturing process, reduce the production costs and increase the competitiveness of the sector. Several studies have demonstrated that near infrared (NIR) spectroscopy enables quick and non-destructive assessment of wood properties (see the reviews of Schimleck et al. 2000, So et al. 2004, Tsuchikawa 2007, Leblon et al. 2013). Moreover, the recent emergence of handheld NIR spectrometers allows in-field and on-site evaluation of wood (Geller and Ramani 2005). They have already been tested to measure wood moisture content, density, blue stain and decay as well as Kraft

pulp yield and cellulose content on standing trees and decked logs in mill yards (Hsieh et al. 2006, Downes et al. 2009, Meder et al. 2009, Downes 2011, Hans et al. 2013).

Among the wood properties, moisture content (MC) and the basic specific gravity (BSG) are two of the most important ones, because they affect several wood manufacturing process efficiencies as well as the physical and mechanical properties of the final products (Fujimoto et al. 2007). In this study, we used a handheld micro-electro-mechanical system (MEMS) digital transform spectrometer (DTS) working in the near-infrared (NIR) range (939.5 - 1796.6 nm) to predict MC (% dry basis) and BSG of quaking aspen (*Populus tremuloides* Michx.) and balsam poplar (*Populus balsamifera* L.) logs. Three sources of environmental variation were taken into account in this study: (1) the logs state (model designed for unfrozen and/or frozen logs), (2) the species (model designed for quaking aspen and/or balsam poplar) and (3) the wood heterogeneity (model designed for sapwood and/or heartwood). The surface roughness was assumed to be constant as the surfaces of each log was refreshed using a chainsaw before taking the measurement. Logs with visible decay or blue stain were excluded and the aging of the wood was ignored in this study. These two last parameters should be considered when using the developed models in a mill yard.

Materials and methods

Sample origin

Samples (i.e., wood disks) were collected from fresh green quaking aspen and balsam poplar logs in the mill yard of an oriented strand board (OSB) mill in Meadow Lake, Saskatchewan, in July 2012. Logs (of approximately 480 cm long) were selected to cover a range of different diameters (that are related to the tree age). A total of 47 logs were selected for quaking aspen and 45 logs, for balsam poplar.

Measurement of wood properties

Two 4 cm thick disks (A and B) were cut at the base of each log with a chainsaw. Disks were protected individually with cellophane wrap in order to limit water loss and shipped to the FPInnovations laboratory in Vancouver (British Columbia) where they were kept frozen for further analysis. Disks from group A were used to measure the basic specific gravity (BSG) according to ASTM D2395–07a (2009). Disks from group B were dried in three different steps to reach different moisture content (MC) levels. At each drying step, the samples were frozen back to - 15°C and the fresh weights of the disks were recorded, for both, unfrozen and frozen disks. The dry weight of each disk was determined at the end of the drying process according to ASTM D4442-07 (2009) in order to be able to determine a posteriori MC at each step.

Near-infrared spectroscopy

As both disks A and B of a given log were extracted at adjacent locations, we assumed that the spectra acquired over disks B were representative of disks A. Therefore, NIR spectra were acquired only on disks B. They were collected with a handheld MEMS-based spectrometer (*Phazir*™, *Thermo Fisher Scientific, Wilmington, MA, USA*) working in the spectral range from 939.5 nm to 1796.6 nm with a spectral resolution of 11 nm. The surface of the wood was cleaned up to remove dust with a steel wire brush before scanning. The *Phazir*™ instrument was configured to average 10 spectra for each scan. A total of 6 scans were collected on the transverse section of each disk: 3 on the sapwood and 3 on the heartwood. Unfrozen disks were scanned after each drying step and after letting the samples cool down to the room temperature (20°C). Frozen disks were scanned just after taking them out from the freezer, one by one to keep the surface frozen (-15°C). Measurements were done on the same six locations on the disks at each step.

Multivariate data analysis

The method used in this study to build the models relating the NIR reflectance to the wood properties was the partial least square (PLS) regression (Wold et al. 1983). All the PLS models presented in this paper were significant at $p < 0.001$ (unless otherwise indicated). Two types of models were designed: the general models that integrate and handle the variability generated by different studied sources of variations (log state, species and wood type) and the specific models that were designed separately for each source of variation. The number of samples used to design the specific models was the same as for the general models (182 for calibration and 90 for validation).

The models were built using untransformed raw spectra. Depending on the set of samples selected to establish the calibration and validation models, the value of the parameters used to assess the performances of the model (RMSE, R^2 and RPD) may change slightly. In order to limit this sampling effect, twenty-five iterations of each model were run with a different random sampling at each iteration for the calibration and validation data sets. The RMSE, R^2 and RPD were averaged between the 25 iterations.

Partial least square discriminant analysis (PLS-DA) (Barker and Rayens 2003) was also used to sort the log data among three MC or BSG classes (low ($MC \leq 45\%$; $BSG \leq 0.350$), medium ($45\% < MC \leq 90\%$; $0.350 < BSG \leq 0.400$) or high ($MC > 90\%$; $BSG > 0.400$)) as well as between the two species and the wood types. The percentage of samples correctly assigned by the PLS-DA to their respective category was computed using a confusion matrix. The classification accuracy was measured using the sensitivity, the specificity and the overall accuracy (Altman and Bland 1994a, b, Kuhn 2008).

All the data analysis was conducted using *R statistical computing software V2.15.3* with the *pls* (Mevik and Wehrens 2007) package for PLS regression (orthogonal scores algorithm) and PLS-DA. The *caret* (Kuhn 2008) package was used to compute the confusion matrix.

Results and discussion

Wood property measurements

The range of moisture content (dry basis) varied between 14 % and 83 % for quaking aspen and between 14 % and 139 % for balsam poplar. The range of moisture content variation for quaking aspen falls within the broader MC range for balsam poplar. The basic specific gravity varies between 0.374 and 0.447 for quaking aspen and between 0.305 and 0.401 for balsam poplar. These ranges are complementary to each other and mixing the two species together increases the range of variation of the basic specific gravity (from 0.305 to 0.447 with an overlap between 0.374 and 0.401).

PLS models

Influence of the log state

The RMSE, R^2 and RPD of the calibration and validation models for MC and BSG obtained for the unfrozen logs were slightly better than those obtained for the frozen logs (**tab. 1**). Ice and frost were present at the surface of the frozen wood and modified the weight of the samples when performing the reference MC measurement. NIR spectra are sensitive to the MC of the samples, but not to the variable amount of ice and frost present at the surface of the samples. This explains the RMSE increases from 1 to 2% between the unfrozen and frozen wood models. The RMSE and R^2 were not very different between the temperature-specific models and the general models for the MC and BSG prediction, such as in the study of Hans et al. (2013). General models show that prediction from MC and BSG from frozen and unfrozen wood are leading to similar results. The number of factors used to build the general models was the same than for the temperature-specific models. Using a higher number of factors in the general models might improve its performance since additional factors could help to take into account the variability produced when mixing the two log states in the same model.

Wulfert et al. (1998) already pointed out that the inclusion of temperature through the calibration design in the models results in reasonable predictions (for mixtures of ethanol, water and 2-propanol as well as heavy oil products) but at the cost of an increased model complexity (number of factors) when compared to models without temperature effects.

Table 1: PLS models for moisture content (MC) (in % dry basis) and basic specific gravity (BSG) prediction according to the log state, the species and the wood type (sapwood or heartwood) [(1)].

Factors	Property	Model	Calibration (N = 182)		Validation (N = 90)		
			$RMSE_C$	R^2_c	$RMSE_V$	R^2_v	RPD
Log state	MC	Unfrozen	8.9	0.91	10.0	0.88	2.93
		Frozen	10.2	0.84	11.8	0.78	2.20
	BSG	Unfrozen	0.019	0.69	0.022	0.60	1.60
		Frozen	0.020	0.67	0.022	0.60	1.59
Species	MC	Quaking aspen	7.2	0.78	7.6	0.75	2.03
		Balsam poplar	9.9	0.89	10.8	0.86	2.75
	BSG	Quaking aspen	0.018	0.26	0.020	0.07[(3)]	1.05
		Balsam poplar	0.019	0.35	0.022	0.18	1.11
Wood type	MC	Sapwood	13.5	0.77	15.0	0.69	1.84
		Heartwood	11.5	0.82	12.7	0.77	2.09
	BSG	Sapwood	0.022	0.60	0.024	0.52	1.46
		Heartwood	0.022	0.58	0.025	0.47	1.39
General[(2)]	MC	6 spectra	10.1	0.87	11.1	0.83	2.48
		2 spectra	11.7	0.83	13.1	0.78	2.17
	BSG	6 spectra	0.020	0.66	0.022	0.57	1.55
		2 spectra	0.020	0.66	0.023	0.55	1.51

[(1)]Number of components used in each model is 9. Values presented are an average of 25 iterations for each model using a different random sampling for the calibration and validation datasets each time.
[(2)] General models are based on spectra collected on quaking aspen and balsam poplar and on frozen and unfrozen wood at different MC levels. Each spectrum is an average between heartwood and sapwood spectra (the number of spectra averaged is indicated in each case).
[(3)] All the models are significant at *p-value* < 0.001, except this one which has a *p-value* of 0.0088.

Influence of the species

The influence of the species on the performances of the models is directly related to the standard deviation (and so the variance) of MC and BSG which are almost 4 and 2 times higher for balsam poplar than for quaking aspen, respectively. Yet, the RMSE in **table 1** indicate that the variance of the residuals is slightly higher for balsam poplar than for quaking aspen translating therefore a better absolute fit of the model for the last species. However, the proportion of total variance explained by the model, and therefore the R^2, is higher for balsam poplar than for quaking aspen. The variances of MC (BSG) in the dataset used to build the general model are intermediate (higher) in comparison to the variance of these properties in the dataset used for the specific models respectively. Meanwhile, the RMSE of the general models stay similar to the one obtained for the specific models, explaining the intermediate and higher R^2 obtained respectively for the MC and BSG general models. This is true for both the calibration and validation models. The higher RMSE obtained for balsam poplar than for quaking aspen might be due to the surface roughness which seemed to be generally more important for the balsam poplar, inducing more variability and noise in the data. Similar trends and conclusions were drawn by Schimleck et al. (2001, 2002) who developed general models including 54 different species and specific models for *Eucalyptus delegatensis* and *Pinus radiata* air-dry density prediction. The general model had the highest R^2. They also indicated that the standard error of calibration (SEC) of the general models were considerably higher when the species were mixed together than when they were separated. Kelley et al. (2004) also compared specific and general prediction models for modulus of elasticity (MOE) and modulus of rupture (MOR) of six softwood species. They pointed out that in the general models, the more heterogeneous set of samples tends to increase the number of components needed for a good model, while the relatively wider range of physical properties covered and the larger dataset tends to reduce it. Fujimoto et al. (2007) predicted the air-dried density, MOE and MOR of hybrid larch on two sets of samples: one with a wide range of density variation (400 to

710 kg m^{-3}) and one with a narrow range of density variation (530 to 550 kg m^{-3}). The models designed from the wide density range dataset all showed better performances than the models from the narrow density range dataset.

Influence of the wood type

In comparison with the general model based on the six spectra averages presented above, the performances of the general model based on two spectra averages (used to compare the wood types) are slightly lower (especially for MC). Mora et al. (2011) also showed, for the prediction of MC and BSG of loblolly pine logs that the model performances improved as the numbers of spectra collected and averaged increased from two to eight. Thygesen (1994) also mentioned that the average spectrum between several spectra collected on a wood disk is better correlated with its average basic density than each spectrum separately. The general models give better results for MC and BSG prediction than specific models. This result is not surprising since it is the mean MC or BSG of the entire wood sample (including heartwood and sapwood) which is predicted. For MC, the specific models for heartwood spectra performed better than the ones for sapwood. This result is in agreement with the MC models obtained by Karttunen et al. (2008) over Scots Pine (*Pinus sylvestris* L.), but not with those obtained by Hans et al. 2013 over black spruce logs. It is well known that the sapwood of black spruce has a higher MC than the heartwood, whereas the heartwood MC of quaking aspen and balsam poplar are known to be higher than the sapwood. For BSG, the better predictions obtained from the general model than from the sapwood or heartwood models are also similar to the results reported by Hans et al. (2013) over black spruce log. However, by contrast to Hans et al. (2013), the model for the heartwood was not as good as the one for the sapwood. It is also important to point out that in some cases scans performed on the sapwood of the wood disks correspond to the juvenile and mature woods respectively. It is well known that the mature wood usually has higher BSG than juvenile wood. This might also affect the BSG model, but the influence of juvenile and mature wood is not considered in this study.

PLS discriminant analysis

PLS-DA was applied to the NIR spectra to perform sorting according to MC, BSG, species and wood type. The sensitivity, specificity and overall accuracy obtained from the confusion matrix computed from the PLS-DA results are presented in **Table 2**. The log sorting in three classes of MC and BSG (low, medium and high) lead to a better overall accuracy for MC (79%) than for BSG (65%). This is in agreement with the PLS models results presented above which showed systematically lower performances for BSG than for MC prediction. In both cases (for MC and BSG), the medium classes had lower sensitivity than the two other MC and BSG classes. This means that a substantial fraction of the logs belonging to the medium class were assigned to either the low or high class. This is probably linked to the fact that MC and BSG are continuous variables and that the split between the three different classes is challenging. However, the sensitivity to the low and high classes and the specificities for the three classes were equal or above 77%.

With regards to the log sorting according to the species, samples were correctly assigned to their respective category with sensitivities of 99% and 97% for quaking aspen and balsam poplar respectively. Our overall accuracy of 98% is comparable to the one (94%) obtained by Haartveit and Flaete (2008) who sorted softwood species (Norway spruce, Sitka spruce (*Picea sitchensis* (Bong.) Carr.), and Lutz spruce (*Picea x lutzii* Little)) using PLS-DA (4 factors). Other studies have showed that NIR spectroscopy was a useful tool for species sorting (Gierlinger et al. 2004, Cooper et al. 2011) and that it could also possibly be used to distinguish samples coming from different origins and sites for the same species (Rana et al. 2008). Our good sorting accuracy can be related to the fact that our species were hardwood species., Tsuchikawa et al. (2003) already showed that the Mahalanobis' generalized distance applied to NIR spectra acquired over samples having moisture contents ranging from oven-dried to fully saturated values can more easily sort hardwood species than softwoods species.

Sapwood and heartwood spectra were correctly assigned to their respective category with sensitivities of 82% and 76% respectively. The overall accuracy achieved was 79%. Haartveit and Flaete (2008) classified the heartwood and sapwood of Scots pine and achieved sensitivities of 97% and 94% respectively (and an overall accuracy of 96%) using PLS-DA (5 factors) and NIR spectra from 800 nm to 2250 nm. Sandberg and Sterley (2009) separated heartwood and sapwood of Norway spruce in dry state from orthogonal signal corrected (OSC) 400-2500 nm spectra using PLS regression with an overall performance of 95%. Similarly, Stirling (2013) reported differentiation of heartwood and sapwood in western hemlock (*Tsuga heterophylla* (Raf.) Sarg.), and amabilis fir (*Abies amabilis* Douglas ex J. Forbes) with greater 90% prediction accuracy based on spectra from 350 to 2500 nm (8 factors). Some studies show that the visible spectrum has an important impact on the model and exclusion of the visible region makes the model weaker and increases the number of components required (Sandberg and Sterley 2009). This might explain the lower performance of our model with regards to other studies since the visible part of the spectrum was not included in our analysis.

Table 2: Accuracies of the PLS-DA models for the log sorting according to their moisture content (MC), basic specific gravity (BSG), species and wood type (*).

Sorting factor	Class	N	Sensitivity	Specificity	Overall accuracy
MC	Low (≤ 45%)	120	0.84	0.88	0.79
	Medium (45% < MC ≤ 90%)	120	0.62	0.89	
	High (> 90%)	120	0.91	0.92	
BSG	Low (≤ 0.350)	130	0.91	0.83	0.65
	Medium (0.350 < BSG ≤ 0.400)	130	0.29	0.86	
	High (> 0.400)	130	0.77	0.78	
Species	Quaking aspen	136	0.99	0.97	0.98
	Balsam poplar	136	0.97	0.99	
Wood type	Heartwood	136	0.76	0.82	0.79
	Sapwood	136	0.82	0.76	

(*) The number of components used in each model is 9. Values presented are an average of 25 iterations for each model using a different random sampling for the calibration and validation datasets each time.

Conclusions

Using a handheld NIR spectrometer to scan the wood cross-section, general PLS models capable of handling several sources of variation encountered in field conditions were calibrated and validated.
The results show that the temperature variations, which engender a shift of the water absorption bands, were incorporated successfully in the general model. Predictions from frozen wood were less accurate than from unfrozen wood but were still of good quality. The calibration of the model over frozen wood is crucial for its operation ability all year round. The models designed from data presenting higher MC and BSG variances have higher RMSEs but show better performances in terms of R^2 and RPD than the models built from data presenting smaller variances. General models are capable of predicting both species properties. The average spectra between sapwood and heartwood give the best prediction for the average MC and BSG of the samples. The models based on the average of 6 spectra collected at the surface of the sample give also better results than models based on the average of 2 spectra. Sorting the logs into classes of MC, BSG (low, medium and high) and/or according to the species can be performed using PLS-DA. This sorting of the logs before entering in the production chain could help optimizing the process in the wood product industry and does not increase significantly the complexity of the mill yard management. Sorting of the wood according to the wood type (heartwood and sapwood) can also be performed.

Acknowledgments

The authors thank K. Groves, Z. Pirouz and G. Chow from FPInnovations as well as K. Phung from the University of British Columbia for their help during the experiments. The study was funded by a NSERC Strategic Grant awarded to B. Leblon et al.

References

Altman, D.G., Bland, J.M. 1994a. Diagnostic test 1: sensitivity and specificity. BMJ 308:1552.

Altman, D.G., Bland, J.M. 1994b. Diagnostic test 2: predictive values. BMJ 309:102.

ASTM Standard. 2009. Vol. 04.10, D4442-07, Direct moisture content measurement of wood and wood-base materials.

ASTM Standard. 2009. Vol. 04.10, D2395–07a, Specific gravity of wood and wood-base materials.

Barker, M., Rayens, W. 2003. Partial least squares for discrimination. J. Chemom. 17(3):166-173.

Cooper, P.A., Jeremic, D., Radivojevic, S., Ung, Y.T., Leblon, B. 2011. Potential of near-infrared spectroscopy to characterize wood products. Can. J. Forest Res. 41:2150-2157.

Downes, G.M., Ebdon, N., Hicks, C., Meder, R. 2009. Developing and evaluating a multi-site and species NIR calibration for the prediction of Kraft pulp yield in eucalypts. Southern Forests 72:151.

Downes, G.M. 2011. Developing and assessing a woodmeal calibration for the Polychromix *Phazir*™, Technical Report 212. Cooperative Research Center for Forestry. Australia.

Fujimoto, T., Yamamoto, H., Tsuchikawa, S. 2007. Estimation of wood stiffness and strength properties of hybrid larch by near-infrared spectroscopy. Appl. Spectrosc. 61(8):882-888.

Geller, Y., Ramani, M. 2005. MEMS-Based digital transform spectrometers. Proceedings paper. SPIE – The International society for optical engineering. American Laboratory, November, pp. 19-21.

Gierlinger, N., Schwanninger, M., Wimmer, R. 2004. Characteristics and classification of Fourier-transform near infrared spectra of the heartwood of different larch species (*Larix* sp.). J. Near Infrared Spectrosc. 12:113-119.

Haartveit, E.Y., Flaete, P.O. 2008. Near infrared spectroscopy (NIRS) as a tool for effective classification of wood. Proceedings of the 51st International Convention of Society of Wood Science and Technology, November 10-12, Conception, Chile.

Hans, G., Adedipe, O., Leblon, B., Stirling, R., Nader, J., Haddadi, A., La Rocque, A., Cooper, P. 2013. Monitoring of moisture content and basic density of black spruce logs using a handheld near-infrared spectrometer. Forestry Chronicle (*in press*).

Hsieh, E., Uy, N., Wallbacks, L. 2006. Development of a portable spectroscopic sensor to measure wood and fibre properties in standing mountain pine beetle-attacked trees and decked logs. Canadian Forest Service. Mountain Pine Beetle Initiative – Working Paper 2006-16. pp. 1-33.

Karttunen, K., Leinonen, A., Sarén, M-P. 2008. A survey of moisture distribution in two sets of Scots pine logs by NIR-spectroscopy. Holzforschung 62:435-440.

Kelley, S.S., Rials, T.G., Groom, L.R., So, C-L. 2004. Use of near-infrared spectroscopy to predict the mechanical properties of six softwoods. Holzforschung 58:252-260.

Kuhn, M. 2008. Building Predictive Models in R Using the caret Package. J. Stat. Soft. 28(5):1-26.

Leblon, B., Adedipe, E.O., Hans, G., Haddadi, A., Tsuchikawa, S., Burger, J., Stirling, R. 2013. A review of near infrared spectroscopy for monitoring wood moisture content and bulk density, Forestry Chronicle (*in press*).

Meder, R., Downes, G.M., Ebdon, N. 2009. Experiences in field assessment of Kraft pulp yield in plantation Eucalypts. TAPPI Engineering, Pulping, Environmental Conference, Memphis, Tennessee.

Mevik, B.H., Wehrens, R. 2007. The pls package: principal component and partial least squares regression in R. J. Stat. Soft. 18(2):1-24.

Mora, C.R., Schimleck, L.R., Clark, A., Daniels, R.F. 2011. Determination of basic density and moisture content of merchantable loblolly pine logs by near infrared spectroscopy. J. Near Infrared Spectrosc. 19(5):391-399.

Rana, R., Muller, G., Naumann, A., Polle, A. 2008. FTIR spectroscopy in combination with principal component analysis or cluster analysis as a tool to distinguish beech (*Fagus sylvatica* L.) trees grown at different sites. Holzforschung 62:530–538.

Sandberg, K., Sterley, M. 2009. Separating Norway spruce heartwood and sapwood in dried condition with near-infrared spectroscopy and multivariate data analysis. Eur. J. *Forest Res.* 128:475–481.

Schimleck, L.R., Raymond, C.A., Beadle, C.L., Downes, G.M., Kube, P.D., French, J. 2000. Applications of NIR spectroscopy to forest research. Appita J. 53(5):458-464.

Schimleck, L., Evans, R., llic, J. 2001. Application of near infrared spectroscopy to a diverse range of species demonstrating wide density and stiffness variation. IAWA J. 22(4):415-429.

Schimleck, L., Evans, R., llic, J. Matheson, A.C. 2002. Estimation of wood stiffness of increment cores by near-infrared spectroscopy. *Can. J.* Forest *Res.* 32:129-135.

So, C-L., Via, B.K., Groom, L.H., Schimleck, L.R., Shupe, T.F., Kelley, S.S., Rials, T.G. 2004. Near-infrared spectroscopy in the forest products industry. Forest Prod. J. 54:6–16.

Stirling, R. 2013. Near infrared spectroscopy as a potential quality assurance tool for the wood preservation industry. Forest. Chron. (in press).

Thygesen, L.G. 1994. Determination of dry matter content and basic density of Norway spruce by near-infrared reflectance and transmittance spectroscopy. J. Near Infrared Spectrosc. 2:127–135.

Tsuchikawa, S., Siesler, H.W. 2003. Near-infrared spectroscopic monitoring of the diffusion process of deuterium-labeled molecules in wood. Part II: Hardwood. Appl. Spectrosc. 57(6):675-681.

Tsuchikawa, S. 2007. A review of recent near infrared research for wood and paper. Appl. Spectrosc. Rev. 42:43–71.

Wold, S., Martens, H., Wold, H. 1983. The multivariate calibration problem in chemistry solved by the PLS method. Lect. Notes Math. 973:286-293.

Wulfert, F., Kok, W.T., Smilde, A.K. 1998. Influence of Temperature on Vibrational Spectra and Consequences for the Predictive Ability of Multivariate Models. Anal. Chem. 70(9):1761-1767.

Quantitative Detection of Void Defects in Log Section Based on Ultrasonic Wave Spread Field

Lihai Wang
College of Engineering and Technology, Northeast Forestry University, Harbin, 150040 China
E–mail: lihaiwang@yahoo.com

Shan Gao
College of Engineering and Technology, Northeast Forestry University, Harbin, 150040 China
E–mail: sgao.nefu@gmail.com gaoshan_2000@126.com

Na Wang
College of Engineering and Technology, Northeast Forestry University, Harbin, 150040 China
E-mail: wangna87@yahoo.com

Jingquan Han
School of Renewable Natural Resources, Louisiana State University AgCenter, Baton Rouge, LA 70803, USA
Email：hjingq1@tigers.lsu.edu

Abstract

This study introduced the concept of the ultrasonic propagation field in wood and verified its applicability through experiments conducted on a log disc. A green *Betula costata* log section was used in the ultrasonic propagation measurements. An ultrasonic wave detector (RSM-SY5) was used to measure the ultrasonic propagation time (UPT) on the cross section of the log sample. After the ultrasonic testing was completed on the non-defective log, five man-made cavities with diameters of 4，8，12, 16 and 20 cm were made sequentially in the heart of the same log and utilized in the ultrasonic test. The even UPT values were then approximately outlined as isolines. Based on the UPT isolines, the ultrasonic propagation field in the log disc was simulated using MATLAB software, and the internal cavity was identified by overlapping the ultrasonic wave fields from different directions. The location and size of the internal cavity defect was proven to be effectively determined by overlying the maps of the ultrasonic wave propagation field through a cross section of the wood. The results indicated that the accuracy of detection values for cavity sizes with diameters of 4, 8, 12, 16 and 20 cm were 83.2%, 84.8%, 94.0%, 95.8% and 96.2%, respectively.

Keywords: Ultrasonic wave; propagation field; cavity defect; quantitative detection; log section

1. Introduction

Internal wood decay is a common structural defect in trees, logs, utility poles and construction timber.

Thus, detecting decay in trees and logs can be of great benefit in assessing wood quality and utilizing forest resources. The applicability of ultrasonic radiation, an emerging non-destructive technology, has been widely demonstrated for assessing wood quality and detecting decay. The ultrasonic wave technique for wood quality assessment is based on wave velocity or transmission time measurements in either the radial or tangential direction. The direct transmission technique for ultrasonic measurement in non-destructive wood testing is related to the measurement of the ultrasonic propagation time (UPT). Direct transmission is believed to be the most appropriate ultrasonic testing technique for quality assessment and decay detection in these types of wood. Ultrasonic tomography of the imaging technique, which can provide an image of any discontinuity, is performed with both velocity (travel time) and attenuation as the contrast-producing parameters (Bucur 2003; Li et al.,2011). Through velocity mapping via two-dimensional ultrasonic tomography, severe decay can be visualized and cavities located (Wang et al. 2009; Dvios 2005; Song et al. 2010). Ultrasonic wave propagation in wood depends on the grain direction and the excitation and is associated with the mechanical anisotropy.

As an acoustic nondestructive testing method, ultrasonic measurement has advantages in the evaluation of wood materials. Based on its applicability and efficiency for assessing wood quality and detecting decay, this study aims to investigate the behavior of ultrasonic wave propagation in wood when the wave encounters a cavity or holes. In addition, the applicability of the ultrasonic wave propagation field to quantitatively detecting the internal cavity defects of a log is discussed and demonstrated. Lastly, a reasonable interpretation for the application of the ultrasonic technique to two-dimensional internal decay scanning is provided.

2. Theoretical Considerations

For the direct transmission technique of ultrasonic measurement, an ultrasonic pulse is transformed from an electronic signal, travels through the specimen and is received by receiver; the pulse is then transformed back into an electronic signal, which can be visualized on an oscilloscope. The time delay, defined as the time that elapses between the emission and reception, is measured on the oscilloscope over the path length of the ultrasonic signals. If one assumes that the wave surface of a sound source transmits along a specific direction and is conveniently detected by the sensor in its propagation area, then overlaying the waves from different directions can yield a packet of ultrasonic wave points at its typical wave surface if the sound source has a limited area (Pellerin and Ross, 2002). Based on the Huygens theorem, the wave packet transmits along each direction, but the velocity vector coordinates only with the phase vector. A sound wave is introduced and spread around; each point of the wave surface in the medium can be taken as a sub-wave source of the secondary spherical wave. Therefore, when an ultrasonic wave transmits in timber, a wave surface will emerge from the sound source along the direction of the velocity vector. Layers of the wave surface spread apart like the filled curves from the same UPT of the wave to yield ultrasonic wave spread or a propagation field.

During the propagation of an ultrasonic wave, the transmission paths alter when they encounter different media and the spread field curves with regularity and twists due to variations in the acoustic impedance. By comparing this phenomenon with the spread field for ultrasound wave propagation in solid wood, defects can be located. By overlaying the profiles with the alteration curves from different

directions, the defect edge can be infinitely approximated and information, such as the location and size of the defect, can be determined.

3 Materials and method

3.1 Experimental materials and device

The samples were obtained from Fangzheng Forestry Bureau, Harbin (long. 125° 42′~ 130° 10′ E, lat. 44° 04′~ 46° 40′ N), China. A 50-cm-long *Betula costata* log section with a 38-cm diameter was produced from a standing tree. The log section, with both ends coated, was stored at room temperature for two months and was then sawn into 10 cm-thick discs in good condition for use in the ultrasonic measurements. After the ultrasonic measurements were completed on an intact wood disc, the disc was immediately made into a cavity defect wood disc with man-made cavities of five diameters (4, 8, 12, 16 and 20 cm) in its heart. An RSM-SY5 non-metallic ultrasonic detector manufactured by the Wuhan Institute of Rock and Soil Mechanics, Chinese Academy of Sciences, was used for the ultrasonic testing of the wood disc at ~20℃. The ultrasonic measurement system included two ultrasonic probes for wood testing (one was transmitter to launch the ultrasonic wave pulse, and the other was receiver to receive the ultrasonic wave). The instrument parameters for this experiment were as follows: the sensor of the trigger mode by which the data recording system was triggered was automatic and independent of the received signal; the sampling frequency was 30 kHz; the sampling point was 2048 with a sampling period of 1 μs, a pulse width of 100 μs and highest and lowest values of pass filtering of 10 and 1000 kHz, respectively.

3.2 Testing procedure

The ultrasonic testing was performed via grid map measurements. The UPT tests were conducted on the cross section of the wood disc to develop a map of the cross section and verify the ultrasonic propagation field in the wood. The center of the cross section of the disc was labeled (0,0,0), and the disc was marked with 4×4-cm grids on the top surface (Figure 1). Four points, located 1 cm below the cross section around the trunk where the bark had been removed, were designated in even intervals and numbered using #1, #2, #3 and #4, successively, as the starting points to fix the transmitter for launching the ultrasound wave. The coordinates of the starting points were as follows: #1, (x,y,z)= (0,−16,−1); #2, (x,y,z)= (−16,0,−1); #3, (x,y,z) =(0,16,−1); and #4, (x,y,z)=(16,0,−1). The receiving probe (the receiver) was taped into each grid intersection and pointed toward the launch probe (the transmitter) with a 45° inclination to the disc surface. In addition, the UPT between the two probes was measured. Immediately after completing all grid intersection ultrasonic tests matching the #1 interval on the non-defective disc, similar tests were performed on the defect disc with the various man-made cavities. For the cavity disc tests, the launch probe was first placed at point #1 (see figure 1) with a receiving probe at each grid intersection to obtain the experimental data. After the point #1 test, the launch probe was sequentially moved to points #2, #3 and #4 with the receiving probe at each grid intersection to perform the test using the same procedure.

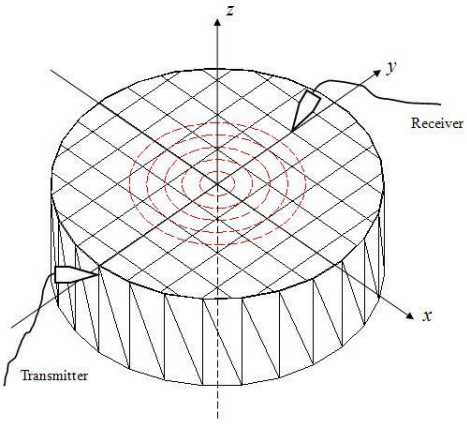

Figure 1-a Schematic diagram of the UPT tests on the thick wood disc

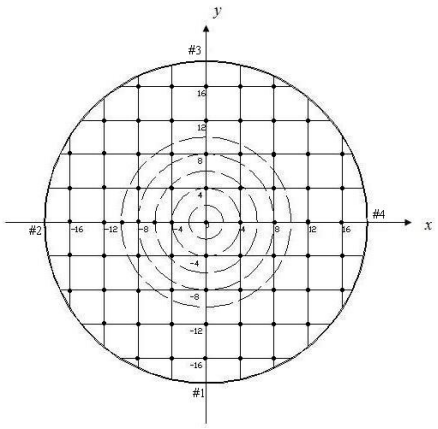

Figure 1-b Testing point distribution on a transverse section

3 Results and analysis

3.1 Computed ultrasonic wave propagation field in non-defective wood

Table 1 lists the UPT data measured on a non-defective disc with the transmitter placed at point #1. Sixty-seven tests are ordered by the UPT value. All tested coordinates with approximately even UPT values are lined as isolines with an interval between isolines of 20 μs. According to the testing data, the UPT isolines from point #1 for the non-defective sample were generated using MATLAB software and are illustrated in Figure 2-a. The plate of the curves that fit the isolines (from launch point #1) was simulated via interpolation and is illustrated in Figure 2-b. As previously stated, the cures plate that yields the UPT isolines distribution was defined as the propagation field of the ultrasonic wave.As illustrated in figure 2-a, launch point #1 is a sound source. The ultrasound wave was launched and spread apart. The overall wave propagation was symmetrically distributed with the line x=0 (Figure 2-a) and maintained its propagation tendency. The curvature of the plots continually increased due to the difference between the waves velocities in the radial and tangential directions. The ultrasonic wave propagated more rapidly in the radial direction than in the tangential direction, verifying the analysis of the propagation field provided in the theoretical portion of this study.

Table 1—UPT values in a non-defective log section with launch probed at point #1

Receiving probe location coordinates	UPT (10^{-6} s)	Receiving probe location coordinates	UPT (10^{-6} s)	Receiving probe location coordinates	UPT (10^{-6} s)	Receiving Probe location coordinates	UPT (10^{-6} s)
(8,−16)	145	(−4,−8)	153	(0,0)	182	(4,8)	280
(4,−16)	103	(−8,−8)	173	(−4,0)	212	(0,8)	260
(0,−16)	78	(−12,−8)	201	(−8,0)	228	(−4,8)	280
(−4,−16)	102	(−16,−8)	276	(−12,0)	255	(−8,8)	281
(−8,−16)	150	(16,−4)	266	(−16,0)	271	(−12,8)	293
(−12,−12)	189	(12,−4)	235	(16,4)	308	(−16,8)	321
(−8,−12)	164	(8,−4)	196	(12,4)	286	(12,12)	339

(−4,−12)	138	(4,−4)	180	(8,4)	265	(8,12)	327
(0,−12)	95	(0,−4)	153	(4,4)	250	(4,12)	314
(4,−12)	132	(−4,−4)	184	(0,4)	229	(0,12)	299
(8,−12)	166	(−8,−4)	203	(−4,4)	244	(−4,12)	315
(12,−12)	190	(−12,−4)	228	(−8,4)	246	(−8,12)	326
(16,−8)	265	(−16,−4)	254	(−12,4)	269	(−12,12)	338
(12,−8)	201	(16,0)	282	(−16,4)	295	(4,16)	351
(8,−8)	173	(12,0)	256	(16,8)	326	(0,16)	345
(4,−8)	155	(8,0)	238	(12,8)	299	(−4,16)	349
(0,−8)	126	(4,0)	216	(8,8)	287		

3.2 Impact of cavity size on the ultrasonic wave spread

Based on the testing data for the cavity defect disc, the distribution of the UPT isolines generated from point #1 is illustrated in Figure 3-a, b, c, d and 3-e with corresponding cavity diameters of 4，8，12，16 and 20 cm, respectively .The layout of the ultrasonic wave propagation field in the defect disc sample differed significantly from that of the non-defective sample (Figure 2-a). Figure 3 indicates that the size of the cavity defect had a significant impact on the ultrasonic wave propagation path and led to a different form of propagation field. When the ultrasonic wave propagated along the x=0 direction at the cross section of the log, the UPT isolines demonstrated a tendency toward inward contraction close to y=0 before the wave passed through cavity in the center. Because the wave had already passed through the cavity, the isoline curves extended in the inverse direction, indicating that the radial velocity of the wave propagation decreased when the wave bypassed the center cavity, but the tangential velocity increased. When observing the entire propagation field, a “lagging behind” phenomenon was found to be led by the cavity. The increases in the UPT time were caused by changes to the propagation path of the ultrasonic wave due to the encountered cavity. As the diameter of the cavity increased, the “lagging behind” phenomenon became more and more remarkable. The degree of curvature for the isolines behind the cavity increased, and the value of the radial transmission time increased as the diameter increased.

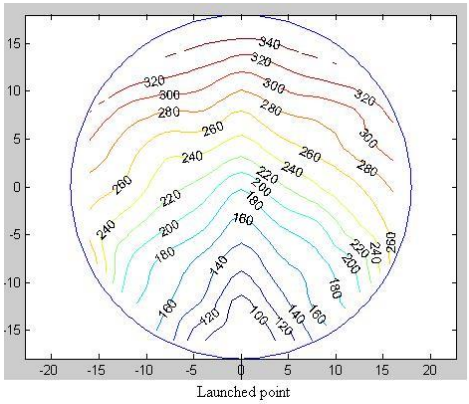

Figure 2- a UPT isolines of the ultrasonic wave in a non-defective disc

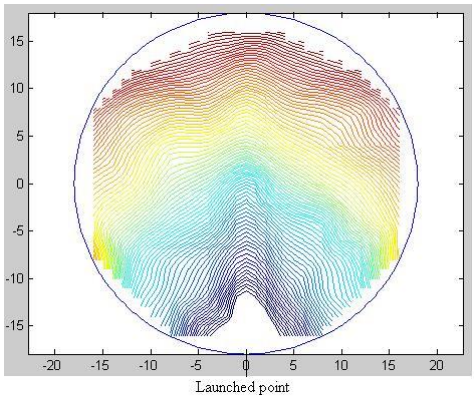

Figure 2-b Simulated propagation field of an ultrasonic wave in a non-defective disc

3.3 Identifying the two-dimensional defects using the wave propagation field

The defect information can be reflected by the superimposed image in various directions to intuitively determine the position, size and shape of the defect in a simple. Therefore, a two-dimensional image of a cavity in a log section was identified by overlaying the ultrasonic wave spread field, which was composed of isolines generated from four different propagation directions (Figure 3). The UPT test data were programmed into images of the wave propagation fields launched from points #1, #2, #3 and #4 using MATLAB software. The two-dimensional identification images for the five types of hole diameters are illustrated in Figure 3-a, b, c, d and e, respectively. The defect information was obtained by overlaying the propagation fields from the different launch points. In the log section with a cavity diameter of 12 cm for example (figure 3-c), the grid lines crisscross in the center of the log cross section to mark the location of the defect or cavity. The defect regions were identified by imposing the distorted propagation field that occurred when the ultrasonic wave encountered a void, hole or cavity. Therefore, the defect boundary can be identified by determining the curve boundary of the deformation field for the ultrasonic wave propagation in each direction.

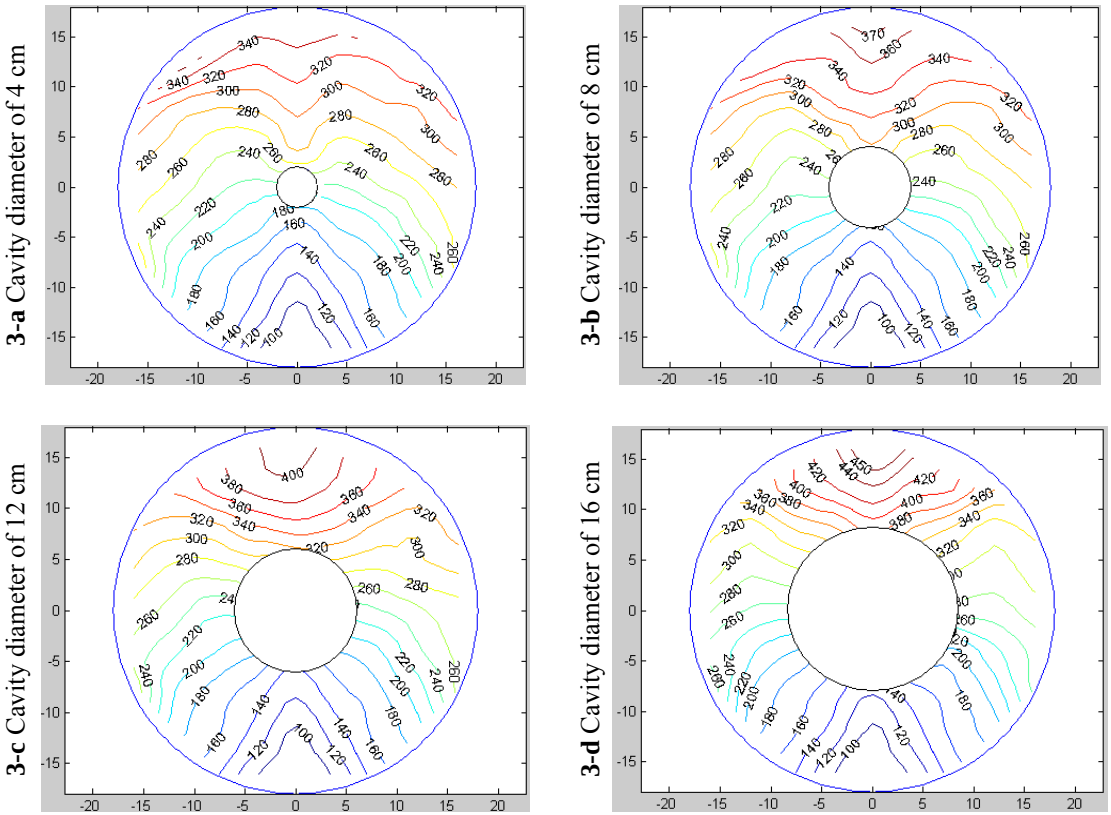

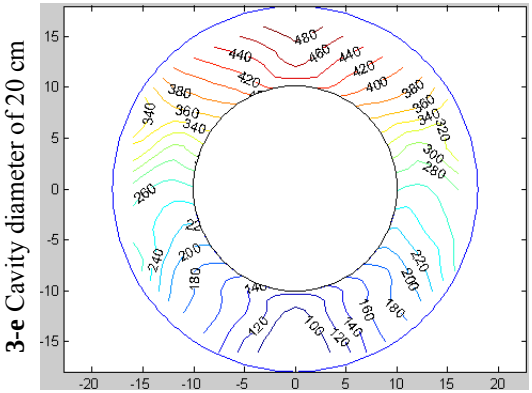

Figure 3—Simulated isolines of the UPT in a log with different sizes of man-made cavities

In contrast to the wave propagation field of the non-defective log, the intermediate point of the deformation curve for the ultrasonic propagation in a defective disc was selected as the edge of the defect area. The defect area of a cavity was outlined by linking the edge points for each propagation direction. Consequently, the size and location of the defect were successfully identified. The ultrasonic wave propagation filed was theoretically explained by the series depicted in figure 4. To quantitatively analyze the accuracy of this identification method, the error of estimation was analyzed by comparing the actual size of the cavity with that detected by applying the ultrasonic wave propagation field. The term S_0 represented the estimated area of the cavity detected, while S_1 represented the actual area, and Δ represented the error of estimation for the cavity. The formula used to calculate the error of estimation is as follows:

$$\Delta = \left| \frac{S_1 - S_0}{S_1} \right| \times 100\%$$

The degree of accuracy in the prediction can be derived as follows:

$$\Delta_0 = (1 - \Delta)\ (\%)$$

For each cavity diameter, Δ_0 is listed in Table 2. As the size of the cavity defect increased, the prediction became more accurate. The accuracy of the detect results was much greater (over 90%) for cavities with diameters over 12 cm, proving that the ultrasonic wave propagation field provided an adequate method for identifying the cavity defect area and providing a rough sketch, and, in a sense, interpreting the law of ultrasonic wave propagation in a cavity defect log.

Table 2— Comparison of the actual and predicted defect areas

Cavity diameter d/cm	Predicted defect area S_0/cm^{-2}	Actual defect area S_1/ cm^{-2}	Error △/%	Degree of accuracy $\triangle_0$/%
4	14.69	12.57	16.8	83.2
8	57.89	50.24	15.2	84.8
12	106.31	113.10	6.0	94.0
16	192.62	201.06	4.2	95.8
20	326.61	314.15	3.8	96.2

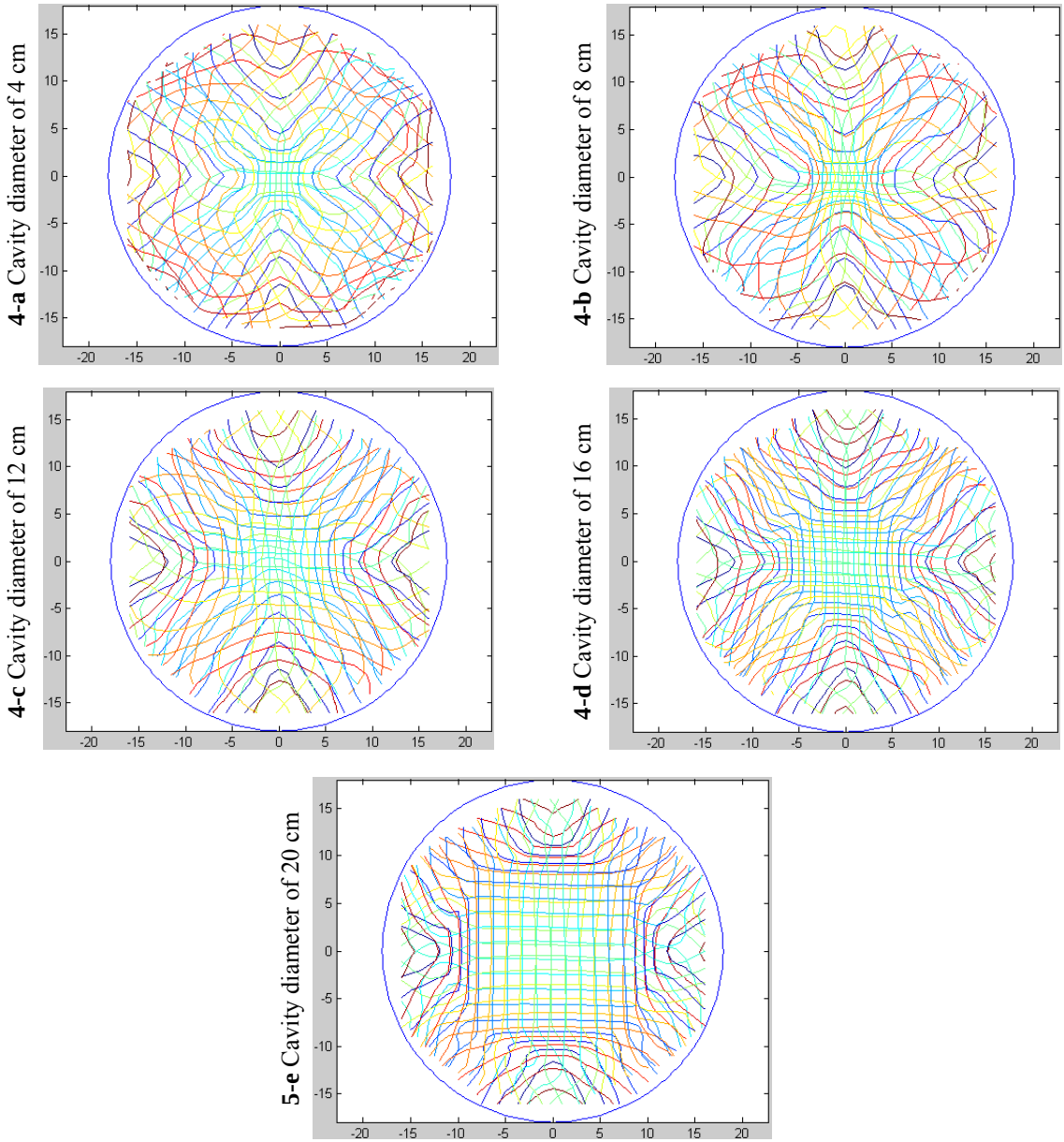

Figure 4—Image created by overlapping the ultrasonic wave propagation field in a log section with cavities of different diameters

4 Conclusions

This study introduced the concept of the propagation field of an ultrasonic wave in a log and verified its applicability for detecting cavity defects. The conclusions can be stated as follows:

1) The ultrasonic wave field composed of UPT isolines was simulated and the location, size and boundaries of the cavities were successfully identified by overlaying the ultrasonic wave fields generated from individual sound resources. 2) The UPT isolines were symmetrically distributed along the ultrasonic wave propagation path. Behind the cavity defect, a tendency toward inward contraction was observed, and the curve was higher on its two ends, but lower in the middle. The entire propagation field exhibited a “lagging behind” behavior initiated when it encountered the cavity. 3) Based on the concept of an ultrasonic propagation field, the detection accuracy for cavities with diameters of 4, 8, 12, 16 and 20 cm was 83.2%, 84.8%, 94.0%, 95.8% and 96.2%, respectively. The

degree of accuracy for the cavity identification increased with increasing cavity size. Highly accurate detection results (above 90%) were obtained for cavities with diameters over 12 cm.

Acknowledgements

This study was supported by the China Special Research Funding Program for Forestry Public Service Sector (Grant No. 201104007) and supported in part by the Fundamental Research Funds for the Central Universities (Grant No. DL12BB31). The authors thank Mr. Shiquan Song for his assistance with the testing.

References

Bucur V.2003.Nondestructive characterization and imaging of wood. Springer, Berlin, Heidelberg, Germany

Bucur V. 2005.Ultrasonic techniques for nondestructive testing of standing trees. Ultrasonics. 43(4): 237-239

Divos F.,P. Divos. 2005.Resolution of Stress Wave based on Acoustic Tomography. Proceedings of the 14th International Symposium on Nondestructive Testing of Wood. Eberswalde, Germany, 309-314

Gao S, Wang X, Wang L, Allison RB.2012.Effect of temperature on acoustic evaluation of standing trees and logs: Part 1 – Laboratory investigation. Wood and Fiber Science, 44(3):286-297

Li L.,X. Wang, L. Wang, R.B. Allison. 2011.Acoustic Tomography in Relation to 2D Ultrasonic Velocity and Hardness Mappings. Wood Science and Technology. (DOI10.1007/s00226-011 -0426-y)

Pellerin F R, Ross J R. 2002.Nondestructive evaluation of wood [J]. Forest Products Society, 135-149.

Wang X .2011. Fundamentals of acoustic measurements on trees and logs and their implication to fiel d application. Pages 25-33 in F Divos, ed. Proc 17th International Nondestructive Testing and Evaluat ion of Wood Symposium, September 14-16, 2011, Sopron, Hungary. University of West Hungary, So pron, Hungary.

Wang X.,J. Wiedenbeck, S. Liang. 2009. Acoustic Tomography for Decay Detection in Black Cherry Trees. Wood and Fiber Science. 41(2): 127-137

Wiedenbeck J, Wiemann M, Alderman D, Baumgras J, Luppold W .2004. Defining hardwood veneer log quality attribute. Gen Tech Rep NE-313. USDA Forest Service, Northeastern Research Station. p 36

Moisture content above fiber saturation point estimated by an acoustic method in freshly cut Radiata pine logs

Andrés Dieste
Forest and Wood Technology Research Centre (CETEMAS)
Finca Experimental "La Mata"
Grado 33820 – Spain
andres-dieste@adinet.com.uy

Laura González
Forest and Wood Technology Research Centre (CETEMAS)
Finca Experimental "La Mata"
Grado 33820 – Spain
lgonzalez@cetemas.es

Abel Vega
Forest and Wood Technology Research Centre (CETEMAS)
Finca Experimental "La Mata"
Grado 33820 – Spain
avega@cetemas.es

Vanessa Baño
Forest and Wood Technology Research Centre (CETEMAS)
Finca Experimental "La Mata"
Grado 33820 – Spain
vbanho@cetemas.es

Abstract

Fresh cut pine logs (Pinus radiata) destined for impregnation were left to dry under atmospheric conditions in Tineo, Northern Spain. The logs were periodically weighed and their acoustic velocity was measured using a Director HM-200 (Fibre-Gen, New Zealand). When the logs reached and estimated moisture content (MC) of approximately 30%, samples were cut to obtain the dry density and the moisture content by gravimetric methods. The MC throughout the experiment was then calculated. A linear regression model was constructed using the MC as dependent variable and the acoustic velocity and the average ambient temperature on the day of measurement as independent variables (R^2=0.661). - Following this methodology, logs with with an acoustic velocity over 4.5 ms-1 were considered safely below FSP. Due to its simplicity, the method is particularly useful to predict the MC in logs above fibre saturation point

Keywords: *Pinus radiata*, moisture content, FSP, acoustic velocity

Introduction

In any managed pine plantations (Pinus radiata), small diameter logs are regularly obtained from thinnings. A common use of this material, once mechanically rounded, is the construction of fences (Ranta-Maunus 1999). Since the natural durability of pine is low, the roundwood is usually treated with wood preservatives. To accomplish good levels of product retention, the logs should be previously dried, ideally below fibre saturation point (FSP) (James W., 1986). Above FSP cells contain free water, resulting in the following problems during impregnation: 1) either more time or more pressure is required to remove the existent free water to reach the same levels of wood preservative retention; 2) the water present in the wood dilutes the impregnating solution, causing a degradation of the product; 3) incomplete drying causes the release of stress in wood after impregnation, with the consequent dimensional stability problems, causing deformations and cracks (Walker J.C.F., 2006).

However, the determination of the moisture content (MC) of the logs presents a technological problem. Logs are usually left to dry under natural conditions in piles. Therefore, it is necessary to determine the MC without incurring in large costs which the sale of the final product will not recoup. The use of hygrometers based on electrical properties is not practical: the moisture content of the logs is well above the measurement range of this equipment. Furthermore, the determination would be punctual and several measurements would therefore be necessary to establish average MC. Acoustic technologies are commonly used for determination of physical and mechanical properties in wood. Several studies have been carried out to establish the relationship between acoustic emissions and drying of lumber and moisture content (Bucur 2006). Easy –to-use techniques based on acoustic technologies are widely accepted in forest technology processes.

The acoustic wave propagation generated by a mechanical impact is readily measurable in a pile of logs. By applying an impact on the surface of the wood three types of wave are generated: longitudinal, shear and surface waves. The longitudinal wave, which travels parallel to the grain, is the most commonly used in wood characterization since it is the fastest and easiest to detect (Wang X., 2011). Wave velocity is determined from the natural longitudinal frequency of vibration of the system: the responses of vibration are represented in the time domain and, using the fast Fourier transformation (FFT), are converted into a function of response of frequency (FRF). This function shows the different peaks of frequency corresponding to the modal shapes of vibration. The natural frequency of vibration is obtained by selecting the peak corresponding to the longitudinal mode of vibration. From this value and the length of log, the wave velocity is calculated (Eq. 1).

$$v = 2Lf \tag{1}$$

where v is the acoustic velocity in logs (ms-1), f is the longitudinal natural frequency of vibration (Hz) and L is the log length (m).

Several authors have used tools based on acoustic emission techniques for the control of the drying process in wood and to assess the effects of MC on wave velocity in wood products (Han et al., 2006, Pellerin et al., 2002). Most of the investigations have been carried out within the hygroscopic range, that is, below FSP. However, it is relevant to study the effect of MC on stress wave velocity above FSP. Gerhards (1975) showed that there is a marked increase in wave stress velocity when wood reaches FSP, attributable to the interaction of water with wood. For Radiata pine boards Moreno Chan et al. (2011) reported that a large portion of the variance of acoustic velocity was due to MC and temperature. Furthermore, they established this relationship above and below FSP.

The objective of this study is to determine the MC in logs above the FSP using acoustic methods based on the longitudinal transmission of wave of vibration.

Materials and methods

Fresh cut 15 year-old pine logs (Pinus radiata) from Northern Spain, destined for vacuum-pressure impregnation with wood preservatives were obtained from thinnings of local plantations. The objective MC) before treatment was in the range of 30%. Length and diameter of each log were measured. Two sets of 15 logs were selected, one in August and the other in November, free of defects and with a similar knot distribution. The logs were sorted by the apical diameter, according to the following classification: 10-14, 15-18 y 19-22 cm. Accordingly, each class had five logs. To study the effect of the season on the drying rate, one set of fresh cut logs was left to dry at ambient conditions from August 2010 to May 2011 and another set from November 2010 to August 2011. Throughout the experiment the velocity of an acoustic wave was measured in the logs using a Director 200 (Fibre-Gen, New Zealand). The sensor of the equipment was pressed against one end of the log and the wood at this same end was hit with a hammer. The acoustic signal travelled through the log and was picked up by the equipment, thus obtaining the time of travel. Using the length of the log, the acoustic velocity was then calculated. The average temperature of the day of the measurement was obtained from weather data (SERIDA, Spain). The MC was determined at least once every month by weighing the logs using a portable balance (PCE-CS 1000, Spain, precision 0.01 g) (Eq. 2).

$$MC_e = \frac{m - (V * \rho)}{V * \rho} \times 100 \tag{2}$$

where MC_e is the estimated moisture content; V is the volume; ρ is the dry density (MC=0%) of Radiata pine obtained from the literature (420 kg m^{-3})

Once MCe was approximately 30%, samples were sawn from the logs, dried to constant mass, and the average MC and dry density was determined for each log. A linear regression model was constructed using the MC as dependent variable and the acoustic velocity, temperature and dry density as independent variables (Eq. 3).

$$MC = \beta_0 + \beta_1 v + \beta_2 t + \beta_3 \rho + u \tag{3}$$

where MC is moisture content; v is the acoustic velocity (ms-1); t is the temperature (°C); ρ is dry density (kgm-3); β0, β1, and β2 are regression coefficients; and u is the error:

$$u = \sqrt{\frac{\sum e_i^2}{n-2}} \tag{4}$$

where ei = Yi - Ŷi

Following Moreno Chan (2011), the variable MC was transformed to its logarithm to achieve a better fit. Values of acoustic velocity below 2.5 ms-1 were attributed to failed measurements and were not considered in the regression model. Outliers were defined as those values higher or lower than three standard deviations from the mean. The resulting data, obtained from343 measurements, was randomly divided into two groups: one set (n=173) was used to construct the model and the other (n=170) to validate it.

The minimum sample size for the regression analysis, considering α=0.05; power=0.8 and f²=0.35 (Eq. 5), was determined to be 34. The number of data points obtained was sufficient, following the criteria presented by Cohen (1992).

$$f^2 = \frac{R^2}{1-R^2} \tag{5}$$

where R^2 = squared multiple correlation of the variables considered

Results and discussion

As expected, it was observed that acoustic velocity decreased with lower moisture content (Figure 1). There was a high negative correlation between MC and acoustic velocity (r= -0.799), which was not found either for ambient temperature (r= -0.322) or for density (r= -0.4823).

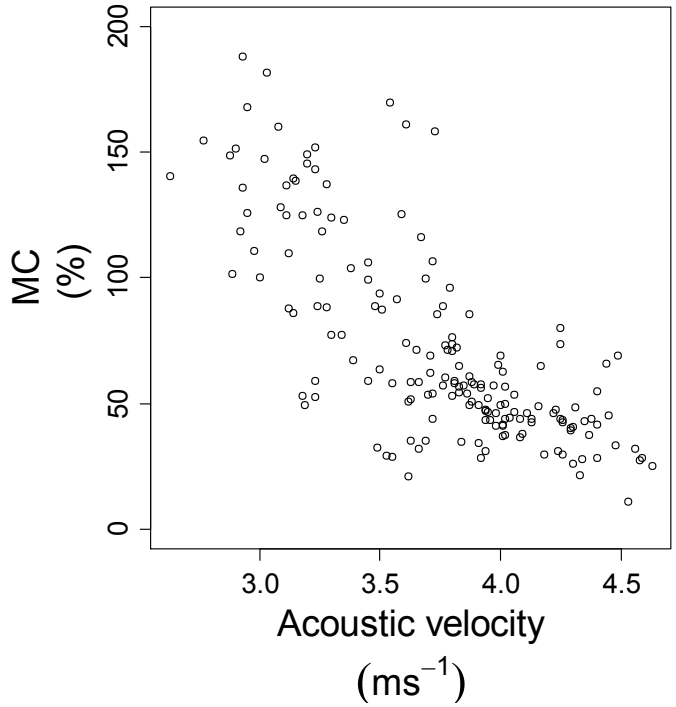

Figure 1— Acoustic velocity versus moisture

Table 1—Linear regressions of LOG10MC as function of acoustic velocity (ms-1), temperature (°C) and dry density (kgm-3). All parameters were significant at p>0.05

Nr.	Equations	n	R²
5	$LOG_{10}MC = 322.2200 - 66.8100v$	171	0.572
6	$LOG_{10}MC = 3.3362 - 0.3830v - 0.0071t$	155	0.661
7	$LOG_{10}MC = 4.174 - 0.327v - 0.0105t - 0.0025\rho$	154	0.726

It was observed that the best model was Eq. 7, which included acoustic velocity, temperature and dry density as independent variables. However, density is not a simple variable to measure since it requires the extraction of samples to process in a suitable laboratory. Therefore, from a practical point of view the most efficient model is the one that includes acoustic velocity and ambient temperature (Eq. 6). Although its R² is lower than for Eq. 7, both variables are easy to measure in the field, rendering a useful estimate

of the moisture content of the logs. At 20°C, 4.5 ms-1 of acoustic velocity predicts an MC of 29.5%, with a confidence interval (α=0.05) between 26.3 and 33.1%. Therefore, every log with an acoustic velocity over 4.5 ms-1 can be considered dry enough for impregnation.

The analysis of the residues allowed the normality and homoscedasticity of model Nr. 6 to be checked (Figure 2)

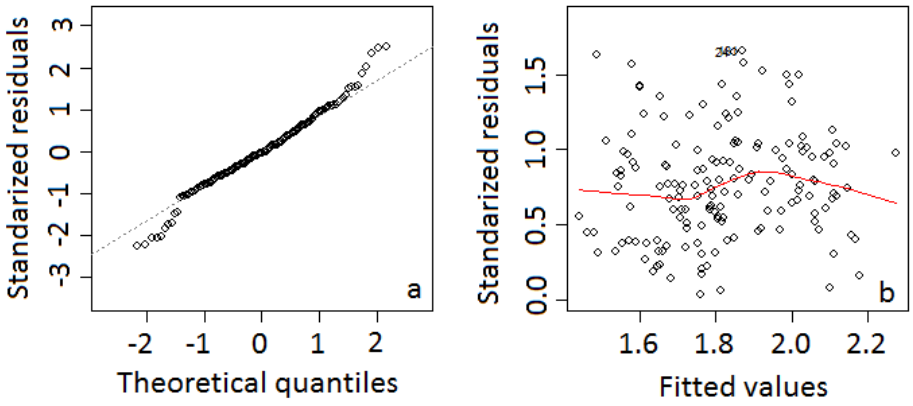

Figure 2—Analysis of residues of linear regression model for the dependent variable LOG10MC: a) normality of the residues; b) heteroscedasticity of the residues

The models were validated, using the subset selected for this purpose, through a cross-validation, equal to Ra2-Rb2.Ra is the correlation between observed and predicted values of the regression subset and Rb is the correlation between observed and predicted values of the independent subset selected for the validation. Cross-validation rate were less than 0.1; therefore, the model obtained was considered reliable (Table 2).

Table 2—Model cross-validation

Model	R_a^2	R_b^2	$\lvert R_a2\text{-}R_b2\rvert$
$LOG_{10}MC = 3.3362 - 0.3830v - 0.0071t$	0.661	0.627	0.034

Conclusions

The use of acoustic velocity to predict the *MC* in logs in a range well above the *FSP* is a reliable technique. Clearly, there is a marked increase in acoustic velocity when the *MC* approaches *FSP*. This represents an advantage over other methods of measuring the MC based on the electric properties of wood, since these are only accurate below *FSP*. Furthermore, the Hitman Director 200 is a portable, easy-to-use tool, which measures *MC* indirectly throughout the log simply by accessing one of the log extremes. In compact log piles, this is a remarkable advantage.

References

Carter, P.; Briggs, D.; Roos, R.; Wang, X. 2005. Acoustic testing to enhance Western Forest values and meet customer wood quality needs". In: Harrington,C.; Constance, A; Schoenholtz, S (eds), Productivity of Western forests: a forest products focus. 121, U.S. Department of Agriculture-Forest Service.

Cohen, J. 1992. Quantitative Methods in Psychology. A Power Primer. Psychological Bulletin Vol. 112.:155-159

Fuentes-Salinas, M. 2000. Estimación del punto de saturación de la fibra (PSF) de las maderas. Revista Chapingo.Serie ciencias forestales y del ambiente 6 (1):79-81

James, W. 1986. Effect of transverse moisture content gradients on the longitudinal propagation of sound in wood. Forest Products Laboratory - USDA FPL 4668

James, W. 2011. Effect of transverse moisture content gradients on the longitudinal propagation of sound in wood. Forest Products Laboratory - USDA FPL 4668

Ranta-Maunus, A. 1999. Round small-diameter timber for construction. Technical Research Centre of Finland (VTT). pp. 191. Espoo

Torres, A. 2011. Guía buenas prácticas en impregnación de madera. Cooperación Técnica MERCOSUR (SGT6). Alemania. 60 pp.

Walker J.C.F. 2006. Primary wood processing - Principles and practice. Springer. pp. 596. Dordrecht.

Log moisture content determination with quantitative magnetic resonance and magnetic resonance imaging

Clevan Lamason
Faculty of Forestry and Environmental Management, University of New Brunswick, Fredericton, NB, Canada, clamason@unb.ca

Bryce MacMillan
Magnetic Resonance Imaging Research Center, Department of Physics, University of New Brunswick, Fredericton, NB, Canada, bryce@unb.ca

Bruce Balcom
Magnetic Resonance Imaging Research Center, Department of Physics, University of New Brunswick, Fredericton, NB, Canada, bjb@unb.ca

Brigitte Leblon
Faculty of Forestry and Environmental Management, University of New Brunswick, Fredericton, NB, Canada, bleblon@unb.ca

Zarin Pirouz
FPInnovations, Vancouver, BC, Canada, zarin.pirouz@fpinnovations.ca

Abstract

Magnetic resonance (MR) spectroscopy and imaging (MRI) are well established techniques employed to provide valuable information on the distribution and concentration of water in biological samples. They are underutilized in the forest products industry in part because of the high costs involved, the large size of the equipment, and the sophisticated knowledge required to operate and maintain the instruments. Recent developments in MR technology, however, are addressing these limitations. One particular development is unilateral (one-sided) MR. This technique has been utilized for several materials science applications, but its potential still needs to be demonstrated in the forest industry. This paper will highlight our work with nondestructive quantitative moisture content (MC) measurements of black spruce (*Picea mariana* Mill.) logs employing 2 recent MR technologies (unilateral MR and SPRITE MRI) developed at UNB. Preliminary results from freeze/thaw and drying studies of black spruce are presented.

Keywords: Log moisture content, nondestructive testing, magnetic resonance, magnetic resonance imaging, moisture content, SPRITE, unilateral magnetic resonance, freeze/thaw

Introduction

In Canada, forestry and forest products are vital to the health, wealth and growth of the economy. Canada's forest products industry is a 57 billion dollar a year industry that represents 12% of the country's manufacturing Gross Domestic Product (FPAC 2012). However, the Canadian forest industry is in turmoil principally due to high production costs that make it difficult to compete with low cost producers and fast fiber growers. To stay competitive and reduce manufacturing costs, the industry must continue to innovate. In particular, it needs to use fast and reliable analytical techniques to improve product quality

and process optimization. Innovation and process optimization are important at numerous stages of the value chain in the forest products industry. These include harvesting, resource management, pulp and fiber yield assessment, scaling and grading of the wood products.

One of the most important properties to be monitored in any wood process is moisture content (MC). Currently, MC is poorly monitored due to the absence of suitable rapid measurement methods. The methods used in the laboratory, and in industry, are either time consuming or destructive. An ideal alternative would be sensors which allow non-destructive, contact-free and real-time measurement of wood moisture.

There are numerous non-destructive techniques available for measuring wood moisture content (Bucur 2003). These techniques use electromagnetic radiation at various wavelengths, such as ionizing radiation (X-ray and gamma rays), visible (VIS) light, near-infrared (NIR), microwaves, ultrasonic waves and magnetic resonance (MR). X-ray sensors require highly trained personnel in order to properly use the instruments. In addition, measurements of wood moisture content using X-ray images have been shown to be influenced by wood density (Wei et al. 2011). NIR radiation can partially overcome this limitation, but its penetration depth in solid wood is limited, ranging from 1 to 5 mm depending on surface roughness and the wavelength employed (Tsuchikawa et al. 1996). Acoustic systems can be used for measuring log moisture content, but they were found to work only for liquid water, i.e., with ambient temperatures above the freezing point (Nader 2007). Furthermore, the relationship between moisture content and acoustics measurements was shown to vary between species, and within the same species (Nader 2007).

Magnetic resonance (MR) and magnetic resonance imaging (MRI) are well known methodologies for molecular structure determination and medical imaging. In each case, MR measures the quantity of hydrogen containing material in the sample of interest, with secondary information on the molecular dynamics and molecular environment. In the context of wood materials, MR and MRI offer the possibility of non-invasive determination of free and bound water concentration in materials spatially resolved (Casieri et al. 2004, MacMillan et al. 2002).

The UNB MRI Centre has developed a novel approach to handheld magnets that permit ‘spot’ measurements of water content at depths up to at least several centimeters inside the material of interest (Marble et al. 2007). This approach permits a small sensor, exterior to the sample, to survey, as required, a large sample. The Centre also developed a new MRI method that allows measurements of short lifetime MR signal components. This paper presents preliminary results on the evaluation of these recent developments on black spruce (*Picea mariana* Mill.) samples in two studies, namely, a freeze/thaw study and a drying study.

MR and MRI theory

MR is a physical phenomenon in which magnetic nuclei are excited by radio frequency (RF) magnetic fields and then detected by induction. The MR phenomenon occurs at a specific frequency, the resonance frequency, which depends on the strength of the magnetic field and on the magnetic properties of the isotope of the atoms. According to the Larmor equation, the resonance frequency is linearly dependent on both the strength of the magnetic field and a nuclear property known as the gyromagnetic ratio (Liang and Lauterbur 2000).

$$\omega = \gamma B_0 \tag{1}$$

where ω is the resonance frequency also known as the Larmor frequency (MHz), γ is the gyromagnetic ratio (42.58 MHz/Tesla in the case of ^{1}H), and B_0 is the static magnetic field strength (Tesla).

In MR, the term *relaxation* describes specific processes by which nuclear magnetization in a non-equilibrium state returns to equilibrium. Two different time constants characterize the longitudinal (spin-lattice) and transverse (spin-spin) relaxations. Most frequently mentioned, T_1 (spin-lattice relaxation time) is a measure of the time required for a spin system to return to thermal equilibrium with its surroundings (lattice). T_1 governs the recovery of the longitudinal magnetization. T_2 (spin-spin relaxation time) is a measure of the decay time of a transverse magnetization due to spin-spin interactions. T_2^* accounts for the effect of both T_2 decay and magnetic field inhomogeneities (Liang and Lauterbur 2000). The MR signal typically decays exponentially with T_2 and T_2^* which are related to the type of water (bound and free) in wood.

MR and MRI in wood

Several MR and MRI studies on wood have been reported in the literature. Conventional MR and MRI techniques were employed to study wood anatomy and structure (Hall et al 1986, Filbotte et al. 1990), wood decay (Filbotte et al. 1990), and wood preservation (Meder et al. 1999). With respect to MC estimation, these techniques have been used to estimate MC in wood pellets (Nyström and Dahlquist 2004) and in drying lumber (Araujo et al. 1992, Hall et al. 1986, Stenstrom et al. 2009). However, these studies consider relatively wet wood because conventional MRI techniques do not allow measuring low moisture contents as they are not sensitive to short lifetime signal components. In contrast, a new MR imaging technique known as *Single Point Ramped Imaging with T_1 Enhancement* (*SPRITE*) was used by MacMillan et al. (2002) to measure water content of drier wood samples (up to 6% MC). *SPRITE* is a pure phase encode MRI technique that does not require echo formation (Balcom et al. 1996). It employs ramped phase encode magnetic field gradient and brief duration broadband radio frequency pulses, which permits rapid image acquisition of short T_2^* signals, such as those obtained from bound water in wood.

For wood studies, another advantage of MR and MRI techniques is that the MR signal from green wood may be separated into three major components: solid wood, bound water and free water (Araujo et at. 1992). The solid wood signal decays rapidly in tens of microseconds and is not usually observable. The solid wood signal is readily separable from the bound water signal, which has a T_2 from one to a few milliseconds. In contrast, the free water has T_2s ranging from tens to hundreds of milliseconds (Riggin et al. 1979, Araujo et al. 1992, MacMillan et al. 2011).

Experiment

Sample preparation

Freeze/thaw study

Black spruce sapwood sample (2.5 cm x 7.5 cm x 7.5 cm) was prepared from an initially frozen green wood disk. The sample had bark on the outer part. It was initially frozen at approximately -20°C, and then allowed to thaw, during the measurements, at ambient temperature.

For the unilateral magnet measurements, the ambient temperature was 3°C. This was achieved by placing the unilateral magnet and the sample inside an insulated and actively cooled box in order to slow down the thawing process. Measurements were taken continuously until the sample thawed completely. Each sample was wrapped in cellophane, and no significant mass loss was observed over the course of the measurements.

For the freezing study, a 0.3 cm x 2.5 cm x 2.5 cm sapwood sample with no visual defects was prepared from the same ‘green’ wood disk as for the thawing study. The sample was also wrapped in cellophane to

prevent mass loss during the course of the measurements. It was left at ambient temperature for about an hour before the start of the measurements. Sample mass was measured before and after measurements and no significant mass loss was observed. For temperature control, the sample was positioned in a heated/cooled air stream inside a glass transfer line specially designed to fit the geometrical specification of the imaging system. The air temperature was controlled with an Omega (*Omega Engineering, Stamford, CT*) CN6072A-P2 temperature controller, employing a platinum resistance temperature device (RTD) in close proximity to the sample. The air temperature was stable to within ±0.3°C.

Drying study

Wood plugs (6 mm in diameter by 25 mm long) were cut from freshly harvested wood and were used for bulk MC measurements using the bench top 10 MHz permanent magnet *Bruker Minispec* instrument (*Bruker Optic GmbH, Rudolf-Plank-Str. 27, 76275 Ettlingen, Germany*). A 4 cm^3 wood sample was cut for the UM measurements, adjacent to the location where the wood plug was cut.

Samples were conditioned step by step at different MCs in a controlled chamber. The mass of each sample was recorded before and after the MR measurements. At the end, the samples were dried in the oven and the MC (% oven-dry weight) were determined according to ASTM D4442-07 (1999).

MR instruments and associated measurements

Figure 1 shows photos of the magnetic resonance instruments employed in this study. Instrument 1 was employed for the imaging measurements in the freezing study. The imaging measurements utilized the *SPRITE* (Single Point Ramped Imaging with T_1 Enhancement) technique (Balcom et al. 1996) acquired with a 100 MHz *Nalorac* horizontal bore superconducting magnet (*Nalorac Cryogenics Inc., Martinez, CA*). A detailed description of *SPRITE* has been published in Balcom et al. (1996), here we summarize a few relevant features. *SPRITE* is a pure phase encode MRI technique that does not require echo formation. Phase encoding in a *SPRITE* measurement permits observation of signals that are tens or hundreds of microseconds in duration. For a centric scan *SPRITE* image employing a uniform RF excitation pulse flip angle, the signal intensity denoted by S, at any point in the image, is determined by Equation 2 (Halse et al. 2003),

$$S = S_0 \, e^{-t_p/T_2^*} \tag{2}$$

where S_0, is the signal intensity at t = 0 and is proportional to the quantity of observable water, t_p is the phase encode time and T_2^* is the apparent signal lifetime. T_2^* is a function of both the intrinsic transverse relaxation time, T_2, and the local magnetic field inhomogeneity ΔB_0 as shown in Equation 3,

$$\frac{1}{T_2^*} = \frac{1}{T_2} + \gamma \Delta B_0 \tag{3}$$

where γ is the nuclear gyromagnetic ratio. Generally for water in wood, $t_p << T_2^*$ meaning that the *SPRITE* signal intensity does not suffer from T_2^* attenuation and the signal intensity is directly proportional to liquid water content. It is important to point out that T_2^* is long for liquids, but short for solids, so that when water freezes, the signal intensity drops dramatically (according to eq. 2), because $t_p >> T_2^*$. Frozen water, such as ice, will no longer be visible in the image.

The images were acquired in 2D employing the *2D Spiral SPRITE MRI* method (Szomolanyi et al. 2001). The measurements were performed at sample temperatures ranging from -1°C to -100°C. The other acquisition parameters were as follows: number of scans = 32, time between steps = 2 ms, time between

spirals = 500 ms, encoding time = 72 µs, maximum gradient = 24.5 G/cm, FOV = 3.8 cm, r.f. pulse width = 1.0 µs, r.f. flip angle = 8°, total acquisition time = 3.2 min.

Aside from the imaging measurements, instrument 3 (4.46 MHz unilateral permanent magnet) was employed in the thawing study. The MRI method resolves 3D space within the sample whereas the unilateral magnet integrates signal from a finite volume within the sample. Both instruments 2 and 3 produced bulk MC measurements utilizing the Carr Purcell Meiboom Gill (CPMG) method. The CPMG method is a spin echo method consisting of a 90^{o} radio frequency (RF) pulse followed by an echo train induced by successive 180^{o} RF pulses.

The unilateral permanent magnet, designed and developed at the UNB MRI Centre, is a lightweight 3 magnet array (Marble et. al. 2007) which offers open access and portability. The unilateral magnet has a homogenous magnetic field of 1 cm^3 volume located approximately 1 cm away from the top of the magnet. The measurement volume is therefore 1 cm^3 and is located 1 cm from the top of the magnet. Some important parameters employed for the unilateral magnet CPMG sequence were: 90 pulse length = 10µs, scans = 512, number of echoes = 128 and acquisition time is about 5 min.

CPMG decay were fitted to a bi-exponential least-square regression using *SigmaPlot* (*Systat Software Inc., USA*). The decay constant is the T_2 relaxation time. Fitting the decay permits determination of the relative hydrogen content associated with each lifetime. The first short lifetime signal component is related to the bound water and the second longer lifetime signal component is related to the free water. The sum of the two signal populations are then be converted into MCs by using a reference sample of known MC. The reference sample, has 30% MC, is made of a mix of H_2O, deuterium oxide and copper sulfate. The MCs estimated at each drying step employing the 4.46 MHz UM and bench top 10 MHz permanent magnet instrument were correlated to the MCs measured by the ASTM D4442-07 method.

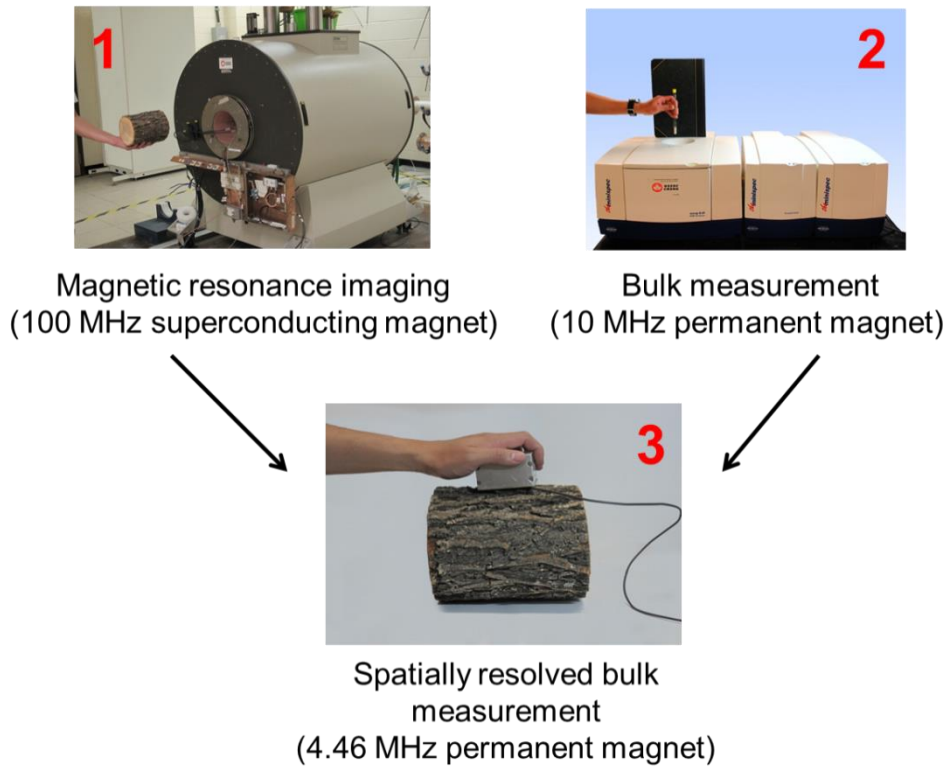

Figure 1 – Magnetic resonance instruments employed. Arrows indicate that #3 utilizes the advantages from #1 and #2.

Preliminary results

Freeze/thaw study

Figure 2 shows the signal intensities acquired by the CPMG method employed by the UM. The total signal increased as the black spruce sapwood sample thaws. Indeed, the liquid water population increases as the sample thaws and the signal intensity is proportional to the amount of liquid water in the sample. Most of the water in the sample is still frozen before 200 min. It is important to note that the UM employed for these measurements has a region of homogenous magnetic field of 1 cm^3 volume that is located approximately 1 cm away from the top of the magnet. This permits excitation and detection of signals inside the sample, but not on the surface of the sample. In the figure, the signal intensity increases after 200 min of thawing. This indicates the start of thawing as the boundary of thawing arose through the sensitive spot (1 cm^3 volume inside the sample). The signal continues to increase after 200 min as the water in the sample melts and the quantity of liquid water increases.

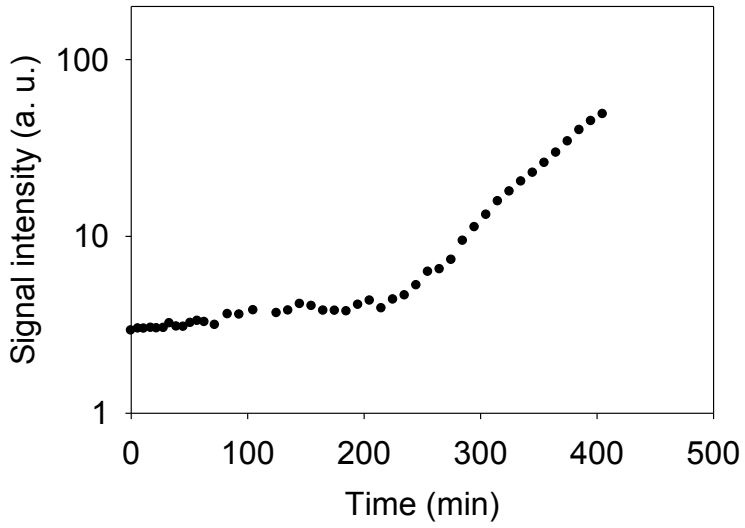

Figure 2 – Semi log plot of signal intensity of the long lifetime components (free water) of the black spruce sapwood as a function of the thawing time. A UM utilizing CPMG measurement was employed. The initial sample temperature was -20°C and the surrounding temperature was 3°C. The ring boundary of thawing arose through the sensitive volume after 200 min.

Figure 3 shows 2D images of a black spruce sapwood sample as it freezes. The images clearly show an abrupt change that occurred when the sample temperature is between -3°C and -5°C. Even at -60°C, the signal is non-zero which means that bound water of this sample is still liquid at this temperature. The 2D images at both -1°C and -3°C temperatures also show distinct signal differences between earlywood and latewood. The signal of the earlywood is twice as high as that of the latewood. The signal difference is associated with the larger size of the lumen of the earlywood tracheids (Panshin and de Zeeuw 1980), which allow them to hold more free water. The *SPRITE* MRI techniques employed determined phase transition of bound water which is otherwise challenging for other techniques, such as the calorimetry based methods.

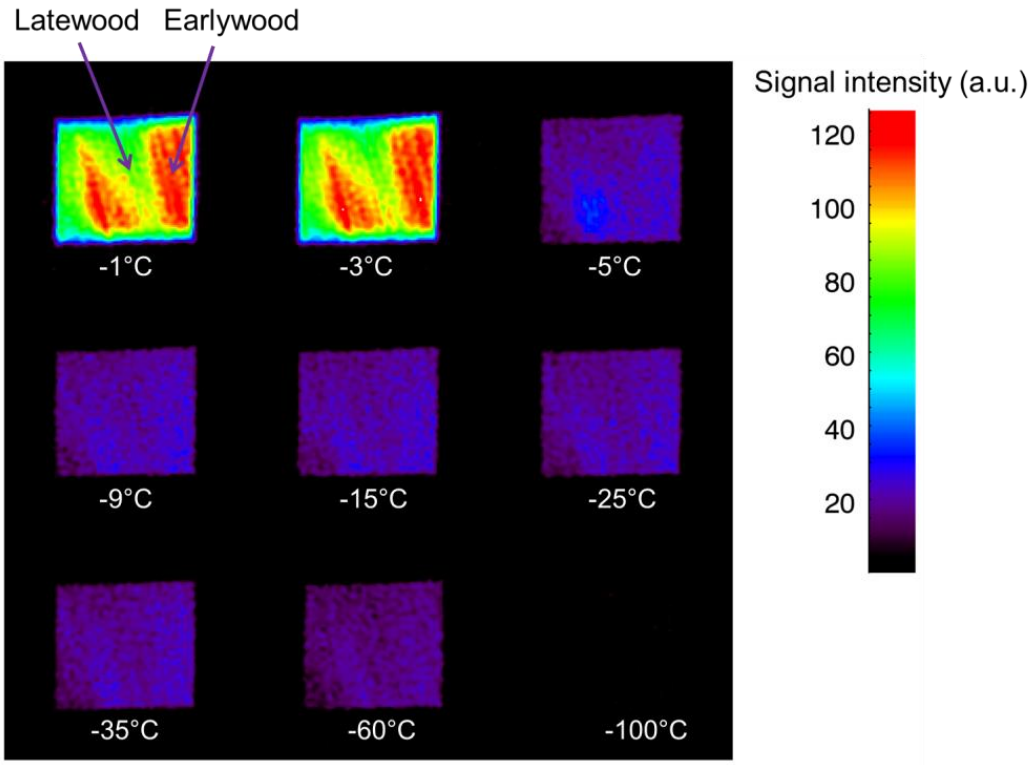

Figure 3 – 2D Spiral *SPRITE* images of a black spruce sapwood sample (2 mm x 25 mm x 25 mm). Each image is 64x64 pixels. High signal intensity corresponds to high concentration of liquid water. Phase transition of free water occurred at -3^{o}C. A nonzero signal for the sample having a temperature ranging from -5 ^{o}C to -60^{o}C suggests that bound water exists in liquid form at these temperatures. Prior to the freezing phase transition of free water, the signal intensity in the earlywood is twice the signal intensity in the latewood.

Drying study

Figure 4 shows that the long lifetime signal intensity of water in black spruce sapwood sample decreases as MC decreases. The MR signal magnitude is proportional to the quantity of liquid water. Figure 4 only considers the long lifetime signal component because the dead time of the RF probe 1 s employed for this particular UM measurement did not allow quantification of short lifetime signals. Thereby, the bound water cannot be quantified and only the free water is quantified.

For the sample of Figure 4, a FSP of 33.3% was determined prior to the UM measurement by employing the 10 MHz bench top permanent magnet instrument. Indeed, this instrument allowed quantification of both short and long lifetime signal components. Therefore, FSP is easily determined by finding the level wherein signal of the long lifetime component is no longer observable and the short lifetime signal component is at its maximum. This occurred at 33.3% MC for the sample of Figure 4.

This FSP value was then used as a benchmark to estimate the MC levels above the FSP. The long lifetime signal component was then converted to MC (above FSP) by utilizing a reference sample with known MC. The resulting MCs as estimated from the UM measurements fits well with the MCs obtained by the gravimetric method (Figure 5). Figure 5 shows a slight overestimation of the gravimetric MCs particularly for low MCs.

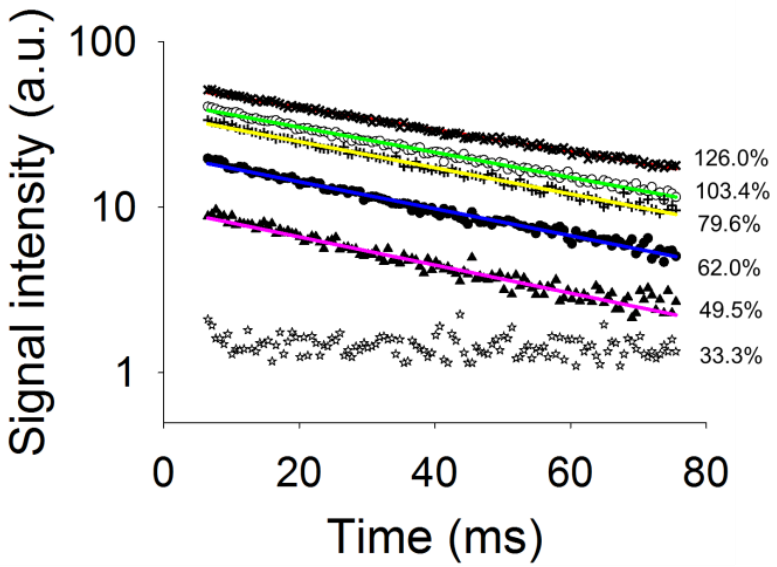

Figure 4 – Semi log plot representing the signal decay of MC of black spruce sapwood employing UM measurements as a function of the estimated MC. The signal intensity decreases as MC decreases. At the fiber saturation point (33.3%) there is no more free water signal. The bound water signal component cannot be observed with the UM device employed.

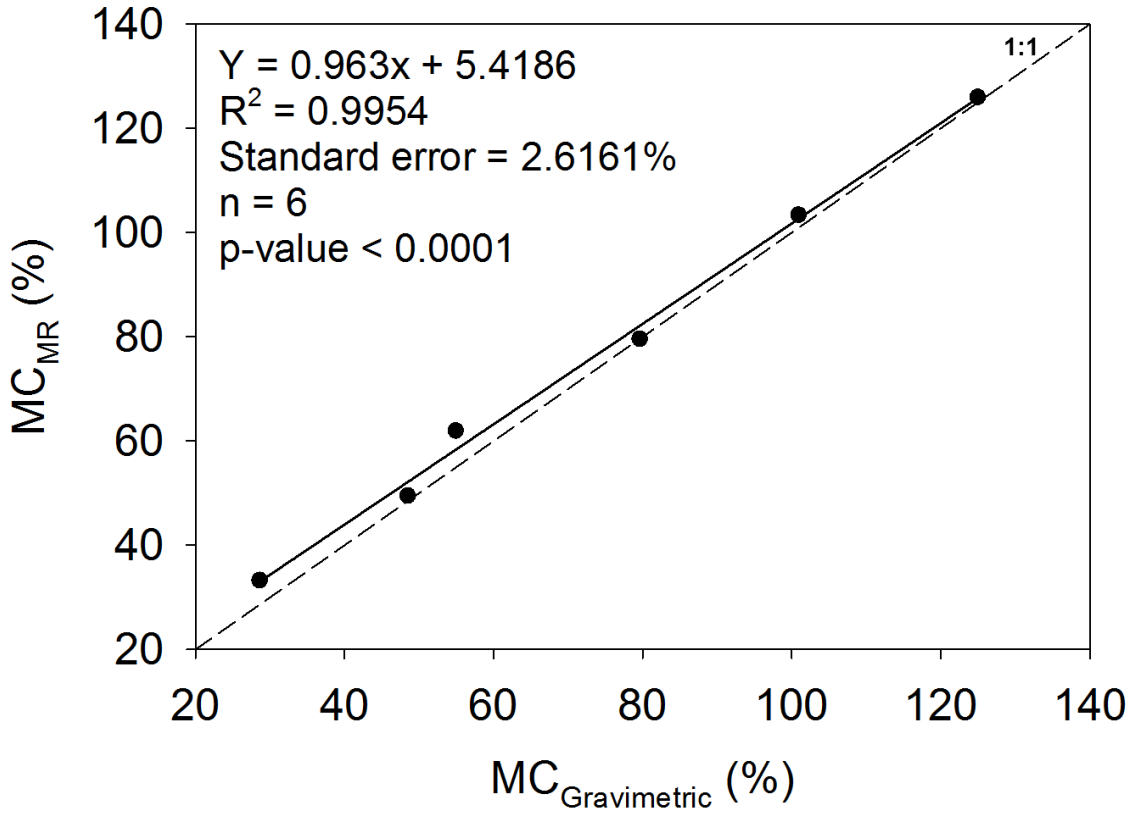

Figure 5 – Comparison between magnetic resonance estimations and gravimetric method MC.

Main findings

We demonstrated the use of unilateral magnetic resonance as a powerful portable tool in monitoring and estimating moisture content in wood samples. The estimation of MC employing the UM above FSP had a good fit with the gravimetric MC, particularly at high MCs.

In addition, unilateral magnetic resonance and *SPRITE* MRI methods can be used to monitor water phase transitions. An abrupt phase transition of free water was observed at -3°C. Unilateral magnetic resonance and *SPRITE* MRI methods allowed measurement of relative quantities of bound and free water in wood. The unilateral magnetic resonance method also allows measurement of water on samples that are not debarked, which is a huge operational advantage. However, MR and MRI cannot measure moisture content of frozen samples because signal from frozen water is undetectable.

Acknowledgments

The authors wish to thank the Natural Sciences and Engineering Research Council of Canada for a Strategic Grant in support of this work. We thank FPInnovations for financial and in kind support. B.J.B. thanks the Canada Chairs program for a Research Chair in MRI of Materials (2009-2016).

References

Araujo, C. D.; Mackay, A. L.; Hailey, J. R. T. [abd others]. 1992. Proton magnetic resonance techniques for characterization of water in wood: application to white spruce. Wood Science and Technology 26:101-113.

ASTM Standard. 2007. Direct moisture content measurement of wood and wood-base materials. Annual book of ASTM Standards, Vol 04.10 D 4442-07. ASTM International. West Conshohocken.

Balcom, B. J.; MacGregor, R. P.; Beyea, S. D. [and others]. 1996. Single point ramped imaging with T_1 enhancement (*SPRITE*). Journal of Magnetic Resonance A, 123(1): 131-134

Brownstein, K. R. 1980. Diffusion as an explanation of observed NMR behavior of water absorbed on wood. Journal of Magnetic Resonance 40(3):505-510.

Bucur, V., 2003. Nondestructive characterization and imaging of wood. Springer Series in Wood Science. Sringer-Verlag Berlin Heidelberg New York, pp. 354.

Casieri, C.; Senni, L.; Romagnoli, M. [and others]. 2004. Determination of moisture fraction in wood by mobile NMR device. Journal of Magnetic Resonance 171(2): 364-372.

Ekstedt, J.; Rosenkilde A.; Hameury, S. [and others]. 2007. Measurement of moisture content profiles in coated and uncoated Scots Pine using magnetic resonance imaging. Proceedings of COST #53 – Quality Control for Wood and Wood Products. October 2007. Warsaw, Poland, pp. 27-32.

Filbotte, S.; Menon, R. S.; MacKay, A. L. [and others]. 1990. Proton magnetic resonance of western red cedar. Wood Fiber Science. 4:362-376.

Forest Products Association of Canada (FPAC). 2012. Industry by the numbers: http://www.fpac.ca/index.php/en/industry-by-the-numbers/

Halse, M.; Goodyear, D. J.; MacMillan, B. [and others]. 2003. Centric scan SPRITE magnetic resonance imaging. Journal of Magnetic Resonance 165: 219-229.

Hall, L. D.; Rajanayagam, V.; Stewart,W. A. [and others]. 1986. Magnetic resonance imaging of wood. Canadian Journal of Forest Research 16(2): 423-426.

Hartley, I. D. 1994. Characterization of water in wood below the fibre saturation point. Ph.D. Thesis. University of British Columbia. Canada. pp147.

Liang, Z-P.; Lauterbur P. C.. 2000. Principle of Magnetic Resonance Imaging – A signal processing perspective. The Institute of Electrical and Electronics Engineers, Inc., New York. pp. 57-76.

MacMillan. M. B.; Veliyulin, E.; Lamason, C. [and others]. 2011. Quantitative magnetic resonance measurements of low moisture content wood. Canadian Journal of Forest Research 41:2158-2162.

MacMillan, M. B.; Schneider, M. H.; Sharp, A. R. [and others]. 2002. Magnetic resonance imaging of water concentration in low moisture content wood. Wood Fiber Science 2: 276-286.

Marble, A. E.; Mastikhin, I. V.; Colpitts, B. G. [and others]. 2007. A compact permanent magnet array with a remote homogenous field. Journal of Magnetic Resonance 186(1): 100-104.

Meder, R.; Franich, R. A.; Callaghan, P. T. 1999. 11B magnetic resonance imaging and MAS spectroscopy of trimethylborate-treated radiate pine wood. Solid State Nuclear Magnetic Resonance 15:69-72.

Nader, J. 2007. Evaluation of two technologies to determine the moisture content of logs. FPInnovations Internal Report, Pointe-Claire, QC, Canada, pp. 14.

Nyström, J.; Dahlquist, E. 2004. Methods for determination of moisture content in woodchips for power plants - a review, Fuel 83(2004), 773–779.

Panshin, A. J.; de Zeeuw, C. 1980. Textbook of Wood Technology. 4th Ed. McGraw-Hill Publishing Company. pp. 722.

Riggin, M. T.; Sharp, A. R.; Kaiser, R. [and others]. 1979. Transverse NMR relaxation of water in wood. Journal of Applied Polymer Science 23:3147-3154.

Stenstrom, S.; Bonazzi, C; Foucat, L. 2009. Magnetic resonance imaging for determination of moisture profiles and drying curves. *In* Modern drying technology. Vol. 2. Experimental techniques. *Edited* by E. Tsotsas and A. S. Mujumdar. Wiley-VCH, Weinheim, Germany. pp. 91-142.

Szomolanyi, P.; Goodyear, D; Balcom, B. [and others]. 2001. SPIRAL-SPRITE: a rapid single point MRI technique for application to porous media. Magnetic Resonance Imaging 19: 423-428.

Tsuchikawa, S.; Torii, M; Tsutsumi, S. 1996. Application of near-infrared spectrophotometry to wood. IV, Calibration equations for moisture content. Mokuzai Gakkaishi. 42: 743–754.

Wei, Q.; Leblon, B; La Rocque, A. 2011. On the use of X-ray computed tomography for determining wood properties: a review. Canadian Journal of Forest Research 41:2120-2140.

Using Parallel Computing Methods to Improve Log Surface Defect Detection Methods

R. Edward Thomas
U.S. Forest Service, Princeton, WV, USA. ethomas@fs.fed.us

Liya Thomas
Pearisburg, VA USA

Abstract

Determining the size and location of surface defects is crucial to evaluating the potential yield and value of hardwood logs. Recently a surface defect detection algorithm was developed using the Java language. This algorithm was developed around an earlier laser scanning system that had poor resolution along the length of the log (15 scan lines per foot). A newer laser scanning system was constructed that had much greater resolution (192 scan lines per foot) along the logs' length. The increased resolution and the slower processing speed of the Java-based algorithm required a new approach. The revised algorithm was designed around the higher resolution data and employs parallel processing technology. The new algorithm processes higher resolution data in less time than required by the original algorithm using the lower resolution scan data. The improved processing power permits a more in-depth analysis of the higher resolution scan data scan data leading to improved detection results.

Keywords: hardwood, log, defect, automated detection, parallel processing

Introduction

For decades hardwood log processing optimization methodologies and techniques have been one of the top priorities in the wood products industry (Chang 1992). After a tree is harvested, it undergoes a rough manual estimation of potential yields and is bucked into several logs. Before a log is sawn into boards, the operator quickly examines it and picks the best opening or highest quality face. During the examination, surface defects are identified, and type, severity, and topological distribution of the defects are determined. Thus, lumber yield is highly subject to time constraints, operator's skill, and conditions at the time of evaluation. Hardwood log defects vary in size, shape, and type, making them difficult to identify. Defects, such as sawn-knot stubs, rotten knots, surface distortion, holes, cracks, gauges, branch sprouts, swelling, worm holes, and animal damage, are imperfections that decrease wood value and utility.
With the advances in scanning equipment, it is possible to develop automated systems that aid the bucking and sawing process. Researchers have experimented with technologies and methods that locate and classify internal as well as external defects on either softwood or hardwood. Systems including those using X-ray/ CT (Computerized Tomography), X-ray tomosynthesis, MRI (Magnetic Resonance Imaging), microwave scanning, ultrasound, and ground penetrating radar have been researched and developed to detect internal defects (Wagner et al. 1989, Guddanti et al. 1998, Zhu and Beex 1994, Devaru et al., Chang 1992, Nordmark and Oja 2004). Advanced computer vision and image processing methods and algorithms were proposed for internal hardwood log defect inspection (Zhu and others 1996, Li and others 1996, Tian and Murphy 1997a, Tian and Murphy 1997b, Kline and others 1998, Bhandarkar and others 1999). Some of these methods and technologies provide high detection rates as the data have extremely high resolution. However, issues such as high cost, low processing speed, data instability, and environmental safety keep them from being commercially available. Another approach is the use of laser

scanning technologies to collect profile data of softwood and hardwood logs. Thomas et al. (2006, 2007) developed a log surface defect detection system, which uses high-resolution laser scan data. In tests of this system, 53 severe defects were detected out of 64 with 9 non-defective regions falsely identified. When calculated as areas, 90.2 percent of the defects were located.

All of these methods required the processing of vast amounts of data, some more than others. In addition, processing the data needs to occur in real time to be of use in a processing environment. As scanners and data collection systems become more advanced, the detail and volume of the data increases, ultimately requiring greater processing resources to yield the desired higher accuracies. Further, successfully solving these problems often exceeds the capabilities of the algorithms used. Most computers sold today have at least two processors, with many having four or more processors. Designing algorithms to take advantage of increased computing power is a must to be able to solve these problems in real time.

Methods

Data Collection

The United States Forest Service constructed a high-resolution three-dimensional laser-scanning system for logs in Princeton, West Virginia. The system has three industrial laser scanning heads designed for the wood processing industry. The scan heads are arranged in an eight foot circle with a 120 degree separation between the scan heads (Figure 1). This allows the three scanners to collect a complete surface scan of the log surface. The log is supported in V-stands every 5 feet at the center of the circle of scanners (Fig. 1). The scanner then over the log and collects a scan line around the circumference of the log every 1/16 inch. Resolution between points within each scan line varies depending on the size of the log, but is typically around 1/8 inch. All points are measured to the nearest 0.001 inch. A dot-cloud image sample of a scanned log is shown in Figure 2. The two vertical white marks in Figure 2 are missing data due to shadowing of the log surface by the V-Stands.

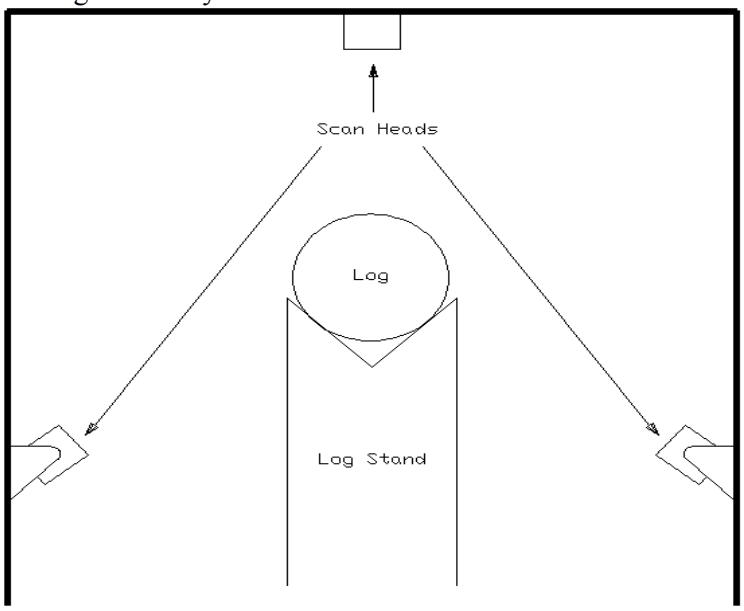

Figure 1—Schematic diagram of high-resolution log scanner.

Thirty-three red oak trees were randomly selected from the MeadWestvaco forest located near Rupert, West Virginia. Each tree was was bucked into log lengths and the logs were laser-scanned then manually diagrammed, where the location and type of the defects were recorded. Ten logs were

randomly selected for this study from a set of 33 logs. The specifications of the selected logs are listed in Table 1.

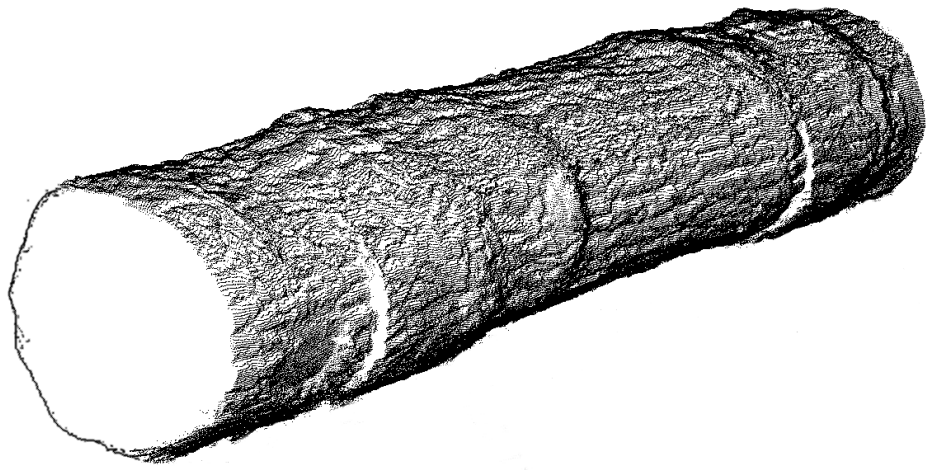

Figure 2—Dot cloud view of log 31C.

Table 1.— Study Log Specifications.

Log	Length (inches)	Large End Diameter (inches)	Small End Diameter (inches)	Total Severe Defects	Total Non-Severe Defects	Total Defects
16D	125.8	17.1	17.0	5	7	12
27B	127.1	20.7	19.1	5	0	5
25E	152.9	15.3	13.1	18	1	19
31C	129.3	16.8	15.7	11	6	17
7A	126.1	20.5	17.2	1	1	0
6B	122.4	17.7	12.4	2	1	3
33B	128.9	17.8	17.3	4	3	7
11C	158.2	14.4	13.3	9	2	11
21C	116.0	18.3	13.9	4	4	8
3C	126.8	14.5	14.1	4	9	13
Average	131.3	17.3	15.3	6.3	3.4	9.5

Sequential Detection Algorithm

The high resolution three-dimensional (3-D) laser-scanned hardwood log data shows minute surface variations, making it feasible to locate external defects. Four major steps are involved:

1) Fit 2-D circles to log cross-sections. Because the scans may be missing data or includes irrelevant deviant data points; a new, robust estimator was developed to reliably estimate the centers and the radii of the fitted circles.
2) Extract radial distances between the fitted circles and log data to indicate local height changes. Radial distances refer to height values on the surface with respect to reference.
3) Locate defects characterized by significant surface rises or depressions.
4) Filter and refine detection results using an expert system.

Robust statistical estimators provide a mechanism to correctly estimate model parameters in the presence of severe outliers (data with large deviants). A new robust non-linear generalized M-estimator (GME) was developed whose objective function makes use of scale estimates (Thomas and Mili 2007). These are calculated using projection statistics and incorporated in the Huber objective function, such that the influence function of the estimator is bounded. This makes it possible to filter out not only the errors in the measurements, but also the errors in the circle model that is applied to a given cross-section data set.

Radial distances are computed between the virtual log produced from the fitted 2-D circles and log data. The radial distances are orthogonal, and as a whole provide a height map of the log surface with respect to the virtual log. These radial distances typically range from -0.5 to 0.5 inch, scaled to range from 0 to 255 gray-levels, and mapped to create a 2-D image (fig. 3). In this process, the log surface is unrolled onto a 2-D coordinate space to create a "skin" representing the pattern of log bark along with bumps and bulges associated with most defects. Next, the log data are processed and interpolated linearly to fill any gaps between data points. This enables our system to locate defects associated with unique characteristics and height change. The defect detection algorithm analyses both contours and 3-D data to locate severe defects at least 0.5 inch high and 3 inches wide.

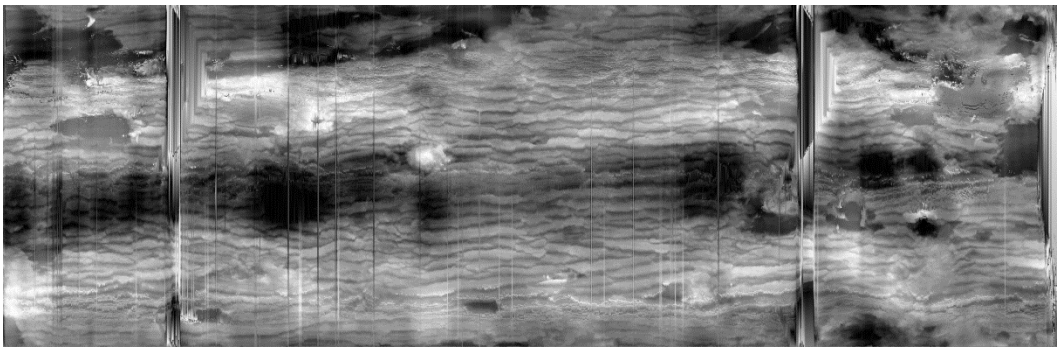

Figure 3—Residual image of log 31C created using the Java algorithm

Six contour levels are computed from the orthogonal distances between a virtual log and any point of the cross section, generating a topographical exterior log map. Examining only the highest and lowest-level contours, defects corresponding to surface rise or depression are detected. Expert knowledge, in the form of defect shape and size characteristics, are applied in a stepwise fashion to rule out regions as potential defects, including regions with sizes smaller than a given threshold, nested in other curves, or long and narrow (determined by the actual width to length ratio of real log dimensions). Some regions are removed for further consideration if they contain a large portion of missing data. The algorithm extends boundaries of an identified region only if a relatively high standing corner of the defect is located. Regions may include an elevated yet non-defective log surface. Typically these regions are covered with tree bark, and thus are associated with distinctive bark patterns.

Using radial distances visualized by the gray-level image presented in Figure 3, the algorithm generates a contour plot and determines the rectangle-enclosed regions of the highest level bounding contour curves that identify potential defects. Some regions are selected if they are large enough (at least 3 inches in diameter) or with a significant height (at least 0.5 inch). The region surrounding selected small regions are examined for the presence of relatively straight-line segments. If the coverage of straight line segments is sufficient, the defect region is adjusted to cover the entire defect surface, rather than just a corner. Such regions are usually the top of a sawn knot, either sound (not rotten), or unsound (rotten). Region-removal rules are given as: regions smaller than a given threshold; regions enclosed in

curves nested in other curves are removed, as there will only be one defect in the same location. Long and narrow regions are normal bark patterns and are ignored. Also ignored are regions smaller than 50 square inches and adjacent to the selected large regions. The marked squares in Figure 3 identify areas with defects.

The Parallel Algorithm

The parallel version of the defect detection algorithm performs the image processing functions and contour analyses in parallel. This version was developed using the following software packages:

a) gcc version 4.6.1 (C Compiler)
b) MPICH2 1.4.1 (Message Passing Interface for parallel application development) (Gropp 2002)
c) OpenCV 2.1.0-7 (Open Source Computer Vision library) (Bradski 2000)

The parallel defect detection algorithm can be built and run using Windows 7[1], a standard C compiler and the Windows versions of the OpenCV and MPICH packages. The test system for the parallel and Java algorithms was conducted on an IBM compatible computer with 24GB of RAM and 8 3.6 Ghz Core2 CPUs running the Mint Linux operating system.

MPICH2 is one of many different programming packages available for developing parallel applications. MPICH2 is one of the most popular implementations of MPI and is available for many operating systems and computer architectures (Pacheco 1997). In addition, MPICH2 is the foundation of several corporate versions of MPI. MPI and MPICH2 allow developers to specify how to divide a processing task such that the different parts of the task are solved concurrently on different processors of the same computer or on processors of other networked computers. There are two common ways of distributing processing across multiple processors. The first method segments the problem into equal pieces and gives a piece to each processor available. Once, each piece is processed, the results are compiled together. In the second approach one processor is designated as the master controller. The master then divides work and collects results from the "slave" processors as work is completed. The parallel application here used the master-slave processing paradigm. In either method, the data to be processed and the results that are collected, are transferred using messages. Hence the name "Message Passing Interface". If one has eight processors, you would have one master and 7 slave processors. Thus, theoretically a parallel-processed job could be solved in $1/7^{th}$ of time required by a single processor algorithm. However, due to the overhead of message passing, the required coordination of processing among all processors, and the portions of the computer program that do not run in parallel, the processing time reduction is always less. How much less depends on maximizing the parts of the original program to run in parallel.

Of the four major defect detection steps, we have concentrated on improving the processing speed of the first two steps. This is because that most of the tasks involved in these steps involve many complex independent operations that are ideal for parallel processing. The first processing step, fitting 2-D circles to log cross-sections, is divided into four smaller tasks:

1) Read in log data.

[1] Windows 7 is a registered trademark of Microsoft, Inc. The use of trade, firm, or corporation names in this publication is for the information and convenience of the reader. Such use does not constitute an official endorsement or approval by the U.S. Department of Agriculture or the Forest Service of any product or service to the exclusion of others that may be suitable.

2) Determine fitting parameters for each log data slice.
3) Box filter fitter parameters between slices.
4) Remove outlier data from each slice.

The second processing step, extracting radial distances between fitted circles and log data to indicate local height changes, is divided into 3 separate tasks:

5) Create image strip for each slice.
6) Fill in missing data "holes" for each slice.
7) Residual image creation from individual image strips.

Of the seven tasks, tasks 2, 4, 5, and 6 are ideally suited for parallel processing. These tasks involve complex processing of individual slices of the laser scan data. More importantly, these operations are independent, (ie. they do not depend on the results of any neighboring slices). To reduce message overhead, the data for 5 slices at a time is transmitted to each processor. When a processor finishes, it transmits the results back to the master processor. The slave processor then receives the next set of 5 slices, if any are remaining. The master processor is responsible for keeping track of which data slices each slave is processing and for collating the results as it receives them. The remaining tasks 1, 3, and 7 are sequential in nature and are not suitable for parallel processing.

The third step, locating defects characterized by significant surface rises or depressions, uses OpenCV to create and analyze the contour data. This library was not written to take advantage of parallel processing, thus this part of the defect detection code is run as a single process. The expert system is the final step that is performed by the Java-based algorithm and is used to reject some areas marked as defective, which are likely not defective. This is accomplished by examining the shape characteristics of the marked defect region to judge if the area is truly a defect. The expert system in the parallel processing version examines only a subset of the conditions that can render an area marked as defective, not truly a defect.

Results

To determine the parallel algorithm advantages and disadvantages compared to the original Java algorithm, the algorithms were run on each of the sample logs and the individual results compared. The specifications of these test logs are described in Table 1. The logs processed are a mix of lower and upper story logs with an average length of 131.3 inches and an average large end diameter of 17.3 inches and a small end diameter of 15.3 inches. Overall there was an average of 6.3 severe defects per log. Defect types considered severe are overgrown, sawn, and unsound knots and clusters, as well as bumps, and holes. In addition, there was an average of 3.4 non-severe defects per log, which includes distortion and adventitious knot defect types.

Tables 2 and 3 contain detection results from the parallel and Java detection algorithms, respectively. Table 4 compares the performance of the two detection methods. Overall, the parallel method had fewer un-detected severe defects, 2.4 versus 3.3 of the Java algorithm. This can be seen in Table 4 where the parallel method had better detection rates in 6 of the 10 logs processed. However, the Java algorithm resulted in significantly fewer false positive defect detections per log, 1.9 versus 4.7 of the parallel method. This difference is due to the Java algorithm's expert system which refines detection results. Perhaps the most significant results in the comparison is processing time. The average processing time per log of the parallel method was 1.009 seconds compared to 49.973 seconds for the Java-based algorithm. In two instances the Java method took longer than one minute to complete, while in five

instances the parallel method required less than one second to process. Thus, the parallel method yields some accuracy, for a greatly decreased processing time.

Table 2—Parallel algorithm detection results.

Log	Total Severe Detected	Total Non-Severe Detected	False Positive Detected	Total Severe Undetected
16D	5	0	4	0
27B	2	0	3	3
25E	11	0	3	7
31C	6	1	2	5
7A	0	1	10	1
6B	1	1	6	1
33B	2	0	5	2
11C	6	0	5	3
21C	3	0	2	1
3C	2	1	7	1
Average			4.7	2.4

Table 3—Java algorithm detection results

Log	Total Severe Detected	Total Non-Severe Detected	False Positive Detected	Total Severe Undetected
16D	3	0	1	2
27B	3	0	1	2
25E	5	0	4	6
31C	2	1	0	9
7A	0	0	2	1
6B	2	1	1	0
33B	2	0	5	2
11C	3	0	0	6
21C	2	1	3	3
3C	1	1	2	2
Average			1.9	3.3

Table 4—Algorithm performance comparison.

Log	Parallel Algorithm Processing Time (seconds)	Java Algorithm Processing Time (seconds)	Parallel Severe Detection Rate (percent)	Java Severe Detection Rate (percent)
16D	1.041	56.500	100	60
27B	0.892	67.910	40	60
25E	1.146	58.959	61	28
31C	1.943	64.075	55	18
7A	0.853	42.534	0	0
6B	1.028	34.559	50	100
33B	0.689	59.891	50	50
11C	1.003	42.069	67	33

21C	0.701	38.248	75	50
3C	0.794	34.985	50	25
Average	1.009	49.973	55	42

Figure 4 is the residual image of log 11C (see Figure 2 for dot cloud view) with the defects as detected using the parallel algorithm. Note that the log support stands created shadows or disruptions on the scan which are visible as two ")" shaped areas on the right edge of the image. These areas were detected as defects and are regarded as false-positive errors.

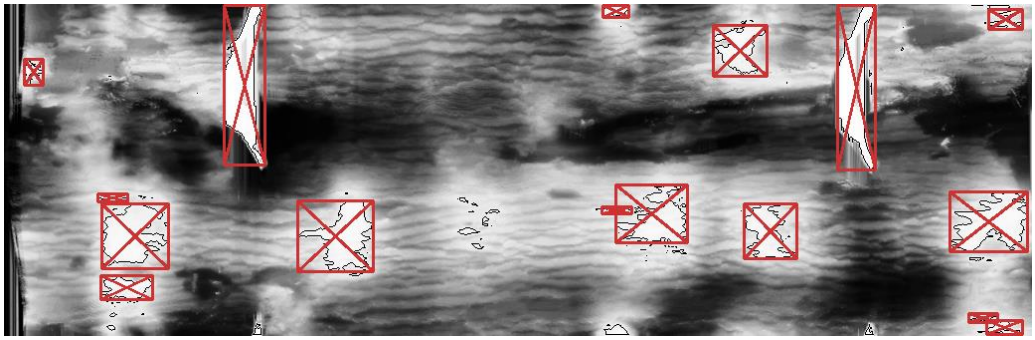

Figure 4—Residual image of log 31C with contour levels and defects identified using the parallel algorithm.

The Java algorithm's expert system is very complex, and is the main reason for the algorithm's low false-positive detection error rate: 1.9 defects per log versus 4.7 defects per log of the parallel algorithm. Approximately 33 percent of the java algorithm's processing time occurs while running the expert system, which on average is about 26 seconds per log. Thus, the expert system also would need to be developed as a parallel algorithm to keep processing times low. The parallel algorithm has a filter that can exclude contours with too many or too few data points. Reducing the parameter to exclude contours with larger contour sizes, resulted in fewer false-positive and detected defects. Increasing the parameter to include the larger contour sizes, resulted in more false-positive as well as more detected defects. The current settings of the system capture most defects, at the cost of greater false-positive.

Summary and Conclusion

The parallel algorithm provided greater detection accuracy on some logs compared to the Java algorithm. This was evident on six of the ten logs processed in the comparison study. However, this was at the cost of greater false positive defect detection where the parallel algorithm indicated that there were almost three additional defects per log, on average, which were not present. In addition, each algorithm detected a total of four non-severe defects on the log sample, but not always on the same log. The greatest advantage of the parallel algorithm is detection speed, on average approximately one second is needed by the parallel algorithm, compared to 49 seconds of the Java algorithm.

The greatest need at present is the development of a parallel expert system to filter and enhance the results of the parallel algorithm. This would greatly reduce the number of false positives as this step in the java algorithm eliminates most false positive results. The expert system also determines which areas are most likely defective and thus improves detection accuracy. The reason that the parallel system detection performance is slightly better in some cases is due to the improved contour analysis algorithms it uses, which is not available for use in Java. In addition, development of the expert system for the

parallel system would allow the tuning parameter, (discussed earlier), to be increased allowing for the detection of more defects, but without the penalty of more false-positive defects.

Due to differences of the contour data structures used by the parallelized and sequential algorithms that identify severe defects, it is better to rewrite the expert system that determines whether an indentified area is really an external log defect. Upon this we may implement a parallelized version of the expert system. A parallel algorithm equally partitioning the identified regions among processors could be developed, each running the same system during the entire process for a significant portion of the execution time. This would greatly reduce processing time for this step. However, the key is to rewrite the rather complicated expert system.

Acknowledgements

The work upon which this publication is based was funded in whole or in part through a grant awarded by the Wood Education and Resource Center, Northeastern Area State and Private Forestry, Forest Service, U.S. Department of Agriculture.

References

Bhandarkar, S.; Faust, T.; Tang, M. 1999. Catalog: a system for detection and rendering of internal log defects using computer tomography. Machine Vision and Applications 11(4): 171–190.

Chang, S. 1992. External and internal defect detection to optimize cutting of hardwood logs and lumber. Technical Report 3, USDA and National Agricultural Library, Beltsville, MD. ISSN 1064-3451. 24 p. Available: http://www.nal.usda.gov/ttic/industry/ hrdwood3.htm.

Devaru, D.; Halabe, U. B.; Gopalakrishnan, B.; Agrawal, S.; Grushecky, S. 2005. Algorithm for detecting defects in wooden logs using ground penetrating radar. Proc. SPIE Vol. 5999, 59990B.

William Gropp. 2002. *MPICH2: A new start for MPI implementations*, In Recent Advances in Parallel Virtual Machine and Message Passing Interface, Dieter Kranzlmüller, Peter Kacsuk, Jack Dongarra, and Jens Volkert.

Guddanti, S.; Chang, S. 1998. Replicating sawmill sawing with topsaw using ct images of a full length hardwood log. Forest Products Journal 48(1): 72–75.

Kline, D.; Widoyoko, A.; Wiedenbeck, J.; Araman, P. 1998. Performance of color camera machine vision in automated furniture rough mill systems. Forest Products Journal 48(3): 38–45.

Bradski, Gary. 2000. The OpenCV library. Dr. Dobbs Journal of Software Tools. http://www.drdobbs.com/open-source/the-opencv-library/184404319. Accessed Feb. 12, 2013.

Li, P.; Abbott, A.; Schmoldt, D. 1996. Automated analysis of ct images for the inspection of hardwood log. In Proceedings of the International Conference on Neural Networks, Washington, D.C., USA. 3: 1744–1749.

Nordmark, U.; Oja, J. 2004. Prediction of board values in Pinus sylvestris sawlogs using X-ray scanning and optical three-dimensional scanning of stems. Scandinavian Journal of Forest Research, 19(5):473-480(8).

Pacheco, Peter S. 1997. Parallel programming with MPI. Morgan Kaufmann Publishers, Inc. San Francisco, CA. 418p.

Thomas, L.; Mili, L. July, 2007. A Robust GM-Estimator for the Automated Detection of External Defects on Barked Hardwood Logs and Stems. IEEE Transactions on Signal Processing 55(7): 3568–3576.

Thomas, L.; Mili, L.; Thomas, E.; Shaffer, C. October, 2006. Defect Detection on Hardwood Logs Using Laser Scanning. Wood Fiber Science Journal 38(4): 682–695.

Thomas, L.; Shaffer, C.; Lamine Mili, L.; Thomas, E. April, 2007. Automated Detection of Severe Surface Defects on Barked Hardwood Logs. Forest Product Journal 57(4): 50–56.
Tian, X.; Murphy, G. 1997a. Automated feature extraction and defect recognition from digital images of tree stems using texture analysis. In Proceedings of the first joint Australia & New Zealand biennial conference on Digital Image & Vision Computing –Techniques and Applications.
Tian, X.; Murphy G. 1997b. Detection of trimmed and occluded branches on harvested tree stems using texture analysis. International Journal of Forest Engineering 8(2): 65–78.
Wagner, F.; Taylor, F.; Ladd, D.; McMillin, C.; Roder, F. 1989. Ultrafast ct scanning of an oak log for internal defects. Forest Products Journal 39(11/12): 62–64.
Zhu, D.; Beex, A. 1994. Robust spatial autoregressive modeling for hardwood log inspection. Journal of Visual Communication and Image Representation 5(1): 41–51.
Zhu, D.; Conners, R.; Schmoldt, D.; Araman, P. 1996. A prototype vision system for analyzing ct imagery of hardwood logs. IEEE Transactions on Systems, Man, and Cybernetics Part B: Cybernetics 26(4): 522–532.

Session 5

Condition Assessment of Historic Wood Structures—Experience from Around the Globe

Evaluation of wood strength with non-destructive and semi-destructive test methods on historical buildings in Northern Italy

Wilfried Beikircher
Department of Engineering Sciences - Timber Engineering Unit, University of Innsbruck, Innsbruck, Austria, Tyrol, wilfried.beikircher@uibk.ac.at

Philipp Zingerle
Department of Engineering Sciences - Timber Engineering Unit, University of Innsbruck, Innsbruck, Austria, Tyrol, philipp.zingerle@uibk.ac.at

Anton Kraler
Department of Engineering Sciences - Timber Engineering Unit, University of Innsbruck, Innsbruck, Austria, Tyrol, anton.kraler@uibk.ac.at

Micheal Flach
Department of Engineering Sciences - Timber Engineering Unit, University of Innsbruck, Innsbruck, Austria, Tyrol, michael.flach@uibk.ac.at

Abstract

Through experience (different research results report the influence) we learned that the strength of wood is associated with the growing region and climatic condition that they are located from. But little information on the aging effect to wood strengths is available. Within the presented research project investigations of timber strength fromhistorical buildings (from 1250 AD to 2011) in a closed area in Northern Italy could be performed. Three non-destructive (Visual examination, Electric resistance, Ultrasound) and two semi-destructive (Drill resistance, Fractometer) measurement methods were used for the investigation. The measurement results for aged wood could be brought into relation to the wood strength of virgin wood. The evaluation shows a wide dispersion of the measuring results. This lack of precision is essentially due to decisive factors of marginal parameters (e.g. temperature and wood moisture) as well as the natural spectre of properties of wood. From this research project cannot be concluded, that the wood strength over the years is changing.

Keywords: strength determination of wood, aged wood, non-destructive testing methods, drill resistance measuring, ultrasonic measurements, Fractometer tests

Introduction

Timber structures have been evaluated for decades since they are a significant part of cultural heritage and the need for their preservation is increasingly significant. In renovating buildings it is essential to assess the condition of timber structures. The most accurate way of determining the mechanical properties of timber are destructive methods. The most relevant results are given by compression -, tension - and bending tests. But those methods need test samples which are mostly not available if historic timber structures have to be assessed. Although the importance of visual assessment of structure elements is highly decisive, the results can be very subjective and dependent on the observers experiences and skills (

Teder et al. 2011). Visual assessment is constrained, especially since members of the timber structue has one or more sides covered and the geometry does not enable the inspection. Therefore other methods are needed to gain reliable results, which are independently on observers' subjective interpretation.
The goal of this project was to determine the change of selected wood properties within the centuries. In cooperation of the cluster Timber & Technology/TIS innovation park, South Tyrol and the Association for the Preservation of Old Wooden Buildings, projects in Northern Italy relating to the time frame from 1250 to 2011 could be assessed. The wood of the timber construction investigated originate from a perimeter of 50 km and therefore the material is highly comparable regarding growing area and climatic conditions. Due to the long time span and the limited availability of wood constructions diverse parts of timber constructions were investigated. The wood tested was mainly part of existing constructions and therefore the selection of the tested area was dependent on the availability and access.
There are several non-destructive (NDM) and semi-destructive (SDM) methods that can be used in the assessment and determination of the quality and properties of timber:

- mechanical (drilling resistance, hardness, intrusion behavior);
- electrical (correlation between electrical resistance and moisture, correlation between electrical resistance and fungal decay);
- acoustic (sound velocity, sound reflection, sound attenuation);
- thermal (heat radiation);
- electromagnetic waves (visible light, IR/NIR radiation, x-ray, neutron radiation, Synchrotron radiation) (Niemz in Teder et al. 2011)

The aim of this work was to investigate the ageing effects on certain wood properties using non-destructive and semi-destructive methods. As NDM the visual inspection for the wood quality in general was used, the moisture content (mc) was determinated by the electrical resistance method and the modulus of elasticity was predicted by measuring the sound velocity. As SDM the drill resistance was measured for determining the year ring width and areas of deterioration and generating relative values for comparing the density estimated. Cores were taken for determining the real year ring width and for Fractometer tests to determine the compression strength. Because most of these methods give only qualitative values the results are only relatively comparable.

Materials

The wood of the timber constructions under investigation originate from a perimeter of 50 km and therefore the material is highly comparable regarding growing area and climatic conditions. Because of the geographical position Norway spruce (Picea abies) and Larch (Larix decidua) were the wood species used in this area and gone under investigation. Due to the long time span and the limited availability of wood constructions diverse parts of timber constructions were investigated. The samples were parts of wooden beams in basement rooms, agricultural storage rooms, family homes made of logwood, wooden roof structures, board stacks and living trees. As there were the limitations aforesaid the number of tests performed vary between one single test up to 20 tests. Table 1 gives an overview of age, origin, wood species and the number of tests performed. A detailed description for the projects under investigation can be found in Kraler et al. 2011.

Table 1—List of the project under investigation and the measurements performed

Dating[1]	Project	abbr.	Wood species	no. of measurements performed		
				Core samples (fractometer tests[2])	Drill resistance	Ultrasonic
1234	Krustnerhaus UG	KRU	Larch	2 (22)	5	3
ca.1250 estimated	Bäckerei Kofler Keller	BAK	Larch	1 (8)	7	7
1346	Krustnerhaus UG	KRU	Larch	3 (28)	14	3
1346	Krustnerhaus EG	KRE	Spruce	0	1	6
1346	Krustnerhaus OG	KRO	Spruce	2 (19)	9	20
1361	Plobenhäusl	PLH	Spruce	2 (18)	12 +2Lab	18
1372	Plobenhäusl	PLH	Spruce	0	8	19
1461	Wirtschaftsgebäude Großstein	WIG	Spruce	4 (27)	11	20
14??	Gotischer Keller (Scheiber)	SCH	Larch	0	6	0
1420	Krustnerhaus UG	KRU	Larch	4 (41)	7	7
1420	Krustnerhaus EG	KRE	Larch	1 (9)	5	0
1420	Krustnerhaus OG	KRO	Spruce	0	0	10
1534	Kasten Pacher Prantach	KAP	Spruce	5 (25)	11	18
ca. 1550	Sandwirt Kellerdecke	SAK	Larch	3 (16)	9	12
ca. 1550	Krustnerhaus Kasten Ulfas	KRK	Spruce	0	6	18
1652	Stall und Stadel	STA	Spruce	0	6	0
1650	Mooserwirt Keller	MOK	Larch	2 (16)	9	9
1761	Dachstuhl Platterhof	PLA	Spruce	0	7	4
1780	Krustnerhaus DG	KRD	Spruce	0	5	14
ca. 1820	Krustnerhaus Veranda	KRV	Spruce	0	5	6
1871	Dachstuhl Moser Josef	DAM	Spruce	2 (13)	7	6
1881	Plobenhäusl	PLH2	Spruce	3 (30)	6	8
ca. 1940	Lodenwalke - Almhütte	LOW	Larch/Spruce	0 /3(18)	1/9	0/20
ca. 1950	Dachstuhl Mooserwirt	MOD	Spruce	2 (21)	9	13
2011	Moos (living tree)	MLH	Spruce	0	3	0
2011	Stuls Schnittholz Stapel	STH	Spruce	0	0	20
2011	Heutiges Holz Labor	HEU_Labor	Larch/Spruce	0/3 (34)	7/4	0/7
??	Aged wood	LAB_Labor	Spruce	17	8	0

[1] exact datings were dated with dendrochronology, ca. dates are informations by the owners
[2] the brackets indicate the number of the fracture measurements out of the core samples

Methods

For the determination of the wood quality following methods were used:

- Visual examination of the wood allows identifying: the wood species, the general quality of the timber parts, components that are missing or broken and in an advanced state of deterioration. For the determination of the strength classes of timber parts the German standard DIN 4074-1 for the visual grading of softwoods was utilized.

- For the determination of the moisture contend the GANN HYDROMETTE HAT 65, which works on the electrical resistance principle, was used. The moisture was measured 3 times at the same wooden part where ultrasound measurements were performed and the mean value was reported.
- The SYLVATEST Duo (Sandoz, 1990) was used for Ultrasound speed measurements. The ultrasound speed is an indicator for the dynamic modulus of elasticity. By performing direct measurements this method allows in combination with the information of the wood species, the moisture content and the density to allocate the timber parts in strength classes. The measurements were performed as indirect measurements and therefore the results are only relative comparable.
- Drill resistance measuring with the device IML-RESI F400S were performed for the relative comparison of the wood density and the determination of the year ring width. At a constant penetration speed into the sampling piece the drill resistance was registered mechanically on a wax paper strip and in addition an electronic device connected to the measuring device digitally stored the drill resistance profile. 5 to 14 drilling measurements in the radial direction were carried out for each project. The drill resistance method allows the determination of the density but reference measurements are necessary for generating absolute values (Rinn et al. 1996).
- 5 mm timber cores were taken with the pole testing drill for hardwood from SUUNTO. The cores were taken for Fractometer tests for obtaining the compressive strength in longitudinal direction. The cores samples were retrieved radially in the surrounding area of 5 cm next to the drill resistance measurement. Depending on the quality and length of the cores 1 to 13 compression tests were performed.

The semi-destructive methods drill resistance, ultrasound measurement and Fractometer tests are described in detail in several publications (Kasal and Anthony 2004; Rug and Seemann 1988; Winter and Held 1996; Teder et al. 2011).

Results and discussion

Visual examination: Larch was found in the basement and in the ground floor and Norway spruce was found in the ground floor and upper floors. The general visual condition of the Larch and Norway spruce material was like new material after 1-2 mm of surface removal. In some cases fungi and insect deterioration was found. But it was surprising that Larch, with the high mc up to 35%, was not attacked by fungi at all.

Whenever possible the construction timber parts were categorized into visual strength classes S7 (S7K), S10 (S10K) or S13 (S13K), according to DIN 4074-1. They are allocated in the EN 1912 to the European strength class categories in EN 338 to S7 = C18 (C16 Larch), S10 = C24 and S13=C30. In most cases the full evaluation was not possible because of the limited access to the parts within the construction; but in general the classification of S10 is expected due to the parts evaluated. The mean year ring width, which indicates the density, was determined by using the drill resistance measurement. All samples fulfilled the limit of 4 mm for class S13.

In the following diagrams the bars represent the mean value of the individual measurements and error bars show the standard deviation.

The moisture content of the wood was determined between 12% and 35% in dependence where the examined part was located (basement, ground floor, upper floor or attic floor). Because of the different environmental conditions the mc variation is very high s. Figure 1 and Figure 3. As all buildings aren't heated, apart from the project MOD, the moisture content fitted to the predominant environmental conditions.

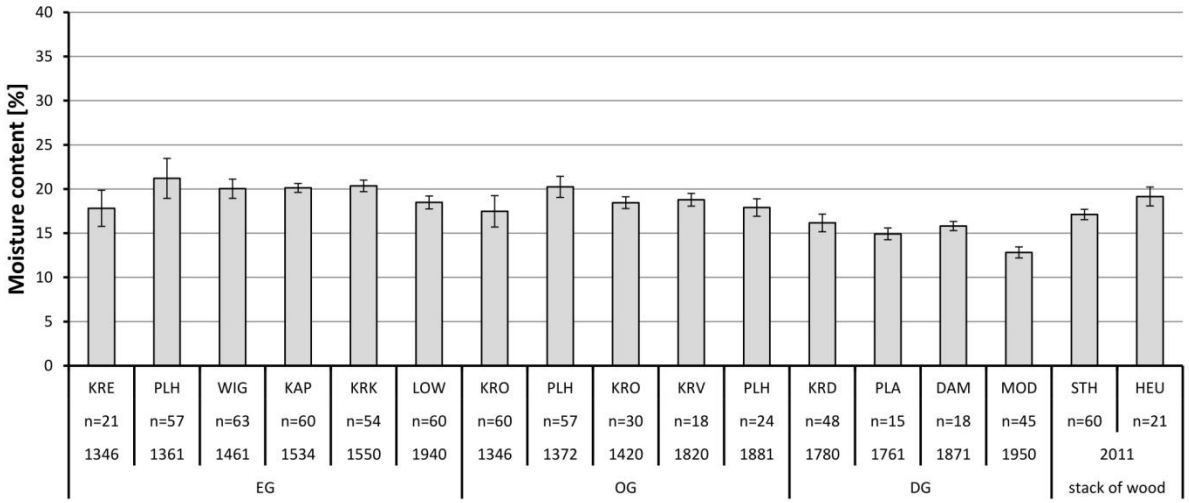

Figure 1—Results of the moisture content measurements for Norway spruce samples; EG = ground floor, OG = upper floor, DG = attic floor

Drill resistance measurements were used to generate the data for the year ring width, which is needed for the visual classification according to DIN 4074-1 and for generating relative values for the density variation. With the drill resistance measurements each measurement is assessed through the integration of the generated drill resistance graph (in %) in the measuring range between 10 mm and 60 mm drilling depth. The results are presented in Figure 2 and Figure 4. The lower values < 12% s. Figure 2 for the projects: KRO, PLH_Labor, KRK, KRD, KRV were not surprising because the wood structure was partially deteriorated by fungi. The rest of the samples under investigation show similar or higher values than the virgin wood from the test series HEU_Labor.

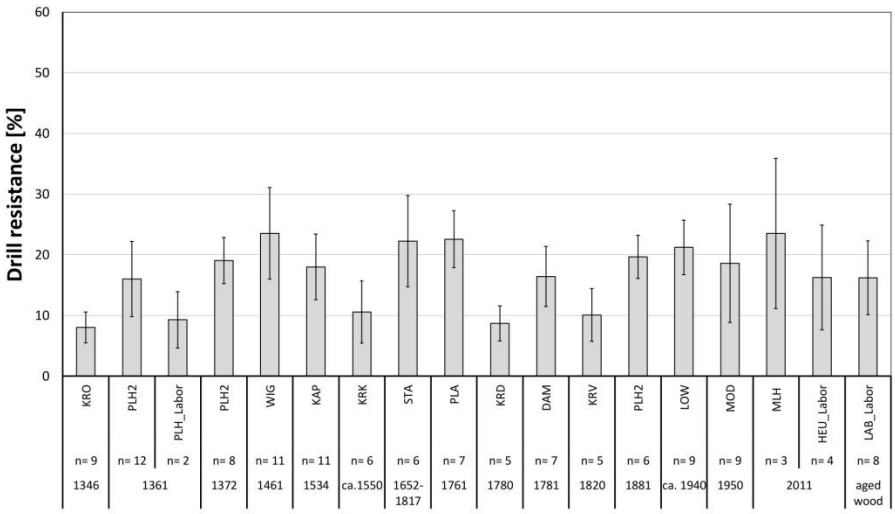

Figure 2—Results of the drill resistance measurements for Norway spruce samples

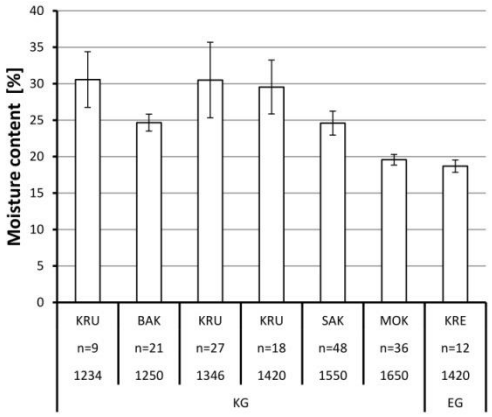

Figure 3—Results of the moisture content measurements for Larch samples; KG = basement, EG = ground floor

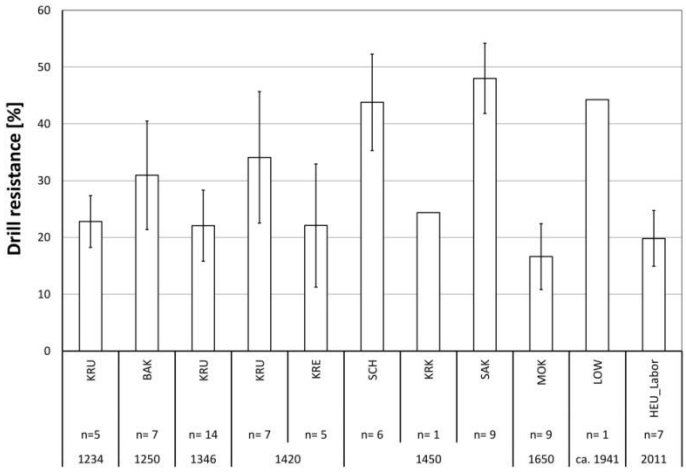

Figure 4— Results of the drill resistance measurements for Larch samples

Preliminary laboratory tests showed that the strength classification out of the testing equipment SYLVATST Duo cannot be used for the indirect ultrasound measurements. The measured sound velocity of indirect measurements is lower than the results out of the direct measurement method. Therefore the results of the sound velocity cannot be used for the calculation of the Young´s modulus or strength classes as presented in literature (Sandoz 1990, Steiger 1996). As results therefore the Ultrasound velocity, in general measured by 2 m distance, is presented in Figure 5 and Figure 7. The results show a wide variation of the ultrasound velocity, but as the STH and HEU series were virgin wood with the classification of S13 it can be said that there is no significant change in the sound velocity by comparison to aged wood. Due to the limited access of the timber parts only in some cases low measurement results can be explained because of damage or the presence of wood defects (PLH, KLE). In some cases the reason of a low measurement result could not be determined; therefore there are limitations of this method for the evaluation of timber parts.

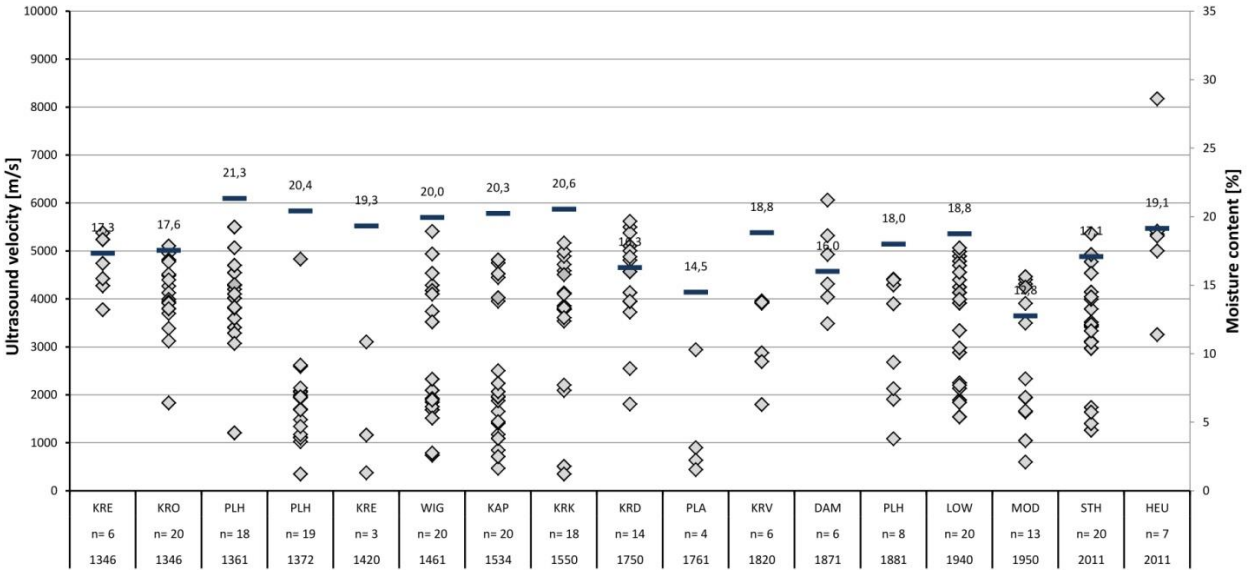

Figure 5—Results of ultrasound measurements and moisture content from Norway spruce samples, the mc is indicated by the horizontal stripe and the rhombs show the single measurements of the ultrasound velocity

Depending on the length and prior damage 1 to 13 compression tests parallel to the grain by using the Fractometer II could be carried out with one drill core sample; only 5 mm in sample length are necessary for one measurement. The measurements started at the wane of the tree following to the center. For every drilling core sample the mean value of the tests was used for comparisons. The results in Figure 6 and Figure 8 show the range of the compression strength. Because damaged samples by fungi or insects were not possible to test, the results show that in general sound aged wood has similar compression strength as virgin wood.

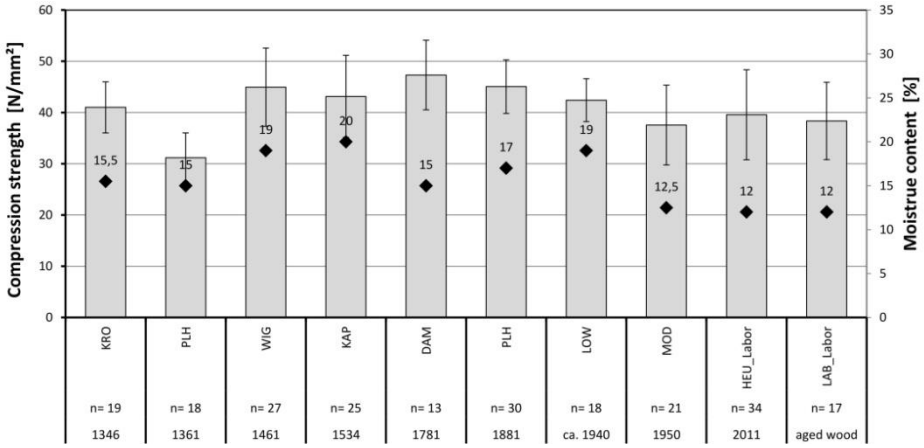

Figure 6—Results of the Fractometer II compression tests for Norway spruce samples, the mc is indicated by the rhomb and the bar show the compression strength with standard deviation

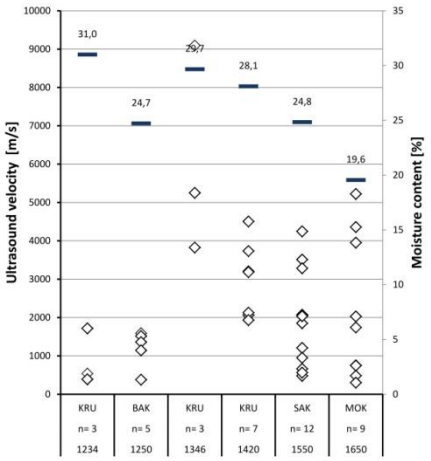

Figure 7—Results of the ultrasound measurements for Larch samples the moisture content; the mc is indicated by the horizontal stripe and the rhombs show the single measurements of ultrasound velocity

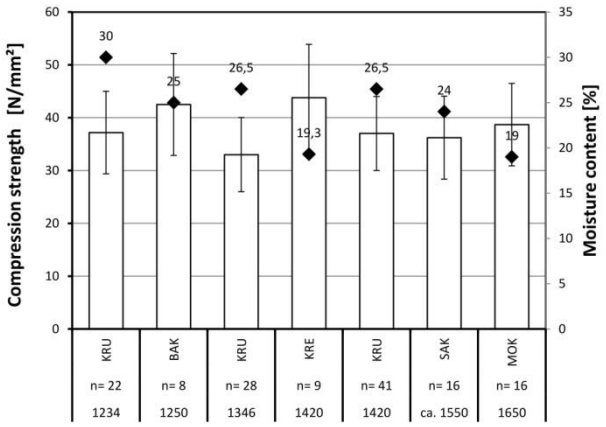

Figure 8—Results of the Fractometer II compression tests for Larch samples; the mc is indicated by the rhomb and the bar show the compression strength with standard deviation

Conclusions

This paper presents a part of the field study of investigations on aged wood in diverse parts of historical buildings in Northern Italy in using non-destructive and semi-destructive test methods to evaluate selected properties of the applied wood. Non-destructive methods are applicable to rapidly screen timber structures

for potential problem areas, or they can be used to provide images of the internal condition of timber constructions. The methods can give reasonable comparative measurements, but suffer from errors resulting from weak correlation between destructive and nondestructive parameters. Semi-destructive methods can give absolute values of the tested parameter, but as in general very small samples are tested, for the determination of the total condition experience of the examiner and additional parameters are necessary.

The visual inspection of timber constructions is the most common method for evaluating the condition of single timber elements, but suffers in the lack of precision and the subjective interpretation of the examiner. In general, because of the limited access, not all parts can be evaluated. For the estimation of strength classes according to DIN 4074 a combination with additional inspection methods for nonvisible deterioration of inner parts is necessary.

The determination of the moisture content with the electrical resistance method is a safe method which is used since a long time. The values determined have a high precision and are adequate for in-situ measurements.

The determination of the mean value of year-ring width and deterioration of inner parts can be detected in using the drill resistance method. Additional the density can be estimated with this method but there are limitations for determination of the absolute value and reference material is needed for relative comparison.

The determination of compression strength parallel to the grain with the Fractometer gives absolute values. This method gives information on the condition of the extracted material and can be used for the determination of the general condition of the timber parts. Due to the very small samples used and the sensibility of damage /destruction also for this method are limitations in transferring the determined strength to the timber elements.

The indirect ultrasound measurement does not give reliable results for determination of the strength class. More research is needed in this field to search for stronger relationship between the indirect and direct measuring method.

The visual inspection and data generated with the non-destructive and semi-destructive methods contribute to receive a more exact strength assessment or sorting of the obstructed woods. But the assessment of strength of the individual members by the used methods can always be imprecise, because of the imperfection of the results of measuring on site. As a result, visual grading methods developed for recent wood may also work for aged wood. However, special attention has to be paid on the grading criteria: fungal decay and infestation of insects because this is sometime difficult to identify on aged wood. Additional mostly the access on the structural parts is limited due to the construction, which lead to an uncertain classification. As a consequence of the investigations performed, an aging effect on the mechanical properties of timber could not be ascertained. Further research will be needed for generating more valuable data by using non-destructive and semi-destructive test methods for the evaluation of timber constructions.

Acknowledgments

This project was enabled by the generous support of cluster Timber & Technology / TIS innovation park, South Tyrol, Italy (commissioning body), the inspiring cooperation with Dr. Harald Haller (selection of projects) and the owners of the buildings from which the samples were taken. We are grateful for their steadfast commitment and support.

References

Kraler, A.; Beikircher, W.; Zingerle, P.2011: Begutachtung von Holzbauten im Passeiertal von 1250 bis Heute, Reserch Report, University of Innsbruck, Timber engineering unit, Jun 2011

Kasal, B.; Antony,W. 2004. Advances in in situ evaluation of timber structures, John Wiley Sons, Ltd; Prog. Struct. Engng Mater.2004; 6:94-103

Rinn, F.; Schweingruber, F.-H.; Schär, R. 1996. RESISTOGRAPH and X-Ray Density Charts of Wood; Holzforschung, Vol. 50, 1996, 4:303-311

Winter, K.; Held, H. 1996. In –situ-Prüfverfahren für verbautes Holz. bau-zeitung 50 (1996) 11, 48-51

Rug, W.;Seemann, A. 1988. Festigkeit von Altholz. Holztechnologie.-Leipzig 29 (1988) 4, 186-190

Teder, M.; Pilt, K.; Milian, M.; Lainurm, M.; Kruuda, R. 2011. Overview of some Non-destructive methods for in situ assessment of structural timber. In:3rd International conference Civil Engineering`11, Proceedings II Materials and Structures, 137-143

Sandoz, J.L. 1990. Triage et fiabilité des bois construction. Validité de la méthode ultrason. Thesis No. 851, EPF Lausanne/IBOIS, 1990

Steiger R. 1996. Mechanische Eigenschaften von Schweizer Fichten-Bauholz bei Biege-, Zug-, Druck und kombinierter M/N-Beanspruchung Sortierung von Rund- und Schnittholz mittels Ultraschall, Institut für Baustatik und Konstruktion (IBK), Eidgenössische Technische Hochschule Zürich (ETH), Phd-Thesis, 1996

ÖNORM EN 1912:2012 11 01: Bauholz für tragende Zwecke - Festigkeitsklassen - Zuordnung von visuellen Sortierklassen und Holzarten

ÖNORM DIN 4074-1:2009 Sortierung von Holz nach der Tragfähigkeit - Teil 1: Nadelschnittholz

ÖNORM EN 338: 2009 Bauholz für tragende Zwecke - Festigkeitsklassen

Combined methodology for ultrasound testing in a timber structure of the 17th century (Granada, Spain)

Jose R. Noya
AIA Intl. Assoc. Architect at Soztak Design, Inc., Chapel Hill (NC),USA, jrnvarch@gmail.com
Department of Mineralogy and Petrology, University of Granada, Spain

Abstract

This research was part of the assessment of the roof of the library of the College of San Pablo in Granada (Spain). The roof structure was an *armadura de par y nudillo,* a timber structure typical of the 17th century. It was difficult to decide whether to preserve or replace two of the structural members. To help this decision, we decided to use ultrasound testing. The objectives were (A) determine the degree of wood decay, (B) determine the strength class and (C) discuss the origin of the decay. After the literature review, a combined methodology was propounded, based on the measurement of the ultrasonic velocities perpendicular to grain. The method was complemented with moisture content measurements and fungal cultures. We concluded that the two structural members were highly deterioriated due to fungi and xylophagous insect attacks. A minimum strenght class of C18 and a maximum of C24 was estimated.

Keywords: ultrasound testing, timber structures, assessment, historic buildings

Introduction

This research was conducted as part of the Master of Science and Technology in Architectural Heritage at the University of Granada in collaboration with the Pedro Salmerón Escobar Architecture and Restoration Studio. Our task in the studio focused on the state of conservation report of the roofs of the San Pablo College and current Law School as part of the Comprehensive Rehabilitation Project of the building. The roof of the library became the primary object of study given its advanced state of decay. According to the studies by Enrique Nuere (Nuere 2001), it corresponds to the typology *armadura de par y nudillo* of the type *lima bordón nones* (figure 1) and was built out of Scots Pine wood at the end of the 17th century. Thus, its high architectural and cultural value would require the conservation of as many of its original structural members as possible in a future repair.

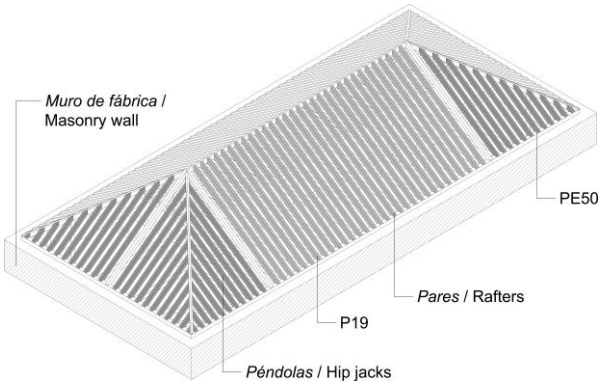

Figure 1—View of the structure. *Armadura de par y nudillo* of the type *lima bordón nones.*

Since at first sight it was difficult to decide whether to conserve or substitute some of these members, we decided to use non-destructive techniques. Ultrasound testing was considered particularly useful for this purpose since it provides a priori information about the mechanical properties and level of decay of the members, it is non-invasive and its portability provides the necessary maneuverability given the restricted space. This being our first attempt at the technique, we decided to study its historic evolution in order to develop a methodology that would best adapt to our particular needs.

Literature review

The use of ultrasound as a non-destructive technique (NDT) originates mainly from tests on concrete during the 1940s. In the late 1950s new research efforts attempted to measure the mechanical properties of wood through the transmission of ultrasonic pulses (Waid and Woodman 1957). Over the following years, several studies showed a correlation between the mechanical and anatomical propererties of wood (Jayne 1959; Pellerin 1965). The ultrasound method developed rapidly during the 1970s and was consolidated in numerous publications from the 1980s to date. Two of those lines of research will be highlighted here:

1. *The statistical comparison of the results of mechanical properties testing on sawn timber and the results obtained through ultrasound.* Elvery and Nwokoye (1970) establish high correlation coefficients between ultrasound speed and some mechanical properties. Sandoz publishes a study (Sandoz 1989) grading the strength class of wood based on the elasticity and rupture moduli using the wave transmission velocity parallel to the wood grain, and demonstrates higher accuracy than with visual grading. In the same study he proposes that ultrasound wave velocity decreases by 0.8% for each 1% increase in wood moisture content.
2. *The use of ultrasound as a NDT for in-situ evaluation of the extent of decay of structural members.* These studies use velocity as an indicator of density loss due to decay (Sandoz and Benoit 2006). They have also been used to detect damage caused by xylophagous insects when velocity was abnormally low (Mantilla et al. 2008). In these studies velocity has generally been calculated using the equation

$$v = \frac{d}{t} \tag{1}$$

where v is the ultrasound velocity, d is the distance between transducers and t is the propagation velocity of the ultrasonic wave.

Numerous studies published in Spain report a high degree of prediction of the mechanical properties of wood based on ultrasound velocity (Acuña et al. 2006; Íñiguez 2007). Pioneer among them is a study on the load bearing capacity of old wood framed floors (Arriaga et al. 1992). These studies have confirmed the reliability of this technique, increasing its application to evaluate the degree of decay in structures in service (Rodrígez et al. 2004) and to grade their strength class (Arriaga et al. 2005). The following correlation between velocity and strength class was proposed according to the *UNE-EN-338* (Arriaga et al. 2002):

Low velocity= 4100 to 4900 m/s: Strength class C14 to C16
Medium velocity= 4900 to 5100 m/s: Strength class C18 (2)
High velocity= 5100 to 5400 m/s: Strength class C22

Finally, a recent study (Acuña et al. 2007), establishes a general equation of the second degree relating the velocity to the angle formed by the transducers and the grain.

$$V_\alpha = a\,\alpha^2 + b\,\alpha + c \quad (3)$$

where V_α is the velocity measured at an angle α, α is the angle formed by the transducers and the grain, and a, b and c are empirically obtained values specific to each species.
The same study proposes the following equation that obtains a high r^2 coefficient for all studied species:

$$V_\alpha = 0.721\,\alpha^2 + (-107{,}92)\,\alpha + 5564.6 \quad (4)$$

Objectives

The research objectives were (A) to determine the degree of wood decay, (B) to determine the strength class according to norm *UNE-EN 338*, and (C) to discuss the origin of the decay.

Materials and Resources

1. Ultrasound Equipment: Model *Steinkamp BP-V Ultrasonic Tester.* It has 50 KHz flat transducers and measures wave propagation time between the transducers.

2. Electric resistance Thermo-hygrometer: Model *Humytester 993 B*. It consists of a handle with insertable electrodes to measure the moisture content of wood.

3. Department of Microbiology of the University of Granada.

Methodology

The study was based on the readings of ultrasound velocities perpendicular to the grain in a manner consistent with previous studies (Sandoz and Benoit 2006; Mantilla et al. 2008: Rodríguez et al. 2004). The methodology was applied to two structural members of the roof: rafter P19 and hip jack PE50, located in vulnerable areas with maximum structural stress. The first two thirds of the members were easily accessible with the ultrasound equipment. The selection of the members was based on the building pathology inspection, which concluded that the greatest stress affected the first two thirds of some of the rafters and hip jacks, just prior to the intersection with the collar ties (figure 1). While PE50 showed fractures and signs of true dry rot, P19 presented no serious damage. The methodology was divided into two main phases: the data collection phase and the data analysis phase. It was complemented with fungal and bacterial cultures.

Data Collection Phase

The data collection phase included all activities conducted *in-situ*. It was divided into two sub-phases: *Markings* and *Measurements*.

Markings

This phase comprised the preliminary steps required to conduct the measurements. First, in order to obtain data from wood in good condition, six structural members were selected with similar features to P19 and PE50 but with no apparent damage, and four points were marked with chalk on each of them. Next, four symmetric point grids were marked, one on each face of P19 and PE50, in the areas of maximum bending moment.

Measurements

A moisture content measurement was conducted on each of the points marked with chalk using the thermo hygrometer, followed by a measurement of ultrasound velocity. The thermo hygrometer was programmed for the species *pinus silvestrys.* The ultrasound readings were conducted using the method of direct transmission perpendicular to the grain (figure 2), placing a transducer on one point and the other transducer on the symmetric point and measuring the propagation time of the ultrasonic wave pulse.

Figure 2— Direct transmission perpendicular to the grain.

Data Analysis Phase

The data analysis phase was conducted *ex-situ* and included tasks related to computational processing of the collected data. First, the data were entered into the Excel 14.0 program using equation 1 to obtain the ultrasound velocity for each point tested. Next, the arithmetic mean of the moisture content registered for each pair of symmetric points was calculated. Initially, the Sandoz relationship was considered for adjusting the velocities to the 12% moisture content. However, upon observation of recent studies (Goia et al. 2005, Calegari et al. 2011), we decided to use the regression line resulting from the relationship between the velocities in the structural members without apparent damage and their moisture content (figure 3).

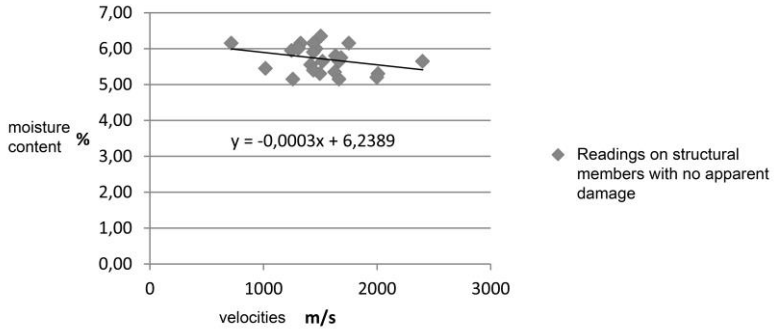

Figure 3— Relationship between the velocities in the structural members without apparent damage and their moisture content.

The adjusted mean velocity of the members without apparent damage was used as reference velocity to evaluate the decay of P19 and PE50. A reduction of 300 m/s was considered indicative of wood decay (Rodríguez et al. 2004). Secondly, the adjusted velocity and moisture data were entered into the Sigma 10 program to obtain isochromatic diagrams. The profiles of P19 and PE50 were represented with Autocad 2012 and superposed on the isochromatic diagrams using Photoshop CS4. The checks and those areas where the velocity could not be measured were represented in black. Thirdly, the following procedure was used to estimate the strength class:

For the velocity parallel to the grain, α=0. We substituted that value in equation 3 and obtained that $V_0 = c$. We used this equivalency in equation 4, obtaining the following expression:

$$V_0 = V_{90} - 0{,}721 \cdot 90^2 - (-107{,}92) \cdot 90 \quad (5)$$

where V_0 is the velocity of ultrasound parallel to the grain, and V_{90} is the mean velocity perpendicular to the grain in the structural members without apparent damage.

Knowing the value of V_0 we could estimate the strength class using equation 2.

Fungal and Bacterial Culture

Since PE50 presented signs of decay, a fungal and bacterial culture was performed to analyze the decay. A sample was extracted from an affected area and placed in an air-tight bag. The sample was inoculated on laboratory plates in various culture media for fungi and bacteria, which were incubated at 28ºC until the microorganism colonies were observable.

Results

The mean perpendicular adjusted velocity in structural members without apparent damage was 1420 m/s. Using equation 5, the parallel velocity V_0 would be 5282.7 m/s. According to equation 2, the wood would have a strength class C22, close to the C18 threshold.

The mean perpendicular adjusted velocity in P19 was 980.97 m/s. The highest velocities were registered around the axis, and the lowest at the knots and edges (figure 4). The mean moisture content was 6.41% with maximum readings close to the edges of approximately 8% and minimum readings at the knots of approximately 3%.

The mean adjusted perpendicular velocity in PE50 was 315.90 m/s (figure 4). It was impossible to obtain velocity readings in the areas with highest decay. The mean moisture content was 5.81%, with maximum readings in the edge area of approximately 10-14%, and minimum readings at the knots of approximately 3%.

Regarding the fungal and bacterial culture, the microscopic and macroscopic observation of the microorganism colonies led to the identification of the fungi *Aspergillus*, *Cladosporium*, two unidentified yeast types and the bacterium *Bacillus SP*.

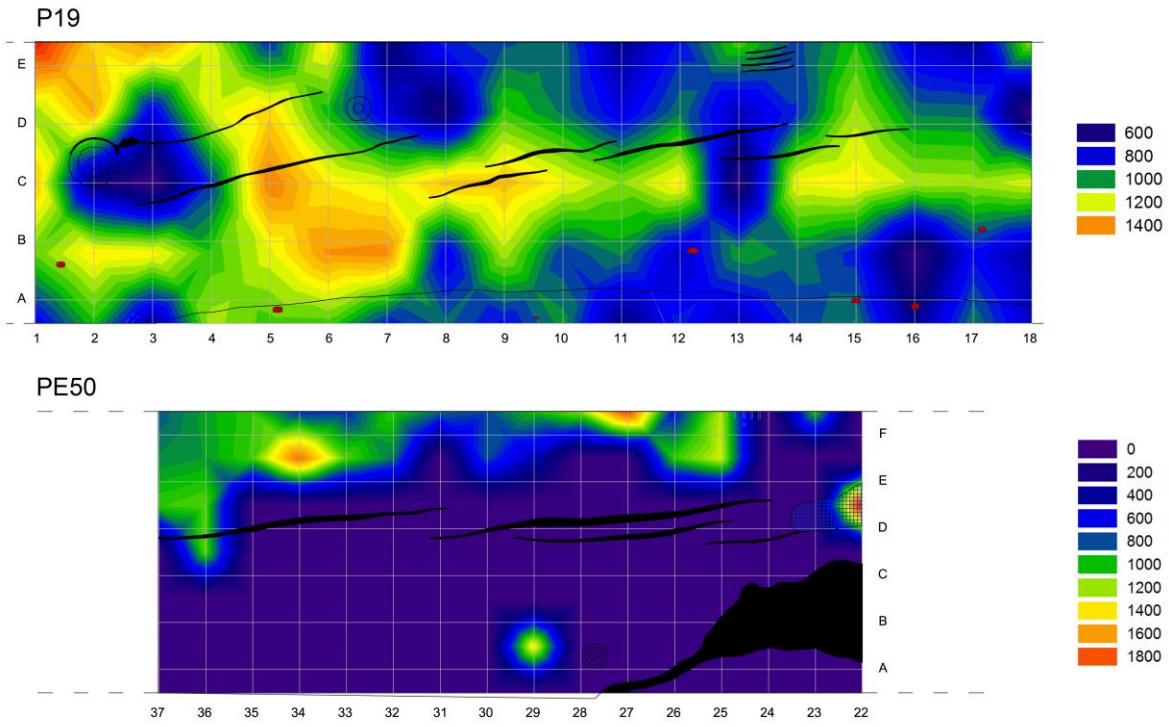

Figure 4— Ultrasound velocities in P19 and PE50.

Conclusions

A. The mean velocity in P19 decreased by 439.03 m/s, and in PE50 by 1104.10 m/s. Thus, both structural members are believed to have a high degree of decay and total or partial substitution is recommended.
B. It was possible to estimate the strenght class as minimum C18 and maximum C22, according to UNE-EN-338.
C. Regarding the origin of the decay, PE50 showed signs of true dry rot or cubic rot where the velocity decreased between 70% and 100%. The ash colored residue could be crumbled and suggested that the decay was caused by the basidiomycete fungus *Serpula lacrymans Lange*, even though it was not possible to isolate it in the fungal and bacterial culture. In the case of P19, the low velocity readings were collected in an area with several elliptical orifices. Given their shape and diameter of approximately 7 mm, they were identified as caused by an attack of xylophagous insects of the *Hylotrupes bajulus L* species. Considering the registered moisture levels, it is believed that neither of the attacks is active.
D. The following problems were identified during the course of the study and will need to be addressed before considering a possible, more extensive research project in the future:
- The coefficient of determination r^2 of the regression line of moisture content-velocity was too low. We believe this could be due to the statistically low number of samples used.
- It is possible that the moisture content readings were not optimal due to insufficient penetration of the thermo hygrometer's electrodes into the wood. Our literature review has not been able to identify an alternate non-invasive technique capable of detecting moisture content *in-situ* with greater precision.
- Equation 4 was obtained from a particular case in which only 5 species were analyzed, and it is uncertain to what degree our wood would perform in a similar way, especially considering that it has been in service for over 300 years.
- The use of a resistograph or a penetrometer would provide density data that would allow higher accuracy in the estimation of the strength class.

- The availability of equipment such as Sylvatest Duo or Microsecond Timer would be very useful for future studies, since it would enable us to obtain readings of velocity parallel to the grain. Additionally, it would allow us to compare our results to those of other studies, since it is a well-known fact that velocity readings vary according to the equipment used.

Acknowledgments

We thank the members of the Pedro Salmerón Escobar Architecture Studio and the faculty and staff of the Department of Mineralogy and Petrology and the Department of Microbiology at the University of Granada for their valuable help and support.

References

Acuña L.; Díez R.; Casado M. [and others]. 2007. La transmisión de ultrasonidos aplicada a la madera estructural. Laboratorio de Maderas de la Universidad de Valladolid. http://www3.uva.es/maderas/mad_0029.htm [Data accessed 7/31/2013]

Acuña, L.; Díez, M.R y Casado, M. 2006. Los ultrasonidos y la calidad de la madera estructural. Aplicación a Pinus pinaster Ait. CIDEU Report. 2: 7-26.

Arriaga, F.; Esteban, M.; Relea, E. 2005. Evaluation of the load carrying capacity of large cross section coniferous timber in standing structures. Materiales de Construcción. 55(280): 43-52.

Arriaga, F.; Peraza F.; Esteban M. [and others]. 2002. Intervención en Estructuras de Madera. AITIM Report. 476 p.

Arriaga, F.; García, L.; Gebremedhin, K.G. [and others]. 1992. Wood structures: Restoration, experimental studies of load carrying capacity of old timber beams. AITIM Report. 1(46): 51-62.

Calegari, L.; Gatto D.A.; Martins, D. 2011. Influence of moisture content, specific gravity and specimen geometry on the ultrasonic pulse velocity in eucalyptus grandis hill ex maiden wood. Ciência da Madeira. 2(2): 64-74.

Elvery, R.H.; Nwokoye, D.N. 1970. Strength assessment of timber for glued laminated beams. Proc Symp on Nondestructive Testing of Concrete and Timber. Institute of Civil Engineering, London, and the British Commission for NDT: 105−110.

Goia, F., Candian, M., Lucchette, F.F. [and others]. 2005. Moisture content effect on ultrasonic velocity in Goupia glabra. Materials Research- Ibero-American Journal of Materials. (8)1:11-14.

Íñiguez, G. 2007. Clasificación mediante técnicas no destructivas y evaluación de las propiedades mecánicas de la madera aserrada de coníferas de gran escuadría para uso estructural. Madrid: Universidad de Madrid. Doctoral Thesis.

Jayne, B.A. 1959. Vibrational properties of wood as indices of quality. Forest Products Journal. (9) 11. 413-416.

Mantilla, E.V.; Rocha, A.; Pires, A. [and others]. 2008. Methodology for analysis of the integrity of historical timber structures attacked by xylophagous insects by means of ultrasound. II Latin American Workshop on Non-Destructive Testing of Wood Products. Cartago, Costa Rica.

Nuere, E. 2001. Nuevo tratado de la carpintería de lo blanco. Madrid: Munilla-Lería. 309 p.

Pellerin, R.F. 1965. The contributions of transverse vibration grading to design and evaluation of 55-foot laminated beams. Proceedings of the 2d Symposium on Nondestructive Testing of Wood. Pullman, WA: Washington State University: 337–348.

Rodríguez, C.; Rubio de Hita, P.; Gómez de Cózar, J.C. [and others]. 2004. Diagnóstico mediante técnicas de ultrasonidos del forjado de madera del refectorio del convento de Santa Clara en Carmona, Sevilla. Informes de la construcción. 55(490): 17-28.

Sandoz, J.L., Benoit, Y., 2006. Acousto-ultrasonic non-destructive evaluation of historical wooden structures. International Conference on Structural Analysis of Historical Constructions. New Delhi, India: 519-526.
Sandoz, J.L. 1989. Grading of construction timber by ultrasound. Wood Science and Technology. 23: 95-108.

Waid, J.S.; Woodma, M.S. 1957. A non-destructive method of detecting diseases in woods. Nature. 180 (4575): 47.

Nondestructive Assessment of Wood Structural Members at Yu Tomb of the Ming Dynasty

Chunhui Liao
School of Technology, Beijing Forestry University, Beijing, China, cloudy_c119@163.com

Houjiang Zhang
School of Technology, Beijing Forestry University, Beijing, China, hjzhang6@bjfu.edu.cn

Xiping Wang
US Forest Service, Forest Products Laboratory, Madison, Wisconsin, USA, xwang@fs.fed.us

Dongqing Li
Beijing Research Institute of Architectural Heritages, Beijing, China, lee5697@vip.sina.com

Abstract

A detailed survey and inspection of the wood components was conducted during a structure renovation project at Yu Tomb of the Ming Dynasty. Visual classficication and nondestructive inspection procedures were employed to assess the physical and mechanical conditions of the wood members taken down from the Memorial Hall and the in-place members of the Three Gates and the Holy Beam. Stress wave timing and resistance micro-drilling tests were found effective in detecting internal structural defects of the wood components in ancient structures and providing scientific data for accurate condition classification. The results of this inspection project provided the architects and construction engineers reliable data to develop a cost-effective renovation plan that can maximize the reuse of the original materials, at the same time ensure the safety of the historic structure.

Keywords: Classification, defects, deterioration, nondestructive assessment, resistance micro-drilling, stress wave, wood component, Yu Tomb

Introduction

Ancient architecture is an important part of historical and cultural heritages in China. The preservation and restoration of old timber structures of highly historical significance has received a great attention in recent decades. Restoration of Yu Tomb (Chinese pinyin: *Yuling*), one of the Thirteen Tombs of the Ming Dynasty, is a recent example. The Ming tombs were put under protection of the Beijing municipal government in 1957. In July 2003, the World Heritage Committee of the United Nations Educational, Scientific and Cultural Organization (UNESCO) officially inscribed the Ming Tombs in Beijing on the World Heritage List as assemblage of the Imperial Tombs of the Ming and Qing Dynasties (UNESCO 2013).

Located in Tianshou Mountain, some 42 kilometers north—northwest of central Beijing, Yu Tomb buried Zhu Qizhen, the 6th Emperor of the Ming Dynasty and his empress. The construction of the tomb started in 1464 (the 8th year of Tianshun). The complex of the mausoleum mainly consists of the Gate of Eternal Favor, the Palace of Eternal Favor, the Soul Gate, the Square City and Soul Tower, wall surrounding the

tomb mound, and the tomb mound (Figure 1). The planning and the design of the mausoleum are simple and reflect the architectural art achievement in the Ming Dynasty.

The main structures of Yu Tomb were rebuilt from 1785 to 1787 (between the 50th to 52nd year of Qianlong). During the period of the Republic of China (1912-1949), the Palace of Eternal Favor was destroyed in the war, and the Gate of Eternal Favor was burned down in 1917 (the 6th year of ROC) (Chen et al. 2005). The Square City and Soul Tower only has skeleton remaining, and the roof is full of dirt and weeds. With the financial support from the Beijing municipal government and authorized by the National Bureau of Cultural Relics, the restoration of Yu Tomb structures was initiated in 2011. Figure 2 shows the site of Yu Tomb before the restoration project. Figure 3 shows the Square City and Soul Tower under repair.

The goal of this renovation project was to restore the damaged structures of the Square City and Soul Tower, the Triple Gates, and the Soul Gate, and save as much original materials as possible. To assist with the architects and construction engineers on developing a renovation plan, Beijing Forestry University was tasked to conduct a detailed condition survey on the wood members in the existing structures. The inspection of the wood components involved in species identification, visual assessment, and nondestructive evaluation of internal defects. The entire process was guided by the Chinese conservation principle for traditional ancient architectures, “Respect history, respect cultural relics, and maintain the original state with least intervention”.

Inspection Procedures and Methodology

The main objects of inspection were the wood components of the Square City and Soul Tower, including columns, lintels, brackets, purlins, and tie beams. A total of 62 wood members were taken down from the structure and stored on ground for visual assessment and nondestructive inspection. The wood members in the Triple Gates and the Soul Gate were inspected on-site while they were in place.

The inspection process was divided into two phases: 1) Visual assessment of appearance and external condition; 2) Nondestructive assessment of internal condition. Visual assessment was first conducted on each individual member by observing, measuring, and mapping the surface defects such as cracks, splits, decay, and structural damages. Longitudinal bending members were also examined for mechanical deflection due to loading. Internal condition of each wood member was assessed using a combination of sounding, stress wave timing, and resistance micro-drilling techniques. The final assessment of the wood structural members was made by analyzing the results from both visual and nondestructive measurements and evaluated based on the classification standards outlined in Table 1.

Classification Standard

We first established the classification standards for assessing the conditions of the wood components based on Chinese Standards GB50165-92 “Technical code for maintenance and strengthening of ancient timber buildings” (SBQTS 1992) and GB/T13942.2-2009 “Durability of wood – Method for field test of natural durability (SAC 2009). The condition of the wood components is generally classified into three categories: Class A—good condition, can be reused directly; Class B—slightly to moderately deteriorated, can be reused after repair; and Class C—severely deteriorated, can not be reused for original function. Table 1 lists the classification criteria and limits for different wood defects existed in the wood components.

Figure 1—Original appearance sketch of Yu Tomb

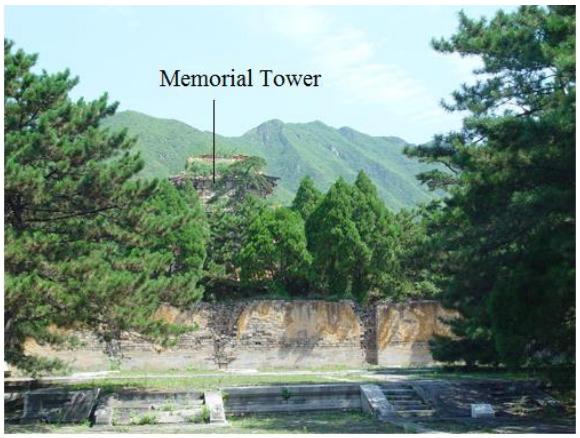

Figure 2—Site of Yu Tomb

Figure 3—Square City and Soul Tower under restoration

Table 1—Classification standards for evaluating wood structural members in ancient timber buildings.

Number	Defect type	Classification criteria	Classification limit		
			Class A: *Excellent*	Class B: *Good*	Class C: *Bad*
1	Surface decay and material loss	On any cross-section, the ratio of decay and material loss area (combined) and the whole area of the cross-section (*k*)	$k \leq 1/20$	$k=1/20\sim1/5$	$k>1/5$
2	Crack	The ratio of crack's length and beam's length (*l*);	$l \leq 1/10$	$l=1/10\sim1/3$	$l>1/3$
		The ratio of crack's depth and the beam's size in the direction (*d*)	$d \leq 1/10$	$d=1/10\sim1/3$	$d>1/3$
3	Deflection	The ratio of deflection and the length of the beam (*k*)	$k \leq 1/200$	$k=1/200\sim1/50$	$k>1/50$
4	Internal decay	On any section, the ratio of decay's area and the whole section's area (*k*)	$k=0$	$k=1/20$	$k>1/20$

Stress wave timing inspection

Wood components that were classified as Class A and B by visual assessment were subsequently inspected for internal condition using a stress wave timing (SWT) technique. SWT measurement for decay detection is based on the concept that stress wave propagation is sensitive to the presence of deterioration of wood members (Pellerin and Ross 2002). Stress waves travel faster through sound wood than they travel through decayed wood. When inspecting columns and purlins, the stress wave velocity was measured in radial direction with a 50-cm interval through the whole length. When inspecting the brackets and corner tie beams, the stress wave velocity was spot-measured at various locations of the beams to determine the soundness of different parts of the member.

Resistance micro-drilling inspection

Wood components that were classified as Class A and B by visual assessment and stress wave timing technique were then further evaluated using a resistance micro-drilling technique. Resistance micro-drilling enables detection of internal deterioration in a timber through measuring the relative resistance in the drilling path. The output of a micro-drilling test is a resistance profile showing density changes along the drilling path. High output characterizes high resistance or high density, and low output characterizes low resistance or low density. Internal decay or cavities in a timber are typically characterized as extremely low resistance or zero resistance in the resistance charts (Ross et al. 2004).

Analysis of inspection results

The baseline stress wave velocities for the two wood species used in Yu Tomb were determined through previous laboratory experiments (Liao, C. et al. 2013). The threshold stress wave velocity in radial direction is 1594 m/s for Nanmu (*Beilschmiedia*) and 1688 m/s for Chinese fir (*Cunninghamia Lanceolata*); The tangential critical velocity of Chinese fir is about 1612.2 m/s. Wood components that have a radial velocity significantly less than the threshold value is considered to have some forms of internal defects. The bigger the velocity difference (comparing with the threshold velocity), the more serious of the internal defects. The existence and extent of the potential defects was further evaluated and confirmed by analyzing the relative resistance profiles obtained through micro-drilling tests.

Results

Species Identification

The tree species of the wood members in Yu Tomb was identified through microscopic examination of small wood samples obtained from various wood components. The results indicated that Nanmu (*Beilschmiedia*) and Chinese fir (*Cunninghamia Lanceolata*) are two main species. Most columns and purlins are Chinese fir, and all beams and brackets are Nanmu**.**

Deterioration Types

Based on visual observation and nondestructive assessment, the wood components were found to have the following types of deteriorations: decay (internal and external), worm holes, breakage (parallel to grain), damage due to cracking, split or compression, deformation, and detachment. As an example, Figure 4 shows the columns and purlins with a range of conditions, from slightly deteriorated to severely deteriorated.

Figure 4—Columns and purlins taken down from the Square City and Soul Tower exhibiting a range of deterioration.

Internal Structural Defects

Internal structural defects of the wood components primarily included rot, cracks along the grain, and ring shakes. Detection and evaluation of such defects were based on the analysis of stress wave timing and resistance micro-drilling results. As an example, Figure 5 shows the schematic diagram of purlin No. 5 (25-cm diameter, 2.5-m long) with defect mapping. Visual observation indicated deep checks and cracks on the surface and decay at one end. Stress wave timing measurements at positions 1 though 7 showed radial stress wave velocities that were significantly less than the threshold value, indicating possible internal defects. It was determined that the low stress wave velocity at positions 1, 2, and 3 were caused by the extended deep checks along the grain as indicated in Table 2. However, from the resistance profiles collected at positions 4-7 (Figure 6), it was clear that the decay observed at the end has extended far into the purlin (colored area). Purlin No. 5 was first classified as Class B based on visual assessment. But with the detection of extensive internal decay, it was re-classified as Class C, which is severely deteriorated and can't be reused.

Table 2—Summary of stress wave timing and resistance micro-drilling tests for purlin No.5 [a]

Test location	Time (μs)	Stress wave velocity (m/s)	Resistance profile index	Condition
1	970	258		Deep check
2	325	769		Deep check
3	200	1250	3019	Deep check
4	215	1163	3017	Internal decay
5	300	833	3016	Internal decay
6	250	1000	3015	Internal decay
7	370	676	3014	Internal decay

[a] The moisture content of purlin No. 5 was measured as 9.7%

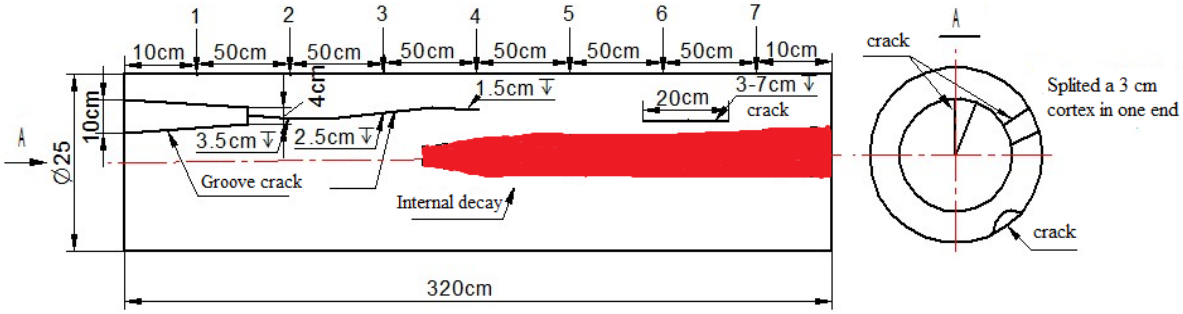

Figure 5—Schematic diagram and defect mapping of purlin No. 5.

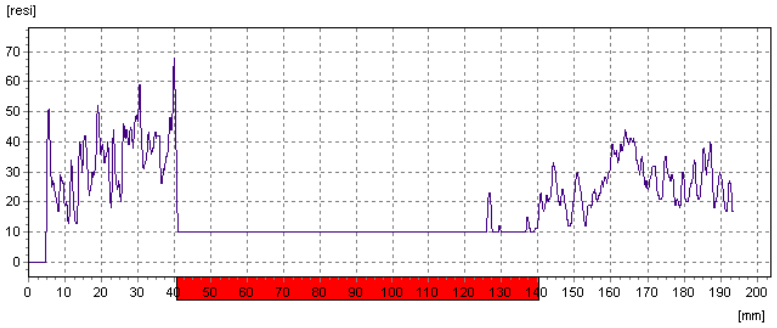

(a) Resistograph at location No.4 for purlin No. 5

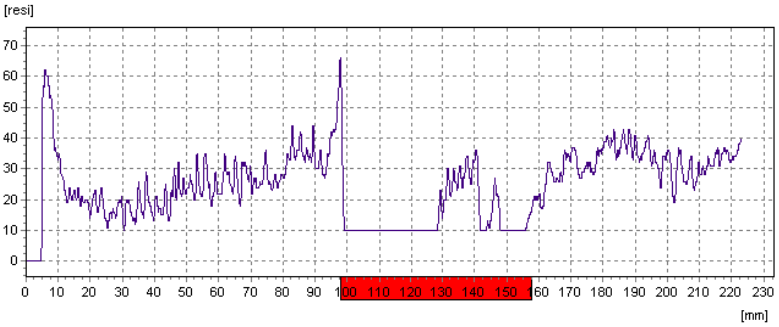

(b) Resistograph at location No.7 for purlin No. 5

Figure 6—Resistograph confirming internal decay in purlin No. 5

Wood Member Classification

Of sixty-two wood members inspected, three were identified as Class A based on the classification standards, twenty-six Class B, and thirty-three Class C. Based on this preliminary result, 29 wood members (both Class A and B) that had the potential to be reused were further inspected using a Fakopp Microsecond Timer and a Resistogarph tool. The three wood members that were originally identified as Class A were down-graded to Class B after some internal defects were detected through subsequent nondestructive tests. Eight Class B wood members were down-graded to Class C because of the large internal defects revealed by nondestructive tests. Therefore, the final classification results are 21 Class B members (can be reused after repaired) and 41 Class C members (should be replaced).

Renovation of Yu Tomb

The inspection and evaluation of the wood components was conducted at the very early phase of the Yu Tomb renovation project. The evaluation results provided basis for the architects and construction engineers to develop a cost-effective renovation plan that can maximize the reuse of the original materials, at the same time to ensure the safety and quality of the structure. During the restoration process, all Class C wood members that were defined as unusable for intended function were kept in a covered storage and served as potential fabric for repairing Class B wood members. All Class B wood members were fully restored to their original function through strengthening, partial replacement, and metal sheet connections. As an example, Figures 7 and 8 show the diagram and repair of the corner tie beam and bracket. Assisted with the inspection results, the contractor removed deteriorated portion in the member and replaced with new materials through gluing and reinforcing with metal sheet connectors. The repaired beams were then coat-treated with preservative solutions before installed back in the structure.

Figures 9 shows both the repaired and replaced wood components that have been reused in the restored structure of the Square City and Soul Tower. Figure 10 shows the overview of the Yu Tomb and the appearance of the Square City and Soul Tower after renovation.

Conclusions

A detailed survey and inspection of the wood components was conducted during a structure renovation project at Yu Tomb of the Ming Dynasty. Visual classficication and nondestructive inspection procedures were employed to assess the physical and mechanical conditions of the wood members taken down from the Memorial Hall and the in-place members of the Three Gates and the Holy Beam. Stress wave timing and resistance micro-drilling tests were found effective in detecting internal structural defects of the wood components in ancient structures and providing scientific data for accurate condition classification. The inspection results indicated that almost all the wood components in the structures of Yu Tomb have deteriated in varying degrees. Decay, worm holes, and damage due to cracking, splitting or compression, were the major structural defects observed. It was determined that 66% of the wood members were severely deterioated and can’t be reused. The remianing 34% of the members had slight to moderate deterioation and can be repaired for reuse in their original funcation. The results of the inspection provided the architects and construction engineers reliable data to develop a cost-effective renovation plan that can maximize the reuse of the original materials, at the same time to ensure the safety and quality of the historic structure.

Acknowledgments

This project was conducted through the research collaboration between Beijing Forestry University and the USDA Forest Products Laboratory (11-MU-11111133-031). The funding support through the Beijing Research Institute of Architectural Heritages is gratefully acknowledged.

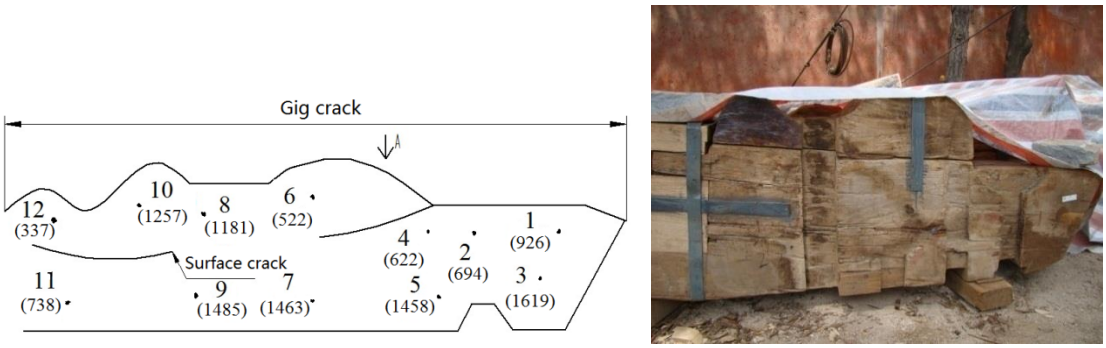

Figure 7—Schematic diagram and repair of a corner tie beam.

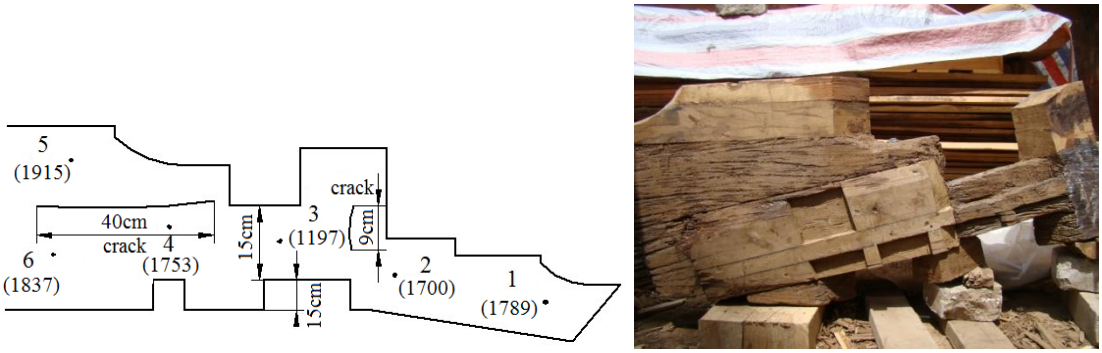

Figure 8—Schematic diagram and repair of a wooden bracket.

Figure 9—Structure restored with repaired and new wood members.

Figure 10—Square City and Soul Tower after renovation.

References

Chen, Y.; Liu, X.; Li, H. 2005. Issues concerning the preserving ancient timber structures. Journal of The Palace Museum. (5): 332-343.

UNESCO. Imperial tombs of the Ming and Qing Dynasties. http://whc.unesco.org/en/list/1004, accessed on July 13, 2013.

Ross, R.J.; Brashaw, B.K.; Wang X.P.; White R.H.; Pellerin, R.F. 2004.Wood and timber condition assessment manual. Forest Products Society, Madison, USA.

Liao, C.; Zhang, H.; Li, D. 2013. Method to calculate the critical velocity of the stress wave in defects detection of ancient architecture wood members. Journal of Northwest Forestry University, (4).

Pellerin, R.F.; Ross, R.J. 2002. Nondestructive evaluation of wood. Forest Products Society. Madison, WI, USA.

The State Bureau of Quality and Technical Supervision (SBQTS). 1992. National Standards of the People's Republic of China, GB50165-92 “Technical code for maintenance and strengthening of ancient timber buildings”, China Building Industry Press, Beijing, China.

Standardization Administration of the People's Republic of China (SAC). 2009. National Standards of the People's Republic of China, GB/T13942.2-2009 “Durability of wood –Part 2: Method for field test of natural durability”, China Standard Press, Beijing, China.

Structural Assessment of the Timber Structure of the Casa Grande Building in the Real Cortijo de San Isidro, Aranjuez, Madrid (Spain)

Francisco Arriaga
ETSI Montes, Universidad Politécnica de Madrid, Madrid, Spain, francisco.arriaga@upm.es

Miguel Esteban
ETSI Montes, Universidad Politécnica de Madrid, Madrid, Spain, miguel.esteban@upm.es

Guillermo Iñiguez-Gonzalez
ETSI Montes, Universidad Politécnica de Madrid, Madrid, Spain, guillermo.iniguez@upm.es

Ignacio Bobadilla
EUIT Forestal, Universidad Politécnica de Madrid, Madrid, Spain, i.bobadilla@upm.es

Daniel F. Llana
ETSI Montes, Universidad Politécnica de Madrid, Madrid, Spain, d.f.llana@upm.es

Mariano Gonzalez-Sanz
Consultant Engineer, Segovia, Spain, marianogonzalezsanz@gmail.com

Abstract

The timber structure of a two-story building from the XVIII century, located in Aranjuez, Spain, was evaluated using nondestructive techniques. These consisted of stress wave measurements and probing tests based on needle penetration depth, to estimate the modulus of elasticity, modulus of rupture and density. A detailed inspection of the timber pieces was carried out to detect biological damage, the dimensions of members and the weight of the construction systems themselves. Nine predictive models for MOE and MOR were applied to the NDT measurements obtained in this building. These models had been proposed by several authors for the same wood species in previous experimental works, but under different conditions in terms of piece sizes, moisture content and the positioning of sensors, etc. Modification factors were applied to measurements in order to give consistent results. The predicted values obtained are similar for the different models used. The range of variation for MOE is ±7% and for MOR ±13%.

Keywords: assessment, case study, non-destructive methods, timber structure

Introduction

In 1776 king Carlos III moved his residence from Madrid to the royal palace in Aranjuez (48 km to the South of Madrid). He bought farmland 6 km from the royal palace for the development and testing of modern agriculture. This same year, a building was constructed for the king´s residence, his entourage and the head of the farm; this building was termed the “Casa Grande” (Big House). Other buildings were also built for the workers and agricultural uses. The whole site (farmland and village) is known as the “Real Cortijo de San Isidro”.

At present, most of the "Casa Grande" is owned by the National Park Department, a public body of the Ministry of Agriculture, Food and Environment. Restoration and consolidation work on the flooring has recently taken place, and there is a project for the restoration of the roof. The building is substantially rectangular in floor plan with a central courtyard, and it is two stories high with masonry and brick walls, Figure 1. Only the Eastern half of the building is under restoration. The first floor has a timber joist structure, except for some parts which these have been replaced with another material. The roof structure consists of a collar roof system (rafters and ties) and trusses (king post trusses) in one of the rooms.

Figure 1—Left: historical center of the "Real Cortijo de San Isidro" village. Right: detail of the "Casa Grande" building.

The aim of this paper is to show the possible consistency of results when applying different predictive models based on non-destructive testing techniques using stress wave velocity measurements and probing to estimate the mechanical properties of structural timber.

Methodology

General data compilation

Species identification: a total quantity of 8 samples of wood were selected for the microscopic identification of the wood species: 2 samples from timber joists and 2 from beams in the floor system of area *G*, Figure 3; and 4 samples from rafters in the roof structure. In all cases the species was characterized as Scots pine (*Pinus sylvestris* L.) or Laricio pine (*Pinus nigra* Arnold); it is not possible to distinguish anatomically between both species. Both are typical coniferous woods used in construction in Central Spain. Considering their location it is more likely that they are Scots pine, and in any case the physical and mechanical properties of both species are very similar.

Visual stress grading: this methodology, which is the most commonly used to define the mechanical properties of new timber, was discarded for practical reasons in this work. Scots pine (and also Laricio pine) timber visually graded as MEG grade according to the UNE 56544 Spanish visual grading standard is assigned to strength class C22 according to the EN 1912 standard. The MEG grade is applied to large cross-section pieces (wider than 70 mm according to UNE 56544 standard), and in practice almost all the timber pieces in existing structures comply with the specifications of this grade (Esteban et al. 2009). It is therefore reasonable to assign strength class C22 as a preliminary estimation.

Geometry: the cross-section of timber pieces in existing structures is not generally a regular rectangular shape, but has wanes and, in some cases, notches to offer better support for the filling material between

joists. In practice, the dimensions of cross-sections are measured as if it were a rectangle in the actual profile. The properties of the cross-section (area, moment of inertia and section modulus) obtained are therefore slightly larger than the actual ones. As an example, Figure 2 shows two cross-sections with typical notched faces where the differences between moment of inertia and section modulus of the rectangle and the actual cross-section are less than 3%.

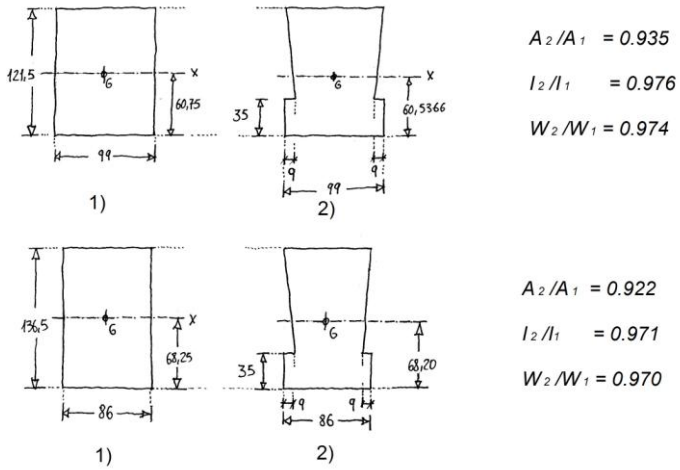

Figure 2—Face notch effect on cross-section properties (A: cross-section area, I: moment of inertia and W: section modulus; 1: rectangle and 2: notched cross-section.

Moisture content: the moisture content (MC) of timber pieces was evaluated using electrical resistance equipment (Gann RTU 600). This measurement was made with two objectives: to detect areas of the structure with high MC and decay processes, and to know the MC in order to adjust nondestructive measurements (for which MC is measured in healthy areas of timber pieces).

Density estimation by probing: Pilodyn 6J Forest equipment was used to estimate the density of timber pieces. This consists of the measurement of the depth of penetration of a 2.5 mm diameter steel needle released with a constant energy of 6 Joules. This measurement was made in healthy regions of timber surfaces.

Stress wave velocity: Microsecond Timer equipment (Fakopp) was used to determine the stress wave velocity. These measurements were made in two different arrangements. When possible, the sensors were situated in opposite faces of the timber piece and at the maximum distance possible in practice. In this case the straight line between sensors and the grain direction form a small angle. This type of measurement is called semi-direct. When the faces of timber pieces were not accessible, the measurement was taken by placing the sensors on the lower face of the timber piece, which is its only accessible surface. This is called indirect measurement. The values of velocity obtained (semi-direct and indirect) were corrected to obtain the reference value of velocity parallel to the grain and from end to end of the timber piece (direct measurement), as is explained at the end of the next Section.

Prediction models for physical and mechanical properties

Stress wave velocity (using the Microsecond Timer) in large cross-section timber of Scots pine has been studied in previous works in order to estimate the bending modulus of elasticity (MOE) and the modulus of rupture (MOR). The following linear regressions have been proposed (Montero 2013):

$$MOE = -13369 + 4.571 \cdot v \qquad (r^2 = 0.53) \qquad (1)$$
$$MOR = -105 + 0.0289 \cdot v \qquad (r^2 = 0.35) \qquad (2)$$

where v is the velocity in m/s obtained in end-to-end (direct) measurement.

The penetration depth obtained with the Pilodyn 6J was used to estimate the density of timber pieces of Scots pine in several works. The data from these works and linear regression equations are given below:

- 116 pieces 150x200 mm in cross-section and 4.2 m in length with a mean value of density of 485 kg/m^3 and a coefficient of variation CoV = 8.8% (Montero 2013):

$$\rho = 630 - 12.72 \cdot P \qquad (r^2 = 0.29) \qquad (3)$$

- 60 pieces 150x200 mm in cross-section and 4.7 m in length and 60 pieces 200x250 mm in cross-section and 5.2 m in length with a mean value of density of 505 kg/m^3 and a CoV = 10% (Iñiguez 2007). The density, ρ (kg/m^3), may be obtained from the following equation:

$$\rho = 712 - 19.07 \cdot P \qquad (r^2 = 0.52) \qquad (4)$$

- 30 pieces 150x200 mm in cross-section and 30 pieces 200x250 mm in cross-section with a mean value of density of 504 kg/m^3 and a CoV = 10% (Iñiguez et al. 2010). The density, ρ (kg/m^3), may be obtained from the following equation:

$$\rho = 726 - 20.54 \cdot P \qquad (r^2 = 0.61) \qquad (5)$$

  where P is the penetration depth of the steel needle in mm. The influence of *MC* in this value has been studied in Douglas-fir species and an increase of 0.19 mm was proposed for each 1% increase in *MC* for the Pilodyn 6J (Smith and Morrell 1986). On the other hand, studies (Calderón 2012) using methods of measuring moisture content closer to the methods used in this work and for the range of 8 to 18% *MC*, show that there is no clear relationship with penetration. Therefore, in this study this adjustment factor was not applied.

The dynamic modulus of elasticity (MOE_d) can be obtained from velocity and density by the following equation:

$$MOE_d = \rho \cdot v^2 \qquad (6)$$

In the previously cited work (Montero 2013) the MOE_d in large cross-section Scots pine timber has also been studied in order to estimate *MOE* and *MOR*, and the following linear regression equations have been proposed:

$$MOE = 804 + 0.7180 \cdot MOE_d \qquad (r^2 = 0.63) \qquad (7)$$
$$MOR = -13.92 + 0.004433 \cdot MOE_d \qquad (r^2 = 0.40) \qquad (8)$$

Other similar research works used ultrasonic waves instead of stress wave. These works propose prediction models for *MOE* and *MOR* based on ultrasound velocity. The velocity of transmission of waves obtained by ultrasound (v_{us}) is slightly higher than that obtained by stress wave (v). The following ratio has been obtained (Gil 2011):

$$v_{us} / v = 1.022 \qquad (9)$$

This ratio was obtained by testing 40 pieces of Scots pine 45x145 mm in cross-section and 4.4 m in length by measuring velocities with ultrasound equipment at a frequency of 23 kHz (Sylvatest Duo) and stress wave with Microsecond Timer (Fakopp). It would then be possible to use prediction models based

on ultrasound velocity, adjusting the velocity obtained by the stress wave procedure; at least when the size of the pieces, quality of timber and distances are similar. Here are some examples of work using ultrasound techniques on Scots pine.

- The velocity of ultrasound waves (Sylvatest) was obtained in 85 pieces of Scots pine 40x150 mm in cross-section and 3 m in length (Hermoso 2001). The mean value of density was 477 kg/m^3 (CoV = 7.6%). The following linear regression was deduced for MOR:

$$MOR = -94.99 + 0.0263 \cdot v_{us} \qquad (r^2 = 0.34) \tag{10}$$

  where v_{us} is the ultrasound velocity in m/s obtained in end-to-end measurement (direct measurement); where $v_{us} = 1.022 \cdot v$.

- Ultrasound velocity (using the Sylvatest Duo) in large cross-section Scots pine timber was studied in the previously cited research work (Iñiguez 2007) in order to estimate the bending modulus of elasticity (*MOE*) and the modulus of rupture (*MOR*), and the following linear regressions were proposed:

$$MOE = -10534 + 4.192 \cdot v_{us} \qquad (r^2 = 0.53) \tag{11}$$
$$MOR = -55.79 + 0.0190 \cdot v_{us} \qquad (r^2 = 0.50) \tag{12}$$

- Finally, research work was carried out using timber beams from a dismantled 18th century building (Esteban 2003, Arriaga et al. 2005, Arriaga et al. 2009). The ultrasound velocity (using Sylvatest Duo) was measured in 25 pieces of Scots pine 141x196 mm in cross-section and 4.5 m in length, with a mean density value of 513 kg/m^3 and CoV = 15%. In this case, the cross-section of timber pieces contains the usual irregularities in existing structures. *MOE* and *MOR* linear regression with ultrasound velocity are as follows:

$$MOE = -13613 + 4.559 \cdot v_{us} \qquad (r^2 = 0.54) \tag{13}$$
$$MOR = -88.68 + 0.0247 \cdot v_{us} \qquad (r^2 = 0.45) \tag{14}$$

All of the previous equations are based on velocity and MOE_d referred to a *MC* of 12% and to a direction parallel to the grain (direct measurement). The following modification factors were used for these adjustments:

- Moisture content: the velocity with reference to 12% *MC* is obtained by the following equation:

$$v_{12} = v_H \cdot [1 + (H-12) \cdot k_H] \tag{15}$$

  where H is a % and $k_H = 0.0075$, is the modification factor for *MC*.

  The effect of *MC* on velocity has been studied in 30 pieces of Spruce (100x140 to 100x220 mm cross section and 2.8 to 4.4 m length), with a decrease in ultrasound wave velocity of approximately 0.8 % for every 1 % increase in *MC*, and for a variation of *MC* in the range from 5 to 30% (Sandoz 1989). Another recent work examined the determination of the effect of *MC* on ultrasound velocity, stress waves and longitudinal vibration by testing 26 pieces of Scots pine - *Pinus sylvestris* L. - (100x150 mm in cross section and 3.0 m length) for a variation of *MC* from 21 to 12%. A decrease in velocity of approximately 0.6% (in ultrasound and stress wave) and 0.7% (longitudinal vibration) was deduced for each 1% increase in *MC* (Montero 2013).

  Velocity is related with MOE_d and density according to equation 6. The EN 384 standard (2010) establishes an increase of 1% for the modulus of elasticity (*MOE*) for each 1% decrease in *MC*, and a

decrease of 0.5% density for each 1% decrease in *MC*. If it is assumed that the influence of *MC* is the same for the static and dynamic *MOE*, the resulting value for velocity would be 0.75%; therefore, the velocity would increase by 0.75% for each 1% decrease in *MC*. This value is close to the 0.7-0.8% interval obtained in the cited works for velocity adjustment. This value was therefore adopted in this work.

- The angle between the sensors and the grain: the velocity with reference to the direction parallel to the grain v_0, is obtained from the velocity measured at an angle α, v_α, by the following equation:

$$v_0 = v_\alpha \, (1+\alpha \cdot k_\alpha) \tag{16}$$

where $k_\alpha = 0.01$, is the angle modification factor. This modification factor was obtained from ultrasound velocity measurements in 80 pieces of Radiata pine 150x200 mm in cross section and 4 m in length (Iñiguez 2008). The velocity parallel to the grain was v_0 = 4859 m/s, the velocity from face to opposite face, over a length equal to 18 times the thickness of the piece, was v_α = 4744 m/s (α = 2.38º). This velocity reduction is equivalent to a decrease of *1* % in velocity for each 1º of slope to the grain. The influence of angle to the grain in ultrasound velocity was also studied for Spanish Scots pine (Acuña et al. 2007) with pieces of approx. 60x400x2000 mm. For an interval of 0º to 6º, the decrease in velocity for each 1º of slope to the grain was 1.49 %. This value is slightly higher than previous findings.

- The modification factor for indirect measurements: when the measurement is made by placing the sensors in the same face of the timber piece (in case only the lower face is accessible) the direct velocity (end to end measurement) v, can be obtained from indirect measurement v_{in} by the following equation:

$$v = 1000 + 0.817 \cdot v_{in} \tag{17}$$

This relationship was deduced by measuring ultrasound velocity in 80 pieces of Radiata pine 150x200 mm in cross section and 4 m in length (Iñiguez 2007, 2008). The velocity parallel to the grain was v = 4859 m/s, and the velocity obtained by positioning the sensors on the same face over a length equal to 18 times the depth was v_{in} = 4724 m/s. The ratio v_{in}/v = 0,972.

The prediction models included in this Section are based on direct and semi-direct but not indirect measurements. However, in the assessment of the building studied in this paper semi-direct and indirect measurements were carried out, and equation 17 was used to adjust velocity to the reference value.

Results and discussion

Figure 3 shows the plan of the first floor joists system and the plan of roof structure (ties and rafter levels) including the designation of areas and numbering of inspected pieces. Table 1 summarizes the geometry and NDT measurements for each inspected area of the building. It is interesting to note that the coefficient of variation of dimensions of the cross-section of pieces varies from 5 to 18 %, except for the collar beam pieces which have a higher value (19 to 25%), probably because they are short secondary pieces, and the carpenters were not worried about their cost/efficiency ratio, Figure 4. On the other hand, the velocity measurements have a much lower CoV (4 to 7%). The depth penetration with Pilodyn present a CoV of from 8 to 30%; this big difference is probably due to variations in the surface health of timber pieces (decay may be present but is not visible).

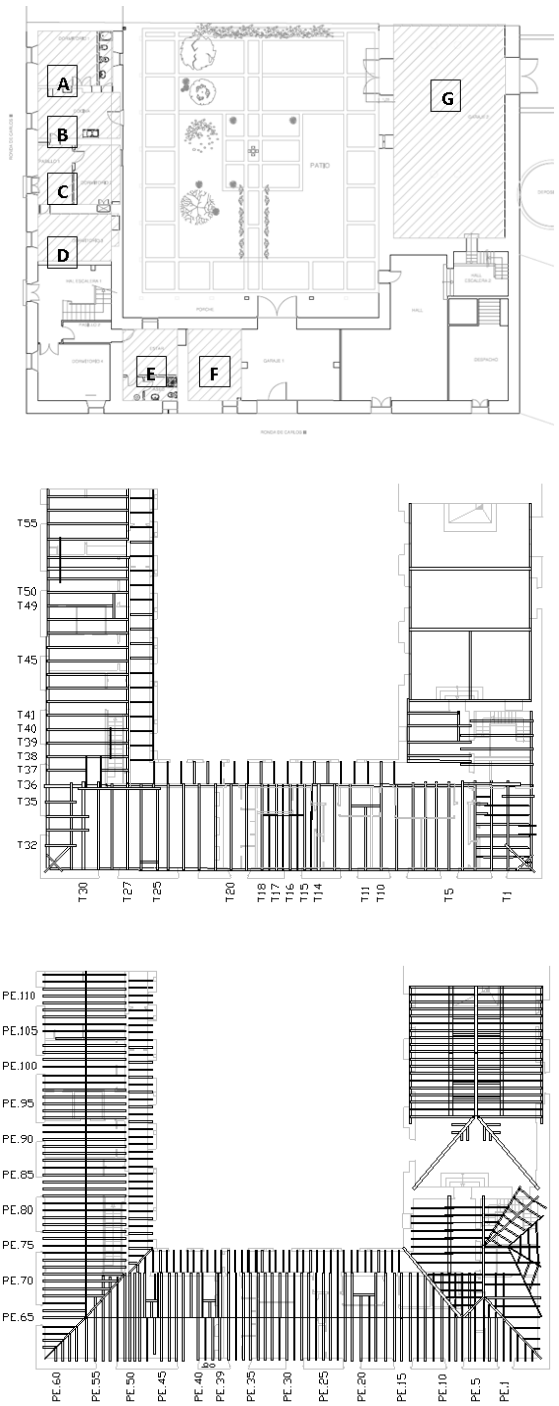

Figure 3—Up: floor joists, Middle: roof ties, Bottom: roof rafters.

The values of density estimated according to equations 3, 4 and 5 give a mean value 515 kg/m^3 (8% CoV), 484 kg/m^3 (1% CoV) and 520 kg/m^3 (7% CoV), for the groups of joists: beams, rafters and ties, respectively.

Table 2 summarizes the *MOE* and *MOR* values estimated for each kind of timber piece (joists, beams, rafters and ties) according to the different prediction models (equations 1, 2, 7, 8 and 10-14). In spite of different prediction models and parameters (velocity or dynamic modulus of elasticity) having been used, the resulting values for *MOE* and *MOR* do not differ noticeably.

The central value and its range for *MOE* are 10115 N/mm^2 ±7% (joists), 10849 N/mm^2 ±8% (beams), 10416 N/mm^2 ±7% (rafters) and 10999 N/mm^2 ±7% (ties). These values are slightly higher than *MOE* assigned to C22 strength class timber (10000 N/mm^2). Furthermore, the central value of the mean values and its range for *MOR* are 40.4 N/mm^2 ±4% (joists), 43.7 N/mm^2 ±3% (beams), 41.9 N/mm^2 ±7% (rafters) and 46.3 N/mm^2 ±9% (ties).

The characteristic value of strength is defined for 5% probability of failure. In this work the number of pieces of each group is very small (not higher than 18).Due to this, the minimum value of predicted *MOR* was considered as an approximation to the characteristic value.

Thus the central value of the minimum values and its range for *MOR* are 27.4 N/mm^2 ±13% (joists), 40.2 N/mm^2 ±5% (beams), 31.6 N/mm^2 ±11% (rafters) and 35.7 N/mm^2 ±7% (ties). As it could be expected, there is a higher variation in results for minimum values than for mean values. The characteristic value for bending strength in the C22 strength class is 22 N/mm^2 , and the minimum estimated values are always above this value.

It is interesting to note that the minimum/mean *MOR* value ratio obtained for beams is 0.92, which is the highest ratio compared with the other types of pieces (joists, rafters and ties). The cross-section of beams is 333x258 mm, which is much greater than that of the other pieces, Figure 5. The quality of timber may also be better, because in such large cross-sections knots are not present at the surface.

Table 1- Summary of recorded data (geometry and NDT measurements).

Area	Piece	Geometry (mm)					NDT measurements						
		n	*b* *CoV*	*h* *CoV*	*l*	*s*	*n*	*MC%* *CoV%*	*P mm* *CoV%*	*v m/s* *CoV*	*Type*	*Dist.* *mm*	α^o
A	joist	6	137 12%	-	5450	308	4	10.8 21%	13.0 8%	4702 6%	I	1925	-
D	joist	7	139 5%	129 18%	5500	449	4	-	9.0 11%	4550 3%	I	1853	-
E	joist	4	118 14%	148 10%	4000	407	4	17.8 16%	8.5 15%	4835 6%	I	1764	-
F	joist	6	131 6%	152 5%	5200	396	-	-	-	-	-	-	-
G	joist	66	140 9%	175 5%	3340+ 1650	338	7	16.1 3%	-	4696 7%	I	1946	-
							3	-	11.5 30%	5076 3%	SD	3411	2.4
	beam	6	333 2%	258 2%	-	-	2	15.6 4%	-	5143 5%	I	1383	-
							6	14.4 12%	11.8 4%	4760 1%	SD	3156	6.0
Roof	rafter	26	112 8%	128 10%	3130	495	13	12.2 6%	9.69 21%	4881 6%	SD	2176	3.0
	tie	8	135 10%	146 9%	5700	1086	9	12.9 10%	11.0 10%	5004 4%	SD	2871	2.8
	c.beam	8	82 25%	74 19%	2050	495	-	-	-	-	-	-	-

n number of measured pieces;
b, h mean values of width and depth of cross-section of the piece, respectively;
l, s mean values of span and distances between axes of joists, respectively;
MC mean value of moisture content in timber pieces;
P mean value of penetration depth of Pylodin needle;
v mean value of stress wave velocity;
Type positioning of sensors for time of flight measurements: I: indirect and SD: semidirect;
Dist. mean value of distance between sensors for time of flight measurements;
α^o mean value of angle between the straight line between sensors and the longitudinal axis of the piece.

A total quantity of 63 timber joists in area *G* were measured in cross-section, giving a coefficient of variation of 9 and 5% for width and depth, respectively, Table 1. This variation in dimensions gives a higher variation in section modulus (CoV=15%) and moment of inertia (CoV=20%). The relative values of section modulus and moment of inertia vary from 1 to 2 and 1 to 2.7, respectively, Figure 6. The variation in load carrying capacity due to variations in cross-section size is much greater than those due to the different prediction models.

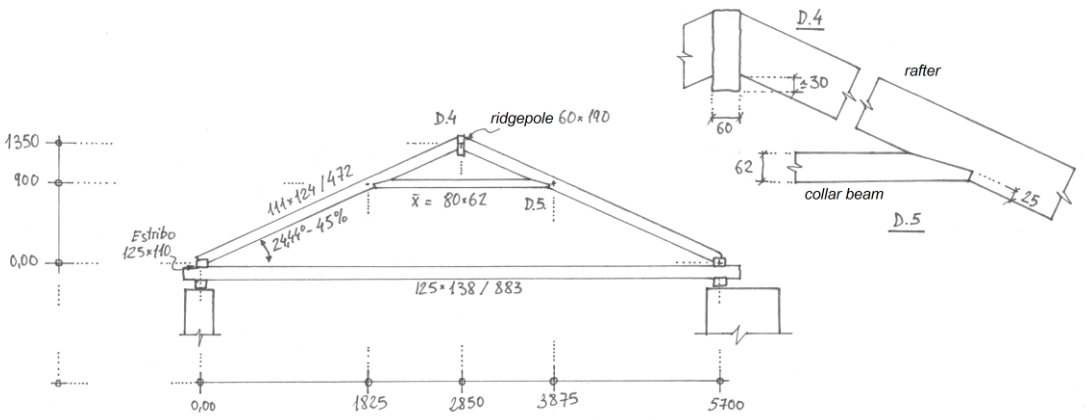

Figure 4—Collar beam roof structure.

Table 2- Summary of results for estimation of the *MOE* and *MOR*.

Type	P.P.	*MOE* (N/mm^2)				*MOR* (N/mm^2)				
		Eq.	mean	CoV%	n	Eq.	mean	CoV%	min	n
Joists	*v*	1	9672	15	18	2	40.7	22	23.9	18
						10	40.5	20	24.9	18
		11	11062	12	18	12	42.1	14	30.8	18
		13	9873	15	18	14	38.6	20	23.9	18
	MOE_d	7	9851	20	8	8	41.9	28	27.4	8
Beams	*v*	1	-	-	-	2	-	-	-	-
					6	10	44.5	9	40.3	6
		11	11701	6	6	12	45.0	6	42.0	6
		13	10568	7	6	14	42.3	9	38.4	6
	MOE_d	7	9996	4	13	8	42.8	6	40.0	6
Rafters	*v*	1	9723	15	13	2	41.0	22	28.8	13
						10	40.8	21	29.5	13
		11	11109	12	13	12	42.3	14	34.1	13
		13	9925	15	13	14	38.8	20	28.2	13
	MOE_d	7	10350	12	13	8	45.0	17	35.0	13
Ties	*v*	1	10319	11	9	2	44.8	16	34.7	9
						10	44.3	15	34.9	9
		11	11668	9	9	12	44.8	11	38.0	9
		13	10532	11	9	14	42.1	15	33.3	9
	MOE_d	7	11236	17	9	8	50.5	23	35.7	9

P.P.	predictor parameter: *v*, velocity and MOE_d, dynamic *MOE* (in this case mean value resulting from equations 3, 4 and 5 was used)
Eq.	equation for prediction
Mean	mean value of *MOE* or *MOR*
CoV	coefficient of variation
min	minimum value of *MOE* or *MOR*
n	number of pieces measured

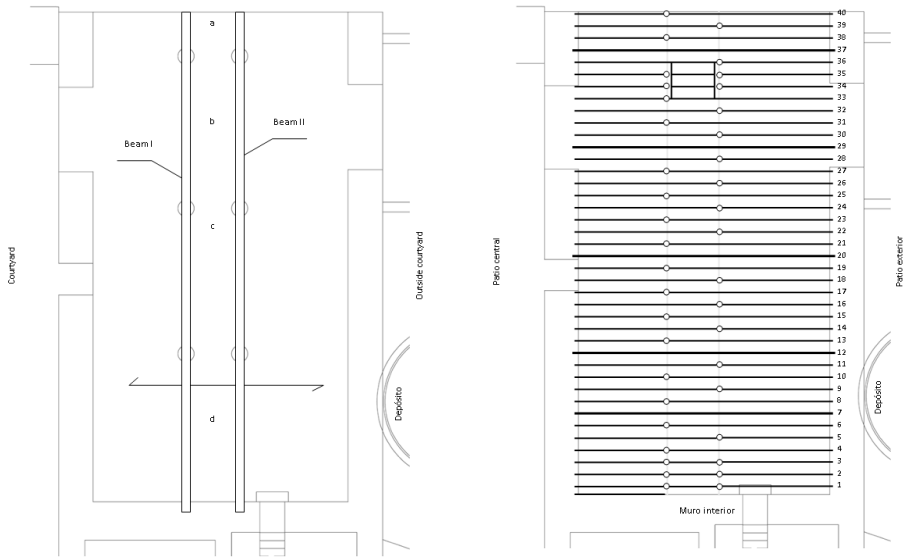

Figure 5—Area G. Left: main beams supported by stone columns. Right: joists with alternate hinged support on the beams.

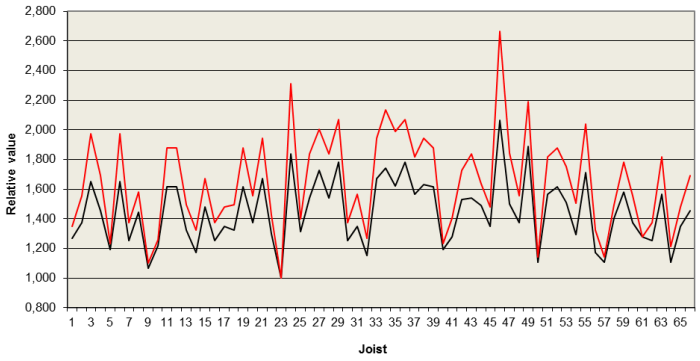

Figure 6—Relative value of Section modulus (black color) and Moment of inertia (red color) for timber joists of area *G*.

Conclusions

Several adjustment factors for velocity measurements were proposed depending on the kind of wave (stress wave and ultrasonic wave), moisture content and sensor positioning (angle with respect to the grain and direct and indirect measurement).

Different prediction models of mechanical properties based on nondestructive methods were applied to the NDT measurements of the timber structural pieces of the building studied. Measurements were adjusted for the factors, and the prediction models lead to very similar values of *MOE* and *MOR*, with a range of variation of 8 and 13%, respectively.

The mechanical property values predicted for different types of pieces (joists, beams, rafters and ties) are very similar and do not differ from each other. There is one exception in the beams, which are of large cross-section, where the prediction gives a higher strength compared with the other types of pieces.

The variation in cross-section dimensions leads to variation of the moment of inertia and section modulus (which are linked to the load carrying capacity, deformation and strength) that is much greater than that obtained by the use of different prediction models.

Acknowledgments

Ministerio de Ciencia e Innovación, Plan Nacional I+D+i 2008-2011. (Ministry of Science and Innovation) Proy.: BIA2010-18858. Asociación de Investigación Técnica de la Madera (Timber Technical Research Association) AITIM. Alfredo Villalba, architect from the Organismo Autónomo Parques Nacionales, Ministerio de Agricultura, Alimentación y Medio Ambiente, España (National Park Department, Ministry of Agriculture, Food and Environment, Spain). Arriaga and Iñiguez-Gonzalez are members of the COST Action FP1101 "Assessment, Reinforcement and Monitoring of Timber Structures".

References

Acuña, L.; Díez, R.; Martín, L.; Casado, M.; Basterra, A.; Ramón, G.; Relea, E. 2007. La técnica de transmisión ultrasónica aplicada a la madera estructural. Asociación Española de Ensayos no Destructivos. 11º Congreso Español de END, Gijón, 2007. pp. 91-102.

Arriaga, F.; Esteban, M.; Relea, E. 2005. Evaluation of the load carrying capacity of large cross section coniferous timber in standing structures. Materiales de Construcción (mater construcc). Vol. 55, nº 280, pp: 43-52.

Arriaga, F,; Iñiguez, G.; Esteban, M.; Bobadilla, I. 2009. Proposal of a Methodology for the Assessment of existing Timber Structures in Spain. Proceedings of the 16th International Symposium on Nondestructive Testing and Evaluation of Wood. Beijing.

Calderón, L. 2012. Estudio sobre la influencia del contenido de humedad de la madera en ensayos no destructivos para *Pinus nigra* Arn., *Pinus radiata* D. Don. y *Pinus sylvestris* L. (Study of the influence of moisture content of wood in nondestructive testing for *Pinus nigra* Arn., *Pinus radiata* D. Don. and *Pinus sylvestris* L.). Final Project Escuela Universitaria de Ingeniería Técnica Forestal, Universidad Politécnica de Madrid.

European standard 2012. EN 1912. Structural timber. Strength classes. Assignment of visual grades and species. European Committee for Standardisation, Brussels/Belgium.

European standard 2010. EN 384. Structural timber. Determination of characteristic values of mechanical properties and density. European Committee for Standardization Brussels/Belgium.

Esteban, M. 2003. Determinación de la capacidad resistente de la madera estructural de gran escuadría y su aplicación en estructuras existentes de madera de conífera (Determination of the load carrying capacity of large cross section structural coniferous timber on existing structures). Doctoral Thesis. Universidad Politécnica de Madrid, ETS de Ingenieros de Montes. 365 p. PDF file: http://oa.upm.es/1404

Esteban, M.; Bobadilla, I.; Arriaga, F.; Iñiguez, G.; García, H. 2009. NDT applied to estimate the mechanical properties of the timber of an ancient structure in Valsaín, Segovia (Spain). Proceedings of the 16th International Symposium on Nondestructive Testing of Wood. 2009, Beijing Forestry University. Pp. 152-157.

Hermoso, E. 2001. Caracterización de la madera estructural de *Pinus sylvestris* L. (Characterization of structural timber of *Pinus sylvestris* L.). Doctoral Thesis. Universidad Politécnica de Madrid, ETS de Ingenieros de Montes.

Iñiguez, G. 2007. Clasificación mediante técnicas no destructivas y evaluación de las propiedades mecánicas de la madera aserrada de coníferas de gran escuadría para uso estructural (Grading by non destructive techniques and assessment of the mechanical properties of large cross section coniferous sawn timber for structural use). Doctoral Thesis. Universidad Politécnica de Madrid, ETS de Ingenieros de Montes. 223 p. PDF file: http://oa.upm.es/415

Iñiguez, G.; Esteban, M.; Arriaga, F.; Bobadilla, I.; Gil, M.C. 2008. The Influence of Specimen Length on Ultrasound Wave Velocity. Proceedings of the 15th International Symposium on Nondestructive Testing of Wood. Forest Products Society. Pp. 155-159.

Iñiguez, G.; Arriaga, F.; Esteban, M.; Bobadilla, I.; González, C.; Martínez, R. 2010. In situ non-destructive density estimation for the assessment of existing timber structures. Proceedings of the 11th World Conference on Timber Engineering. Riva del Garda, Trento, Italy.

Gil, MC. 2011. Influencia del tamaño y la calidad de la pieza en la estimación de las propiedades mecánicas de la madera de *Pinus sylvestris* L. para uso estructural mediante técnicas no destructivas (Size and quality effect on nondestructive techniques for mechanical properties estimation of structural timber of *Pinus sylvestris* L.). Final Project. ETS Ingenieros de Montes, Universidad Politécnica de Madrid.

Montero, M.J. 2013. Clasificación de madera estructural de gran escuadría de Pinus sylvestris L. mediante métodos no destructivos. (Grading of structural large cross-section timber of Pinus sylvestris L. by nondestructive methods). Doctoral Thesis. Universidad Politécnica de Madrid, ETS de Ingenieros Agrónomos. 345 p.

Montón, J. 2012. Clasificación estructural de la madera de Pinus radiata D. Don procedente de Cataluña mediante métodos no destructivos y su aplicabilidad en la diagnosis estructural. (Structural grading of Pinus radiata D. Don timber from Catalonia using nondestructive methods and their applicability in structural diagnosis). Doctoral Thesis. Universidad Politécnica de Cataluña, EU Politécnica de Cataluña. 160 + 309 pp.

Sandoz, J.L. 1989. Grading of construction timber by ultrasound. Wood Sci. Tech. vol 23: 95-108.

Smith, S.M.; Morrell, JJ. 1986. Correcting Pilodyn measurement of Douglas-fir for different moisture levels. Forest Products Journal, Vol 36 No1, pp. 45-46.

UNE 56544:2011 Clasificación visual de la madera aserrada para uso estructural. Madera de coníferas. Visual grading for structural sawn timber. Coniferous timber. Asociación Española de Normalización (AENOR), Madrid, Spain.

Nondestructive assessments of the timber roof structure of the “São Francisco Church” in Florianopolis, Brazil

Leandro Dussarrat Brito
Department of Structural Engineering – SET, Laboratory of Wood and Wooden Structures – LaMEM, University of São Paulo – USP, São Carlos School of Engineering – EESC, São Carlos, São Paulo, Brazil, dussarrat@sc.usp.br

Carlito Calil Junior
Department of Structural Engineering – SET, Laboratory of Wood and Wooden Structures – LaMEM, University of São Paulo – USP, São Carlos School of Engineering – EESC, São Carlos, São Paulo, Brazil, calil@sc.usp.br

Abstract

The objective of this paper was to use the main methods of nondestructive techniques (NDT) during the works of inspections "in situ" for the evaluation of timber roof structural members of the "São Francisco Church" in Florianopolis, Santa Catarina State, in Brazil. For this, in the inspections of the timber structural members, were used nondestructive techniques (NDT) of the visual inspection for evaluations of visual characteristics due to the presence of defects; sounding with hammer, probing test; moisture content survey; and resistance micro drilling with Resistograph IML-RESI-F500-S for evaluations of internal conditions in cross sections of the main timber structural members selected. The results generated by resistograph were plotted against the amplitude of the intensity levels of resistance to drilling in wood, on the entire cross section drilled. The criteria of choice for localized points for surveys were conducted in regions previously detected, either on visual inspection, on sounding, on probing test and after moisture content survey, in all timber roof structural members that showed signs of superficial fungal rot and holes or cavities with features derived from termites and beetles, and regions of support beams, as these regions had moisture conditions favorable to proliferation of organizations bio deteriorative. The use of resistograph in nondestructive techniques (NDT) inspections to internal evaluations of the wood has demonstrated a very efficient method, fast and simple, indicating a good prediction of deterioration level in the internal cross sections inspected.

Keywords: structures, timber, inspection, assessment, decay, nondestructive techniques

Introduction

This paper presented the main pathological manifestations observed by nondestructive assessments of the timber roof structural members of the “São Francisco Church” in Florianopolis, Brazil.

General information

Restoring existing structures for reuse of the building is a major trend in the global issue of sustainability, (CÓIAS, 2011). With this attitude you can reduce waste generation and material consumption that would result from the process of constructing a new building at the place of that old one existing. In this context

have been used instrumental methodologies for inspections and maintenance of timber structures. Like subsidy in various countries have been used several nondestructive techniques (NDT) to inspections and assessments of the timber structures.
Neglecting or becoming irregular maintenance, predisposes to the timber structure of the roof to the development of deterioration or wear of the elements that compose it, and imply the need for rehabilitation with reinforcements, recoveries for the use intended, or even the condemnation of the structure. In this context, it has been researched methodologies for technical inspection and rehabilitation of structures of timber structures in the "Laboratory of Wood and Timber Structures" (LaMEM), the School of Engineering of São Carlos (EESC), University of São Paulo (USP).

Objective

This work has as main objective to present the main methods of nondestructive techniques (NDT), used in inspections of structure of the timber roof structure, to identify and evaluate possible pathologies present. It is essential to carry out periodic inspections on timber structures, to evaluate and identify signs of possible pathological manifestations, and indicate possible solutions preventive maintenance or corrective, to ensure the durability requirements for useful life of timber structures extension and securing those structures on the current conditions of use.

Theoretical foundation

Agents of wood decay

The wood decay is a process that adversely change wood properties. In broad terms, it can be attributed to two primary causes: biotic (living) agents and abiotic (nonliving) agents, respectively referred in (HIGHLEY and SCHEFFER 1989); (RITTER and MORRELL 1990); (ARRIAGA et al 2002); (CALIL JR. 2006); (MACHADO et al 2009); (CALIL JR. and BRITO 2010).

The Biotic agents of decay are living beings, such as organisms that attack wood include bacteria, fungi (Mold and stain fungi; brown rot fungi; white rot fungi; Soft rot fungi), insects (Termites; Subterranean Termites; Beetles), and marine borers (pholads, shipworms, Limnoria) cited in (HIGHLEY and SCHEFFER 1989); (RITTER and MORRELL 1990); (ARRIAGA et al 2002); (CALIL JR. 2006); (MACHADO et al 2009); (CALIL JR. and BRITO 2010). These organisms require certain conditions for survival, such as moisture, oxygen, temperature, and suitable source of food, usually wood. Although the degree of dependence of these parameters is variable, each must be present to decay to occur, referred in (HIGHLEY and SCHEFFER 1989) and (RITTER and MORRELL 1990). Some of these organisms use the wood as a food source, while others use it for shelter, (RITTER and MORRELL 1990).

The abiotic agents of decay include ultraviolet light, metal corrosion by-products, mechanical abrasion, impact, strong acids or bases, wood damaged by fire, anomalies design structural and constructions, cited in (HIGHLEY and SCHEFFER 1989); (RITTER and MORRELL 1990); (ARRIAGA et al 2002); (CALIL JR. 2006); (MACHADO et al 2009); (CALIL JR. and BRITO 2010). Damage by abiotic agents can be mistaken for biotic attack, but the lack of visible signs of fungi, insects, marine borers, plus the general appearance of the wood, can alert the inspector to the nature of the damage. Although destructive in their own right, abiotic agents can also damage the preservative treatment, exposing untreated wood to attack by biotic agents (RITTER and MORRELL 1990).

Nondestructive techniques for inspections and evaluation

Nondestructive evaluation is the science of identifying the physical and mechanical properties of materials without changing its end-use capabilities and then using this information to make decisions regarding appropriate applications. Nondestructive evaluation (NDE) technologies have contributed significantly toward detect structural problems. Table 1 show many tests and techniques evaluation categorized as nondestructive by PELLERIN and ROSS (2002).

Table 1 – Nondestructive techniques (PELLERIN and ROSS 2002).

Avaliação não destrutiva da madeira (NDT)	
Evaluation of visual characteristics	Chemical tests
Color Presence of defects	Composition Presence of treatments - Preservatives - Fire retardants
Physical tests	Mechanical tests
Electrical Resistance Dielectric properties Vibrational properties Wave Propagation Acoustic emissions X-ray	Flexural stiffness Proof loading - Bending - Tension - Compression Probes/coring

The main nondestructive techniques (NDT) for inspections in timber structures in order to estimate the damage to the wood caused by biotic agents of decay, such as beetles, termites and fungi, are usually simple and require minimal equipment. Methods for detecting deterioration in timber structures are divided into two categories: those for exterior deterioration and those for interior deterioration. In both cases, specific methods or tools are appropriate for certain types of damage, and their usefulness varies depending on the type of structure, (HIGHLEY and SCHEFFER 1989); (RITTER and MORRELL 1990). The techniques for detecting exterior deterioration highlight the technique of visual inspection (NDT) with records images; probing test or pick test is one of the simplest, a pointed pick, awl, or screwdriver is driven a, and as a chisel or punch to discover layers in regions not visible, to detect extent of the attack and find the galleries (cavities) in order to determine the severity of the damage; measuring the moisture content with the moisture meter. The techniques for detecting internal deterioration stand out, with sounding test with hammer, cited in (HIGHLEY and SCHEFFER 1989); (RITTER and MORRELL 1990); (ARRIAGA et al 2002), supplemented with microdrilling with Resistograph to evaluate the resistance to perforation the wood and can be used alone or in combination (ARRIAGA et al 2002); (ARRIAGA et al 2002); (PELLERIN and ROSS 2002); (BRITO and CALIL JR. 2013).

Although, a variety of inspection methods may be employed, in practice the inspector uses only a few tools. The methods or tools are often dictated by budget, previous experience, and the types of problems that are encountered. No equipment can replace a well-trained inspector who has a broad knowledge of wood systems. The timber structure inspectors have the difficult task of accurately assessing the condition of an existing structure. They must understand the biotic and physical factors associated with wood deterioration as well as the relative rate at which these processes occur in a given environment. Timber inspection is a learned process that requires some knowledge of wood pathology, wood technology, and timber engineering, (RITTER and MORRELL 1990).

Methodologies

Technical Visits

To do the assessments were performed inspections with technical visits "in situ" to identify possible pathological manifestations found and evaluate the current conditions of the timber roof structural members. For this work were used the Nondestructive Technique (NDT) by Visual Inspection to evaluations of visual characteristics due to detecting the presence of external pathological manifestations and the Resistograph IML-RESI-F500-S to detect internal deterioration.

Assessments of the timber roof structures

The nondestructive techniques used in this work were by Visual Inspection to evaluate the characteristics related to external structural problems, that is, assessments of the pathological manifestations of timber structural members, deterioration due wood humidity and deterioration due fungi and insects attacks. And the Resistograph related to internal structural problems. Figures 1 to 13 shows the major types of structural problems detected.

Biotic agents of deterioration these timber roof structures

a b c

Figure 1 - External view with indicative absence of preventive maintenance: Visual signs of potential deterioration with Plants growth.

a b c

Figure 2 - Moisture stains and discoloration caused by stain fungi.

a b c

Figure 3 - Visual signs of potential deterioration in end beam removed that show with visual characteristics of wood infected with white rot fungi in an advanced stage, decayed is abnormally light colored with dark streaks. These characteristics occur because the white rot fungus feeds upon the cellulose, hemi-cellulose, and the lignin and makes the wood white and stringy.

a b c

Figure 4 - Beams with visual characteristics of wood infected with brown rot fungi decayed has a darkened color with a cracked, brittle surface that resembles charred wood, as cited in [RITTER & MORRELL, 1990]. These characteristics occur because the brown rot fungus degrades the cellulose and hemi-cellulose leaving the lignin as a framework which makes the wood dark brown and crumbly. These beams were in regions susceptible to moisture concentrations, as can be noticed visual characteristics of moisture stains. The top of the wood beam C32 were infected with termites in an advanced stage.

a 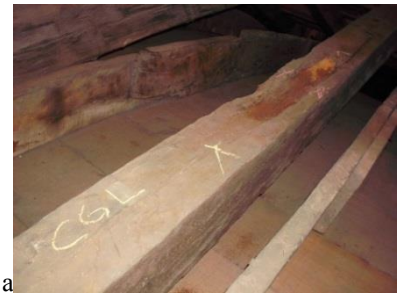 b c

Figure 5 – Beams with visual characteristics of wood infected with soft rot fungi. Note the shallow depth of decay in the Beam C6L.

Note: In cases where it is necessary identify the type of fungi, it are recommended analyzes biological in laboratory. Soft rot in wood often appears brown and can be confused with decay caused by brown rot fungi.

a b c

Figure 6 - Visual signs of potential deterioration in beams with termites and the wood damage they caused. Note in the tunnels, cavities and holes the frass and debris accumulations that are indicatives of termites in activity.

a b c

Figure 7 - Visual signs of potential deterioration in beams with termites and the wood damage they caused (continued).

a b c

Figure 8 - Beams with visual characteristics of wood infected with beetles. Note that the tunnels, cavities and holes of the beetles are bigger than of the termites. The beetle larvae tunnel through the wood, without discoloring it, and leave behind a flourlike frass.

a b c

Figure 9 – Longitudinal check in beams caused by potential deterioration with infestations of the termites and the wood damage they caused.

a b c

Figure 10 – In specific regions was detected severe pathologic manifestations by visual inspection technique followed by probing test and sounding test with hammer, was used the mapping with Resistograph-IML-RESI F500-S for these internal assessments timber structural members. This example is a timber beam that had superficial pathological manifestations, such as holes, termite tunnels and longitudinal checks external, however the diagram Resistograph-IML-RESI F500-S in the cross section microdrilling showed good resistance to drilling wood, with indicative only superficial pathological manifestations.

Figure 11 – This diagram by Resistograph-IML-RESI F500-S show an example of internal voids problems in cross section with potential deterioration in timber beams with cavities and termites tunnels in longitudinal check.

Figure 12 – Pathological manifestations with indicative of maintenances and incorrect conceptions (part 1): a) timber beams with insufficient cross section; b) beams with deformation by creep c) lateral buckling side timber beam.

Figure 13 – Pathological manifestations with indicative of maintenances and incorrect conceptions (part 2): a) Anomalies in joints b) incorrect notch favors the splitting (thru) checks c) incorrect reinforcement with splice joint inefficient.

Conclusions

Most of the types of deterioration have been analyzed using visual inspection and also mechanical equipment like Resistograph microdrilling technique. Detailed evaluation and technical report has been carried out with the support of the "Laboratory of Wood and Wood Structures" (LaMEM), São Carlos School of Engineering (EESC), University of São Paulo (USP).

It is concluded that for the evaluation of structural elements of wood, visual inspection technique has proved very efficient for the detection of abnormalities visible to diagnose pathological manifestations surface, to estimate the damage to the wood caused by abiotic agents such as checks, splits, cracks, deformations, and by biotic agents, such as beetles, termites and fungi, are usually simple and require a minimum equipments.

In this work, it was possible to detect pathologies in various timber structural members, which could be avoided with regular inspections and preventive maintenance.

There was finding the lack of preventative maintenance and control timber roof structures, by professional inspector specialist timber structure in this historic church in Florianópolis, Brazil.

There are in Brazil, numerous historic churches that need to be restored. In this way the assessment, maintenance and rehabilitation of timber roof structures must be an important subject for the future of timber structures in Brazil.

The routine sequential for recommendation at the inspection process of timber structures, can be used the techniques as indicated below the:

- ✓ visual inspection technique, with records photos;
- ✓ probing test or pick test with mortise chisel;
- ✓ moisture meter;
- ✓ sounding technique with hammer;
- ✓ microdrilling with resistograph;

Acknowledgements

The authors thank CNPq (National Council for Scientific and Technological Development.) for its financial backing of this work.

References

ARRIAGA, F.; PERAZA, F.; ESTEBAN, M.; BOBADILLA, I.; GARCÍA, F. 2002. Intervención en estructuras de madera. ISBN: 8487381243. Ed. AITIM, Madrid, España.

ABNT NBR 7190:1997. Projeto de estruturas de madeira. Rio de Janeiro. Brasil.

BRITO; L. D.; CALIL JR., C. 2013. Use Resistograph IML-RESI-F500-S for inspection NDT to internal assessments of structural timber elements. CINPAR 2013 - IX International Congress on Pathology and Recovery Structures. João Pessoa, Brazil.

CALIL JUNIOR., C. et al, 2006. Manual de projeto e construção de pontes de madeira. ISBN: 85-98156-19-1. Suprema, São Carlos, Brasil. Free download: <*http://www.set.eesc.usp.br/_portal/pt/livros/361-manual-de-projeto-e-construcao-de-pontes-de-madeira*>

CALIL JUNIOR., C.; BRITO, L. D. 2010. Manual de Projeto e Construção de Estruturas com Peças Roliças de Madeira de Reflorestamento. ISBN: 978-85-8023-000-0. Depto. de Eng. de Estruturas, EESC/USP. São Carlos, Brasil. Free download: <*http://www.set.eesc.usp.br/portal/pt/livros/371-manual-de-projeto-e-construcao-de-estruturas-com-pecas-rolicas-de-madeira-de-reflorestamento*>

CÓIAS, V. 2011. Qualificação dos profissionais e das empresas para a qualidade na reabilitação de estruturas de madeira. CIMAD 11 – 1º Congresso Ibero-Latino Americano da Madeira na Construção. Coimbra, Portugal.

HIGHLEY, T. L.; SCHEFFER, T. 1989. Controlling decay in waterfront structures. Evaluation, Prevention, and Remedial Treatments. Department of Agriculture, Forest Service, Forest Products Laboratory. FPL-RP-494. Madison, WI, U.S.A.

MACHADO, J. S.; DIAS, A.; CRUZ, H., CUSTÓDIO, J. E. P.; PALMA, P. M. C. 2009. Avaliação, Conservação e Reforço de Estruturas de Madeira. ISBN9789896420659. Ed. Verlag Dashöfer, Portugal.

PELLERIN, R. F.; ROSS, J. 2002. Nondestructive Evaluation of Wood. Forest Products Society, Madison, WI, USA.

RITTER, M. A.; MORRELL, J. J. 1990. Timber bridges. Department of Forest Products, Oregon State University, USA.

Condition survey and repair of wooden bridges in the Czech Republic

Veronika Hunková
Department of Wood Processing, Faculty of Forestry and Wood Technology, Mendel University, Brno, Czech republic, veronika.hunkova@mendelu.cz

Abstract

There are about twenty covered wooden bridges from the 18th and 19th century in the Czech Republic. All of them are protected. Over the last ten years some of their owners performed some repairs. Careful methods of condition survey and reparation were used in accordance with their historical value. In this paper two of them are presented. The whole process of the survey, evaluation and repair techniques are described. The acoustic measurement was used on the footbridge in the village of Švařec and a new simple instrument for the survey was used for the bridge in Prudká. The instrument was designed for teaching of survey performance and this was the test of its applicability on a real wooden structure. The paper contains an example of the methods used for the repair of the historical bridge and recommendations for Prudká footbridge at the end.

Keywords: wooden bridge, assessment, repair, monument, protection

Introduction

Approximately twenty historical wooden bridges and footbridges have been preserved in the Czech Republic. Three of them are on the river Svratka. They are among the protected national heritage sites and all reconstructions should be performed under the supervision of National Heritage Institute (NPU). The highest footbridge is located in the village of Švařec. It is followed by a road bridge in Černvír. The last footbridge is located in the village of Prudká and it is used by pedestrians and cyclists alike.

Footbridge in the village of Švařec

The footbridge in Švařec (Fig. 1) was built in 1873 by the local people. This period was also confirmed dendrochronologically (felling time was determined in between 1869 and 1870) (Kloiber et al. 2005). The footbridge is 22.6 m long and its passage width is 1.6 m. The height of the footbridge is 3 m, the height of the ridge above the river Svratka reaches 5 m. The footbridge is supported by two stone pillars of 2 m of height. Fir and spruce wood was used for the construction.

The main bearing elements are two double beams. The lower ones of the diameter of approx 45 × 35 cm and the total length of 22.6 m are laid on bedding timbers. On top of them, four lower diameter beams (30 × 28 cm) are laid. They are of half length and are firmly connected with the lower ones by bolts with in-built beech connectors. Two long bolts bind the main bearing beams perpendicularly towards their length over the stone pillars. Furthermore, the vertical posts bearing purlins are connected to the stringers with the use of bolts. Apart from that, they are tenoned in the beams. Three floor beams in total are located under the main supports. Two of them are located behind the bedding timbers and one is hung on wrought iron straps on double bearing beams in the middle of the footbridge. Supports which ensure transversal reinforcement of the structure are tenoned in the floor beams. The reinforcement is used as a handrail and supports the roof.

Figure 1 — Footbridge in Švařec (a) and view of its aisle (b)

Diagonal straps (two lower and two upper ones), which are tenoned into the central post and the upper ones are fixed into purlins through dovetail halving, are used for the longitudinal reinforcement of the structure. These elements are also tenoned in the side posts. The purlins are fitted with rafters. The rafters are connected at the top with halving with a pin and strutted with a collar tie (also halving). The first, the middle, and the last several rafters are supported with an X-tie. The saddle roof is covered with five rows of split shingles.

Condition

Preliminary survey was performed in 2004. Significant deflection of the footbridge was obvious at the first sight. The measured values at the northern and southern beams were 15 and 17 cm. Significant damage by house longhorn beetle (*Hylotrupes bajulus*) and brown rot was found (Fig. 2a,b). One of the reasons was the tailed-in bedding timbers at beams. The bedding timbers were heavily damaged and the moisture was transferred directly to the beams (Fig. 2a). Furthermore, the damage of floor beams was clearly obvious. Their protection by wooden boards against weather conditions was insufficient (Fig. 2c).

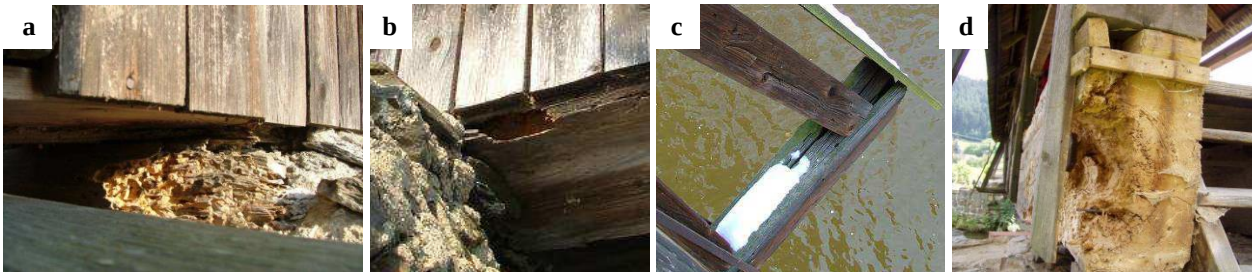

Figure 2 — Bedding timber on left bank pillar (a), hole in south main beam (b), snow on floor beam in middle part (c), western head of main beam on western side (d)

Further survey required an approval of the National Heritage representatives, since it was necessary to remove the lining. Therefore, this survey was only performed the next year. After the removal of the footbridge siding and floor, really poor condition of beams was found (Fig. 2d). On the basis of National Heritage Institute request, experts (Kloiber et al. 2005) were invited to perform non-destructive survey to find the extent of damage. The measurements were performed with the use of the device Arborsonic, which measures ultrasound penetration through wood. The measurements were performed in perpendicular as well as longitudinal direction towards the axis of the beams.

The survey showed that the assumed remaining mass is insufficient after the transfer of load. Some of the posts damaged by house longhorn beetle were intended for replacement. All of the posts had been

replaced within the previous repairs. All of them were closer to the western bank. This also corresponds with more extensive damage of the beams. The representatives of National Heritage Institute neither agreed with the replacement of the main beams by glued beams, nor with the use of different material than wood. A new problem appeared regarding the availability of the material, i.e. such wooden logs from which it would possible to produce beams of the necessary dimensions (approx 45 × 35 cm and length of 22.5 m). The reconstruction was postponed until the following year.

New beams were produced according to a statics opinion (Hrdlička 2006) in the same way as the original ones, i.e. from two finished beams laid on each other in opposite directions. This eliminated their thinning. The total 90 cm height is kept along the whole length of the beams. The beams were produced with extra 4.5 cm camber in order to compensate the deflection. The connection of beam into a grid bearer was performed with the use of 36 threaded rods M16 with square washers and nuts. In contrast to the original, vertically embedded, beech connectors (Fig. 3a,b), oak pins were selected and embedded horizontally (Fig. 3c). There are 34 connectors in total and they are placed in between threaded rods, with the exception of the middle part of the footbridge.

Reconstruction

The disassembling of the structure took nearly a week. It was performed very carefully. Thanks to this fact, all wooden elements which did not need to be changed for not being damaged by woodborers were saved. Similarly, the majority of metal parts, including nails, were extracted.

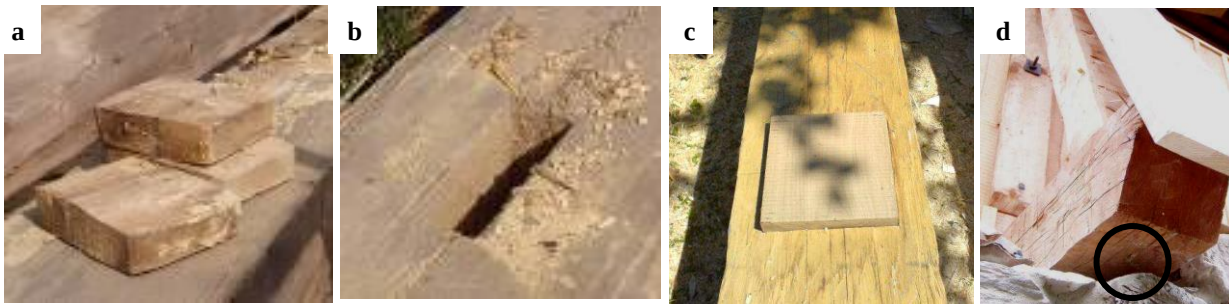

Figure 3 — Connectors in the original (a,b) and new lower bearing beam (c), opening in floor beam for the drainage of rainwater (d)

What followed was the repair of stone pillars by concrete mortar. The heights of the stone pillars were reduced. The bedding of beams would be ventilated better. The edges of the pillar are sloped towards the edges to allow easier drainage of rainwater and the splashing water would be taken from the bridge structure. Apart from that, anchoring bolts were built in the pillars. According to the statics calculation, the beams were finished and the holes for connectors (Fig. 3c) were prepared. They were laid on top of each other by a crane, drilled and bolted. All this was performed on the bank for safety reasons.

The assembly of the structure was done similarly to how the builders assembled it in the past. New elements were prepared on the bank, but the fine finishing was done during the assembly. New floor beams were drilled through at the place of tenons of a tenoned brace (Fig. 3d). The resultant opening will allow drainage of water coming in the mortise and speed up drying. In addition, the footbridge was given a new shingle roof, siding, and the floor. All wooden elements of the structure were treated by protection coating. After the reconstruction, the deflection of beams was measured and its value was 2.5 m.

Figure 4 — The finishing works at Footbridge in Švařec in 2006 (a) and degradation of the eastern upper beam head of the northern beam in 2012 (b)

Conditions in 2012

The last inspection of the structure condition was performed in 2012. Since the reconstruction in 2006, no significant damage by wood-decaying fungi or by wood-borers has been found. Slight damage is found at the upper beam head at the eastern side of the footbridge (see photo in Fig. 4b). The siding and the shingle roof are in good condition and provide the footbridge with sufficient protection against weather. Some bolts were loose and were tightened up during the inspection. With the use of a total station we measured a deflection of 40 mm at the southern beam and 49 mm at the northern beam.

Discussion

The original bearing beams consisted of two beams above each other connected by bolts and connectors. There were 6 bolts and 5 connectors. The reconstruction used 7 times more of these elements. In 2005, the deflection reached 16 and 17 cm. The damage of wood was very high and the strength was lower than 50 %. The mortises were damaged by pressure and connectors in the mortises were loose and some of them were damaged by wood-decaying fungi or by wood-borers. Nobody has definitely tightened the wrought bolts for several decades (due to the long-term corrosion it was even impossible to loose them). It is impossible to expect that the beams could form a single bearing beam. If the calculation is made in the same way as it was made in the statics opinion (the same load and calculation method) that the whole load is only applied on a single bearing beam of the profile of 45 × 36 cm, the resultant deflection is approx 36 cm.

All the above mentioned facts lead to a question whether it is really necessary to use the calculation according to the existing standards for the repair of a heritage monument. Regarding the footbridge in Švařec, the appearance of a historical monument as well as the work of carpenters deteriorated. Although, they produced hewn beams by historical technologies, but, at the entry, everyone notices a dense row of bolts and not the excellence of carpentry work. Can there be a structural designer who is willing to back the dimensions generated by a method of trial and error of our ancestors and approve the reconstruction as a copy. The dimensions of the original elements have been proven by hundreds years of use and stayed at their place even after their load bearing capacity was reduced to less than half.

Footbridge in the village of Prudká

The wooden footbridge connecting the railway station Prudká and the local paper mill was built by the owner of the paper mill for their employees in 1899 (Fig. 5). The time period of the construction was also confirmed dendrochronologically (Nováková, 2008). At the moment, the inheritance rights are not clear and the owner is not known. The footbridge is maintained by the employees of the local paper mill and by the local residents. The repairs are just provisional and do not comply with national heritage principles.

Figure 5 — Footbridge in Prudká in 2012, view from left bank (a) and inside (b)

The footbridge rests on the right bank on a oblong shape stone pillar, in the middle on a wooden pile bent, and on the left bank on an abutment wall. Each footbridge bay consists of two main fir bearing beams and one spruce stringer. The bridge deck is approx three metres above the river. The bearing beams are doubled above the wooden pile bent. The oak pile bent consists of three pilots and four transversal beams. The pilots are protected by plated ice aprons from oak wood. The footbridge structure is supported by bedding timbers on the pillar and abutment wall. The floor beams under the longitudinal bearing beams are located at the places of posts. They are fixed to the queenpost trusses by wrought straps. The bearing system of the footbridge is represented by two pairs of queenpost trusses. The queenpost trusses are connected with a top chord by a tenon. Diagonal stripes are tenoned in between posts and purlins. The footbridge is divided into six parts, each of the average length of 5.6 m. 0.72 m-wide view part is between 2 m-high boarding and the roof gutter. The saddle roof of the footbridge is currently covered by tar paper. The covered part of the footbridge is 33 m long, 2.40 m wide and 3.90 m high.

Condition

In 1999, the roof of the footbridge was repaired together with several heavily damaged elements of the vertical structure. A reconstruction of the degraded main bearing beam head on the left bank was to follow. However, due to the above mentioned reasons, the reconstruction never took place.

Figure 5 — Supported bearing beam at the pile bent (a), supported post and brace by oak planks (b), connection of additional beam with floor beam (c)

The damage of this bearing beam reached such degree that a provisional repair was made in 2005. A new unfinished beam was laid next to the bearing beam. It was supported by oak planks at the pile bent and floor beams (Fig. 5a,c). The post and brace, which were tenoned into the original bearing beam, were supported in the same way (Fig. 5b). At the same time, all cross beams and floor beams were replaced.

The last inspection of the structure was performed in 2013. Apart from the visual evaluation, a new instrument was used for tuition of civil engineering surveys. The instrument is in the phase of experimental verification. The instrument was developed for the tuition and therefore the following requirements were set: simplicity, appropriate accuracy, and low price.

The simplicity of the principle was required, so that students can see and understand how the instrument works. When using it, they should get the feeling for wood and its damage (so that it would not be a "magic box" from where the results come out themselves). The simplicity was also desirable for its production, so that it could be easily assembled in school workshop by individual students.

The requirement for accuracy for this instrument included the resolution in three degrees of damage (if possible in the whole profile of the wooden element):
- no or slight damage, requires no intervention
- medium, requires further survey or reconstruction
- total destruction.

Low price is obviously the requirement of our time, when the crisis has an impact on universities as well. Purchase of instruments in large amount is usually impossible. Low number of instruments leads to a limited access of students to them, and the students are unable to get familiar with the given issues. All the available methods require considerable experience with surveys, so that the interpretation of results could be correct. If students have more opportunities to improve their knowledge and feeling for surveys, it is always easier to learn to work with other instruments and evaluate the measured data better.

Instrument scheme

The instrument scheme is shown in Fig. 6. A sharp point (1) is fixed to the perpendicular beam (2), the position can be easily adjusted at the place of their crossing (3). An indicator (4) comes out of the place for the measurement of the position of the horizontal bar on a scale (5). The scale (5) is fixed to the base (6). The base (6) contains an opening for the point (7) and two draw springs (8) are fixed to the base. The springs (8) connect the base (6) with the beam (2).

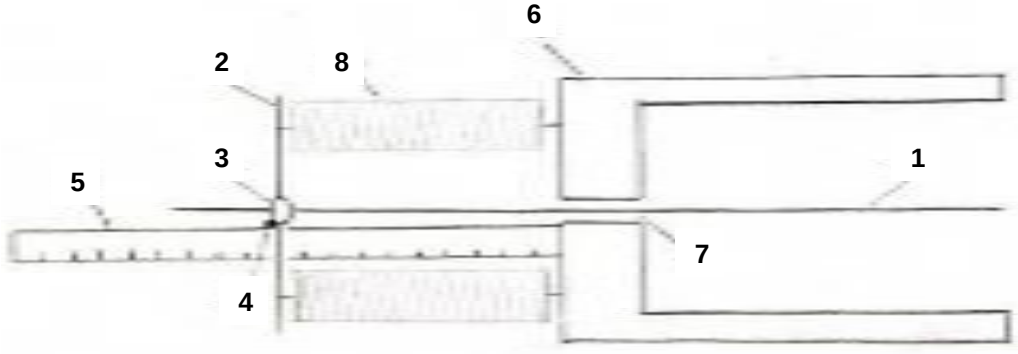

Figure 6 — Instrument for determination of the degree of damage of wooden elements

Measuring process

The point is fixed at the crossing (3), so that it would lie on the surface of wood (at the bottom of a drilled hole) and there would be no clearance between the springs (8) and the base (6) (but they cannot be stretched). The springs (8) are pulled behind the bearing beam (2) to the determined length (given by the end of the scale (5)). After release, the point (1) is shot into the wood and the depth of the penetration is found on the scale (5).

Based on the performed experiments, the limits of the degree of damage (obvious in Table 1) were set.

Table 1—Estimate of the degree of damage in relation to the point

Depth of point penetration (mm)	Degree of damage (-)
5–9	no or slight damage, requires no intervention
10–14	medium, requires further survey or reconstruction
>15	total destruction

Results of wooden footbridge measurement

The instrument was used for the verification of wood condition in the heads of the main beams. 6 mm probes were drilled every 30 cm from the fronts of bearing beams, the depth of 5 cm. In order to make the results more comprehensive, a scheme was drawn and the results were hatched. In addition, a visual examination of the holes by endoscope was made.

Based on the performed measurements for all heads, it was found that the bearing beams on the right bank are in relatively good condition. Only the main bearing beam is damaged up to approx 1/3 of its profile at its end (Fig. 7b). The bearing beam supports only one post at this place. Small provisional repair was made there in the past and the post was supported. In contrast, the bearing beams at the abutment wall show significant damage of wood. It includes the provisionally repaired bearing beam in the past. Two other ones are damaged by brown rot in the centre of their profiles. Fortunately, brown rot neither reaches over the bedding timber, nor past the place with the connection of the brace (Fig. 7a).

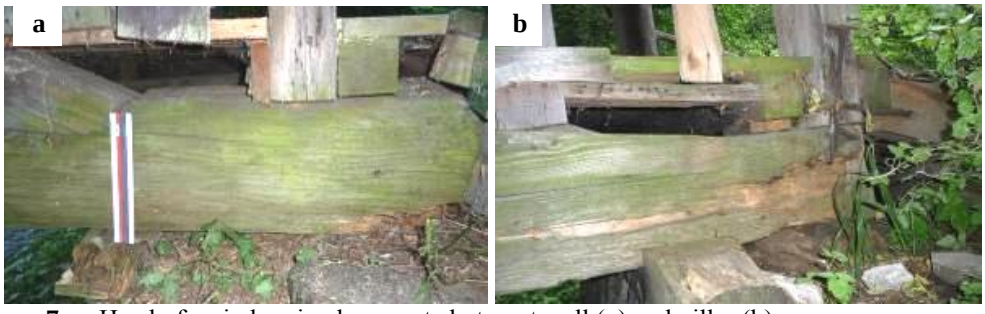

Figure 7 — Head of main bearing beams at abutment wall (a) and pillar (b)

Reconstruction design

The most damaged main bearing beam at the left bank should be replaced along its whole length. The provisional beam which is placed next to the main one should be replaced. The other bearing beams with damaged heads should be repaired with the replacement of the damaged parts. Ideally, all-wood connections should be provided. An example of such solution is the reconstruction of a bridge in Černvír.

This road bridge was built in 1713 and is the oldest wooden bridge in the Czech Republic (Fig. 8a). Its reconstruction took place in 2005 to 2010. Bearing beam heads were also damaged by brown rot in this bridge (Fig. 8c). The designed connection is shown in Fig. 8b,d (Hrdlička 2006). It is a tenon with oblique ends and a narrowing secured with locust pins. Similar connections (oblique tenon or a splice secured by wooden pins) are currently used in the Czech Republic for the reconstructions of important monuments. It has been proven in many reconstructions that precisely performed joints are able to carry given load and even higher load in many cases than commonly used joints with steel elements. They also meet the National Heritage requirements: they do not change the appearance of the structure and keep carpentry alive.

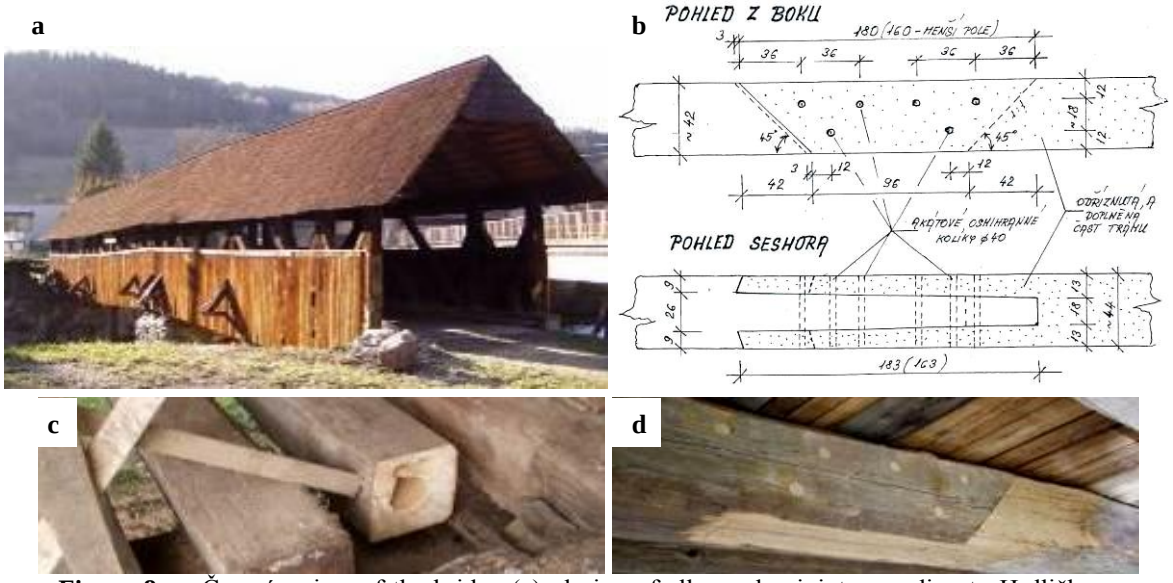

Figure 8 — Černvír: view of the bridge (a), design of all-wooden joint according to Hrdlička (b), head of a stringer damaged by rot (c), and performed connection (d)

Conclusion

The article describes two wooden bridges over the river Svratka in the Czech Republic. The footbridge in Švařec has been repaired. Ultrasound measurement was used for the examination of its condition. Beams for the reconstruction were hewn and connected by wooden connectors. However, the use of a large number of modern bolts is rather questionable.

The footbridge in Prudká has unclear ownership rights, therefore waiting for reconstruction. Thus, it would be a suitable place for testing a new teaching instrument for the determination of wood condition. It appeared that it is useable in the filed work, shows sufficient accuracy for preliminary surveys, and can be used as a supplement to other non-destructive methods. An endoscope can be used immediately. The instrument is simple and cheap and allows students to get the feeling for wood and its faults.

Based on the extent of damage, the repair methods were designed. As an example the method used in the wooden bridge in Černvír was mentioned. That method used carpentry joints. This procedure is in the Czech Republic supported by the National Heritage representatives, since the result is not only aesthetically acceptable, but also functional and, helps to keep hand-made carpentry craft alive.

Acknowledgments

This paper is published with the support of the project „Inovace technických a dřevařských disciplín pro vyšší konkurenceschopnost“ (reg. No. CZ.1.07/2.2.00/28.0019).

References

Bláha, J.; Kloiber, M.; Kyncl, T. 2005. Stavebně technický průzkum ve Švařci. Brno.

Hrdlička, O. 2006. Statický posudek dřevěné lávky ve Švařci. Kladno.

Hrdlička, O. 2006. Statický posudek mostu v Černvíru. Kladno.

Nováková, L. 2008. Historická dřevěná lávka v Prudké. Bakalářská práce. MENDELU v Brně.

Use of ultrasonic attenuation spectroscopy to detect internal small defects for maintenance of historic building

Jung-Kwon Oh
Department of Forest Sciences, Seoul National University, Seoul, Korea, jkoh75@hotmail.com

Jun-Jae Lee
Department of Forest Sciences, Seoul National University, Seoul, Korea, junjae@snu.ac.kr

Abstract

The early stage of insect damage is too small to be detected by conventional TOF-based ultrasonic techniques. Besides, inconsistent contact pressure of transducer let analysis of attenuation difficult when inspecting cultural heritage. In this study, it was investigated whether or not the ultrasonic attenuation spectral analysis can detect small artificial defects simulating early stage of insect damage, under varied contact pressure. The artificial defects were made by drilling 3mm diameter holes and the through-transmission ultrasound measurement was carried out under severely varied contact pressure. Spectral analysis with 2nd derivative pretreatment predicted the number of holes with much lower error of prediction (RMSE : 1.609) than the conventional methods (RMSE : 5.925). This result indicates that the spectral analysis has a high possibility in detection of insect damage in cultural heritage.

Keywords: Ultrasound, Attenuation spectroscopy, insect damage, cultural heritage

Introduction

In wooden cultural heritage building, insect damage, such as termite damage, is one of the most serious problems. Usually, insects prefer early wood rather than latewood, because early wood is softer and easier to eat than latewood, and so insects make narrow and long tunnels from the ground to the top of the column. Because this hole can be a path of other biological attack and the damage can be expanded, early detection is required for conservation of the building. But the early stage of the damage is quite small in a cross section.

Through-transmission elastic wave is very powerful tool to provide valuable information on the internal state of wood. The time of flight (TOF) is sensitive to the defects in wood (Sandos et al. 2000).; based on this knowledge, TOF-based computed tomography (CT) was developed and commercialized for standing tree inspection(FAKOPP 3D Acoustic tomography, Fakopp, Hungary, PICUS Sonic tomography, argus electronic gmbh, Germany). The CT technology reconstructs cross section views by the filtered back projection (FBP) algorithm and TOF of waves passing through various paths in the cross section. This CT technique can provide higher detectability by inspection of more wave paths (Divos and Szalai 2002). Nevertheless, this technology cannot detect early stage of insect damage because of its size. Kim et al. (2008) reported that a 13mm diameter defect or larger could be detected by TOF-based CT in which ultrasound was used, but the diameter of insect damage in early stage is smaller than this resolution.

Most of elastic wave technology detects defects by TOF of the earliest received wave passing through the wood of interest. In addition to TOF, attenuation is a parameter in wave transmission analysis that is influenced by internal defects, which is especially reflected in studies on non-wood materials (Aduda and Rawlings 1996, Jeong and Hue 1995). In the case of wood, Tallavo et al. (2012) investigated attenuation according to the direction of the transducers and distinguished a deteriorated wood pole by statistical dissimilarities. Sandos et al.(2000) also investigated the relationship between induced saw cut depth and wave velocity, peak amplitude, and energy of the received signal. Several studies on attenuation have used peak amplitude and energy (Tallavo et al. 2012, Lee et al. 2011, Lee et al. 2013). The results of these studies indicated that attenuation can be a good predictor in internal defect detection. Because TOF analysis cannot provide enough detectability to detect small insect damage, another predictor, attenuation, needs to be analyzed.

Ultrasonic attenuation spectroscopy is one of the methods to analyze attenuation. Fundamentally, the wavelengths that are long (low frequency) relative to defect size are not affected by defects but relatively short wavelengths (high frequency) are attenuated (Tucker 2013). Chambers and Tucker (1999) applied ultrasonic spectroscopy to bond-quality inspections of nozzles in a space shuttle; however, we found very few studies using ultrasonic spectroscopy on wood. Tiitta et al. (1998) reported that the high frequency content of the signal is virtually absent and the amplitude of the peak frequencies is also substantially reduced. Jordan et al. (1998) tried to classify wood species by the machine learning algorithm (neural network) of the ultrasonic technique, and showed possibility to use ultrasonic attenuation spectral analysis with the machine learning algorithm in order to obtain the micro-structure information.

In use of attenuation characteristics in wood, one of the most difficult problems to be solved is energy loss of ultrasound between wood and transducer. Because the loss can not be measured in testing, exact attenuation is difficult to evaluate. In inspection on cultural heritage, any harm is not allowed during inspection of cultural heritage. Because painting on its surface is also cultural heritage, any spots by liquid, even water, are not allowed during NDT testing. Therefore, elastomeric couplant (dry couplant) is commonly used instead of liquid type couplant. When using this type of couplant, the pressure employing transducers is another factors to evaluate attenuation. For analysis of attenuation in cultural heritage, an apparatus to press transducers with consistent pressure was developed which consists of shoe and spring (Lee et al. 2013). Even this apparatus cannot provide consistent contact condition in perfect because of many unexpected test condition, such as various shape of objects, surface condition and undesired spring deformation.

In summary, existing TOF-based techniques do not have sufficient detectability to detect the early stage of insect damages because of its size. Attenuation spectral analysis was expected to provide better detectability than the TOF-based technique, but in case of inspection on cultural heritage buildings, varied contact pressure can make a negative effect on the attenuation measurement. Therefore, in this study, through-transmission ultrasonic tests were carried out under severely-varied contact pressure at every ultrasonic measurement. Prior to developing small insect damage detecting model, it was investigated whether or not attenuation spectral analysis can detect that small defects under varied contact pressure.

Materials and Methods

Experiments

Specimen preparation

Insects usually make small holes along the length of the wood members (Fig. 1a). Red pine (*Pinus densiflora*) round timbers without any biological deterioration were prepared, and the diameter of the

round timber was 96 mm. In order to simulate insect damage, drill holes were bored in the direction of the timber length from one end (Fig. 1b).

The attenuation of the waves traveling in longitudinal direction is much smaller than in the other directions. If the specimen length was too short, then the waves could be repeatedly reflected at both ends. These repeatedly reflecting waves could have an unexpected effect on this study. Therefore, approximately 1300mm length specimens were used without trimming. The long specimens might provide long enough paths for the reflected waves not to reach the receiving transducer by being attenuated while traveling through the wood in longitudinal direction. By this experimental set-up, it was expected that the undesired effects of the reflection at the other end could be minimized.

There must be large variation in ultrasound behavior between wood pieces. This variation can decrease the accuracy of final model. However, this study was intended to investigate whether or not the spectral analysis can detect small defect under varied contact pressure. The variation between wood pieces can make it difficult to investigate the effect of contact condition. Therefore, only two specimens were prepared for the experiment, instead at each specimen, many spectrums were obtained under various contact pressure.

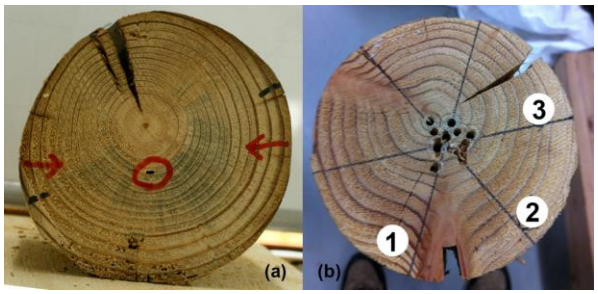

Figure 1—Replication of insect damage by drill holes (a: Hidden insect damage, b: Artificial insect damage replicated by drill holes- Number showed 3 paths of ultrasound in ultrasonic measurement)

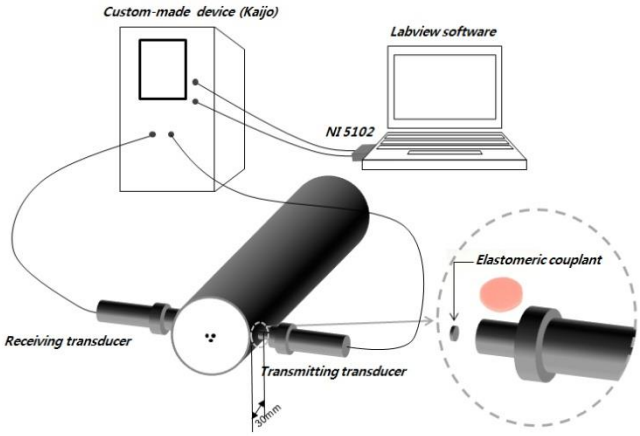

Figure 2—Schematic drawing of ultrasonic test set-up

Through-transmission ultrasound measurement

In this study, two piezoelectric transducers (central frequency: 80kHz, Kaijo Co. Ltd., Japan) were used to generate ultrasound and to receive the signal. These transducers had approximately 33% bandwidth (54kHz~106kHz). A custom-made device and transducers were used to generate ultrasonic wave (central frequency 80kHz, Kaijo Co. Ltd., Japan). The device has functions of purse generator, amplifier, data acquisition and TOF calculator & TOF display. The raw voltage signals were transferred into laptop computer through an interface card (NI 5102, National Instrument Inc, USA). The full signal of through-transmitted waves were captured and recorded by LabVIEW software (LabVIEW, National Instrument Inc, USA)(Fig. 2). As a couplant, elastomeric couplant (Elastomer, Olympus Co., USA) was glued on both transducers.

At first, the ultrasonic test was carried out on the sound round timber in three radial directions as shown in Fig. 1b. The transmitting and receiving transducers were positioned at opposite sides of the specimen (Fig. 2). In each direction, 10 ultrasonic waveforms were obtained. and the tested cross section was located 30 mm away from an end (Fig.2).

Contact pressure employing transducers can affect the attenuation characteristics of the waves (Beall 2002). It is not possible to keep it perfectly consistent; hence, the contact pressure was applied by hand to

have varied pressure level, from very small pressure to let the transducer touch to wood to high pressure (approximately 0.4N/mm^2). Also, in order to obtain sufficient number of observations, transducers were detached and pressed again at every measurement. By this test procedures, 10 waveforms were obtained at a direction, and the pressure of the 10 waveforms were not the same, even though they were obtained from the same path.

After obtaining 30 waveforms on a sound specimen, a 3mm-diameter hole was bored at the center of a cross section. Then, 30 waveforms were obtained at the cross section of interest. Then, a second hole of the same diameter was bored. The procedure of obtaining a waveform and boring another hole was repeated until the number of holes reached nine. All of the holes penetrated only early wood and were made as close to the center as possible. The holes were bored to a depth of 50mm. Because holes was bored close to the center, ultrasound always passed through the holes. The contact area was 346mm^2 (diameter of couplant was 21mm).

Modeling to detect internal defects

Pretreatments

All of the waveform obtained were converted from the time-domain to the frequency-domain by the Fast Fourier Transform (FFT, Matlab R2012a Mathworks USA). Two pretreatments were applied to minimize the effect of the contact condition: two types of scaling and two types of derivative (1st and 2nd derivative).

As the first scaling pretreatment, the maximum amplitude of the frequency-domain spectrum was identified, then all of the amplitude components for each frequency were divided by the maximum amplitude (Eq. 1). The second scaling pretreatment was performed by scaling based on the received wave energy, in which the received wave energy was calculated using Eq. 2, and all of the amplitude components for each frequency were divided by the energy (Eq. 1).

$$A^*(f) = \frac{A(f)}{k} \tag{1}$$

$$E = \int_f A(f)df = \sum_f A_f \tag{2}$$

where, $A(f)$ is the amplitude at a specific frequency of f and $A^*(f)$ is the scaled amplitude at a specific frequency of f. The term k is the maximum amplitude of the frequency-domain or the received energy (E). Savitzky-Golay (S. Golay) (Savitzky and Golay 1964) derivative was applied to scaling-pretreated spectrum. This pretreatment is based on performing a least squares linear regression fit of a polynomial around each point in the spectrum to smooth the data. The derivative was then the derivative of the fitted polynomial at each point. The derivative math pretreatment is often used to reduce the nonzero bias in near-infrared spectroscopy (Burns and Ciurczak 2001). The derivative was calculated with 5 point (1667Hz) segment smoothing by linear fitting by Matlab software.

Partial least squares (PLS) regression analysis

Drill holes were bored in the center of an end in order to replicate insect damage, and the degree of deterioration was evaluated by the number of holes. In the statistical model, the number of holes was used as a dependant variable. In order to compare the new spectral analysis models with the existing model, the relationship between the number of holes and the conventional ultrasonic parameters of TOF, energy of received signal and maximum amplitude were investigated.

Frequency domain attenuation (362 data) was used as independent variables (M1 in Table 1). M2 to M4 model was made by adding conventional parameters (wave speed, energy and maximum amplitude) in M1model (Table 1). Before modeling, three kinds of scaling pretreatments (without scaling, Max.-amplitude-based and energy-based scaling) and 3 kinds of derivative pretreatments (without derivative, 1st derivative and 2nd derivative) were applied. In total, 36 models were tested (3 scalings, 3 derivatives and 4 independent variable sets).

Table 1— Independent variables in the statistical model used to detect the number of holes in wood.

Model	Independent Variables	Number of Independent Variables
M1	Spectrum[1)]	362
M2	M1 and Wave Speed	363
M3	M2 and Energy	364
M4	M3 and Max. Amp.	365

[1)] Frequency-domain.

As a statistical model, the PLS regression model was applied. Out of 600 datasets, 300 datasets were randomly selected as a training dataset and the remaining 300 datasets were used for validation (two-fold validation). Each 36 model was optimized by the accuracy in validation. The 36 modeling cases were compared with each other in accuracy of validation and the best model was chosen, where accuracy of the validation was evaluated by root mean square error of prediction (RMSE).

Results and discussions

Prediction by existing predictors

Wave speed is one of the best predictor to detect internal defects. Table 2 showed the relationship between the wave speed and the number of holes; however, the coefficient of determinant was only 0.190 (RMSE : 5.925).

Several researchers have reported that the energy of the received signal and maximum amplitude are sensitive to the defects (Lee et al. 2011, Lee et al. 2013, Biernacki and Beall 1993); however, in this study, the accuracy of these parameters was also very low as shown in Table 2.

Table 2 —Accuracy in prediction of the number of holes by conventional parameters

Conventional parameters	Accuracy	
	R^2	RMSE
Wave Speed (1/TOF)	0.190	5.925
Energy	0.220	5.395
Max. Amp.	0.105	8.374

The varied contact condition may be one of the reason of the low accuracy of the conventional parameters and these low accuracy indicate that conventional parameters under varied contact conditions may not detect such the small diameter damages in cultural heritage. Besides, the defect size in this experiment was very small. A general rule of thumb is that a discontinuity must be larger than one-half the wavelength to stand a reasonable chance of being detected; in case of 80kHz ultrasound traveling in perpendicular to the grain direction, larger than 10mm defect can be detected but the size of the hole in this study was only 3mm diameter.

Attenuation spectral analysis

Effects of pretreatments

Originally, the scaling pretreatment was intended to remove the effects of the varied pressure used to make transducer contact to wood. However in most cases that the scaling process was applied, the accuracy was lower than the model without scaling pretreatments (Table 3). Table 2 showed a relationship between the receiving energy and the number of holes. Even though coefficient of determinant was only 0.220, it indicates that the energy is one of the important predictors for defect

detection and the received signal was more attenuated with the increase in the number of holes. The Scaling pretreatment removes the difference in overall attenuation regardless of the number of hole by dividing all of the spectrums by the maximum amplitude or energy. Losing this important predictor (overall attenuation) seemed to lower the accuracy. Even though the scaling pretreatment removed the effect of varied contact condition of transducers, the effect seems to be smaller than the contribution to the prediction of overall attenuation. Therefore, we concluded that the scaling pretreatment was not appropriate for modeling internal defect detection.

Table 3— According to model, accuracy in prediction of the number of drill holes[1)]

Model	Derivative Pretreatment	Scaling Pretreatment					
		Not Applied		Based on Max. Amp.		Based on Energy	
		R^2	RMSE[2)]	R^2	RMSE	R^2	RMSE
M1	Not Applied	0.582	1.858	0.564	1.897	0.590	1.839
	1st Derivative	0.637	1.731	0.635	1.736	0.625	1.759
	2nd Derivative	0.673	1.642	0.615	1.781	0.658	1.679
M2	Not Applied	0.590	1.840	0.528	1.974	0.566	1.891
	1st Derivative	0.647	1.706	0.638	1.727	0.644	1.714
	2nd Derivative	0.686	1.609	0.642	1.718	0.675	1.637
M3	Not Applied	0.595	1.829	0.549	1.929	0.531	1.966
	1st Derivative	0.662	1.671	0.629	1.748	0.647	1.707
	2nd Derivative	0.670	1.651	0.647	1.707	0.677	1.633
M4	Not Applied	0.563	1.900	0.549	1.929	0.544	1.940
	1st Derivative	0.642	1.718	0.630	1.747	0.637	1.730
	2nd Derivative	0.668	1.655	0.636	1.734	0.676	1.635

[1)] Prediction results for validation data set by a regression model determined with training data set
[2)] Root mean square error of prediction.

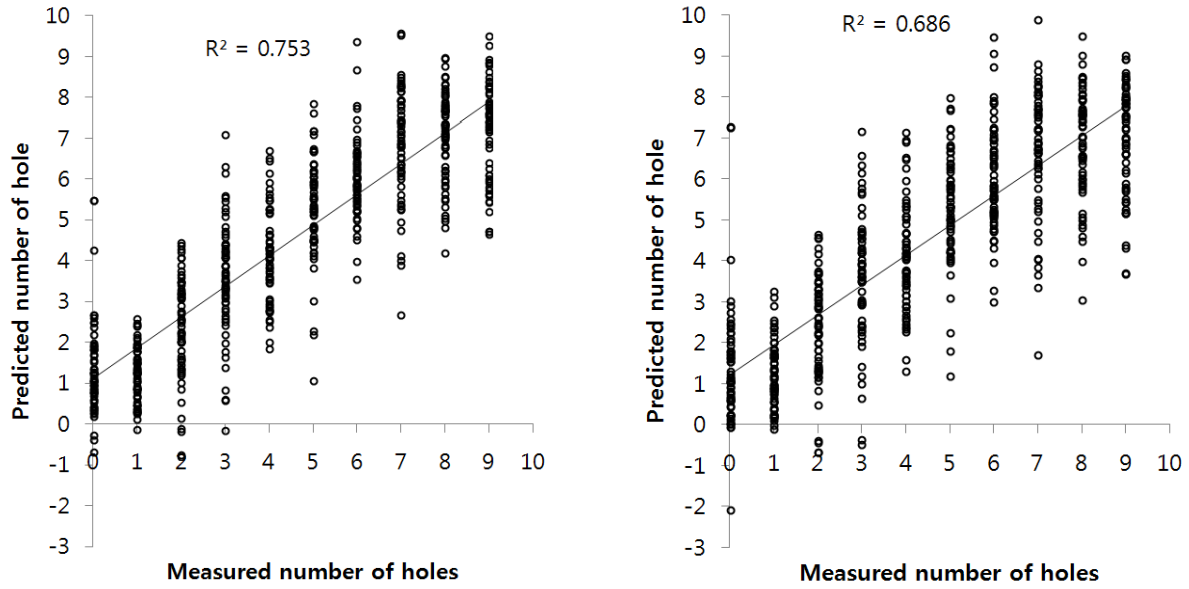

(a) (b)

Figure 3 — Prediction of the number of holes by PLS with the attenuation and wave speed (M2, 2nd derivative, scaling pretreatment was not applied). a: training set, b: validation set.

Another pretreatment, the derivative, increased the accuracy. This derivative is very common pretreatment in spectral analysis which can remove noise by smoothing effect and reduce the nonzero bias (Burns and Ciurczak 2001, Fujimoto et al. 2010). The nonzero bias can be caused by varied contact

condition such as surface condition and contact pressure employing the transducers. The overall received energy (received signal integral) can be varied by applied contact pressure and surface condition. This non-uniformity of received energy can drop the accuracy of the model as well as robustness. The derivative pretreatment leads to focus on relative change rather than the amplitudes at each frequency. Because this experiment used severely-varied contact condition on purpose, the received energy must be very varied. Based on the comparison of RMSE between models, the derivative pretreatment seemed to effectively reduce the effect of contact condition. Besides, the spectrum must have some noise and S. Golay derivative pretreatment smoothes the spectrum, as a result the noises are removed. The effect of contact condition and noise reduction seemed to be the reason why derivative pretreatment increased the accuracy. The 2nd derivative showed higher accuracy than 1st derivative. From M1 to M4, the 2nd derivative showed approximately 10% lower error of prediction (RMSE) than the analysis without derivative pretreatment. As Table 3 shows, the best model was M2 model with 2nd derivative pretreatment. This model showed lowest RMSE (1.609). Fig. 3 showed the results of M2 model with 2nd derivative pretreatment.

Feasibility of ultrasonic attenuation spectral analysis in detecting internal insect damage

In terms of accuracy, the use of attenuation by spectral analysis significantly increased the accuracy in detecting small defect in wood. The TOF showed 5.925 of RMSE but spectral analysis showed much lower error of prediction (1.858 of RMSE). When wave speed and spectrum were used together as independent variables (M2 in Table 3), the RMSE decreased to 1.840. In addition, 2nd derivative pretreatment lower the RMSE up to 1.609. This error of prediction was much lower than conventional parameters (Table 2). This comparison demonstrated that the attenuation spectral analysis would be worth in internal defect detection in NDT inspection of cultural heritage building.

Conclusions

Insect damage is one of the most serious damage in cultural heritage. In the early stage, the insect makes a small tunnel along the length of wooden member. This small diameter hole is too small to detect by conventional methods. In order to detect such that small deterioration, attenuation needs to be analyzed but not-uniform contact condition of transducers makes it difficult. On purpose, the transducers were contacted to wood with varied pressure at every measurement and the number of 3mm-diameter drill hole was predicted by PLS regression. From this test set-up, this study investigated whether or not spectral analysis can detect internal small diameter hole under un-uniform contact pressure of transducers.

To remove the effect of contact condition, two pretreatments were applied. Out of the two, scaling pretreatment was not effective but derivative pretreatment showed approximately 10% higher accuracy than the models without the pretreatment. Because derivative pretreatment makes the model be developed based on relative change rather than amplitude at each frequency, the derivative pretreatment seems to effectively reduce the negative effect of not-uniform contact condition on attenuation analysis.

In this study, the diameter of drill hole was only 3mm and this experiment was carried out under very severely varied contact pressure. Nevertheless the spectral analysis showed higher accuracy (RMSE : 1.609) than conventional method (RMSE : 5.925). Based on this result, it was concluded that the spectral analysis has a high possibility in detection of internal insect damage in cultural heritage.

References

Aduda B.O., Rawlings R.D. 1996. Spectral analysis of acousto-ultrasonic waves for detect sizing, NDT&E International 29(4):237-240

Beall F.C. 2002. Overview of the use of ultrasonic technologies in research on wood properties, Wood Sci Technol 36:197-212

Biernacki J.M., Beall F.C. 1993. Development of an acousto-ultrasonic scanning system for nondestructive evaluation of wood and wood laminates, Wood and Fiber Science 25(3):289-297

Bucur V. 1995. Acoustics of wood, CRC Press, ISBN 0-8493-4801-3:76-77

Burns D.A., Ciurczak E.W. 2001. Handbook of near-infrared analysis, Marcel Dekker Inc. : 97

Chambers J.K., Tucker J.R. 1999. Bondline analysis using swept-frequency ultrasonic spectroscopy, http://www.uspec.com/Insight0399.PDF Assessed May 10 2013

Divos F., Szalai L. 2002. Tree evaluation by acoustic tomography, proceedings of the 13th International Symposium on Nondestructive Testing of wood, UC Berkeley, USA, Aug. 19-21 :251-256

Fujimoto T., Kurata Y., Matsumoto K., Tsuchikawa S. 2010. Feasibility of near-infrared spectroscopy for online multiple trait assessment of sawn lumber, J Wood Sci 56:452-459

Jeong H., Hsu D.K. 1995. Experimental analysis of porosity-induced ultrasonic attenuation and velocity change in carbon composites, Ultrasonics 33(3):195-203

Jordan R., Feeney F., Nesbitt N., Evertsen J.A. 1998. Classification of wood species by neural network analysis of ultrasonic signals, Ultrasonics 36:219-222

Kim K.M., Lee J.J., Lee S.J., Yeo H. 2008. Improvement of wood CT images by consideration of the skewing of ultrasound caused by growth ring angle, Wood Fiber Science 40(4):572-579

Lee S., Lee S.J., Lee J.S., Kim K.B., Lee J.J., Yeo, H. 2011. Basic study on nondestructive evaluation of artificial deterioration of a wooden rafter by ultrasonic measurement, J Wood Sci 57:387-394

Lee S.J., Lee S., Pang S.J., Kim C.K., Kim K.M., Kim K.B., Lee J.J. 2013. Indirect detection of internal defects in wooden rafter with ultrasound, J Korean Wood Sci Technol, 41(2):164-172

Sandoz J.L., Benoit Y., Demay L. 2000. Wood testing using Acousto-ultrasonic, Proceedings of World Conference on Timber Engineering.

Savitzky A., Golay M.J.E. 1964. Smoothing and differentiation of data by simplified least square procedures. Anal Chem 36:1627–1639

Tallavo F., Cascante G., Pandey M.D. 2012. A novel methodology for condition assessment of wood poles using ultrasonic testing, NDT&E International, 52:149-156

Tiitta M., Beall F.C., Biernacki J.M. 1998. Acousto-ultrasonic assessment of internal decay in glulam beams, Wood Fiber Science 30(3) :259-272

Tucker J.R., 2013. Ultrasonic Spectroscopy for Corrosion Detection and Multiple Layer Bond Inspection, http://www.uspec.com/UltraSpecPaper.PDF Accessed May 10 2013

Structural Evaluation of the Second Oldest Glued-Laminated Structure in the United States

Douglas R. Rammer
Engineering Properties of Wood, Wood based Materials and Structures, US Forest Service Forest Products Laboratory, Madison WI, USA drammer@fs.fed.us

Jorge de Melo Moura
Department of Architecture and Urbanization, Universidade Estadual de Londrina, Londrina, Paraná' Brazil jordan@uel.br

Abstract

The second glued-laminated structure built in the United States was constructed at the USDA Forest Products Laboratory (FPL) in 1934 to demonstrate the performance of wooden arch buildings. After decades of use the structure was decommissioned in 2010. Shortly after construction, researchers structurally evaluated the glued-laminated arch structure for uniform loading on the center arch. This structural system evaluation was added to the existing laboratory work on glued-laminated arches to develop the foundation on which the current glued-laminated arch design criteria is based. After decommisioning, recovered arches were tested in the laboratory to evaluate the loss of structural performance. Loss of structural performance was evaluated by comparing original and current deformation. Based on a preliminary visual and structural assessment, the degradation of structural performance was minimal in the arches, except for one arch that was exposed to a significant amount of water resulting from fighting a building fire.

Keywords: Glued-laminated, arch, historical, structural evaluation, ultrasound

Introduction

General information

In the 1930's the USDA Forest Products Laboratory was engaged in a research program to develop glued-laminated wood beams (Wilson and Cottingham 1952) and arches (Wilson 1939). A seminal project for the glued-laminated research was the construction of an arch building on FPL's campus in winter of 1934 (Figure 1). This building was 13.7 m wide by 48.8 m long and consisted of nine arch lines spaced 4.8 m apart. The base to crown height was 5.7m. Three different arch configurations were utilized. The five central arches were glued-laminated arches with a rectangular cross section having a constant width but a varying depth that was greatest at the knee, near the roof and wall junction, and least at the foundation and roof peak. Adjacent to each span is a wooden arch of double "I" section composed of plywood webs and glued-laminated flanges with a constant width and varying depth, similar to the glued laminated arches. End spans were built with heavy timber trusses connected with shear plate connectors. Spanning between the arches were stress-skin panels consisting of top and bottom plywood panel, glued and nailed to nominal 38 by 140 mm solid sawn lumber. This stiff box configuration assists in spreading forces to adjacent arches.

After decades of use, this structure was deconstructed in the fall of 2010 (Figure 3). Since these arches represent the first generation of both construction adhesives and glued-laminated development, the

durability of these arches was evaluated. As part of the overall nondestructive research program, the individual arches were loaded to determine the extent of structural degradation over the past 75 years.

Figure 1—Construction of the USDA Forest Products glued-laminated arch building in the winter of 1934

Figure 2—Deconstruction of FPL's glued-laminated arch building.

Initial Arch Performance

In the fall of 1935, after erection of the structure, the glued-laminated arch structure was incrementally loaded to 140kN with sand bags that were placed uniformly and centered over the full arch span. The load is equivalent to a 295 kN/m^2 on the tributary roof area to one arch and 42% higher than the assumed design live load. Both the immediate and sustained deformations were measured for approximately 224 days between September 1935 and May 1936. Deformations were measured on the loaded arch at the peak and quarter points, while only the peak deformations were measured for the two adjacent arches. Based on these measurements, it was determined that some of the applied uniform load was distributed to the adjacent arches by the stressed-skin panels. Data from this structural evaluation was used to establish both the short term and long-term test procedures used in this study and validated the structural models.

Experimental Procedures

Load Configuration

As stated previously, shortly after the arched structure was constructed, a uniformly distributed load was applied to the center arch line of the structure. For comparison testing of a single arch under a similar

loading configuration, this load distribution affect must be accounted for. Application of a uniformly distributed load is troublesome and such loading is typically approximated by a series of concentrated load points.

To conduct experiments on a single half arch in this study, the amount of load redistributed in the original building to adjacent arches was determined. Additional work was needed to determine the location and number of concentrated loads to simulate a uniform loading on the arch arm. This was accomplished through structural analysis of both the original building and a single half arch using MASTAN2 (2006).

Figure 3—Loading of FPL glued laminated arch building and measurement techniques for live loading of building.

For the model of the complete building, each arch was sub-divided into 32 beam elements, each with its cross sectional area and moment of inertia equivalent to those of the mid-span element properties. The upper and lower arch connections were assumed to be hinges, with the base connection having translation restraint. A uniform load, equivalent to the total weight of the sand bags, was applied along the length of the arch arm. The roof system of the arched building consisted of glued plywood and solid sawn stress-skin panels that span the tops of the arches. The lower plywood panel was attached to the arch with six-penny nails spaced every 140 mm. These stress skin members were represented as beams spaced every 1.2 m with section properties using an effective width according to EC5 procedures (Porteous and Kermani 2007). Since the panels were discontinuous over the arch and nails were used to connect the panels to the arch, semi-rigid connections were assumed at the end of the stress-skin beam elements. Effective connection stiffness was adjusted until the model and measured crown deformation of the loaded and adjacent arch along with the ¼ point deformation of the loaded arch were visually matched. Based on the analysis, instead of applying the original 140kN loading to the single full span arch, the laboratory loading was reduced to 106kN to account for the load distributional effects of the roof.

Similarly, a single half arch model was created to determine the number and location of concentrated loads to approximate a uniformly distributed load applied to the arch arm. A linear elastic structural analysis was performed of a single arch that had been sub-divided into 52 beam elements with variations in cross sectional properties. This iterative process continued until the difference between the displacements and moments of the different concentrated and uniform loading conditions were visually minimized. Figure 4 shows the arch deformation for both the series of concentrated loads and the uniformly distributed load conditions, which justifies the approach.

The original loading was uniform across the entire width of the building resulting in peak displacements that were only vertical and rotational. Due to the symmetry of the original testing, only half an arched span was loaded in the laboratory. The peak connection was simulated by welding the original

connection plates to a stiff plate that ran on a linear bearing system. This linear bearing facilitated the vertical movement of the arch peak and the connection plates allowed for rotation of the arch end.

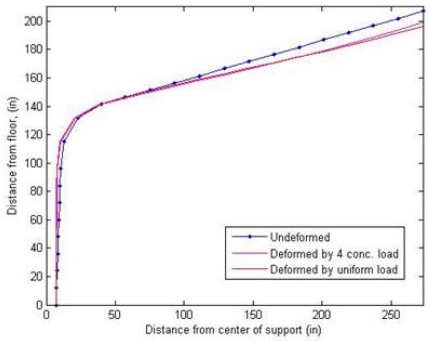

Figure 4—Loading on FPL glued-laminated arch building and measurement techniques for live loading of building.

Loading Protocol

Load was applied to the arch using two 245-kN MTS actuators in tandem under load control until the maximum load was reached. Loads were applied in the following four cycle pattern highlighted in Table 1 with no pauses at the transitions between cycles. For arches 3 and 10, the cycle 3 sustained loading times were extended to 138 and 168 hours, respectively. Figure 5 shows the images of the test setup to achieve the 4-point concentrated load condition.

Table 1—General Loading Protocol for Arches

Cycle	Loading	Sustained	Unloading
1	5 min	10 min	5 min
2	5 min	10 min	5 min
3	5 min	72+ hours	5 min
4	5 min	10 min	5 min

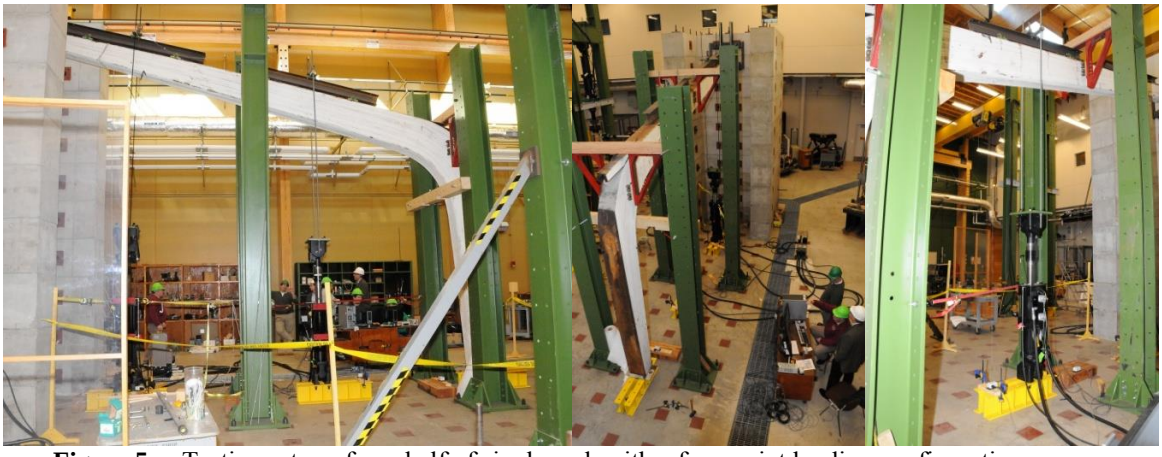

Figure 5— Testing setup of one half of single arch with a four-point loading configuration.

Measurements

Both load and deformation were continually recorded for the duration of the tests, at variable rates. During the loading and unloading of the arches readings were every second, while during the sustained

load readings were taken at longer intervals, but not in excess of 30 seconds. Vertical deformations were measured at all quarter points and one horizontal deformation of the arch leg was measured 3.3 m above the support.

Experimental Response

Short Term Loading

Arches were to be loaded with 2 short-term cycles, followed by a sustained load, and finished with one more cycle of short term loading. A typical response to the short term loading cycles are shown in Figure 6a. Note the initial cycle had the greatest deformation response due to the seating of the arch while subsequent short term loadings, cycle 2 and cycle 3 showed nearly identical behavior. Cycle 3short team loading indicated no structural stiffness degrade due to sustained loading just prior. Only arch 5 showed abnormal behavior and only one short term loading was conducted,
Figure 6b. After loading, an inspection revealed that the base of the arch leg had considerable delamination and decay which caused excessive compressive deformation at the base connection. In 1993, the building experienced a fire event. In the course of fighting the fire significant amounts of water pooled at the base of this arch and likely caused the end delamination since the adhesives were not moisture resistant.

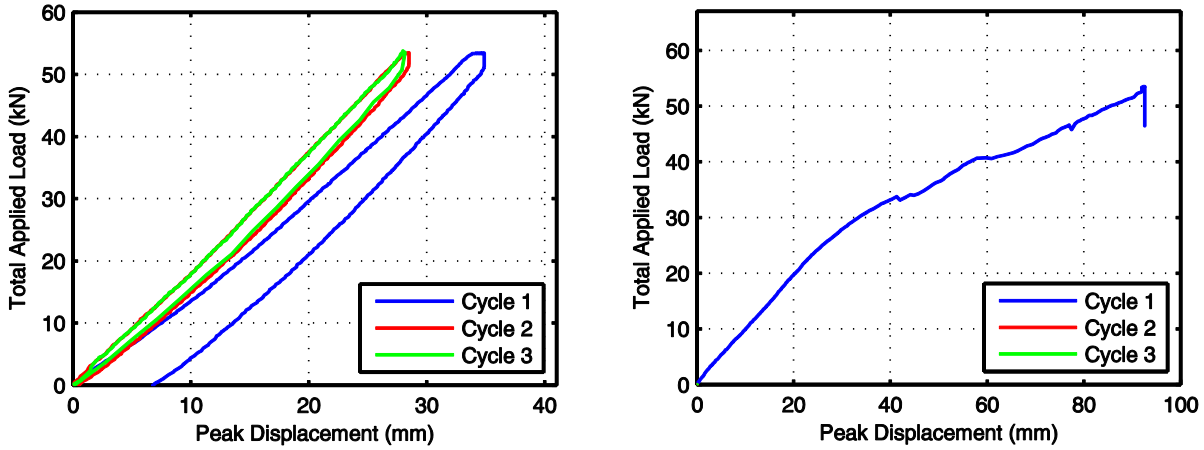

Figure 6— Short term load response for (a) Arch 3 and (b) Arch 5.

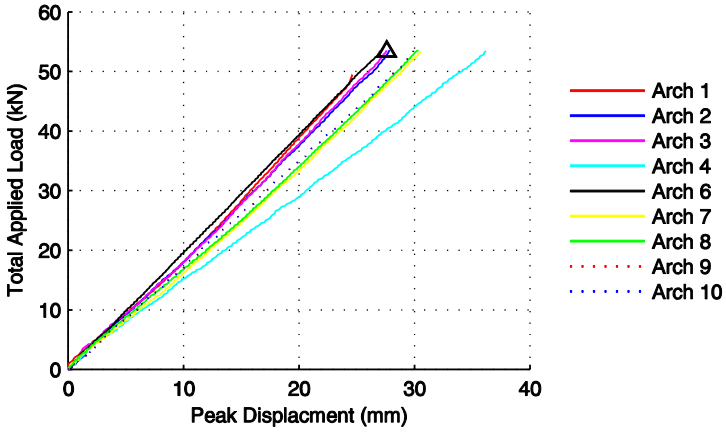

Figure 7— Third cycle, short term, load response for all arches, except 5.

Peak deformation versus applied load, for the third cycle of loading, is plotted in Figure 7 for all arches. Figure 7 indicates all of the arches show a linear response with load, but three distinct observations can be made: 1) arches 1 thru 3 and 6 are grouped together and showed the highest stiffness, 2) arches 8 thru 10 are grouped together at a different and slightly lower stiffness response, and 3) arch 4 stands alone with the lowest linear response. While no reasonable explanation was identified for these groupings, we believe Arches 1 thru 3 and 6 most closely represent the original structure due to the high stiffness, and therefore, are the ideal reference data points for analytical comparisons.

Long Duration Loading

In addition to the short term loading, at least 72 hours of sustained load was applied to the structure between the second and third loading cycles. This longer-term loading provided insight into the potential increase to deformation by sustained loading. During the original loading condition, peak deformation increased about 15 to 20 percent after the first 60 days of loading, while the rate of deformation decreased. After 60 days, the original deformation rate increased but this rate of change was likely due to drying deformations associated with the heating of the building and periodic winter snow loads. To compare the effect that sustained loading has on deformation for all arches we calculated the ratio of the instantaneous measured deformation to deformation when maximum load was first applied. Figure 8 plots this ratio versus time for all measurement locations, for both 72 and 160 hours load durations. Both graphs reveal that larger measured deformations (Peak, ¾ pt, and midspan) gave similar and consistent ratios over the monitoring period. The change in measured deformation was greatest in the first 24 hours of loading, the deformation rate decreased with continued loading, and the deformation increased over the entire monitoring period by about 10 percent. Figure 9 shows the effect of sustained loading on the peak deformation over 72 hours, for all tested arches. For all the arches, the percent of deformation increase was lower than 15 percent and the rate of deformation change was decreasing. These observations lend credence to the statement that measured building deformation changes in the original structure after 60 days were caused by drying of the glued-laminated arches and periodic snow loads, not the original applied loading.

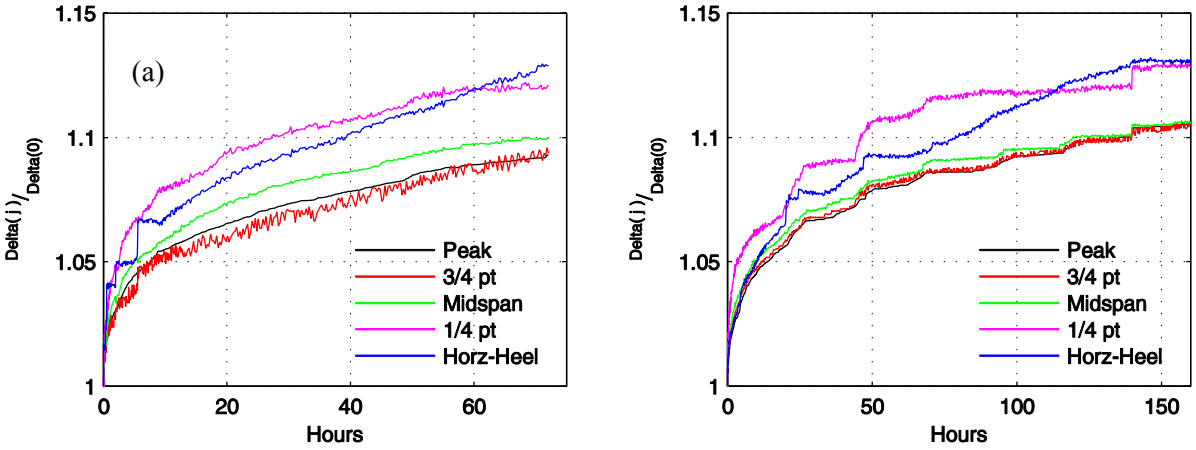

Figure 8— Sustained load deformation response for all measurements for 72 and 160 hours.

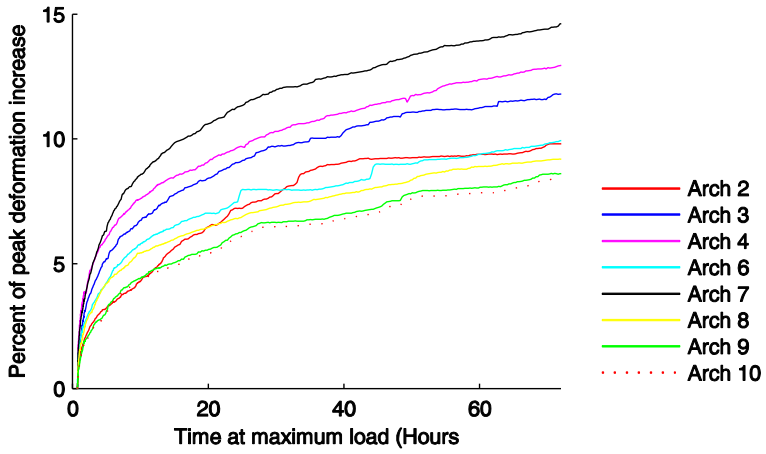

Figure 9— Sustained load response of the peak deformation for all arches, except Arch 5.

Analytical Response

A simple linear elastic model of a single arch was created using MASTAN2, (2006). Though the intention was to simulate uniform loading with four concentrated loads and make a direct comparison, the applied loads were placed at different locations in the laboratory testing. The structural model was reanalyzed for the new loading condition. When the original structure was constructed, two additional arches were manufactured but were tested with a thrust load and from the remains; ASTM D143 property tests were conducted. These material tests estimated a modulus of elasticity of 13.1 GPa. For comparison purposes, the maximum deformation obtained during the laboratory testing of the arches for the final load cycle will be evaluated. Table 2 presents the analytical deformation at the measured deformation locations along with the average, minimum and maximum deformations at maximum load. In general, the model deformations are lower than the average but greater than the minimum measured deflections. Percent difference of the analytical and measured deformations showed similar trends. Figure 7 shows that the model peak deformation (open triangle symbol) and the stiffest group of arches (1,2,3,6) are visually the same.

Table 2—Comparison of Analytical model to experimental measurements

	Deformations (mm)				Percent difference		
Location	Analytical	Average	Min	Max	Average	Min	Max
Peak	27.6	29.3	24.6	36.2	-5.8	12.2	-23.8
¾ Point	20.4	20.1	19.7	27.2	1.5	3.6	-25.0
½ Point	11.7	13.8	12.4	16.8	-15.2	-5.6	-30.4
¼ Point	3.2	5.1	4.7	6.4	-37.3	-31.9	-50.0
Thrust	-7.8	-6.8	-5.7	-9.3	14.7	36.8	-16.1

Connection Issues

The most consistent problem observed after deconstruction of the glued-laminated arch structures was the condition of the crown connection. Figure 10 shows the crown connection consisted of steel side plates attached to the each arch arm with three 25.4-mm bolts in a triangular pattern. Measurements revealed inner bolt end spacing was 2.5d, lower than the minimum 4d required by contemporary design standards. As a result, most of the arch had cracks, splits, or wood plugs emanating from the inner bolts. Figure 10 also shows missing wood material associated with the lower bolt line though this condition was less common. Unlike the middle bolt, sufficient end spacing was provided. There is two possible

explanations for this damage. One, after the failure of the inner bolts, the remaining capacity of the connection was insufficient to carry a maximum event load that occurred during the service life to the structure. Two, the connection was damage during deconstruction due to possible out of plane twisting of the arch while it was lowered to the ground (Figure 2). In either case, the damage to the connection had little influence on the vertical loading response of the arches because the splits did not go completely through the cross section. Under a lateral loading scenario, or as the arches reach maximum loading conditions, the connection condition could have a strong influence on behavior.

Figure 10— Peak connection in building and glued-laminated peak with connection plate removed

Conclusions

After 75 years of service, ten glued-laminated arches were recovered for structural evaluation from the deconstruction of the second glued-laminated building built in the United States. Strength loss was assessed by comparing the deformations of single half-arches with a structural model. The structural model was developed and validated using data generated from a 1935 study where the application of a 6-month, in-situ loading of the central span of the original arch structure. Loading of the laboratory half span arches consisted of three cycles of short-term loading and one long-term loading of at least three days. Comparison of the model and experimental deformation reveal that 8 of the 10 arches performed with little or no stiffness loss. One arch had considerable decay and delamination of its leg, and therefore, loading protocols were not completed. Finally, some failures of the glued-laminated edges at the peak connection were observed and attributed to insufficient end spacing of the bolts.

References

Wilson, T.R.C. 1939. The Glued Laminated Wooden Arch. USDA Technical Bulletin No. 691.

Wilson, T.R.C. and Cottingham, W. S. 1952. Tests of glued-laminated wood beams and columns and development of principles of design. Forest Prod. Lab. Rep. R1687.

MASTAN2, version 3.3, developed by Ronald D. Ziemian and William McGuire, 2006

Porteous, J. and Kermani, A. 2007. Structural Timber Design to Eurocode 5. Blackwell Publishing.

Session 6

Nondestructive Evaluation of Composite Materials—Nanocellulosic Films to Glued Laminated Timber

Nondestructive Measurement of Dynamic Modulus for Cellulose Nanofibril Films

Yan Qing
School of Materials Science and Engineering, Central South University of Forestry and Technology
US Forest Service, Forest Products Laboratory, Madison, Wisconsin, USA, yqing@fs.fed.us

Robert J. Ross
US Forest Service, Forest Products Laboratory, Madison, Wisconsin, USA, rjross@fs.fed.us

Zhiyong Cai
US Forest Service, Forest Products Laboratory, Madison, Wisconsin, USA, zcai@fs.fed.us

Yiqiang Wu
School of Materials Science and Engineering, Central South University of Forestry and Technology, wuyiqiang@csuft.edu.cn

Abstract

Nondestructive evaluation of cellulose nanofibril (CNF) films was performed using cantilever beam vibration (CBV) and acoustic methods to measure dynamic modulus. Static modulus was tested using tensile tension method. Correlation analysis shows the data measured by CBV has little linear relationship with static modulus, possessing a correlation coefficient (R^2) of 0.282. However, the data tested by acoustic method correlated well with the static modulus, approaching a correlation coefficient of 0.6. Irregular sample shape largely contributed to these obtained results. The dynamic modulus, especially measured by acoustic method, is likely an effective tool in non-destructive evaluation of mechanical properties for CNF nanomaterials.

Keywords: Cellulose nanofibril films, Cantilever beam vibration, Acoustic method, Tensile test

1. Introduction

As the most abundant biopolymer on the earth, cellulose and its derivations are attracting a high level of attention. In the 1980s, cellulose nanofibrils were created by subjecting plant pulp fibers to repeated mechanical defibrillation (Herrick et al., 1983; Turbak et al., 1983). Compared to conventional natural fibers, these nanofibrils exhibit a diameter less than 100 nm, and approach several micrometers in length. Abundant and eco-friendly, cellulose nanofibrils have other unique advantages, such as outstanding mechanical strength, excellent visible light transmittance, low thermal expansion, and desirable barrier capability for low molecular substances (Siró and Plackett, 2010). Until now, many attempts were dedicated to seeking industrial applications of cellulose nanofibils in a broad variety of fields like special packaging, engineered polymeric composites, medical carriers, flexible conductive substrates, and energy storage (Nyström et al., 2010; Olsson et al., 2010; Okahisa et al., 2009).

Theoretically, it was calculated that nanofibrils have a Young's modulus of approximately 150 GPa (Iwamoto et al., 2009). However, due to their superfine dimensions, measurement of mechanical properties of nanofibrils using traditional approaches is still challenging. A testing method via atomic force microscopy (AFM) was successfully applied to measure mechanical strength of individual

nanofibrils at the nanoscale level (Cheng and Wang, 2008; Iwamoto et al., 2009). Similar to a three-point bending test, the samples were initially suspended on a silicon wafer possessing several regular micro-grooves. A cantilever tip was used to apply a small test load on the nanofibrils at an appropriate position. The deflection and load obtained were used to estimate the exact mechanical strength. However, determination of deflection and distinguishing the test position are complicated and sensitive. Static mechanical properties tested from nanofibril films, on the other hand, indirectly provide evaluation of such individual nanofibrils.

Many nondestructive methods involving vibrational and acoustic assessments have been used to predict the mechanical properties of forest products (Ross et al., 2004; Wessels et al., 2011). The measured dynamic modulus is reported correlating highly to the static modulus tested by bending or tensile tension (Wang et al., 2007; Wang et al., 2012). Hunt and Turk (2008) developed a cantilever beam vibration apparatus for thick wood fiber composites such as fiberboard and particleboard. However, to the best of our knowledge, there is scant literature regarding dynamic modulus measurement of cellulose nanofibril films or its composites. Here, the dynamic modulus of various cellulose nanofibril films prepared from different species of cellulose nanofibrils was tested by means of cantilever beam vibration and acoustic method. Based on the statistical analysis of correlation between obtained dynamic and tensile modulus, an optimized approach was selected which provides an alternative in estimating the mechanical properties of cellulose nanofibrils and CNF composites nondestructively.

2. Materials and methods

2.1 Materials

Five species of cellulose nanofibrils denoted as R, RM, ER, ERM, and TEMPO were used in the study to prepare different films. The TEMPO nanofibril was produced by chemical treatment at neutral condition (Saito et al., 2009), involving 2, 2, 6, 6-tetramethylpiperidinyl-1-oxyl (TEMPO) mediated oxidation with hypochlorite and chlorite as common reactants. The R and RM nanofibrils were mechanically refined in a stone grinder for 6h, and RM was followed by 20 times microfiluidization pass-through. While, ER and ERM nanofibrils were previously treated by enzyme hydrolysis for 1.5h, and subsequently treated by mechanical fibrillation like the R and RM variants. Detailed descriptions for above mentioned nanofibrils were offered in our previous work (Qing et al., 2013).

2.2 Preparation of CNF films

The CNF films were prepared by filtrating CNF suspensions, followed by air- and then oven-drying of wet films. The nanofiber solution, diluted into 0.2% solid concentration, was filtrated using a 142 mm Milipore ultrafiltration System (Millipore, Millipore Corporation, USA) under 0.55 MPa air pressure. OmniporeTM filter membranes with micropore size of 0.1 μm (JVWP14225, JV, Millipore Corporation, USA) were used in the apparatus, and were supported by the filter paper. The wet films were peeled from the membrane and stacked first between waxed paper and then filter paper, and maintained between two metal plates. The package was air dried at room temperature for 24h and then oven dried at 60 ^{o}C for 8h under a load of approximately 250 N. These films were then conditioned in a 50% relative humidity chamber at a temperature of 23 ^{o}C until tested. The final tensile test, dogbone-shape specimens (seen in Figure 1) were cut to conform to ASTM D638-10 type V by means of a special die.

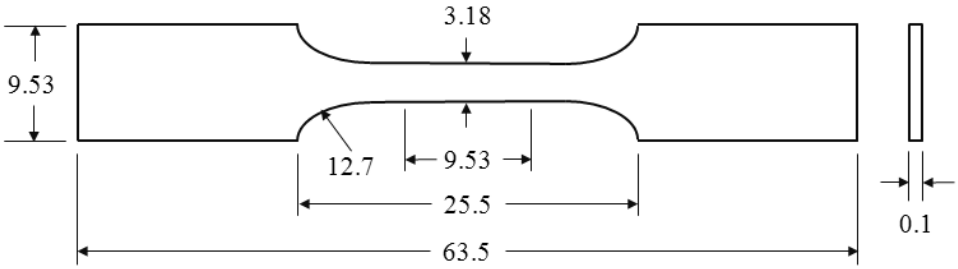

Figure 1—Dimensional profile of ASTM tensile specimens. (Unit: mm)

2.3 Cantilever beam vibration (CBV) measurement

Cantilever beam vibration (CBV) modulus was measured using a USDA Forest Service, Forest Products Laboratory (FPL) designed apparatus, a general profile of which was given in Figure 2. A specific description including mechanism, manual instruction, and applications is available in the reference (Turk et al., 2008). As shown in Figure 2a, the ASTM tensile specimens were clamped at three different positions and subjected to a free vibration which was induced by an initial displacement of 6, 7 and 8mm, respectively. The clamped lengths were 10, 19, and 32 mm, respectively. A laser detector automatically collected the vertical displacement with a sampling frequency of 1000 Hz. More than 5 replicate tests were conducted at each condition. Figure 3 illustrates a representative specimen vibration response, exhibiting typical free-vibration damping.

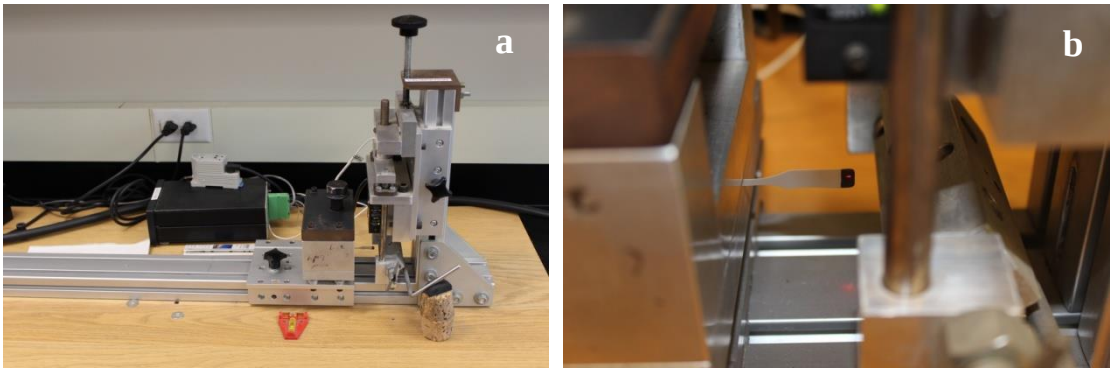

Figure 2—Cantilever beam vibration apparatus (a) and specimens clamped at the grip (b)

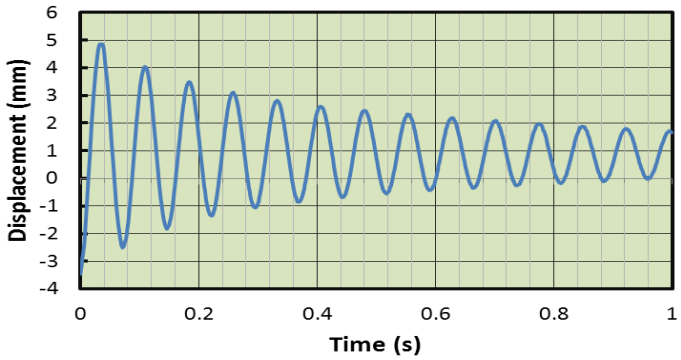

Figure 3—A typical specimen free-vibration response

The frequency of the first model of free vibration of a cantilever beam is given in the following equation (Harris 2002).

$$\omega = 2\pi f = \left(\frac{1.875}{l}\right)^2 \sqrt{\frac{EI}{\rho_A A}}$$

Where f is detected frequency (Hz), l is unclamped length of cantilever beam (m), E is dynamic modulus (Pa), I is area moment of inertia of the vibration beam (m^4), ρ_A is density of vibration beam (kg/m^3), and A is the cross area of vibration beam (m^2).

2.4 Acoustic modulus measurement

The acoustic modulus was calculated based on the equation $DMOE_{aco} = v^2 \rho$, where v is the acoustic velocity transmitted in the testing material, and ρ is the actual density of testing material (Ross et al., 2004). To measure the acoustic velocity, a JAMES v-meter (seen in Figure 4) was used. The transmit times of regenerated ultrasonic pulses traveled in a defined distance which ranged from 20, 30, 40 to 50mm were determined, respectively. The acoustic velocity was defined as slope of the distance scatter data and its corresponding time. At each condition, more than 5 specimens were tested.

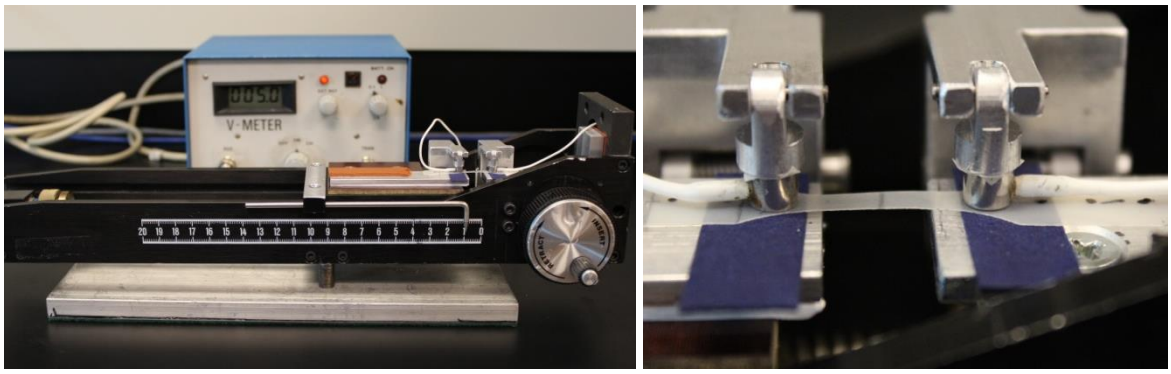

Figure 5—Profile of acoustic velocity testing apparatus

2.5 Tensile tests (static modulus)

The tensile properties of different CNF films were tested by an Instron 5865 universal material testing apparatus (Instron Engineering Corporation, MA, USA) with a 500 N load cell, according to ASTM D638-10. The specimens were cut to conform to ASTM D638-10 type V dog bone shape using a special cutting die (Qualitest, FL, USA) and were subsequently conditioned for a minimum of 1 week at 50% RH and 23 °C prior to testing. Testing was performed within the conditioned chamber in order to maintain specimen equilibration. The specimens were pre-loaded with 5 N of force to remove slack, and the tests were performed with a crosshead speed of 1 mm/min. At least 6 specimens were tested for each condition. An LX 500 laser extensometer (MTS Systems Corporation, MN, USA) was used to determine the displacement with sampling frequency of 10 Hz. The laser recorded the displacement between two strips of reflective tape initially placed approximately 8 mm apart on the necked-down region of the dog-bone specimens. Strain was calculated from the determined displacement and initial gage length. Tensile modulus was calculated as the slope of the stress-strain curve in the stress region of 30-70 MPa.

3. Results and Discussion

3.1 Cantilever beam vibration

Table 1 gives dynamic modulus of various nanofibril films measured by cantilever beam vibration. It is clearly seen that there were significant differences in dynamic modulus as the clamp length varied. However, the tested values differed slightly when the samples were clamped at the same length, even with different initial displacements to induce free vibration. Considering the cellulose nanofibril films were homogeneous, apart from the nanofibril itself, the clamp length appears to play an important role in the evaluation of dynamic modulus.

Unlike conventional forest product samples such as fiberboard and plywood, the test samples here had unique shape, and were extremely light. It was thought these factors would affect the natural free vibration. The hypothesis was supported by a similar test of aluminum strips (64L×9.53W×0.1mmT). When clamped at three different lengths of 10, 19, and 32mm, the measured dynamic modulus varied largely, even though the homogeneous aluminum has a reported theoretical dynamic modulus of 65-70 GPa. It is believed the clamped length would influence the stiffness of test samples with such dimension and weight. As a result, the measured dynamic modulus varies widely.

Additionally, the tested cellulose nanofibril films were not perfectly flat because of residual growth stress and unique sizing. The warping originated naturally from the above factors and contributed to the difference in measured dynamic modulus.

Table 1—Tensile and CBV dynamic modulus for various nanofibril films.

Materials	Tensile modulus (GPa)	Dynamic modulus (GPa)		
		Clamped at10 mm	Clamped at19 mm	Clamped at 32 mm
TEMPO	11.71 (1.56)	10.46 (1.62)	6.17 (0.74)	17.58 (1.99)
R	8.29 (1.34)	6.37 (0.09)	4.12 (0.12)	11.47 (0.96)
RM	10.48 (2.11)	6.75 (0.86)	4.31 (0.53)	11.89 (1.57)
ER	14.25 (3.17)	10.66 (1.44)	6.29 (0.56)	17.65 (1.48)
ERM	14.43 (1.76)	8.89 (0.55)	4.05 (0.25)	14.31 (0.40)

Values in parenthesis represent standard deviation

To figure out how well the measured CBV dynamic modulus can be correlated to static modulus, the nondestructive samples were then subjected to tensile testing. The specific values are displayed in Table 1. The correlation between CBV dynamic and static modulus are shown in Figure 5. The correlation coefficient of these data sets is relatively low, approaching R^2 values less than 0.3. This indicates a huge, existing challenge in predicting mechanical properties of cellulose films using conventional CBV methods. As illustrated above, improvement of sample preparation and enhancing the accuracy of displacement and free vibration detection are warranted for future investigations. However, this CBV testing provides valuable insight into nondestructive prediction of cellulose nanofibril properties.

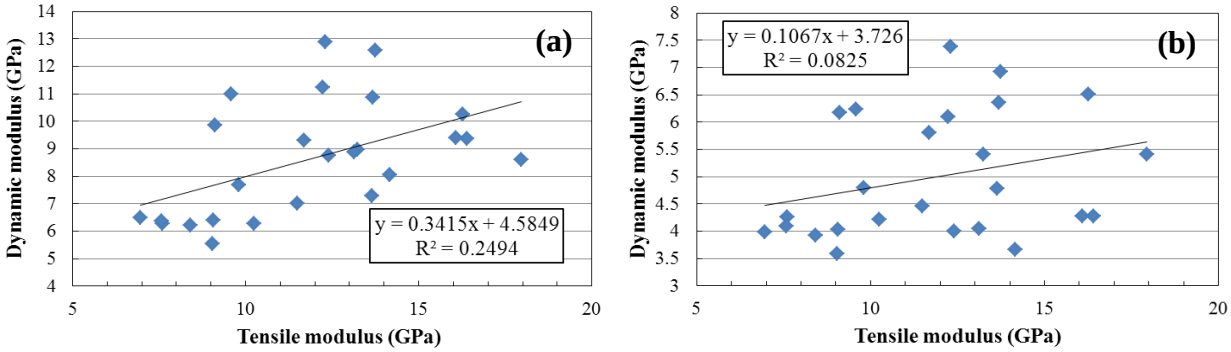

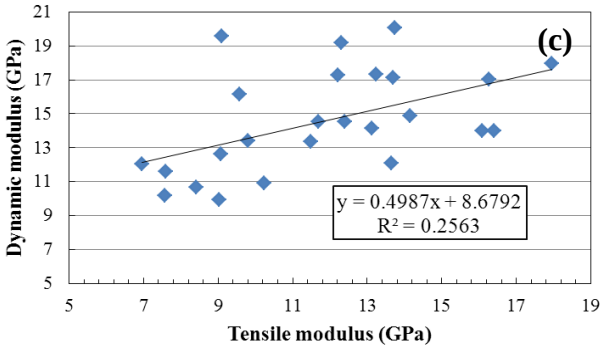

Figure 5—Correlation between CBV dynamic and tensile modulus. (a), (b), and (c) represents clamped length at 10, 19 and 32 mm, respectively.

3.2 Acoustic dynamic modulus

As comparison, the acoustic approach was also applied in testing dynamic modulus. The measured values are shown in Table 2. Because this dynamic modulus is simply equal to density times the acoustic velocity squared, one should be pay more attention to the determination of such velocity transmitted in testing samples. Therefore, 6 different methods, denoted as Method 1 to 6 respectively, were developed to compute acoustic velocity. Method 1 was that which the velocity is identical to the slope of a linear trendline of transmitted distance against time. When considering the initial state should be at the coordinate origin, in Method 2 the linear trendline started at zero. However, the correlation coefficient (R^2) is less than 0.6, which is relatively low. Velocity in Method 3 is an average value calculated from four different predetermined transmitted distances. Due to small tested distance (not more than 50 mm), Methods 4 to 6 attempted to decrease interruption of transverse waves in the least distance and thus improve the accuracy of intrinsic velocity. Method 4 is a simple velocity calculated from greatest testing distance of 50 mm. Similar to Method 1, the velocity measured from Method 5 is the slope of the linear trendline of transmitted distance against time. However, the first two distances were subtracted from corresponding intercepts which are obtained from Method 1. In Method 6, the velocity is equal to the slope of the linear trendline of such data sets with the greatest two distances and coordinate origins.

Table 2—Tensile and acoustic dynamic modulus for various cellulose nanofibril films

Materials	Tensile modulus (GPa)	Dynamic modulus (GPa)					
		Method 1	Method 2	Method 3	Method 4	Method 5	Method 6
TEMPO	11.71 (1.56)	5.12 (0.37)	12.08 (0.83)	20.40 (1.33)	11.40 (1.03)	13.58 (1.00)	10.73 (0.75)
R	8.29 (1.34)	3.84 (0.29)	8.75 (0.49)	13.92 (0.40)	8.18 (0.36)	9.87 (0.57)	7.78 (0.43)
RM	10.48 (2.11)	4.02 (0.26)	9.63 (0.50)	16.37 (1.07)	8.82 (0.65)	10.77 (0.60)	8.49 (0.46)
ER	14.25 (3.17)	5.03 (0.19)	12.59 (0.50)	22.40 (2.10)	11.62 (0.28)	14.08 (0.46)	11.09 (0.36)
ERM	14.43 (1.76)	5.10 (0.19)	12.14 (0.40)	21.03 (0.81)	11.41 (0.60)	13.57 (0.47)	10.80 (0.40)

Values in parenthesis represent standard deviation.

The correlation between acoustic dynamic and tensile modulus is shown in Figure 6. Interestingly, the coefficient of correlation is approximately 0.6, much greater than was calculated in CBV dynamic modulus measurement. The result indicates that nondestructive measurement using acoustic approach is better than CBV testing in the prediction of mechanical properties of cellulose nanofibril film materials. As interpreted above, these nanofibril films are of unique dimension which would block an intrinsic free vibration. On the contrary, such characteristics might have little effect on the transmission of ultrasonic waves. However, the determination of velocity is another challenge. As comparison, Method 6 appears to provide a more effective and efficient approach to detect an exact transmitted velocity in such testing samples. Figure 7 gives a comprehensive comparison of dynamic and tensile modulus.

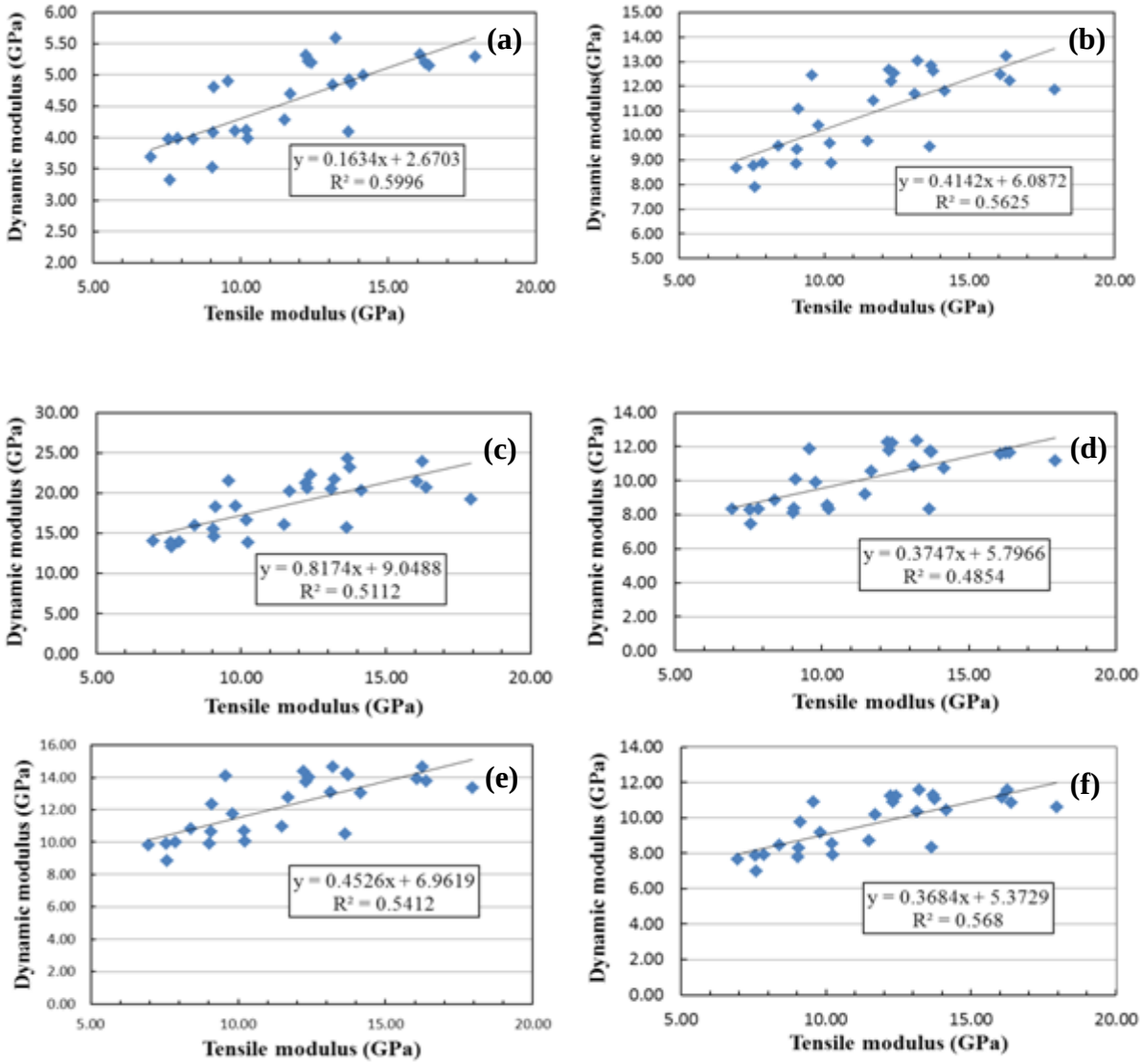

Figure 6—Correlation between acoustic dynamic and tensile modulus. (a), (b), (c), (d), (e), and (f) represents dynamic modulus calculated from method 1, 2, 3, 4, 5, and 6, respectively.

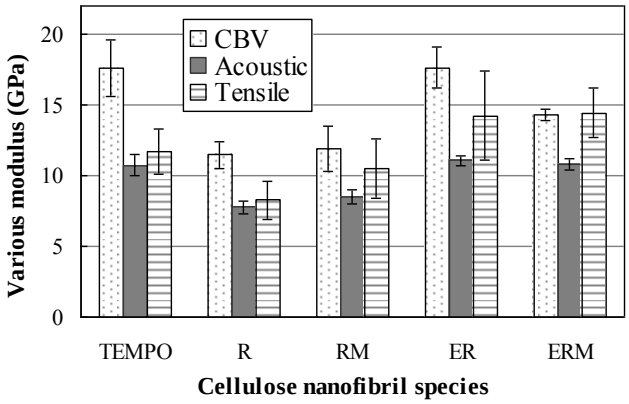

Figure 7—Comprehensive comparison of dynamic and tensile modulus.

Conclusions

Nondestructive evaluation involving cantilever beam vibration and acoustic methods was performed to measure the dynamic modulus of cellulose nanofibril films. The comparison of resulting dynamic modulus and static modulus tested using tensile tension was investigated. Results show a correlation coefficient (R^2) of 0.282 and indicate the data measured by CBV has little linear relationship to static modulus. However, the data tested by acoustic method correlated well with the static modulus, approaching a correlation coefficient of 0.6. The irregular and special sample shape could contribute largely to the obtained result. The dynamic modulus, especially measured by acoustic method, is likely an effective indictor to evaluate the mechanical properties of cellulose nanofibril materials in nondestructive testing.

References

Cheng, Q.; Wang, S. 2008. A method for testing the elastic modulus of single cellulose fibrils via atomic force microscopy. Composites part A: Applied Science and Manufacturing, 39(12):1838-1843.

Harris, C.M. ed. 2002. Harris's shock and vibration handbook, 5th edition. New York:Mcgraw-Hill:1568 p.

Herrick, F.W., Casebier, R.L.; Hamilton, J.K.; et al. 1983. Microfibrillated cellulose: Morphology and accessibility. Journal of Applied Polymer Science: Applied Polymer Symposium, 37(9):797-813.

Iwamoto, S.; Kai, W.; Isogai, A.; et al. 2009. Elastic modulus of single cellulose microfibrils from tunicate measured by atomic force microscopy. Biomacromolecules, 10(9):2571-2576.

Nyström, G.; Mihranyan, A.; Razaq, A.; et al. 2010. A nanocellulose polypyrrole composite based on microfibrillated cellulose from wood. The Journal of Physical Chemistry B, 114(12): 4178-4182.

Olsson, R.T.; Azizi Samir, M. A. S.; Salazar-Alvarez, G.; et al. 2010. Making flexible magnetic aerogels and stiff magnetic nanopaper using cellulose nanofibrils as templates. Nature Nanotechnology, 5(8):584-588.

Okahisa, Y.; Yoshida, A.; Miyaguchi, S.; et al. 2009. Optically transparent wood-cellulose nanocomposite as a base substrate for flexible organic light-emitting diode displays. Composites Science and Technology, 69(11-12):1958-1961.

Qing, Y.; Sabo, R.; Zhu, J.Y.; et al. 2013. A comparative study of cellulose nanofibrils disintegrated via multiple processing approaches. Publishing.

Ross, R.J.; Erickson, J.R.; Brashaw, B.K.; et al. 2004. Yield and ultrasonic modulus of elasticity of red maple veneer. Forest Products Journal, 54(12):220-225.

Saito, T.; Hirota, M.; Tamura, N.; et al. 2009. Individualization of nano-sized plant cellulose fibrils by direct surface carboxylation using TEMPO catalyst under neutral conditions. Biomacromecules, 10(7):1992-1996.

Siró, I.; Plackett, D. 2010. Microfibrillated cellulose and new nanocomposites materials: A review. Cellulose, 17(3):459-494.

Turk, C.; Hunt, J.F.; Marr, D.J. 2008. Cantilever-beam dynamic modulus for wood composite products: part 1 appartus. Research Note FPL-RN-0308. Madison, WI: U.S. Department of Agricutue, Forest Service, Forest Produts Laboratory. 5 p.

Turbak, A.; Snyder, F.W.; Sandberg, K.R. 1983. Microfibrillated cellulose, a new cellulose product: properties, uses, and commercial potential. Journal of Applied Polymer Science: Applied Polymer Symposium, 37(9):815-827.

Wessels, C.B.; Malan, F.S.; Rypstra, T. 2011. A review of measurement methods used on standing trees for the prediction of some mechanical properties of timber. European Journal of Forest Research, 130:881-893.

Wang, X.; Carter, P.; Ross, R. J.; et al. 2007. Acoustic assessment of wood quality of raw forest materials- a path to increased profitability. Forest Products Journal, 57(5):6-14.

Wang, Z.; Li, L.; Gong, M. 2012. Measurement of dynamic modulus of elasticity and damping ratio of wood-based composites using the cantilever beam vibration technique. Construction and Building Materials, 28:831-834.

Nondestructive Evaluation of Coir-fiber Cement Composites

Joana Mendes Ferraz
Department of Forest Engineering, Faculty of Technology, University of Brasilia, Brasília, DF, Brazil
joanamendesferraz@gmail.com

Cláudio Henrique Soares Del Menezzi
Department of Forest Engineering, Faculty of Technology, University of Brasilia, Brasília, DF, Brazil,
cmenezzi@unb.br

Mário Rabelo de Souza
Forest Products Laboratory, Brazilian Forest Service, Ministry of Environment, Brasília, DF, Brazil,
mario.souza@florestal.gov.br

Abstract

The paper aimed at evaluating the utilization of a nondestructive technique to predict mechanical properties of coir-fiber cement composites. Three treatments were evaluated: addition of 4% $CaCl_2$, hot water immersion at 80°C, and immersion into NaOH aqueous solution. Twenty-four panels were manufactured, and 102 samples were cut from this material and nondestructively tested using stress wave technique. Dynamic modulus of elasticity (E_d) and stress wave velocity (sw_v) were determined and used so as to predict the mechanical properties of the panels. According to the results, the models were highly statistically significant ($p<0.0000$) for all mechanical properties, but adjusted R^2 values presented high variability – from 0.214 to 0.665. In general, models fitted to flexural properties were more reliable (0.658-0.665), followed by compression strength (0.48-0.49) and internal bonding (0.214-0.276). Although the E_d variable generated the best models, only sw_v presented potential to predict mechanical properties.

Keywords: fiber-cement composites, treated coir fiber

Introduction

Nowadays, cement-wood composite presents major importance on civil construction market due to its low cost and easy production, as its composition includes residues from timber and agro-industries, thus being a viable alternative for these residues. Moreover, these composites have found great worldwide acceptance since this mixture combines desirable properties of lignocellulosic material and cement (Coates 1994). These composites can be used as: linings, floors, screens, external coatings, specialized coatings for acoustical isolation, protection elements against fire, etc (Olorunnisola 2008).

The lignocellulosic portion of these composites is obtained from several sources such as wood and agricultural residues, fast-growing wood species and annual crops. However, these materials contain substances (sugars, extractives, etc) that inhibit cement setting, which can lead to a composite with worsened properties. Therefore, the usual approach to overcome this limitation is adding compatibilizers or treating the organic raw material before mixing with cement. Specifically for coir fiber (*Cocos nuceifera*), Ferraz et al. (2012) observed extreme inhibition of cement setting and suggested that

pretreatment must be applied before considering this material for manufacturing cement-bonded composites.

The utilization of nondestructive methods to evaluate wood/fiber cement composites has been studied by several authors. Aamr-Daya et al (2008) employed longitudinal ultrasonic vibration and observed that the addition of 10% of flax in the mixture with cement imparted significant decrease in the dynamic modulus of elasticity. Turgut (2007) found that ultrasound velocity was drastically reduced (2900 m/s to 2000 m/s) when wood sawdust was added to cement composite bricks. Similar results were found by Turgut and Algin (2007). NDT methods have been also used to monitor cement setting as performed by Rodrigues and Beraldo (2010) and Beraldo and Balzamo (2009). The relationship between nondestructive testing and mechanical properties has been investigated by Teixeira and Moslemi (2001) and Araújo et al. (2011). In general, the results were encouraging since the regression models presented R^2 over 0.55. The ultrasonic method has been identified as a promising technique in order to measure porosity in mortars (Goueygou et al. 2009). In this context, the present paper, along with two others (Ferraz et al. 2011 and Ferraz et al. 2012), comprises a series of papers concerning the characterization of coir-fiber composites. Specifically, we aimed at analyzing the utilization of the stress wave nondestructive method as to estimate the mechanical properties of coir-fiber cement composites manufactured with addition of compatibilizers and pretreated raw material.

Materials and Methods

Composite Manufacturing

Initially, a bale of green coir fiber (*Cocos nucifera* L.) was obtained from the enterprise Coco Comandatuba Ltda., located in Ilhéus, Bahia State, Brazil. Afterwards, the fibers were processed in a hammer mill with 6-mm mesh opening. After the classification, this processed material was used to manufacture coif-fiber cement composites. Three treatments were assessed so as to reduce inhibiting effects: addition of 4% $CaCl_2$ in the cement-fiber mixture, pre-treatment consisting of fiber immersion into hot water at 80°C for 90 minutes, and another consisting of fiber immersion into NaOH aqueous solution at 5% for 72h. Two cement:fiber ratios (3:1 and 4:1) were also evaluated for each treatment. Therefore, six treatments were assessed and four boards were manufactured for each one, presenting nearly the following dimensions: 350 mm x 350 mm x 12.5 mm (length, width and thickness) and 1,200 kg/m³ nominal density (Figure 1). Further details concerning manufacturing can be found in Ferraz et al. (2011). Afterwards, the boards were placed in an air-conditioned room for 28 days at controlled conditions (20±3ºC; 65±1% RH) to fulfill the curing process.

Figure 1—Coir-fiber cement composite after manufacturing and specimens cut from each board to be nondestructively tested before mechanical testing.

Nondestructive Evaluation and Mechanical Testing

Twenty-eight days after setting, five specimens measuring 350 mm x 50 mm (length x width) were taken from each board (Figure 1). Initially, these specimens were nondestructively tested using the stress wave method (Metriguard Stress Wave Timer model 239A). The material was hit three times by a pendulum and the transit time (t, μs) as well as the average value were used to calculate the stress wave velocity (sw_v, m/s), according to equation 1. Stress wave dynamic modulus of elasticity (E_d, MPa) was determined according to equation 2.

$$sw_v = \frac{L}{t \times 10^{-6}} \tag{1}$$

$$E_d = \frac{sw_v^{\,2} \times \rho}{g} \times 10^{-5} \tag{2}$$

where L is span (m), ρ is the material density (kg/m^3) and g acceleration of gravity (9.8 m/s^2)

After the nondestructive evaluation, the specimens were tested up to rupture so as to determine: modulus of rupture (f_m), modulus of elasticity (E_M), compression strength (f_c), tension perpendicular to the board surface according to NBR 14810-3 (ABNT, 2002). The latter is usually named internal bonding (IB). Five replicates were made per property/board. Further details regarding the composite's properties assessment can also be found in Ferraz et al. (2011).

Statistical Analysis

Nondestructive properties (sw_v, E_d) were used as independent variables (x) to estimate the mechanical properties (f_m, E_M, f_c, IB) of the coir-fiber composites. Initially, the treatments (N=120) were analyzed altogether using simple linear regression ($y=a+bx$). Afterwards, this analysis was run for each treatment ($CaCl_2$, NaOH, hot water) separately (N=40), but the five following further non-linear models were also tested: S-curve, power, compound, quadratic and cubic (equations 3-7). The best model was chosen taking into account: level of significance coefficients, coefficient of determination (R^2), calculated F value and standard error of estimate (SEE). The effects of the applied treatment and cement:fiber ratio on the nondestructive properties of the composites were studied through analysis of variance (ANOVA) followed by Tukey´s test run to compare means.

$$\ln(y) = b_0 + \left(\frac{b_1}{x}\right) \tag{3}$$

$$\ln(y) = \ln(b_0) + (b_1 \times \ln(x)) \tag{4}$$

$$\ln(y) = \ln(b_0) + (\ln(b_1) \times x) \tag{5}$$

$$y = b_0 + b_1 x + b_2 x^2 \tag{6}$$

$$y = b_0 + b_1 x + b_2 x^2 + b_3 x^3 \tag{7}$$

Results and Discussion

Figure 2 shows the results of nondestructive variables according to the pre-treatment and cement:fiber ratio studied. Tukey´s test revealed that stress wave velocity was statistically different for the three treatments evaluated. Composites manufactured with hot water pretreated coir presented higher swv value followed by $CaCl_2$ and NaOH. Consequently, the respective Ed followed the same trend, although $CaCl_2$ and NaOH treatments showed statistically similar values. It was found that the addition of fiber (4:1 to 3:1) did not affect any nondestructive variable. Stress wave velocity values found are lower than those observed by Araújo et al. (2011) while studying bamboo-cement and bamboo-gypsum bonded composites: 1800 m/s to 2000 m/s. Beraldo and Balzamo (2009) found values ranging from 1141 m/s (natural) to 1428 m/s ($CaCl_2$ added).

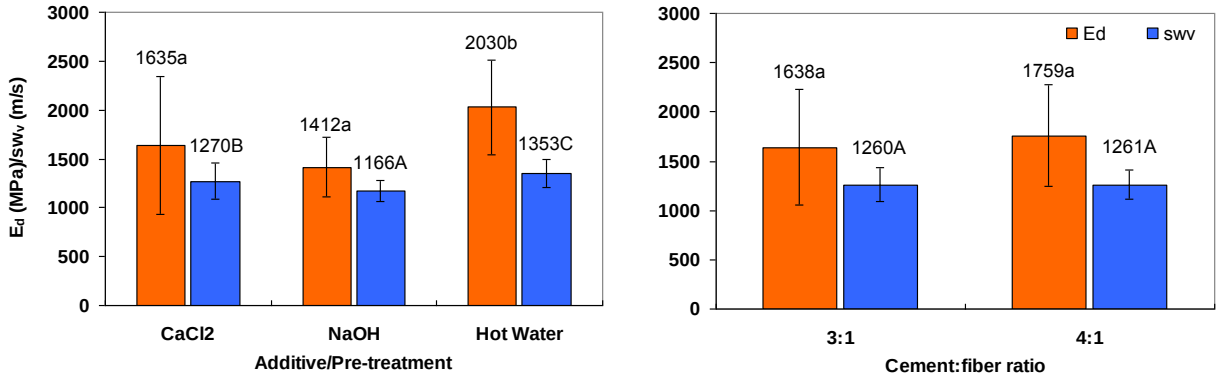

Figure 2—Stress wave dynamic modulus of elasticity (E_d) and wave velocity (sw_v) of coir-fiber cement composites according to treatment and cement:fiber ratio. (Note: mean values followed by the same letter do not statistically differ according to Tukey´s test at α=0.05).

As previously mentioned, the mechanical properties of this material can be found in Ferraz et al. (2011). The correlation between those values and nondestructive variables are presented in Table 1. It is clear that all evaluated properties are highly correlated. Dynamic modulus of elasticity (E_d) presented values ranging from 0.525 (IB) to 0.815 (E_M), while sw_v values ranged from 0.462 to 0.811, regarding the same properties.

Table 1—Pearson correlation (r) between nondestructive properties and mechanical properties and density.

Property	E_d	sw_v	f_m	E_M	ρ	f_c
sw_v	0.985**					
f_m	0.693**	0.700**				
E_M	0.815**	0.811**	0.845**			
ρ	0.884**	0.797**	0.493**	0.654**		
f_c	0.635**	0.582**	0.324**	0.436**	0.650**	
IB	0.525**	0.462**	0.025^{NS}	0.292**	0.577**	0.331**

Note: NS: non-significant; ** significant at α=0.01.

Teixeira and Moslemi (2001) employed stress wave oscilloscope and stress wave timer to nondestructively evaluate four types of wood-fiber cement composites. The correlation between static and dynamic modulus of elasticity ranged between 0.535 and 0.694, which was considered satisfactory for wood based composites. It is noteworthy the relatively good results found for stress wave velocity. Although they were lower than those found for E_d, it was verified that when only sw_v is used, it is possible to identify the trends of the composite properties. This is important since this type of composite is usually dense (>1,200 kg/m^3), which restrains its handling for measuring and weighting, mandatory variables to calculate the dynamic modulus of elasticity.

Table 2 presents the linear models fitted to explain coir-fiber composites' variation in mechanical properties. In this analysis, the treatments were analyzed altogether (N=102), without any type of treatment segregation. All models were highly statically significant (*p<0.0001*) and all four mechanical properties could be modeled using nondestructive variables. Nevertheless, the models' coefficients of determination ranged considerably: from 0.214 to 0.665. As expected, stiffness (E_M) presented better predictability than that observed for strength (f_m, f_c, IB). This can be explained because the theory behind nondestructive testing is based on elastic properties of the material, and strength properties are determined beyond this limit.

Table 2—Models fitted to explain composite properties variation of the whole tested treatments (N=102).

Property	Predictor	Model	F	R^2	SEE
E_M	E_d	$-421.98 + 0.728E_d$	190.47**	0.665	280.17
	sw_v	$-2172.06 + 2.387sw_v$	182.86**	0.658	281.11
f_m	E_d	$0.039 + 0.001E_d$	92.35**	0.481	0.803
	sw_v	$-3.494 + 0.005sw_v$	92.96**	0.489	0.778
f_c	E_d	$-0.108 + 0.001E_d$	66.24**	0.403	0.926
	sw_v	$-3.162 + 0.004sw_v$	48.67**	0.339	0.971
IB	E_d	$0.001 - 0.081E_d$	36.24**	0.276	0.151
	sw_v	$0.001 - 0.434sw_v$	25.03**	0.214	0.158

Note: ** significant at α=0.01; SEE: standard error of estimate.

Teixeira and Moslemi (2001) considered that R^2 values around 0.6 are suitable for wood composites. However, it means that nearly 40% of the variation in the properties cannot be explained by the models. Thus, further variables should be tested. These authors employed multivariate linear regression and the models' predictability improved considerably. In the present work, no further analysis was tried. The results regarding flexural properties (E_M and f_m) are similar to those obtained by Araújo et al. (2011). They manufactured bamboo (*Guadua magna*) cement and gypsum bonded composites and found significant models with similar coefficient of determination presented here: 0.62 to 0.69 (cement) and 0.37 to 0.75 (gypsum).

The models fitted using only stress wave velocity presented promising results. Beraldo and Balzamo (2009) found an excellent result (R^2=0.94) using ultrasonic pulse velocity to predict compression strength of *Eucalyptus grandis*-cement composites. On the other hand, Araújo et al. (2011) found R^2=0.69 for the relationship between stress wave velocity and modulus of rupture in bending of bamboo-cement composites. Nevertheless, the result was worse (R^2=0.37) for composite bonded with gypsum.

Further analysis was performed for each treatment separately and the results are presented in Table 3. In this analysis, only Ed was used as independent variable. Some $CaCl_2$ samples had to be removed because they yielded very poor mechanical property values and were identified as outliers. It can be observed that the models' coefficients of determination could be bettered in comparison with previous regression analysis. For instance, the model to predict E_M could reach R^2=0.809 ($CaCl_2$) while that for f_m reached 0.747 (hot water).

The comparison between treatments shows that the properties of the composite manufactured by adding $CaCl_2$ could be modeled at much higher level (mean R^2=0.613) than those presenting NaOH (0.399) or hot water (0.309) pretreated coir fiber. Additionally, the internal bonding (IB) was only modeled for the $CaCl_2$ treatment. It was found that nonlinear regression models yielded better predictability. The main type of model was S-curve (9 models), followed by compound (1) and power (1).

Table 3—Models fitted to explain composites properties variation within each treatment studied.

Treatment	Property	Model	F	R^2	SEE
$CaCl_2$	E_M	(P) ln (y) = ln (0.007) + (1.513 ln (E_d))	80.54**	0.809	0.324
(N=24)	f_m	(S) ln (y) = 1.073 - (734.12/E_d)	23.61**	0.554	0.256
	f_c	(S) ln (y) = 1.296 - (798.56/E_d)	12.59**	0.399	0.381
	IB	(C) ln (y) = ln (0.033) + (ln (1.001)E_d))	42.51**	0.691	0.489
NaOH	E_M	(S) ln (y) = 7.684 - (1836.36/E_d)	29.35**	0.471	0.342
(N=39)	f_m	(S) ln (y) = 1.891 - (1598.66/E_d)	33.63**	0.505	0.278
	f_c	(S) ln (y) = 1.197 - (1109.79/E_d)	9.29**	0.221	0.367
	IB	NS	-	-	-
Hot Water	E_M	(S) ln (y) = 8.891 - (3682.84/E_d)	106.34**	0.763	0.284
(N=39)	f_m	(S) ln (y) = 2.892 - (3637.03/E_d)	97.19**	0.747	0.293
	f_c	(S) ln (y) = 1.945 - (1915.34/E_d)	14.56**	0.306	0.398
	IB	NS	-	-	-

Note: ** significant at α=0.01; P: power model; S: s-curve model; C: compound model; SEE: standard error of estimate.

Conclusions

The mechanical properties of coir-fiber cement composites manufactured by different types of treatments could be modeled at reasonable level using the stress wave nondestructive method. It was found that up to 65% of variation in the properties could be explained by dynamic modulus of elasticity or stress wave velocity. These results were improved when regression analysis was separately performed for each treatment. Composite manufactured by adding $CaCl_2$ presented better results. The utilization of stress wave velocity only showed promising results, which means lower level of labor during nondestructive evaluation. Finally, it can be concluded that the stress wave method is suitable to predict the mechanical properties of these types of fiber-cement composite.

Acknowledgments

The authors thank the Coordination for the Improvement of Higher Education Personnel (CAPES) for granting the Scholarship to the first author and for the travel grant conferred to the second author to attend this conference.

References

Aamar-Daya, E.; Langlet, T.; Benazzouk, A.; Quéneudec, M. 2008. Feasibility study of lightweight cement composite containing flax by-product particles: Physical-mechanical properties. Cement & Concrete Compostes. 30(10): 957-963.

Araújo, P.C.; Arruda, L.M.; Del Menezzi, C.H.S.; Teixeira, D.E.; Souza, M.R. 2011. Lignocellulosic composites from Brazilian giant bamboo (*Guadua magna*). Part 2: properties of cement and gypsum bonded particleboards. Maderas: Ciencia y Tecnologia. 13(3): 297-306.

Beraldo, A.L.; Balzamo, H. 2009. Compuestos no-estructurales de cementos comerciales y aserrín de maderas Argentinas. Maderas: Ciencia y Tecnología. 11(3): 233-250.

Coates, G. R. 1994. Product application of wood-cement particleboards including applied finishes. In: Proceedings International Inorganic-bonded Wood and Fiber Composite Materials Conference, Washington: 189-192.

Ferraz, J.M.; Del Menezzi, C.H.S.; Souza, M.R.; Okino, E.Y.A.; Martins, S.A. 2012. Compatibility of pretreated coir fiber (*Cocos nucifera* L.) with Portland cement to produce mineral composites. International Journal of Polymer Science, 7p.

Ferraz, J.M.; Del Menezzi, C.H.S.; Teixeira, D.E.; Martins, S.A. 2011. Effects of treatment of coir fiber and cement/fiber ratio on properties of cement bonded composites. BioResources. 6(3): 3481-3492.

Goueygou, M.; Lafhaj, Z.; Soltani, F. 2009. Assessment of porosity of mortar using ultrasonic Rayleigh waves. NDT&E International. 42(5): 353-360.

Olorunnisola, A.O. 2008. Effects of pre-treatment of rattan (*Laccosperma secundiflorum*) on the hydration of Portland cement and the development of a new compatibility index. Cement and Concrete Composites. 30(1): 37-43.

Rodrigues, M.S.; Beraldo, A.L. 2010. Caracterização física e mecânica de argamassas à base de cimento Portland e cinza de casca de arroz residual. Engenharia Agrícola. 30(2): 193-204.

Teixeira, D.E.; Moslemi, A.A. 2001. Assessing modulus of elasticity of wood-fiber cement (WFC) sheets using nondestructive evaluation. Bioresource Technology. 79(2): 193-198.

Turgut, P.; Algin, H.M. 2007. Limestone dust and wood sawdust as brick material. Building and Environment. 42(9): 3399-3403.

Turgut, P. 2007. Cement composites with limestone dust and different grades of wood sawdust. Building and Environment. 42(11): 3801-3807.

Investigation of water sorption in multilayer boards, glued with different adhesives by means of neutron imaging, DVS and synchrotron microscopy

Peter Niemz, ETH Zurich, Institute for Building Materials, Wood Physics, Zurich, Switzerland, niemzp@ethz.ch

Sergio Sanabria, ETH Zurich, Institute for Building Materials, Wood Physics, Zurich, Switzerland, ssananbria@ethz.ch

Walter Sonderegger, Paul Scherrer Institute, Villigen, Switzerland, walter-sonderegger@bluewin.ch

David Mannes, Paul Scherrer Institute, Villigen, Switzerland, David.Mannes@psi.ch

Abstract

Diffusion processes into multilayered samples of Norway spruce have been measured and quantified by means of neutron imaging (NI). The influence of different adhesives on the diffusion process was investigated. For each sample configuration, neutron transmission images were used to measure time dependent water profiles in the diffusion direction. Using Fick's second law, diffusion coefficients in spruce wood and in the adhesive joints were calculated in function of the moisture content. The adhesives (1C PUR) show until three orders of magnitude lower values for the diffusion coefficient than spruce wood. UF leads to a smaller barrier effects with respect to wood and 1C PUR. A correlation with the sorption properties of isolated adhesive films was detected. The diffusion through the adhesive films showed a clear dependency on the moisture content. The results were compared with high resolution synchrotron light microscopy images from bond lines and sorption isotherms from adhesive films.

Keywords: neutron imaging, synchrotron microscopy, dynamic sorption analysis, diffusion, adhesives, bond lines

Introduction

In recent years, glued solid wood materials such as glued laminated timber or multilayered solid wood panels have gained in importance. In this context, the diffusion of water vapor within wood and the barrier effect of adhesive joints are of high relevance in the field of building physics. This is particularly the case when the hygroscopic behavior and the water transfer in building elements as well as the humidity exchange with the room is regarded. While diffusion processes of wood have been the subject of many investigations (e.g. Stamm 1959a, 1959b, Skaar 1988, Frandsen *et al.* 2007), the influence of adhesive joints on the diffusion processes has scarcely been studied. One of the few studies done on this topic was carried out by Frühwald 1973. He investigated in detail the influence of bond lines of a phenolic resin between the veneers of beech plywood by varying the number of bond lines and films per line.
The aim the present study was to investigate the phenomenon of the moisture-depending diffusion resistance of different adhesives: urea formaldehyde resin (UF) and one-component polyurethane (1C PUR). Neutron radiography was used to detect the water content within wood (according to Mannes *et al.* 2009). The advantage of this non-destructive method is its high sensitivity to hydrogen what allows the visualizing of time-dependent water diffusion processes in wood.

Material and method

Material

A total of 20 samples from Norway spruce (*Picea abies* [L.] Karst.) of approximately 120 mm (length) x 15 mm (width) x 30 mm (height) were prepared for testing bound water diffusion. The diffusion process run from the top to the bottom of the sample. Two of the samples were used to determine the diffusion in the radial and tangential direction of solid wood. The other 18 samples were added with one to five bond lines at half height or rather regularly distributed over the height in order to investigate the influence of bond lines on the diffusion processes. For these samples, the diffusion in the spruce wood occurs in the tangential direction.
The applied adhesives are used for load-bearing timber structures, UF (cold gluing) in dry conditions and 1C PUR even in humid conditions. All adhesive joints were bonded at 20°C and 65% RH. Table 1 gives an overview.

Table 1—Overview of selected tested samples and the applied adhesives at the beginning of the measurements (oven-dry) and the mean moisture content ($MC_{mean.end}$)) respectively water concentration ($_{Cmean.end}$ at the end of the measurements after 70 days exposed to a differentiating climate (20°C/85% RH to 0% RH)

Material/Adhesive	No.	Direction of diffusion	Joint No. (-)	Oven-dry density (kg/m^3)	$MC_{mean.end}$ (%)	$C_{mean.end}$ (g/cm^3)
Spruce wood	1	Tangential	-	418	12.8	0.054
	2	Radial	-	402	12.5	0.050
Urea	3	Tangential	1	398	12.5	0.050
	4	Tangential	3	441	10.6	0.047
	5	Tangential	5	457	9.6	0.044
PUR	6	Tangential	1	403	12.0	0.048
	7	Tangential	3	430	7.9	0.034
	8	Tangential	5	476	6.1	0.029

Experimental setup

The experiments were performed at the neutron radiography facility NEUTRA of the spallation neutron source SINQ at the Paul Scherrer Institute (PSI) in Villigen, Switzerland (Lehmann *et al.* 2003). The samples were tested in two series over a period of about ten weeks. During this time, the preliminarily oven-dried samples were exposed to a differentiating climate (20°C/85% RH to almost 0% RH). The moisture of the samples was measured with neutron radiation after defined time intervals in order to follow the diffusion process into the sample. The measurements took place after 0, 1, 3, 7, 23, 29, 59, 74 days. Thereby, at the beginning of the tests the samples (dried at 103°C until weight constancy) were insulated with aluminum tape on the four edges, leaving only the top and the bottom planes (the orthogonal planes of the required diffusion direction) unsealed. Each sample was then fixed on a cup filled with silica gel that was closed with a slotted aluminum plate. The sample was arranged above the opening of the slot, which had the same length and width as the sample (Figure 1). The first neutron radiation measurement was still made with the dry sample to obtain a reference image. For the measurement, the cup with the sample was positioned in front of the neutron detector (a combination of a neutron sensitive Li doped ZnS scintillator and a CCD-camera). The tangential-longitudinal plane (and in one case the radial-longitudinal plane) of the sample was so exposed to a parallel beam of neutron radiation for a defined time. The neutron scintillator converts the neutron signal into visible light, which is led via a mirror onto a cooled 16 bit CCD camera (Mannes (2009).

Figure 1—Cup with silica gel and the sample above, isolated on four sides with aluminum tape.

Data evaluation

The attenuation of the neutron radiation within a sample can be described by the exponential law of radiation attenuation (Beer-Lambert law, see Mannes (2009). Evaluation of the diffusion coefficient follows the method described in Mannes (2009), Sonderegger (2011) using a 2nd order linear partial differential equation (*PDE*) of the diffusion corresponding to Fick's second law.
The aim of the measurements was to detect the distribution of the water content within the sample in the diffusion direction. Table 1 shows the tested samples and the mean water content of the samples as MC and as water concentration.
Sorption isotherms of cured adhesive films were determined using a DVS Advantage apparatus (DVS, Surface Measurement Systems Ltd (SMS), London according to the method described by Wimmer et al. (2013).

Results and discussion

Diffusion

Table 2 and the Figures 2-4 show the results. It was found that the diffusion coefficients of the adhesives (1C PUR) were up to three orders of magnitude lower than those of spruce wood. UF had a smaller barrier effect compared to wood, which in contrast to 1C PUR, clearly depends on the MC.

Table 2—The parameters of the diffusion coefficients of wood and adhesive according $D_{o.w}$, $D_{o.a}$ = diffusion coefficients at initial MC of wood and adhesive respectively; α_w, α_a = constants describing moisture dependency; σ = surface emission coefficient, M_∞ = equilibrium MC

Material/Adhesive	No.	Bond line (No./Thickness)	$D_{o.w}$ (m^2/s)	$D_{o.a}$ (m^2/s)	M_∞ (%)
Spruce tangential	1	-	1.83E-12	-	16.0
Spruce radial	2	-	4.67E-12	-	16.1
Urea-1	3	1 / 0.1	3.94E-12	2.72E-13	17.1
	4	3 / 0.1	1.82E-12	8.70E-13	15.9
	5	5 / 0.1	2.85E-12	3.79E-13	16.6
PUR-1	6	1 / 0.1	4.69E-12	8.52E-13	16.4
	7	3 / 0.1	4.11E-12	8.71E-13	16.1
	8	5 / 0.1	1.93E-12	4.47E-13	15.5

The influence of the number of bond lines on the diffusion process is shown in Figure 2. For the samples with a single bond line, the diffusion process has nearly finished after 74 days. Observation of samples with three and five bond lines reveal that the diffusion process just reaches the bottom of the sample, and in the case of 1C PUR with 5 bond lines, the water only reaches as far as the fifth bond line. This indicates a high diffusion resistance of the hardened adhesives particularly for the 1C PUR and is also visualized with the steps in the distribution of the MC at each bond line. The diffusion coefficient of UF over the whole range of the measured MC is about one order of magnitude lower than that of spruce wood.

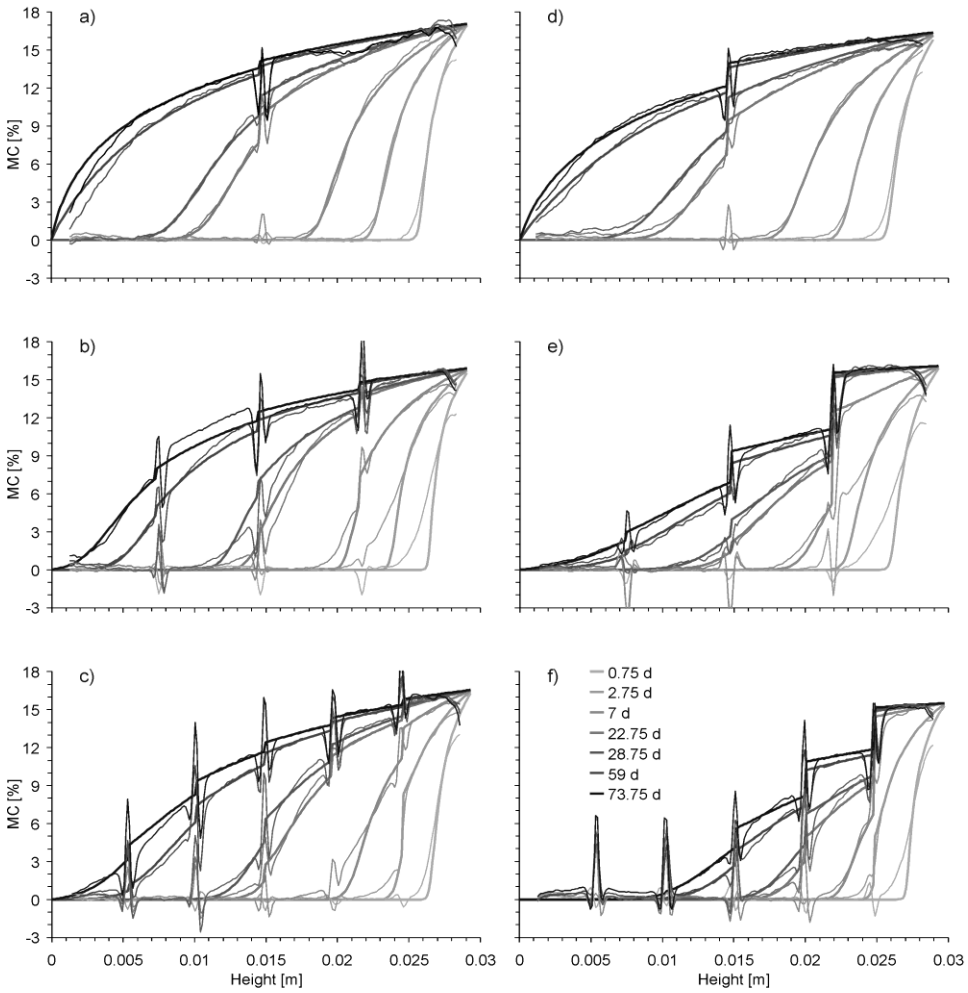

Figure 2—Vertical profiles of the MC through the samples with 1, 3 and 5 adhesive joints of series 1 during the diffusion experiment (experimental results = fine lines; model curves = fat lines): a – c) UF, d – f) 1C PUR

Regarding 1C PUR, the difference between the diffusion coefficients of wood and adhesive increases from one to about three orders of magnitude with increasing MC. Moreover, the diffusion coefficient of 1C PUR shows only a slight dependency on the MC and partly even a negative slope (concerning the increase of the diffusion coefficient with increasing MC). The diffusion coefficients of UF show a high dependency on MC similar to the spruce wood whereas 1C PUR shows only low dependency on MC.

Hass et al. (2010) investigated the influence of hardening and observed micro cracks within UF joints and pores within PVAc joints due to shrinkage (Figure 3). Therefore, it is conceivable that cracks and pores increase the diffusion coefficient with increasing MC, too.

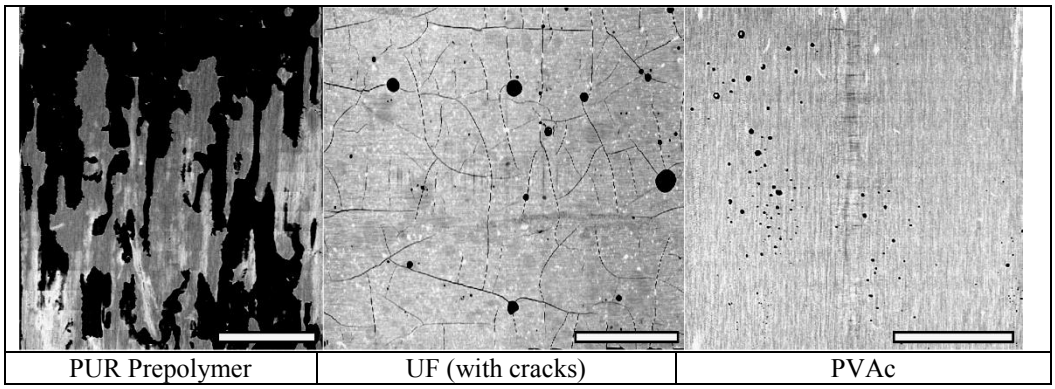

Figure 3—Bond line imperfections for different adhesives (Synchrotron (Foto: Hass 2012))

Sorption properties of adhesives

The different adhesive films investigated reveal also a significant difference in their sorption properties. Polyurethane only absorbed 3.5 % moisture, at medium uptake speed. Fish glue and hide glue showed a much higher water uptake in relation to 1 CPUR (Figure 4).

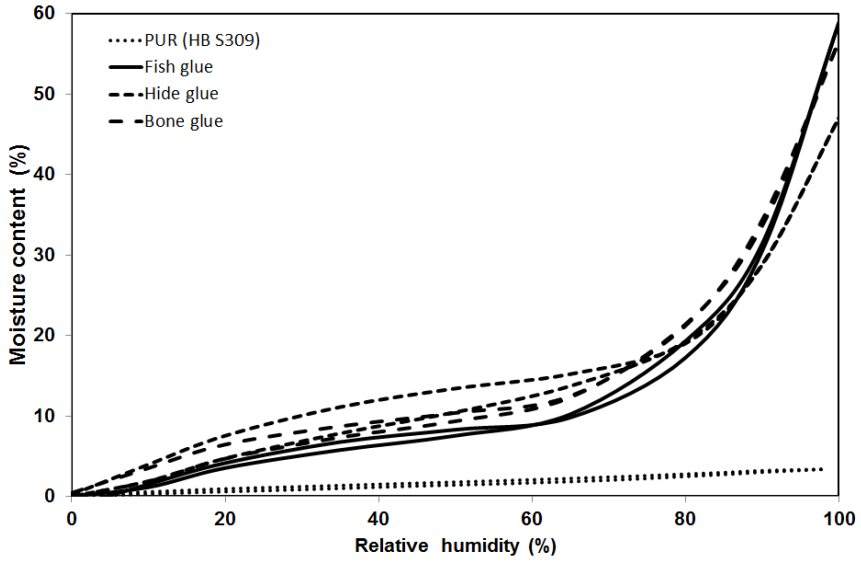

Figure **4—Sorption isotherms of the studied adhesives tested on adhesive films** (Wimmer et al. (2013))

Conclusions

It was possible to detect time dependent diffusion processes within wooden samples containing bond lines by localizing and quantifying the water content in the diffusion direction. On the basis of the received data, both, the MC dependent diffusion coefficients of the spruce wood as well as of the bond lines, were calculated in the form of an exponential function relative to MC with good agreement to the measured data. The diffusion resistance of the bond lines strongly depends on the adhesive type and on the MC. 1C PUR shows up to three orders of magnitude lower diffusion coefficients at high MC compared to spruce wood and has a high barrier effect on water sorption over the whole measured MC range. In contrast UF has a lower barrier effect and clearly depends on the MC. This can be correlated with bond line imperfections.

In ongoing investigations at ETH we aim to correct swelling/shrinking effects of wood or wood based materials. This finally leads to improved results regarding the moisture distribution. A developed method "Adaptive Digital Image Correlation" (ADIC) applies Digital Image Correlation processing directly on neutron transmission images to determine deformations. The natural variability of wood leads to reproducible gray level patterns in successive neutron images, which are used for subset referencing. Adaptive assessment based on the tracking of small changes between adjacent pixels, hard constraints filter out false correlation hits.

References

H.L. Frandsen, H.L.; Damkilde, A.; Svensson, S. 2007. A revised multi-Fickian moisture transport model to describe non-Fickian effects in wood, Holzforschung 61(5): 563-572.

Fruhwald, A. 1973. Ein Beitrag zur Kenntnis des diffusionstechnischen Verhaltens von Furnierplatten und kunstharzbeschichtetem Holz, Dissertation, University of Hamburg, Hamburg

Lehmann E.; Vontobel , P.; Wiezel, L. 2001. Properties of the Radiography Facility NEUTRA at SINQ and its Potential for Use as European Reference Facility, Nondestructive Testing and Evaluation 16: 191-202.

Hass, Ph.2012. Penetration behavior of adhesives into solid wood and micromechanics of the bond line. PhD thesis, ETH Zurich, 133p

Mannes, D. 2009. Non-destructive testing of wood by means of neutron imaging in comparison with similar methods.PhD thesis, ETH Zurich

Mannes, D.; Sonderegger, W.; Hering, S.; Lehmann, E.; Niemz, P. 2009. Non-destructive determination and quantification of diffusion processes in wood by means of neutron imaging, Holzforschung 63(5): 589-596.

Skaar, K. 1988. Wood-water relations, Springer-Verlag, Berlin/Heidelberg/New York

Stamm, A.J.1959a. Bound-water diffusion into wood in the fibre direction, Forest Prod J 9(1): 27-32.

Stamm, A.J., 1959b. Bound-water diffusion into wood in across-the-fibre directions, Forest Prod J 10(10): 524-528.

Wimmer, R.; Kläusler, O.; Niemz, P., 2013. Water sorption mechanisms of commercial wood adhesive films. Wood Sc. Technol 47(4):763-775

Sonderegger, W. 2011. Experimental and theoretical investigations on heat and water transport in wood and wood based materials. PhD thesis, ETH Zurich

A Kinematic and Acoustic Emission Methodology for Investigation of Progressive Damage Behavior of Triaxially Braided Regenerated Cellulose Composites

Rani F. ElHajjar
Assistant Professor (Corresponding), Department of Civil Engineering and Mechanics, College of Engineering & Applied Science, University of Wisconsin, Milwaukee, WI 53211, USA. Contact: elhajjar@uwm.edu

Issam I. Qamhia
Graduate Research Assistant, Department of Civil Engineering and Mechanics, College of Engineering & Applied Science, University of Wisconsin, Milwaukee, WI 53211, USA.

Abstract

In this study we investigate the unnotched and notched tensile mechanical properties of triaxially braided regenerated cellulose composites. The mechanical response, kinematic fields and acoustic emissions for unnotched coupons are simultaneously obtained in this experimental approach. Mechanical loading, three dimensional digital image correlation and acoustic emission methods are used to investigate the damage propagation behavior. The analysis of the acoustic waveforms is performed through temporal characterization of the acoustic emissions and individual waveform analysis for identification of the failure modes. Coupling the digital image correlation is used to study the kinematic behavior and strain fields near the notches, for the notched samples, and to understand the distributed nature of failure in these specimens and to correlate observed events in load drops in the mechanical response.

Keywords: Regenerated Cellulose, 3D Braided Composites, Digital Image Correlation, Acoustic emission.

Introduction

Natural fibers are attractive reinforcements in composite materials for several product applications due to their renewable and biodegradable nature (Cheng, Wang et al. 2009; Soykeabkaew, Nishino et al. 2009; Graupner and Mussig 2011). Braided composites are made of a type of textile composites that can be produced in 2D and 3D fabric textures and have improved out-of-plane properties and impact resistance. The fiber preform produced by braiding operations is unique and can be impregnated with thermosetting resin using different methodologies such as resin transfer molding, vacuum assisted transfer molding or in prepreg forms. Increasing the through-the-thickness yarn interlacing properties under components of out of plane resistance reduces the susceptibility to delaminations Miravete, Clemente et al. (2000). Braided preforms can also be used to form complex shapes at high rates through automation techniques (Scholz, Dost et al. 1997). The net shape capability and the improved out-of-plane resistance led to wide applications of braided composites relative to uniaxial fabric and filament wound composites (Poe, B. et al. 1997).

Triaxially braided preforms are designed by using three fiber orientations in certain quantities and directions to obtain desired properties. The parameters that mostly affect their behavior are the size of the axial and braider yarns, braider angle, and the axial yarn spacing. The mechanical properties of the composites are typically determined from the fiber, matrix, interface and fabric architecture. Tow undulations in the bias yarns present challenges in direct application of classical lamination plate theories to obtain the mechanical properties of the composites. Several methods have been proposed to model the elastic response including macro-mechanical and micromechanical approaches energy methods, finite element and classical lamination plate theory methods (Yang, Ma et al. 1986; Masters, Foye et al. 1993; Naik 1994; Byun 2000; Quek, Waas et al. 2003). Yang et al. (Yang, Ma et al. 1986) developed a fiber inclination model as a methodology for predicting the elastic properties of three-dimensional textile structural composites. A general purpose micromechanics analysis based on an iso-strain assumption by using a 3-D stress averaging technique within a representative unit cell (RUC) was also proposed by Naik et al. (Naik 1994; Naik, Ifju et al. 1994) to compute the overall composite properties. Quek et al. (2003) proposed a RUC of the braided architecture that considered the undulations and angles of the bias tows by separating the composite into three separate layers for the axial yarn and the two bias yarns with subsequent averaging. A modified equation was proposed by Shokrieh and Mazloomi (2010) to better capture the shear properties. In both models, the thicknesses of all three layers were assumed to be identical. El-Hajjar et al. (2013) evaluated the simple, discrete yarn and three-layer analytical representations for application on triaxially braided models for glass fiber composites. The correlation with experiments indicated that the three layer representation approach yielded consistent results.

The discrete 3-layer analytical model presenting yarns architecture as a total equivalent stiffness matrix of the triaxially braided composite in a unit cell is used to verify the experimental results;

$$[C^{RUC}] = t^{+\theta}\left[C_{global}\right]^{+\theta} + t^{-\theta}\left[C_{global}\right]^{-\theta} + t^{0}\left[C_{global}\right]^{0} \qquad \text{eq. 1}$$

Where $t^{+\theta}$, $t^{-\theta}$ and t^{0} are specified as the thickness of each layer to the thickness of the laminate.

In this study, the tensile behavior in a quasi-isotropic triaxially braided regenerated cellulose composite with a high-bio content epoxy resin is investigated. A resin infusion methodology is used to prepare the specimens. The mechanical properties are predicted by a 3-layer discrete analytical model using a micro to macro mechanics approach. A digital image correlation technique is used to investigate the load redistribution using a full-field study of the deformation behavior. Damage initiation and propagation through the unnotched braided composite specimens are examined by a passive acoustic emission technique.

Experimental Methods

The fiber system used in this study is a quasi-isotropic triaxially braided preform (BioMid; GSC and ENC, Inc., Burnaby, BC, Canada) with (-60, 0, 60) fiber orientation in a single ply. The braid was specially manufactured by A&P Technology (Cincinnati, Ohio, USA). The center-to-center spacing between the axial yarns was 5.2 mm, whereas the spacing between the bias yarns was at 2.6 mm. The percentage by weight in the axial yarn and in each bias yarn is equal. Similar properties in the axial and transverse directions will result from using these weight ratios, angles and spacing. Following the braiding process, the braided sleeve was subsequently slit into a flat sheet to allow for further processing. The regenerated fibers were stored at room temperature and a humidity level of 30%. A vacuum assisted resin infusion method was used to manufacture the composite panels with minimal levels of porosity. The panels were prepared from triaxially braided regenerated cellulose fibers and an epoxy resin system (Super Sap 100/1000; Entropy Bio-Resins, Gardena, California, USA). The bio-based epoxy used is classified as a United States Department of Agriculture (USDA) Bio Preferred Product using ASTM

D6866 (ASTM 2007) and is reported by the supplier to have a 37% bio-content. For the early fabrication trials, a wet layup technique was used. The fibers, specifically the axial yarn, weren't fully infused, however, possibly due to the swelling of the fibers, which led to an increased difficulty in processing. A cross section of a composite panel prepared by resin infusion is shown in Figure 1.

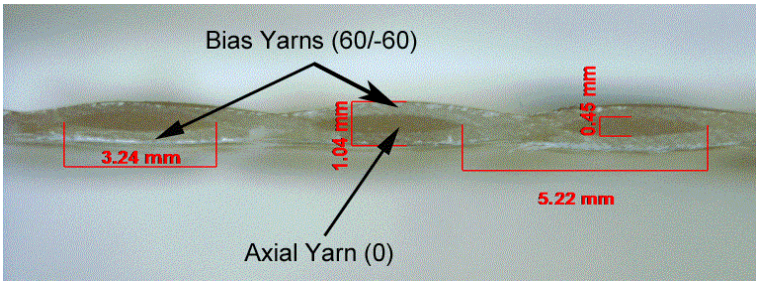

Figure 1- Micrograph of the cross section of the cured composite

The panels produced were 200 mm by 305 mm and were infused under room temperature conditions. The fiber volume fraction of the composite is determined by using the volume measurements of the matrix and fiber constituents (ASTM 2009). The average fiber volume fraction for the prepared composites is 0.60 ± 0.02. Panels were cut into 305 mm long by 38 mm wide coupons in transverse and longitudinal directions. For the notched specimens, the specimens were 152 mm long x 76 mm wide. Two notches were machined parallel to the short edge toward the center of the sample; one at each side leaving an effective width of 36mm.The elastic properties were obtained by testing the specimens in tension according to ASTM ID: D3039 (ASTM 2007) standard for tensile properties of polymer reinforced fiber composites. Mechanical loading was carried out on an electromechanical test system with a 97.8 kN (22.0 kips) capacity. A displacement-controlled test was carried out at a displacement rate of 1.3 mm/min. For accurate strain measurements; an extensometer was used for recording the elastic deformation behavior along a 25mm length at the middle of the specimens.

Simultaneous mechanical testing, 3D-Digital Image correlation (DIC), and Acoustic Emission (AE) tests were carried out on a subset of the specimens, mainly unnotched specimens. For the notched specimens, a 25 mm gauge length was used to ensure all bias yarns are fully gripped. DIC was used to capture the strains on the surface of the composite specimen and to confirm the loading curves obtained by simple mechanical loading. The DIC technique uses a random speckle pattern applied to the specimen that is captured by using a couple-charged device (CCD) camera. These images are then processed by using correlation algorithms to compare strained maps with a reference image taken before the loading is applied. The procedure has been previously applied by the authors by comparing strain results obtained from 3D-DIC with finite element predictions for carbon/epoxy laminates with through thickness cutouts (El-Hajjar and Petersen 2011). The digital image correlation tests were performed by using the Dantec Dynamics Q-400 system. A resolution of 5 megapixels was used for the two CCD cameras, together with a 30 mm Schneider Xenoplan lens. Acoustic emission was used to investigate damage initiation and damage propagation through the cumulative energy versus of the recorded emissions. A Mistras 2001 data acquisition system was used for recording the data, including waveforms. A Physical Acoustics WS-alpha transducer was used for measuring the AE signals. The sensor has an operating frequency of 100-1000 kHz with a 63.74dB peak sensitivity occurring at 523.23 kHz. In order to improve the quality of the captured signals; a pre-amplifier coupled with a bandpass filter adjusted to pass frequencies in the range of 10-1200 kHz was used.

Results and Discussion

Braided composites can present challenges during characterization and mechanical testing due to the unique architecture of the braids of the regenerated cellulose composite. The type of damage that initiates in the specimens and the instance it takes place in the time history are interesting to understand. Many of these damage events do not show up clearly in the loading curves. The use of techniques such as DIC and acoustic emission help in a better assessment of the behavior of the composite. The loading curves for longitudinal and transverse specimens loaded in tension are shown in Figure 2. The stress versus strain curves show that two regions can be identified for the loading curves; in which the first is linear elastic and the second is a region with a lower stiffness. This behavior under tension loading is similar to that seen for other regenerated cellulose composites, eg. Lyocell/epoxy composites (El-Hajjar and Qamhia 2013). The stiffness properties are extracted within the 0 to 0.6 percent of the strain range from extensometer readings. Figure 2 also show a good correlation between the discrete 3-layer analytical model prediction and the experimental results for both the transverse and axial directions. Differences in stiffness between experimental and model results were found to be less than 4% in both longitudinal and transverse directions (Table 1). The model can be further used to predict the effects of fiber volume fraction, crimp angle or aspect ratio on the behavior of the composites. The Poisson ratios, ν_{xy} and ν_{yx} were also estimated by the analytical model (table 1).

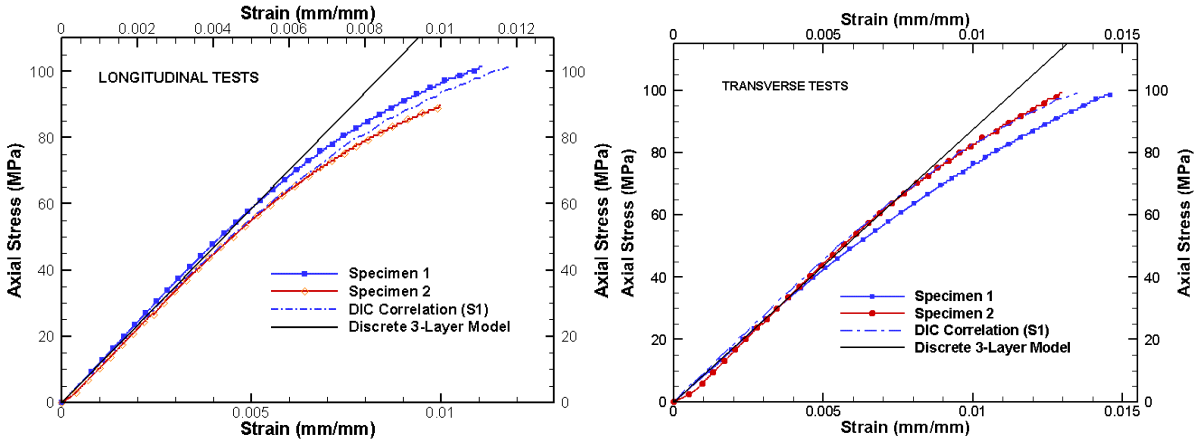

Figure 2- Stress versus strain of RCF/epoxy quasi-isotropic composites (longitudinal and transverse)

The initiation of damage in the transverse specimens starts at a much lower stress level compared to the first emissions observed in the longitudinal specimens (Figure 4). Matrix cracking is most likely the reason for the initial emissions. For the longitudinal specimens, the final cumulative energy at failure is 35% higher than transverse specimens. The fracture of the axial fibers oriented in the direction of loading is believed to be causing these higher emissions. The incidence of high acoustic emissions can be used to indicate the point at which irreversible damage occurs. However, a distinction between initial and final ply failure cannot be easily observed.

The strain fields from DIC are shown in Figure 2 to show the correlation with the extensometer measurements. The 3D Digital Image Correlation results show a high correlation between loading curves obtained by mechanical loading and the full-field strain measurements. The strain fields were averaged over the area of the specimen and were used to obtain the Poisson ratios, ν_{xy} and ν_{yx} (Table 1). The failure progression in longitudinal and transverse coupons is shown in Figure 4. The load in the tension test for the longitudinal specimens is uniformly distributed as shown in Figure 4(a). Consequently, the interlaminar shear stresses as a result of increasing the shearing stresses in the axial and bias yarn interface are believed to be the causes of the interfacial matrix cracking (Littell, Binienda et al. 2009). The

transverse specimens show large areas of low stress in the regions between the axial yarns (Figure 4(b)). Deflections in the out-of-plane of the image as the transverse coupons are loaded in tension can contribute these patterns. The stresses associated with this deformation pattern can contribute to edge damage.

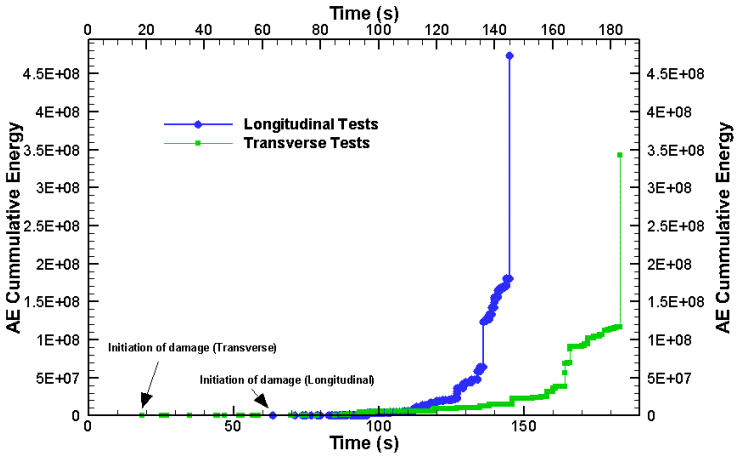

Figure 3- Cumulative energy plots of RF/epoxy quasi-isotropic composites for longitudinal and transverse samples

Table 1 - Predicted and experimental results for triaxially braided regenerated cellulose/epoxy composite system

Mechanical Property	Discrete 3-Layer Model	Experiments
E_x GPa (Msi)	11.67 (1.69)	11.22 (1.63)
E_y GPa (Msi)	8.74 (1.27)	9.06 (1.31)
ν_{xy}	0.296	0.303
ν_{yx}	0.351	0.401

A comparison of the damage initiation determined through acoustic emissions indicates that the initiation of damage occur at a much earlier load in the unnotched specimens than the notched specimens. This observation can be attributed to the edge deformations seen in Figure 4 especially related to the transverse specimens. The presence of notches on both sides concentrates the deformations in a smaller area. This limits the influences of the edge and also results in less variability in the test results. Thus, a higher initiation damage load levels results in the notched transverse specimens. However, the increased stress concentration at the notch is likely lead to a slightly reduced ultimate strength in both longitudinal and transverse orientations (Figure 5).

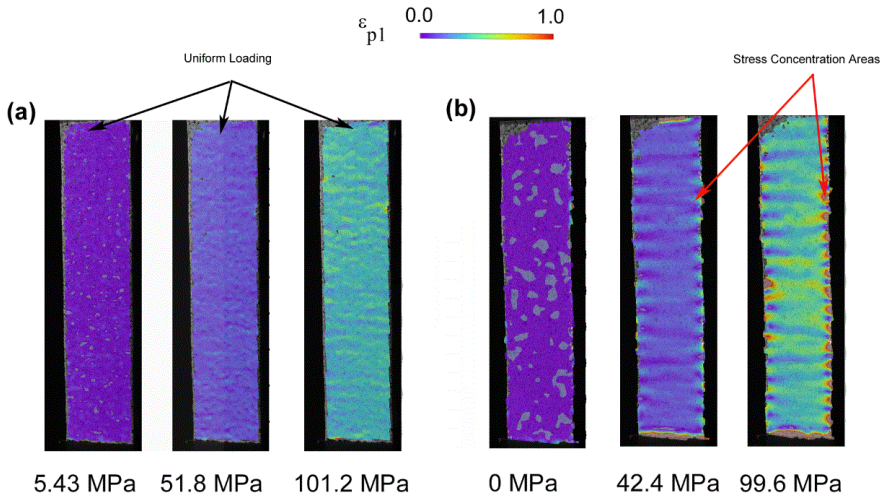

Figure 4- Progression of principal strain distribution in (a) longitudinal specimen (b) transverse specimen

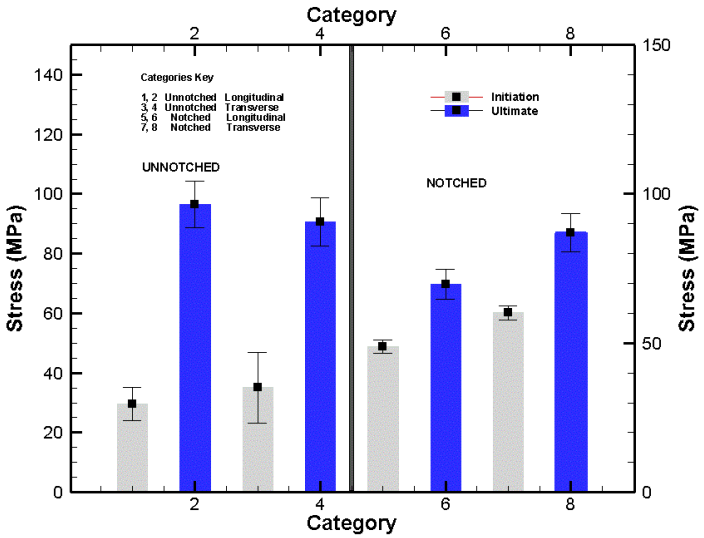

Figure 5- Initiation and ultimate failure of unnotched and notched RF/epoxy specimens

Conclusions

In this study, the tensile mechanical behavior of composites prepared from quasi-isotropic triaxially braided regenerated cellulose with a high-bio content epoxy resin were investigated. Two manufacturing procedures of the composites were investigated: simple layup and resin infusion. The resin infusion setup was found to be the most successful in fabricating the quasi-isotropic triaxially braided materials with the higher fiber volume fractions up to 60%. The swelling of the natural fibers also needs to be accounted for in any manufacturing approach through processing optimization studies. For the unnotched specimens, the initial elastic stiffness results are approximately 20% higher in the longitudinal direction than the transverse direction. One possible reason for that is that there is no direct load transfer from the grips to all the bias yarns in the specimen, which lead to testing difficulties with the transverse specimens. Another explanation can be deducted by inspecting the results of the full field strain measurements

obtained by DIC technique. These results show an abnormal behavior at the specimen edges of the transverse coupons, which cause limitations of the rectangular coupon in capturing the transverse deformation behavior in these specimens. A significant out-of-plane deformation results from this abnormal behavior, creating areas of stress concentration at the edges from which failure can propagate, and reducing the effective width of the specimen. The acoustic emissions are measured and used to examine the damage initiation and propagation through the braided composite. Acoustic emission can be used to detect events that do not show on the stress-strain behavior. The comparison of results between longitudinal and transverse specimens show that damage initiation start at lower stresses in the transverse direction compared to the longitudinal specimens. More energy is dissipated due damage, however, in the longitudinal direction due to the breaking of fibers in the axial yarn. The acoustic emissions can be used to establish limiting failure stresses and strains corresponding to the onset of significant internal damage.

Acknowledgements

This research was supported through a grant from the UWM Research Growth Initiative.

References

ASTM (2007). D3039 Standard test method for tensile properties of polymer matrix composite materials. West Conshohocken, PA, ASTM International.

ASTM (2007). D6866 Standard Test Methods for Determining the Biobased Content of Solid, Liquid, and Gaseous Samples Using Radiocarbon Analysis. ASTM International.

ASTM (2009). D2734 Standard Test Methods for Void Content of Reinforced Plastics. West Conshohocken, PA, ASTM International.

Byun, J.-H. (2000). "The analytical characterization of 2-D braided textile composites." Composites Science and Technology **60**(5): 705-716.

Cheng, Q., S. Wang, et al. (2009). "Effects of process and source on elastic modulus of single cellulose fibrils evaluated by atomic force microscopy." Composites Part A: Applied Science and Manufacturing **40**(5): 583-588.

El-Hajjar, R. and D. R. Petersen (2011). "Adhesive Polyvinyl Chloride Coatings for Quantitative Strain Measurement in Composite Materials." Composites Part B-Engineering **42**(7): 1929-1936.

El-Hajjar, R. F. and I. I. Qamhia (2013). "Modeling and characterization of the moisture-dependent bilinear behavior of regenerated cellulose composites." Journal of Wood Science.

El-Hajjar, R. F., S. S. Shams, et al. (2013). "Closed form solutions for predicting the elastic behavior of quasi-isotropic triaxially braided composites." Composite Structures **101**(0): 1-8.

Graupner, N. and J. Mussig (2011). "A comparison of the mechanical characteristics of kenaf and lyocell fibre reinforced poly(lactic acid) (PLA) and poly(3-hydroxybutyrate) (PHB) composites." Composites Part a-Applied Science and Manufacturing **42**(12): 2010-2019.

Littell, J. D., W. K. Binienda, et al. (2009). "Characterization of Damage in Triaxial Braided Composites under Tensile Loading." Journal of Aerospace Engineering **22**(3): 270-279.

Masters, J. E., R. L. Foye, et al. (1993). Mechanical properties of triaxially braided composites: experimental and analytical results. Philadelphia, PA, American Society for Testing and Materials.

Miravete, A., R. Clemente, et al. (2000). "3-D textile reinforcements in composite materials." CRC Press LLC,2000 Corporate Blvd,NW,Boca Raton FL 33431,USA.

Naik, R. A. (1994). "Analysis of woven and braided fabric reinforced composites." NASA CR-194930.

Naik, R. A., P. G. Ifju, et al. (1994). "Effect of Fiber Architecture Parameters on Deformation Fields and Elastic Moduli of 2-D Braided Composites." journal of composite materials **28**(7): 656-681.

Poe, C., D. H. B., et al. (1997). "A Review of the NASA Textile Composites Research." NASA Langley Technical Report.

Quek, S. C., A. M. Waas, et al. (2003). "Analysis of 2D triaxial flat braided textile composites." International Journal of Mechanical Sciences **45**(6–7): 1077-1096.

Scholz, D. B., E. F. Dost, et al. (1997). Advanced Technology Composite Fuselage - Materials and Processes, Langley Research Center.

Shokrieh, M. M. and M. S. Mazloomi (2010). "An analytical method for calculating stiffness of two-dimensional tri-axial braided composites." Composite Structures **92**(12): 2901-2905.

Soykeabkaew, N., T. Nishino, et al. (2009). "All-cellulose composites of regenerated cellulose fibres by surface selective dissolution." Composites Part A: Applied Science and Manufacturing **40**(4): 321-328.

Yang, J.-M., C.-L. Ma, et al. (1986). "Fiber Inclination Model of Three-Dimensional Textile Structural Composites." journal of composite materials **20**(5): 472-484.

Detection and analysis of the stress relaxation properties of thin wood composites using cantilever-beam bending

Houjiang Zhang
School of Technology, Beijing Forestry University, Beijing 100083, China, hjzhang6@bjfu.edu.cn

John F. Hunt
USDA Forest Products Laboratory, WI 53726-2398, USA, jfhunt@fs.fed.us

Yan Huang
School of Technology, Beijing Forestry University, Beijing 100083, China, huangyan0815@126.com

Abstract

At present, the discussion on the stress relaxation properties of wood and wood materials is usually investigated in tension, mid-point bending and dual cantilever bending methods. This paper aims to study the stress relaxation properties of thin wood composites using a cantilever-beam bending method. According to the stress relaxation tests, we found this detection method could be feasible. From the stress relaxation plots the initial rate is fast and then slows down after some time. We compared the stress relaxation and the relaxation coefficient for specimens from particleboard, high density fiberboard, medium density fiberboard, and wood fiber plastic boards. We looked at 2 hours test vs 3 hour test to determine if it might be possible to determine stress relaxation over a 2 hour time span. The stress curves for the high-density fiberboard and the particle board are more consistent between specimens. The test stress curves of the medium density fiberboard are a little less consistent. The wood fiber plastic specimens were harder less consistent in the data to determine the relaxation coefficient. The relaxation coefficient value corresponded to the stress relaxation, where minimal stress relaxation occurred in the specimens then the coefficient value was also lower and if the stress relaxation was higher, then the coefficient value was also higher. This is preliminary work to determine the potential for obtaining the relaxation characteristics using a simple log model. There is a need to further study the stress relaxation for composite boards using a different model but the cantilever bending method may be a useful method for determining this characteristic.

Keywords: thin wood composites, cantilever-beam bending, stress relaxation, relaxation coefficient

Introduction

Thin wood composites defined in this paper includes fiberboard, particleboard, wood-fiber plastic, reconstituted veneer, pulp molded products that measure between 1 to 5mm (Zhang et al. 2010). These composites materials can be used widely for products such as box boards, container boards, non-load-bearing building panels of building materials, architectural, and decorated panels. The performance or structural needs are different for each application requiring an understanding of the mechanical properties of these wood composites. The main mechanical properties of thin wood composites include static elastic modulus, dynamic elastic modulus, storage modulus, loss modulus, shear modulus, and stress relaxation

properties. Detecting these mechanical properties of thin wood composites has a very important meaning in production and application fields.

In the past, stress relaxation of wood and wood materials has been investigated by many scientists (Attic et al. 1968, Cheng 1985, Feng and Zhao 2010, Larson 1999). Three kinds of testing methods were mainly used by them, including tension test (Cao et al. 2006, Xie and Zhao 2004), mid-point bending test (Ikuho et al. 2002) and dual cantilever bending test (Ebrahimzadeh et al. 1993). The key mechanism of the test methods is to give and keep an initial deflection to the specimen, and then measure the stress reduced with the time. However, using cantilever-beam bending method, to detect the stress relaxation properties of wood or wood materials has not found. This paper aims to similarly introduce a detection method on the stress relaxation properties of thin wood composites based on the cantilever beam bending theory.

SUMMARY ON STRESS RELAXATION OF WOOD COMPOSITES

The stress relaxation occurs in wood composites when a static displacement is applied to a board or panel where the strain is constant (constant displacement) and the stress continues but at a decreasing rate. The curves of constant strain and decreasing stress rate are shown in Figure 1 (Feng and Zhao 2010). The stress relaxation is a static viscoelasticity phenomena, that changes with the environmental conditions (Cheng 1985). The major factors that influence stress relaxation are temperature, moisture content, strain levels, density, and grain direction. Brown et al used eight species of dried lumber and determined that the approximate relaxation coefficient *m* was inversely proportional to density as measured using horizontal grain pressure gauge (Cheng 1985).

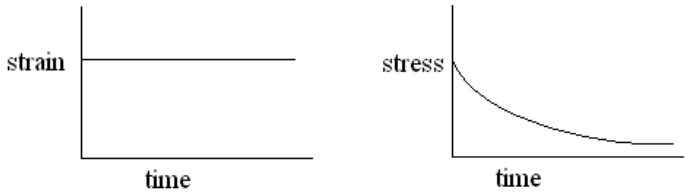

Figure 1—Constant Strain and Stress relaxation of wood materials

TEST METHOD

Test apparatus

Test apparatus is based on the cantilever beam bending load and deformation theory. The test apparatus includes two main parts: the mechanical structure part and the data processing part. The apparatus composition is shown in Figure 2 (a), and the apparatus photo is shown in Figure 2 (b).

The mechanical structure part clamps the specimen in a hanging vertical position, a static displacement is made by displacing the end of the specimen using a hook. A load cell, connected with the hook, is used to measure the load applied to the end of the beam. The data processing part consists of a signal conditioning box, a computer and a data processing software. Function of the data processing part are sensing load signal, conditioning load signal, A/D change and processing the data. The signal box consists of a linear DC power, an amplifier of load cell, an A/D card, etc. The software, written by Labview (Deng and Wang 2004), is used to acquisition and process the data, to get the stress relaxation properties of the specimens.

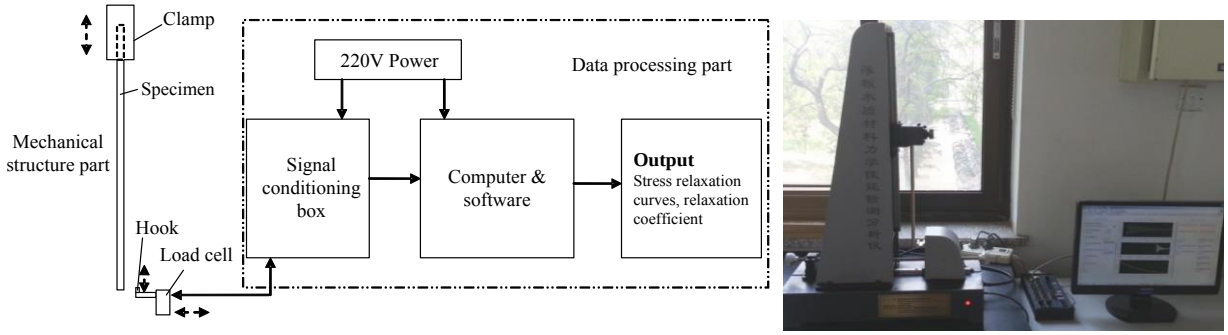

(a) Composition diagram (b) Photo

Figure 2—Cantilever beam test apparatus

Test theory

As shown in Figure 3, the specimen was clamped as a cantilever beam. A perpendicular hook was used to set the initial distance at the end of the specimen, *y*, resulting in a displacement load, *P*. Based on the engineering mechanics (Liu 2004), maximum tension stress and compression stress occur at the two surfaces of cross section A-A, and there is an equation (1).

$$\sigma = \frac{6Pl}{bh^2} \tag{1}$$

Where, σ is the maximum stress (MPa), *P* is static load (N), *l* is cantilever length (mm), *b* is width of the specimen (mm), *h* is thickness of the specimen (mm). The maximum stress was determined at initial load at the given displacement, then continued to be measured as a function of time.

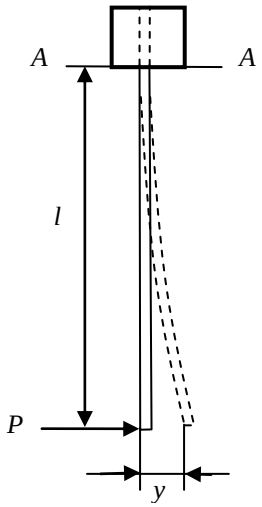

Figure 3—Static bending of a cantilever beam

Kitazawa used equation (2) to determine the stress relaxation rate of solid wood (Cheng 1985).

$$\sigma_t = \sigma_1(1 - m\log t) \tag{2}$$

In this formula, *t* represents time (min); σ_t represents the maximum stress at time *t* (MPa); σ_1 represents the maximum stress at time of 1 minute (MPa); *m* is relaxation coefficient. In the tests of this paper, the

initial tension bending stress was set to approximately 10%-20% of modulus of rupture (MOR) of the materials. By rearranging equation (2) we can obtain the estimated relaxation coefficient m, equation (3).

$$m = \frac{1}{\log t}(1 - \frac{\sigma_t}{\sigma_1}) \tag{3}$$

Experimental materials

In this stress relaxation study, four kinds of specimens were used, including particleboard (PB), medium density fiberboard (MDF), high-density fiberboard (HDF) and wood fiber plastic board (WFP). The sizes, symbol and number of specimens are listed in Table 1. For the specimens can be clamped as cantilever-beams, total lengths of the specimens were equal to *l*+50 mm.

Table 1—Type, size, symbol and number of the specimens

Set	Type	Size of specimens (*h* × *b* × *l*, mm)	Symbol	Number of specimens
1	Particleboard	5×50×290	PB 5	5
2	Medium density fiberboard	4.6×50×290	HDF 4.6	5
3	High-density fiberboard	3.7×50×290	MDF 3.7	5
4	Wood fiber plastic board	2×50×180	WFP 2	5

RESULTS AND ANALYSIS

Test results

The following are the results from the cantilever bending beam test. Load was measured after an initial 20mm displacement was applied and held at the free end of the beam. After the initial displacement, load was continuously recorded for 2 to 3 hours. Beam stress was determined from the load using equation (1) and plotted as a function of time. Constant displacement testing resulted in stress that gradually decreased with time. While the displacement was the same for all boards in this study, there were slight differences in load to reach the 20 mm displacement and therefore there were slight differences in stress calculations. For visual comparison purposes, the stresses were normalized to 100 percent maximum stress for each board. The results of the normalized data are shown in Figures 4, 5, 6, and 7. Of the total five specimens from each composite type, four specimens were held for two hours, and the 5th specimen was held for 3 hours. The test data for each of the 3-hour stress relaxation tests are shown in table 2. After the tests, the specimens retained a curved shape due to creep and stress relaxation within the boards. Continuous calculation of the relaxation coefficients, m, for all the boards were also plotted vs. time in Figures 4, 5, 6, and 7.

Table 2—Maximum stress vs. time based on the measured load for a 20mm displacement

		stress relaxation—stress value（MPa）vs. time						
Set	Specimen	0 min	30 min	60 min	90 min	120 min	150 min	180 min
1	PB 5-5	14.02	12.51	12.25	12.059	11.90	11.75	11.70
2	HDF 4.6-5	19.94	17.46	17.16	16.96	16.85	16.74	16.59
3	MDF 3.7-5	15.65	14.17	13.91	13.74	13.55	13.45	13.36
4	WFP 2-5	7.26	6.10	5.84	5.80	5.65	5.65	5.65

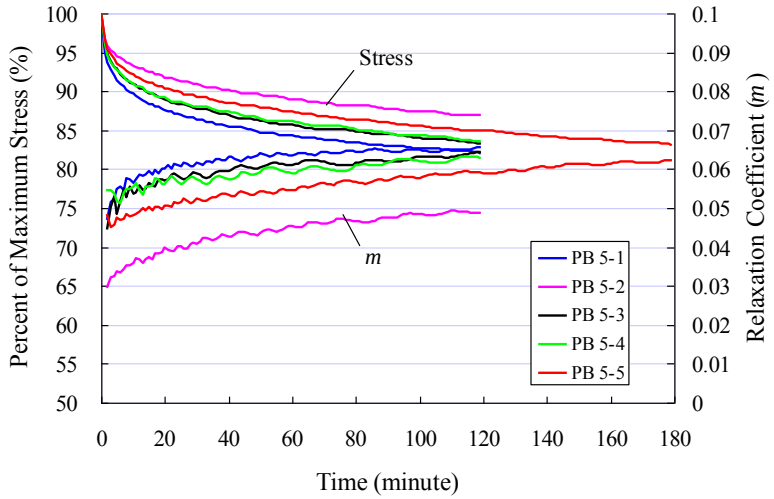

Figure 4—Percent stress relaxation for Particleboard (PB) set with corresponding coefficient *m*.

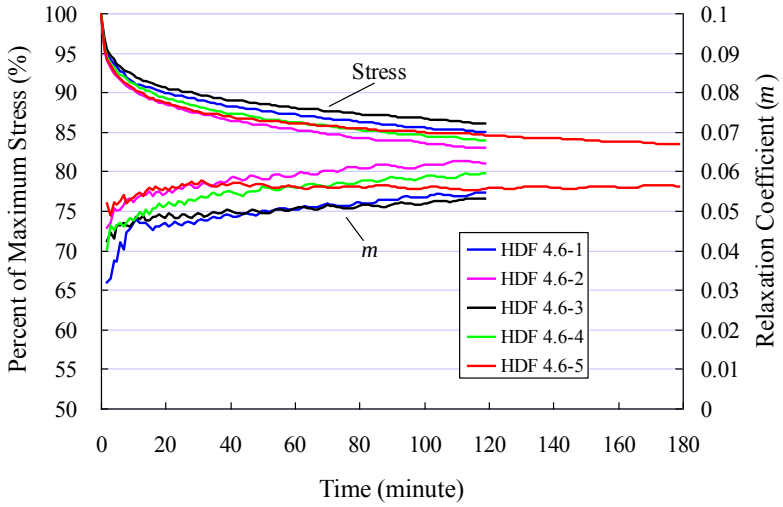

Figure 5—Percent stress relaxation for High Density Fiberboard (HDF) set with corresponding relaxation coefficient *m*.

Result analysis

From the stress relaxation tests, Figures 4, 5, 6, and 7, we can see the reduction in stress for all the board sets for a constant displacement. There were slight differences in the load and hence the stress calculated for each board. The normalized plots show the slight differences in the boards. We believe the variability in the stress curves was due to material properties variation within the board sets. But, it can be seen that the same basic curves are shown for each set. The stress relaxation curves for the HDF and the PB boards are more consistent than MDF and WFP boards. It is possible the thicker boards were more uniform and thus provide similar stress relaxation and as a result produce similar curves. We believe the additional noise for the MDF and WFP boards for the stress relaxation curves may be due in-part to internal stress release inside the panel as well as material property variations. The extent of stress relaxation as a function of time over 180 minutes can be seen in table 3. It can also be seen that the MDF 3.7-5 had the minimum stress relaxation of all the specimens. After 3-hours, the stress value decayed only to 85.4% of

the initial stress. From table 2, the MDF specimen had higher stress values than PB specimen, yet the stress relaxation was different. PB 5-5 and HDF 4.6-5 boards each had maximum stress relaxation of 83.5% and 83.2% of initial stress, respectively. The WFP 2-5 board had the lowest stress relaxation effect which might have been expected due to plastic's basic creep properties that are greater than wood. After 180 minutes, the stress value decreased to 77.8% of the initial stress.

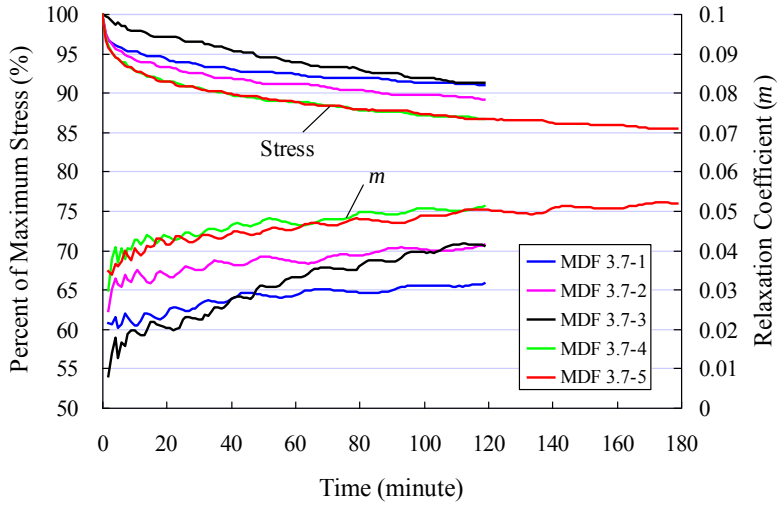

Figure 6—Percent stress relaxation for Medium Density Fiberboard (MDF) set with corresponding relaxation coefficient *m*.

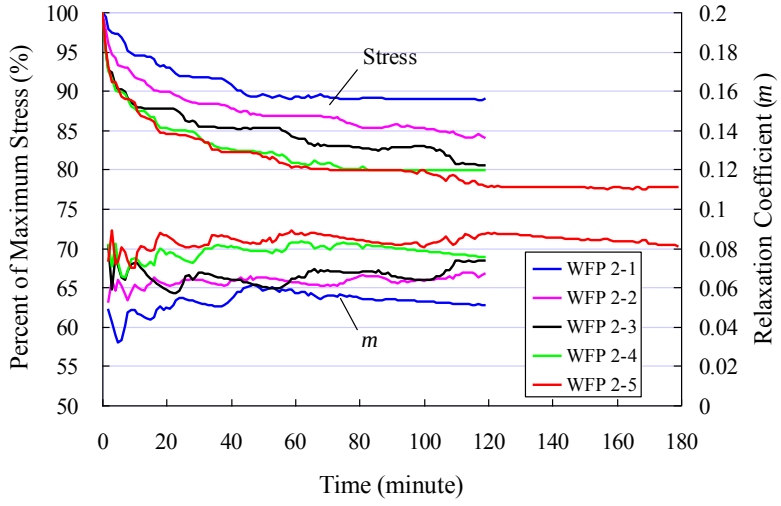

Figure 7—Percent stress relaxation for Wood Fiber Plastic (WFP) set with corresponding relaxation coefficient *m*.

The relaxation coefficient, *m* (equation (3)), whether plotted as actual stress vs. time or with maximum percentage stress vs. time, both provided the same *m* values and resulted in the same *m* plots. The coefficient was low for the initial stress relaxation but as time proceeded, an equilibrium condition began to emerge. *m* for all four board types had similar yet slightly different values. For our tests, equilibrium for the coefficient seemed to occur after about 120 minutes. It was also noted that the coefficient value corresponded to the stress relaxation, where minimal stress relaxation occurred in the specimens then the *m* value was also lower and if the stress relaxation was higher, then the coefficient value was also higher.

This effect needs to be studied to determine how relaxation is related to maximum stress values. We believe the initial high stress relaxation curves from the composite panels are a result of the composite characteristics as compared to the model which was developed for solid wood, equation (2). Composite materials have different stress relaxation mechanisms and may need to have a different model to better determine initial as well as long-term stress relaxation.

Table 3—Percent maximum stress over time over 180 minutes

Set	Samples	0 min	30 min	60 min	90 min	120 min	150 min	180 min
1	PB 5-5	100%	89.3%	87.4%	86.0%	84.9%	83.9%	83.5%
2	HDF 4.6-5	100%	87.6%	86.1%	85.1%	84.5%	84.0%	83.2%
3	MDF 3.7-5	100%	90.6%	88.9%	87.8%	86.6%	86.0%	85.4%
4	WFP 2-5	100%	83.9%	80.4%	79.9%	77.8%	77.8%	77.8%

CONCLUSIONS

(1) The stress relaxation properties of thin wood composites using the cantilever beam principle is potentially feasible. From the tests, we can see stress relaxation properties and the attenuation extent of stress with time.

(2) From the curves of stress relaxation, we can see the attenuation extent of stress is initially greater and slows down. It may be possible that a test time of two hours could provide an initial stress relaxation values. More analysis is needed to see if this is true.

(3) The stress relaxation curves of HDF and PB are more uniform. The stress relaxation curves of MDF are slightly irregular, but more samples are needed to determine average behavior. The stress relaxation curves of the WFP material are worst and needs more investigation as to why.

(4) The relaxation coefficient *m* changes with time until about 120 minutes after testing. The fluctuation of *m* is in accordance with the stress relaxation properties. The coefficient *m* value is related to the stress level. Higher the stress change, the lower the *m* value.

(5) The relaxation coefficient, m, could be used to reflect the stress relaxation properties of wood composites. It has the potential to better identify the stress relaxation properties of different boards. If the value of *m* is higher, the stress relaxation decreases at a faster rate and results in more creep behavior. Conversely, if the value of *m* is smaller, there is less stress relaxation and less creep.

Acknowledgments

The authors would like to thank the forestry industry research special funds for public welfare projects of Chinese State Forestry Administration for funding this research, grant #: 201304512.

References

Attic P. Schniewind, Richmond, Cal. 1968. Recent Progress in the Study of the Rheology of Wood. Wood Science and Technology. 2: 188-206.

Cao Jinzhen, Manhua Xie, Guangjie Zhao. 2006. Tensile stress relaxation of copper–ethanolamine (Cu–EA) treated wood. Wood Science and Technology. 40: 417-426.

Cheng Junqing. 1985. Science of Wood. Beijing: China Forestry Publishing House. (in Chinese)

Deng Yan, Wang Lei. 2004. Testing technology and application of Labview 7.1. Beijing, China: China Machine Press. (in Chinese)

Ebrahimzadeh P. R., D. G. Kubat. 1993. Effects of humidity changes on damping and stress relaxation in wood. Journal of Materials Science. 28: 5668-5674.

Feng Shanghuan, Zhao Youke. 2010. The summary of wood stress relaxation properties and its influencing factors. Wood Processing Machinery. 3: 37-40. (in Chinese)

Ikuho Iida, Koichi Murase, Yutaka Isbimaru. 2002. Stress relaxation of wood during the elevating and lowering processes of temperature and the set after relaxation. Journal of Wood Science. 48: 8-13.

Larson R. G. 1999. The structure and rheology of complex fluid. Oxford University Press. New York.

Liu Hongwen. 2004. Mechanics of Materials. Beijing, China: China Machine Press. (in Chinese)

Xie Manhua, Zhao Guangjie. 2004. Effects of periodic temperature changes on stress relaxation of chemically treated wood. Forestry Studies in China. 6(4): 45-49.

Zhang Houjiang, Guo Zhiren, Hunt John F., Fu Feng. 2010. Measuring modulus of elasticity for thin wood composites by using the dynamic method. Journal of Beijing Forestry University. 32(2): 149-152. (in Chinese)

Evaluation of Elastic Properties of Spruce Lumber and Glulam by Nondestructive Methods

Zsigmond Vas
Transilvania University of Brasov, Romania

Ferenc Divós, Levente Dénes
University of West Hungary, Sopron, Hungary

Abstract

The main objectives of this study were to compare the elastic properties of spruce laminae and glulam structures made of them determined by destructive (four point static bending strength) and different nondestructive methods. Dynamic longitudinal vibration and bending vibration frequency determination techniques were used for modulus of elasticity determination parallel with theoretical calculations based on the multilayer symmetric orthotropic laminates theory. For glulam manufacturing, laminae having higher modulus of elasticity were placed as outside layers to manufacture homogeneous and heterogeneous structures. The degrees of correlation obtained from the different nondestructive testing methods and theoretical estimations were then analyzed and compared with the static bending results. The results indicate a good correlation between dynamic and static modulus of elasticity values as well as with computed values. The lowest standard deviation was obtained for the theoretical values as was expected and the static values demonstrate a standard deviation of 800 MPa. Based on the results of this study, the load-bearing capacity of glulam can be designed using the elastic properties of the laminae determined by nondestructive methods or theoretical computations.

Keywords: Nondestructive method, longitudinal vibration, multilayer structures, glulam, symmetric theory

Assessment of Stress Wave Analysis for Quantifying Decay in Above Ground Field Exposures

Glenn M. Larkin and Peter E. Laks
School of Forest Resources and Environmental Science
Michigan Technological University
Houghton, MI 49931, USA

Abstract

Laboratory obtained longitudinal stress wave MOE (MOE_{sw}) was previously compared to other methods (static bending, longitudinal compression strength, weight loss, and visual evaluation) and proved to be the most suitable to quantify decay in southern pine exposed above ground in field tests. Longitudinal stress wave analysis was evaluated for its utility as an in-field tool to measure decay in above ground field exposures. Specimens were exposed at seven field sites in the USA. Data was collected in the field after 3, 6, 9, 12, and 18 months of exposure. A subset of the specimens was removed after each measurement and re-tested in the lab. Field measured MOE_{sw} (with moisture content correction factors) gave the same results as reconditioned specimens evaluated in a lab setting. The merits of stress wave analysis for general use in quantifying decay in above ground field exposures are discussed.

Introduction

The most commonly used methods to measure decay are based on weight loss and/or visual evaluation. Both fail to detect early decay and usually require long-term exposure to decay fungi to obtain sufficient data to determine product performance (Wilcox 1978, Hardie 1980). Mechanical strength test methods have been used in both laboratory and field tests to evaluate decay (Nicholas and Crawford 2003, Nicholas and Militz 2008). These techniques have limitations. Most notably they require bulky equipment, have specimen geometry constraints, and may be destructive, necessitating a large number of replicates. An alternative is to use non-destructive acoustical test methods to monitor decay *in situ* during field exposures.

Percussion stress waves, ultrasound, and vibration are established technologies used to grade lumber, assess the condition of structures and living trees (Bucar 2006). These methods have been reviewed (Kaiserlik 1978) and used to evaluate the progression of decay and termite attack in southern pine exposed in ground contact field exposures (Pellerin et al. 1985, DeGroot et al.

1998, Wang et al. 2007) and above ground field exposures (Nicholas et al. 2012). In the ground contact studies, correlations to compression strength, weight loss, and visual evaluations were used to demonstrate method applicability. Laboratory measurements of field exposed above ground specimens showed that stress wave derived longitudinal MOE (MOE_{sw}) performed favorably as a measure of decay compared with stiffness in bending and longitudinal compression strength (Larkin and Laks, unpublished results). This paper further examines MOE_{sw} as a method for in-field use to monitor decay in accelerated above ground exposures.

Experimental

Specimen Selection and Preparation

Southern pine (*Pinus* spp.) lumber was purchased from CzechMate Lumber (Willowbrook, IL, USA) in December 2003. Clear, straight-grained, and defect free boards with 2-4 rings/cm (6-10 rings/inch) were selected to comply with AWPA Standard E7 (AWPA 2003). Approximately 5000 individual specimens were machined to dimensions of 254 mm (l) x 37.4 mm (r) x 6.4 mm (t), and marked at the mid-section with an indelible, UV-stable marker. Each was visually examined to eliminate specimens with heartwood or juvenile wood. Length was measured along the longitudinal mid-line of the radial plane, while width and height were measured at the halfway along the specimen's length, and densities were calculated from volume and weight. There was a normal distribution of densities, and specimens were culled from the tails. Stress wave time (μs/m) was measured on the remaining specimens, and a second sort resulted in a normal distribution of stress wave times. Specimens were again culled from the tails; then MOE_{sw} was calculated from stress wave velocity and density. The third sort resulted in a normal distribution of MOE_{sw}, and less than 1% of the specimens were culled from the tails. The remaining 2000 specimens were oven-dried at 105^{o}C for 24 hours and their dry weights were

measured immediately upon removal from the oven. Test specimens were randomly selected and divided into groups for field exposure, and an unexposed control. Among different groups of specimens, there were no statistical differences in the unexposed density (mean = 609.9 kg/m^3, SE = 1.26 kg/m^3, P = 0.561), stress wave velocity (mean = 4913.1 m/s, SE = 4.03 m/s, P = 0.637), and MOE_{sw} (mean = 13.4 GPa, SE = 0.01 GPa, P = 0.814). The intent was to produce a set of specimens with minimal variability with the hope that this would carry through to the field exposure and the procedures used to measure decay.

Field Exposures and Evaluations

Untreated southern pine specimens were exposed above ground at field sites in the USA. Two of the sites were Alberta, MI, (cool temperate) and Hilo, HI, (warm tropical). These sites represent the lower and upper boundaries of decay hazards at Michigan Tech Wood Protection Group field test sites. Some results from these sites will be presented in this paper. Results from other sites will be published elsewhere. Alberta, MI, field exposure occurred from April 2004 to October 2005. Hilo, HI, field exposure occurred from February 2004 to August 2005. Specimens were placed in racks parallel to the ground at a height of 60 cm (24 in) above ground level. The racks [122 cm (L) x 50 cm (W)] were constructed from schedule 40 PVC pipe with a 2.54 cm inner diameter and arranged in two rows with an inside width of 24 cm between rails which had a 100 cm long, 0.85 cm slot that faced inward and aligned to allow insertion of specimen ends. The installed specimens were held in place by the slots and spanned the distance between the rails. Approximately 1.25 cm at each end of the specimens was inserted into the slots. The bottom of the rails had drain holes to allow water to escape.

Specimens were inspected in the field after 3, 6, 9, 12, and 18 months of exposure. They were visually evaluated for decay and insect attack using the AWPA rating scale (AWPA 2012a).

Then they were weighed, their dimensions were measured, and MOE_{sw} was determined. After evaluation, specimens were either removed for laboratory tests, or returned to the exposure rack. Nine specimens were removed for lab measurements at the 3, 6, 9, and 12-month inspections. All remaining specimens were returned to the lab after the 18-month inspection.

MOE_{sw} was determined from density and stress wave velocity measurements. Stress wave velocity in the longitudinal direction was measured with a Metriguard Model 239A stress wave analyzer equipped with a laboratory clamp set (Metriguard, Pullman, WA, USA). Plexiglass (2041.1 m/s) and aluminum (4526.7 m/s) bars with the same dimensions as the southern pine specimens (228.6 mm span) were used as reference materials to check the measurement accuracy and precision of the stress wave timer before use, and as an intermediate check after every 25 specimens during use. A calibration could not be performed because the initial stress wave velocity of the southern pine fell outside the range of the reference materials. Stress wave velocities of decayed southern pine fell within the range of the reference materials.

All MOE_{sw} measurements were adjusted to 27.1% moisture content, the critical point where there was an inflection in MOE_{sw} and measured density in laboratory studies of unexposed controls. The moisture content adjustment was made using the established correction value of 2% per 1% MC for MOE_{sw} (Wood Handbook 2010).

Apparent moisture content for specimens measured in the field was calculated from the difference of the field measured weight and pre-exposure oven-dry weight. Weight loss for retrieved specimens was calculated from the difference of the pre- and post-exposure oven-dry weights. The specimens were oven-dried for 24 hours in a forced air laboratory oven at 105^{o}C and immediately weighed upon removal.

An abiotic weight loss was determined by leaching unexposed specimens using the AWPA E11 (AWPA 2012b) laboratory leachability test, modified to accommodate specimen volume differences. Instead of the usual 0.30 L of water used for 19 mm cubes, nine specimens were leached with 4.0 L. Water changes occurred at 6, 24, 48, 96, 144, 192, 240, 288, and 336 hours. After the last water change, the specimens were oven-dried and weighed as above to calculate percent weight loss.

Statistical Analysis

Visual evaluation, MOE_{sw}, and weight loss were evaluated by comparing the means of exposed and unexposed specimens. Statistical analysis was performed with SigmaPlot 12 (Systat Software, Inc., 2011). The difference between means within each method was tested with one-way ANOVA procedures. The means at each interval for the field-measured specimens were compared using repeated measures one-way ANOVA. When an ANOVA analysis was statistically significant at a level of 0.05, comparison of the means was performed using the Holm-Sidak test to evaluate pairwise differences among all means of exposed and unexposed specimens. It provided the most statistical power in picking out differences among the means. A comparison of the means was also performed between values at each time interval and the unexposed controls. When evaluating weight loss, a comparison of the means that included the leached abiotic weight losses was performed.

Results and Discussion

Determination of Decay

Decay in untreated southern pine specimens exposed above ground over a period of 18 months was evaluated using weight loss, visual, and non-destructive test methods. The results are shown in Tables 1 and 2, expressed as percent residual value of the unexposed controls to allow direct

comparisons among the methods. As was previously shown in laboratory measurements (Larkin and Laks, unpublished results), the in-field MOE_{sw} measurements detected decay in three or six months at Hilo, HI, and Alberta, MI, respectively. This result is consistent with the ten-fold higher decay hazard for the Hawaiian exposure site. Weight loss detected decay at Hilo, HI, after 12 months and did not detect decay at Alberta, MI, during the 18-month exposure period. Visual evaluations failed to detect decay at either of the test sites.

Four different MOE_{sw} measurements sets were examined to evaluate the method transfer from the laboratory into the field:

1. All specimens measured in the field.
2. Removed specimens measured in the field.
3. The last set of specimens to be removed was measured in the field at each inspection.
4. Removed specimens measured in the laboratory.

Field measurements were under ambient conditions over a wide range of moisture contents. Laboratory measurements were made after reconditioning to target moisture content of 12%. All results were adjusted to 27.1% as described above. A one-way ANOVA analysis revealed no statistically significant differences among the four sets of measurements within each of the test sites. Repeated measures one-way ANOVA analysis for the last set of removed specimens demonstrated that this group behaved in a statistically similar manner to each of the removed specimen sets during the course of the field exposures in Hawaii and Michigan. The starting point (the unexposed control) is the same for all four sets of MOE measurements. The end point converges to the 18-month evaluation for each of the three in-field sets (Figures 1 and 2). However, there is the potential for differences at the 3, 6, 9, and 12-month measurement intervals

and with the laboratory measurements. One-way ANOVA analysis at each of these intervals had no statistical differences among the four MOE_{sw} sets.

There were no statistical differences observed for any of the sets of MOE_{sw} measurements. Therefore, direct in-field MOEsw measurements were sufficient to measure the progression of decay in southern pine specimens exposed in accelerated above ground field exposures at Alberta, MI, and Hilo, HI.

Conclusions

Weight loss and visual evaluation do not perform well as measures of decay in accelerated above ground field exposures of southern pine. Neither method is suitable for detection of the early stages of wood decay. Laboratory MOE_{sw} measurements of removed specimens is suitable as a measure of decay in accelerated above ground field exposures of southern pine. It was able to detect the early stages of wood decay. There was no statistical difference between laboratory and in-field MOE_{sw} measurements. Subsets of the in-field measurements were not statistically different from the entire population of specimens. Field measured MOE_{sw} (with moisture content correction factors) gave the same results as reconditioned specimens evaluated in a lab setting. MOE_{sw} method transfer from the laboratory to in-field use was feasible for monitoring decay in accelerated above ground field exposure of southern pine at two field sites with large differences in decay hazard.

References

AWPA 2003. *AWPA Standard E7-01: Standard method of evaluating wood preservatives by field tests with stakes.* In: AWPA Book of Standards. American Wood Preservers' Association, Granby, TX, USA.

AWPA 2012a. *AWPA Standard E16-09: Standard field test for evaluation of wood preservatives to be used out of ground contact: Horizontal Lap-Joint Method*. In: AWPA Book of Standards. American Wood Protection Association, Birmingham, AL, USA.

AWPA 2012b. *AWPA Standard E11-12: Standard method for accelerated evaluation of preservative leaching*. In: AWPA Book of Standards. American Wood Protection Association, Birmingham, AL, USA.

Bucar, V. 2006. Acoustics of Wood, 2nd Edition. Springer-Verlag, Berlin, Germany, 393 pp.

DeGroot, R.C., Ross, R.J., Nelson, W.J. 1998. *Non-destructive assessment of wood decay and termite attack in southern pine sapwood*. Wood Protection 3: 25-34.

Hardie, K. 1980. *A review of strength testing as a measure of biodeterioration of wood and wood based materials.* International Biodeterioration Bulletin 16(1): 1-8.

Kaiserlik, J. 1978. *Nondestructive testing methods to predict the effect of degradation on wood: a critical assessment*. GTR-FPL-19. USDA Forest Service, Forest Products Laboratory, Madison, WI, USA.

Nicholas, D.D., Crawford, D. 2003. *Concepts in the development of new accelerated test methods for wood decay*. In Goodell, B., Nicholas D.D., Schultz T.P. (Eds.), *Wood Deterioration and Preservation: Advances in our Changing World*. ACS Symposium Series 845, American Chemical Society, Washington, DC, 288-312.

Nicholas, D.D., Militz, H. 2008. *Concepts in the development of new accelerated test methods for wood decay*. In: Schultz, T., Militz, H., Freeman, M.H., Goodell, B., Nicholas, D.D. (Eds.), Development of Commercial Wood Preservatives: Efficacy, Environmental and Health Issues. ACS Symposium Series 982, American Chemical Society, Washington, DC, 142-151.

Nicholas, D.D., Shi, J., Schultz, T. 2009. *Evaluation of variables that influence dynamic MOE in wood decay studies.* Document IRG/WP 09-20409. International Research Group on Wood Preservation. Stockholm, Sweden.

Pellerin, R.F., DeGroot, R.C., Esenther, G.R. 1985. *Nondestructive stress wave measurements of decay and termite attack in experimental wood units*. In: Proceedings of the 5th nondestructive testing of wood symposium, September 9-11, 1985, Washington State University, Pullman, WA p. 319-352.

Systat Software, Inc. 2011. *SigmaPlot 12*. Chicago, IL, USA.

Wang, X., Page-Dumbrose, D., Jurgensen, M.F., Ross, R.J. 2007. *Field assessment of wood stake decomposition in forest soil*. Holzforschung 61: 605-610.

Wilcox, W.W. 1978. *Review of the literature on the effects of early stages of wood decay on wood strength*. Wood and Fiber, 9(4): 252-257.

Forest Products Laboratory. 2010. *Wood Handbook: Wood as an engineering material*. GTR-FPL-190 USDA Forest Service, Forest Products Laboratory, Madison, WI, USA. 508 pp.

Table 1. Mean Residual Measures of Decay for Southern Pine Exposed Above Ground at Alberta, MI

Measure of Decay	Mean Longitudinal MOE_{sw}				Weight	Visual Evaluation
Exposure (Months)	Laboratory (Removed)	Field (Removed)	Field (Last Set)	Field (All)	Field (Removed)	Field (Removed)
0	99.6 (0.3)[a]	99.6 (0.3)	99.6 (0.3)	99.6 (0.3)	100	100
3	97.5 (0.9)	97.8 (1.2)	96.5 (0.8)	97.5 (0.5)	98.8 (1.0)	100
6	95.7 (0.9)	95.8 (1.6)	91.6 (2.0)	94.3 (0.9)	98.3 (2.0)	100
9	88.4 (0.9)	88.3 (2.4)	90.3 (1.8)	89.9 (1.2)	98.0 (1.0)	100
12	86.8 (0.8)	86.9 (1.0)	86.5 (1.4)	86.6 (0.9)	97.8 (1.2)	100
18	86.9 (0.9)	86.1 (1.5)	86.1 (1.5)	86.1 (1.5)	95.9 (2.0)	99.0 (1.0)

[a] values in parentheses indicate standard error

Table 2. Mean Residual Measures of Decay for Southern Pine Exposed Above Ground at Hilo, HI

Measure of Decay	Mean Longitudinal MOE_{sw}				Weight	Visual Evaluation
Exposure (Months)	Laboratory (Removed)	Field (Removed)	Field (Last Set)	Field (All)	Field (Removed)	Field (Removed)
0	99.8 (0.6)[a]	99.8 (0.6)	99.8 (0.6)	99.8 (0.6)	100	100
3	93.1 (1.0)	92.5 (0.9)	86.9 (1.9)	92.8 (1.0)	98.2 (1.0)	100
6	86.3 (1.3)	86.0 (0.8)	83.5 (0.9)	85.0 (0.6)	96.3 (1.0)	100
9	78.7 (0.8)	78.9 (0.7)	76.0 (1.4)	78.5 (0.8)	96.1 (1.0)	100
12	73.0 (1.3)	73.9 (1.3)	72.8 (1.3)	73.3 (0.9)	93.5 (1.0)	99.0 (1.0)
18	68.8 (1.3)	68.2 (1.4)	68.2 (1.4)	68.2 (1.4)	92.0 (2.0)	97.0 (2.0)

[a] values in parentheses indicate standard error

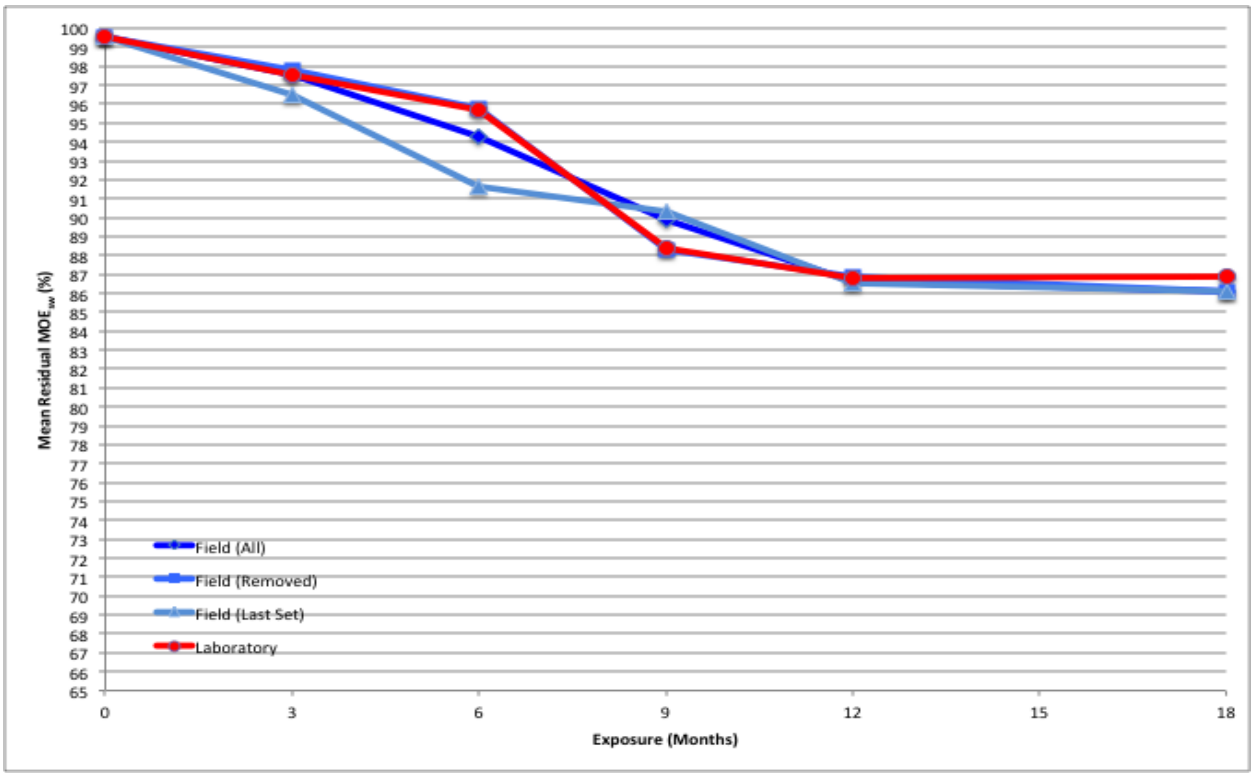

Figure 1. Mean residual stress wave derived MOE (MOE_{sw}) of in-field and laboratory measurement sets for southern pine specimens exposed at Alberta, MI for a period of 18 months. See text for descriptions of the sets.

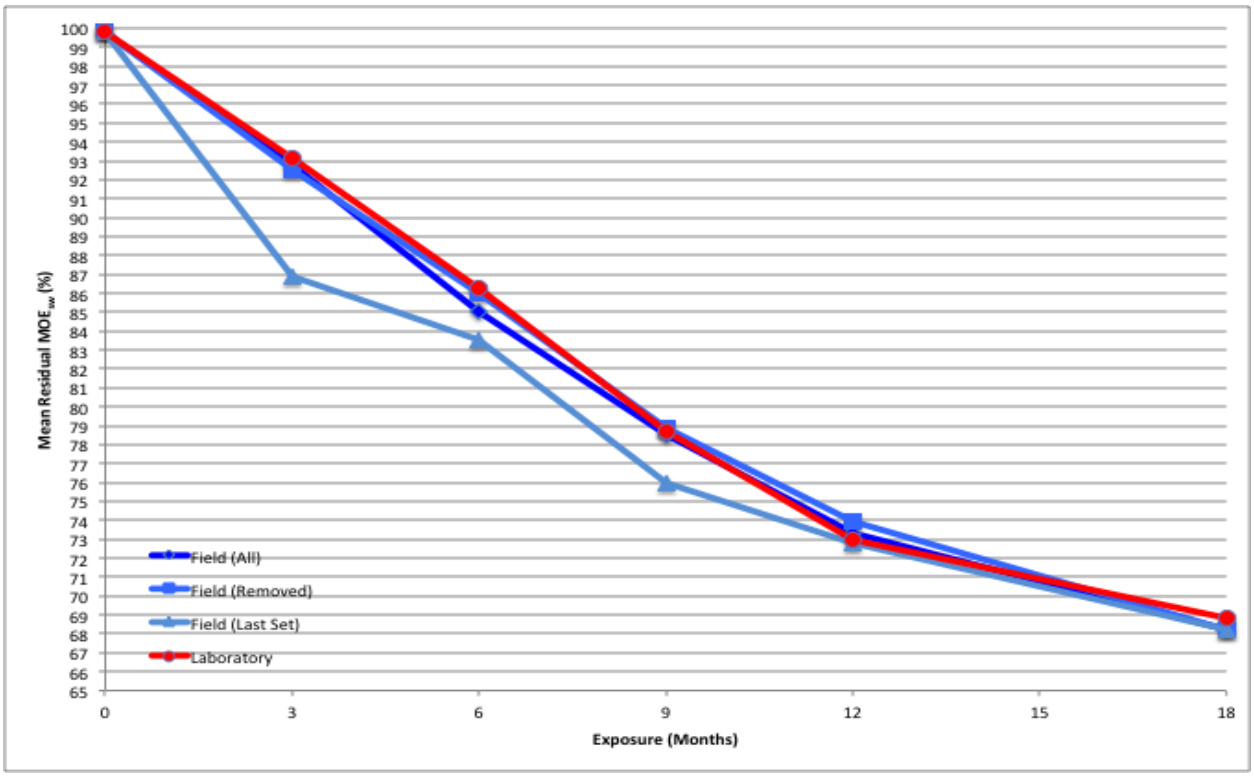

Figure 1. Mean residual stress wave derived MOE (MOE$_{sw}$) of in-field and laboratory measurement sets for southern pine specimens exposed at Hilo, HI for a period of 18 months. See text for descriptions of the sets.

Nondestructive chemical imaging of wood at the micro-scale: advanced technology to complement macro-scale evaluations

Barbara L. Illman
Director of IMBT, U.S. Forest Service Forest Products Lab, Madison, Wisconsin, USA, billman@fs.fed.us

Julia Sedlmair
Physicist, University of Wisconsin-Madison, Synchrotron Radiation Center and U.S. Forest Service Forest Products Laboratory, Madison, Wisconsin, and The Pennsylvania State University, University Park, Pennsylvania USA, jsedlmair@src.wisc.edu

Miriam Unger
Chemist, University of Wisconsin-Milwaukee and University of Wisconsin-Madison, Synchrotron Radiation Center, Madison, Wisconsin USA, MiriamUnger@gmx.de

Carol Hirschmugl
Professor, Department of Physics, University of Wisconsin-Milwaukee, Milwaukee, Wisconsin; and University of Wisconsin-Madison, Synchrotron Radiation Center, Madison, Wisconsin USA, chirschmugl@gmail.com

Abstract

Chemical images help clarify understanding of wood properties, durability, and cell wall deconstruction for conversion of lignocellulose to biofuels, nanocellulose and other value added chemicals in forest biorefineries. We describe here a new method for nondestructive chemical imaging of wood and wood-based materials at the micro-scale to complement macro-scale methods based on X-rays, acoustics, and georadar. Chemical detection, mapping and digital image construction were obtained with a high resolution Fourier transformed infrared microspectroscopy facility that obtains infrared light from a recently constructed beamline at the University of Wisconsin Synchrotron Radiation Center, Madison, Wisconsin USA. This pioneering Infrared Environmental Imaging (IRENI) facility is equipped with a unique design for illuminating and analyzing samples, enabling rapid FTIR data collection, high spatial resolution (pixel size of 0.54×0.54 μm^2), and computer-generated images of lignin, hemicellulose and cellulose in wood cell wall layers of commercially important *Pinus taeda* L. and *Populus deltoides* Bartr.

Keywords: wood, poplar, pine, chemical imaging, FTIR, lignocellulose, IRENI, synchrotron

Introduction

Nondestructive infrared based chemical images can replace time consuming destructive handling and fixative procedures that alter the nature of wood architecture and chemistry. Technological advances in microspectroscopy, computer capacity and specialized imaging software provide a unique opportunity for *in situ* and *in vivo* analysis, revealing wood chemistry and architecture at the micro- and nano-scale levels. Our approach has been to develop procedures with x-ray and infrared spectroscopy to image internal chemistry of solid materials (Hirschmugl and Gough 2012; Nasse et al. 2011a; Illman and Bajt 2003:

Illman and Dowd 1999). Here we describe chemical images of commercially and environmentally important pine and poplar wood using the one of-a-kind synchrotron-based IRENI (Infrared Environmental Imaging) high resolution Fourier transformed infrared (FTIR) microspectroscopy beamline facility at the University of Wisconsin Synchrotron Radiation Center (SRC). Infrared radiation interacts with the dipoles and functional groups of molecules of a sample in a non-invasive and non-destructive way, resulting in detectable absorbance spectra for construction of chemical images with micro-scale resolution.

Chemical images will provide information about wood weathering, fasteners, adhesives, coatings, fungal decay and artifacts. Additionally, chemical images of wall deconstruction will aid the design of protocols to breakdown cell walls for conversion of lignocellulose to liquid biofuels, nanocellulose and chemical feedstock. The objective here is to image lignin, hemicellulose and cellulose in wood of two important model softwood and hardwood species, pine and poplar.

Methods

Commercial kiln dried pine (*Pinus taeda* L.) and poplar wood (*Populus deltoides* Bartr.) were sectioned (10µm thick) with a Reichert sliding (sledge) microtome, stored at room temperature between two standard glass microscope slides and transferred to BaF_2 disks (PIKE Technologies, Madison, WI, USA) for data collection.

Wide-field infrared microspectroscopy was performed at the IRENI beamline facility (Figure 1) using a Bruker Hyperion 3000 and a focal plane array detector (FPA) with a programmable mapping stage coupled to a Fourier Transform Infrared (FTIR) vertex 70 spectrometer. The novel IRENI beamline configuration collects a section of synchrotron radiation (320 mrad × 25 mrad) generated by a bending magnet, collimates 12 light beams that are arranged in a 3×4 matrix side by side to illuminate the sample, creating a virtually homogeneously illuminated sample area of 40 µm × 60 µm using a 74x objective (Nasse et al. 2011a; Nasse et al. 2011b).

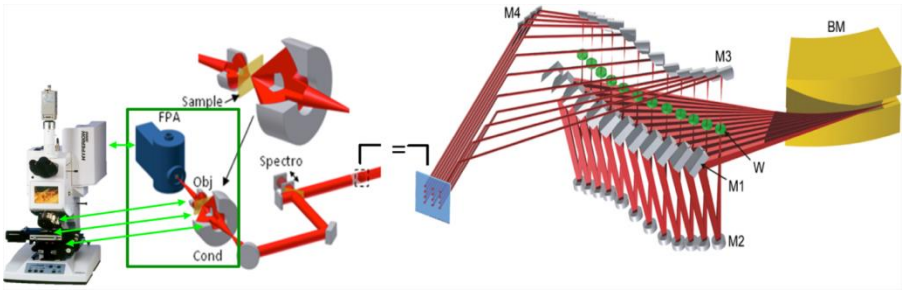

Figure 1. Schematic of the IRENI synchrotron beamline facility, going from right to left: From a bending magnet a section is extracted and subdivided into 12 beams that are collimated into a 3x4 matrix via a system of mirrors (M1-M4). The condenser is used to defocus the beams, resulting in homogeneous illumination at the sample plane. A 74x objective images the sample onto a 128x128 FPA with an effective pixel size of $0.54\mu m^2$ x $0.54\mu m^2$. The end station microscope is a Bruker 3000.

Infrared spectra were collected in transmission mode with a 74x-objective (NA = 0.65) in combination with a condenser of similar NA, determining that the geometric pixel size limit of the detector should not exceed 0.59 μm^2. The FPA (grid of up to 128×128 detectors) has a pixel size of $0.54\mu m^2$ in transmission mode that results in slight oversampling, enabling high spatial resolution at all wavelengths within minutes. Concurrent collection of thousands of infrared spectra in a single shot FPA image covering an area up to 50 μm^2 (96 x 96 pixels) results in a total of 9, 216 spectra. The spectral bandwidth ranged from 4000 cm^{-1} to 800 cm^{-1}.

Analysis of the data was carried out using OPUS (http://www.brukeroptics.cz/downloads.html) and IRidys (www.iryidys.com) running on IGOR Pro (www.wavemetrics.com). Wavemetrics' IGOR Pro was used to extract the spectra, integrate over spectral peaks and display 2-dimensional chemical maps.

Results and Discussion

Cellulose, lignin and hemicellulose were identified by characteristic absorption bands (Pandey1999, Pandey2003, Marchessault1962, Fackler2010, Fengel1992, Kumar2009, Gorzsás 2011) within the wood fingerprint region and illustrated with chemical imaging. A spectral signal was selected from multiple signals for each polymer in order to simplify the demonstration of the process and benefits of IRENI chemical images. At the assignment for cellulose (1372 cm^{-1}), hemicellulose also absorbs but the signal is weak. Absorption at 1506 cm^{-1} was selected for lignin, and 1740 cm^{-1} for hemicellulose. The absorption band assignments represent the most probable and most commonly made classifications. In contrast to spectra of chemical standards, the spectra of lignin, cellulose, hemicellulose and other wood chemicals overlap in cell walls and even the extracted polymers are not pure. The intertwined polymer fibers and chemical linkages make heterogeneous wood one of the most difficult specimen to study.

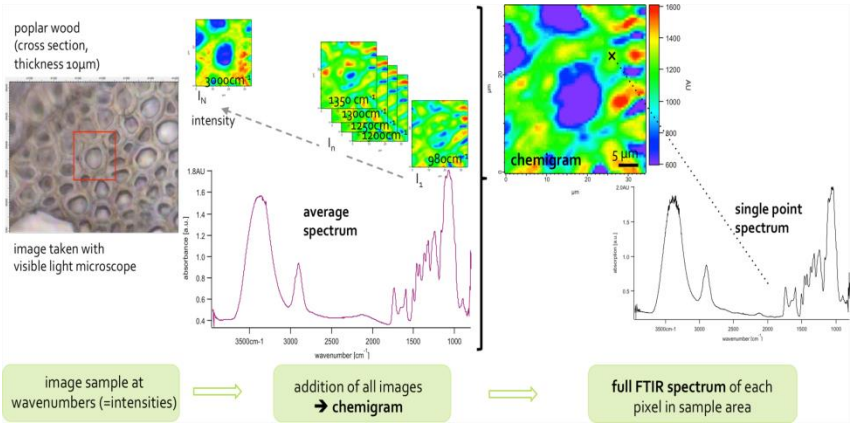

Figure 2. Acquisition of a full FTIR spectral image of poplar. Far left panel: sample area is indicated with a red square (34µm side length) on the light micrograph. Middle: images over entire mid-IR spectrum are obtained in one measurement and added to form chemigram. Right: chemigram with full FTIR spectrum in each pixel, and a single point spectrum from cell wall.

The process for generating IRENI micro-spectro-chemical images from an average spectrum and from a single point spectrum is shown in Figure 2.

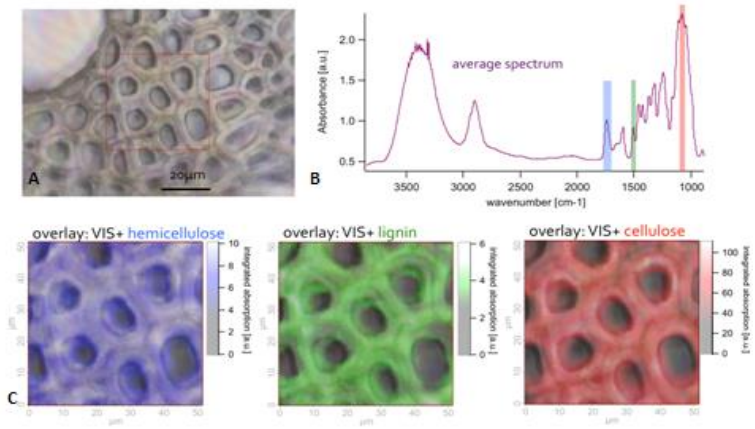

Figure 3. Chemical images of lignin, hemicellulose and cellulose in transverse section of poplar.

Figure 3 shows a light micrograph (A) of a transverse section of poplar wood with the sample region designated by a red square box (34µm side length). Specific spectral regions assigned to hemicellulose (blue), lignin (green) and cellulose (red), are shown in the average FTIR spectrum (B) of the sample, and used to generate chemical images (C). Transparencies (65%) of the images were overlaid on the sample region of the light micrograph. The lumen is gray. The color intensities illustrate the distribution and relative concentration of the polymers in cell walls of pine tracheids. Differences in the relative spectral intensity of cellulose, hemicellulose and lignin in pine and poplar are being examined elsewhere. In Figure 4, similar images for pine wood are shown over twice the sample area as Figure 3 to demonstrate the potential mapping capabilities of this system.

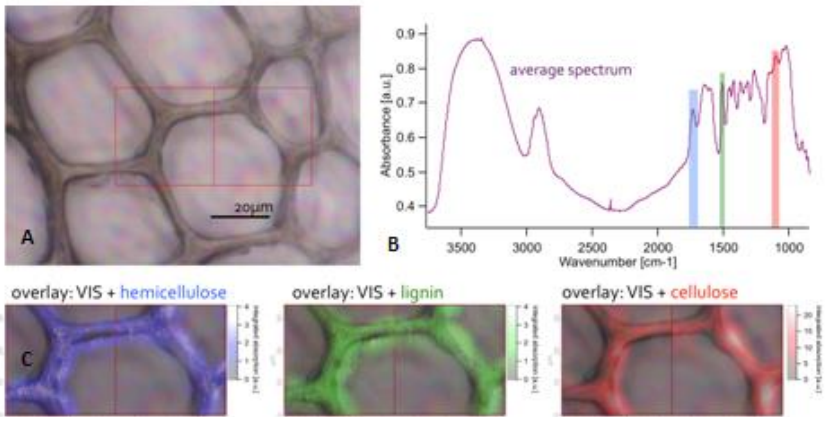

Figure 4. Chemical images of pine wood. A) Light micrograph of a transverse section of pine wood with the FTIR sample region outlined by a red box. B) The average FTIR spectrum with the integration of specfic spectral regions assigned to hemicellulose (blue), lignin (green) and cellulose (red). (C) Chemical images are displayed as transparencies (63%) overlaid on the red box sample region of the light micrograph.

Clearly, the results presented here are a small fraction of the 9, 216 (poplar) and 8,192 (pine) spectra collected for each spectral area of these samples. Data mining for multiple absorption bands promises to reveal new chemical and structural information at the micron scale. Preliminary experiments characterizing adhesive and chemical modifications are encouraging.

Conclusions

The multiple beam FTIR synchrotron beamline IRENI nondestructively measured chemical components of wood, allowing the extraction of specific spectra for hemicellulose, lignin and cellulose and the generation of chemical images with high spatial resolution. Preparation of samples was easy, cost effective, and required no special treatment, staining or storage. Micro-chemical-spectroscopy at IRENI offers many advantages over other techniques. Pixel size at IRENI is 0.54 x 0.54 μm^2 whereas typical table top FPA and synchrotron IR imaging systems are only 5 x 5 μm^2. Collection of full spectra over large sample area gives more accurate data than traditional techniques where a single spectrum from a sample is collected and averaged. Our current research includes fungal decay, adhesive bonding, chemical modification and moisture effects. This presentation will include examples of wood cell wall degradation and treatment of archeological wood.

Acknowledgments

This work was supported by the USDA Forest Service Forest Products Lab, the U.S. National Science

Foundation under awards CHE-1112433, and DMR-0619759, and is based on research conducted at the Synchrotron Radiation Center, University of Wisconsin–Madison, which is supported by the National Science Foundation under award DMR- 0537588, and by the University of Wisconsin– Milwaukee and University of Wisconsin–Madison. The authors wish to thank Thomas A. Kuster, Forest Products Lab, for assistance with microtoming wood for 2-D images.

References

Fackler, K. et al. 2010. Localisation and characterisation of incipient brown-rot decay within spruce wood cell walls using FT-IR imaging microscopy. *Enzyme Microb. Technol*. **47**(6), 257–267, 2010.

Fengel, D. 1992 Möglichkeiten und Grenzen der FTIR-Spektroskopie bei der Charakterisierung von Cellulose. *Das Papier* **46**(1), 7–11.

Gorzsás, A. 2011 Cell-specific chemotyping and multivariate imaging by combined FT-IR microspectroscopy and orthogonal projections to latent structures (OPLS) analysis reveals the chemical landscape of secondary xylem. *Plant J.* **66**(5), 903-914.

Hischmugl, C.J.; Gough, K.M. 2012. Fourier Transform Infrared Spectrochemical Imaging: Review of Design and Applications with a Focal Plane Array and Multiple Beam Synchrotron Radiation Source. *Appl. Spectrosc.*, **66**(5), 475-490.

Illman B.L., Dowd, B.A. 1999. High resolution microtomography for density and spatial information about wood structures. In: Bonse, U., ed. Developments in X-Ray Tomography II. SPIE **3772**, 198-204.

Illman, B.L. 2003. Synchrotron applications in wood preservation and deterioration. In: *Wood Deterioration and Preservation: Advances in our Changing World*. B. Goodell, D.D. Nicholas, T.P. Schultz, eds. ACS Symposium Series 845. American Chemical Society, Washington, D.C., 337-345.

Kumar, R. et al. 2009 Physical and chemical characterizations of corn stover and poplar solids resulting from leading pretreatment technologies. *Bioresource Technol.* **100**(17), 3948–3962.

Marchessault, R. 1962 Application of infra-red spectroscopy to cellulose and wood polysaccharides. *Pure Appl. Chem.* **5**(1-2), 107–130.

Nasse, M.J. et al. 2011a. High-resolution Fourier-transform infrared chemical imaging with multiple synchrotron beams. *Nature Methods*, **8**(5), 413-416.

Nasse, M.J. et al. 2011b. Multi-beam synchrotron infrared chemical imaging with high spatial resolution: Beamline realization and first reports on image restoration. *Nucl. Instr. Meth. A*, **649**, 172-176.

Pandey, K.K. 1999 A study of chemical structure of soft and hardwood and wood polymers by FTIR spectroscopy. *J. Appl. Polymer Sci.* **71**(12), 1969–1975.

Pandey, K.K., Pitman, A.J. 2003 FTIR studies of the changes in wood chemistry following decay by brown-rot and white-rot fungi. *Int. Biodeterior. Biodegrad.* **52**(3), 151–160.

Ross, R. ed 2011. Wood handbook - Wood as an engineering material. USDA Forest Service, Forest Products Laboratory, Madison, WI. Gen. Tech. Rep. FPL-GTR-113.

Session 7

Nondestructive Evaluation of Structural Materials I— New Techniques and Approaches

Visual Timber Grader Device

Carlito Calil Neto
Laboratory of Wood and Wood Structures (LaMEM), University of Sao Paulo, Sao Carlos, Sao Paulo, Brazil, netousp@gmail.com

Carlito Calil Junior
Laboratory of Wood and Wood Structures (LaMEM), University of Sao Paulo, Sao Carlos, Sao Paulo, Brazil, netousp@gmail.com

Abstract

Differences in load resistance of over 100% are commonly found between two pieces of wood of the same species and same dimension, for two reasons: First, strength is strongly correlated with density of the wood; and second, other natural growth characteristics, in particular the nodes, have an adverse effect on resistance, and the extent and location of these are different in each piece timber. Moreover, maximum economy of material is achieved when variation of characteristics in a given class is limited and all parts are used to their full potential. This paper aims to present a patented device, small, cheap, and easy to use, for the classification of wood in accordance with the ASTM D 4761 standard. The classification process uses rules for classifying pre-sized wooden structural elements of various cross sections accounting for growth defects and density, and thus can improve utilization, safety, and economy in using the structural material.

Keywords: Device, visual, timber, grader

Introduction

The American system of visual classification structure was developed as a result of the search by designers for allowable stresses of the material that met the criteria for safety and economy. In 1923, the USDA Forest Service Forest Products Laboratory published a set of rules for classification, with some resistance values. These resistance values determined for classifying the best cut wood of a tree, were used essentially unchanged for 20 years.

World War II brought dramatic changes in the system of visual classification, and resistors project had a temporary increase. The U.S. Army has employed an extra 85% in resistance design. After World War II, some of the increases in resistance become permanent. At the same time, growth in demand for timber imposed pressure in the classification system, and other changes were made to the most efficient use of forest resources.

The most recent change was the creation of the standard PS 20-70 (American Softwood Lumber Standard), which took effect in September 1970. This standard incorporates several features, including fresh and dry dimensions for the determination of the shrinkage of wood. Under the requirements of PS

20-70, a national rule classification (National Grading Rule) was written determining characteristics uniform classification for all species of conifers in the size of rafters and boards.

According BREYER et al (1998) in 1978, a major research project entitled "In-Grade Test Program" was undertaken jointly between the timber industry and the U.S. Forest Products Laboratory (FPL). The purpose of the program "In-Grid" was the test pieces of wood visually classified. Approximately 73,000 beams of structural dimensions were tested in bending, tension and compression parallel to grain. According Galligan & MCDONALD (2000), sampling was conducted using the main wood species in the United States and Canada. To assist with testing elements of structural dimensions, two standards were written ASTM: ASTM D1990 (Standard Practice for Establishing Allowable Properties for Visually Graded Dimension Lumber From In-Grade Test of Full-Size Specimens) and ASTM D4761 (Standard Test Methods for Mechanical Properties of Lumber and Wood-Base Structural Material). The visual grading rules for many species were kept, and the name "In-Grid" includes the elements tested with wood available in the market in accordance with ASTM D4761.

Since 1991, the American standard sizing of structural elements, NDS (National design specification for wood contruction) began adopting as design values for beams and plates the results obtained in the "In-Grid".

In Brazil classification studies structural timbers were held in São Paulo University and recent Brazilian Standard NBR7190/2011 include with recommendations for the use of wood classified.

OBJECTIVE

Nowadays there are automated machines for classification for woods but with costs too high for use with structural elements of wood normally used in Brazilian constructions. Under these conditions, the main objective of this work is to propose a classifier that can sort by wood density and size in with very low cost and portable that could be carried in the pocket.

MAIN TEXT

The visual rating is based on the premise that the mechanical properties of a piece of wood are different from the mechanical properties of a piece of wood that is free from defects due to growth characteristics, and such characteristics can be viewed and judged by the human eye. With the aid of classification rules, the growth characteristics are used to select the wood into quality classes.

The classification rules are given by a percentage relative to the size of the face are measuring where that is, depending on analysing this face and its size, the size of acceptable defects will be greater or smaller. The visual timber grader device is divided into two "knives", and in each there are several knife blades of varying lengths depending on the size of the face to be classified and 1 cm thick. Made of transparent polymer for better visualization node, each blade has an opening angle of 360 degrees. This device can be various lengths, depending on what the size of the face that you want to sort. The choice of knife is used to define what will be considered part of the timber (the wide face and narrow face and corner of wide face) and each of the blades are marked sizes of defects acceptable according to the Brazilian standard for classification of wood NBR7190 / in 2011.

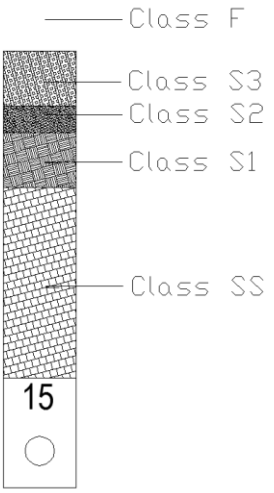

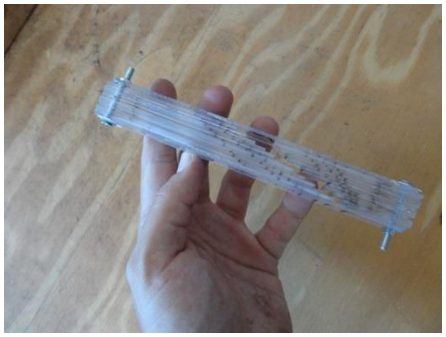

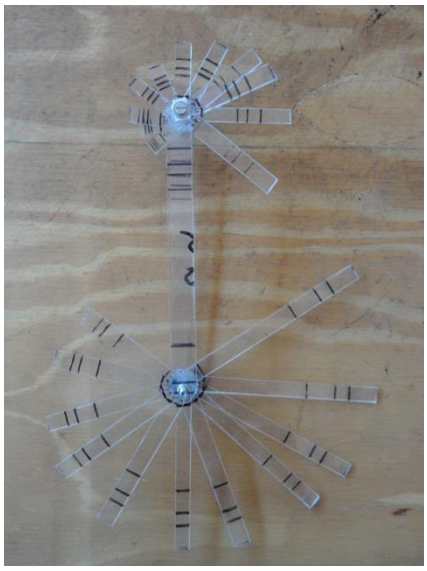

Figure 1: knife blade

Figure 2: Classifier timber device

At the beginning of the slide there is a number (2, 3, 4, 5, 6, 7, 8, 9,10, 11, 12, 13, 14, **15**, 16, 17, 18, 19, 20) means that the size this of the face which classifies.

Example classification: the wooden beam below we classify the piece of wood from the cross section of 10 cm wide (wide face) by 5 cm thick (narrow face) with the use of the device. For this we must first identify where the node are located, and what side should we use from the classifier timber device. Once identified we will use the "knife" right for each type of node we want to classify, to the wide face we use "switchblade" node broad face with the blade of 10 cm (for the face measures 10cm wide) to the corner of face and narrow face, we must use the "knife" in the corner of face and narrow face, with the blade 5 cm (for the narrow face measures 5 cm).

Figure 4: Using the classifier timber device

To sort the wood as dense and non-dense we must first identify the tops of lumber. We then place the blade of the knife assembly smaller with the letter D in the growth rings and see if we can put 4 or more growth rings.

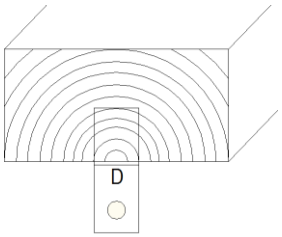

Figure 5: Using the knife D from classifier timber device

CONCLUSIONS

Today, the measurement of defects is performed visually, ie without the aid of any tool. In visual grading are observed diameter of knots and wood density, measured by the size of a knot and the number of growth rings. The classifier timber device proved to be a small outfit, low cost and good workability, be doing the work easier and fast for this kind of work.

Acknowledgments

The authors thank the University of Sao Paulo and the Laboratory of Wood and Wood Structures (LaMEM) for the support for this research.

References

ASTM (1998). West Conshohoken, PA: American Society of Testing and Materials.

ASTM D198-97. “Standard Methods of Static Test of Timber in Structural Sizes”.

ASTM D245-93. “Standard Practice for Establishing Structural Grades and Related Allowable Properties for Visually Graded Lumber”.

ASTM D1990-97. “Standard Practice for Establishing Allowable Properties for Visually Graded Dimension Lumber From In-Grade Test of Full-Size Specimens”.

ASTM D4761-96. “Standard Test Methods for Mechanical Properties of Lumber and Wood-Base Structural Material”.

Curry, W.T. (1969). “Mechanical Stress Grading of Timber. Timber Papers Nº 18”, Forest Products Research Laboratory, in: Conference on Non-Destructive Testing of Concrete and Timber, London.
Galligan, L. W. ; Mcdonald, K. A. (2000). “Machine grading of lumber – Practical concerns for lumber producers”. Gen. Tech. Rep. FPL-GTR-7 USDA, Department of Agriculture, Forest Service, Madison, WI.39 p.
Green, D. W. (1998). “Techline - Strength of Visually Graded Structural Lumber”. Was., D.C., FPL – FS – USDA, Department of Agriculture, Forest Service, Madison.

Grenn, D. W. ; Kretschmann, D.E. (1999). “Wood handbook—Wood as an engineering material - Chapter 6 - Lumber Stress Grades and Design Properties”. Was., D.C., FPL – FS – USDA, Department of Agriculture, Forest Service, Madison.Madsen, B. (1992). “Structural Behaviour of Timber”. Timber Engineering Ltd. Vancouver, Canadá.

NBR 7190 (1997). Projeto de Estruturas de Madeira. Rio de Janeiro, ABNT

Pigozzo, J. C. ; Pletz, E. ; Rocco Lahr, F. A. (2000). “Aspectos da classificação mecânica de peças estruturais de madeira”. VII Encontro Brasileiro em Madeiras e Estruturas de Madeira, São Carlos,SP.
Southern Pine Inspection Bureau (1994). “Standard Grading Rules for Southern Pine Lumber”. Pensacola,Fla.

Virtual grading of boards using high-speed CT data compared to visual board grading

Rafael Baumgartner
Department of Forest Utilisation, Forest Research Institute of Baden-Württemberg, Freiburg, Germany
rafael.baumgartner@forst.bwl.de

Norvin Laudon
Department of Forest Utilisation, Forest Research Institute of Baden-Württemberg, Freiburg, Germany
norvin.laudon@forst.bwl.de

Franka Brüchert
Department of Forest Utilisation, Forest Research Institute of Baden-Württemberg, Freiburg, Germany
franka.bruechert@forst.bwl.de

Udo H. Sauter
Department of Forest Utilisation, Forest Research Institute of Baden-Württemberg, Freiburg, Germany
udo.sauter@forst.bwl.de

Abstract

In the past, sawmill industry optimised the sawing with respect to volume recovery using the outer shape of the logs. A recently developed high-speed CT scanner capable of sawmill speeds makes it possible to sort according to internal quality by analyzing the internal features of the log prior to sawing.

In this study, a set of Norway spruce logs was CT-scanned and sawn to boards for panel production. These boards are produced by an initial breakdown, kiln drying and finally a second sawing process. An identification and marking pattern was used to track the position of the boards through each of the processing steps. The defects on the final boards were manually measured and the boards graded to visual grades. These grades were compared to virtual grades by locating the boards in the CT data using their actual positioning in the log. Internal defects in the logs were identified by automated defect detection algorithms working on the CT-data. These defects were intersected with the virtual board surfaces and graded according to the same rules as applied in the manual measurements.
This study shows that virtual grading can be simulated before initial breakdown and leads to similar results as visual grading of the fresh boards directly after sawing. Any features or defects which might develop after the initial breakdown, i.e. during the drying process, cannot be detected using this methodology. Virtual grading is also highly dependent on the defect detection and therefore the grading results can be improved by improvements to the detection algorithm.

Key words: sawn timber, grading, x-ray

Introduction

In the past sawmill industry optimised the cutting in respect to volume recovery using outer shape parameters of the logs. Inner quality could not be automatically measured so far. In 2011 a CT-scanner for sawmills was introduced to the public (Giudiceandrea 2011), which runs at an industrial speed of 120 m/min. This high-speed CT allows looking inside the logs and detecting various defects. With the

detected defects it is possible to optimise the cutting regarding quality. Berglund (2013) achieved a value increase of 13% on average by changing the cutting angle from “horns down” to the optimum with respect to knots.
Evaluation of optimisation has always the problem that the link to real boards is missing, because a log can only be sawn in one or the other way. For a chosen angle the sawn boards can never be proven to be the optimum for a specific log, as all other angles can only be simulated and the log cannot be cut a second time. Therefore an optimisation is only trustable if simulated grading is closely related to the real grading.
In this study the focus is on showing that position of a board in a log can be followed through primary breakdown, drying and secondary breakdown. This allows grading the surfaces on real boards and on the matching virtual surfaces in CT data. By comparing the two outcomes it is possible to evaluate the virtual grading of board surfaces in CT data.

Material and methods

In an industrial trial 74 Norway spruce (*Picea abies* (L.) Karst.) logs were cut to 148 cants using a cutting pattern with just two cants (Figure 3). Each cant was further cut to 5 pieces of sawn veneer after drying (Figure 1). These veneer pieces are an intermediate step in the production of three layer panels. The logs used for this trial had been sorted prior to cutting to fulfil a dimension requirement and only logs without rot are used for this product.

Figure 1— Five pieces of sawn veneer cut from one cant.

All logs were scanned with the Microtec CT.log at FVA prior to cutting. This CT is not running in industrial speed, thus the high speed data had to be created with simulation software using cone beam reconstruction. In longitudinal direction the voxel size was 10 mm, in the other two dimensions 1 mm. The algorithm proposed by Johansson et al. (2013) was run on these 3D data to detect knots. For grading the knots were intersected with the surfaces of the sawn veneer pieces. Figure 2 shows the colour image of a board surface under the virtual surface from CT data with the detected defects outlined.

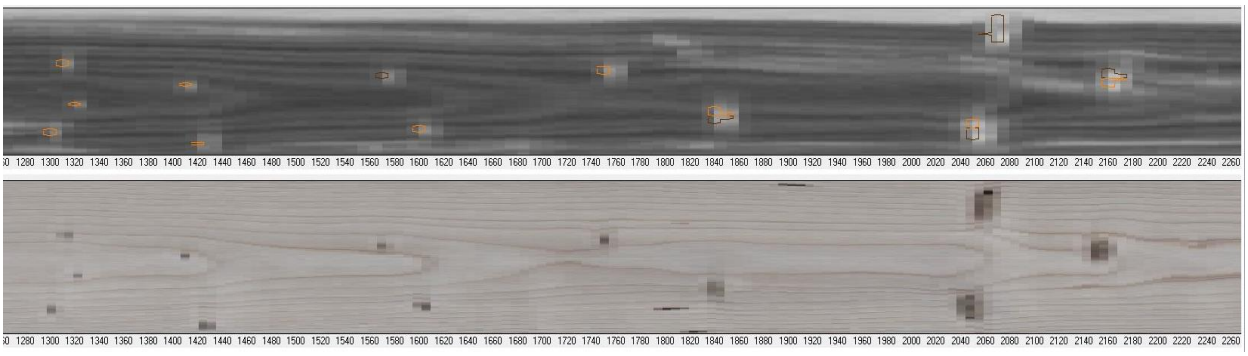

Figure 2— Colour image of one surface (bottom) and CT image with detected defects (sound knots orange and black knots brown) of the same virtual surface (top)

To find the surfaces of the cants or more importantly of the sawn veneers in the CT data the following marking system was used: On the butt end of each log a hole in longitudinal direction was drilled. This hole is visible in the CT image (black point in figure 3 between 12 and 1 o'clock marked with an arrow). A black line was drawn on the butt end cross section from the pith to this hole. The angle of this line and the pith position were measured on the cants before drying. With these measurements the cants can be positioned in the CT data (figure 3 on the left). For fine tuning of the position of the sawn veneers colour images were used.

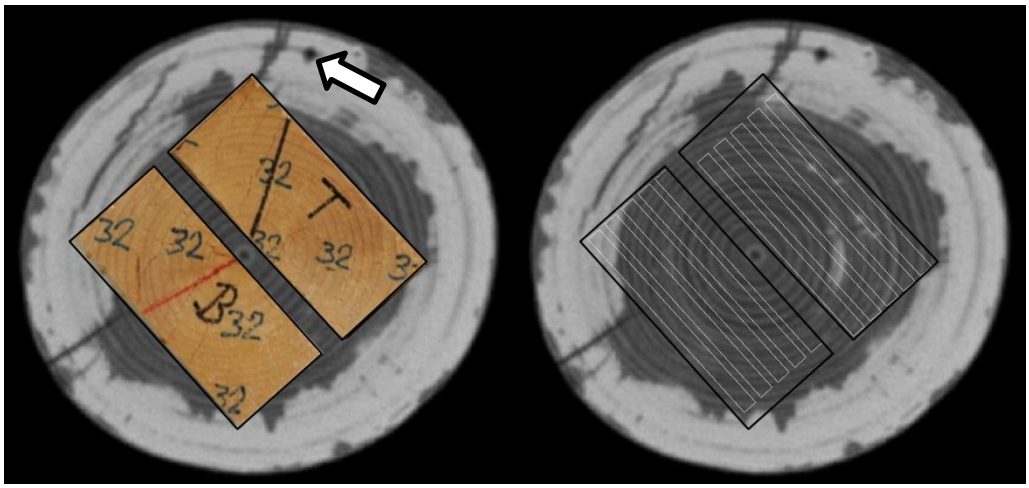

Figure 3— Colour images of the front face of the cants positioned in a CT image of the log (left) and position of sawn veneer in the cants in the same CT image (right)

For this study a subsample of 23 cants from 16 logs was taken, i.e. for 7 logs both cants were used, for 9 logs only one of the two cants was used. This approach allowed gathering all data for some logs, but still received a high variation for the features. With 5 pieces per cant this resulted in 115 pieces of sawn veneer with 230 flat surfaces.

Both flat surfaces of all veneer pieces were graded twice. First the surfaces were graded according to the knots automatically detected in the CT data. The second grading was done manually by measuring the largest sound and black knots on every surface.

The grading was carried out according to EN 13017-1 (2000) into the classes "A", "B" and "C" ("0" and "S" were not used) using the rules for knots only. EN 13017-1 (2000) is the relevant standard to which the three layer panels are sorted at the end of the production. According to this standard sound knots are allowed in class "A" up to a diameter of 40 mm and are not limited for class "B" and "C". Black knots are

not allowed in class “A”; in class “B” black knots are “occasionally allowed”, which was transformed to a limit of 20 mm; in class “C” size of knots is not limited.

Results

Each surface was graded twice, manually on real veneers and automatically from CT-data. Figure 4 shows pie diagrams of the distribution of the classes derived from all flat surfaces (two per board) graded to the same class.

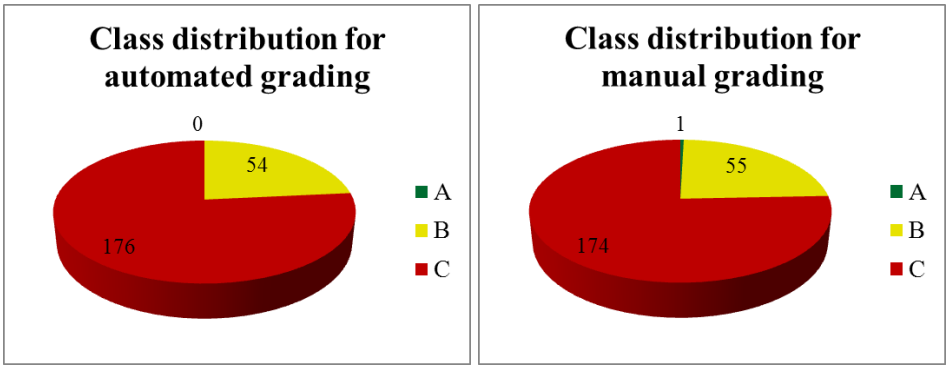

Figure 4— Frequency of the different classes for manual and automated grading

To compare the two grading operations more precisely it is necessary to compare the grades for each surface separately. Table 1 shows a confusion matrix of matching and mismatching assessment of the board surfaces, where all the surfaces were counted, that have the same manual and the same automated grade. For example, 31 surfaces were grade C for the automated procedure, but manually graded to be B.

Table 1—Confusion matrix for grading

	manual A	manual B	manaul C
automated A	0	0	0
automated B	0	24	30
automated C	1	31	144

32 of 230 surfaces (14%) were graded better by CT than by manual inspection (i.e. false negatives in the defect detection of automated grading). 30 surfaces (13%) were graded to a worse grade by CT (i.e. false positives in the defect detection of automated grading). All together 62 (30+1+31) surfaces (27%) were graded differently, and consequently 168 (24+144) surfaces (73%) were graded to the same grade.

Discussion

The data set used in this paper originated from a trial, which intended to be as close to the usual sawmilling process as possible. Of course an interruption was introduced by CT scanning, as the logs had to be transported to the CT scanner, scanned and brought back to the sawmill after the scans. Nevertheless the used marking system allowed to follow the orientation of the products during the whole process. Therefore grading of real and virtual surfaces can be compared.
The frequency of class A, B and C is similar for manual grading (1 A, 55 B, 174 C) and automated grading (0 A, 54 B, 176 C) (Figure 4). That is a difference of 1, 1 and -2 for grades A, B and C respectively. 27% were graded differently, while 73% were graded into the same class. Differences in grading can result from different sizes of the knots in manual and automated measurements. The differences are mainly caused by the detection of the dead knot border, i.e. the distance from the pith where the knot dies. This leads to some dead knots to be graded as sound knots in the automated

procedure, and some sound knots to be graded as dead knots. To improve this, the detection of the dead knot boarder has to be improved in the algorithm.
An additional reason for inaccuracies in the grading is the positioning precision of board surfaces in the CT data. The logs were marked, and pith and angle were measured on the cants manually which can introduce a small error in the position of the cants in relation to the logs. An additional error is caused by drying the cants. Due to the anisotropy of wood the shrinkage can be different in different directions and though for instance bow and twist of the cants can be produced. The sawn veneers were cut from the planed cants what means that the outer surfaces are straight planes in deformed cants. In the logs these surfaces have an irregular shape for deformed cants. Of course the deformation was held to a minimum by stacking in the kiln, but nevertheless for some cants it might have occurred. This means that for some veneers the surfaces graded in CT-data might be one or two millimetres off on one or the other end in relation to the manually measured surfaces. Therefore it might be possible that a knot appears dead on the surface of the real veneer, but appears sound in CT data, or vice versa.
The data set used in this trial includes mostly C grades. The reason are black knots which are limited for class B and not allowed in class A in EN 13017-1. EN 844-12 defines a black knot as a knot that is partially or fully black. Following this rule strictly every knot was identified as black knot, if there was only a tiny portion of disintegration from stem wood. But dependent on the value for use it might be more appropriate to limit only loose knots or dead knots, which can produce holes. That means knots that are only intergrown to a small portion or not intergrown at all would cause grade C, where other knots would be allowed for grade B or dependant on size even for grade A. That would mean that grade distribution of all the veneers would move to the better grades. Generally scientific grading results tend to lower grades than manual grading in practice, as in practice overall positive appearance might overrule one small negative defect.

Conclusions

This study showed that generally a grading of virtual surfaces is possible. The result of automated grading is similar to the manual grading. Using the rules for knots is just one part in grading of sawn products. By adding more defects a complete grading can be executed using CT data of logs. Of course this is limited to features that are already present in the logs. Drying splits, for instance, develop during drying and therefore cannot be detected in the CT data of the fresh logs, as they are not present at that time.
In the data set used the reason for downgrading was mainly “black knots”. Therefore an improvement for virtual sorting of the veneers for three layer panels could be achieved by improving the position of the dead knot border.
The product used in this trial is not very common in sawmill industry, but on the other hand showed that even a product, which was further processed after drying, can be virtually graded except for drying splits. For other products, especially with less processing, the results of automated grading prior to sawing can only be closer related to manual grading.

References

Berglund, A.; Broman, O.; Grönlund, A.; Fredriksson, M. 2013. Optimizing log rotation with an industrial computed tomography scanner. Computers and Electronics in Agriculture, 90: 152–158

EN 844-12: 2000. Round and sawn timber - Terminology - Part 12: Additional terms and general index

EN 13017-1: 2000. Solid wood panels - Classification by surface appearance - Part 1: Softwood

Giudiceandrea, F.; Ursella, E.; Vicario, E.; 2011. A high speed CT scanner for the sawmill industry. 17th International nondestructive testing and evaluation of wood symposium.

Johansson, E.; Johansson, D.; Skog, J.; Fredriksson, M. 2013. Automated knot detection for high speed computed tomography on Pinus sylvestris L. and Picea abies (L.) Karst. using ellipse fitting in concentric surfaces, Computers and Electronics in Agriculture, 96: 238-245

Moisture content image of subalpine fir board from near infrared hyperspectral images

Ataollah Haddadi-Goyaghaj
Faculty of Forestry and Environmental Management, University of New Brunswick, Fredericton, NB, Canada, ata.haddadi@unb.ca

James Burger
Burgermetrics, Riga, Latvia, james.burger@burgermetrics.com

Brigitte Leblon
Faculty of Forestry and Environmental Management, University of New Brunswick, Fredericton, NB, Canada, C:\Documents and Settings\pambyrd\Local Settings\Temporary Internet Files\Content.Outlook\MEV2EGRP\:bleblon@unb.ca,

Zarin Pirouz
FPInnovations, Wood Products, Vancouver, BC, Pirouz@fpinnovations.ca

Kevin Groves
FPInnovations, Wood Products, Vancouver, BC, Kevin.Groves@fpinnovations.ca

Joseph Nader
FPInnovations, Forest Operations, Pointe-Claire, QC, Canada, joseph.nader@fpinnovations.ca

Abstract

In this study, moisture content (MC) images of subalpine fir (*Abies lasiocarpa* Hook) boards were derived from near infrared hyperspectral images acquired by a line scan camera in the 947-1637 nm range. 107 samples with the size of 4×4×4 cm^3 were prepared. The samples were dried to various MC levels in several steps, and in each drying step hyperspectral images and weight measurements were collected. After processing all the images, the extracted spectra were then split into a calibration and a validation data set to build and validate a partial least square (PLS) regression model between the near infrared absorbance spectra and the measured MCs. We achieved an acceptable estimation accuracy with an RMSE of 11% for the validation data set. The model was then applied to the sample images and to the whole board images in order to produce 2D MC images of boards.

Keywords: board, hyperspectral imaging, moisture content, near infrared, PLS, subalpine fir

Introduction

Moisture content (MC) is one of the most important properties of wood products since it affects transportation costs as well as several processes, such as drying, resistance to biological deterioration and dimensional stability (Panshin and DeZeeuw 1980).

Oven-drying of wood samples is the most universally acceptable method for estimating MC, but it is destructive and time-consuming (Mora et al. 2011a; 2011b; Skaar 1972). An alternative is to use systems that are based on radiation measurements, such as near infrared spectroscopy (NIRS). In most of the cases, these systems only provide spot measurements as shown over black spruce (*Picea mariana* Mill.) frozen and unfrozen disks (Hans et al. 2013) and loblolly pine (*Pinus taeda* L.) disks (Mora et al. 2011a; 2011b; 2008). Thereby, they cannot measure the spatial variability of moisture content in the board. By contrast, hyperspectral imaging systems allow measuring wood physical and chemical properties through a non-destructive, contactless and real-time method as well as providing the spatial distribution of these wood properties across the products.

Hyperspectral imaging systems have been tested to identify compression wood in Norway spruce (*Picea abies* L.) and Scot pine (*Pinus sylvestris* L.) lumber (Hagman 1997; Nyström and Hagman 1999) and in Norway spruce stem cross-sections (Duncker and Spiecker 2009). They also have been tested for estimating density, microfibril angle and stiffness of loblolly pine wood strips (Jones et al. 2007). More recently, they have been used to map the chemical composition (Thumm et al. 2010), and MC and density of loblolly pine disks (Mora et al. 2011b). They were also used to map MC of European beech (*Fagus sylvatica* L.) and Scots pine (*Pinus sylvestris* L.) disk cross sections (Kobori et al. 2013).

This paper presents preliminary results on the development of a method to estimate MC images of subalpine fir (*Abies lasiocarpa* Hook) boards from near infrared hyperspectral images (NIR-HSI). Subalpine fir is native to western Canada and is gaining economic importance as the supply of lodgepole pine is reduced by the mountain pine beetle infestation. It is marketed as kiln-dried lumber and part of the SPF species group (spruce-pine-fir), which are used for structural components. Drying subalpine fir boards is difficult because they may contain wet-pockets (Watanabe et al. 2012). The drying rate of boards with wet-pockets is relatively low, as these boards require more drying time to reach a desired MC. Given that wet-pockets only occur in certain regions of the board, using a spot measurement system for estimating the MC leads to incorrect determination. Therefore, there is the need to use imaging systems that allow a good estimation of the spatial variability of the board MC, and thus a better optimization of the kiln drying process.

Materials and methods

Sampling and moisture measurements

The samples used for this study were extracted from 14 subalpine fir *(Abies lasiocarpa* Hook) boards having a size of 12×4×275 cm^3. All boards were first planed and were cut in two or three samples at different locations by a handheld circular saw and then recut to three smaller samples with the size of 4×4×4 cm^3. Samples were not chosen from the end of the boards and samples with visual defects, such as decay and big knots, were excluded from the measurements.

In total, one hundred and seven samples were prepared. In order to provide a wide range of MCs, these samples were dried and measured in multiple steps. At each step, the sample weight was measured using an electronic scale. At the last drying step, the oven-dry weight was measured and the moisture content (in percentage of the dry weight) of each sample was determined by:

$$MC(\%\text{dry basis}) = (M_{wet} - M_{dry})/M_{dry} * 100 \quad (1)$$

Where M_{wet} is the wet weight (g) of the sample and M_{dry} is the weight (g) of the oven-dry sample. The resulting range of moisture content (% dry basis) varied between 0% and 140%, with a mean value of 44.03% and a standard deviation of 28.82%.

Image acquisition

Hyperspectral images of wood were acquired using the *HyperSee* software (*Burgermetrics, Latvia*, www.burgermetrics.com) working with a *Specim´s* hyperspectral camera (*Spectral Imaging Ltd., FIN–90571 Oulu, Finland*). The system is a combination of a *N17E ImSpector* imaging spectrograph, and a temperature stabilized *InGaAs* camera.

The camera takes images by pushbroom type line scans in 320 pixels and 256 wavelength channels. The first four and the last 41 wavelengths were too noisy, so they were ignored during image acquisition and only wavelength channel #5 to #214 were considered. The extracted spectrum for each pixel can be considered as continuous between 947 and 1637 nm since the spectral sampling is 4nm. In addition to the camera and spectrograph, two more components should operate properly to get a high quality hyper cube image: the conveyor and the illumination unit.

The line-scan camera measure spectral information in one spatial dimension. The second spatial dimension is acquired by moving the target linearly, perpendicular to the camera imaging line. The height and focus of the camera were modified by trial and error to get sharp and high quality images with a minimum of one mm pixel size over the entire wood sample which allows observing the differences between latewood and early wood on the imaged samples. For both the small samples and the whole board, the camera was positioned at 48 cm height and has a fore lens having a focal length of 22.5 mm and a constant field of view (FOV) of 17.5°. Such setting allows scanning 15 cm width objects. The pixel size in the direction of the scan line was 0.6 mm.

A sufficient and homogeneous light over sample was provided by three ASD (http://www.asdi.com/) *PRO LAMP* studio lights around the imaging line of the camera. It is important to ensure that that the light source is stable during image acquisition.

To reduce image acquisition time and avoid unintentional drying of the small samples during imaging, samples were imaged in groups of 15 to 21. After 8 drying steps, 838 small images and their corresponding MC values were collected. We also acquired images of each whole board using the same camera setting. In both the small samples and the whole boards, the images were acquired on the radial section of the wood. Examples of the images that are acquired on both the small samples and the boards are presented in **Figure 1**.

a) small sample images *b) whole board*

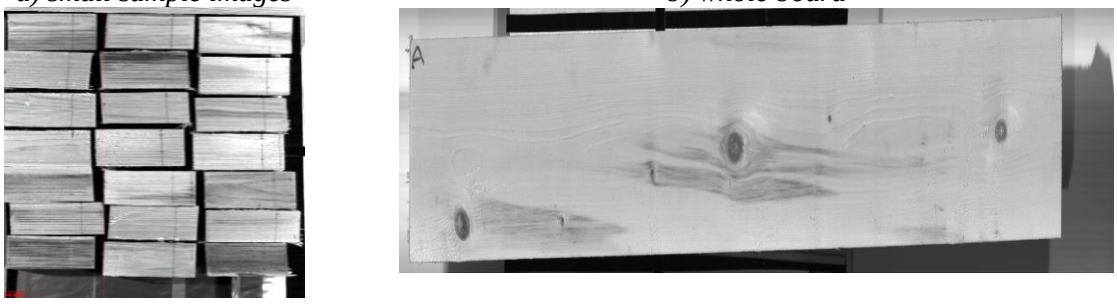

Figure 1—image of small samples and the whole board.

Image processing

The image processing included the following steps: 1) image calibration, 2) recovering bad pixels that produce extreme reflectance values at some wavelengths, 3) delineating the small samples on each image;

and 4) removing outlier spectra. The whole image processing was performed in *MATLAB 7.12.0 (970 West 190th Street, Suite 530, Torrance, CA 90502, U.S.)* and *ENVI-IDL* image processing software (*Exelis Visual Information solution, Boulder, Colorado, USA*).

The first step was to calibrate the camera detector and convert the image digital numbers into reflectance values. This step requires acquiring two images, one of a white reference panel and one of a black reference panel, both panels having known reflectance. Then the absorbance was calculated by log(1/R), where R is the reflectance. The near infrared wood spectra exhibited random reflectance maxima and minima at some wavelengths, called here "*bad pixels*". These extreme reflectance values can be recovered from the reflectance values of neighboring wavelength channels. Since the position of the bad pixels is the same in all images, they can be found using the black and white panel images and the reflectances of their neighborhood pixels can be used for recovering the corrected reflectance values of these "bad pixels" in all the images acquired of the wood samples. Overall, 2692 bad measurements in a measured frame (wavelength*pixel), which is 4% of the total number of measurements, were found and considered for recovering. After finding the wavelengths corresponding to extreme reflectance, the corresponding reflectance should be replaced by a corrected value. The corrected reflectance values were computed using a median filter. The median filter is applicable to non-linear data and considers the statistical data distribution (Richards and Jia 2006). The output excludes the values which do not fit the statistical pattern of the local neighborhood. It should be noted that only bad wavelengths were recovered, as the median filter was not applied to the whole spectrum, as shown in **Figure 2**.

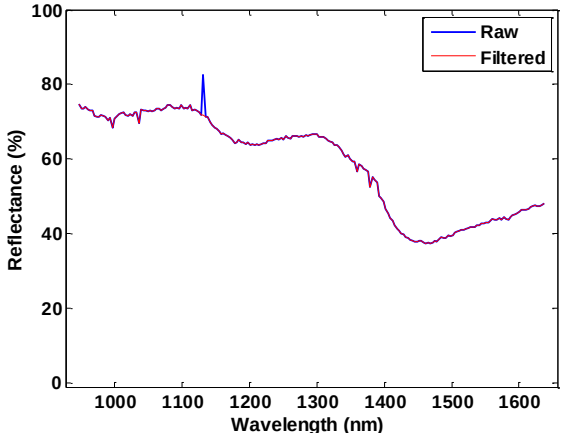

Figure 2—Raw and median-filtered spectra

Given that each image corresponded to 15 to 21 small samples, it needs to be divided into one separate file for each wood sample for further processing. This operation was performed manually in *ENVI* using a rectangle of 35 pixels by 50 pixels.

Among all of the sample image spectra, however there are some abnormal spectra which their pattern is different with the wood spectra called here "outliers". To find these outliers, we used a combination of the principal component analysis (PCA) and the *boxplot* method of Laurikkala et al. (2000). First, the spectra are transformed using PCA into a new space that has uncorrelated axis. PCA transformation allows easily identifying the outliers as being the spectra that are located outside the cloud which is made by the "good" spectra in the plane of the two first components. The Mahalanobis distance between the cloud median and the individual data can then be calculated. The distances are then used into the *boxplot* method to find the range of acceptable distance. The outliers are spectra that have a distance higher than the maximum distance range. Using the *PCA-boxplot* method, we found about 200 outlier spectra over the 1700 spectra of each small sample image (i.e. about 12% of the spectra) which were excluded from further analysis. The final spectra were directly used in the PLS modeling without any further denoising processing.

PLS modeling

Since there is one single MC value per sample, but more than 1000 spectra for each sample, each data consists of the mean spectrum of each sample image and its corresponding MC. The whole data set was split randomly into two datasets: a calibration one to calibrate the model relating the spectral information to MC and a validation one to validate the model. There are several multivariate linear analysis methods that can be used to build the model. We used here the partial least squares (PLS) regression because it is quick, accurate and suitable for data with many variables such as spectral data. It is especially useful when the data show a high level of multicollinearity, such as in our case, because the spectral reflectance values are not completely independent from each wavelength to another one.

PLS transfers the input variables to uncorrelated variables called principal components (PC). Since the first PCs have high information content and the last ones express noise and less important information content, the method only uses the first significant PCs to produce the regression method (Rosipal and Kramer 2006). In our case, we use the number of components that minimizes the root mean square error (RMSE) between measured and predicted MCs for the validation data set. We found that 8 was the number of components that corresponds to the minimum RMSE. A model with 8 components explained about 84% of the variation in MCs value. A high number of components are not optimal as it just increases the noise and variance of the weights of the predictors which leads to over-fitting.

The quality of both the calibration and validation was assessed using the following statistics: 1) coefficient of determination (R^2) between measured and predicted MC values and its associated *p*-value and significance level; and 2) the RMSE between measured and predicted MC.

Results and discussions

In order to relate the MC to the spectral data, we built a PLS model with the calibration data set. It gives an R^2 of 0.84 and an RMSE of 11.67 %. When it is validated over the other data set, the resulting R^2 is 0.83 and the RMSE is 11.84% (**Figure 3**). In both cases, the R^2 is significant at p-value < 0.001. The scattering plots for the model shows a better correlation between NIR spectra-predicted and measured MCs at low MC levels than at high levels of MC values. The RMSE for the validation model with the MC values of less than 50% is reduced from 11% to 8%. The better model for low MC levels can be due to the fact that samples with high MC levels have more variable.

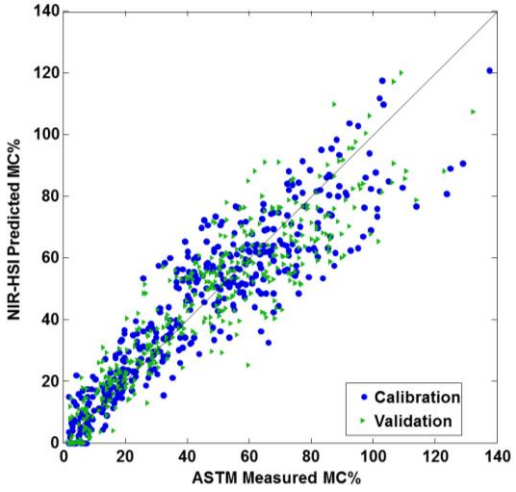

	Calibration	Validation
N	419	419
RMSE	11.67%	11.84%
R2	0.84	0.83
p-value	< 0.001	< 0.001

Figure 3—PLS model built with 8 components

Our obtained R^2 and RMSE values are lower than those published in Kobori et al. (2013) who used HSIs in the visible and near infrared spectral domains. They are on the same order as the ones obtained by Mora et al. (2011b) who used HSIs acquired in the 1005-1645 nm range to predict MCs of loblolly pine disks. In Mora et al. (2011b)'s study, the estimated MCs were in the range of 45% to 65% (dry basis), whereas in our case, the range of variation for the estimated MCs is higher (from 0% to 140%). Our PLS modeling results are especially good given that they were obtained by NIR images acquired on radial surfaces, which usually result in poorer PLS models than those computed with spectral measurements made over the transversal section (Leblon et al. 2013).

Figure 4 shows the MC image derived from some wood sample images that were selected to represent the whole MC range of the samples. For each image, beside the measured MC value and the mean estimated MC value, the figure also presents the histogram of MC distribution showing the variation of the MC over the small sample. The histogram width gives some information about the precision of the PLS model (Burger and Geladi 2006). The MC variation was greater for high MC values than for low MC values. As the board is drying, the distribution of the MCs becomes more homogeneous and the rate of water loss is decreasing.

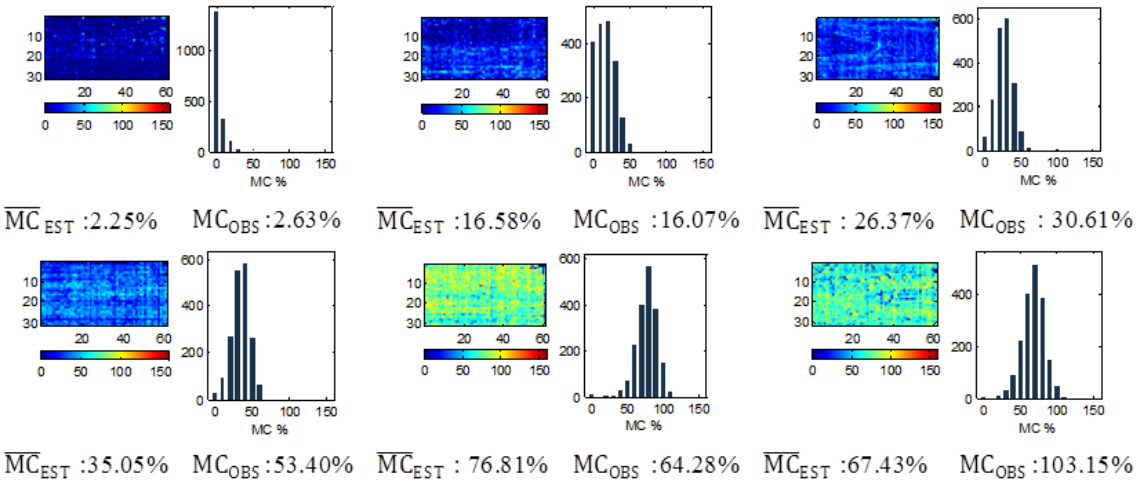

Figure 4—2D images of moisture content for small samples and their corresponding MC histogram. The samples have been selected to represent the whole range of MC variations

The good agreement between measured and estimated MC values confirms an acceptable accuracy of the PLS model. This model can then be used with image data acquired over the whole board to produce a 2D MC image that provides the distribution of MC across the board, such as the one of **Figure 5**. Beside the variation in MCs, the images also show the growth rings with the distinct early wood and latewood and also some defects such as knots which have lower MC than the other parts of the board. Additionally in some parts of the board, we can see the wet-pockets which appear as clear spots in the first image of **Figure 5**.

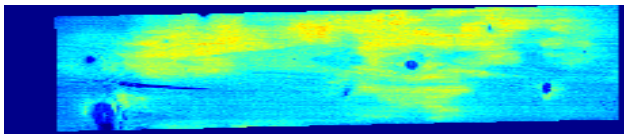

A

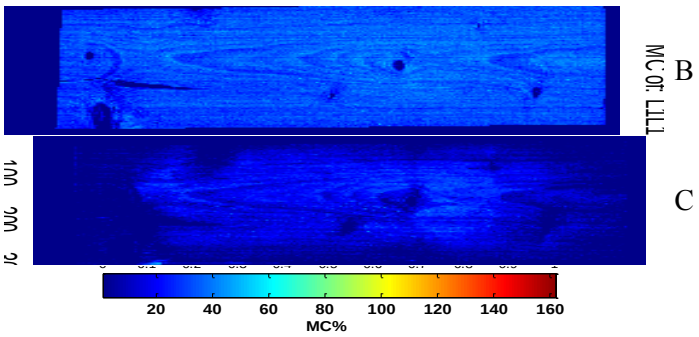

Figure 5—2D image of moisture content for a whole board. The average MC of A, B, and C is 66.29%, 30.43%, and 8.31% respectively. The image of D is the same board in X-ray images

Conclusion

A PLS model was developed to estimate MC variation on the surface of subalpine fir boards based on NIR spectra extracted from hyperspectral images. The method is based on NIR radiation that has a limited penetration depth in solid wood, from 1 to 5 mm depending on surface roughness and the wavelength used (Sykes et al. 2005). However, we were able to achieve an estimation accuracy is 11% for the validation data set, which is acceptable for applications such as presorting boards before drying, and the accuracy improves to 8% when MC is less than the FSP. The MC distribution across board is particularly relevant to species such as subalpine fir which have wet-pockets and are difficult to dry due to high variability of MC within the board.

Although in our study we only derived board MC images from NIR hyperspectral images, similar methods can also be applied to produce 2D images for other chemical components in wood. This will be the subject of future work.

Acknowledgements

The authors thank G. Chow from FPInnovations as well as K. Phung (UNB) for their help during the experiments. The study was funded by a NSERC Strategic Grant awarded to Leblon et al.

References

Burger, J.; Geladi, P. 2006. Hyperspectral NIR image regression. Part II: Dataset preprocessing diagnostics, J. Chemometrics, 20: 106–119.

Duncker, P.; Spiecker, H. 2009. Detection and classification of Norway spruce compression wood in reflected light by means of hyperspectral image analysis. IAWA J. 30(1):59-70.

Hans, G.; Leblon, B.; La Rocque, A.; Stirling, R.; Nader, J.; Cooper, P. 2013. Monitoring moisture content and basic specific gravity of black spruce logs using a handheld MEMS-based near infrared spectrometer, Forestry Chronicle (*accepted*).

Hagman, O. 1997. Multivariate prediction of wood surface features using an imaging spectrograph, Holz als Roh und Werkstoff, 55: 377-382.

Kobori, H.; Gorretta, N.; Rabatel, G.; Bellon-Maurel, V.; Chaix, G.; Roger, J.M. Tsuchikawa, S. 2013. Applicability of Vis-NIR hyperspectral imaging for monitoring wood moisture content (MC), Holzforschung 2013; 67(3): 307–314, DOI 10.1515/hf-2012-0054.

Laurikkala, J.; Juhola, M.; Kentala, E. 2000. Informal identification of outliers in medical data. In: 14th European Conference on Artificial Intelligence and 5th International Workshop on Intelligent Data Analysis in Medicine and Pharmacology IDAMAP-2000 Berlin, 22 August, 2000, ECAI-2000, 24-28.

Leblon, B.; Adedipe, O.; Hans, G.; Haddadi, A.; Tsuchikawa, S.; Burger, J.; Stirling, R.; La Rocque, A.; Pirouz, Z.; Groves, K.; Nader, J. 2013. A review of near infrared spectroscopy for monitoring wood moisture content and bulk density, Forestry Chronicle (*accepted*).

Mora, C.R.; Schimleck, L.R.; Clark III, A.; Daniels, R.F. 2011a. Determination of basic density and moisture content of merchantable loblolly pine logs by near infrared spectroscopy, J. Near Infrared Spectroscopy. 19(5): 391-399.

Mora, C.R.; Schimleck, L.R.; Yoon, S, Thai, C.N. 2011b. Determination of basic density and moisture content of loblolly pine wood disks using a near infrared hyperspectral imaging system, J. Near Infrared Spectroscopy, 19(5): 401-409.

Nyström, J.; Hagman, O. 1999. Real-time spectral classification of compression wood in *Picea abies*, J. Wood Sci. 45:30-37.

Panshin A.J.; DeZeeuw C. 1980. Textbook of wood technology: structure, identification, properties, and uses of the commercial woods of the United States and Canada. 4th Ed. McGraw·HiI1 Book Co., New York, p. 772.

Richards, J.A.; Jia, X. 2006. Remote sensing digital image analysis, Springer-Verlag Berlin Heidelberg, p. 439.

Rosipal, R.; Kramer, N. 2006. Overview and recent advance in partial least square, Springer-Verlag, Berlin, pp. 34-51.

Skaar, C. 1972. Wood-water relations, Springer-Verlag, Berlin, p. 283.

Sykes, R.; Bailian, L.; Goldfarb, B.; Kadla, J.; Chang, H.M. 2005. Prediction of loblolly pine wood properties using transmittance near infrared spectroscopy, Can. J. For. Res. 35: 2423–2431.

Thumm, A.; Riddell, M.; Nanayakkara, B.; Harrington, J.; Meder, R. 2010. Near infrared hyperspectral imaging applied to mapping chemical composition in wood samples. J. Near Infrared Spectroscopy 18(6): 507-515.

Watanabe, K.; Mansfield, S.; Avramidis, S. 2012. Wet-pocket classification in *Abies lasiocarpa* using visible and near infrared spectroscopy, European Journal of Wood and Wood Products, 70: 61-67.

Comparison of local variation of modulus of elasticity determined on basis of scanned fiber angles and full strain field measurements

Min Hu
Department of Building and Energy Technology, Linnaeus University, Sweden, Email: min.hu@lnu.se

Marie Johansson
Department of Building and Energy Technology, Linnaeus University, Sweden, Email: marie.johansson@lnu.se

Anders Olsson
Department of Building and Energy Technology, Linnaeus University, Sweden, Email: anders.olsson@lnu.se

Bertil Enquist
Department of Building and Energy Technology, Linnaeus University, Sweden, Email: bertil.enquist@lnu.se

Abstract

Laser scanning of fiber angles has shown to be a powerful tool to establish bending MOE profiles along boards. This study aims at investigating the accuracy of the MOE variation determined on basis of fiber angles obtained from laser scanning. Material employed was a board of Norway spruce of dimension 50×150×3900 mm. Firstly fiber angles on four surfaces were identified using a WoodEye scanner and based on the fiber angles the MOE profile which was calibrated according to the longitudinal resonance frequency was established. Thereafter the board was subjected to bending and during loading an image correlation system, ARAMIS, was engaged to detect the strain field. Subsequently the strain field was used to obtain the MOE variation. The MOE profiles determined in two different ways were compared and they showed close compliance. However, differences were found as well. The research thus contributes to further improvement of a newly suggested grading method.

Keywords: Finite element analysis, Strength grading, Fiber angle scanning, Strain field, Image correlation

Introduction

Most strength grading machines on the European market are based on the relationship between a measured MOE for each board and the bending strength. An assumption often made is that the measured MOE is valid for the whole board. In reality, knots and other defects cause large variation in stiffness along boards and if this variation could be taken into account better predictions of strength could be reached. Many studies have shown that with better knowledge of local variation of the MOE, a higher coefficient of determination (R^2) with respect to bending strength could be obtained (e.g. Isaksson 1999). In this context, measurement of fibre angles using laser scanning has shown to be a powerful tool. As wood is a strongly orthotropic material, with high stiffness in the fibre direction, deviation in fibre orientation around for example knots causes considerable reduction in the bending stiffness. With knowledge of fibre orientation from laser scanning it is thus possible to calculate a

bending stiffness profile along an individual board. Moreover, this can be done at a speed corresponding to the production speed at sawmills and hence it can be utilized for commercial strength grading purposes.

The aim of the present study is to study the MOE profile established based on full-field displacement measurement along a board during a bending test and compare this profile with the MOE profile based on fibre angles from laser scanning as suggested by Olsson et al. (2013). A 3D non-contact deformation measurement system ARAMIS® was employed to capture the displacement field of one surface of a board exposed to pure bending. The displacements were detected at known stress levels and therefore a MOE profile could be established and compared with the one established on basis of fibre orientation information.

Material

A board of Norway spruce was chosen for the study from a sample collected from southern Sweden. The choice was made because of the board's relatively large defects/knots and distinct weak sections along the longitudinal board direction. Dynamic test has been carried out on this board earlier (Hu et al. 2011), and the dynamic MOE (cf.Table 1) in accordance with the first axial natural frequency has been registered. The relevant material properties are found in Table 1. Before the tests, the board was conditioned in a climate room with a temperature of 20˚C and a relative humidity of 65%.

Table 1--The relevant material parameters of the specimen.

Material parameter	Value
Dimension	50×150×3900 mm
Density	454kg/m^3
1st axial frequency	637Hz
Dynamic MOE	10.98GPa

Method and measurements

The laboratory measurements provided data of 1) 3D coordinates on one surface of the board before and after deformation and 2) fiber angles on four surfaces of the board. The test set up and measuring procedures are further described below. In addition to the laboratory tests, the study also comprises numerical calculation and FE modeling which were implemented using the software MATLAB/CALFEM®.

Strain measurement on board subjected to static bending

As mentioned before, an image correlation system ARAMIS was used to capture the deformation field along the board. ARAMIS is a contact free measuring system which provides 3D surface coordinates. It recognizes surface structure of the studied object in digital camera images and allocates coordinates to image pixels. ARAMIS records images before, during and after deformation and the first image recorded represents the undeformed state. The recorded digital images are applied for calculating the deformations (GOM 2009).

To facilitate a constant bending moment along the whole board, for creating a MOE profile based on the strain measurements, the board was lengthened by finger jointing an extra 550 mm long board at each end of the original board (cf. Figure 1). The bending test as sketched in Figure 1 was arranged as four-point bending where the board was symmetrically loaded at two points over a span of 3900 mm. In such a case, the mid span i.e. the whole original board was exposed to a pure constant bending moment without shear. The board was loaded at five different load/stress levels, i.e. five load stages were applied, and the correponding load/stress level of each load stage are reported in Table 2. To record deformation along the whole mid span, twelve ARAMIS projects, each covering a measuring area of 480 × 480 mm on the object surface, were created along the board for each load stage. This

gave a resolution of the ARAMIS measurement that was approximate 3 mm in both *x*- and *y*-direction. With the aid of another contact free measurment system, TRITOP, the twelve separate ARAMIS projects were combined into one project shareing a global coordinate system (Oscarsson 2012).

Table 2 The load stages of ARAMIS measurment.

Stage no.	0	1	2	3	4
Nominal load *F* [kN]	0.5	2.0	4.0	5.5	7.0
Nominal stress σ [MPa]	1.5	5.9	11.7	16.1	20.5

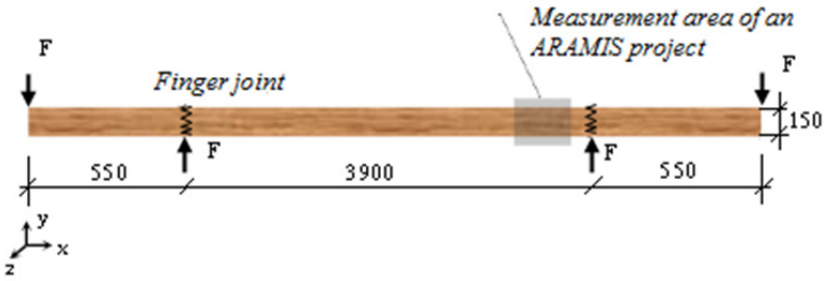

Figure 1 Four point bending test setup, length unit [mm].

Fiber angle detection using a WoodEye scanner

A WoodEye scanner from Innovative Vision AB was used to detect the fiber angles on the board surfaces. A WoodEye scanner is mainly equipped with four sets of multisensor cameras, dot and line lasers and conveyor belts. To detect the fiber orientation on wood surfaces it ultilizes the so called tracheid effect which means that the most extended principal axis of light intensity distribution around a laser dot is oriented in the direction of the fiber. Figure 2 shows an example how the fiber directions on a wood surface are identified using the tracheid effect. The photograph to the left shows a wood surface including a knot; the middle image shows how the light from dot lasers spread on the wood surface and the right plot displays the identified fiber orientation. The local fiber angles on four surfaces of a wooden board are registered when a board is fed through the scanner. The resolution employed for the scanning data, i.e. the distance between laser dots, is 0.8 mm in *x*- direction (along the board) and 3.6 mm in *y*- direction (across the board, cf. Figure 1). For further information regarding the WoodEye scanner, reference is made to Olsson et al. (2013).

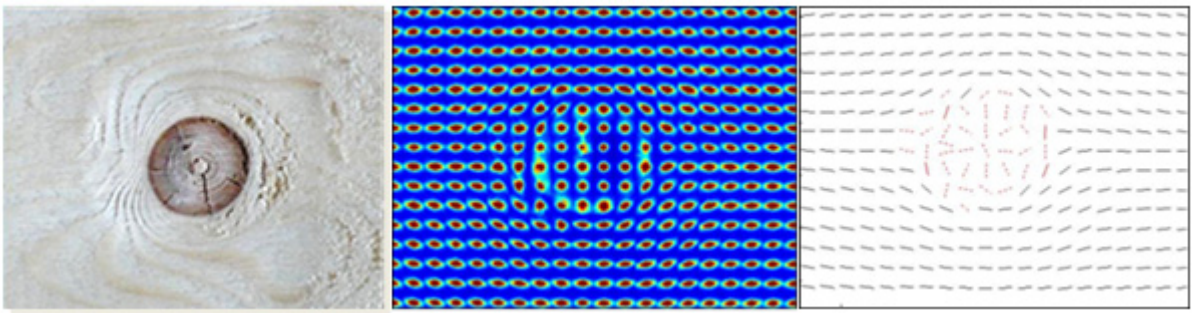

Figure 2 A wood surface containing a knot (*left*); an image illustrating the tracheid effect (*middle*); the fiber orientation on the wood surface identified by ultilizing the tracheid effect (*right*) (Olsson et al 2013).

Calculation of bending MOE based on ARAMIS data

The displacement data from ARAMIS of load stage 1 and 4, of which the nominal normal stress levels are 5.9 MPa and 20.5 Mpa, respectively, was used to establish the MOE profile. The calculation was carried out as follows:

- The object surface was divided into small rectangular subareas which conformed to the spatial resolution of the ARAMIS displacement data, and the data was rearranged in the form of a matrix. Each column/row in the matrix represented data points located on one vertical/horizontal line. In addition, each column of subrectangulars as a whole was regarded as a 'section' representing an unique position in *x*- direction.
- The relative displacements of adjacent data point were used to calculate strains. However, the so calculated strain field includes a lot of noise, cf. Figure 3 (top).
- To suppress the noise, a smoothing function was applied. It calculates the average strain over a selected surrounding area and assigns the average value to the subrectangular in question. The strain field after smoothing is shown in Figure 3 (down), where the average value is calculated over an area of 12×12 mm.
- Thereafter, a linear regression line for the strains of each section was estimated, and the position of the neutral layer, denoted $\bar{y}$, was set to coincide with the *y* coordinate where the linear strain achieved the value of zero. The linear regression of two selected sections are shown in Figure 3 to provide a general idea of how well the regression models fit the calculated strains. In accordance with Euler-Bernolli beam therory, the bending stiffness *EI* of each section was obtained as:

$$EI = \frac{M(y_m - \bar{y})}{\varepsilon_m} \quad (1)$$

  where *M* is the bending moment, y_m and ε_m is a *y* coordinate and the corresponding strain value, respectively, on the line of regression. The *EI* profile for the whole board was obtained by considering *EI* values of all sections along the board.
- At last, the bending MOE profile was obtained as:

$$\boldsymbol{MOE = \frac{EI}{I_h}} \quad (2)$$

  where I_h is the nominal second moment of inertia. Note that it is dependent only on the dimension of the cross section.

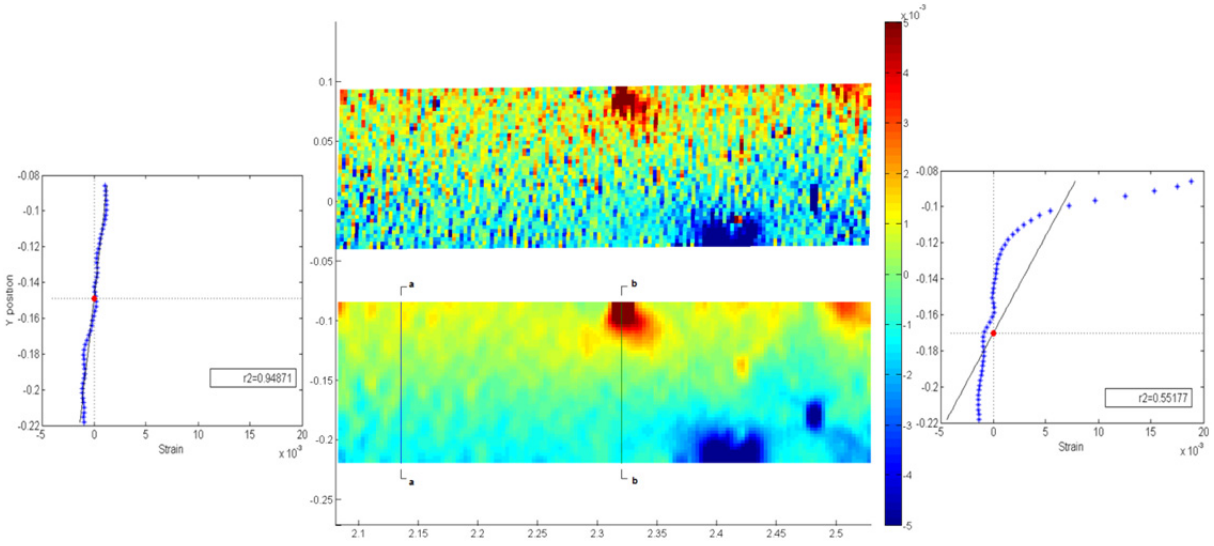

Figure 3 Illustration of the effect of the smoothing function and the linear regression implemented on the smoothed strains. The middle part shows color plots of strains in the longitudinal direction of the board calculated on basis of an ARAMIS project before (*top*) and after (*down*) application of the smoothing function. The graphs at both sides show the scatter plot of the smoothed strains and the corresponding regression line for section *a-a (left)* and *b-b (right)*. The red dots in the graphs indicate the position of the neutral axes. *r2* values displayed are the coefficients of determination of the regression model.

Calculation of bending MOE on basis of fiber angle

Olsson et al. (2013) suggests a scheme for calculating bending MOE profile based on the fiber angles and shows that rather accurate prediction of bending strength can be performed on basis of such

profiles. In the method presented four surfaces of boards are scanned with dot lasers in a WoodEye scanner. Transformations taking material properties in different directions into account give basis for calculation of local material stiffness in board direction which in turn gives basis for establishing a MOE profile valid for bending. Important assumptions in the method are that: a) density (ρ) and the MOE in the fiber direction (E_l) are constant within a board, b) other stiffness parameters than E_l are linear functions of E_l, c) fiber angles detected on surfaces are located in the *l-r* plane, d) the fibers are oriented in a plane which coincide with the wood surfaces, i.e. the so called diving angles are assumed to be zero and e) the fiber angles detected on a surface are representative for the fiber orientation to a certain depth within the board. Thus, except the density ρ, which is determined as the mass of the board divided by its volume, the only parameter that has to be determined individually for each board is E_l. This parameter is determined by an eigenfrequency analysis on a simple finite element beam model. The model employs the transformed MOE variation along the board and E_l is obtained by achieving the same natural frequency from the model as the one determined experimentally. The steps taken to calculate the MOE profile can be described as follows:

- The fiber orientation in each data point with spatial resolution of 0.8 ×3.6 mm is calculated.
- The material properties are transformed from the local direction to the board direction, whereby particularly the material stiffness in the longitudinal direction of the board, $E_x(x,y)$, is calculated.
- The global bending stiffness based on the transformed MOE variations are used in a simple finite element model for an eigenfrequency analysis to achieve the same resonance frequency as the one determined experimentally, whereby the value of E_l and accordingly $E_x(x,y)$ get calibrated for the particular board in study.
- By applying assumption e) mentioned above, i.e. that for a given position (x, y), a same value of E_x applies over a certain thickness (in z- direction), the cross-sectional bending stiffness with respect to z- axis could be calculated as:

$$\boldsymbol{EI = \iint E_x\,(y - \bar{y})^2 dA} \qquad (3)$$

- Finally, the bending MOE for each position along the board was obtained as:

$$\boldsymbol{MOE = \frac{EI}{I_h}} \qquad (4)$$

  where I_h is the nominal second moment of inertia which is dependent only on the dimension of the cross section.

For a more detailed description of the procedure, reference is made to Olsson et al (2013).

Results and discussions

The MOE profiles estimated from the strain and fiber angle measurements, with their respective maximum resolution, as well as an image of the four surfaces of the actual board are shown as the top part of Figure 4. In the full resolution plot despite the rippled pattern observed on both curves, which is due to the high resolution and noise, it appears that the weak sections according to calculated MOE profiles based on fibre angle data from WoodEye and from strains detected by ARAMIS, respectively, are closely correlated. To even out some of the noise, 80 mm moving average of the MOE is performed and the resulting curves are presented as the second plot of Figure 4. When comparing the curves with the board image it is found that the MOE profiles drop at positions where knots are observed on the board surface. Based on different methods a mean value of the MOE for the whole board can be calculated (cf. Table 3). It should be noted that the mean MOE calculated from ARAMIS strain is given as a range which is due to the load uncertainty during the measurement. As stated earlier, it was necessary to move the cameras along the board and create twelve ARAMIS projects to cover the whole S2 surface and for each load stage this process took 30 minutes. We aimed at applying a constant load, but some variation in the applied load level could not be avoided. Overall the load level of each stage might vary ±200 N which corresponds to ±0.97 GPa in the estimated MOE. At this point, small discrepancies are found for the mean values of evaluated MOE presented in Table 3.

Table 3—The mean value of MOE based on the the first longitudinal resonance frequency, the fiber angle data and the strain(in *x*- direction) measurements respectively.

Method	Resonance frequency	Fiber angle	Strain
Mean MOE [GPa]	10.98	11.32	12.20±0.97

The color image in the middle of Figure 4 shows the strain field in *x*- direction of S2 which indicates compressive strains at the top and tension strains at the bottom. It is also possible to observe strain concentrations around knots which are visible on the wood surface. As shown in Figure 4, regarding the position of weak sections and the absolute value, some parts of two curves end up with a very good agreement and some parts do not. One discrepancy can be seen in the left part of the curves where the MOE based on strain data gives a higher maximum level than the one based on fiber angles. The model based on fiber angles assumes a constant E_l along the whole board which for this particular board is probably not true. The higher mean MOE in the left end of the board pointed out by the ARAMIS strain result might be caused by the growth conditions for the tree.

For the individual drops in the curves it is also possible to see very good agreement in some positions and worse agreement in other positions. This is related to the calculation model and to the type of knot groups present in different sections. Typical examples for two different type of knot groups are shown by the highlighted zones, A and B, at the bottom of Figure 4. In the longitudinal board direction, the knots in zone A are spread out, whereas knots in zone B are positioned in a narrow band.

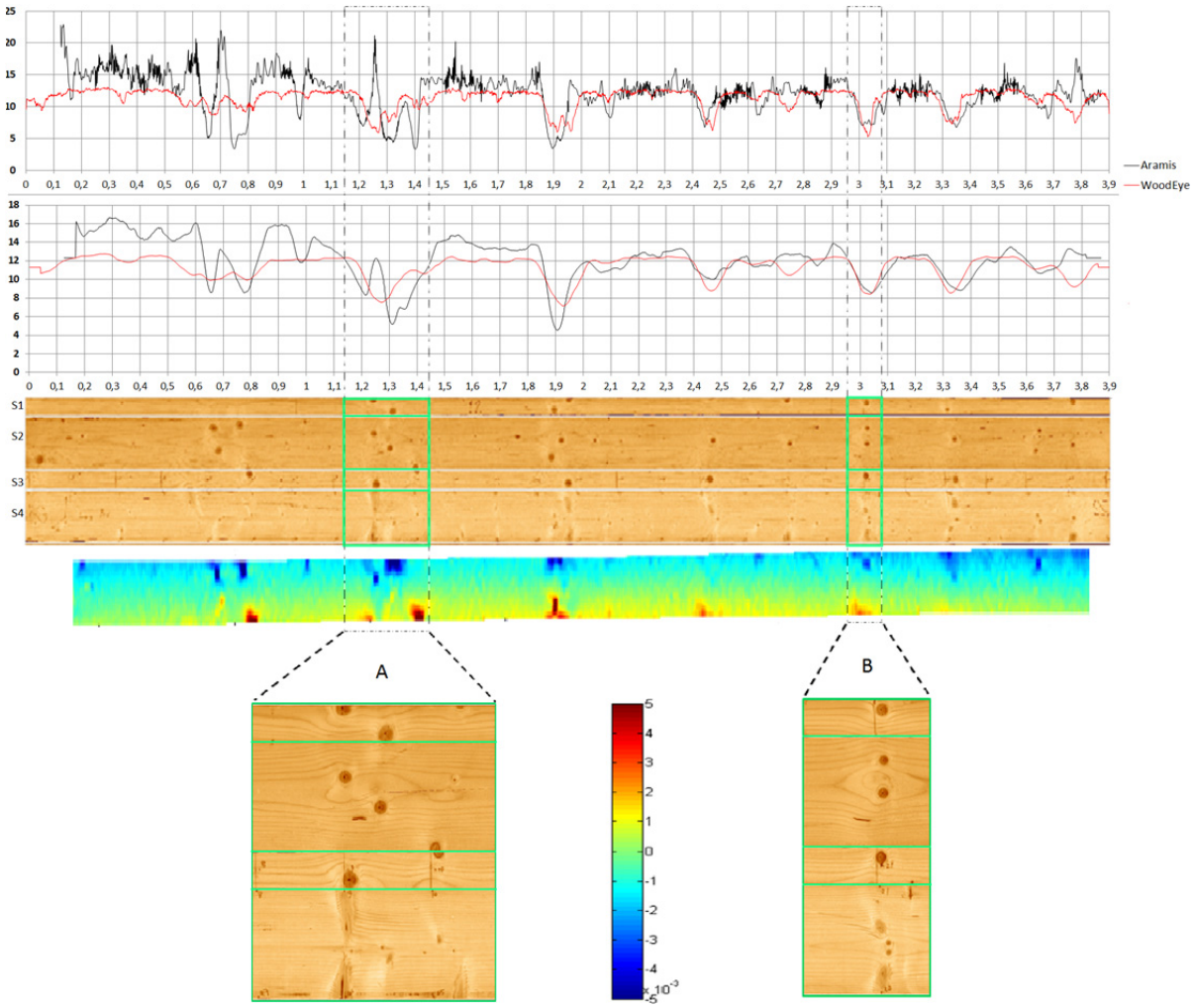

Figure 4— Diagrams of the estimated MOE profiles based on fiber angle scanning and strain measurements (denoted "WoodEye" and "ARAMIS", respectively), photographs of the board surfaces and the estimated *x*- strain based on ARAMIS data. *Key:* the top two diagrams show

MOE variation with the maximal resolution (*up*) and with a resolution of 80 mm (*down*). The middle parts show the photographs of all four surfaces marked as S1~S4 of the board, extracted from the WoodEye scanner. The next plot shows the strain field on the S2 surface after the smoothing function is applied, and the color scale employed is shown below. The two pictures at bottom illustrate the enlargement of two segments of the board surfaces.

Zone A thus contains a knot cluster that is spread out over 150 mm in longitudinal board direction while zone B embraces a knot cluster that is well collected in longitudinal direction. On the lower edge of the strain image large tension strains can be detected even without knots visible on the S2 surface. This is an influence of the knot which is visible on the S3 surface. It shows that based on strains measured on only one surface of the board the strains detected using ARAMIS system is capable of capturing the weaknesses in the board which are not visible on the surface in study. The same effect can also be observed for zone A where the knots on S1 and S3 have an influence on the strains field of S2. For zone B the MOE profiles calculated based on both strain and fiber angle data show the same minimum value at the same location. All the knots in zone B are located almost at the same position in the longitudinal board direction. Therefore a very good agreement on position is obtained. For zone A different patterns of the two MOE profiles are found. Two sharp drops appear in the 'ARAMIS profile' but only a single drop in the 'WoodEye profile'. The knots in zone A is more spread out in the longitudinal direction. When we look at the strain pattern it is possible to see that there are large effects of knots at two sections corresponding to the two drops in the 'ARAMIS profile'. While the laser scanning measurement shows disturbances in the fiber angles in the area between the knots which result in one wide flat drop in the MOE profile.

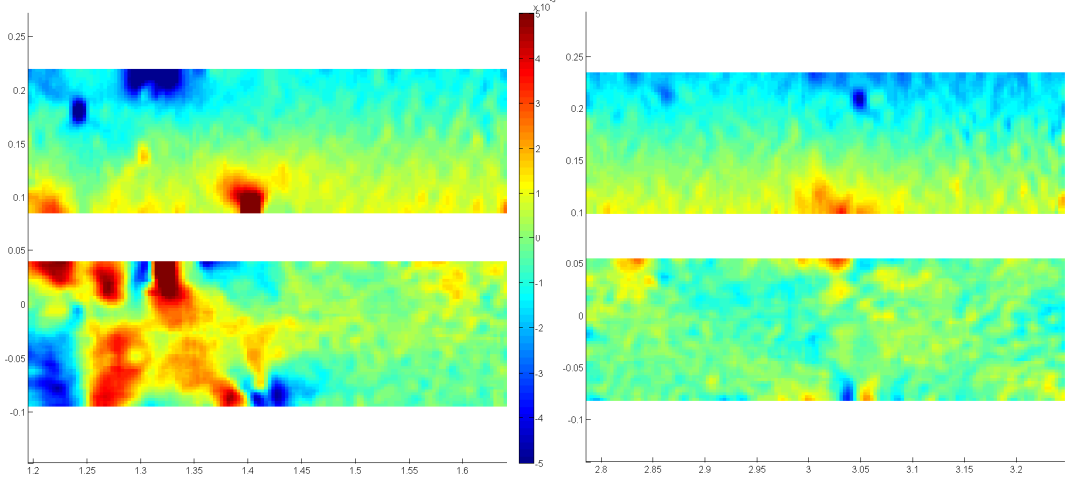

Figure 5- The *x* strains (*up*) and shear strains (*down*) around knot cluster in zone A (*left*) and B (*right*).

As mentioned above ARAMIS system measures 3D deformation, thus it is possible to study the shear strains. Referring to Figure 5 although the pure bending according to Euler-Bernoulli beam theory which should result in very small shear, it is obvious that large shear deformations occurred in the material. The shear strains are especially visible around knot cluster A. For knot cluster B, i.e. with knots in a group are located along a vertical line perpendicular to the longitudinal board direction, the occurring deformations are such that they can be properly modeled with the beam theory. While the knots in a group are more spread out in the longitudinal direction, however, large shear strains occur due to irregularities in the material directions and properties, which cannot be fully captured by the beam theory and thus the calculated bending stiffness overestimates the true local stiffness.

Conclusions

Only one surface of the board was examined by ARAMIS and the strain field detected depends, on a local scale, very much on the knots visible on the examined surface. Therefore a high resolution MOE profile, calculated on basis of the strain field detected of one surface of the board, would differ from a MOE profile calculated on basis of the strain field of the other surface. On a more global level,

however, information from just one surface of the board for evaluation of bending stiffness should be sufficient since the curvature of the board, except on a very local scale, is almost equal on the two sides of the board in bending. Thus the reliability of a MOE profile, calculated using the strain data of only one surface, depends on the scale considered. Whether the scale corresponding to the 80 mm moving average employed in the present analysis represents a resolution that is coarse enough or not in this respect may be questioned. Having this kept in mind, good agreement regarding the position and magnitude of weak section is obtained where a group of knots are clustered more closely together in longitudinal board direction while it becomes worse where a group of knots is more spread out in longitudinal direction. The MOE profile established on basis of fiber angles from laser scanning in the way described shows an overall good agreement with the MOE profile established on basis of strains detected by ARAMIS. Therefore the present research supports conclusions drawn in previous research, namely that MOE profiles established on basis of fibre angle information in the way described may be used for rather accurate strength prediction of boards. The present research also reveals, however, that the local stiffness, in regions with clusters of knots spread out in longitudinal board direction, can not be properly captured by the beam theory that the method employs. This conclusion should be the starting point for further development of the method towards improved measures of local stiffness leading to even more accurate predictions of bending strength.

References

T. Isaksson (1999). Modeling the variability of bending strength in structural timber – Length and load configuration effects. Division of structural engineering, Lund Institute of Technology.

A. Olsson, J. Oscarsson, E. Serrano, B. Källsner, M. Johansson and B. Enquist (2013). Prediction of timber bending strength and in-member cross-sectional stiffness variation on basis of local wood fiber orientation. European Journal of Wood and Wood Products. DOI 10.1007/s00107-013-0684-5.

M. Hu, M. Johansson, A. Olsson, C. Bengtsson and A. Brandt (2012) Grading of sawn timber using the vibration technique - Locating imperfections based on flexural mode shapes. 17th international nondestructive testing and evaluation of wood symposium. 269-276.

H. Petersson (2010). Use of Optical and Laser Scanning Techniques as Tools for Obtaining Improved FE-input Data for Strength and Shape Stability Analysis of Wood and Timber. IV European Conference on Computational Mechanics, May 2010, Paris.

GOM mbH (2007) ARAMIS User manual- Software, Version 6.1 and higher.

J. Oscarsson (2012), Strength grading of structural timber and EWP laminations of Norway spruce- Development potentials. Licentiate thesis, school of engineering, Report No.15, Linnaeus university, Växjö, Sweden.

S. Ormarsson (1999) Numerical Analysis of Moisture-Related Distorsions in Sawn Timber. Doctoral thesis, Chalmers University of Technology, Gothenburg.

J. M. Dinwoodie (2000) Timber: Its nature and behavior. E & FN Spon, New Fetter Lane, London.

Digital image analysis software to *Pinus taeda* L. lumber classification

Ricardo Rall
Department of Computer Science, Technological College - FATEC, Botucatu, São Paulo, Brazil, rrall@fatecbt.edu.br

Adriano Wagner Ballarin
Department of Rural Engineering, College of Agronomical Sciences - Sao Paulo State University – FCA/UNESP, Botucatu, Sao Paulo, Brazil, awballarin@fca.unesp.br

Antonio Cesar Germano Martins
Sao Paulo State University – UNESP, Sorocaba, Sao Paulo, Brazil, amartins@sorocaba.unesp.br

Abstract

The use of *Pinus* in Brazilian lumber industry has been growing in recent years and, in 2011, the use was up to 27.3 million m³. This industry has sought more efficient ways to guarantee the quality of its products, with special attention to the inspection work, which plays an important role in the production process. This paper reports the development of alternative digital image analysis software to detect, quantify many kinds of defects and classify *Pinus* lumber. The material used in test was obtained from six trees of *Pinus taeda* with 37-year-old – Horto Florestal de Manduri – SP, Brazil. The trees yielded 110 boards, on which were visually analyzed and manually quantified knot, pith and pitch pockets s in accordance to NBR 12297 (Brazilian standard). The method used in the processing of digital images of these boards was composed of the following stages: image acquisition of the boards, pre-processing of images, image segmentation, recognition and characterization of the defects and classification of the boards. The results revealed that none of the techniques, when applied separately, was satisfactory in detection of knots, pith and pitch pockets, been necessary the combination of them to these detections as well as for the recognition of several encased knots with decay. The digital image analysis software, developed in Java, streamlined the process of detection, quantification of defects and classification of the boards with a hit percentage of 84.5% when compared to visual classification.

Keywords: wood, *Pinus taeda* L., classification, image processing, lumber.

Introduction

One of the strongest reasons for the introduction of the genus *Pinus* in Brazil was the need for commercial plantations for industrial supplies, targeting the mechanical processing for the production of sawn or laminated wood, for panels, pulp and paper (Kronka et al. 2005). This genus has approximately 100 species and is native from temperate and tropical regions. Commercially, in the US market, the species *P. taeda* belongs to group called Southern Pine, which includes several species such as Longleaf Pine (*P. palustris*), Shortleaf Pine (*P. echinata*), Loblolly Pine (*P. taeda*) and Slash Pine (*P. elliottii*) (USDA FOREST SERVICE 2002).

The most common defects observed in this type of wood are the presence of knots, fiber inclination, warping, cracks and splitting (Stanalker and Harris 1989). Knots, originated from branches, interrupt the direction of the

fibers, causing deviations, with more or less pronounced slopes around them and can be classified according to the area occupied in the cross section of the piece.

The mechanical weakening due to the presence of the knot in pieces of lumber is significant. Knots especially change the strength properties, depending on the ratio of the cross section of the piece that they compromise, its location and the stress distribution in the peace (Stanalker and Harris 1989). The effect is higher in tensile strength than in compression one. In bending, the effect of the knot depends on face (tensioned or compressed), in which it is located (Stanalker and Harris 1989).

According to NBR 11700 - Lumber from conifer reforestation for general use - classification (ABNT 1991a) among other lumber defects, the knots are used for the classification of wood in five classes (super, extra, first, second and third classes). In Brazilian sawmills, this classification is usually performed by skilled workers. However, this inspection may require substantial skill and visual acuity, and these tasks are often monotonous, boring and even dangerous.

An automated inspection system can operate tirelessly and promote more consistent and accurate quality patterns for the inspected products. Further, its usage also permits the observation of defects too subtle for human detection and higher speeds in the process.

This study aimed to develop alternative software for machine vision to detect the defects in coniferous lumber - boards, using techniques of digital image processing and checking its sensitivity and specificity by comparing their results to visual measurements.

Material and Methods

Preparation of the boards

Six trees of *Pinus taeda* L with approximately 37 years olds were randomly sampled from Horto Florestal located in Manduri-SP-Brazil (latitude 23 º 00 'south, longitude 49 º 19' west and 700m height),. The trees were cut to 110 boards with approximate dimensions of 225 cm long, 2.5 cm thick and various widths, according to the diameter of the wood trees. The boards were dried in industrial dryer to the equilibrium moisture content of 12%.

In the College of Agronomical Sciences - Sao Paulo State University UNESP - Botucatu / SP, the boards were passed lengthwise through a standard planning machine and crosscut to 200 cm, with the maintenance of their variable widths between 13.5 and 32.6 cm (mean 21.5 cm).

Visual classification of boards

The visual classification of the boards was performed using the NBR 12.297 - Lumber from conifer reforestation, for general use - measuring and quantifying defects (ABNT 1991b) and NBR 11700 (ABNT 1991a). The visual classification was required to ascertain the efficiency of machine vision software developed and provide parameters for evaluating the applicability of the standard and information about possible defects found on the boards.

Digital images acquisition

The illumination of the environment for digital images acquisition was performed with four fluorescent lamps model Daylight T12 1.20 m length - 40 W each. The homogeneity of the illuminance was guaranteed using a digital lux meter, model 300 Thal (Multivisi).

Digital images of the boards were acquired with a digital camera Lumix, Panasonic, DMC-LZ26, with maximum resolution of 6 megapixels and 6x optical zoom, installed on a tripod (Mirage, Lander model) at 1.0 m high and 1,1m away from the board.

Development of the software for processing digital images

The software was developed in Java, with the J2SE Development Kit 5.0 Java Developer Kit (JDK), using the interface Netbeans version 6.8 to the software development, library Java Advanced Imaging (JAI) and Fiji and Image J software, available free of charge manufacturers' websites.

The segmentation of images was performed using various methods such as region growing, thresholding, binary operation XOR. Morphological operations like thresholding targeting were not able to completely eliminate the background and, in some cases, eliminated part of the region of interest. It was necessary to use morphological operations of opening and closing, in order to eliminate noises in the image. For this, we used a square kernel, which preserves boundary of objects. The kernel size was chosen 3x3. Some tests were performed with larger sizes, but the processing time was longer and there was no improvement in the result. The morphological operations were based on the definitions of Gonzalez and Woods (2004), and these operations were derived from two basic operations: erosion and dilation, which in general results in "shrinkage" and "enlargement" of objects or areas of interest of the image.

The recognition and interpretation of the images were made from the determination of morphological chromatic, textural (entropy and contrast) and structural characteristics of the objects under analysis (knot, pith and pitch pockets).

Measurement of morphological characteristics

Morphological measurements were taken in pixels and stored in millimeters, using the scale factor ("Scale Options" software). Some morphological measurements were implemented:
• Length and average width (three measurements) of the board
• Area and perimeter of the object
• Length and width of the object (contained in the smallest rectangle)
• Maximum width of the pith.
• Shape Factor (ratio between its width and length of the object)

Measurement of chromatic characteristics

The software has implemented the following measurements of chromatic characteristics:
• Number of pixels similar to the background (color blue) – denotes occurrence of knothole
• Means, medians, standard deviations and mode for each band (R, G and B)
• Percentile 5% lower – detection of decayed knots by dark marks
• Textural characteristics entropy and contrast – co-occurrence matrix – method of the four angles (Haralick et al 1973)

Measurement of structural characteristics

The structural feature used was the percentage of edge coincident with the edge of the board. This measure detected objects that arise at the edge of the board (sawn knots or pith e.g.). This measurement was useful to identify false positive objects (marks of planning machine e.g.) detected by the software that did not match to knots, pith and pitch pockets.

At last, the final classes of the boards (super, extra, first, second and third classes) obtained from the software were compared with those obtained in the visual manual.

Results

In a total, 110 boards were analyzed by visual inspection and by the software developed for the classification of wood for defects.

When used alone (isolated), none of the techniques employed by the software was satisfactory in the detection of knots and pith. However, the combination of various techniques enabled significant success in these tasks. Detection of knots and pith were possible with the application, in sequence, of the following techniques: thresholding segmentation, region growing, and XOR operations, finally, morphological operations.

Figures 1, 2, 3 and 4 show the steps used in the detection of defects (knots and pith).

The efficiency of the software in the classification of boards relating to knots, pith and pitch pockets was assessed by comparison with the visual classification and the results are reported in Table 1.

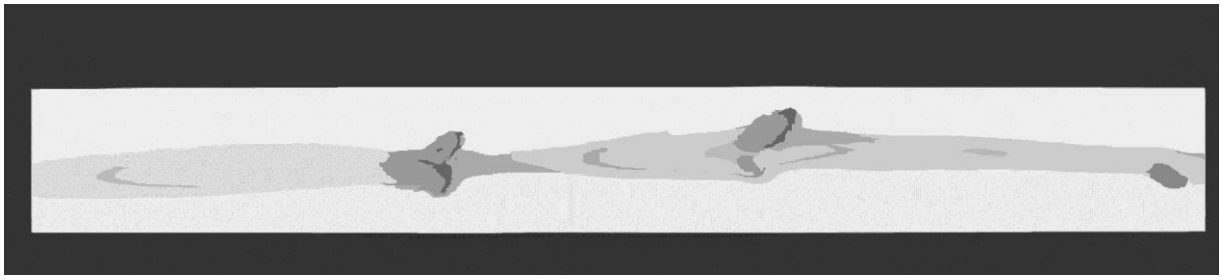

Figure 1 – Grayscale picture of the original board.

Figure 2 - Segmentation by thresholding and region growing. a) knot case; b) pith case.

Figure 3- Colorful original board.

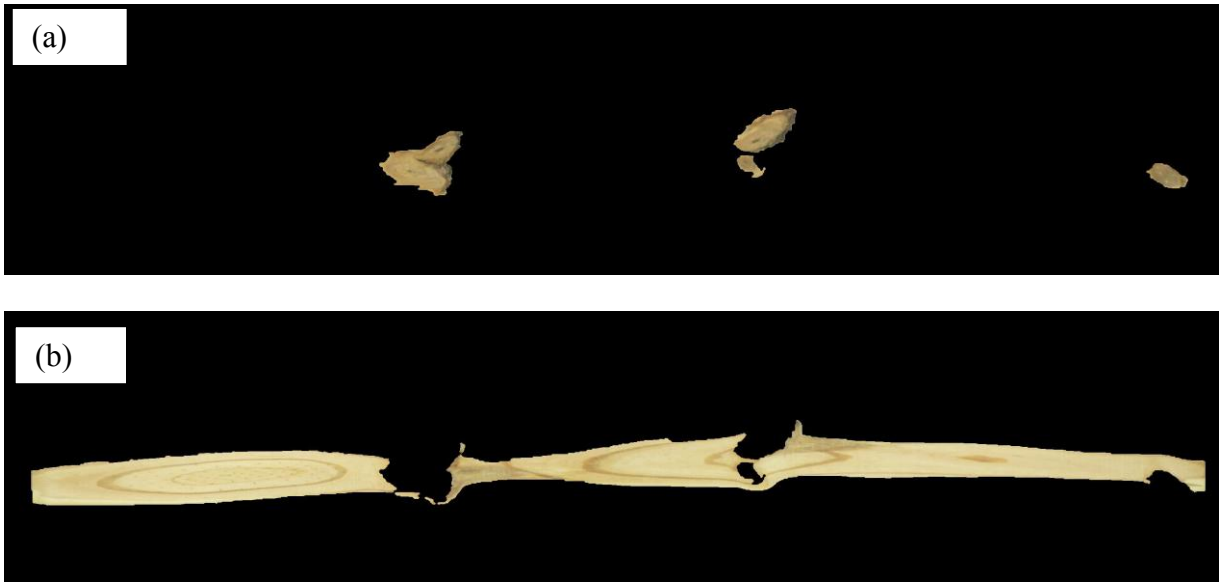

Figure 4 - XOR and morphological operations. a) knot case; b) pith case.

Table 1 – Confusion matrix comparing the classifications of the manual and the software

		Manual classification						
		Third class	**Second class**	**First class**	**Extra class**	**Super class**	**Total**	**Inclusion error (%)**
Software classification	**Third class**	16	2				18	0.0
	Second class	6	24	1			31	19.4
	First class		2	37			39	5.1
	Extra class		1	2	1	1	5	60.0
	Super class			1	1	15	17	11.8
	Total	22	29	41	2	16	110	
	Omission error (%)	0.0	6.9	2.4	0.0	6.3		84.5

Table 1 illustrates, for example, that for the first class, the software sorted 39 boards and 37 corresponded in fact to this class, as demonstrated by the classification. The two boards that did not correspond to that class - false positives - resulted in inclusion error of 5.1% (2 boards in 39). Inclusion errors reached high values in the extra class. In addition to the misclassification of the software, a reduced number of boards classified in that class favored the occurrence of an error as high. In other cases, the errors found were lower.

A similar analysis can be conducted to evaluate the errors of omission, which detects the false negatives. The analysis also showed that 1 out 41 boards visually classified as first class, was omitted by the software, leading to an error of omission of only 2.4% (1 in 41 boards).

In a comprehensive analysis, we evaluated the software had a hit of 84.5% (93 boards in 110). Kauppinen (1999), pioneering work on the subject, using a classifier to six types of defects on pine boards, got hit rate of 66%. For the classification of defects in eucalyptus wood, Khoury et al. (2006), using artificial neural networks, depending on the block size of the image, obtained accuracy rates of 83.1% (blocks of 64x64 pixels) and 76.6% (32x32 pixels). Also studying eucalyptus wood, Gomes et al. (2008) had a success rate of 81%.

Conclusions

From the results obtained, it can be concluded that none of the techniques, when applied alone, was satisfactory for the detection of knots. Among the combinations studied, which brought the best result in the overall detection of knots was targeting region growing and thresholding, followed by the binary operation XOR and morphological operations of opening and closing to eliminate noise.

The software for digital images processing, developed in Java, streamlined the processes of detection and classification of defects (knots, pith and pitch pockets) and the final classification of the boards, with a hit percentage of 84.5%. With this performance and characteristics, may become part of a device to be fully developed in Brazil, necessarily less expensive than those currently available, to better adapt to the reality of our small and medium-sized sawmills.

References

Associação Brasileira de Normas Técnicas. 1991a. Madeira serrada de coníferas provenientes de reflorestamento para uso geral – classificação. NBR 11.700. Rio de Janeiro. 6 p.

Associação Brasileira de Normas Técnicas. 1991b. Madeira serrada de coníferas provenientes de reflorestamento, para uso geral – medição e quantificação de defeitos. NBR 12297. Rio de Janeiro. 6 p.

Gomes, J. M. ; Pinto, F.A.C.; Della Lucia, R.M. [and others]. 2008. Desenvolvimento e avaliação de um protótipo classificador de tábuas usando técnicas de visão artificial. Revista Árvore, 32(5): 949-959.

Gonzalez, R.C.; Woods, R.E. 2004. Digital image processing using Matlab. New Jersey: Pearson Education Inc. Upper Saddle River: 337 – 358.

Haralick, R. M.; Shanmugam, K.; Dinstein, I. 1973. Textural features for image classification. IEEE Transactions on Systems: man and cybernetics, 3(6): 610-621.

Kauppinen, H. 1999. Development of a color machine vision method for wood surface inspection. Oulu, Finland: University of Oulu, 133p. M.S. thesis.

Khoury Jr., J.K.; Pinto, F.A.C.; Quieroz, D.N. [and others]. 2006. Redes neurais para reconhecimento de defeitos de madeira serrada de eucalipto em imagens digitais. Scientia Florestalis, 70: 85-96.

Kronka, F. J. N.; Bertolani, F.; Ponce, R. H. 2005. A cultura do Pinus no Brasil. São Paulo: Páginas e Letras: 156 p.

USDA Forest Service. Pinus taeda.
http://www2.fpl.fs.fed.us/TechSheets/softwoodna/htmldocs/pinustaeda.html [Access in Nov 12, 2009].

Camera based real time wood evaluation software in application

László Szalai
Institute of Informatics and Economics, Faculty of Wood Sciences, University of West Hungary, Sopron, Hungary, szalai@inf.nyme.hu

Abstract

The paper presents an application of the camera based optical evaluation system we developed. The software uses a special image processing method and statistical analysis to recognize the grain orientation of wood, as well as its defects. The system generates calculated values for the analyzed material at regular intervals, while feeding. The camera is focused on the surface and records the grain orientation, knots and decay on the fly. After processing the full length of the material the special algorithm is capable of determining the quality value of wood for sorting, even at high feed rates.

Keywords: non-destructive, lumber grading, scanning, grain orientation, knot

Introduction

Today, in the era of high-quality production it is becoming important for a sawmill (or wood based panel company) to work with selected and certified wood according to the European criteria. Several standards exists to qualify timber strength in Europe. These standards (EN 408, EN 338) are coming to the focus of production companies, because without the use of these standards it is difficult to break into the European market.

In many cases the strength classification of lumber is still through the conventional human visual method, which means that a worker visually determines the size of the defects contained in the timber. The other - more exact – method is the destructive testing of wood, in which samples are taken and physically broken by an expensive testing machine. Then wood is classified into different strength classes according to its properties. This latter method has disadvantages of slowness and the fact that after this process the timber becomes unusable.

A not too old approach is the nondestructive testing of wood. Its biggest advantage is that during the process the timber is not broken. This test method has many subtypes, including the investigation of the speed (Divós et al. 2002) of sound - as well as other connected sound method like vibration, the radiation of wood (X-ray, CT, etc.) and scanning-based methods.

In my research scanning was used for the nondestructive testing of wood and was modeled a factory timber feeding machine in the laboratory and was created a tool which is able to classify what goes through it by image analysis.

Materials and methods

During my research spruce (Picea abies) timber (20 cm x 5 cm x 3 m) was used as raw material, which was cut by traditional circular saw technology. The timber was relatively straight at first sight, its twist and bow where less than 5 percent, so it was suitable for feeding with a winch.

The system’s basic setup is shown in Figure 1.

Wood scanning is done from below and above, using cameras in real time. At the end of the scanning, the system is able to decide the quality class of the wood based on the grain orientation and indicate it according to the EN 338 standard values. We do not measure the elastic modulus of the wood but we try to reach an equivalent classification.

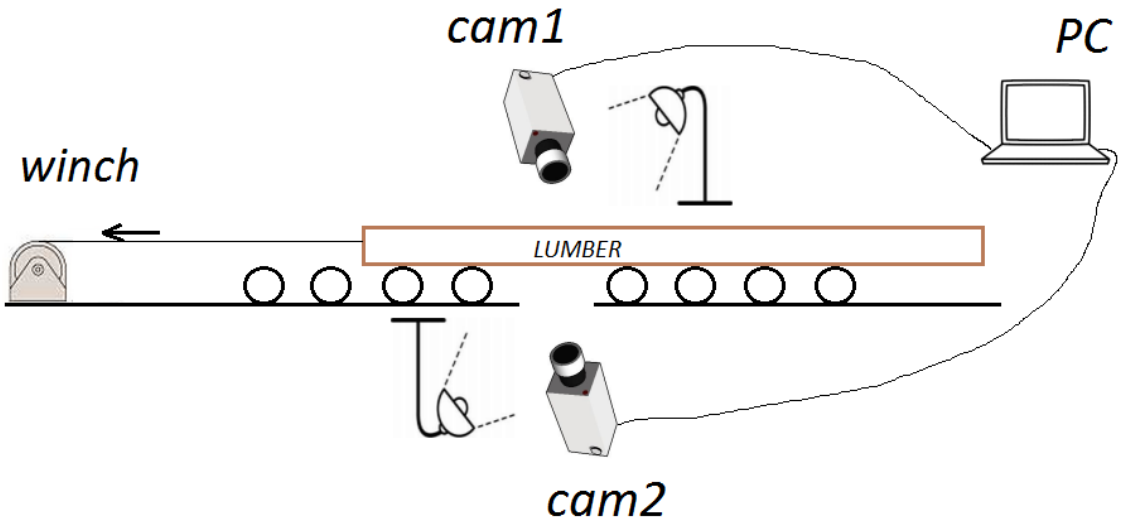

Figure 1 – The setup of the lumber surface analyzer

The timber moves on a feeding roller table in the longitudinal direction with the help of a winch. It pulls with a constant speed. The surface of the timber is illuminated from above and below with a homogeneous light. Two cameras scan the sawn surfaces above and below. The images are transmitted from the cameras to the computer that analyzes it. The cameras are good quality webcams that can be easily purchased in commercial trade. Their specifications include HD resolution and 30 frame per second capturing speed. I have not used the HD resolution during the investigation. A higher frequency of 30 fps was utilized instead, because of the high feed rate. I set the camera resolution to 640x480 pixels. The processing computer was a normal desktop level PC with dual core processor. This is also available at a low price. It is important to note that the cameras' distance from the timber should be no more than 40 centimeters.

Grain orientation theoretical considerations

Only pine wood material was tested by the system. Its grain orientation meets the requirements most closely. 80% of the tested timber was cut radially, and 20% was cut tangentially. All pieces of timber had conspicuous grain orientation. The grain and the defects of the pine appeared on the surface. Important defect include mainly the knot, since it obviously affects the grain orientation (Divós and Sismándy-Kiss 2011).

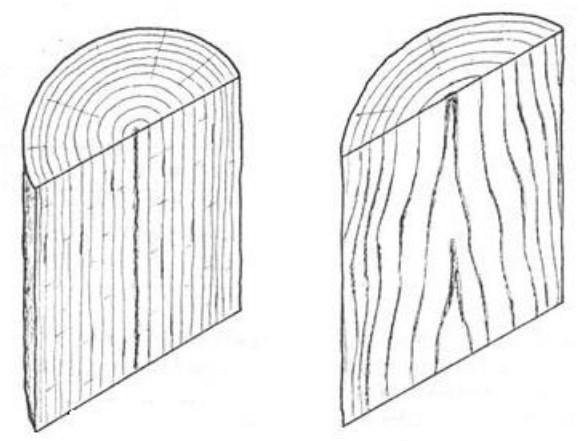

Figure 2 – The grain orientation of the intact wood

The Figure 2. shows the grain orientation of the wood after sawing. In case of the intact timber we can see nearly parallel lines on the radial surface. In the case of a tangential surface, the so-called crown figure appears. Crown figure is the visual grain structure on the surface which comes from cutting through the annual rings. In the investigated wood material this crown figure was mostly intensified at the knotty regions.

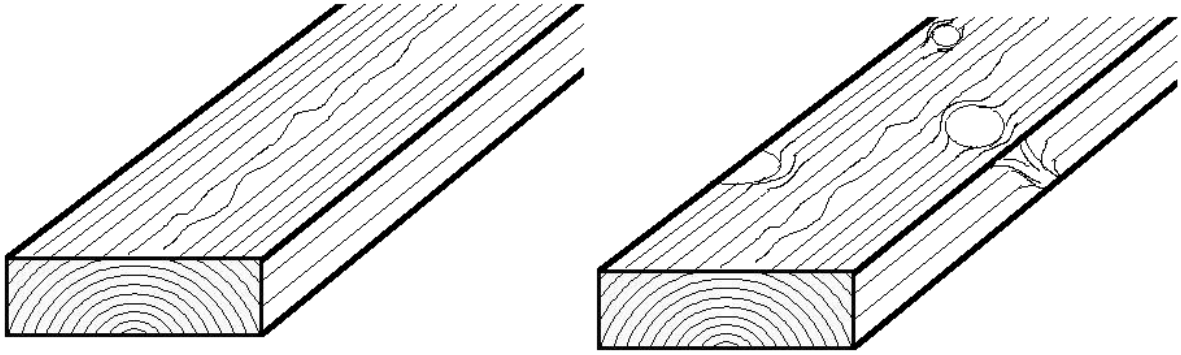

Figure 3 – Effect of the knots

Figure 3 shows the effect of the knots on the grain as seen on the surface. The sample on the left is intact with normal grain orientation, typically parallel lines on the surface. In the sample on the right there are knots that influence the grain orientation so the lines are no longer parallel.

Processing in real time

As I mentioned, the camera that scans the surface of the timber being fed, sends the video stream that the computer subsequently analyses. The basis of the analysis is simple. An algorithm processes the relevant part of the current video frame at regular intervals and calculates a value based on its grain orientation. This is continued step by step throughout the full length of the timber. The smaller the segment width for which this factor is determined, the more accurate is the obtained measurement.

The width of the segments is calculated as follows (1):

$$w = \frac{fr}{fps * cf} \tag{1}$$

Where w = the width of the analyzed segment (m), fr = feed rate (m/s), fps = frames per second, and cf is a correction factor. The correction factor depends on the lighting conditions, quality of the camera

and the computer's performance. Experience shows that it ranges from 0.6 to 0.9 in value. In higher-speed systems it approaches 0.9.

For example, in case of a 2 m/s feed rate, 0.7 correction factor and 30 fps camera speed, the width of the segments must be analyzed at approximately 10 cm.

The system can operate in single or dual camera mode. If only one side is analyzed, the accuracy will be worse. The calculated value of the segment can be determined by the values of the two sides in dual camera mode.

The algorithm of the predictor parameter

The determination is based on the vectorized grain orientation.

Figure 4 – Vectorization of the grain

As shown in Figure 4, the image analysis captures a snapshot (in the middle) from the video stream (on the left), and performs the frame vectorization (on the right). Thereafter, the image is evaluated. Figure 5 outlines the analysis process.

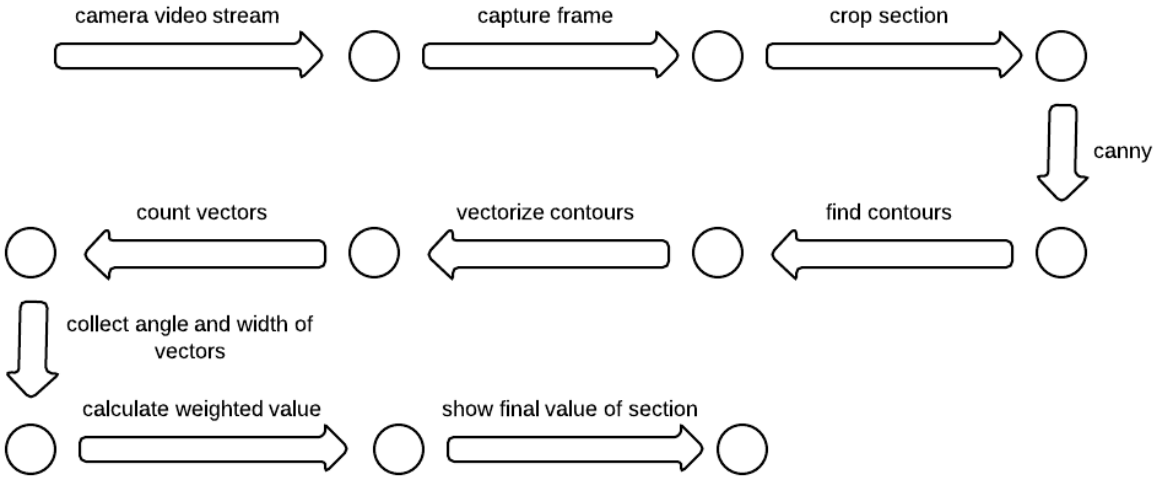

Figure 5 – Process of the determination of the final quality value

Figure 5 shows that in specified intervals the camera frame is captured and then we crop the segment for analysis. Then, a modified Canny edge detector algorithm determines the contours around the color changes on the surface. Later it vectorizes the contours. The fine-tuning of this algorithm and its adjusting to the measured wood is the most important point of the evaluation. After determining all the

contour numbers, based on the angle and length of the vectors, weighted value is calculated as the quality factor of the current segment.

We count the length of the 10-80◦ vectors and we do the same with the 0-10◦ and the 80-90◦ vectors.

$lh = \sum (L80\text{-}90)$ $lv = \sum (L0\text{-}10)$ $la = \sum (L10\text{-}80)$

Where *lh* = length of horizontal vectors, *lv* = length of vertical vectors, *la* = length of angularly vectors.

The quality factor of the section is calculated by the following formula (2):

$$sv_n = \frac{\mathrm{lh}*\mathrm{c1}+\mathrm{la}*\mathrm{c2}}{100*(\mathrm{lh}+\mathrm{lv}+\mathrm{la})} \quad (2)$$

Where the *sv* = quality factor, *c1* and *c2* correction parameters. The fine-tuning of the correction parameters is also an important, for example, depends on the sharpness of the grain structure, the color of the surface of the wood, the method of sawing and planing, and the quality.

If the grain orientation is healthy, the number of the slanted vectors will be few and short. If there are knots and irregular grain orientation, the number of the slanted vectors grows. I note, that the choice of the correction factors and filter parameters of the Canny edge detector algorithm for a strongly crown-figured wood is not trivial. In case of a greater number of test pieces, test measurement and validation are necessary.

In dual-camera mode, the captured frames should be synchronized, and the evaluation must be done on matching segments. In this case, the final quality value of the current segment is calculated by the average of the two sides.

Results

After timber surface scanning, the software shall prepare the analysis of the sections for the full length of the test piece, and determine the quality value for each section, and the wood profile. We can see this in Figure 6.

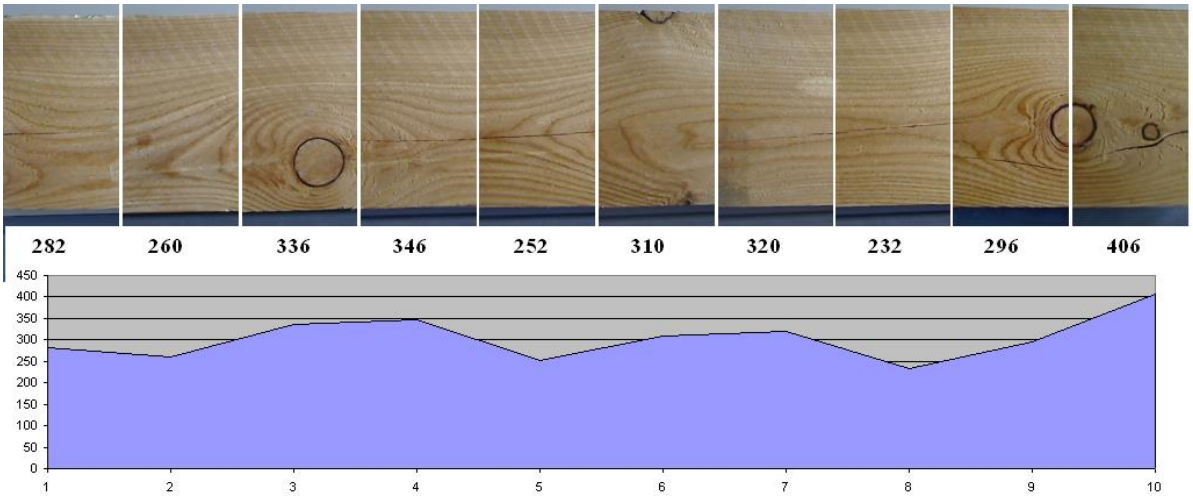

Figure 6 – Quality values and profile

The quality profile is a curve that consists of the quality values calculated for the different sections. If the profile contains similar and small values, then the grain orientation of the timber is normal, intact. In knotted materials, peaks appear in the profile that show the defects localized on the surface.

The average quality factor defines the strength class of the timber. The test was made on 50 samples of spruce timber. First, the quality profile was determined on all the timbers with the single camera system, then the values were checked based on the EN 338 with the help of the Portable lumber grader.

	Grade				
device	**C16**	**C18**	**C20**	**C22**	**C24**
Portable lumber grader (EN 338)	10	8	7	20	5
grain orientation analyzer	10	10	8	16	6
Efficiency (%)	*100*	*80*	*87*	*72*	*83*

On average the match was 84 %.

Of course, the dual-camera solution gets more accurate values but this test was not completed until the writing of this paper.

Conclusions

As you can see, nondestructive optical testing of wood is possible with cheap and readily available IT tools. As tests were made in laboratories, additional tests need to be done before its usage in the industry. The stability of the system can be critical mostly in industrial environments. The laboratory test revealed that with spruce timber, the quality grading can be accomplished even with the single camera version. This evaluation is based on the analysis of the grain orientation. The efficiency is nearly 85 %, compared to the Portable lumber grader. The dual camera version is expected to get more accurate results. The determination of the right correction factors for the algorithm may cause difficulties, as the analysis is very sensitive to these. This method can also be applied to the evaluation of glued laminated timber. Research has started in this area as well.

Acknowledgements

The work was partially supported by the TAMOP-4.2.2.C–11/1/KONV-2012-0015 (Earth-system) project sponsored by the EU and European Social Foundation.

References

Divós, F., Csóka, L., Szalai, L., Gyenizs, P., 2002. Fűrészáru szilárdság szerint történő osztályozása és gyakorlati alkalmazása. I. rész. FAIPAR L. évf. 2. szám, 19-24

Divós, F., Csóka, L., Szalai, L., Gyenizs, P., 2002 “Fűrészáru szilárdság szerint történő osztályozása és gyakorlati alkalmazása”. II. rész. FAIPAR L. évf. 2. szám, 12-15

Divós, F., Sismándy-Kiss, F., 2010. Strength Grading of Structural Lumber by Portable Lumber Grading – effect of knots. The Future of Quality Control for Wood & Wood Products, Edinburgh, Scotland.

Divós, F., Sismándy-Kiss, F., 2011. Strength Grading of Structural Lumber – Effect of Damping and Knots . 17th International Nondestructive Testing and Evaluation of Wood Symposium, Sopron, Hungary.

EN 338, 2009. Structural timber. Strength classes.

EN 408, 2003. Timber structures. Structural and glued laminated timber. Determination of some physical and mechanical properties.

Session 8

Nondestructive Evaluation of Structural Materials II— Enhancements to Traditional Methods and New Applications

Effects of temperature and inner cavity defects on stress wave propagation through green wood

Huadong Xu
College of Engineering & Technology, Northeast Forestry University, Harbin , China,
huadongxu@yahoo.com

Lihai Wang
College of Engineering & Technology, Northeast Forestry University, Harbin , China,
lihaiwang@yahoo.com

Abstract

An experimental approach was used to study the stress wave propagation through the radial section of green wood (ussuri poplar). Some measuring points were firstly drawn on the radial section of wood specimen. The stress wave time was then measured point by point using an Arbotom system, while wood specimen was frozen or unfrozen, intact or defective respectively. The stress wave velocity was calculated using the wave propagation distance divided by time, and the effects of temperature on the stress wave velocity was then discussed. The stress wave time isolines on the radial section of intact and defective specimen were simulated and compared finally. The results showed that temperature had significant effects on the stress wave velocity. The wave velocity decreased gradually as temperature (subzero to above zero) increased. Additionally, cavity defect can distinctly change the stress wave time isolines on the radial section of wood. The stress wave time from the exciting point to the region behind the cavity in defective wood is lager than in intact wood. Stress wave seems to propagate along the edge of cavity not to pass the cavity directly.

Keywords: wood, stress wave, temperature, defects, propagation velocity

Introduction

Stress wave nondestructive technique has been used to test the wood quality for a few decades. It has proved that stress wave is one of the most popular and effective methods for assessing the wood quality in the world (Kang and Booker, 2002; Ross et al, 1994; Mattheck and Bethge, 1993). However, stress wave propagation in wood may be affected by some special factors. The first important factor is wood defect. Wood is a typical natural and anisotropic biomaterial that generally contains some growth defects in the form of knots, grain deviation and cracks. This material is also vulnerable to damage such as fungal decay and termite attacks due to mechanical and environmental effects. Such forms of defects mostly change the local mechanics properties of wood, such as modulus of elasticity (MOE), and further affect stress wave propagation in wood (Divos and Szalai, 2002). The second factor is grain angle. Wood generally contains three typical main axes: longitudinal, radial and tangential direction. The wood qualities and inner structures at these three axes and at an angle rotating from the axes are significantly different. Thus the stress wave propagation through wood also may be affected by the grain angle (Kabir, 2001; Armstrong et al, 1991). The third factor is temperature. Temperature may change the water phases in wood and further has an effect on the stress wave propagation. Bachle et al.(2006) and Sandoz (1993) have proved

that temperature has a significant effect on the acoustic wave propagation in wood. Actually, there are other factors to influence the stress wave propagation in wood, such as moisture content.

Some previous researches have discussed the effects of grain angle, moisture content and temperature on stress wave or ultrasonic wave propagation in wood(Kabir, 2001; Armstrong et al, 1991). But most of the work employed small clear wood specimens as research objects to do experiment and only discussed one or two influencing factors. Little relative researches selected green timber as research object to study the stress wave propagation in wood and systematically analyze the effects of grain angle, temperature and defect on stress wave propagation. Additionally, there are many researches on the applicability and reliability of stress wave techniques for evaluating the wood quality or detecting the inner defect in standing trees or wood structure (Bulleit, 1985; Bucur, 2005; Wang et al, 2001). However, very little research studies the effects of wood defects on stress wave transmitting time isolines or traveling path.

In this study, through measuring the stress wave time (SWT) and computing the stress wave velocity (SWV) in intact green wood at frozen and unfrozen status respectively, the effects of temperature on SWV will be further discussed on the basis of previous researches firstly. Then, the different size defects are simulated by removing mass from intact wood specimens, and the effects of cavity defects on SWT will be analyzed in order to grasp the change of the stress wave propagation path when it meet with the cavity defects. At last, the SWT isolines on the radial section of intact and defective specimen were simulated and compared.

Material and methods

Material

In a local sawmill in Fangzheng forestry bureau, Heilongjiang, China, an ussuri poplar (*Populus ussuriensis*) log is longitudinally sawn along the pith into some quarter-sawn timbers, one of which is selected as the experiment specimen. The length and thickness of wood specimen are 76cm and 7cm, and the long and short widths are 35cm and 34cm respectively, as shown in Figure 1. The moisture contents of heart wood and sapwood of wood specimen are 83.3% and 99.5%.When wood specimen was not tested, it was covered with a plastic bag and placed in a refrigerator to prevent the change of moisture content.

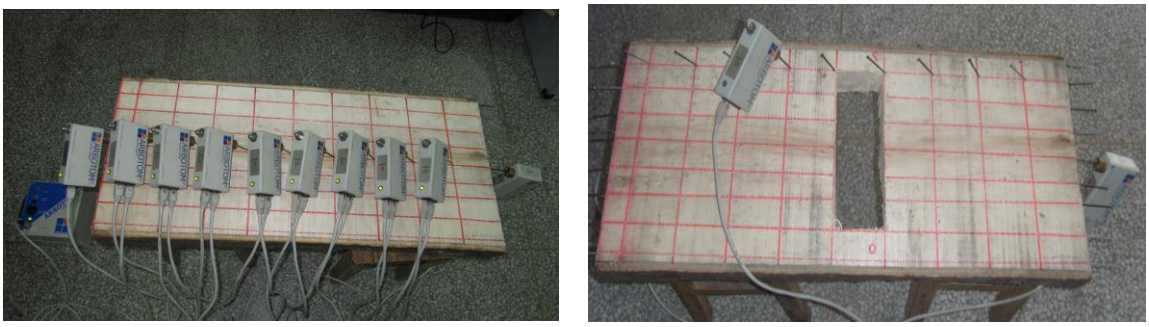

(a) (b)

Figure 1— Green wood specimen and stress wave time (SWT) tester. (a)A multi-channel Arbotom system was used to test intact wood; (b) A double channel Arbotom system was used to test wood with cavity.

Methods

As shown in Figure 2, not including bark, there are nine measuring points along radial direction at 4cm interval, and nine measuring points along longitudinal direction at 8cm interval on the radial section of wood specimen. The distance between last two columns points is 4cm, for example the distance from point 82 to point 99. Additionally, six measuring points are drawn between point 1 and point 18. Totally, there are one hundred and six measuring points on the radial section of lumber. O and P will be used to determine the location of the cavity drilled in the wood specimen.

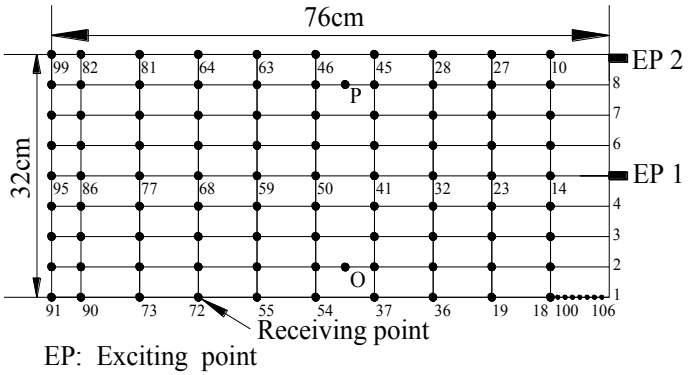

Figure 2— Arrangement of measuring points

An Arbotom system, Rinntech Company, was used to test the SWT through lumber radial section, see Figure 1. Measurement included three steps: First, in room temperature (20℃), the SWT in intact specimen was tested point by point while EP1and EP2 were selected as the exciting point respectively; Second, the intact specimen was controlled at -30℃,-20℃,-10℃,-5℃,0℃and 5℃ respectively in a refrigerator, the SWT was then tested point by point at every temperature; Third, a rectangular cavity with different size was drilled in the specimen in sequence, and the SWT through defective wood was then tested in the same method. The location and area of cavity are shown in Figure 1(b) and Table 1. Stress wave velocity (SWV) was the propagation distance divided by time.

Table 1 The location and area of the rectangular cavity artificially drilled in wood specimen

	Four corner points	Area(cm^2)	Ratio of cavity area to lumber radial section area (%)
Cavity 1	38、44、P、O	96	3.95
Cavity 2	38、44、47、53	192	7.90
Cavity 3	29、35、47、53	384	15.79
Cavity 4	29、35、36、62	576	23.68

Results and Discussion

Effect of temperature on stress wave velocity

Figure 3 shows the effect of temperature on the average velocity of radial stress wave (RSW) and longitudinal stress wave (LSW) in heart wood and sap wood. Longitudinal SWV are higher than radial SWV both in frozen and unfrozen wood. As temperature decreases, the average velocities of both radial and longitudinal stress wave increase. However, it is not a linear relation between SWV and temperature, both the longitudinal and radial SWV have an abrupt jump near 0℃ temperature. This is because the specimen is green wood, which moisture content is more than fiber saturation point (FSP). When wood specimen contains a lot of free water, free water will change from liquid to solid as wood temperature is below 0℃(Kärenlampi et al, 2005), ant then it will affect the stress wave propagation in wood.

Table 2 is the SWV data in intact wood at each measuring temperature. Table.2 shows the average velocities of RSW and LSW in heart wood and sapwood at -30℃ are 131.19%, 14.95% and 18.69% respectively higher than at 20℃; at -30℃ are 25.96%, 4.32% and 3.85% respectively higher than at -5℃; and at -5℃ are 83.54%, 10.19% and 14.29% respectively higher than at 20℃. These data indicate the radial SWV is more significantly affected by temperature than the longitudinal SWV. In addition, SWV has larger change as temperature decreases from 20℃ to -5℃ than as temperature decreases from -5℃ to -30℃.

Table 2 The average stress wave velocity (SWV) in wood at different measuring temperature

Temperature (℃)	Average propagation velocity (m/s)		
	LSW in heartwood	LSW in sapwood	RSW
20	2241	2160	450
4	2339	2232	536
0	2370	2339	624
-5	2469	2469	826
-10	2489	2480	921
-15	2524	2539	979
-20	2539	2544	983
-30	2576	2564	1040

Note: LSW is longitudinal stress wave; RSW is radial stress wave.

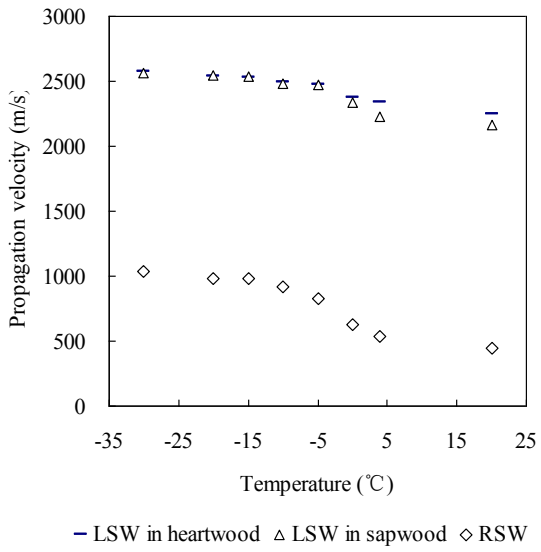

Figure 3— Effect of temperature on stress wave velocity (SWV) in green wood

Effect of cavity defect on stress wave propagation

Effect of cavity defect on longitudinal stress wave time

Table 3 summarizes the longitudinal SWT at different path in intact and defective wood. Figure 4 shows the longitudinal SWT at each path in defective wood is different with that in intact wood. It is larger in defective wood than in intact wood, and increases as cavity size increases.

In addition, in intact wood, the longitudinal SWT at different path is almost the same with each other. However, it is obviously different with each other when wood contains the same size cavity. The longitudinal SWT from point 5 to point 95 is the largest, 540μs for Cavity 1; but from point 2 to point 92 and from point 8 to point 98 are only 329μs and 325μs for Cavity 1. For not traveling over the cavity, the longitudinal SWT from point 1 to point 91 and from point 9 to point 99 in defective wood are almost the same as in intact wood.

Why is the transmitting time of longitudinal stress wave at each path different under the same long path and the same size cavity? The reason may be stress wave propagates along the edge of cavity not pass the cavity directly. Then the propagation distance of stress wave from point 5 to point 95 is the largest when wood specimen contains cavity, so the SWT is the highest.

Table 3 The longitudinal stress wave time (SWT) in wood with cavity

EP—RP	Longitudinal SWT (μs)				
	Intact	Cavity 1	Cavity 2	Cavity 3	Cavity 4
1-91	325	322	322	322	324
2-92	320	329	331	341	339
3-93	315	360	376	383	398
4-94	333	435	448	461	475
5-95	333	540	556	561	596
6-96	324	486	484	480	511
7-97	319	415	345	378	405
8-98	320	325	340	331	350
9-99	320	322	325	323	320

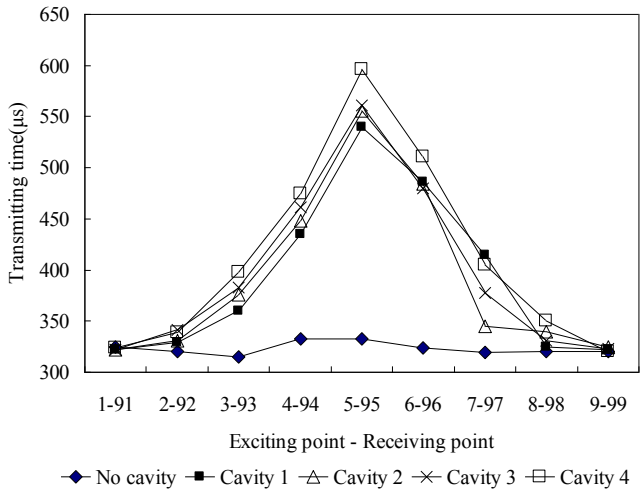

Figure 4— Effect of cavity defect on the longitudinal stress wave time (SWT) in wood at different path at room temperature

Effect of cavity defect on stress wave time isolines

Figure 5(a) is the SWT isolines on the radial section of intact wood when EP1 is excited. Figure 5(a) shows that stress wave transmits gradually from wood pith to the farther area in the radial section of lumber when EP 1 is knocked on. However, the speed of stress wave in different direction is different. In longitudinal, stress wave travels most fast; in radial, stress wave travels most slowly; in the transition area from longitudinal to radial, the SWT decreases gradually. In other words, there are more isolines per unit length in radial than in longitudinal, as shown in Figure 5(a). The SWT isolines in radial section of

lumber when EP2 is knocked on are shown in Figure 5(b). Similarly, stress wave also transmits gradually from exciting point to farther area, and travels most fast in longitudinal and most slowly in radial.

Figure 5(c) is the SWT isolines on the radial section of defective wood when EP1 is excited. Compared with Figure 5 (a), Figure 5(c) indicates the SWT isolines on the radial section of defective wood are significantly different with that of intact wood. When wood specimen contains cavity, the SWT isolines behind the rectangular cavity can form two "circular regions". The SWT from the EP1 to these two regions is larger than to other region of wood radial section. Compared to the SWT from the EP1 to these two regions in intact wood, the SWT in defective wood is it's two times. In addition, the SWT from EP1 to other region behind the rectangular cavity except those two regions is larger than that in intact wood specimen.

Similarly, compared with Figure 5 (b), Figure 5 (d) shows the SWT from EP2 to the area behind the cavity in defective wood is larger than in intact wood. The SWT isolines in defective wood can also from a "circular regions" near the farthest corner of rectangular cavity from EP2. Compared to the SWT from the EP2 to this region in intact wood, the SWT in defective wood is it's one point five times. In addition, the SWT from EP2 to other region behind the rectangular cavity in defective wood is also larger than in intact wood.

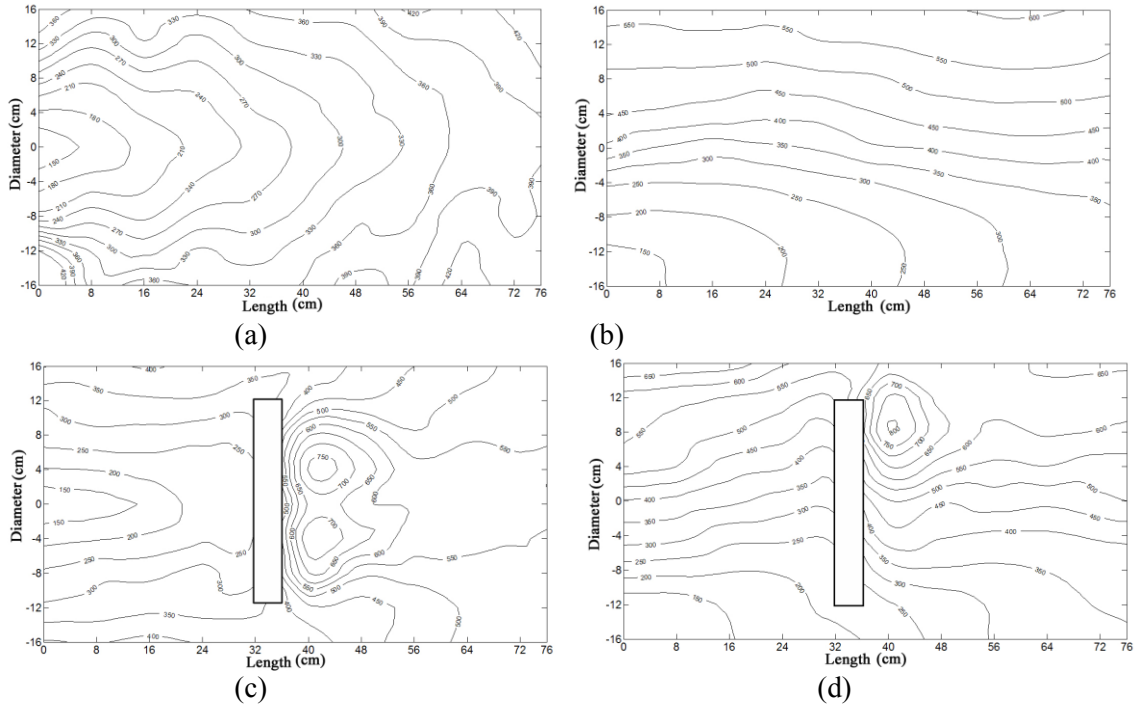

Figure 5— Effect of cavity defect on stress wave time (SWT) isolines on the radial section of green wood. (a) and (b) are the SWT isolines on the intact wood when EP1 and EP2 are excited respectively; (c) and (d) are the SWT isolines on the wood with Cavity 1when EP1 and EP2 are excited respectively.

Conclusions

By measuring and analyzing the stress wave time (SWT) through the radial section of ussuri poplar green wood, the effects of subzero temperature and cavity defect on the stress wave propagation are studied, some main conclusions are as follows:

(1)Temperature also has a significant effect on stress wave propagation in green wood. As temperature (from above zero to subzero) decreases, the SWV increases. The SWV in green wood has an abrupt "jump" near 0℃temperature.

(2)Compared with intact wood, the SWT isolines on the radial section of defective wood are obviously different. The SWT from the exciting point to the region behind the cavity in defective wood is lager than in intact wood. In addition, stress wave seems to propagate along the edge of cavity not pass the cavity directly.

Acknowledgments

This work was financial supported by "the Fundamental Research Funds for the Central Universities of China (DL12BB18)".

References

Armstrong, J. P.; Patterson, D.W.; Sneckenberger, J. E. 1991.Comparison of three equations for predicting stress wave velocity as a function of grain angle, Wood and Fiber Science 23(1): 32-43.

Bachle, H.; Walker, J. 2006. The influence of temperature on the velocity of sound in green pine wood, Holz als Roh- und Werkstoff, 64: 429–430

Bulleit, W. M. 1985.Modeling stress wave passage times in wood utility poles, Wood Science and Technology 19:183-191.

Bucur, V. 2005. Ultrasonic techniques for nondestructive testing of standing trees, Ultrasonics 43:237-239.

Divos, F.; Szalai, L. 2002.Tree evaluation by acoustic tomography, Proceedings of the 13th International symposium on nondestructive testing of wood, Berkeley, Madison, pp. 251-256.

Kabir, M. F. 2001. Prediction of ultrasonic properties from grain angle, Journal of the institute of wood science, 15(5): 235-246.

Kang, H.; Booker, R. E. 2002.Variation of stress wave velocity with MC and temperature, Wood Science and Technology 36:41-54.

Kärenlampi, P.; Tynjälä, P.; Ström, P. 2005. Phase transformations of wood cell wall water, Journal of Wood Science 51:118-123.

Mattheck, C. G.; Bethge, K. A. 1993.Detection of decay in trees with the Metriguard Stress Wave Timer, Journal of Abroriculture, 19(6):374-378.

Ross, R. J.; Ward, J. C.; TenWolde, A. 1994.Stress wave nondestructive evaluation of wetwood, Forest Products Journal 44(7/8):79-83.

Sandoz, J. L. 1993.Moisture content and temperature effect on ultrasonic timber grading, Wood Science and Technology 27:373–380.

Wang, J.; Biernacki, J. M.; Lam, F. 2001. Nondestructive evaluation of veneer quality using acoustic wave measurements, Wood Science and Technology 34:183-191.

Preliminary results of a structural timber grading procedure in Spain based on nondestructive techniques

Guillermo Iñiguez-Gonzalez
ETSI Montes, Universidad Politécnica de Madrid, Madrid, Spain, guillermo.iniguez@upm.es

Daniel F. Llana
ETSI Montes, Universidad Politécnica de Madrid, Madrid, Spain, d.f.llana@upm.es

María J. Montero
ETSI Montes, Universidad Politécnica de Madrid, Madrid, Spain, mj.montero@upm.es

Eva Hermoso
CIFOR-INIA, Madrid, Spain, hermoso@inia.es

Miguel Esteban
ETSI Montes, Universidad Politécnica de Madrid, Madrid, Spain, miguel.esteban@upm.es

José L. García de Ceca
CIFOR-INIA, Madrid, Spain, ceca@inia.es

Ignacio Bobadilla
EUIT Forestal, Universidad Politécnica de Madrid, Madrid, Spain, i.bobadilla@upm.es

Raquel Mateo
AITIM, Madrid, Spain, r.mateo@aitim.es

Francisco Arriaga
ETSI Montes, Universidad Politécnica de Madrid, Madrid, Spain, francisco.arriaga@upm.es

Abstract

The main aim of this paper is to present the preliminary works undertaken to establish a common procedure for the use of nondestructive techniques to evaluate the properties of sawn timber.

NDT parameters were measured for the main structural Spanish species: Scots pine (*Pinus sylvestris* L.), laricio pine (*Pinus nigra* Arn. Ssp. *salzmannii*), radiata pine (*Pinus radiata* D. Don.), maritime pine (*Pinus pinaster* Ait.) and sweet chestnut (*Castanea sativa* Mill.). The commercial equipment and techniques used were: Sylvatest Duo and Trio (ultrasound technique), Microsecond Timer (stress wave), Hitman and PLG (vibration analysis), Pilodyn 6J Forest (penetration resistance) and SWRM (screw withdrawal force).

A data sheet to collect all the results was designed, taking into account test procedures and adjustment factors. NDT results are being compiled and a protocol is being drawn up, in order to standardize the test procedures and to homogenize the data analysis.

Keywords: non-destructive methods, large cross section, sawn timber, Spanish species

Introduction

The evaluation of material properties by means of nondestructive techniques is not a new concept. The fundamental hypothesis for the NDT of wood materials was initiated by Jayne (Jayne 1959). He proposed that the energy storage and dissipation properties of wood, which can be measured nondestructively by using several techniques, are controlled by the same mechanisms that determine the static behavior of such material (Ross and Pellerin 1994). Since the first research works (Bell et al. 1950; Galiginaitis et al. 1954; James 1962; McKean and Hoyle 1962; Senft et al. 1962; Pellerin 1965) good results have been achieved.

Concerning the use of NDT in Spain, the first experiences apart from visual grading were conducted at the beginning of the 1990s to grade maritime pine sawn timber using portable ultrasonic equipment (Martínez 1993). There is also some research experience in the assessment of old timber structures (Arriaga et al. 1992), and to quantify weight loss due to rotting using ultrasound velocity (Bucur et al. 1993). It was not until the year 2000 that the Spanish timber research community started to investigate NDT. A historical review starting with visual grading methods can be consulted in Carballo (Carballo et al. 2009).

Research works since then have mainly focused on the use of portable and commercial equipment to grade sawn timber (Hermoso 2001; Conde 2003; Arriaga et al. 2006; Íñiguez 2007) or used in the assessment of historical buildings (Esteban 2003).

The main Spanish species studied were: radiata pine, Scots pine, laricio pine and maritime pine. There is also experience with testing hybrid poplar *Populus x euramericana*, Douglas fir (*Pseudotsuga menziesii* (Mirb.) Franco) and sweet chestnut (*Castanea sativa* Mill.).

The most common techniques applied were: ultrasonic and stress wave, vibration analyses, penetration resistance, screw withdrawal force and drilling resistance (Esteban et al. 2007). Commercial and portable equipment were usually used.

Although it is relatively easy to conduct a NDT test, it is important to note that several factors affect NDT parameters. These factors can be divided into two categories: factors resulting directly from wood properties, such as knot size, slope of grain, moisture content, etc. and, on the other hand, factors related to the test procedures and devices used, like transducer coupling, path length and the size and shape of specimens.

Factors affecting ultrasonic measurements in wood have been widely studied (Bucur and Böhnke 1994). There are several research works on the effect of moisture content on ultrasound velocity (Sandoz, 1993) and correction factors proposed for vibration and ultrasound velocity (Moreno-Chan et al. 2010; Unterwieser and Schickhofer 2010). The influence of temperature on ultrasound propagation velocity is less important than moisture (Bucur, 2006). Specimen geometry can significantly affect velocity wave measurements (Divos et al. 2005) and wave propagation mode.

In structural sawn timber some correction factors are proposed for Spanish Scots and laricio pine using ultrasound waves by Arriaga (Arriaga et al. 2009).

Due to this large and diverse use of NDT, the authors propose to establish a common NDT procedure in the evaluation of Spanish structural timber properties. The main objective of this paper is to present the preliminary works conducted in order to achieve this objective.

Methodology and material tested

According to authors' compilation works, the main structural Spanish sawn timber species studied by NDT are radiata pine, Scots pine, laricio pine, maritime pine and sweet chestnut.

The commercial equipment and techniques applied are: Sylvatest Duo and Trio (ultrasound wave); Microsecond Timer, Arbotom and IML Micro Hammer (stress wave); Hitman HM200 and PLG (vibration analysis); Pilodyn 6J Forest (penetration resistance); Screw Withdrawal Resistance Meter SWRM (screw withdrawal force); IML resistograph and Rinntech resistograph (drilling resistance) and SIR10H-1,6GHz antenna GSSI (Ground-penetrating radar).

To standardize the nondestructive tests and to permit the comparison of results between species and different equipment within Spain, a three year research project conducted by the authors is running (Proy.: BIA 2010-18858. Ministerio de Ciencia e Innovación. Plan Nacional I+D+i 2008-2011).

Its first objective is to group all the main NDT results recorded in recent years by different research groups around the country, and then to create a homogenized data base to define equations and correction factors for Spanish species and commercially available equipment. Additionally, work on developing an agreed NDT test protocol are running to homogenize future data records.

Finally, regulatory approval of this nondestructive evaluation protocol using a standardization process will be necessary. The end users of NDT and research authorities will need these standardization results (Carballo et al. 2009; De Visser and Galligan 2011).

Beyond the standardization process carried out by the European Technical Committee CEN/TC 124 (embodied in EN 14081-4:2009), practical experiences in other countries apart from Brazil are unknown. A nondestructive testing standard (NBR 15521) for the mechanical classification of dicotyledonous sawn wood by means of ultrasonic testing was approved there in 2007.

The previous research work by this paper's authors studied the assessment of existing timber structures in Spain using NDT, and presented a proposed methodology, including some adjustment factors (Arriaga et al. 2009).

Using that experience and focused on new material, an Excel data sheet has been designed to create a homogenized data base.

The summarized information for each specimen contained in this data sheet is:

- General information (number, code, species, source and laboratory).
- Geometry (moisture content (MC), nominal and real dimensions).
- Visual grading (visual grade according to one or more visual standards).
- Pilodyn 6J Forest (radial and tangential penetration depth).
- SWRM (radial and tangential screw withdrawal force).
- Sylvatest (length and time of end to end propagation, direct and indirect tests).
- Microsecond Timer (length and time of end to end propagation, direct and indirect tests).

- PLG (longitudinal and transversal frequencies and mass).
- Bending test according to EN 408 (MOE, MOR and density).

The data base is now composed of 6,066 samples from research projects conducted by different Spanish researchers and institutions from 1996 to date.

The preliminary results of 687 samples from three different species (radiata, Scots and laricio pine), are presented in this paper. Section sizes and the number of specimens of each species are shown in table 1.

Table 1- Number of specimens according to size and species

Species	Cross-section (mm)	Number of pieces	Number
radiata pine	80 x 120	150	305
	150 x 200	80	
	150 x 250	75	
Scots pine	100 x 150	26	262
	150 x 200	176	
	200 x 250	60	
laricio pine	150 x 200	60	120
	200 x 250	60	
Total			687

Different correction factors were used for the NDT measurements:

- Moisture content (MC):

For ultrasonic wave velocity (Steinkamp BP-V equipment), a correction factor with a decrease in velocity of approx. 0.8% was applied for each 1% increase in MC, within a range of 5 to 30% MC (Sandoz 1989).

For the Microsecond Timer and PLG, a correction factor of a 1% decrease in velocity was applied for each 1% increase in MC (Authors' proposal).

For density and MOE (bending test EN 408), a correction factor with a 0.5% increase on density was applied for each 1% increase in MC, and a 1% decrease in MOE for each 1% increase in MC (EN 384).

- The length effect: a reference value of ultrasound wave velocity, V_{ref}, is applied for a length of 3.6 m. This value may be calculated from the velocity measured for length L (m), V_L, by the equation: $V_{ref} = V_L \cdot [1+(L-3.6) \cdot k_L]$, where $k_L = 0.014$ for Scots pine and 0.026 for laricio pine (Arriaga et al. 2009).

- The position of the sensors respecting the grain: a correction factor is applied for the angle adjustment of velocity of ultrasound waves in the range from 0º to 6º, of $k_\alpha = 0.01$, obtaining $V_0 = V_\alpha \cdot (1+\alpha \cdot k_\alpha)$ (Arriaga et al. 2009).

Results and discussion

Based on the first collection of data, which is composed of 687 samples, table 2 summarizes the results obtained for species and tests:

Table 2- NDT and bending test results

Species	Penetration depth (Pilodyn)					
	Radial		tangential		average	
	mean (mm)	CV (%)	mean (mm)	CV (%)	mean (mm)	CV (%)
radiata pine	11.3	18.92	11.3	24.48	11.3	19.41
Scots pine	11.7	21.67	11.1	20.79	11.4	19.68
laricio pine	9.7	24.23	9.5	24.34	9.6	22.58

Species	Screw withdrawal force (SWRM)					
	Radial		tangential		average	
	mean (kN)	CV (%)	mean (kN)	CV (%)	mean (kN)	CV (%)
radiata pine	2.13	21.32	2.03	23.58	2.08	19.72
Scots pine	1.48	30.70	1.53	28.89	1.51	28.50
laricio pine	2.31	22.20	2.37	24.28	2.34	22.28

Species	Sylvatest velocity					
	$Vel_{EEsyl12}$		direct		indirect	
	mean (m/s)	CV (%)	mean (m/s)	CV (%)	mean (m/s)	CV (%)
radiata pine	4933	8.04	4895	8.88	4782	8.89
Scots pine	4925	5.69	4804	5.07	4686	5.12
laricio pine	4807	8.28	-	-	-	-

Species	Microsecond Timer velocity					
	$Vel_{EEmst12}$		direct		indirect	
	mean (m/s)	CV (%)	mean (m/s)	CV (%)	mean (m/s)	CV (%)
radiata pine	4719	9.61	4591	9.32	4488	9.47
Scots pine	4945	4.92	5013	5.16	4897	5.08
laricio pine	-	-	-	-	-	-

Species	PLG velocity (longitudinal frequency)	
	Vel_{Lplg12}	
	mean (m/s)	CV (%)
radiata pine	4434	8.77
Scots pine	4480	6.15
laricio pine	4272	9.54

Species	Bending test (EN 408)					
	Density (Den_{12})		MOE_{glo12}		MOR	
	mean (kg/m^3)	CV (%)	mean (N/mm^2)	CV (%)	mean (N/mm^2)	CV (%)
radiata pine	491	10.78	8876	21.82	34.71	39.27
Scots pine	491	9.83	9750	16.64	40.21	27.34
laricio pine	588	14.06	10524	23.05	43.45	35.90

Statistical analyses were used to study the normality of the variables prior to further analyses. All variables showed normal probability distributions. Figure 1 shows the MOE frequency histogram for all species (bending test).

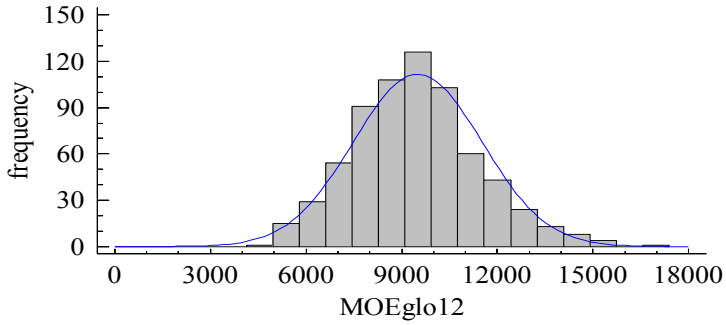

Figure 1- Frequency histogram for MOE_{glo12} (N/mm^2)

On the other hand, statistically significant differences between "species" were found in the one-way analysis of variance, as was expected. This is due to the intrinsic differences between species. Figure 2 shows an example of this for MOE.

Statistical diagnosis of each one-way analysis of variance confirms the validity of the assumptions of normality of distribution, homoscedasticity and independence.

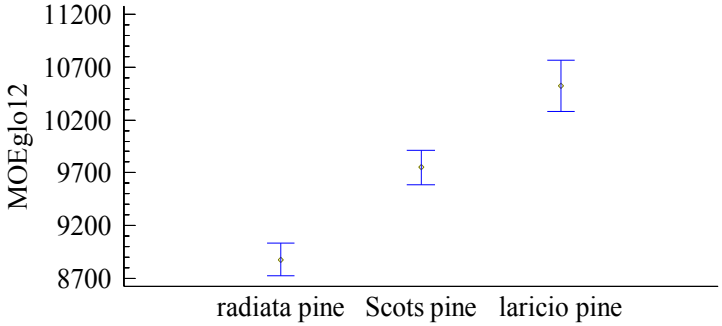

Figure 2- Means plot of one-way analysis of variance: MOEglo12 (N/mm2) vs. species

The ability of the different non-destructive values to function as predictors of the density, MOE and MOR of material is evaluated by means of multiple linear regression analysis. The equations are shown below.

The validity of the assumptions of normality distribution, linearity, homoscedasticity and independence by the equation model was tested and accepted.

Penetration depth and screw withdrawal resistance vs. density:

Penetration depth and screw withdrawal resistance as predictors of density are evaluated using the arithmetic mean of radial and tangential values:

For Pilodyn: $Den_{PLG12} = 688.059 - 9.8479 \cdot Depth_{PIL12} - 68.5543 \cdot Z_{rad} - 66.6052 \cdot Z_{sil}$ $R^2=0.42$

For SWRM: $Den_{PLG12} = 438.668 + 66.1475 \cdot Force_{SW12} - 68.1009 \cdot Z_{rad} - 28.7329 \cdot Z_{sil}$ $R^2=0.52$

Where: Den_{PLG12}: the global density of the piece adjusted to 12% moisture content, in kg/m^3; $Depth_{PIL12}$: the arithmetic mean of radial and tangential readings of penetration depth, in mm; $Force_{SW12}$: the arithmetic mean of radial and tangential readings of resistance, in kN; Z_{rad}: this is equal to 1 if the species

of timber is radiata pine; Z_{sil}: equal to 1 if the species of timber is Scots pine; and if the species is laricio pine, Z_{rad} and Z_{sil} are equal to 0.

Wave velocity vs. static modulus of elasticity (MOE):

Ultrasound, stress and vibration wave velocities as predictors of the MOE, are evaluated. The models used are:

For Sylvatest: $MOE_{glo12} = -8360.82 + 3.93105 \cdot Vel_{EEsyl12} - 2157.67 \cdot Z_{rad} - 1261.37 \cdot Z_{sil}$ $R^2=0.57$

For MST(*): $MOE_{glo12} = -10204.0 + 3.93982 \cdot Vel_{EEmst12} + 557.242 \cdot Z_{rad}$ $R^2=0.62$

For PLG: $MOE_{glo12} = -6487.35 + 3.988 \cdot Vel_{Lplg12} - 2323.92 \cdot Z_{rad} - 1638.61 \cdot Z_{sil}$ $R^2=0.58$

Where: MOE_{glo12}: static modulus of elasticity, in N/mm^2; $Vel_{EEsyl12}$: longitudinal ultrasound velocity, in m/s; $Vel_{EEmst12}$: longitudinal stress waves velocity, in m/s; Vel_{Lplg12}: velocity achieved with longitudinal frequency, in m/s; Z_{rad}: equal to 1 if the species of timber is radiata pine; Z_{sil}: equal to 1 if the species of timber is Scots pine; and if the species is laricio pine, Z_{rad} and Z_{sil} are equal to 0.

(*): model valid only for radiata and Scots pine

Wave velocity vs. modulus of rupture (MOR):

Ultrasound, stress and vibration wave velocities as predictors of the MOR, are evaluated. The models used are:

For Sylvatest: $MOR = -42.2589 + 0.0178433 \cdot Vel_{EEsyl12} - 11.0134 \cdot Z_{rad} - 5.47812 \cdot Z_{sil}$ $R^2=0.29$

For MST(*): $MOR = -36.5938 + 0.0156393 \cdot Vel_{EEmst12} + 5.40959 \cdot Z_{rad}$ $R^2=0.20$

For PLG: $MOR = -33.6838 + 0.0180851 \cdot Vel_{Lplg12} - 11.7415 \cdot Z_{rad} - 7.18882 \cdot Z_{sil}$ $R^2=0.29$

Where: MOR: modulus of rupture, in N/mm^2; $Vel_{EEsyl12}$: longitudinal ultrasound velocity, in m/s; $Vel_{EEmst12}$: longitudinal stress waves velocity, in m/s; Vel_{Lplg12}: velocity achieved with longitudinal frequency, in m/s; Z_{rad}: equal to 1 if the species of timber is radiata pine; Z_{sil}: equal to 1 if the species of timber is Scots pine; if the species is laricio pine, Z_{rad} and Z_{sil} are equal to 0.

(*): model valid only for radiata and Scots pine

Conclusions

Work compiling nondestructive testing values in timber is being undertaken in Spain. This has the purpose of collecting existing test results from different groups of researchers, after which cross-sections and species which are lacking from the data base will be added.

A testing protocol has also been designed and proposed. This has the purpose of making the results of future nondestructive tests by different researchers comparable.

The results of testing 687 specimens have been already collected and homogenized. Preliminary adjustment factors such as moisture content, length and slope of grain, have been proposed and are included in the data base.

As expected, the results of density prediction using penetration depth or screw withdrawal force as non-destructive parameters, have been shown to be acceptable in the structural evaluation of members, obtaining 0.42 and 0.52 of R^2, respectively. Using the mean value of two measurements (radial and tangential), plus species differentiation, better correlations are achieved.

There is a good relationship between wave velocity and the modulus of elasticity of timber (R^2 over 0.57). These results show that it is possible to use different methods as good indicators of the general quality of pieces. Better determination coefficients will be obtained when the dynamic elasticity modulus is used instead of wave velocity alone.

The weaker relationships between nondestructive testing results and the modulus of rupture (R^2 around 0.20), mean that wave velocity is not such a good index of the strength of material as others. This is because local defects have more influence on strength than the general quality of pieces. Although this was suspected previously, it has been sadly confirmed by these results.

Although this study does not yet include sufficient material to propose a grading method of timber based on nondestructive testing results, it does mark the route to this goal.

Acknowledgments

Ministerio de Ciencia e Innovación: Proy.: BIA 2010-18858. Plan Nacional I+D+i 2008-2011. Proy.: BIA 2006-14272. Plan Nacional I+D+i 2004-2007. Proy.: AGL 2002-00813. Plan Nacional I+D+i 2000-2003. CIFOR-INIA, Timber Structures Laboratory, Madrid (Eva Hermoso / Rafael Diez). UPC-INCAFUST, Cataluña (Joaquín Montón / Jordi Gené). AiTiM, Madrid (Fernando Peraza). Universidad de Valladolid, Campus Palencia (Milagros Casado / Luis Acuña). CETEMAS, Asturias (Vanessa Baño / Abel Vega). Francisco Arriaga and Guillermo Iñiguez-Gonzalez are members of the COST Action FP1101 "Assessment, Reinforcement and Monitoring of Timber Structures".

References

Arriaga, F; García, L.; Gebremedhin, K.G.; Peraza, F. 1992. Grading and load carrying capacity of old timber beams. International Summer Meeting, American Society of Agricultural Engineers. Charlotte, North Carolina, USA.

Arriaga, F.; Íñiguez, G.; Esteban, M.; Fernández-Golfín, J.I. 2006. Structural Tali timber (Erythrophleum ivorense A. Chev., Erythrophleum suaveolens Brenan.): Assessment of strength and stiffness properties using visual and ultrasonic methods. Holz als Roh- und Werkstoff, 64. P. 357 - 362.

Arriaga, F.; Íñiguez, G.; Esteban, M.; Bobadilla, I. 2009. Proposal of a methodology for the assessment of existing timber structures in Spain. 16th International Symposium on Nondestructive Testing of Wood. Beijing, China.

Bell, E.R.; Peck, E.C.; Krueger, N.T. 1950. Young's modulus of wood determined by a dynamic method. Report 1775. Madison, WI: U.S. Department of Agriculture, Forest Service, Forest Products Laboratory.

Bucur, V.; Böhnke, I. 1994. Factors affecting ultrasonic measurements in solid wood. Ultrasonics, 32 (5). P. 385 - 390.

Bucur, V.; Navarrete, M.A.; de Troya, M.T.; Sánchez, E.; Garros, S.; Diez, R. 1993. Fungy decay in wood by combined non-destructive testings. Ultrasonics International 93 Conference Proceedings, Vienna, Austria, 6-8 July 1993. P. 287 - 290.

Bucur, V. 2006. Acoustic of wood. 2nd Edition. Springer. Germany.

Carballo, J.; Hermoso, E.; Díez, R. 2009. Ensayos no destructivos sobre madera estructural. Una revisión de 30 años en España. Revista forestal (Costa Rica) 6 (17), 2009.

Conde, M. 2003. Caracterización de la madera estructural de Pinus nigra Subsp. Salzmannii (Characterization of structural timber of Pinus nigra Subsp. Salzmannii). Doctoral Thesis. Universidad Politécnica de Madrid, ETS de Ingenieros de Montes. 209 p.

De Visser, D.; Galligan, W. 2011. Design property assessment of single members in existing structures - NDE challenge. Proceedings 17th International Nondestructuve Testing and Evaluation of Wood Symposium. Sopron, Hungary.

Divos, F.; Denes, L.; Íñiguez, G. 2005. Effect of cross-sectional change of a board specimen on stress wave velocity determination. Holzforschung, 59. P. 230-231.

EN 384:2010. Structural timber. Determination of characteristic values of mechanical properties and density.

EN 408:2010. Timber structures. Structural timber and glued laminated timber. Determination of some physical and mechanical properties.

EN 14081-4:2009. Timber structures. Strength graded structural timber with rectangular cross section. Part 4: Machine grading. Grading machine settings for machine controlled systems.

Esteban, M. 2003. Determinación de la capacidad resistente de la madera estructural de gran escuadría y su aplicación en estructuras existentes de madera de conífera (Determination of the load carrying capacity of large cross section structural coniferous timber on existing structures). Doctoral Thesis. Universidad Politécnica de Madrid, ETS de Ingenieros de Montes. 365 p. PDF file: http://oa.upm.es/1404

Esteban, M.; Argüelles, R.; Arriaga, F.; Íñiguez, G.; Bobadilla, I. 2007. Current state of research on structural timber in Spain. Informes de la construcción. Vol. 59, 506, 15-27. Abril-junio 2007.

Galiginaitis, S.V.; Bell, E.R.; Fine, A.M. 1954. Nondestructive testing of wood laminates. Final Report. Louisville, KY: Office of Naval Research, Institute of Industrial Research, University of Louisville.

Hermoso, E. 2001. Caracterización mecánica de la madera estructural de Pinus sylvestris L. (Mechanical characterization of structural timber of Pinus sylvestris L.). Doctoral Thesis. Universidad Politécnica de Madrid, ETS de Ingenieros de Montes. 277 p. PDF file: http://oa.upm.es/644

Íñiguez, G. 2007. Clasificación mediante técnicas no destructivas y evaluación de las propiedades mecánicas de la madera aserrada de coníferas de gran escuadría para uso estructural (Grading by non destructive techniques and assessment of the mechanical properties of large cross section coniferous sawn

timber for structural use). Doctoral Thesis. Universidad Politécnica de Madrid, ETS de Ingenieros de Montes. 223 p. PDF file: http://oa.upm.es/415

James, W.L. 1962. Dynamic strength and elastic properties of wood. Forest Products Journal, 12 (6): 253-260.

Jayne, B.A. 1959. Vibrational properties of wood as indices of quality. Forest Products Journal. 9(11): 413-416.

Martínez García, J. J. 1993. Características mecánicas de la madera de Pinus pinaster Ait. obtenidas a partir de ensayos con piezas de tamaño estructural. Doctoral Thesis. Universidad Politécnica de Madrid, ETS de Ingenieros de Montes.

McKean, H.B.; Hoyle, R.J. 1962. Stress grading method for dimension lumber. Special Tech. Pub. 353. Philadelphia, PA: American Society for Testing Materials.

Moreno-Chan, J.; Walker, J.C.; Raymond, C.A. 2010. Effects of moisture content and temperature on acoustic velocity and dynamic MOE of radiata pine sapwood boards. Wood Sci Technol (2010) 45:609–626.

NBR 15521: Ensaios não destrutivos - Ultra-som - Classificação mecânica de madeira serrada de dicotiledôneas. (Non-destructive testing - Ultrasonic testing - Mechanical classification of dicotyledonous sawn wood). April 2007. Brasil.

Pellerin, R.F. 1965. A vibrational approach to nondestructive testing of structural lumber. Forest Products Journal. 15(3): 93-101.

Ross, R.J.; Pellerin, R.F. 1994. Nondestructive testing for assessing wood members in structures: A review. Gen. Tech. Rep. FPL-GTR-70 (Rev.). Madison, WI: U.S. Department of Agriculture, Forest service, Forest Products Laboratory. 40 p.

Sandoz, J.L. 1989. Grading of construction timber by ultrasound. Wood Sci. Tech. Vol 23: 95-108.

Sandoz, J.L. 1993. Moisture content and temperature effect on ultrasound timber grading. Wood Science and Technology 27:373-380. 1993.

Senft, J.F.; Suddarth, S.K.; Angleton, H.D. 1962. A new approach to stress grading of lumber. Forest Products Journal. 12(4): 183-186.

Unterwieser, H.; Schickhofer, G. 2010. Influence of moisture content of wood on sound velocity and dynamic MOE of natural frequency - and ultrasonic runtime measurement. Eur. J. Wood Prod. (2010) 69: 171-181.

Optimization of machine strength grading of structural timber by means of bending MOE profiles with high resolution

Jan Oscarsson
SP Wood Technology, SP Technical Research Institute of Sweden, Växjö, Sweden, jan.oscarsson@sp.se

Anders Olsson
Dep. of Building and Energy Technology, Linnæus University, Växjö, Sweden, anders.olsson@lnu.se

Bertil Enquist
Dep. of Building and Energy Technology, Linnæus University, Växjö, Sweden, bertil.enquist@lnu.se

Abstract

Most machine strength grading methods are based on rather poor statistical relationships between edgewise bending strength and modulus of elasticity (MOE), the latter determined either as flatwise bending MOE measured over a length of about one meter, or as global axial dynamic MOE. Furthermore, European Standards stipulate that local MOE in both edgewise bending and tension shall be determined at a critical section and over a length of five times the depth of the piece. However, a study of tensile strain fields determined on side board surfaces using contact-free measurement technique showed that stiffness reduction occurs very locally. This characteristic was used for development of a new indicating property (IP) defined as local edgewise bending MOE and determined by means of scanned fibre direction fields and stiffness integration over cross-sections. A maximum coefficient of determination equal to 0.77 was obtained between strength and such an IP determined over a length of about the member's half depth.

Keywords: coefficient of determination, contact-free, fibre angle, indicating property, laser scanning, machine strength grading, strain fields

Introduction

Machine strength grading of structural timber is based on statistical relationships between strength and non-destructively measured wood characteristics such as density, annual ring width, modulus of elasticity (MOE) and occurrence of knots. Structural properties are also influenced by, inter alia, reaction wood, top ruptures, fibre angle and fibre disturbances. It is well known (*e.g.* Hoffmeyer 1995) that the best indicating property (IP) of strength in both bending and tension is the MOE which can be measured in different ways. Most grading machines are based on flatwise bending or axial dynamic excitation. In the first case, a three-point bending test is carried out continuously as a piece is passing through a grading machine. The span length varies, typically between 600 and 1200 mm, depending on the make of the machine. Load P and deflection δ is registered and local static MOE (E_{flat}) is determined as

$$E_{flat} = Pl^3 /(48 I_f \delta) \quad (1)$$

where l is the span length and I_f is the second moment of inertia in the flatwise direction. In the second case, a piece is set into axial vibration by means of a hammer blow at one end. The resonance frequency

of the first axial mode of vibration is determined on the basis of the impulse response measured by either a microphone or a laser vibrometer. The global (*i.e.* average) axial dynamic MOE ($E_{a,1}$) is calculated as

$$E_{a,1} = 4\rho(f_{a,1}L)^2 \tag{2}$$

where ρ is the density, $f_{a,1}$ is the determined resonance frequency and L is the length.

Another global MOE can be determined on the basis of resonance frequencies corresponding to edgewise bending modes. Such modes include shear, but shear deformations have very little influence on resonance frequencies of lower bending modes. According to Bernoulli-Euler beam theory, in which shear deformations are disregarded, a bending MOE ($E_{b,1}$) corresponding to the resonance frequency ($f_{b,1}$) of the first edgewise bending mode can be estimated using

$$E_{b,1} = 0.96\rho L^4 f_{b,1}^2 / h^2 \tag{3}$$

where h is the depth of the piece, see Figure 1. There are grading machines based on edgewise bending excitation on the European market, but their application is limited.

The European Standard EN 408 specifies a test method for determination of strength and local as well as global static MOE in edgewise bending. A test set-up based on the standard is shown in Figure 1. The critical section, *i.e.* the section at which failure is expected to occur, shall be in a position between the two point loads. For a set-up according to Figure 1, the local static edgewise MOE (E_m) is calculated from

$$E_m = 6hl_1^2(F_2 - F_1)/[16I_e(v_2 - v_1)] \tag{4}$$

where l_1 is the length equal to $5h$ over which the local deformation v is measured, I_e is the edgewise second moment of inertia, F_2-F_1 is an increment of the sum of the two point loads and v_2-v_1 is the corresponding increment of local deformation. The global static edgewise MOE ($E_{m,g}$) is obtained from

$$E_{m,g} = 1242(F_2 - F_1)/[b(w_2 - w_1)] \tag{5}$$

where b is the piece thickness and w_2-w_1 is the increment of global deformation.

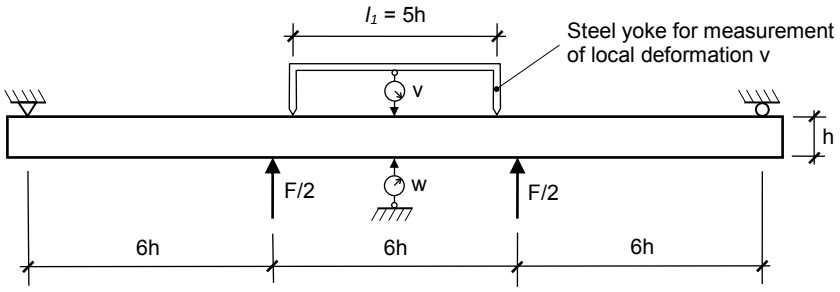

Figure 1—Test set-up according to EN 408 for determination of bending strength (σ_m), and static edgewise bending MOE, local (E_m) as well as global ($E_{m,g}$).

The standard EN 408 also includes a test method for determination of both strength ($\sigma_{t,0}$) and local static MOE ($E_{t,0}$) in tension parallel to the grain, the latter determined at the critical section as

$$E_{t,0} = l_1(F_2 - F_1)/[A(w_2 - w_1)] \tag{6}$$

where A is the cross-sectional area, F_2-F_1 is a load increment and w_2-w_1 is the corresponding increment of local deformation measured over a length (l_1) equal to five times the width, see Figure 2 (right).

In previous research (Olsson *et al.* 2012; Oscarsson 2012) the MOE measures presented in eqs. (1)-(5) were determined for a sample of 105 strength graded Norway spruce planks of dimension 45×145×3600 mm, sampled at Södra Timber's sawmill in Långasjö, Sweden. At the time of testing, the mean moisture content (MC) was 13%. The results presented in Table 1 show that the strongest relationship in terms of coefficient of determination (R^2) between bending strength and MOE was achieved for local static MOE in edgewise bending (E_m), determined in accordance with EN 408. This relationship (R^2=0.74) was considerably stronger than those obtained for $E_{a,1}$, $E_{b,1}$ and E_{flat}, respectively, which, as described previously, are applied in commercial strength grading. Thus, the results in Table 1 indicate that more accurate strength grading would be achieved if grading methods based on IPs reflecting local edgewise MOE were available. The foundation for such a method has recently been published (Olsson *et al.* 2013). In the research presented below, this method was applied for the purposes of investigating to what extent R^2 between strength and local MOE is dependent on the length over which the MOE is determined, and for which such length optimum relationship in terms of R^2 is achieved. In addition, a study of tensile strain fields, determined on surfaces of Norway spruce side boards by means of a contact-free measurement technique based on white-light digital image correlation (DIC), provided valuable information concerning stiffness variation along the length of the boards.

Table 1—Mean value, standard deviation, and relationship in terms of R^2 with bending strength (σ_m) for five different MOE measures, see eqs. (1)-(5), obtained from investigating 105 planks of Norway spruce of dimension 45×145×3600 mm (Olsson *et al.* 2012; Oscarsson 2012).

Method for assessment of MOE	Symbol	Mean [GPa]	Standard dev. [GPa]	R^2 between MOE and σ_m
Locally, static edgewise bending (EN 408)	E_m	11.0	2.8	0.74
Globally, static edgewise bending (EN 408)	$E_{m,g}$	10.6	2.3	0.72
Axial dynamic excitation	$E_{a,1}$	12.4	2.6	0.59
Edgewise dynamic excitation	$E_{b,1}$	12.7	2.7	0.65
Locally, static flatwise bending	E_{flat}	9.7	1.9	0.62

Materials

Test results obtained for two samples of timber, one of boards and one of planks, were utilized in this research. Both samples have been applied in previous but different investigations. The plank sample is described above. The board sample consisted initially of 56 Norway spruce side boards of dimension 25×120×3900 mm. The boards, which were of sawfalling quality, were delivered to Linnæus University from the sawmilling company Södra Timber, subsequently split and cut to dimension 25×56×3000 mm, and then used in an investigation concerning the possibility of grading glulam laminations of Norway spruce side boards in a wet state (Oscarsson *et al.* 2011). In that investigation, global axial dynamic MOE ($E_{a,1}$) and density was determined both in a wet state and after drying to a MC of 12-14%. Local static MOE in tension ($E_{t,0}$) and tensile strength ($\sigma_{t,0}$) were determined in accordance with EN 408 after the dried boards had been stored at a standard climate of 20°C/65% relative humidity for seven months. The test set-up is shown in Figure 2 and the relationships between stiffness measures and tensile strength are found in Table 2. As for the plank sample, the largest R^2 was achieved for the locally determined static MOE. For nine of the split boards, two-dimensional strain fields occurring on one of the flatwise surfaces during the tensile strength tests were determined on the basis of surface deformations measured using two master-slave connected contact-free measurement systems based on DIC technique, see Figure 2 (left).

Table 2—Mean value, standard deviation, and relationship in terms of R^2 with tension strength ($\sigma_{t,0}$) for three different MOE measures, see eqs. (2) and (6), obtained from investigating 116 side boards of Norway spruce of dimension 25×56×3000 mm (Oscarsson *et al.* 2011).

Method for assessment of MOE	Symbol	Mean [GPa]	Standard dev. [GPa]	R^2 between MOE and $\sigma_{t,0}$
Locally, static tension (EN 408)	$E_{t,0}$	9.59	3.40	0.68
Axial dynamic excitation, wet state	$E_{a,1,wet}$	10.84	2.58	0.55
Axial dynamic excitation, dried state	$E_{a,1,dried}$	13.04	2.93	0.52

Methods and measurements

Tensile tests and strain field determination

The set-up for the tensile tests and DIC measurements carried out for nine of the split boards is shown in Figure 2. The testing machine was of make MFL with a hydraulic force generation, 2.0 m length of stroke and a 3.0 MN load cell. The distance between the grips was ~1500 mm and the load was applied in force control mode. To ensure high measurement resolution of the long and narrow surface to be measured (56×~1500 mm), two identical DIC ARAMIS systems from GOM, Germany, were applied. Each system, including two cameras, separately measured deformations occurring on slightly more than half the visible board length, see Figure 5b. Prior to the tests, separate 3D coordinate systems were defined for each DIC system through a calibration procedure based on the two cameras being positioned at angles and distances that depend on the size of the object to be measured. The difference in angle meant that stereoscopic images were obtained from each system. The master-slave application implied that pictures were taken simultaneously by both pair of cameras at an interval of three seconds during a load test. Each double pair of pictures represented a *load stage* to which unique strain fields corresponded. Based on the stereoscopic images, 3D coordinates of a large number of measuring points on the surface were determined for every load stage and the strains at each such point was calculated using ARAMIS software. The distance between measuring points was 3.6 mm in longitudinal board direction and 1.8 mm in lateral direction.

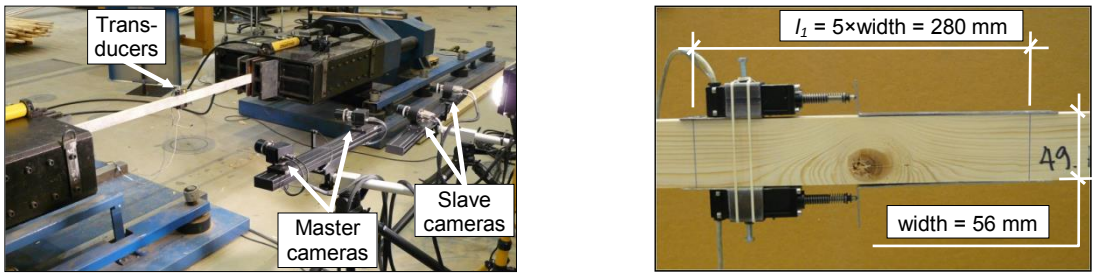

Figure 2—Set-up for tension tests according to EN 408 and for DIC measurements (left), and transducers for deformation measurements at assumed critical board section (right).

To visualize strains along the entire board length jointly and simultaneously, a third coordinate system to which the other two could be transformed was needed. For this purpose, another GOM measurement system called TRITOP was used. A set-up, see Figure 3 (left), including orientation crosses, a scale bar and 27 reference point markers fixed to a metal sheet, was arranged. On the basis of digital pictures of the set-up taken from several angles using a photogrammetric camera, the third 3D coordinate system was defined using TRITOP software. This implied that the markers on the sheet shared a fixed coordinate relationship, a characteristic that was utilized for the coordinate transformation. When a master-slave measurement was prepared, the sheet was put behind the board, see Figure 3 (right). As the pictures of the first load-stage were taken, the markers were also caught and their positions in each ARAMIS coordinate system determined. By that, a relationship between TRITOP coordinates and ARAMIS coordinates was

established and the transformation could be carried out accordingly. The transformed measurement results from the two ARAMIS systems were subsequently combined and jointly visualized, see Figures 5c-d.

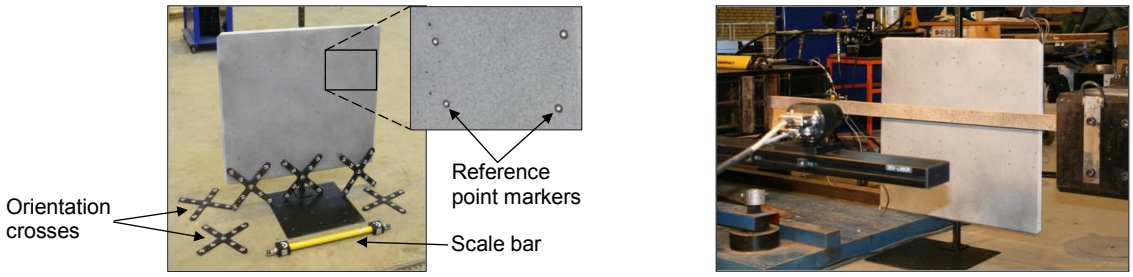

Figure 3—Set-up for determination of TRITOP coordinate system (left) and set-up for establishment of relationship between ARAMIS coordinates and TRITOP coordinates.

Determination of bending MOE profiles and local IP

In the previous research referred to in Tables 1-2, the highest R^2 between strength and stiffness was achieved for MOE determined locally in accordance with EN 408. As mentioned in the *Introduction*, it can be assumed that more accurate grading will be achieved if grading methods based on locally determined edgewise IPs were available, and that such a method had recently been presented (Olsson *et al.* 2013). In this new method, an optical scanner of make WoodEye is applied for lengthwise dot laser scanning of timber surfaces. By means of the tracheid effect, information about the angle φ between local fibre direction and the member's longitudinal direction is obtained, see Figure 4 (left). Even small angles will cause considerable impairment of the structural properties, since wood is a strongly orthotropic material with superior performance in the longitudinal fibre direction. Scanned high resolution information about φ provides a basis for transformation of material properties relating to the fibre direction to local material properties referring to the member's direction. Local MOE in the latter direction provides data for integration of MOE profiles valid either for edgewise bending or in the axial direction of the member. According to Olsson *et al.* (2013), the IP for a certain member is defined as the lowest *bending* MOE found along the piece. Important assumptions in the new method are that

- the density, ρ, and the MOE in the fibre direction, E_l, are constant within a member,
- other stiffness parameters are linear functions of E_l,
- fibre directions measured on the wood surface are located in the longitudinal-tangential plane,
- the fibre direction coincide with the wood surface, *i.e.* the diving angle is set to zero, and
- the fibre direction measured on a surface is valid to a certain depth, *i.e.* the fibre angle φ shown in Figure 4 (left) is assumed to be valid in the volume defined by the area dA (Figure 4, middle) times the length dx (Figure 4, left and right).

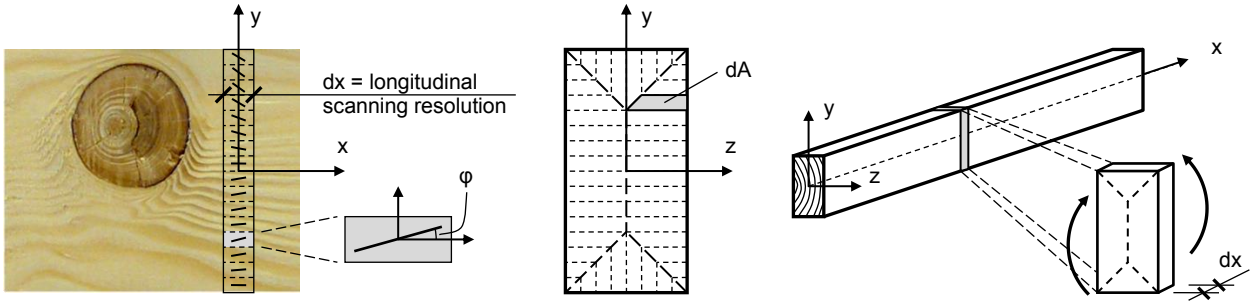

Figure 4—Local fibre directions scanned on a member's surface (left), cross-section divided into sub-areas (middle) implying that the exhibited angle φ is valid within the volume $dA \times dx$, and segment of length dx (right) the edgewise bending MOE of which is calculated by stiffness integration over the segment's cross-section.

Thus, E_l is the only property, apart from ρ, that has to be determined individually for each member. This is done such that an axial eigen value analysis on a simple one dimensional finite element model of the piece results in the same longitudinal resonance frequency as the one determined experimentally.

Results and discussion

DIC measurements

The results of the DIC measurements are presented in Figure 5 using *contour plots* and *section diagrams.* A *contour plot* means that the strain distribution is visualized for a certain load stage, on the basis of a defined colour scaling. *Sections* are defined in camera images as lines on the measured surface and strains and displacements along such lines can be plotted in corresponding *diagrams*. An example of typically achieved results is shown in Figure 5. The exhibited strains correspond to a tensile stress of 26.4 MPa. An image of the measured surface is shown in Figure 5a. Contour plots showing longitudinal tensile strains, ε_x, achieved separately by the two DIC systems are exhibited in Figure 5b. The combination of these plots is visualized in Figure 5c which also includes the position of two defined sections and of the origin of the TRITOP coordinate system. Longitudinal tensile strains along the sections are presented in Figure 5d.

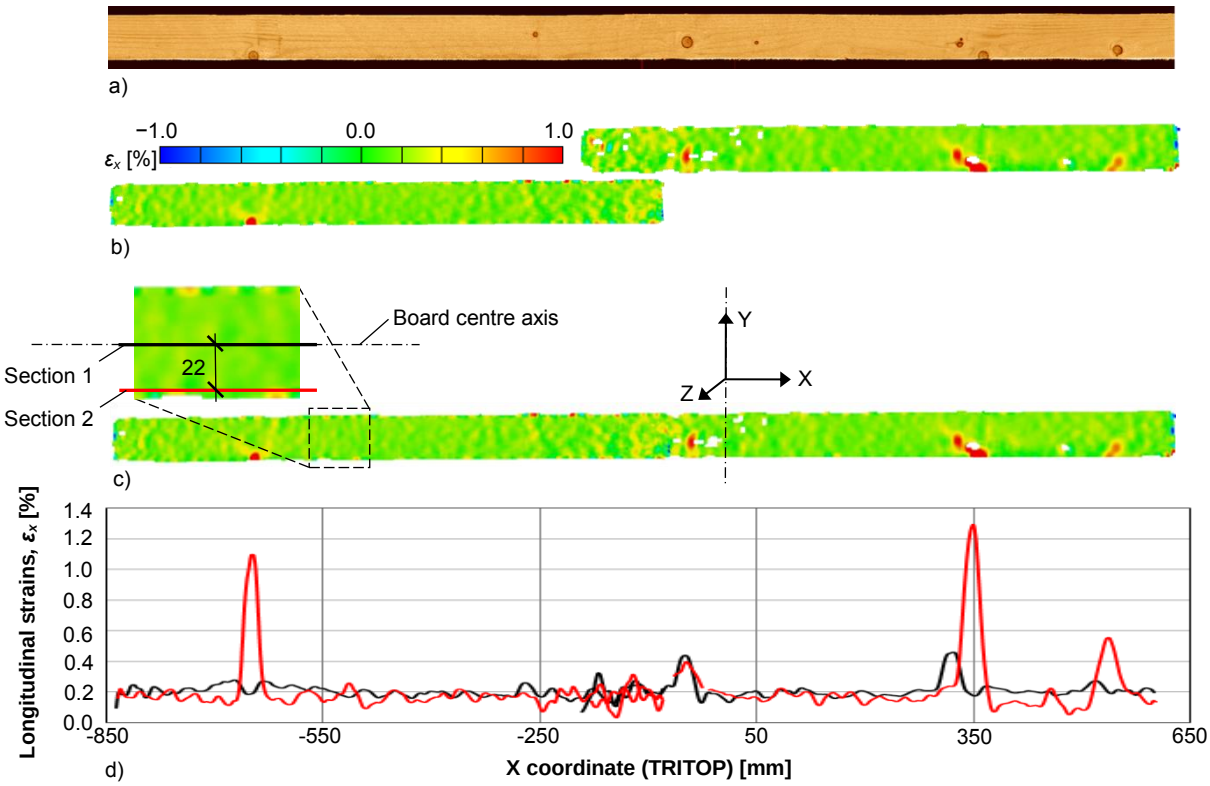

Figure 5—DIC measurement results for board no. 28B at a tensile stress of 26.4 MPa: a) flatwise board surface, b) contour plots of longitudinal strains, ε_x, determined by master system (left) and slave system (right), c) combined contour plot, positions of defined sections (left detail), and position of TRITOP coordinate system (right detail), and d) longitudinal strains, ε_x, along Sections 1-2.

The most important result of the DIC measurements is that the reduction of MOE at critical knots occurs very locally. It was found that the length of such reduction, indicated in Figure 5d by the increase of longitudinal strain at TRITOP x-coordinates -650 mm and 350 mm, roughly corresponded to the board's width. This length is just 20% of the one of five times the width that according to EN 408 shall be applied

for determination of local MOE in tension, see eq. (6). Thus, on the basis of the displayed results, it can be concluded that the method of EN 408 will result in an overestimation of local tensile MOE at critical knots, since the stipulated measurement length of 280 mm, see Figure 2 (right), will include clear wood parts in which the stiffness is unaffected by the presence of knots. In this context, knots are of particular importance, since failures in timber members are very often related to such defects. A more thorough description of the DIC measurements and results are found in Oscarsson (2012).

Bending MOE profiles and optimum relationship between IP and bending strength

Typical edgewise bending MOE profiles obtained for an investigated plank are shown in Figure 6. The scanning resolution in longitudinal direction, *i.e.* the distance between dot laser measurements, was 0.8 mm. The left profile exhibits a bending MOE profile calculated for maximum resolution, *i.e.* a resolution equal to the scanning resolution. The right profile displays a moving average MOE calculated over an interval equal to half the depth of the piece. The latter means that each MOE value along the profile is calculated as the average value of the surrounding 72 mm. A comparison of the two graphs shows that the IP's dependency on the length of the moving average interval is strong. The IP corresponding to full resolution was 5.5 GPa, whereas a higher value (IP=7.6 GPa) was reached for the moving average profile. The relationship between IP and length interval of moving average was studied in more detail. Of particular interest was the IP achieved for the interval of 725 mm, equal to five times the depth, *i.e.* the length over which local MOE in both bending and tension is determined according to EN 408. This IP was as high as 12.0 GPa, whereas the actual local bending MOE according to EN 408 was 10.6 GPa.

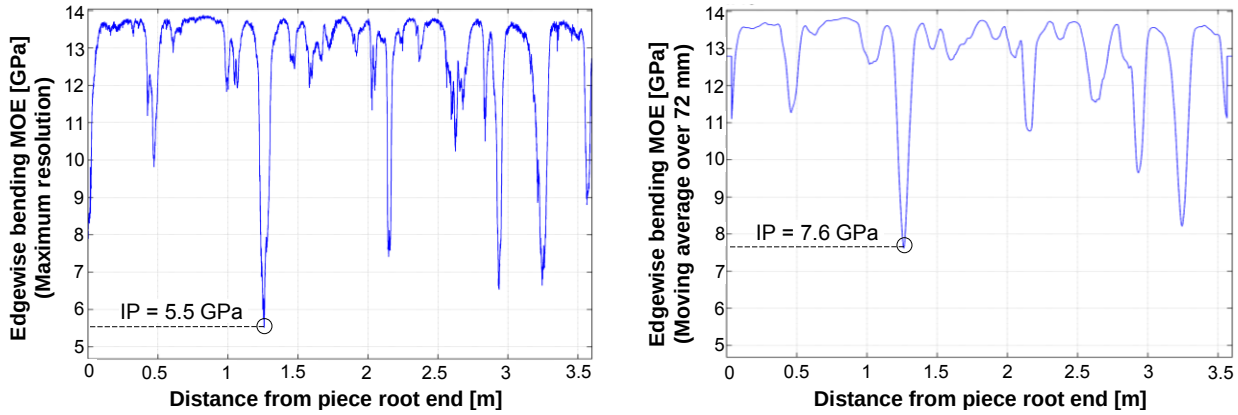

Figure 6—Bending MOE profiles for plank no. 34 corresponding to maximum resolution (left) and to a moving average calculated over a length interval of half the depth of the plank (right), respectively.

For the board sample, profiles of both bending and axial MOE were studied and corresponding IPs in terms of lowest MOE along each board determined. As for the planks, the IP's dependency on the length of the moving average interval was noted. Consequently, it was also interesting to investigate to what extent the variation of length interval influenced the R^2 between IP and strength. For both samples, MOE profiles of bending and axial MOE, respectively, were calculated for different length intervals and corresponding IPs were determined. The results presented in Figure 7 show that, for both samples, higher R^2 was achieved for IPs based on bending. For the board sample, which was tested in tension, this may seem surprising. An explanation may be that edge knots cause uneven stress distribution over the cross-section resulting in edgewise deformations. The results also show that maximum R^2 values were achieved for IPs determined over a length interval of about half the width/depth. A comparison between these R^2 values and those presented in Tables 1-2 reveals interesting facts, partly discussed in Olsson *et al.* (2013). The maximum R^2=0.68 for the plank sample (Figure 7, left) is higher than those referring to $E_{a,1}$, $E_{b,1}$ and E_{flat} in Table 1, implying that the new grading method can provide a grading accuracy that exceeds what is achieved by common methods on the market. However, R^2 determined on the basis of static edgewise

bending MOEs according to EN 408 (E_m and $E_{m,g}$ in Table 1) are stronger than 0.68. Since the MOEs determined on the basis of the standard reflect "real" MOEs, it can be concluded that there is a potential for improvement as regards the assumptions on which the new grading method is based. Yet, the maximum R^2=0.77 for the board sample is considerably stronger than those presented in Table 2, which is probably due to the fact that the strength of narrow pieces is much dependent on the occurrence of single large knots and that this characteristic is properly caught by means of the new method.

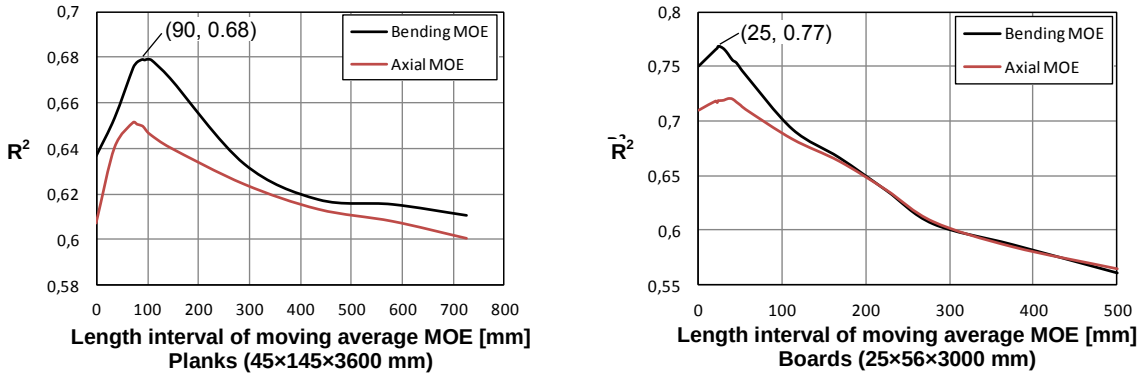

Figure 7—Relationship between length interval of moving average MOE and R^2 between strength and IP.

Conclusions

The research presented in this paper shows that determination of local MOE in accordance with EN 408 results in an overestimation of the MOE. By means of the new grading method (Olsson *et al.* 2013) in which MOE profiles are applied for IP determination, it was found that maximum R^2 between strength, in bending as well as in tension, and IP was achieved for IPs determined as moving average *bending* MOE calculated over a length interval of approximately half the depth/width of investigated timber members.

References

EN 408. 2010. Timber structures – Structural timber and glued laminated timber – Determination of some physical and mechanical properties. European Committee for Standardization.

Hoffmeyer, P. (ed.) 1995. Strength grading adds value, Part 2 – Available technique. Technical University of Denmark, Lyngby, Denmark. Technical Report 335-1995 (in Danish, Norwegian and Swedish).

Olsson, A.; Oscarsson, J.; Johansson, M.; Källsner, B. 2012. Prediction of timber bending strength on basis of bending stiffness and material homogeneity assessed from dynamic excitation. Wood Science and Technology. 46(4): 667-683.

Olsson, A.; Oscarsson, J.; Serrano, E.; Källsner, B.; Johansson, M.; Enquist, B. 2013. Prediction of timber bending strength and in-member cross-sectional stiffness variation on the basis of local wood fibre orientation. European Journal of Wood and Wood Products. 71(3): 319-333.

Oscarsson, J.; Olsson, A; Johansson, M; Enquist, B; Serrano, E. 2011. Strength grading of narrow dimension Norway spruce side boards in the wet state using first axial resonance frequency. International Wood Products Journal. 2(2): 108-114.

Oscarsson, J. 2012. Strength grading of structural timber and EWP laminations of Norway spruce – Development potentials. Licentiate thesis, Report No. 15, School of Eng., Linnæus Univ., Växjö, Sweden.

Ultrasound as a tool in defining the reuse potential of wood poles

Flaviane Flor de Faria Freitas
Master Student, Laboratory of Nondestructive Testing (LabEND), School of Agricultural Engineering (FEAGRI), University of Campinas (UNICAMP), Campinas, São Paulo, Brazil, flavianeff@gmail.com

Raquel Gonçalves
Associate Professor, University of Campinas (UNICAMP), College of Agricultural Engineering (FEAGRI) and Coordinator of the Laboratory of Nondestructive Testing (LabEND), Brazil, raquel@agr.unicamp.br

Elcio Coelho Jr.
Undergraduate Student, Laboratory of Nondestructive Testing (LabEND), School of Agricultural Engineering (FEAGRI), University of Campinas (UNICAMP), Campinas, São Paulo, Brazil, e_coelho1@hotmail.com

Abstract

Discarding of wood that comes from poles and crossarms is a challenge for managers of electric power distribution companies, for this wood was treated with potentially toxic chemical products. In Brazil, the National Policy on Solid Waste (PNRS) guidelines indicates that the companies are responsible for any damage that may be provoked by improper management of their residues or rejects. The objective of this paper was to evaluate the uses of ultrasound to determine the reuse potential of poles in function of the non-compromised material volume. Eight wooden poles were used for the experiments, retrieved from the electric network by the dealer due to some deterioration problems presented. The poles were thoroughly examined by ultrasound following guidelines already used for pole inspection. The results indicate that analysis tool is adequate and efficient in indicating the reuse potential of poles that are no longer fit to remain in the network.

Keywords: electrical network structures, solid residues, treated wood

Introduction

The disposal of wood from unsuitable poles is nowadays, in Brasil, a bigger problem, since such wood is treated with potentially toxic chemical products. If they are sold, auctioned or donated, those who purchase these types of wood can direct them to health-compromising usages, due to possible leaching of toxic elements (chrome, copper and arsenic), by toxic emissions arising from their burn, or by contact with humans, if used in creating furniture or other domestic or commercial artifacts.

As of August 2nd 2010, a law has been approved (numbered 12305), which establishes guidelines of the National Policy on Solid Waste (PNRS). In said law, issues concerning the final destination of solid residues are presented, as well as the cycle of life for different products, which includes reuse, recycling, recovering, and transformation into inputs and/or other products, in order to avoid or minimize adverse environmental impacts. Additionally, this law mentions reversed logistic, which is composed of instruments, actions, and procedures which allow restitution of solid residues to the business industry.

This insures reuse of such residues in their cycle, other productive cycles, or other environmentally correct final destinations. It also establishes that the dealers are to be responsible for the rejects, as well as the use of the disposal material.

In Canada, 3/4 of all discarded poles are reused in different applications, such as finishing on gardens, retaining walls on the coasts, etc. (TRADA TECHNOLOGY & ENVIROS CONSULTING Ltd, 2005). In December 2008, California's Environmental Protection Agency presented a standard to control reuse or clean disposal of treated wood, such as poles. In England, a similar standard exists since 2003.

Brazilian Energy Dealers have been replacing crosshead timber with other materials, such as light concrete or polymeric materials, but it is difficult to compare them to wood, when it comes to the relationship between resistance and weight. Besides, using structures such as cementitious matrix does not avoid environmental issues. On the contrary: cement production takes up a lot of energy, in addition to being responsible for about 7% of the planet's CO_2 emissions. According to data used by the Intergovernmental Panel on Climate Changes (IPCC), 1 ton of CO_2 is emitted into the atmosphere for each ton of cement produced. In 2007 alone, Brazil produced 44 millions of tons of cement, which resulted in an emission of 29.4 millions of tons of CO_2. For that reason, this material should be used responsibly. Increasing its life cycle through reuse, for instance, can be one of the minimization alternatives to the environmental damages.

Based on these matters, both the Laboratory of Nondestructive Testing (LabEND) and the Laboratory of Materials and Structures (LME) are conducting a research called "*Matriz High Tech de Reuso e Descarte Limpo*", sponsored by CPFL. Their goal is to develop a diagnostic of the solid residues generated by CPFL, and propose promising options for the reuse of discarded materials. One of the research group's suggestions to avoid environmental problems of the disposal of wooden poles is to reuse such material directly in another of the dealer's processes, reducing the smaller pieces, and using them in a new matrix.

Researchers have identified that wooden poles discarded from the electric power network present proper mechanical characteristics which allow their reuse (CLAUSEN, MUEHL e KRZYSIK, 2006; COOPER 1996; LEICHTI, MEISENZAHL e PARRY, 2005; LI, SHUPE e HSE, 2004, MUNSON e KAMDEM, 1998).

Therefore, within the context of the aforementioned project, the P&D research will evaluate, from methodological, resistance and rigidity points of view, the reuse of wooden poles - discarded from the electric power network - for creation of crosshead timber. In that context, the objective of this study was to evaluate ultrasound usage to determine the reuse potential of poles, in function of the non-compromised material volume.

Methodology

Eight Eucalyptus wooden poles were used in the development of this research: six from *Eucalyptus citriodora* and two from *Eucalyptus saligna*. All poles had been retrieved from the electric network and provided by CPFL.

Initially, the poles were scoped at every 200 mm from the base, with the pole's initial outbreak as ground zero. The embed stretch was not considered. Two radial positions were marked in each measurement line (D1 and D2).

Before beginning ultrasound testing, the equipment was calibrated with an acrylic bloc, for which the velocity was known. The circumferences of the poles were also measured in each marked line, to calculate the diameter (wave path length), and, subsequently to determine de wave propagation velocity.

Measurement of the wave propagation time on both radial positions of each marked line - on the transverse sections of the poles - was made with ultrasound equipment (USLab, AGRICEF, Brazil) and 45Hz longitudinal transducers (Figures 1a and 1b).

The poles were inspected by ultrasound to evaluate if they had enough wood volume with residual compatible resistance for pole sawing and production of crossarms. The methodology used for this procedure was the one proposed in Research and Development projects (P&D) previously conceived by the research group, financed by CPFL (P&D no. 121 and 133). The radial velocity propagation results were compared to the pole classification zones established during the previous study of said research (P&D 121 and 133). This classification indicates the velocity borne to which the pole presents residual resistance above critical values. These values were established by the energy dealer and, due to that, the pole parts that presented radial velocity for wave propagation above established limits were considered adequate, being then sent to sawing process for crossarms.

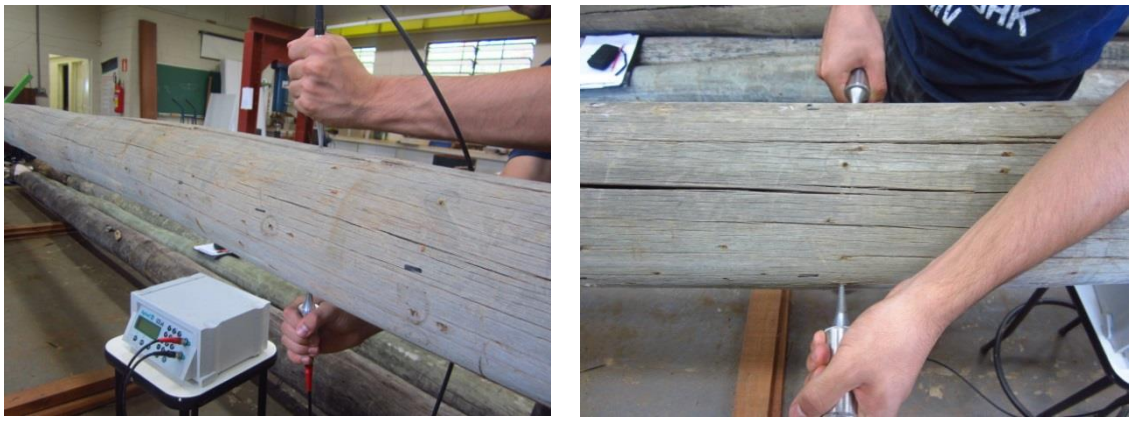

(a) (b)

Fig.1 - Ultrasound testing on poles, on D1 and D2 positions.

The parts of the poles that were considered adequate (previous step) were firstly cut transversely into 2 m long logs. At sawmill, the logs go through the stripping of their slabs (Figure 2a), followed by sawing, which leaves them with compatible dimensions to the crossarms. The transverse section of the crossarms used for this study had 90 mm x 90 mm (5 pieces) in compliance with the Technical Specification of CPFL 2900 (2009), and 112 mm x 90 mm (7 pieces), in compliance with NBR 8458 (2010).

During the sawing process, the crossarms were visually evaluated, in order to verify if the process of separation of the poles and of the regions of the poles using ultrasound had had satisfactory results. Figure 3 shows a prepared crossarm, after sawing.

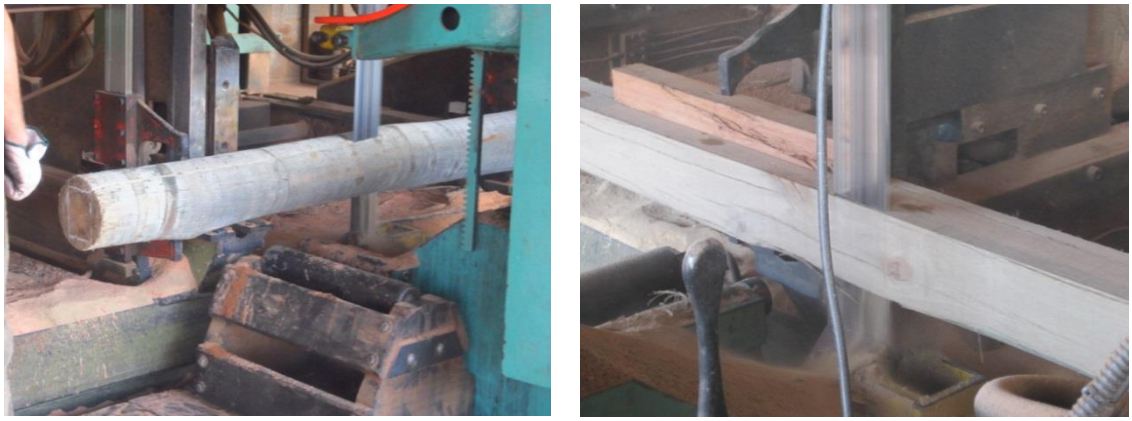

(a) (b)

Fig. 2 - slab removal (a) and sawing (b)

Fig. 3 – Crossarm obtained after partial pole sawing.

Results

The velocity results were put in a table for all eight inspected poles, considering both radial measurement positions (D1 and D2).

Viable poles for sawing for crossarms production were the ones that presented at least 11 consecutive measurement points with velocities above the critical value - of lengths above 2 m. This critical value was established in the research group's previous project with the energy dealer.

Table 1 summarizes the poles analysis by means of ultrasound wave propagation velocities.

Table 1— Numbering, diameter (ϕ), number of measurement lines with ultrasound (n), results concerning the velocity analysis and the number of crossarms retrieved from each pole (N)

Pole/ ϕ	n	Consecutive measurement points with velocities indicating good conditions	N
1 190 mm	26	6 points (≅1,2 m of well-preserved wood) from 21st° point (≅4,2 m from outbreak)	0
2 190 mm	31	31 points (≅6,2 m of well-preserved wood)	2
3 248 mm	27	0 points (0 m of well-preserved wood)	0
4 210 mm	28	28 points (≅5,6 m of well-preserved wood)	2
5 178 mm	29	28 points, being 11 on the first part and 17 on the second (≅2,2 m of well-preserved wood on the first part and 3,40 m on the second part)	2
6 226 mm	25	24 points from the second point after outbreak (≅4,8 m of well-preserved wood)	2
7 250 mm	25	0 points (≅ 5 m of well-preserved wood)	4
8 170 mm	29	3 widely spaced points on the pole's length.	0
		Total amount of crossarms	**12**

Throughout this research, ultrasound experiments will be conducted on these crossarms, in order to classify them according to criteria established by a previous project with the energy dealer, as well as humidity and density tests, and static bending tests, in order to verify if they are in accordance with the acceptance criteria established by the energy dealer NBR 8458 standard (2010) and the Technical Specification from CPFL 2900 (2009).

Initial (only with part of the sample) results of these analysis, show that no crossarms had signs of biological or insects attack, but some of them present cracks and apparent density below the minimum value (810 $kg.m^{-3}$) established by energy dealer. The mean moisture content were near 12% and the longitudinal ultrasound velocity was above 5000 $m.s^{-1}$, indicating , by previous results (P&D 133), that the crossarms have strength superior to the minimum values established for their acceptance.

Conclusions

This study has evidenced the viability of the ultrasound experiment on inspections of poles discarded from the network, in order to identify the zones in which reuse would be possible for crossarms production.

Acknowledgements

We thank the Companhia Paulista de Força e Luz (CPFL Energia) for financing this research and the Master scholarship. We also thank the National Council of Technological and Scientific Development (CNPq) for the undergraduate research scholarship and the College of Agricultural Engineering (FEAGRI) to the laboratory infrastructure.

References

Associação Brasileira de Normas Técnicas – NBR 8458/1984 – Cruzetas de madeira para redes de distribuição de energia elétrica. 13p. Rio de Janeiro (RJ), 1984.

BRASIL. Lei nº 12305, de 2 de agosto de 2010. Institui a Política Nacional de Resíduos Sólidos (PNRS); altera a Lei 9605, de 12 de fevereiro de 1998; e dá outras providências. Available at: < http://www.planalto.gov.br/ccivil_03/_ato2007-2010/2010/lei/l12305.htm>. Access in Aug 14th 2010.

CLAUSEN, C. A.; MUEHL, J. H.; KRZYSIK, A. M. Properties of structural panels fabricated from bioremediated CCA-treated wood : Pilot scale. **Forest Products Journal**, Madison/USA, v. 56, n. 3, p. 32-35, March 2006.

COMPANHIA PAULISTA DE FORÇA E LUZ. **CPFL 2893**: Cruzetas de madeira preservada e não preservada para redes aéreas de distribuição de energia. Brazil, 2009. 25, p.

COMPANHIA PAULISTA DE FORÇA E LUZ. **CPFL 2900**: Cruzetas de Madeira Preservada e Não Preservada 2000mm. Brazil, 2009. 5, p.

COOPER, P. et al. The Potential for Re-Use of Preservative-Treated Utility Poles Removed From Service. **Waste Management & Research**, v. 14, n. 3, p. 263-279, June 1996.

LEICHTI, R. J.; MEISENZAHL, M.; PARRY, D. Structural timbers from retired Douglas-fir utility poles. **Forest Products Journal**, Madison/USA, v. 55, n. 3, p. 32-35, March 2005.

LI, W.; SHUPE, T. F.; HSE, C. Y. Physical and mechanical properties of flakeboard produced from recycled CCA-treated wood. **Forest Products Journal**, Madison/USA, v. 54, n. 2, p. 89-94, Feb. 2004.

MUNSON, J. M.; KAMDEM, D. Reconstituted particleboards from CCA-treated red pine utility poles. **Forest Products Journal**, Madison/USA, v. 48, n. 3, p. 32-35, March 1998.

TRADA TECHNOLOGY & ENVIROS CONSULTING Ltd. Options and risk assessment for treated wood waste. The Waste & Resources Action Programme, UK, 2005.

Adequacy of Standards of Wood Grading Using Ultrasound to the Standard of Structural Design

Gisleiva Cristina dos Santos Ferreira
Assistant Professor, College of Technology (FT), University of Campinas (UNICAMP), Campinas, São Paulo, Brazil, gisleiva@ft.unicamp.br

Raquel Gonçalves
Associate Professor, University of Campinas (UNICAMP), College of Agricultural Engineering (FEAGRI)and Coordinator of the Laboratory of Nondestructive Testing (LabEND), Campinas, São Paulo, Brazil. raquel@agr.unicamp.br

Rafael de Souza Favalli
Graduate Student, Laboratory of Nondestructive Testing (LabEND), School of Agricultural Engineering (FEAGRI), University of Campinas (UNICAMP), Campinas, São Paulo, Brazil, rs.favalli@gmail.com

Cinthya Bertoldo
PhD Student, Laboratory of Nondestructive Testing (LabEND), School of Agricultural Engineering (FEAGRI), University of Campinas (UNICAMP), Campinas, São Paulo, Brazil, cinthyabertoldo@gmail.com

Abstract

To meet the needs of designers who use the guidelines for structural design (NBR 7190, 1997) as a reference for calculations, the classifying table of the Brazilian standard that proposes mechanical grading of timber using ultrasound test (NBR 15521, 2007), includes, besides longitudinal modulus of elasticity E_M, expected values for the characteristic values of strength of compression parallel to grains ($f_{c0,k}$) and for the average modulus of elasticity obtained in compression parallel to grains tests (E_{c0}). The objective of this research was to evaluate the adequacy of the f_{ck} and E_{c0} values, predicted while using the NBR 15521 (2007) standard, as well as the framing of characteristic values of strength of stress parallel to grain ($f_{t0,k}$) and average stress modulus of elasticity (E_{t0}) obtained with specimens from the same sample. The results indicated that the expected values for f_{c0k} and for E_{c0} were adequate, but it is difficulty to correctly infer the results for stress using the relations with compression proposed by NBR 7190 (1997).

Keywords: wave propagation, compression parallel to grain, stress parallel to grain, Eucalyptus grandis.

Introduction

The Brazilian standard NBR 15521 (2007) proposes mechanical grading of hardwood lumber by means of ultrasound wave propagation tests. This standard was developed based on results of tests in structural lumber from hardwood tropical species with an average age of 45 years.

The grading established in this standard can be done in three different ways, depending on the moisture content condition of the wood at the moment of testing. These conditions are as follows: wood with moisture content above fiber saturation point, adopted as being 30%; wood in equilibrium condition,

considered as having moisture content between 11% and 13%, and wood with intermediate moisture content between the saturated and the equilibrium conditions.

When using direct longitudinal ultrasound wave propagation, parallel to the fibers, as a grading parameter, tests to obtain velocity must be conducted on the saturated condition (V_{LLsat}). For wood in the equilibrium condition, the grading parameter must be the stiffness coefficient (C_{LL}), calculated with both the apparent density value (ρ) and the longitudinal velocity (V_{LL}) in the equilibrium moisture content ($C_{LL} = \rho\ V_{LL}^2$). To perform grading in wood with intermediate moisture content, between the saturated and the equilibrium conditions, the standard indicates a correction equation for determining velocity in the saturated condition, which enables similar grading to the first case (saturated wood condition).

The primary parameter for the grading of wood adopted by this standard (NBR 15521, 2007) is the stiffness of structural lumber, represented by the longitudinal modulus of elasticity (E_M) obtained through static bending in the equilibrium moisture content (12%).

On the other hand, the Brazilian Standard for Designer Wooden Structures (NBR 7190, 1997) based its structural calculations and strength classes on values obtained through compression tests parallel to the fibers (f_{c0}) conducted on small and clear specimens.

To meet the needs of researchers, who use the Designer Standard (NBR 7190, 1997) as a reference for calculating wooden structures, the grading table presented on the Ultrasound Grading Standard (NBR 15521, 2007) incorporates expected values for characteristic strength in compression parallel to the fibers ($f_{c0,k}$) and for the average modulus of elasticity in compression parallel to the fibers ($f_{t0,k}$), as well as the primary grading parameter - the modulus of elasticity in bending (E_M at moisture content of 12%). Furthermore, the Designer Standard indicates equations that connect the parallel compression parameters to other necessary parameters for designing, such as characteristic strength ($f_{t0,k}$) and modulus of elasticity (E_{t0}) in tension parallel to the fibers.

This study meant to evaluate the adequacy of $f_{c0,k}$ and E_{c0} predicted by the grading of structural pieces by means of ultrasound (NBR 15521, 2007) for *Eucalyptus grandis* wood. Additionally, the adequacy of the inference equations of the characteristic strength ($f_{t0,k}$) and the modulus of elasticity (E_{t0}) in tension parallel to the fibers proposed by the NBR 7190 (1997) was also evaluated.

Methodology

Five 34-year-old *Eucalyptus grandis* trees were used in this study, from a forest located in Lençóis Paulista/SP. Three 3,5 m long beams were retrieved from each tree, for a total of 15 logs. The first log was retrieved from the base (called *b*), the second one from 7 m from the base (called *m*), and the third from 14 m from the base (called *t*).

The logs were sawed in boards of approximately 3.5 m long (Figure 1), which generated 255 beams with 0.05 m x 0.10 m transverse section and 2.5 m long, 476 prismatic compression specimens (40 mm x 40 mm x 120 mm), and 617 tension specimens (25 mm x 10 mm x 250 mm with reduced central section).

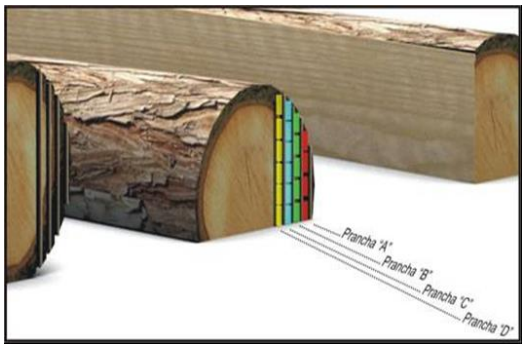

Figure 1— Log sawing outline Fonte Massak (2010)

Ultrasound equipment was used when testing (USLAB, Agricef, Brazil) in the saturated condition, in order to obtain velocity (V_{LLsat}). During the tests, longitudinal wave and 45 kHz frequency transducers were positioned on the extremities (longitudinal propagation) on three points of the transverse section, in agreement with the NBR 15521 (2007) (Figure 2). The transducer coupling to the pieces was made using medicinal gel.

Figure 2—Ultrasound longitudinal measurements on the beam

In this standard (NBR 15521, 2007), the minimal length for testing on the pieces was indicated, in function of the transducer being used. For transducers with frequency between 41 kHz and 50 kHz, the minimum piece length is 0.30 m. Since the beams were 2.5 m long, the study is within established limits. It is imperative to abide to these limitations, so that the velocity values are not affected by the relation between path length and wave length, which would alter the result of the grading (Bucur, 2006, Bartholomeu *et al.*, 2003).

The beams underwent drying and acclimatization in climatic chamber with temperature and relative moisture content control, and when they reached moisture content of 12% they were testing again, for obtain the velocity in this new moisture content condition. The dimensions and weight of each beam were obtained as well, in order to calculate the apparent density (ρ). Once the velocities and densities for the beams in equilibrium condition were known, it was possible to determine the stiffness coefficient (C_{LL}).

The beam static bending tests were made in a frame with 50 kN capacity, and the vertical deformation measurements were obtained on the central point by means of linear position transducer with 0.001 mm resolution, attached to a data acquisition system which allows readings of load and automatic deformation Therefore, a data log was created for each test, which afterwards was used to calculate strength (f_m) and modulus of elasticity (E_M) in static bending.

The specimens were also acclimatized at moisture content of 12% and tested in compression (Figure 3a) and tension parallel to the fibers (Figure 3b) by means of a Universal Machine (DL 30000, EMIC,

Brazil), in order to obtain the rupture stress (f_{c0}, e f_{t0}) and the modulus of elasticity (E_{c0} e E_{t0}). To obtain the modulus of elasticity, the specimens were prepared with extensometers from the machine itself, in order to attain the deformations.

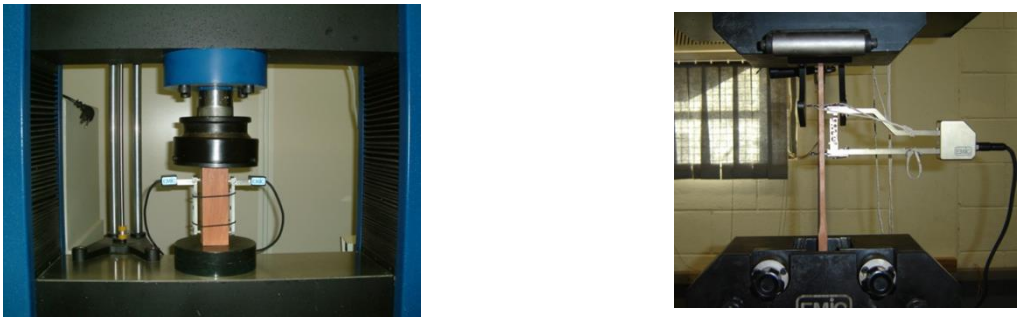

a b

Figure 3— Compression (a) and tension (b) tests on the specimens

The beams and specimens retrieved from each log were considered lots, or samples. For each lot, the characteristic strengths in bending (f_{mk}), compression ($f_{c0,k}$) and tension ($f_{t0,k}$) were determined, as well as the average modulus of elasticity in bending (E_M), compression (E_{c0}) and tension (E_{t0}).

For each lot, the strength classes from the NBR 7190 (1997) were ranged with values of f_{c0k} obtained through tests of compression specimens. With this grading, it was possible to obtain the value ranges for f_{ck} and E_{co} expected for the woods in that lot. This expected value range was compared to the expected value range on the NBR 15521 (2007) grading, by means of saturated velocity (V_{LLsat}) and stiffness coefficient (C_{LL}) obtained in beams ultrasound tests.

The expected value ranges comparison through both grading standards was conducted regarding three categories. Category 1 was assigned when the values predicted by the NBR 15521 (2007) for the analyzed parameter (f_{c0k} or E_{c0}) were in the same range as the values predicted by the NBR 7190 (1997). Category 2 was assigned when the values predicted by the NBR 15521 (2007) for the analyzed parameter (f_{c0k} or E_{c0}) were in a superior range to the values predicted by the NBR 7190 (1997). Category 3 was assigned when the values predicted by the NBR 15521 (2007) for the analyzed parameter (f_{c0k} or E_{c0}) were in an inferior range to the values predicted by the NBR 7190 (1997). Kretschmann and Hernandez conducted a similar analysis and, according to these authors, since the grading beams are adopted in function of the 5-percentile, the results enclosed in Categories 1 and 3 are considered *successes*, because values higher than predicted for the most part are expected. Results enclosed in Category 2 are considered *errors*, and are only tolerated in 5% of the results, since they constitute a security problem.

The tension test results (f_{t0k} and E_{t0}) couldn't be used when comparing grading, since these parameters are not incorporated in the grading standards under analysis. However, considering that the NBR 7190 (1997) presents connections between the tension proprieties and the compression proprieties ($f_{c0,k}/f_{t0,k} = 0,77$ and $E_{c0,m} = E_{t0,m}$), these connections were analyzed, in order to verify if they could be used to infer tension proprieties by means of the NBR 15521 (2007).

Results

The results from the compression (f_{c0} and E_{c0}) and tension tests were used to determine the characteristic strengths ($f_{c0,k}$ and f_{t0k}) and the average modulus of elasticity (E_{c0} and E_{t0}) for the lots. Since the NBR

7190 (1997) uses f_{c0k} as an entry parameter, this parameter alone was used to classify lots in conformity to this standard (Tables 1 and 2).

The beam velocity results in the saturated condition (V_{LLsat}) and the stiffness coefficient in the equilibrium condition (C_{LL}) were used to classify the beams according to the NBR 15521 (2007) grading ranges. Through this grading, it is possible to obtain the inference of the expected characteristic strength ($f_{c0,k}$) and the average modulus of elasticity (E_{c0}) on the lot (Tables 1 and 2).

The comparison between the NBR 15521 (2007) and the NBR 7190 (1997) grading was made in function of the expected value ranges for each parameter. Grading are always indicators of value ranges, not of absolute values, which is why this type of comparison was adopted. Therefore, a lot that underwent compression parallel to the fibers in static test, obtaining a result of $f_{c0,k} = 33.6$, for instance, would be put in class C 30 of the NBR 7190. For the tested lot, the value of $f_{c0,k}$ expected is from 30 to 40 MPa. If when classifying the beam by means of ultrasound according to the NBR 15521 (2007) the class obtained is UD 35, the expected value for $f_{c0,k}$ is from 35 to 40 MPa, which means that both standards classified the lot similarly (Tables 1 and 2).

For an estimate of f_{c0k}, the grading based on saturated velocity and stiffness coefficient (Table 1) obtained by means of beam ultrasound tests (NBR 15521, 2007) had the same practical results, which means that in 20% of the lots the predicted values for f_{c0k} were superior to those obtained by grading based on specimen compression tests (Category 2 of grading, or security problem).

For estimated E_{c0} (Table 2), the grading in Category 2 was lower, both for those based on saturated velocity (6.7%) and those based on stiffness coefficient (0%) obtained by means of beam ultrasound tests (NBR 15521, 2007). In this case, the ultrasound grading based on stiffness coefficient had an increased grading on Category 3 (from 6.7% to 33.3%) for estimated E_{c0}. This result can't be considered an error, because it is not a security problem. However, it implies underestimation of the stiffness of the material.

The average relation between $f_{c0,k}$ and $f_{t0,k}$ was very distant from the standard's proposed value (0.77). It presented a value of 0.47, its minimum being 0.30 and its maximum being 0.64 for all 15 lots. Therefore, using this relation to obtain f_{c0k} through f_{t0k} - thus proceeding with the NBR 7190 (1997) grading - was not deemed convenient. On the other hand, using the real values of this relation would have no practical sense.

For average E_{c0} and E_{t0} on the lot, taking into account the fact that the NBR 7190 (1997) considers these values as being equal, a statistical analysis of the compared results for both samples was conducted. The statistical test implemented was the confidence interval between the averages differences, which contains zero (-102.3 to +4,929.4) and, therefore, indicated that the lot equality can't be rejected with a 95% confidence level. Although the lot averages were considered statistically equivalent, the average relation E_{c0}/E_{t0} was of 1.17, with a coefficient of variation of 9.3%, with the smallest relation being 0.92, and the bigger, 1.32. In only one of the lots E_{c0} was smaller than E_{t0}. This indicates that, when inferring a value range for E_{t0}, using the same value of the E_{c0} would be a security problem, since the value would be overestimated.

Table 1 – Comparison of the expected results for the characteristic strength ($f_{c0,k}$) of the lots, obtained through the NBR 7190 (1997) and the NBR 15521 (2007)

Lot	$f_{c0,k}$ range of the NBR 7190 based on $f_{c0,k}$ of the specimens tests	$f_{c0,k}$ range of the NBR 15521 based on V_{LLsat} of the beam tests	Comparison	Overview of the grading based on V_{LLsat}	$f_{c0,k}$ range of the NBR 15521 based on C_{LL} of the beam tests	Comparison	Overview of the grading based on C_{LL}
1b	30 to 40	35 to 40	Category 1		35 to 40	Category 1	
1m	40 to 60	50 to 55	Category 1		40 to 45	Category 1	
1t	40 to 60	50 to 55	Category 1		40 to 45	Category 1	
2b	40 to 60	35 to 40	Category 1		35 to 40	Category 3	
2m	40 to 60	50 to 55	Category 1		40 to 45	Category 1	
2t	30 to 40	55 to 60	Category 2		40 to 45	Category 2	73.3% Category 1
3b	40 to 60	30 to 40	Category 1	80% Category 1	40 to 45	Category 1	
3m	20 to 30	50 to 55	Category 2	and	45 to 50	Category 2	20% Category 2
3t	40 to 60	50 to 55	Category 1	20% Category 2	45 to 50	Category 1	and
4b	30 to 40	25 to 30	Category 1		30 to 35	Category 1	6.7% Category 3
4m	30 to 40	35 to 40	Category 1		35 to 40	Category 1	
4t	30 to 40	35 to 40	Category 1		35 to 40	Category 1	
5b	30 to 40	30 to 35	Category 1		35 to 40	Category 1	
5m	40 to 60	45 to 50	Category 1		45 to 50	Category 1	
5t	30 to 40	45 to 50	Category 2		45 to 50	Category 2	

V_{LLsat} = velocity obtained by means of ultrasound tests on the saturated beam,
C_{LL} = stiffness coefficient obtained by means of ultrasound test on the beam in equilibrium moisture content;
Category 1 = values predicted by the NBR 15521 (2007) for the analyzed parameter ($f_{c0,k}$) on the same value range predicted by the NBR 7190 (1997);
Category 2 = values predicted by the NBR 15521 (2007) for the analyzed parameter ($f_{c0,k}$) on the superior value range predicted by the NBR 7190 (1997);
Category 3 = values predicted by the NBR 15521 (2007) for the analyzed parameter ($f_{c0,k}$) on the inferior value range predicted by the NBR 7190 (1997);

Table 2 – Comparison of the expected results for the average modulus of elasticity (E_{c0}) of the lots, obtained through the NBR 7190 (1997) and the NBR 15521 (2007)

Lot	E_{c0} range of the NBR 7190 based on $f_{c0,k}$ of the specimens tests	E_{c0} range of the NBR 15521 based on V_{LLsat} of the beam tests	Comparison	Overview of the grading based on V_{LLsat}	E_{c0} range of the NBR 15521 based on C_{LL} of the beam tests	Comparison	Overview of the grading based on C_{LL}
1b	14500-19500	15000-16500	Category 1		15000-16500	Category 1	
1m	19500- 24500	19500-20500	Category 1		16500-18500	Category 3	
1t	19500- 24500	19500-20500	Category 1		16500-18500	Category 3	
2b	14500-19500	15000-16500	Category 1		15000-16500	Category 1	
2m	14500-19500	19500-20500	Category 1		16500-18500	Category 1	
2t	14500-19500	20500-21200	Category 2	86.6% Category 1	16500-18500	Category 1	
3b	14500-19500	14000-15000	Category 1		16500-18500	Category 1	66.7% Category 1
3m	19500- 24500	19500-20500	Category 1	6.7% Category 2	18,500-19,500	Category 3	and
3t	19500- 24500	19500-20500	Category 1	and	18,500-19,500	Category 3	33.3% Category 3
4b	14500-19500	12000-14000	Category 3	6.7% Category 3	14000-15000	Category 1	
4m	14500-19500	15000-16500	Category 1		15000-16500	Category 1	
4t	14500-19500	15000-16500	Category 1		15000-16500	Category 1	
5b	14500-19500	14000-15000	Category 1		15000-16500	Category 1	
5m	19500- 24500	18500-19500	Category 1		18500-19500	Category 3	
5t	14500-19500	18500-19500	Category 1		18500-19500	Category 1	

$f_{c0,k}$ = characteristic strength obtained through compression on the parallel directin to the fibers;
V_{LLsat} = velocity obtained by means of ultrasound tests on the saturated beam ;
C_{LL} = stiffness coefficient obtained by means of ultrasound test on the beam in equilibrium moisture content;
Category 1 = values predicted by the NBR 15521 (2007) for the analyzed parameter ($E_{c0)}$ on the same value range predicted by the NBR 7190 (1997);
Category 2 = values predicted by the NBR 15521 (2007) for the analyzed parameter ($E_{c0)}$ on the superior value range predicted by the NBR 7190 (1997);
Category 3 = values predicted by the NBR 15521 (2007) for the analyzed parameter (E_{c0}) on the inferior value range predicted by the NBR 7190 (1997);

Conclusions

The $f_{c0,k}$ inferred by the ultrasound test on beams (NBR 15521, 2007) match the value range predicted by the NBR 7190 (1997) on 80% of the cases. For the average modulus of elasticity (E_{c0}), 97% of the values were within range.

The $f_{t0,k}$ inferred through the relation with the $f_{c0,k}$ results obtained through grading is not suitable, because the relations vary too much.

Adopting E_{t0} as being the same as the E_{c0} obtained through grading is not appropriate, since the overall results of E_{t0} were inferior to E_{c0}, which indicates that equality would represent a security problem.

Acknowledgements

We thank the National Council of Technological and Scientific Development (CNPq) for the undergraduate research scholarship; São Paulo Research Foundation (FAPESP) for financial support to this research (Proc. 2009/10319-9) and for PhD scholarship (Proc. 2011/00904-1).

References

ASSOCIACÃO BRASILEIRA DE NORMAS TÉCNICA – NBR 15521/2007 – Ensaios Não Destrutivos – Ultrassom – Classificação mecânica de madeira serrada de dicotiledôneas, 8p. Rio de Janeiro (RJ), 2007.

ASSOCIACÃO BRASILEIRA DE NORMAS TÉCNICA – NBR 7190/1997 – Projeto de Estruturas de Madeira, 107p. Rio de Janeiro (RJ), 1997.

Bartholomeu, A.; Gonçalves, R.; Bucur V. . (2003).Dispersion of ultrasonic waves in Eucalyptus lumber as a function of the geometry of boards . Scientia Forestalis, n. 63, p. 235-240, jun

Bucur, V. (2006).Acoustics of wood. Springer-Verlag, Berlin, Germany.

KRETSCHMANN, D.; HERNANDEZ, R. Grading timber and glued structural members. Primary wood processing: principles and practice. Dordrecht, Springer, 2006. pages 339-390.

Massak, M. Influência da idade da árvore na velocidade de propagação de ondas de ultrassom em peças estruturais de madeira de reflorestamento. (2010). 62f. Tese (Mestrado) – Faculdade de Engenharia Agrícola, Universidade Estadual de Campinas, Campinas.

The classification of large cross section sawn timber in the structural use of *Pinus silvestris* L. using NDT together with visual grading

Eva Hermoso
INIA-CIFOR, Forest Products Department. Madrid, Spain, hermoso@inia.es

María J. Montero
ETSI Montes, Universidad Politécnica de Madrid, Madrid, Spain, mj.montero@upm.es

Miguel Esteban
ETSI Montes, Universidad Politécnica de Madrid, Madrid, Spain, miguel.esteban@upm.es

Raquel Mateo
AITIM, Madrid, Spain, r.mateo@aitim.es

Daniel F. Llana
ETSI Montes, Universidad Politécnica de Madrid, Madrid, Spain, d.f.llana@upm.es

Abstract

Several studies have been carried out in Spain in order to draw together non destructive techniques suitable for structural timber grading. The subject of this paper is to discuss the possibility of using the non-destructive techniques based on wave transmission and visual grading and to propose an improved classification system.

This study is based on 116 pieces (200x150x4200 mm) of *Pinus sylvestris* L. Using ultrasonic and stress wave techniques, a classification into two different groups is proposed. The grades based on wave velocity have been compared and combined with the visual grades according to the UNE 56544 standard.

Significant differences have been found in the mechanical properties obtained just for the velocity grades, but not in the visual grades. However, the velocity grades can be used to improve the visual grading, as is shown when they are combined.

Keywords: Visual grading, ultrasonic wave; stress wave; large cross section; sawn timber; *Pinus sylvestris* L.

Introduction

The first grading system of wood for structural use based on visual methods was developed in 1923 and was published by the Forest Product Laboratory (USA) (Fernández-Golfín et al, 2001). Twenty years later appeared the first modifications to improve the efficiency of the grading. Since then, several corrections and improvements have been made to the different standards for the visual grading of timber. One of the main difficulties in the application of this method is taking into account the weighting of the different defects or singularities of the wood in order to predict its quality.

Since the 1990's up to current times, different studies have been carried out in Spain on the grading of structural timber (Fernández-Golfín, 1998; Conde, 2007; Hermoso, 2001, 2003, 2007; Adell, 2005; Íñiguez, 2007). The current standard for Spanish coniferous timber for structural use is the UNE

56544 "Visual grading of sawn timber for structural use. Coniferous timber", which establishes a visual grading classification applicable to sawn timber for structural use of rectangular sections from Spanish conifers which include the red pine timber (*Pinus sylvestris* L.). The last version of this standard was published in 2007 and the main innovation was the consideration of the new MEG grade for large cross sections.

The visual grading is based on the evaluation of the external singularities that are shown on the surface of the pieces: defects due to the anatomy of the wood or due to the sawing process, biological damage or deformations. The current national standards are based on pieces with sections in thickness from 30 to 100 mm and width up to 300 mm.

The main advantages of visual grading are the simplicity of the method, the low costs and the immediacy of the results. Furthermore, it can complement other methods. Nevertheless, the inconveniences can be adduced to be the conservative results and thus the underestimated values obtained for the mechanical properties of the wood, as well as the subjectivity of the operator.

The other non destructive technique used in this work is based on the velocity of the transmission of mechanical waves through wood. There are different methods depending on the origin or the type of wave, the way of measuring the signal or the type of device used for processing the signal. All of the methods are based on the same physical fundamentals. The advantages of these techniques are the reliability of the measurements, the relatively low cost of the equipment, the possibility of portable equipment and its ease of use.

After the visual grading, the non destructive techniques based on the propagation of an stress wave - used since 1929- are the oldest references cited. In the 1940s, Floyd Firestone in USA, Donald Sproule in England and Adolf Trost in Germany, developed and improved the technique based on ultrasonic waves for the detection of defects in different materials, as well as to detect submarines and for other military applications (Sziliard, 1982).

Since then, the advances in acoustic techniques (sonic or ultrasonic, depending on the frequency of the wave) have found successful applications in industry and in construction as basic tools for quality control, mainly in the field of steel structures (the control of welded joints), as well as in concrete, and in the case of timber, applications in the grading of sawn timber or in the inspection of existing structures (Monton, 2012).

Material and test methods

This study has been carried out on a sample of 116 pieces of Scots pine (Pinus sylvestris L.) sawn timber from El Espinar, Segovia (Spain). The nominal dimensions of the pieces were 150 x 200 x 4200 mm. This species was selected for this study because it is one of the most used in the construction of structures in Spain. The dimensions are within the range most demanded by the market and are frequently found on existing and ancient timber structures. These dimensions are also close to those of other samples of timber pieces used in previous studies about large cross sections.

The pieces were tested under a moisture content close to 12 %, which is the reference value cited in the Spanish and European standards. The moisture content was measured by hygrometer according to the UNE-EN 13183-2 standard.

The first step of the study was the visual grading of all the pieces according to the Spanish standard UNE 56544:2007, suitable for sawn timber with squared section of the main Spanish coniferous species for structural use. This standard defines a large cross section (more than 70 mm width) and a visual grade as MEG (in Spanish "Madera Estructural Gruesa"). The pieces that don’t meet the specifications for the MEG grade are classified as rejects R.

The second step consisted of measuring the velocity of an ultrasonic wave through the pieces using a Sylvatest Duo device. The velocity was measured in parallel direction to the grain from edge to the edge, and was adjusted to the 12% moisture content according to the specifications of the equipment manufacturer (0.8 %).

In the same way, other measurements of acoustic wave velocity were collected using the Microsecond Timer (Fakopp) device. Three values of the time of flight were taken and the mean value of the readings was then used to calculate the velocity (while absolute differences between readings were lower than 3 microseconds). The values of velocity were adjusted to the 12 % value of moisture content according to this equipment manufacturer (1 %).

The third NDT technique used in this study consists of determining the natural frequency of vibration of every piece using the Portable Lumber Grader (Fakopp) device. The software of the equipment allows to calculate the velocity of the wave by the Fourier transform. At the same time, a scale is also connected to the equipment to allow to calculate the weight and, therefore, the density.

Finally, all the pieces were tested according to the UNE-EN 408:2010 in order to determine the mechanical properties by means of the bending test, specifically the global modulus of elasticity (MOEGlo) and the bending strength or the modulus of rupture (TDR).

Results and discussion

Visual Grading

The results obtained with the current visual grading are in Table 1:

Table 1- Visual grading results.

	Nº	%
Madera Estructural Gruesa (MEG)	78	67
Rechazo (R)	38	33
TOTAL	116	100

For neither of these groups are there significant differences in material properties: the global modulus of elasticity, adjusted to 12% moisture content (MOEGlo12) and the bending strength or the modulus of rupture (TDR), with even better results obtained in the rejects, as can be seen in Figures 1 and 2 and in the table 2:

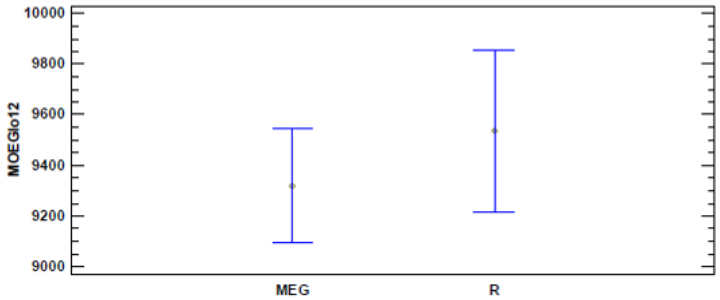

Figure 1- Visual grades distribution for MOEGlo12 (N/mm^2)

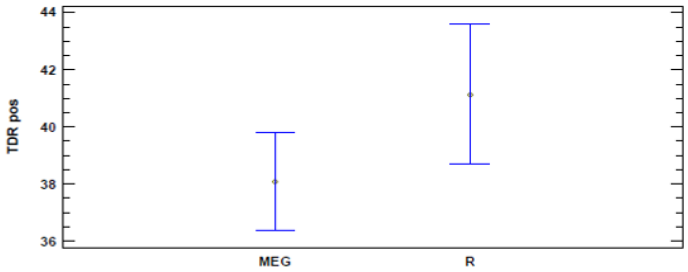

Figure 2- Visual grades distribution for TDR (N/mm^2)

Table 2- Mean values of mechanical properties for visual grades.

CV	DenGlo12 media (kg/m^3)	MOEGlo12 medio (N/mm^2)	TDR media (N/mm^2)
MEG+R	502	9391	39,09
MEG	498	9537	38,09
R	510	9320	41,14

Other non destructive techniques

Regardless of challenging the adequacy of the visual grading standard (which is the subject of another study), in view of the results following the specifications set today, the possibility of a new grading using other non destructive techniques has been considered.

After performing a factor analysis, the results show that the wave velocity of the three techniques used are good indicators to estimate the modulus of elasticity (MOE) and the modulus of rupture (TDR).

For each technique, in order to establish structural qualities, a limit value of wave velocity was defined. It was selected with different percentiles of distribution. The percentages that were studied are: 10% (v10), 15% (v15), 20% (v20) y 25% (v25). For example, the wave velocity v10, divides the sample into two groups: rejects, with a wave velocity lower than the limit v10, and selected wood, with the pieces with a velocity higher than this value v10. For each velocity limit the difference between the mechanical properties of wood rejected, accepted and complete sample was evaluated.

The 25% percentile is the one for which significant differences were obtained in all techniques and all groups for both the modulus of elasticity and the modulus of rupture. That is why this limit is selected, to calculate the values of the classification step using Sylvatest, Microsecond Timer (MST) and PLG:

- Sylvatest: v25 sylvatest = 4.700 m/s
  S1: pieces with stress wave velocity v > 4.700 m/s
  S2: pieces with stress wave velocity v < 4.700 m/s

- MST: v25 MST = 4.802 m/s
  MT1: pieces with stress wave velocity v > 4.802 m/s
  MT2: pieces with stress wave velocity v < 4.802 m/s

- PLG: v25 PLG = 4.224 m/s
  PLG1: pieces with stress wave velocity v > 4.224 m/s
  PLG2: pieces with stress wave velocity v < 4.224 m/s

In figures 3 and 4 are shown the mechanical properties results of classification according to several pieces of equipment and to new criterion:

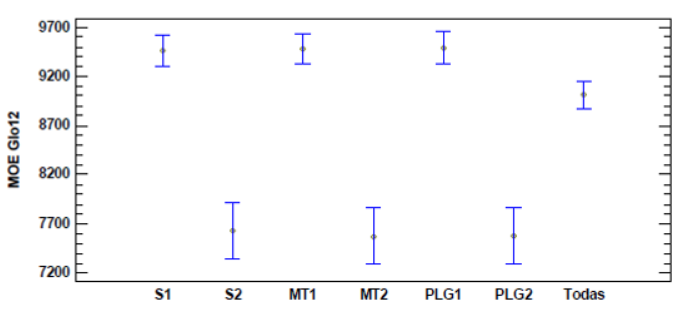

Figure 3- de MOEGlo12 (N/mm^2) and stress wave velocity classes ANOVA

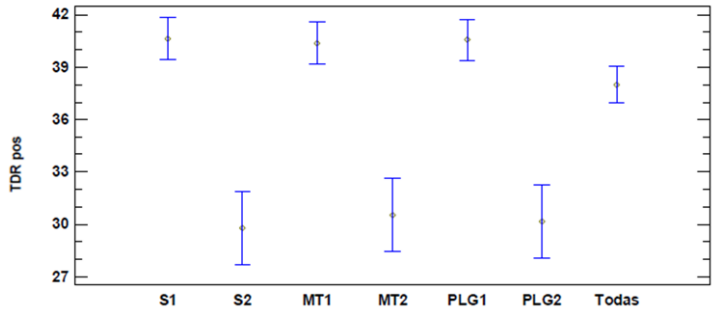

Figure 4- TDR (N/mm^2) and stress wave velocity classes ANOVA

Table 3- Mechanical properties according to velocity classes (25 percentile).

	ALL	S1	S2	MT1	MT2	PLG1	PLG2
MOEGlo12 (N/mm^2)	9007	9461	7634	9480	7574	9489	7577
TDR (N/mm^2)	37,98	40,62	29,80	40,38	30,56	40,55	30,19

According to table 3, if 25% of the pieces with less stress wave velocity are not considered, there is a classification improvement. So mean modulus of elasticity then is from 9.007 N/mm^2 to 9.461 N/mm^2 and 9.489 N/mm^2, depending on the technique used. For strength, this improvement is from 40,38 to 40,62 N/mm^2.

As a result of this analysis, it is concluded that the propagation velocity of a stress wave can be used as a grading parameter as it is able to separate adequately pieces of high quality with a hit rate of 75%.

Visual strength grading methods together with other non destructive techniques

Seeing the possibilities of non destructive methods for structural timber grading, there appears to be the possibility of improving the present hit rate of the visual strength grade methodology by combining them. With this aim, a new classification in MEG or R pieces that also meets the greater or equal threshold 25 percentile velocity of Sylvatest, MST and PLG, was carried out defining a new class called MEG+v and the rejects, that do not overcome that threshold of velocity, are called R+v. Table 4 and figures 5 and 6 show the results of the combination.

Table 4- Mean values of mechanical properties for visual+velocity grades.

CV+v	Nº piezas/%	Mean MOEGlo (N/mm^2)	Mean TDR (N/mm^2)
TOTAL	116/100	9391	39,09
MEG+v	104/90	9526	39,97
R+v	12/10	8223	31,47

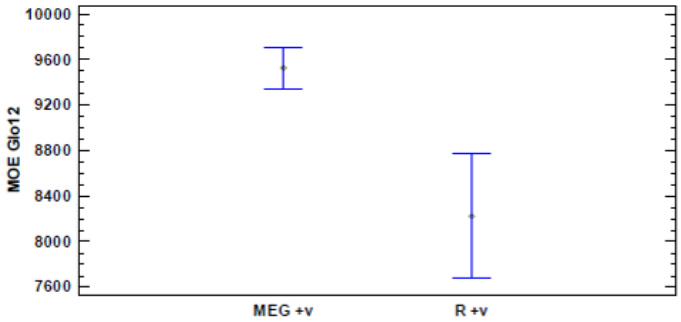

Figure 5- MOEGlo12 results from CV+v

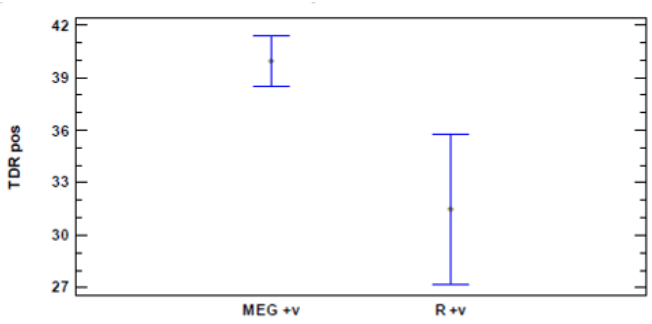

Figure 6- TDR results from CV+v

Conclusions

The application of visual specifications for timber grading does not support significant differences in the mechanical properties among structural classes.

It is possible to set up a velocity of transmission of wave threshold by means of non destructive methods to define an effective timber grading. This threshold of velocity would be that corresponding to 25 percentile of the distribution of values.

The application of combined methodologies such as visual strength grade joined to wave velocity as the result of non destructive tests, allows improve the hit rate and the definition of structural classes of different mechanical properties.

Acknowledgements

Ministerio de Ciencia e Innovación: Proy.: BIA 2010-18858. Plan Nacional I+D+i 2008-2011. Proy.: BIA 2006-14272. Plan Nacional I+D+i 2004-2007. Era-Net WoodWisdom Proy. WW-2009-1-11. CIFOR-INIA, Timber Structures Laboratory, Madrid (Eva Hermoso/Rafael Diez).

References

Adell Almazán, F.J. 2005. Comparación de las normas de clasificación de Madera estructural española (UNE 56544) y alemana (DIN 404) para madera de pino Silvestre (Pinus sylvestris, L.) de procedencia alemana. Proyecto fin de carrera. Escuela Técnica Superior de Ingenieros de Montes. Universidad Politécnica de Madrid.

Conde, M. 2007. Improving the prediction of strength and rigidity of structural timber by combining ultrasound techniques with visual grading parameters. Materiales de construcción. Vol 57. No 288. pp.49-59.

Fernández-Golfín, J.I.; Díez, M.R.; Hermoso, E. 2001. Análisis y estado del arte de la técnica de clasificación mecánica por máquina de la madera aserrada structural (Revisión). Revista de Investigación Agraria. 10 (1). Pp. 5-9.

Fernández-Golfín, J.I.; Díez, M.R.; Gutiérrez, A. 1998. Caracterización mecánica de la madera aserrada de uso estructural, clasificada visualmente de acuerdo con la Norma UNE 56.544. Materiales de construcción. Vol. 48. Nº 252: pp. 45-59.

Hermoso, E. 2001. Caracterización mecánica de la madera estructural de *Pinus sylvestris* L. Doctoral Thesis. Universidad Politécnica de Madrid. ETS de Ingenieros de Montes. 253pp.

Hermoso, E.; Fernández-Golfín, J.I.; Díez, M.R. 2003. Mechanical characterization of timber according to European standards from Spanish provenances of Scots Pine. Investigación Agraria sistemas y Recursos Forestales, Vol. 12, no 3, pp 103-110.

Hermoso, E.; Carballo, J.; Fernández-Golfín, J.I. 2007. Revisión de la caracterización estructural de la madera de Pinus radiata D. Don del norte de España acorde a las modificaciones normativas. II Congreso Iberoamericano de investigación y desarrollo de productos forestales. pp 1-10.

Íñiguez, G. 2007. Clasificación mediante técnicas no destructivas y evaluación de las propiedades mecánicas de la madera aserrada de coníferas de gran escuadría para uso estructural. Doctoral Thesis. Universidad Politécnica de Madrid, ETS de Ingenieros de Montes.

Montón, J. 2012. Clasificación estructural de la madera de Pinus radiata d. Don procedente de Catalunya mediante métodos no destructivos y su aplicabilidad en la diagnosis estructural. Doctoral Thesis. Universitat Politècnica de Catalunya.

Szilard, J. 1982. Ultrasonic Testing: Non conventional testing techniques. Chichester (ENG.). New York: Wiley. ISBN: 04-7127-938-2.

Session 9

Material Characterization I—Acoustic-Based Techniques

Determination of the Mechanical Properties of *Castanea Sativa* Mill by Ultrasonic Wave Propagation and Comparison with the Compression Method

Carlos Vázquez
PhD student, Department of Agroforestry Engineering, University of Santiago de Compostela, Campus Universitario. 27002 Lugo, Spain, +34686844575: c.vazquez@outlook.com

Raquel Gonçalves
Associate Professor, College of Agricultural Engineering (FEAGRI), University of Campinas (UNICAMP), College of Agricultural Engineering (FEAGRI), raquel@feagri.unicamp.br

Manuel Guaita
Professor, Department of Agroforestry Engineering, University of Santiago de Compostela, Campus Universitario. 27002 Lugo, Spain, +34686844575: m.guaita@usc.es

Cinthya Bertoldo
PhD Student, College of Agricultural Engineering (FEAGRI), University of Campinas (UNICAMP), Campinas, São Paulo, Brasil, cinthyabertoldo@gmail.com

Abstract

Ultrasonic wave propagation is a nondestructive method for the determination of mechanical properties. As an orthotropic material, wood presents different properties according to the direction to the grain. Often, only the longitudinal Young's modulus (E_L) is determined, but many projects, using current software tools, require knowledge of the radial and tangential Young's moduli (E_R and E_T), the longitudinal-radial, longitudinal-tangential and radial-tangential shear moduli (G_{LR}, G_{LT} and G_{RT} respectively) and the Poisson's ratios for all planes (v). The mechanical properties of 13 specimens of *Castanea sativa* from three different Spanish regions were determined. Ultrasonic results for three of the specimens were compared with results obtained by the traditional compression method for the determination of the mechanical properties of wood. The determination of all the elastic constants by compression testing on three of the specimens did not reveal significant differences between both methods for any of the constants.

Key words: orthotropic, constants, stiffness, wood, moduli.

Introduction

In the Iberian Peninsula, some species with very good features are not being used because their mechanical properties have never been determined.

As an orthotropic material, wood presents different properties depending on the direction to the grain. Many projects using current software tools require knowledge of all the mechanical properties. Therefore, the following constants must be determined: three Young's moduli (E_L, E_R, E_T), three shear moduli (G_{LR}, G_{LT}, G_{RT}) and six Poisson's ratios (v_{LR}, v_{LT}, v_{RL}, v_{RT}, v_{TL}, v_{TR}). These elastic constants compose the elasticity matrix. Currently, rapid and efficient methods for the determination of the properties of materials are promoted, and the ultrasonic technique readily determines the stiffness and elastic properties of materials.

Some authors, such as Bucur (1983, 2006), Bucur and Archer (1984) and Keunecke et al. (2007) highlighted the benefits of the ultrasonic technique for the determination of the properties of wood.

Since the 1980s, there has been a search for methods that allow the use of the Christoffel's equations (Bucur, 2006) to determine all the elastic constants of fibrous materials, including wood. Improvement in results depends on the development of equipment and transducers for use in wood.

Preziosa et al. (1981) and Preziosa (1982) were pioneers in the use of the ultrasonic technique for the determination of the stiffness matrix of wood. François (1995) proposed the use of a polyhedral specimen with 26 faces to measure the elastic constants of wood. Polyhedral specimens with 26 faces allow the determination of all the elements in the stiffness matrix from a single specimen.

Gonçalves et al. (2011) performed ultrasonic and compression tests on the same specimens and determined the elastic constants of wood –three Young's moduli (E_L, E_R, E_T), three shear moduli (G_{LR}, G_{LT}, G_{RT}) and six Poisson's ratios (ν_{LR}, ν_{LT}, ν_{RL}, ν_{RT}, ν_{TL}, ν_{TR}). Some of the authors cited above compared their measurements with the values obtained from static tests, but Gonçalves et al. (2011) were the only authors who compared the results obtained on the same specimens with both methods.

The goal of this paper is to determine the three Young's moduli (E_L, E_R, E_T), the three shear moduli (G_{LR}, G_{LT}, G_{RT}) and the six Poisson's ratios (ν_{LR}, ν_{LT}, ν_{RL}, ν_{RT}, ν_{TL}, ν_{TR}) of Spanish *Castanea sativa* Mill. by means of ultrasonic testing, and to compare the results with the values obtained by bending (for Young's modulus E_L) and compression testing.

Materials and methods

Materials

To conduct ultrasonic testing, a 'Panametrics-NDT EPOCH4' ultrasonic wave pulser (Olympus /Panametrics NDT Inc. San Diego, CA) was used. The ultrasonic wave pulser has two sets of 1MHz longitudinal and transverse wave transducers. To perform measurements, a couplant gel must be applied between the transducers and the specimen. In this case, starch glucose was used as coupling medium, because of the good results presented by Gonçalves et al. (2011), mainly for transverse waves.

Time of wave propagation was measured on 13 polyhedral specimens (Figure 1) of *Castanea sativa* with 26 faces, as suggested in François (1995) and tested by Trinca (2011). Propagation time was used to calculate the velocity of wave propagation for both longitudinal and transverse waves.

Specimens were conditioned in a chamber at 20ºC and 65% humidity, in compliance with standard UNE 56528.

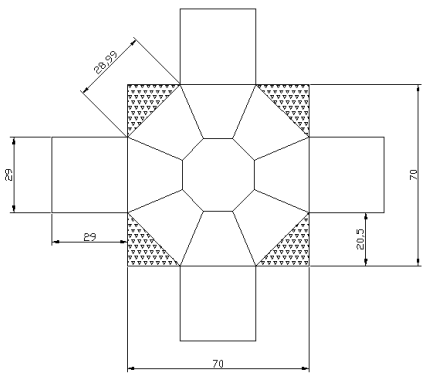

Figure 1- Plan view of a polyhedron with 26 faces, measured in mm

For compression tests, 18 prismatic specimens with dimensions of 20x20x60 mm were extracted from three *Castanea sativa* beams with dimensions of 70x150x3000 mm, each with a different Spanish origin, namely Asturias, Galicia and *Cataluña*. Every polyhedral specimen used for the determination of mechanical properties by ultrasonic testing was obtained from the three beams. Specimens were conditioned in a chamber at 20ºC and 65% humidity in compliance with UNE 56528. Micro-Measurements C2A-13-250LW-350 and C2A-13-250LT-350 strain gauges were used to measure specimen strain.

Compression tests were conducted in a testing frame 200kN from PEMADE laboratories, and data was collected using a Quantum X-HBM data acquisition system, a laptop computer and Microtest data collection software.

Methods

Ultrasonic testing

Extraction and preparation of specimens (polyhedra)

To obtain specimens with the three directions well defined, the rings of the selected sample must be as parallel as possible, and its radius must be large. In addition, each face of the polyhedron must be sufficiently large to allow for full direct contact with the transducer (13 mm), and the specimen must not contain pith or knots. The specimens were named CT, A and G according to their region of origin, *Cataluña*, Asturias and Galicia, respectively.

Ultrasonic and bending testing

Using polyhedral specimens allowed us to measure various wave velocities, which are required to determine the stiffness matrix (Fig. 2).

Figure 2- An example of wave propagation time measurement

The stiffness matrix [C] was determined based on the velocities using the Christoffel tensor (Bucur, 2006).

The compliance matrix [S] has been determined as the inverse of the stiffness matrix $[C]^{-1}$.

Static bending tests were performed on the beams (70x150x3000 mm), from which the polyhedral specimens were cut. Bending tests were performed according to standard UNE-EN 408:2011 to obtain the longitudinal Young's modulus for each beam. The Young's moduli obtained were then compared with the stiffness coefficients obtained using ultrasound in the longitudinal direction.

Compression testing

Extraction and preparation of specimens

From each beam, six specimens were cut, three in the directions of the axes, and three with 45º inclinations in each plane (Fig. 3). To measure strain during testing, strain gauges were placed on the specimens.

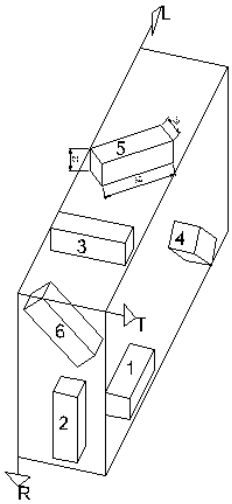

Figure 3- Scheme for the extraction of specimens at the axes and the inclined planes (Gonçalves et al., 2011). 1, Longitudinal 2, Radial 3,Tangential 4, Longitudinal-Radial 5, Longitudinal-Tangential 6, Radial-Tangential

Tests

The specimens positioned at the longitudinal axis were tested under compression, according to standard UNE 56535, for the determination of compression stress parallel to the grain. For this arrangement, constants E_L, v_{LR} and v_{LT} were obtained.

The specimens positioned in the radial and tangential directions were tested according to standard UNE 56542 for the determination of compression stress perpendicular to the grain. For this arrangement, constants E_R, v_{RL} and v_{RT}, E_T, v_{TR} and v_{TL} were obtained.

Finally, the specimens positioned at the inclined longitudinal-tangential, tangential-radial and longitudinal-radial planes were tested according to UNE 56542. For this arrangement, constants G_{LT}, G_{TR} and $G_{LR,}$ were obtained, respectively.

To determine the elastic constants, data was analysed with Microsoft Excel, and lines were fitted to the ε/σ graphs with R^2 above 0.99 using equations cited by Gonçalves (2011). Young's moduli in the axial direction (E_L, E_R, E_T) were determined from the slope of the stress/strain curve (σ/ε), and data was fitted so that the curve was linear in a section between 20 - 60% of maximum stress with a correlation coefficient (R^2) above 0.99.

Results and Discussion

Ultrasonic testing

The results for the elastic constants were determined from the compliance matrix for each polyhedron. To verify the results, we used the data obtained from static bending tests (E_M) performed previously on the same beams from which the specimens were extracted (Table 1).

The stiffness modulus C_{LL} (termed dynamic modulus by other authors like Íñiguez, 2007) obtained through nondestructive testing and the Young's modulus obtained by static bending testing are highly

correlated with a correlation coefficient of 0.89, a good result in comparison with the values obtained by other authors such as Íñiguez (2007), who reports lower correlation coefficients (0.74) for structural-size samples and other species. Considering that longitudinal modulus E_L is calculated using the complete matrix, E_L values should be similar to the values obtained under bending. The mean difference between the values of E_L and E_M is 3% (Table 1).

Gonçalves *et al.* (2011) inverts the complete stiffness matrix to determine longitudinal Young's modulus of *Apuleia leiocarpa*, *Goupia glabra* and *Eucalyptus saligna* wood, and obtains values 1%, 2%, and 4% higher than the values obtained in static tests for the same species.

The statistical difference between the Young's modulus determined by the ultrasonic method (E_L) and the Young's modulus determined by static bending (E_M) has been assessed by using a difference of means test at 95% confidence level. Considering that the difference between means is in the range [-121 to 1024], which contains the zero value, the values of the moduli determined from ultrasonic testing and static bending testing are considered statistically equivalent at 95% confidence level.

Table 1-Results from ultrasonic testing

Specimen	*Means*	*CV (%)*
$E_L(N/mm^2)$	**10,985**	23.2
$E_R(N/mm^2)$	**1,452**	16.2
$E_T(N/mm^2)$	**774**	12.0
$G_{TR}(N/mm^2)$	**257**	20.5
$G_{TL}(N/mm^2)$	**788**	10.5
$G_{LR}(N/mm^2)$	**1,131**	10.5
v_{RL}	**0.066**	44.8
v_{TL}	**0.056**	20.1
v_{LR}	**0.554**	57.0
v_{TR}	**0.372**	10.4
v_{LT}	**0.803**	31.4
v_{RT}	**0.693**	6.2
E_M *bending* (N/mm^2)	**10,674**	18.6

To compare the rest of the elastic constants, which have not been obtained in static tests, but shear moduli, we have assessed the order of magnitude of the relationship between the means of the constants as represented in the terms of the compliance matrix, as suggested by Bodig and Jayne (1982), and we have verified whether the order of magnitude is similar to the expected order (Table 2).

Table 2- Relationship between the terms of the compliance matrix (10^{-5})

	$\frac{v_{RL}}{E_R}$	$\frac{v_{LR}}{E_L}$	$\frac{v_{TL}}{E_T}$	$\frac{v_{LT}}{E_L}$	$\frac{v_{TR}}{E_T}$	$\frac{v_{RT}}{E_R}$
Castanea sativa	4.58	5.04	7.20	7.31	48.11	47.74
Bodig and Jayne (1982)	1.52 - 5.13	1.34 - 4.27	1.79 - 6.14	1.59 - 6.48	20.68 - 128.00	21.37 - 104.33

In addition, the values of the Poisson's ratio have been compared to the mean values (Table 3) reported by Bodig and Jayne (1982), who report average values for the Poisson's ratio, but large variability for those constants.

Table 3- Values of the Poisson's ratio for dicotyledons reported by Bodig and Jayne (1982), and values obtained for *Castanea sativa* using polyhedral specimens

	ν_{RL}	ν_{TL}	ν_{LR}	ν_{TR}	ν_{LT}	ν_{RT}
Castanea sativa	0.066	0.056	0.55	0.37	0.80	0.69
Bodig and Jayne (1982)	0.044	0.027	0.37	0.33	0.50	0.67

Compression testing

The results of compression and ultrasonic tests of specimens CT3, A1 and G6 (Table 4) have been compared, to check whether there are any differences between them.

Table 4-Means and coefficients of variation of the constants for the ultrasonic and compression methods

			E_L (N/mm^2)	E_R (N/mm^2)	E_T (N/mm^2)	G_{RT} (N/mm^2)	G_{LT} (N/mm^2)	G_{LR} (N/mm^2)	ν_{TR}	ν_{TL}	ν_{RL}	ν_{LR}	ν_{LT}	ν_{RT}
Result	compression	*Mean*	9,757.33	1,336.48	707.47	484.69	822.30	1,082.09	0.47	0.04	0.08	0.47	0.52	0.82
		Coeff.var.(%)	29.55	19.53	6.55	52.85	24.51	26.56	10.79	66.14	54.98	3.69	11.83	19.14
	ultrasound	*Mean*	9,973.12	1,441.38	789.80	298.94	760.44	1,139.47	0.39	0.05	0.08	0.60	0.66	0.70
		Coeff.var.(%)	22.27	27.69	21.50	24.45	14.75	17.89	16.47	20.17	18.65	50.90	43.18	3.62

The results of E_L obtained by compression and ultrasonic testing have been compared with the values obtained for Young's modulus under bending. In addition, the other constants have been compared with the values expected according to Argüelles, Arriaga and Martínez (2000), who report the following values for Spanish deciduous species: $E_T = E_L/13.5$, $E_R = E_L/8$, G_{RT} = 366 N/mm^2, G_{TL} = 971 N/mm^2, G_{RL} = 1,260 N/mm^2, ν_{LT} = 0.46, ν_{TR} = 0.38, ν_{LR} = 0.39, ν_{RT} = 0.67, ν_{TL} = 0.033, ν_{RL} = 0.048.

The differences between the means have been analysed at 95% confidence level, to check whether significant differences are found between the results obtained by the ultrasonic method and the results obtained by the compression method, and between both of them and the expected results (Table 5).

Table 5-Means and coefficients of variation of the constants for the ultrasonic and compression methods

			E_L (N/mm^2)	E_R (N/mm^2)	E_T (N/mm^2)	G_{RT} (N/mm^2)	G_{LT} (N/mm^2)	G_{LR} (N/mm^2)	ν_{TR}	ν_{TL}	ν_{RL}	ν_{LR}	ν_{LT}	ν_{RT}
Result	compression	*Mean*	9757.33	1,336.48	707.47	484.69	822.30	1,082.09	0.47	0.04	0.08	0.47	0.52	0.82
		Coeff.var.(%)	29.55	19.53	6.55	52.85	24.51	26.56	10.79	66.14	54.98	3.69	11.83	19.14
	ultrasound	*Mean*	9,973.12	1,441.38	789.80	298.94	760.44	1,139.47	0.39	0.05	0.08	0.60	0.66	0.70
		Coeff.var.(%)	22.27	27.69	21.50	24.45	14.75	17.89	16.47	20.17	18.65	50.90	43.18	3.62

The results of E_L obtained by compression and ultrasonic testing have been compared with the values obtained for Young's modulus under bending. In addition, the other constants have been compared with the values expected according to Argüelles, Arriaga and Martínez (2000), who report the following values for Spanish deciduous species: $E_T = E_L/13.5$, $E_R = E_L/8$, G_{RT} = 366 N/mm^2, G_{TL} = 971 N/mm^2, G_{RL} = 1,260 N/mm^2, ν_{LT} = 0.46, ν_{TR} = 0.38, ν_{LR} = 0.39, ν_{RT} = 0.67, ν_{TL} = 0.033, ν_{RL} = 0.048.

The differences between the means have been analysed at 95% confidence level, to check whether significant differences are found between the results obtained by the ultrasonic method and the results obtained by the compression method, and between both of them and the expected results. The results of this test show that for ultrasound and compression tests and for ultrasound and expected results there are no statistical differences. For compression test and expected values there are statistical differences only for $\nu_{LR.}$.

For each specimen, the results of ultrasonic tests also have been compared to the results of compression tests, and each of these results has been compared to the expected values (Table 6).

Table 6-Means of the relationships between the results obtained with both methods and comparison with expected values according to Arriaga et al. (2000)

Constant	E_L (N/mm^2)	E_R (N/mm^2)	E_T (N/mm^2)	G_{RT} (N/mm^2)	G_{LT} (N/mm^2)	G_{LR} (N/mm^2)	ν_{LR}	ν_{LT}	ν_{RT}	ν_{TR}	ν_{TL}	ν_{RL}
Ultras/compres	1.04	1.07	1.11	0.70	0.95	1.14	1.29	1.29	0.87	0.83	1.59	1.23
Compres/expected	0.95	1.09	0.97	1.32	0.85	0.86	1.21	1.12	1.22	1.23	1.21	1.69
Ultras/expected	0.98	1.20	1.09	0.82	0.78	0.90	1.55	1.44	1.04	1.02	1.47	1.60

The results obtained with the ultrasonic method show deviations from the expected values similar to those obtained with compression testing, except for parameters v_{TL}, v_{LR} and v_{LT} (Table 6). Particularly, as compared to the expected values, the mean error for v_{LR} in compression tests is much lower than the error found in ultrasonic tests (Table 6). However, the difference of means test reveals significant differences from expected values for v_{LR} in compression tests and not in ultrasonic tests because v_{LR} is very uniform and always above the expected values in compression tests, which suggests that the expected value for v_{LR} may be lower than the real value of v_{LR} for *Castanea sativa*.

Conclusions

- The Young's moduli determined by ultrasonic testing and static bending testing on the same beams were statistically equivalent.
- The coefficient of correlation between stiffness modulus (C_{LL}) and Young's modulus in static bending (E_M) was 0.89.
- Poisson's ratios determined by ultrasonic method were in the expected orders of magnitude, based on Bodig and Jayne (1982).
- The statistical analysis did not reveal significant differences between the compression method and the ultrasonic method for any elastic constant.
- The comparison of the results for constants v_{TL}, v_{LR} and v_{LT} and the expected values revealed that the values produced by the compression method are considerably nearer to the expected values reported by Argüelles, Arriaga and Martínez (2000) than the results of the ultrasonic method.
- The ultrasonic method shows great potential for nondestructive determination of the mechanical properties of wood.

Acknowledgements
To FAPESP (Proc. 2013/00438-6) and CAPES by supporting the exchange of researchers

References
AENOR (1988). UNE 56542:1988; Características físico-mecánicas de la madera. Determinación de la resistencia a la compresión perpendicular a las fibras. [Physical-Mechanical Properties of Wood. Determination of Compression Strength Perpendicular to the Grain.] AENOR, Madrid

AENOR (1977). UNE 56535:1977; Características físico-mecánicas de la madera. Determinación de la resistencia a la compresión axial. [Physical-Mechanical Properties of Wood. Determination of axial compression strength.] AENOR, Madrid

AENOR (1978). UNE 56528:1978; Características físico-mecánicas de la madera. Preparación de probetas para ensayos. [Physical-Mechanical Properties of Wood. Preparation of Specimens for Testing.] AENOR, Madrid

AENOR (2011). UNE EN 408:2011; Estructuras de madera. Madera aserrada y madera laminada encolada para uso estructural. Determinación de algunas propiedades físicas y mecánicas. [Timber Structures. Sawn and Glued Laminated Timber for Structural Use. Determination of some Physical-Mechanical Properties.] AENOR, Madrid

Argüelles R; Arriaga F; Martínez J J (2000). Estructuras de madera, diseño y cálculo. [Design of Timber Structures] AITIM, Madrid, Spain

Bodig J; Jayne B A (1982). Mechanics of wood and wood composites. Van Nostrand Reinhold, New York

Bucur V (1983). An ultrasonic method for measuring the elastic constants of wood increment cores bored from living trees. Ultrasonics, 21(3), 116-126

Bucur V (2006). Acoustics of wood. Springer-Verlag, Berlin, Germany

Bucur V; Archer R R (1984). Elastic constants for wood by an ultrasonic method. Wood Science and Technology, 18, 255-265

François M (1995). Identification des symmetries matérielles de matériauxa anisotropes. PhD Thesis. Université Paris 6, LMT, Cahan, France

Gonçalves R; Trinca A J; cerri D G P (2011). Comparison of elastic constants of wood determined by ultrasonic wave propagation and static compression testing. Wood and Fiber Science, 41(1), 64-75.

Iñiguez G (2007). Clasificación mediante técnicas no destructivas y evaluación de las propiedades mecánicas de la madera aserrada de coníferas de gran escuadría para uso estructural [Classification by Nondestructive Methods and Assessment of the Mechanical Properties of Large Conifer Sawn Timber for Structural Use.] PhD Thesis, Universidad Politécnica de Madrid, Spain

Keunecke D; Sonderegger W; Pereteanu K; Lüthi T; Niemz P (2007). Determination of Young's and shear moduli of common yew and Norway spruce by means of ultrasonic waves. Wood Science and Technology, 41, 309-327

Preziosa C (1982). Méthode de détermination des constantes élastiques du matériau bois par utilisation des ultrasons. Université d'Orléans, Orléans

Preziosa C; Mudry M; Launay J; Gilletta F (1981). Détermination des constantes élastiques du bois par une méthode acoustique goniométrique. Comptes rendus de l'Académie des Sciences II, 293(2), 91-94

Trinca A J (2011). Metodologia para determinação das constantes elásticas da madeira por ultrassom. PhD Thesis, Faculdade de Engenharia Agrícola, Universidade Estadual de Campinas, Brasil

Acoustic Emission and Synchrotron Radiation X-ray tomographic in-situ microscopy of sub-macroscopic damage phenomena in wood

Franziska Ritschel
Wood Physics Group, Institute of Building Materials, ETH, Swiss Federal Institute of Technology, Zürich, Switzerland, fritschel@ethz.ch

Michaela Zauner
Wood Physics Group, Institute of Building Materials, ETH, Swiss Federal Institute of Technology, Zürich, Switzerland, mzauner@ethz.ch

Sergio J. Sanabria
Wood Physics Group, Institute of Building Materials, ETH, Swiss Federal Institute of Technology, Zürich, Switzerland, ssanabria@ethz.ch

Andreas J. Brunner
Laboratory for Mechanical Systems Engineering, Empa, Swiss Federal Laboratories for Materials Science and Technology, Dübendorf, Switzerland, andreas.brunner@empa.ch

Peter Niemz
Wood Physics Group, Institute of Building Materials, ETH, Swiss Federal Institute of Technology, Zürich, Switzerland, niemzp@ethz.ch

Abstract

Spruce wood specimens (*Picea abies* (L.) Karst.) exposed to stepwise tensile load parallel and perpendicular to fiber orientation until failure were monitored simultaneously with in-situ Acoustic Emission (AE) measurement and Synchrotron Radiation X-ray Tomographic Microscopy (SRXTM). The AE method enables high time resolution (sub-ms) of damage initiation and accumulation. The SRXTM allows three-dimensional volumetric high-resolution visualization of the inner wood cellular structure, providing information on microscopic structural changes leading to ultimate failure in stressed wood. To achieve a maximum resolution of 1.85 μm^3 per voxel, specimens were prepared with a predefined breaking point in the form of a taper. The applicability of this approach was demonstrated by comparing the visualized structural changes in the SRXTM reconstruction with the AE signatures. Significant differences were observed among the tested load directions, which could be tracked in space and time with SRXTM and AE, respectively.

Keywords: Damage Accumulation; Synchrotron Radiation X-ray Tomographic Microscopy; Acoustic Emission; In-Situ; Tension

Introduction

The investigation focuses on the damage progress in wood materials at microscopic scale. Thus, for the very first time, destructive tests on wooden specimens were monitored in-situ by the combination of Acoustic Emission (AE) measurement (Debaise et al. 1966, Ansell 1982, Beall 2002, Bucur 2006) and Synchrotron Radiation X-ray Tomographic Microscopy (SRXTM) (Trtik et al. 2007, Forsberg et al. 2008, Zauner et al. 2012). The high time resolution of AE measurement is beneficial for detection of micro-mechanisms, their interactions and accumulation leading to macroscopic failure. Nevertheless, the challenge is to assign the features of the detected signals to their microscopic source mechanism (Grosse and Ohtsu 2008). Especially the high resolution in connection with the high brilliance and therefore shorter recording time of synchrotron based tomographic microscopy enables volumetric sub-cellular insight (Mannes et al. 2010). The combination of both methods enables virtually real-time studies on the damage mechanisms. Hence, AE signal parameters and waveforms could be correlated with visualized microstructural changes, i.e. fiber breakage, fiber delamination or shear mechanisms between fibers.

Materials and Method

Investigation on damage evolution was carried out on specimens of clear spruce wood (*Picea abies* (L.) Karst.) of 30 mm x 5 mm x 2.6 mm (length x width x thickness) dimension. Two sample types are distinguished by the fiber-load-angle: The "radial specimen" was loaded perpendicular to fiber and the "longitudinal specimen" was loaded parallel to fiber. One specimen surface was cut by a microtome blade to improve the coupling of the piezoelectric AE sensors. To ensure crack initiation, the specimens are taper shaped (cross section of 4 mm^2 down to 1 mm^2) and additionally a predefined notch was cut by a scalpel tip within the volume of interest monitored by SRXTM (Figure 1).

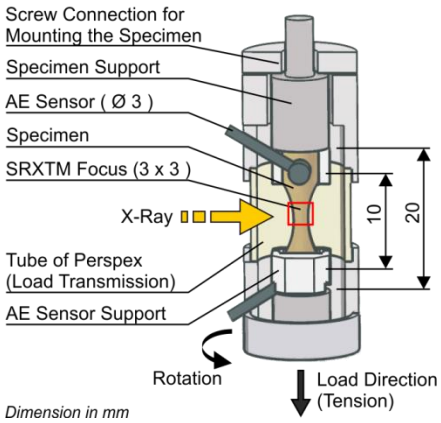

Figure 1—Experimental design

Trial tests were performed at the TOMCAT, the synchrotron beamline at the Paul Scherrer Institute in Villingen, Switzerland. The load application was performed by traverse control, whereby the traverse is moving downwards for tensile testing (Figure 1). The sample holder mount was realized by pasting on (epoxy adhesive) both ends of the wood specimen into two specimen supports that are Aluminum tins with a connection thread. These tins enable an interlocking mount of the specimens in the testing device. For load transmission, a plug system of three tubes is put over the specimen and is fixed by a thread washer at the upper end. This three-pieced plug system enables the mounting of the piezoelectric AE sensors (Figure 1). The center tube is made of Poly-methyl-methacrylate (PMMA, Perspex). The PMMA is suitable because of its low absorption of the radiation, and additionally, since its compression strength reaches 110 N / mm^2.

The tensile tests were monitored with a digital AE-system (type AMSY 6, Vallen Systeme GmbH). Two miniature sensors (type M31 from Fuji Ceramics Corp.) with a coupling area of 3 mm diameter were mounted on the specimen's surface sustaining the scalpel tip. The precisely machined sensor supports enable the even mounting of the AE sensors' piezo bearing face on the specimen's surface. The AE sensors are sensitive in the frequency range of 300 kHz to 800 kHz. The acquisition of digital waveforms was performed with a sampling rate of 10 MHz (409.6 µs signal duration including 200 samples pre-trigger). The threshold was set to 33.2 dB_{AE}.

For the SRXTM monitoring, the energy of radiation was set to 20 keV. The measurements were performed in phase contrast mode. One CCD camera of 2048 x 2048 pixels recorded the scintigrams; the objective (UPLAPO4x) provided a field of view of 3 x 3 mm^2. For one tomography, the specimen was rotated 180° (1501 projections, 32 dark field projections, 150 white field projections, duration of about 20 min). In average, climatic condition was +20° and 22 % relative humidity.

In principle, the tensile tests were performed stepwise by stopping the traverse position manually as soon as AE occurred. Prior and after each load step, the quality of AE coupling was checked by auto-calibration (using each sensor subsequently as emitter and sensor, respectively). When stopping the traverse, immediately the load decreases indicating that the wood is in relaxation. Thus, the motion within the structure significantly degrades the quality of the tomography. Hence, 1-2 min idle time was adhered to, monitored by AE, to minimize the risk recording artifacts of relaxation within the tomograms. The spatial resolution of the structural reconstruction yields 1.85 $µm^3$ per voxel. The synchronization of load application, tomography and AE monitoring is via post processing.

Results and Discussion

By means of two examples (one sample of each specimen type) challenges and chances combining both, AE and SRXTM, are presented and discussed. The radial specimen was loaded in three steps (Table 1, Figure 2a) with a traverse speed of 0.002 mm/min. Almost no AE signals were detected at the first and second step. Only shortly before ultimate failure (4 N/mm^2) in step 3, an average AE activity of 115 signals per sensor was recorded (Table 1). During the idle time subsequent to step 3, the radial specimen failed due to relaxation. This ultimate failure generated 107 AE signals per AE sensor.

Table 1—AE monitoring of spruce tensile loaded perpendicular to fiber (radial test)

	Engineering tensile stress	Traverse displacement	Average number of signals per sensor
	N/mm^2	µm	-
Preload	0.40	-	0
Step 1	2.03	3.167	1
Step 2	3.18	1.850	1
Step 3	4.04	1.537	115.5
Failure	3.98	1.537	107

The AE measurement precisely detects structural changes in a high time resolution (sub-ms). Specifically, in step 3 (Figure 2b), the increasing diversity in AE signals, i.e. identified by amplitude values vs. testing time, reflects the complex damage progresses. Further, the accumulation of various AE signals at discrete time sequences indicates significant damage events as result of several mechanisms. For instance, during the 3rd loading of the radial sample, a load drop indicating pre-failure is accompanied by a number of AE signals at the discrete time of 2300.4 s. The amplitudes ranging between 0.05 mV and 50 mV reveal the

diversity in damage, since the signal amplitude can be used as a rough measure for the intensity of the source mechanism.

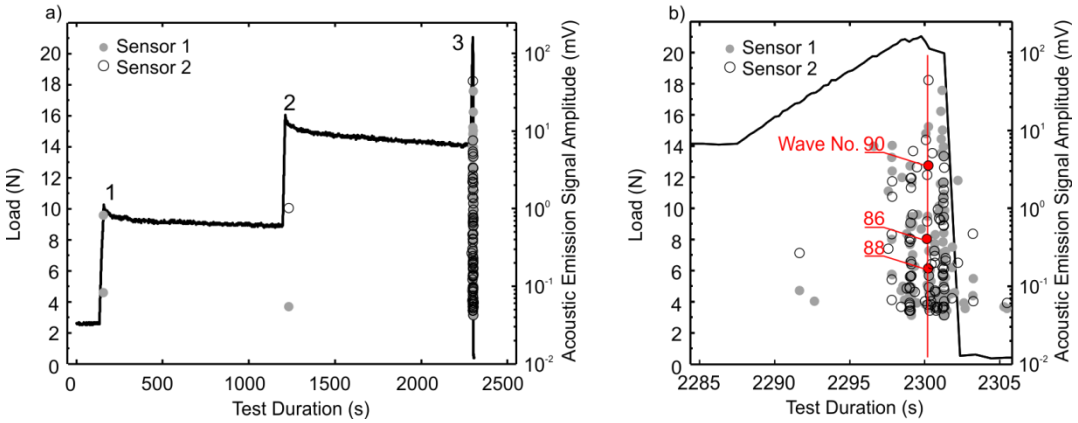

Figure 2—Tensile test on the radial specimen (a). Load and AE signal amplitude versus test duration. Ultimate failure of the specimen at load step 3 with high time resolution (b). Waveforms and frequency spectrum of the highlighted AE signals at 2300.4 s are presented in Figure 3.

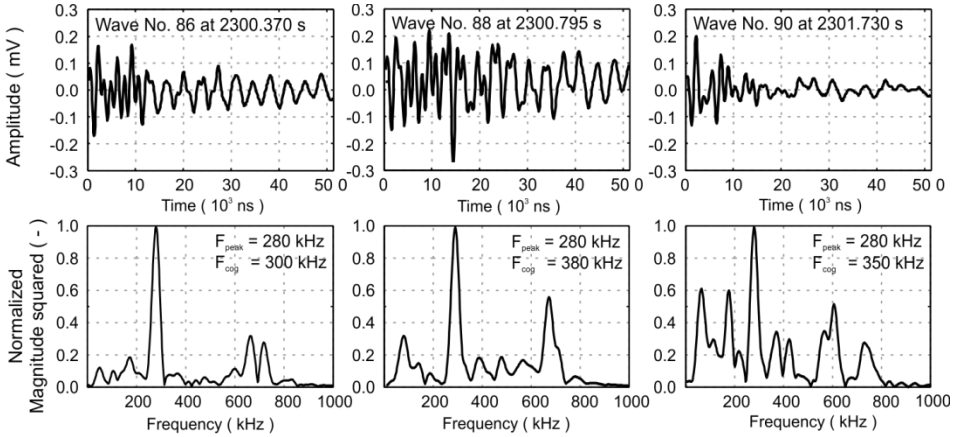

Figure 3—Waveforms and frequency spectra including values of peak and center of gravity frequencies of selected AE signals detected at 2300.4 s while tensile loading the spruce wood specimen perpendicular to fiber (radial test).

Furthermore, the spectra of the AE signals contain signatures of their source mechanisms. Thus, a first characterization was done by determining the first peak frequency and the center of gravity frequency. For this, the frequency spectra were extracted by Fast Fourier Transformation applying a Hamming window function. A first evaluation found the first 512 samples of the transient signals (original recorded AE signal length of 4096 samples) sufficient for disclosing the signals' waveform characteristics. According to this, the first 512 samples of each waveform and the assigned frequency spectra are presented for three selected AE waveforms (Figure 3) that occurred within a time interval of 136 ms close to the discrete time of 2300.4 s (Figure 2). Please note, that the amplitude of the waveform sections in Figure 3 are not equal to those of all AE signal amplitudes vs. test duration plotted in Figure 2, since the first 512 samples of the waveform not yield the peak amplitude of the entire AE signal containing 4096 samples. However, the three high-lighted AE signals show the same peak frequency of 280 kHz. Due to the different shapes of the frequency spectra, different center of gravity frequencies were estimated (Figure 3). Therefore, the characteristics of the spectra reveal variability of the source mechanism.

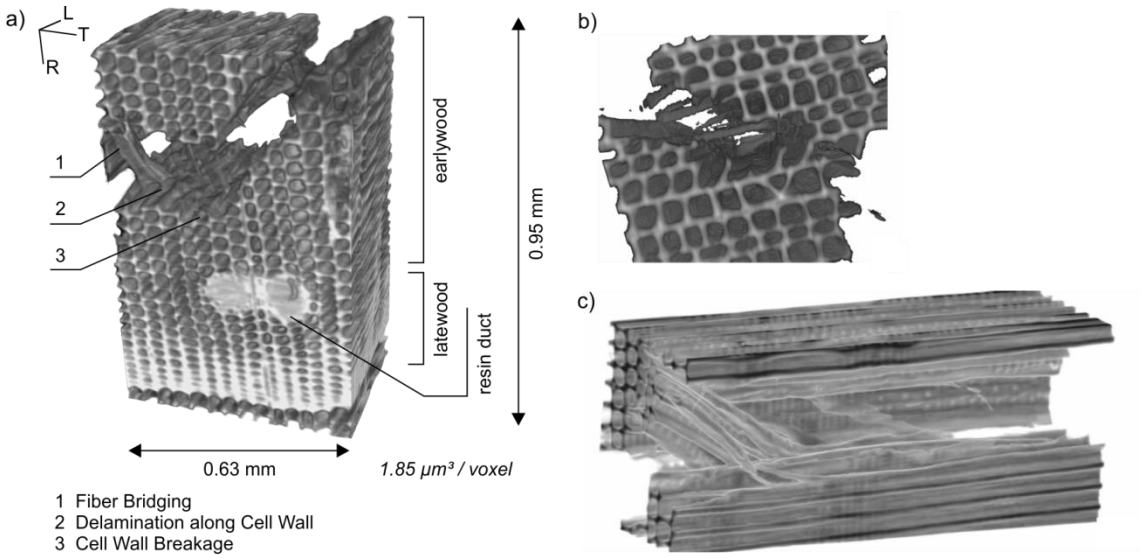

Figure 4—Reconstruction of failed radial specimen (a). The section including fiber-bridging (b) and the isolated fiber-bridging in 3D (c).

The reconstruction of the tomography is consistent with the AE results, showing no indication of damage after the first and second load step. However, the reconstruction of the failed specimen (after load step 3) reveals a complex fracture pattern including several damage mechanisms (Figure 4). As expected, the fracture passed through the earlywood tracheids yielding a number of transwall and intrawall cracks, as well as fiber-bridging of cracks by fiber bundles (Figure 4b-c).

Table 2—AE monitoring of spruce tensile loaded parallel to fiber (longitudinal test)

	Engineering tensile stress	Traverse displacement	Average number of signals per sensor
	N/mm^2	µm	-
Preload	2.60	-	0
Step 1	24.05	6.0	3
Step 2	48.21	4.6	5
Step 3	66.25	3.8	52.5
Step 4	79.65	4.6	65
Failure	89.98	8.2	interruption

The longitudinal specimen was loaded in five steps (Table 2, Figure 5a) with a traverse speed of 0.02 mm/min. Only a few AE signals of low amplitude were detected in load steps 1 and 2. Further, above 70 % of ultimate strength (90 N/mm^2), achieved in step 3, an averaged AE activity of at least 52 signals per sensor was recorded (Table 2). The extended idle time between load step 3 and 4 (Figure 5a) was caused by technical malfunctions on-site. Moreover, in load step 4, the coupling of the sensor 1 was lost and impossible to recover during the test. However, during load step 4 (90% of ultimate strength), sensor 2, with coupling still intact, recorded 65 signals. After the traverse stop in load step 4, the curved shape of the load signal indicates a first damage. The specimen failed during load step 5. Unfortunately, at this time, the coupling of sensor 2 was lost as well and AE results from the ultimate failure were not recorded. However, a more precise view on load step 4 (Figure 5b) shows significant accumulation of AE events at the discrete time of 5551.9 s (time interval of 18 ms). This AE detection preceded the

subsequent first damage after the traverse stopped (Figure 5a). The distribution in AE signal amplitudes (0.5-5.0 mV) indicates significant damage accumulation.

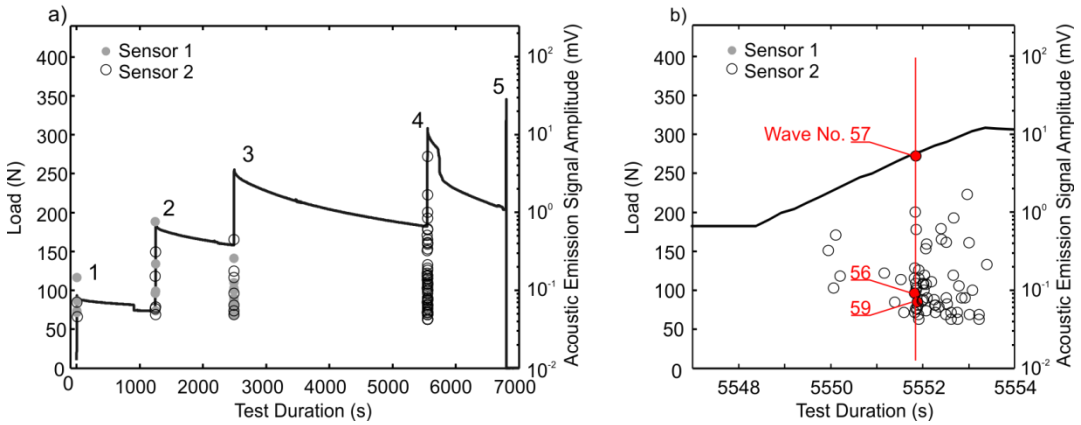

Figure 5—Tensile test on the longitudinal specimen (a). Load and AE signal amplitude are presented in function of the test duration. Load step 4 with higher time resolution (b). Waveforms and frequency spectrum of the high-lighted AE signals at 5551.9 sec are presented in Figure 7.

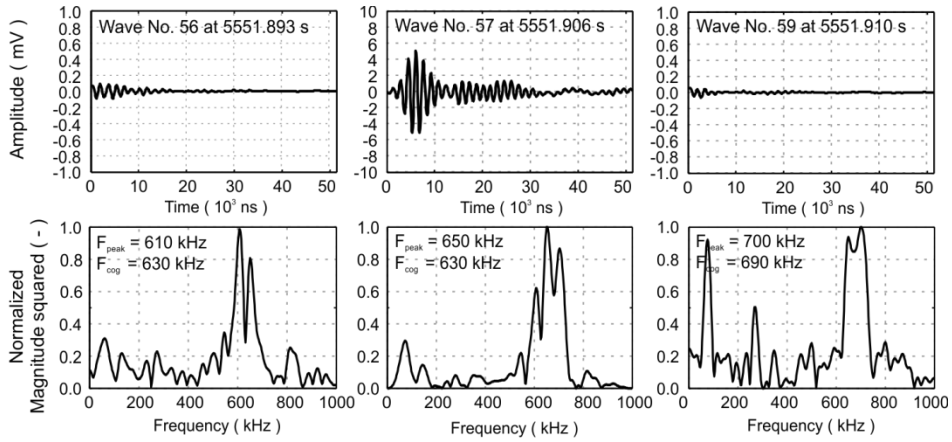

Figure 6—Waveforms and frequency spectra including values of peak and center of gravity frequencies of selected AE signals detected at 5551.9 s while tensile loading the spruce wood specimen parallel to fiber (longitudinal test).

Moreover, the spectral content of selected waveform sections detected at the discrete time of 5551.9 s reveal further differences. In contrast to the selected AE signals of the radial sample, the AE waveforms of the identified damage event in the longitudinal sample mainly contain higher frequencies (Figure 6). The peak frequency is above 600 kHz and here, the center of gravity frequency is approximately in the same range as well.

The tomographic reconstruction relating to load step 4 (Figure 7) substantiates that the crack path, almost exclusively limited to the earlywood, was stopped by the latewood tracheids (Figure 7a). Thus, the preceding AE accumulation close to 5551.9 s contains damages of earlywood features (Figure 7b-c). In accordance to the tomographic observations (load step 1, 2) of the radial specimen, the reconstructions of the longitudinal specimen also show no structural damages for the load steps 1-3. Nevertheless, since micro cracks in cell walls are not detectable with the resolution of 1.85µm^3 per voxel, structural changes cannot be completely excluded yet.

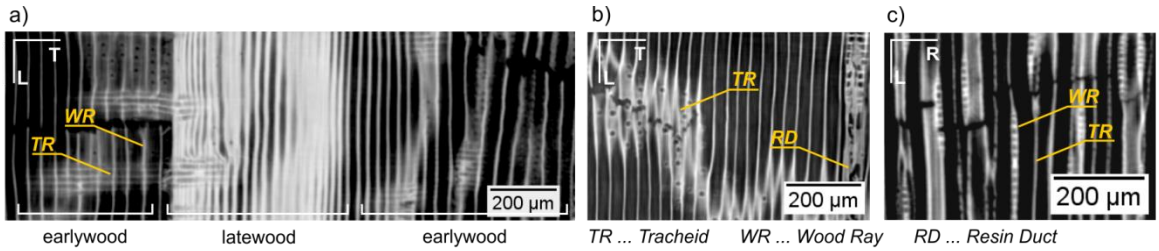

Figure 7—Reconstruction of failed spruce specimen loaded parallel to fiber (longitudinal test)

Conclusion and Outlook

The microscopic damage evolution in spruce wood (*Picea abies* (L.) Karst.), that was exposed to tensile load (in radial and longitudinal direction), was focused on by evaluating damage evolution from in-situ acoustic emission (AE) and structural details from synchrotron based tomographic microscopy (SRXTM).

Due to structure-function relation and the applied fiber-load-angles, the tomographic reconstructions substantiate the different crack paths accompanied by several damage mechanisms (Figure 4, 7). Accordingly, while focusing on the potential assignation to their origin source mechanism, the AE analysis deals with the different features of the AE signals. For instance, the amplitude of the entire recorded AE waveforms (signal length of 409.6 µs) reaches higher maximal values (< 50 mV) for the AE monitoring of the radial specimen (Figure 2) compared with the longitudinal specimen (< 10 mV, Figure 5). Furthermore, AE signals contain descriptive characteristics in their frequency spectrum. In case of the radial specimen, the presented AE waveforms revealing significant structural changes show peak frequencies and center of gravity frequencies below 400 kHz. In contrast, the AE of longitudinal specimens shows peak frequencies as well as center of gravity frequencies above 600 kHz. Further, it has to be taken into account that the recorded AE signals are affected by propagation in the anisotropic wood material and by reflections from the boundaries due to the small specimen size. However, in future analysis the recognition of waveform signatures will be estimated by the method of unsupervised pattern recognition (Sause et al. 2012).

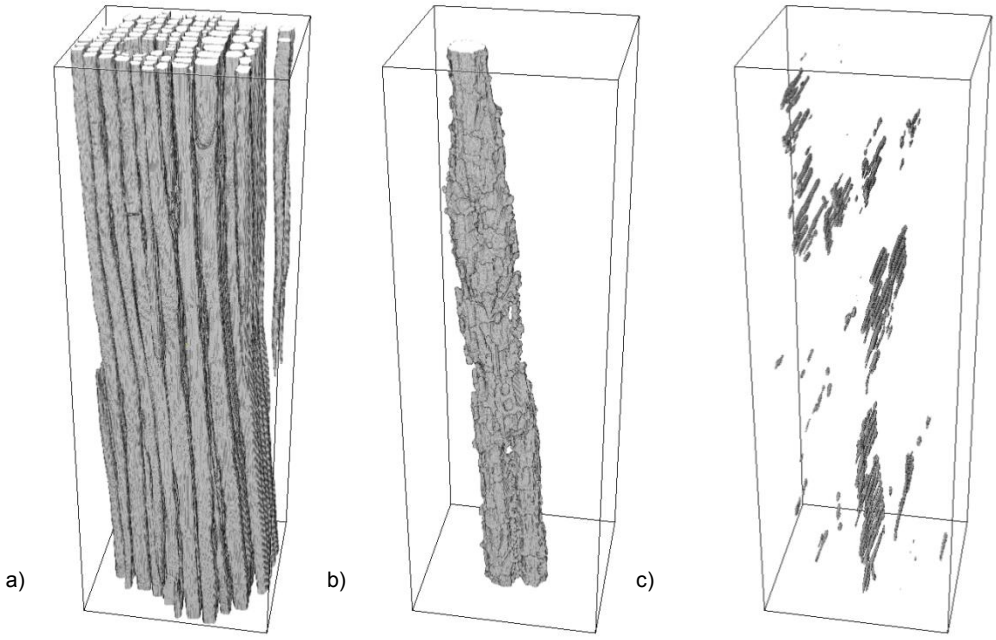

Figure 8—Segmentation of a) wood tracheids, b) resin canal and c) wood rays from SRXTM dataset.

Moreover, the analysis of the reconstruction from the SRXTM monitoring will focus on description of structural deformation at microscopic scale. Thus, in further trials at the TOMCAT beamline, more detailed reconstructions of the wooden structure were already achieved with a resolution of < 1µm^3 per voxel. Out of these results, a dedicated segmentation and geometric parameterization of specific wood cells is currently being performed (Figure 8). In future work, the structural information of each load state might yield more precise insight into the damage evolution at microscopic scale.

Acknowledgement

The authors acknowledge the financial support of the Swiss National Science Foundation under grant SNF-Project 127134. Thank goes to the team of Prof. M. Stampanoni at the TOMCAT beamline (PSI Villingen), especially to Prof. Bernd Pinzer. Also we would like to thank P. Jenni and T. Schnider for the realization of the experimental equipment and our colleagues N. Aigner, D. Fernandez, Dr. P. Hass, O. Kläusler, K. Kranitz, C. Lanvermann, F. Michel, S. Schlegel for support throughout the measurement campaign.

References

Ansell, M.P. 1982. Acoustic emission from softwood in tension. Wood Science Technology 16: 35–58.

Beall, F.C. 2002. Overview of the use of ultrasonic technologies in research on wood properties, Wood Science and Technology 36(3):197-212.

Bucur, V. 2006. Acoustics of wood. Berlin, Springer-Verlag: Chapter 10.

Debaise G.R., Porter A.W., Pentoney R.E. 1966. Morphology and mechanics of wood fracture. Materials Research & Standards 6(10):493–9

Forsberg, F.; Mooser, R.; Arnold, M.; Hack, E.; Wyss, P. 2008. 3D micro-scale deformations of wood in bending: Synchrotron radiation mu CT data analyzed with digital volume correlation. Journal of Structural Biology 164(3): 255-262

Grosse, C.U.; Ohtsu, M. 2008. Acoustic Emission Testing in Engineering – Basics and Applications. Berlin, Springer-Verlag: Chapter 12.

Hass, P.; Wittel, F.K.; McDonald S.A.; Marone, F.; Stampanoni, M.; Herrmann, H.J.; Niemz, P. 2010. Pore space analysis of beech wood: The vessel network. Holzforschung 64(5): 639-644

Mannes, D.; Marone, F.; Lehmann, E.; Stampanoni, M.; Niemz, P. 2010. Application areas of synchrotron radiation tomographic microscopy for wood research. Wood Science and Technology. 44(1): 67-84.

Sause, M.G.R.; Gribov, A.; Unwin, A.R.; Horn, S. 2012. Pattern recognition approach to identify natural clusters of acoustic emission signals. Pattern Recognition Letters 33(1): 17-23.

Trtik, P.; Dual J.; Keunecke, D.; Mannes, D.; Niemz, P.; Stähli, P.; Kaestner A.; Groso, A.; Stampanoni, M. 2007. 3D imaging of microstructure of spruce wood. Journal of Structural Biology 159(1): 46-55.

Zauner, M.; Keunecke, D.; Mokso, R.; Stampanoni, M.; Niemz, P. 2012. Synchrotron-based tomographic microscopy (SRµCT) of wood: development of a testing device and observation of plastic deformation of uniaxial compressed Norway spruce samples. Holzforschung 66(8): 973-979.

Effect of Temperature and Moisture State Changes on Modulus of Elasticity of Red Pine Small Clear Wood

Shan Gao
College of Engineering and Technology, Northeast Forestry University, Harbin, China
Gaoshan_2000@126.com (*Corresponding author*)

Xiping Wang
USDA Forest Service Forest Product Laboratory, Madison, Wisconsin, USA, xwang@fs.fed.us

Lihai Wang
College of Engineering and Technology, Northeast Forestry University, Harbin, China
lihaiwang@yahoo.com

Abstract

This study examined the response of dynamic and static modulus of elasticity (MOE) of red pine small clear wood to a temperature change from -40 to 40 ℃. The 25.4×25.4×407 mm red pine specimens used in this study were selected from those used in a previous laboratory investigation of acoustic properties. The moisture content (MC) of the specimens ranged from 0% to 118.3%. The dynamic MOE was calculated based on measured acoustic velocity and the wood density at the time of acoustic measurement. The static MOE was measured by conducting a static bending test in a laboratory-controlled environment chamber with wood temperature changing from -40 to 40 ℃. Our results indicated that both static and dynamic MOE of wood were affected by temperature and the state of moisture in wood. Above freezing point, MOE decreased linearly at a slow rate as wood temperature increased. Below freezing point, MOE increased at a rapid rate as wood temperature dropped. We found that MC of wood had a significant compounding effect on the MOE-temperature relationships. Temperature effect was much more significant in green wood than in dry wood. Mathematical models were developed to predict the percentage change of MOE relative to the standard temperature of 20 ℃ for wood temperature below and above freezing point. It is concluded that dynamic MOE of wood based on acoustic measurements can be used as a good predictor of static MOE for nondestructive evaluation of wood under a range of wood temperatures.

Key words: **A**coustic velocity, dynamic modulus of elasticity (MOE), static MOE, small clear wood, temperature, moisture content, freezing point.

Introduction

Past research has proven the concept of acoustic measurement on standing trees and logs as a nondestructive evaluation method to evaluate wood quality through the value chains of forest operation and wood products manufacture (Wang et al 2007). Acoustic velocity is now recognized as a measure for predicting the stiffness or modulus of elasticity of wood and wood products derived from measured logs or standing trees. As acoustic measurements are increasingly being conducted on tree stems and logs in forests and log yards, the effects of wood moisture content and environmental condition on acoustic measures has received considerable attention. In a recent laboratory investigation, we studied how acoustic velocity and energy loss response to wood temperature changes on small clear wood samples, especially around freezing point. We found that wood temperature has a significant effect on acoustic velocity in frozen wood. Below the freezing point, acoustic velocity increased as wood tem-

perature decreased. When wood temperature was well above freezing, velocity in green wood was not significantly affected by temperature change. It was also found that wood moisture content had a significant compounding effect on the velocity-temperature relationships. Temperature effect was much more significant in green wood than in dry wood.

When acoustic velocity measure of trees and logs are used to predict the stiffness of wood, a similar temperature and moisture content effect is expected to be seen in dynamic MOE. But how does the dynamic MOE response differently to the changes of temperature and moisture content than static MOE is not clear yet. The objectives of this study were to further investigate the effects of temperature and moisture content/state on dynamic and static MOE of red pine small clear specimens and develop analytical models for adjusting predicted MOE to account for temperature differences when acoustic measurements are performed in different climates or different seasons.

Background

A series of studies have reported the effect of temperature on mechanical properties of wood. Gerhards (1982) summarized the studies on the immediate effects of moisture content and temperature on several mechanical properties of clear wood. Comben (1964) investigated the effect of temperature on strength and elasticity of ash, balsa, and Douglas-fir under 12%, 18%, 20%, and green conditions. He found that as wood temperature decreased from 17 to -73℃, the static MOE increased 32% under 12% MC and 78% for green wood.

Sellevold et al. (1975) examined the response of dynamic MOE and internal friction of beech wood beams at a various equilibrium moisture contents from 0 to 96% to the temperature changing from 25 to -130℃. A marked transition was found on the curve of the percentage change of MOE relative to 25℃ with the temperature at around -90℃ and around 0℃ for the wood of moisture contents at or above the FSP. The magnitude of the transition decreased with the decreasing moisture content. They reported a 23% increase in MOE with the decreasing temperature from 25 to -70℃ for wood of 15% MC and 55% for wood of 98% MC.

Mishiro and Asano (1984 a, b) investigated the effects of temperature and moisture content on bending properties of spruce in the temperature range -180 to 60℃ with moisture content below FSP (0% to 28.5%) and above FSP (50 to 210%). Both MOE and bending strength were found to increase as temperature decreased. They noticed that the relationships between bending properties and temperature were apparently influenced by the wood moisture content. For green wood, the property-temperature relations were characterized as segmented linear relationships with distinctively different slopes in three temperature ranges: -140 to -20℃, -20 to 0℃ and 0 to 60 ℃. Above 0℃, MC above fiber saturation point did not significantly influence the properties-temperature relations; but below 0℃, MC showed a strong compounding effect on the bending properties.

Fridly et al. (1992) evaluated the mechanical properties of 38 by 89 mm structural Douglas-fir lumber in several hygrothermal states and found about 14 % loss in median modulus of rupture (MOR) but little change in MOE when the lumber specimens were heated form 23 to 55 ℃.

DeGeer and Bach (1995) conducted static bending tests on different grades of 38 by 89 mm spruce-pine-fir (SPF) lumber at 20℃, -15℃ and -30℃ with MC from 15% to 17%. They reported a fast increase in MOE for the temperature change from 20 to -15℃, while a much smaller change observed for the temperature change from -15 to -30℃. They attributed the change in MOE and MOR with changing temperature to the phase change of the moisture in the lumber.

Green and Evans (2008) evaluated the immediate effect of temperature on flexural MOE of green and dry structural lumber from 66 to −26℃. They observed an increase in MOE with decreasing temperature for both green and dry lumber. For lumber at 4 and 12% MC levels, a linear relationship was used to relate the increase in MOE to decrease in temperature. For green lumber, a segmented linear re-

gression was developed to describe the change in MOE of green lumber with changing temperature. The slope of the MOE-temperature relationship was steeper below 0℃ than above.

Chan et al (2010) performed acoustic wave measurements on 200 × 80 × 55 mm radiata pine sapwood boards at a temperature range of -71 to 58℃ and a MC range of 17% to 159%. Acoustic velocity decreased linearly with increasing temperature and an abrupt discontinuity occurred around freezing pint of water for the wood with MC above FPS. A similar relationship was also found between calculated dynamic MOE and temperature.

Materials and Methods

Materials

The materials used in this study were selected from the small clear red pine specimens (25.4 × 25.4 × 407 mm) that were used for a previous laboratory investigation on acoustic properties (Gao et al. 2012). The entire set of the specimens were in different moisture levels: Group 1 was green condition (fresh-cut and stored in a freezer before test); Group 2 and 3 were conditioned to 24 and 12% equilibrium moisture content (EMC); and Group 3 was oven-dried to 0% MC. We initially selected 12 specimens for this study, 3 from each group. The specific MC of three green specimens was 118.3%, 91.4% and 78.6% respectively. These specimens were wrapped with plastic film individually and stored in a refrigerator at – 20℃before test.

Ultrasonic measurement

A Sylvatest Duo (CBS-CBT, Les Ecorces, France) unit was used to measure the ultrasonic velocity in the selected wood samples at a temperature range of -40 to 40 ℃. A sealed foam box was constructed and used as an environmental chamber throughout the testing process. Dry ice and hot water were used as a cooling and heating source during testing. A detailed procedure for controlling wood temperature is described in Gao et al. 2012.

Static bending test

To perform static bending tests over a wide range of temperature conditions, we built a special environmental chamber which was mounted on the universal testing machine (Figure 1). The chamber was constructed with a sealed foam box which fitted into the center-point loading setup on the machine, with the wood specimen, end supports, and the loading head enclosed into the chamber. A wood specimen wrapped with plastic film was supported over a 35.6-cm span by two metal supporting plates (51 by 51 mm) which were resting on two wood blocks. A liquid carbon dioxide tank was used as a cooling source to provide low temperature carbon dioxide gas into the chamber.
Two 30W light bulbs were used as a heating source to heat the wood specimen inside the chamber. The temperature of specimen was controlled by regulating air circulation using two small electric fans running at the opposite corners of the chamber. Two thermocouples (TC) were inserted into the wood specimen at different position to monitor the wood temperature change. TC No. 1 was fixed at the mid-span and center depth and TC No.2 at the quarter span and quarter depth. TC No. 3 was placed in the chamber to measure the air temperature. During the testing process, a microprocessor thermometer (Omega Model HH23, OMEGA Engineering, Inc., Stamford, CT) was used to monitor the wood temperatures (TC No.1 and No.2) and the air temperature in the lower chamber (TC No.3). A solenoid connected CO_2 cylinder was used to control the flow of liquid CO_2 gas from cylinder to specimen chamber through a copper tube line. A temperature controller (Chromalox) was used to control CO_2 gas circulation to keep the desired wood temperatures.

Static bending test was conducted on each specimen under a center-point loading according to ASTM 143-94 (ASTM, 2006). The modulus of elastic of wood was calculated from the following equation ():

$$MOE = \frac{L^3 \Delta P}{4bh^3 \Delta D} \quad (1)$$

Where L is the span length, b and h are the base and height of the specimen respectively, ΔP is the load increment and ΔD is the deflection increment under ΔP.

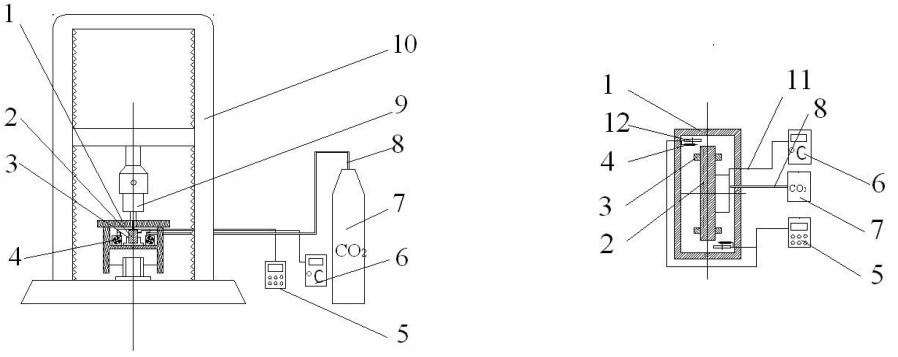

(a) Schematic of the static bending test setup equipped with a temperature control system.

(b) Schematic of the environmental chamber with a temperature control system.

Figure1—Schematic of the bending test system for measuring MOE of red pine at various temperatures (1-Environmental chamber; 2-Wood specimen; 3-End supports; 4-Electronic fan; 5-Temperature controller; 6-Microprocessor thermometer; 7-Liquid carbon dioxide cylinder; 8-Copper tube; 9-Cross-head; 10-Instron machine; 11-Thermocouple wire; 12-Heating bulb)

Testing process was started by releasing the liquid CO_2 gas from the cylinder to the chamber till the wood temperature reached -40℃. Static bending test was conducted at a wood temperature of -40℃ first and then repeated at every 10℃ increment till the wood temperature increased to 40℃. When the chamber temperature reached the room temperature, the electronic heaters (light bulbs) were turned on to gradually raise the wood temperature up to about 40℃. During each testing cycle, two electric fans were manually control the air circulation so that the targeted temperatures were reached with uniformity, which was indicated by close readings of three thermocouples (TC No.1, No.2 and No.3). After the testing process was completed, we re-measured the dimension and the weight of each specimen to calculate the wood density, and monitored MC change during testing.

Results and Discussion

Response of static MOE to temperature change

Table 1 summarizes the physical characteristics of the red pine specimens tested. Due to system break-down and limited machine time available, we tested six specimens in total: three in group 1, each had distinctively different MC; one for each other groups. The MC of the specimens was in a range of 0.3% and 112.9%. The time used to complete one test cycle was about 8 to 10 hours. No noticeable change was observed in weight and dimension for each specimen. Wood moisture loss during the test cycle was minimal (0.9-1.2 % for Group 1, 0.7 – 1.4% for Group 2, 0.1 – 2.1% for Group 3, and 0.2% for Group 4). Wood density was derived based on the weight and dimension of the specimen at the beginning of static bending test.

Figure 2 shows the load-deflection curves of a green specimen (No.1) obtained at a wood temperature range from -40 to 40 ℃, with a 10℃ increment. It is apparent that the slope of the linear curves (within the elastic region), which indicates the stiffness of the specimen, increased as wood temperature dropped from 40 ℃ to -40 ℃. We also observed a significant shift on the slope of the load-deflection cure between 0 ℃ and -10 ℃. This was consistent with what we observed on acoustic velocity shift for the same specimen around the freezing point (Gao et al. 2012).

Table 1—Physical properties of the red pine small clear specimens selected for static bending test.

Group No.	Specimen No.	MC (%)	Density (kg/m^3)	Dimension			Weight (g)	Oven-dry Weight (g)	Ring count (no./mm)
				Height (mm)	Base (mm)	Length (mm)			
	1	112.9	858.28	25.68	25.12	407.02	225.35	105.85	2.9
I	2	90.1	730.91	25.30	25.81	407.12	194.27	102.19	2.6
	3	76.4	723.18	25.20	25.55	407.10	189.55	107.47	3.6
II	4	24.5	517.90	26.16	25.10	407.00	138.39	111.19	1.9
III	5	15.2	463.27	29.08	25.58	407.00	140.26	121.75	1.6
IV	6	0.3	465.69	23.93	23.95	407.14	108.66	107.95	1.9

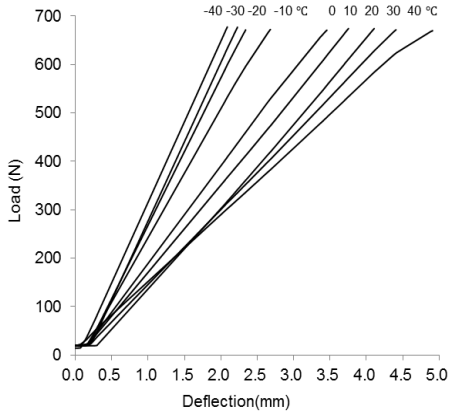

Figure 2—Load-deflection relationships of a green wood specimen (No. 1) at various temperatures.

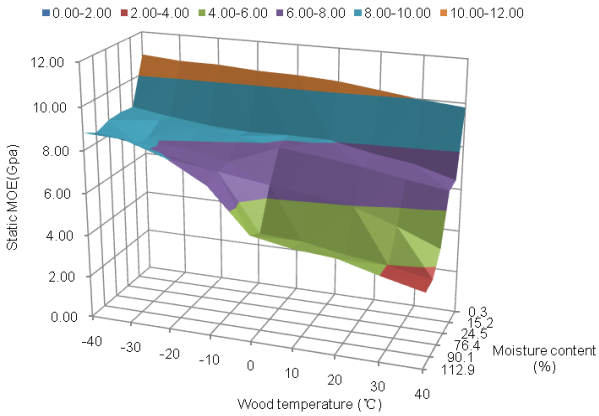

Figure 3—Effects of temperature and moisture content on static modulus of elasticity

Figure 3 shows the response of static MOE of the specimens with different MC to the wood temperature changes. The static MOE increased continuously as wood temperature dropped from 40 ℃ to -40 ℃. The change rate of static MOE was different at different temperature zones (above 0℃, -10 to 0℃, and -10 to -40 ℃) and affected by the wood moisture condition. The freezing point of water (0℃) was clearly a turning point for the trends of static MOE-temperature relationships in green wood. As wood temperature changed from 40 ℃ to -40 ℃, the percentage increase in static MOE was from 92.34 to 149.56 % for green specimens, 30% for specimen of 24% MC, 26.8% for specimen of 12%MC, and 11.3% for specimen of 0%MC.

With respect of moisture effect, 24% MC (FSP of red pine) presented as a demarcation point in the static MOE-MC relationships. For dry wood (below FSP), the static MOE decreased dramatically with increase of MC. This trend was generally same for the entire temperature range tested. For green wood (above FSP), the static MOE decreased slightly with the increasing MC when wood temperature was above freezing, but it stayed relatively constant when wood was below freezing.

Overall, our results indicated that wood temperature, moisture content, and moisture state (frozen or non-frozen) had a compounding effect on the static MOE of wood. The effect of temperature on static MOE was most prominent for green wood and below freezing point. Our findings are basically in agreement with those reported by Mishiro and Asano (1984a, b). The sudden raise in MOE around freezing point was attributable to the phase transformation of the free water in wood cells. Mishiro and Asano (1984a, b) used the rule of mixtures to explain their results and predicted wood properties by considering the percentage of water in saturated cell wall and air voids and frozen water in the cell lumen. In addition, our experimental data showed that temperature changes contributed more to the static MOE change when wood temperature was below freezing, and moisture content changes con-

tributed more to the static MOE change when wood temperature was above freezing.

Analytical models

Relative static MOE and dynamic MOE

To examine the significance of the temperature impact on MOE and minimize the difference in prediction across percentile levels of the property distribution, an analytical model based on the percentage of change in MOE relative to the MOE at a base temperature of 20 ℃ was used to describe the relationship between MOE and temperature. The percentage of change in MOE is defined as

$$\Delta MOE(\%) = \left(\frac{MOE_T - MOE_0}{MOE_0}\right) \times 100 \qquad (2)$$

where MOE_T is MOE at the temperature T and MOE_0 is the MOE at 20 ℃ (Barrett et al. 1989; Green and Evans, 2008; Gao et al, 2012, 2013).

Figure 4 illustrates the percentage of change in measured static MOE relative to 20℃ (relative static MOE) at different temperatures. A significant change in relative static MOE with temperature was observed below freezing point for green wood. Above freezing, the relative static MOE increased gradually as the wood temperature decreased. An abrupt increase in relative static MOE occurred when wood temperature dropped just below the freezing point. Then the change became slow as the temperature fell below -10℃. For wood specimens with a MC below the FSP, the relative static MOE was not significantly affected by temperature.

Our previous study has demonstrated that temperature has significant effect on acoustic velocity of small wood specimen. The mathematic models were developed to describe the relationship between acoustic velocity and temperature (Gao et al. 2012). Based on the acoustic velocity and density of the specimens, the corresponding dynamic modulus of elasticity was derived and the percentage of change in dynamic MOE relative to 20℃ with temperature was illustrated in the Figure 5. The relative dynamic MOE showed a similar changing trend with temperature as the relative static MOE. This further proved the hypothesis initiated by Jayne (1959) that the energy storage and dissipation properties of wood materials in a stress wave test are controlled by the same mechanisms that determine the static behavior of such material.

Prediction models of relative static and dynamic MOE

The relative MOE and temperature relationships can be characterized by the following segmented linear regression models at two different temperature ranges:

$$\Delta MOE = k_d T + h_d \quad (\%) \quad (-40℃ \leqslant T \leqslant -10℃ \text{ or } 0℃ \leqslant T \leqslant 40℃) \qquad (4)$$

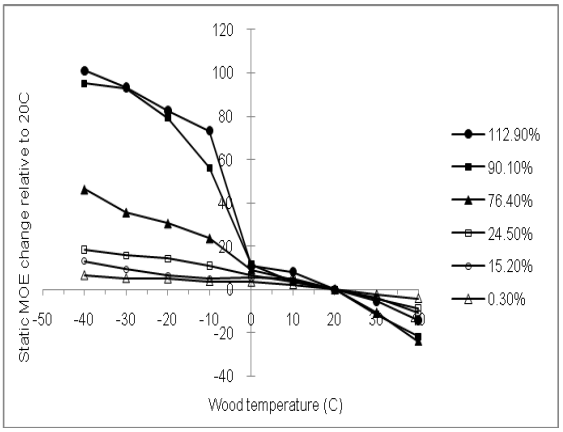

Figure 4—Relationship between relative static MOE and temperature.

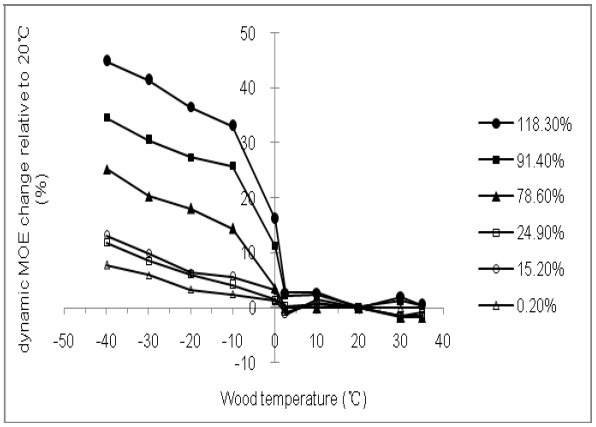

Figure 5—Relationship between relative dynamic MOE and temperature.

Table 2—Coefficients of regression models of relative MOE –temperature

$\Delta MOE_d = k_d T + h_d$ (%)					$\Delta MOE_s = k_s T + h_s$ (%)				
MC	T≤-10℃		T≥0℃		MC	T≤-10℃		T≥0℃	
	k_d	h_d	k_d	h_d		k_s	k_s	k_s	k_s
118.3%	-0.400	28.94	-0.054	2.267	112.9%	-1.260	47.45	-0.816	12.74
91.4%	-0.295	22.17	-0.056	2.390	90.1%	-0.906	64.66	-0.640	12.89
78.6%	-0.347	10.83	-0.084	1.117	76.4%	-0.749	15.50	-0.836	12.74
24.9%	-0.257	1.221	-0.097	1.749	24.5%	-0.238	80859	-0.381	6.985
15.2%	-0.261	2.257	-0.107	2.368	15.2%	-0.211	3.500	-0.361	6.000
0.2%	-0.185	0.264	-0.165	0.084	0.3%	-0.086	3.002	-0.171	3.000

Figure 6 shows the linear regression lines for relative static and dynamic MOE and temperature relationships at two temperature zones: -40℃≤T≤-10℃ and 0℃≤T≤40℃.The straight line between 0 ℃ and -10 ℃ simply represents the transition of relative MOE and no statistical regression line can be obtained because of limited data points.

The regression coefficients of the linear models for relative static and dynamic MOE versus temperature at different MC levels are listed in Table 2. The coefficient of determination for the static ΔMOE ranged from 0.91 to 0.99 in the temperature range of -40 to -10℃ and from 0.90 to 0.99 in the temperature range of 0 to 40℃. The coefficients of determination for the dynamic ΔMOE ranged from 0.95 to 0.99 in the temperature range of -40 to -10℃and from 0.22 to 0.95 in the temperature range of 0 to 40℃.

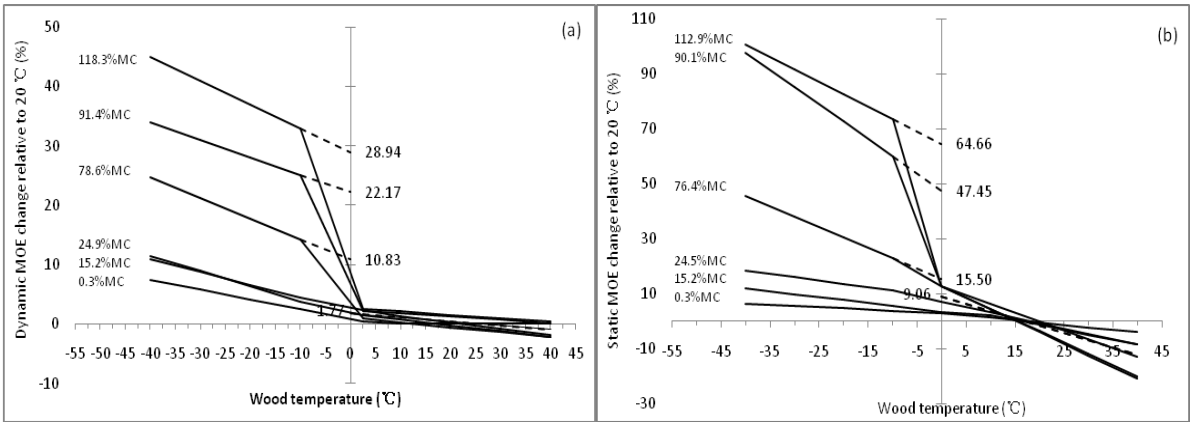

Figure 6—Linear regressions demonstrating the effect of temperature on percentage of change in static and dynamic MOE relative to 20℃.

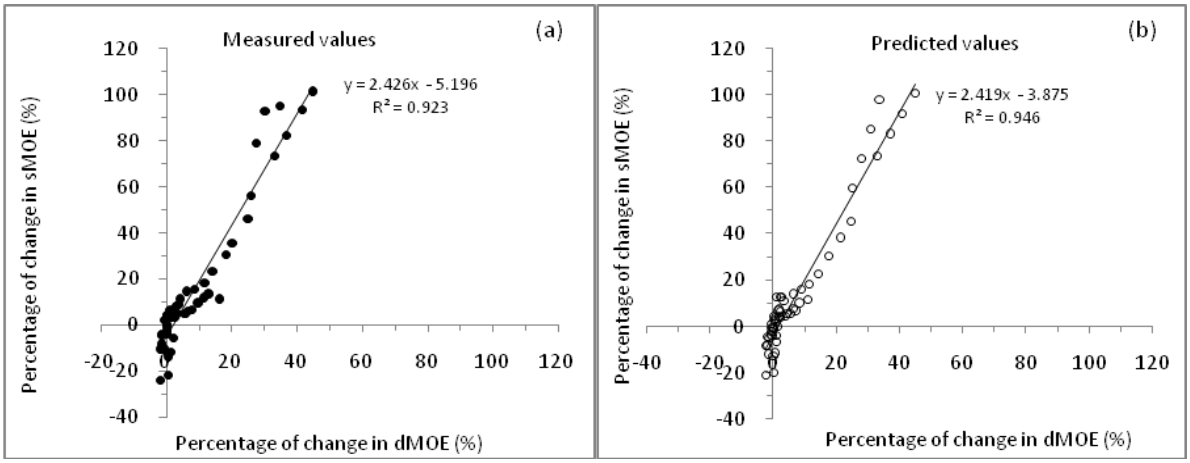

Figure 7—Relationships between relative dynamic MOE and relative static MOE of red pine specimens.

Figure 7 shows comparisons between relative static MOE and relative dynamic MOE of the red pine specimens. Very good linear relationships existed between measured changes in dynamic MOE and static MOE, with a coefficient of determination of 0.92 (Figure 8a) and between predicated changes in dynamic MOE and static MOE, with a coefficient of determination of 0.946 (Figure 8b). Therefore it is logical that the dynamic MOE based on acoustic velocity can be used as a good predictor of the static MOE for nondestructive evaluation of wood at a range of wood temperatures.

Conclusions

This study examined the response of dynamic and static modulus of elasticity (MOE) of red pine small clear wood to a temperature change from -40 to 40 ℃ and developed analytical models to predict the percentage of changes in MOE at different temperatures relative to a standard temperature (20℃). Based on the results, we conclude the following:

1. Modulus of elasticity of wood was affected by temperature and the state of moisture in wood. Above the freezing point, MOE of wood (non-frozen) decreased linearly at a slow rate as wood temperature increased. Below freezing point, MOE increased at a rapid rate as wood temperature dropped.

2. Moisture content of wood had a significant compounding effect on the MOE-temperature relationships. Temperature effect was much more significant in green wood than in dry wood. MOE of green wood changed abruptly around the freezing point, due to the phase transformation of free water in the cell lumens.

3. Mathematical models were developed to predict the percentage change of MOE relative to standard temperature of 20℃ in two temperature zones: -40℃≤T≤-10℃ and 0℃≤T≤40℃.

4. The relative dynamic MOE showed a similar changing trend with temperature as the relative static MOE. Dynamic MOE can be used as a good predictor of the static MOE for nondestructive evaluation of wood at a range of wood temperatures.

Acknowledgement

This project was supported by the Fundamental Research Funds for the Central Universities (Grant No. DL12BB31) and was conducted under the cooperative research agreement between Northeast Forestry University, Harbin, China, and the USDA Forest Products Laboratory (FPL). We thank Dr. Robert Ross for his great support to this project and also thank Mr. James T. Gilbertson of FPL for his technical assistance during the testing.

References

ASTM (2009) D143-09. Standard test methods for small clear specimens of timber. American Society for Testing and Materials, West Conshohocken, PA, USA.

Barrett JD, DW Green, JW Evans (1989) Temperature adjustments for the North American in-grade testing program *In*: Proc. In-grade Testing of Structural Lumber. DW Green, BE Shelley and HP Vokey, eds. Proc. 47363, Forest Proc. Soc. Madison, WI. pp 27-38

Comben AJ (1964) The effect of low temperature on the strength and elastic properties of timber. Journal of the Institute of Wood Science 13:44-55.

DeGeer D and L Bach (1995). Machine stress grading of lumber at low temperatures. Natural Resources Canada, Canadian Forest Service, Northern Forestry Centre, Edmonton, Alberta. Canada-Alberta Partnership Agreement in Forestry Report 127. 20 p.

Fridley KJ, Tang RC, Soltis LA (1992) Hygrothermal effects on mechanical properties of lumber. Journal of Structural Engineering 118(2):567-581.
Chan JM, Walker JC, Raymond CA (2010) Effect of moisture content and temperature on acoustic velocity and dynamic MOE of radiata pine sapwood boards. Wood Sci Technol 45:609-626.

Gao S, Wang X, Wang L, Allison RB (2012) Effect of temperature on acoustic evaluation of standing trees and logs: Part 1 – Laboratory investigation. Wood and Fiber Science 44(3): 286-297

Gao S, Wang X, Wang L, Allison RB (2013) Effect of temperature on acoustic evaluation of standing trees and logs: Part 2 –Field investigation. Wood and Fiber Science 45(1): 15-25

Green DW, Evans JW (2008) The immediate effect of temperature on the modulus of elasticity of green and dry lumber. Wood and Fiber Science 40(3):374 -383

Jayne BA (1959) Vibrational properties of wood as indices of quality. Forest Products Journal 9(11):413-416.

Mishiro A, Asano I (1984a) Mechanical properties of wood at low temperature: Effect of moisture content and temperature on bending properties of wood I. Moisture content below the fiber saturation point. Mokuzai Gakkaishi 30(3):207-213

Mishiro A, Asano I (1984b) Mechanical properties of wood at low temperature: Effect of moisture content and temperature on bending properties of wood II Moisture content beyond the fiber saturation point. Mokuzai Gakkaishi 30(4):277-286

Sellevold JE, Radjy F, Hoffmeyer P, Bach L (1975) Low temperature internal friction and dynamic modulus for beach wood. Wood and Fiber 7(3):162-169

Silins U, Lieffers VJ, Bach L. (2000) The effect of temperature on mechanical properties of standing lodgepole pine trees. Trees 14:424–428

Wang X, Carter P, Ross RJ, Brashaw BK (2007) Acoustic assessment of wood quality of raw forest materials – A path to increased profitability. Forest Products Journal 56 (5): 6-14.

Influence of Temperature and Moisture Content in Non-destructive values of Scots pine (*Pinus sylvestris* L.)

Daniel F. Llana
ETSI Montes, Universidad Politécnica de Madrid, Madrid, Spain, d.f.llana@upm.es

Guillermo Iñiguez-Gonzalez
ETSI Montes, Universidad Politécnica de Madrid, Madrid, Spain, guillermo.iniguez@upm.es

Francisco Arriaga
ETSI Montes, Universidad Politécnica de Madrid, Madrid, Spain, francisco.arriaga@upm.es

Peter Niemz
Wood Physics, Institute for Building Materials, ETH Zürich, Switzerland, niemzp@ethz.ch

Abstract

Good results evaluating material properties using non-destructive testing (NDT) techniques have been achieved for decades. Several studies to understand the influence of temperature and moisture content on NDT have concluded different effects. In this study, NDT parameters were measured on the principal structural Spanish sawn timber species, Scots pine (*Pinus sylvestris* L.).
NDT were conducted on 216 specimens of nominal dimensions 20 by 20 by 400 mm. Specimens were divided into several groups and studied at six different temperatures and four different moisture contents. Commercial equipment and techniques applied were Sylvatest Duo (ultrasonic wave technique), Steinkamp BPV (ultrasonic wave technique), and Grindo Sonic Mk5 "Industrial" (vibration analysis technique). Differences in NDT values within specimens at different temperatures and moisture contents were obtained.
Main results of this study and relationships that describe changes in NDT values by effect of temperature and moisture content are presented.

Keywords: Ultrasonic wave, vibration analysis, temperature, moisture content, climate conditions

Introduction

Evaluation of the influence of climate parameters on timber mechanical properties and on non-destructive testing (NDT) is not a new concept (James 1961; Gerhards 1982; Niemz 1993; Arriaga 2009).

Although it is relatively easy to conduct a NDT test, it is important to note that several factors affect NDT parameters. The applicability of ultrasound techniques in practice requires full knowledge of the effect of environmental conditions, which is why this present paper focuses on the influence of equilibrium moisture content (EMC) below fibre saturation point (FSP) and temperature (T) over *Pinus sylvestris* L.

Factors affecting ultrasonic measurements in wood have been profusely studied (Bucur 1984; Bucur 1994). There are several research works on the effect of EMC and T on ultrasound velocity and correction factors proposed for vibration and ultrasound velocity (Sandoz 1991; Moreno-Chan 2010; Unterwieser 2010).

The ultrasound velocity parallel to the fibres decreases dramatically with EMC up to the FSP (Sakai 1990; Kang 2002; Oliveira 2005; Bucur 2006; Gonçalves 2008), approximately eight times more than the EMC effect when EMC > FSP (Sandoz 1993). The same effect above and below the FSP was found for stress waves (Wang 2008).

Ultrasonic velocity generally increases linearly with decreasing T (+50 to -30ºC) and EMC below FSP (Bucur 2006).

The influence of T on acoustic properties is magnified when the EMC of wood increases (Sandoz 1993). The overall trend of the changes in velocity is similar for all dry wood (below FSP), below and above freezing point (Gao 2011).

Other studies focused on stress waves and concluded that the stress wave speed decreased reciprocally with increasing EMC and decreased linearly with increasing T. The T has the same effect on stress wave parameters on both studied species (softwood and hardwood), however the effect of EMC is different (Matthews 1994).

Different correction factors for EMC on NDT measurements were proposed for several authors. Considering 12% EMC as the reference value.

For ultrasound technique (Steinkamp BP-V) records, a correction factor with a decrease in velocity of approx. 0.8 % with an increase of 1 % of EMC, in the range of 5 to 30 % EMC, was proposed for spruce (Sandoz 1989).

For ultrasonic velocity, a correction factor with a decrease in velocity of 0.53% with an increase of 1% in EMC, in the range below 28% EMC, was proposed for spruce (Steiger 1996).

For ultrasonic velocity (Steinkamp BP7 45 kHz) of Parana pine, a correction factor equation was proposed. From it was obtained a decrease in velocity of 0.45% with an increase of 1% in EMC, below FSP (Gonçalves 2008).

For ultrasound technique (Sylvatest) and vibration technique (Viscan) records, correction factors with a decrease in ultrasound velocity of 0.60%, a decrease in dynamic modulus of elasticity (Edyn) of vibration of 0.87% and an increase of density of 0.42%, accompanying a 1% increase in EMC, in the range below 28% EMC, were proposed for spruce (Unterwieser 2010).

Less works were found dealing with adjustment factors of T on NDT measurements.

For ultrasound technique (Sylvatest) records, a correction factor was proposed with a decrease in velocity of approx. 0.08 % with an increase of 1 ºC (12% EMC), in the range of -20 to 60 ºC (Sandoz 1993). The same correction factor was proposed by Steiger in the range from 20 to 40 ºC (Steiger 1996).

Material and methods

The materials used consisted of 216 small clear specimens of nominal dimensions 20x20x400 mm, cut from 24 dry timber pieces of dimensions 150x50x4400 mm at 20ºC and 65% of Scots pine (*Pinus sylvestris* L.) from Valsain, Segovia, Spain. The specimens were grouped into 9 batches of 24 specimens each and were tested in the ETH laboratories in Zurich, Switzerland.

The influence of EMC was studied over four batches of 24 specimens each, conditioned for 45 days before testing at a temperature of 20 ± 2ºC and at four different air relative humidities (55%, 65%, 75%, and 85% ± 5%). Table 1 summarizes these batches.

Table 1 - Specimens for study of EMC effect according to climate conditions.

Batch	Air Humidity (%)	T (ºC)	Number of specimens
H55T20	55 ± 5	20 ± 2	24
H65T20	65 ± 5		24
H75T20	75 ± 5		24
H85T20	85 ± 5		24
TOTAL			**96**

The influence of T was studied using six batches of 24 specimens, each conditioned to normal conditions of 20 ± 2ºC and 65 ± 5% of air relative humidity. Then the specimens were wrapped individually in plastic bags. Each batch of 24 wrapped specimens was conditioned at different temperatures (50, 30, 20, -10, -20 and -40 ± 2ºC) using a Feutron KPK 200 GmbH chamber. The temperature of the specimens was monitored with internal sensors and recorded with a commercial data loger Almemo 2890-9 Ahlborn. Table 2 summarizes these batches.

Table 2 - Specimens for study of T effect according to climate conditions.

Batch	Air Humidity (%)	T (ºC)	Number of specimens
H65T50	65 ± 5	50 ± 2	24
H65T30		30 ± 2	24
H65T20		20 ± 2	24
H65T-10		-10 ± 2	24
H65T-20		-20 ± 2	24
H65T-40		-40 ± 2	24
TOTAL			**144**

Several measurements using NDT were carried out at each climate condition.

Time of flight value was measured with two ultrasonic commercial devices. Sylvatest Duo (using conical sensors of 22 kHz frequency) and Steinkamp BP-V (using conical sensors of 50 kHz frequency). Measures were made end to end (longitudinal direction parallel to the grain) on each specimen, with a constant sensor coupling pressure.

According to the time results of ultrasound devices, the wave velocities (length/time) and Edyn were calculated using equation 1:

$$E_{dyn}=\rho \cdot V^2 \cdot 10^{-6} \quad (1)$$

Where: E_{dyn} is the dynamic modulus of elasticity, in N/mm^2; ρ is the density, in kg/m^3; and V is the velocity of the ultrasound wave, in m/s.

For the vibration analysis (with a commercial device Grindosonic Mk5 "Industrial") the specimen was simply supported at two nodal points at a distance of 0.224 l from the end; l being the total length of the specimen. The midspan of the specimen was hit with a small hammer and the impact induced an oscillation in the vertical (transverse) direction. The transverse frequency was registered by an accelerometer and Edyn was obtained according to equation 2 (Görlacher 1984).

$$E_{dyn,v}=\frac{4\,\pi^2 \cdot l^4 \cdot f_0^2 \cdot \rho}{m_n^4 \cdot i^2} \cdot \left(1+\frac{i^2}{l^2} \cdot K_1\right) \cdot 10^{-12} \quad (2)$$

Where: $E_{dyn,v}$ is the dynamic modulus of elasticity, in N/mm^2; l is the length of the specimen, in mm; f_0 is the transverse frequency, in Hz; ρ is the density, in kg/m^3; m_n^4 is the constant = 0.5006x10^3; i is the radius of gyration, in mm; K_1: constant = 49.48.

After measurements were completed, the EMC of each specimen was determined using the oven dry method according to standard EN 13183-1. Four different average EMC (10.88, 12.00, 15.58 and 17.38 %) were obtained for each batch conditions (H55T20, H65T20, H75T20 and H85T20), respectively.

Results and discussion

The effect of EMC on non-destructive parameters is summarized in table 3.

Table 3 - NDT results for different EMC.

		NDT					
Batch	**EMC (%)**	Vel Sylvatest Duo		Vel Steinkamp BPV		Edyn Grindosonic Mk5	
		mean (m/s)	CV (%)	mean (m/s)	CV (%)	mean (Hz)	CV (%)
H55T20	**10.88**	5927	4.95	5572	4.20	13566	15.84
H65T20	**12.00**	5867	4.67	5505	4.04	13276	17.08
H75T20	**15.58**	5742	4.15	5455	3.71	12971	14.61
H85T20	**17.38**	5632	4.30	5325	3.83	12313	15.62

Statistical analyses were done in order to study the normality of variables prior to further analyses. All variables showed normal probability distributions. Figure 1, shows the frequency histogram for velocity of ultrasounds.

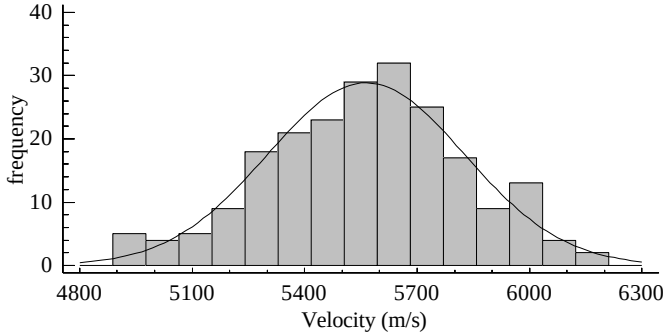

Figure 1 - Frequency histogram for velocity. Steinkamp BPV.

A clear tendency of change in properties with EMC was found, as was expected. This effect has been found in many similar studies (Gerhards 1982, Sandoz 1991, Steiger 1996, Gonçalves 2008). Despite the EMC of the studied batches being really close, some parameters exhibit statistically significant differences between two non-consecutive batches, determined from the one-way analysis of variance. Figure 2 shows an example of ultrasound velocity.

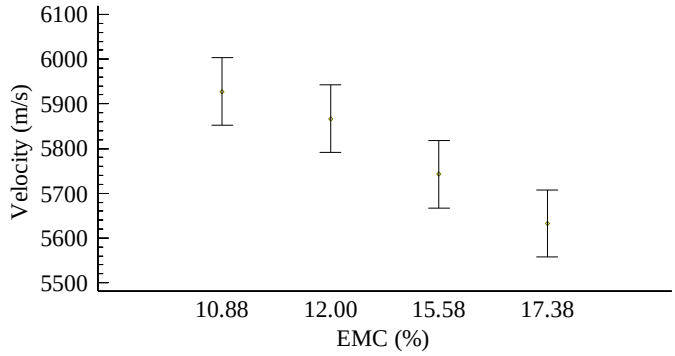

Figure 2 - Means plot of one-way analysis of variance: velocity Sylvatest vs. EMC.

Statistical diagnosis performed on each one-way analysis of variance confirms the validity of the assumptions of normality of distribution, homoscedasticity and independence.

The effect of T on non-destructive parameters is summarized in table 4.

Table 4 - NDT results for different T.

		NDT					
Batch	**T (ºC)**	Vel Sylvatest Duo		Vel Steinkamp BPV		Edyn Grindosonic Mk5	
		mean (m/s)	CV (%)	mean (m/s)	CV (%)	mean (Hz)	CV (%)
H65T50	**50**	5777	4.53	5455	4.11	12963	16.86
H65T30	**30**	5891	4.56	5545	3.90	13623	16.39
H65T20	**20**	5867	4.67	5505	4.04	13276	17.08
H65T-10	**-10**	6012	4.38	5671	3.95	14020	17.24
H65T-20	**-20**	6109	4.98	5704	4.38	14024	17.08
H65T-40	**-40**	6189	4.41	5841	3.86	14746	15.39

The one-way analysis of variance revealed statistically significant differences between some batches below 0ºC, but this difference does not appear between batches above 0ºC. Different tendencies above and below 0ºC has been found for some authors on ultrasound velocity (Gao 2011) above FSP, but it were not found works obtaining different tendencies in dry wood. Thus a different tendency above and below 0ºC was found. Figure 3 show an example for velocity of ultrasound waves using Steinkamp BPV.

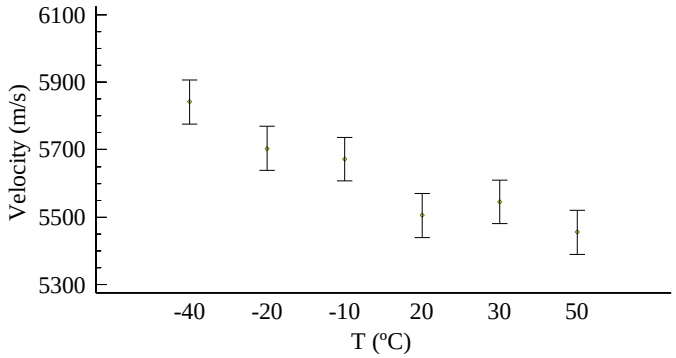

Figure 3 - Means plot of one-way analysis of variance: velocity Steinkamp vs. T.

Adjustment factor for EMC

Linear regressions were done using the average value of different variables of each batch and EMC in order to study EMC tendencies (Figure 4), as a result, several equations were obtained (equations 3 to 5):

Vel Sylvatest = 6392 - 43 EMC R^2=0.99 (3)

Vel BPV =5920 - 33 EMC R^2=0.90 (4)

Edyn freq = 20313 - 191 EMC R^2=0.95 (5)

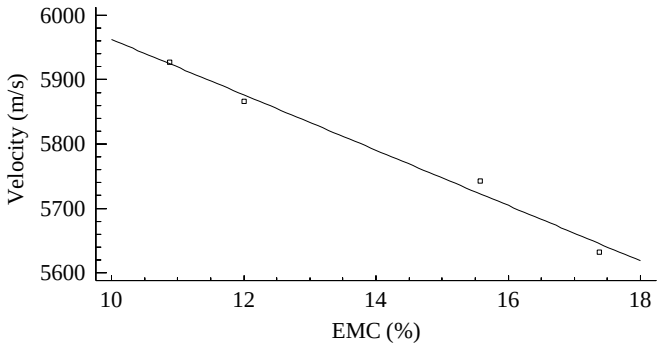

Figure 4 - Linear regression: velocity Sylvatest vs EMC.

The influence of EMC (between 10.88 and 17.38 %) on ultrasonic waves and vibration were determined. From equations 3 to 5, and considering 12% EMC as the reference value, adjustment factors (6 to 8) were obtained for each variable.

For ultrasound Sylvatest Duo: $V_{12} = V_H / [1-k_{H1} (H-12)]$ $k_{H1}= 0.0073$ (6)

For ultrasound Steinkamp BPV: $V_{12} = V_H / [1-k_{H2} (H-12)]$ $k_{H2}= 0.0059$ (7)

For vibration Grindosonic MK5: $Edyn_{12} = Edyn_H / [1-k_{H3} (H-12)]$ $k_{H3}= 0.0106$ (8)

Where: V_{12} is the ultrasound velocity in the longitudinal direction, at 12% EMC, in m/s; V_H is the ultrasound velocity in the longitudinal direction, at H EMC, in m/s; H is the EMC, in %; k_{Hi} is the EMC adjustment factor; Edyn is the dynamic modulus of elasticity obtained by vibration, in N/mm^2

For ultrasound velocities a decrease by 0.73% was achieved, using the Sylvatest Duo device, and 0.59%, using the Steinkamp BP-V device with an increase of 1% in EMC. If it is compared with other studies this adjustment factor is slightly greater than ones proposed by other authors for Sylvatest in Spruce (Steiger 1996, Unterwieser 2010) and lower than 0.8% proposed by Sandoz for Steinkamp BPV(Sandoz 1989). In addition, with an increase of 1% in EMC, the Edyn, estimated using the vibration technique , decreased by 1%, this adjustment factor is slightly greater than 0.87% proposed by Unterwieser (Unterwieser 2010) but in this case a different device was used.

Adjustment factor for T

Linear regressions were done between the average values of different variables of each batch and T, in order to study tendencies occurring with T changes (Figure 5), consequently several equations (below zero) were obtained (equations 9 to 11):

Vel Sylvatest = 5966 - 6 T R^2=0.98 (9)
Vel BPV =5591 - 6 T R^2=0.97 (10)
Edyn freq = 13689 - 25 T R^2=0.92 (11)

Different tendency above and below zero for different variables are shown in figure 5. This difference was found in every variable.

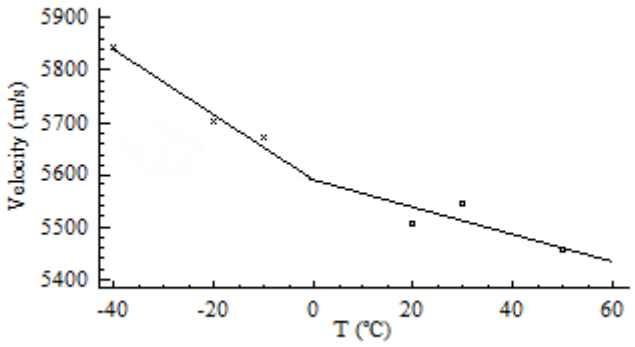

Figure 5 - Linear regressions: velocity Steinkamp BPV vs T.

Influence of T (between -40 and 0 ºC) on ultrasonic waves and vibration was evaluated at 12% EMC. From equations 9 to 11, and considering 0ºC as the reference value, adjustment factors (12 to 14) were obtained for each variable.

For ultrasound Syl: $V_0 = V_T / [1-k_{T1} (T-0)]$ $k_{T1}= 0.0010$ (12)

For ultrasound BPV: $V_0 = V_T / [1-k_{T2} (T-0)]$ $k_{T2}= 0.0011$ (13)

For vibration: $Edyn_0 = Edyn_T / [1-k_{T3} (T-0)]$ $k_{T3}= 0.0018$ (14)

Where: V_0 is the ultrasound velocity in the longitudinal direction, at 0ºC, in m/s; V_T is the longitudinal ultrasound velocity at temperature T, in m/s; T is the temperature, in ºC; k_{Ti} is the temperature adjustment; Edyn is the dynamic modulus of elasticity estimated by vibration, in N/mm^2

With an increase of 1ºC, a decrease of around 0.1% and 0.18% was recorded for ultrasound velocities and Edyn respectively. Ultrasound velocities adjustment factor 0.1% is slightly greater than 0.08% proposed by Sandoz (Sandoz 1993)

The effects of T are less significant than the EMC effects in common conditions of inspection of structures (from 0 to 30 ºC and from 8 to 30 % of EMC).

Conclusions

The present study shows that non-destructive measurements (wave velocity and frequency) of Scots pine are affected by equilibrium moisture content and temperature conditions. These results are consistent with findings from previous studies on spruce and fir.

Influence of equilibrium moisture content on ultrasound velocities and dynamic modulus of elasticity in the range 10 to 18% could be considered lineal.

Adjustment factors for the influence of equilibrium moisture content on Scots pine were obtained for non-destructive testing. In the case of ultrasound techniques, a slight difference between devices was found, Steinkamp (using sensors of 50 kHz frequency) presents smaller correction factors than Sylvatest (using sensors of 22 kHz frequency) and the reason could be founded in the different frequencies.

Influence of temperature on non-destructive testing shows a different tendency above and below 0 ºC. A clear lineal tendency was found below 0ºC and no significant tendency was found above 0 ºC for dry timber.

Adjustment factors for influence of temperature were proposed for non-destructive testing in the range -40 to 0ºC and considering 0ºC as the reference value. No differences between ultrasound devices were found.

Acknowledgments

Ministerio de Ciencia e Innovación. Plan Nacional I+D+i 2008-2011. Proy.: BIA 2010-18858.

Institute for Building Materials, Wood Physics Group, ETH Zürich.

References

Arriaga, F., et al., 2009: Proposal of a methodology for the assessment of existing timber structures in Spain. 16th International Symposium on Non-destructive Testing of Wood. Beijing, China.

Bucur, V., 1984: Relationships between grain angle of wood specimens and ultrasonic velocity. Catgut Acoustical Society Newsletter, 41. P. 30 - 35.

Bucur, V., Böhnke, I., 1994: Factors affecting ultrasonic measurements in solid wood. Ultrasonics, 32 (5). P. 385 - 390.

Bucur, V., 2006: Acoustic of wood. 2nd Edition. Springer. Germany.

EN 13183-1:2002: Moisture content of a piece of sawn timber. Part 1: Determination by oven dry method.
EN 13556:2003: Round and sawn timber. Nomenclature of timbers used in Europe.
Gao, S., et al., 2011: Modeling temperature and moisture state effects on acoustic velocity in wood. Proceedings 17th International Non-destructive Testing and Evaluation of Wood Symposium. Sopron, Hungary.
Gerhards, C. C., 1982: Effect of moisture content and temperature on the mechanical properties of wood: an analysis of immediate effects. Wood and Fiber, 14 (1), 1982, pp. 4-36.
Gonçalves, R., Leme, O.A., 2008: Influence of moisture content on longitudinal, radial and tangential ultrasonic velocity for two Brazilian wood species. Wood and Fiber Science, 40 (4), 2008, pp.580-586.
Görlacher, R., 1984: Ein neues Meβverfahren zur Bestimmung des Elastizitätsmodulus von Holz [A new measuring procedure for determining modulus of elasticity of wood]. Holz als Roh und Werkstoff. 42 (1984) 219-222.
James, W.L., 1961: Internal friction and speed of sound in Douglar-fir. Forest Products Journal, XI (9), 1961: 383-390.
Kang, H., Booker, R. E., 2002: Variation of stress wave velocity with MC and temperature. Wood Science and Technology 36 (2002) 41-54.
Matthews, B., et al., 1994: The effect of moisture content and temperature on the stress wave parameters. Proceedings of the 1st European Symposium on Non-destructive Evaluation of Wood. Sopron, Hungary, 21-23 September 1994, pp. 261-269.
Moreno-Chan, J., et al., 2010: Effects of moisture content and temperature on acoustic velocity and dynamic MOE of radiata pine sapwood boards. Wood Sci Technol (2010) 45:609–626.
Niemz, P., 1993: Physik des Holzes und der Holzwerkstoffe [Physics of wood and wood-based materials]. DRW-Verlag, Germany.
Oliveira, F., et al., 2005: Moisture content effect on ultrasonic velocity in *Goupia glabra*. Materials research, vol. 8, No.1, 11-14, 2005.
Sakai, H., et al., 1990: Effect of moisture content on ultrasonic velocity and attenuation in woods. Ultrasonics, vol 28, 1990, pp. 382-385.
Sandoz, J.L., 1989: Grading of construction timber by ultrasound. Wood Sci. Tech. Vol 23: 95-108.
Sandoz, J.L., 1991: Nondestructive evaluation of building timber by ultrasound. 8th International symposium on Non-destructive testing of wood. Vancouver.
Sandoz, J.L., 1993: Moisture content and temperature effect on ultrasound timber grading. Wood Science and Technology 27:373-380. 1993.
Steiger, R., 1996: Mechanische Eigenschaften von Schweizer Fichten-Bauholz bei Biege-, Zug-, Druck- und kombinierter M/N-Beanspruchung [Mechanical properties of Swiss spruce in bending strength, tensile strength, crushing stress and M/N combine]. Doctoral Thesis. ETH Zürich.
Unterwieser, H., Schickhofer, G., 2010: Influence of moisture content of wood on sound velocity and dynamic MOE of natural frequency - and ultrasonic runtime measurement. Eur. J. Wood Prod. (2010) 69: 171–181.
Wang, X., 2008: Effects of size and moisture content on stress waves E-rating of structural lumber. 10th World Conference on Timber Engineering. Miyazaki, Japan.

Assessing the Dimensional Stability of Two Hardwood Species Grown in Turkey with Acoustic Measurements

Turker Dundar
Faculty of Forestry, Istanbul University, Istanbul, Turkey, dundar@istanbul.edu.tr

Xiping Wang
USDA Forest Service, Forest Products Laboratory, Madison, WI, USA, xwang@fs.fed.us

Nusret As
Faculty of Forestry, Istanbul University, Istanbul, Turkey, nusretas@istanbul.edu.tr

Erkan Avcı
Faculty of Technology, Mugla University, Mugla, Turkey, erkanavci@mu.edu.tr

Abstract

The objective of this study was to examine the potential of acoustic measurement as a rapid and nondestructive method to predict the dimensional stability of oak (*Quercus petrea*) and chestnut (*Castanea sativa*) that are commonly used in floor industry. Ultrasonic velocity, specific gravity, and radial, tangential and volumetric shrinkages were measured on seventy-four 20- by 20- by 30-mm specimens obtained from freshly cut oak and chestnut stems at forestlands located in northwest part of Turkey. The ultrasonic velocities of the specimens decreased with increasing equilibrium moisture content (EMC). We found that specific gravity was not a good predictor of the transverse shrinkages as indicated by relatively weak correlations. Ultrasonic velocity, on the other hand, was found to be a significant predictor of the transverse shrinkages for both oak and chestnut. The best results for prediction of shrinkages of oak and chestnut were obtained when the ultrasonic velocity and specific gravity were used together. The multiple regression models we developed in this study explained 77% of volumetric shrinkages in oak and 72% of volumetric shrinkages in chestnut. It is concluded that both ultrasonic velocity and specific gravity be employed as predicting parameters to evaluate the dimensional stability of wood during manufacturing process.

Keywords: dimensional stability, shrinkage, ultrasonic velocity, oak, chestnut

Introduction

As building and engineering materials, wood has advantages of being economical, low in processing energy, renewable, strong, and aesthetically pleasing. However, some wood characteristics limit its use, among them are swelling and shrinking of wood as it takes up and loses moisture (Rowell and Banks 1985). Dimensional stability is a measure of the extent of swelling or shrinkage resulting from moisture movement in wood below fiber saturation point (FSP). Dimensional stability of the wood products during use affects their function and service life and is therefore of huge economic value to the forest industry. Dimensional changes of wood caused by sorption are anisotropic and dependent on the anatomical direction in the wood (Skaar 1988). Wood shrinkage also depends on microstructural and molecular features of the cell wall. These include the microfibril angle (MFA), the angle at which the cellulose fibrils wind in the cell walls, as well as the physical properties of the surrounding matrix. Longitudinal shrinkage of wood is generally quiet small (0.1% – 0.2% of the green condition when oven dried). This

small change is often neglected in the manufacture and subsequent use of the wood products. However, transverse shrinkages in tangential and radial directions are of major importance. Tangentially, wood shrinks from 6% to 12% of the green dimension when dried from green to the oven-dry condition for hardwood (FPL 2010); while in the radial direction the corresponding shrinkage is roughly one half of the tangential shrinkage for a given wood specimen. This differential of radial-tangential shrinkage is one of the primary factors causing shape distortion during seasoning of lumber and during ultimate use. This is one of the most important challenges for hardwood floors where the dimensional stability is critical.

Traditionally shrinkage has been correlated with density (Suchsland 2004). This correlation is not particularly strong and represents a general trend for sound wood of different species (Suchsland 2004, Leonardon et al. 2010). X-ray lumber density scanning is successful in grading structural lumber based on prediction of stiffness and strength, but no shrinkage prediction capability was established (Schajer 2000). Some studies investigated the potential of near infrared (NIR) spectroscopy as a tool for shrinkage prediction. It was reported that for 5-year old *Eucalyptus urophylla* × *E. Grandis* hybrids, tangential shrinkage could be modeled with 82% accuracy by NIR (Bailleres et al. 2002) , whereas weak correlations with radial shrinkage (0.45) and longitudinal shrinkage (0.35) precluded similar predictions. For mahogany (*Swietenia macrophylla*), 63% of the variation in volumetric shrinkage could be predicted by NIR (Taylor et al. 2008).

A number of studies also suggest that acoustic wave techniques may be used to assess the dimensional stability of structural lumber. Wang and Simpson (2006) evaluated the potential of acoustic analysis as presorting criteria to identify warp-prone boards before kiln-drying. Dimension lumber (38 × 89 × 2440 mm) sawn from open-grown small-diameter ponderosa pine trees was acoustically tested lengthwise at green condition. They found that the amount of warp in the form of crook and bow that developed during drying decreased as green board measurements of acoustic speed and acoustic MOE increased and rate of wave attenuation decreased. The results also showed a statistically significant correlation between acoustic properties of the boards and the grade loss because of exceeding warp limits. Ivkovic et al. (2009) investigated a range of wood properties that can be measured with relative ease and low cost for their ability to predict wood stiffness, strength, and shrinkage in juvenile wood of radiata pine. With respect to shrinkage prediction, they found that density and MOE had a weak relationship with radial and tangential shrinkages ($r^2 = 0.13 – 0.16$), while acoustic velocity and MOE had a strong negative non-linear relationship with longitudinal shrinkage of the inner ring samples ($r^2 = 0.78$ and 0.58 respectively). Based on their findings, they recommended that acoustic velocity combined with increment core density be used as practical measurement parameters for predicting stability in young trees.

The objective of this study was to assess the potential of ultrasonic measurement as a rapid and nondestructive method to predict the dimensional stability of oak and chestnut grown in Turkey. The specific objectives were to 1) determine radial and tangential shrinkages of oak and chestnut; 2) examine the relationships between transverse shrinkages and specific gravity, ultrasonic velocity, and peak energy of ultrasonic signals; 3) determine the best nondestructive parameters for predicting transverse shrinkages of oak and chestnut.

Materials and methods

Specimen preparation

Oak (*Quercus petrea*) and chestnut (*Castanea sativa*) wood that are commonly used in floor industry were used as wood materials. A 5-cm-thick disk was taken from 0.3-m stem height of freshly cut tree stems from forestlands located in northwest part of Turkey for both tree species. A total of four disks, two

from each species, were transported to Istanbul University, Faculty of Forestry immediately. The disks were placed in a plastic bag in order to maintain green condition. The wood specimens for shrinkage measurements were prepared from pith to bark along north-south direction of the disks. The sizes of the specimens were 20 by 20 by 30 mm with the 30-mm dimension along the grain. A total of 74 specimens were obtained, including 36 oak and 38 chestnut. A special care was taken to prevent moisture loss from the samples throughout the sample preparation process.

Experimental procedure

The initial weight and dimensions of all specimens at green condition were immediately measured and recorded. The weight was measured to the nearest 0.01 g and the dimension was measured to the nearest 0.01 mm.

A Sylvatest Duo (CBS-CBT, Les Ecorces, France) device operating at a frequency of 22 kHz was used to measure the ultrasonic velocity and peak energy of the received signal in each specimen. The transmitter probe and the receiver probe were positioned at the opposite faces of a specimen with a constant pressure (50 N) applied to the probes to improve the coupling between the probes and wood. The measurements were made in both radial and tangentialdirection. For each measurement, the transmitter probe emitted five consecutive pulses through the specimen. An average ultrasound propagation time (UPT) and average peak energy of the receiving signal were recorded after each measurement. The ultrasonic velocity (V) of the specimen was calculated based on the average UPT value and the distance between two probes (L):

$$V=L/UPT \qquad (m/s) \qquad (1)$$

After initial measurements, all specimens were then sequentially subjected to 90%, 80%, 65%, 50%, and 40% relative humidity (RH) at a constant temperature of 20°C in a climatic room until they reached constant weight, then followed by oven dry at 103±2 °C for 48 hours to reach a 0% MC. When each MC level was reached, the weight and dimension of each sample were measured, followed by ultrasonic measurements in both radial and tangential directions using the Sylvatest Duo device.

Data analysis

In this study, tangential, radial, and volumetric shrinkages of the specimens were determined from green condition of initial measurement to oven dry condition. The specific gravity (SG) of the specimens was determined based on 12% equilibrium moisture content (EMC) volume and oven dry weight. Single and multiple variable statistical regression analysis were used to determine the following relationships: (1) ultrasonic velocity versus wood moisture content (MC); (2) ultrasonic velocity versus tangential, radial and volumetric shrinkages; (3) specific gravity versus tangential, radial, and volumetric shrinkages; (4) specific gravity and ultrasonic velocity versus tangential, radial, and volumetric shrinkages.

Results and discussion

Table 1 summarizes the statistics of specific gravity (SG), radial shrinkage (RS), tangential shrinkage (TS), volumetric shrinkage (VS), and tangential to radial shrinkage ratio (TS/RS) for oak and chestnut specimens. The mean specific gravity was found to be 0.612 for oak and 0.515 for chestnut, which is in a good agreement with the values given in the Turkish literature for same species (Berkel 1970; Bozkurt and Goker 1985). The shrinkage values presented in this table are from FSP to oven dry condition. It was found that tangential shrinkage was 47% higher than radial shrinkage for both oak and chestnut. The differences were significant at 0.01 level of probability.

Table 1— Specific gravity and transverse shrinkages of oak and chestnut.

Species	No. of specimens	Initial MC (%)	Specific gravity (12%MC)	Shrinkage from FSP to 0% MC (%)			
				Radial (RS)	Tangential (TS)	Volumetric (VS)	Ratio (TS/RS)
Oak	36	56.4	0.612 (0.063) [a]	5.1 (1.11)	10.8 (1.74)	15.6 (2.23)	2.1
Chestnut	38	69.5	0.515 (0.052)	3.8 (0.77)	8.1 (0.99)	12.0 (1.34)	2.1

[a] The number in parenthesis is standard deviations.

Table 2— Results of linear regression analysis of shrinkage and specific gravity relationships for oak and chestnut.

y Shrinkage (%)	*x* Specific Gravity	Regression model: $y = a + bx$				
		a	*b*	r^2	SEE	*p*
			Oak			
Tangential (TS)	SG 12%MC	-0.268	17.096	0.373	1.402	<0.001
Radial (RS)		-1.762	11.185	0.387	0.889	<0.001
Volumetric (VS)		-0.405	24.785	0.484	1.618	<0.001
			Chestnut			
Tangential (TS)	SG 12%MC	-	-	0.041	-	0.222*
Radial (RS)		-0.053	7.447	0.255	0.673	0.001
Volumetric (VS)		-6.033	11.521	0.204	1.204	0.004

* Not significant

Ultrasonic velocity in relation to moisture content

Figure 1 shows the relationships between ultrasonic velocity and moisture content for oak and chestnut. Ultrasonic velocities in both tangential and radial direction were found to increase continuously as moisture content decreased. This is similar to the influence of moisture content on modulus of elasticity (Green and Kretschmann 1994; Kollmann and Cote 1968). A polynomial regression was found best fit to the experimental data ($r^2 = 0.99$ for radial shrinkage in both oak and chestnut, $r^2 = 0.97$ for oak, and $r^2 = 0.94$ for chestnut in tangential direction). This is in agreement with the velocity trend from what reported in other studies (Mishiro 1996).

Relationship between specific gravity and shrinkages

The degree of correlation between shrinkage and specific gravity was evaluated by linear regression analysis. The results were given in Table 2. The relationships between SG and shrinkage values were found to be relatively low but significant ($p<0.01$) except for the shrinkage of chestnut specimens in tangential direction ($r^2 = 0.04$) which was non-significant. The coefficients of determination were higher for oak ($r^2 = 0.373$ to 0.484) than chestnut ($r^2 = 0.041$ to 0.204) (Figure 2).

Relationship between ultrasonic velocity and shrinkages

Figure 3 shows the relationships between shrinkages and ultrasonic velocity. The radial and tangential shrinkages decreased linearly with increasing ultrasonic velocity for oak. The correlation was stronger in radial direction ($r^2=0.67$) than in tangential direction ($r^2=0.52$). A similar relationship was found in chestnut with a coefficient of determination (r^2) of 0.70 in radial direction and 0.56 in tangential direction as shown in Fig. 3.

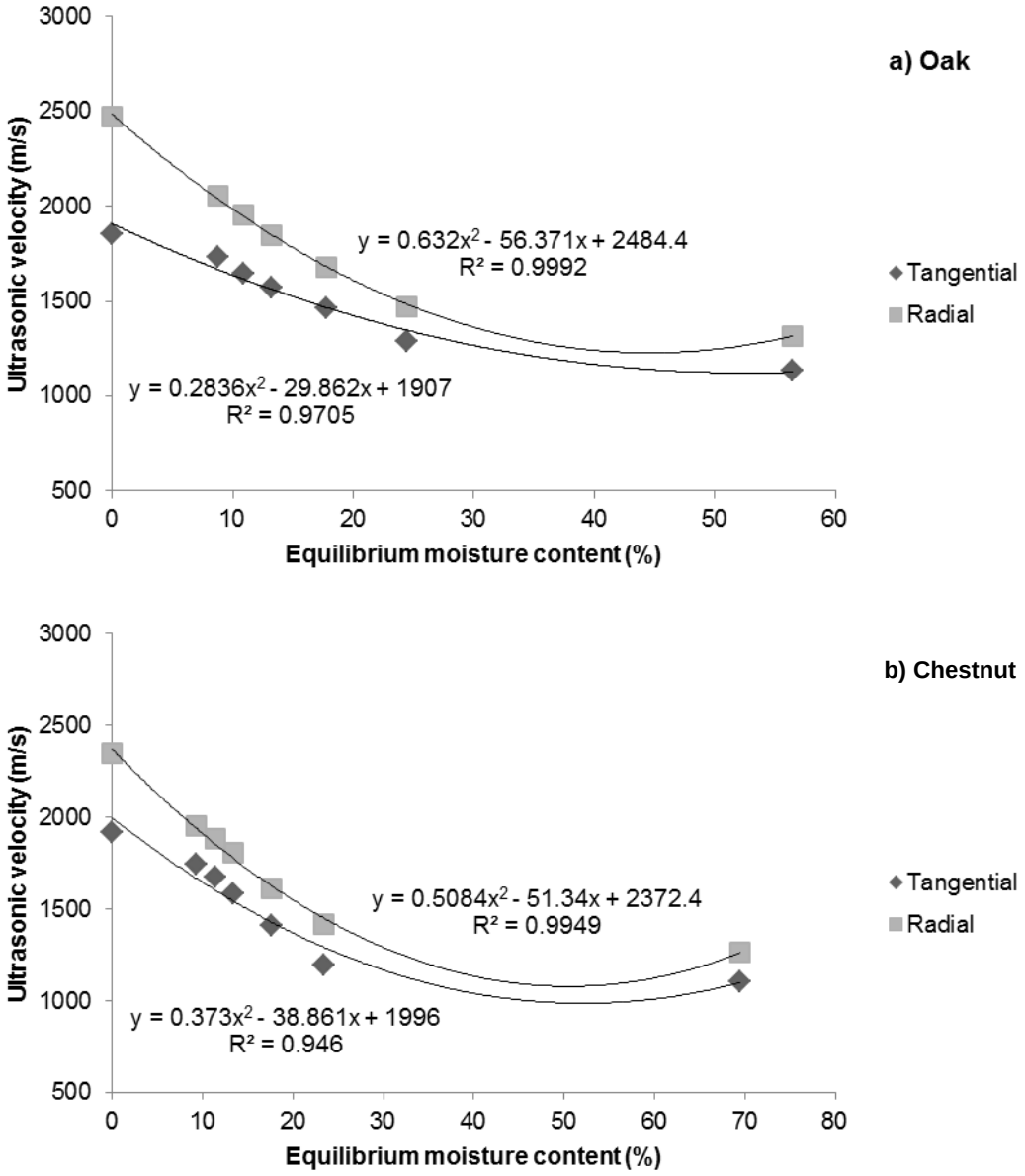

Figure 1—Relationships between ultrasonic velocity and equilibrium moisture cintent for oak and chestnut.

The results of linear regression analysis for the shrinkage and ultrasonic velocity relations are tabulated in Table 3. Note that the shrinkage–velocity data obtained in radial and tangential directions fit the same general trend within each species. Examination of the shrinkage–velocity models indicated that the linear correlation coefficients (*b*) were close in radial and tangential directions for both oak and chestnut.

The velocity calculated as average of tangential and radial velocity explained 65% of the volumetric shrinkage for oak and 64% of the volumetric shrinkage for chestnut according to the linear regression model. This indicated that ultrasonic measurement has a good potential to be used as a nondestructive method for predicting shrinkage.

Table 3— Results of linear regression analysis of ultrasonic velocity and shrinkage relationships for oak and chestnut.

y Shrinkage (%)	*x* Ultrasonic velocity	Regression model: $y = a + bx$				*p*
		a	*b*	r^2	SEE	
			Oak			
Tangential (TS)	V_T	23.136	-0.011	0.525	1.220	<0.001
Radial (RS)	V_R	20.632	-0.012	0.670	0.653	<0.001
Volumetric (VS)	V*	44.669	-0.024	0.650	1.332	<0.001
			Chestnut			
Tangential (TS)	V_T	15.514	-0.007	0.563	0.661	<0.001
Radial (RS)	V_R	12.187	-0.007	0.702	0.426	<0.001
Volumetric (VS)	V	26.053	-0.012	0.641	0.809	<0.001

* Calculated as average of V_T and V_R.

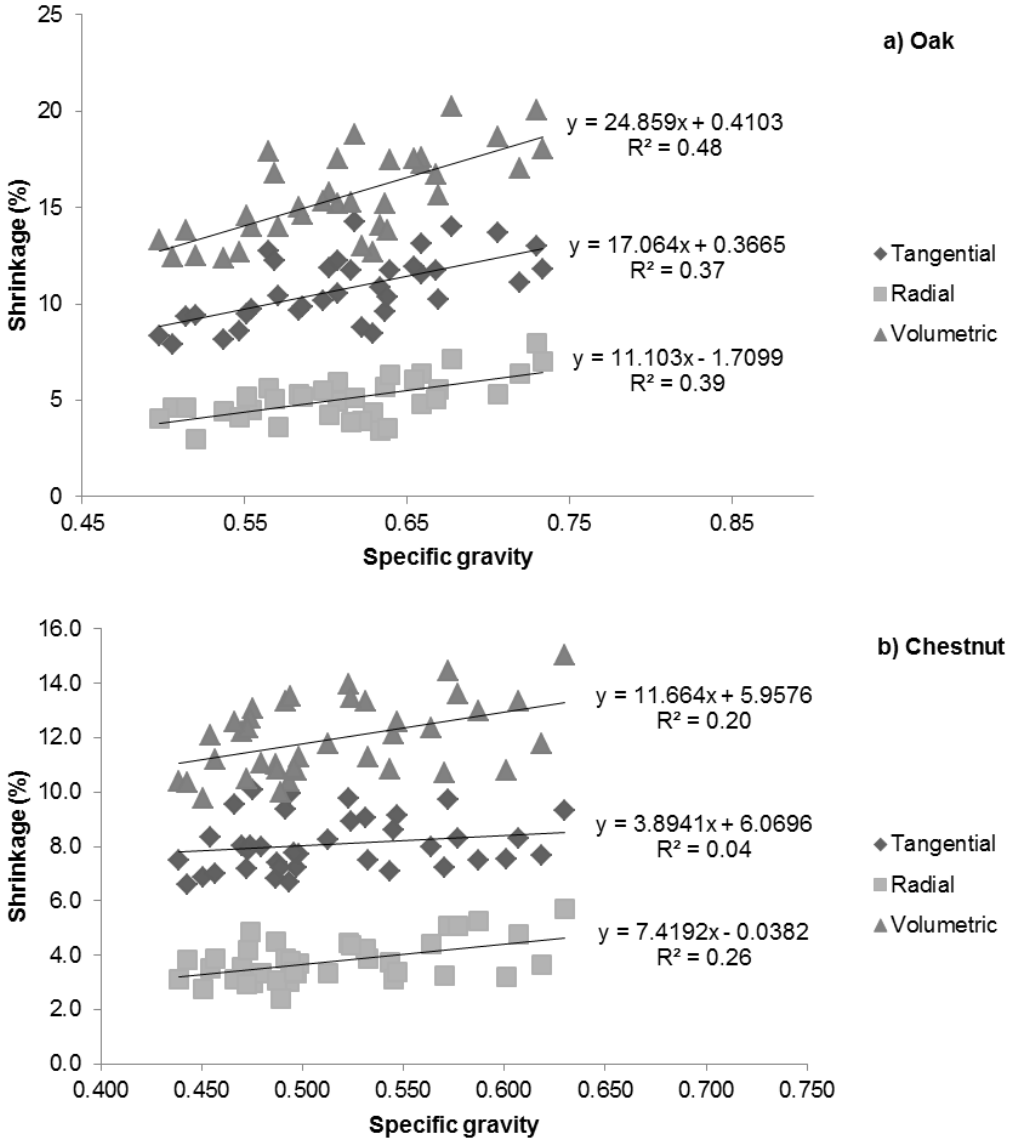

Figure 2—Relationships between shrinkages and specific gravity for oak and chestnut.

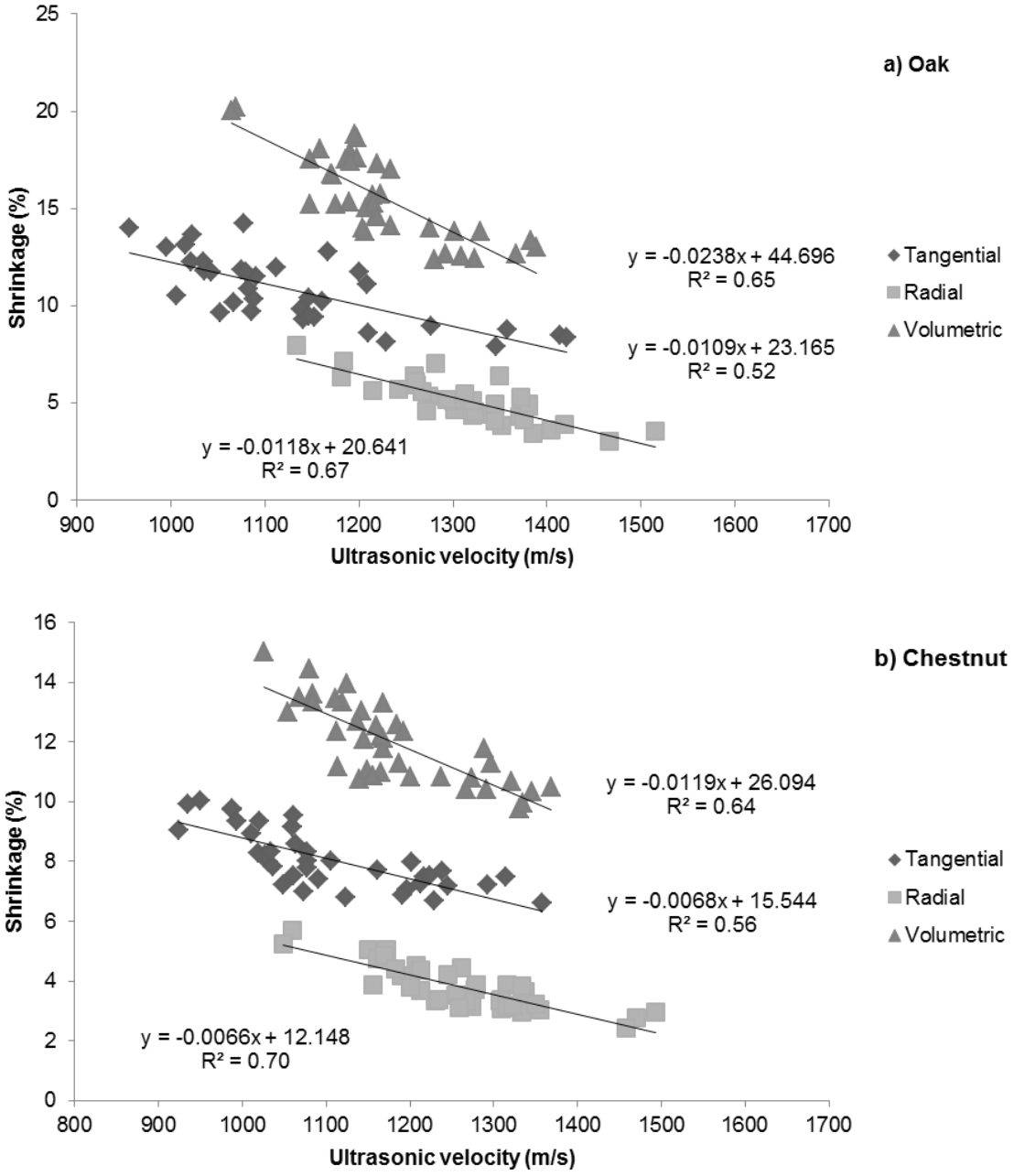

Figure 3—Relationships between ultrasonic velocity and shrinkages for oak and chestnut.

Multiple variable regression model

The results of multiple variable linear regression analysis of the relationships between shrinkage and ultrasonic velocity and SG are shown in Table 4. The coefficients of determination increased considerably in all directions except for the tangential direction of chestnut when the ultrasonic velocity and SG were used together to predict shrinkages. For example, the ultrasonic velocity explained 65% for oak and 64% for chestnut alone (Table 3), it was raised 77% for oak and 72% for chestnut when the ultrasonic velocity and SG were used together (Table 4).

Table 4— Results of multiple variable regression analysis of shrinkage, ultrasonic velocity and specific gravity relationships for oak and chestnut.

y Shrinkage (%)	x_1 Specific gravity	x_2 Ultrasonic velocity	Regression model: $y = ax_1 + bx_2 + c$					*p*
			a	*b*	*c*	r^2	SEE	
					Oak			
Tangential (TS)	SG 12%MC	V_T	10.000	-0.009	12.274	0.627	1.097	<0.001
Radial (RS)		V_R	7.690	-0.010	13.663	0.839	0.463	<0.001
Volumetric (VS)		V	14.148	-0.018	29.031	0.770	1.095	<0.001
					Chestnut			
Tangential (TS)	SG 12%MC	V_T	3.230	-0.007	13.778	0.592	0.648	<0.001
Radial (RS)		V_R	3.247	-0.006	9.681	0.743	0.401	<0.001
Volumetric (VS)		V	7.196	-0.011	21.202	0.716	0.729	<0.001

Prediction of transverse shrinkages

The results of this study showed that specific gravity alone was not a good predictor of shrinkage as indicated by weak correlations. Ultrasonic velocity, on the other hand, was found to be a significant predictor of transverse shrinkages and therefore has a good potential to be used as a field method to evaluate the dimensional stability of standing trees. However, the best results for prediction of shrinkages of oak and chestnut were obtained when the ultrasonic velocity and SG were used together. Figure 4 shows the plot of predicted shrinkages values and measured shrinkage values for oak and chestnut. The multiple parameter prediction model explained 85% of radial shrinkage, 62% of tangential shrinkage, and 76% of volumetric shrinkage in oak. As for chestnut, it explained 74% of radial shrinkage, 60% of tangential shrinkage, and 71% of volumetric shrinkage.

Conclusions

Ultrasonic velocity in both tangential and radial direction was found to increase continuously as moisture content decreased. A polynomial regression was found best fit to the experimental data.

Specific gravity was found to have relatively weak relationships with shrinkages and was not a good predictor of shrinkage. Both tangential and radial shrinkages decreased linearly in a similar trend with increasing ultrasonic velocity. A single linear regression model relating shrinkage to ultrasonic velocity was proposed to predict radial, tangential, and volumetric shrinkages using ultrasonic velocity.

The best results for prediction of shrinkages of oak and chestnut were obtained when the ultrasonic velocity and SG were used together. The multiple parameter prediction model explained 85% and 74% of radial shrinkage, 62% and 60% of tangential shrinkage, and 76% and 71% of volumetric shrinkage in oak and chestnut, respectively.

The results of this study indicated that ultrasonic velocity was a significant predictor of transverse shrinkages and therefore has a good potential to be used as a field method to evaluate the dimensional stability of wood. The best prediction of the transverse shrinkage of oak and chestnut can be achieved when both ultrasonic velocity and specific gravity are used as predicting parameters through multiple variable regression models.

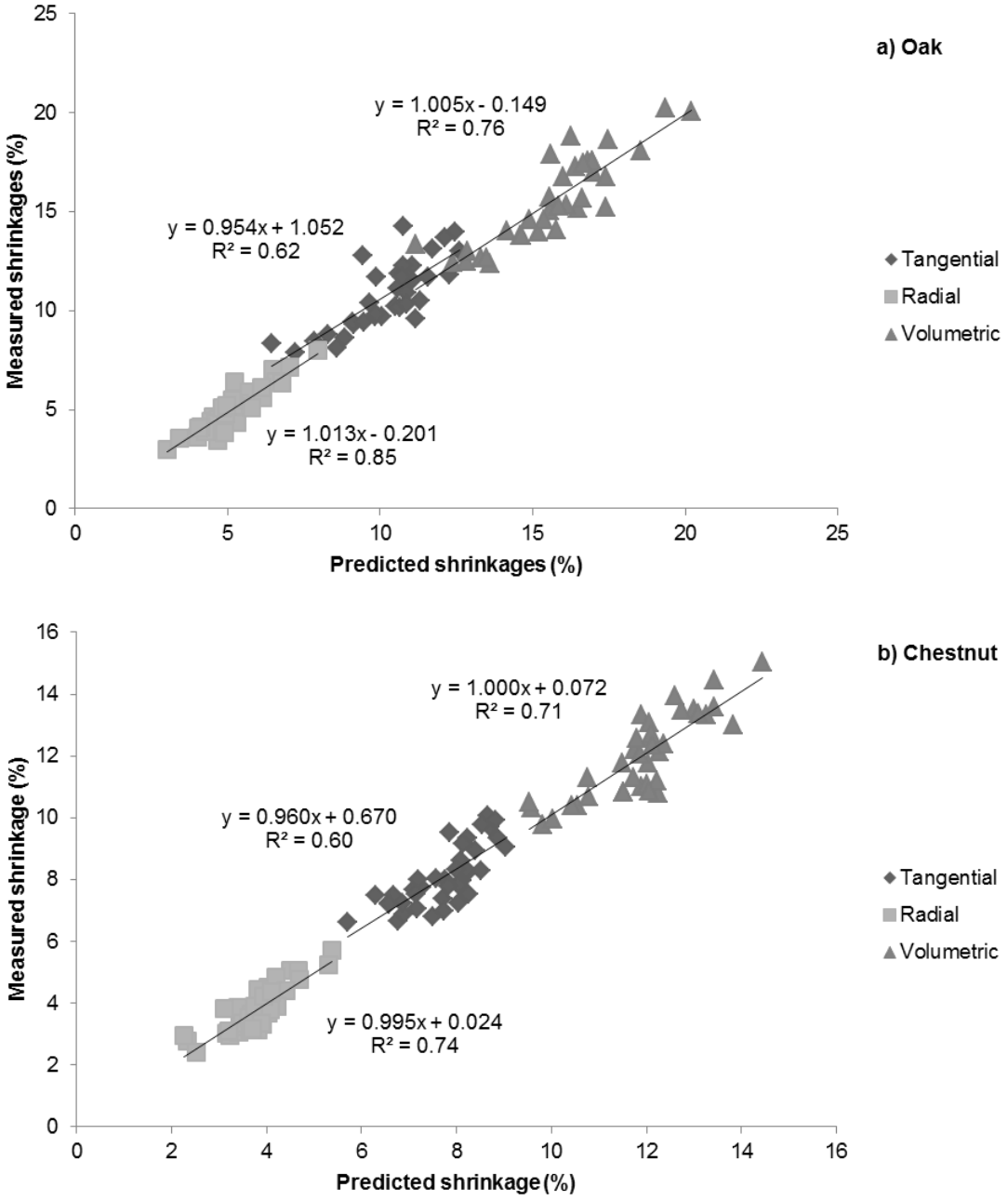

Figure 4— Relationships between predicted shrinkages and measured shrinkages for oak and chestnut.

References

Bailleres, H.; Davrieus, F.; Pichavant, F.H. 2002. Near infrared analysis as a tool for rapid screening of some major wood characteristics in a eucalyptus breeding program. Annals of Forest Science, 59: 479-490.

Berkel, A. 1970. Ağaç malzeme teknolojisi Cilt I. I.U. Orman Fakultesi Yay.No. 145, Istanbul, 480p.

Bozkurt, A.Y.; Göker, Y. 1985. Fiziksel ve mekanik ağaç malzeme teknolojisi. I.U. Orman Fak. Yay.No. 311, Istanbul, 355p.

FPL 2010. Wood handbook—Wood as an engineering material. General Technical Report FPL-GTR-190. USDA Forest Service, Forest Products Laboratory, Madison, WI. 508 p.

Green, D.; Kretschmann, D. 1994. Moisture content and the properties of clear southern pine. Research Paper FPL-RP-531. USDA Forest Service, Forest Products Laboratory, Madison, WI. 28 pp.

Ivkovic, M.; Gapare, W.J.; Abarquez, A.; Ilic, J.; Powell, M.B.; Wu, H. 2009. Prediction of wood stiffness, strength, and shrinkage in juvenile wood of radiate pine. Wood Science and Technology, 43: 237-257.

Kollman, F.F.P; Cote, W.A. 1968. Principles of wood science and technology Vol. 1, Solid Wood. Springer Verlag, Berlin, Germany. 535 pp.

Leonardon, M.; Altaner, C.M.; Vihermaa, L.; Jarvis, M.C. 2010. Wood shrinkage: influence of anatomy, cell wall architecture, chemical composition and cambial age. European Journal of Wood Products, 68: 87-94.

Mishiro, A. 1996. Ultrasonic velocity and moisture content in wood II. Ultrasonic velocity and average moisture content in wood during desorption (1): Moisture content below the fiber saturation point. Mokuzai Gakkaishi, 42: 612-617.

Rowell, R.M.; Banks W.B. 1985. Water repellency and dimensional stability of wood. General Technical Report FPL-50. USDA Forest Service, Forest Products Laboratory, Madison, WI, 24p.

Schajer, G. 2000. Lumber strength grading using X-ray scanning. Forest Products Journal, 51(1): 43-50.

Skaar, C. 1988. Wood-water relations. Springer series in wood science. Springer Verlag, Berlin.

Suchsland, O. 2004. The swelling and shrinking of wood—A practical technology primer. Forest Products Society, Madison, WI. 194 pp.

Taylor, A.M.; Baek, S.H.; Jeong, M.K.; Nix, G. 2008. Wood shrinkage prediction using NIR spectroscopy. Wood and Fiber Science, 40: 301-307.

Wang, X.; Simpson, W.T. 2006. Using acoustic analysis to presort warp-prone ponderosa pine 2 by 4s before kiln-drying. Wood and Fiber Science, 38(2): 206-214.

Acoustoelasticity of Wood Determined by Static Bending Experiments

Cinthya Bertoldo
PhD student, Laboratory of Nondestructive Testing (LabEND), School of Agricultural Engineering (FEAGRI), University of Campinas (UNICAMP), Campinas, São Paulo, Brazil, cinthyabertoldo@gmail.com

Raquel Gonçalves
Associate Professor, Laboratory of Nondestructive Testing (LabEND), School of Agricultural Engineering (FEAGRI), University of Campinas (UNICAMP), Campinas, São Paulo, Brazil, raquel@feagri.unicamp.br

Rafael Lorensani
PhD student, Laboratory of Nondestructive Testing (LabEND), School of Agricultural Engineering (FEAGRI), University of Campinas (UNICAMP), Campinas, São Paulo, Brazil, rafaelmansini@hotmail.com

Abstract

Acoustoelasticity is the variation of the waves' propagation velocity in function of the variation stress. The acoustoelastic constant is determined by the relation between the relative variation of the velocity and the stress variation. For wood, in spite of certain progresses, there is not, yet, conclusive results regarding values of the acoustoelastic constant. Therefore, the objective of this research was to verify the acoustoelastic behaviour of wood during bending tests. Eighteen beams of three different Eucalyptus species were instrumented with extensometers in four different positions in height, and the velocity variation of longitudinal waves was followed on these four positions by means of ultrasound measurements in parallel and perpendicular directions to the fibers. Variations of velocity were more significant and coherent in the parallel direction to the fibers, in which the velocity presents falling tendencies as the stresses rises, both in the tension zone and the compression zone.

Keywords: Ultrasound; *Eucalyptus*; Longitudinal waves

Introduction

Acoustoelasticity is the wave propagation velocity variation due to stress state, and it has been studied in several materials. If there is any possibility of determining a coefficient to connect the velocity variation, between loaded and unloaded states, it would be best to obtain the strain state of a piece being loaded by means of wave propagation methods.

There already are more conclusive studies for materials that have an isotropic behavior, such as steel. However, for materials with orthotropic behavior, such as wood, the few studies in existence are not very conclusive.

Ultrasound waves that propagate perpendicularly to the loading direction are polarized on the two main stresses directions, due to stress-induced anisotropy. Both shear waves present different velocities, which is something that doesn't occur in a stress-free material. This phenomenon is called acoustoelastic birefringence (HASEGAWA and SASAKI, 2000), and it is a counterpart to the photo elastic effect observed in researches that use specially-designed models for this kind of phenomenon evaluation. The acoustoelasticity has been used for determining stresses in metals and aluminum

(ANDRINO *et al.*, 2002; ANDRINO, 2007; CAETANO, 2003; PEREIRA Jr., 2011). The articles that are based on aluminum are particularly important, since aluminum is also considered to be an orthotropic material.

The acoustoelastic constant is found through the variation between velocity and stress (Equation 1). Therefore, in case determining this constant for a given species of wood is possible, it can be used to determine the stress state of a structural element.

$$K = \frac{\frac{V - V_0}{V_0}}{\sigma} \qquad (1)$$

In which σ is the compression or traction stress; V is the velocity on the piece under stress and V_0 is the initial velocity on the piece with no stress.

In the research by Hasegawa and Sasaki (2000), the tests were made on specimens that were subjected to compression and tension loading, applied on the direction parallel to the fibers, and ultrasound measurements were made on the perpendicular direction to the charge's application. The authors used longitudinal transducers and shear transducers and, for the shear transducers, the wave polarization was constantly made in the direction of the application of the load. The ultrasound measurements were made on the radial direction, with the transducers positioned on the tangential surface. The authors used *strain gages* (5 and 10 mm long) to determine the distance variation between the transducers, brought by the effect of the Poisson's ratio. These values were used to correct the length course when calculating velocity.

The results obtained by Hasegawa and Sasaki (2000) showed that the shear velocities decreased from the beginning to the end of the compression tests. As the stress grew (levels up to 70% of the rupture), the ultrasound velocity decreased visibly. In traction, the results were different. The shear velocities began to grow as the stress grew (until approximately 35 MPa) and, above that stress level, started to decrease. In longitudinal velocity, Hasegawa and Sasaki (2000) found that, as stress grew, the velocity decreased, whether in traction or compression.

Preliminary acoustoelasticity tests were made by a research group in the College of Agricultural Engineering (FEAGRI) of UNICAMP, using bending tests (ORMONDE *et al.*, 2006). The bending tests were made in structurally-dimensioned beams. The ultrasound tests were made with wave propagation in the perpendicular direction (radial and tangential) to the traction and compression strain generated by bending. Results showed that, as well as what Sasaki *et al.* obtained, the velocity variation with stress variation was bigger for conifers than for hardwood. Longitudinal wave velocity in a perpendicular direction to loading increases when compression and tension are increased in hardwood and decreases when traction tension increases. In conifers, on the other hand, the process is reverse.

Thus, the objective of this research was to verify the acoustoelastic behavior of *Eucalyptu*s wood during static bending tests.

Material and methods

Three different Eucalyptus species were used in this study - *Eucalyptus grandis* (10 years old), *Eucalyptus citriodora* (8 years old) and *Eucalyptus pellita* (26 years old). For each of the species, six beams with structural section of 0.05 m x 0.10 m and 2.5 m long were used. The beams were tested after acclimatization, with about 12% humidity.

Tests were made using Ultrasound equipment (EPOCH 4, Panametrics, USA) with plane-faced longitudinal wave transducers and 1000 kHz frequency; and ultrasound equipment (USLAB, Agricef,

Brazil) with exponential-faced longitudinal transducers. Longitudinally, it was not possible to use the Panametrics equipment, since it doesn't have enough power to perform readings in large course lengths. Readings in the perpendicular direction to loading could have also been made with USLab equipment, but, as the measurements were made during beam loading, it was simpler to test using two different equipments with simultaneous measurements. Besides, small stress alterations could occur when loading is paused for ultrasound measurements, which would make longitudinal measurement different from perpendicular measurements from loading, stress-wise.

Starch glucose was used as a coupling for the plane-faced transducers, which, according to Gonçalves *et al.* (2011), presents good results in ultrasound tests in wood.

First, each beam was polished on both sides of the central area (mid-span), smoothing the surface for bonding *strain gages* and for readings through EPOCH 4 equipment. After polishing, better coupling between the transducer and the beam enhances precision in ultrasound readings.

Right after the polishing step, the *strain gages* were bonded on the ultrasound wave propagation time reading positions, for subsequent velocity calculation (Figure 1).

Figure 1. Bonding of the *strain gages* on the traction and compression zones of the beam.

Once the extensometers were bonded to the wood, the cable welding step started. Each *strain gag*e has two strings and each one of those strings had to be welded to a cable that couples to the data acquisition system (Figure 2). Eight *strain gages* were bonded to each beam, four in each parallel surface (beam's height): two on the superior part (compressed zone), and two on the inferior part (traction zone). It was also necessary to fasten the extensometer cable on the beam with duct tape, to limit movements that could break or loosen the extensometers, as well as to avoid accidents (Figure 2).

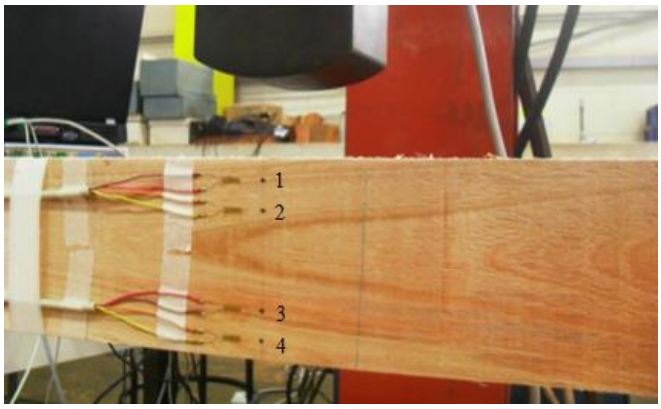

Figure 2. Assemblage of *strain gages* with cables and points of ultrasound measurements.

First, the beams underwent wave propagation time measurements in unloaded condition, in order to obtain initial velocity (V_0).

Loading application on the beams was made with a frame with hydraulic activation of the charge. The static scheme used in testing was bi-supported (reaction supports),center-point loading and distance between the reaction supports (span) of 21 times the height.

During loading, ultrasound wave propagation time readings were made in parallel and perpendicular directions to the fibers, both in direct testing (transducers positioned in parallel surfaces). Longitudinal and perpendicular directed to the fibers measurements were made considering the strain *gages'* positioning. When measuring perpendicularly to the fibers, it was not possible to measure in the same extensometer point. For that reason, reading was made as close as possible, as shown in Figure 2, where there is a point marking the center of the transducer during ultrasound measurements.

Figure 3.a illustrates tests in the perpendicular direction to the fibers by means of ultrasound equipment (EPOCH4, Panametrics, USA), and plane-faced transducers with 1000 kHz, while Figure 3.b shows tests in the parallel direction to the fibers by means of ultrasound equipment (USLab, AGRICEF, Brazil), and exponential-faced transducers with 45 kHz. A small hole to insert the transducer's tip was made for exponential-face transducer tests.

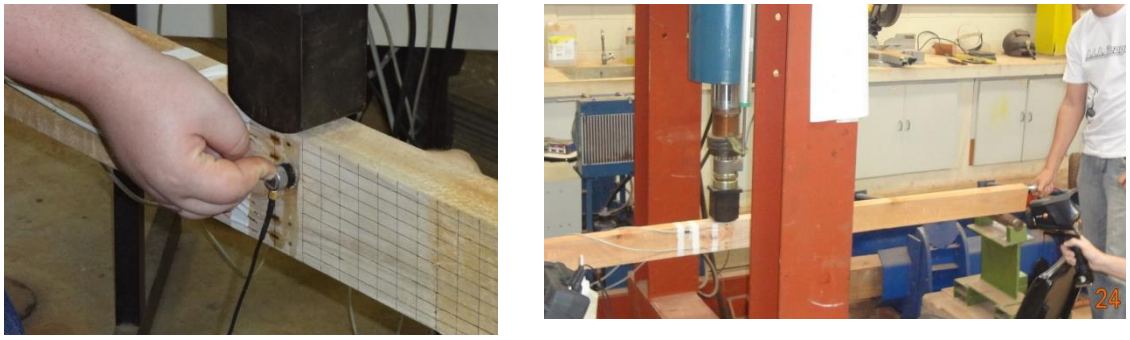

a b

Figure 3. Ultrasound tests made during beam loading on perpendicular (a) and parallel (b) directions to the fibers.

Theoretical stress expected for each of the zones on which the extensometers were bonded (Figure 1) were determined through equations 2 and 3.

$$M = \frac{P\,L}{4} \qquad (2)$$

In which M is the moment considering the bi-supported scheme and center-point loading, P is the applied load and L is the span.

$$\sigma = \frac{M}{I} y \qquad (3)$$

In which I is the moment of inertia and y is the distance from the stress determination point and center of mass.

During bending tests, the extensometer instrumentation allowed specific longitudinal deformation obtention (ε) in all 4 measurement zones (Figure 1). The test also allowed calculation of the modulus of elasticity (E_M) of the beams. Knowing these values, it was possible to obtain the acting stress for each measurement zone, which in this study we will call experimental stress (σ), using Equation 4.

$$\sigma = E_M \epsilon \qquad (4)$$

In which σ is the experimental stress, ε is the specific longitudinal deformation and E_M is the modulus of elasticity.

Results and discussions

For isotropic materials like steel, the velocity variation with stress (in tension tests) behaves linearly, but that has not been observed in wood beams which underwent bending tests.

For longitudinal velocity in parallel direction to the fibers, it was possible to observe velocity's decrease tendencies with increased stress, but it was not linear throughout the stress range. There were also different variation magnitudes between the beams. Figure 4 presents two examples of variation behavior in velocity (parallel to the fibers) with stress, obtained for most part of the beams.

In longitudinal velocity in perpendicular direction to the fibers (radial or tangential), variations in velocity were, all in all, quite smaller than in longitudinal direction. There was also a greatly variable behavior between the beams than observed in propagation in the direction of the fibers (Figure 4.b). In some cases almost there was no variation of the velocity (Figure 4b).

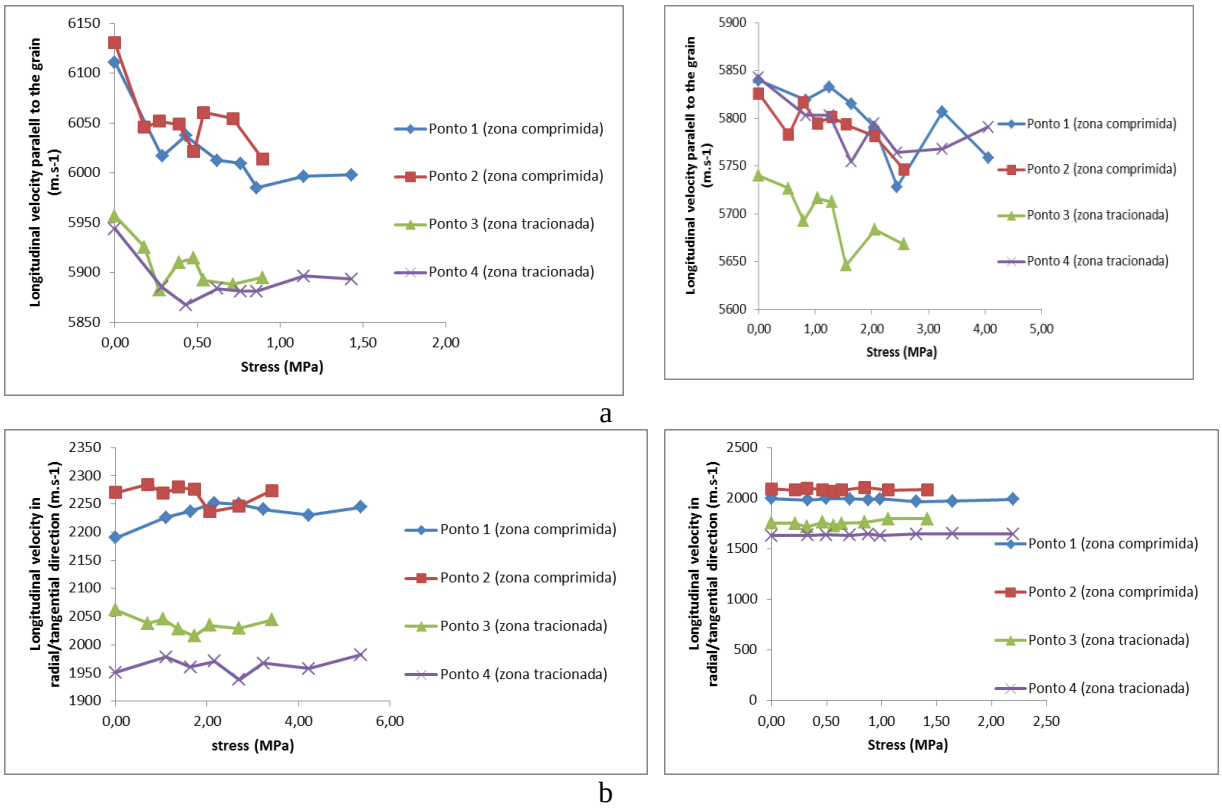

Figure 4 - Examples of velocity variation behavior with stress on measurement points

Drying defects are common in *Eucalyptus*, and longitudinal bow and twist was noted in some of the beams tested for this research. This condition violates the plane sections theory. This issue can be verified, for instance, by means of the stress x strain graphic (Figure 5), which considers all four measurement zones. The graphic on Figure 5 illustrates the behavior of the average deformity values in the compressed and bended areas. This graphic confirms that there is nonconformity in the compressed section regarding the values in zones 1 and 2. Deformation in the edges (zone 1) is inferior to deformation in the internal fibers. This nonconformity in deformation can occur with beam distortions during testing, which happen due to drying defects.

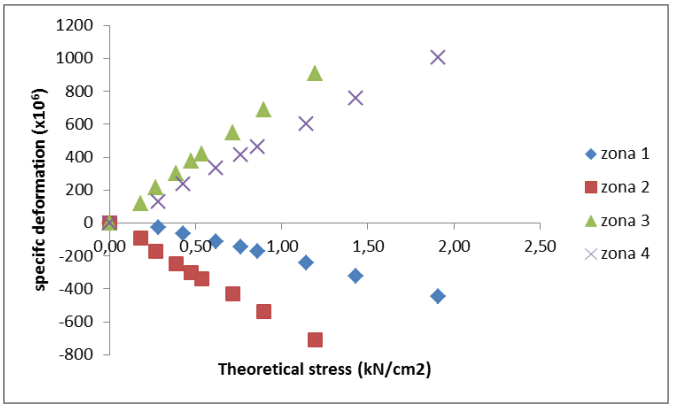

Figure 5 - Example of theoretical stress x strain obtained in each measurement zone (*Eucalyptus grandis*)

The transverse section stress diagram, calculated though Equation 4 and the average deformations found in parallel surfaces (Figure 6), shows nonconformity in stress values for the compressed section. It also indicates significant differences between the experimental and theoretical stresses, considered, in this case, only for maximum loading. These differences would be related to the problems during experimental deformation measurements mentioned previously.

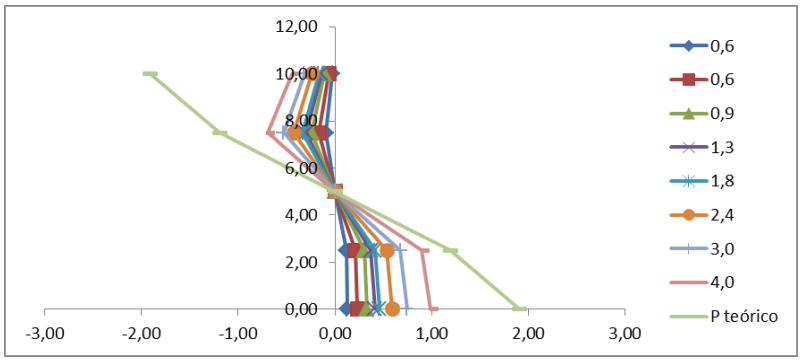

Figure 6. Experimental stress diagram for each loading level and theoretical stress diagram considering maximum loading level (*Eucalyptus grandis*)

Considering the velocity variation behavior in function of the stress, the acoustoelastic constants were determined only to the longitudinal velocity in parallel direction to the fibers.

The average elastic constants of each specimen were calculated, in each measurement zones, from the results obtained for each stress variation range. Then, the average for the values obtained in each species was determined, on both the compressed and traction areas. The calculations were made considering the theoretical and experimental stress (Table 1). The acoustoelastic constant values get more similar when the theoretical and experimental stress's behaviors are more alike. Spurious values, obtained due to lack of linearity between the velocity variation on different stress ranges, mentioned previously, were discarded.

Table 1. Average acoustoelastic constants and coefficients of variation (CV - in parentheses) for all three species, obtained using theoretical and experimental stress.

Species	Type of stress	Compression zones	Tension zones
Eucalyptus grandis (10 years old)	Theoretical	0.0028 (33.7%)	- 0.0033 (80.2%)
	Experimental	0.0038 (38.6%)	- 0.0037 (76.2%)
Eucalyptus citriodora (8 years old).	Theoretical	0.0026 (51.6%)	- 0.0035 (53.4%)
	Experimental	0.0032 (54.7%)	- 0.0040 (60.2%)
Eucalyptus pellita (26 years old)	Theoretical	0.0042 (21.7%)	- 0.0035 (69.6%)
	Experimental	0.0043 (24.5%)	- 0.0025 (57.9%)

It can be observed that the acoustoelastic coefficients present high coefficients of variation, which can be explained by the lack of linearity between velocity variation and stress variation.

The acoustoelastic coefficient value was more stable for the compressed area in species *Eucalyptus pellita*. In this case, the constant value was also greatly superior, when compared to the other two species. This behavior can be related to the age of the trees. For *Eucalyptus pellita*, they were mostly adult wood, while the other species presented juvenile wood. If this hypothesis is correct, adult trees can be expected to have a bigger variation in velocity with stress than younger trees.

This difference in values of the acoustoelastic constants and of the coefficients of variation was not observed in the traction section, especially when theoretical stress was used in acoustoelastic constant calculations. When using theoretical stress, reversal of the behavior in traction area was observed, for the value of the constant for *Eucalyptus pellita* was inferior to the rest.

Although some beams presented reversed behavior, it can be observed that, for the most part of them, the wave propagation in longitudinal direction decreases with increased stress, both in compression and traction zones.

The acoustoelastic constant calculation (Equation 1) was made considering the stress signal, and for that reason, the constant is positive in compression zones, and negative in traction zones. Similar results were found by Hasegawa and Sasaki (2000).

Conclusion

The acoustoelasticity issue in wood is a subject that still need further scrutinizing, so that more conclusive results can be reached. However, in this preliminary research, it was possible to determine important methodological aspects to be observed in this group's subsequent researches like, for instance, the importance of rectilinear beams for bigger precision in determining stress state. It was also possible to observe that the use of theoretical stress does not seem to entail important differences when calculating acoustoelastic constants, which means discarding the use of extensometers can be considered, which could allow a bigger sampling, since instrumented testing is more laborious and costly.

Acknowledgements

We thank the São Paulo Research Foundation (FAPESP) for financial support to this research (Proc. 2009/10319-9) and for the PhD scholarship (Proc. 2011/00904-1) and the National Council of Technological and Scientific Development (CNPq) for the undergraduate and Master scholarships. We also thank the Higher School of Agriculture "Luiz de Queiroz" (Esalq/USP) and Professor Mario Tomazelo for the material donated to this research.

References

ANDRINO, M. H.; CAETANO, S. F.; SANTOS, A. A. 2002. Avaliação das Tensões em Chapas de Alumínio 7050 Utilizando o Efeito Acustoelástico. In: 6a CONFERÊNCIA SOBRE TECNOLOGIA DE EQUIPAMENTOS (COTEQ), 10p., Salvador.

ANDRINO, M. H. 2007. Aplicação de Ondas Longitudinais Criticamente Refratadas para a Medição de Tensões em Dutos. 203 p. Tese (Doutorado) – Faculdade de Engenharia Mecânica, Universidade Estadual de Campinas, Campinas.

CAETANO, S. F. 2003. Determinação das Constantes Acustoelásticas para Aço API 5L X70 para Gasodutos. 167 p. Dissertação (Mestrado) – Faculdade de Engenharia Mecânica, Universidade Estadual de Campinas, Campinas.

HASEGAWA, M.; SASAKI, Y.; IWATA, T. 2000. Acoustoelastic effect of wood III: effect of applied stresses on the velocity of ultrasonic waves propagating normal to the direction of the applied stress. Journal of Wood Science 46, p.102-108.

ORMONDE, P. C.; GONÇALVES, R. 2006. Avaliação do Fenômeno Acustoelástico na Madeira por Meio de Ultra-som, 05/2006, 1° Seminário sobre a Aplicação de Ensaios não Destrutivos na Madeira e Materiais a Base de Madeira,Vol. 1, pp.1-6, Itatiba, SP, Brasil.

PEREIRA Jr., P. 2011. Influência da Anisotropia gerada por laminação sobre a medição de tensões por ultrassom em ligas de Alumínio 7050. Monografia para Exame de Qualificação. Faculdade de Engenharia Mecânica, UNICAMP.

SASAKI, Y.; IWATA, T.; ANDO, K. 1998. Acoustoelastic effect of wood II: effect of compressive stress on the velocity of ultrasonic waves parallel to the transverse direction of wood. J Wood Sci 44:21−27.

Conversion Mode of the Ultrasound Wave

Robson Van Dijk
Master Student, Laboratory of Nondestructive Testing (LabEND), School of Agricultural Engineering (FEAGRI), University of Campinas (UNICAMP), Campinas, São Paulo, Brazil, robson.dijk@agr.unicamp.br

Raquel Gonçalves
Associate Professor, University of Campinas (UNICAMP), College of Agricultural Engineering (FEAGRI) and Coordinator of the Laboratory of Nondestructive Testing (LabEND), Brazil, raquel@agr.unicamp.br

Julio Soriano
Assistant Professor, University of Campinas (UNICAMP), College of Agricultural Engineering (FEAGRI) and Coordinator of the Laboratory of Nondestructive Testing (LabEND), Brazil, julio.soriano@agr.unicamp.br

Cinthya Bertoldo
PhD Student, Laboratory of Nondestructive Testing (LabEND), School of Agricultural Engineering (FEAGRI), University of Campinas (UNICAMP), Campinas, São Paulo, Brazil, cinthyabertoldo@gmail.com

Abstract

Depending on the distance between the transducers, the ultrasound propagation velocity values in indirect measurement can be different from direct measurements, which complicate the interpretation of the inspection's results. The objective of this research was to evaluate, using a big length beam (7000 mm), the velocity's behavior obtained by the direct and indirect measurement. The test was performed using three plane side transducer frequencies (25 kHz, 45 kHz and 80 kHz) and varying the distances between the transducers every 100 mm. The results showed that from relations $L/\lambda \cong 5{,}0$ the velocity obtained on both types of measurement is equivalent to all the transducer frequencies, but the behavior of the wave dispersion differs among them, being less dispersive to the 25 kHz transducer and more dispersive to the 80 kHz transducer.

Keywords: direct experiment, indirect experiment, compression wave, surface wave

Introduction

Wood, as well as every other material, deteriorates and loses its resistance capacity with time, thus requiring periodical inspection. Among the inspection methods, those based on non-destructive techniques have increasingly become accredited, for their timeliness and low costs. The non-destructive technique that stands out is the one based on ultrasonic wave propagation.

However, wave propagation and, consequently, propagation velocity, can be influenced by dispersion phenomenons (BARTHOMOMEU et al, 2003), which can occur due to several reasons - such as piece dimension and transducer positioning during inspections. These issues influence studies that aim at

obtaining correlation model between wave propagation velocity and stiffness and strength proprieties, because most of the correlation models are obtained though direct measurements (longitudinal waves), in which the transducers are positioned in opposite surfaces. However, this measurement method is not very common when inspecting working structures, because it is not customary to have access to two opposite surfaces of the inspected element, which leads to the need for indirect (superficial) measurements.

Since superficial wave propagation is not the same as volume wave (longitudinal) propagation, the velocity results can be different, which complicates analysis of the inspections' results. Erroneous analysis may lead to interpretation mistakes.

Another important issue regards correlations between wave propagation velocities and wood proprieties. These correlations are usually obtained by means of direct tests (compression waves), and, if used with velocity values obtained indirectly, they can also lead to interpreting mistakes in wood strength and stiffness.

However, some studies point out that, in indirect measurements, once the minimum distance is observed between transducers, taking into account the path length (L) and the wave length (λ), the superficial wave presents a propagation velocity equivalent to the longitudinal wave propagation velocity (BARTHOMOMEU et al, 2003, BUCUR, 2006).

Therefore, the objective of this study was to evaluate the velocity equivalence between direct and indirect measurements conducted with different transducer frequencies (25 kHz, 45 kHz and 80 kHz).

Material and Methods

One beam from Cabreúva specie wood (*Myrocarpus frondosus*) with transverse section of 500 mm x 153 mm and 6,950 mm long was tested in the equilibrium moisture content condition ($\cong$ 12%).

The ultrasound tests were conducted with ultrasound equipment (USLab, AGRICEF, Brazil), and plane-faced transducers with frequencies of 25 kHz, 45 kHz and 80 kHz.

Initially, the longitudinal propagation velocity was determined through direct measurement (parallel to the fiber). For such, wave propagation time measurements were conducted with the transducers positioned in opposite surfaces, in three different heights of the transverse section (Figure 1), as specified by the NBR 155215 (2007).

Figure 1 – Direct (longitudinal) wave propagation time measurements

For indirect tests, the emission transducer was secured at 100 mm from the edge of the piece, while the receiving transducer was moved every 100 mm, until it reached the opposite edge (Figure 2). Every measurement was made three times on each point (repetitions), using medicinal gel as coupling.

Figure 2. Indirect (superficial) wave propagation time measurements

In order to evaluate wave dispersion, an additional test was conducted on the beam, using only the 45 kHz transducer. The emission transducer was set on the superior surface, at the left extremity of the beam, while the receiving transducer went through every point of the measurement grid (Figure 3), which had been divided into three lines (distance between the lines was 55 mm) and columns separated by 100 mm, from beginning to end of the beam (7.0 m).

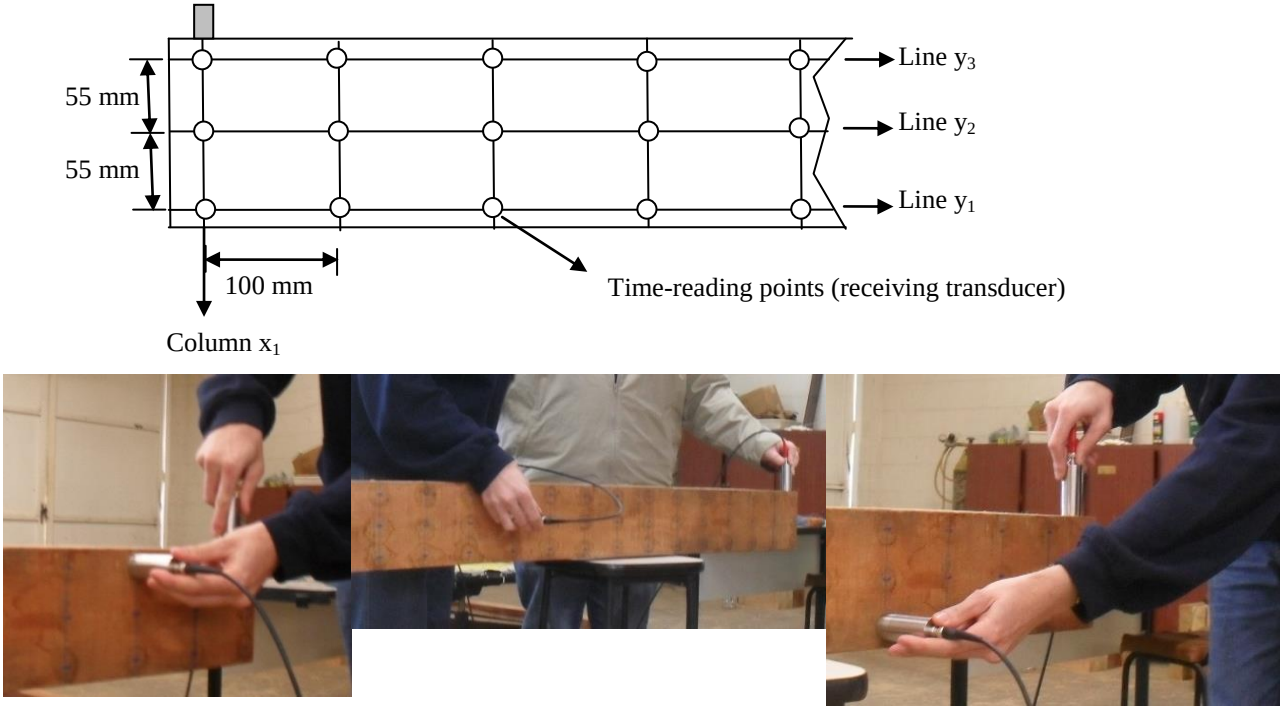

Figure 3. Outline of measurements and beam tests for wave dispersion analysis

Results

The velocities obtained using different transducer frequencies were not exactly the same, but the biggest difference was of 3% between the velocities obtained with the 80 kHz transducer and the 25 kHz transducer (Table 1). Taking into account the velocities obtained with all the transducer velocities, the coefficient of variation was 1.6%. These low coefficients of variation in velocities for the three measurement points obtained with each frequency (Table 1) indicate that the beam was homogeneous, with no indication of internal defects. Visual analysis did not flag any defects either.

Table 1— Longitudinal velocities ($m.s^{-1}$) in direct tests, and coefficient of variation (%) of velocities for the three measurement points

Parameters	Transducer frequency		
	25 kHz	**45k Hz**	**80k Hz**
Average velocity	4,631	4,580	4,490
Coefficient of variation (%)	0.38	0.53	0.20

In the indirect measurements, the statistical analysis when comparing the averages using the velocity results obtained in each transducer distance (from 100 mm to 6,900 mm) indicated that there is no equivalency between the velocities in the different frequencies. For this analysis, the *Multiple sample comparison*, which compares the results for the three frequencies through multiple statistical and graphic tests, was used. Since the *P-value* on the ANOVA table was lower than 0.05, there is a significant statistical difference for the confidence level of 95% between the average of the three frequencies. To determine which frequencies were different among themselves, the *Multiple Range Test* was used (Table 2), which indicated that all the frequencies were statistically different because they belong in different

groups. This result suggests that wave behavior in function of transducer distance depends on the frequency of the transducer, which was already expected, because the wave length varies according to the frequency.

Table 2 — Results of the *Multiple Range Test* (95% confidence level)

Frequencies (kHz)	Data quantity	Average velocity ($m.s^{-1}$)	Group
25	69	4,080	a
45	69	3,898	b
80	69	3,443	c

Considering the average values of the longitudinal velocities (direct measurement) obtained for each frequency, the wave lengths were approximately 180 mm for the 25 kHz transducer, 100 mm for the 45 kHz transducer, and 57 mm for the 80 kHz transducer. Using the distance relationships between the transducers (L) and the wave length (λ), it is possible to evaluate, for all three transducer frequencies, the velocity behavior obtained directly and indirectly on the beam (Figures 4, 5 and 6).

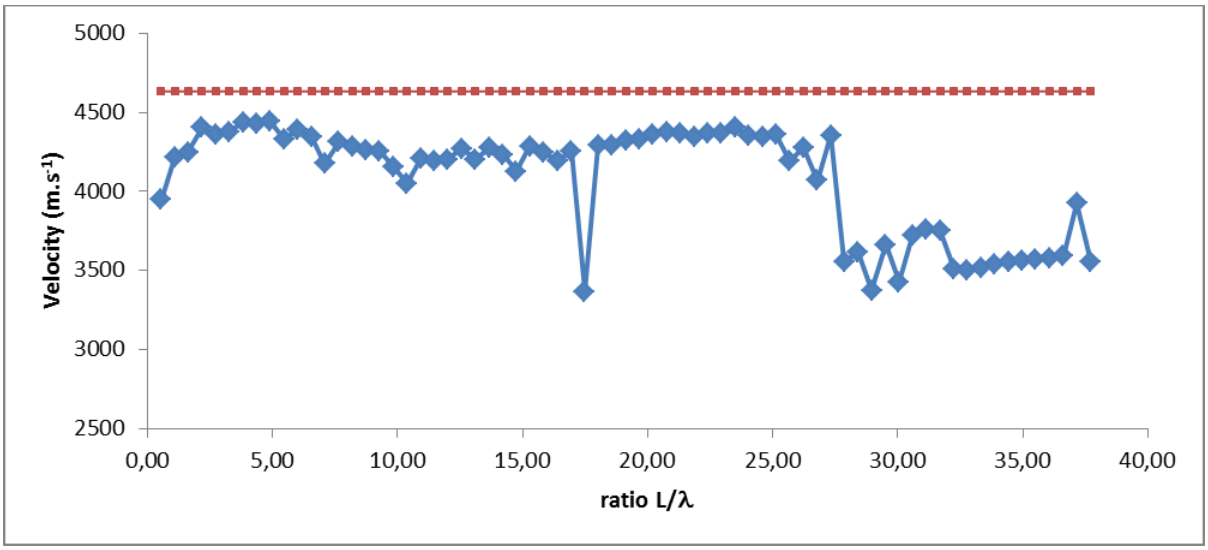

Figure 4 – Velocity behavior in function of the relationship between transducer distance (L) and wave length (λ) for the 25 kHz transducer

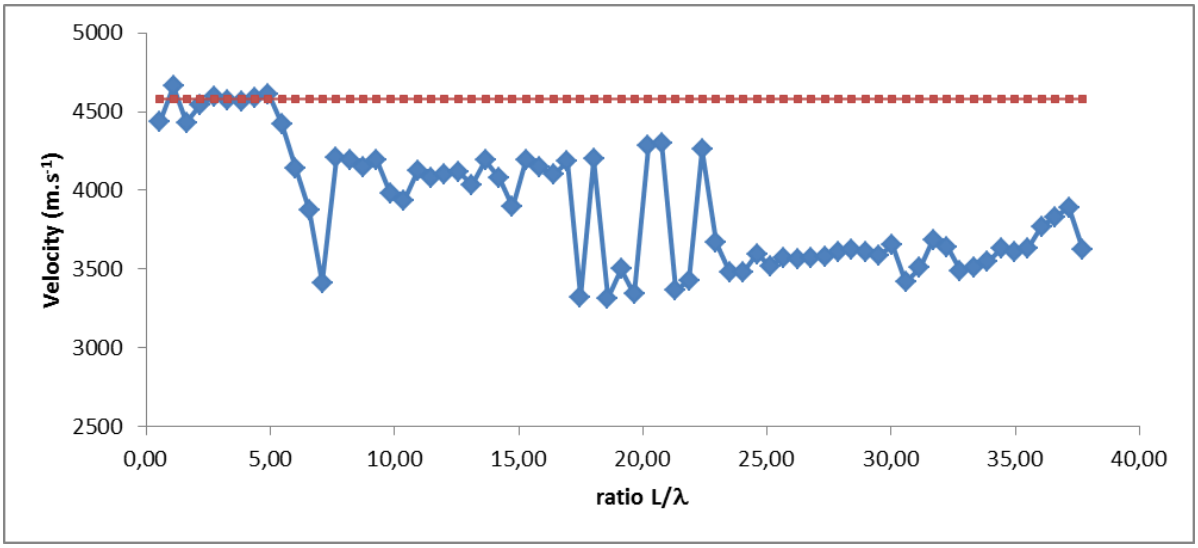

Figure 5 – Velocity behavior in function of the relationship between path length (L) and wave length (λ) for the 45 kHz transducer

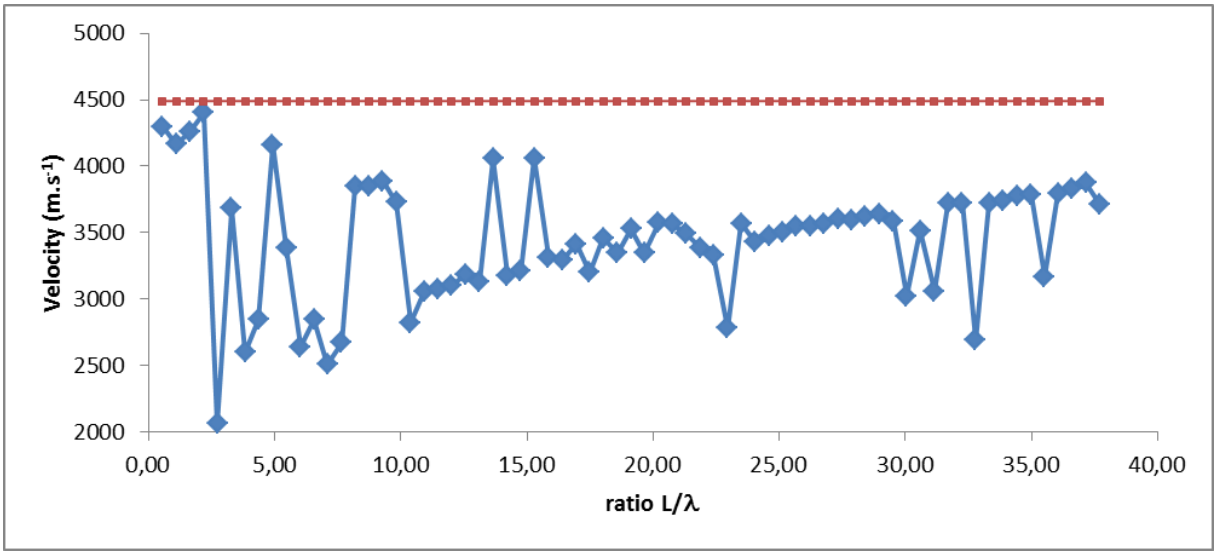

Figure 6 – Velocity behavior in function of the relationship between path length (L) and wave length (λ) for the 80 kHz transducer

For all the frequencies, disregarding oscillations, there are three behavior levels for the velocity obtained indirectly. The first level (up to $L/\lambda \cong 3$) indicates a very similar behavior for all three transducer frequencies, with increased velocity values obtained indirectly as L/λ increases. The intermediate and final levels also present similar behavior between the different frequencies, with velocities obtained directly around 10% and 30% lower than the velocities obtained directly, respectively. The behavior difference for the intermediate and final levels is the relationship L/λ from which these baselines occur.

More specifically, for 25kHz frequency, the velocity obtained indirectly did not reach the velocity value obtained directly (Figure 4) for none of the relationships between transducer distance (L) and wave length (λ). The differences were around 10% for the L/λ varying from 3.0 to 27.0, and 30% from $L/\lambda \cong 27$.

For 45 kHz frequency, the velocity obtained indirectly was only similar as the one obtained directly on a small section (from $L/\lambda \cong 3$ to 5). From $L/\lambda \cong 5$ to 22, it was about 10% lower, and from $L/\lambda \cong 22$, it was 30% lower.

For 80 kHz frequency, the velocity obtained indirectly was only similar as the one obtained directly on $L/\lambda \cong 3$, presenting great instability on the remaining sections, with an average 30% lower than the velocity obtained directly on the remainder of the beam.

The reduction on the velocity values obtained in indirect measurements can be related to wave dispersion. Taking into account the measurements conducted on the perpendicular surface of the beam (Figure 3), one can notice that, for the 45 kHz transducer, only a small initial section presented velocity values for the superior part of the beam (near the indirect measurements) that resembled the values found through direct (longitudinal) measurements - Figure 7.

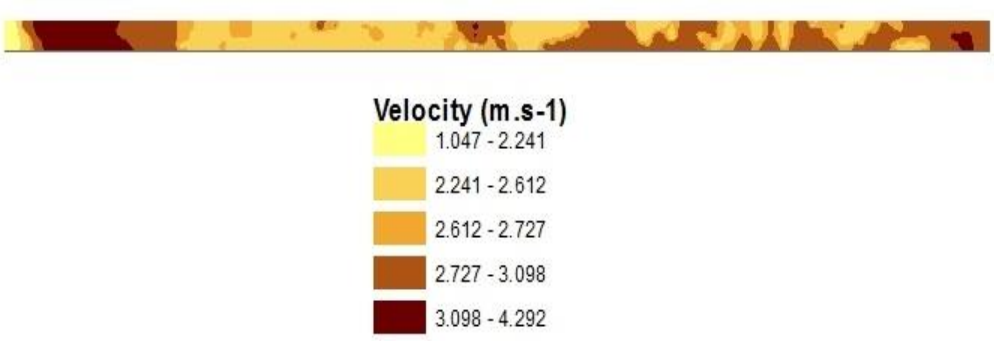

Figure 7. Wave dispersion in indirect measurements with 45 kHz transducer.

Although the velocity value obtained indirectly with the 25 kHz transducer did not reach the velocity value obtained directly, the results were more stable, and only after $L/\lambda \cong 25$ relationships were the velocity results influenced by dispersion.

Conclusions

For all three frequencies analyzed, it was verified that

- Using transducer distances smaller than twice the wave length was not appropriate, because the velocities were not constant, and increased as the transducer distance increased.

- There is a limit value for transducer distance, above which the velocities obtained indirectly are about 30% inferior to those obtained directly, and that this phenomenon should be connected to wave dispersion.

- There is an intermediate stretch between transducer distances, between twice the wave length and the point from which wave dispersion begins, in which the velocities obtained indirectly present smaller differences than 10%, regarding the velocities obtained directly.

Acknowledgements
To the Coordination for Enhancement of Higher Education Personnel - CAPES for the financial support and masters scholarship, to the São Paulo Research Foundation - Fapesp, for financial support (Proc. 2012/22599-9) and the PhD scholarship (2011/08612-0), and to the School of Agricultural Engineering (FEAGRI, Unicamp), for infrastructure.

References
BARTHOLOMEU A, GONÇALVES R, BUCUR V. 2003. Dispersion of ultrasonic waves in Eucalyptus lumber as a function of the geometry of boards. Scientia Forestalis n.63, p.235-240.

BUCUR, Voichita. 2006. Acoustics of Wood. Editora Springer Verlage – N.Y. 393p.

Session 10

Material Characterization II—Near Infrared, Neutron Imaging, and Other Techniques

Esclerometer test methods for estimating the density of wood

Julio Soriano
Assistant Professor, University of Campinas (UNICAMP), College of Agriculture Engineering (FEAGRI), Campinas, SP, Brazil, julio.soriano@feagri.unicamp.br

Raquel Gonçalves
Associate Professor, University of Campinas (UNICAMP), College of Agricultural Engineering (FEAGRI), Campinas, São Paulo, Brazil, raquel@agr.unicamp.brr

Alex J. Trinca
Postdoctoral Researcher, University of Campinas (UNICAMP), College of Agricultural Engineering (FEAGRI), Campinas, São Paulo, Brazil, ajtrinca@mxb.com.br

Nadia S. Veiga
Master student, School of Agricultural Engineering (FEAGRI), University of Campinas (UNICAMP), Campinas, São Paulo, Brazil, nadiasveiga@gmail.com

Ingrid Z. Martins
Undergraduate student, School of Agricultural Engineering (FEAGRI), University of Campinas (UNICAMP), Campinas, São Paulo, Brazil, ingrid.martins@feagri.unicamp.br

Abstract

Wood density is a physical property that needs to be known for the development of engineering designs and for determine the stiffness matrix in nondestructive testing. The conventional method for determining such property shows difficulties for some applications by requiring the extraction of specimens. In this research is studied the tendency of the correlation wood density, obtained by the conventional method, and the esclerometer impact obtained by using a portable device. Three species of tropical wood was used, and for each one were extracted 12 prismatic specimens (80mm x 200mm x 300mm) with moisture content established. These prisms were subjected to the esclerometer test and specimen was extracted for determination of density by the conventional method. The results obtained allowed the observation that the correlation established between density and esclerometer impact is significant and would be possible estimate the wood density nondestructively using this methodology.

Keywords: nondestructive testing; tropical wood; moisture established

Introduction

The conventional methods for determining the density of wood require fabrication of specimens, for which mass and volume must be measured. It is well known that this physical propriety of wood is of fundamental importance for transportation sectors, paper and furniture industries, and for composition of loadings in construction design. Unlike other common structural materials, like steel or concrete, wood presents a wide variation in density, thanks to its diversity of species. In the case of hardwood species,

density depends on the thickness of the fiber walls, as well as the portion of voids occupied by vases and parenchyma (USDA 2010).

Certain mechanical proprieties can be connected to wood density. To exemplify this, equations that expressed the dependence between hardness and density (Wiemann and Green 2007, Lahr et al. 2010) were developed. Concerning nondestructive tests, it may be pointed out that the elastic constants of the wood, according to Cristoffel's Equations (Bucur 2006), relate to wave propagation velocity and density of wood.

For known wood species, it is possible to estimate density by means of tables with values pre-determined in laboratory. However, activities concerning inspection of structures in which unknown species can be used are more common. This situation indicates the importance of developing techniques and equipment that allow estimates the wood density outside of the laboratory, without the need to extract specimens. With the prospective *in situ* proposal, results obtained with drilling device reportedly don't offer a good estimate of wood density (Machado et al. 2003). To estimate wood density in live trees, the Resistograph equipment was described as advantageous when compared with the traditional volumetric method, due to its low cost and timeliness. The Resistograph is also considered advantageous in live trees because allows evaluating the whole diameter of the tree, instead to Pilodyn, which only evaluates the range of the drill (Isik and Li 2003).

Esclerometry is a non-destructive testing technique known for its applications on concrete structures. For each esclerometric impact, the rebound's coefficient can be obtained, which represents the relation between the restored energy and the energy applied by the device (Proceq 2009). Previous researches of application of this technique in wood were developed in pieces of *E. Saligna* species, and led to the conclusion that this technique was able to distinguish the proprieties in the longitudinal and normal directions to the fibers (Soriano et al. 2011a). In spite of that result, it is well known that several mechanical properties are influenced by direction of the grain, moisture content and species (Wiemann and Green 2007).

In the present study, the results of esclerometric impacts, applied to three different tropical wood species (*Cedrela ssp, Apuleia leiocarpa , Dipteryx odorata*) were connected with their respective densities in order to contribute to the development of new nondestructive techniques that can be applied in situ.

Material and Methods

Pieces from three tropical species (*Cedrela ssp, Apuleia leiocarpa , Dipteryx odorata*) with very distinct densities were obtained, for which the references (IPT 1989) for the specific gravity (moisture content 15%) are 530kg.m^{-3}, 830kg.m^{-3}and 1.090kg.m^{-3}, respectively. For each specie, 12 prismatic pieces 300 mm long (parallel to the fibers) were retrieved from 12 different pranks with transverse sections 80 mm x 200 mm. The *Cedrela ssp* and *Apuleia leiocarpa* species' pieces were stabilized in kilns, since they initially presented elevated moisture content, 47.5% e 78.8%, respectively. The *Dipteryx odorata* species' pieces had already been stabilized with 12.4% moisture content, below the fiber saturation point.

The prisms were identified and given the referential demarcations for the tests. To apply the impacts on the longitudinal and tangential directions, five points were demarcated on the center line of each corresponding surface (Figure 1). Thus, 10 impacts were applied on each of these anatomical directions. On the radial direction, 18 impacts were applied, 9 of which in each corresponding surface of the prism. The distance between the impact application points was 50 mm. The coefficients of impact that are to be represented in this paper by QL (longitudinal direction), QR (radial direction) and QT (tangential direction) are dimensionless quantities.

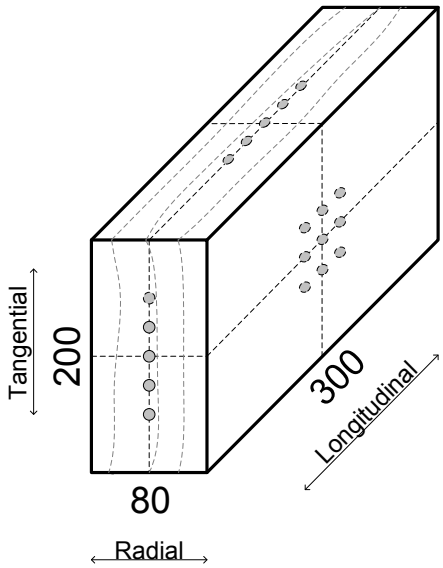

Figure 1— Prism with identification of the anatomical directions, and the esclerometric impact application points (dimensions in mm). The points were 50 mm apart from each other.

The esclerometry was performed using portable equipment (Digital Silver Schmidt BN, PROCEQ, Switzeland). Due to the dimensions of the specimens, they had to be attached to a hydraulic machine for esclerometric impact application. In a previous study of esclerometric method applied to wood (Soriano et al. 2011b), it was suggested that a load estimated from 15% of average strength of compression normal to the fibers be applied for specimen attachment, which would insure the behavior of the material in elastic limit.

Figure 2 – Esclerometer test on a prism attached to hydraulic machine

To determine density and moisture content of each specie, from the prisms that underwent esclerometric testing, 12 specimens were made, in conformity with the Brazilian standard (ABNT NBR 7190, 1997), with 20 mm x 30 mm transverse section and 50 mm long. A kiln was used on the drying procedures to determine the moisture content (Model 315 SE, Fanem, Brazil), as well as a precision scale (Model AS 5500, Marta, Brazil). On the drying process, the specimens remained in the kiln (Figure 3)at a 103º C +/-

2º C temperature, until stability is reached, that is, when the variation between two consecutive mass readings presents a result lower than 0.5%.

Figure 3 - Specimens in the kiln to determine the moisture content.

A Kollmann diagram was used to correct the density obtained by means of apparent density tests on moisture content of 12% (Panshin and Zeeuw 1980). The Equation 1 (Brazilian standard NBR 7190 1997) was used to correct the values of esclerometric impact.

$$f_{12} = f_{MC\%}\left(1 + \frac{3(MC\%-12)}{100}\right) \quad (1)$$

In which f_{12} is the strength estimated at a moisture content of 12%, $f_{MC\%}$ is the strength obtained through testing, and MC is the percentage of moisture content obtained though testing.

Results and discussions

Average values for 12 specimens per species were obtained for the moisture content and apparent density tests, which are presented on Table 1. The densities were corrected for the reference moisture content of 12%, using the Kollmann diagram as a parameter. Therefore, to compare with the esclerometry results, 490 kg.m^{-3} (*Cedrela ssp*), 810 kg.m^{-3} (*Apuleia leiocarpa*) and 1007 kg.m^{-3} (*Dipteryx odorata*) densities were used.

Table 1 – Average values of moisture content (MC) and apparent density (ρ)

MC (%)	CVar (%)	ρ (kg.m^{-3})	CVar (%)	ρ (12%) (kg.m^{-3})
		Cedrela ssp		
24.91	7.63	530	4.80	490
		Apuleia leiocarpa		
17.00	20.72	830	3.77	810
		Dipteryx odorata		
12.40	9.96	1007	6.40	1007

Average impact values (Q) per species and per each of the anatomical directions - Longitudinal (L), Radial (R) and Tangential (T) - were obtained from esclerometric tests, which are presented on Table 2. For each species tested, the highest average impact values were found in the Tangential direction (QT), and the lowest on the longitudinal direction (QL).

Minitab Statistical Software was used for statistical analysis, with homogeneity verification of results through ANOVA function of the Fisher test (with a confidence level of 95%). For each one of the species,

the statistical analysis showed a lack of homogeneity for the average esclerometric impact values, which means that the esclerometric method managed to differentiate the quantities according to the anatomical directions.

Table 2 – Average esclerometric impact values obtained by the tests and corrected values for reference moisture content (12%)

MC	Longitudinal			Radial			Tangential		
	QL	Homogeneous Groups*	CVar (%)	QR	Homogeneous Groups*	CVar (%)	QT	Homogeneous Groups*	CVar (%)
				Cedrela ssp					
24.91	17.0	A	17.6	23.9	B	12.2	27.6	C	12.2
12	21.1	-	-	29.6	-	-	34.2	-	-
				Apuleia leiocarpa					
17.00	28.5	C	7.1	32.6	D	6.8	36.1	E	4.5
12	33.5	-	-	38.4	-	-	42.5	-	-
				Dipteryx odorata					
12.40	35.3	E	14.3	39.1	F	9.7	42.5	G	8.1
12	35.7	-		39.6	-	-	43.0	-	-

*Similar letters indicate homogeneous groups.

In order to analyze correlations such as densities, the esclerometric impact values were corrected for reference moisture content of 12% (Table 2). For these corrections, Equation 1 was used and, for results obtained on *Cedrela ssp* species, the limite value for moisture content of 20% was used as reference, since for superior moisture content values wood strength is believed to suffer small variations (Brazilian standard NBR 7190 1997).

The experimental results for all three species are represented on Figure 4, in which the exponential adjustment model was represented. Table 3 presents the linear and exponential equations and their correlation coefficients. From the adjustments obtained through the regressions (Table 3) it can be asserted that the exponential model explain better the estimation of wood density by esclerometer impact (Q), due to superior coefficients of correlation (R) presented.

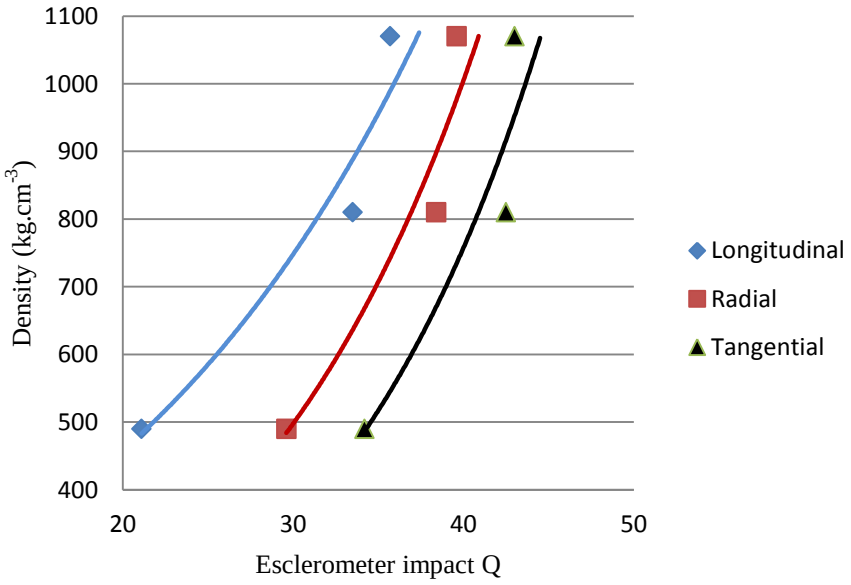

Figure 4 – Experimental density and esclerometer impact results for all three anatomical directions and exponential adjustment model.

Table 3 – Regression model density (ρ) as a function of Esclerometer impact on Longitudinal (QL), Radial (QR) and Tangential (QT) for reference moisture content (12%).

Direction	Correlation model	
	Linear	Exponential
Longitudinal	$\rho = 0.035QL - 0.2632$ $R = 0.95$	$\rho = 0.1715e^{0.0491QL}$ $R = 0.97$
Radial	$\rho = 0.0499QR - 1.0001$ $R = 0.94$	$\rho = 0.0605e^{0.0703QR}$ $R = 0.97$
Tangential	$\rho = 0.0538QT - 1.3577$ $R = 0.92$	$\rho = 0.0358e^{0.0763QT}$ $R = 0.95$

Finally, it should be noted that for the three directions anatomical correlations between the two studied properties are well representative and relatively high correlation coefficients were obtained, either by adjusting linear or exponential. These results allow the use of correlations for the longitudinal direction and also application on the normal direction to the fibers, being advantageous from the standpoint of applicability for inspection pieces *in situ* that only the radial and tangential directions will be accessible for impact application.

Conclusions

In this study of three tropical wood species, it is possible to conclude that:

The correlation between density and esclerometric impact was greatly represented by linear and exponential adjustment models, with coefficients of correlation varying between 0.92 and 0.97, which allows estimations of wood density by means of esclerometry.

For each anatomical direction resulted in a most appropriate equation to adjustment the results from esclerometric impacts and wood density.

The present study must be broadened with species with intermediate densities to the ones tested. The influence of the moisture content on the correlation models must also be investigated.

Acknowledgements

We thank the National Council of Technological and Scientific Development (CNPq) for the undergraduate research scholarship, to the Coordination for Enhancement of Higher Education Personnel (CAPES) for the master scholarship and the Founding of Support to Research (FAEPEX) from University of Campinas for the financial support.

References

ABNT . 1997. Design of timber structures. NBR 7190. Brazilian Association of Technical Standards. Rio de Janeiro. (in Portuguese).

Bucur, V. 2006. Acoustics of Wood. Berlin: Springer. 393p.

IPT - Institute for Technological Research of the State of Sao Paulo. 1989. Sheets characteristics of Brazilian woods. São Paulo: IPT. 418p. (in Portuguese)

Isik, F.; Li, Bailian. 2003. Rapid assessment of wood density of live trees using the resistograph for selection in tree improvement programs. Canadian Journal of Forest Research. 33: 2426-2435.

Lahr, F.A.R.; Chahud, E.; Fernandes, R. A. [and other]. 2010. influence of density in hardness parallel and normal to the grain for some Brazilian tropical tree species. Scientia Forestalis, 38(86): 153-158 . (in Portuguese)

Machado, J. S.; Costa, D.; Cruz, H. 2003. Evaluation of pine timber strength by drilling and ultrasonic testing. Proceedings, Symposium Non-Destructive Testing in Civil Engineering. http://www.ndt.net/article/ndtce03,papers/p047/p047.htm. [Jul 2009].

Panshin, A. J.; Zeeuw, C. 1980. Textbook of wood technology: structure, identification, properties and uses of commercial woods of the United States and Canada. N York: McGraw-Hill. 722p.

PROCEQ©. 2007. Silver-Schmidt. (manual of operation).

Soriano, J.; Gonçalves, R.; Bertoldo, C. [and other]. 2011a. Application of esclerometer test method in specimens of eucalyptus saligna. Proceedings, International Symposium on Nondestructive Testing and Evaluation of Wood '16, Sopron. 6p.

Soriano, J.; Gonçalves, R.; Bertoldo, C. [and other]. 2011b. Application of esclerometer test method in specimens of eucalyptus saligna. Revista Brasileira de Engenharia Agrícola e Ambiental 15(3): 322-328. (in Portuguese)

U.S. Department of Agriculture, Forest Service, Forest Products Laboratory . 2010. Wood handbook - Wood as an engineering material. General Technical Report FPL-GTR-190. Madison, WI: 508 p.

Wiemann, M.C.; and Green, D.W. 2007. Estimating Janka hardness from specific gravity for tropical and temperate species. Technical Report, USDA, 26 p.

Dynamic mechanical analysis (DMA) as a tool for characterization and non-destructive testing of wood

Robert Widmann
Structural Engineering Research Laboratory, Empa – Swiss Federal Laboratories for Materials Science and Technology, Duebendorf, ZH, Switzerland, Robert.widmann@empa.ch

Andreja Kutnar
Andrej Marušič Institute, University of Primorska, Koper, Slovenia, andreja.kutnar@upr.si

Abstract

In this paper the methodology of dynamic mechanical analysis (DMA) for wood is being discussed. It is intended to provide valuable information about possible parameter settings.
Dynamic mechanical analyze (DMA) is a technique for the determination of the viscoelastic behavior of a sample under cyclic loading and varying conditions, e.g. temperature, humidity and frequencies. In terms of testing wood and wood based composites with this technique, such data – obtained on small specimens – are valuable for analyzing the change of its properties in conjunction with e.g. elevated temperatures. This is of interest regarding studies of e.g. thermal modification/degradation, accelerated aging, structural behavior under fire or creep of glue lines.
DMA technique has already been used for wood. Most of the studies were focused on the results e.g. regarding the above mentioned fields of interest. When our team started to use DMA for wood we learned that the test method can have a strong influence on the results and only limited information can be found on that. Therefore, in an ongoing project the influence of important parameters like test set-up, support conditions, static and dynamic load level as well as inclination of temperature ramps on the measured viscoelastic behavior of wood is being studied. In this paper the results obtained up to now are presented and the application of DMA in a case study regarding thermal modification of beech specimens is demonstrated.

Keywords: dynamic mechanical analysis (DMA), wood, viscoelasticity, test method

Introduction

DMA Principal

Dynamic mechanical analysis (DMA) is a technique for the determination of the viscoelastic behavior of a sample under a cyclic loading and varying conditions, e.g. ramps or increments in temperature and/or frequencies (Menard 2007). DMA usually delivers three mechanical parameters related to energy storage and dissipation: elastic (storage) modulus E', viscous (loss) modulus E'', and damping tanδ. It is a well established technique in the field of characterizing polymers. In particular the determination of thermomechanical transitions of the material can be well observed with this method. Therefore DMA is along with differential scanning calorimetry (DSC) the most often used method to evaluate the glass transition temperature T_g of a (polymeric) material. At this temperature a transition of a material from a hard and brittle state ("glassy") into a molten state ("rubbery") or vice versa occurs. The ratio of the loss modulus E'' to the storage modulus E' expressed as tan δ reaches a maximum at or around the glass transition T_g. As wood is a composite containing the polymeric components cellulose, hemicellulose, and lignin, it is obvious that DMA can also be used for the characterization of wood (Birkinshaw et al 1986,

Backman A.C. and Lindberg K.A. 2001, Salmén, L. 1984). However, DMA has been often used in studies where wood is combined with other polymers, like e.g. with adhesives or as a component of wood plastic composites, but studies using DMA for the analysis of wood itself are much less numerous. Apart from the "traditional" DMA studies with wood being a part of an above mentioned composite it is also of interest to use DMA technology in conjunction with studies of wood regarding e.g. drying at elevated temperatures, thermal modification/degradation, accelerated aging or structural behavior under fire.

In Figure 1 two graphs of DMA measurements are shown. The graph at the left hand side shows the measurement of an epoxy-type adhesive which can be also used for gluing CFRP to wood. The other graph shows the DMA measurement of a spruce specimen under similar conditions. It is obvious that the changes of E', E" and tan δ due to temperature variation are much more pronounced for the epoxy than for the wood. It can also be observed that damping of wood and its variation is much lower (tan δ = 0.012 – 0.022) compared to the epoxy.

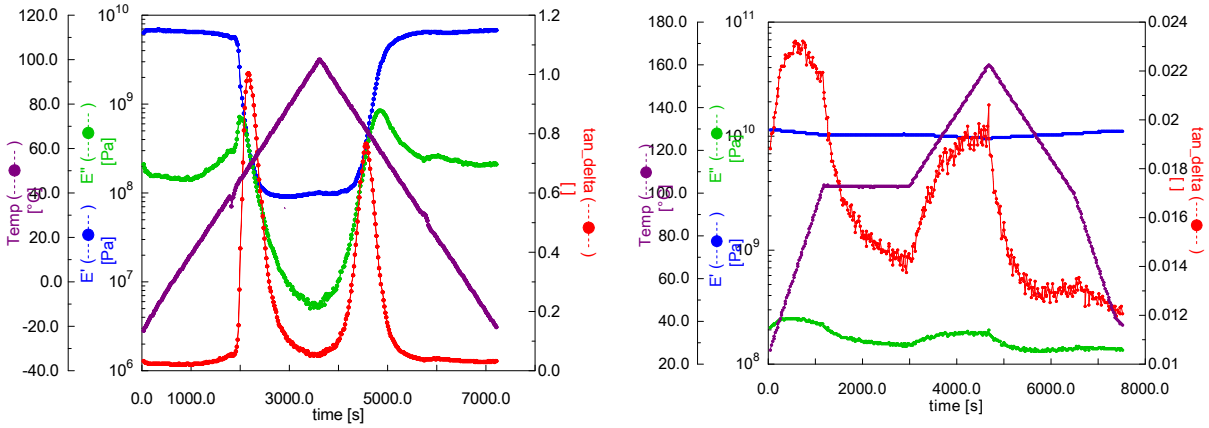

Figure 1— Typical graphs following DMA measurements. Left: Epoxi-type adhesive and right: spruce specimen. Both were tested in 3-point bending.

This fact is of a certain importance as already only relatively small absolute variations of *E*" can lead to relatively big relative variations of tan δ. On the one hand this is an advantage as the method is very sensitive but on the other hand already minor adjustments of the DMA equipment like e.g. the movement of the stage in order to keep a certain preloading level can influence the results significantly as will be shown further down.

Equipment

There are different manufacturers of DMA equipment, two of the most important being TA Instruments and PirkinElmer. All studies presented in this paper are based on measurements with a TA RSAIII Rheometrics System Analyzer (Figure 2). The basic technical specifications of the system are shown in Table 1.

Table 1 — Technical specifications of the TA Instruments RSA III Rheometrics System Analyzer

Motor		Transducer		Environmental Controller	
Frequency	10^{-6} Hz to 80 Hz	Phase angle resolution	+/- 0.1°	Temp. range	-150°C to +600°C
Max Force	35 N (3500 g)	Force resolution	0.2 mg	Temp. rate	0.1 to 50°C/min
Amplitude	+/- 1.5 mm			Oven gas	Air and/or N2
Strain resolution	+/- 0.05 mm			No moisture control	

Figure 2— TA Instruments RSA III Rheometrics System Analyzer with open convection oven (left), spruce specimen before thermal treatment/DMA in a 3-point bending set-up with a 40 mm span (top right) and a larch specimen in a tension set-up (bottom right).

From the specifications shown in Table 1, in particular from the strain and force resolutions, it can be seen, that this equipment is very interesting for testing small sized wood specimens. It is not really possible to carry out static tests in this equipment. However, if or tests the lower possible frequency range between 10^{-3} Hz and 10^{-6} Hz is being used this can be regarded as quasi static.

Test configurations

The TA Instruments RSA III offers the following test configurations (see also Figure 3):

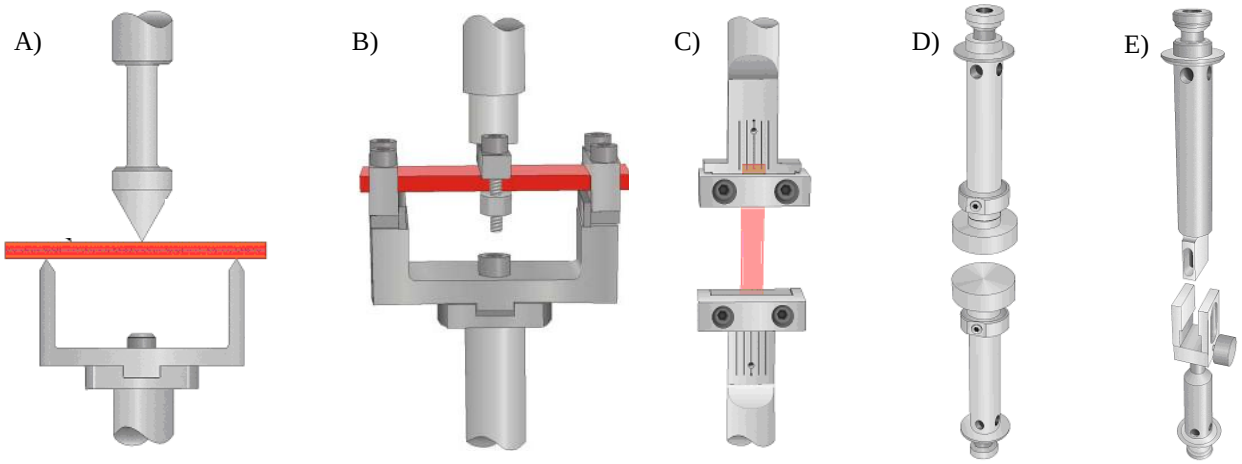

Figure 3— Test configurations and tools. Source: User manual TA RSAIII. • A) 3-point bending, B) clamped 3-point bending, C) tension, D) compression and E) shear.

The choice of which test set-up is the best one to be used for a certain application mostly depends on the specimen geometry and stiffness. For testing wood in principal any geometry would be possible, however the choice in this case is limited due to stiffness. The relevant values are indicated in the operation manual of the device. According to this manual the stiffness should be chosen as follows:

"The RSA III measures sample deformation (strain) by taking the difference between the motor and transducer displacement signals. The measurement is sensitive to limits in strain resolution, as well as variations in motor, and transducer, calibration and linearity. Under "ideal" conditions, the sample deformation is relatively large, and as such, the transducer displacement is much smaller than the motor displacement applying the force. The difference between the two (used to obtain sample displacement) is therefore a large number, and the relative error associated with the measurement is small. However, this error becomes significant when very stiff samples (low sample compliance) are tested, and the transducer displacement becomes close to the motor displacement. In this case, the difference between the two displacements is small, and the relative error is large, and of similar magnitude as the measurement. This condition is indicated by the measured strain value being significantly smaller than the commanded strain value. As a practical guideline, actual strain should be greater than 30 percent of the commanded strain. If actual strain is much lower, the sample needs to be made less stiff by lengthening it and making it narrower and/or thinner."

Most suitable for testing wood are the first three of the above mentioned set-ups. Compression tests would require very small specimen sizes and shear tests (in a sandwich configuration) most probably will result in big data errors that will occur due to shrinking and swelling of the wood. Three-point bending and clamped 3-point bending could be used for testing wood parallel and perpendicular to the grain whereas tension with "reasonable" specimen dimensions can only be tested perpendicular to the grain. For the wood specimens used in our studies (Spruce *Picea abies* and Beech *Fagus sylvatica* with a longitudinal MOE in the range of 10 GPa and MOE perpendicular in the range of 0.3 MPa) and tested under tension or 3-point bending resulted in the specimen dimensions indicated in **Table 1**Table 2.

Table 2 — Specimen dimensions

Test Set-up	Orientation	Length [mm]	Width [mm]	Thickness[mm]
Tension	parallel	25 - 30	5 - 8	0.9 - 1.2
3-point bending	Parallel and perp.	25 - 40	5 - 8	0.9 - 2.5

Our measurements showed that with these dimensions the compliance requirements of the system can be met even thought the specimen dimensions for 3-point bending with short spans do not comply with the recommended sizes according to ISO 6721-5.

Test parameters

For the different test set-ups special requirements have to be met. For tension and 3-point bending a static preload has to be set in order to guarantee that the dynamic load doesn't lead to a stress reversal (buckling) in the case of tension or to a zero-load in the case of 3-point bending. This static load has to be greater than the maximum dynamic load amplitude at any time of the test. The TA RSAIII equipment and the relevant software TA Orchestrator offer three different possibilities for the application of a preload:

- Constant static force
- Static force tracking dynamic force
- Estimation of static force on base of the complex modulus $E^* = (E'^2 + E''^2)^{1/2}$

For all three ways of the application of a preload the consequences of this preload have to be considered. First of all the sum of static preload and dynamic load may not exceed the linear elastic range of the material at any time of the test. This often requires that the preload is being adapted in an ongoing test, when e.g. the modulus decreases under a certain limit due to increased temperatures or in our case due to ongoing wood modification and/or degradation. There are several options within the TA Orchestrator software to account for this softening and to adapt the pre load respectively. Even if these options are chosen carefully, the reaction of the device might have an influence on the results. An example for this is shown in Figure 4. Spruce specimens were thermally modified in the oven of a TA RSAIII Rheometric system analyzer. It was the aim to monitor the ongoing modification by observing the progress of the basic DMA data storage modulus, loss modulus and tan δ. In this case the effect of different modification times for a constant modification temperature should be studied. The two presented results are part of a complete series, one with a short (120 min) and the other with a long (1920 min) modification (or holding-) time T_h. It can be observed that all three parameters are affected by changing temperatures and also over time. For the given graph resolution the storage modulus *E*' changes only slightly, while E" and tan δ show bigger variations and tan δ for the initial phases follows mainly the progression of the loss modulus *E*".

The focus of the study was on the evaluation of the viscoelastic behavior of the specimen while being modified under a constant temperature. For the test with the longer modification time apart from some signal noise two pronounced discontinuities can be observed at about t = 580 min and t = 750 min. Both cases can be dedicated to an adaptation of the pre load by the system. A consequence of this behavior is that the most effected data E" and tan δ are shifted in such way, that they can't be used for analyzing the thermal modification process (as initially intended) without filtering the original data. However, the application of an appropriate filter seems to be difficult in that case and relevant data would have to be generated before a filter tool could be applied.

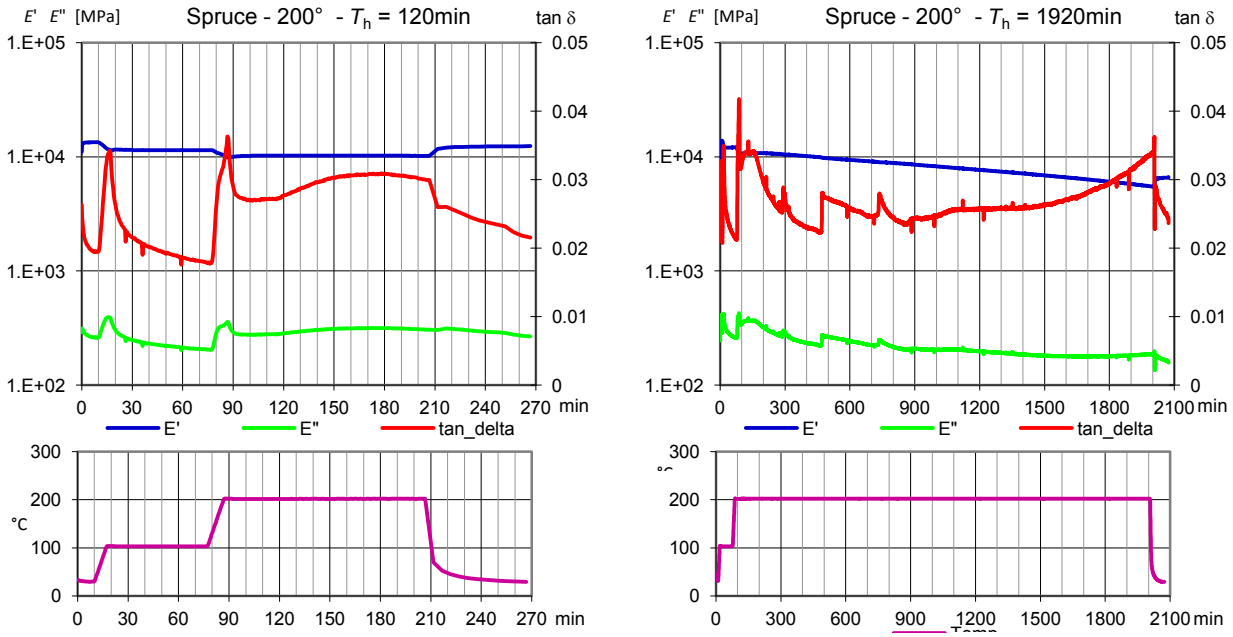

Figure 4— Thermal modifications of Spruce specimens in a TA RSA III Rheometrics System Analyzer with two different holding times T_h.

Other options to avoid such effects are an optimized procedure for the adaption of the pre load or to choose a test set-up that does not require a preload, like clamped 3-point bending. However, both options

aren't without difficulties. For test set-ups that require a preload it is practically always necessary to adapt this preload according to the alteration of the stiffness properties of the material during the test. If the preload wouldn't be changed, pronounced discontinuities like shown above might be avoided. But on the other side pronounced creep might result in this case from excessive (pre) loading and thus also influence the test results in an unwanted way. We weren't able to find a final solution that meets all our needs up to now but the study is being still carried on.

The choice of another test set-up (here: clamped 3-point bending) might help to overcome the mentioned problems that result from the application of a preload. However, it can be expected that other difficulties will play a role. Clamped 3-point bending is compared to tension and normal 3-point bending a system that is statically indeterminate. The clamping can and will lead to the formation of additional stresses if the specimen changes its dimensions during the test, as will be the case for wood that is being thermally modified. In addition the clamping force can be reduced due to the same reason. Anyhow, it will be one of the next steps within the project to evaluate the suitability of this set-up for testing wood.

Case study: observation of thermal wood modification process

In a study the viscoelastic behavior of wood that undergoes a thermal modification was evaluated regarding the influence of time and temperature on the intensity of the modification (Kutnar et al 2013). In the following the evaluation of the influence of temperature is being shown with special regards to the applied methods.

Method

The relevant test parameters are summarized in Table 3.

Table 3 — Test parameters

Parameter	Unit	Details
Wood species		Beech
Test set-up		3-point bending
span	mm	25
Oven gas		air
Temperature	°C	103, 180 – 250 in 10°C steps
Temperature ramp rate	°C/min	0.5, 10
Soak time	min	150, 300, 450, 1080, 2160
Relative humidity at temp.	%	~ 0
Target strain	%	0.02
Auto tension		Activated (compression)
Force control		Static force tracking dynamic force
Static force / dynamic force		1.15
Dynamic load frequency	Hz	1.0
DMA data		Storage modulus, loss modulus, tanδ, temperature, force, displacement, strain, creep
Wood data		Mass, dimensions, density, colour

Results

The following graph (Figure 5) shows the progression of the three parameters storage modulus E', loss modulus E'' and the damping tanδ versus time for beech specimens that were modified under 200°C and 250°C and a soak time of 150 minutes. The modification temperature was reached after 15 minutes (200°C) and 21 minutes (250°C) respectively, which is best indicated by a peak value of tanδ. At the lower temperature both, storage modulus and loss modulus slightly increase until the end of the treatment

while at the higher temperature both values decrease strongly. It can also be observed, that the storage modulus which is practically the Young's Modulus appears to be relatively low.

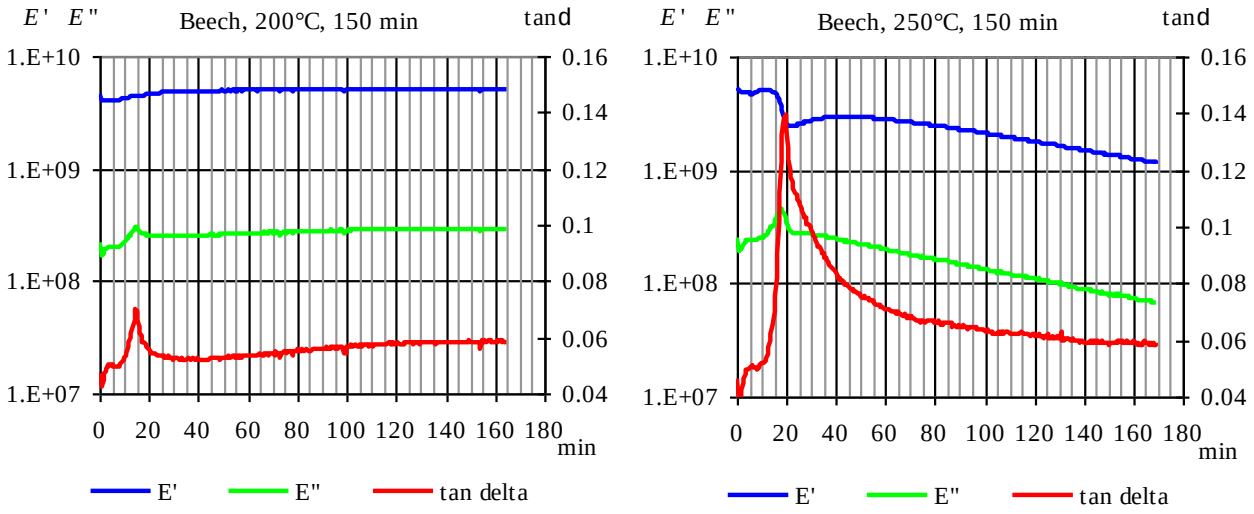

Figure 5— DMA of beech specimens that were subjected to thermal modifications with different holding times. The temperature ramp was conducted with a rate of 10°C/min up to the desired modification temperature.

It has to be mentioned, that the absolute values of the modules have to be converted. The software of the DMA equipment calculates the modules on base of the measured sample compliance C (Eqn. 1) with an assumed constant cross section as entered into the test set-up. Due to shrinkage the cross section $A = w \cdot t$ and the moment of inertia $I = w \cdot t^3/12$ decrease significantly and with this the compliance C increases during the modification. This results in overestimated absolute values of the modules. Table 4 shows the values for one series with beech. In columns c and d it can be seen the loss of mass and density which is more pronounced with elevated temperature. However, the main focus of the study is on the rheometric data that are shown in columns e to l of Table 4. The measured storage modules (also shown in Figure 5) increase for lower temperatures and decrease with higher temperatures over time which can be seen in column g of Table 4. If the storage modulus is corrected according to the reduced cross section the temperature influence is still visible (Table 4, column k).

$$C = g_c \cdot l^3 / (400 \cdot E^* \cdot t^3 \cdot w) \qquad (1)$$

With: C = compliance [mm/kg], g_c = gravitational constant [98.1 Pa/g]
l = length [mm], t = thickness [mm] w = width [mm], E^* = complex modulus [(GPa],

Table 4 — Results of the tests, influence of temperature, 0.02% commanded dynamic strain, B = beech, S = spruce

a	b	c	d	e	f	g	h	k	l
No.	T	δ_{m0}	$\delta\rho_0$	E'_{init}	E'_{fin}	$\delta E'_{app}$	$E'_{fin,corr}$	$\delta E'_{eff}$	$\delta E''_{eff}$
	°C	%	%	GPa	GPa	%	Pa	%	%
B01	200	-5.4	-2.5	5.08	6.23	22.6	7.35	44.7	69.1
B06	210	-8.5	-4.7	7.82	6.53	-16.6	8.06	3.1	4.2
B03	220	-13.7	-4.2	8.27	5.40	-34.7	7.40	-10.5	-7.6
B04	230	-21.5	-10.8	5.90	3.59	-39.2	5.29	-10.3	14.9
B07	240	-25.5	-10.9	8.16	2.83	-65.3	4.65	-43.1	-44.8
B08	250	-33.1	-12.2	5.96	1.46	-75.5	2.94	-50.7	-42.2

δ_{m0} = change of dry mass, $\delta\rho_0$ = change of dry density, E'_{init} = initial storage modulus, measured at 100°C, E'_{fin} = final storage modulus, $\delta E'_{app}$ = apparent change of storage modulus, $E'_{fin,corr}$ = corrected final storage modulus, $\delta E'_{eff}$ = effective change of storage modulus, $\delta E''_{eff}$ = effective change of loss modulus.

Conclusions

Based on preliminary tests on spruce and beech specimens in a DMA equipment the following conclusions could be made:

- DMA is a very sensitive technique for the determination of a materials viscoelastic behavior. Besides its standard use for studying polymers it can also be used to evaluate wood that undergoes changes in material properties due to thermal modification/degradation.
- From the variety of available test set-ups tension and 3-point bending configurations proved to be well suitable for testing wood.
- The importance of several test parameters, like static preload and auto-stress level, and their influence on the results was demonstrated and discussed. The study is in a too early stage to be able to give final recommendations for an optimum parameter setting.

References

Backman A.C. and Lindberg K.A. (2001). Differences in wood material response for radial and tangential direction as measured by dynamic mechanical thermal analysis. Journal of Material Science 36, 3777 - 3783

Birkinshaw M., Buggy M. And Henn G. G. (1986). Dynamic mechanical analysis of wood. Journal of Materials Science Letters 5, 898 - 900

ISO 6721-5 (1996). Plastics – Determination of dynamic mechanical properties – Part 5: Flexural vibration – Non-resonance method. International Organization for Standardization, Geneva, Switzerland

Kutnar; A., Widmann; R., Brémaud I. (2013) Preliminary studies for use of dynamic mechanical analysis (DMA) to verify intensity of thermal wood modifications. International Wood Products Journal, DOI: http://dx.doi.org/10.1179/2042645313Y.0000000044

Menard, K (2007). Dynamic mechanical analysis: A practical introduction. 2nd Edition, CRC Press, Boca Raton, USA

Salmén, L. (1984). Viscoelastic properties of in situ lignin under water-saturated conditions. Journal of Materials Science. 19: p. 3090-3096.

Development of a grain angle meter to measure slope-of-grain on wood objects such as baseball bats

Harry E. Moore
Researcher, R&D, Metriguard Inc., USA, harrym@metriguard.com

Ryan D. Baldwin
Researcher, R&D, Metriguard Inc., USA, rbaldwin@metriguard.com

Abstract

The correlation between wood grain angle and strength and stiffness in both tension and bending has long been understood. A proven method for the measurement of this grain angle is by sensing the direction of the maximum dielectric constant of a wood specimen.

In order to determine the grain angle of a cylindrical, or conical wood object, a hand-held meter has been developed with a guide system designed to track the curved surface. These guides keep the dielectric sensor both parallel to the axis and tangent to the surface of a cylindrical wood object. To accurately track a conical surface as found on baseball bats, these guides are allowed to float with respect to the meter body. In addition, the optimum dielectric sensor footprint was discovered following experiments with various sizes, shapes and curvatures for the sensor.

Finally, and in the case of baseball bats, the diameter of the dielectric sensor was optimized to track the grain angle along the bat's handle, which is the narrowest section of the bat, and consequently the most susceptible location for failure.

These grain angle meters are now being successfully employed by baseball bat manufacturers to produce the strongest bats possible.

Keywords: bat testing, grain angle, dielectric sensor, slope of grain, grain angle meter, Metriguard Model 512

Background

While school and amateur baseball have migrated to aluminum and composite bats, tradition-bound professional baseball has used wooden bats throughout its history. One downside of wooden bats is their susceptibility to failure upon impact with the ball. Bat failures sometimes result in multiple pieces which can endanger personnel both on and off the field. Pieces from multiple piece bat failures have become projectiles which have caused serious injury to spectators and players alike.

An increased number of multiple piece failures of wood bats in Major League Baseball led to an investigation of the cause. Evaluation of the trend revealed a higher incidence of multiple-piece failures of bats made from sugar (hard rock) maple. Examination of the fracture line of most multiple piece

failures revealed slope-of-grain, or grain angle, greater than a few degrees on the tangential face of the bat, to be the major contributor to the failure (Hernandez 2009) (Figure 1.)

Figure 1−Example of a multiple piece bat failure, showing high slope-of-grain along the bat's fracture surface.

Traditionally, bat stock was cut by splitting the wood which resulted in the surfaces of the stock aligning with the grain angle. This method resulted in excellent grain angle alignment in the finished bat. However, sawing the stock is now more common; this method is insensitive to the grain angle and yields finished bats with more irregular grain angle.

Another consideration affecting the performance of wood bats is the orientation of the grain with respect to the impact surface. The tangential face is the preferred face to contact the ball as the impact strength of wood is highest on this face. (The radial face is the preferred face on ash bats as they have a tendency to separate at growth rings if hit on the tangential face.) The grain angle on the radial face is the major determiner of the impact strength on the opposite or tangential face and vice versa. Under real world conditions, the strength of both faces comes into play as the ball may strike the bat off center and/or the player may hold the bat at a sub-optimal angle.

It is well known that the strength of wood decreases dramatically with an increase in the grain angle relative to the long axis of a wood member (Forest Products Laboratory 2010b). Researchers determined that limiting the grain angle to 1 in 20 (< 3 degrees) or less would result in significantly fewer maple bat failures (Forest Products Laboratory 2010a.)

Limiting the slope-of-grain in wooden objects requires the ability to see and measure grain angle within a range of only a few degrees. Some species of wood, like white ash, are ring-porous and have large enough grain structure to readily see grain angle alignment with the bat. Unfortunately, some species used to make baseball bats, such as maple and birch, are diffuse-porous species and are so tight-grained that grain angle on the tangential face is not visually discernible. A method was devised to measure the grain angle on the tangential face of diffuse-porous sugar maple and yellow birch bats which involves placing a dot of ink on the tangential face and using a protractor to measure the direction of the ink flow along the grain (Roberts 2012). This measurement method is simple and economical, but it is slow, susceptible to interpretation and mars the specimen. In addition, the grain angle of these diffuse-porous species may vary significantly by several degrees along the specimen length and even within the width of the ink blot. Using a single, small ink blot, therefore, may not be the best method for identifying bats with slope-of-grain that contribute to multiple piece bat failure. Another shortcoming of the ink blot test

is it must be done before finishing. Evaluation after manufacture is limited to only the initial ink blot if the bat has a clear finish, or not at all if the surface is stained or painted.

The difficulties with the measurement of slope-of-grain on the tangential face of diffuse-porous sugar maple bats led to the development of an instrument to measure the grain angle on a straight or tapered cylindrical wood object to reduce multiple piece failures of wood baseball bats in Major League Baseball.

Grain Angle Meter Development

With the development of an accurate and repeatable instrument to measure the grain angle of a flat wood specimen using a dielectric sensor (Bechtel and Allen 1997), it was a logical extension of this technology to apply it to curved wood surfaces such as bats, pool cues, golf clubs and the like.

This grain measurement technology is based on the difference in dielectric constant of wood between the parallel direction (lower dielectric constant) and perpendicular (higher) to the grain (USDA 2007.) The dielectric constant is simply the ability of a material to concentrate an applied electric field. Measuring dielectric constant can be as simple as measuring the current flow between two conductors with an alternating voltage applied. The grain angle meter compares the currents measured between a series of conducting surfaces when a rotating electric field is applied. Comparing these currents results allows an accurate determination of the grain angle relative to the axis of the instrument.

The challenge has been adapting the flat dielectric sensor plate to allow it to maintain contact with, and track along, a curved surface. To measure the grain angle of a curved surface, a series of dielectric plates of differing dimensions and curvatures was examined. If was found that the curved sensors, while best at maintaining close tracking to the specimen, were influenced by the grain angle perpendicular to the direction being measured. In other words, the tangential and radial grain angles of the specimen could not be isolated. Elliptical sensors were tested but found to distort the symmetry of the electric field and gave no advantage.

The final instrument design (Figures 2 and 3) includes a small, square dielectric plate that was found to be best suited to concentrate the electric field at the axis of contact between the instrument and the specimen. A spring loaded V guide allows the operator to press the instrument to maintain intimate contact with the curved surface. A calibration procedure was developed to correct distortion of the angle displayed caused by the curved surface.

The Metriguard Model 512 Grain Angle Meter design allows the grain angle meter to average the angles of all grain directions in approximately 1” diameter and 1/8” below the surface. Surface penetration allows the use of the grain angle meter on bats and other wood objects that have been previously surface treated with stains, varnishes and paints. Testing has revealed that not all black paints are compatible with the meter.

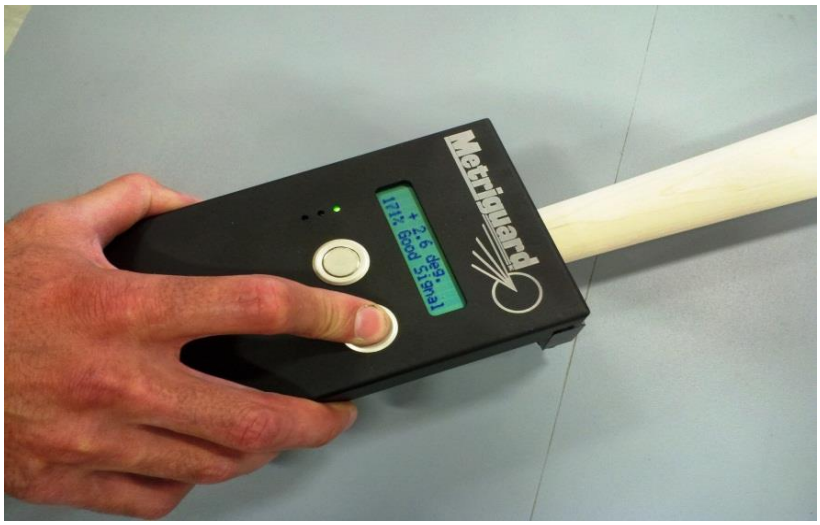

Figure 2—The Metiguard Model 512 grain angle meter in use on the handle of a baseball bat. Continuous readings can be taken as the instrument is moved along the bat.

Figure 3—Bottom view of meter showing the square sensor plate and spring loaded V specimen guides.

Grain Angle Meter Evaluation

Evaluating this technology is challenging because of the difficulty of establishing the “true” grain angle of a specimen. Grain angle varies over even short sections of wood specimens and each specimen has unique grain patterns so establishing a baseline to compare measurement methods is problematic.

The ink blot test for grain angle, which can be a simple but effective method of finding this “true” angle, is limited by the fact that grain angle may vary significantly in a very small area. The ink blot is about the size of a small coin and within that area the grain angle can vary by several degrees (Fig 4). Choosing a line to measure the grain angle on is subjective and may not be consistent over multiple evaluations. Further, the ink blot test measures grain angle in only one dimension and is therefore not able to recognize changes in grain angle below the wood surface. The ink blot test is an easy and economical method of measuring grain angle at a single point on the surface of a wood element but is not as useful in determining the grain angle of a larger area.

Figure 4—An ink blot reveals wood grain angle which can vary within even a small area.

The Model 512 Grain Angle Meter addresses the issue of localized grain variation by averaging readings over a one inch diameter sensor. In addition, the dielectric sensor includes evaluation of grain angle to a depth of approximately 1/8” so some component of the grain angle below wood surface is included in the measurement. Comparison of the ink blot measurement and the dielectric meter measurement requires that specimens with visually consistent grain angle be selected.

Another issue arises when trying to measure the grain angle of a fractured wood specimen to determine the” true” grain angle. Firstly, grain angle in a wood element can vary significantly along its length.

Figure 5 shows a fractured section of a maple dowel after impact testing which exhibits significant changes in grain angle along the length of the piece.

Secondly, when subjected to bending forces, a wood specimen is warped which inserts a bias in the measurement. It is possible to gain an approximation of this bias angle by noting the warp angle of the outer edge of the sample near the breaking point and subtracting this angle from the angle of the fracture. Determining the "true" grain angle of a wood specimen is a subjective process and as such, assessing the performance of the dielectric grain angle meter requires careful selection of test materials and methods.

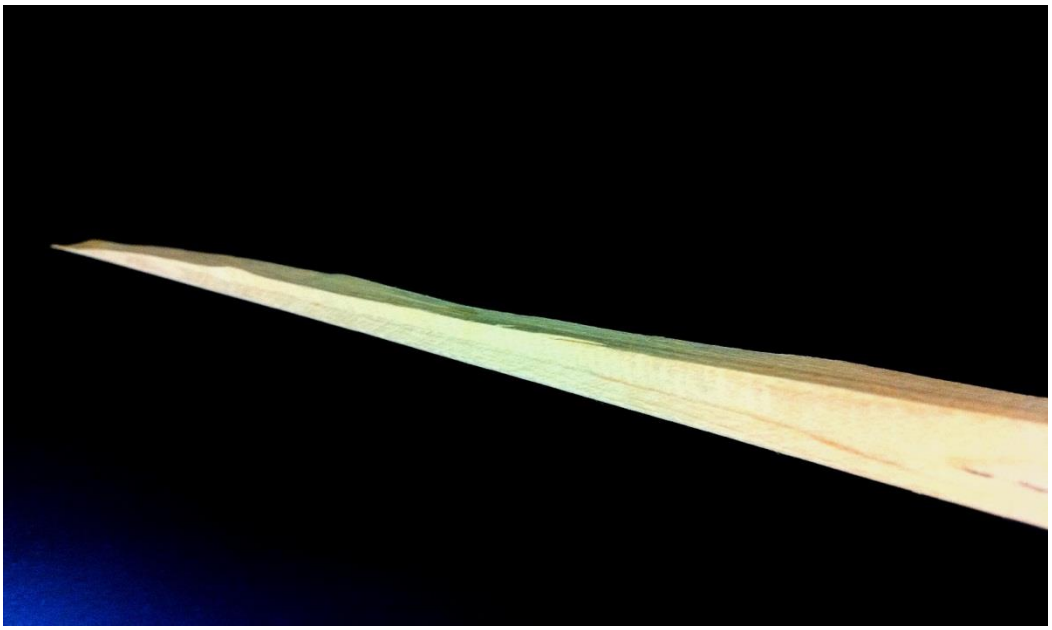

Figure 5—A fractured wood specimen after impact testing demonstrating the significant changes in grain angle along the length.

A study was conducted to compare the ink blot measured slope-of-grain with that measured by the Model 512 grain angle meter. Twenty 1" maple dowels were selected for the study. In order to try to minimize the presence of localized grain angle variation, a section of each dowel which was visually consistent was selected for the application of the ink blot. The ink blot was applied on the tangential face of the dowel, revealing the grain angle for measurement with a protractor. The grain angle meter was placed on the dowel over the ink blot at the same location. Grain angle measurements for each dowel using the two different measurement methods were found to be very comparable (Fig 6).

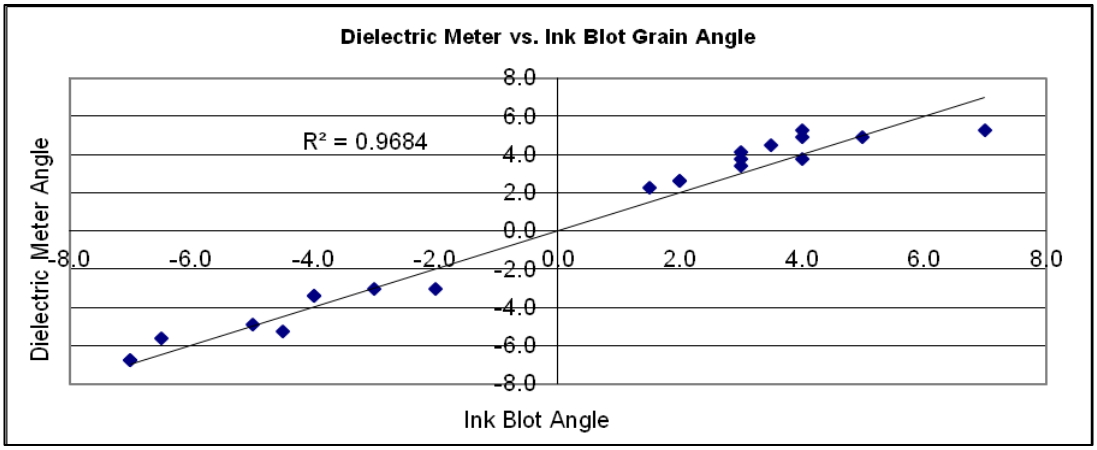

Figure 6—Comparison of 20 grain angle measurements on one inch maple dowels made with a dielectric meter and an ink blot test.

Another method of evaluating the performance of the dielectric grain angle meter involves inducing fracture along the grain of a wood specimen and measuring the grain angle of the fractured face and comparing the measurement with the reading from the meter. Figure 7a demonstrates the use of the Model 512 on a 1" maple dowel, indicating slope-of-grain of 6.3 degrees. Figure 7b shows approximately 6 degrees slope-of-grain along the fracture face of the same 1" maple dowel after impact testing.

Figure 7a—The dielectric grain angle measurement on a 1" maple dowel.

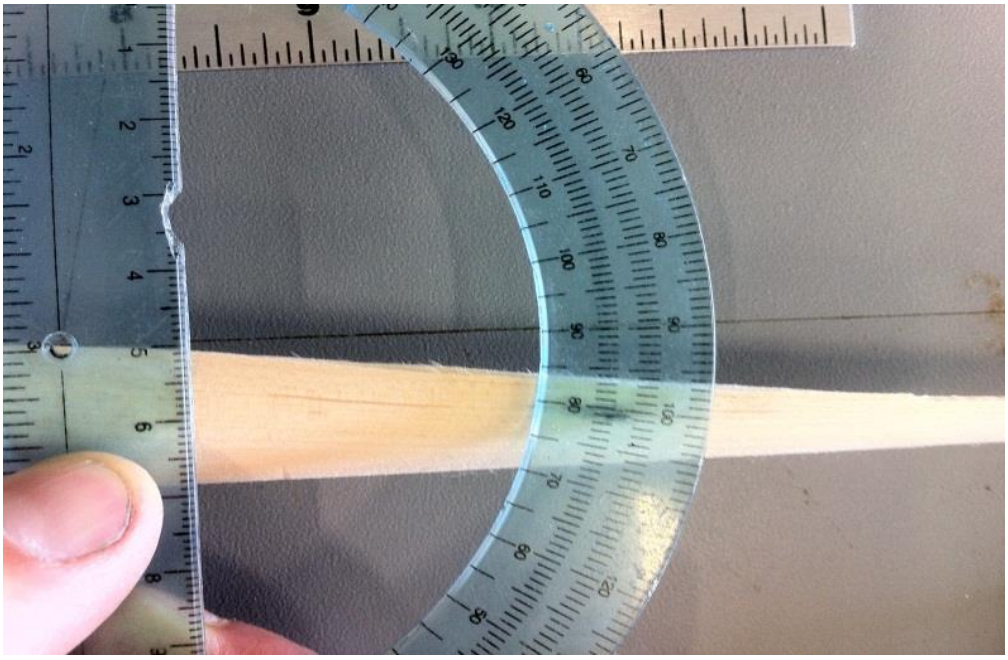

Figure 7b—A protractor was used to measure the fracture angle of the same 1" maple dowel after impact testing.

In one study on square billets stock used in the manufacture of pool cues, testing was conducted to verify the predictability of the fracture angle on flat stock taken to failure against the average grain angle measured by the dielectric meter. Figure 8 shows good correlation between the dielectric grain angle measurement and fracture angle measurement.

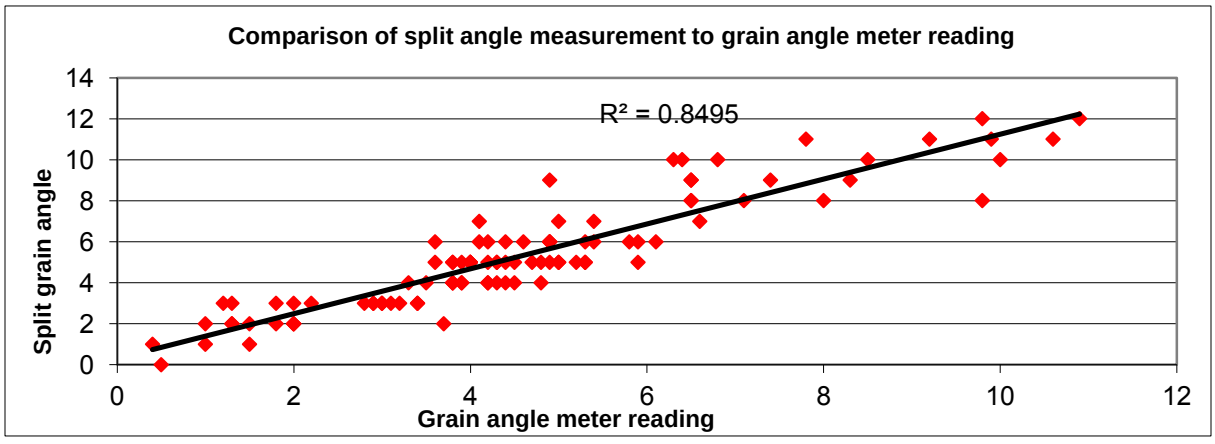

Figure 8— Comparison of grain angle measured by a dielectric grain angle meter and fracture angle measurement after impact testing.

Conclusions

A dielectric grain angle meter that will quickly and reliably measure grain angle on straight and tapered cylindrical wood objects has been developed (Metriguard Model 512) based on previous technology which is used in a grain angle meter for flat surfaces (Metriguard Model 511). The new device can make accurate and reliable measurements of grain angle which can be used to predict strength performance of dowels, tool handles, pool cues, baseball bats and other sports equipment. Measurements with the grain angle meter have been found to compare well with grain angle measurements from both ink blot tests and along the fracture face of wood specimens after impact testing.

The Model 512 addresses shortcomings of the ink blot testing adopted and mandated by Major League baseball for the purpose of reducing multiple piece bat failures and improving safety. In contrast with the ink blot test, the meter samples grain angle over a larger area, is not limited to a single, subjectively selected line to measure the grain angle, and easily allows multiple readings in the area of interest. Evaluation of grain angle after finishing is also possible with the dielectric grain angle meter in contrast with the ink blot which cannot be evaluated when covered by stains or paints. Use of the meter leaves no marks that would detract from the appearance of the wood product.

Using the Model 512 dielectric grain angle meter allows for checking grain angle of baseball bats at all stages of manufacture and use which can help reduce multiple piece bat failures and improve safety for Major League baseball.

References

Baldwin, R., Logan J., and Moore H., (2012), *Method and Apparatus for Measuring the Grain Angle of a Round Wood Object*, U.S. Patent Application No. US20120146617 A1.

Barringer, Felicity, (2013), *Science Lowers Shattering Risk at Home Plate*, The New York Times July 25, 2013.

Bechtel, F., and Allen, J. (1987). *Methods of Implementing Grain Angle Measurements in the Machine Stress Rating Process.* Proceedings of the Sixth Nondestructive Testing of Wood Symposium, Washington State University.

Bechtel, F., Allen, J., and Logan, J. (1990). *Apparatus and Method for Measuring Wood Grain Angle*. U.S. Patent No. 4,972,154.

Bechtel, F., Allen, J., and Logan, J. (1997). *Dielectric Sensor Apparatus*. U.S. Patent No. 5,654,643.

Forest Products Laboratory, (2010a), *Strengthening America's Pastime, Scientists Work to Keep Baseball Players and Fans Safe*, FPL press release.

Forest Products Laboratory. (2010b). *Wood Handbook – Wood as an Engineered Material*. Forest Products Laboratory General Technical Report FPL-GTR-190.

Green, D.W. (2001). *Wood: Strength and Stiffness*. USDA Forest Products Laboratory, Madison, WI. USA.

Hernandez, R., (2009), *Review of 2009 Baseball Bat Regulations*, RockBats, LLC Technical Note.

Roberts, Quinn, (2012*), Huge strides being made in reducing broken bats*, MLB.com

US Dept. of Agriculture, (2007), *The Encyclopedia of Wood*, Skyhorse Publishing, New York, NY

Methods disclosed in this paper are the subject of pending U.S. patent claims and prospective foreign patent rights.

Development of a portable hardness tester for wood using displacement transducer

Adriano Ballarin
Department of Rural Engineering, College of Agronomical Sciences, Botucatu, Sao Paulo, Brazil, awballarin@fca.unesp.br

Albert Assis
Graduate Student, College of Agronomical Sciences, Botucatu, Sao Paulo, Brazil, albert_assis@fca.unesp.br

Hernando Lara Palma
Department of Forest Sciences, College of Agronomical Sciences, Botucatu, Sao Paulo, Brazil, larapalma@fca.unesp.br

Abstract

Hardness is largely used in material specifications. Specifically for timber, Janka hardness is traditionally performed by quantifying the necessary force to promote a predefined indentation of a small steel sphere in wood, in a simple, quick and easy test. More recently, international studies have reported the use of Brinell hardness for timber quality assessment in field conditions, especially due to the lower magnitude of the involved force. Two generation of portable equipment with these purposes were already developed by the Research Group on Forest Products from FCA/UNESP, Brazil for dynamic evaluation of hardness, with very good correlations with Janka hardness and several other mechanical properties of the material. This paper presents results obtained in the development of the third generation of this equipment, which uses displacement transducer in order to automate the indentation evaluation in wood. Functional tests of the equipment were carried out using seven species of Eucalyptus. Results already obtained revealed strong correlation to Janka hardness and confirmed the potential of the equipment in the classification of wood.

Keywords: Janka hardness, Brinell hardness, portable equipment, displacement transducer

Introduction

Hardness is largely used in material specifications. Among the major strength properties of wood, hardness reveals its potentialities (good correlation to other mechanical properties and quickness of results) and can be used as a non-destructive tool in the characterization of species from reforestation (Ibama 1993, Colenci 2002).

General methods to evaluate hardness in materials are gathered in two major groups (Holmberg 2000). In the first one, hardness is evaluated by the required force to promote a defined surface indentation (penetration) of a piece (a metal sphere, e.g.). The well known Janka hardness uses this principle. In the second group hardness is evaluated in terms of the indentation (deformation) promoted by a particular piece that is forced at the surface of the material with a pre-defined force. The dimensions and shapes of the pieces and the magnitude of the force are determined by the method adopted.

For evaluation of hardness in wood, considering its viscoelastic properties, especially its resilience, and its low elastic modulus to yield stress ratio (E/Y) perpendicular to the grain, one can easily note greater appropriation of Janka hardness when compared to Brinell hardness. When the force that

promoted the indentation is removed, the material automatically recovers the elastic part of the total deformation applied, and, for Brinell hardness, the evaluation of the indentation (usually the diameter of the spherical shape at the surface of the material) maybe imprecise, unless the measurement is performed immediately before the force is removed.

Despite the major appropriation of Janka hardness to wood measurements several researchers (Colenci 2006, Bektas et al. 2001) have suggested Brinell method for the evaluation of hardness in wood in field condition, considering the lower magnitude of the forces involved in the indentation and the additional difficulty to control, the depth of the metal sphere indentation required on Janka hardness method.

Two generation of a portable equipment with these purposes were developed by the Research Group on Forest Products from FCA/UNESP, Brazil for dynamic evaluation of hardness in wood - Portable Hardness Tester for wood - DPM.

The first generation of this equipment was reported as a low cost tester - when compared to commercially available alternatives – with great functionality in the operation; in addition, showed good correlation with the results of Janka hardness and good performance in timber classification process (Colenci 2006, Ballarin et al. 2010, Ballarin et al. 2012).

The second generation was developed with the main objective of automate the indentation evaluation using accelerometers. The results also revealed a possible association of the acceleration, velocity and displacement of the equipment to viscoelastic parameters of the timber (Ballarin et al. 2012), however some limitations were observed, mainly imposed by the technique of indirect evaluation of indentation (by integration) used.

This paper presents results obtained in the development of the third generation of this equipment – DPM 3 - which uses displacement transducer in order to automate the indentation evaluation in wood.

Material and Methods

The Portable Hardness Tester - DPM-3 (Figure 1) – patents pending - is an electro-mechanical equipment whose operating principle is similar to Brinell hardness test, i.e., a cap with spherical format and known diameter is indented into wood using a known energy. In this case, energy mobilized to promote indentation is obtained by the free fall of a mass and the hardness value is determined by the relationship between the energy used and the area of the spherical surface that will be printed on the material evaluated (indentation) according to the expression:

$$H = \frac{E}{\pi.D.h} \quad (1)$$

where H is hardness strength ($kJ.m^{-2}$), E is the energy resulted from the fall of the mass (kJ), D is the diameter of the metal sphere (m) and h is the deep of the indentation promoted (m).

The measurement of the indentation is made by a displacement transducer connected to an electronic circuit responsible for signal processing, calculation and immediate display of hardness.

Seven species of eucalyptus were used to perform the experimental tests. Sixteen specimens (5cm x 5cm x 15cm) were obtained for each specie evaluated, totalizing 112 specimens. Table 1 presents the major characteristics of the wood species analyzed.

The Janka hardness tests were performed in the direction perpendicular to the grain of wood on a universal servo controlled testing machine EMIC, model DL 30000, following, in general, the

requirements of the NBR 7190 (ABNT, 1997). Hardness H was estimated alternatively by the Portable Hardness Tester – DPM3 using Equation 1.

Figure 1 – Portable Hardness Tester – DPM-3 – a) general view; b) operation; c) detail of the digital display, showing the hardness H and the indentation.

Table 1 - Main characteristics of the groups of Eucalyptus wood

Group	Specie	Age of the Plantation (years)	Average density(*) ($kg.m^{-3}$)
1	*E.maculata*	35	810
2	*E.microcorys*	35	770
3	*E. tereticornis*	40	950
4	*E. citriodora*	44	980
5	*E. saligna*	50	690
6	*E. dunnii*	20-23	750
7	*E. viminalis*	20	720

(*) – Apparent density based on mass and volume at 12%MC – values reported by suppliers

Results and Discussion

Using the displacement transducer, the Portable Hardness Tester DPM-3 promoted fast and easy readings, revealing consistent values of indentation. Immediately after the indentation, the value of hardness H (Equation 1) provided by the software was displayed.

The indentation was determined under load (and not on unloading), avoiding the influence of the recovery. Furthermore, by measuring the indentation instead of the indented area, the DPM3 avoided "sinking in" phenomenon effects. Both, recovery and "sinking in" effects were reported by Doyle and Walker (1985) as limitations of the conventional Brinell hardness tests for wood.

Table 2 presents descriptive statistics of the measurements of Janka and Portable Hardness Tester – DPM3 hardness.

Table 2 — Descriptive Statistic of hardness measurements

Descrip. Stat.	Hardness Janka (MPa)	Portable Hardness Tester-H ($kJ.m^{-2}$)
Mean	68,53	41,69
Sd	24,34	7,43
Min	26,70	26,10
Max	135,40	56,21
CV	35,53	17,83
N	112	112

Relating to results from Tables 2, it is observed lower coefficient of variation (CV) of the results obtained from the Portable Hardness Tester (17.83). Results from conventional Janka hardness tests presented almost the double variation. In a first moment, this occurrence could be associated to low sensitivity of the equipment to technological differences presented by species. Despite this, strong correlation was obtained in the association showed in Figure 2.

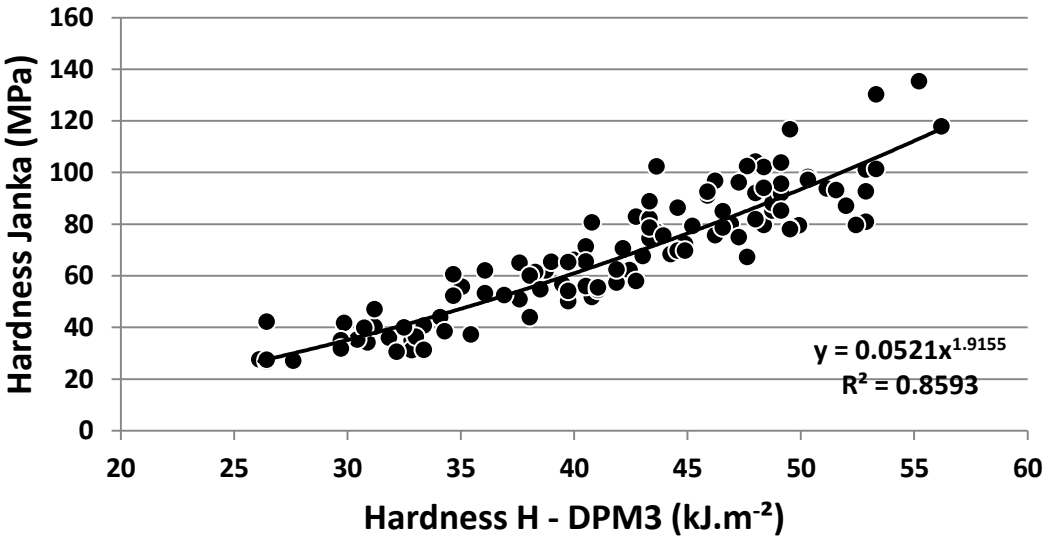

Figure 2: Hardness Janka versus Hardness H evaluated by the Portable Hardness Tester – DPM3

The determination coefficient (R^2) expressed moderate to strong association between hardness H (DPM3) and conventional hardness Janka, that was in the same magnitude of those obtained by Ballarin et al. (2012), Colenci (2006) and Bektas el al (2001).

Figure 2 shows a greater dispersion of the results for higher levels of hardness, that may be attributed to the rational function [$f(x)=k.x^{-1}$] that governs Brinell hardness and particularly the hardness H

(Equation 1). In fact, for higher levels of hardness (lower indentations levels, in other words) minor variations in the indentation promote large variations in the hardness value.

It can also be observed that the correlation between Janka and H hardness was not linear. One possible approach to this occurrence can be pointed considering the increasing compression zone of compressed wood beneath the indenter, reported by Doyle and Walker (1985). Wood requires less resistance to indenter in initial levels of indentation as the compression level of the fibers at this stage is still low. To the extent that the fibers will compress, one compression zone is created beneath the indenter, thereby increasing the resistance to indentation. This phenomenon, mobilized by Janka test (indentation of 5.64mm) but not by the test using Portable Hardness tester (lower indentation levels, as can be seen in Table 3) was particularly observed in the load-displacement diagram of Janka test for harder woods.

Table 3 – Descriptive Statistic of the indentation promoted by DPM-3

Descrip. Stat.	Indentation (mm)
Mean	1.55
Sd	0.31
Min	1.11
Max	2.39
CV(%)	19.83
N	112

As already mentioned, the values of indentation reported in Table 3 were evaluated under load and in the first indentation (used on the evaluation of hardness H), once the equipment monitored the full phenomenon of the indentation, from the first indentation to the full damping. Mean indentation was 1.55mm (varying from 1.11 mm to 2.39mm), considerably lower than the fixed indentation of 5.64mm, utilized on Janka test – conventionally adopted as the radius of a circle with diametrical area of $1cm^2$.

Looking for a better understanding of the relationship between the hardness H and the Janka hardness a new association between the results was evaluated and presented in Figure 3, considering the Janka hardness obtained with the half indentation adopted conventionally by the Janka test in international standards. As mentioned by Helinska-Raczkowska and Molinski (2003), the Polish standard PN 90/D-04109, in accordance with International Standard ISO 3350-1975E, admits Janka Hardness test with half the original indentation, i.e., 2.82 mm, considering that with the full indentation (5.64mm) there is the possibility of wood rupture around the indenter, fact that has been observed in some tests of this experimental program with Janka tests.

This new association revealed a stronger correlation ($R^2 = 0.913$) and a lower dispersion of results, when compared to those observed in Figure 2. These results reinforced the original proposal of the equipment to perform indentations shallower than those promoted by Janka test.

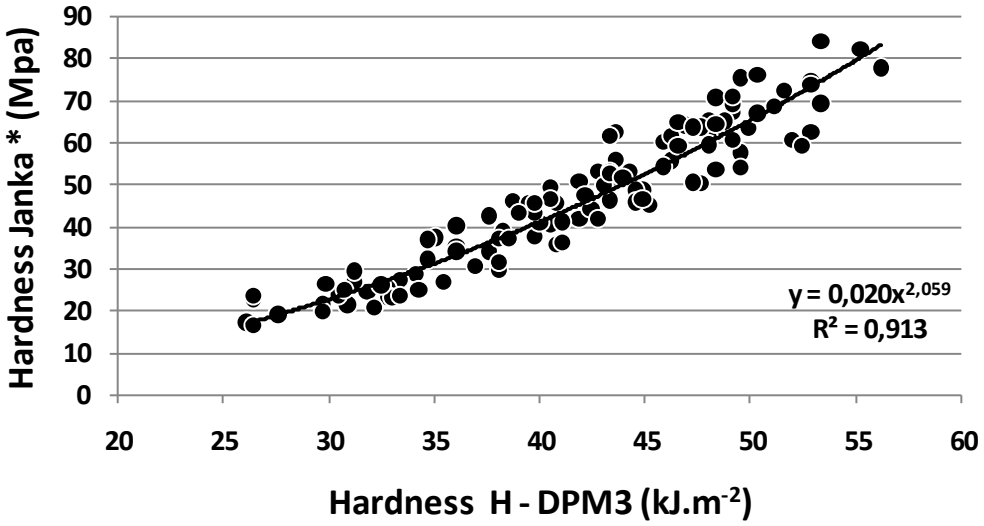

Figure 3: Hardness Janka* (indentation of 2,82mm) versus Hardness H evaluated by the Portable Hardness Tester – DPM3

Conclusions

From this experimental program to test a Portable Hardness Tester with displacement transducer the following main conclusions can be established:

- The Portable Hardness Tester – DPM3 promoted fast, easy and reliable readings of the indentation, as well as evaluation of hardness H;
- The classical problems of Brinell hardness of the "sinking in" phenomenon and the recovery of indented area were solved by the equipment using under loading measurement of the indentation (and not of the indented area);
- Hardness H measured from the equipment revealed moderate to strong association to conventional Janka Hardness (R^2=0.86) and strong association to Janka test performed using indentation of 2.82mm (R^2=0.91)

Acknowledgments

The authors express their gratitude for the financial support given by FAPESP – Sao Paulo State Agency for the development of this project (08/08414-0) and by Energy in Agriculture Graduate Program –FCA/UNESP – Sao Paulo State University.

References

Associação Brasileira de Normas Técnicas. 1997. Projeto de estruturas de madeira. NBR 7190. Rio de Janeiro.

Bektas, I.; Alma, M.H.; As, N. 2001. Determination of the relationships between Brinell and Janka hardness of eastern beech (Fagus orientalis). Forest Products Journal, 51(11/12):.84-87.

Ballarin, A. W.; Almeida, P.A.O.; Lara Palma, H.A., Colenci, R. A. 2010. Portable hardness tester for timber classification. In: WCTE 2010 – Word Conference on Timber Engineering, 8p.

Ballarin, A.W.; Almeida, P.A.O.; Lara Palma, H.A. 2012. Estimating hardness of eucalyptus wood with a portable hardness tester. In: WCTE 2012 – World Conference on Timber Engineering, 4p.

Colenci, R.A. 2002. Qualificação mecânica de madeiras para uso como dormente ferroviário. Botucatu, SP: Sao Paulo State University, 90p. M.S. thesis.

Colenci, R. A. 2006. Desenvolvimento de equipamento para avaliação em campo da dureza de madeiras para dormente ferroviário. Botucatu, SP: Sao Paulo State University, 83p. PhD thesis.

Doyle, J.; Walker, J.C.F. 1985. Indentation hardness of wood. Wood and Fiber Science. 17(3): 369-376

Helinska-Raczkowska, L.; Molinski, W. 2003. The effect of the Janka ball indentation depth on the hardness number determined for selected species. Folia Forestalia Polonica. 34: 27-36

Holmberg, H. 2000. Influence of grain angle on Brinell hardness of Scots pine (Pinus sylvestris L.). Holz als Roh-und Werkstoff. 28: 91-95

Instituto Brasileiro do Meio Ambiente e dos Recursos Renováveis. 1993. Amostragem e propriedades físico-mecânicas de madeiras amazônicas. Brasília: IBAMA, Coleção Meio Ambiente – Serie estudo floresta, nº 1.

Contactless high precision measurement of deformation in wood without artificial markers

Alfred Rinnhofer
JOANNEUM RESEARCH, Machine Vision Applications, Steyrergasse 17, 8010 Graz, AUSTRIA,
alfred.rinnhofer@joanneum.at

Jean-Philippe Andreu
JOANNEUM RESEARCH, Machine Vision Applications, Steyrergasse 17, 8010 Graz, AUSTRIA,
jean-philippe.andreu@joanneum.at

Abstract

Precise, contactless, area-wide and real-time measurements of wood deformations are essential to the wood research community. Instead of of traditional measuring devices (strain gauges, extensometers, etc...), high resolution digital cameras can be used to very precisely track the motion of the wood under testing load. Using a calibrated stereo rig even enables evaluation of wood deformations in 3D. The implementation of motion tracking algorithm of the wood texture on dedicated parallel computing platforms allows getting real-time measurements. Such a measuring system also has the advantage to be easily integrated in existing testing environments.

Keywords: precise, contactless, area-wide, real-time, 3D measurements, digital cameras, stereo, calibration, motion tracking

Introduction

In many applications, a precise, contactless, area-wide and real-time measurement of wood deformations will bring essential knowledge on wood structural parameters. The field of applications goes from laboratory evaluation to inline testing in industrial proof loading machines.
High resolution digital cameras are used to take images of the wood surface and track the motion of its surface. Existing measurement systems are also featuring digital cameras but do require markers or sprayed patterns on the surface under inspection in order to work properly. The system presented in this paper does not need those means: the natural wood texture under proper illumination combined to the tracking of densely sampled surface points allows a precise computation of the surface motion.
Between image frames, either the minimal displacement of every single tracked point of interest (local deformations), or the relative motion from distant (up to several tenth of meters) wooden parts (global deformation) can be measured in real time. Resolution, accuracy (in μm range) and the size of the observed area are dependent of the camera models and lenses used.
Depending on the speed, accuracy and stability required, different tracking algorithms can be selected.
While positioning multiple cameras along a wooden beam during a stress test will provide an elongation profile thus enabling the identification of the weakest beam section, using a stereo rig enables evaluation of deformations in 3D. Depending on the wood species and surface treatment, proper illuminations will be applied to improve the image quality thus facilitating the detection of the surface points of interest.
In this paper, through two different applications, we will demonstrate the effectiveness of our image processing methods for computing global and local deformations on wooden surfaces. We will present results on accuracy and speed and point out possible future fields of application.

Computing Motion

Computing object motion over a series of digital images could be performed by tracking its trajectory over that series of images. In its simplest form, tracking can be defined as the problem of estimating the trajectory of an object in the image plane as it moves around a scene. An object is generally not tracked as a whole but instead a representative set of features derived from its appearance.
The two key components to any feature tracker are accuracy and robustness. The accuracy component relates to the local accuracy of the tracking while the robustness component relates to sensitivity of the tracking with respect to changes of lighting, motion, etc… Intuitively, in order to handle large motions, one would preferably consider a large tracking area but the cost of local accuracy. There is therefore a natural tradeoff between local accuracy and robustness when choosing the size of the tracking area.

Motion Models

As the object moves the intensity of its image representation change in a complex way. Two motion models are usually considered: a purely translational one when the inter-frame displacements are small and an affine one (more capable of handling image warping) otherwise. In our case, since the objet motion compared to the frame rate is rather small (small inter-frame translation), we will adopt a pure translational model.
We have to mention that opting for a somewhat simpler translational model does not equate with a reduced accuracy. It has been shown that attempting to determine affine deformation parameters in the case of small inter-frame translation is not only useless but can lead to poor solutions (Tomasi and Kanade 1994).

Computation

Assuming small inter-frame displacements, the tracking can be performed by optimizing some matching criterion with respect solely to translation. As shown in (Lucas and Kanade 1981) given two successive images *I* and *J*, computing the displacement vector $\vec{d}$ at the position *x* over the area Ω it done by minimizing the residual error ε:

$$\varepsilon = \int_{\Omega} \left[I\left(x - \vec{d}\right) - J(x) \right]^2 w \, dx \qquad (1)$$

Note that in this expression, *w* is a weighting function and could be set to 1.0 or alternatively, could be a Gaussian-like function that emphasizes the central area of the integration window. In practice, to get an accurate solution, it is necessary to iterate multiple times on this minimization procedure (in a Newton-Raphson fashion). At each step *i* of the procedure, the area Ω is translated by the current displacement vector $\vec{d}_i$ computed by Equation (1), until a convergence is finally reached. In order to keep all computation at a sub-pixel accuracy level, it is necessary to be able to compute brightness values of Ω at locations between integer pixels. For that purpose bilinear interpolation is used.
That iterative implementation of the optical flow computation algorithm proposed by (Lucas and Kanade 1981) provides a good local tracking accuracy.

Aperture Problem

Optical flow is the apparent motion of brightness patterns in the image. Generally, the optical flow corresponds to the motion field, but not always. We are only able to measure the component of optical flow that is in the direction of the intensity gradient but not the component tangential to the intensity gradient. This ambiguity is known as the *aperture problem*. For instance, if the motion field of a wooden beam is purely longitudinal along its grain (i.e. tangential to the intensity gradient), the optical flow could

not measure the motion. So, in order to eventually alleviate that problem, some other periodic features than medium/low frequency patterns (like the grain) could be used. For instance the surface of rough sawn timber offers a lot of rapidly changing patterns (high frequency patterns) which can be used to help solving that *aperture problem* of the optical flow.

Illumination

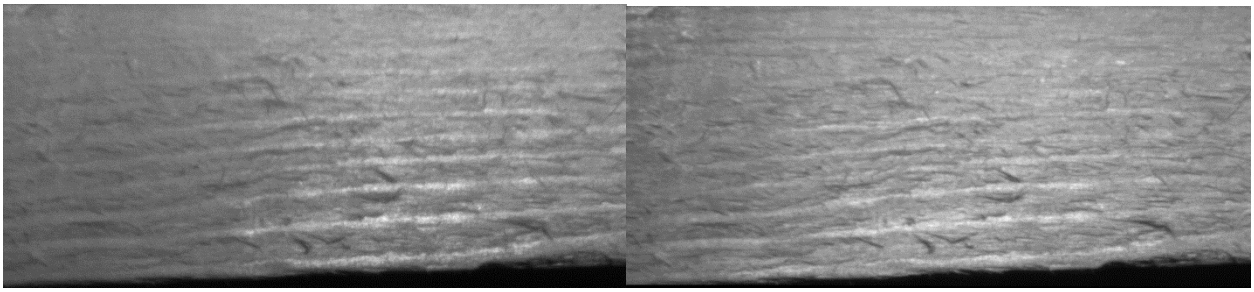

Figure 1—Left: tungsten halogen lamp illumination. Right: led illumination.

Not only is the quality of the grain patterns influencing the recovery of the motion field, the illumination is also having an important impact on the accuracy of the optical flow. Figure 1, shows the same wood surface under two different illuminations. On the left side the surface was illuminated with a tungsten halogen lamp while on the right side it was illuminated with a LED stripe. While the LED illuminated surface shows a lot of fine details, in the image of the tungsten lamp illuminated surface the local contrasts are rather low. This is caused by the fact, that the infrared part of the light is penetrating the surface, scattered in the outermost layers and conducted back to the surface. Since normal B/W cameras are also sensitive in the infrared range (to achieve a higher sensitivity), the recording of this additional infrared image reduces the contrasts and high frequencies in the image which normally is a key feature of a well-focused sharp image. Small, directed light sources with no infrared radiation at an angle, which produces well defined shadows from isolated fibers, are a good setup for such applications.

Load-Elongation Measurement

Experimental Setup

In autumn 2012 a contactless load-elongation experiment was carried out on spruce beam during the 5th COMET Area Meeting in Graz (Austria). Parallel to this contactless measurement an inductive position sensor was also used for comparison purpose.
As shown on Figure 2, the experimental setup was consisting of two high definition (1360x1024 pixels) B/W digital cameras with their corresponding LED illumination bars positioned along the beam.

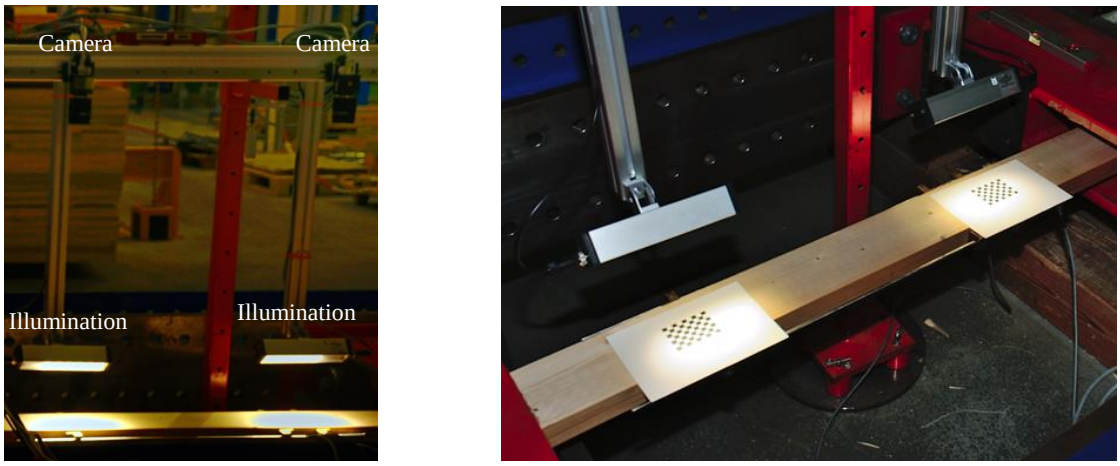

Figure 2—Left: Camera and illumination setup. Right: camera calibration with a planar chess-board target.

The cameras were positioned perpendicular to the beam surface at the distance needed for reaching the wanted accuracy.
In order to get a very precise pixel size and compensate for the distortions of the camera lenses, the cameras were carefully calibrated by the using a planar chess-board calibration target as described in (Zhang1999). In that experimental set-up, the pixel size computed after calibration was 48µm.

Results and comparison with an inductive position sensor

Optical measurements were performed on a densely sampled surface of the beam under each of the cameras. Areas down to 8x8 pixels (representing a surface of 0.15 mm² with a pixel size of 48µm) were tracked over time. A statistics (percentile ranking) over all displacement vectors within the area of the inspected surfaces resulted in the global optical elongation measurement.
Figure 3 shows the correlation between optical (our camera system) and mechanical (inductive position sensor) measurements. The difference between the two measuring methods shows little difference and a strong correlation.

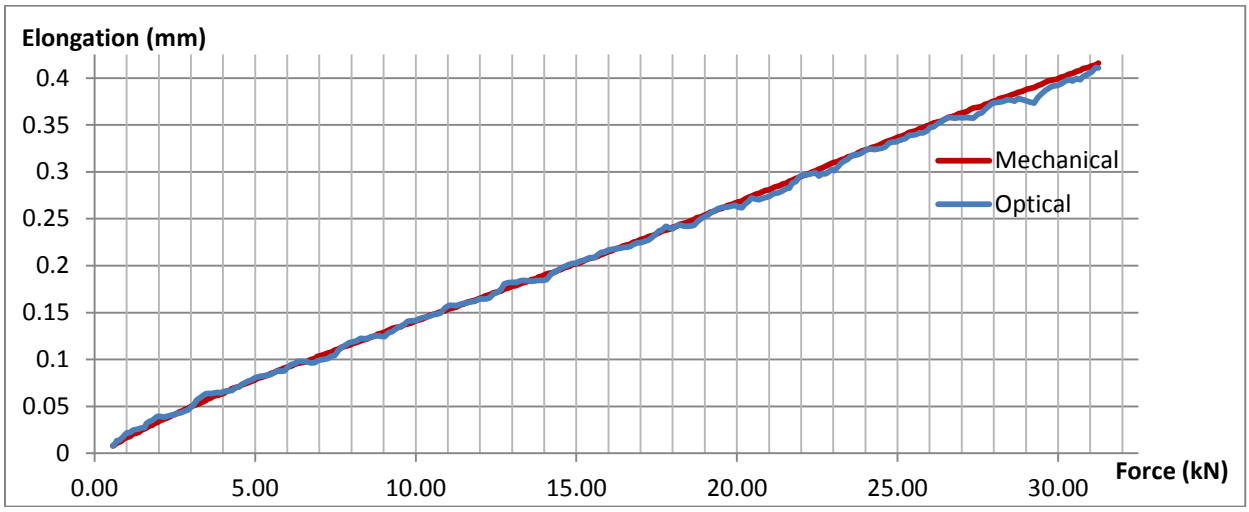

Figure 3—Comparison between mechanical (red color) and optical (blue color) elongation measurements with respect to the force applied to the beam

On this peculiar example the numerical difference between the two methods over the duration of the experiment (from 0 to more than 30kN) has a mean of 1.6 µm and a standard deviation 3.9µm.
One other advantage of the optical thus contactless method is that the measurement could be conducted until the material under inspection breaks what is difficult with a mechanical measuring system, due to the sudden energy released during breaking.

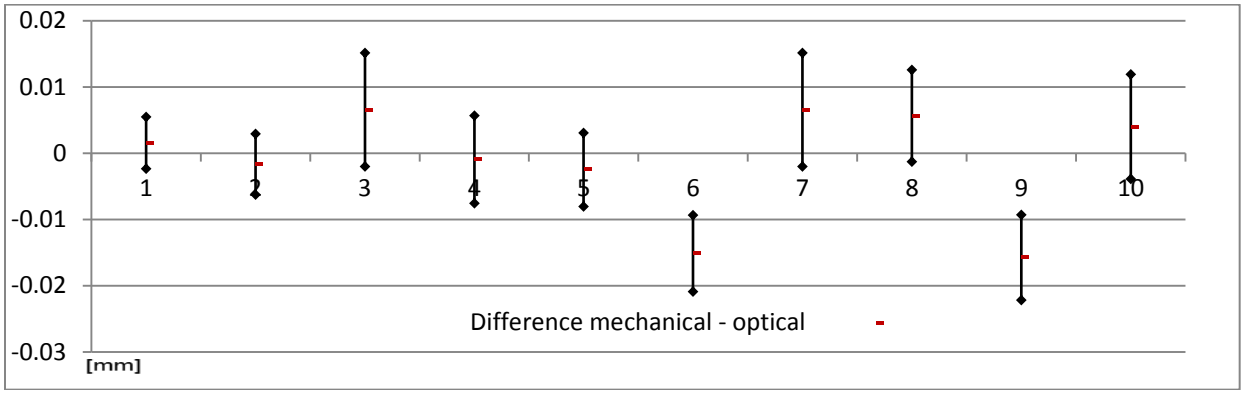

Figure 4—Difference (mean ± standard deviation) between optical and mechanical measurement of a series of 10 different beams.

The comparison of the two measuring methods was extended to a series of ten beams (Figure 4). Over those ten measurements, one can see that the difference (mean and standard deviation) between the measurements is still very low thus proving the soundness of our optical measuring system.

Real Time 3D Deformation Measurements

Exhibition Setup

Based on an exhibition setup used for CONTROL 2011 in Stuttgart (Germany), a real time 3D deformation measurement system using a stereo rig composed of two cameras was built.
Deformations on hardwood are too tiny for the human eye to discern, require some time to appear and are not elastic. So in order to simulate 3D deformations on a wooden surface for the audience of the international fair, an elastic plastic foil on which a wood pattern was printed was used instead of a real piece of wood. Due to its elasticity that foil could be stretched from its sides and poked on its back side by a lever (see Figure 5) throughout the duration of the exhibition.

Figure 5—Left: Exhibition setup. Right: movement of the stretching frame and back side lever poking the foil perpendicular to its surface thus inducing 3D deformations

For measuring the local deformations on each of the image delivered by the stereo rig, the algorithm previously presented was used. Once the displacements were computed, they were combined via triangulation (Hartley and Sturm 1997) to obtain a measure in 3D.
In order to reach real-time computation (15 frame pairs per second) of the deformations in 3D, the resolution of the two cameras was reduced to 680x512 pixels and the algorithm previously presented had to be reprogrammed on a parallel computing platform. This was achieved by using CUDA (NVIDIA Corp. 2007) which enables dramatic increases in computing performance by harnessing the power of dedicated graphics processing units (GPUs).
As in the previous experiment, both cameras were calibrated using a planar chess-board calibration target and the extrinsic parameters of the stereo rig (the coordinate system transformations from 3D world coordinates to 3D camera coordinates) were computed. In that exhibition set-up, the pixel size computed after calibration was 0,25mm.

Results and precision

Optical measurements were performed on 32x32 pixels areas (representing a surface of 64mm² with a pixel size of 0,25mm). For each camera, all surface samples were tracked over time and their corresponding displacement vectors were registered and displayed (Figure 6, left).

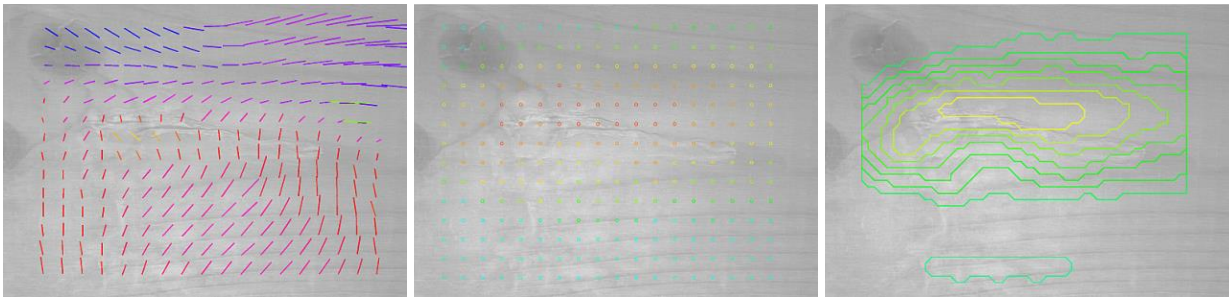

Figure 6—Left: Magnified local deformation vectors. Middle: Punctual distance calculation displayed with a temperature color map (the redder the nearer, the bluer the farther). Right: Distance isolines displayed using a temperature color map.

Then the center point of each surface sample (deformation displacement taken into account) seen from one of the camera was triangulated with the corresponding center point of the same surface sample seen from the other camera. This results in 3D distance measures of all of the center point with respect to the stereo rig. That distance could be either displayed as a punctual measurement (Figure 6, middle) or as isolines (contour lines) that could be fitted to the surface consisting of these 3D distance measurement points (Figure 6, right).

Some words have to be said about the accuracy of the 3D measurements. Logically, the 3D measurements depend on the quality of pixel pair matching and on the method used for their triangulation. Since triangulation is always performed under some noise a robust triangulation algorithm like the one presented by (Hartley and Sturm 1997) should be used. Still other physical parameters are influencing the accuracy of the reconstruction: namely the base dimension of stereo rig and its distance to the object under inspection. Figure 7 displays reconstruction accuracy curves depending of those two parameters (stereo rig base dimension and object distance) with two different pixel pair matching accuracy.

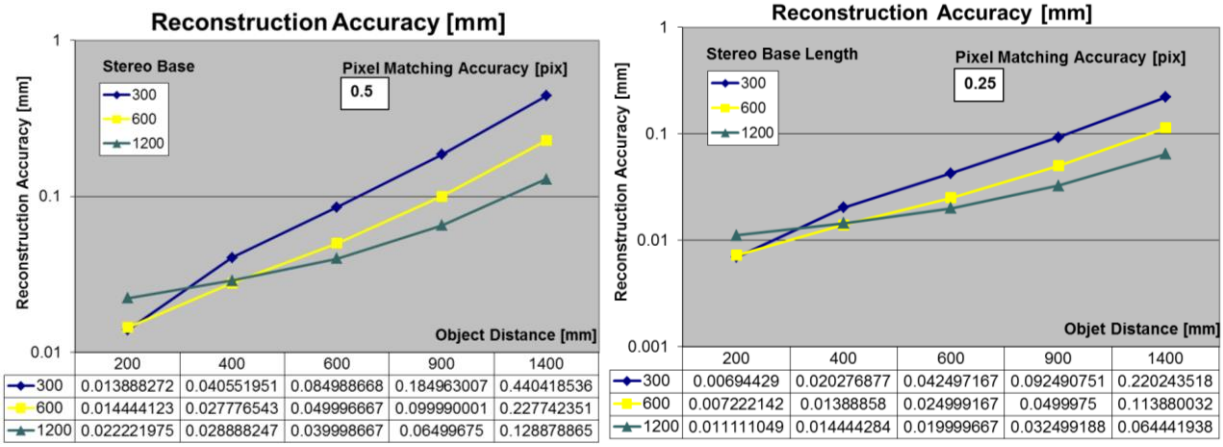

Figure 7—3D reconstruction (triangulation) accuracy depending on the width of the stereo base, the object distance to the stereo rig and the pixel matching accuracy: 0.5 pixels on the left side, 0.25 pixels on the right side.

One can clearly see that the broader the stereo rig base dimension (ranking from 300mm to 1200mm on Figure 7), the better for the accuracy. Logically the same can be said about the distance from the object to the stereo rig: the nearer the object the better the accuracy. Still one has to keep in mind that increasing the stereo rig base dimension decreases the field of view of the two cameras, thus a tradeoff should be struck between these two parameters. Increasing the pixel pairing accuracy from half a pixel to a quarter pixel roughly doubles the final reconstruction accuracy. Depending on the parameters of the setup and on the algorithm accuracy (i.e. for pairing pixels), a 3D reconstruction accuracy ranging from 10µm to 100µm could be reached.

Conclusions

Through two different setups, we have demonstrated that precise, contactless, area-wide and real-time measurements of wood deformations could be achieved by using high resolution digital cameras, proper illumination and dedicated parallel computing platforms for tracking the motion of wood surfaces.
While the accuracy is depending on the camera resolution, the lenses used, the distance of the camera to the object and the precision of the pixel pairing algorithm we have shown that measuring within the µm range could be achieved.
Due to his reduce bulk this optical measuring system has also the advantage to be easily integrated in existing testing environments. Its contactless nature and the fact that measurements are performed at real-time speed enable its use for non-destructive as well as destructive tests.

Acknowledgments

This work is part of the COMET project holz.bau which was funded by the Austrian ministries BMWFJ and BMVIT, and the Steirische Wirtschaftsförderungsgesellschaft mbH, Land Steiermark.

References

Hartley, R.I.; Sturm P.F. 1997. Triangulation. In: Computer Vision and Image Understanding, 68(2): 146-157.

Lucas, B. D.; Kanade, T. 1981. An Iterative Image Registration Technique with an Application to Stereo Vision. In: Proceedings of the 7th International Joint Conference on Artificial Intelligence (IJCAI '81): 674-679.

NVIDIA Corp. 2007. NVIDIA CUDA Compute Unified Device Architecture Programming Guide.

Tomasi, C.; Kanade, T. 1994. Good Features to Track. In: Proceedings of the IEEE Conference on Computer Vision and Pattern Recognition: 593-600.

Zhang, Z. 1999. Flexible Camera Calibration by Viewing a Plane from Unknown Orientations. In: Proceedings of the International Conference on Computer Vision (ICCV'99): 666-673.

Session 11

Structural Condition Assessment I—NDT Fundamentals and Assessment Methods

Monitoring the Deterioration of Wood and Wood Products with Acoustic Nondestructive Testing Techniques

Gregory T. Schueneman, Robert Ross, Rodney C. DeGroot
USDA Forest Products Laboratory, Madison, WI USA

Abstract

Deterioration of wood may be caused by various biological agents that derive their nourishment from constituents of a woody cell. This results in significant reduction in load carrying capacity of the wood, which in turn may result in structural failure. Considerable effort has been devoted to examining the use of acoustic methods for monitoring deterioration in wood and wood products. The objective of this paper is to reveiw (1) basic acoustic test methods and corresponding data analysis techniques and (2) research results on the use of acoustic methods for monitoring deterioration in wood and wood products.

Keywords: Acoustic, wood, wood products, nondestructive evaluation

Options for NDE Assessment of Heat and Fire Damaged Wood

Robert H. White
U.S. Forest Products Laboratory, Madison, WI, USA, rhwhite@fs.fed.us

Brian Kukay
Montana Tech/ The University of Montana, Butte, MT, USA, BKukay@mtech.edu

James P. Wacker
U.S. Forest Products Laboratory, Madison, WI, USA, jwacker@fs.fed.us

Abstract

Depending on the duration and temperature, heat can adversely affect structural properties of wood. While severe temperatures will result in damage that is visually obvious, damage to wood in terms of structural performance extends to wood that visually appears to be unaffected or only mildly affected. The loss in structural capacity includes both reductions for the duration of the elevated temperature exposure and reductions that are permanent even after normal temperatures are restored. While extensive work has been done to develop techniques for assessing, using nondestructive evaluation (NDE), the residual capacity of wood affected by biological degradation, a comparative small amount of work has been done on NDE of wood exposed to elevated temperatures. NDE techniques for assessing biological degradation include forced vibration, resistance micro-drilling technology, stress wave evaluation, ultrasonic testing, radiography, and near infrared technologies. These techniques and others will be reviewed for their applicability to heat damaged wood.

Keywords: wood, fire, post-fire, damaged wood, NDE, nondestructive evaluation, residual load capacity

Introduction

Heat can adversely affect the structural properties of wood. While severe temperatures will result in damage that is visually obvious, the damage to wood in terms of structural performance extends to wood that visually appears to be unaffected or only mildly affected. The loss in structural capacity includes reductions for duration of the elevated temperature exposure and those that are permanent after normal temperatures are restored. Evaluation methods are needed to assess the extent of damage from exposure to elevated temperatures. Applications for such nondestructive evaluation (NDE) techniques include fire-damaged wood, wood near heat generating utilities or industrial operations, and wood subjected to high temperature processes.

While extensive work has been done on NDE techniques for assessing the residual capacity of wood affected by biological degradation, only limited work has been done on NDE for wood exposed to elevated temperatures. One exception was research done in the late 1980's and early 1990's on NDE for the elevated temperature damage to fire-retardant-treated (FRT) plywood roof sheathings (Ross et al. 1991, Winandy 2001). NDE technologies have also been used in research projects to investigate the damage due to production processes, e.g. heat treatment, and investigate the chemistry of thermal degradation.

Effect of elevated temperatures on wood

From 200 to 300°C, the wood components of hemicelluloses and lignin begin to undergo significant degradation (Browne 1958). Significant depolymerization of the cellulose component of wood occurs between 300 and 350°C. Thermal degradation of the wood to a char residue causes reductions in the density of the wood and the shrinkage of the surface char layer.

The National Design Specification (NDS®) for Wood Construction (American Wood Council 2012) advises that prolonged heating to temperatures above 66°C (150°F) can cause a permanent loss of strength. While days of heating at 66°C can have a permanent effect on mechanical properties, the immediate temperature effect on mechanical properties is reversible for heating periods that are limited to hours at temperatures below 100°C (Kretschmann 2010). In contrast to the immediate impact on strength properties of individual wood members at elevated temperatures, the permanent loss in compressive strength occurs at higher temperatures than a comparative loss in tensile strength (Schaffer 1977). The NDS supplied multipliers that are applied to the tabulated stresses for wood that will experience sustained exposure to temperatures of 100°F to 150°F are more severe (0.5 to 0.8) for bending and compressive stresses than they are for compressive or modulus of elasticity (MOE) (0.9). The irreversible effects of elevated temperatures on mechanical properties depend on moisture content, heating medium, temperature, exposure period, and the species and size of the piece involved (Kretschmann 2010).

Issues in evaluating heat and fire damaged wood

Irreversible effects of elevated temperatures for a given duration are primarily on the strength properties and a considerable smaller effect on the stiffness properties (Kretschmann 2010). Elevated temperature exposure changes the correlation between the MOE and the modulus of rupture (MOR). Thus, a difficulty for NDE based on determining elastic properties is that the property of most interest in terms of safety (i.e. strength properties) are more sensitive to elevated temperature exposure than the properties being measured.

A difficulty in evaluating wood for damage from elevated temperature exposure is the inherent variability in the properties of wood both in terms of the original strength properties and the properties being examined as indicator of strength loss. Rather than predicting specific values of MOE and MOR, results for many of these techniques are better for comparing damaged members to similar members that are outside the area of elevated temperature exposure.

NDE options

Visual and density determinations

The most obvious NDE determination of damage due to thermal degradation is visual. There can be various degrees of browning of the wood. Pyrolysed wood retains the original cellular structure as observed via light microscopy or scanning electron microscopy (Zickler et al. 2006). Zicherman and Williamson (1981) examined the microstructure of fire-damaged wood and found the demarcation between damaged and undamaged wood to be extremely narrow (several cell layers in thickness). Schroeder (1999) concurs with this observation of a narrow pyrolysis zone and attributed observations of a wider band to chemically-borne moisture migration. For woods with resin contents, extrusion of the resin is evidence of exposure to elevated temperatures.

As discussed, one detrimental outcome of the thermal degradation is the reduction in the density for wood exposed in temperature range of 200 to 350°C. Taking into account both mass and volumetric changes, the change in density equates to 60% of original density at temperature of 340°C (Zickler et al. 2006). From 600 to 900°C, the char density increases to about 80% of original density. Later at 1800°C, the density drops back to 70% of original density (Zickler et al. 2006). Thus, one option for NDE evaluation is to measure the density itself. A core sample can be removed to examine the density gradient.

Screw withdrawal

An extensive investigation of screw withdrawal as a NDE tool was for the evaluation of FRT wood damaged due to prolonged exposure to elevated temperature in roof applications has been conducted (NAHB National Research Center 1990, Winandy et al. 1998, Ross et al. 1991). The screw-withdrawal test relates the maximum extraction load to residual flexural properties. In an initial FPL study of thermally degraded FRT plywood, the regression of screw withdrawal resistance and bending strength had a correlation coefficient of 0.88 (Ross et al. 1991). In a more extensive study on FRT thermally degraded plywood (Winandy et al. 1998), the data from different treatment/thickness could not be grouped into a single universal model to predict the bending strength but models were developed for specific sub-groups.

The results obtained through screw-withdrawal tests were thought to be of value when comparing to similar members in the fire-damaged structure that have obvious degrees of degradation or residual load capacity. Kukay et al. (2008, Kukay and Todd 2009) developed equations including variables for moisture content, specific gravity, moment of inertia, maximum screw withdrawal load, cross-sectional orientation with respect to the pith, treatment group (charred or un-charred), and various interactions between these variables. They concluded that the results obtained through screw-withdrawal tests are best represented when the results are limited to comparisons to similar members that have obvious degrees of residual load capacity. Variability of the results stem from changes in: the predrilled pilot-hole size, the screw insertion depth, the screwtip to screw shank diameter, and the rate of extraction. For these reasons, care was needed when interpreting and extrapolating the results from screw-withdrawal tests. General correlations are likely to lack adequate precision to establish actual property values.

Micro indentations, penetration, hardness

In contrast to the screw withdrawal techniques that depend on a depth of thermal degradation, techniques based on hardness provide an indicator of thermal degradation near the surface of the wood member. The micro-indentation technique is much like that of a traditional hardness test. A 1.5 mm (lengthwise), 0.5 mm diameter pin is pressed into the wood member with a very precise loading. Hardness is the force required to indent a material a specified amount. There are various methods in wood hardness testing including the Janka method and the one specified by Branco et al. (2009). The amount of the pin that penetrates the wood has been used to generalize the mechanical properties of individual members. The penetration test, a variation of the micro indentation test, utilizes a larger pin. This test measures the amount of strikes of a rebound hammer that is required to drive the large pin into the member a certain distance. The Pilodyn test uses the depth of penetration of a spring-loaded pin as a measure of degree of degradation (Ross and Pellerin 1994).

Zickler et al. (2006) conducted nanoindentation tests on spruce wood that had been pyrolysed to temperatures up to 2400°C. The reduced elastic modulus remained fairly constant to temperature of about 280°C but then rapidly dropped to a broad minimum at 400°C. Starting at 500°C, the reduced elastic modulus increased to values (40 GPa) at 900°C, much higher than the room temperature values (~12 GPa), until decreasing again starting at about 2300°C. Likewise, hardness increases from 0.4 GPa at 220°C to approximately 4.5 GPa at 700°C and a reduction in values occurs starting at 2000°C. The

indentation ductility index remained constant at about 0.8 until 300°C where it dropped to ~ 0.1 at around 500°C. Zickler et al. (2006) concluded that below 400°C, decomposition leads to a minimum of the elastic modulus. Above 400°C, there is a gradual transition from a visco-plastic biomaterial into a brittle, glass-like carbonaceous residue with maximum values at around 800°C. Above 2000°C, plastic deformability improves.

Resistance micro-drilling technology

An innovative technique that provides relative density gradients through the width of the member is resistance micro-drilling. Modern drill-resistance equipment usually consists of a power drill, a specialized drill bit, and a software/hardware interface to facilitate data collection and data analysis. Drill resistance tests are performed in much the same fashion as drilling a pilot hole, or a series of pilot holes into wood members. The results from a drill resistance test, however, are plotted as a function of penetration-depth zones that exhibit less resistance and can be noted for areas of possible decay. Drill-resistance tests have been traditionally classified as a quasi-nondestructive (semi-destructive) test as minor localized damage (~3 mm holes) is imposed on the member of interest during testing. Drill-resistance tests are a function of drill-bit insertion depth. Generally speaking, a decrease in drill resistance or rather, an increase in the drill-penetration rate can be correlated to areas of decay, and aid in the determination of the thickness of the residual shell (Emerson, et al. 1998).

Until recently there had been little research to apply micro-drilling to the evaluation of fire damaged wood. As part of a study on evaluating fire damaged components of historic covered bridges, four 127 mm x 305 mm glulam beams were subjected to a low temperature fire exposure in a fire test furnace. In a quick assessment of the application of technology to fire damaged wood, resistance micro-drilling measurements were made on charred beam near the mid-length of the beams in a vertical orientation. The fire-charred outer portion of the glulam beam has considerably less density than sound wood and was easily detected with this NDE tool. The resulting relative density profiles were utilized to estimate (1) the remaining depth of uncharred wood and (2) the thickness of the thermal damaged wood layer. It was much more difficult to estimate the thickness of the thermal damaged wood layer.

Sound/ Stress wave

Stress-wave evaluation is based on sound-wave physics. Stress waves (also referred to as sound waves) are generated from an impact on the surface of a member that is under investigation. Impact sound waves are measured as a function of their time to travel from one side of the member to the other side. The dynamic modulus of elasticity or apparent MOE (Pa) is considered equal to the wave speed (m/s) raised to the second power times gross density (kg/m^3) (Ross & Pellerin 1994). As with some other NDE methods, stress wave is a better predictor of MOE than it is for MOR. In tests of logs, Wang et al. (2004) found that both static and dynamic MOE decreased continuously as the log diameter decreased, apparently due to difference in the tree growth rate. The moisture content of the member must be known before the analysis can be completed. Since this test relies on stress waves quickly propagating through the member, it is essential that the exact distance between the first and second probes is known. Boundary conditions and their effects on wave behavior need to be considered (Ross et al. 1991). Stress-wave evaluation tests have long been used to detect decay in wooden members. They have more recently been used as indicators of residual wood stiffness for individual members.

Garcia et al. (2012) used stress wave for nondestructive determination of the MOE of wood before and after heat treatment. The dynamic modulus of elasticity decreased by about 13% in the most severe treatment (230°C for 4 h) but not for the milder treatments.

A strong relationship was found between energy absorption as measured by stress wave techniques and residual strength of degraded FRT wood but the speed of sound was insensitive to the degradation (Ross, et al. 1991). As part of a study on evaluating fire damaged components of historic covered bridges, four 127 mm x 305 mm beams were subjected to a fire exposure in a fire test furnace that resulted in a narrow char layer but a deep layer of elevated temperatures that penetrated beyond the base of the char layer by nearly 25 mm. As a result of the fire exposure, average measured values indicate: a 54% reduction in the maximum recorded load, a 46% reduction in strength (MOR) based on the residual cross-sectional area and a corresponding 20% reduction in stiffness (MOE). The results are based on a standard three point bending test with an increasing load applied at the lengthwise center of each beam. Sound wave measurements were taken near the top and bottom of each beam. The values and corresponding results were repeatable; resulting comparisons of the transmission rates indicated a reduction due to fire exposure. But the reductions in the times for fire exposure were not greater than the differences between the fastest and slowest times for the different specimens prior to fire exposure.

Ultrasonic

Ultrasonic inspection techniques consist of high-frequency stress waves that disperse quickly over a short distance in wood. Ultrasonic inspection has been used in manufacturing to estimate product quality and can also be used to detect common strength-reducing defects such as knots, slope of grain, and decay. MOE is computed from the sound wave measurements. Measurements for MOE are only valid for longitudinal measurements but the velocity and frequency domain signal amplitude are useful for defect detection in the transverse direction (Klinkhachorn et al. 1999).

Klinkhachorn et al. (1999) developed a portable ultrasonic device and conducted a few preliminary tests on charred yellow poplar specimens. There were little changes in the time delay or the velocity due to the charring of the two or four surfaces of the specimens but the area under Power Spectral Density (PSD) plots changed significantly as the result of the charring. Reinprecht and Panek (2012) have shown that ultrasound technology can be used to detect differential density in wooden members. In their study, sawdust was used to model rot in wood. The ultrasound waves that propagated through the media were significantly slower in comparison to a solid member.

Chemical analysis

Chemical analysis represents a different approach to NDE analysis of thermally degraded wood in that the effects being measured are the changes in the chemical composition of the wood. For initial exposures to heat, the extractives and the hemicelluloses are likely to be the first to be affected. Wood extractives such as fatty acids, fats, and waxes migrate to the surface of heat treated wood (Nuopponen, et al. 2003). Nuopponen et al. (2003) used FTIR spectroscopy to examined Scots pine that had been heat treated under steam at temperatures of 100 to 240°C. At temperatures of 100 to 180°C, the resin acids in the radial resin canals moved to the surface of the heat-treated wood and disappeared from the wood surface at higher temperatures (Nuopponen et al. 2003). While not providing a measure of strength loss, consideration of extractive content can provide indication of the level of temperature exposure.

In the thermal degradation process, the hemicelluloses are among the first of the three main wood components to be affected (LeVan and Winandy 1990). Potential parameters include holocellulose and alpha cellulose content and degree of polymerization (Ross et al. 1991). Hemicellulose measurements have potential to provide direct measure of strength loss since the xylose, galactose, and arabinose content were sensitive to the loss of mechanical properties (Winandy 2001). Arabinose was the most sensitive indicator of early strength loss. In a study on cyclic long-term temperature exposure at 82°C, 30% RH, only arabinose showed a consistent reduction with increased durations of heating (Green and Evans

2008). The cellulose is the last component to be affected by the elevated temperatures. Various investigators have used x-ray techniques to examine the crystallinity of the cellulose.

Reductions in the pH (increased acidity) of the wood are a potential indicator of thermal degradation and strength loss. Lebow and Winandy (1999) investigated pH of wood as technique for evaluating thermally degraded FRT plywood. Although some correlation ($R^2 = 0.74$) was observed between pH and strength loss in FRT plywood, this method was less sensitive to degradation in untreated plywood. In the investigation of options for assessing thermally degraded FRT plywood, expense and the specialized testing are often cited as disadvantages of the chemical analysis approach (NAHB National Research Center 1990, American Plywood Association 1989).

Near infrared

NIR technology works by analyzing the interactions between materials and electromagnetic radiation. The wavelength and line speed are both variables that are noted when creating prediction models for applications that historically have related to the detection of decay and other wood processing issues. Spectral analysis tests use infrared radiation to identify end products of chemical processes including thermal degradation. The NIR technology can be used to accurately measure the chemical composition, mechanical properties, and a select few anatomical properties of wood (Brashaw et al. 2009). Bachle et al. (2010) and Esteves and Pereira (2008) have investigated NIR spectroscopy to evaluate the properties of heat-treated wood. Other researchers have used this technique to predict surface moisture distribution as well as wet pockets. The ability to detect local variants as well as general material distributive properties like moisture content make this technique appealing to applications beyond quality control.

Mechanical Testing

Mechanical testing is a more direct approach to evaluating the effect of elevated temperatures on mechanical properties. In terms of NDE, this normally involves some sort of proof loading to determine the MOE. A bending proof load test was one of the options developed for the assessment of FRT plywood roof sheathing (NAHB Research Center 1990, Ross et al. 1991). As part of the study on fire-damaged components of historic covered bridges, a proof loading method specific to field application to fire-damaged wood components was developed (Kukay et al. 2013). Mechanical testing options include destructive methods such as removal of selected members for testing or removal of small samples for laboratory mechanical testing. Destructive testing will provide a direct measurement of modulus of rupture while proofing loading techniques only provide direct measurements of modulus of elasticity.

Acknowledgments

Portions of this paper were extracted from a final report submitted by Brian Kukay, Charles Todd, Tyler Jahn, Jenson Sannon and Logan Dunlap of *Montana Tech of the University of Montana* for a study on *Evaluating Fire-Damaged Components of Historic Covered Bridges*. This study is part of the Research, Technology and Education portion of the **National Historic Covered Bridge Preservation** (NHCBP) Program administered by the Federal Highway Administration. This study is conducted under a joint agreement between the Federal Highway Administration – Turner Fairbank Highway Research Center, and the Forest Service – Forest Products Laboratory.

References

American Plywood Association. 1989. Fire-retardant-treated plywood roof sheathing: In-situ testing. Tacoma, WA: APA.

American Wood Council. 2012. ASD/LRFD NDS® National Design Specification® for Wood Construction with Commentary. Leesburg, VA: AWC.

Bachle, H.; Zimmer, B.; Windeisen, E.; Wegener, G. 2010. Evaluation of thermally modified beech and spruce wood and their properties by FT-NIR spectroscopy. Wood Sci. Technol., 44:421-433.

Branco, J.; Piazza, M.; Cruz, P. 2010. Structural analysis of two King-post timber trusses: Non-destructive evaluation and load-carrying tests. Construction and Building Materials. 24(3):371-383.

Brashaw, B. K. [and others]. 2009. Nondestructive testing and evaluation of wood: A worldwide research update. Forest Products Journal, 59(3):7-14.

Browne, F. L. 1958. Theories of the combustion of wood and its control. Report 2136, Madison, WI: United States Department of Agriculture, Forest Service, Forest Products Laboratory.

NAHB National Research Center. 1990. Homebuilders guide to fire retardant treated plywood: Evaluation, testing, and replacement, Upper Marlboro, MD: National Association of Home Builders National Research Center.

Emerson, R. N. [and others]. 1998. Nondestructive evaluation techniques for timber bridges. In: Proc. 5th World Conference on Timber Engineering, Montreaux, Switzerland, Lausanne, Switzerland: Presses polytechniques et universitaires romandes, pp. 670-677.

Esteves, B.; Pereira, H. 2008. Quality assessment of heat-treated wood by NIR sspectrocopy. Holz Roh Werkst, 66:323-332.

Garcia, R. A. [and others]. 2012. Nondestructive evaluation of heat-treated Eucalyptus grandis Hill ex Maiden wood using stress wave method. Wood Sci. Technol., 46:41-52.

Green, D. W.; Evans, J. W. 2008. Effect of cyclic long-term temperature exposure on the bending strength of lumber. Wood and Fiber Science, 40(2), pp. 288-300.

Klinkhachorn, P.; Halabe, U. B.; GangaRao, H. 1999. Portable ultrasonic device to monitor timber properties: Assessment of charred timber members. In: Proc. 28th International Conference on Fire Safety, Columbus, OH, pp. 89-93.

Kretschmann, D. E. 2010. Mechanical Properties of Wood. In: Wood Handbook, Wood as an Engineering Material . Madison,WI: USDA, Forest Service, Forest Products Laboratory, p. 46.

Kukay, B. [and others]. 2008. Post-fire assessments, methodology, and equations for directly determining wood's residual flexural properties. Forest Products Journal, 58(1-2):40-46.

Kukay, B.; Todd, C. 2009. Determining wood's residual flexural properties using nondestructive testing. Wood Design Focus, 19(2):8-12.

Kukay, B.; White, R. H.; Todd, C. S.; Tyler, J. 2013. Evaluating fire-damaged components of timber bridges and structures. In: Proceedings, Structures Congress 2013, Pittsburgh, PA, Virginia: American Society of Civil Engineers, pp. 758-767.

Lebow, S. T.; Winandy, J. E. 1999. Effect of fire-retardant treatment on plywood pH and the relationship of pH to strength properties. Wood Science and Technology, 33:285-298.

LeVan, S. L.; Winandy, J. E. 1990. Effects of fire retardant treatments on wood strength: A review. Wood and Fiber Science, 22(1): 113-131.

Nuopponen, M.; Vuorinen, T.; Jamsa, S.; Viitaniemi, P. 2003. The effects of a heat treatment on the behaviour of extractives in softwood studied by FTIR spectroscopic methods. Wood Sci. Technol., 37: 109-115.

Reinprecht, L.; Panek, M. 2012. Ultrasonic technique for evaluation of biodefects in wood: Part 1-Influence of the position, extent, and degree of internal; artificial rots. International Wood Products Journal, 3(2):107-115.

Ross, R. J.; Cooper, J.; Wang, Z. 1991. In-place evaluation of fire-retardant-treated plywood. In: Proc. Eighth International Nondestructive Testing of Wood Symposium. Vancouver, WA: Washington State University.

Ross, R. J.; Pellerin, R. F. 1994. Nondestructive testing for assessing wood members in structures: A review, FPL-GTR-70, Madison, WI: USDA, Forest Service, Forest Products Laboratory.

Schaffer, E. 1977. State of structural timber fire endurance. Wood and Fiber, 9(2): 145-170.

Schroeder, R. A. 1999. Post-fire analysis of construction materials. Ph.D. Dissertation, Berkeley, CA: University of California.

Wang, X. [and others]. 2004. Diameter effect of stress-wave evaluation of modulus of elasticity of logs. Wood and Fiber Science, 36(3):368-377.

Winandy, J. E. 2001. Thermal degradation of fire-retardant-treated wood: Predicting residual service life. Forest Products Journal, 51(2):47-54.

Winandy, J. E.; Lebow, P. K.; Nelson, W. 1998. Predicting bending strength of fire-retardant-treated plywood from screw-withdrawal tests, FPL-RP-568, Madison, WI: USDA, Forest Service, Forest Products Laboratory.

Zicherman, J. B.; Williamson, R. B. 1981. Microstructure of wood char Part 1: Whole wood. Wood Science and Technology, 15(4):237-249.

Zickler, G. A.; Schoberl, T.; Paris, O. 2006. Mechanical properties of pyrolysed wood: a nanoindentation study. Philosophical Magazine, 86(10):1373-1386.

X-Ray technology for the assessment of existing timber structures

Steffen Franke
Department of Architecture, Wood and Civil Engineering, Bern University of Applied Sciences, Biel, Switzerland, bettina.franke@bfh.ch

Bettina Franke
Department of Architecture, Wood and Civil Engineering, Bern University of Applied Sciences, Biel, Switzerland, steffen.franke@bfh.ch

Robert Widmann
Empa, Structural Engineering Research Laboratory, Duebendorf, Switzerland, robert.widmann@empa.ch

Abstract

For the assessment of timber structures, which is a permanent task to evaluate the normal function, non-destructive testing methods are preferred but the value of the information is limited due to the performance of the applied method. X-Ray is a non-destructive technology which allows a view into the structural member, where especially internal damages like cracks, holes or plastic deformations of mechanical fasteners can be detected. The mobile X-Ray technology is a non-destructive testing method with a good accuracy for detailed information. The digital analysis of the radiograms allow in-situ measurements. The method and its possibilities for non-destructive testing of timber structures are presented. The presentation based on practical examples gives an overview of the ability and the limits of this method. It shows that the mobile X-Ray technology offers a high potential for an effective assessment.

Keywords: X-ray, non-destructive testing, timber, connection,

Introduction

The structural assessment of timber structures is caused by different reasons, such as regular inspections, structural modifications, changes in serviceability or historic preservation. The assessment of timber structures should always begin with a visual inspection of the complete building for the analyses of the supporting structure. The following assessment of the single members, connections or specific details will take place only after this step. An advantage in assessing timber structures is that abnormalities are normally relatively easy to detect due to discoloration, cracks or plastic deformations. Especially in combination with the measurement of the moisture content, first specification can already be done. Depending on the abnormalities found, specific testing methods are available and can be used. The test methods can generally be classified into nondestructive, semi-destructive and destructive test methods. For the general survey of the building and its detailed assessment, an overview of common methods is given in Table 1. Further explanation can be found in e.g. Aicher (2008), Görlacher (1996), Kasal & Tannert (2010), Köhler et al. (2011), Rinn (1992), Steiger (2009) and Vogel et al. (2009).

Table 1 - Common assessment methods for timber structures

Nondestructive testing methods	Semi-destructive testing methods	Destructive testing methods
Visual inspection	Resistance drilling	Test of glue line quality
Survey	Penetration resistance tests	Mechanical testing for strength prediction
Moisture content	Withdrawal resistance test	
Crack detection and mapping	Drill core specimens	
Ultrasonic wave or echo method	Endoscopy	
Chemical investigations		
X-Ray		

Non-destructive testing methods are preferred, but the value of the information is limited due to the performance of the applied assessment method. Especially the occurrence of internal damages like cracks, holes, fitting inaccuracy or plastic deformations of mechanical fasteners cannot be detected reliably with these common methods. However the X-ray technology allows a view to the inside of a structural member or a connection. The application of the X-ray technology on wooden structures was investigated and the results and limitations are presented in this paper.

X-ray technology

Method

Since the discovery of X-rays in the late 19th century, this technology has been used for medical imaging which is its most famous application. Later, other applications were added for this technology e.g. in materials science and technology. Since mobile X-ray systems are available, this technology has also been used for the in-situ assessment of structures, as shown in Vogel (2012), (Brashaw et al. (2009), Wei et al. (2011), Pease et al. (2012), Kruglowa (2012), Lechner (2013). The adoption of this technology provides the possibility to look inside the member with a high resolution according to the measuring area of 30 by 40 cm for the film used. The X-ray technology is a non-destructive testing method and works quasi contactless. The use of a mobile X-ray technology in combination with the specific digital scanner allows in-situ assessment of existing structures.

The safety requirements for the use of the mobile X-ray system do not restrict the practical use on existing timber structures. The mobile X-ray system used works with hard X-ray pulse generator but with a very low dose as against stationary X-ray systems known. Furthermore the exposure transmitter is only active, meaning X-rays are only generated, while ”taking” the picture. This process takes only a few seconds and before and after no X-ray exposure happens. In practical use, the safety zone is specified as follows: 3

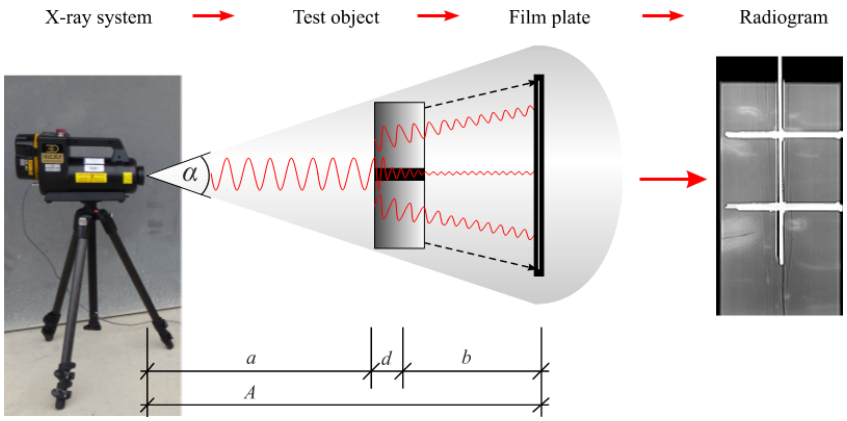

Fig. 1 - Principle process of X-ray technology and investigations

meters around the transmitter, 30 meters in measuring direction and 11 meters perpendicular to it. The users carry a personal dosimeter to register any irradiation.

Theory and Calculation

X-rays are a form of electromagnetic radiation. The X-rays are absorbed depending on the material respectively their density. The X-ray absorption parameter is defined by the Beer-Lambert law as follows:

$$I = I_0 \cdot e^{-\mu d} \tag{1}$$

Where I is the intensity after radiography in [W/m^2], I_0 the intensity before radiography in [W/m^2], d the thickness in [m] of the material and μ the X-ray absorption coefficient in [m^{-1}]. For wood, the X-ray absorption coefficient is defined as follows:

$$\mu = \mu' \cdot \rho \tag{2}$$

With μ' as the mass absorption coefficient in [m^2/kg] and ρ the density of the material in [kg/m^3]. The absorption capacity depends on the density of the material, the atomic mass, atomic number and the depth of the material, Purschke (1989).

The X-ray radiography depends on the pulse intensity of the X-rays, the distance of the test object to the transmitter as well as to the film plate and also the thickness of the material. The principle of the process is shown in Fig. 1, where the test object is located between the X-ray transmitter and the film plate. The X-rays transmitted travel through the test object and will be absorbed with different intensities before they hit the film plate. The material specific absorption of the X-rays leads to the so called radiogram which will finally be transferred into a grayscale picture. The volume of the three dimensional test object will be reproduced as a two dimensional picture.

Applications and limits of the mobile X-ray technology

Laboratory analyses of the system

The principle of the X-ray process is similar to taking a picture with a photo camera. While the quality of a photo depends on the depth of field, sharpness of movement and focus, these parameters are not comparable for X-ray systems. For X-ray photography, the pulse intensity, the distances of the test specimen between the transmitter and the film plate and the thickness respectively density of the object influence or restrict the results, resolution and accuracy of the method. Some of these parameters were

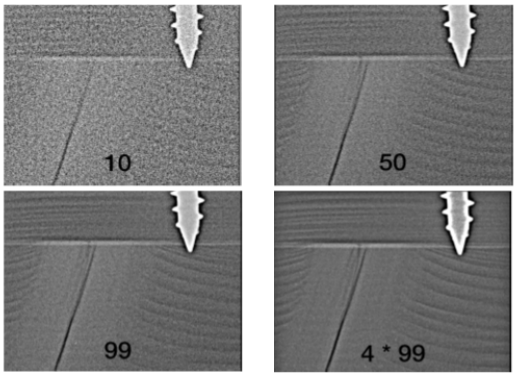

Fig. 2 - Radiograms with different number of pulses

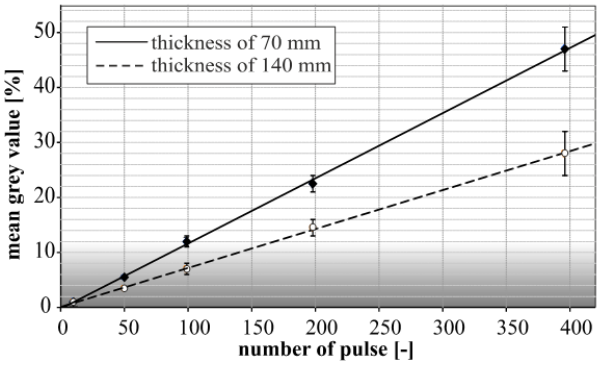

Fig. 3 - Effect of number of pulses, the shadowed area marks the not useful configurations for the used wood

investigated and are described following. The X-ray unit XR 200 with a maximum photon energy of 150 KVP and X-ray dose per pulse of 0.026 - 0.040 mSv was used for the investigations.

According to Eq. (1), the intensity I on the film plate increases linearly with the intensity of the transmitter I_0. The gray value of one pixel is proportional to the intensity and will increase respectively. Fig. 2 shows radiograms taken with different numbers of pulses from a steel screw tip inserted in a wood block as test object. The test object made of European Spruce with a density of 480 kg/m^3 and about 15 % moisture content had a constant thickness d of 70 mm. For a larger thickness of an identical material the absorption of the X-rays increases, so that for radiograms with comparable quality, the number of pulses has to be increased as well. The effect of the number of pulses was analyzed for two different thicknesses of the wooden block and is shown in Fig. 3.

For the optimization of the test set-up, the influence of the distance a between the transmitter and the test object and the distance b between the test object and the film plate (Fig. 1) was verified regarding accuracy and sharpness of the radiograms. The same test object with a steel screw inserted in the wood block, as mentioned before, with a thickness of 70 mm was used. An increase of the distance b (with constant A) results in the projection of a smaller area where the object is represented enlarged but with less sharpness and more noise, as shown in Fig. 4. On the other hand, the reduction of distance a leads to a clear “burned” spot and unusable radiograms. A minimum distance a of about 1 meter was necessary for the test configuration with a film plate of 30 by 40 cm. The relation between the two distances a and b is summarized in Fig. 5.

Finally the thickness of the test object was verified from 70 mm up to 350 mm. Hereby the number of

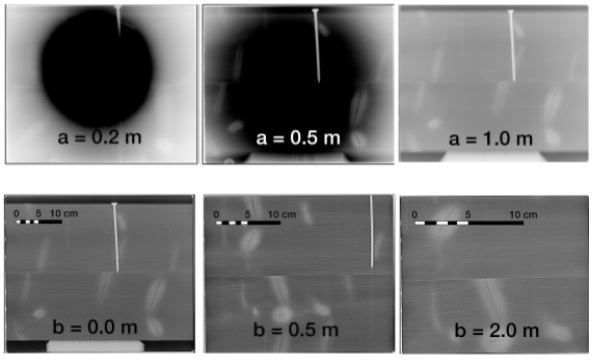

Fig. 4 - Radiograms with different distances, top row distance a and bottom row distance b

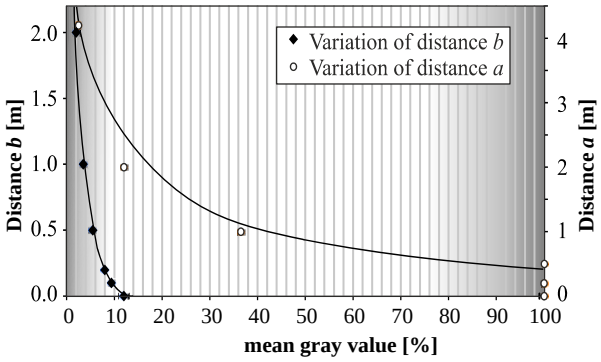

Fig. 5 - Effect of distances a and b, the shadowed area marks the not useful configurations

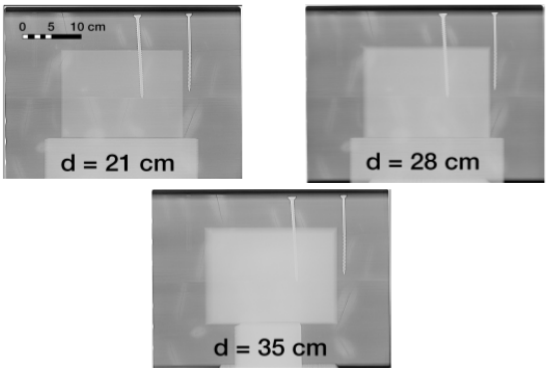

Fig. 6 - Radiograms with different thicknesses of the test object

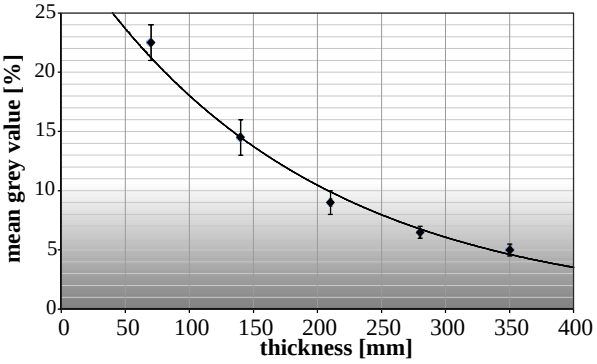

Fig. 7 - Effect of thickness, the shadowed area marks the not useful configurations

pulses with 2*99, distances A with 2.0 m and b with 0.0 m were kept constant. The radiograms of the test object with the metal screw inserted in the wood block with different thicknesses are shown in Fig. 6. The contrast of the radiogram decreases with the increase of the thickness of the specimen. Typical timber structural elements with thicknesses up to 200 mm can be assessed with the used system. For greater thicknesses the contrast vanishes and only objects with distinctly different densities, e.g. parts of steel embedded in wood are visible in the radiogram. The relation between the mean gray value and the thickness is shown in Fig. 7 as summary.

Assessment of wood and connections

The first investigations were done in the laboratory with samples of historical wood to wood connections as well as with mechanical connections. Fig. 8 shows a wood to wood connection with an internal hardwood dowel. Not only the two wood species, European spruce and beech, can be clearly distinguished but also characteristic features within one material like knots and annual grow rings are clearly visible. Furthermore the fitting accuracy of such a connection can be checked. In this case gaps are

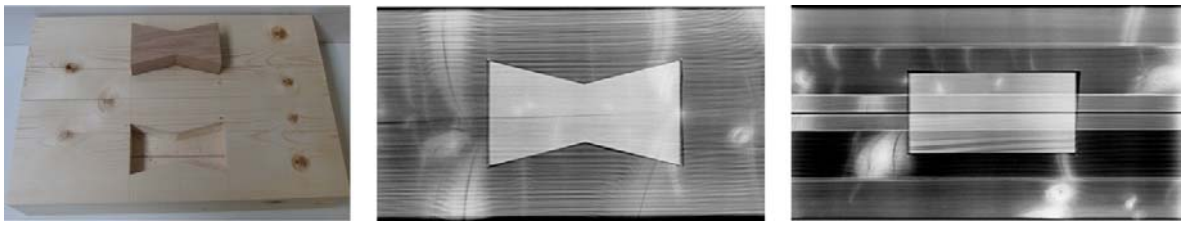

Fig. 8 - Wood to wood connection with a hardwood (beech) dowel embedded in softwood (spruce) members

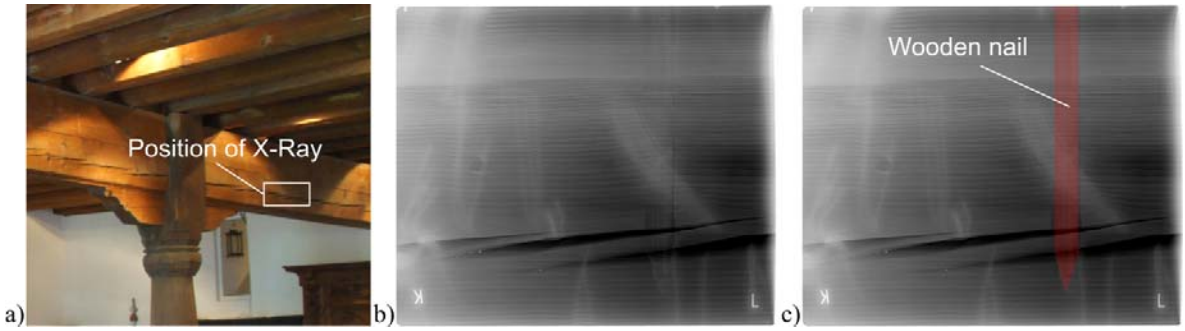

Fig. 9 - Wood nail in a historic multi layered wooden member, a) position of the measurement, b) original radiogram, c) wooden nail marked in radiogram

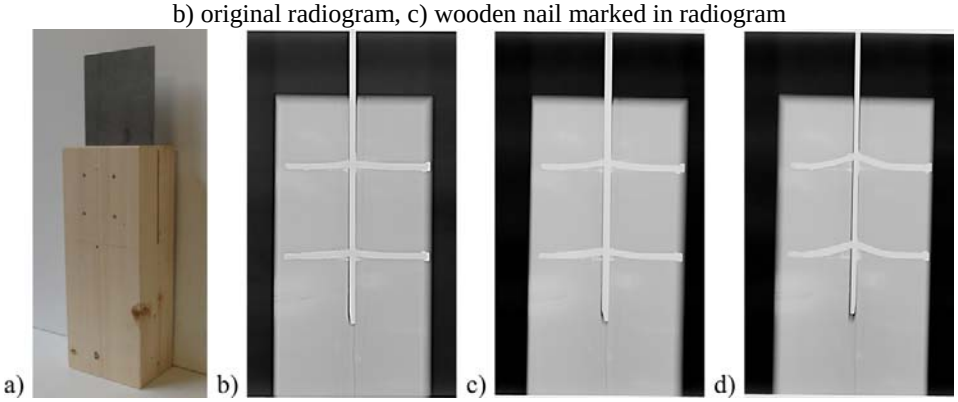

Fig. 10 - Connection with mechanical fasteners, a) Test specimen, b) unloaded connection, c) and d) connection with plastic deformations

clearly detectable. As a practical application, a historical timber construction in a castle was investigated. Wooden nails could be detected during the assessment of a multi layered beam construction, as shown in Fig. 9.

The assessment of timber connections with mechanical fasteners is shown in Fig. 10 for a dowelled connection with inner steel plate. The test specimen shown was loaded/unlodaded in certain steps at the laboratory and X-rayed after each load step. For every case, the visual inspection of the outside area (heads of the fasteners) did not indicate any irregularities. But the radiograms show that inside the connection plastic deformations according to the Johansen theory, Johansen (1949), already occurred, as shown in Fig. 10c)-d). The visible plastic deformations of the fasteners indicate an overloading and a failure of the connection which could not have been observed from outside.

Assessment of repaired glue lines and fungal/insect decay

Glulam is a common used engineered wood product for large span timber constructions. The assessment of these structures is a permanent task in order to ensure the integrity and performance. In some cases, glue lines or cracks have to be repaired or supports and high stressed areas have to be reinforced. The assessment of restructured glue lines was therefore investigated with the mobile X-ray system within a research project. A glulam member with two repaired glue lines was X-rayed in different directions to check the quality of the restoration. In the first radiogram, taken in a direction perpendicular to the glue-line plane and shown in Fig. 11b), a clear void at the outside of the beam can be seen. But the allocation to one of the glue-lines or even the evaluation if there are more failures in the same direction is not possible. Fig. 11c) shows the radiogram of the same section but taken under an angle of about 45° to the glue-line plane. Here, the two repaired glue-lines can be distinguished from each other and the failure spots and injection holes are clearly visible for each glue-line. In this case, both glue-lines show the voids

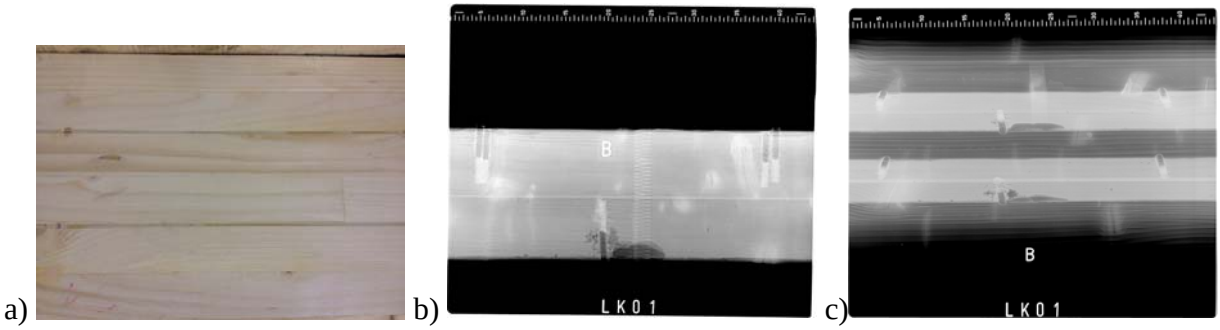

Fig. 11 - Gulam member with two repaired- cracks, a) test specimen, b) X-ray direction perpendicular to the glue-line (top view), c) X-ray direction inclined to glue-line

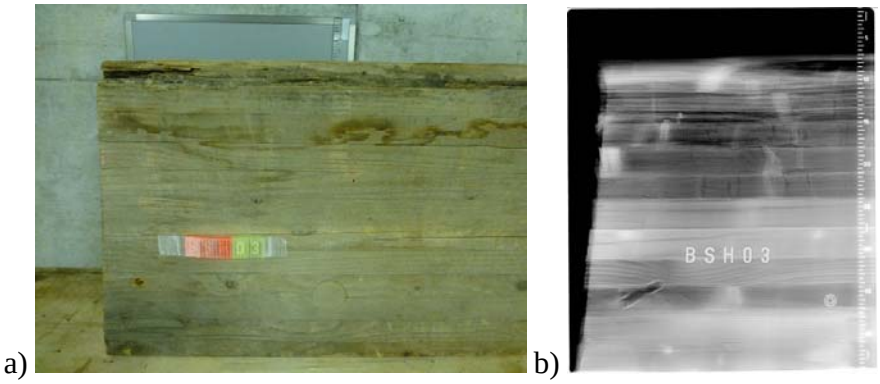

Fig. 12 - Fungal decay in X-ray, a) test specimen, b) radiogram

at the same position. Furthermore, the assessment of this member also shows further small voids and bubbles along the glue-line plane. Such images can help the engineer to determine the quality of a repaired glue line and on base of this to assess its load bearing capacity. In another practical application, also voids and bubbles within a glued-in rod connection could be detected.

In general fungal or insect decay can be observed within the visual inspection. But in some cases structural elements are covered or only viewable from one side, so that the mobile X-ray system can be used for detailed analyses or specification of assumptions. Fig. 12 shows as example a glulam member with fungal decay in the top lamellae. The typical cubic failure structure is visible in the radiogram observed and allows to estimate the dimension of the decay.

Summary and conclusion

The X-ray system has been used in laboratory tests and practical situations at existing structures. It led to excellent results which allowed detailed analyses going further as common non-destructive assessment methods. It was shown that the mobile X-ray technology offers a high potential for an effective assessment of existing structures including connections and structural timber members. Deformations of mechanical fasteners like the formation of plastic hinges due to overloading are visible as well as the macroscopic structure of wood, knots or different wood species. Also glued connections like finger joints or restructured glue-lines were checked for quality and/or damages. Voids or bubbles but also cracks due to overloading could clearly be detected.

The practical examples presented, give an overview of the ability and the limits of this method and show that the mobile X-ray system is a novel successful non-destructive testing method of timber structures. With increase of the differences of the density of the investigated materials, the contrast is getting more and more intensive. However, reliable analyses of the resulting radiograms should be done by people who have experiences with the system and are professionals in timber structures in order to be able to identify irregularities from inaccuracies even in less contrast radiograms.

Acknowledgment

The project work was supported by the Federal Office for the Environment (FOEN). We would like to thank also the master student Mr. Scherler for his effort and contribution to these results within his project paper.

References

Aicher, S. 2008. Verfahren und Aussagemöglichkeiten bei der Begutachtung von Holzkonstruktionen in Fachtagung Bauwerksdiagnose, Berlin, Germany.

Görlacher, R. 1996. Hölzerne Tragwerke: Untersuchen und Beurteilen in: Sonderforschungsbereich 315: Erhalten historische bedeutsamer Bauwerke, Verlag Ernst & Sohn, Berlin, Germany.

Kasal, B., Tannert, T. 2010. In situ assessment of structural timber, State of the art report of the Rilem technical committee 215-AST, Springer Verlag, Dordrecht, Heidelberg, London, New York.

Köhler J., Fink, G., Toratti, T. 2011. Assessment of failures and malfunctions, Publication of COST Action E55-Modelling of the performance of timber structures, Shaker Verlag GmbH, Aachen.

Rinn, F. 1992. Chancen und Grenzen bei der Untersuchung von Konstruktionshölzern mit der Bohrwiderstandsmethode, Bauen mit Holz, 94/9.

Steiger, R. 2009. Zustandserfassung und Zustandsbeurteilung, in EMPA/HSR-Conference, Rapperswil, Switzerland.

Vogel, M., Tannert, T., Hansen, H., Kehl, D., Kraus, S. 2009. Überprüfungsmethoden geschädigter Holzkonstruktionen, Research report, Bern University of Applied Sciences, Biel, Switzerland.

Vogel, M., Scharmacher, F. 2012. Qualitätskontrolle von Holzkonstruktionen – Mobiles Röntgen. Holzforschung Schweiz 2012/1, pp. 9-11.

Brashaw, B.K., Bucur, V., Divos, F., Goncales, R., Lu, J., Meder, R., Pellerin, R.F., Potter, S., Ross, R.J., Wang, X., Yin, Y. 2009. Nondestrucitve testing and evaluation of wood: A wordlwide research update, Forest Products Journal 2009/59, pp.7-14.

Wei, Q., Leblon, B., La Rocque, A. 2011. On the use of X-ray computed tomography for determining wood properties: a review, Can. Journal for Res. 2011/41, pp. 2120-2140.

Pease, B.J., Scheffler, G.A., Janssen, H. 2012. Monitoring moisture movements in building materials using X-ray attenuation: Influence of beam-hardening of polychromatic X-ray photon beams, Construction and Building Materials 36 pp. 419-429.

Kruglowa, T. 2012. In-situ assessment of density and material proberties in timber structures by non-destructive and semi-destructive testing, Thesis, Chalmers University of Technology , Gothenburg, Sweden.

Lechner, T. 2013. Assessment of density in timber using X-ray equipment, International Journal of Architectural Heritage, 2013/7, pp. 416-433.

Purschke, M. 1989. Verbesserung der Detailerkennnbarkeit in Röntgendurchleuchtungsbildern durch digitale Bildrestauration, Doctoral thesis, Technical University of Berlin, Germany.
K.W. Johansen, Theory of timber connections. Int. Association for Bridge and Structural Engineering (IABSE) Publications, 9 (1949), pp. 249-262.

In Situ Structural Timber Strength Measurement Advances Using Qualitative Resistography and Quantitive Resisto-Fractometry

Paul S. E. Probett **MIFPI, AsocRICS, MBOINZ, MNZIBS, NZCB.**
Clinton S. Craig
Blake J. Probett

INCODO Ltd, Tauranga, New Zealand, mail2us@incodo.co.nz

Abstract

In situ and on site evaluation of timber used for structural purposes has largely been based on methodologies that give qualitive assessments that describe condition aspects, rather than providing measurable "strength" data. This is largely due to the absence of site-friendly equipment and processes that provide the various "strength" values engineers need for meaningful structural evaluation. Even when such methodologies are used, sample size, the degree of destructive investigation and the difficulties in quickly relating ultimate values to yield strength and/or to various local or international code requirements present issues. This document describes a paired methodology based on electronic resistography, used alone and in concert with incremental core type fractometry coupled by using software that permits a high degree of integration of results.

This is acknowledged to be a starter paper with limitations, based on preliminary and limited research undertaken in house by a very small company, in a remote corner of the globe, undertaken by field technicians looking for solutions to a real experienced problem. It highlights, arguably, a novel direction in this area whereby specific strength characteristics of wooden structural elements can be determined on site. Largely it identifies tools and methodologies with a strong emphasis on site applications.

Keywords: digital Resistograph, digital Fractometer, fractometry, resisto-fractometry, control tests, yield strength, Woodchecker, in situ, on-site, timber strength.

Introduction

Background

As late as 2010 a comprehensive analysis by Kasal and Tannert [1] underscored that, while there were a large number of methodologies for assessing timber in situ, most had limitations. Data generated generally indicated varying aspects of timber condition, - but useable compressive, bending, and tensile strength values were not easily derived, and where they were, samples usually needed to be processed at a remote testing facility and/or samples needed to be substantial in number and dimension. Resultant delays in reports, cost of testing, acceptability of damage to structures in obtaining samples and representivity of samples are common issues.

Resisto-Fractometry

'Resisto-fractometry' is an in-house quasi-technical term coined that reflects the object the team had in fusing two separate technologies so as to:

1) Develop a control sample based method using a digital microdrill (specifically an IML Resistograph PD) whereby graphic profiles from suspect or questionable integrity areas were compared against known sound wood of the same specie and from the same structure. The use of control graphic profiles to compare subsequent profiles obtained from concern areas made identifying of anomalies more easy and gave a greater degree of confidence in identifying sound timber profiles. This improved qualitive timber condition evaluation when the Resistograph was used in isolation.

2) 4.9 mm core samples were tested for compressive strength parallel to grain (using an IML electronic Fractometer) to provide qualitive strength data. The check methodology involved taking core samples approximately 20 mm from microdrill test points on the same grain plane to build a higher degree of confidence in the likely compressive strength implied by the electronic resistographic data. This required the in-house development of software to facilitate the various comparative sets of data generated and to derive averaged ultimate and averaged yield strength values. It also required sourcing a good and increasing selection of ISOs, ASTMs and similar local building code requirements relating to timber strength requirements and including their specifics in reports generated.

Developmental Summary

Very clear correlation between a standard Resistograph profile and x-ray density of a sample from the same location have been shown by others. In addition the general correlation between density and overall timber strength characteristics has been commented on by many. It was noted that while Fractometer technology has been available for some time, it had reportedly not been used to compare against resistographic data and vice versa. Scientific literature is, apparently, silent in regard to inputs from digital Fractometers (portable compression testing unit with 60 MPa capacity that in base form, compresses 5mm length sections of 4.9-5.0 mm timber core pellets, parallel to grain, to determine ultimate strength results). Research indicates that the Digital Fractometer Print used is the only site-friendly digital compression tester currently available.

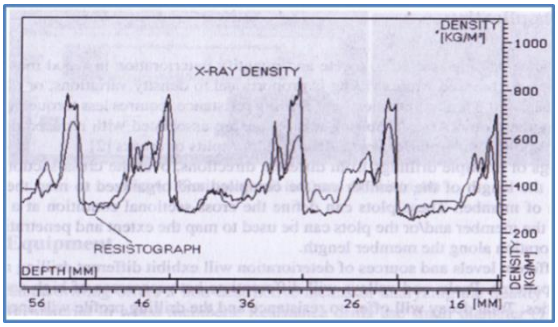

Fig 1- Graph [1] illustrating similarity of profiles between Resistograph readings and x-ray density readings of same sample

An additional function of Fractometer s includes determining bending strength of parallel to grain cores. However comparing Fractometer core sample compression strength profiles to Resistograph profiles has been the subject of little to no appreciable research. This was largely understood to be

because until recently, a) Resistographs and Fractometers were mechanical only b) the Fractometer in particular has for some time been viewed more as an arborist's tool for wet timber. A third issue was that core samples used with a Fractometer need to be very cleanly cut to obtain consistent results. While cores were traditionally extracted using incremental borer type augers, this type of core drill tends to penetrate quickly and tear the outer face of dry wood samples (particularly soft specie early wood such as that of Pinus Radiata). This causes them to fail somewhat prematurely under parallel to grain compression tests. Use of a high speed dendochronological type coredrill such as the Berliner type was found to significantly reduce the number of compromised compression tests. It also enabled removal of cores from more difficult points in buildings and structures. The handles of a standard incremental borer restrict application i.e. when removing samples from bottom plates of walls, whereas a drywood corer is designed to fit a standard lightweight power drill.

Fig 2a, 2b - Comparison of 'Berliner' type dendochronological high speed dry wood core drill and standard hand operated auger incremental borer. **Fig 2c –** Core with damaged external surface

Initial comparisons between Resistograph graphic profiles and those obtained using the Fractometer presented a good to very good commonality.

Control based resistography

Digital Resistography

The local driver for the development of this approach was the need to determine the amount of degradation of enclosed light timber wall framing in leaky homes. Assessment as to what framing needs to be replaced (in New Zealand) has largely been based on the recording of high moisture levels, visible staining or degradation. Occasionally this is supplemented with some largely non-representative microbiological analysis of fungi presence / damage coupled with occasional spot testing for preservative presence, type and residual salts levels. Generally this required a large number of cut-outs in walls to quantify damage and determine remediation scope. A frequent comment was that if a dwelling did not need a reclad before the inspection(s) it usually needed one afterward as seamless repairs to the exterior of monolithically finished claddings are inherently difficult.

Resistography allowed assessments to be less intrusive (2.0 mm holes in skirting or hidden behind peeled back wallpaper) and more intensive, providing a better indication of overall condition and has been found to be particularly useful in locating hidden decay between framing timbers.

A key issue was wood variability: Most light timber framed construction in New Zealand over the last 50 or more years has been plantation grown Pinus Radiata. With selective breeding programs extending back to the early 1930's growth characteristics have changed. Plantations are grown in climatically different areas and varied soils. In recent years timber average bending strengths of

newer generation trees has decreased, requiring increased timber beam depths in code type documents.

This led to developing a control based approach for each dwelling being checked.

Control Comparison Approach

The methodology developed is to take 3-5 or more test readings on internal walls that were known to be sound timber, checking graphs for commonality, representivity and lack of anomalous indications and then selecting one of the lower amplitude but sound profiles as the control sample. Using developed software, this was then overlaid as a graphic template profile over all the following tests of comparable timber in the same building - effectively a control graph against which subsequent tests were compared.

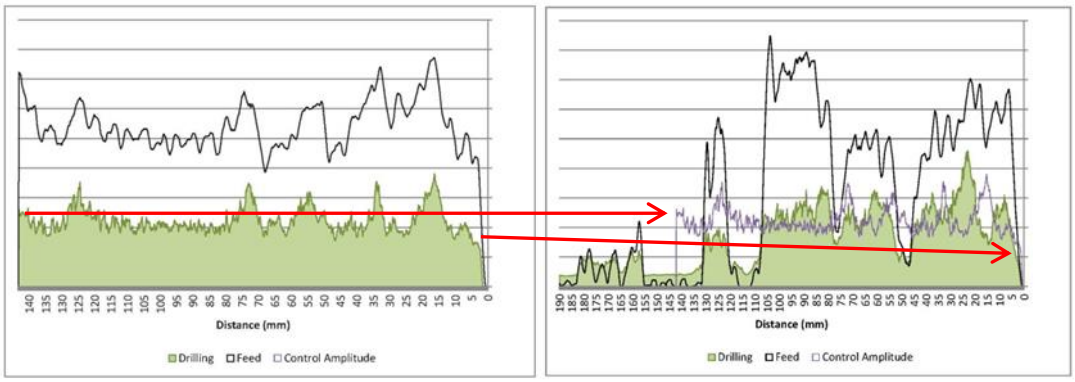

Fig 3a, 3b - Representative control graph at left overlaid as on right hand graph in purple as a template. Note: Graphs read from right to left, Right hand graph indicates anomalous material at 50 mm mark and from 110 - 200 mm

Where the technology permitted, wireless Windows based tablets are used to process data and generate reports on site in real time. The aim being to complete a report on site and export wirelessly to end users.

Caution: While this is a logical development of the technology, resistography in isolation must still be considered a qualitative tool.

Fractometry

Resistographic and Fractometric Data Comparisons

The determining by others that resistographic profiles were nearly identical with x-ray density profiles provided the base step to the integration of data from the two units. It was obvious that when cores are taken from the side of structural timber, irrespective of whether the core is radial or tangential, the compression of the side of the core, if aligned correctly would always mean compression parallel to grain with similar earlywood and latewood peaks. Reason being that while such a core sample being taken would be perpendicular to grain, when the core is cut into sections to fit into the Fractometer the compressive force is applied at 90 degrees, so each 5 mm core would effectively be being tested parallel to grain, i.e force being applied parallel to grain direction on the curved edges of the core “pellets”.

It was postulated that if a core sample for use in a Fractometer was removed and taken parallel to a Resistographic drill point and the data compared, there may be a reasonable degree of correlation.

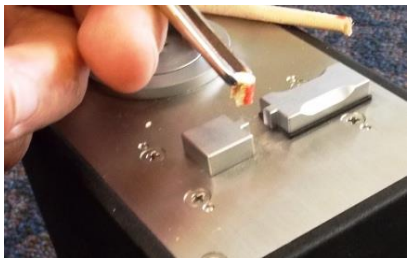

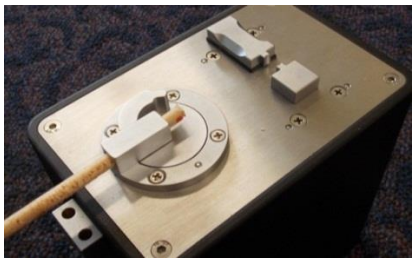

Fig 4a, 4b - Digital Fractometer with 'pellet' being inserted into jaws at left. Optional bending strength feature with timber core being placed at right

Fig 5a, 5b - Core sample in jaws with force being applied from left and right. Second photo with failure occurring prematurely by shearing as timber grain not in alignment with plane of jaws.

Much of the testing undertaken was based on 90 x 45 mm p.rad framing. With each core being 90mm long and sectioned with a scalpel into 5mm tablets – providing 18 samples, each of which was compressed to determine ultimate strength.

Note: A digital Fractometer such as the IML Print unit applies up to 60MPa force. Load is increased in a stepped manner at increments of 0.005 mm. With Pinus Radiata samples, failure commonly occurred within 100 incremental steps. When the swinging arm feature on the top of the unit is used it provides bending strength data on cores. New Zealand plantation based timber is considered unsuitable for such testing given the wide early wood bands – often exceeding 30 mm.

Resisto-fractometry

Resistographic and Fractometric Data Comparisons and Integration

Initial tests showed a very good comparison between individual pairs of resistographic data and fractometric data profiles. However when both sets of data were applied to the same graph there was the issue of aligning values on the y-axis, as resistographic data is displayed as a percentile degree of amplitude, while the fractometric data is a simple success of compression strength values in MPa. In addition it was appreciated that testing would frequently be undertaken involving drilling through skirting/trim and plasterboard/sheetrock before accessing the structural frame elements. The degree of graphic profile alignment was found to be high but variables such as the quality of the core extracted, and the accuracy of alignment of samples in the Fractometer (parallelity with grain) needed to be addressed carefully. Some offset of results was noted occasionally with graphs appearing similar but not aligning as closely at the greatest depth of tests. This was attributed to the

need for Resistograph and Fractometer tests to be separated by approximately 10 mm (difficulty in drilling a hole in a hole or right beside a hole). New Zealand Pinus Radiata is not especially straight grained wood, particularly non-clear specimens that have been downgraded for framing usage. While side by side drilling may be seen to be at the same grain plane at the drills' points of entry, compound changes in grain flow at depth are considered to influence results slightly. Reportedly microdrill bits can wander as they penetrate timber of varying hardness and density. It is considered likely that more slowly growing, straight grained timber would provide more consistent results. It follows that correlations between results will obviously have a degree of variance depending on timber specie.

Software Development (Woodchecker)

Software was developed in-house to move raw data to end user report formats and allow overlaying of graphic results from the two technologies. To compensate for these graphic overlay offset effects, the software included 'sliders' to, a) enable the Fractometer data to be moved laterally to align with the same point of origin of the framing being evaluated - i.e same start point, and b) allowed the Resistograph based percentile graph to be increased in amplitude by an appropriate factor to more closely align with the height profile of the Fractometer graph.

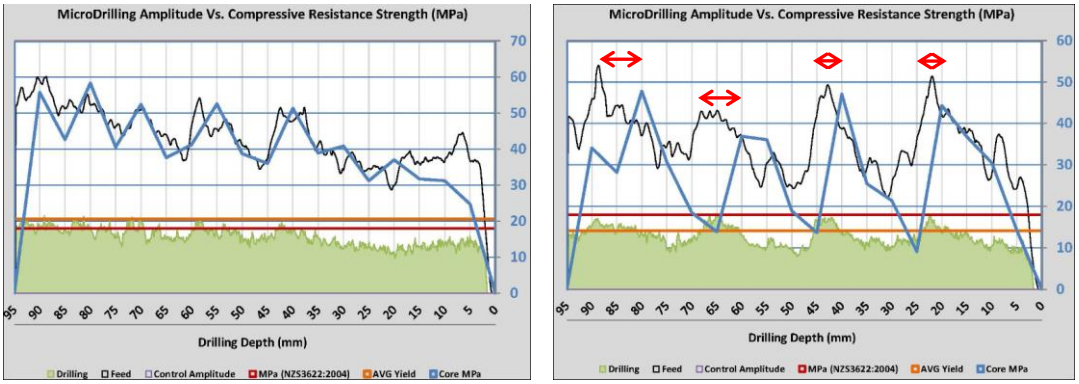

Fig 6 – Resistographic total data (black upper line) with Fractometric data overlaid (blue) Average yield strength as horizontal orange line. Code strength document (NZS:3622) as horizontal red line. Note offset of data in graph 2 of Resistograph amplitude and accompanying Fractometer MPA peaks, likely differences in grain planes.

Features included permitting adjustments to be made as, a) the *y* axis of a Resistograph is basically a percentile measurement while the Fractometers scale was MPa, and, b) the Resistograph PD takes readings at the rate of 1/mm while the Fractometer takes readings at the rate of 200/mm per 5mm tested sample. The resultant overlaid graphs for a typical 100 mm width framing timber have 1000 and 20 nodes respectively.

It should be appreciated that the key object of the developments remains determining a methodology that would objectively advance on site timber condition evaluation and strength measurement relative to a local leaky building crisis. Again, looking for solutions to local problems: two of the three largest cities in New Zealand have experienced significant earthquakes in the last two years, with Christchurch losing much of its CBD. A program to evaluate whether 190,000 older buildings meet 30% of current earthquake code requirements is commencing. It is hoped that having equipment, software and the methodologies described in this paper, can enable prompt, realistic, virtual, NDT, quantitive strength measurement of critical structural timber components, leading to a reduction in the need for the usual conservative strength assumptions.

Fractometer data presentation

It is readily acknowledged that the need for further development of fractometry and resisto-fractometry is essential to give validity to the outlined methodology. Coupled with the test/measurement processes developed it was also became apparent that the software that integrated data could be enhanced to provide both a tool for users of the technology in the field, as well as a means for increasing the scope and range of other in situ timber "strength' measurements needed for calculation purposes.

Software development

The software was initially developed for in-house use but has been developed to include:

a) Bluetooth import of data friendly

b) Data export options to cloud based hosting sites.

c) An integrated database that allows data from multiple sources / locations to be merged. This would be useful for research and analytical work - for example a nationwide integration of testing of utility poles with remote data pooled and centrally analysed to develop pole replacement prioritisation and scheduling.

d) An open report template allowing data to be entered on site progressively using tablet or laptops and that includes marked photographic or drawing records identifying test points and results.

e) Provision of compression strength individual and whole of sample strength graphs.

f) A method of selecting an appropriate and recognized method of converting ultimate strength values to useable recognized yield strengths – particularly important for assessment of older structures with bolted or similar connections.

g) A method of selecting from a range of building/structural code values so that the degree of compliance of tests can be easily appreciated by end users of reports, particularly decision makers who may lack an appreciation of the beauties and subtleties of timber strength measurement. Alternatively user specified values can be chosen

h) A modular base to the software that allows for adaptions and developments of fractometry that may increase the types of on-site / in situ timber strength tests available.

Research Directions

It is considered that the four tools (speed programmable electronic Resistograph, electronic Fractometer, dendochronological quality core drills and Woodchecker software) provide the basic equipment for arguably a somewhat novel direction in in situ /on site timber strength evaluation and measurement.

In addition a specie by specie comparison of "paired" resistographic and fractometric tests, focusing on a comparison of averaged amplitude vs averaged parallel to grain compressive strength is considered warranted. This will allow sets of statistical analyses that would determine the degree of confidence one can have in resistography as a largely standalone means of providing timber parallel to grain compressive strength. Therefore part of current research is aimed at determining the degree

of correlation between the averages of three variables 1) Resistograph amplitude average 2) Adjacent Fractometer test average ultimate strength of timber, and 3) Average yield strength derived from Fractometer data. Samples are taken within 20 mm to determine statistically whether there is an appreciable degree of correlation – that would allow resistography in isolation to provide a qualified indicative or even a, possible actual strength range. It is hoped formulae similar to the following will be developed for a range of familiar timber strength measurements.

$$a = fp \pm Evar$$

For s specie where: a equals average amplitude percentage of Resistographic test, fp equals average compression strength parallel to grain Evar equals the statistical degree of expected variance in samples strength and where Resistograph penetrative speed is l /mm/sec and rotational speed is m rpm.

Currently development of a drywood core bit with 300 mm x 45 mm sample size and not requiring a full length pilot hole is being considered. Such a core from a large section structural timber element would theoretically allow two core samples up to 300 mm long for parallel to grain compression testing and up to thirty number 40-45 mm samples for bending strength and or compression strength perpendicular to grain.

Summary

Novelty and independent review of methodologies

It is readily and clearly conceded that the preceding outlines an approach that may be novel, but is yet to be repeated or reviewed by persons more learned, experienced, financed and equipped than the writer. As at the time of writing, digital Resistographs with programmable set horizontal feed and rotational speed settings are becoming more common, while electronic Fractometers remain few and far between and dendro quality core drills are not easily sourced.

However it is suggested that the consistently positive results of the 1,000 plus tests undertaken comparing Resistograph and Fractometer profiles do provide a basis for considering that research at a higher level, based on the methodology and equipment described in this paper, will provide good subject material for research by others and hopefully a quick, useful and cost effective method for quantifying specific timber strength characteristics of existing structures and enhancing the degree of confidence in Resistographic tests.

References

1 Kasal and Tannert. 2010 RILEM *State of the Art Reports: In Situ Assessment of Structural Timber*

2 Rinn, F., Schweingruber, F.H., and Schar, E. Resistograph and X-ray density charts of wood. Comparative evaluation of drill resistance profiles and X-ray density of different wood species. *Holzforschung*, Vol. 50, pp. 303-311, 1996.

Preserving timber structures with non-destructive evaluation of critical joinery

Paul Crovella
Department of Sustainable Construction Management and Engineering, State University of New York College of Environmental Science and Forestry, Syracuse, NY, USA, plcrovella@esf.edu

Dr. George Kyanka
Department of Sustainable Construction Management and Engineering, State University of New York College of Environmental Science and Forestry, Syracuse, NY, USA, ghkyanka@esf.edu

Abstract

A non-destructive method of evaluating the rotational stiffness of timber joints was applied to two historic timber structures. Results from the testing showed that more than half the members had joint stiffness values of $\alpha > 1$. For the first structure tested, the average percent error for members with $\alpha > 1$ was 31%. When values of wood density and Modulus of Elasticity were determined in the lab rather than estimating, the percent error for one member was reduced from 55% to 26%. For the second structure tested, the method provided lower percent error for joints with $\alpha > 1$ than for joints with $\alpha > 1$. The second structure had larger percent error in the measurements than the first structure. This is believed to be due to the non-geometric (natural) shape of the members used in the construction. Further research is needed to properly validate the method across different structure types and sizes.

Keywords: Timber Frame joint, non-destructive evaluation, rotational stiffness

Introduction

Overview

In structural rehabilitation of timber-framed bridges, churches, mill buildings, homes, and barns, an engineering analysis is often necessary to determine the load bearing capacity. To perform this analysis the properties of the wood and the properties of the connections must be determined (Brungraber, 1985). There are a number of accepted non-destructive methods for determining in-situ mechanical properties of wood (Ross et al., 2004, Kasal et al., 2009). However, there are no commonly accepted methods for non-destructively determining the strength and stiffness of timber connections (Anthony, 2008). This paper presents results on the use of a frequency-based method to non-destructively determine the initial rotational stiffness of timber joints in two timber structures.

Literature Review

In identifying critical research needs for the American Society of Civil Engineers Structural Engineering Institute, Ron Anthony wrote “Under design loads, seldom do wood members fail in a structure unless they are severely deteriorated. Failures generally occur at connections. Yet we have a wealth of knowledge about wood properties, but not the behavior of connections. Unfortunately, connections are critical in structure performance,…,and yet we do not have a reliable means to assess their condition or capacity.” (Anthony, 2008) Bo Kasal (Kasal, 2011) in summarizing state-of-the-art in in-situ lumber evaluation for the 2011 Structural Health Assessment of Timber Structures Conference, identified the first

need for further work as "Detection of fastener deterioration and deformation". Determination of all strength and stiffness properties of timber joinery is ultimately necessary. This paper presents results on determination of just one of those properties, in-plane rotational stiffness. This property may be an indicator for overall joint quality for rehabilitation (Brungraber, 1985). Alternately, it may the value of critical interest for the structural analysis. Dave Fischetti (Fischetti, 2009) in the book Structural Investigation of Historic Buildings states that "Structural Engineers are aware that it is very difficult to produce a true hinge or a true fixed joint in the actual structure. Joints in timber trusses may act somewhere between those two, causing a very different distribution of forces than produced by the analysis."

A non-destructive method for determining the rotational stiffness of timber joints using the natural frequency of vibration of the beam has been developed and tested in the laboratory (Crovella and Kyanka, 2011). This paper presents results from applying this method in two timber structures.

Method

Structures for Testing

Circa 1900 post and beam barn

Eight secondary structural members in a 56' x 30' x 20' barn shown were evaluated. The principal structural members were solid sawn 8" x 8" members, and the secondary members were 4" x 6", both Eastern Hemlock (*Tsuga Canadensis)*. Moisture content of the members averaged 11.1% with a range from 10.3 to 11.9%. The secondary members were mortised into the principal members and secured with a single peg (wood dowel). The eight members tested (B1,B2,B3,B4,C3,C4,D3,D4) are indicated in Figure 1.

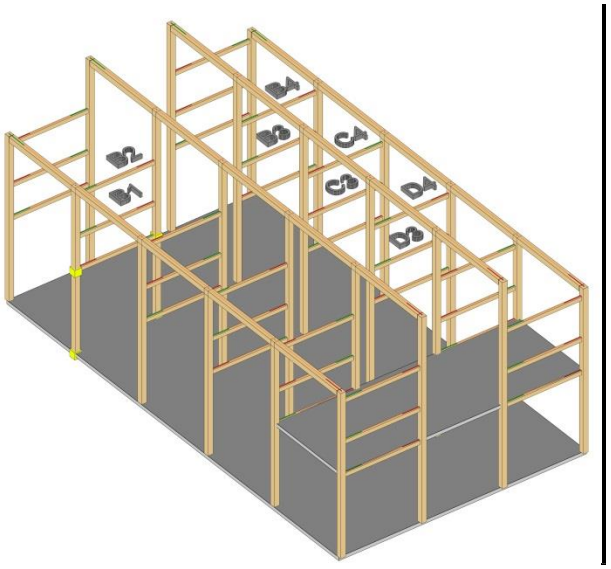

Figure 1—Elements of circa 1900 barn that were tested

For each of these elements, a single axis accelerometer was attached to the top center of the member, and then the member was struck with a soft-faced mallet to excite vibration in the elastic range. The free vibration time history was recorded on a portable computer (Audacity, 2011), and then custom software was used to perform a Fast Fourier Transform. The fundamental natural frequency of vibration was identified from the frequency plot, and used with the beam properties to determine input values for an analysis using the finite element method. Ansys® finite element software was used to produce a dynamic

analysis and the rotational stiffness of the member joints (in the vertical plane) was varied until the natural frequency matched the recorded values.

Next, each member was loaded with a series of weights to produce an elastic deflection less than L/1000, and the midpoint deflection was measured.

Using the frequency and deflection measurements, as well as mechanical properties of the member, a comparison was made between joint stiffness as determined by vibration, and by closed-form solution using deflection. For more details on the method, refer to the description from Crovella and Kyanka (Crovella and Kyanka, 2011).

For this building, the species was visually identified and graded (No 3 Eastern Hemlock) and assigned values for Modulus of Elasticity (MOE) (based on the National Design Specifications for Wood Structures) and density (based on the Wood Handbook) at an assumed 12% MC. Further, a sample of material was removed from one of the members (B1) to determine density and MOE with laboratory tests.

1936 Pack Lodge Visitor Center

The second building tested had light frame wall construction, with a log truss roof structure. Two 24' log trusses spanned the main hall. These scissor trusses were constructed from ~8" diameter Eastern Spruce (*Picea glauca, Picea rubens, Picea mariana*) with the bottom chords intersecting at a center post. The average moisture content was 12.6% with a range from 11.7 to 13.6. The joints appeared to be a combination of wooden joinery and steel fasteners. The four sections of the truss bottom chords were evaluated to determine their rotational stiffness using both the frequency and deflection methods (as described above).

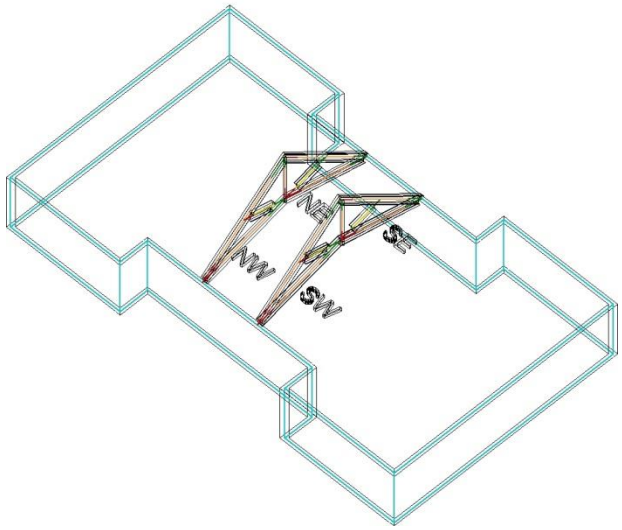

Figure 2 – Bottom chord members of Pack Lodge that were tested

Results

Testing of the circa 1900 barn provided a total of eight similar members with stiffness results for both deflection and frequency.

Table 1 - Circa 1900 Barn Joint Stiffnesses

Member	Joint stiffness (lb-in/rad) based on deflection	Joint stiffness (lb-in/rad) based on frequency
B1	2,200,000	1,000,000
B2	1,300,000	1,100,000
B3	130,000	100,000
B4	25,000	60,000
C3	1,000,000	700,000
C4	600,000	600,000
D3	850,000	400,000
D4	25,000	0

Testing of Pack Lodge provided four similar members (truss bottom chords) with stiffness results for both deflection and frequency.

Table 2 - Pack Lodge Truss Joint Stiffnesses

Member	Joint stiffness (lb-in/rad) based on deflection	Joint stiffness (lb-in/rad) based on frequency
NE	12,000,000	2,500,000
NW	6,000,000	9,000,000
SE	700,000	1,400,000
SW	51,000,000	21,000,000

Discussion

Circa 1900 Barn

Analysis of joints by relative stiffness

The results from testing of the circa 1900 barn showed a general correspondence between larger and smaller values with the two methods. The percent error in the frequency measurement varied from 140% for B4 to 0% for C4. The average percent error was 52%. The method showed which joints have higher rotational stiffness relative to the bending stiffness of the member. This stiffness can be classified by the ratio of the rotational stiffness of the joint (k) to the bending stiffness of the member (EI/L). When separated by those members with kL/EI ratios greater than 1 (5 members), the percent error of the method is reduced to 31%, for members with kL/EI ratios less than 1 (3 members), the error increases to 88%. This separation at kL/EI of 1 is useful for the purpose of analysis, generally for kL/EI values less than 1, joint stiffness can be considered to be negligible. Thus the method provides more precision in the range where it most impacts structural behavior. Graphical representation of these ranges can be found in Figure 3. This figure shows that 0.1 change in normalized frequency corresponds to changes in orders of magnitude of rotational stiffness for kL/EI less than 1. For kL/EI values greater than 1, a 0.1 change in normalized frequency corresponds to less than one order of magnitude change.

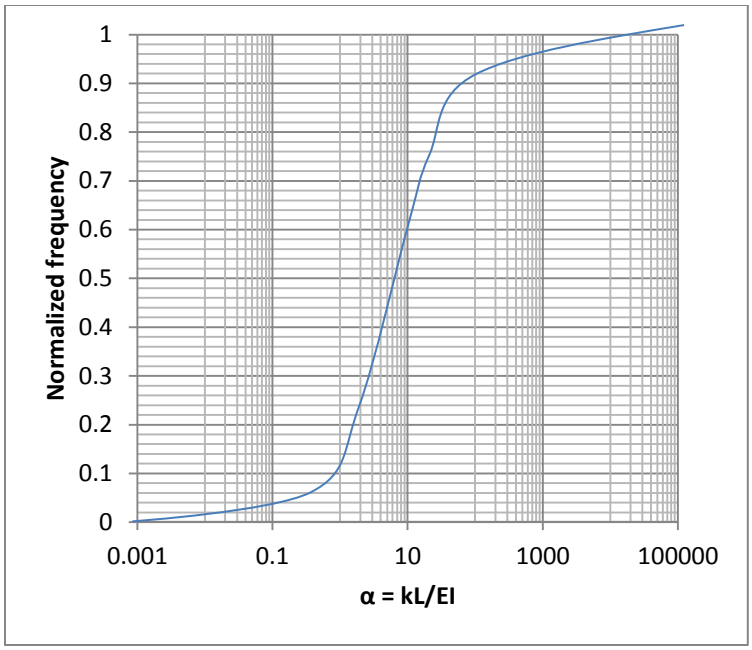

Figure 3 – Effect on natural frequency of increasing rotational joint stiffness (normalized frequency is the ratio of the frequency measured minus the frequency of a pinned member to the frequency of rigid member minus the frequency of a pinned member).

Testing assumptions of MOE and density

The greatest percent error (55%) in the members with kL/EI ratios greater than 1 was found in B1. Two assumptions that introduce inaccuracy in the method are the values for MOE and density. In order to better understand the potential precision of the method, a wood sample was removed from member B1, and tested according to ASTM D143 to determine the MOE. A sample was also removed to determine density using the oven-dry method. Using these measured values of MOE and density, the calculations for joint stiffness due to deflection and frequency can be corrected. As a result, the joint stiffness for deflection was reduced, and the joint stiffness for frequency was increased, reducing the percent error from 55% to 26% (Table 3)

Table 3 – Joint stiffness calculations based on assumed and tested values

Values used for calculations	Joint stiffness (lb-in/rad) based on deflection	Joint stiffness (lb-in/rad) based on frequency	% Error
Assumed values of MOE (900,000 psi) and density (26.2 pcf)	2200000	1000000	55
Measured values of MOE (1,010,000 psi) and density (31.3 pcf)	1750000	1300000	26

Pack Lodge

The results from testing the Pack Lodge visitors center produced results with greater variability than the circa 1900 barn. The percent error varied from 100% to 50%. The average percent error was 72%. Three of the four members had stiffness ratios of kL/EI greater than 1. The largest percent error (100%)

was in the member with the kL/EI value less than 1. The average percent error in members with kL/EI greater than 1 was 63%.
A number of difficulties arose in applying the method to this structure. The non-geometric forms of the members made accurate determination of member properties difficult. These peeled logs were neither straight, nor uniform in their cross section or taper. The dimensions of the members were determined by measuring the circumference at each end and in the middle. These three values were averaged, and then the average circumference was used to calculate an equivalent circular diameter. The cross section varied along the length, with significant shape defects due to the natural form. Values of the Moment of Inertia calculated for these members varied by 45% for members that appeared nearly equal in size. The crook (variation from a straight line) along the length of the member made determination of length a more difficult operation. Finally, the shape of the joints made the definition of the end point more difficult, further complicating the process (Figure 4).

Figure 4 – Pack Lodge bottom chords showing the boundary conditions

Conclusions

The use of a frequency technique to determine the rotational stiffness of joints in a timber structure may be two-fold. First, for a structural analysis of a building, it may be necessary to determine which members should be modeled as pin connected, and which members should be modeled as semi-rigid with a specific value for rotational stiffness. For the two buildings tested, the frequency method showed an overall correlation to deflection, and was able to determine joints of greater and lesser stiffness. The precise stiffness value of joints is of interest when the kL/EI ratio is greater than 1. The frequency method has improved precision in this range, and averaged 32% for solid sawn members. This percent error was able to be reduced by approximately half by measuring, rather than assuming, values for MOE and density.

The method has greater difficulty determining stiffness values for irregularly shaped members, whose overall lengths, etc. are harder to define.

A second use for this method is to determine which joints may be particularly weak and in need of closer inspection and repair. Work done by Brungraber (Brungraber, 1985) and Yue (Yue, 2011) have shown a correlation between lower rotational stiffness and lower ultimate rotational strength. Using this frequency method may allow for rapid location members of lower rotational strength for focused attention in

restoring timber structures. However further research is needed in this area before proposing an acceptable technique.

References

American Forest & Paper Association. 2012. National Design Specifications for Wood Construction supplement – Design Values for Wood Construction.

Anthony, Ronald W. 2008. Maintenance and Rehabilitation – Assessing and Extending the Life of Existing Wood Structures. Paper presented at the Structural Engineering Institute Pre-Congress Workshop "Wood Engineering Challenges in the New Millennium: Critical Research Needs" for the annual international meeting of the American Society of Civil Engineers, April 23-24, 2007 in Vancouver, BC, Canada.

ANSYS® Academic Research, Release 8.0, ANSYS, Inc.

Audacity 1.2.6 free download available at http://audacity.sourceforge.net/

Brungraber, R. 1985. Traditional Timber Joinery: A Modern Analysis. PhD dissertation, Stanford University, Palo Alto, CA.

Crovella, P. L. and G. H. Kyanka. 2011. Use of vibration techniques to determine the rotational stiffness of timber joints. Proceedings of the Structural Health Assessment for Timber Structures Conference. Lisbon, Portugal. 12pp.

Fischetti, David C. 2009. Structural Investigation of Historic Buildings John Wiley and Sons. 275 p.

Forest Products Laboratory 1999. Wood handbook : wood as an engineering material.. General technical report FPL ; GTR-113. Madison, WI : U.S. Department of Agriculture, Forest Service, Forest Products Laboratory: xi, [463] pages : ill. ; 28 cm..

Kasal, B., R. Anthony and M. Drdacky. 2009. In-Situ Evaluation of Historic Wood and Masonry Structures 130 p. http://www.rilem.net/proContents.php?pro=pro062

Kasal, B. 2011. State-of-the-art in in-situ evaluation of structural timber – some critical observations. Saporiti, J. editor. Proceedings of the Structural Health Assessment of Timber Structures. 2011, June 16-17 Lisbon, Portugal.

Ross, R. J., Brashaw, B. K., Wang, X., White, R. H., and Pellerin, R.F. 2004. Wood and Timber Condition Assessment Manual, Forest Products Society, Madison, WI.

Schmidt, R. J. and R.B. MacKay. 1997. Timber frame tension joinery. Report on research sponsored by the Timber Frame Business Council. Washington, D.C.

Yue, Zhi. 2011. A Study on Traditional Chinese Wood Joint Differences as a Supplement for Wood Structure Code. Saporiti, J. editor. Proceedings of the Structural Health Assessment of Timber Structures 2011 June 16-17 Lisbon, Portugal.

Approved Concept for Inspection of Modern and Historic Timber Structures: Theory and Practical Experiences

Frank Rinn

Abstract

Based on the development of resistance drilling in 1986 and combined with other methods, such as visual inspection, wood moisture measurements, and stress-wave timing, a comprehensive concept for inspection of timber structures and documentation of the results was developed in conjunction with experts from several other professions. Since 1987, several thousand historic and modern timber structures have been inspected: for example, buildings (castles, churches, family houses, sport/swimming halls), bridges, poles, harbors, and playground equipment. The major goal of the specific type of color-coded inventory sketches was to comprehensively show all relevant results of the inspection and at the same time revealing these findings in a way that can be understood by architects, engineers, carpenters, and heritage administrations in a quick and easy way without having to read text reports. The biggest difference from ordinary concepts is the step from damage documentation to condition inventory. As a consequence, costs of restorations and maintenance typically dropped by about 50% because of significantly higher planning safety (achieved by significant, reliable, and clear results).

Keywords: Timber inspection, resistance drilling, color coded condition inventory

Introduction

More than 2.5 Mill historic half-timbered buildings and more than 5 Million buildings with wooden ceiling beams have to be preserved in Germany as good as possible due to regulations on historical monuments as the cultural heritage. More than 200 Billion Euro are spend for buildings in Germany every year. Approximately 60% of the building budget is spent for restoration and repair of existing buildings. However, the education of architects and engineers still mainly focusses on design of new buildings.

Between 1 and 3 Billion Euro are spent each year for preservation of historical monuments, mostly at least partially financed by taxes or lottery funds.

Approximately 5% of new houses are built with structural timber (+10% p.a.). The inspections of 'new' timber buildings (built > 1950) is growing, due to poor quality of design, wrong use and missing maintenance.

As a consequence, the need for non-destructive timber inspection increases. However, specific boundary conditions have to be regarded:

- Architects and engineers are still mostly paid a percentage of the total costs (thus are not primarily interested in saving costs, especially if public money is involved).
- If a building is 100, 200 or even more years old and does not show significant deformation, the timber structure is supposed to be strong enough and then only decayed parts of the structure have to be replaced. That's all! There is no need for structural analysis and calculation of load carrying capacity.
- If there are significant obvious deformations or the future use of the building will bring in more load (less than 5% of all cases) then stiffness and strength of beams have to be determined.

Based on the market, the client's needs and the given boundary conditions, we developed a concept how to inspect timber structures in a fast, efficient and reliable way.

Major objection and tasks of our inspections

Non-destructively creating an easy to understand and clearly visible status report on timber structure condition without harming other (historic) fabric:

- create/modify sketch of construction covering all relevant timber beams
- determine dimensions of timber cross-sections and connections
- reliably identify decayed and intact parts of beams and connections
- (sometimes: determine MOE and estimate MOR)
- visualize results in color inventories (rather than writing long text reports)

The inspection concept was developed in cooperation with architects, engineers, carpenters and administrations. Meanwhile, several thousand buildings have been successfully inspected.

Major steps of the inspection are

1. Create new or modify existing sketches of the construction.
2. Visually inspect all accessible parts (condition, external defects, dimensions of beams, previous repairs) - often major part of total work to be done.
3. Technical measurements:
    - 3.1 moisture content measurement
    - 3.2 resistance drilling (with calibratable machines only, such as Resistograph®)
    - 3.3 stress wave timing (for example using impuls hammer or Arbotom®).
4. Documentation of all results and all relevant information about timber condition into a few graphical sketches by avoiding long text reports.

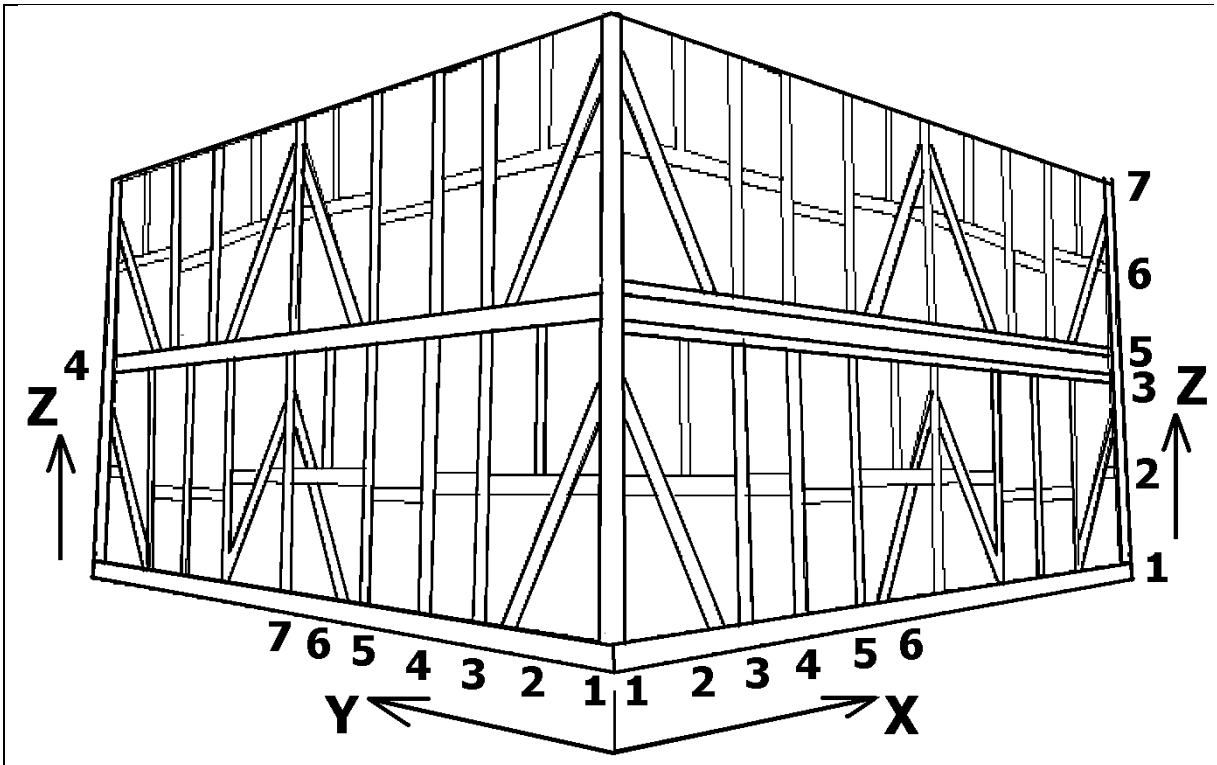

Fig 1.: Example for coordinate system numbers to clearly identify timber axis and joints.

Basic sketch for colored inventory

All relevant beams have to be shown in at least one of the sketches. A coordinate system reliably identifies each beam and connection.
The demands made for an inventory regarding the timber construction can be easily formulated:

1 All pieces of timber relevant for the statics of the construction must be drawn in at least one plan.

2 When possible, no piece of timber should be drawn on top of any other.

3 The relative position of the beams to each other must be correct.

4 Great deformations relevant to the static construction must be included.

Unfortunately, it can be determined that existing inventories often do not fulfill these conditions. The common ground plans at approx. 1 meter height over the ceiling beams are useless for this purpose. It has proven better to draw up a new schematic sketch of the construction according to the above-mentioned conditions instead of trying to correct existing plans.

In some cases it makes sense to examine the hidden timbers in the ceiling by means of thermography. Up to now, this technique can predominantly be used in winter, because great differences in temperature are required.

Visual (ordinary) inspection

This first part of the inspection is often the major part of the total working time and usually consists of the following steps:

1. Look for external decay (by fungi or insects).
2. Knock on all beams and connections with ordinary hammer
3. Use handcraft tools to check in all suspicious holes/connections
4. Take samples from insect or fungal decayed parts and determine decay species.

5. Check quality of previous repairs and replacements.
6. Look for and measure major deformations.
7. Try to find reasons for decay and other defects.
8. Document all results in colored sketches.
9. Determine points where technical inspection is required.

At the end of the visual ('conventional') inspection, the colored sketch already contains a lot of information but has many white spaces where condition of the corresponding beams is still unknown.

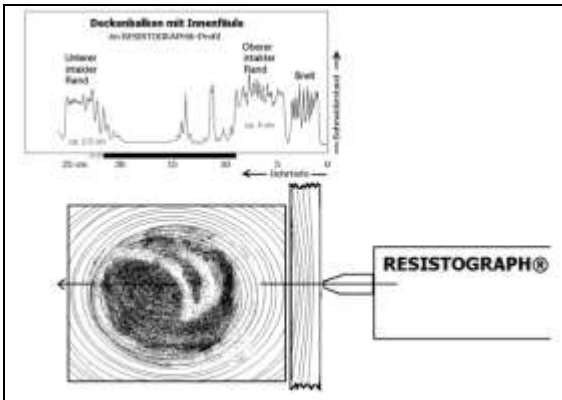

Fig. 2: Resistance drilling using calibratable machines allows the experienced user to reliably identify decay even in hidden timber, such as ceiling beams below floor.

Technical inspection

When visual inspection was not able to clear all questions or of hidden beams have to be evaluated, technical methods are used in order to answer the remaining open questions:

1. Relative moisture content.
2. Drill resistance measurements
   a. find hidden beams behind stucco or below flooring
   b. assess depth of obvious outside decay or cracks (e.g. in glue-lam)
   c. check internal condition (of visible and hidden beams and connections)
   d. determine gross density (after calibrating drilling machine)
3. Stress wave timing: speed of sound, detect hidden cracks or connections
4. Combine (not only numeric) results, e.g. density * speed ^{2} = MOE
5. Document all measurement points and all results in colored inventories.

Having inspected a timber structure visually and technically may lead to great results but does not help preserving historic fabric or making repair efficient if the experts planning and executing the repair work do not understand the results in an easy and clear manner.

Based on the success of the application of resistance drilling for inspecting timber starting 1986, we then developed a concept how to document inspection results that provides more precision and reliability but is, at the same time, more easy to understand for both engineers and carpenters.

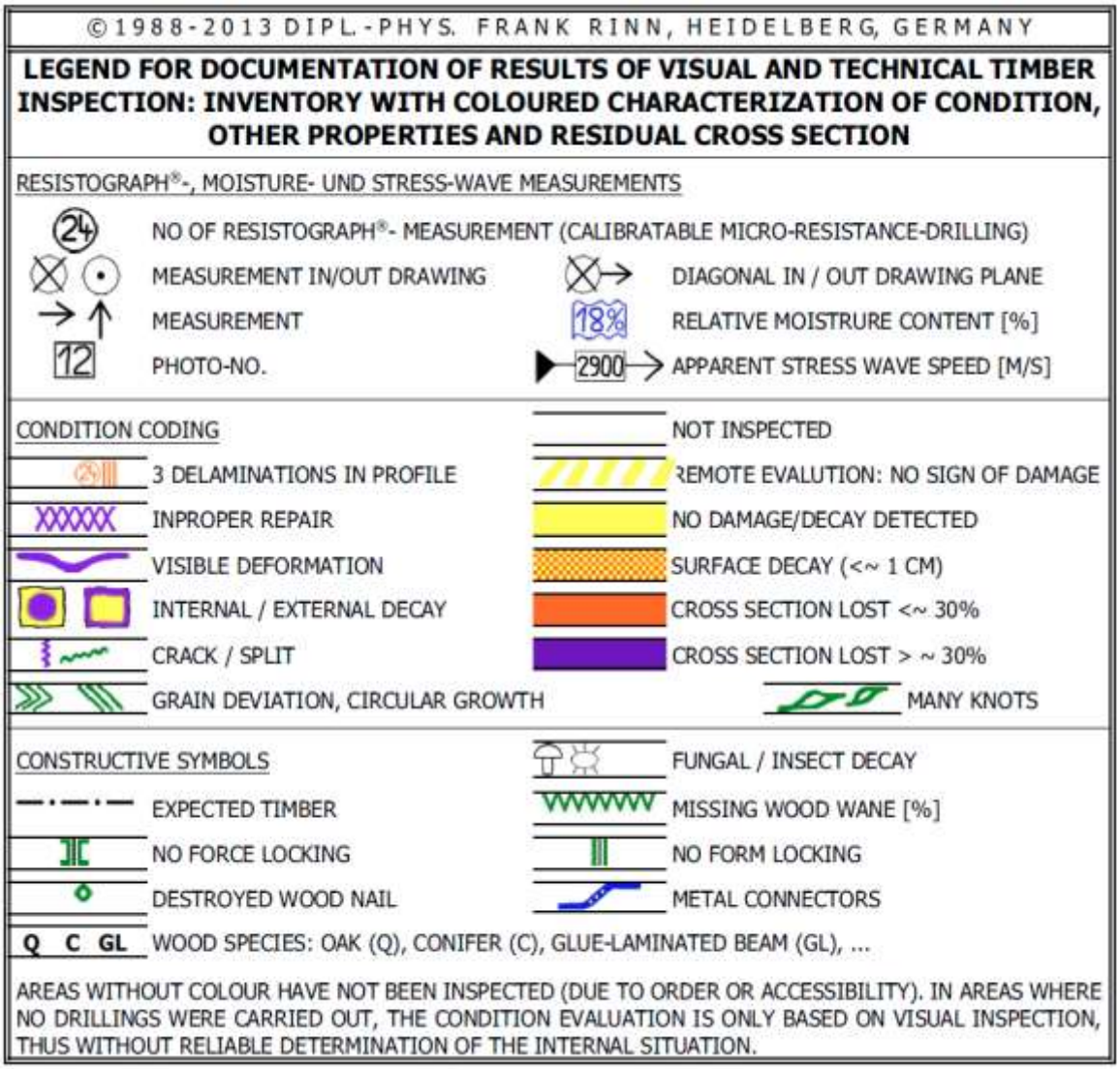

Fig. 3: Legend of colored inventory sketches showing the condition of timber in three major colors and describing additional signs for specific symptoms identified at a beam or structure.

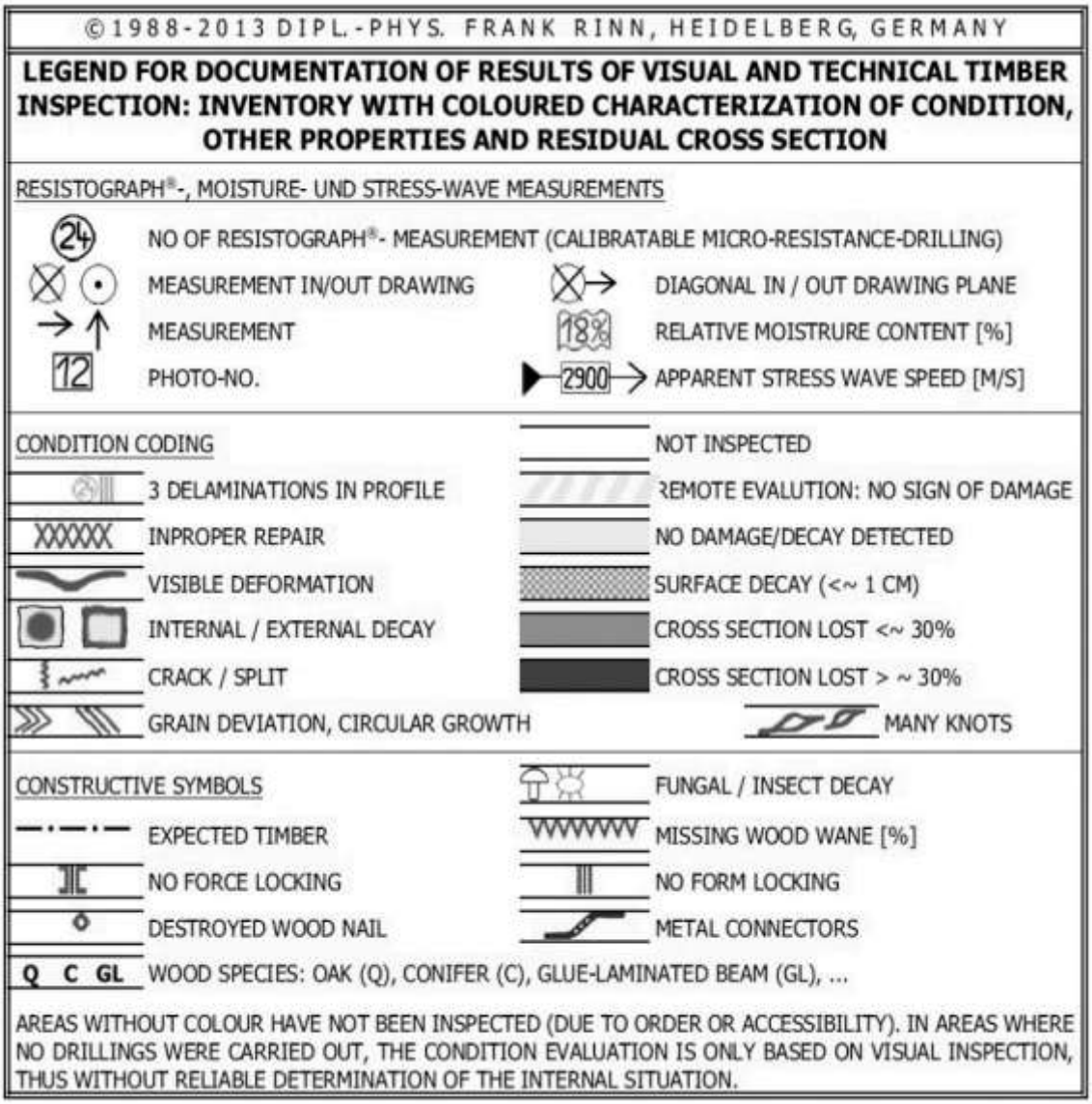

Fig. 4: Black and white copy of the condition legend still providing three major condition markers reliably differentiated by different grey scales.

Documentation concept

The first step forward coming from black and white sketches of timber structures with shadings for marking decay was to use colors. But, in order to make the drawings as easy as possible to read, the number of main colors had to be as small as possible, at most three or four.

At the time we developed our concept (late 1980ies / early 1990ies), color copies were still quite expensive, especially if printing in larger than standard letter sizes. The colors thus had to be selected in a way that allows black and white copies still providing the major information about decay and condition (Fig. 3). Consequently, we selected red (extensively decayed), orange (mean decay), and yellow (intact) as the major colors – because they can be differentiated easily on the first view and because black and white copies still show the three colors reliably in differentiated types of grey (Fig. 4).

The traffic-light color scheme, green for intact), yellow for partially decayed, and red for strongly decayed parts, was no option because of several reasons: in a black and white copy, green was commonly darker than red, leading to a wrong impression about the condition of the corresponding parts. In addition, structural engineers in Germany commonly used green for marking structurally relevant, local aspects and symptoms, such as cracks.

The biggest step forward was introducing a color for marking parts of timber that were inspected (either visually, by tapping and/or resistance drilling) and where found to be intact and sound. This means, if a beam was tested in whatever kind and no sign of decay was found, this beam is marked with a certain color.

For the first time, this way it was possible to distinguish between the sections of a timber structure that were not inspected (no color) and the parts that were inspected without finding damages (yellow). This may sound as a tiny little aspect but changed a lot because from then on later planning and working steps did know what parts of the structure they can rely on without doubting whether these parts had been checked or not (because there was no decay marked).

Another big step forward was combining as many parts of the usually many individual sketches of a structure as possible into one single overview drawing: this reduced the total number of sketches representing the condition of a structure often from 10 to 1 or 2 – making it much easier for engineers and architects as well as for carpenters getting an overall impression about the condition of the bridge or structure as a whole. In addition, the overview given by a single sketch with a color coded condition inventory allows the identification of connections between sources and reasons of different spots or areas of decay. That means, these overview inventories provide a base for a much deeper understanding of the structure as a whole instead of only working locally on repair of individual parts.

Fig. 5:
Typical timber bridge to be inspected because of decay (although made by tropical hardwoods).

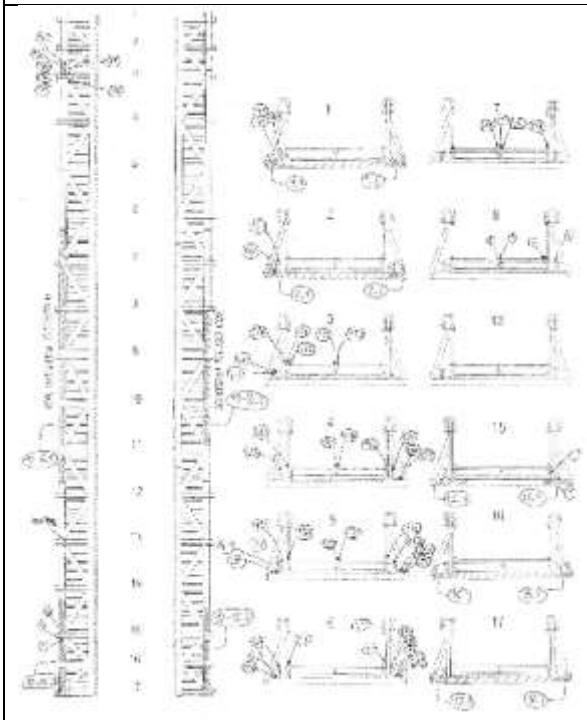

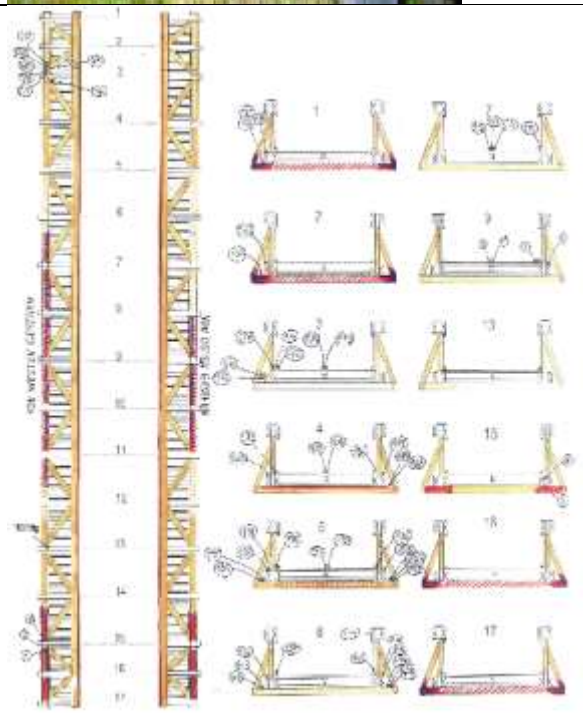

Conventional black and white damage map of a timber bridge. Originally it was common to mark decayed parts with a certain kind of shading and a label that refers to the text list position of the corresponding description of the found damage.
Such a drawing consisted usually of 18 individual sketches of each axis and was accompanied by many pages of text within the report.

Colored version of an inventory map showing wood condition in different colors. The colors do not only reveal where decay was found but furthermore show what parts of the structure were found and proven to be intact. Because colors allow the reader to much easier identify damaged areas, such a combined sketch replaces many conventional drawings.

Practical working steps

Commonly we prepare the basic drawings of structures before the technical inspection starts. Such structural sketches have to show all relevant timber parts that belong to at least one plane of the structure or are connected with this plane. While doing that, we try to avoid showing different beams in one sketch that in reality overlay each other and represent different planes – because it is impossible to show correct colors if these beams have different conditions and thus would have to be characterized by different colors overlaying each other.

Usually, the sketches are prepared in a larger size and scale for enabling the inspector on site to put in all relevant information while inspecting - as one of our major goals was to avoid text notes but reveal all relevant aspects in the sketch. And, all evaluations should be done on the spot without having to go back to office and again work on profile analysis and come to a conclusion that, for example, additional assessments are required. This is time consuming and inefficient. Our goal was to always come to a final conclusion about the condition of timber on site while inspecting because only on site at the structure you can just tap or drill another time at another spot in order to confirm unclear results or suspicious symptoms. The highest (cost and time) efficiency we always achieved when the inspection came to a final conclusion on the site and when all relevant results were documented in the color coded inventory map on site. This drawing has then only to be reproduced in the office and surrounded by a short text note.

The reproduction of the colored on-site drawing is usually done by a reduction factor of 4. These squeezed sketches then represent the most significant part of the report. In addition, the report usually contains some illustrating pictures and a short text summary with recommendations. Even the recommendations for repair work can be partially included in the color coded sketch because lines may be implemented indicating where and how damaged beams should be cut and/or replaced.

All this fits to the traditional German saying: “A good drawing is the language of a good engineer”.

Fig. 6: Example for a simple, combined plan presentation of a half-timbered building. On top of the facade the complete rafter plane of this side is drawn. Such a combination allows for one, the recognition of possible reasons for damage, if, for example, the leaky roof has caused damages to the rafter foot points as well as to the purlin and the post head underneath it in the facade. In individual inventory plans with individual rafter axis and facade drawings, such correlations are often overlooked.

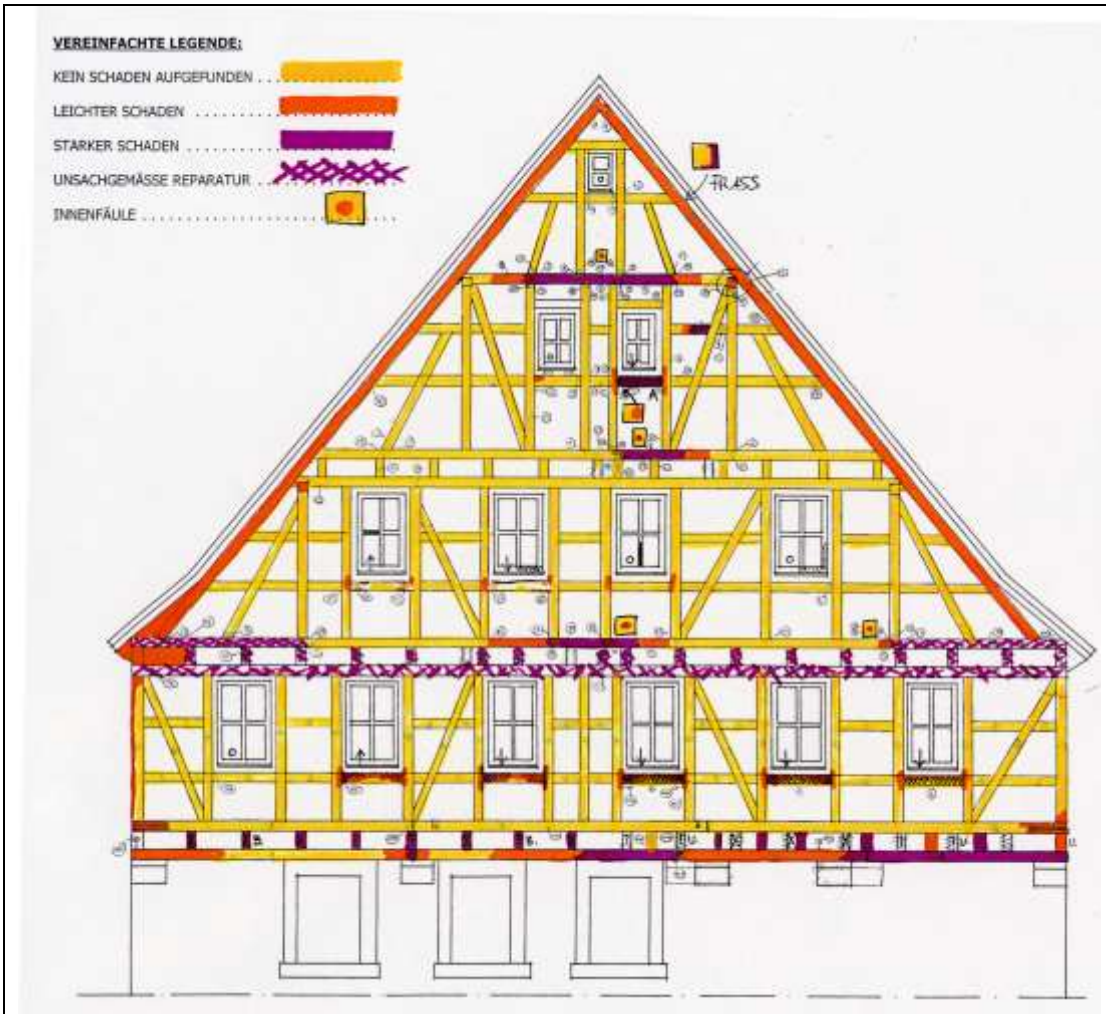

Fig. 7: Overview sketch with a simplified color coded condition inventory. This inspection was carried out by one person on one day including the drawing of the inventory what is usually done on site.

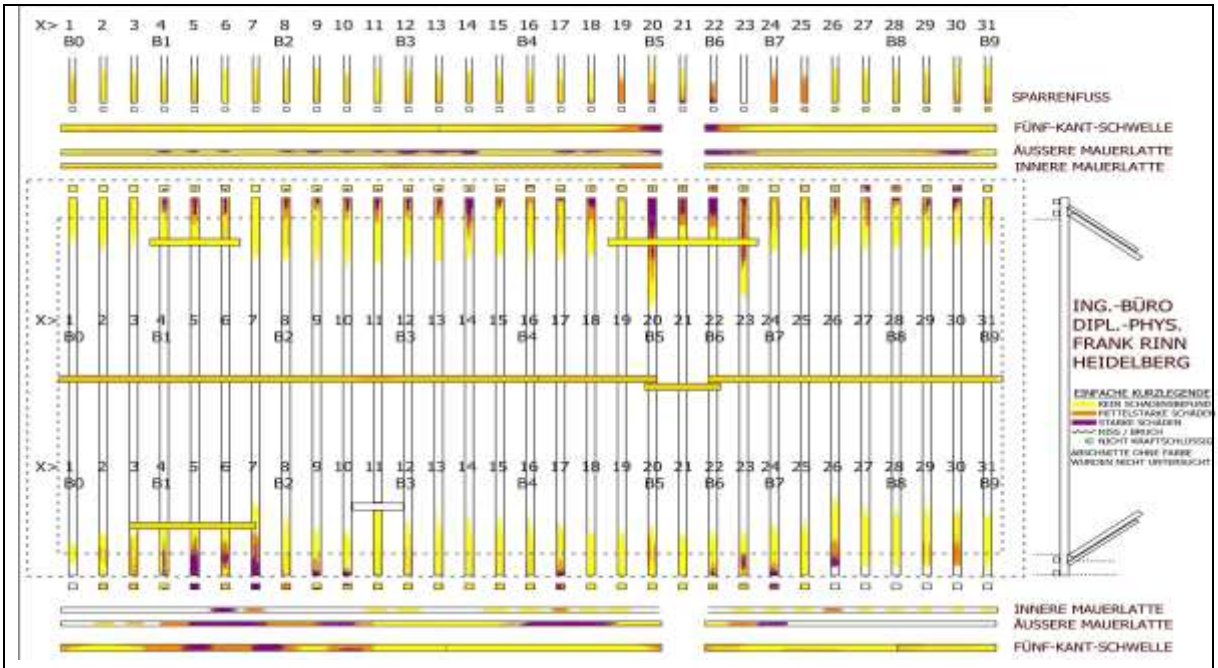

Fig. 8: Ceiling beams of a historic church plus underneath wall beams and the foot parts of looming rafters. This one sketch replaced several dozen sketches of all axes of conventional documentations.

Consequences

Practical application of this concept in several hundred real market projects of very different size scales proved its suitability and led to a significant increase of planning safety and furthermore to dramatically reduced total costs.

References and further reading

Dackermann, U., K. Crews, B. Kasal, J. Li, M. Riggio, F. Rinn, and T. Tannert. 2013. In situ assessment of structural timber using stress-wave measurements. Materials and Structures. June 2013. DOI 10.1617/s11527-013-0095-4.

Fischer, H.-B., Rinn, F. 1996: Bestandsplan mit farbiger Zustandskartierung der Holzkonstruktion. Bauen mit Holz 11 (1996): 852-858.

Rinn, F. 1988: A new method for measuring tree-ring density parameters. Physics diploma thesis, Institute for Environmental Physics, Heidelberg University, 85pp.

Rinn, F. 1990. Device for material testing, especially wood inspection by drill resistance measurements. German Patent 4122494.

Rinn, F. 1993: Gucken, Klopfen, Bohren. Zerstörungsfreie Bohrwiderstandsmessung als Teil der ingenieurtechnischen Holzuntersuchung. Bausubstanz, 5 (1993): S. 49 - 52.

Rinn, F. 1993: Catalogue of relative density profiles of trees, poles and timber derived from RESISTOGRAPH micro-drillings. Proc. 9th int. meeting non-destructive testing, Madison 1993.

Rinn, F. 1994. Resistographic visualization of tree ring density varia-tions. International Conference Tree Rings and Environment. Tucson, AZ, 1994. Printed in: Radiocarbon 1996, pp. 871-878.

Rinn, F. 1994: One minute pole inspection with RESISTOGRAPH micro drillings. Proc. Int. Conf. on wood poles and piles. Ft. Collins, Colora-do, USA, March 1994.

Rinn, F. 1994: Resistographic inspection of building timber. Proc. Pacific Timber Engineering Conference. Gold Coast, Australia, July 1994.

Rinn, Frank (2006): Konzept für Zustandsanalysen von Holzkonstruk-tionen. bauen mit holz 10/2006. S. 26-33.

Rinn, F. 2012: Basics of micro-resistance drilling for timber inspection. Holztechnologie 53(2012)3. - S. 24 - 29

Tannert, T., R. W. Anthony, B. Kasal, M. Kloiber, M. Piazza, M. Riggio, F. Rinn, R. Widmann, and N. Yamaguchi. 2013. In situ assessment of structural timber using semi-destructive techniques. DOI 10.1617/s11527-013-0095-4.

Detection and Assessment of Wood Decay in Glulam Beams Using a Decay Rate Approach: A Review

C. Adam Senalik
USDA Forest Products Laboratory, Madison, WI, United States of America, csenalik@gmail.com

Abstract

A glulam beam is subjected to X-ray computer tomography and acousto-ultrasonic measurements to detect and assess wood decay. A glulam beam without visible indications of wood decay was taken from field use. A modified impulse-echo technique is employed as an inspection method requiring access to only one side of the beam. It is observed that decay-rate analysis of the collected signals allows detection and assessment of wood decay. The decay-rate approach leads to an overall rate of false calls of 7.2%. Considering the variability that exists in wood including the presence of splits, orientation and thickness of growth rings, etc., this relative low rate of false calls makes this approach very attractive. The results of the decay-rate analysis are found to be consistent with decay located using X-ray computer tomography. This paper is a review of findings first presented in (Senalik et al. 2010).

Keywords: Wood decay, structural lumber, glulam beams, X-ray computer tomography, impulse-echo

Introduction

While much has been done to preserve wood and wood composites, even the best preservative techniques available today have not been able to truly halt the natural decay process. The process of decay varies with species, but follows a sequential process of incipient, intermediate, and advanced decay. Incipient decay normally occurs with little visible change of the wood, although the dynamic strength properties are greatly reduced. The other extreme, i.e., advanced decay, is characterized by wood with no intrinsic strength.

Several nondestructive testing methods have been attempted to detect and evaluate incipient decay. The inherent variability of wood such as grain angle, density, moisture content variations, and presence of features such as knots, splits, and resin pockets mask the presence of incipient decay. An ultrasonic through-transmission approach was developed in (Senalik et al. 2008). It was shown that the frequency of maximum amplitude and ultrasonic velocities were sensitive to wood decay. However, often only one lateral side of the wooden beam is available for testing and evaluation. The ultrasonic pulse-echo configuration does not lend itself to this test, mainly because of the high levels of ultrasonic attenuation in wood and because of the growth ring channeling effects, (i.e., guiding wave effects). As a result, a modified impulse-echo decay rate approach was developed where the energy is delivered by dropping a steel sphere onto a steel plate previously coupled to the glulam beam. A good literature review of impulse-echo approaches is provided in (Sansalone 1997), (Reis and Habboub 2000), and (Senalik et al. 2009). This paper is a review of findings first presented in (Senalik et al. 2010).

Experimental description

One Douglas-Fir glulam beam with a cross-section of 7.5in by 5in (19.1cm by 12.7cm) was salvaged from a construction site. The glulam beam was made from five 5in by 1.5in (12.7cm by 3.8cm) laminas,

which were laminated to yield the final glulam beam. Visual inspection of the original beam did not show any indications of decay. A 45 inches (114 cm) long segment of this beam was then cut for this study. In this 45 in (114 cm) long segment, the only observed indication of decay was at the end of the beam in lamina 2 where an interior small hole was observed. However, the level of decay could not be assessed using visual inspection. In addition, a small (millimeter-wide) longitudinal crack, i.e., split, on the top surface was also observed. Before testing, the beam was marked with a one inch square (2.54mm square) grid for subsequent X-ray and ultrasonic measurements.

X-ray computer tomography was used to characterize the wood decay in the glulam beam. Tomographic views were made every centimeter along the beam length. The examined beam possessed decay at all severity levels ranging from sound wood to advanced decay. Based upon the cross-section tomographic views, a determination was made it as to the severity of decay at each location within the beam. The third lamina of the beam possessed a transition region between sound wood and advanced decay, which provided a location to evaluate the ability of the decay-rate technique to identify incipient decay.

Data was collected using a modified impact-echo data acquisition system. The voltage signal from an accelerometer (Model PCB309M12 with a resonance frequency of 120 kHz) mounted near the point of impact was filtered using a Butterworth filter with a band pass of 500 Hz to 500 kHz. Each test data set consisted of 8192 data points collected at a sampling rate of 1 MHz. Data was recorded after the voltage exceeded the trigger voltage of 19 mV. A steel ball bearing of diameter 12.70 mm and mass of 8.33 grams was used as the impactor. The steel ball bearing was dropped from a height of 200 mm onto the center of a circular steel plate with a mass of 6.27 grams, a thickness of 6.35 mm, and a diameter of 12.71 mm. Using MatLab filtering tools, the recorded waveforms were further band filtered using a Butterworth filter between the frequencies of 500 kHz and 500 kHz.

The accelerometer was placed adjacent to the impact plate, and both were centered with respect to the width of each lamina. Care was taken to prevent contact between the impact plate and the accelerometer. Both the impact plate and the accelerometer were coupled to the lamina surface using Celvacene heavy, high vacuum grease. The presence of the plate prevented marring of the lamina top surface by the steel sphere and eliminated variability of the impact spectral power distribution caused by the presence of the growth rings on the top surface. The impact plate also increased the area across which the wave energy was distributed. The beam was fixed into a position such that a portion of the beam was cantilever to the test rig support. The location of testing was always within the cantilever portion of the beam in order to minimize signal loss due to leakage into surfaces abutting the beam.

Decay Rate Analysis

In this study, five measurements for each different location along each lamina were made. Five waveforms were collected using 8192 data points using a sampling rate of 1 MHz, and an average waveform was created. A window of 1024 points was moved across the waveform point by point and the corresponding FFTs were calculated. Using an FFT containing 1024 points, the frequency amplitudes ranging from 976 Hz to 19.53 kHz with increments of 976 Hz were calculated. A spectrogram of frequency magnitudes with respect to time was generated for each frequency. An exponential decay curve was fitted to the magnitude versus time curves for each frequency as shown in Figure 1a. The exponent is considered to be the attenuation rate of the magnitude with respect to time for each frequency. An average of the attenuation rates for the frequencies in a frequency band of 500Hz to 20 KHz (ranging from 976 Hz to 19.53 kHz with increments of 976 Hz) was then calculated. Figure 1a shows the decay of the amplitude corresponding to 12.72 kHz (solid line) and the dashed line represents the exponential fit (r^2 = 0.87) for data collected from lamina 3 at location 686 mm (27 in), which led to a decay rate value of

1.26 Nepers/ms. Figure 1b shows the decay rate of amplitudes of all the FFT frequencies at the same location.

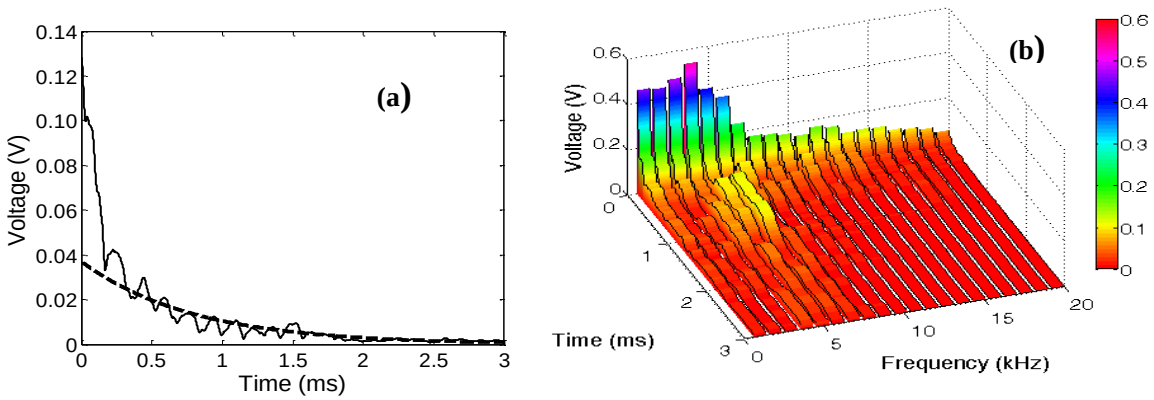

Figure 1 - Frequency voltage decay versus time at location 27 (686 mm) of Lamina 3. (a) The solid line represents the decay of one of the amplitudes (corresponding to 12.72 kHz) and the dashed line represents the corresponding exponential fit (r^2 = 0.87). The data was collected from Lamina 3 at location 686 mm (27 in). This frequency component has a decay rate value of 1.26 Nepers/ms; (b) Voltage amplitude versus time for frequencies 500 Hz to 20 kHz (FFT amplitudes) at the same location.

Figure 2 shows an histogram of the average exponential decay rate for sound and decayed wood showing the corresponding probability density functions, which are assumed to follow a normal distribution. The distribution corresponding to sound wood has a mean of 1.0 Nepers/ms and a standard deviation of 0.06 Nepers/ms while the distribution corresponding to decayed wood has a mean of 1.2 Nepers/ms and a standard deviation of 0.08 Nepers/ms.

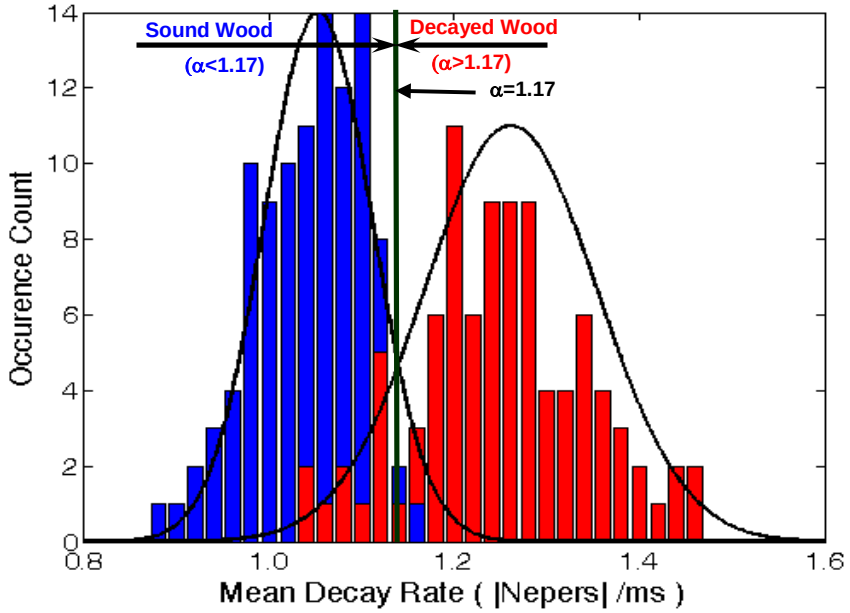

Figure 2 - Histogram of the mean exponential decay rate for sound and decayed wood showing corresponding probability density functions.

Figure 2 shows that the two normal distributions, intercept each other at the value of 1.17 Nepers/ms. Assuming that this average attenuation coefficient would be considered to serve as a decision criteria to differentiate between sound wood and decayed wood, the criteria would lead to 5.7% of false negative

calls (decayed wood considered to be sound wood) and to 3.5% false positive calls (sound wood considered to be decayed). This leads to an overall rate of false calls of 7.2%.

Conclusions

To detect and assess wood decay within a glulam beam, a modified impulse-echo technique is used in conjunction with a decay-rate analysis of the collected signals. The impulse-echo technique involves dropping a steel sphere onto a steel plate coupled to the surface of the beam. Wave data is collected using an accelerometer mounted near the point of impact. A spectrogram of the collected voltage signal is constructed. The voltage magnitude is fitted to an exponentially decreasing curve. An exponent magnitude greater than 1.17 Nepers/ms is a positive indicator of the presence of internal decay. The decay rate approach has an overall rate of false calls of 7.2%. Considering the variability that exists in wood including the presence of splits, orientation and thickness of growth rings, etc., this relative low rate of false calls makes this approach very attractive. The results provided by the modified impulse-echo decay-rate approach are consistent with indications of decay obtained using X-ray computer tomography. Furthermore, the modified impulse-echo results appear to indicate that the approach is sensitive to early stages of decay.

Acknowledgements

This research was made possible by the support from the National Science Foundation under Grant No. CMS 02-01305.

References

Reis, H., Habboub, A.K. 2000. Nondestructive Evaluation of Dimension Stone Using Impulse Generated Stress Waves: Part 1 – Theoretical Aspects and Experimental Prospects. ASTM 1394, K. R. Hoigard, Ed., American Society for Testing and Materials, West Conshohocken, PA, pp. 3-23.

Reis, H., Habboub, A.K. 2000. Nondestructive Evaluation of Dimension Stone Using Impulse Generated Stress Waves: Part 2 – Estimation of Complex Moduli. ASTM 1394, K. R. Hoigard, Ed., American Society for Testing and Materials, West Conshohocken, PA, pp. 24-38.

Reis, H., Habboub, A.K. 2000. Nondestructive Evaluation of Dimension Stone Using Impulse Generated Stress Waves: Part 3 -- Microstructure Characterization. ASTM 1394, K. R. Hoigard, Ed., American Society for Testing and Materials, West Conshohocken, PA, pp. 39-54.

Sansalone, M. 1997. Impact-Echo: The Complete Story. American Concrete Institute-Structural Journal, Vol. 94, No. 6. pp.777-786.

Senalik, C.A., Beall, F.C., O'Dell, K., and Reis, H. 2008. Detection and Assessment of Wood Decay in Glulam Beams Using a Through-Transmission Ultrasonic Approach. Proc. SPIE 6932.

Senalik, C.A., McGovern, M.E., Beall, F.C. and Reis, H. 2009. Detection and Assessment of Wood Decay in Glulam Beams Using a Modified Impulse-Echo Approach. Proc. SPIE 7292, 72920Y.

Senalik, C.A., Beall, F.C. and Reis, H. 2010. Detection and Assessment of Wood Decay in Glulam Beams Using a Decay Rate Approach. Insight-British Institute of Non-Destructive Testing, Vol. 52, No. 10. pp 553-560.

An electrical interface for vibration energy harvesting from wood floor

Shuai Pang
School of Technology, Beijing Forestry University, Beijing, P.R.China, psh1988@126.com
Jiangming Kan
School of Technology, Beijing Forestry University, Beijing, P.R.China, kanjm@bjfu.edu.cn
Wenbin Li
School of Technology, Beijing Forestry University, Beijing, P.R.China, leewb@bjfu.edu.cn
Huixiang Wang
School of Technology, Beijing Forestry University, Beijing, P.R.China,361383428@qq.com

Abstract

Vibration energy from wood floors is of great significance. People's walking on the wood floors can generate potential large energy with rational utilization. Piezoelectric energy harvesting (PEH) is an efficient way of vibration energy harvesting. This paper introduced the performance of two different mechanical structures for PEH. A circuit for collecting and storing energy was applied and analyzed. The results show that different mechanical structures can be applied in different situations. The structure with one side fixed and the other fixed to some extent and shaking with the exciter may be a good choice for collecting vibration energy from wood floors since the generated voltage of the piezoelectric element is stable and reasonable in low frequency conditions. Meanwhile, with the structure and circuit mentioned in the paper, piezoelectric energy can be well stored for further application.

Keywords: wood floor, PEH, structure, electrical interface, vibration.

Introduction

Vibration is everywhere and has high energy density, so a variety of studies have been made on the application and conversion efficiency of it.

In the research on practical uses, special shoes that can collect energy from people's walking have not been used well since researchers failed to make the collected energy able to charge the telephone or other portable electronic devices (Kymissis et al. 1998， Mateu and Moll 2005). Wireless sensors can be charged to operate but they can't work only with vibration energy (Yoon et al. 2005). A sustainable dance floor can compress 10mm when being stepped on to create electricity. The compression is enough to produce up to 35 Watt of sustained output per module (Sustainable Dance Club 2011). To collect the vibration energy in practical use is promising. Researchers are trying to make the vibration energy better used in practice.

In the research on increasing the efficiency of vibration energy harvesting, researchers found that PEH is more efficient compared with magnetic and static ways(Sodano et al. 2004). Different piezoelectric materials, size, mechanical structures are of different generating electricity performance (Wanglu et al. 2012). As the voltage of the generated electricity is sinusoidal, different performances of various rectifiers have been studied including the full-bridge rectifier(Jeon et al. 2005), voltage doubling rectifier (Dallago et al. 2007), CMOS full-bridge rectifier (LiQiang 2011) , etc. The matching resistor theory is also a focus of improving the performance of the harvesting (Ottman 2002). Synchronized switch harvesting on inductor (SSHI) technique is a hotspot consisting of parallel-SSHI and series-SSHI. The key point of the technique is to control the switch when the piezoelectric beam reaches its maximum displacement but it usually needs extra power and precise detecting devices (Lefeuvre et al. 2006). Self-powered SSHI technique has appeared but it has higher harvested power than the standard harvesting technique when its output open voltage is larger than 6V (Junrui Liang and Wei-Hsin Liao, 2012). Voltage stabilization is also a part of the electrical interface and the storage of the energy is essential.

PEH is an efficient way of harvesting energy harvesting. This paper introduced the performance of two different mechanical structures for PEH and focused on the optimization of PEH from wood floor. The electrical interface which connects the piezoelectric element to the terminal electric load is a critical point in the optimization of a PEH system. The performance of a collecting and storing circuit has been analyzed.

Experiments

In the experimental environment, we attempted to simulate people's walking on wood floors by using the vibration exciter functioning on the piezoelectric element.The experimental devices include a signal generator GFG-8015G, a power amplifier B&K 2706, a vibration exciter B&K 4809, a designed fixed station, an oscilloscope NEC omniace RA110, multimeters and so on. The sketch of experimental setup is shown in Figure 1.

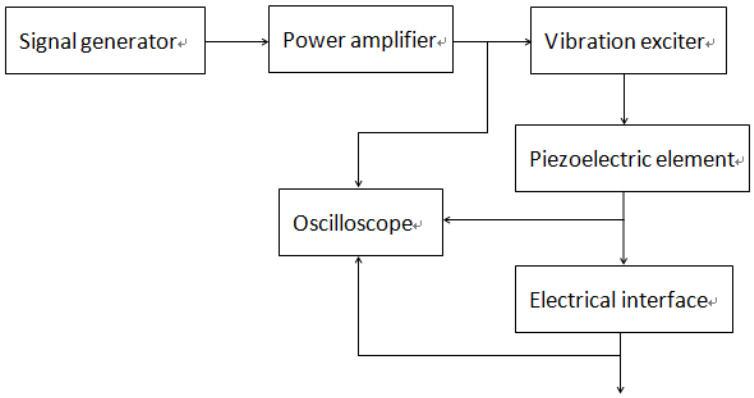

Figure 1---Sketch of experimental setup

Piezoelectric element

The piezoelectric transducer is composed of the copper base plate and the PZT-5H ceramics. The plate is bimorph. Its working model is d31 whose generated voltage is perpendicular with the applied stress. More detailed parameters are shown in Table 1. The parameters were confirmed by measurements except modules of elasticity. If the piezoelectric element is larger, the capacity of generating electricity will be bigger.

Table 1---Parameters of the materials

Materials and dimension	PZT-5H	Copper
Density($Kg \cdot m^{-3}$)	6790	8300
Modules of elasticity(GPa)		131
Thickness(mm)	0.2	0.2
Width(mm)	50	50
Length(mm)	50	70

Two mechanical structures

The two mechanical structures' simplified schematic diagrams are shown in Figure 2. Model a is that one side of the piezoelectric element is fixed and the other side is fixed to some extent and shaking with the exciter. Model b is that just one side is shaking with the exciter and the other side is free.

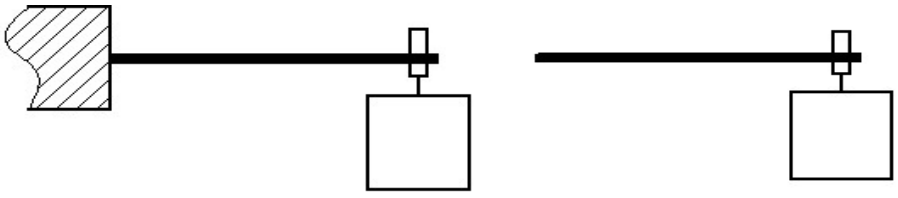

(a) (b)

Figure 2---Two modes of mechanical structures

As shown in Figure 1, The signal generator can produce a certain frequency of sine wave. The power amplifier makes the wave large enough to shake the exciter. The piezoelectric plate shakes with the exciter and the generated sine output voltage of the plate can be seen with the oscilloscope.

Frequency of the system

The natural frequency is shown in equation (1), and we can calculate w_n through the parameters in Table 1 and by the equations from (1) to (5). From equation (1), we can conclude that increasing the mass of m_1 can reduce the natural frequency. In our experiments, there is no m_1, so m_1 is equal to zero.

$$w_n = \sqrt{\frac{k}{m_1 + m_2}} = 2\pi f_n \tag{1}$$

$$\delta = \frac{Pl^3}{3EJ} \tag{2}$$

$$k = \frac{P}{\delta} \tag{3}$$

$$m_2 = \frac{33ql}{140} \tag{4}$$

$$J = \frac{bh^3}{12} \tag{5}$$

Where k is the spring stiffness, m_1 is the weight of mass fixed at the free end of the beam, m_2 is the equivalent weight of the cantilever's free end, δ is the deflection, P is static load of the cantilever's free end, E is modulus of elasticity, J is the moment of inertia, q is the mass per meter, l is the length of the cantilever beam, b is the width of the cantilever beam and h is the thickness of the beam (Yinmin Zhang,2008). l is 61mm in the experiment.

f_n is calculated to be 22.9Hz, which is consistent with the simulation result using ANSYS 14.0. The resonant frequency in damping conditions is shown in equation (6):

$$w = \sqrt{1 - 2\xi^2} w_n \tag{6}$$

The electrical interface

In the experiment, structure of model a mentioned above is used to generate electricity since it works well in low frequency. The chips LTC3588-1 and CBC3112 were used for collection and storage of energy. LTC3588-1 is for piezoelectric energy harvesting power supply. It owns an integrated low-loss full-wave bridge rectifier. With input operating range from 2.7V to 20V, the output voltage can be selected to one of the following voltage: 1.8V, 2.5V, 3.3V and 3.6V. And the continuous output current can be up to 100mA, which is much larger than the original output current in μA level. We choose 3.6V to carry out our experiment. CBC3112 is the world's first intelligent thin film energy storage device. A 12μAh thin film

energy storage is integrated. 3.6V is in the range of the input of CBC3112. The experimental electrical circuit is shown in Figure 3.

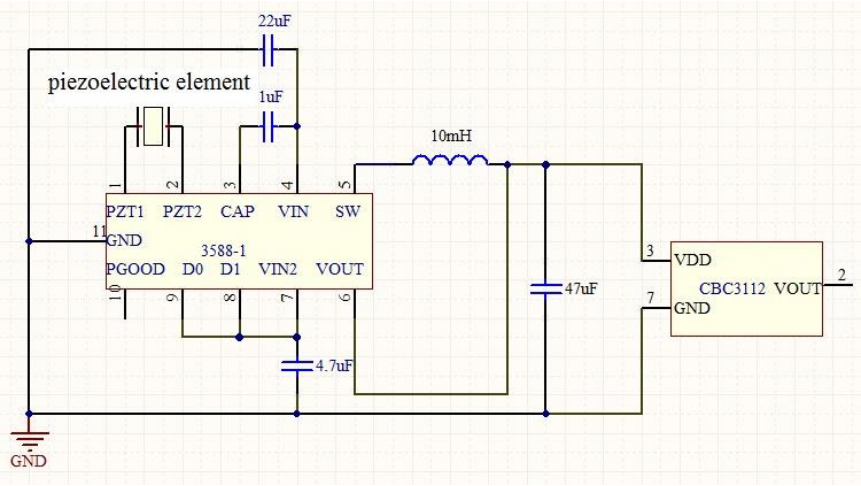

Figure 3---The experimental electrical circuit

Results

For each mechanical model, in different amplifier's output voltage and different frequency, the generated peak voltage was recorded. Figure 4 and Figure 5 respectively show the relationship between frequency and the generated peak voltage with model a and model b structure as shown in Figure 2. Meanwhile, Figure 6 shows the performance of the two models when the output voltage of the power amplifier is 3V. Figure 4 and Figure 5 demonstrate that the larger the input of the piezoelectric transducer is, the larger the output of it. Figure 6 shows that different mechanical structures have different performances .They can be used in different situations. If the environmental vibration frequency is lower than 15 Hz, model a is better to collect energy since its output voltage is large than that of model b. But if the environmental vibration frequency is easy to reach the resonant frequency, it's better to use model b.

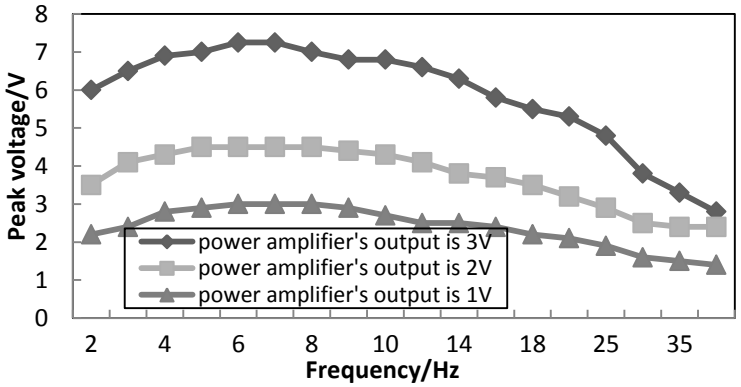

Figure 4---Relationship between frequency and the generated peak voltage with model a

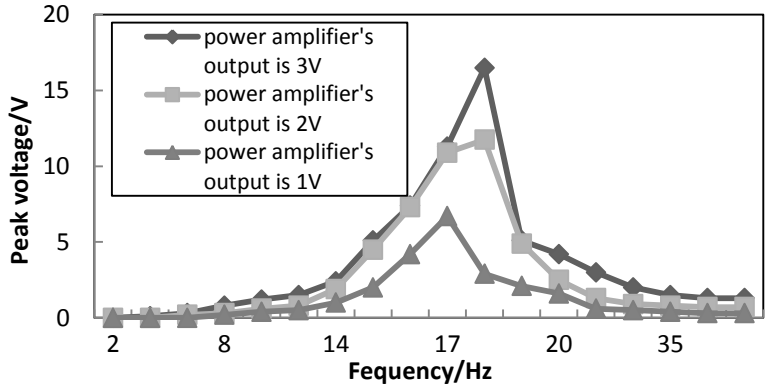

Figure 5---Relationship between frequency and the generated peak voltage with model b

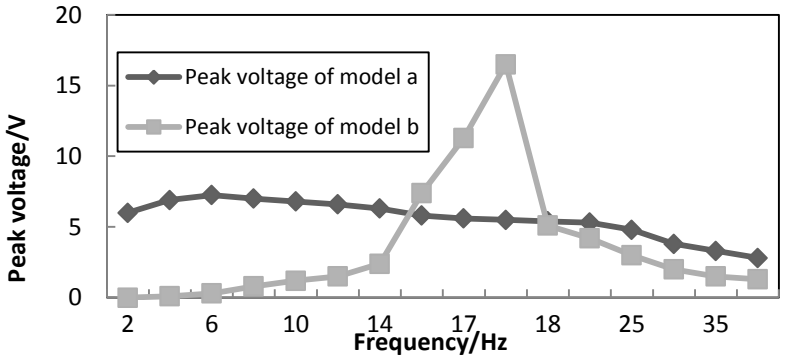

Figure 6---Comparison of two models' frequency and generated peak voltage relationship

When the piezoelectric element is relatively still which means the exciter doesn't shake it but there is also vibration in the environment, the resistor is ranging from about 26MΩ to 38MΩ. The resistor is changing when the piezoelectric element is shaking. The output voltage of the piezoelectric element can be changed by adjusting the frequency and the output of power amplifier. Because the resistor of the piezoelectric element is in the level of MΩ, the output current is limited to the level of μA.

Using LTC3588-1, the output current of the chip can be up to 100mA. With CBC3112, the energy can be stored in a short time for further use. It's seen that the output voltage of CBC3112 can be from 2.06V to 3.90V in about 5 minutes as shown in Figure 7. So the energy can be well collected and stored.

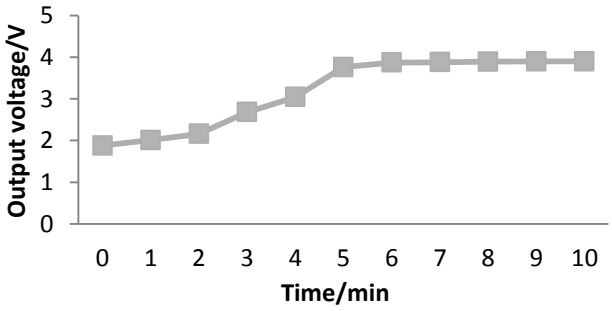

Figure 7---Storage performance of CBC3112

Conclusions and Discussions

In this paper, two mechanical structures used for PEH have been analyzed. Structure of model a is more suitable for the wood floor system as the frequency of people walking on the floor is low and the generated output voltage of the piezoelectric element with the structure is stable and reasonable which is helpful for the later collection and storage of energy.

Various kinds of frequencies added to the piezoelectric element should be tested further to see the performance of generating electricity. The design of the mechanical system should make sure it can be better fit to the surroundings, especially considering the frequency. The resonant frequency can cause the largest displacement of the piezoelectric element, but that doesn't mean it's the optimal frequency to choose. Too large deformation may reduce the performance of the piezoelectric element in a short time since the piezoelectric element may be damaged. In experimental situations, each time only one frequency can be selected, but in reality, there're various kinds of frequencies which are hard to analyze. So in practical use of wood floor system, more experiments in the design of the structure should be carried out, not only to acquire as much energy as possible but to ensure stability.

The resistor matching theory is not suitable to use since the resistor of the piezoelectric element is so big that matching the resistor of the load with that of input is impractical and may cause extra energy loss. How to collect and store the energy more efficiently is worth researching. To create and use integrated micro circuit chips instead of discrete component circuits is a good way to reduce the loss of the circuit.

Acknowledgements

The research is supported by the college students' innovation project of BJFU named Research of Vibration Generators under grant 121012.

References

Kymissis, J.; Kendall, C.; Paradiso, J.; Gershenfeld, N. 1998. Parasitic power harvesting in shoes. In: Proceedings, Second International Symposium On Wearable Computer, Pittsburgh, PA,USA :132–139.

Mateu, L.; Moll, F. 2005. Optimum piezoelectric bending beam structures for energy harvesting using shoe inserts. Journal of Intelligent Material Systems and Structures. 16(10) 835–845.

Yoon, H.S.; Washington, G. ; Danak, A. 2005. Modelling, optimisation, and design of efficient initially curved piezoceramic unimorphs for energy harvesting applications. Journal of Intelligent Material Systems and Structures. 16(10) 877–88.

Sustainable dance club , http://www.sustainabledanceclub.com/ .

Sodano H A; Inman D J; Park G. 2004. A review of power harvesting from vibration using piezoelectric materials. Shock Vib Dig. 36:197-205.

Wanglu Z; Goponath RP,;Lei Zuo. 2012. An efficient vibration energy harvester with a multi-mode dynamic magnifier. Smart Materials and Structures. 21(1).

Jeon Y.;Sood R.; Jeong J. H; Kim S.-G. 2005. MEMS power generator with transverse mode thin film PZT. Sensors and Actuators A: Physical, vol. 122, no. 1, pp. 16–22.

Dallago E.; Frattini G.; Miatton D.;[and others].2007. Integrable high-efficiency AC-DC converter for piezoelectric energy scavenging system, in Proc. IEEE Int. Conf. Portable Information Devices, 1–5.

LiQiang. 2011. A low voltage -high efficiency CMOS rectifier for low power battery-less System. School of electronics and electric engineering.

Ottman G.K; Hofman H.F.; Bhatt A.C.[and others].2002. Adaptive Piezoelectric Energy Harvesting Circuit for Wireless Remote Power Supply. Transactions on power electronics,17(5):669-676.

Lefeuvre E.; Badel A.; C. Richard C;[and others] .2006.A comparison between several vibration-powered piezoelectric generators for standalone systems. Sensors and Actuators A 126:405–416.

Junrui Liang; Wei-Hsin Liao. 2012. Improved Design and Analysis of Self-Powered Synchronized Switch Interface Circuit for Piezoelectric Energy Harvesting Systems. Transactions on Industrial Electronics, 59(4):1950-1960.

Yinmin Zhang. 2008. Mechanical vibration.8-70.

Tabesh A; Frechette L G. 2010. A low-power stand-alone adaptive circuit for harvesting energy from a piezoelectric micropower generator． IEEE Transactions on Industrial Electronics，57(3) : 840－849.

Session 12

Structural Condition Assessment II—New Techniques and Field Experiences

New construction NDT device for *in situ* evaluation of wood using compression stress-deformation measurements parallel to grain

Michal Kloiber, Miloš Drdácký
Academy of Sciences of Czech Republic, v. v. i., Institute of Theoretical and Applied Mechanics, Centre of Excellence Telč, Telč, Czech Republic, kloiber@itam.cas.cz, drdacky@itam.cas.cz

Jan Tippner, Václav Sebera
Mendel University in Brno, Faculty of Forestry and Wood Technology, Department of Wood Science, Brno, Czech Republic, seberav@gmail.com, jan.tippner@gmail.com

Abstract

Our work presents a new type of non-destructive diagnostic tool for *in situ* evaluation of wood inbuilt in constructions. This new approach enables to determine strength and stiffness parameters of wood parallel to grain based on measurement of force required for pushing jaws inside the predrilled hole apart. Such technique has not been used yet, so it represents an innovative approach. For a verification of the proposed technique, the standard compression tests (following EU standards) parallel to the grain were carried out on a universal testing machine. Comparative results show a good agreement between the newly proposed tool and standard tests on spruce (*Picea abies* L.). To understand and explain mechanical phenomena the proposed tool is based on, the finite element analyses were performed in advance. FE model assumed orthotropic and elastic material model. Results of the FE probabilistic analyses explained relationships among parameters gained by proposed NDT diagnostics and predicted material properties.

Keywords: non-destructive testing, wood, in-situ testing, compression strength.

Introduction

The range of current methods and devices has lacked a solution enabling a researcher to measure mechanical properties of wood using gently destructive investigation of its behaviour when loaded by a miniature loading jack inserted in a predrilled hole. During its application, the dependence of deformation on the loading caused by symmetrically placed jaws being pushed apart in a predrilled radial hole with 12 mm in diameter is measured (Drdácký and Kloiber, 2013). The semi-destructive drilling of the hole in the tested material also enables an evaluation of the wood condition (e.g. based on the core, the sawdust, videoscopy, etc.). The described principle of this new method for the assessment of mechanical properties has become a basis for a construction of a new device. The presented paper introduces the new device and shows the results of numerical simulations and measurements conducted with the purpose of verification the function of the new device by comparing it with standard destructive compression tests following EU standards. Probabilistic analyses based on the numerical modelling in ANSYS software show sensitivity of output measured force and stiffness on input material properties in common modes of device use. The verification of the possible *in-situ* establishment of conventional strength and modulus of deformation parallel to grain was carried out using beams with 200×240 mm in cross-section, so that the maximum objectivity of the experiment was guaranteed. Moreover, more measurements using other semi-destructive methods described in the following chapter were done in the close vicinity of the holes for jaws pushing apart tests.

Materials and methodology

Construction of the new device

The device (Fig. 1, 2) is designed to measure mechanical properties of wood using non-destructive or semi-destructive investigation of its behaviour when loaded by a small size jack inserted in a pre-drilled hole. The device can be used both in a laboratory and in the field to determine the condition and quality of timber. The device provides the dependence of deformation on the tension brought about by pressing symmetrically placed jaws apart in a pre-drilled radial hole with 12 mm in diameter.

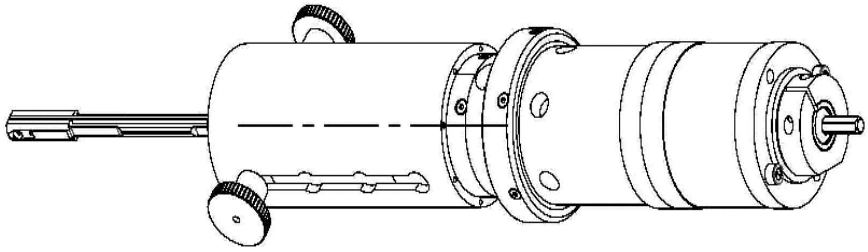

Figure 1 – Axonometric projection of the newly designed device

The advantage of the device is the possible gradual recording of the force and shift of jaws (loading jack) at different depths corresponding to the required dimensions of commonly investigated constructions. The device is laid on the tested unit (usually a constructional element of a rectangular profile) by means of a cylindrical shell, which allows for measuring in four positions of the pre-drilled hole. The shell arresting is provided by two grooved screws, for positions (core depths) 5–25 mm, 35–55 mm, 65–85 mm, and 95–115 mm. When the measuring part of the device is inserted in the drilled hole and the device is laid on the tested element, the rounded jaws (Fig. 2) are pushed apart into the walls of the hole. The maximum depth of possible loading on both sides is 1.5 mm. The rounded jaws are 5 mm wide and 20 mm long. The jaws also include flexible arms whose movement during pushing is provided by a push-apart bronze wedge fitted to the lower end of the drawbar by means of a pin and screw. The apex angle of the wedge is 15°. This angle is not self-locking and to release the jaws it is sufficient to release the push-apart force (Drdácký and Kloiber, 2013).

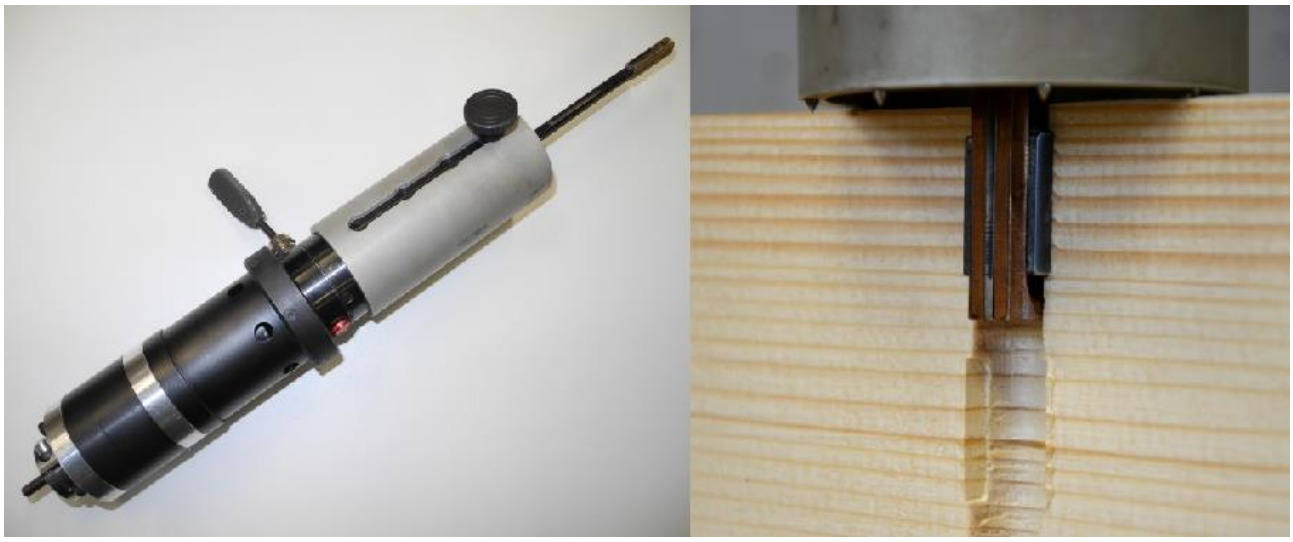

Figure 2 left – overall view of the newly designed device, **right** – detail of the drawbar with the wedge and rounded jaws

The force of the drawbar drawing is continually recorded. It is calibrated to the real force of the loading jack and simultaneously related to the measured distance of movement of the jaws (Fig. 3). The signals are wireless transmitted to a portable computer where they are processed.

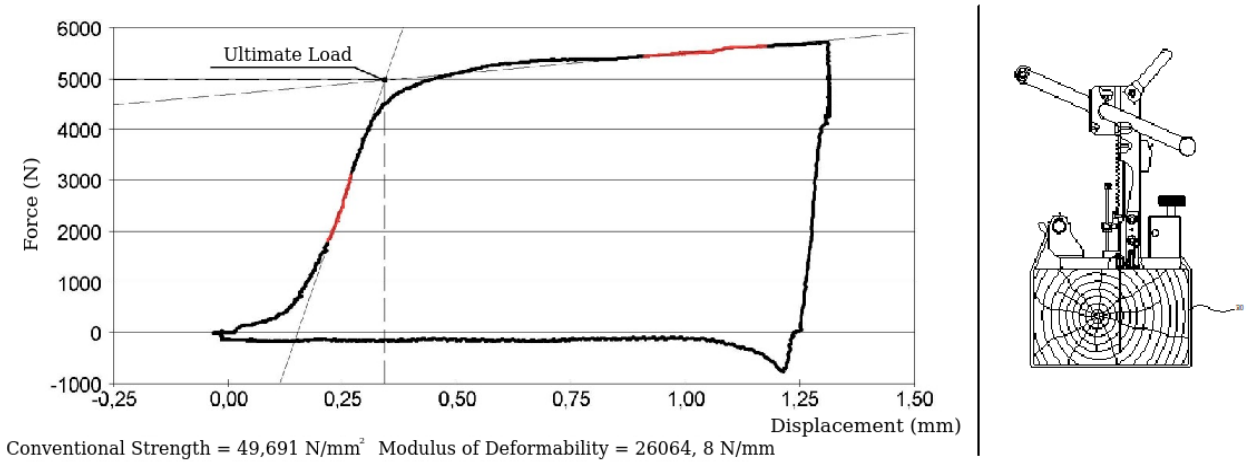

Figure 3 left – An example of the device output: a record of the force needed to push the jaws apart in relation to the measured shift (displacement) of the jaws; **right** – the detail of the device for pin pushing

The other used devices

Other semi-destructive methods used for measuring were the measuring of mechanical resistance of wood against microdrilling and measuring of mechanical resistance of wood against pin pushing (Fig. 3 right). Microdrilling was carried out using *Resistograph*, which is based on the resistance of the material against the penetration of a small borer with 1.5–3.0 mm in diameter. The movement of the borer is constant and revolutions do not change (Rinn, 1994; Rinn et al., 1996). The output is a profile of energy consumption, or relative resistance, including the elimination of the borer energy consumption of friction in deeper layers. The peaks in the graphical record correspond to higher resistance or wood density; the lower points are related to a lower relative resistance of wood (Drdácký et al., 2006).

The other alternative was measuring of resistance against gradual penetration of an object – a pin (Fig. 3 right) – to a depth relevant for the dimensions of common wooden constructional elements. The method is based on continuous monitoring and recording of the power related to the measured depth of pin pushing (Kloiber et al., 2012). The device is autonomous, portable, and it allows for the establishment of properties in the entire cross section of the wooden elements thanks to the sufficient length of the pin; moreover, in contrast to microdrilling, it retains the character of a loading test. The output of measuring is a graph of the development of the force necessary for pin pushing. Based on the size of the resistance force, the mechanical resistance of the material can be established. Detailed information about the construction of this device and comparison with destructive timber testing can be found in Kloiber et al. (2013).

Experiment

The verification of the prediction of mechanical properties using the measuring by semi-destructive devices was carried out by measuring of sixteen 8 m long beams made of Norway spruce (*Picea abies* L. Karst.), commonly used in historical constructions in the Czech Republic. The cross-section of the beam was 200×240 mm, which corresponds to the dimensions usually appearing in timber inbuilt in historical constructions. After gradual drying of all sixteen beams and their conditioning to 12% moisture content, holes were made by a borer with 12 mm in diameter. Two holes were made in each beam. The boring was done in purely radial direction and the distance between the holes was 100 mm. The depth of the boring was about 130 mm, which enabled us to perform the measuring using the jaw pushing apart in the hole in four layers: layer 1 (5–25 mm), layer 2 (35–55 mm), layer 3 (65–85 mm), and layer 4 (95–115 mm), see Fig. 2 right. The depths of the layers are given by the device construction. The measuring part of the device was then inserted in the radial hole and the device was laid on the tested piece of timber using a cylindrical shell. The jaws were pushed apart parallel to the grain while the drawbar was drawn out with the push-apart wedge on which the jaws moved. The prints of the jaws in the timber are obvious in Fig. 2, which also shows the distances between the individual layers of measurement across the element. In total, we measured 128 positions (16 beams, always 2 holes) using the newly constructed device.

Mechanical properties were determined using the record of the measured data in the form of a stress-strain diagram with the record of the force used for the drawbar drawing out, (Fig. 3). Axis x represents the displacement when the jaws are pushed, axis y shows the force necessary for the jaws to be pushed. The maximum force (F_{max}) in Fig. 3 - Yield point, was established from the intersection of tangents of the elastic and the plastic parts of the stress-strain diagram. Conventional compressive strength ($CS_{C\,(L)}$) was determined from the proportion of the ultimate load and the area of the pushed jaws. The modulus of elasticity cannot be calculated directly from the diagram; the modulus of deformability was established using the angle of the curve fit through the linear part of the force record and deformation. In the places adjacent to the bored holes, we performed measuring using the device for pin pushing (pin with 2.5 mm in diameter, 120 mm long). Basic characteristics measured were: work (S) as the area below the curve [N.mm] of the force record in dependence on pin displacement, length (L) [mm], time of pin displacement [s], and the maximum and minimum force [N]. To assess the mechanical resistance of timber against pin pushing, the average force (F_{AVG}) [N] was used, calculated as the quotient of work S and length of displacement L, which best correlates with mechanical properties (Tippner et al., 2011). The Resistograph 2450p recorded the amount of energy needed to keep the constant drilling speed. The output is the profile of energy consumption, or the relative resistance, including the elimination of the borer energy consumption of friction in deeper layers. The graphical output needed to be evaluated explicitly in order to compare it with physical and mechanical properties, therefore, a script was designed in MATLAB to calculate a parameter marked as Resistance Measure *RM* [Bits], i.e. a resistance value that corresponds to the area below the curve divided by the length of the measured section (Kasal and Tannert, 2010).

The function of the semi-destructive devices was verified using experiments based on the comparison of the measured quantities from the particular devices and those established by testing of standard samples by destructive tests on the universal testing device Zwick Z050 in compliance with the standard test procedure. The results were processed by TestXpert v 11.01. The basic parameters included into analysis for device verification were: wood density (*Density*), wood strength in compression parallel to the grain ($S_{C\,(L)}$), and the modulus of elasticity in compression parallel to the grain ($MOE_{(L)}$). The tests were performed in compliance with standard European regulations using 20x20x30 mm samples taken at individual positions adjacent to places of measuring by the semi-destructive devices. Two samples with dimensions 20x20x30 mm (compression parallel to the grain) were made for each place of measuring by the device for jaws pushing apart. The data was further processed in Statistica 10.0 (survey analysis of data, verification of distribution normality, independence of elements of the selection, correlation analysis, linear and non-linear regression).

FE modelling

The finite element analysis was used to predict the behaviour of the device and sensitivity of measured outputs to common factors. This paper presents using of probabilistic analyses to describe the influence of grain declination and properties of materials. The influence of the bottom of a hole to reaction forces in the case of measuring near the bottom was analyzed as well. The 3D model was made in ANSYS Mechanical APDL 14.5 software with using the Ansys Parametric Design Language. The final unsymmetrical geometry model consists of the wood specimen (cube 50 x 50 x 50 mm) with a hole of 12 mm diameter and the jaws simplified to prismatic deformable bars. The FE model uses a regular sweep mesh with quadratic hexahedral solid elements (SOLID186) in all domains. The interaction between jaws and wood was defined by symmetric contact pairs using contact (CONTA 174) and target (TARGE170) elements on the surfaces. Material model of specimen was based on the elastic orthotropic properties of Norway spruce with respect to literature data (derived ratios of constants) and the experimentally obtained density and $MOE_{(L)}$. The material of jaws is considered as elastic isotropic steel. Boundary conditions were applied as displacements on back sides of the moving jaws and boundary areas of wood specimen as well. Nonlinear large displacement contact analysis was performed to compute displacements, strains, stresses and reaction forces in 50 substeps of load step with the jaws imprint. Parametric definition of model allowed to test influence of 5% changing of grain declination (in all 3 possible directions, in practice slight turning of the device in the hole, drilling in non-radial direction) on reaction forces, comparison of measuring in different depth of a hole. Further, the ANSYS Probabilistic Design System was used to describe correlation between all moduli of elasticity and reaction forces. Randomizing by Monte Carlo method was used in probabilistic analyzes, input range of parameters was defined with Gaussian distribution by average value of parameter and standard deviation (matches coefficient of variance 0.15 in all cases, which corresponds to common variability of mechanical properties of wood). Analysis counts 300 cycles.

Results and Analysis

Fig. 4 illustrates the distribution of strains in transversal and longitudinal slices of the model for the measurement near the bottom of the hole and the measurement in a high position (where the bottom surface is assumed as infinite). Despite the small contact area of jaws, there is a large theoretical area of impacted material, which suggests a good potential for estimation of non-local properties. Common measurement in distance 5 mm above the hole bottom gives us unbiased results of reaction forces.

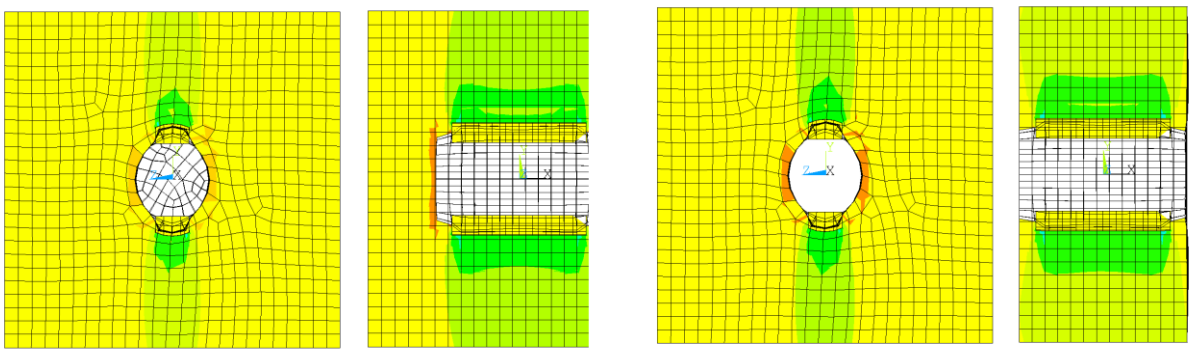

Figure 4 – Strains in the direction of applied forces for the longitudinal and transversal slices of FE model for the measurement near the hole bottom (left) and measurement in a high position (right)

Tab. 1 shows correlation coefficient between input parameters retrieved by probabilistic FE analysis. Tab. 1 shows the statistical interdependence between the parameters involved, including input and output variables. Spearman rank order correlation coefficients are shown. For the values closer to zero, the two variables are weakly correlated, for the values closer to 1, the two variables are highly correlated. Table shows only results for the reaction force in the direction of loading. Reactions in other directions were small: the direction of hole axis is about 0.2 % of reaction force in loading direction and reactions in tangential direction of tested material slightly higher (about 1%) but still negligible. The values of coefficients of correlations show strong influence of longitudinal modulus of elasticity (correlation coefficient 0.96). A weak correlation for the case of all other parameters was found. Negligible influence was described also for modulus of elasticity of the jaws material – steel. In practical conclusion: 15% changes of material properties cause changes of reaction forces only in the case of longitudinal elastic modulus and other material properties have no effect; 5% changes of grain declination caused by turning of device in the hole or drilling in non-radial direction has also no effect on reaction forces (on the force based outputs from measurement respectively). Presented linear analysis was not able to describe all necessary behaviour of the process due the high plasticity of real imprint of jaws to wood. The FE model including plasticity phenomena with description of influence on conventional strength will be subject of further papers.

Tab. 1 – Correlation coefficients from sensitivity FE analysis – F_R (as reaction force) vs. E_L, E_R, E_T (as normal moduli of elasticity), G_{RT}, G_{LT}, G_{RL} (as shear moduli of elast.), A_L, (declination in longitudial direction or turning of device in hole), A_T, A_R (declination in tangential and radial direction or deviation of hole axis from radial direction)

	E_L	E_R	E_T	G_{RT}	G_{LT}	G_{LT}	A_L	A_T	A_R
F_R	**0.959**	0.013	0.048	0.035	0.073	0.014	0.030	0.019	0.027

Experimental values of the 16 beams (strength in compression parallel to the grain, conventional compressive strength, modulus of elasticity parallel to the grain, modulus of deformability) are presented in Fig. 5. The results of analyses prove statistically significant differences between the beams. Mainly beams 2, 9, 17 manifested considerably higher measured properties of wood than the other beams. Considerably lower measured properties than is common in spruce wood were found in beams 4 and 5. The progress of the values of strength in compression parallel to the grain $S_{C(L)}$ corresponds to the progress of the values of conventional compressive strength $CS_{C\,(L)}$. Similarly, there is a very good correspondence between values of $MOE_{(L)}$ and $MOD_{(L)}$ of all measured beams (Fig. 5). Influence of material stiffness (longitudinal Young's modulus) and computed reaction force in relation to displacement was also revealed by sensitivity FE analysis (very strong correlation). The absolute differences between values of the parameters measured on

testing specimens and values obtained from the new device could be also explained by sensitivity analysis. The influence of other parameters cannot be neglected in the complicated mode of jaws' imprint into wood (see correlation coefficients from PDS analyses above). The higher values of properties from "imprint" method probably correspond to high stiffness of material. The similarities between data distributions of standard tests and output parameters were also recorded by the other two semi-destructive devices.

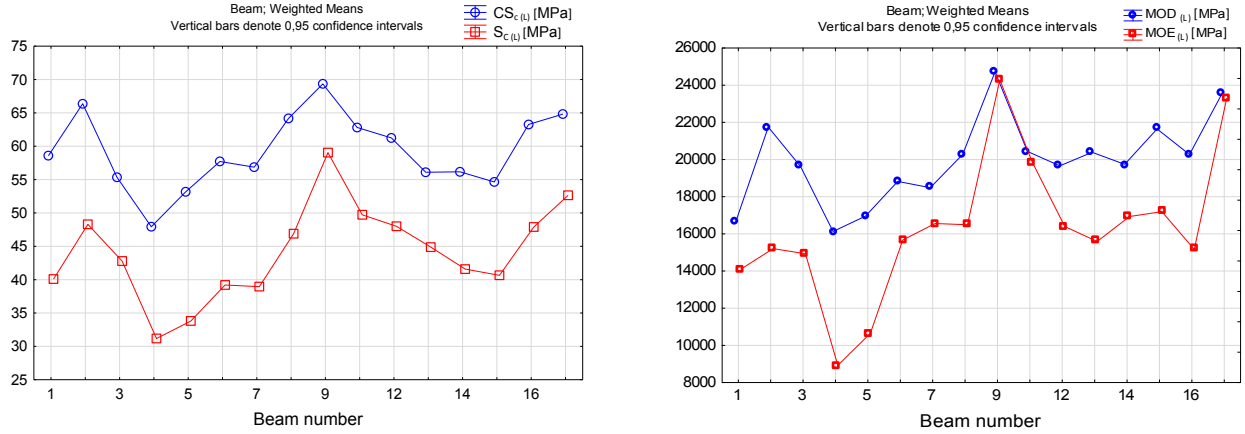

Figure 5 left – Compressive strength $S_{C\,(L)}$ and conventional compressive strength $CS_{C\,(L)}$ parallel to grain for individual beams (pushing jaws in the hole apart); **right –** modulus of elasticity $MOE_{\,(L)}$ and modulus of deformability $MOD_{\,(L)}$ parallel to grain for individual beams (pushing jaws in the hole apart)

Tab. 2 shows correlations between the parameters (*Density*, $CS_{C\,(L)}$, $MOE_{\,(L)}$) and measuring by semi-destructive devices ($CS_{C\,(L)}$, $MOD_{\,(L)}$, F_{AVG}, *RM*). Especially the relation to density can be considered strong for all semi-destructive devices. Compression strength parallel to the grain can be accurately established using the newly constructed device for jaws pushing apart. Also the method of pin penetration enables us to assess mechanical properties of the timber very well. The resistance measure calculated from the graphical record of microdrilling is a universal parameter, which correlates with density mainly, but the establishment of mechanical properties based on this is not convincing. This behaviour of the methods based on resistance drilling can be explained by the principle/mode of material disruption close to timber machining, in contrast to pin penetration, where the loading mode and disruption are closer to loading while testing of mechanical properties, and mainly in contrast to jaws pushing apart, where the loading and the disruption are very close to loading and disruption caused by compression tests parallel to the grain.

Tab. 2 – Correlations between the explored parameters (*Density*, $CS_{C\,(L)}$, H_L) and the measuring by semi-destructive devices ($CS_{C\,(L)}$, F_{AVG}, *RM*, F_{MAX}, *Depth*).

	$CS_{C\,(L)}$	$MOD_{\,(L)}$	F_{AVG}	*RM*
Density	0.87	0.61	0.81	0.90
$S_{C\,(L)}$	0.92	0.88	0.82	0.62
$MOE_{\,(L)}$	0.75	0.87	0.74	0.46

The relationship between the conventional compression strength parallel to the grain $CS_{C\,(L)}$ and the selected properties of wood *Density*, $S_{C\,(L)}$ is described by linear regression (Fig. 6). The coefficients of determination R^2 show very close dependences.

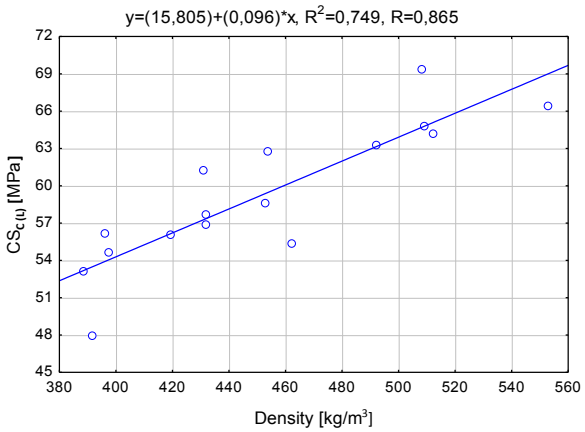

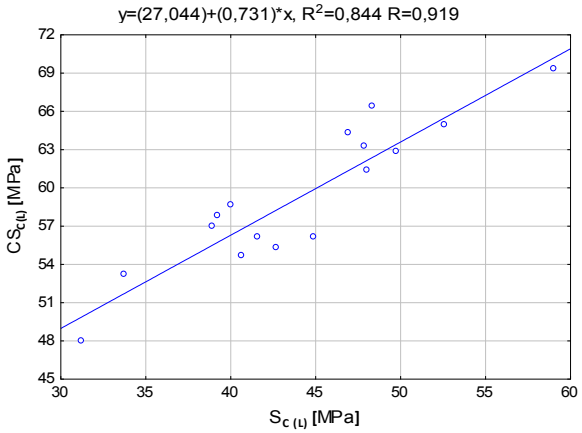

Figure 6 left – Dependence of density and $CS_{C\,(L)}$ compressive strength parallel to the grain; **right** – dependence of $S_{C\,(L)}$ and $CS_{C\,(L)}$ conventional compressive strength parallel to the grain (both show data from proposed device)

The relationship between the modulus of deformation $MOD_{(L)}$ and modulus of elasticity parallel to the grain $MOE_{(L)}$ is described by linear regression (Fig. 7). Its coefficients of determination R^2 show very close dependences here too.

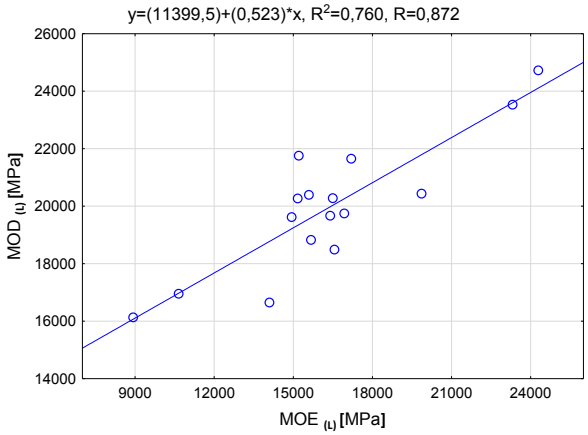

Figure 7 – Dependence of modulus of deformability $MOD_{(L)}$ and modulus of elasticity $MOE_{(L)}$ parallel to grain (new proposed device)

Similarly, the density and $S_{C\,(L)}$ can be derived using the average force of pin pushing (Fig. 8). The density can also be derived well using the resistance measure of microdrilling (Fig. 9 left). Only the compression strength parallel to the grain derived from the resistance measure seems to be weakly convincing (Fig. 9 right).

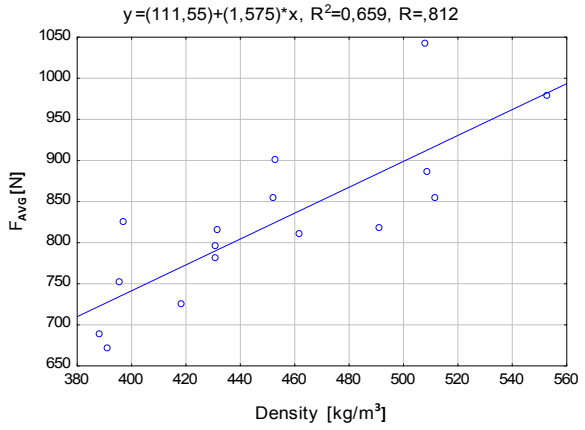

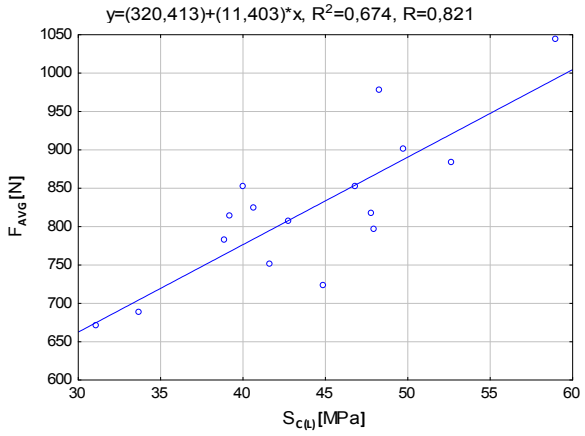

Figure 8 left – Dependence of average force F_{AVG} on $S_{C\,(L)}$ (pin pushing); **right** – dependence of average force F_{AVG} on density (pin pushing)

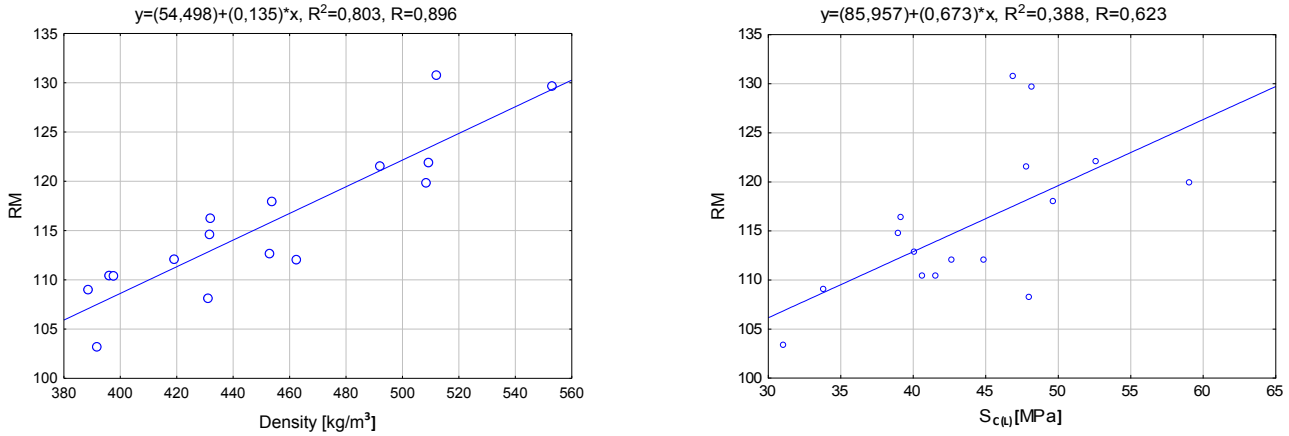

Figure 9 – Dependence of density and resistance measure *RM* (microdrilling); **right –** Dependence of $S_{C\,(L)}$ and resistance measure *RM* (microdrilling)

Conclusions

This paper presents the construction and usage of a new device for *in-situ* assessment of inbuilt timber. The use of the device, which is sufficiently sensitive to natural differences among the individual beams, has been verified. The theoretical analysis of relationships between input material properties and output evaluated parameters was performed by probabilistic FE analysis. The longitudinal modulus of elasticity has the strongest impact on the output force (from which output parameters of device are derived) (correl. coeff. 0.96); the radial and tangential moduli and also shear moduli have non-negligible influence (coefficients lower then 0.1). The influence of angle inaccuracy in drilling of hole (practically 5%) has no impact on reaction forces (correl. coeff. lower than 0.1). The FE model also shows a negligible difference in forces obtained by measurement near the hole bottom and measurements in higher positions. As regards experimental verification, strong correlations were mainly found between $CS_{C(L)}$ and conventional compression strength parallel to the grain and $S_{C(L)}$ strength of standard samples (correl. coeff. 0.92). The relationships were closer described by practically usable linear regression models. The compression strength parallel to the grain correlates with the other explored parameters, e.g. density (correl. coeff. 0.87). The other parameter for the assessment of mechanical properties using the new device was $MOD_{(L)}$ modulus of deformability, which correlates very well with $MOE_{(L)}$ modulus of elasticity parallel to the grain (correl. coeff. 0.87). The construction of the new device is light and the fact it does not require electric grid, it can be easily used in the field. In contrast to other methods, the new device enables us to establish mechanical properties in the depth profile of the assessed elements very accurately.

As regards the other method, very good correlations were found between density and *RM* resistance measure (correl. coeff. 0.90), density and F_{AVG} average force (0.81), further between $S_{C\,(L)}$ wood strength in compression parallel to the grain and F_{AVG} average force (0.82), $MOE_{(L)}$ modulus of elasticity parallel to the grain and F_{AVG} average force (0.74). Less significant correlations were found for *RM* resistance measure and mechanical properties $S_{C\,(L)}$ wood strength in compression parallel to the grain (0.62) and $MOE_{(L)}$ modulus of elasticity parallel to the grain (0.46).

Acknowledgments

This paper was created with a financial support from grant project DF11P01OVV001 “Diagnostics of damage and life span of Cultural Heritage buildings”, NAKI program, provided by the Ministry of Culture and institutional support RVO 68378297.

References

Drdácký, M., Kloiber, M. 2013. In-situ compression stress-deformation measurements along the timber depth profile. In: 2nd International Conference on Structural Health Assessment of Timber Structures (SHATIS’13), Trento, Italy.

Field Performance of a Two-Lane Bridge Composed of 30-m-Long Glulam Arch-Truss and Stress–Laminated Deck

Kwang-Mo Kim, Chang-Deuk Eom, Sang-Joon Lee
Korea Forest Research Institute, Seoul, Korea

Abstract

In December 2012, the first timber road bridge in Korea was installed on a river crossing of the main road in the Micheongol National Natural Recreation Forest (Yangyang, Gangwon). Two glulam arch-trusses were installed at both sides of the road to make a 30-m-long simple span structure. A stress laminated glulam deck was settled on the steel cross beams between the two trusses. The field monitoring program for this bridge began in January 2013 and includes measuring vertical and horizontal displacements of the bridge. The surface of glulam members and connections are also being observed periodically to detect the initiation of any defect. Any change of prestress are also being recorded to verify the performance of the stress-laminated deck. Truck loading test were scheduled for March 2013. Because we just start this monitoring program, we do not have enough measured data to draw any conclusions, and this paper will focus on the applied methods for field monitoring of the timber bridge.

Keywords: Timber bridge, glulam arch-truss, stress-laminated deck, field monitoring

Novel air-coupled ultrasound method for climatic-induced delamination imaging in individual bonding planes of historic glued timber

Sergio J Sanabria[a,*], Philipp Schütz[b], Jürg Neuenschwander[b], Robert Widmann[c], Peter Niemz[a]

[a]Wood Physics Group, Institute for Building Materials, ETH Swiss Federal Institute of Technology Zurich, Schafmattstrasse 6, CH-8093 Zurich, Switzerland, ssanabria@ethz.ch, niemzp@ethz.ch
[*]Corresponding author (T +41 44 633 91 38, F +41 44 632 1174)

[b]Laboratory for Electronics/Metrology/Reliability, Empa, Swiss Federal Laboratories for Materials Science and Technology, Überlandstrasse 129, CH-8600 Dübendorf, Switzerland, philipp.schuetz@empa.ch, juerg.neuenschwander@empa.ch

[c]Laboratory for Structural Engineering, Empa, robert.widmann@empa.ch

Abstract

The proliferation of glued timber construction raises increasing concern about safety problems related to in-service delamination of glue lines. In this work, a portable installation is presented based on a recently patented air-coupled ultrasound slanted lateral transmission (ACU, SLT) method. In comparison with the previous normal transmission (ACU NT) technology, the novel ACU SLT method is capable of separately associating lamination defects to individual bonding planes of arbitrarily high glued timber stacks. Moreover, the mechanically scanned transducers require only access to the lateral faces of the laminated timber beams. The impact of the natural variability of wood in the ultrasound signal is discussed and effectively minimized by combining ultrasound images acquires with specific transducer orientations. The installation was applied to assess a recently dismantled 90 year old roofing glulam member with significant climatic-induced delamination. The results are compared with feeler gauge visual inspection, laboratory X-ray computed tomography (CT) assessment and standard shear strength testing of stitch probes. The ACU SLT method was capable of assessing the geometry of delaminations not detected with the feeler gauge but consistently shown in the X-ray tomograms. Low-strength stitch probes were consistent with low signal amplitude regions in the ACU SLT images, the latter allowing full-scale non-destructive assessment of the structural member.

Keywords: climatic-induced delamination, historic glued laminated timber, air-coupled ultrasound, X-ray computed tomography, multi-layer laminates, heterogeneous wood anisotropy

Introduction

Several building collapses, which were related to the delamination (debonding) of the glued laminated timber (glulam) support members have raised concern on the safety problems related to adhesive bonding (Bautechnik 2006, Blass and Fresse 2010). Bonding related failure is related to both manufacture errors (not moisture-resistant or not properly cured glue lines), and in-service swelling and shrinkage strains in the bonding planes. The latter are a consequence of unfavorable load combinations (e.g. snow, wind and gravel filling on flat roofs) and gradients in moisture and temperature due to extreme climate variations between winter and summer months. Although the complex debonding mechanisms have been a matter of

considerable study, the available theories still do not allow the prediction of the initiation and propagation of delaminations in real glulam constructions (Bucur 2011). The improvement of bonding assessment is currently mainly addressed from the adhesive manufacturer side, with the development of climate-resistant gluing products. The quality control of the end glulam product is routinely performed on the basis of stitch samples, for which strength parameters are measured with standardized destructive tests (EN391 2001); this only allows identifying major production drifts.

The condition assessment of in-service glulam beams requires non-destructive testing methods, which allow the identification of delaminations at an early stage, and their mapping to specific bonding planes of the laminate. The methodologies should be reliable, inexpensive and portable. The most common on-site practice is still visual inspection. The depth of open edge cracks is estimated with a tenth of millimeter thick feeler gauge at conspicuous bonding planes and positions along the beam length.

In the last years, a considerable research effort has been dedicated to the development of methods capable of imaging inner delamination flaws. X-rays are able to penetrate thick structural members, off-the-shelf portable radiographic systems are available which have been applied to assess inhomogeneities (e.g. knots, metallic elements) in glulam constructions (Hasenstab et al. 2004). However, these systems provide a reduce sensitivity to debonding. A significantly higher contrast is obtained with three-dimensional computed tomography (CT) reconstruction (Hu & Gagnon 2007), which combines radiographic projections in a full range of orientations between sample and radiation path, leading to measurement time and geometric constraints, which mostly limits application to laboratory environment. (Sanabria et al. 2011) proposed a limited-angle CT reconstruction approach, which requires only a reduced number of projections quasi-parallel to the bonding planes, this method is potentially portable.

Ultrasonics is a well-established portable tool for the assessment of glued joints, with a very high sensitivity to delaminated interfaces. The main challenges for structural wood testing are one hand to achieve reproducible coupling of ultrasound energy into the tested members. On the other hand interactions of ultrasound waves with gluing interfaces need to be separated from the complex wave propagation in wood. Two fields of development dominate the actual research panorama. A shear wave pulse-echo array transducer from reinforced-concrete industry has been applied to single-sided *in situ* inspection of glulam. Reproducible measurements are achieved with dry-contact (DCU) spring-loaded coupling, ultrasonic images are generated by mechanically positioning the transducer in a grid of scanning points. Surface waves and back-wall echoes are applied to detect edge cracks and large scale delamination sections in individual bonding planes (Hasenstab 2009, Dill-Langer et al. 2011, Neuenschwander et al. 2013, Krause et al. 2013). The second field of development is the air-coupled ultrasound technology (ACU), which does not require contact between transducers and sample. This removes reproducibility errors and allows for continuous transducer scanning over the test sample surfaces with arbitrary transducer orientation and step size. The ACU method has been industrially applied for a while in the wood-based composite industry (Fuchs 2011). A recently completed four-year Swiss National Science Foundation research project has addressed the application of this technology to bonding quality assessment in glulam (Sanabria 2012). An ACU bonding assessment system capable of transmission through up to 500 mm thick glulam was developed. Conventional normal transmission (NT) imaging performs an integrated assessment of the full bonding stack (Sanabria et al. 2011b, Sanabria et al. 2011c). Moreover, a novel slanted lateral transmission setup (SLT) was developed and patented, which allows to generate independent bonding defect maps of specific bonding planes (Sanabria et al. 2013, Sanabria et al. 2013b). For both contact and non-contact methods, future research directions aim at improving the lateral resolution and reliability of the assessment by means of advanced data evaluation techniques based on a quantitative understanding of the wave propagation phenomena in wood structures (Dill-Langer et al. 2011, Neuenschwander et al. 2013, Krause et al. 2013, Sanabria 2012).

This work aims at providing an actual picture of the capabilities of the ACU technology to assess climatic-induced delaminations in real glued timber objects, in comparison with other available bonding assessment methods. First, selected examples of ACU NT imaging are briefly presented. Secondly, the ACU SLT method was applied to perform condition assessment on a section of a 90 year old roofing glulam member. The same member was assessed with visual inspection (feeler gauge), an industrial X-ray computed tomography system and standard shear strength testing. Moreover, an assessment of the same sample with dry-contact ultrasound (DCU) has been published elsewhere (Neuenschwander et al. 2013). Thus the investigations provide an excellent and to the best of our knowledge unprecedented basis of comparison of all available non-destructive bonding assessment technologies on a real timber structure.

Assessment of climatic-induced delaminations with ACU NT method

The ACU normal transmission method (NT) setup is illustrated in Fig. 1 and Fig. 2. A collimated ultrasound beam is transmitted perpendicularly through the laminate between a transmitter-receiver (Tx-RX) transducer pair. The transducers are scanned as a fixed unit in a raster fashion along the length and width of the laminate. A reduction of the signal amplitude level detected at the receiver is associated to the presence of defects. The method provides an integrated assessment (defect/defect-free) of the complete bonding stack.

Figure 1 demonstrates the detection of delaminations induced by strong climate variations in a two-layer laminate. The sample was manufactured by gluing together two 20 mm thick lamellas made from different wood species, one made from Norway spruce (*Picea abies* Karst.), a softwood, and the other one made from European beech (*Fagus sylvatica* L.), a diffuse porous hardwood, so that internal stresses were induced in the lamination plane. A one component polyurethane adhesive (HB 181, Purbond AG, Sempach Station, Switzerland) was used. The samples were exposed to exterior climate conditions for several months until delaminations occurred. The depth of the delaminations was then measured with both ACU normal transmission (NT) and a 100 µm thick feeler gauge. An ACU amplitude drop by 10 dB was chosen as threshold to segmentate glued and delaminated regions, which provided a good compromise between defect detectability and wood natural variability. The delamination depths estimated with ACU were slightly larger than the ones measured with the feeler gauge. The ACU image shows additional delamination indications (DI) at positions not accessible by the feeler gauge.

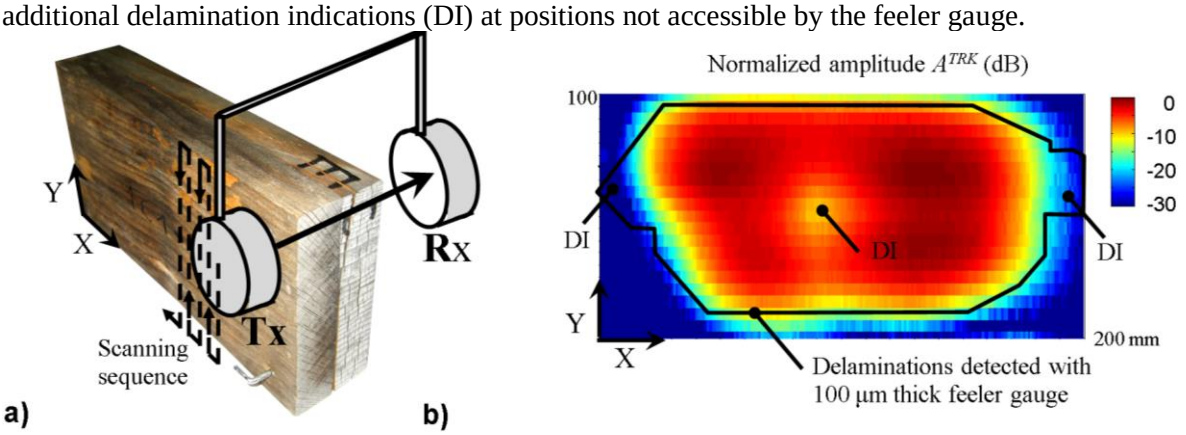

Figure 1 —ACU NT imaging of delaminations induced by strong climate variations. a) Test sample. b) ACU NT image. The transition between well-glued and delaminated regions measured with feeler gauge is marked (solid line).

Figure 2 demonstrates the detection of cracks in a test square solid wood beam from Norway spruce, which was sawn and planed to a cross-section of 170 x 170 mm^2. The cracks were induced by drying stresses when the solid wood was conditioned from green state in a standard climate (T = 20°C, RH =

65%). Two ACU NT images were generated by successively scanning the transducers along two perpendicular planes, represented by the transducer pairs T1-R1 and T2-R2 (Fig 3a). The cracks lead to a high reduction of the ACU signal if aligned perpendicular to the insonification direction (Fig 3b-bottom), and to no remarkable ACU amplitude variations if aligned perpendicular to the insonification direction (Fig. 3b-top). The additional cracks and wood heterogeneities (knots) shown in the photograph of the sample affected only a small portion of the sample length (X), and thus do not show a significant effect on the ACU images. The dimensions of the crack area observed in the ACU image (Fig 3b-bottom) were in qualitative agreement with the ones observed in the optic images of the surfaces of the sample (Fig. 3a).

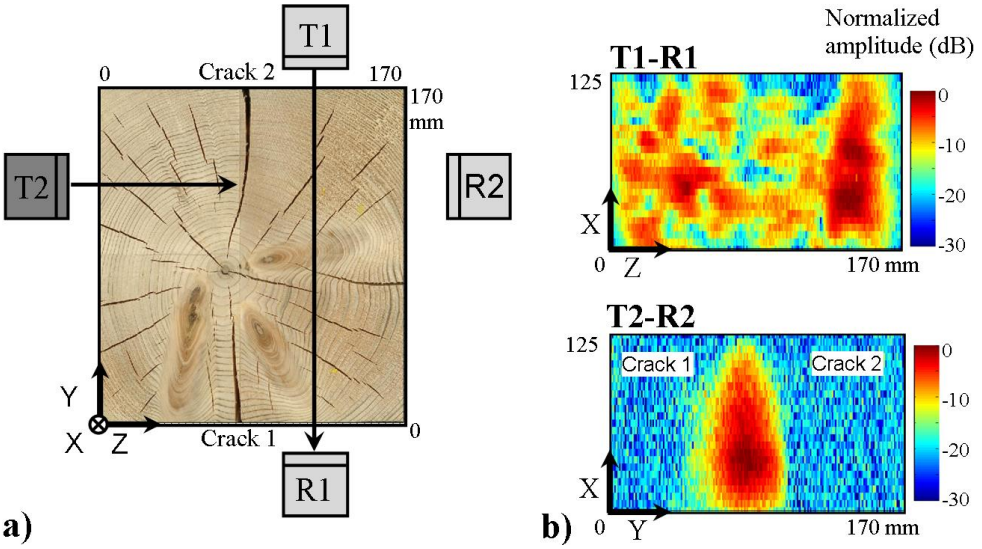

Figure 2 —ACU imaging of drying cracks in solid wood. a) Photograph of the sample and ACU NT setup. b) ACU NT image measured with transducer pair T1-R2, with insonification parallel to cracks 1 and 2. c) ACU NT image measured with transducer pair T2-R2, with insonification perpendicular to cracks 1 and 2.

Assessment of historic glulam beam with ACU SLT and X-ray CT

A historical glulam beam sample (1020 x 146 x 384 mm3) was obtained from the roofing support of an aircraft hangar erected in Lucerne, Switzerland, in 1922 (Fig. 3a). The beam is made from Norway spruce (*Picea abies* Karst.) and consists of 14 lamellas glued together with a Casein adhesive, exhibiting considerable climatic-induced delamination. Further infos are detailed in (Neuenschwander et al. 2013).

Figure 3b illustrates the principle of the ACU slanted lateral transmission (SLT) setup. The ACU transmitter (Tx) and receiver (Rx) transducers are positioned at two opposite lateral faces of the sample, with a small inclination ψ with respect to the assessed bonding planes, which leads to a controlled refraction angle $\hat{\psi}$ within the glulam beam. The transducers are scanned in height (X) and length (Y) directions of the glulam sample. This setup limits the physical interaction of the ultrasound beam with a reduced portion Δh of the glulam height, which allows the separate testing of a reduced number of (or just one) bonding planes. The robustness of the assessment is improved by combining ultrasound images obtained with specific ψ settings (here ψ_1= 2.3°, ψ_2= 4.4° and ψ_3= 6.1°, represented in Fig. 3b by the transducer pairs T1-R1, T2-R2, T3-R3), so that specific Δh values are obtained (typically multiples of the mean timber lamella thickness d). With a correct geometric interpretation, all images provide consistent delamination position indications. The distinct wave paths excited by ψ_1, ψ_2 and ψ_3 provide *spatial diversity*, minimizing the influence of local scatterers (e.g. wood knots, annual ring structure) in the bonding assessment.

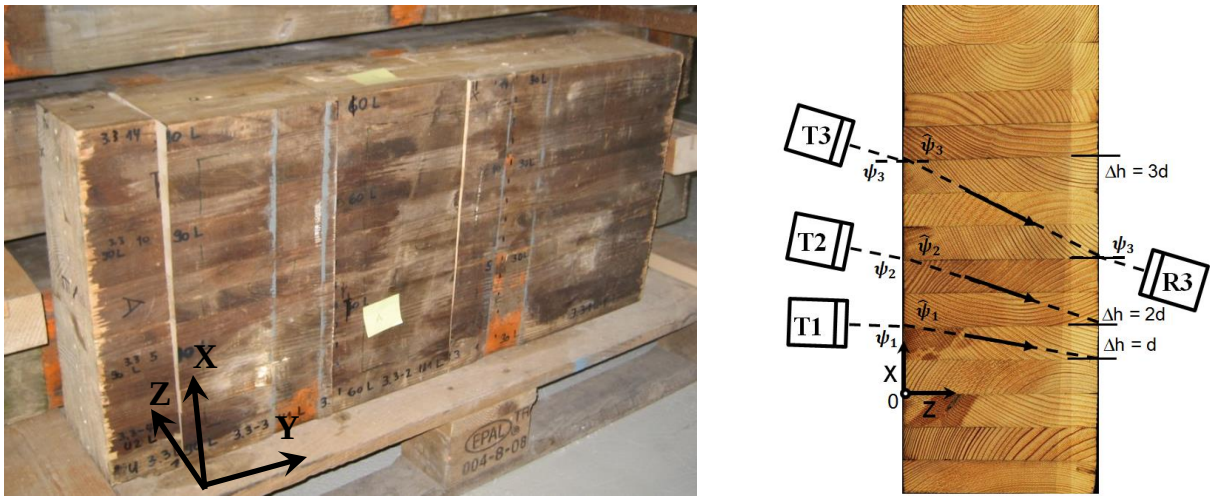

Figure 3 – a) Historic roofing glulam. b) ACU SLT inspection with 3 specific insonification angles $\boldsymbol{\psi_1}$, $\boldsymbol{\psi_2}$, $\boldsymbol{\psi_3}$, the receiver transducer R1 and R2 are drawn analogously to R3.

After the ACU SLT measurements, the accessible edge open delaminations were exhaustively assessed with a 10 mm wide 100 µm thick feeler gauge. Next, the glulam member was cut into three blocks, which were tested in lab with an industrial X-ray CT system (Schütz et al. 2013). It consists of a 450 kV X-ray tube and a flat panel detection which provides a cubix voxel size with 170 µm length, the effective lateral resolution is of about 3 voxels. Figure 5 shows selected CT tomoslices along and across the bonding plane #3. At Y = 180 mm no delamination indications were found, whereas at Y = 260 mm debonding between the two timber lamellas is clearly visible. This is clearly reflected in the gray level distribution in the bonding plane, which shows dark areas in the delaminated areas. The two white spots (arrows) correspond to internal steel nails. A dedicated glue line segmentation was implemented, which minimizes the influence of the annual ring structure and includes the non-planarity of the glue lines (in preparation).

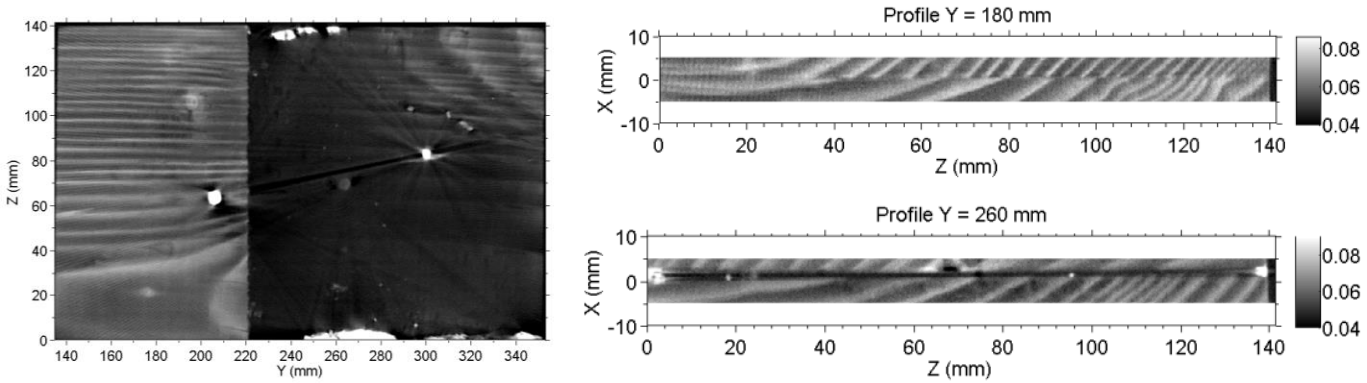

Figure 4 — X-ray CT assessment of bonding plane #3. Left: Gray level distribution in bonding plane. Right: Tomoslices across the bonding plane at two selected Y positions.

Figure 5 compares lamination assessment results obtained with ACU SLT, X-ray CT and feeler gauge for specific bonding planes. For all methods, the assessment results are expressed with a percentage bonding quality estimator (%), which represents the assessed delamination section, with 0% corresponding to full-width delamination and 100% to defect-free bonding. For ACU SLT, delaminated positions are defined

by thresholding the combined ultrasound image below a defined amplitude value (typically -6 dB from the mean value).

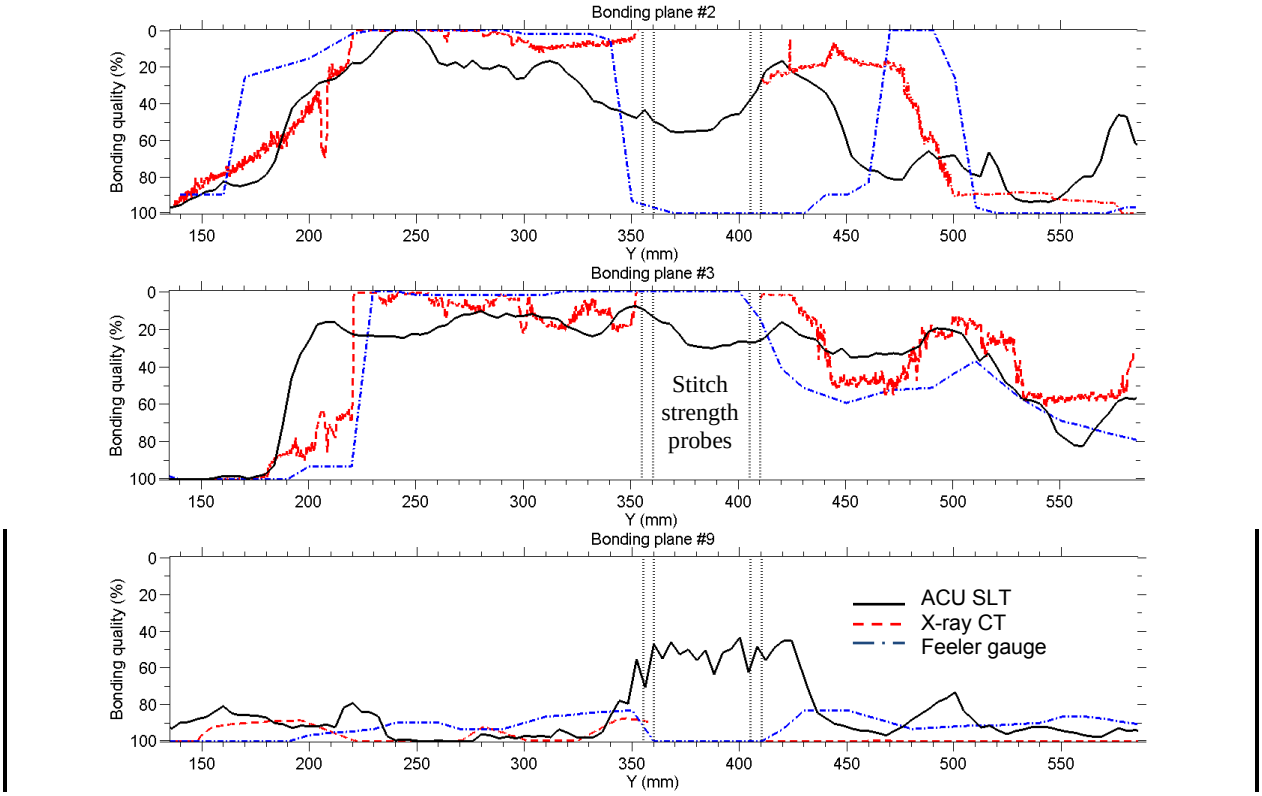

Figure 5— Delamination assessment along three selected bonding planes.

From the selected observations of Fig. 5 several general observations are extracted, a complete discussion of the assessment results is under preparation. All methods consistently identify the large scale delaminations in the bonding planes #2 and #3, as well consistently providing a defect-free assessment in bonding plane #9. The ACU SLT method provides best sensitivity to delamination, even for infinitesimal gaps. The main limitations of ACU SLT are in lateral resolution, according to Sanabria et al. 2013 a minimum delamination section of 50% with a length of 100 mm is required for ACU SLT detection in commercial glulam beams, this rule of thumb is seemingly as well applicable here. For example, in bonding plane #2 (at Y = 150-250 mm and Y = 400-500 mm) the feeler gauge and X-ray CT respectively predict a 50 mm longer delamination area than assessed by ACU.

The X-ray CT assessment provides best lateral resolution and provides most complete information about the inner wood structure. It allows for example to identify the initiation of delamination at bonding plane surface heterogeneities, such as wood knots. However, it is unable to detect delamination gaps well-below the lateral resolution. This is evident in the bonding plane #2 (150-200 mm and 450-500 mm), where the 100 µm feeler gauge reveals a larger delamination area than detected by X-ray CT, or at bonding planes #3 (175-225 mm), where the ACU SLT method reveals a longer delamination area.

The feeler gauge assessment provides best accuracy in the sizing of edge open cracks. For example, the shallow cracks (<20% section) in bonding plane #9 (Y = 200-350 mm and Y = 400 to 600 mm) are well-below the lateral resolution sensitivity of ACU SLT and the gap sensitivity of X-ray CT. In comparison to ACU SLT and X-ray CT, surface wave detection with dry-contact ultrasound (DCU) provides better lateral resolution to edge open cracks, allowing detection of delaminations deeper than 20 mm. Yet, the detectability of inner flaws requires in general larger delaminated sections (>80%) and is less robust,

being prone to false hits (Neuenschwander et al. 2013). The visual inspection with feeler gauge fails to detect inner lamination flaws or cracks with a rough non-straight profile. This is evident in bonding plane #2, where the delamination region between Y = 340 and 370 mm, partially detected by X-ray CT, is not assessed by the feeler gauge. As well in bonding plane #9, the ACU SLT method provides an indication of partial delamination (Y = 350-400 mm) which is not assessed by the feeler gauge. The same in bonding plane #3, where the delamination section between Y = 180-220 mm is undersized.

Strength (N mm^{-2})

Bondline	Z = 0	Z = 72	Z = 145
2	3.52	0	1.4
3	0	0	0
...			
9	4.44	3.5	0

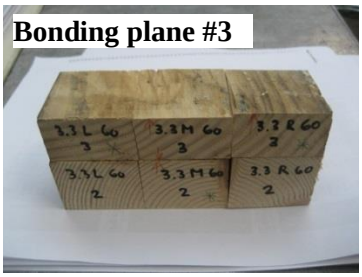

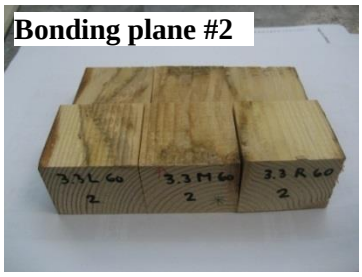

Figure 6— Shear strength testing of stitch probes extracted from Y = 355 to Y = 410 mm (Fig. 4).

This observations are confirmed by the shear strength stitch probes cut out from the structure between Y = 355-410 mm (Fig. 6). The sample width was cut into 3 sections, which were separately tested. Shear strength values are provided (N mm^{-2}), the wood fracture percentage (WFP) was for all shown stitch probes <10%, meaning that the fracture occurred exclusively at the glue lines. The fracture surfaces shown in the photographs reveal discoloration at delamination regions. In the case of bonding plane #3 the full section was delaminated at the beginning of the test (strength = 0 N mm^{-2}), which was successfully detected with ACU SLT, X-ray CT and feeler gauge (Fig. 5). In the case of bonding plane #2, the delamination occurred internally, which explains that it could only be detected with ACU SLT an X-ray CT, but not with feeler gauge. The main highlight of stitch probe testing is that actual strength values are provided, allowing not only detection of delamination but as well of low-strength bonding. The main limitation is its destructive nature. This limits the testing to a small portion of the sample length, which leads to misleading results. This is clearly the case in bonding plane #9, where the partially delaminated stitch probe section was successfully detected with ACU SLT. Yet considering the assessment results in Fig 5, the stitch probe does not reflect the considerably better bonding quality along the main part of the beam length.

Conclusions

In comparison to the other non-destructive delamination testing technologies, ACU SLT scores high in defect detectability, outperforming X-ray CT in delamination gap sensitivity and feeler gauge assessment in detectability of inner flaws. Individual bonding planes can be separately tested. The main limitations are in defect lateral resolution, as a rule of thumb >50% section and >100 mm long defects can be detected. The method may be well complemented by testing of edge open delaminations, based either on surface waves (dry-contact ultrasound) or simple feeler gauge assessment at conspicuous regions. X-ray CT provides the largest amount of inner structure data (annual rings, wood knots, etc.) and thus remains a valuable tool to investigate the link between these structures and the mechanisms of delamination initiation and propagation. The lateral resolution of industrial CT systems is sufficient to detect most of delaminated regions the development of limited-angle CT systems based on off-the-shelf portable X-ray radiographic systems has unexplored potential. Future major developments in ultrasound testing of timber structures go in the direction of a more sophisticated data evaluation based on a better quantitative understanding of wave propagation phenomena in wood, as observed in the converging research directions of three independent research groups dedicated to the field. First experiences show a groundbreaking potential (Dill-Langer et al 2011, Sanabria 2012, Krause et al 2013).

Acknowledgments

This research was supported by the Swiss National Science Foundation (contract 200021-115920), the Laboratory for Electronics/Metrology/Reliability in Empa (Dr. Urs Sennhauser) and the Wood Physics Group of ETH Zurich. The historic glulam beam sample was kindly provided by the Berne University of Applied Sciences: Architecture, Wood and Civil Engineering, Switzerland (Mareike Vogel). Thomas Schnider, Roman Furrer are gratefully credited for their contributions in the manufacture of test samples and acquisition of experimental data, respectively.

Reference list

Bautechnik (2006). Gutachten zu den Ursachen des Einsturzes der Eissporthalle in Bad Reichenhall vergelegt. *Bautechnik 83* (9):667-668, 2006.

Blass H J, Frese M (2010). Schadensanalyse von Hallentragwerken aus Holz. Tech. Rep., Karlsruher Institut für Technologie (KIT), Karlsruhe, Germany, 2010.

Bucur V, ed. (2011) *Delamination in wood, wood products and wood-based composites*, Springer, Berlin, Germany, 2011.

Dill-Langer G, Stritzke C, Aicher S (2011). Inspection of glue lines in glued laminated timber by means of ultrasound methods: experiments and modeling. In Proc.: 17th Int. Nondestructive Testing and Evaluation of Wood Symposium, University of West Hungary, Sopron, Hungary.

EN 391 (2001). Glued laminated timber – delamination test of glue lines.

Fuchs M (2011) New technologies for glow and blister detection widens on-line evaluation of board characteristics by implementing new calibration methods. *Transactions of Famena,* 34 (4):33-46.

Garab J, Toth A, Szalai J, Bejo L, Divos F (2010) Evaluating glued timber beams using a non-destructive testing technique. *Transactions of Famena,* 34(4):33-46.

Hasenstab A, Osterloh K, Robbel J, Krause M, Ewert U, Hillemeier B (2004). Mobile Röntgenblitzröhre zum Auffinden von Holzschäden. In: 2004 DGZFP-Jahrestagung, Salzburg, Germany.

Hasenstab A (2009). Defects in wood non-destructive locating with low frequency ultrasonic echo technique. In: NCDTE'09, Non-Destructive Testing in Civil Engineering, Nantes, France.

Hu L J, Gagnon S (2007) X-ray based scanning technique for non-destructive evaluation of finger-joint strength. In Proc: 15th Int. Nondestructive Testing and Evaluation of Wood Symposium, Forest Products Society, Deluth, MN, USA.

Krause M, Effner U, Nowak T, Müller S, Vergin D (2013). 3D-SAFT Imaging von Streuern in Brettschichtholz. In: 2013 DGZFP-Jahrestagung, Dresden, Germany.

Neuenschwander J, Sanabria S J, Schütz P, Widmann R and Vogel M (2013). Delamination detection in a 90-year-old glulam block with scanning dry point-contact ultrasound. *Holzforschung* doi:10.1515/hf-2012-0201.

Sanabria S J, Wyss P, Neuenschwander J, Niemz P, Sennhauser U (2011) Assessment of glued timber integrity by limited-angle microfocus X-ray computed tomography. *European Journal of Wood and Wood Products* 69:605-617.

Sanabria S J, Furrer R, Neuenschwander J, Niemz P, Sennhauser U (2011b). Air-coupled ultrasound inspection of glued laminated timber. *Holzforschung* 65:377-387.

Sanabria S J, Furrer R, Neuenschwander J, Niemz P, Sennhauser U (2011c). Monitored assessment of structural integrity of multilayered glued laminated timber beams with air-coupled ultrasound and contact ultrasound imaging. In Proc.: 17th Int. Nondestructive Testing and Evaluation of Wood Symposium, University of West Hungary, Sopron, Hungary, 359-366.

Sanabria S J (2012). *Air-coupled ultrasound propagation and novel non-destructive bonding quality assessment of timber composites*. PhD Thesis, ETH Zurich, Zurich, Switzerland.

Sanabria S J, Furrer R, Neuenschwander J, Niemz P, Sennhauser U (2013). Novel slanted incidence air-coupled ultrasound method for delamination assessment in individual bonding planes of structural multi-layered glued timber laminates. *Ultrasonics* 53(7): 1309-1324.

Sanabria S J, Neuenschwander J, Sennhauser U (2013). Air-coupled ultrasonic contactless method for non-destructive determination of defects in laminated structures. Patent WO 2013/023987 A1.

Schütz P, Miceli A, Jerjen I, Flisch A, Hofmann J, Broennimann R, Sennhauser U (2013). Reducing environmental scattering in industrial computed tomography by system redesign. *NDT & E International* 58:36-42.

Influence of Wood Thickness on Attenuation of Soft X-ray for Developing Portable X-ray CT

Chul-Ki Kim
Department of Forest Science, Seoul National University, Seoul, Korea, aries8924@hanmail.net

Jung-Kwon Oh
Department of Forest Science/Research Institute for Agriculture and Life Sciences, Seoul National University, Seoul, Korea, jkoh75@hotmail.com

Jun-Jae Lee
Department of Forest Science/Research Institute for Agriculture and Life Sciences, Seoul National University, Seoul, Korea, junjae@snu.ac.kr

Abstract

Portable x-ray apparatus were used to reconstruct density CT image to investigate density distribution and detect artificial deterioration in wood which would be affect physical properties or wood quality. Soft x-ray as well as portable x-ray apparatus was used to apply in field, and its attenuation characteristic was investigated in this study. Because of scattering in wood, mass attenuation coefficient of soft x-ray decreased as penetrating depth in wood increased. From the results, equation of mass attenuation coefficient related with penetrating depth in wood, $\mu = -0.214\ln(t) + 0.7251$, was derived to convert radiograph to density radiograph. And it has been confirmed that the accuracy of density CT image was improved when reconstructed density CT using that equation was compared with real air-dry density. The RMSE for the entire small specimens which were made to know real air-dry density of the round timber was 0.041 g/cm^3. And RMSE for the midsection, exterior of the round timber was 0.012, 0.054 g/cm^3, respectively. Although exterior of specimen was underestimated as digital detector couldn't detect amount of x-ray attenuation after passing the short distance in wood, inner detect and density distribution seem to be properly evaluated using portable x-ray apparatus with soft x-ray.

Keywords: X-ray, mass attenuation coefficient, density CT image, non-destructive testing

Introduction

A great abundance of wooden construction have passed down for a long time in Korea. According to National Research Institute of Cultural Heritage Administration in Korea, some of those cultural properites seemed to be deteriorated by living organism (wood-ratting fungi, termite) or environmental factor (ultraviolet rays, moisture). It is especially hard to detect the deteriorations caused by living organism, because they usually began at inner part of wood. Moreover, those deterioration would affect physical properties or wood quality as one of most important factor in wood properties is density.

Non-destructive testing & evaluation (NDT&E) have been developed to inspect internal state of wood. X-ray is effective methods to investigate inner state of wood or wood based material, compared with other NDT&E like acoustic techniques. Because x-ray has higer resolution than acoustic technuques when is was used to evaluate inner state of wood. And it can provide an information of density from its frequency and charateristic of attenuation. Futhermore, cross sectional image of object which called

computed tomography (CT) image could be reconstructed using many x-ray photographs taken around a single axis of rotation.

To verify wood density, the researches about x-ray attenuation in wood have been done for several decades. Olson et al. calculated the change of mass attenuation coefficient for measurements of conifer wood density. The ideal x-ray energy between 5.13 and 5.69 keV for 1 mm thick wood samples provides the maximum attenuation difference between earlywood and latewood. Nakada et al. used soft x-ray imaging to study the moisture content distribution in clear Japanese cedar according to direction. It is also a useful method to obtain an information about not only density distribution but the size or location of defect in wood by x-ray computed tomography (CT) image, which could be reconstructed using a lot of radiographs obtained with rotating x-ray apparatus. Macedo et al. reported that image quantification of CT image in terms of dry bulk density could be obtained for tree different x- and gamma-ray energies (28.3, 59.5 and 662.0 keV). Lindgren et al. was reconstructed density CT image of clear wood to know physical properties according to three direction (radial, tangential and longitudinal direction) in wood. Moberg, Oja and Temnerud analysis CT image to provide a description of internal knot and resin pocket, which could be used to raise the production yield rate of lumber.

Despite those advantages, it is hard for x-ray or CT technique to be used in place where cultural properties or tree are located. Because most of x-ray or CT equipment which had been used to study for wood science was not developed for field applicability. Those and shield are not easy to be moved and their radiation intensity is too hard to shield site. However, the radiation exposure could be prevented by being for apart from x-ray source without radiation shielding, if low energy intensity x-ray is chosen to be used in place. And those low energy intensity x-ray could be generated by portable x-ray tube which is commercially produced for NDT and security inspections. So, it has been thought that the first step to solve field applicability problem is using soft x-ray from portable x-ray apparatus. In this study, the term of soft x-ray is used for low energy intensity x-ray which is not collimated beam.

The behavior of attenuation for soft x-ray which has continuous spectrum is different from hard x-ray which had been used previous studies. Attenuation of soft x-ray is governed by penetrating depth of object as well as its density, because soft x-ray from portable apparatus is continuous spectrum x-ray, in which the longer wavelength part tend to be attenuated by scattering rather than absorption (Ko et al. 2005). So it could be said that it is important to understand attenuation of soft-ray. Because density measurement by soft x-ray has a large difference from the actual density as penetrating depth is changed. From these reasons, the effect of penetrating depth on density prediction for soft x-ray was experimentally investigated in this study. The result of density CT image using behavior of attenuation of soft x-ray was also presented.

Materials and Methods

Materials

Two sets of specimens were prepared in this study; the first set was prepared for determination of attenuation coefficient, and the second set was for the validation of CT reconstruction which uses different mass attenuation coefficient according to penetrating depth.

For the determination of mass attenuation coefficient according to penetrating depth, four clear wood species were prepare; cedar (*Crypfomeria japonica*), larch (*Larix leptolepis*), pitch pine *(Pinus rigida*), and red pine (*Pinus koraiensis*). For each species, ten specimens were prepared, and Table 1 shows the size, density and moisture contents for the specimens.

Table 1—Clear wood details for attenuation of continuous x-ray

Species	Size[1] (mm)			Density[2] (g/cm^3)		MC (%)
	Width	Height	Length	Aver.	S.D.	
Cedar	31.51	33.37	80.00	0.32	0.04	12
Larch	32.87	38.58		0.50	0.07	
Pitch pine	31.50	33.58		0.51	0.02	
Red pine	32.90	39.95		0.40	0.03	

[1] Average dimension for ten specimens for each species
[2] Air-dry density at MC 13%

For the second test setup, a round wood with artificial hole was prepared to confirm accuracy of CT reconstruction. The species of round wood was pitch pine (*Pinus rigida*) and its air-dried density and moisture content was 0.43 g/cm^3, 12%, respectively. Fig. 1 (a), (b) shows the schematic drawing of round timber.

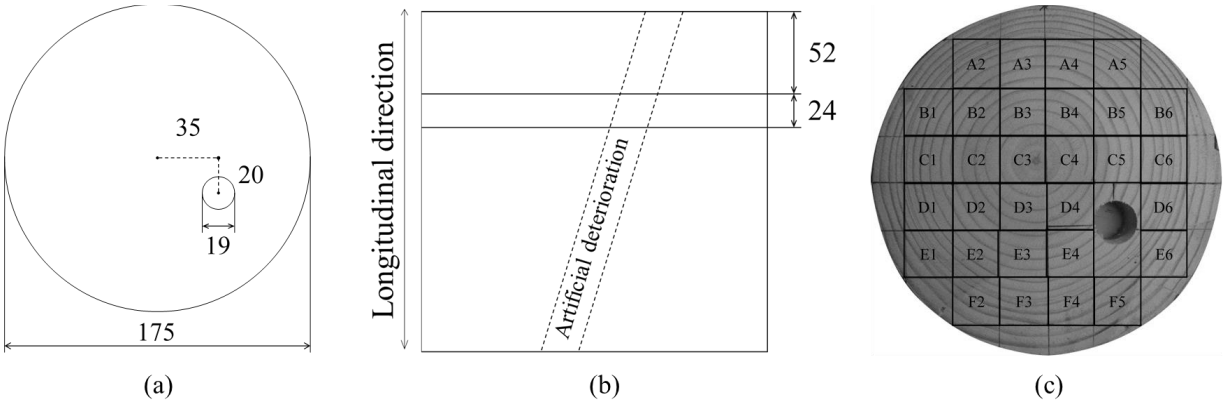

Figure 1—Round wood with artificial hole for CT image reconstruction. Its species, air-dry density and MC was pitch pine (*Pinus rigida*) 0.51 g/cm^3, 12 %, respectively. (Unit: mm) (a) Diameter and location of artificial hole in top of round wood, (b) Location of disk with 24 mm height to verify accuracy of CT image in side view of round wood, (c) Small specimens which was measured by dimension method in top of disk

An x-ray tube, K-4 (Softex, Japan), of which the maximum tube voltage and currents were 60 kV and 5 mA was used in this study. The tube voltage and current were 37 kV and 2 mA for getting mass attenuation coefficient and reconstructing density CT image. The digital detector, NX 06 (RF system, Japan) was used in this study, which is composed of scintillators and 12 CCD (Charge Coupled Device) and those are combined into one unit. The maximum resolution of digital detector was about 318.97 pixels/mm^2. Those portable x-ray apparatus were set up at CT installation which have been made for laboratory scale test.

Methods

Based on experience of inspection on heritage building, the intensity of x-ray was chosen (37 kV and 2 mA). Digital detector was exposure radiation for 5 seconds to get radiographs, and then digitalized JPGE files were automatically saved in laptop computer.

Correlation of mass attenuation coefficient with penetrating depth

Absorption of x-ray which has the lower energy and continuous wavelength was measured to find characteristic attenuation, as changed penetrating depth of clear wood. It is reported that the intensity of transmitted x-ray decreases exponentially if the beam is collimated, monochromatic (Kaelbel 1967), and eq. 2 and eq. 3 can derived from eq. 1 as follow

$$I = I_0 e^{-\mu\rho t} \tag{1}$$

$$\ln(I) = -\mu\rho t + \ln(I_0) \tag{2}$$

$$\rho = \frac{\ln(I_0 / I)}{\mu t} \tag{3}$$

where, I is intensity of attenuated x-ray (mSv), I_0 is intensity of initial x-ray (mSv), μ is the mass attenuation coefficient (cm^2/g), ρ is air-dried density (g/cm^3), t is penetrating depth of x-ray in wood (cm). Although x-ray which was used in this study has continuous wavelength distribution, eq. 2 was used to derive mass attenuation coefficient (μ).

The logistic regression equation, eq. 4 as follow, was derived from the result of mass attenuation coefficient with penetrating depth to convert radiographs into density radiographs

$$\mu = -a\log(t) + b \tag{4}$$

where, a and b is coefficient of the logistic regression equation.

Reconstruction of density CT image and verification of its accuracy

To reconstruct density CT image, one hundred eighty radiographs were taken during round wood were turned every 2 degrees on the CT installation. The tube voltage and current was 37 kV and 2 mA. Using mass attenuation coefficient and penetration distance of x-ray in round wood, the radiographs were converted into density radiographs. But the penetration distance to make density radiographs was calculated from assumption that round wood is a perfect circle. After that, CT image was reconstructed by filtered back projection (FBP) algorithm which were programmed and Matlab R2007 (Mathworks inc, USA).

To verify accuracy of CT image, round wood was cut into disk with 24 mm height. Then, the disk was cut thirty small specimens, as shown fig. 1 (c), and air-dry density was measured by dimension method. Air-dry density of small specimens, which could be measured by dimension method, was compared with density value in CT image to verify accuracy of density CT image.

Results and discussions

Characteristic absorption of x-ray which has lower energy and continues wavelength distribution

Mass attenuation coefficient for the whole penetrating depth was 0.1844 with the eq. 2 to calculate mass attenuation coefficient, as shown fig. 2. And mass attenuation coefficient decreased as penetrating depth of x-ray in wood increased (Table 2). It means that the quantity of x-ray which had reached at digital detector increased as penetrating depth of x-ray increased. Because the intensity of x-ray was attenuated by scattering as well as absorption, when the penetrating depth was long (Ko et al. 2005). So, it seemed

that repeated scattering x-ray in wood, including unabsorbed x-ray, was detected at digital detector. The least coefficient of determination was 0.97 when penetrating depth was 6.50 cm.

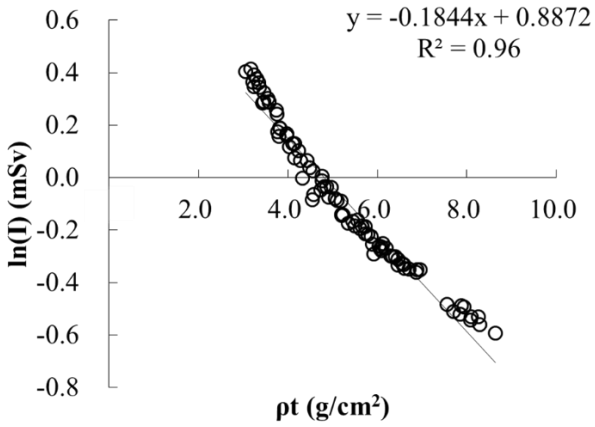

Figure 2— Mass attenuation coefficient of wood, which was come from eq. 2 according to tube voltage.

Table 2—Mass attenuation coefficient according to penetrating depth of soft X-ray

Penetrating depth (cm)				Mass attenuation coefficient (cm^2/g)	$R^{2\ 2)}$
Aver.	Max.	Min.	CV[1)]		
6.50	6.29	6.58	0.020	0.3218	0.97
6.72	6.71	6.73	0.001	0.3045	0.99
7.78	7.69	7.98	0.008	0.3018	0.99
9.45	9.44	9.47	0.001	0.2515	0.99
9.87	9.85	9.98	0.003	0.2332	0.99
12.60	12.59	12.62	0.001	0.1854	0.98
13.15	13.14	13.17	0.001	0.1572	0.98
15.72	15.36	15.99	0.015	0.1386	0.99
16.44	16.42	16.46	0.001	0.1241	0.99

[1)] Coefficient of variation = standard deviation/aver.
[2)] Coefficient of determination for mass attenuation coefficient

From these results, it thought that it is necessary to make the equation of mass attenuation coefficient according to the penetrating depth of x-ray, when radiograph was converted into density radiograph using the low energy and continuous wavelength distribution x-ray. Because density could be overestimated, if mass attenuation coefficient, which had been came of shorter penetrating length than it really is, was used. There is logistic regression equation of mass attenuation coefficient which was used to make density radiography according to penetration depth as $\mu = -0.214\ln(t) + 0.7251$, where, μ is the mass attenuation coefficient (cm^2/g) and t is penetrating depth of x-ray in wood (cm). The coefficient of determination (R^2) of the equation was 0.98.

Verification of density CT image

A set of 180 density radiographs, which had been taken during turning round wood every 2 degrees on CT installation, was made in two different ways; the first method was that constant mass attenuation

coefficient (0.1844) was used without considering penetrating depth, and the other was the way to use the equation of mass attenuation coefficient according to penetrating depth was used.

Two kinds of density CT image were reconstructed as shown fig. 3. These density CT images was compared with air-dry density of small specimens which were shown in fig. 1 (c).

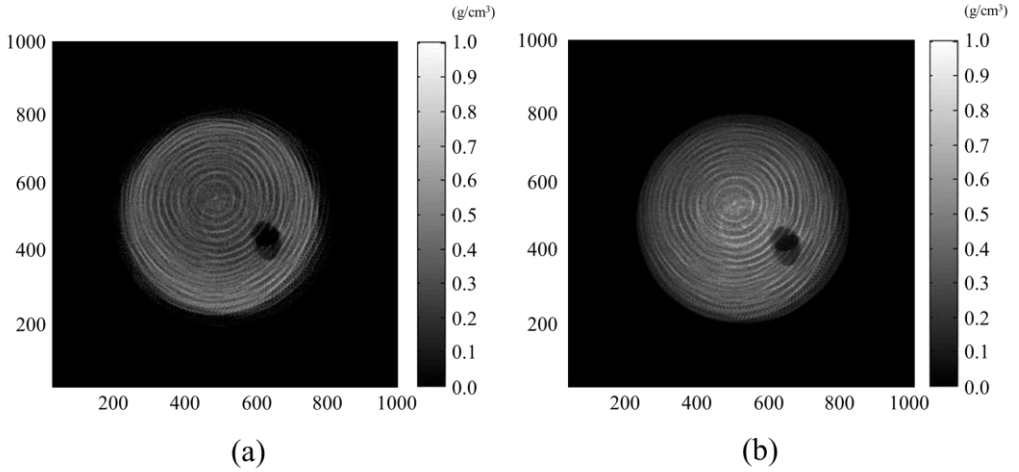

Figure 3— Density CT image using mass attenuation coefficient. (a) was reconstructed CT image by using constant mass attenuation coefficient (0.1844), and (b) was reconstructed CT image by using the equation of mass attenuation.

In density CT image using constant mass attenuation coefficient (fig. 3), the midsection of specimen was underestimated, but in the exterior parts, the results was opposed to that. It thought that it is cause by mass attenuation coefficient. The value of constant mass attenuation coefficient, 0.1844, was similar when x-ray penetrate clear wood with about 12.5 cm. So, it was overestimated in the exterior parts of specimens as constant mass attenuation coefficient (0.1844) which is smaller than actual mass attenuation was used to convert into density radiograph using eq. 3. RMSE (Root Mean Square Error) of the entire small specimens was 0.165 g/cm^3. And RMSE for the midsection was 0.082, and it was smaller than that for the exterior parts.

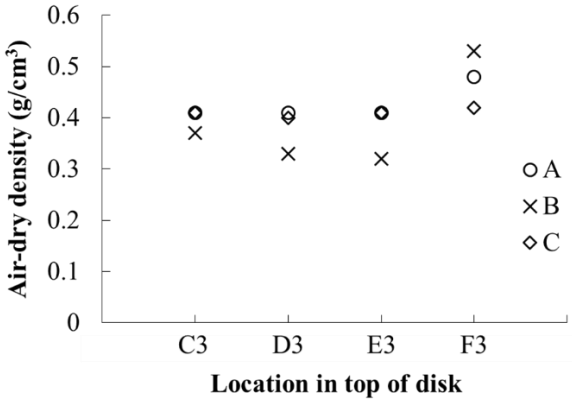

Figure 4— Comparison between air-dry density by measuring dimension method and predicted air-dry density by evaluating CT image in top of disk (fig. 1 (c)). A is the air -dry density by measuring dimension method, B is predicted air-dry density by evaluating CT image reconstructed by using constant mass attenuation coefficient (0.1844), and C is also predicted air-dry density by evaluating CT image reconstructed by using the equation of mass attenuation coefficient.

In case of density CT image using the equation of mass attenuation coefficient, RMSE for the entire small specimens was 0.041 g/cm^3. And RMSE for the midsection, exterior was 0.012, 0.054 g/cm^3, respectively. It could be said that the accuracy to predict inner density using CT image was improved as shown in fig. 4. However, the exterior parts of specimen was underestimated because digital detector couldn't locate amount of attenuation after passing the short distance. In other words, it could be considered that there was no wood when digital detector didn't detect a change of x-ray amount after x-ray penetrate the specimen. So, the exterior parts of specimen seemed to be underestimated.

Although the accuracy of estimation for the edge part of specimen was not particularly good, inner detect and density distribution seem to be properly evaluated using portable x-ray equipment with x-ray having low intensity and continuous wavelength. So, it can be used in site, because deterioration like heart rot, termite damage was usually started near heartwood.

Conclusions

This study was carried out to investigate the influence x-ray path length on attenuation of soft x-ray to reconstruct density CT image using portable x-ray apparatus. From this study, mass attenuation coefficient which is related with attenuation of x-ray decreased as penetrating depth of soft x-ray in wood increased. And it has been confirmed that the accuracy of density CT image which was reconstructed with 180 density radiographs was improved using mass attenuation coefficient according to penetrating depth. From these results, portable x-ray apparatus could be used to reconstruct CT image for field applicability.

Acknowledgments

This study was carried out with the support of 'Bio-industry Technology Development Program (project No. 111054-3)' provided by Korea Institute of Planning and Evaluation for Technology in Food, Agriculture, Forestry and Fisheries (iPET)

References

Divos, F.; Divos, P. 2005. Resolution of stress wave based acoustic tomography. In: 14th international symposium on nondestructive testing of wood, Shaker Verlag, Germany: 307-314.

Kaelbel, E.F. 1967. Handbook of X-rays. 130 p. McGraw-Hill, USA.

Korean society of physics for radiosurgery. 2005. Radiation physics (in Korean) 211 p. Komoonsa, Korea.

Lindgren, O.; Davis, J.; Wells, P.; Shadbolt, P. 1992. Non-destructive wood density distribution measurements using computed tomography. Holzforschung. 50(7): 295-299.

Macedo, A.; Vaz, C.M.P.; Pereira, J.C.D; Naime, J.M.; Cruvinel, P.E.; Crestana, S. 2002. Wood density determination by x- and gamma-ray tomography. Holzforschung. 56(5): 535-540.

Moberg, L.; 2000. Models of Internal Knot Diameter for Pinus sylvestris. Scand. J. For. Res., 15(2): 177-187.

National Research Institute of Cultural Heritage. 2012. Conservation of wooden objects. 20-25 p. Pointtech, Korea.

Nakada, R.; Fujisawa, Y.; Hirakawa, Y. 1999. Soft X-ray observation of water distribution in the stem of Cryptomeria japonica D. Don Ⅰ: General description of water distribution. J wood sci, 45(3): 188-193.

Nakada, R.; Fujisawa,Y.; Hirakawa, Y. 1999. Soft X-ray observation of water distribution in the stem of Cryptomeria japonica D. Don Ⅱ: Types found in wet-area distribution patterns in transverse sections of the stem. J wood sci, 45(3): 194-199.

Nicolotti, G.; Socco, L.V.; Martinis, R.; Godio, A.; Sambuelli, L. 2003. Application and comparison of three tomographic techniques for detection of decay in tree. J. of Arboric., 29(2): 66-78.

Olson, J.R.; Liu, C.J.; Tian, Y.; Shen, Q. 1988. Theoretical wood densitometry: Ⅱ. Optimal X-ray energy for wood density measurement. Wood Fiber Sci., 20(1): 187-196.

Oja, J.; Temnerud, E. 1999. The appearance of resin pockets in CT-images of Norway spruce (Picea abies (L.) Karst.). Holzforschung, 57(5): 400-406.

Schmidt, O. 2010. Wood and fungi. 157 p. Springer, Germany.

Overview of the National Timber Bridge Inspection Study

James P. Wacker
Forest Products Laboratory, USDA Forest Service, Madison, Wisconsin, USA, jwacker@fs.fed.us

Brian K. Brashaw
Natural Resource Research Institute, University of Minnesota-Duluth, Duluth, Minnesota, USA
bbrashaw@nrri.umn.edu

Frank Jalinoos
Turner-Fairbank Highway Research Center, Federal Highway Administration, McLean, Virginia, USA,
frank.jalinoos@dot.gov

Abstract

As many engineers begin to implement life cycle cost analyses within the preliminary bridge design phase, there is a significant need for more reliable data on the expected service life of highway bridges. Many claims are being made about the expected longevity of concrete and steel bridges, but few are based on actual performance data. Because engineers are least familiar with timber bridges, their expected longevity is often unfairly estimated at only 25-30 years. A national scale project has been developed for the United States, led by the USDA Forest Products Laboratory and the U.S. Federal Highway Administration. In this project, a group of 6 bridge inspection teams, representing the major climate zone types in the U.S., each inspected at least 20 timber bridges. Nondestructive inspection techniques included visual, probing, sounding, stress wave, and resistance micro-drilling. The study results will help to provide a better understanding of the design, performance, and durability characteristics of timber bridge structures. This paper will highlight the overall inspection findings, which were instrumental in reliably estimating the expected service life for timber bridge superstructures and help support future designs that employ life cycle and sustainable features.

Keywords: bridge, inspection, nondestructive evaluation, service life, durability, condition

Introduction

As many engineers begin to implement life cycle cost analyses within the preliminary bridge design phase, there is a significant need for more reliable data on the expected service life of highway bridges. Many claims are being made about the expected longevity of concrete and steel bridges being 75 years or more, but few are based on actual performance data. Because engineers are least familiar with timber bridges; their expected longevity is typically unfairly estimated at 20 years. Additional research is needed on a national scale that provides more reliable data about the true longevity of timber bridges in the U.S. and allows for more accurate life-cycle assessments.

In order to generate more quantitative and unbiased bridge performance data, the Federal Highway Administration (FHWA) recently launched a new initiative called the Long-Term Bridge Performance Program (LTBP). The LTBP is national program and it includes detailed inspection, periodic evaluation and monitoring of approximate 200 bridges over a 20-year period. The LTBP program concentrates on “work-horse” highway bridges. This includes steel, reinforced and pre-stressed concrete bridges of

stringer/multi-beam or girder, multiple box beam or girders and slab design types constituting 75% to 80% of the National Bridge Inventory (NBI). Under the LTBP program, a representative sample of bridges will be evaluated in a cluster/reference bridge sampling method. Each reference bridge will anchor a cluster of 5 or more bridges that are within a small geographical location (along linear highway corridor or scattered about a geographic region approximately 30 miles wide) and subject to similar climate and traffic conditions. The reference bridges will involve 1) detailed and arm-length visual inspection (VI); 2) advance nondestructive evaluation (NDE); 3) global testing (load testing, modal testing, and continuous monitoring); and, 4) destructive material sampling. The cluster bridges will involve arm-length VI. The LTBP has developed an open, scalable, and extensive data management system called the "Bridge Portal". This database is capable of integrating LTBP data with other sources, such as NBI, PONTIS, weather, and traffic. Unfortunately, the LTBP currently does not include timber bridges in their current scope. This research study was developed to generate more reliable bridge performance data and establish a framework for long-term timber bridge performance monitoring. This background information will be needed if timber bridges are to be incorporated into the LTBP in the future.

National Bridge Statistics

Timber bridges are an indispensable component of the U.S. highway system especially on secondary rural roadways. The current December 2010 National Bridge Inventory (NBI) database includes 604,426 bridge structures (including culverts) with a span length greater than 20 ft (6 m), with approximately nearly 8 percent utilizing timber as a primary structural component for the superstructure (Table 1). Many of these structures have been in-service for decades and have performed well structurally, but have been deemed structurally deficient or functionality obsolete. In addition, many bridge inspectors are not as familiar with timber as a bridge material and tend to downgrade their condition rating in the NBI. The net result is that many timber bridges have been assigned poor load ratings, or posted for restricted loads, when their actual condition is satisfactory. The long-range impact is that many engineers hold the misconception that timber is a low durability bridge material having an estimated service life of less than 25 years.

Table 1—National bridge statistics as of December 2010.

Concrete	Steel	Timber	Masonry	Aluminum	Other	Total
391,161	185,148	24,267	1,743	1,459	648	604,426
All timber superstructure		Timber deck on steel stringers		Total – timber as primary component		
24,267		24,492		48,759 (8% of total bridges)		

Source: www.fhwa.dot.gov/bridge/britab.cfm

There are promising examples of length-of-service that support the long-term durability of timber bridges. The Forest Service (FS) maintains nearly 3,000 timber road bridges in their transportation network. Many of them are sawn timber superstructures that were installed in the post-WWII era and are still in-service after several decades. The FS also has a fairly large population of early glulam bridges built in the 1950s that are still providing vital transportation links in the Pacific Northwest. The railroads have used timber components for bridges for over 100 years and have several sawn timber structures that have been in-service for more than 75 years. Recently, long-term performance of stress laminated timber bridges was also reported (Wacker et al 2003). However, what is lacking in the literature is a scientific study on the long-term performance of timber highway bridges in the U.S.

The geographical distribution of the NBI inventory data shows that 19 States have greater than 500 bridges (Figure 1). States with more than 1,500 timber bridges include Louisiana, Iowa, and Minnesota; States having 1,000–1,500 timber bridges include Texas, Oklahoma, Mississippi, Kansas, Missouri, and Nebraska. States having 500–1,000 bridges include North Dakota, California, Oregon, Washington,

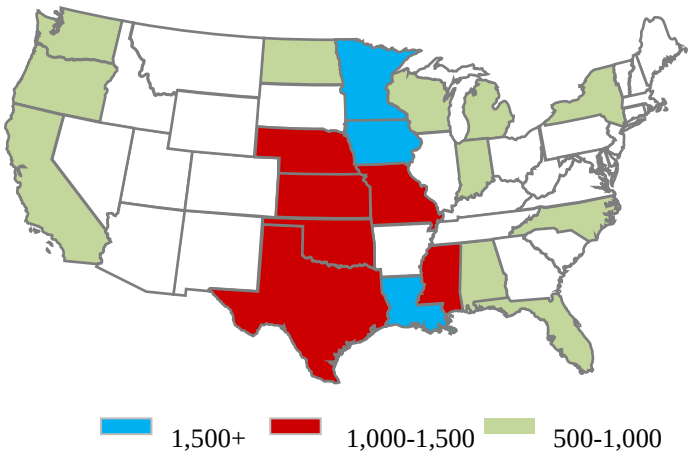

Figure 1—States with significant timber bridge inventories.

Wisconsin, Michigan, Indiana, Alabama, New York, North Carolina, and Florida. The remaining 31 states have less than 500 timber bridges in their bridge inventory.

There are a variety of timber bridge superstructure types (Figure 2). The main categories are longitudinal decks, stringer systems, and others. Longitudinal decks include nail-laminated, spike-laminated, stress-laminated (using either sawn lumber or glulam laminations), and longitudinal glulam bridges. The spike-laminated and longitudinal glulam deck superstructures consist of partial-width panels that are interconnected with transverse stiffener beams attached at intervals along the bridge length. The total bridge span ranges typically between 6 and 31m (20 and 100 ft.).

Nail-laminated deck

Glulam stringer and transverse deck

Longitudinal glulam deck

Stress-laminated deck

Glulam deck arch

Glulam suspended arch

Figure 2—Examples of various timber bridge superstructures.

Objective and Scope

The primary objective of this study is to assess the condition and performance of more than 100 existing timber highway bridges representing the main climate regions in the continental United States. A secondary objective of this study was to establish the baseline framework for evaluating future performance of timber bridges nationwide. The study results will help to provide a better understanding of the design, performance, and durability characteristics of timber bridge structures, which can improve future bridge design and preservation practices and ultimately extend service life. Lastly, the findings should assist with timber bridge service life expectancy when compared with alternative bridge materials.

Research Methods

Project Team Overview

A team approach was used to inspect timber bridges in all USA regions. USDA Forest Products Laboratory and the U.S. Federal Highway Administration partnered with several other organizations to complete the field bridge inspection work. Each organization represented a US region and would be responsible for inspecting bridges in their respective regions. Figure 3 also shows the general geographic region assigned to each partner organization.

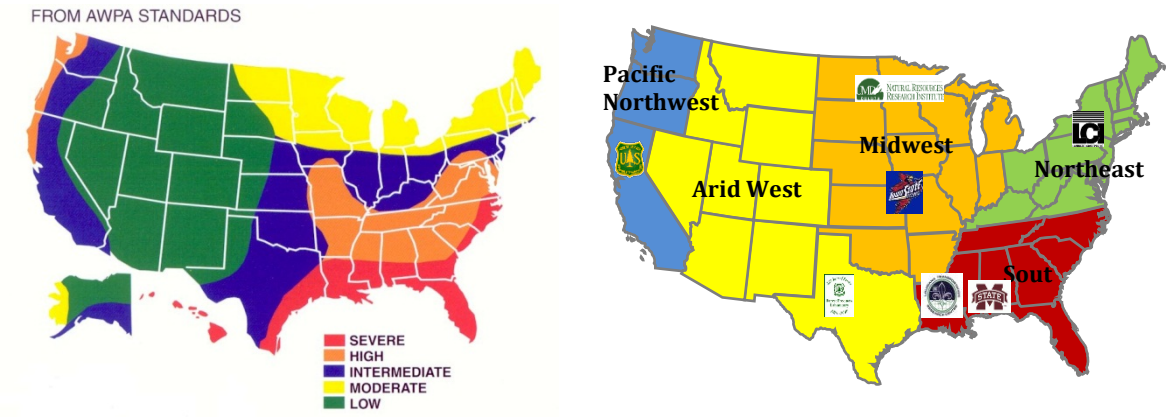

Figure 3—Project team designations for the various wood decay hazard climate zones in the continental US.

Selection of Bridge Candidates

Team members were asked to assess the inventory of timber bridges in their region and select candidate bridges for field evaluations. Teams were required to select timber bridge clusters within a multi-county region that had the same superstructure design type and preferably of similar age. Each project team selected approximately 20 bridges for inspection. This list was reviewed and approved by the project coordinators and used to assemble a national perspective for the candidate bridge selections and determine age and bridge type overview.

Bridge Inspection Work

The bridge inspection methods utilized involved a combination between visual, hammer sounding, moisture content surveys, stress wave timing, and various probing/drilling techniques. These techniques were reviewed among all teams prior to field inspection to emphasize uniformity among the various

inspection teams. More detailed description of these bridge inspection methods are currently available (Ritter 1990).

Inspection Results

At this time, field inspections have been completed and all data is being compiled for drafting a comprehensive final report. Table 2 provides a summary of the number and type of timber bridges inspected by each team. Typical inspection work being conducted at a field bridge is shown in Figure 4. A resistance micro-drill was utilized at locations where either high moisture contents were detected or other anomalies that were identified through visual inspection, hammer sounding, and/or stress wave timing investigations.

Table 2—Summary of bridges inspected in this national bridge inspection study.

US Region	State	County	No.	Bridge Types
Pacific West (*28 total*)	California	Del Norte	3	Glulam girder/nail-, glulam, & concrete
		Siskiyou	3	Glulam girder/nail-lam deck
	Oregon	Klamath	3	Sawn girder/plank deck
		Washington	7	Sawn girder/plank deck
	Washington	Yakima	7	Sawn girder/plank deck
		Grays Harbor	5	3 Sawn girder/plank (plus concrete deck) 1 glulam girder/glulam deck
Midwest (*36 total*)	Minnesota	Saint Louis	5	Spike-laminated deck
			5	Timber deck/steel girder
		Freeborn/Jackson	4	Sawn girder/plank deck
	Wisconsin	Sawyer/Price	5	Sawn girder/plank deck
	Iowa	Blackhawk	7	Sawn girder/plank deck
		Bremer	5	Sawn girder/plank deck
		Clarke	5	Spike-laminated deck
Northeast (*15 total*)	New York	Steuben-Chemung-Tioga	5	Glulam Stringer/transverse glulam deck
		Alleghany	6	Longitudinal glulam deck
	Maryland	Queen Anne/Dorchester	4	Spike-laminated deck
South (*60 total*)	Mississippi	Lafayette	8	Sawn girder/plank deck
	Alabama	Pickens	4	Sawn girder/concrete deck
	Tennessee	Crocket/Madison	7	Sawn girder/plank deck
	Louisiana	District 2	4	Sawn girder/plank deck
		District 8	5	Sawn girder/plank deck
		District 62	5	Sawn girder/plank deck
	Alabama	Shelby	5	Sawn girder/plank deck
	Georgia	Colquitt	5	Sawn girder/plank deck
		Stephens	5	Sawn girder/plank deck
	North Carolina	Johnston	4	Sawn girder/concrete deck
		Durham	3	Timber deck/steel girder
		Wake	5	Sawn girder/plank deck
		GRAND TOTAL =	**130**	

Summary and Conclusions

Over 130 timber bridges were inspected as part of a national study jointly administered by the USDA Forest Products Laboratory and the U.S. Federal Highway Administration. A team of project partners conducted the in-depth field inspections using a variety of methods. Many bridges have shown to be in remarkably good condition after more than 5 decades of service. The use of advanced NDE inspection tools when inspecting timber highway bridges provides a more reliable indication of its structural

condition. These findings have provided for a better understanding of the design, performance, and durability characteristics of timber bridge structures. Lastly, this study provides foundation for future long-term monitoring efforts and improved service life predictions for timber bridges in the US.

Figure 4—Inspection of a timber bridge superstructure located in Washington using a resistance micro-drilling unit.

Acknowledgments

The authors would like to acknowledge the key technical support of the other project partners:

Tom Williamson, T-Williamson Engineering Inc.
David Strahl and Lola Hislop, USDA Forest Service-Pacific Northwest Region
Vijaya Gopu, Louisiana Transportation Research Center and University of New Orleans
Matt Smith, Laminated Concepts Inc.
Travis Hosteng and Brent Phares, Iowa State University
P. David Jones, Mississippi State University
Clayton Bennett, Georgia Department of Transportation
Henry Black, North Carolina Department of Transportation
Alabama Department of Transportation

Thanks are also due to several local bridge personnel who assisted with these bridge inspection efforts.

References

Ritter, M. 1990. Timber Bridges-Design, Construction, Inspection, and Maintenance. Engineering Management Series EM-7700-8. Washington, DC: U.S. Department of Agriculture, Forest Service, 944 p.

Wacker, J.P.; Calil Jr, C.; Hislop, L.E.; Lee, P.D.H.; Kainz, J.A. 2003. Long-Term Performance Monitoring of Hardwood Timber Bridges in Pennsylvania. Res. Pap. FPL–RP–612. Madison, WI: U.S. Department of Agriculture, Forest Service, Forest Products Laboratory. 56 p.

Distribution of Shear Strengths in Wood Estimated from Normalized Withdrawal Resistances of Probes

Nobuyoshi Yamaguchi
Department of building materials and components, Building Research Institute, Tsukuba-city, Ibaraki-pref., Japan, yamaguch@kenken.go.jp

Abstract

Withdrawal resistances of probes using metric-screws with short thread have been developed by author as a semi-destructive in-situ assessment method of wood. Wood is un-homogeneous material. For the purpose to evaluate effect of the grain on the withdrawal resistances, withdrawal resistances measurements and shear loading tests were conducted for piece specimens cut off from a lumber of three species. Distribution of densities, shear strengths and withdrawal resistances in these lumbers were obtained. Comparison of distributions of shear strengths and withdrawal resistances resulted that the grain affects less for the shear strengths and withdrawal resistances. The methods to predict densities and shear strengths from normalized withdrawal resistances (NWR) with regression coefficients were proposed. Correlations between the measured and predicted densities and shear strengths were reasonable. The method to assess integrity of wood using NWR is proposed. The judgment method using the predicted shear strengths and the nominal shear strengths of wood species are also proposed.

Keywords: assessment, withdrawal resistance, shear strength, grain

Introduction

In situ assessment of structural timber in existing structures contributes to maintain availability of existing structures. Judgments of sustainable use or replacement of wood members are often required during the assessments of structures. Assessment methods applied for existing structures are classified into non-destructive and semi-destructive testing methods. Many assessment methods had been proposed and developed (Ross, 1994; Divos,1999; Kasal,2010). In-situ assessment method by withdrawal resistance of probes using metric screws with short threads was proposed and have been developed by author (Yamaguch,2011, 2013). Single withdrawal resistance measurement for wood, and coaxial multiple withdrawal resistance measurement method which is able to obtain distribution of withdrawal resistances in the cross-section of wood were developed. This measuring method using the probes with short thread is possible to obtain withdrawal resistances of target points in deep from the surface of wood. Furthermore withdrawal resistances of the wood behind gypsum boards or plaster finishing are also able to be measured by this method through a hole applied on those boards or finishing. As wood is un-homogeneous material and includes annual rings, effect of the annual ring on these withdrawal resistances should be analyzed. Experimental research using piece specimens cut off from a lumber of three wood species was conducted to analyze the effect of annual ring of wood on the withdrawal resistances.

Methodology

Specimens

Specimens for the withdrawal resistance measurements and shear loading tests were prepared. Species of the specimens were Sugi (Cryptomeria japonica), Hinoki (Chamaecyparis obtusa) and Douglas-Fir (Pseudotsuga menziesii, abbr;D-Fir). Moisture contents of these Sugi, Hinoki and D-Fir specimens were around 8, 9 and 11% by moisture meters. Densities of them were around 0.38, 0.45 and 0.53 g/cm^3 in air condition. Figure-1 shows three groups of piece specimens cut off from un-degraded lumber sequentially. Figure-2 shows a group of piece specimens (30x30x30 mm) which is arranged to three columns (left, center, right), rows (upper, middle, lower) and lines (1st , 2nd , 3rd) of nine piece specimens each. Nine piece specimens of a line have different angle of the grain and are named from No.A to I. Figure-3, -4 and -5 shows nine piece specimens in a line of Sugi, Hinoki and D-Fir respectively, those in a line show a cross-section of lumber. Sugi and Hinoki specimens shown in Figure-3 and -4 have a pith between the piece specimens of No.E and H. D-Fir specimen shown in Figure-5 has no pith. Directions of shear loading were both of longitudinal direction (L-dir) and transverse direction. As transverse direction includes all of radial, tangential direction of the grain and intermediates between them, transverse direction is named RT-dir. Piece specimens belongs to 1st and 3rd lines were used for shear loading tests of L-dir and RT-dir respectively. Piece specimens belong to 2nd line specimens were used for withdrawal resistance measurements of RT-dir.

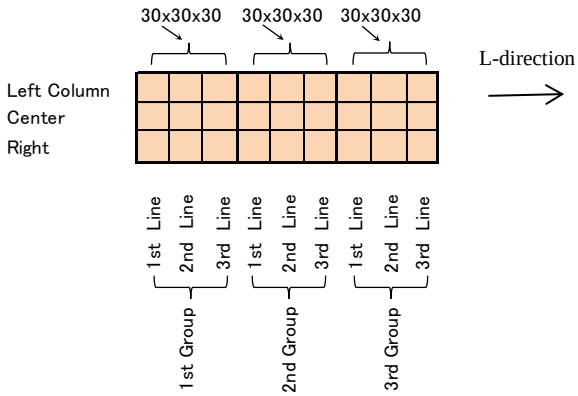

Figure 1—Three groups of piece specimens

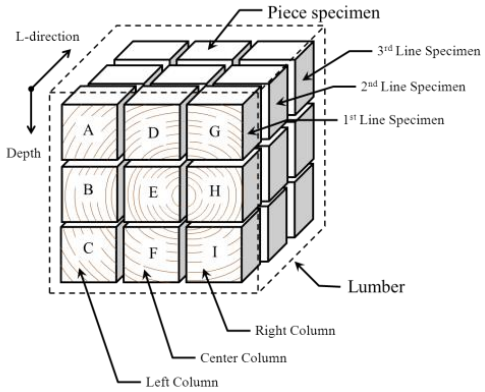

Figure 2—Piece specimens cut off from lumber

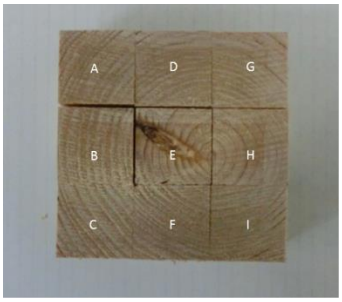

Figure 3— Piece specimens and cross-section of Sugi

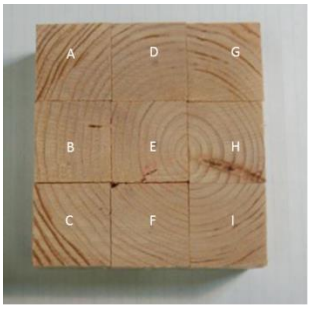

Figure 4— Piece specimens and cross-section of Hinoki

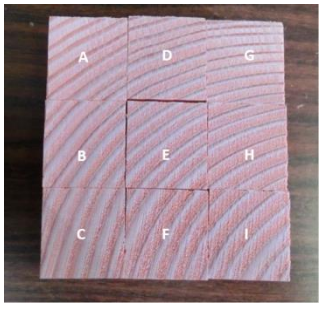

Figure 5— Piece specimens and cross-section of D-Fir

Withdrawal resistance measurement

Probes

Withdrawal resistance measurements used metric-screw type probes with 12.85mm length thread, which are shown in Figure-6. These probes were manufactured from commercially available metric threaded rods, shape of these thread is adjusted to the ISO 261 and 724. The probes have a short-thread which is

made up removing the rest of thread from threaded rods by machines. Diameters of the probe threads are constant along the probe axis. Dimension of the probe is shown in Figure-6. Diameter (peak to peak) of the thread is 3.87mm. Diameter of the remaining shafts is 2.8mm. Distance between the pitches of the threads is 0.7mm. The probes were screwed into piece specimens downwardly and withdrawn upwardly.

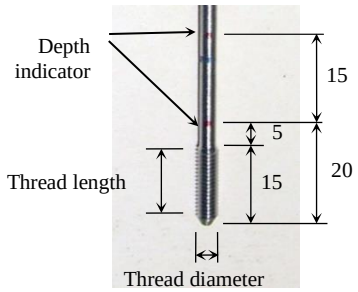

Figure 6—Dimension of probe

Measurement procedures

To begin with measurements, a pre-drilled hole of 3mm (2.94mm) in diameter was made in the center of piece specimens. The probe was screwed into the pre-drilled hole by electric-driver. Penetration depth of the probe tip was 20mm. The depths in the specimens were controlled by the depth indicators marked on the probe shaft which are shown in Figure-6. The probe was pulled out slowly by the portable withdrawal equipment powered by electric-driver. Withdrawal resistances were measured by the load cell installed in the equipment simultaneously. Figure-7 and -8 show a pre-drilled hole and position (depth) of the thread in piece specimens. All the withdrawal direction was upward of piece specimens shown in Figure-3, -4 and -5. Withdrawal direction was transverse of wood (RT-dir of the grain). Withdrawal resistances between the probe and wood occur on the outer cylindrical plain around the probe threads. The outer cylindrical plain is round shear plain. Measurement depths of the withdrawal resistances are defined as the distances between the surface of piece specimens and the middle of the cylindrical shear plain. Depth of the withdrawal resistance measurement was 12.5mm. There are some cutting stock (saw width and finishing loss) between piece specimens as shown in Figure-2. The measurement depths of layered piece specimens in a column (ex. No.A, B and C) before cut off from a lumber were estimated 15, 50 and 85mm.

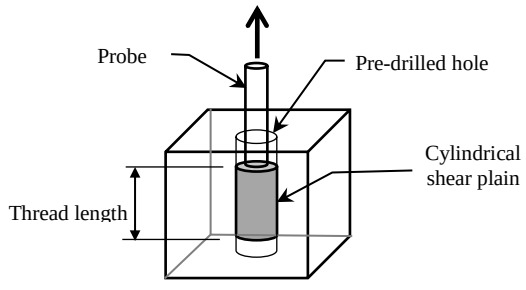

Figure 7—Cylindrical shear plain between pre-drilled hole and probe thread

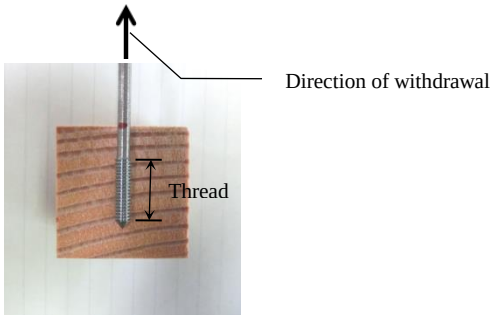

Figure 8—Grain direction of piece specimen and withdrawal direction of the probe

Estimated shear strength (NWR)

Measured withdrawal resistances are affected by area of cylindrical shear plain around the probe threads. Removing the effect of dimension of the probe threads, measured withdrawal resistances were normalized by the outer cylindrical area of the threads. Normalized withdrawal resistance (NWR) is obtained by Equation-1. NWR indicates estimated shear strength of wood on the cylindrical shear plain shown in Figure-7. Direction of estimated shear strength (NWR) was RT-direction of wood in these tests.

$$\tau = \frac{P}{R_t \times \pi \times L_t} \quad (1)$$

τ	: Estimated shear strength (NWR)	[N/mm^2]
P	: Withdrawal resistance	[N]
R_t	: Diameter of the thread (peak to peak)	[mm]
L_t	: Length of the thread of probes	[mm]
π	: Circular Constant	

Shear loading tests

Dimension of piece specimens for shear loading tests was 30x30x30mm, and the size of chair for shear loading was 10x10mm based on JIS Z 2101. Shear strengths of L-direction and RT-direction were measured in case using Sugi and Hinoki. In case using D-Fir, shear strengths of L-direction was only measured. Figure-9 indicates specimen for shear loading tests and flat shear plain in these tests. This shape of the shear pain is different from that of withdrawal resistances shown in **Figure-7**.

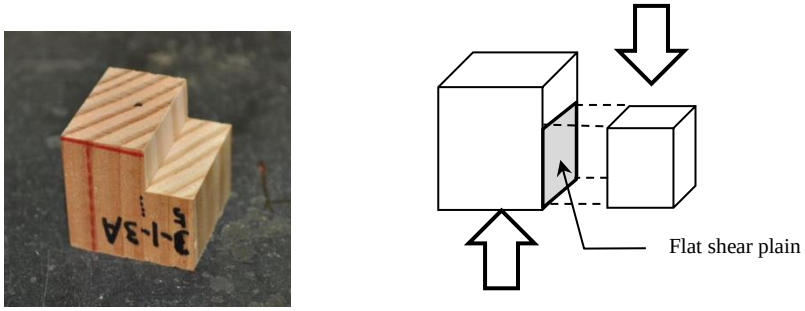

Figure 9— Specimen for shear loading test and flat shear plain

Results and Discussion

Density, shear strength(L) and NWR along L-direction

Average values and coefficient of variation (COV) of measured densities, shear strengths for L-dir (L) and NWR are summarized in Table 1. Number of each measurement of densities, shear strengths (L) and NWR was six, three and three respectively. Nominal values (average) of densities and shear strengths (L) of these species described in 'Wood Handbook (FFPRI, 2004)' are also shown in Table 1. Measured average density of D-Fir was greater than the nominal value. Measured average shear strengths (L) of these three species were greater than those of nominal values considerably. COV values more than 10% are emphasized in Table 1. COV greater than 10% was only one in case of densities. COVs greater than 10% were three and eight in case of shear strengths (L) and NWR. Variation of measured shear strengths (L) and NWR were greater than those of densities in all species. Variation of measured densities, shear strengths (L) and NWR in Sugi were much more than those of other species. Average densities, shear strengths (L) and NWR obtained from the three specimens in three groups of specimens are used in the analysis.

Table 1—Average and COV of density, shear strength(L) and NWR along L-direction

		Species	Sugi			Hinoki			D-fir		
		Position	Left	Center	Right	Left	Center	Right	Left	Center	Right
Average	Density (g/cm^3)	Upper	0.34	0.37	0.33	0.43	0.44	0.45	0.56	0.53	0.54
		Middle	0.39	0.39	0.34	0.44	0.48	0.51	0.53	0.52	0.49
		Lower	0.39	0.45	0.37	0.43	0.44	0.46	0.54	0.49	0.48
		Ave.	0.38			0.45			0.52		
		Nominal	0.38			0.44			0.46 – 0.50		
	Shear Strength (L) (N/mm^2)	Upper	9.6	9.2	9.3	10.9	11.5	12.7	12.8	12.8	10.5
		Middle	10.7	11.4	10.8	10.4	12.1	13.8	11.9	12.6	11.0
		Lower	11.9	15.2	11.3	10.6	10.1	11.3	13.4	12.7	11.6
		Ave.	11.0			11.5			12.2		
		Nominal	6			7.5			7.8 – 10.4		
	NWR (N/mm^2)	Upper	4.7		4.9	7.6	7.3	8.2	13.1	12.1	11.7
		Middle	5.2		4.3	7.2	7.5	9.0	11.7	11.6	10.9
		Lower	5.8	9.4	6.5	6.8	6.8	6.7	11.8	9.7	9.6
		Ave.	5.8			7.5			11.4		
COV (%)	Density (g/cm^3)	Upper	2.3	11.0	1.1	0.6	2.8	2.7	2.2	1.1	1.5
		Middle	5.4	3.4	2.7	1.4	6.2	8.1	2.2	1.5	1.4
		Lower	1.1	3.6	1.2	0.6	1.2	8.6	1.5	1.8	3.2
		Ave.	3.5			3.6			1.8		
	Shear Strength (L) (N/mm^2)	Upper	4.9	2.3	2.4	5.1	6.8	1.4	2.2	3.6	3.5
		Middle	8.8	3.6	12.3	6.8	9.9	9.8	0.8	12.3	8.9
		Lower	3.1	26.9	1.5	2.6	8.3	0.3	1.3	4.4	4.2
		Ave.	7.3			5.7			4.6		
	NWR (N/mm^2)	Upper	4.0		9.0	3.5	7.3	9.4	13.2	3.8	5.6
		Middle	15.6		22.6	12.4	6.7	3.0	6.6	3.3	1.3
		Lower	7.5	29.4	16.0	3.4	5.5	11.6	8.7	3.4	14.5
		Ave.	14.9			7.0			6.7		

Prediction of density using NWR with regression coefficients

Relationships between densities and NWR of Sugi, Hinoki and D-Fir are shown in Figure-10. Linear approximation formula and coefficients of correlation of these species are also shown in Figure-10 respectively. Square of coefficients of correlation (R^2) between densities and NWR are reasonably good in Sugi, Hinoki and D-Fir. Densities of these species in air dry condition are predicted by NWR with these coefficients of regression.

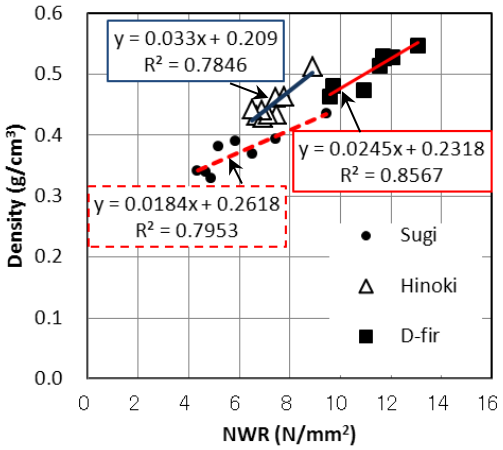

Figure 10—Prediction of density from NWR in Sugi, Hinoki and D-Fir

Distribution of shear strengths in cross-section

Figure 11, 12 and 13 show distributions of measured shear strengths (L) by shear loading tests of Sugi, Hinoki and D-Fir specimens. Figure 14, 15 and 16 show distributions of estimated shear strength (NWR) by withdrawal resistance measurements of Sugi, Hinoki and D-Fir specimens. Depths in these figures are corresponding to the depths in lumber. In case of specimen No.B and H, shear plains of shear loading tests or penetration direction of withdrawal measurements are perpendicular to the grain. In case of specimen No.D and E, those are parallel to the grain. These results used average of three values obtained from three groups of piece specimens. Apparent effect of the grain was not observed on both distributions of the measured shear strengths (L) and the estimated shear strengths(NWR).

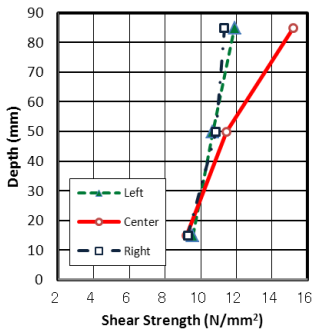

Figure 11—Measured shear strength(L) of Sugi

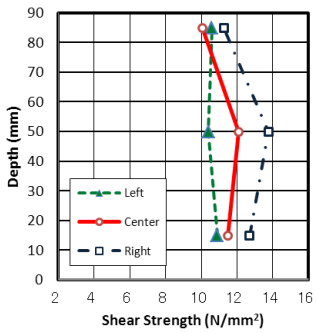

Figure 12—Measured shear strength(L) of Hinoki

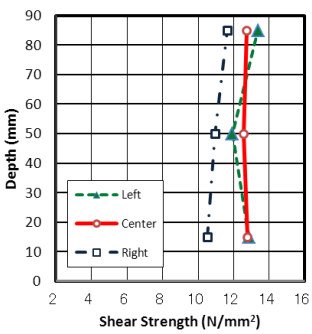

Figure 13—Measured shear strength(L) of D-Fir

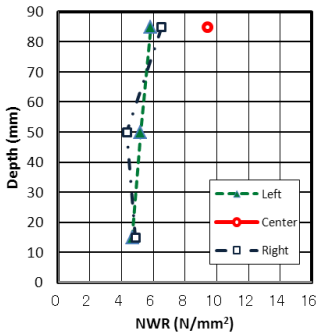

Figure 14— Estimated shear strength (NWR) of Sugi

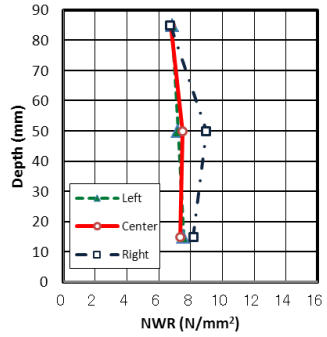

Figure 15— Estimated shear strength(NWR) of Hinoki

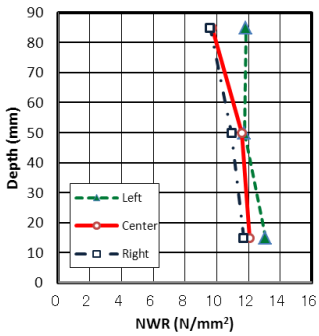

Figure 16— Estimated shear strength(NWR) of D-Fir

Prediction of shear strength(L) using NWR with regression coefficients

Relationship between shear strengths and NWR are shown in Figure-17, 18 and 19. Shear strengths of L-dir and RT-dir, average shear strengths of them (RT&L) are plotted in these figures. Shear strengths (L) of Sugi and Hinoki are much greater than NWR of them, but shear strengths (L) of D-Fir are close to the NWR. It is considered differences between shear strengths (L) and NWR would be related to the differences of those shapes of the shear plain. Species may also affect them. Linear approximation formula and the square of the correlation coefficients (R^2) are shown in Figure-17 and 18. Assuming the relationship between shear strengths (L) and NWR is linear in any NWR, shear strengths (L) are predicted from these linear approximation formulas. Shear strengths (L) of Sugi and Hinoki are predicted using NWR and the coefficients of regression indicated in Figure-17 and 18. Those of D-Fir are predicted from measured NWR without using coefficients of regression.

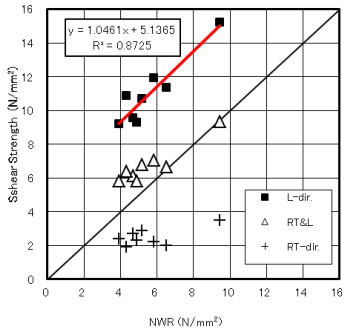

Figure 17—Shear strengths and NWR of Sugi

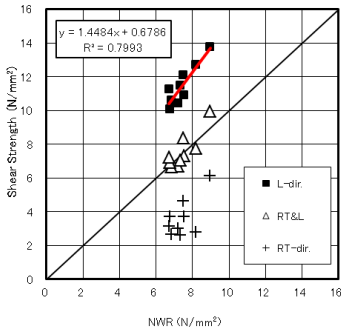

Figure 18—Shear strengths and NWR of Hinoki

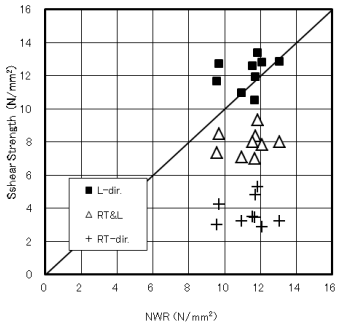

Figure 19—Shear strengths and NWR of D-Fir

Integrity judgment based on NWR

To assess the integrity of wooden members based on withdrawal resistances, NWR are compared to those of benchmark wood species/group under investigation. Both shear plains of tests and benchmark is same (cylindrical). Variation of NWR would be greater than that of densities, it is recommended to use average NWR for the judgment from multiple withdrawal resistance measurements.

Integrity judgment based on predicted shear strength (L)

To assess integrity of wood members based shear strengths, predicted shear strength(L) were compared to the nominal shear strength (L) described in 'Wood Handbooks (FFPRI, 2004)'. Figure 20,21 and 22 show linear approximation formulas for the prediction of shear strengths (L) of Sugi, Hinoki and D-Fir. Nominal (average) shear strengths (L) of these species are also indicated in these figures respectively. The intersections of these linear approximation lines and nominal shear strengths (L) indicate threshold values of NWR in Figure 20 and 21. The nominal shear strength (L) is the threshold value of NWR in Figure 22. Additional consideration is required to use five percentile values of the nominal shear strengths (L) instead of average value. Allowable shear strengths for structural calculations are not suitable for the threshold values in the integrity judgment, because allowable shear strengths are too conservative for the integrity judgment. In case to judge replacement of wood members, structural calculation of the members is needed. Densities and shear strengths (L) predicted from NWR are valuable for the further prediction of mechanical properties as MOR, compression strength, etc. These predicted mechanical properties of wood members would be used for the structural calculation of existing timber structures.

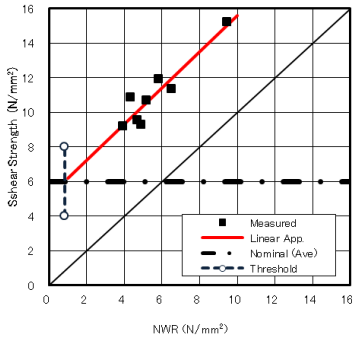

Figure 20—Nominal shear strength and criteria on NWR (Sugi)

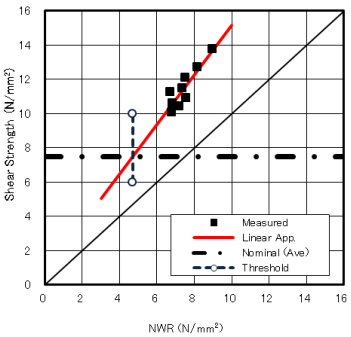

Figure 21— Nominal shear strength and criteria on NWR (Hinoki)

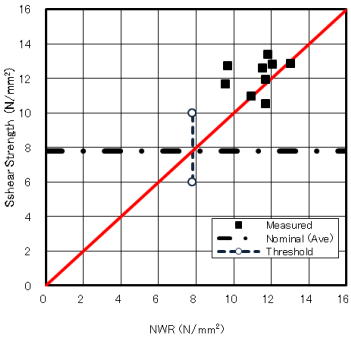

Figure 22— Nominal shear strength and criteria on NWR (D-Fir)

Conclusions

In order to assess integrity of wood members, withdrawal resistance measurement method using metric-screw probes with short threads was proposed. Comparing distributions of measured shear strengths and withdrawal resistances in cross-section of wood, grain of wood affects less for the shear strengths (L) and withdrawal resistances. Comparing densities and NWR, densities of wood were predicted from NWR with good accuracy. Integrity judgment method comparing NWR of test and benchmark specimens was proposed. Shear strength (L) of wood was also predicted from NWR and coefficients of regression with reasonable accuracy. Another integrity judgment method was also proposed, which compares nominal shear strength (L) in 'Wood Handbook' and predicted shear strength (L) from NWR with coefficients of regression. In case to judge replacement of wood members, predicted density and shear strength (L) are significant values for the further prediction of other mechanical properties of wood as MOR, compression strength, etc. These predicted mechanical properties of wood members will be valuable for the structural calculation of existing timber structures.

References

Divos F.; Nemeth L.; Bejo L. 1999. Evaluation of the wooden structure of a baroque place in Papa, Hungary, Proceedings of 11th international symposium on non-destructive testing and evaluation of wood, Washington State University, USA, 153-160.

FFPRI. 2004, Wood Handbook(Mokuzai kogyo handbook) Ver.4, Forestry and Forest Products Research Institute, Japan, Maruzen

Kasal B.; Tannert T. 2010. In situ assessment of structural timber, RILEM State of the Art Reports, Volumn 7, Springer.

Ross, R.J.; Pellerin, R.F. 1994. Nondestructive testing for assessing wood members in structures, General Technical Report FPL-GTR-70, Forest Products Laboratory, US Department of Agriculture.

Yamaguchi N.2011. In-situ assessment method of wood based on shear stresses obtained from withdrawal resistances of screw-type probes, Proceedings of 17th international symposium on non-destructive testing and evaluation of wood, Sopron (Hungary).

Yamaguchi N. 2013. In situ assessment method of wood using normalized withdrawal resistances of metric-screw type probes (SHATIS'13), Trento (Italy).

Nondestructive Evaluation of a 75-Year Old Glulam Arch

Marko Teder
Dep. of Rural Building, Inst. of Forestry and Rural Engineering, Estonian University of Life Sciences, Kreutzwaldi 5, Tartu 51014, Estonia, marko.teder@emu.ee

Xiping Wang
USDA Forest Service Forest Products Laboratory, One Gifford Pinchot Drive, Madison, WI 53726, USA, xwang@fs.fed.us

Abstract

The purpose of this study was to explore the possibilities of using existing nondestructive evaluation (NDE) methods to assess delamination and decay of glulam structures. A glulam arch removed from a research building after more than 75-year service was used as a test specimen. The glulam arch section was tested using stress wave timing, ultrasonic wave propagation, and resistance micro-drilling methods at a series of locations. The arch was subsequently cut open for visual inspection and small compression and shear samples were obtained for strength testing. It was found that wave propagation times or wave velocities measured across the laminations were good indicators of internal decay. Stress wave timing and ultrasonic propagation methods were able to detect moderate to large delamination, but not micro-delamination. Resistance micro-drilling was found not effective in detecting delamination. Further research is planned to evaluate the possibility of using pulse-echo method to detect internal delamination of glulam members.

Key words: glued laminated timber (glulam), stress wave, ultrasonic wave, resistance micro-drilling, strength, modulus of elasticity.

Introduction

The use of glued laminated timber (glulam) has become widespread all over the world extending the modern wooden building capabilities. Solid wood members are increasingly being replaced by modern engineered timber laminates glued and stacked together, enabling timber structures to carry more loads (for instance in large-span roofs). As innovative construction techniques for timber buildings are continuously being developed, the need for modern assessment methods are increasing to assure or extend the service life of the glulam structures, especially due to the problems related to the adhesive bonding causing delamination in glulam elements. Delamination usually results from manufacturing failures, improper bonding, overloading during the service life of a structure, or by moisture changes causing stresses. Since the visual assessment is typically confined to the surface conditions and provides only limited information on internal wood condition and the bond lines between laminates in glulam timber, more advanced methods need to be explored and developed for field inspection of glulam timber components in modern buildings.

In the fall of 2010, a glulam arch structure at the USDA Forest Products Laboratory (FPL) was deconstructed after more than 75 years of use. Since these arches represent the first generation of both construction adhesives and glued-laminated development, the glulam arches were preserved as research specimens for various groups at FPL to evaluate the durability and residual strength of these aged arch members. The objective of the study reported herein was to assess the physical conditions of the arch members and evaluate the effectiveness of several nondestructive testing methods,

including stress wave timing, ultrasonic wave propagation, and resistance micro-drilling, for detecting delamination and decay in wooden glulam beams.

Materials and Methodology

Old Glulam Arch Structure

A research building incorporating glued laminated wooden arches was erected on the USDA Forest Products Laboratory's campus in 1934 (Figure 1). As one of the first examples of glulam structures in the United States, this building represented FPL's early efforts on developing arches from thin, individual wood laminations that could be bent into flowing shapes. In addition to its primary service function, this building was also intended to demonstrate the adaptability of wood to modernism in both design and construction. The construction embodied special features developed or adopted through research at the FPL. One special feature was to create unobstructed floor space and ample overhead clearance for sawmill and other industrial projects. For this reason, arched supports were chosen in preference to column-and-girder or standard truss construction (Wilson 1939).

Three types of arch supports were used in the building—one solid glulam, one of double I-beam section, and one of trussed arch held together at the joints with split-ring and hinge-and-plate connectors. Five solid arches and two each of the composite types were built and symmetrically disposed in the building, solid arches at the middle bays, double I-beam arches next, and trussed arches at the ends. The halves of the large glued arches were bent at the knee but were straight below and above the knee, and were held together at the apex with bolted plates. Flanged plate bearings for all arches were provided at the foundations.

Throughout the years the building was used for various research applications and the interior was configured to meet those needs. In 1993, while drying fiber an intense fire was started on the west end of the building. During this event, several of the arch members were exposed to elevated temperature and fire conditions. Those affected members were repaired/strengthened by retrofitting one or two sister members following the fire event. The repaired arch members have performed well since the fire event.

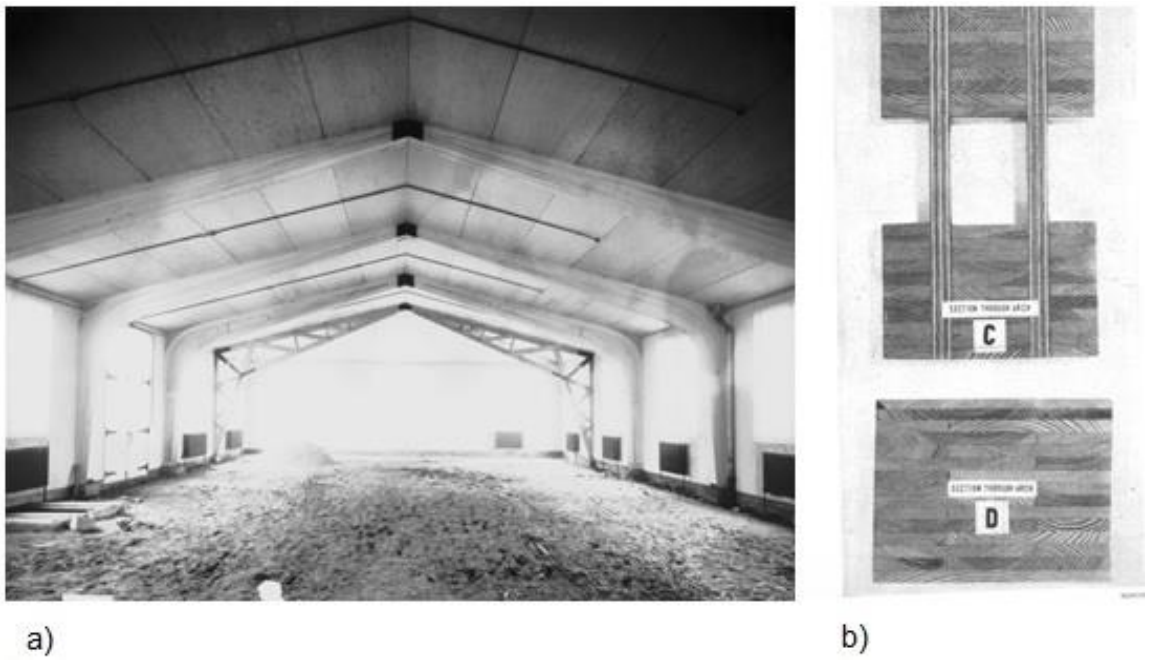

Figure 1—a) Inside view of the USDA Forest Products Laboratory service building, b) Cross-section views of C-type and D-type glulam used as the bearing structural components in the building.

Experimental Procedure

The solid glulam arches were glued up of laminations of 1.4-cm (9/16-in.) material to a width of 29.2-cm (11 ½ -in.) and a thickness of 30.5-cm (12-in.) at the base, 61.0-cm (24-in.) at the knee, and 20.3-cm (8-in.) at the apex. Each layer was made of 10.2 cm (4-in.) and 20.3-cm (8-in.) pieces, with the edge joints staggered in alternate laminations. Through a preliminary stress wave and ultrasonic timing inspection, we were able to determine the general physical conditions of all the solid glulam arch sections removed from the building. Glulam arch section No. 5 was found to contain a wide range of decay and delamination due to moisture intrusion and exposure to the elevated temperatures in fire. We selected this section as a specimen for an in-depth study.

Extensive non-destructive testing was performed on the selected glulam arch section using several different types of NDE techniques, including stress wave timing, ultrasonic transmission, pulse-echo, and resistance micro-drilling. Figure 2 shows the glulam specimen under testing and locations that NDE measurements were conducted. The physical condition of the section changed through the length, thus we began the measurements at the cross-section 50 mm from the decayed end (lower end), followed by 200 mm and then by 300 mm increments (Figure 2b). At each of these locations, measurements were taken at three levels which were designated as A, B and C for upper, middle, and lower levels respectively. The experiments were carried out in a laboratory at 21 °C and 50% relative humidity.

Upon completion of nondestructive measurements, the glulam section was cut open at each tested cross-section, resulting 13 glulam blocks B, C, D, …, and N (block A was severely decayed, delaminated, and fall into pieces after cutting). Visual inspection was conducted at each opened cross-section to identify decay, cracks and any delamination that can be visually seen. A high-resolution digital image of each cross-section was subsequently obtained to document the internal conditions of the glulam section. Following visual inspection of the cross-sections, shear and compression samples were cut from the blocks to obtain the residual mechanical properties of the glulam arch section through destructive testing.

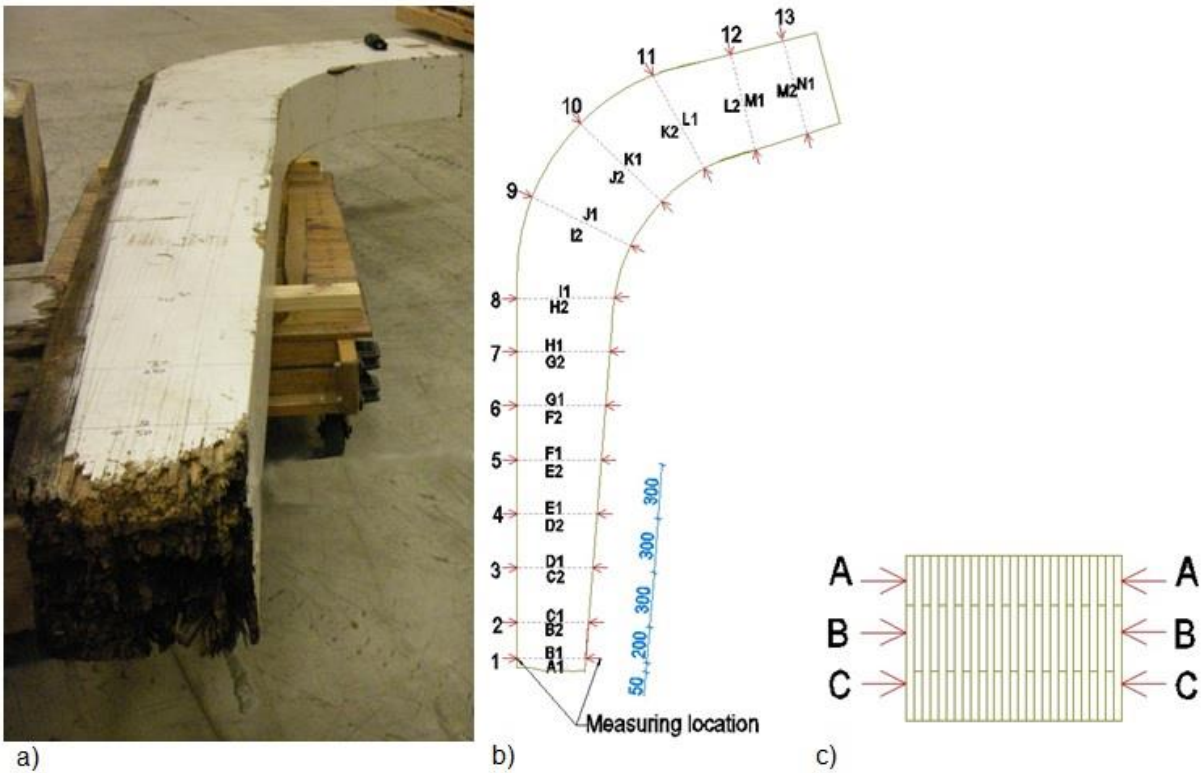

Figure 2—a) Glulam arch under testing; b) Plan view showing measurement locations; c) Cross-section view showing measurement locations (A, B, and C were 45, 135 and 225 mm from the edge of the cross-section respectively).

Testing of glulam arch section

Stress wave timing

Stress wave timing (SWT) measurement for decay detection is based on the concept that stress wave propagation is sensitive to the presence of deterioration of wood members (Pellerin and Ross 2002). Stress waves travel faster through sound wood than they travel through decayed and delaminated wood. Conducting stress wave timing measurement on a glulam member requires access to two opposite sides of the member for attaching sensor probes. The glulam arch section was tested through the thickness (perpendicular to the laminations) using a Fakopp stress wave timer. The sensor probes were inserted into opposing faces of the glulam at the same cross-section and same level. Stress waves were generated through a hammer impact.

Ultrasonic transmission

Sylvatest Duo device equipped with two 22 kHz transducers was used to measure the ultrasonic velocity across the thickness of the glulam (perpendicular to the laminations). The transmitter probe and the receiver probe were positioned at the opposite faces of the glulam with a relatively constant handheld pressure applied to the probes to improve the coupling between the probes and wood. For each measurement, the transmitter probe emitted five consecutive pulses through the glulam. An average ultrasound propagation time (UPT) and peak energy of the receiving signal were recorded after each measurement. The ultrasonic velocity (V) of the specimen across laminations was calculated based on the average UPT value and the thickness of the glulam at the cross-section (distance between two probes):

$$V = \frac{L}{UPT} \text{ (m/s)}$$

Resistance micro-drilling

Resistance micro-drilling tests were conducted after the acoustic measurements. Resistance micro-drilling enables detection of internal deterioration in a timber through measuring the relative resistance in the drilling path. The output of a micro-drilling test is a resistance profile showing density changes along the drilling path. The high output characterizes high resistance or high density and the low output characterizes low resistance or low density. Internal decay or cavities in a timber is typically characterized as extremely low resistance or zero resistance in the resistance charts (Kotlinova et al. 2008). An IML PD-400 Resistograph unit was used to obtain resistance profiles at the same locations where stress wave timing and ultrasonic measurements were conducted.

Testing of small lamination samples

To evaluate the compression strength of the glulam arch and the shear strength of the bond lines after 75 years of service, we cut small samples from the glulam blocks according to the specifications of the ASTM D905-08 and D143-09 standards. Twenty five 50 by 50 by 200 mm compression samples were obtained from blocks C, D, E, F, and G, five from each block (Figure 3a). Fifty 38 by 50 by 50 mm shear samples were cur from blocks B, C, D, E, F, G, and N (Figure 3b), five from each block for blocks C, D, E, F, and G, ten from block N and fifteen from block B. But thirty five samples were good enough for successful testing. Both compression and shear samples included 3 bond lines. Special care was taken to ensure that the bond line being tested for shear was located in the center line and the loading surfaces were smooth, parallel to each other, and perpendicular to the height (Figure 3b).

Ultrasonic measurements

The compression and shear samples were first acoustically evaluated using a Sylvatest Duo device before destructive testing. For compression samples, ultrasonic measurements were conducted in both radial (3 points) and longitudinal directions. For shear samples, ultrasonic measurements were conducted in radial directions (2 points). The transmitter probe and the receiver probe were positioned at the opposite faces of a sample with a constant pressure (196 kPa) applied to the probes to improve coupling between the probes and wood.

Mechanical testing

Compression-parallel-to-grain test was conducted on each compression sample using an Instron machine in accordance with ASTM D143-09 standard. Modulus of elasticity (MOE) and compression strength (CS) parallel to grain were subsequently determined for each compression sample.

Shear samples were tested using the same Instron machine by compression loading in accordance with ASTM D905-08 standard. The shear strength of the bond line was determined based on the maximum compression load and the bond line area between the two laminations.

All the experimental data was processed and analyzed using MS Excel and STATISTICA 12.

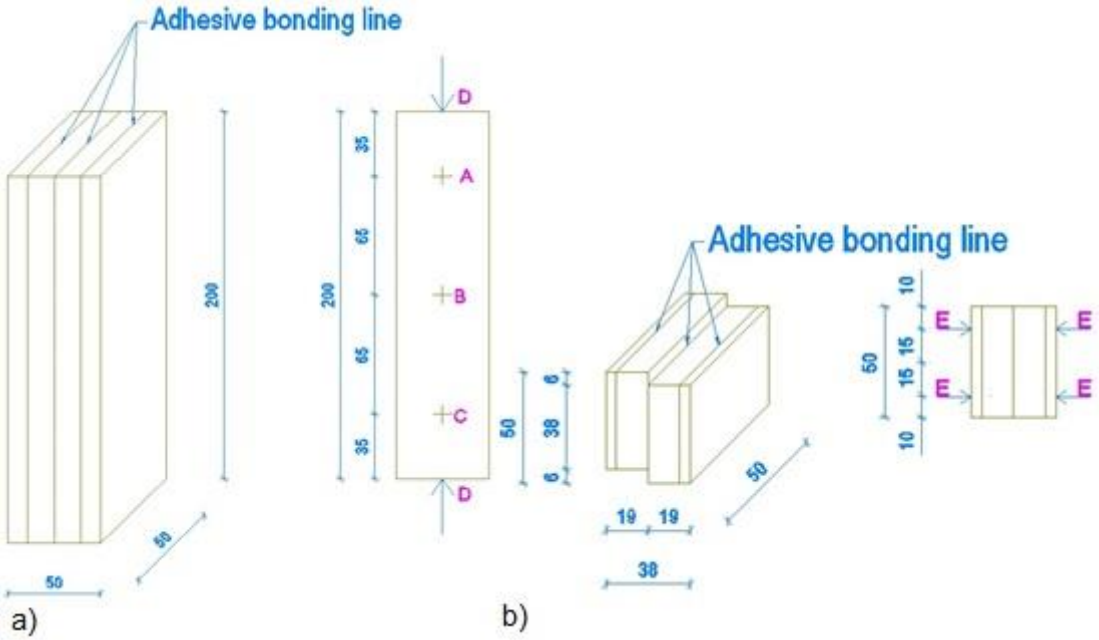

Figure 3—Small samples cut from the glulam blocks for mechanical testing. a) Compression test sample with ultrasonic measurements at point A, B, C and D; b) Shear test sample with ultrasonic measurement at point E.

Results and Discussion

NDT assessment of the glulam arch section

The results of ultrasonic and stress wave timing measurements from the glulam section are illustrated in Figure 4 and Figure 5 in the form of time/velocity distribution along the length. Two methods produced similar mappings of the condition in terms of acoustic measures. Ultrasonic measurement results indicated potential structural defects at location 1 for entire cross-section, at location 2 for upper (A) and middle (B) areas, and at location 10 for lower (C) area. Similarly, stress wave measurement results identified structural problems for the entire cross-sections of location 1 and 2, and the lower area (C) of location 10.

After the glulam arch was cut open along the measurement lines, moderate to severe delamination and decay were found at locations 1 and 2, which confirmed the evaluation results of acoustic measurements. Delamination was observed in few outer laminations at location 10, which caused abnormal ultrasonic and stress wave readings as illustrated in Figure 4 and 5. The delamination in this arch section was likely caused by the exposure to high temperature during the fire event occurred in 1993.

Figures 6 and 7 show the images of the glulam cross-sections at locations 1 and 2 superimposed with the resistance profiles of three drilling paths A, B, and C. It is clear that high relative resistance in the profiles corresponded to the solid laminations and low relative resistance corresponded to the deteriorated or decayed laminations in the glulam arch. Despite of being able to detect degraded areas of glulam, our results indicated the otherwise for using resistance micro-drilling to detect internal delamination. By comparing the visually identified delamination and internal checks with the relative resistance measured, we found that most delamination was not observable in the resistance profiles. Even though some of the low valleys in the resistance profiles clearly corresponded to the big delamination per visual assessment, the relatively high resistance at the low valley would make it difficult to judge whether it is delamination or early wood.

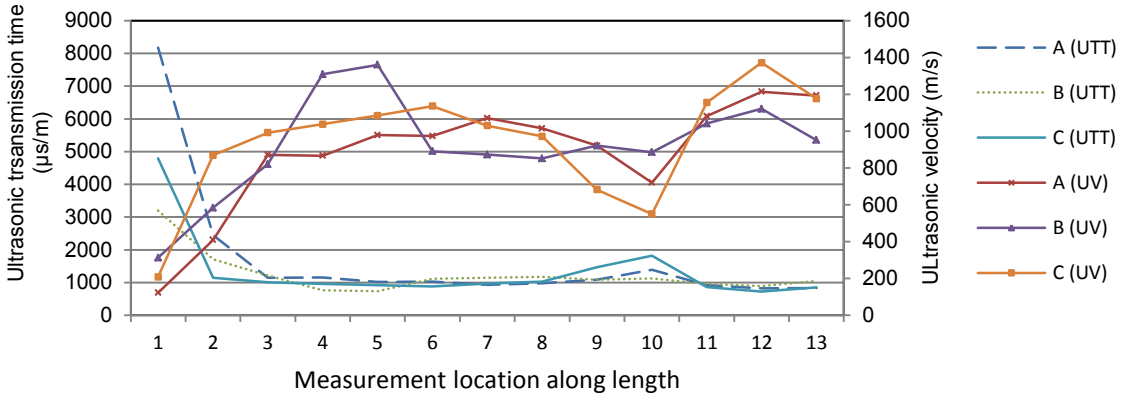

Figure 4—Ultrasonic transmission time and ultrasonic velocity measured across laminations of the glulam arch section (Notes: UTT – ultrasonic transmission time, UV – ultrasonic velocity).

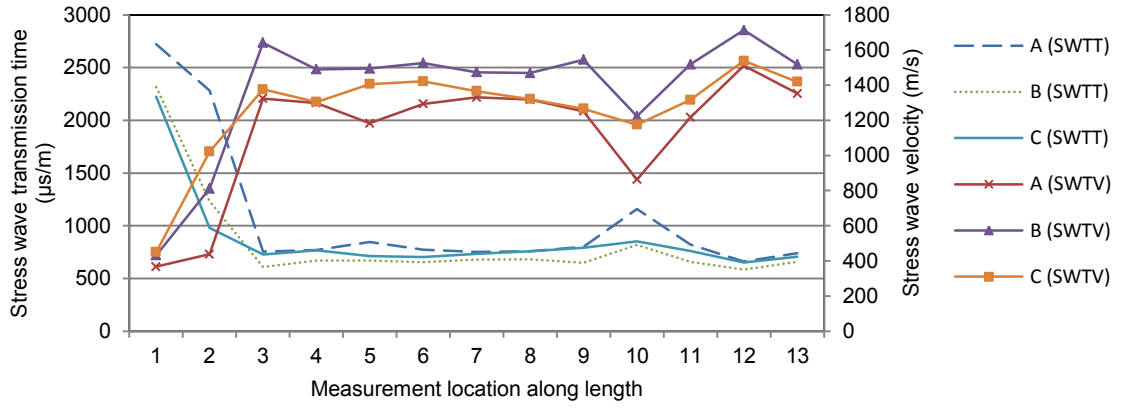

Figure 5—Stress wave transmission time and stress wave velocity measured across laminations of the glulam arch section (Notes: SWTT – stress wave transmission time, SWTV – stress wave transmission velocity).

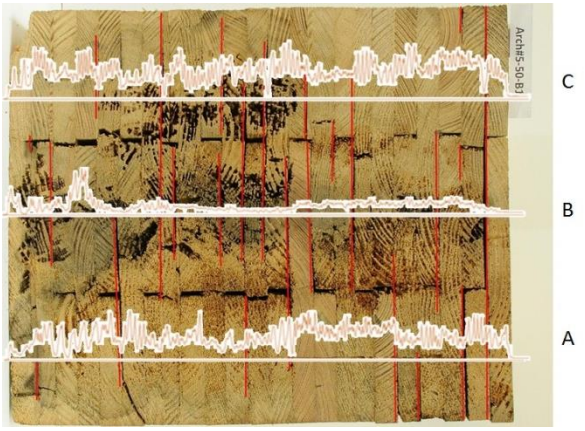

Figure 6— Image of the glulam cross-section at location 1 superimposed with the resistance profile of three drilling paths (Red lines indicate delamination by visual inspection).

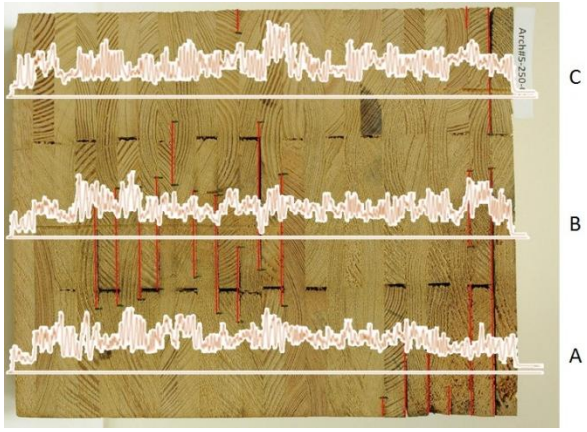

Figure 7— Image of the glulam cross-section at location 2 superimposed with the resistance profile of three drilling paths (Red lines indicate delamination by visual inspection).

Residual strength of the glulam arch

Figure 8 shows the compression strength (CS) of the compression samples at different locations (along length) and positions (through thickness) in the glulam arch. At each location (from C to G), the first 5 bars show the distribution of CS in thickness direction, with the very first bar represents the CS value of the wood close to the outer layers. The sixth bar (shaded) is the average CS at each location. The testing results indicated that the outer laminations (first bar) of the arch consistently had low compression strength, especially at C, D, and E areas. Given the history of fire event in the building and the visual signs of fire exposure (dark color), it is clear that the part of the glulam arch (outer laminations) has been deteriorated due to exposure to the elevated temperature. Assume that the laminations with relatively higher CS were intact (for example, 2nd, 3rd, fourth and fifth bars at location C1-C2), then the strength reduction of the outer laminations is estimated to be from 12.1% to 36.4%. Excluding the deteriorated portion, the average CS of the glulam arch was in the range of 71.7 to 75 MPa, which was significantly higher than the values given in the Wood Handbook for some pine species. This suggests that the intact glulam arch was still in a good quality condition after 75-years of service.

Figure 9 shows the modulus of elasticity (MOE) of the compression samples at different locations (along the length) and positions (through thickness) in the glulam arch. The testing results indicated that the fire event had very little impact on MOE of the outer laminations for most locations, except E1-E2, where MOE reduction was 16.7% (1st bar) and 6.5% (2nd bar). Excluding the deteriorated portion (outer laminations), the average MOE of the glulam arch was in the range of 7.67 to 8.08 GPa.

Similarly, Figure 10 shows the shear strength of the shear samples at different locations (along the length) and positions (through thickness) in the glulam arch. The testing results indicated that the shear strength of the bond lines varied greatly, indicating a significant delamination issues existed in the glulam arch, particularly in sections from B to E. Some shear samples cut at B, C, and D sections were separated after cutting and some were tested as almost zero strength.

Table 1 summarizes the results of linear correlations between ultrasonic propagation time (UPT) and compression and shear strength of the glulam samples. Ultrasonic propagation time measured in longitudinal direction of the glulam had no correlation with compression strength. UPT measured in radial direction (perpendicular to grain) had a moderate correlation with both compression strength (R^2=0.419) and shear strength (R^2 = 0.433). The results from small glulam samples indicated that ultrasonic measurements on glulam beams are not effective in predicting the compression and shear strength of the glulam beams.

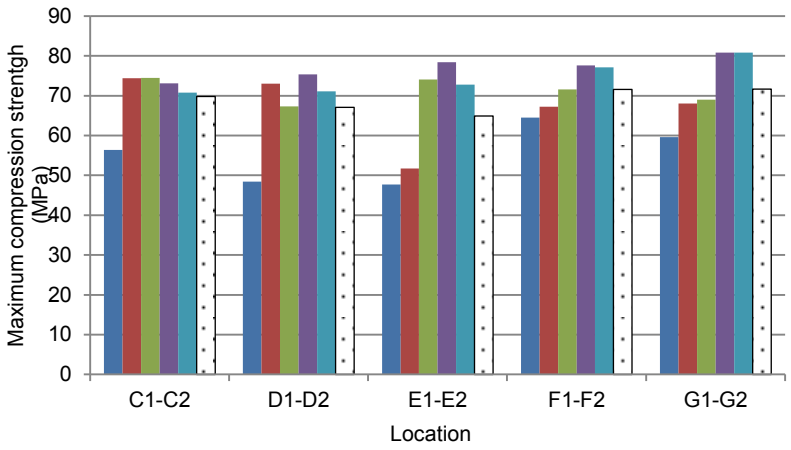

Figure 8—Maximum compression strength (parallel to grain) of small samples obtained from the glulam arch (Note: Shaded colums represent mean values).

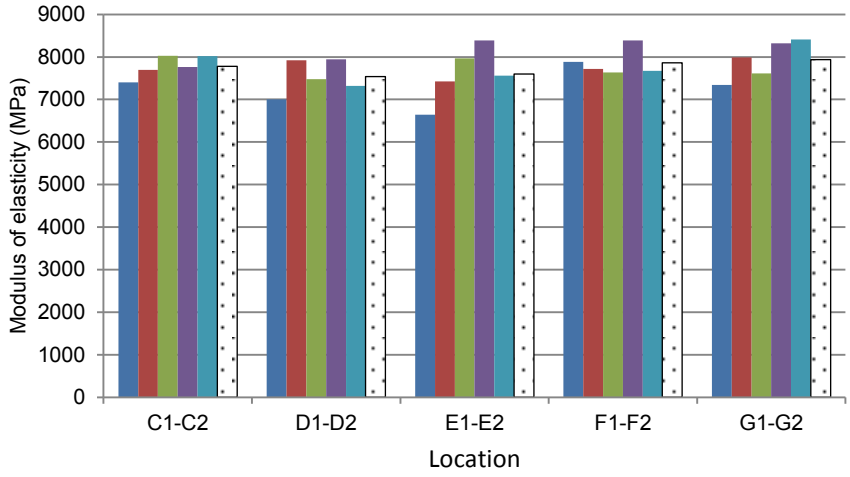

Figure 9—Modulus of elasticity (in compression) of small samples obtained from the glulam arch (Note: shaded colums represent mean values).

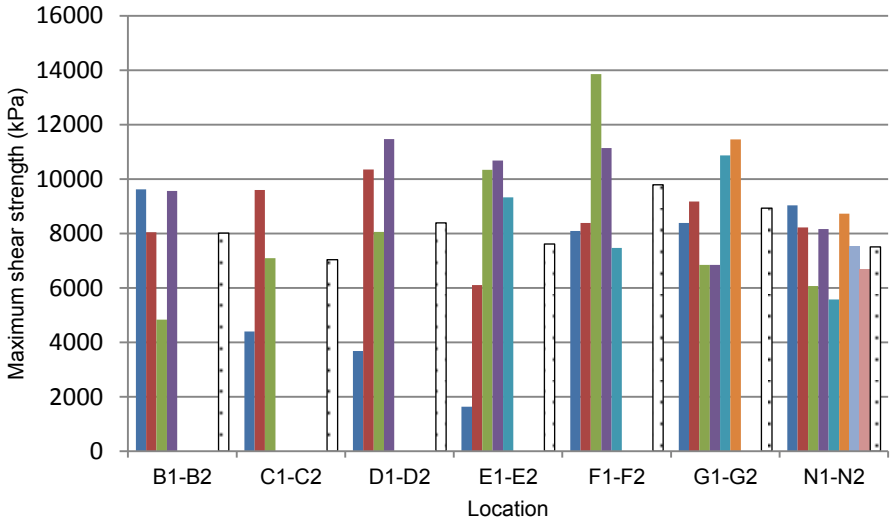

Figure 10—Maximum shear strength of small samples obtained from the glulam arch (Note: shaded colums indicate mean values).

Table 1—Results of the linear correlations between ultrasonic propagation time (UPT) and the compression and shear strength of the glulam samples (linear regressioon model: $y = ax + b$) [a]

Specimen	*Y*	*X*	*a*	*b*	R^2	p-value
Compression samples	CS	UPT_R	-21.60	83452	0.419	<0,001
	CS	UPT_L	-136.7	153473	0.277	0,0069
Shear samples	SS	UTT_R	-7.318	13327	0.433	<0,001

[a] UPT_R—ultasonic propagation time perpendicular to grain; UPT_L—ultrasonic propagation time along the grain (longitudinal); CS—compression strength; SS—shear strength.

Conclusions

Stress wave timing, ultrasonic wave propagation, and resistance micro-drilling methods were used to evaluate the physical conditions of a glulam arch removed from the USDA Forest Products Laboratory research building, after more than 75 years of use. The purpose of this laboratory study was to explore the possibilities of assessing glulam structural condition in situ with some existing NDE methods. Based on the results from this investigation, we concluded the following:

1. Both stress wave timing and ultrasonic propagation methods are effective in detecting internal deterioration of glulam components in building. Wave propagation times or wave velocities measured across the laminations in a glulam member are good indicators of internal decay.
2. Stress wave timing and ultrasonic propagation methods were able to detect moderate to large delamination in glulam, but not micro-delamination.
3. Resistance micro-drilling is effective in detecting decay, but not successful in detecting delamination in glulam.
4. Exposure to elevated temperature during the past fire event had a significant impact on the compression and shear strength of the glulam arch evaluated, but not on the modulus of elasticity. The intact portion of the glulam arch remained having high strength.
5. Further research is needed to look into the possibility of using pulse-echo method to detect internal delamination of glulam members.

Acknowledgments

The authors would like to thank Steve Schmieding, technician and photographer of the USDA Forest Products Laboratory (FPL), Dr. Junguo Zhang, visiting professor from Beijing Forestry UNiversity, and Jim Gilbertson, technician of the USDA Forest Products Laboratory (FPL) for providing assistance. Marko Teder's stipend for studies and research at FPL was provided by Foundation Archimedes European Social Fund's DoRa programme.

References

ASTM. 2008. Standard test method for strength properties of adhesive bonds in shear by compression loading. D905-08. American Society for Testing and Materials, West Conshohocken, PA.

ASTM. 2009. Standard test methods for small clear specimens of timber. D134-09. American Society for Testing and Materials, West Conshohocken, PA.

Kotlinova, M.; Kloiber, M.; Vasconcelos, G.; Lourenco, P. J. B. B.; Branco, J. M. G. 2008. Nondestructive testing of wood. Portugal.

Pellerin, RF; Ross RJ. 2002. Nondestructive evaluation of wood. USA, WI, Madison: Forest Products Society. 210 p.

Wilson, T. R. C. 1939. The glued laminated wooden arch. Washington, DC: U.S. Department of Agriculture, Forest Service, Forest Products Laboratory. 123 p.

Session 13

Poster Session

Energy Harvesting and Nondestructive Evaluation

Robert Ross
USDA Forest Products Laboratory, Madison, WI

Jiangming Kan
Beijing Forestry University, Beijing, P.R. China

Abstract

Energy harvesting is the process by which energy derived from external sources (e.g., solar, thermal, wind, and kinetic sources) is captured and stored for small, wireless autonomous devices, such as those used in wearable electronics and wireless sensor networks. A substantial amount of research has investigated energy harvesting for a wide range of applications—from harvesting energy from the boots of soldiers to power their portable electronic field equipment, to harvesting energy to power in-service sensors for monitoring transportation structures. Energy harvesting technologies could potentially be applied to power in-place nondestructive monitoring systems for wood structures. This presentation will (1) review several energy harvesting technologies and (2) discuss their potential use for wood structures.

Keywords: Wood, energy harvesting, nondestructive evaluation

Torsional Shear Tests on Laminated Veneer Lumber Using a Universal-Type Test Machine

Bonnie Z. Yang
Mississippi State University, Starkville, MS

Peggi Clouston, Alex Schreyer
University of Massachusetts Amherst, Amherst MA

Abstract

A universal-type test machine was configured to apply torsion load-to-failure to estimate orthotropic shear strengths of full-size laminated veneer lumber (LVL). The objective of the study is to provide insight and detail regarding a lesser known torsion test setup, while at the same time estimating torsional shear strength of 1.9E Eastern Species LVL, hitherto unknown. It was found that at large angles of twist, approximately 23° or more, the test apparatus experienced slippage at the bearings and had the potential to become unstable due to high lateral forces. This was not an obstacle for calculating shear strength of LVL in this study, a relatively noncompliant material, but likely would be an issue for more compliant materials. The mean inplane and through-thickness plane shear strengths of 1.9E Eastern Species LVL were estimated to be in the range of 7.2–11.2 MPa and 5.9–7.3 MPa, respectively.

Keywords: Torsion, shear strength, laminated veneer lumber, experiment, orthotropic material

Interference of Pith in Ultrasonic Tomography

Alex Julio Trinca, Raquel Gonçalves, Danilo Miguel Agustino, Robson van Dijk
University of Campinas (UNICAMP), College of Agricultural Engineering (FEAGRI), Campinas, São Paulo, Brazil

Abstract

Ultrasonic tomography is a technique broadly used to determine internal defects in trees. Commercial tomography equipment is available on the market, but tomography can also be performed in a less sophisticated manner using conventional ultrasound equipment and post-processing images by means of specialized software. The relative low cost of the equipment and its portability have been decisive factors in expanding the application of this technique. Widespread use of the technique has encouraged collaboration among research groups in advancing its use and adapting the technique to situations and forest types in various countries. The pith is a material with different anatomic characteristics and properties, resulting in lower ultrasonic wave propagation velocity than that of wood. The objective of this study was to identify the interference of pith in tomography images. Discs from *Pinus* sp. wood with centered or dislocated pith were used for this study. We found that the differentiated characteristics of the pith influence the results related to other internal defects analyzed, thus confusing the interpretation of dimension and location of these defects. These results served as the basis for including that variable in algorithms in order to correct the image.

Keywords: Pith, ultrasonic tomography, wood

Non-destructive methods to estimate the physical aging of Superpan

Santiago Sevilla
Forestry Engineer Student; EUIT Forestal, Universidad Politécnica de Madrid; Madrid; Spain.

After the success achieved by using non-destructive methods in previous research projects, to estimate physical and mechanical aging of particle and fiberboards, the study of the relationships between aging, physical and mechanical changes, and non-destructive measures on particle boards with an exterior fiber coating (Superpan), are proposed in this paper. A total number of 96 pieces of Superpan were tested to analyze its real physical and mechanical properties, and the same properties estimated using non-destructive methods (screw withdrawal and ultrasonic and stress wave velocity), during a physical laboratory aging test.
Measurements of the propagation wave velocity with the sensors in parallel, end to end, and forming an angle of 45 degrees, with both sensors in the face of the board, in order to contrast different layers, have been recorded.
After the results of statistical analysis, it can be concluded that there is a strong relationship between the non-destructive measurements carried out, and the decline in physical and mechanical properties of the panels due to aging. It has been also found that the Superpan ages better than standard particle board, and similarly or even better than the standard fibreboard.
Authors propose several models to estimate board´s physical and mechanical properties and aging degree, with coefficients of determination R^2 over 0.9. The best results are obtained with the stress wave method (R^2= 0.98), although ultrasonic method results are highly representative as well (R^2= 0.97).

Keywords: Screw withdrawal, stress wave velocity, ultrasonic waves, mechanical properties, physical properties, aging tests.

Coauthors:

Ignacio Bobadilla; Forestry Engineer, PhD.; EUIT Forestal, Universidad Politécnica de Madrid; Madrid; Spain.
Roberto Martínez López; Forestry Engineer; ETSI Montes, Universidad Politécnica de Madrid; Madrid; Spain.
Miguel Esteban Herrero; Forestry Engineer, PhD.; ETSI Montes, Universidad Politécnica de Madrid; Madrid; Spain.
Daniel F. Llana; Agricultural Engineer; ETSI Montes, Universidad Politécnica de Madrid; Madrid; Spain.

Preservative conservation of historical musical instruments – A review

Voichita Bucur

Materials Science and Engineering Division, CSIRO, Clayton South, Victoria 3169, Australia
voichita.bucur@csiro.au

Abstract

Preventive conservation is understood as any measure that prevents damage or reduces the potential of it. The aims of conservation are: the revelation, the investigation and the preservation. Compared to other artefacts, in conservation of historical musical instruments there is an increase risk of damage introduced by the diversity of materials on which the musical instruments are built. The aging effects on musical instruments have different origins such as the changes induced by ageing in materials properties, the oxidative degradation induced by the surrounding temperature and humidity of the air, the photochemical degradation induced by lights with different wavelength and the effects of discoloration of wood, or the biodegradations caused by fungi and insects. Climate change over the next century is likely to have some effects on environment therefore musical instruments which are cultural heritage objects which are non renewable resources need to be preserved in a controlled microclimate. The restoration of a harpsichord is discussed.

Keywords: musical instruments, conservation, wood

Introduction

Preventive conservation of musical instruments is understood as any action that prevents damage or reduces the potential of it**.** The competing aims of conservation are: the revelation, the investigation and the preservation (Caple 2009). The revelation has the capacity to reveal by showing the meaningful appearance of an object exposed in a museum; the investigation analyse the object with different methods (visual, nondestructive, non contact, analytical, etc) to recover historical, physical, chemical, etc. information; the preservation maintains the object in its present physical state preventing possible deterioration. (Barassi and Laini 1987, Basile 1989)

Compared to other artefacts, in conservation of historical musical instruments there is an increase risk of damage introduced by the diversity of materials on which the musical instruments are built (Uzielli 2009, 2011, Fioravanti and Mecca 2011). Preservative conservation of historical musical instruments requires permanent approaches to identify and reduce the potential hazards through the control of the surroundings for preventing the aging effects. The aging effects on musical instruments have different origins such as the changes induced by ageing in materials properties, the oxidative degradation induced by the surrounding temperature and humidity of the air, the photochemical degradation induced by lights with different wavelength and the effects of discoloration of wood, or the biodegradations caused by fungi and insects, and other pollutants (Unger et al. 2001). Climate change over the next century is likely to have some effects on environment, therefore cultural heritage objects which are non renewable resources need to be preserved.

While data on the behaviour of specimens of different materials such as wood, metal, leather, ivory, painted and varnished surfaces exist in technical literature, data on the behaviour of these materials incorporated in musical instruments are relatively scarce. There is a lack of fundamental research of the effect of restoration and conservation operations on musical instruments (ie. long term effect of string tensions on withstand, the effect of pitch, cleaning, repairing of cracks on soundboard behaviour, acoustical quality and revarnish of bow string instrument, etc Bucur 2013). It is also to underline the importance of historical knowledge about the craftsmanship and art history in different historic periods and the limits of modern techniques utilisation in restoration and conservation of musical instruments.

Musical instruments conservation science requires multidisciplinary approaches. As noted by Wouters (2008) the conservation science of objects belonging to world's cultural heritage have the following major objectives:

- To understand historic literature data revealing the choice of sources and products, the manufacturing technology and the extrapolation of these data into a present day scientific framework
- To recognise the phenomena related to manufacture and deterioration at any level of observation: visual, microscopic, molecular
- To create databases for reference collections and standards
- To understand the 'usefulness' of intervention in relation to destructiveness and innovation
- To develop fundamental research and high –level interactivity with professionals from different disciplines

The effect of indoor air pollution on musical instruments conservation

Because of possible climate change trends over the next century and the increasing pollution level in industrialized countries and all over the world, the effect of indoor air pollution on cultural and historical materials has been thoroughly studied (Camuffo 1998, Cassar 2005). For the protection of built cultural heritage in Europe climate maps have been generated for the near future (2010 – 2039) and for the far future (2070 – 2099), with a baseline period 1961-1999 (Sabbioni et al. 2006). While the effects of climate change have been investigated with reference with human health, ecosystems and cultural heritage, the preservation of musical instruments is not mentioned among the cultural treasures to be preserved. Indoor air pollution on cultural and historical materials is directly related to the possible effects of climate change (Ryhl-Svendsen 2006, Cass et al. 1991).

The intensity of indoor air pollution depends on outdoor state of the air (outdoor concentration of pollutant, air humidity, temperature, biological purity) the ventilation system (air exchange rate, deposition velocity), the indoor concentration of pollutants (pollution generation by the displayed materials and the walls of the building), the surface and volume of room.

Risks of biological attacks

Wood is a natural composite material which can survive very long time in dry and stable environment as seen in old Japanese temples. As pointed out by Nilsson and Rowell (2009) wood natural structure interacts permanently with the environment – air temperature and relative humidity and contaminants - oxygen, ultraviolet energy, micro-organism, chemicals of different pH.

Fungi, bacteria and insects act through the basic processes of biological degradation such as oxidation, hydrolysis, dehydratation, reduction and free radicals reactions (Gambetta 1987). Of course, these main degradations processes can interact with musical instruments. Mould, stain, decay fungi and insects attacks occur in wood when musical instruments are stored under unappropriated

conditions of air temperature and high relative humidity. Not all types of biological attacks are equally devastating.

Fungal attack

Wood destroying fungi, wood staining fungi and surface moulds are the three main classes of fungi destroying wood (Ungar et al. 2000). Wood decay is the major damage caused by fungi. Fungal species differ in their biochemical systems of cell wall components degradation (cellulose or lignin), their morphology and their tolerance to aggressive environmental conditions (Schwarze 2007). For musical instruments the moulds are the most potential destructors. Moulds are fungi present at wet wood surface, living with simple carbon compounds and producing hyphae of different colours such as black (*Aspergillus* sp), green (*Gliocladium* spp. *Penicillium* spp.) orange (*Monila* spp) or red (*Fusarium* spp), which can be removed by brushing or planing. Stains (*Ascomycotina*, *Deuteromycotina, Alternaria alternate*, *Cladosporium*) are degrading discolorations caused by pigmented hyphae of fungi causing little damage to prosenchyma cells in wood. Spores penetrate trough ruptured tracheids and rays. The hyphae propagate through pits and colonize parenchyma rays or longitudinal parenchyma surrounding the resin canal by direct pit penetration.

Insects attack

Insects in wood are vectors of stain and decay fungi. Insects colonize wood for habitation and food source, producing discrete tunnels or surface channels. Insects are life cycles beginning with an egg progressing in larval, pupal and adult stage. The insects are included in the class of *Arthropoda* and those damaging wood are from the orders Isoptera (termites), Coleoptera (beetles). The life cycle of insects can be between 3 and ten years. For musical instruments Coleoptera are the most dangerous during the larval stage. Larvae of *Anobium punctatum* requires as nutrient cellulose and proteins, *Hylotropes bajulus* requires protein, cellulose and hemicelluloses and vitamine B, *Lyctus brunneus* requires starch, protein, sugar. The main damages caused by insects in wood in general are pin and grub holes, and network of galleries.

Deterioration of keyboard instruments

In this section we choose to discuss the case of keyboard instrument, a harpsichord made by I. Couchet in 1652, today in Musée de la Musique in Paris, France. During the last decades a large number of antique harpsichords have been restored to playing condition and new replicas of authentic instruments have been built.

In Europe the harpsichord makers were famous in 16th, 17th and 18th centuries and superb instruments have been built by makers that today can be grouped around several schools – the Italian, the French, the Flemish, the German, the English and Irish and the Iberic (Spain and Portugal), the Dutch and the Scandinavian (Germain 2002, Fletcher and Beebe 2010).

The harpsichord is one of the richest decorated musical instruments in western music, with a very large selection of materials (wood, semi-precious stones, mother –of-pearl, tortoiseshell, applied metals- brass marquetry, ivory, bone, leather).

Wood is the main material used for the harpsichords. Different species have been used for the soundboard like cypress, spruce, fir, depending on local availability of lumber (Dugot 2008). For the

bridge maple was preferred, for the spine maple, walnut or oak. The bentside was in maple or in coniferous veneered with mahogany.

Inappropriate conservation conditions can determine the development of important defects or ruin completely the instrument. The most frequent defects are soundboards cracks, detachment of the bridge or ribs due to shrinkage and swelling of wood in rib and soundboard (Fig 1).

Figure 1 Frequent defects in harpsichords observed during long time conservation

a)Treble side soundboard crack propagating over bellyrail (photo Beebe - Harpsichords Australia)	b) Crack along the spine and dislocation of bass end(photo Beebe – Harpsichords Australia)

Figure 2 Internal structure of the harpsichord (photo courtesy Le Conte et al 2012 , fig 2, page S 162)

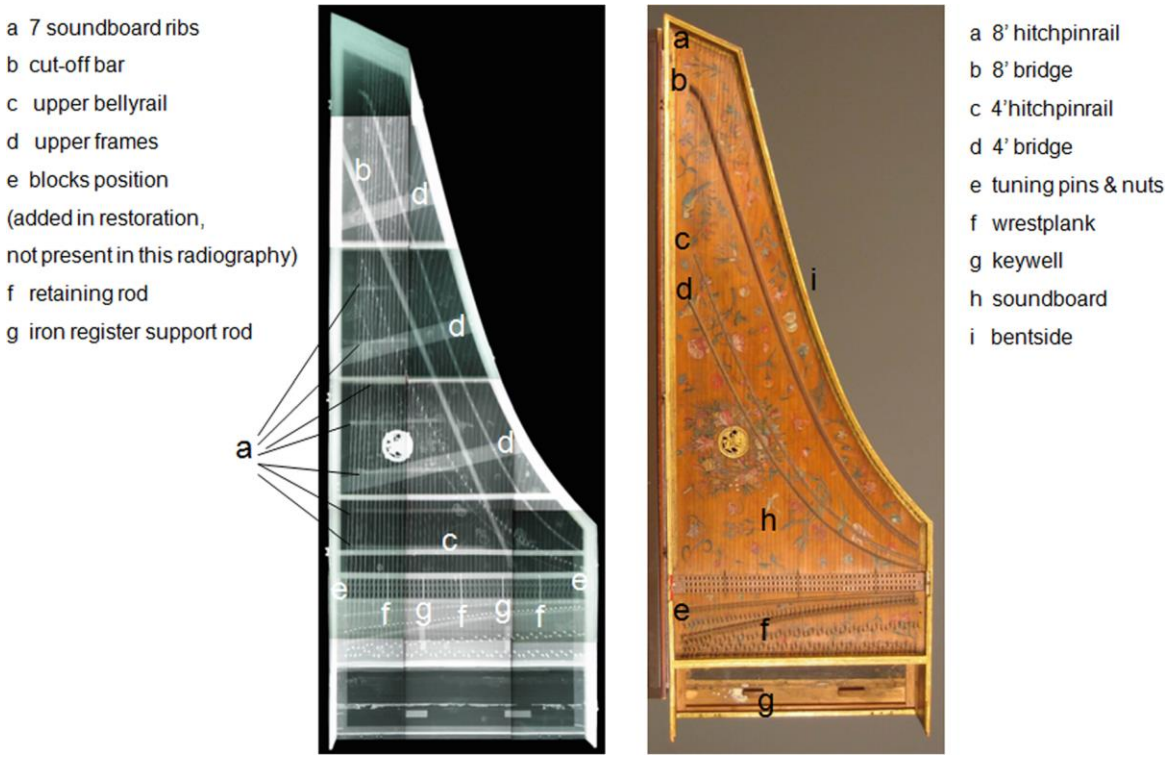

The internal structure of the harpsichord in shown by X ray radiography in Fig 2. For restoration intervention it was necessary to determine the influence of different structural elements vibrations on soundboard behaviour.

X ray radiography allows visualising the internal structure of the instrument, for determining the exact geometry of the instrument and, for defining a mechanical model for a static structure with 150 strings and 6700 N applied on 3 mm variable thickness soundboard.

Finite element modelling allows visualisation of stiffnesses or displacements, showing zones in bending or twisting. Harpsichord behaviour was studied with finite element modelling to identify the vibration modes of different structural elements. Other parameters taken into consideration are: the thickness of the soundboard 3mm, variable; the pitch for A was 392 Hz- French XVIIth century pitch for strings; the strings inducing static forces; the simply supported boundary conditions for the whole surface of the bottom of the harpsichord; the modal frequencies between 1 and 500 Hz, the reference plane for displacement between spline top and bentside.

Figure 3 shows the theoretical values deduced from modelling and the measured values for restored harpsichord. Theoretical values of the vertical displacement of the soundboard are between +1.3 mm and – 2.6 mm (Fig. 3a). With soundboard included in the whole instrument, the shear stress distribution which is the most dangerous for cracks development in the soundboard varied between 3.24 N/m^2 to – 3.37 N/m^2 (Fig 3c).

The most fragile zones of the soundboard are in the central part, shown in blue. During different steps of restoration for soundboard cracks reparation, the strings have been gradually removed. Measured soundboard displacements were between 1.0 mm and -1.8mm (Fig 3b). Figure 3 d shows two mode shapes of the soundboard vibration. The measured range of shear stress distribution is between 3.24 N/m^2 to – 3.37 N/m^2

Figure 3 Theoretical values deduced from modelling and measured values for the restored instrument.

Legend a) calculated vertical displacement of the soundboard, b) measured vertical displacement of the soundboard c) shear stress distribution of the soundboard when included into the harpsichord d) two modes (Le Conte et al 2012 Fig. 3, page S 163).

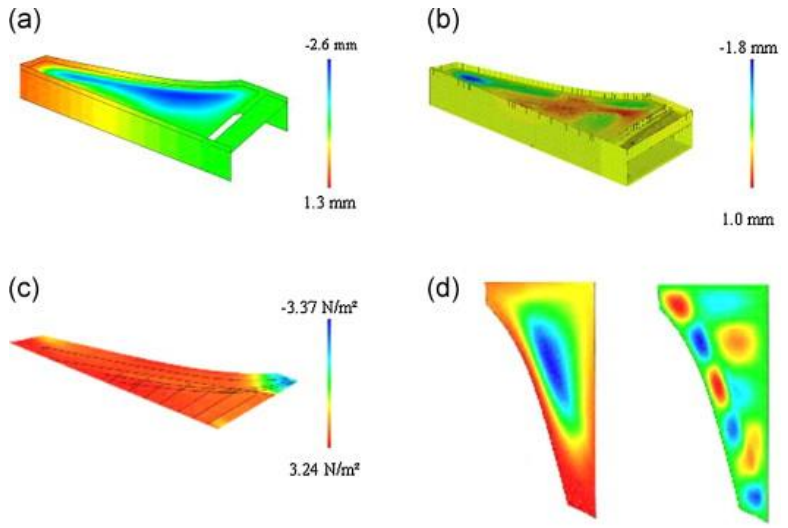

From the analysis of theoretical and experimental data it was deduced the necessity of reinforcements of the zone between the wrestplank and the upper bellyrail. This intervention should avoid cracks development into the soundboard and decrease the displacement of the upper bellyrail.

Traditional approach of the restoration practice for the consolidation of the structure of the harpsichord and to compensate the inevitable shrinkage of the whole structure is to introduce brass gap- spacers and wooden blocks inside the box. This intervention could modify the acoustic qualities of the instrument, but in the same time the mechanical stability of the harpsichord need to be guaranteed.

The influence of brass elements and new wooden blocks on stress distribution was studied with finite element analysis as shown in Fig 4 .

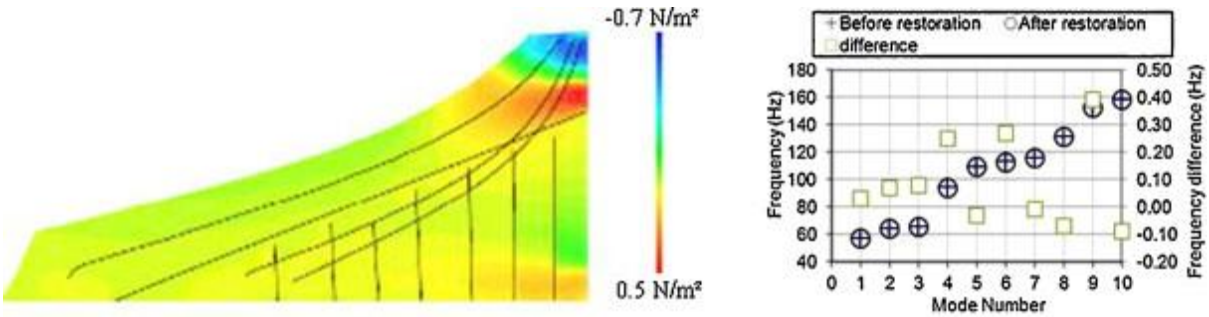

Figure 4 Difference in stress distribution between the initial state and the consolidated soundboard (a) and variation of mode number as a function of frequency before and after restoration of the harpsichord. (Le Conte et al 2012. Fig 4, page S 164)

If we have in mind that the objective of restoration intervention was to reduce the stress in the structure with minimum structural modification, then we can observe a reduction of shear stress gradient in the bottom right corner of the soundboard. More gap-spacers added les shear stress in the soundboard, but a reasonable equilibrium needs to be established to allow soundboard vibration.

To preserve acoustic qualities of the harpsichord, the vibration modes and frequency range of the soundboard before and after restoration need to be in theory identical, or, in practice as closed as possible. To demonstrate this statement, vibration modes shift - before and after restoration- has been compared. Figure 4 b shows negligible frequency shifts for the first ten modes. (ie. Modes 1, 2 and 3 show an average shift of -0.10 Hz; modes 5, 6, 7 show a shift between 0.1 and 0.2 Hz, mode 10 show a shift of 0.4 Hz., etc). As expected increasing frequency sift for higher modes was observed but in a low range.

Maintenance of historic musical instruments

Maintenance procedure of historic musical instruments was and still is a subject of contradictory discussions among the curators and musicians depending whether the instruments are in playing conditions or not (Barclay 1997, 2009, Gétreau 2001, 2002). Playing instruments causes wear and degradation and require continual maintenance in the frame of two concepts 'the acceptable risk' induced by the maintenance procedure and 'the historic value' of the instrument. Because of their complexity and of the diversity of materials used, keyboard instruments require the intervention of a very specialized operator. Wood framed keyboard instruments are particularly vulnerable to environmental conditions of temperature and air humidity. The adhesives used for historic instruments are collagen based, very susceptible to damage due to high air relative humidity. The strings must be of traditional materials, the normal initial pitch of the instrument should be respected. Fluctuations of more than 10% in air relative humidity can induce damage of the instruments. The plucked instruments – lutes, guitars, mandolins and the frames of harps are even more delicate than bowed instruments.

Acknowledgments

I would like to thank Materials Science and Engineering Division, CSIRO Australia for sponsoring this research.

References

Barassi E, Laini EM 1987. For a European chart for restoration. Conservation, restoration and reuse of historic musical instruments (Per una Carta Europea del Restauro. Conservazione, restauro e riuso degli strumenti musicali antichi). *Quaderni della Rivista Italiana di Musicologia*, 15: 119 – 126

Barclay R 1997. Hearing the original instrument. *Conservation J.* Issue 25, 4 p. www.vam.ac.uk/content/conservation-journal/issue-25/hearing-the-original-insdtrument/

Barclay R 2009. *Criteria to consider when planning methodology and approach in intervention on historic Instruments*. Actes de la journée d'étude- Le bois : instrument du patrimoine musical – Cité de la musique, Paris, France – 29 mai 2008 : 95 -101

Basile G 1989. What is restoration? Conservation of works of art: how, when, and why (Che cos'il restauro. Come quando, per che conservare le opera d'arte). Editori Riuniti, Roma

Beebe C 2013. Carey Beebe Harpsichords , Sydney, Australia - Harpsichords Australia http://www.hpschd.nu/index.html?nav/nav-2.html&t/welcome.html&http://www.hpschd.nu/c/43.html

Bucur V 2013 *Materials for musical instruments* (in preparation)

Caple B 2009. The aims of conservation. In '*Conservation. Principles, dilemmas and uncomfortable truths'*. Eds. A Richmond and A Bracker. Elsevier, Amsterdam: 25-31

Camuffo D 1998. *Microclimate for cultural heritage.* Series Developments in Atmospheric Science 23, Elsevier, Amsterdam

Cassar M 2005. *Climate change and the historic environment.* Nottingham, The Russel Press

Cass GR, Nazaroff WW, Tiller C, Whitemore PM 1991. Protection of works of art from damage due to atmospheric ozone. *Atmospheric Environment* 25A: 441 - 451

Gambetta A 1987. Biodeterioration of wood in musical instruments and methods of protection (Biodegradamento del legno degli strumenti musicali and metodi di protezione). In E. Barassi and E M Laini Per una Carta Europea del Restauro. Conservazione, restauro e riuso degli strumenti musicali antichi. *Quaderni della Rivista Italiana di Musicologia*, 15: 119 – 126

Germann S 2002. The Historical Harpsichord. Harpsichord decoration, vol 4 Pendragon, Hillsdale, New York

Gétreau F 2002. Considerations on keyboard conservation and policy for facsimiles and replicas in France. *Proc. Convegno Bartolomeo Cristofori : la spinetta ovale del 1690. Incontro di studio per il progetto di restauro*. Firenze, Italia, 21-22 Ottobre, Strumenti a tastiera: copie e restauro.

Gétreau F 2001. The conservation of acoustical specifications: a long ignorance in public collections of ancient instruments. *Proc. 17th Int. Congress on Acoustics, Rome*

Dugot J 2008. Types of woods used in instrument making in Europe of 16th and 17th centuries. *Actes de la Journée d'étude- Le bois: instrument du patrimoine musical*. Cité de la Musique, Paris, France, 29 mai : 11p

Fioravanti M, Mecca S (Eds) 2011 *The Safeguard of Cultural Heritage- A challenge from the past for the Europe of tomorrow'* Firenze University Press

Fletcher N, Beebe C 2010. Harpsichord and clavichord. In '*The science of string instruments'* Ed. TD Rossing. Springer Verlsag, New York: 123 - 143

Le Conte S, Le Moyne S, Ollivier F, Vaiedelich S 2012. Using mechanical modelling and experimentation for the conservation of musical instruments. *J. Cultural Heritage* 135: S161-S164

Nilsson T, Rowell R 2009. Historical wood–structure and properties. In **'***Wood Science for Conservation of Cultural Heritage–Florence 2007***'.** Proc. International Conf. held in Florence 2007 **-** *L. Uzielli Ed.* Firenze University Press**:** *11-15*

Ryhl-Svendsen M 2006. Indoor air pollution in museums: a review of prediction models and control strategies *Reviews in Conservation* 7: 27-41

Sabbioni C, Cassar M, Brimblecombe P 2006. Global climate change impact on built heritage and cultural landscape. In ' *Heritage, Weathering and Conservation'* Eds. Gomez-Heras and Vasquez-Calco, Taylor & Francis Group, London : 395-401.

Schwarze FWR 2007. Wood decay under the microscope *Fungal Biology Reviews* 21, 4: 133–170

Unger A, Schniewind A, Unger W 2001. *Conservation of wood artefacts: a handbook*. Springer Verlag, Berlin

Uzielli L 2011. The material science applied to the conservation of wooden cultural heritage : future perspectives. In Fioravanti M, Mecca S Eds. ' *The Safeguard of Cultural Heritage- A challenge from the past for the Europe of tomorrow'* Firenze University Press:140-142

Uzielli L Ed. 2009. *Wood Science for Conservation of Cultural Heritage – Florence 2007* Proceedings of the International Conference held in Florence 2007 - Firenze University Press

Wouters J 2008. Reflections on the position of science in multidisciplinary approaches. *Chemistry Internat Newsmagasine for IUPAC* 30, 1, January-February: 6p. media.iupac.org/publications/ci/2008/3001/1_wouters.html

An electrical interface for vibration energy harvesting from wood floor

Shuai Pang
School of Technology, Beijing Forestry University, Beijing, P.R.China, psh1988@126.com
Jiangming Kan
School of Technology, Beijing Forestry University, Beijing, P.R.China, kanjm@bjfu.edu.cn
Wenbin Li
School of Technology, Beijing Forestry University, Beijing, P.R.China, leewb@bjfu.edu.cn
Huixiang Wang
School of Technology, Beijing Forestry University, Beijing, P.R.China,361383428@qq.com

Abstract

Vibration energy from wood floors is of great significance. People's walking on the wood floors can generate potential large energy with rational utilization. Piezoelectric energy harvesting (PEH) is an efficient way of vibration energy harvesting. This paper introduced the performance of two different mechanical structures for PEH. A circuit for collecting and storing energy was applied and analyzed. The results show that different mechanical structures can be applied in different situations. The structure with one side fixed and the other fixed to some extent and shaking with the exciter may be a good choice for collecting vibration energy from wood floors since the generated voltage of the piezoelectric element is stable and reasonable in low frequency conditions. Meanwhile, with the structure and circuit mentioned in the paper, piezoelectric energy can be well stored for further application.

Keywords: wood floor, PEH, structure, electrical interface, vibration.

Introduction

Vibration is everywhere and has high energy density, so a variety of studies have been made on the application and conversion efficiency of it.

In the research on practical uses, special shoes that can collect energy from people's walking have not been used well since researchers failed to make the collected energy able to charge the telephone or other portable electronic devices (Kymissis et al. 1998， Mateu and Moll 2005). Wireless sensors can be charged to operate but they can't work only with vibration energy (Yoon et al. 2005). A sustainable dance floor can compress 10mm when being stepped on to create electricity. The compression is enough to produce up to 35 Watt of sustained output per module (Sustainable Dance Club 2011). To collect the vibration energy in practical use is promising. Researchers are trying to make the vibration energy better used in practice.

In the research on increasing the efficiency of vibration energy harvesting, researchers found that PEH is more efficient compared with magnetic and static ways(Sodano et al. 2004). Different piezoelectric materials, size, mechanical structures are of different generating electricity performance (Wanglu et al. 2012). As the voltage of the generated electricity is sinusoidal, different performances of various rectifiers have been studied including the full-bridge rectifier(Jeon et al. 2005), voltage doubling rectifier (Dallago et al. 2007), CMOS full-bridge rectifier (LiQiang 2011) , etc. The matching resistor theory is also a focus of improving the performance of the harvesting (Ottman 2002). Synchronized switch harvesting on inductor (SSHI) technique is a hotspot consisting of parallel-SSHI and series-SSHI. The key point of the technique is to control the switch when the piezoelectric beam reaches its maximum displacement but it usually needs extra power and precise detecting devices (Lefeuvre et al. 2006). Self-powered SSHI technique has appeared but it has higher harvested power than the standard harvesting technique when its output open voltage is larger than 6V (Junrui Liang and Wei-Hsin Liao, 2012). Voltage stabilization is also a part of the electrical interface and the storage of the energy is essential.

PEH is an efficient way of harvesting energy harvesting. This paper introduced the performance of two different mechanical structures for PEH and focused on the optimization of PEH from wood floor. The electrical interface which connects the piezoelectric element to the terminal electric load is a critical point in the optimization of a PEH system. The performance of a collecting and storing circuit has been analyzed.

Experiments

In the experimental environment, we attempted to simulate people's walking on wood floors by using the vibration exciter functioning on the piezoelectric element.The experimental devices include a signal generator GFG-8015G, a power amplifier B&K 2706, a vibration exciter B&K 4809, a designed fixed station, an oscilloscope NEC omniace RA110, multimeters and so on. The sketch of experimental setup is shown in Figure 1.

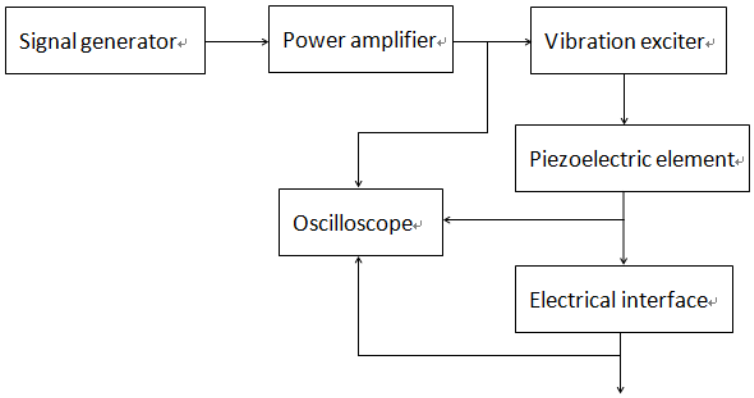

Figure 1---Sketch of experimental setup

Piezoelectric element

The piezoelectric transducer is composed of the copper base plate and the PZT-5H ceramics. The plate is bimorph. Its working model is d31 whose generated voltage is perpendicular with the applied stress. More detailed parameters are shown in Table 1. The parameters were confirmed by measurements except modules of elasticity. If the piezoelectric element is larger, the capacity of generating electricity will be bigger.

Table 1---Parameters of the materials

Materials and dimension	PZT-5H	Copper
Density($Kg \cdot m^{-3}$)	6790	8300
Modules of elasticity(GPa)		131
Thickness(mm)	0.2	0.2
Width(mm)	50	50
Length(mm)	50	70

Two mechanical structures

The two mechanical structures' simplified schematic diagrams are shown in Figure 2. Model a is that one side of the piezoelectric element is fixed and the other side is fixed to some extent and shaking with the exciter. Model b is that just one side is shaking with the exciter and the other side is free.

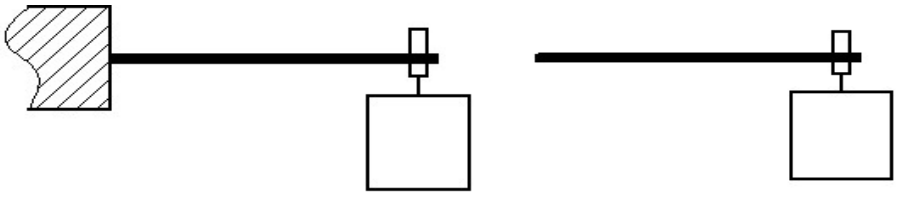

(a) (b)

Figure 2---Two modes of mechanical structures

As shown in Figure 1, The signal generator can produce a certain frequency of sine wave. The power amplifier makes the wave large enough to shake the exciter. The piezoelectric plate shakes with the exciter and the generated sine output voltage of the plate can be seen with the oscilloscope.

Frequency of the system

The natural frequency is shown in equation (1), and we can calculate w_n through the parameters in Table 1 and by the equations from (1) to (5). From equation (1), we can conclude that increasing the mass of m_1 can reduce the natural frequency. In our experiments, there is no m_1, so m_1 is equal to zero.

$$w_n = \sqrt{\frac{k}{m_1 + m_2}} = 2\pi f_n \tag{1}$$

$$\delta = \frac{Pl^3}{3EJ} \tag{2}$$

$$k = \frac{P}{\delta} \tag{3}$$

$$m_2 = \frac{33ql}{140} \tag{4}$$

$$J = \frac{bh^3}{12} \tag{5}$$

Where k is the spring stiffness, m_1 is the weight of mass fixed at the free end of the beam, m_2 is the equivalent weight of the cantilever's free end, δ is the deflection, P is static load of the cantilever's free end, E is modulus of elasticity, J is the moment of inertia, q is the mass per meter, l is the length of the cantilever beam, b is the width of the cantilever beam and h is the thickness of the beam (Yinmin Zhang,2008). l is 61mm in the experiment.

f_n is calculated to be 22.9Hz, which is consistent with the simulation result using ANSYS 14.0. The resonant frequency in damping conditions is shown in equation (6):

$$w = \sqrt{1 - 2\xi^2} w_n \tag{6}$$

The electrical interface

In the experiment, structure of model a mentioned above is used to generate electricity since it works well in low frequency. The chips LTC3588-1 and CBC3112 were used for collection and storage of energy. LTC3588-1 is for piezoelectric energy harvesting power supply. It owns an integrated low-loss full-wave bridge rectifier. With input operating range from 2.7V to 20V, the output voltage can be selected to one of the following voltage: 1.8V, 2.5V, 3.3V and 3.6V. And the continuous output current can be up to 100mA, which is much larger than the original output current in μA level. We choose 3.6V to carry out our experiment. CBC3112 is the world's first intelligent thin film energy storage device. A 12μAh thin film

energy storage is integrated. 3.6V is in the range of the input of CBC3112. The experimental electrical circuit is shown in Figure 3.

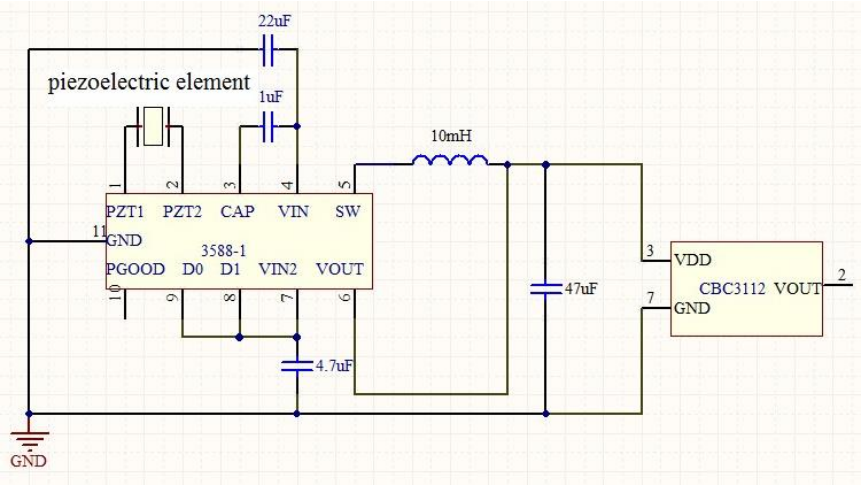

Figure 3---The experimental electrical circuit

Results

For each mechanical model, in different amplifier's output voltage and different frequency, the generated peak voltage was recorded. Figure 4 and Figure 5 respectively show the relationship between frequency and the generated peak voltage with model a and model b structure as shown in Figure 2. Meanwhile, Figure 6 shows the performance of the two models when the output voltage of the power amplifier is 3V. Figure 4 and Figure 5 demonstrate that the larger the input of the piezoelectric transducer is, the larger the output of it. Figure 6 shows that different mechanical structures have different performances .They can be used in different situations. If the environmental vibration frequency is lower than 15 Hz, model a is better to collect energy since its output voltage is large than that of model b. But if the environmental vibration frequency is easy to reach the resonant frequency, it's better to use model b.

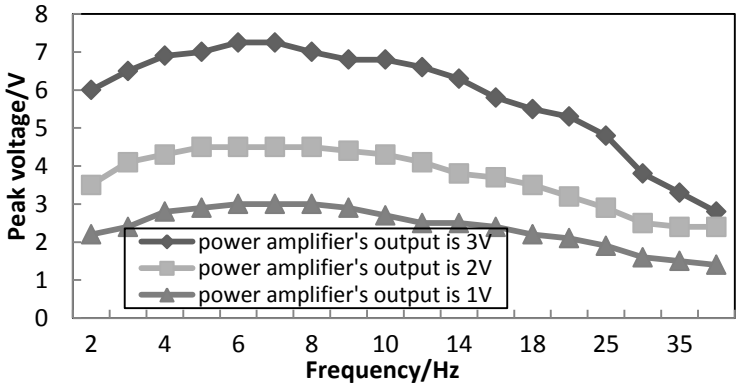

Figure 4---Relationship between frequency and the generated peak voltage with model a

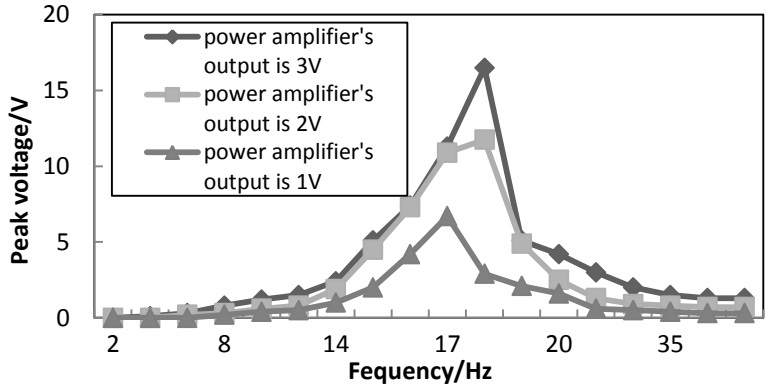

Figure 5---Relationship between frequency and the generated peak voltage with model b

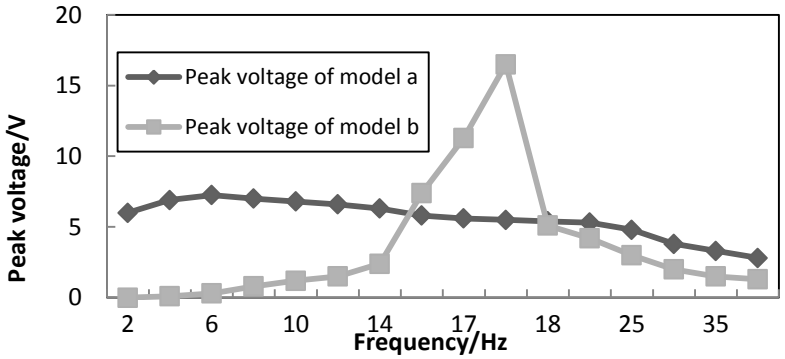

Figure 6---Comparison of two models' frequency and generated peak voltage relationship

When the piezoelectric element is relatively still which means the exciter doesn't shake it but there is also vibration in the environment, the resistor is ranging from about 26MΩ to 38MΩ. The resistor is changing when the piezoelectric element is shaking. The output voltage of the piezoelectric element can be changed by adjusting the frequency and the output of power amplifier. Because the resistor of the piezoelectric element is in the level of MΩ, the output current is limited to the level of μA.

Using LTC3588-1, the output current of the chip can be up to 100mA. With CBC3112, the energy can be stored in a short time for further use. It's seen that the output voltage of CBC3112 can be from 2.06V to 3.90V in about 5 minutes as shown in Figure 7. So the energy can be well collected and stored.

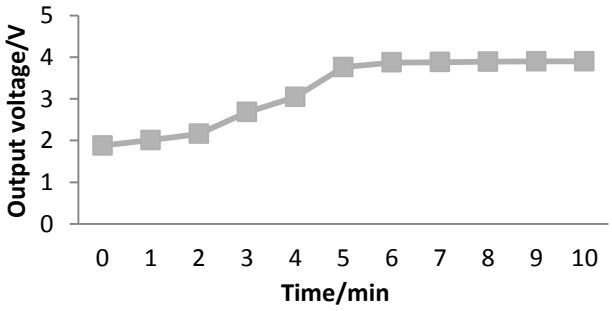

Figure 7---Storage performance of CBC3112

Conclusions and Discussions

In this paper, two mechanical structures used for PEH have been analyzed. Structure of model a is more suitable for the wood floor system as the frequency of people walking on the floor is low and the generated output voltage of the piezoelectric element with the structure is stable and reasonable which is helpful for the later collection and storage of energy.

Various kinds of frequencies added to the piezoelectric element should be tested further to see the performance of generating electricity. The design of the mechanical system should make sure it can be better fit to the surroundings, especially considering the frequency. The resonant frequency can cause the largest displacement of the piezoelectric element, but that doesn't mean it's the optimal frequency to choose. Too large deformation may reduce the performance of the piezoelectric element in a short time since the piezoelectric element may be damaged. In experimental situations, each time only one frequency can be selected, but in reality, there're various kinds of frequencies which are hard to analyze. So in practical use of wood floor system, more experiments in the design of the structure should be carried out, not only to acquire as much energy as possible but to ensure stability.

The resistor matching theory is not suitable to use since the resistor of the piezoelectric element is so big that matching the resistor of the load with that of input is impractical and may cause extra energy loss. How to collect and store the energy more efficiently is worth researching. To create and use integrated micro circuit chips instead of discrete component circuits is a good way to reduce the loss of the circuit.

Acknowledgements

The research is supported by the college students' innovation project of BJFU named Research of Vibration Generators under grant 121012.

References

Kymissis, J.; Kendall, C.; Paradiso, J.; Gershenfeld, N. 1998. Parasitic power harvesting in shoes. In: Proceedings, Second International Symposium On Wearable Computer, Pittsburgh, PA,USA :132–139.

Mateu, L.; Moll, F. 2005. Optimum piezoelectric bending beam structures for energy harvesting using shoe inserts. Journal of Intelligent Material Systems and Structures. 16(10) 835–845.

Yoon, H.S.; Washington, G. ; Danak, A. 2005. Modelling, optimisation, and design of efficient initially curved piezoceramic unimorphs for energy harvesting applications. Journal of Intelligent Material Systems and Structures. 16(10) 877–88.

Sustainable dance club , http://www.sustainabledanceclub.com/ .

Sodano H A; Inman D J; Park G. 2004. A review of power harvesting from vibration using piezoelectric materials. Shock Vib Dig. 36:197-205.

Wanglu Z; Goponath RP,;Lei Zuo. 2012. An efficient vibration energy harvester with a multi-mode dynamic magnifier. Smart Materials and Structures. 21(1).

Jeon Y.;Sood R.; Jeong J. H; Kim S.-G. 2005. MEMS power generator with transverse mode thin film PZT. Sensors and Actuators A: Physical, vol. 122, no. 1, pp. 16–22.

Dallago E.; Frattini G.; Miatton D.;[and others].2007. Integrable high-efficiency AC-DC converter for piezoelectric energy scavenging system, in Proc. IEEE Int. Conf. Portable Information Devices, 1–5.

LiQiang. 2011. A low voltage -high efficiency CMOS rectifier for low power battery-less System. School of electronics and electric engineering.

Ottman G.K; Hofman H.F.; Bhatt A.C.[and others].2002. Adaptive Piezoelectric Energy Harvesting Circuit for Wireless Remote Power Supply. Transactions on power electronics,17(5):669-676.

Lefeuvre E.; Badel A.; C. Richard C;[and others] .2006.A comparison between several vibration-powered piezoelectric generators for standalone systems. Sensors and Actuators A 126:405–416.

Junrui Liang; Wei-Hsin Liao. 2012. Improved Design and Analysis of Self-Powered Synchronized Switch Interface Circuit for Piezoelectric Energy Harvesting Systems. Transactions on Industrial Electronics, 59(4):1950-1960.

Yinmin Zhang. 2008. Mechanical vibration.8-70.

Tabesh A; Frechette L G. 2010. A low-power stand-alone adaptive circuit for harvesting energy from a piezoelectric micropower generator． IEEE Transactions on Industrial Electronics，57(3) : 840－849.

Advanced NDE Evaluation Tools for Historic Covered Bridges

James Wacker
USDA Forest Products Laboratory

Joseph Klett, Frank Jalinoos
Federal Highway Administration

Xiping Wang, Robert J. Ross
USDA Forest Products Laboratory

Abstract

Nondestructive evaluation (NDE) and structural health monitoring (SHM) technologies have been used on a limited basis for condition evaluation of timber bridges. Similar to concrete, steel, and masonry bridges, visual inspection (VI) is the predominant method used for the inspection of these structures. However, VI along with probing and picking tools, is subjective and qualitative in nature and its limitations for inspection of the aging infrastructure have been well recognized. There are well established technologies used to inspect other materials; however, their application for timber-covered bridges has been quite limited. Additionally, in the past 10–15 years, many advanced digital signal processing (DSP) tools have been developed, which has substantially improved the imaging and interpretation of the field results. This study would assess, validate, and adapt few of these advanced imaging tools and techniques for field condition assessment of wood members. This paper will provide an overview of this ongoing project and describe some of the challenges with inspecting larger bridge timbers.

Keywords: Historic, covered bridge, inspection, tools, nondestructive, decay, moisture

Characterization of *Pinus pinaster* wood by means of ultrasound

Cinthya Bertoldo Pedroso
PhD Student, Laboratory of Nondestructive Testing (LabEND), School of Agricultural Engineering (FEAGRI), University of Campinas (UNICAMP), Campinas, São Paulo, Brazil, cinthyabertoldo@gmail.com

Raquel Gonçalves
Associate Professor, University of Campinas (UNICAMP), College of Agricultural Engineering (FEAGRI)and Coordinator of the Laboratory of Nondestructive Testing (LabEND), Campinas, São Paulo, Brazil. raquel@agr.unicamp.br

Maria Eduarda Moreira
Undergraduate student, Laboratory of Nondestructive Testing (LabEND), School of Agricultural Engineering (FEAGRI), University of Campinas (UNICAMP), Campinas, São Paulo, Brazil, dudammoreira@gmail.com

Esther Merlo Sanchez
Empresa Madeira Plus, Galícia, Spain, Esther.merlo.sanchez@gmail.com

Oscar Santaclara
Empresa Madeira Plus, Galícia, Espanha, oscar.santaclara@gmail.com

Abstract

The characterization of wood involves determining 12 properties – 3 longitudinal elasticity moduli (E_L, E_R, E_T), 3 shear moduli (G_{LR}, G_{LT}, G_{RT}) and 6 Poisson ratios (ν_{LR}, ν_{LT}, ν_{RL}, ν_{RT}, ν_{TL},ν_{TR}). The objective of this paper was to determine, by means of wave propagation tests, all 12 elastic constants of the *Pinus pinaster* wood grown in Spain. Seven specimens of polyhedral geometry with 26 sides, as well as longitudinal and transverse transducers with frequency of 1 MHz were used for the tests. The longitudinal elasticity module (E_L) was statistically equivalent to the elasticity modules obtained in static bending test (E_M) and *compression test parallel to the grain* (E_{c0}). Specimens of compression parallel to the grain were instrumented to allow determining the ν_{LT} and ν_{LR} Poisson ratios. The results showed that only the ν_{LT} Poisson ratio obtained in the polyhedral and the compression tests were statically equivalent.

Keywords: ultrasound, polyhedral specimen, Poisson coefficient, longitudinal elasticity module
.

Introduction

Increasingly precise and potent computer programs have made knowledge of material properties essential. Acquiring this knowledge is particularly difficult when dealing with wood, for as an orthotropic material, it has different proprieties in the three main directions (Longitudinal, Radial and Tangential). Knowing its behavior implies determining 12 elastic parameters – 3 longitudinal elasticity modules (E_L, E_R, E_T), 3 transverse elasticity modules (G_{LR}, G_{LT}, G_{RT}) and 6 Poisson coefficients (ν_{LR}, ν_{LT}, ν_{RL}, ν_{RT}, ν_{TL},ν_{TR}).

All these properties can be determined through static testing, but such tests are costly and arduous. Mascia (1991) and Furlani (1995) presented a methodology for determining Compliance matrix by means of static compression test. For such test, 6 prismatic specimens were used in each repetition. From the three specimens retrieved from the symmetry axis, the three longitudinal elasticity modules can be obtained, as well as the six Poisson coefficients. The three shear modules can be found due to the three angle-retrieved specimens on all three symmetry planes. Six strain gages are bonded to each specimen (Figure 1)

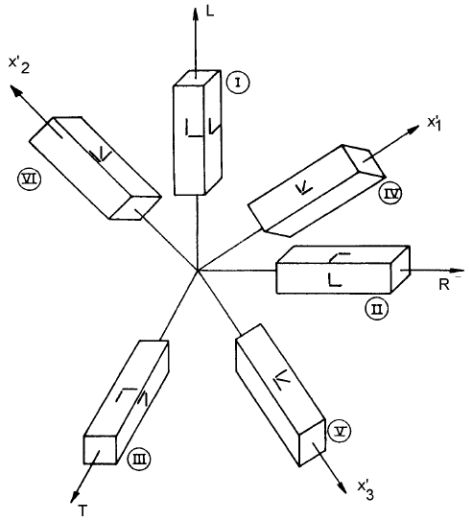

Figure 1. Positioning of the specimen and the strain gages to determining of the Compliance matrix in static compression tests. Source: Mascia (1991)

François (1995) suggested a 26-faced polyhedron as a specimen to determine the elastic constants of wood by means of wave propagation. The advantage of this specimen is that it allows obtaining all the elements of the Stiffness matrix using a single polyhedron.

Trinca (2011) evaluated the test's methodology using ultrasound to determine the elastic constants in wood by means of three specimen geometries: prismatic, multi-faced disc, and 26-faced polyhedron. The author concluded that all three geometries present equivalent results, while the 26-faced polyhedron presents reduced sampling and ease of specimen production.

Material and methods

Seven cubic specimens with 70 mm edges, angled according to the Longitudinal (L), Radial (R) and Tangential (T) axis, were retrieved from seven different beams of *Pinus pinaster* from Galician forests in Spain. The cubic specimens were acclimatized, in order to reach 12% humidity. Afterwords, they underwent measurements and weighting to determine their apparent density at 12% humidity (ρ_{12}). Seven polyhedrons were produced from the cubes, which were used in characterization tests in *Pinus pinaster* by means of ultrasound (Figure 2). For polyhedron production, a worktable disc saw was oriented to cut at a 45° inclination on the different faces of the cubes. The cube dimension was adopted in function of the transducers' diameters, which should be circunscript on the reading face of the polyhedron.

Figure 2 - 26-faced polyhedron used in ultrasound tests for characterization of *Pinus pinaster* wood.

Measurement of the dimensions of the different axis, which correspond to the ultrasound wave path lengths (LL, TT, RR, LR, LT, TR), was made with a digital parking meter (MITUTOYO, Digimatic Caliper).

The tests were made with an ultrasound equipment (EPOCH 4, Panametrics, USA), and longitudinal and transverse wave transducers, both plane-faced and with a 1000 Hz frequency (Figure 3). Starch glucose was used as a coupling for the plane-faced transducers, which, according to Gonçalves *et al.* (2011), presents good results in ultrasound tests in wood.

By means of the longitudinal transducer, wave propagation times on directions L, R and T were obtained, which were used to calculate the longitudinal velocities in the longitudinal, radial and tangential directions (V_{LL}, $V_{RR}$and V_{TT}).

Considering the same directions, but by means of the shear transducer, all the wave propagation and polarization times were obtained, on the directions LR, LT, RL, RT, TR and RT. The results were used to calculate the transverse velocities on the Longitudinal-Radial, Longitudinal-Tangential and Radial-Tangential planes (V_{LR}, V_{LT}, V_{RL}, V_{RT}, V_{TR} e V_{RT}).

To determine the relative velocities for wave propagation out of the symmetry axis, the propagation time was obtained on the faces that presented 45° inclination in relation to each plane. Shear transducers were used in this test.

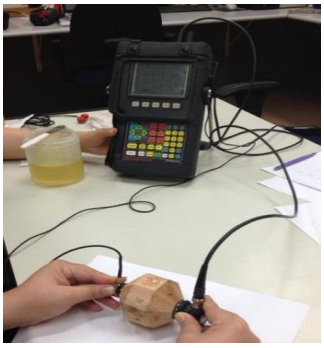

Figure 3 - Ultrasound testing in 26-faced polyhedron.

Once the velocities found, the stiffness matrix coefficients [C] were determined using the Christoffel equations. Matrix inversion ($[C]^{-1}$) leads to the Compliance matrix [S], which contains all 12 elastic parameters sought.

In order to compare them to the ultrasound tests' results, static compression tests were made. Ten specimens with 20 mm x 20 mm and 60 mm length were used in this test, angled according to L, R and T

axis, at equilibrium humidity (12%). The compression specimens were made with *Pinus Pinaster* wood from 4 different trees from Spanish forest. This material did not belong to the same beam sampling that generated the polyhedrons. The results were only partially compared: with compression test on the specimens angled according to L, R and T axis and loading in the parallel direction to the fibers, only the elasticity module in the longitudinal direction (E_L) and the Poisson coefficientsν_{LR} and ν_{LT} can be determined.

The compression tests parallel to the fibers were made in a universal testing machine (DL 30,000, EMIC, Brazil). The deformations occurred during testing were obtained through 5 mm long strain gages (KFG-5-120-C1-11, KYOWA, Japan) with a 2.10 +/-1.0% gage factor and a 119.8 +/-0.2 Ω. resistance gage.

Each specimen was prepared with 6 strain gages - always in 2 parallel faces - for deformation readings in the same direction for both faces, and in each of the directions (longitudinal, radial and tangential). Figure 4 illustrates the strain gages' position on the specimens. The strain gages' terminals were welded to the data acquisition cables.

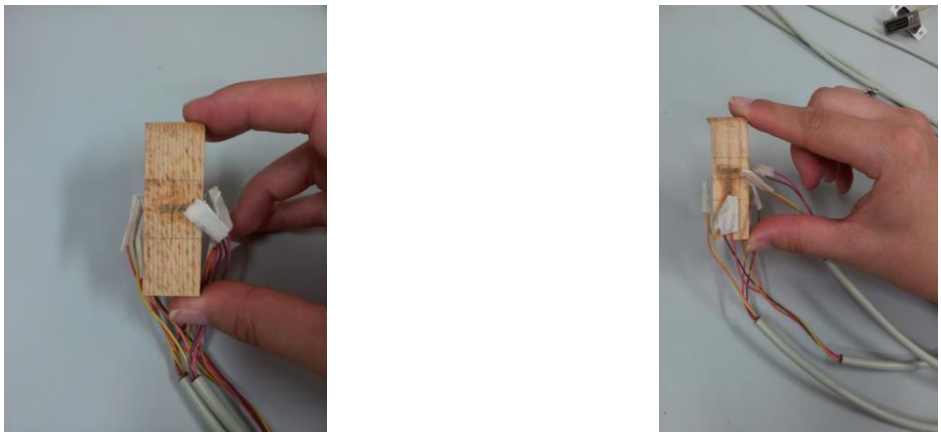

a b

Figure 4 - Strain gages positions for radial (a), longitudinal (b) and tangential (b) deformations of the compression specimens.

When loading was applied in the longitudinal (L) direction, the stress for the longitudinal direction (σ_L) was found, as well as the specific deformations' measurements in the longitudinal (ε_L), radial (ε_R), and tangential (ε_T) directions (Figure 5). Thus, from each specimen, it was possible to determine the elasticity module for the longitudinal direction (E_L) and the Poisson coefficients υ_{LT} and υ_{LR}, using Equations 1, 2 and 3, respectively.

$$E_L = \sigma_L/\varepsilon_L \quad (1)$$

$$\upsilon_{LT} = \varepsilon_T/\varepsilon_L \quad (2)$$

$$\upsilon_{LR} = \varepsilon_R/\varepsilon_L \quad (3)$$

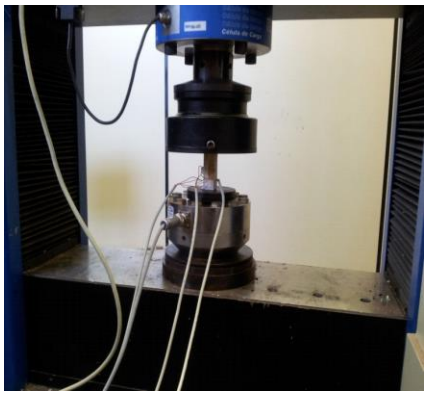

Figure 5 - Compression test parallel to the fibers on the instrumented specimens.

The calculated values from the equations 1, 2 and 3 were used to compare the characterization parameters of *Pinus pinaster*, obtained by the Compliance matrix calculated by inverting the Stiffness matrix determined on ultrasound testing on the 26-faced polyhedrons.

Results and discussions

The wave propagation velocity results obtained with the longitudinal and transverse transducers were used in the Christoffel equations for calculating the Stiffness matrix, which, when inverted, enables obtention of the 12 elastic parameters of *Pinus pinaster* wood (Table 2). To help result comparison, Table 2 also presents the average values suggested by Bodig and Jayne (1982) for the Poisson coefficients. It is important to point out that, for the Bodig and Jayne (1982) study, elastic parameter results for several species of wood were used, with great variations within the same species as well as between different species, which means their average values must assist only as references.

Table 2 - Elastic parameters values obtained by inverting the Stiffness matrix

	Specimen									
	3044	**3026**	**3040**	**3025**	**3001**	**3002**	**2899**	**Averages**	**CV (%)**	**Bodig**
E_L (Mpa)	12,748	13,548	13,751	12,059	12,124	9,000	13,258	12,355	13.1	
E_R (Mpa)	1,338	1,400	1,648	1,463	1,206	1,287	1,602	1,420	11.4	
E_T (Mpa)	762	583	733	848	571	637	664	686	14.7	
G_{TR} (Mpa)	244	219	227	270	236	238	259	242	7.3	
G_{TL} (Mpa)	666	714	753	866	743	852	852	778	10.1	
G_{LR} (Mpa)	1,110	868	932	1,082	1,028	1,256	1,253	1,076	13.8	
υ_{LR}	0.78	0.69	0.67	0.82	0.78	0.44	0.81	**0.71**	18.8	**0.42**
υ_{RL}	0.08	0.07	0.08	0.10	0.08	0.06	0.10	0.08	16.2	0.04
υ_{LT}	0.43	0.78	0.74	0.48	0.75	0.52	0.91	**0.66**	27.6	**0.42**
υ_{TL}	0.03	0.03	0.04	0.03	0.04	0.04	0.05	0.04	17.2	0.03
υ_{RT}	0.71	0.86	0.69	0.64	0.92	0..84	0.85	0.79	13.3	0.47
υ_{TR}	0.41	0.36	0.31	0.37	0.44	0.42	0.35	0.38	11.7	0.35

The Poisson coefficient values obtained by means of ultrasound testing were superior to those proposed by Bodig and Jayne (1982). This result has also been found by Preziosa et al (1981 e 1982), Bucur & Archer (1984), Trinca (2011), Gonçalves (2011) and Ozyhar (2013).

The average values of the Poisson coefficient determined by means of parallel compression tests (Table 3) were more similar to the values proposed by Bodig and Jayne (1982), which suggest the value of 0.42 for both coefficients (ν_{LR} e ν_{LT}) (conifers). However, there's a great value discrepancy between the specimens (ν_{LT} fluctuated between 0.189 and 0.906, and ν_{LR} between 0.190 and 0.531).

Table 3 - Elastic parameters values obtained by means of compression tests parallel to the fibers.

Identification	**E_{c0} (Mpa)**	**υ_{LT}**	**υ_{RL}**
2061 1D	9,515	0.328	0.398
2061 3D*	24,408	0.592	0.470
2077 2D	20,329	0.459	0.522
2077 3D*	18,603	0.906	0.531
2077 3I	25,894	0.718	0.374
2084 2D	14,619	0.349	0.441
2084 3I*	15,075	0.417	0.353
2086 2D	10,078	0.234	0.455
2086 3D*	6,057	0.189	0.427
2086 3I	8,053	0.253	0.190
Average	15,263	0.444	0.416
C. V.	45.3%	51.9%	23.6%

*slightly reclined specimen rings

Although being from the same species and the same county (Spain), one must remember that the compared results between ultrasound and compression tests were not obtained from the same specimen sampling. Thus, said compared results (Table 4) must take into account the natural variability of wood.

The elasticity module determined by compression test parallel to the fibers was 24% superior to the same parameters determined by means of ultrasound (Table 4). Acoustoelastic constant values obtained by means of ultrasound are always somewhat superiors to those obtained through static test on the same specimen. This is due to the difference between both types of test (isothermal and adiabatic). For this research, the tests were performed in different specimens, which makes this point moot.

Table 4 - Average value comparison of the modulus of elasticity and Poisson coefficients obtained with compression test (E_{c0}) and ultrasound test (E_L), with respective coefficients of variation (CV)

	Test	
	Compression (CV%)	**Ultrasound (CV%)**
E_{c0}/E_L MPa	15,263 (45.3)	12,355 (13.1)
υ_{LT}	0.44 (51.9)	0.66 (27.6)
υ_{LR}	0.42 (23.6)	0.71 (18.8)

Using the average confidence intervals (Table 5) from the obtained results for the elastic parameters by means of ultrasound and compression, it is verified that, for E_L, the values obtained by means of ultrasound are completely contained within the compression values' confidence interval, which indicates statistical equivalence of the results. For the Poisson coefficients, only a part of the values obtained by

means of ultrasound is contained within the compression values' confidence interval, which limits statistical equivalence.

Table 5 - Confidence intervals (IC) of the modulus of elasticity results obtained by means of ultrasound (E_{Lu}) and compression (E_{Lc}); Poisson coefficients on LT plane obtained by means of ultrasound (ν_{LTu}) and compression (ν_{LTc}) and Poisson coefficients on LT plane obtained by means of ultrasound (ν_{LRu}) and compression (ν_{LRc})

Parameter	Confidence interval on average	
$\mathbf{E_{Lu}}$	10,858	13,853
$\mathbf{E_{Lc}}$	10,315	20,211
$\mathbf{\nu_{LTu}}$	0.49	0.83
$\mathbf{\nu_{LTc}}$	0.28	0.61
$\mathbf{\nu_{LRu}}$	0.59	0.84
$\mathbf{\nu_{LRc}}$	0.35	0.49

Two statistical tests were used in order to statistically confirm the equivalence between the results obtained by means of ultrasound and compression tests: confidence interval from the average difference and *t* test. Both these tests evaluate the equivalence of the results considering the variability within each sample.

For the Longitudinal Elasticity module, the average difference between the results obtained by means of ultrasound (E_{Lu}) and compression (E_{Lc}) lies between -8,637 and +2,822. Therefore, zero belongs to the interval, and there is no significant statistical difference between the averages. *T* test was made on the same result group, and indicated values of $P = 0.30 > 0.05$. Therefore, once again, the equivalence hypothesis can't be rejected. For both tests, a 95% trust level was implemented.

For the Poisson coefficient on LT plane, the average difference between the results obtained by means of ultrasound (ν_{LTu}) and compression (ν_{LTc}) lies between -0.0089 and + 0.437. Therefore, zero belongs to the interval, and there is no significant statistical difference between the averages. *T* test indicated values of $P = 0.059 > 0.05$. Therefore, for a trust level of 95%, the equivalence hypothesis can't be rejected. For the Poisson coefficient on LR plane, the average difference between the results obtained by means of ultrasound (ν_{LRu}) and compression (ν_{LTc}) lies between + 0.177 and + 0.41. Therefore, zero does not belong to the interval, and there is significant statistical difference between the averages. *T* test indicated values of $0.000089 < 0.05$. Therefore, for a trust level of 95%, the equivalence hypothesis was rejected.

Conclusion

The statistical analysis made with confidence interval tests in average differences and *t* test indicates that the equivalence hypothesis cannot be rejected, ergo the longitudinal elasticity module and the Poisson coefficient (ν_{LT}) obtained by means of ultrasound were statistically equivalent to those obtained by means of compression tests in parallel direction to the fibers on same species samples.

Acknowledgements

The authors thank the National Council of Technological and Scientific Development (CNPq) for the undergraduate research scholarship, the São Paulo Research Foundation (FAPESP) for the PhD scholarship (Proc. no 2011/00904-1), and College of Agricultural Engineering (FEAGRI) for the infrastructure.

References

BUCUR , V; ARCHER R.R.; Elastic constants for wood by an ultrasonic method. Wood Sci. Technol 18: 255-265, 1984.

FRANÇOIS, M. (1995) **Identification des symmetries materielles de materiaux anisotropies**.França**,** Tese de Doutorado – Universidade de Paris, 137p**.**

FURLANI, J.E.. **Um estudo sobre a variação numérica do coeficiente de Poisson na madeira, considerando a anisotropia do material**. Campinas,Tese de Mestrado –Faculdade de Engenharia Civil , Departamento de Construção Civil/ UNICAMP, 1995.

GONÇALVES, R.; TRINCA, A. J.; CERRI, D. G. P. Comparison of elastic constants of wood determined by ultrasonic wave propagation and static compression test. **Wood and Fiber Science**, v. 43 (1), p. 64-75, 2011.

MASCIA, N.T. (1991) **Considerações à respeito da anisotropia na madeira**. São Carlos, Tese de Doutorado - Escola de Engenharia de São Carlos/USP, 295p.

OZYHAR, T.; HERING, S.; SANABRIA, S.J.; NIEMZ, P. Determining moisture-dependent elastic characteristics of beech wood by means of ultrasonic waves. **Wood Sci Technol**, 47: 329-341, 2013. DOI 10.1007/s00226-012-0499-2

PREZIOSA, C.; MUDRY ,M.; LAUNAY, J.; GILLETTA, F.; Détermination des constantes élastiques du bois par une méthode acoustique goniométrique. CR Acad Sci Paris 293(2):91-94, 1981.

PREZIOSA, C.; Méthode de détermination des constantes élastiques du matériau bois par utilisation des ultrasons. Université d'Orléans (Orléans),1982.

TRINCA, A. J. **Metodologia para determinação das constantes elásticas da madeira por ultrassom.** Tese (Doutorado em Engenharia Agrícola) – Na área de concentração de Construções Rurais e Ambiência, Faculdade de Engenharia Agrícola, Universidade Estadual de Campinas, Campinas (SP), 2011.

Ultrasonic Tomography in Detecting Knots

Alex Julio Trinca, Raquel Gonçalves, Camila Stephanie Fernandes Linhares
University of Campinas (UNICAMP), College of Agricultural Engineering (FEAGRI), Campinas, São Paulo, Brazil

Abstract

Ultrasonic tomography is broadly used to analyze the internal condition of trees. There are, on the market, options of industrial tomographs, but tomography can also be less sophisticated, using conventional ultrasound associated with specialized software that allows post-processed imaging. In this case, the low costs of both the equipment and processes can be vital to studying and diffusing this technique. Detecting knots in wooden logs is very important to some sawing processes, such as plywood production. The objective of this paper was to preliminarily evaluate the ultrasonic tomography, using conventional ultrasound equipment and post-processed imaging to identify knots. Twenty-two *Pinus* sp. discs were used in the tests. Each disc's contour was determined, which allowed determining the coordinates (*X,Y*) of the measurement mesh points (diffraction). The wave propagation times for the measurement zones were obtained through the ultrasound test. The coordinates (*X,Y*) spreadsheets of the points referring to the transducer's positioning (emitter and receptor), with their respective wave propagation times, were inserted into the ImageWood software (developed by the research group) to generate the image of each disc. Although the images did not reproduce the exact contour and position of the knots, it was possible to correctly identify the zone in which they were positioned, leading to the conclusion that the simplified methodology (conventional ultrasound equipment) was adequate. The results will be used to compose the algorithm currently being studied by the research group.

Keywords: Ultrasound, post-processed image, *Pinus* sp.

Algorithms for the Generation of Ultrasonic Tomography

Alex Julio Trinca, Raquel Gonçalves, Andre Viana Lima,
Marco Antonio Garcia de Carvalho, Enrique da Silva Filiange
University of Campinas (UNICAMP), College of Agricultural Engineering (FEAGRI), Campinas, São Paulo, Brazil

Abstract

Researching techniques that allow the evaluation of the internal condition of trees or timber has been the focus of many researchers. Ultrasonic tomography presents advantages such as being a nondestructive technique that does not involve radioactive materials, having quick responses and a relatively low cost compared with other tomographic techniques. However, the obtained precision depends largely on the algorithms used when processing data obtained on the experiment. The development of dedicated algorithms, as well as collaborating with the advances of knowledge and the technology appropriation, allows different countries to develop more adequate equipment to their realities and the characteristics of the forest and arboreal species. The objective of this research was to develop the basis for creation of a program that results in images with better precision to represent internal defects in Brazilian native species or exotic species grown in Brazil. Discs from the native species *Aspidosperma desmanthum* and *Tabebuia* sp. and from exotic *Pinus* sp. were adopted for this study. The focus characteristics of the analysis were the presence of knots and dislocated pith. The parameter used in identifying the characteristics was the velocity of ultrasonic waves propagation. The results allowed the generation of a matrix, applied on the IFT (Image Foresting Transform) and Precision Recall methodologies, which allows incorporating the data to the algorithms in elaborating images of the internal condition of the wood. This methodology uses the Software Image Wood (developed at FEAGRI – UNICAMP) as a base, and has shown satisfactory results.

Keywords: Tree inspection, internal wood condition, velocity of wave propagation

ADEQUACY OF THE *EUCALYPTUS* GRADING USING BRAZILIAN STANDARD PROPOSED FOR NATIVE TROPICAL SPECIES

Rafael Gustavo Mansini Lorensani
Master Student, University of Campinas (UNICAMP), College of Agricultural Engineering (FEAGRI), Laboratory of Nondestructive Testing (LabEND), Campinas, São Paulo, Brazil. rafael.lorensani@agr.unicamp.br

Raquel Gonçalves
Associate Professor, University of Campinas (UNICAMP), College of Agricultural Engineering (FEAGRI)and Coordinator of the Laboratory of Nondestructive Testing (LabEND), Campinas, São Paulo, Brazil. raquel@agr.unicamp.br

Esther Merlo Sanchez
PhD, Empresa Madeira Plus, Galícia, Espanha, Esther.merlo.sanchez@gmail.com

Tarik Ottoboni Negreiros
Undergraduate Student, University of Campinas (UNICAMP), College of Agricultural Engineering (FEAGRI), Campinas, São Paulo, Brazil. t_ottoboni@inbox.com

Alex Julio Trinca
Postdoctoral Researcher, University of Campinas (UNICAMP), College of Agricultural Engineering (FEAGRI), Laboratory of Nondestructive Testing (LabEND), Campinas, São Paulo, Brazil. ajtrinca@mxb.com.br

Abstract

The Brazilian standard that provides guidelines for grading of wood using ultrasound (NBR 15521, 2007) was designed with samples of native tropical timber with an average age of 45 years. There are many *Eucalyptus* species in Brazil with adequate proprieties for timber application. However, due to the country's climatic conditions, their growth is accelerated and they have been commercialized at a too young age. The objective of this research was to evaluate the adequacy of the grading proposed by the NBR 15521 (2007) on *Eucalyptus*. The grading through NBR 15521 (2007) was not suitable for wood from young trees (8 and 10 years old). For wood from adult trees (over 20 years old), when reduction coefficient of 1.18 was applied in the velocity values, the grading was adequate and could be used for Eucalyptus.

Key words: Elasticity module, planted forests, ultrasound

Introduction

The Brazilian standard that proposes classification of timber by means of non-destructive ultrasound wave propagation test, the Brazilian National Standards Organization (ABNT/NBR 15521, 2007), was conceived using rigidity properties of native tropical woods with an average age of 45 years. This standard proposes classifying of wood through ultrasound wave propagation velocity bands, or stiffness coefficient bands, associated with the elasticity properties obtained in static bending tests. Therefore, it proposes that through ultrasound tests (velocity range or stiffness coefficient) its elasticity module in bending be determined, which would allow classifying the structural piece.

However, in Brazil, wood from planted forests have been largely used. These woods are, usually, marketed at a much lower age than the one set by ABNT/NBR 15521 (2007) in its sampling for statistical determination of the classification bands. Additionally, the planted forest's trees have rapid

growth in Brazil, due to the high levels of sunlight and the high temperatures, which favor biological activity. According to the literature, this growth condition may cause a different anatomic structure in trees (microfibril angle and latewood density), when compared to the anatomic structure of native tropical species. This issue, combined with the marketing of young wood, calls for an evaluation of the adequacy of classification proposals formulated based on results obtained in adult tropical species, such as the ABNT/NBR 15521 (2007).

Kretschmann & Hernandez (2006) point out that planted species of rapid growth (like *pinus* and *eucalyptus* in Brazil and other tropical climate countries) have not been greatly accepted due to suspicion regarding their mechanical proprieties, which makes mechanical classification very important in confirming these species' proprieties. The authors indicate that the high microfibril angles could be the main cause of low strength and stiffness in wood with rapid growth.

The main objective of this research was to evaluate the stiffness classification of *Eucalyptus* timber of different species and ages, in function of the propagation velocity of ultrasound waves and stiffness coefficient.

Material and methods

The tests were conducted on wood from 13 *Eucalyptus* trees, from which logs were obtained and then sawed into beams (Table 1).

Table 1 - Tested species with respective age and quantity of beams used during the research.

Species	Age	Number of trees	Number of beams	Precedence
E. grandis	34 years old	5	247	*Duraflora* Company, Lençois Paulista, SP, Brazil
E. grandis	8 years old	2	22	Experimental Forest of the Higher School of Agriculture "Luiz de Queiroz" (ESALq/USP), Anhembi, SP, Brazil
E. citriodora	10 years old	2	15	
E. pellita	26 years old	2	55	
E. globulus	28 years old	2	35	Galician forest, Spain

The ultrasound tests were conducted with ultrasound equipment (USLab, AGRICEF, Brazil), and 45 kHz plane-faced transducers positioned on the extremities of the beams, so that the compression wave could be propagated longitudinally (direct measurement). The measurements were made in three points of the transverse section (superior, middle and inferior) (Figure 1). Before the tests were started, the ultrasound equipment was calibrated with an acrylic bloc, for which the longitudinal wave propagation velocity is known (2,750 $m.s^{-1}$). The transducer coupling to the pieces was made using medicinal gel.

The beams were initially tested in green condition, in order to obtain the propagation velocity values in the saturated beam (V_{LLsat}). After ultrasound tests, the beams underwent chamber drying with temperature and humidity control until they reached equilibrium moisture (around 12%), when they were tested again for velocity in the dry condition (V_{LL}) obtention, which is used when calculation stiffness coefficient (C_{LL}). In this moisture content (around 12%), the beams were also tested in static bending.

Figure 1— Longitudinal measurements with ultrasound

The stiffness coefficient C_{LL} (MPa) was calculated with Equation 1.

$$C_{LL} = \rho_{12\%} \times V_{LL}^2 \times 10^{-6} \qquad \text{Equation 1}$$

In which: $\rho_{12\%}$ is the apparent density in wood with moisture around 12 % (11 % - 13%); expressed in $kg.m^{-3}$; V_{LL} is the wave propagation velocity in wood with moisture around 12 %, expressed in $m.s^{-1}$.

The beam static bending tests were made in a frame with hydraulic actuator with a 500 kN load, in order to determine the elasticity module E_M. The tests were conducted in compliance with the ASTM D198-08 (2008).

The classification bands adopted by NBR 15521 adjusted the regression model to the minimum value (prediction limit of 5% or lowered curve). Therefore, the predicted values for E_M would match the characteristics values. However, the standard doesn't specify if the classification must be done individually, or by batchs. Therefore, the classification analysis was done for both - using individual beam values in one case, and the characteristics values in the other.

For individual classification, once the results in the green condition (V_{LLsat}) and the stiffness coefficient in the equilibrium condition (C_{LL}) were known, the beams were classified in compliance with the NBR 15521 (2007) classification bands.

The average velocity correction coefficient was determined in function of the results of this classification, both in the green and dry conditions. After applying the velocity correction coefficients on all beams, a new individual classification was made, in compliance with the NBR 15521 (2007) stiffness classes, considering the corrected velocities in the green condition (V_{LLsat}) and the corrected stiffness coefficients (C_{LL}) in equilibrium condition.

When classifying with the characteristics values, all the beams from a tree were considered one batch. The characteristic value for the elasticity module (E_{Mk}) was calculated with a 5-percentil of the batch.

Once the ultrasound classification results, obtained through previously explained methods, were known, the E_M or E_{Mk} interval expected was obtained.

Since the beams were tested in static bending, the results for modulus of elasticity of the beam E_M and for batch E_{Mk} were compared to those expected by the ultrasound classification, and the results of said classification were categorized in three different categories, as proposed by Kretschmann & Hernandez (2006):
- *Category 1* – E_M predicted with values within the interval expected by the classification.
- *Category 2* – E_M predicted with values below the interval expected by the classification.
- *Category 3* – E_M predicted with values above the interval expected by the classification.

Since the classification bands are adopted in function of the downgraded model (5-percentil), the results framed in Categories 1 and 3 are considered *successes*, because values higher than predicted

for the most part are expected. Results framed in Category 2 are considered *errors*, and are only tolerated in 5% of the results.

Results and discussions

Initially, the data was evaluated regarding normality, using skewness and kurtosis values obtained with the statistical program Statgraphics. Since the parameter's values were within the -2 to +2 interval, the normal distribution hypothesis was not rejected.

According to beam classification, through green velocity (V_{LLsat}) as well as through stiffness coefficient (C_{LL}), it can be asserted that many results are framed in *Category 2*. In this case, the beams were classified in a superior class than the one obtained by static bending tests, which indicated a security problem when using this classification (Figures 2 and 3).

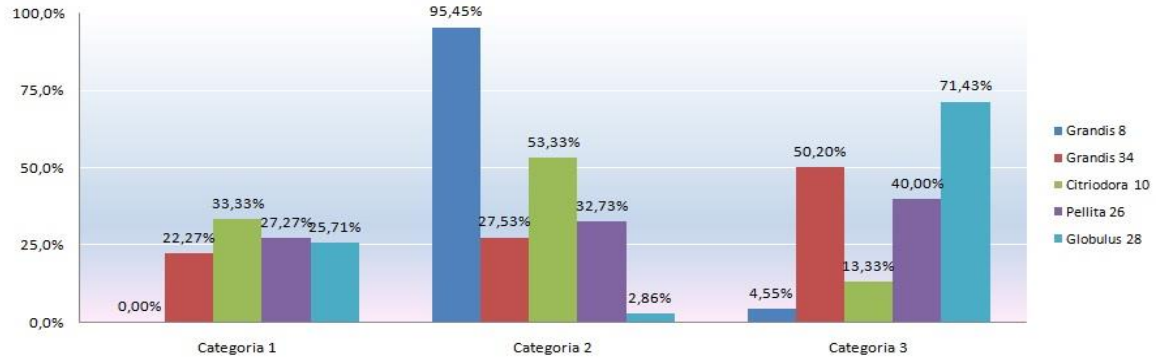

Figure 2 – Classification categories through modulus of elasticity (E_M) of the eucalyptus timber, using the individual velocity values in the green condition (V_{LLsat}).

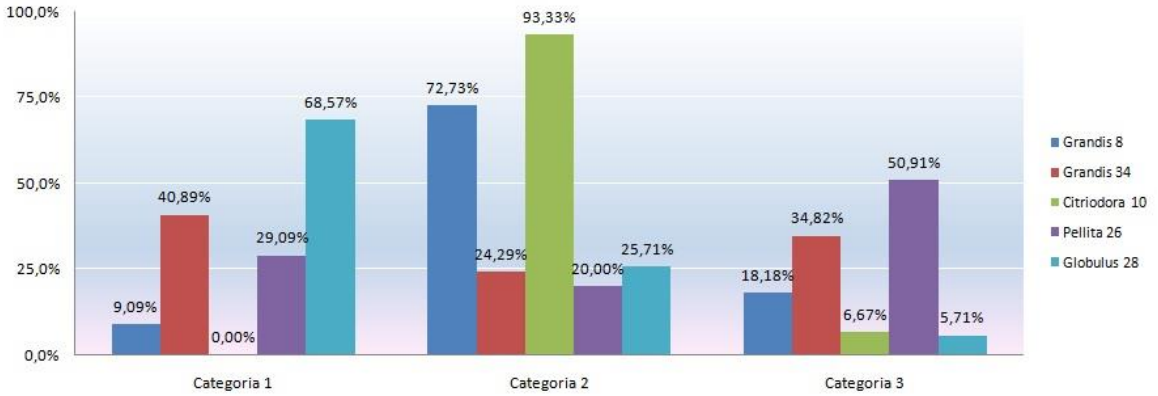

Figure 3 – Classification categories through modulus of elasticity (E_M) of the eucalyptus timber, using the individual stiffness coefficients values in 12% moisture content (C_{LL}).

With this security issue, it was verified that it is possible to apply the velocity correction factor, both for the saturated and dry conditions. Applying this correction factor would only be possible if the velocity presented the same variation tendency with rigidity in *Eucalyptus* and in tropical wood, with a constant bias. To determine this correction coefficient, the average values for $E_{M,}$ obtained in the beams of each species, were used to determine the classification class for NBR 15521 (2007). The estimated green velocity value ($V_{LLsat,est.}$) was used as the minimum velocity in the average elasticity module classification band, and the relationship between average V_{LLsat} obtained in test for each species and the $V_{LLsat,est.}$ was calculated with this velocity value.(Table 2).

Table 2 – Relationship between estimated green velocity ($V_{Lsat,est}$) in function of modulus of elasticity E_M classification (obtained in tests) for NBR 15521 (2007) classes, and the average green velocity (V_{LLsat}) obtained in beam tests for each species.

Species / age	$E_{M\ 12\%}$ [MPa]	$V_{LLsat\ est}$ [m.s^{-1}]	$V_{LLsat,\ medium}$ [m.s^{-1}]	Relationship
E. grandis 8 years old n = 22 beams	8,034 (3.512)	< 3,040	4,116	1.35
E. grandis 34 years old n = 247 beams	15,549 (2,715)	3,690	4,158	1.13
E. citriodora 10 years old n = 15 beams	14,724 (2,293)	3,690	4,187	1.13
E. pellita 26 years old n = 55 beams	11,133 (3,970)	3,040	3,754	1.23
E. globulus 28 years old n = 35 beams	13,801 (1,581)	3,690	3,865	1.05
Average relationship				**1.18**

Values in parenthesis correspond to the standard deviation

When the average relationship was applied to correct the saturated and dry velocity values, it was verified that the classifications in Category 2 were always lower than 5% for the older species, but that for the younger species - although reduced - the percentages were, overall, still higher than 5% (Figures 4 and 5).

Figure 4 – Distribution of the classification categories of *Eucalyptus* beams, using the corrected velocity in saturated condition by factor 1.18 as a classification parameter.

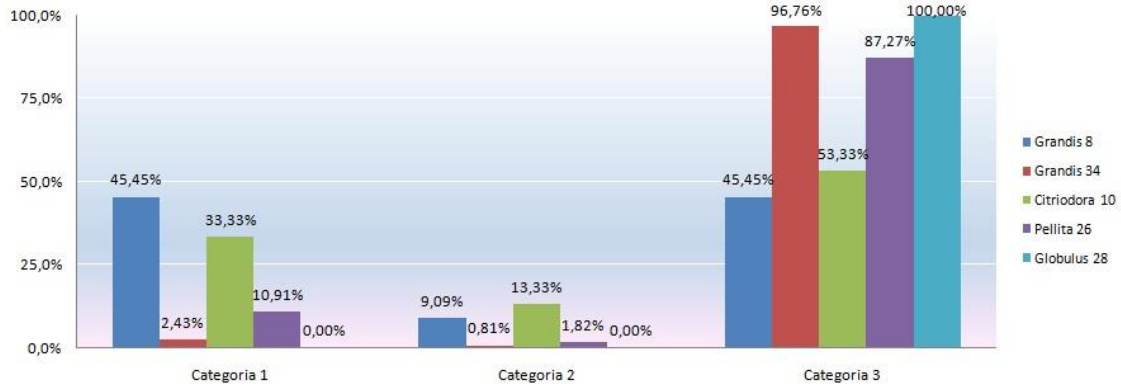

Figure 5 – Distribution of the classification categories of *Eucalyptus* beams, using the stiffness coefficient obtained with dry condition velocity corrected by factor 1.18 as a classification parameter.

Conclusions

The NBR 15521 (2007) classification bands, based on velocity on green wood or stiffness coefficient (calculated with wood velocity in the equilibrium condition), were not adequate to classify *Eucalyptus* timber, neither for the younger nor for the older species, since the percentage of beams with overestimated elasticity modules (Category 2 in classification) was higher than 5%.

The reduction coefficient of 1.18 applied to the velocities (saturated and dry), obtained on beams from adult trees, was adequate to classifying *Eucalyptus* wood with the NBR 15521 (2007) classification bands, since the percentage of beams with overestimated elasticity modules (Category 2 in classification) was lower than 5%, both with saturated velocity and stiffness coefficient as entry parameters in the classification bands.

Acknowledgements

We thank the National Council of Technological and Scientific Development (CNPq) for the masters and undergraduate scholarships, the São Paulo Research Foundation (FAPESP) for the postdoctoral scholarship (Proc. 2011/08286-5), for the exchange program support with Spanish researchers (Proc. 2011/08612-0) and for resources used in beam transportation and sawing (Proc. 2009/10319-9). We also thank the Company Duraflora and the Higher School of Agriculture "Luiz de Queiroz" (Esalq/USP) for the material donated to research and the College of Agricultural Engineering FEAGRI/UNICAMP for laboratory infrastructure.

References

AMERICAN SOCIETY FOR TESTING AND MATERIALS. ASTM D198-08: Static tests of Timbers in Structural Sizes. Philadelphia, Pa, USA, 2008.

ASSOCIAÇÃO BRASILIERA DE NORMAS TÉCNICAS. NBR 15521: Ensaios não destrutivos — Ultra-som — Classificação mecânica de madeira Serrada de dicotiledôneas. Rio de Janeiro, 2007. 107 p.

ASSOCIAÇÃO BRASILIERA DE NORMAS TÉCNICAS. NBR 7190: Projeto de estruturas de madeira. Rio de Janeiro, 1997. 107 p.

COSTA, A. L. C. VELOCIDADE DE PROPAGAÇÃO DE ONDAS DE ULTRA-SOM NA MADEIRA PARA DIFERENTES CONDIÇÕES DE UMIDADE. 2005. 103 f. Tese (Doutorado) – Faculdade de Engenharia Mecânica, Universidade Estadual de Campinas, Campinas.

KRETSCHMANN, D.; HERNANDEZ, R. Grading timber and glued structural members. Primary wood processing: principles and practice. Dordrecht, Springer, 2006. Pages 339-390.

LOGSDON, N. B. (1992). Estudo comparativo sobre a maneira de obter a densidade aparente a 12% de umidade. In: ENCONTRO BRASILEIRO EM MADEIRAS EESTRUTURAS DE MADEIRA, 4, São Carlos, SP. 1992. Anais. São Carlos, LaMEM/EESC/USP. v. 4, p. 31-42.

Behavior of Different Types of Adhesives in Bonding Extensometers in Tests with Wood

Tarik Ottoboni Negreiros, Rafael Gustavo Masini Lorensani, Raquel Gonçalves, Julio Soriano
University of Campinas (UNICAMP), College of Agricultural Engineering (FEAGRI), Campinas, São Paulo, Brazil

Abstract

It is usual to use comparisons with static tests in research that use nondestructive techniques and, in many cases, extensometers are used to follow up the strain. To bond strain gages, one usually uses the same type of adhesives used for metals and concrete, even if these materials have very different elasticity properties. The objective of this paper was to analyze the behavior of four different types of adhesives (epoxy base, cyanacrylate base, rubber base, and silicone base) in bonding strain gages to specimens tested in compressions parallel to the fibers. A Brazilian native species of wood, Goupia glabra, was used for the experiments, whose average density was 870 kg m^{-3}. The experiments were conducted in nine specimens with nominal dimensions of 50 mm by 50 mm by 150 mm, to which the strain gages were bonded with the different types of adhesives paired up to minimize the influence of the intrinsic variability of wood's proprieties, as well as the variation in distribution of stresses to the specimens during charging. The experiment machine's extensometer was used in comparing the results. The deformations were measured and the modulus of elasticity was calculated with epoxy and cyanacrylate, which were statistically equivalent to those obtained from the experiment machine's extensometer. The least adequate behavior was that of silicone.

Keywords: Epoxy, cyanacrylate, rubber, silicone

Inspection of Demolition Wood Using Ultrasound

Robson van Dijk, Raquel Gonçalves, Julio Soriano
University of Campinas (UNICAMP), College of Agricultural Engineering (FEAGRI), Campinas, São Paulo, Brazil

Abstract

Wood has been established as a building material throughout human history, and it has lately been considered one of the most sustainable ones, being a renewable material, having low incorporated energy, and being able to store carbon. Considering these aspects, using demolition-originated wood is more valued, for it extends this noble material's useful life by postponing its liberation of carbon to nature. One of the viably used techniques in inspecting demolition wood that addresses its reuse is ultrasound. However, many aspects can interfere in this type of test, which can lead to mistakes when interpreting the inspection's results. The objective of this paper is to present and discuss an inspection case study conducted by means of longitudinal waves with different measurement types (direct, semi-direct, and indirect), different transducers (plane and dry point contact faces), and different frequencies (25, 45, and 80 kHz). In this paper, discussion of results is based on theoretical aspects related to wave propagation, with, for instance, relations between the wave length and the defect's dimension, or the run length, revealing the importance of knowledge and application of these bases to the inspection procedures.

Keywords: Direct measurements, semi-direct measurements, indirect measurements, longitudinal waves

Inspection of Demolition Wood Using Ultrasound

Frank Rinn
RINNTECH, Heidelberg, Germany

Abstract

Resistance drilling has been applied by professionals in tree and timber inspection since 1987. First prototypes of 1984 used a spring-loaded recording mechanism but delivered systematically wrong and unreliable profiles. Electric recording was better but not perfect. The profiles of electronically regulated and recorded drills have since been shown to be linearly correlated to wood density, thus clearly and reliably revealing variations between earlywood and latewood zones as well as changes between intact and decayed or hollow parts. However, knowledge about the method's technology and about wood anatomical properties are critical for being able to interpret the profiles correctly. For decades, stress-wave timing has been a well-established method for modulus of elasticity (MOE) assessments. A comparison of the results of the application of these two methods at the same beams shows that different material properties, such as density and MOE, have different influences on the measured parameters. Wood moisture content, for example, leads to a higher drill resistance but a lower stress-wave speed.

Keywords: Stress-wave timing, resistance drilling, wood moisture, wood density, MOE

Theory and Practical Condition Inspection of Laminated Timber Structures

Frank Rinn
RINNTECH, Heidelberg, Germany

Abstract

After several severe and catastrophic accidents with many deaths, more German authorities realized the need for a proper inspection of modern timber structures using glue-lam beams. Inspection of laminated timber requires specific methods because their size, structural use, connection, and internal material properties are very different from full-size beams. To distinguish between soft wood and decay, for example, it is mandatory to use high-resolution, electronically regulated resistance drilling clearly and reliably revealing wood density: only by comparing the changes between earlywood and latewood zones of the tree rings it is possible to reliably identify signs of decay. In addition, resistance drilling has been shown to be the sole quasi-nondestructive method for checking whether there are enough steel connections in invisible internal areas of joints. However, in-depth knowledge of the method and wood anatomical features is required for a proper application, interpretation, and evaluation. Sometimes it makes sense to combine this method with stress-wave timing and wood-moisture measurements. By studying examples from practical applications, the required knowledge can be obtained.

Keywords: Laminated timber, condition inspection, resistance drilling, stress-wave timing

Relationship between longitudinal and transversal natural vibration frequencies on structural timber of Spanish *Pinus radiata* D. Don and *Pinus sylvestris* L.

Eva Hermoso; Forestry Engineer, PhD.; CIFOR-INIA; Madrid; Spain.

Raquel Mateo; Forestry Engineer; AITIM; Madrid; Spain.

María J. Montero; Agricultural Engineer; ETSI Montes, Universidad Politécnica de Madrid; Madrid; Spain.

José L. García de Ceca; Forestry Engineer, PhD.; CIFOR-INIA; Madrid; Spain.

Daniel F. Llana; Agricultural Engineer; ETSI Montes, Universidad Politécnica de Madrid; Madrid; Spain.

Measurements of natural frequency vibration are a non destructive technique that is applied on structural wood to estimate its mechanical properties. This paper is about the analysis of the relationship between longitudinal and transversal measurements on this technique due to the better management of the latter.

The study was carried out in 140 specimens of *Pinus radiata* timber, from País Vasco (Spain), with two different cross sections: 70 beams with 150x250x4500 mm^3 and 70 beams of 200x250x4500 mm^3, and 218 specimens with 150x200x4200 mm^3 of *Pinus sylvestris* timber from Segovia (Spain)

The equipment used was PLG (Portable Lumber Grader) of Fakopp Co. In addition to the vibration methods, it was carried out bending test according to UNE-EN 408 for determination of static modulus of elasticity.

The relationship between dynamic modulus of elasticity, obtained by longitudinal vibration method, and the static modulus of elasticity is as good as has been demonstrated in previous researches. However, the relationship between the modulus of elasticity obtained by longitudinal frequency and the modulus of elasticity from transversal frequency is not as good as expected, but better in *Pinus sylvestris* than *Pinus radiata.* Moreover, there is a weak relationship between the longitudinal and transversal frequencies. Thus, to use transversal non destructive measurements to derive longitudinal behaviour of timber from its natural frequency of vibration, it would require a specific analysis for each wood species for structural uses.

Key words: vibration techniques, mechanical properties, *Pinus radiata, Pinus sylvestris*

Mechanical properties of clear poplar wood vs. cracked and drilled bars

A. Yavari[1], M. Roohnia[2], A. Tajdini[3]

Abstract

In this study, mechanical properties of rectangular clear poplar bars as well as cracked and drilled ones with nominal dimension of 2×2×36 cm (R×T×L) were evaluated.
Impact of three-step hole production (a three millimeter turned to a bigger hole with the diameter of five millimeters and finally to its biggest size with 8 millimeter diameter) was appraised on tangential surface of the beams visible from two surfaces with vibration method on free bar.
Stepwise drilling (three steps of drilling) showed that as the bigger the holes, the lesser the amount of ACE on tangential and radial directions, and quality (average of Q) decreased, while on the other hand damping (tand LR) increased.
Influence of crack expanding (three steps crack propagation from 6cm, which turned to 12cm and finally 18cm) was examined on radial surface of the bars with vibration method on free bar.
With crack propagation of poplar bar (three steps of 6 cm expanded to 12 and finally to 18cm) evaluated from free vibration method on free bar using individual impacts on each tangential (LT) and radial (LR) plane, the results indicated average velocity of (Ave. V) (LT) declined while damping tand LR increased.

Keywords: ACE; Damping; Velocity

Introduction

Defects lead to reduction in net cross section and their presence, introduces stress concentrations in wood member. The amount of strength reduction depends on the size and location of defects (*Structural Wood Design*, Abyi Aghayere and Jason vigil). Crack occurring in the structural elements causes a local variation in stiffness, affecting the dynamic behavior of the structure to considerable degree (Chati et al. 1997). The use of low-frequency ultrasonic echo technology with longitudinal and transverse waves, for the investigation of wooden construction components, is described. There, by ultrasound echo, it is possible to detect the damage from the undamaged side of the specimen. The drilling resistance method is used as reference procedure, detecting the back walls of the specimens as well as the inserted cavities inside the structures (B. Hillemeier May 2005, University of Applied Sciences, Germany). Free vibration testing was used to generate the two initial mode shapes for damage detection in timbers, and it was proved that the chosen 3 wavelet was suitable and sufficiently sensitive to identify the location, extent and number of different damages (Hu et al, 2006). The best technique, to detect a defect initially, depends on the defect size, which must be found and the size of the structure to be inspected. The FMMIS method is used for segmentation image to achieve a good classification performance, and achieving a defect detection rate of 95% with 6% false positive rate on 300 test wood image (*A Review of External Wood Defect Detection* Nik Kamariah Nik Ismail, Jasni Mohamad Zain, University Malaysia Pahang). Evaluating of shear modulus through LT and LR vibration in clear beams was verified. Therefore, the introduced differences might be an indicator of the defect. Greater differences between shear modulus evolutions of a proper bar may indicate greater defects, i.e. holes (Roohnia et al. 2010).

[1] Ali Yavari, Science and Research Branch, Islamic Azad University - IRAN, ali_yavari100@yahoo.com
[2] Mehran Roohnia, Karaj Branch, Islamic Azad University - IRAN, mehran.roohnia@kiau.ac.ir
[3]Ajang Tajdini, Karaj Branch, Islamic Azad University – IRAN, ajang.tajdini@kiau.ac.ir

Materials and method

Rectangular 2×2×36cm timbers of *Populus Deltoides* (randomly collected from Zanjan, Iran) were cut from bark to pith and then conditioned in 65 percent relative humidity and 21°C. Using MATLAB software Mechanical properties of unharmed samples were analyzed, (Based on Timoshenko bar equations and Bordonne Solution)[4]. Then, mechanical properties of cracked and drilled bars[5] were

[4]

$$a_k = \left(\frac{MOE}{\rho}\right) - \left(\frac{MOE}{K \times G_{ij}}\right) b_k \quad (1)$$

$$b_k = \frac{4\pi^2 l^2 f_k^2 F_{2k}}{X_k} \quad (2)$$

$$a_k = \frac{[4\pi^2 l^2 f_k^2 (1 + \alpha F_{1k})]}{\alpha X_k} \quad (3)$$

$$X_k = m_k^4 \quad (4)$$

$$\alpha = \frac{I}{Al^2} \quad (5)$$

where I is the moment of inertia, A, cross-sectional area, leanings, length of the specimen, K shape coefficient (the value of 5/6 can be used for a rectangular cross section), G_{ij} shear modulus in the plane of vibration (GLT or GLR), r specific gravity, f_k frequency of the k_{th} the mode of vibration obtained from fast Fourier transform spectrum; and m_k the results is given in the following equation:

$$m_k = \frac{(2k+1)\pi}{2} \quad (6)$$

$$F_{1k} = \Theta^2(m_k) + 6\Theta(m_k) \quad (7)$$

$$F_{2k} = \Theta^2(m_k) - 2\Theta(m_k) \quad (8)$$

$$\Theta_{(m_k)} = \frac{[m_k \tan(m_k) \tanh(m_k)]}{[\tan(m_k) - \tanh(m_k)]} \quad (9)$$

evaluated individually. The impact of 3step hole production (3millimeter, 5millimeters, and finally the biggest size with 8millimeter diameter), on tangential surface of the beams visible from two surfaces and crack expanding (3 steps of crack propagation including 6cm then turned to 12 cm and finally 18 cm) was evaluated on radial surface of the bars with vibration method on free bar.

5
Higher correlation coefficients of the estimated trend lines in Equation 1 benefit the specimens with more homogeneity, where the Timoshenko model has been fitted initially to isotropic materials, and next to the clearest specimens. The selection was made based on trends with correlation coefficients higher than 0.99. Sampling was made selectively, numbers of wooden-sample and wholesome in shape were selected from spruce.

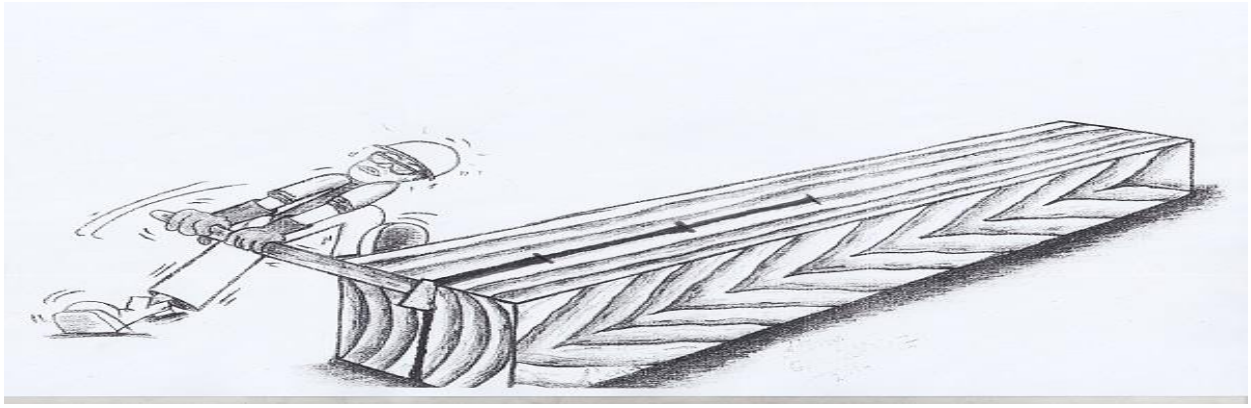

Fig (1) Schematic view of 3 steps of crack propagation including 6cm then turned to 12cm and finally 18cm on radial surface of the bar.

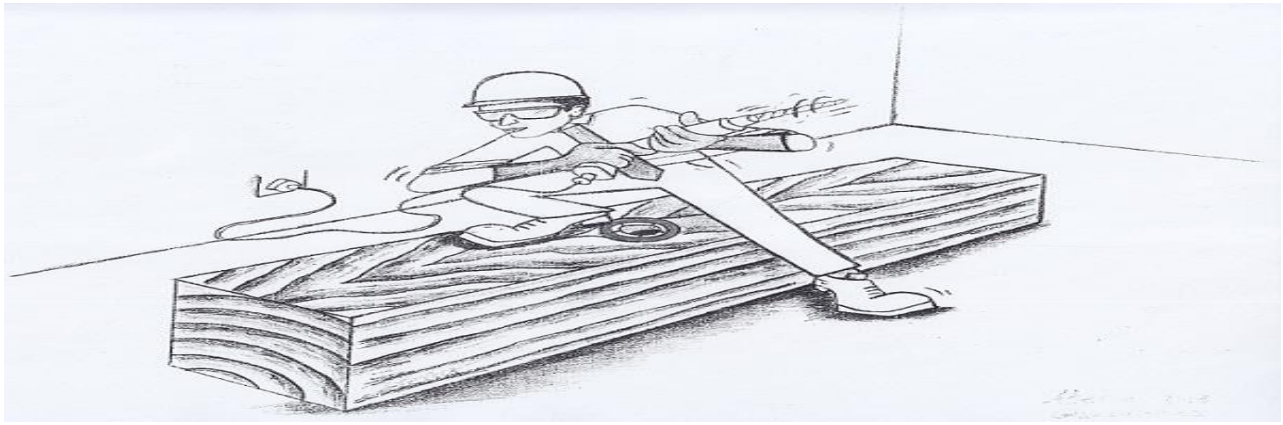

Fig (2) Schematic view of three step hole production (a 3 millimeter turned to a bigger hole with the diameter of 5 millimeters and finally to its biggest size with 8-millimeter diameters) on tangential surface of the beam visible from two surfaces.

RESULT AND DISCUSSION

The result showed:
A) With crack propagation of poplar bar (three steps of 6cm expanded to 12 and finally to 18cm) evaluated from free vibration method on free bar using individual impacts on each tangential (LT) and radial (LR) plane, the results indicated a decline in average velocity of (Ave. V) (LT) while damping tand (LR) increased, Fig (3).
B) The results of studies of the ACE (R) and ACE (T) show that as the diameters of the holes increase, the amount of ACE decreases; eventually, in an eight millimeters hole (in the most damaged samples), this amount would be minimized, Fig (4).
C) As the defects get worse (from 0 to 18cm cracks) the velocity decreases, Fig (5).
D) With propagation of defect (as holes get bigger on tangential surface), the amount of Delta E increases, Fig (6).

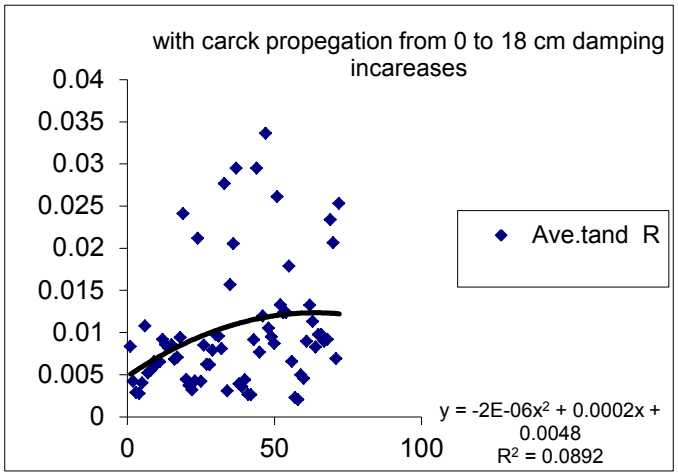

Fig (3) with crack propagation from zero to 18 cm damping increases.

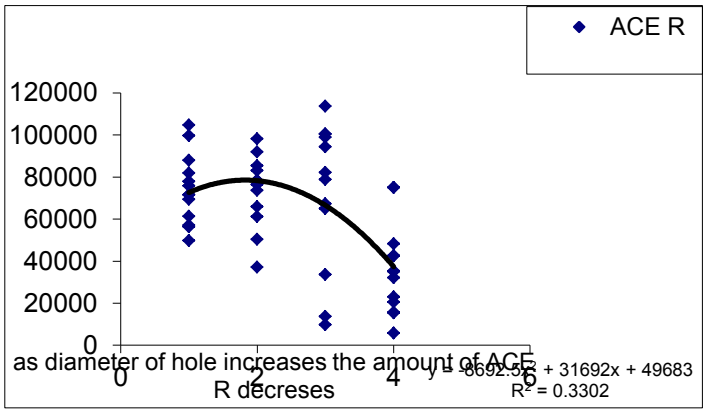

Fig (4-A) as diameter of the hole increases the amount of ACE (R) decreases.

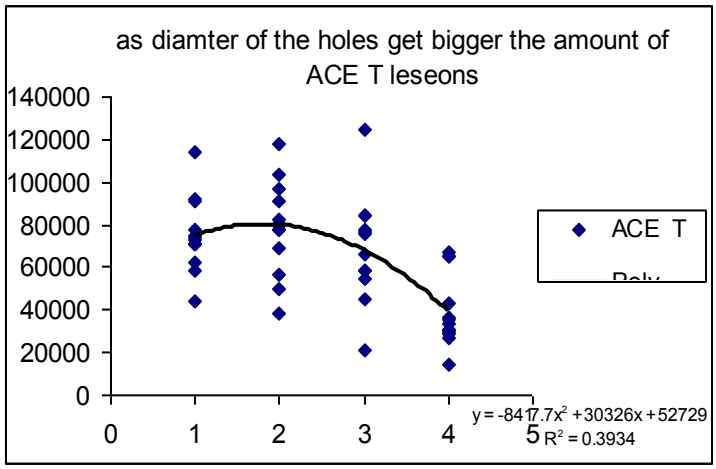

Fig (4-B) as diameter of the hole get bigger the amount of ACE (T) lessens.

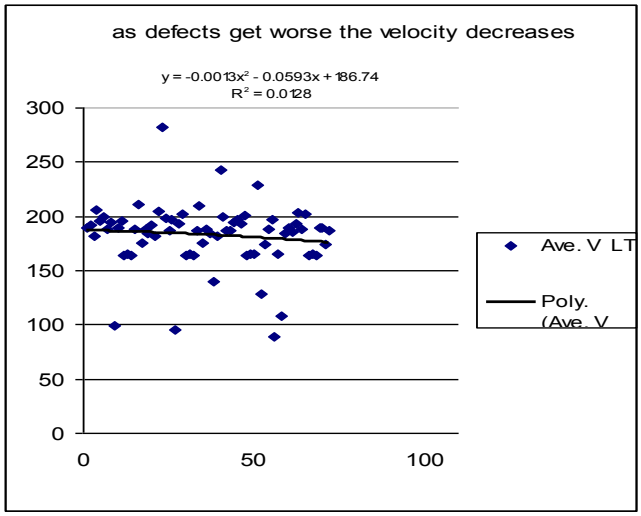

Fig (5) velocity decreases as defects get worse

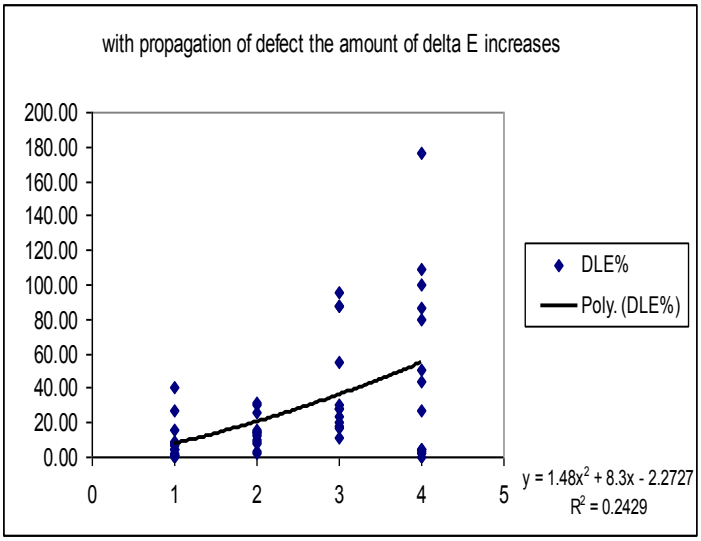

Fig (6) the amount of delta E increases with crack propagation.

CONCLUSION

The effect of step-wise holes with different diameters of zero, three, five and eight millimeters on tangential surface and step-wise cracking (3 steps of crack propagation including 6cm turned to 12 cm and finally 18 cm) on radial surface of the bars by one way analysis of variances (ANOVA) and Duncan were used for grouping the analyzed parameters. In Table 1 and Table 2 the results showed that, when the bars were impacted on tangential surface the drilling holes, on their largest diameters could affect the elastic parameters, as it was expected.

Therefore, it can be concluded that fingerprints of holes and checks on elastic parameters (ACE (R), ACE (T), Delta percentage E, Ave tand, Ave. V (LT)) in proper directions might be applicable for hole and check identification, but the intensity, type and location of the defects were not envisaged.

Table I - ANOVA for the effects of the step-wise (0 to 8 mm) holes on mechanical properties

ANOVA

		Sum of Squares	df	Mean Square	F	Sig.
Ave. Tand. R	Between Groups	.000	3	.000	2.207	.095
	Within Groups	.004	68	.000		
	Total	.004	71			
Ave. V.R	Between Groups	10994.794	3	3664.931	3.749	.015
	Within Groups	66480.566	68	977.655		
	Total	77475.359	71			

Table 2 - Duncan multiple comparison tests for the effect of Ave Tand R

Duncan

		Subset for alpha = 0.05	
Hole	N	1	2
1	13	.01	
2	13	.01	
3	12	.01	
4	13		.01
Sig.		.322	1.000

Table 3- Duncan multiple comparison tests for the effect of AVE. Q. T

Duncan

Hole	N	Subset for alpha = 0.05	
		1	2
4	13	112.05	
2	13		232.61
1	13		233.32
3	12		240.02
Sig.		1.000	.825

Table 4- Duncan multiple comparison tests for the effect of ACE.R

Duncan

Hole	N	Subset for alpha = 0.05	
		1	2
4	13	35833.11	
3	12		71520.70
2	13		73686.07
1	13		74219.28
Sig.		1.000	.786

Table 5- ANOVA for the effects of crack expanding (three steps of crack propagation including 6cm then turned to 12cm and finally 18cm) on radial surface of the bars.

ANOVA

		Sum of Squares	df	Mean Square	F	Sig.
Ave.Tand.R	Between Groups	.000	3	.000	2.207	.095
	Within Groups	.004	68	.000		
	Total	.004	71			
Ave.V.R	Between Groups	10994.794	3	3664.931	3.749	.015
	Within Groups	66480.566	68	977.655		
	Total	77475.359	71			

Table 6- Duncan multiple comparison tests for the effect of Ave. Tand.R

Duncan

Check	N	Subset for alpha = 0.05	
		1	2
1	18	.01	
2	18	.01	.01
4	18	.01	.01
3	18		.01
Sig.		.119	.359

Table 7- Duncan multiple comparison tests for the effect of Ave. V.R

Duncan

Check	N	Subset for alpha = 0.05		
		1	2	3
3	18	154.54		
4	18	163.52	163.52	
2	18		177.50	177.50
1	18			186.57
Sig.		.392	.184	.387

REFERENCES

Aghayere, Abyi, Jason vigil, 2007. *Structural wood design*

Chati, M., R. Rand, S. Mukherjee. *Modal analysis of cracked beams*. Department of Theoretical and Applied Mechanics, Cornell University, Ithaca, New B. Hillemeier, May 2005, University of Applied Sciences, Germany.

Hu et al., 2006. *A statistical algorithm for comparing mode shapes of vibration testing before and after damage in timbers*

Hu, C., Afzal, M. T. (2006). *A statistical algorithm for comparing mode shapes of vibration testing before and after damage in timbers*. Journal of Wood Science, 52 (4), 348 - 352

Nik Kamariah Nik Ismail, Jasni Mohamad Zain, University Malaysia Pahang(asni , Mohamad

Roohnia, M. Tajdin I. A. and Manouchehri N., 2010, *Effect of drilling as artificial defects on dynamic shear modulus of wood*

Zain and Nik Kamariah, Nik Ismail, 2009. *A Review of External Wood Defect Detection*

Nondestructive Evaluation of Acoustic Performance of Dalbergia Sissoo used in Making Clarinet

Amir Mohammad Abdolahian Sohi
Department of Wood Science and Technology, Science and Research Branch, Islamic Azad University, P.O.Box 14515/775, Tehran, Iran, amas_ci@yahoo.com

Abstract

The aim of this paper is to Nondestructively Evaluate the Acoustic performance indicators such as Acoustic Coefficient and Sound Velocity of Dalbergia Sissoo (SHISHOM) beams in making Clarinet, using Free- Free Flexural vibration. Although nowadays plastic or some other materials is used in making Clarinet, but the unique acoustical properties of Rosewood and its aesthetic appeal still make it the best material of choice for Clarinet. As in south part of IRAN, there are some regions which have Dalbergia Sissoo, thus the feasibility of using SHISHOM in making Clarinet was under question. The results revealed that Acoustic Coefficient and Sound velocity, as two important indicators of acoustic performance, of SHISHOM were not only equal with the other Rosewood beams but also had higher values than them. Therefore, Dalbergia Sissoo (SHISHOM) is a good choice and somewhat suitable material in making Clarinet. So, IRAN as a country with vast history of music and also a variety of musical instruments can have lot to say with Dalbergia Sissoo in Clarinet making industry.

Keywords: Acoustic Coefficient, Sound Velocity, Dalbergia Sissoo, Flexural Vibration

Introduction

It appears probable that the progenitors of man, either the males or females or both sexes, before acquiring the power of expressing their mutual love in articulate language, endeavored to charm each other with musical notes and rhythm (Darwin1871) So far we can only speculate, when our early ancestors started to perform music, on the role of music in our biology and evolution (Cross, 2001), and when the first musical instruments were made and from which materials.
Humans seek beauty and desire in art, so wood is used as the material for musical instruments. Although the materials of the musical instruments have been replaced by iron, plastic, and many other materials, wooden musical instruments retain a characteristic sound color and acoustic properties. So, many musical instruments continue to be made from wood.(Bucur 2006)
The clarinet is a woodwind instrument. It comes in many different sizes, with different pitch ranges. Though there are more than a dozen different modern clarinet types, the most of them used in orchestras and bands. (Figure 1) The standard clarinet consists of five parts—the mouthpiece, the barrel or tuning socket, the upper (or lefthand) joint, lower (or right-hand) joint, and the bell. A thin, flattened, specially shaped piece of cane called a reed must be inserted in the mouthpiece before the instrument can be played. Different notes are produced as the player moves his fingers over metal keys which open and close air holes in the clarinet's body. There is a vast history behind clarinet from Egypt as early as 3000 B.C, to Eastern Europe, and Sardinia 1690 (Conrad 2004). But The design of the clarinet was improved by the end of the eighteenth century, and today shape of it, is the result of these long history.

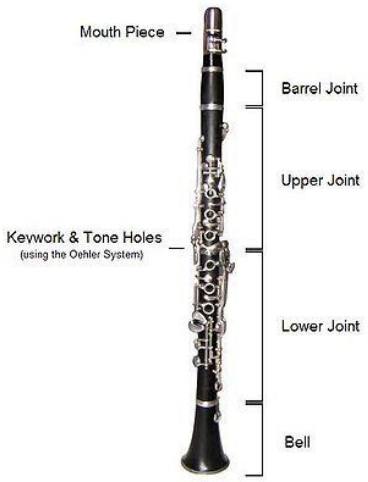

Figure 1—The Construction of Clarinet.

Even if during barock or classical area many woodwinds were built using local wood species as boxwood maple or plum, the tradition has shifted to the use of hard exotic woods. Grenadilla, Rosewood, African Black Wood *(Dalbergia Melanoxylon)* or Ebony are now of very common use .During the twentieth century, the number of industrially produced woodwinds has increased and the ask for more and more quantity of Rosewood leads to the use of too young trees as well to a quality decrease of the wood itself. Clarinet bodies have been made from a variety of materials including wood, plastic, hard rubber, metal, resin, and ivory. But the vast majority of professional musicians believe that the unique acoustical properties of wood and its aesthetic appeal still make it the best material of choice for Clarinet. So, the best and appropriate clarinets used by clarinettist are made from African hardwood especially African Black Wood *(Dalbergia Melanoxylon).* Although, there are a lot of suitable African hardwood, but among them *Dalbergia Melanoxylon* because of its suitable acoustical properties has been incomparable and has the extent used.

Iran as one of the ancient country has a vast history of music and a variety of musical instruments. Among them, there are lots of Woodwind, String, and Percussion… instruments which have been passed on from generation to generation for centuries. Besides in south part of IRAN, there are some regions which have Dalbergia Sissoo, SHISHOM.

Therefore, in this paper the feasibility of using Dalbergia Sissoo, SHISHOM as an Iranian Dalbergia, in making Clarinet was under question. We focused on Acoustic Coefficient (K) and Sound velocity (V), as two important indicators of acoustic performance. This work will lead to a better knowledge of the acoustic behavior of Dalbergia Sissoo , so that the practicable and feasibility of Dalbergia Sissoo in making clarinet were investigated. Hence, IRAN can have lot to say with Dalbergia Sissoo in Clarinet making industry.

Materials and Methods

Specimens

The wood for making Clarinet, studied in this research was SHISHOM (Dalbergia Sissoo) which was in the same species that was chosen by prosperous Clarinet makers around the world. SHISHOM trees are abundant in the sothern part of Iran.

Twenty (20) clear bars were selected from this species in accordance with ISO 3129 standard. 1 meter in lenght and 3 centimeter diameter bars were cut beginning from breast height diameter of the tree. The specimens were conditioned at 22ºC and 65% relative humidity (R.H.) for two week.

Flexural Vibration Test

To obtain the properties of *Young's modulus and acoustic coefficient,* free-free flexural vibration tests were performed, in accordance with fast Fourier transform analyses and Timoshenko beam theory (Bordonné 1989, Brancheriau et al., 2002, Brémaud 2008). *Sound Velocity (V)* was calculated using MATLAB® 7.1 software. *Density* was calculated simultaneously using the direct method. The specimens rested on soft thin rubber, and individual impacts were made on the cross section to generate flexural vibration. Sounds were recorded using Audacity® software at a sampling rate of 44100 Hz (Figure 2).

Figure 2 — Schematic view of the most common setup for free vibration on a free-free bar test. Sound was recorded at one free end, and hammer impact excites the bar on the other free end (ASTM C1548-02)

Then, the three first modes of vibration were obtained from Fast Fourier Transform spectrum (Figure3).

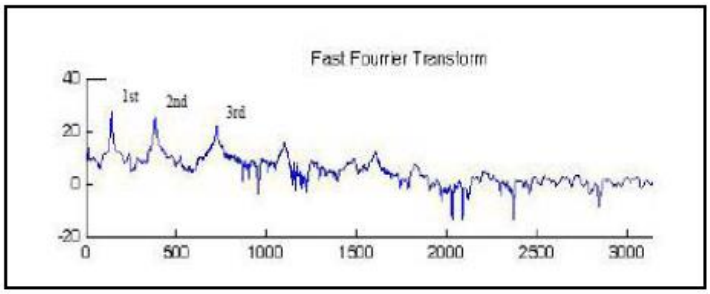

Figure 3— Fast Fourier Transform (FFT Spectrum) - Three first modes of vibration. Y-axis corresponding to Amplitude in dB and X-axis the frequency in Hz.

Young's moduli were calculated using the Timoshenko beam equations (Bordonné 1989, Brancheriau et al., 2002, Roohnia et al., 2010) Eq. (1), and the acoustic coefficient was then obtained from the modulus of elasticity (E) and density.

$$a_n = \left(\frac{E}{\rho}\right) - \left(\frac{E}{K \times G}\right) b_n \qquad (1)$$

where $\boldsymbol{\rho}$ is density (kg/m3), E is modulus of elasticity (Pa), and $\boldsymbol{G}$ is shear modulus (Pa), $\boldsymbol{K}$ is shape index (for prism 0.883) and $\boldsymbol{a}$n and $\boldsymbol{b}$n are:.

$$a_n = \frac{[4\pi^2 l^2 f_n^2 (1 + F_{1n})]}{m_n^4} \qquad (2) \qquad \text{and} \qquad b_n = \frac{4\pi^2 l^2 f_n^2 F_{2n}}{m_n^4} \qquad (3)$$

where f_n is the frequency of the nth mode, and m is the nth result of $\cos(m_n)\cdot\cosh(m_n)=1$.

$$F_{1n} = \Theta^2(mn) - 6\Theta\ (mn) \qquad (4)$$

$$F_{2n} = \Theta^2(mn) - 2\Theta\ (mn) \qquad (5)$$

$$\Theta_{m_n} = \left| \frac{m_n.\tan(m_n).\tanh(m_n)}{\tan(m_n)-\tanh(m_n)} \right| \qquad (6)$$

Considering the a_n and b_n parameters Eq.(2) and Eq.(3), the Young's moduli were obtained from a linear regression. The acoustic coefficient was then obtained from Eq. (7) (Tsoumis 1991, and Yoshikawa 2007):

$$K = \sqrt{\frac{E}{\rho^3}} \qquad (7)$$

where K represents the acoustical coefficient, E corresponds to the modulus of elasticity in MPa, and ρ is the density in g/cm3. The Sound Velocity (V) which describes the speed of longitudinal waves in wood, also characterizes the transverse vibrational frequencies, is defined as the root of the material's Young's modulus, E (Mpa), divided by the material's density ρ (g/cm^3). (Bremaud 2008, Obataya 2000).

$$V = \sqrt{\frac{E}{\rho}} \qquad (8)$$

Results

The results of studied parameters: Density (ρ) , Young's modulus (E), Acoustic Coefficient (K), and Sound Velocity (V) for Shishom are shown in Table 1.

Table 1— Data of studied parameters

	Density (ρ) gr/cm^3	Young's modulus (E) Gpa	Acoustic Coefficient (K)	Sound Velocity (V) m/s
1	1.11	17.8	190.18	569
2	1.18	18.9	188.99	621
3	1.09	19	187.81	605
4	1.01	17.7	184.98	589
5	1.13	18.7	178.91	567
6	1.13	18.1	186.76	548
7	1.09	18.5	183.45	609
8	1.12	19	185.65	579
9	1.14	18.7	187.77	591
10	1.09	17.9	179.41	611
11	1.09	19	184.43	602
12	1.11	19.1	184.56	571
13	1.12	17.7	179.91	579
14	1.12	17.7	179.89	563
15	1.16	18.4	181.89	581
16	1.14	18.1	186.25	609
17	1.13	17.8	183.33	598
18	1.15	19	186.99	574
19	1.18	18.4	185.28	556
20	1.11	18.7	181.93	607
Means	1.11	18.41	186.05	588

Clarinet was made by African Black Wood *(Dalbergia Melanoxylon)* for many years. Makers use their experience to select the best woods that could be used to make Clarinet. (Table 2)

Table 2— Data of African Black Wood (Refrence: Wood Database, lumber identification, 2012 http:/www.wood-database.com/lumber identification.)

	Density (ρ) gr/cm^3	Young's modulus (E) Gpa	Acoustic Coefficient (K)	Sound Velocity (V) m/s
Means	1.08	17.95	119.83	128

Table 1 defined four main properties of Shishom which characterized it in the world of Clarinet making: first its Density and second its Young's Modulus and then its Acoustic Coefficient and Sound Velocity as the two important acoustic factors to choose woods for making clarinet. On the other hand, acoustic properties of African Black Wood *(Dalbergia Melanoxylon)* are shown in table2. It can be figured out, acoustic properties of Shishom *(Dalbergia Sissoo)* are not lesser than African Black Wood *(Dalbergia Melanoxylon)*, and in all of them have the higher value.

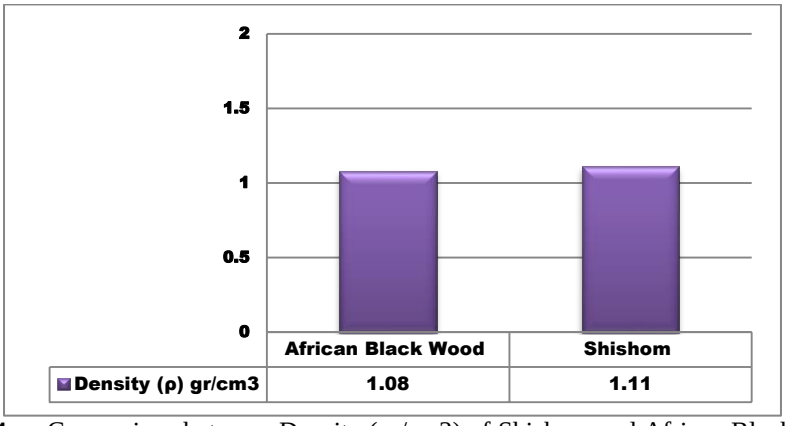

Figure 4 — Comparison between Density (gr/cm3) of Shishom and African Black Wood.

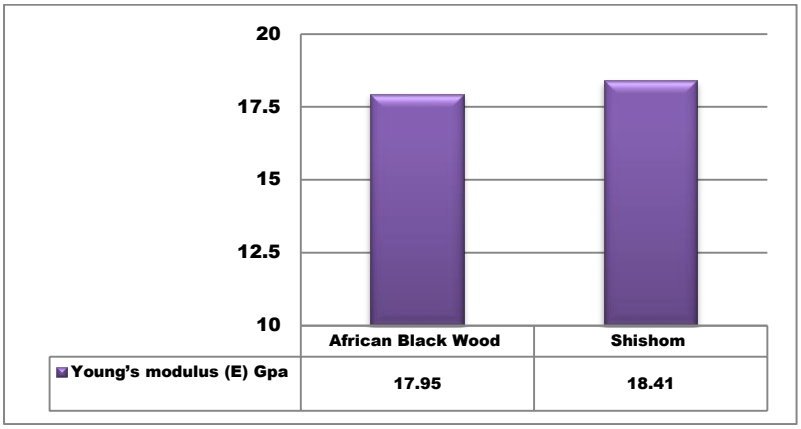

Figure 5 — Comparison between Young's Modulus (Gpa) of Shishom and African Black Wood.

Comparative studies between density and young's modulus were defined that the means of Shishom specimens density were higher than African Black Wood (Figure 4). There was not a little difference between the means of density in both of them. So, this will lead to pay attention to the density of Shishom as important parameter in making Clarinet. Furthermore, Shishom had also higher Young's modulus in comparison with African Black Wood (Figure 5). So, higher Density and Young's modulus of Shishom must consider.

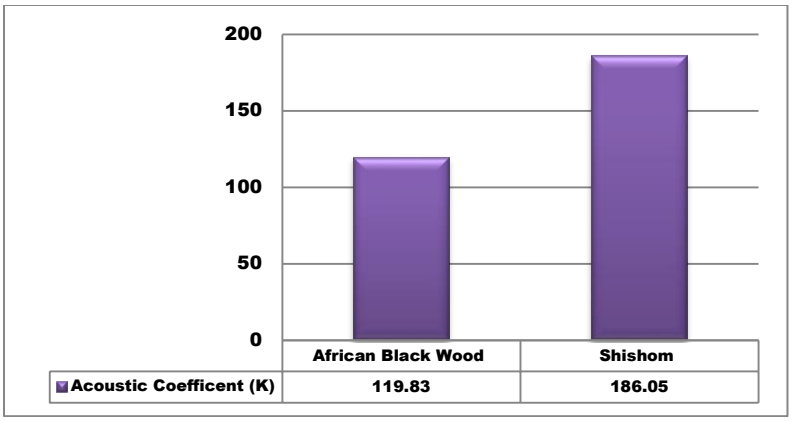

Figure 6 — Comparison between Acoustic Coefficient (K) of Shishom and African Black Wood.

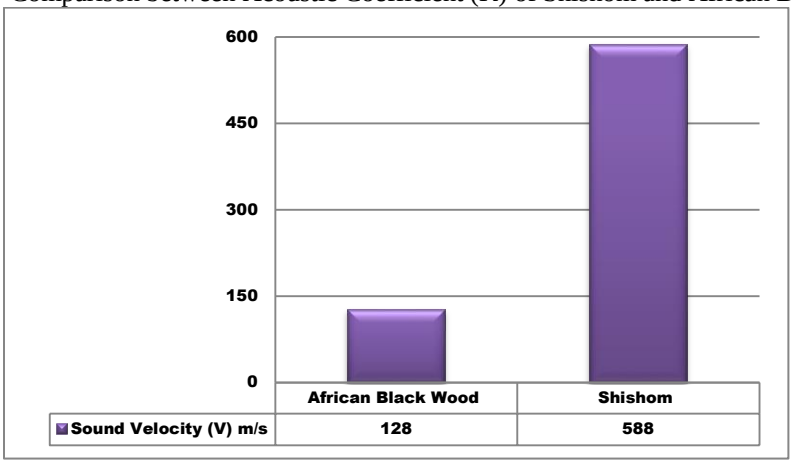

Figure 7 — Comparison between Sound Velocity (V) m/s, of Shishom and African Black Wood.

Comparing the results of acoustic coefficient and sound velocity of both defined that Shishom had higher acoustic coefficient and sound velocity than African Black Wood. (Figure 6 and 7) Higher acoustic coefficient and sound velocity of Shishom were consequence of its higher young's modulus and the portion of this parameter in the acoustic coefficient and sound velocity formula.

Discussions

The results showed that Shishom like African Black Wood as a traditional material for making Clarinet have a density more than 1.00 gr/cm3. Talgorn et al (2010) have also summarized ideal Clarinet bar type which was characterized by a high density. Thus, when playing, the wood's high density could reduce the swaying wave which could affect the player's performance. As it defined Density of Shishom is somewhat higher than African Black Wood and this will lead to one of its privilege for using in Clarinet making.

Young's modulus, which does not depend on frequency, generally increases with increasing density of the wood, which becomes vital when considering use of the wood for the musical instruments materials. Talgorn et al (2010) have summarized that the ideal bar type which was characterized by a high Young's modulus for a bar cut along the grain. The pitch depends on the square root of the ratio of E and q. The ratio is also referred to as the specific Young's modulus (E/q) [Holz 1974, 1996]. African Black Wood as a traditional material for making Clarinet has a Young's modulus more than 17 GPa. It could be summarized that the value of Young's modulus of wood which is used to make the Clarinet might be greater than 17 GPa. On the other hand, Shishom specimens have a Young's modulus greater than 18 GPa. While their density were higher than traditional material for making Clarinet. This will lead to know that Shishom could be use as one material for making Clarinet, because of its greater Young's modulus.

But, this implies that there are other factors that contribute to the quality of the wood used for making Clarinet.
Sounds wave have better quality in the mediums in consequence of the high Young's Modulus of the mediums [Bremaud. 2007]. The results showed that Shishom specimens have a higher Sound Velocity than African Black Wood. This is the results of its higher Young's modulus. Thus, sounds have better propagation in Shishom..
Acoustic coefficient is the ratio between Young's modulus and density, and it is another factor to show the acoustic performance of the woods. Higher acoustic coefficient will lead to a better acoustic performance Yoshikawa. 2007]. The results showed that African Black Wood have lower acoustic coefficient than Shishom specimens. It was figured out that Shishom in mechanical properties (Density and Young's Modulus) and also two main acoustic properties (Sound Velocity and Acoustic Coefficient) have higher value than African Black Wood and It means that Shishom is a good choice for making Clarinet.

Conclusion

This research was carried out to determine the significant acoustic properties of the Dalbergia Sissoo (Shishom) required making Clarinet. When the Clarinet is being played, it must do two things. First, it must maintain a specific normal frequency by vibrating. Second, it has to resonate and distribute sound waves into the surroundings, which come from the mechanical vibration. African Black Wood is the traditional material for making Clarinet for many years. The results from this research clearly indicate that the Acoustic quality of the wood for making Clarinet and its resonator Bar must have two main characteristics besides high Density and Young's Modulus. These are Acoustic Coefficient (K), and Sound Velocity (V). Thus, high Acoustic coefficient, and high Sound velocity can lead to a better acoustic performance of the wood required to make Clarinet.
Furthermore, African Black Wood as a traditional material to make Clarinet is one of the preserved species and makers have lots of problems to supply their demand. So, comparative studies between African Black Wood and Shishom (as an abundance species in south of Iran) were explored. The results from this research clearly indicate that Shishom have better values in Young's modulus, Density, Acoustic coefficient, and Sound velocity than African Black Wood. So, Shishom had a better acoustic performance than African Black Wood.
Therefore, Dalbergia Sissoo (SHISHOM) is a good choice and somewhat suitable material in making Clarinet. So, IRAN as a country with vast history of music and also a variety of musical instruments can have lot to say with Dalbergia Sissoo in Clarinet making industry.

References

Bordonné, P.A. 1989. Measurement of Dynamic Modulus of Wood by Free Flexural Vibration Test. Nancy University. 154-156 p. PhD Thesis

Brancheriau, L. 2002. Natural vibration analysis of clear wooden beams: a theoretical review. Journal Wood Science and Technology. 36 .347–365

Brémaud, Iris. 2007. A database linking woody species, vibrational properties, and uses in musical instruments of the world .International Symposium on Musical Acoustics. Barcelona, Spain.

Brémaud, I. 2008. Mechanical characterization of woods and instruments making: origins and compilation of variability. Journal d'étude Le bois : instrument du patrimoine musical – Cité de la Musique, 24- 46 p.

Bucur, V. 2006 .Acoustic of wood, Springer-Verlag, Berlin Heidelberg, Germany. 343p.

CONARD, N. J. 2004. Eine Mammutelfenbeinflo¨ te aus dem Aurignacien des Geißenklo¨ sterle. Archa¨ologisches Korrespondenzblatt 34: 447–462.

CROSS, I. 2001. Music cognition, culture and evolution. Annals of the New York Academy of Sciences 930: 28–42.

DARWIN, C. 1871. The descent of man and selection in relation to sex. John Murray, London, England.70p.

Holz. D. 1974. On some important properties of non-modified coniferous and leaved woods in view of mechanical and acoustical data in piano soundboards. Archiwun Akustyki Journal. 9:37–57

Holz. D. 1996. Acoustically important properties of xylophone-bar materials: can tropical woods be replaced by European species? Acta Acustic Journal. 82:878–884

Obataya, E. 2000. Vibrational properties of wood along the grain. Journal of Material Science 35 :2993 – 3001.

Roohnia, M. Yavari, A. Tajdini, A. 2010. Elastic Parameters of Poplar Wood with End-Cracks, J. Annal Forest Science. 67(409):1- 6.

Talgorn B, Gibiat V, Dubrisay D, Selmer J,Halary JL. 2010. Acoustic and Mechanical Modified Wood Characterization for Woodwind Use. Proceedings of 20th International Congress on Acoustics, Sydney, Australia: 23-27.

Tsoumis, G. (1991) . Science and technology of wood, 1st Ed., Van Nostrand Reinhold, New York. 204-207p.

Wood- Sampling Methods and General Requirements for Physical and Mechanical Tests – 1975-11-01- International Standard ISO 3129.

Wood Database, lumber identification, 2012 http:/www.wood-database.com/lumber identification.

Yoshikawa, Sh. 2007. Acoustical classification of woods for string instruments, Journal of Acoustic Socity 122: 568-573.

Patented nondestructive evaluation technology developed by the Forest Service for use in the wood products industry

Robert J. Ross
USDA Forest Service Patent Program, 1 Gifford Pinchot Drive, Madison, Wisconsin
rjross@fs.fed.us

Xiping Wang
USDA Forest Service Patent Program, 1 Gifford Pinchot Drive, Madison, Wisconsin
xwang@fs.fed.us

Janet I. Stockhausen
USDA Forest Service Patent Program, 1 Gifford Pinchot Drive, Madison, Wisconsin
jstockhausen@fs.fed.us

Linda K. Schramer
USDA Forest Service Patent Program, 1 Gifford Pinchot Drive, Madison, Wisconsin
lkschramer@fs.fed.us

Joseph Wszalek
USDA Forest Service Patent Program, 1 Gifford Pinchot Drive, Madison, Wisconsin
jwszalek@fs,fed.us

Ieng-Yi Chen
USDA Forest Service Patent Program, 1 Gifford Pinchot Drive, Madison, Wisconsin
lengyichen@fs.fed.us

Abstract

Nondestructive Evaluation (NDE) technology is now a valuable part of the harvesting and manufacturing process for improved quality and consistency of the wood products produced. The Forest Service (FS) has developed and patented several NDE technologies applicable to the wood products industry. These patents allow wood harvesters and manufacturers to measure the physical and mechanical properties of wood material while still using the wood for its intended use. These patents put FS in a unique position to promote the research, development, and use of NDE technology, and to encourage environmentally-responsible practices, within the lumber and wood industry.

Keywords: patent, nondestructive evaluation, technology, Forest Service

Introduction

Traditionally, testing the physical and mechanical properties of wood and wood products was expensive, impractical on a large scale, and required either taking physical samples from the source or destroying the

material. However, recent developments in the field of Nondestructive Evaluation (NDE) technology allow for fast, reliable, and inexpensive testing of live and cut wood that does not harm or damage the product. NDE technology has become a critical part of the harvesting, manufacturing, and research, relating to wood products. The economic benefits of improved quality and consistency when using NDE on wood products are considerable. The Forest Service (FS), part of US Department of Agriculture, holds patent rights to NDE technologies (a*ppendix 1*) that make it possible for wood producers, harvesters, and manufacturers to measure the physical and mechanical properties of wood material while still using the material for its intended use. Additionally, FS encourages environmentally responsible practices within the lumber and wood industry and the use of NDE is one way to accomplish that goal.

Technology transfer in the Forest Service

The federal government fosters research and development of technology to promote collaboration between the federal laboratories, universities and/or industrial cooperators. Transfer of technology to the marketplace is the goal, as this creates jobs and the American economy benefits. These activities are governed by federal laws. The first law in a continuing series on federal technology transfer is the Stevenson-Wydler Technology Innovation Act of 1980 which promotes and defines technology transfer. The Act made it easier for federal laboratories to transfer technology to nonfederal parties and provided outside organizations with a means to access federal laboratory developments. The primary focus of the Stevenson-Wydler Act was to get federal laboratories more involved in the technology transfer process, which in turn helped with the dissemination of information from the federal government. The law requires laboratories to take an active role in technical cooperation.

The next applicable law is the Bayh-Dole Act of 1980 which established more boundaries regarding patents and licenses for federally funded research and development. Small businesses, universities, and not-for-profit organizations were allowed to obtain title to inventions developed with federal funds. Government-owned and government-operated (GOGO) laboratories were permitted to grant exclusive patent licenses to commercial organizations.

A particularly useful law is the Federal Technology Transfer Act of 1986 which was the second major piece of legislation to focus directly on technology transfer. All federal laboratory scientists and engineers are required to consider technology transfer an individual responsibility, and technology transfer activities are to be considered in employee performance evaluations. In addition, the law enabled government-owned and government-operated (GOGO) laboratories to enter into Cooperative Research and Development Agreements (CRADAs) and to negotiate licensing arrangements for patented inventions made at the laboratories. It also required that government-employed inventors share in royalties from patent licenses. Further, the law provided for the exchange of personnel, services, and equipment among federal laboratories and nonfederal partners. Other specific requirements, incentives and authorities were added, including the ability of GOGO laboratories to grant or waive rights to laboratory inventions and intellectual property, and permission for current and former federal employees to participate in commercial development, to the extent that there is no conflict of interest.

Lastly, Executive Order 12591 (1987) was signed which facilitates access to science and technology by requiring that federal laboratories and agencies assist universities and the private sector by transferring technical knowledge. The Order required agency and laboratory heads to identify and encourage individuals who would act as conduits of information among federal laboratories, universities, and the private sector. It also underscored the government's commitment to technology transfer and urged GOGOs to enter into cooperative agreements to the limits permitted by law. The Order also promoted commercialization of federally funded inventions by requiring that, to the extent permitted by law,

laboratories grant to contractors the title to patents developed in whole or in part with federal funds, as long as the government is given a royalty-free license for use.

Background on the NDE industry

NDE technology allows wood producers, harvesters, and manufacturers to measure the physical and mechanical properties of a piece of wood without destroying the wood's future utility. NDE technology serves the integral function of optimizing the volume and quality of output from each tree saving both time and money in research, product evaluation, resources, and troubleshooting. NDE technology, and in particular scanning technology, is essential to measure sawn, peeled, sliced, or chipped products and to optimize sorting and further conversion. *See Figures 1 and 2 below*. NDE technology also allows for the optimal use of materials with varying internal properties and ensures that resulting products can be provided with consistent properties. NDE technology can evaluate each individual log or piece of wood and determine the most appropriate use for that log's shape and growth characteristics.

Figure 1 - An ultrasonic wood scanning machine, assigned to FS in U.S. Patent 6, 276, 209, "System and method of assessing the structural properties of wooden members using ultrasound." This NDE technology uses vibrations to measure the internal structure of wooden planks.

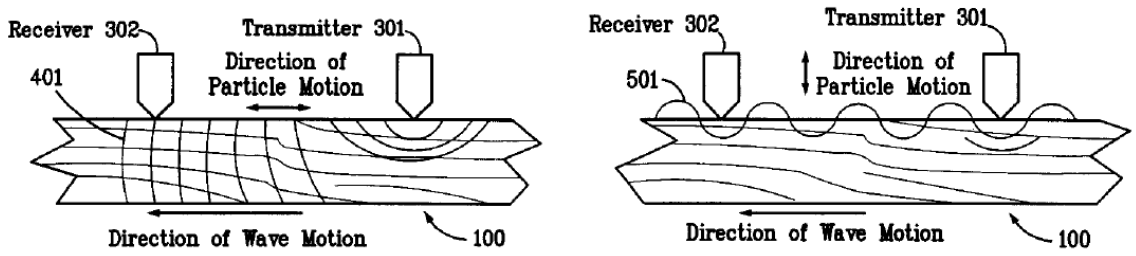

Figure 2 - A schematic showing the mechanism by which the NDE technology measures the wood's internal quality as shown in U.S. Patent No. 6,276,209 which ws jointly developed by FS and an industrial collaborator.

NDE technology contributes significantly to the U.S. economy. The total U.S. market for NDE technology was valued at nearly $2.5 billion in 2010, and is expected to be more than $2.3 billion by 2015 (BBC Research 2010). The wood products industry supports over a million jobs in the U.S. alone (Ritter and Skog 2011) so NDE technology is a key component of the domestic job market.

Impact on the NDE Industry

Originally, scanning technology had been used only in sawmills and veneer plants to maximize volumetric yield, detect usable area, and eliminate wane in edging of boards. Now, by using the FS developed NDE technology, harvesters and processors can evaluate the internal quality of logs and trees prior to processing. Knot detection, grain direction, growth rate, and density are all key factors in determining timber value, and the timber industry can use its knowledge of these factors to maintain high-quality output and to maximize market value. Despite the value of on-site NDE technology, however, few harvesters or processors have the financial means or research capacity to develop their own NDE technology.

Additionally, FS collaborates with universities and companies to develop new NDE technologies. These collaborations benefit all the parties involved: it allows the universities to do additional relevant research and companies to develop their technology more quickly. It also can provide mechanisms for protecting any intellectual property developed during the collaboration. *See Figure 3 below*.

Figure 3 - A schematic showing fibre-gen's "Hitman" automated system in which the NDE technology is mounted on field machinery and located within the harvester head and allows foresters to select and cut lumber based on wood stiffness because it enables real-time acoustic testing in operations.

For example, FS, a university, and an industrial collaborator jointly own NDE patents for standing timber. *See Figure 4 below.* The industrial collaborator is now commercializing the technology.

Figure 4 - A handheld NDE device capable of measuring the internal quality of standing timber. This product was developed using U.S. FS Patent No. 7,418,866 which was jointly developed and is jointly owned by FS and an industrial collaborator.

Conclusion

FS has played an invaluable role in the development and promotion of NDE technology throughout the wood products industry. Acoustic testing has become the industry standard for stiffness measurement. These technologies have made it possible to produce products that are more consistent and higher quality. The FS patents allow companies to participate in the NDE market and the FS's long history of academic

and commercial collaboration has developed technology that is revolutionizing the wood products industry.

References

BBC Research LLC. 2010. Nondestructive Testing http://bccresearch.wordpress.com/2010/11/23/u-s-market-for-ndt-technologies-to-reach-2-3-billion-in-2015/

Ritter MA, Skog K, Bergman R. 2011. Science supporting the economic and environmental benefits of using wood and wood products in green building construction. U.S. Department of Agriculture, Forest Service.

U.S. Patent No. 6,276,209 entitled, “System and Method of Assessing the Structural Properties of Wooden Members.”

U.S. Patent No. 7,418,866 entitled, “Method and Apparatus for Evaluation of Standing Timber.”

NONDESTRUCTIVE EVALUATION PATENT PROSECUTION HISTORY
ROSS, et. al.
Updated July 30, 2013

Parent Application

SN:	06/843,717
Date Filed:	March 25, 1986
Title:	Method and Apparatus for Non-destructive Evaluation of the Mechanical Properties of Composite Materials
Inventors:	Pellerin & Ross
Issued:	June 13, 1989
Patent No.:	4,838,085
Status:	**Expired** on 6/13/2006. All maint. fees paid through expiration.
Assignee:	Washington State University Research Foundation, Inc.

Continuation in Part of S/N: 06/843,717

SN:	07/365,218
Date Filed:	June 12, 1989
Title:	Non-destructive Evaluation of Structural Members
Inventors:	Pellerin & Ross
Issued:	June 18, 1991
Patent No.:	5,024,091
Status:	**Expired** on 6/12/2009. All maint. fees paid through expiration.
Assignee:	Washington State University Research Foundation, Inc

Parent Application

SN:	07/857,146
Date Filed:	March 25, 1992
Title:	Method and Apparatus for Evaluating the Drying Properties of Un-Dried Wood
Inventors:	Ross
Issued:	May 3, 1994
Patent No.:	5,307,679
Status:	**Expired** on 5/3/2002 for failure to pay maint. fee
Assignee:	US Forest Service

Child Application

SN:	08/147,522
Date Filed:	Nov. 5, 1993
Title:	
Inventors:	Ross
Status:	**Abandoned**

Parent Application

SN:	07/912,391
Date Filed:	July 13, 1992
Title:	Method and Apparatus for In Situ Evaluation of Wooden Members
Inventors:	Ross, DeGroot, Geske, Nelson, Malinauskas, Cuevas
Issued:	March 14, 1995
Patent No.:	5,396,799
Status:	**Expired** on 3/14/2003 for failure to pay maint. fee
Assignee:	US Forest Service

Title (Utility 09/151,432):	Ultrasonic Apparatus for Characterizing Wooden Members Using a Measurement of Wave Distortion
Title (Utility 09/196,674):	Method and Apparatus for Detecting and Characterizing Splits in Logs
Title (Utility 09/196,674):	Method and Apparatus for On-Line Monitoring of Log Sawing
Title (Divisional 09/800,551):	Method and Apparatus for On-Line Monitoring of Log Sawing
Title (Divisional 09/882,446):	Method and Apparatus for Detecting and Characterizing Splits in Logs
Title (International):	Ultrasonic Apparatus for Characterizing Wooden Members
Inventors:	Shafer and Ross
Assignees:	USDA, U.S. Natural Resources Inc. (formerly Perceptron Inc.)

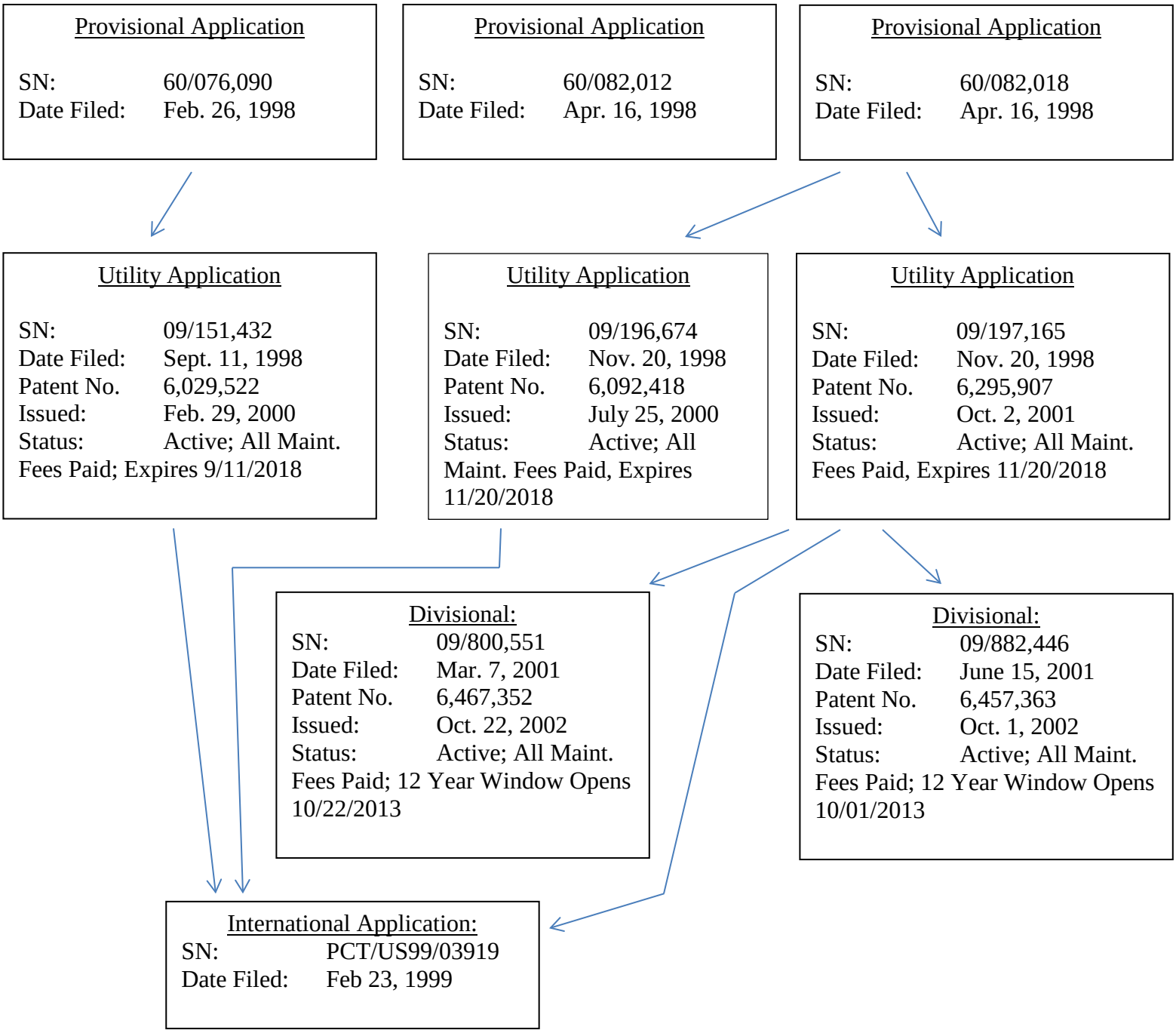

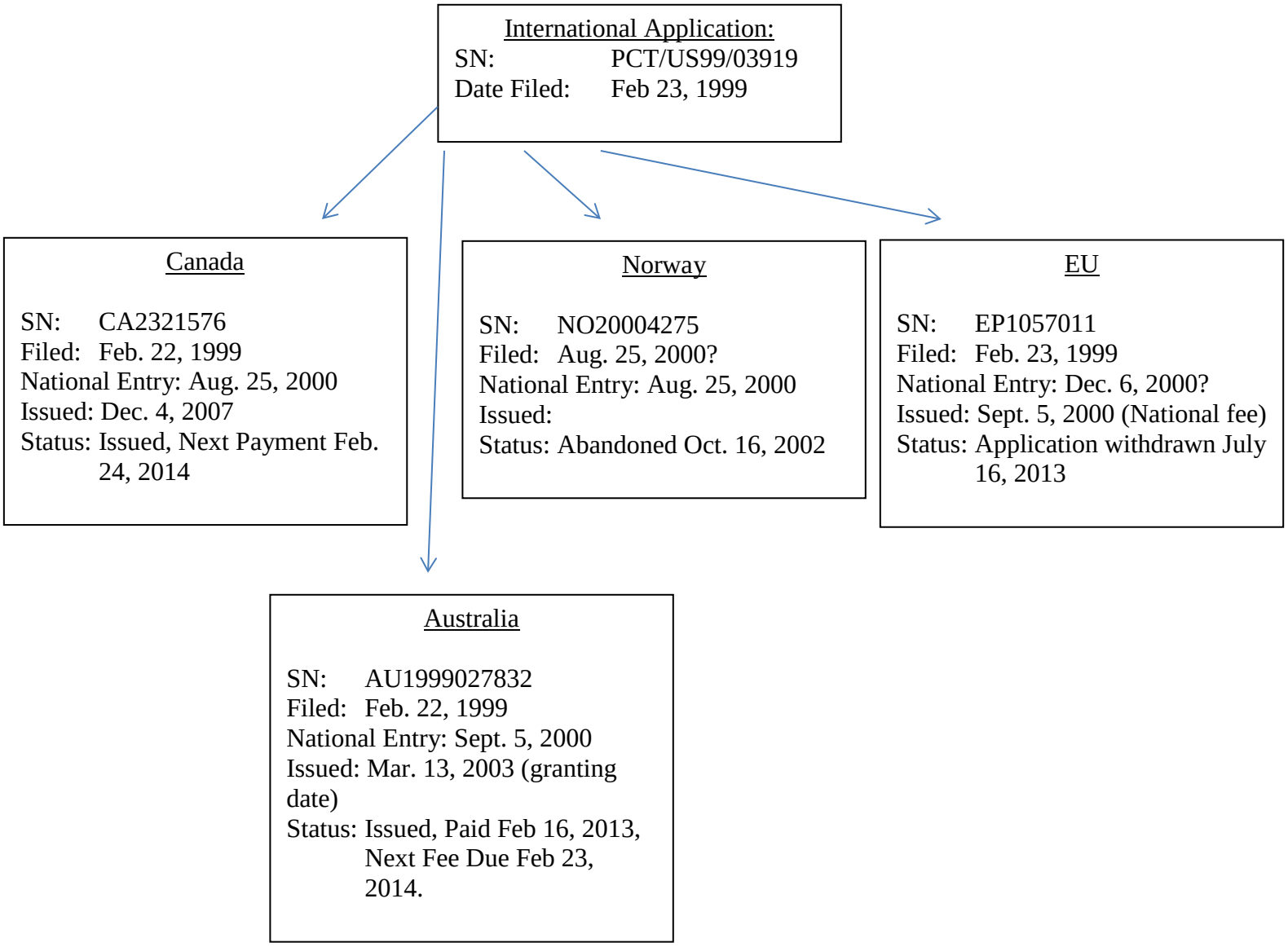
International Application:
SN: PCT/US99/03919
Date Filed: Feb 23, 1999
Canada
SN: CA2321576
Filed: Feb. 22, 1999
National Entry: Aug. 25, 2000
Issued: Dec. 4, 2007
Status: Issued, Next Payment Feb. 24, 2014
Norway
SN: NO20004275
Filed: Aug. 25, 2000?
National Entry: Aug. 25, 2000
Issued:
Status: Abandoned Oct. 16, 2002
EU
SN: EP1057011
Filed: Feb. 23, 1999
National Entry: Dec. 6, 2000?
Issued: Sept. 5, 2000 (National fee)
Status: Application withdrawn July 16, 2013
Australia
SN: AU1999027832
Filed: Feb. 22, 1999
National Entry: Sept. 5, 2000
Issued: Mar. 13, 2003 (granting date)
Status: Issued, Paid Feb 16, 2013, Next Fee Due Feb 23, 2014.

Title: System and Method of Assessing the Structural Properties of Wooden Members Using Ultrasound
Inventors: Schafer, Ross, Erickson, and DeGroot
Assignees: US Natural Resources Inc (formerly Perceptron Inc.), and USDA Forest Service

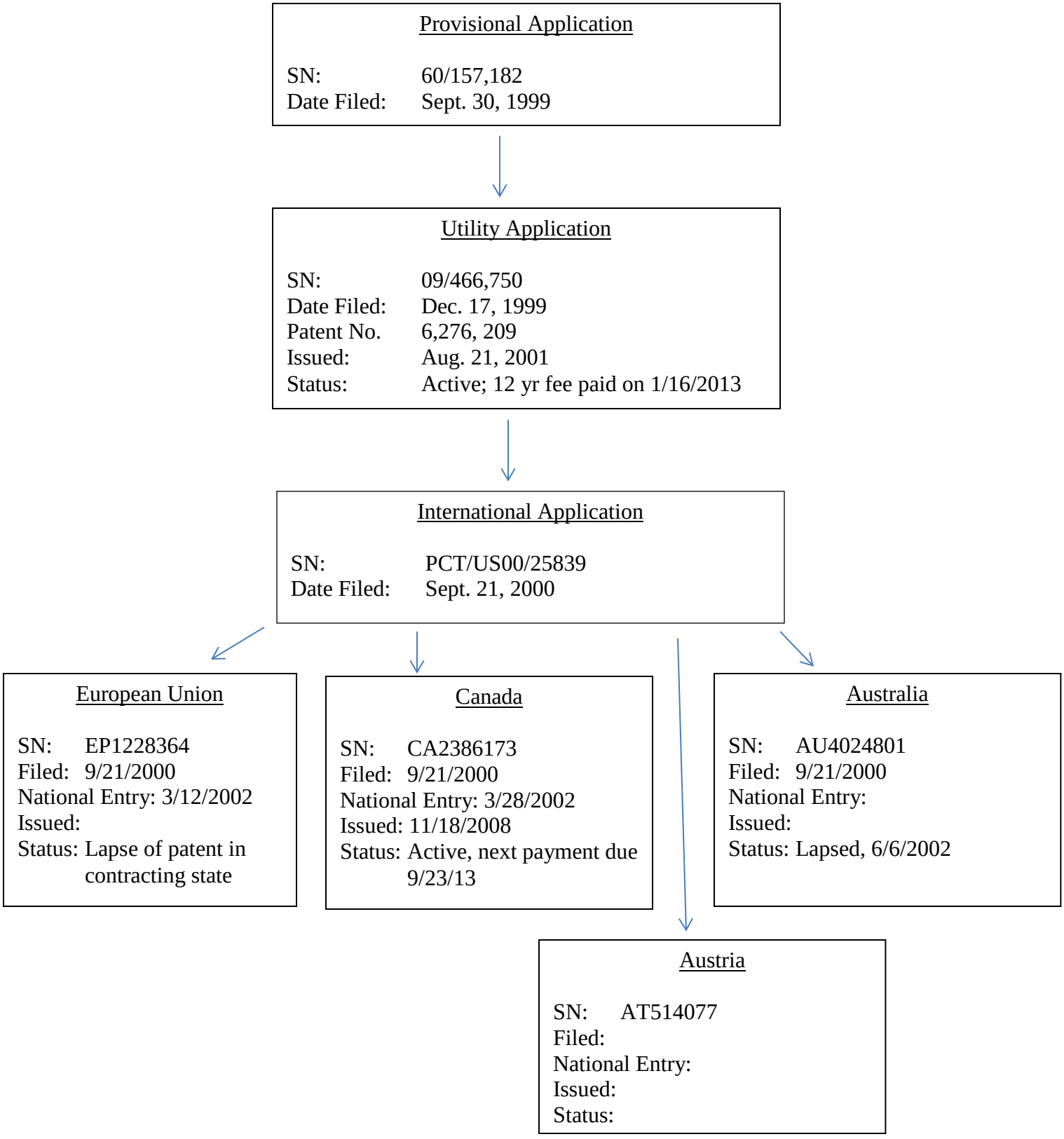

Title: System and Method for Performing Nondestructive Evaluation Techniques on a Log or Round Timber
Inventors: Wang, Ross, Mattson, Erickson, Forsman, Geske & Wehr
Assignees: Michigan Technological University and USDA Forest Service

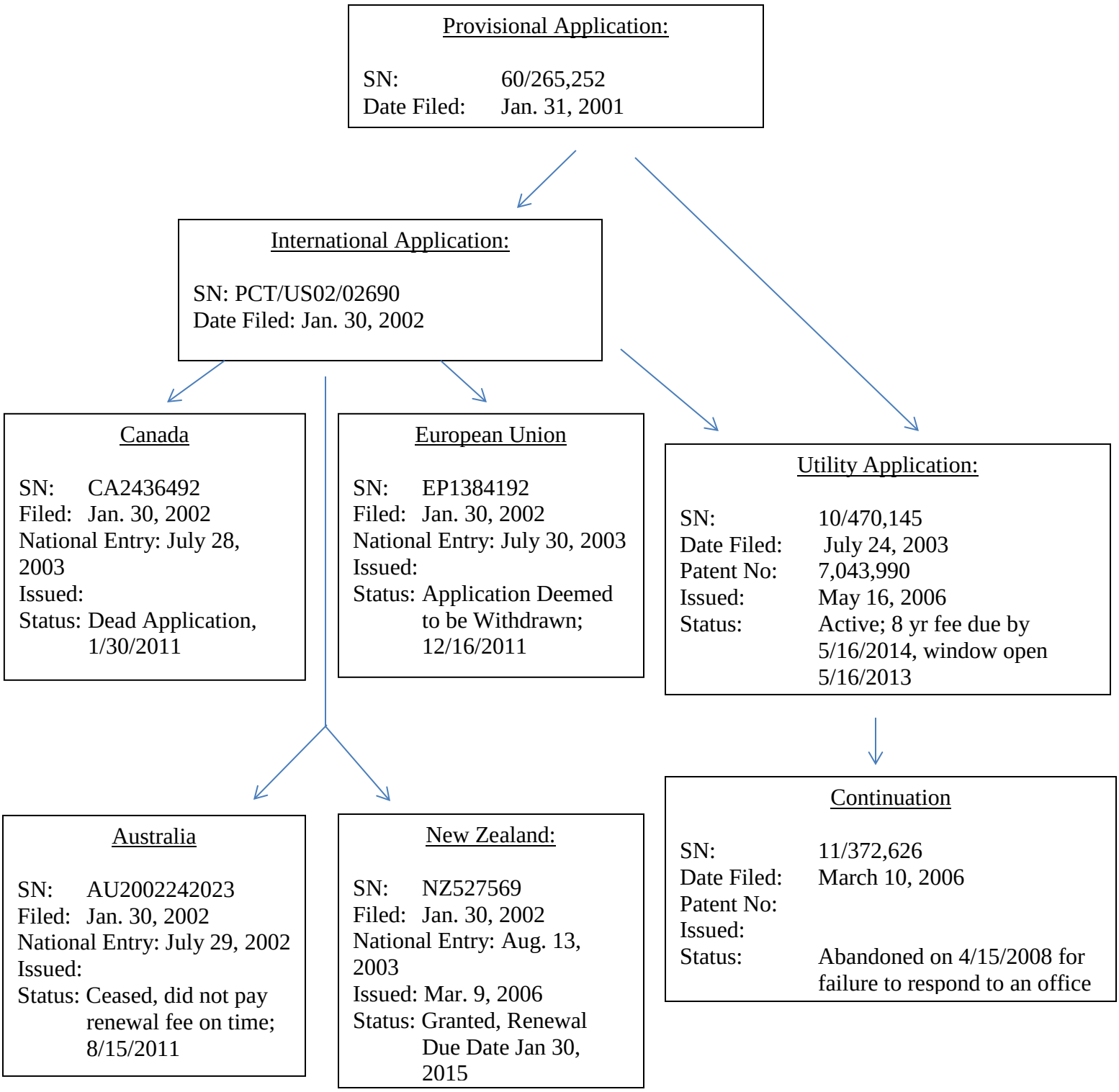

Title: Method and Apparatus for the Evaluation of Standing Timber
Inventors: Wang, Ross, Carter, Sharplin
Assignees: University of Minnesota, fibre-gen, and USDA Forest Service

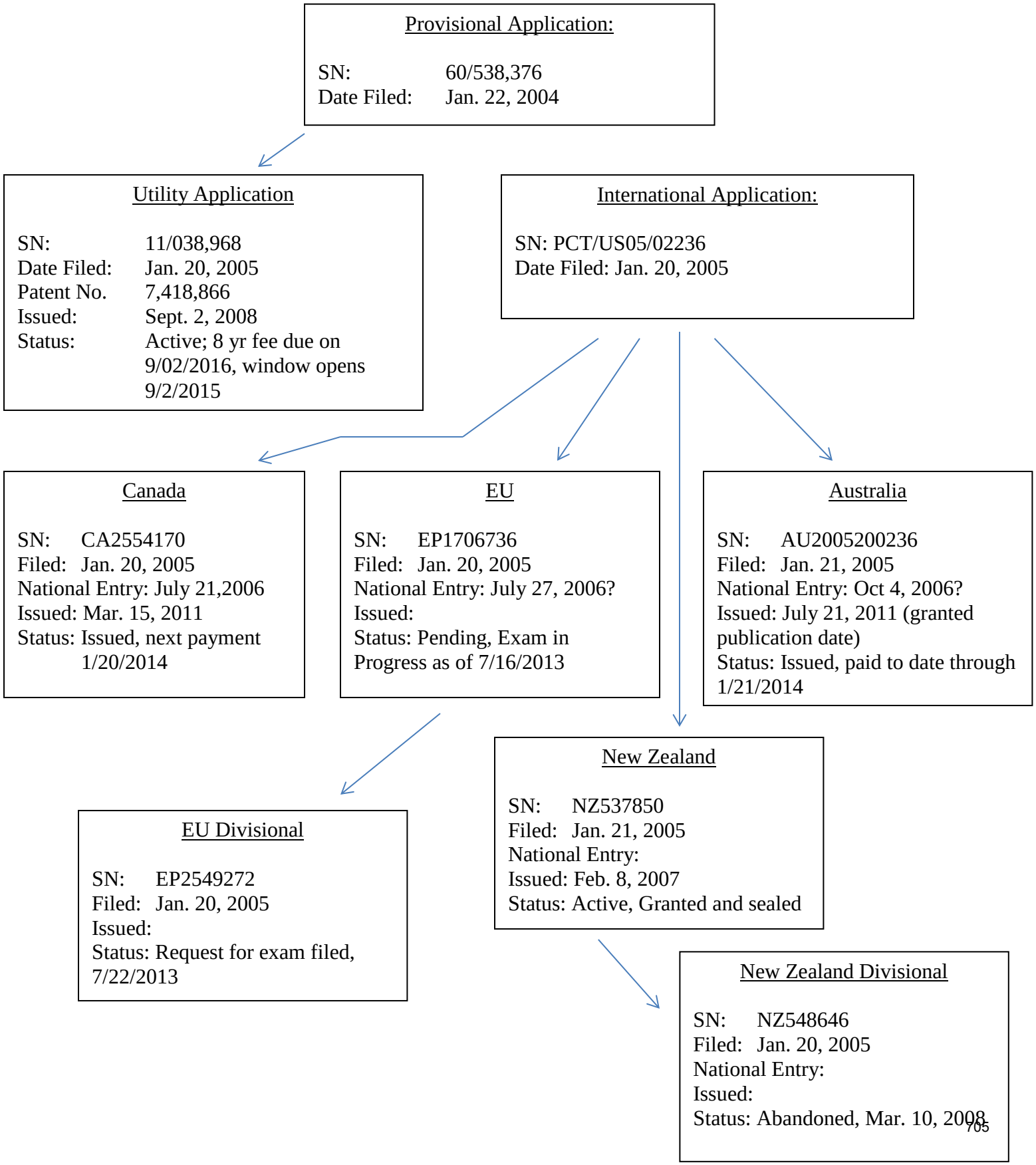

Indirect Detection of Internal Defects in Wood with Ultrasound

Sang-Joon Lee
Dept. of Forest Products, Korea Forest Research Institute, Seoul, Korea, lsjoon@forest.go.kr

Chul-Ki Kim
Dept. of Forest Sciences, Seoul National University, Seoul, Korea, aries8924@hanmail.net

Sung-Jun Pang
Dept. of Forest Sciences, Seoul National University, Seoul, Korea, pangsungjun@snu.ac.kr

Jung-Kwon Oh
Dept. of Forest Sciences, Seoul National University, Seoul, Korea, jkoh75@hotmail.com

Kwang-Mo Kim
Dept. of Forest Products, Korea Forest Research Institute, Seoul, Korea, lovewood@forest.go.kr

Ki-Bok Kim
Center for Safety Measurement, Korea Research Institute of Standards and Science, Daejeon, Korea, kimkibok@kriss.re.kr

Jun-Jae Lee
Dept. of Forest Sciences, Seoul National University, Seoul, Korea, junjae@snu.ac.kr

Abstract

There are several limitations for applying the conventional TOF (time of flight) analysis of ultrasound even it can give useful and fast results. Only initial period of received ultrasonic signal was concerned for determining the TOF. Several wood scientists have been paid attention to analyze various ultrasonic parameters such as EV (energy value) and PL (pulse length). Many of these approaches have been done under controlled circumstances with small clear wooden specimens.

The purpose of this research was development of quantitative ultrasonic test methodology for detecting internal defects in wood especially members of ancient wooden building. Applicability in field test as well as accuracy should be carefully concerned. And connection part between wooden members and/or contacted or hidden part by wall of ceiling or other construction materials make it hard to apply direct way of ultrasonic test. Therefore indirect way of ultrasonic test needed to be applied. Test methodology with newly developed prototype of ultrasonic system was proposed. Results shows that ultrasonic parameters including RMS voltage and TOF-amplitude show relatively high prediction accuracy with internal defects of tested wooden members.

Keywords: ultrasound, wooden ancient building, indirect detection, TOF(time of flight), ultrasonic parameter

Biological Factors Affecting Wood Durability Performance in Buildings

Kalle Pilt
Estonian Mycology Research Centre, Tartu, Estonia

Uwe Noldt
Thünen Institute of Wood Research, Hamburg, Germany

Ave Sadam
Estonian Mycology Research Centre, Tartu, Estonia

Abstract

Many factors affect durability of wood in existing timber structures. One of the most important factors affecting durability is biological, especially the wood-rotting fungi and wood-destroying insects. This paper gives an overview about fieldworks on Ruhnu Island, Estonia, and investigations on damages of house longhorn beetle, deathwatch beetle, and common furniture beetle in the churches built in 1642 and 1912 AD, respectively. Because both churches are architectural heritage buildings, only nondestructive methods in measuring mechanical properties of timber structures could be used, such as the Resistograph IML-RESI F400. The modeling of timber structures was analyzed with the modern computer design program ArchiCad 12 and engineering program Autodesk Robot Structural Analysis v. 22. Engineering calculations were taken from European Standards. The extent of various damages in two churches built at different time but located in the same environmental conditions was analyzed during discussions. The damage by insects differ by extent and by habitat. In the results, the possibilities of preliminary work for the restoration of old timber structures in architectural heritages are described.

Keywords: Timber wood, durability, fungi, fungus, insect, beetle, cultural heritage, *Serpula lacrymans*, architectural heritage, wood-boring insects, nondestructive method

Near-Infrared Calibrations for Wood Density and Modulus of Elasticity for *Eucalyptus nitens* from Tasmania (Australia)

Mario Vega, Matthew Hamilton
University of Tasmania, Hobart, Tasmania, Australia

Geoff Downes
Forest Quality Pty. Ltd., Hobart, Tasmania, Australia

Chris Harwood
CSIRO

Paul Adams
Forestry Tasmania

Brad Potts
University of Tasmania, Hobart, Tasmania, Australia

Abstract

Eucalyptus nitens is widely planted in temperate regions of the world and the second most planted eucalypt in Australia. There are 208,000 ha planted on the island of Tasmania, mainly for pulpwood, but 10% of the estate has been thinned and pruned for timber and veneer production. However, these plantations are yet to be harvested commercially for these products, and a better understanding of their wood characteristics is required. Wood density and modulus of elasticity (MOE) are key traits that affect the value of E. nitens timber and veneer products. Large-scale assessment of the plantation resource for these traits requires the development of cost-effective sampling techniques for studying within- and between-tree variation. We developed near-infrared (NIR) calibration models for density and MOE based on 1-mm interval scans of the radial face of intact, air-dried wood samples. The reference data for the model development were obtained from SilviScan assessment at the same scale. These NIR models were derived from 56 breast-height cores from two sites, one in the northeast and the other in southeast of Tasmania. The r^2 for these models was moderate when applied on the site where they were developed (density r^2 = 57.5 and 54.0%; MOE r^2 = 75.1 and 65.1%). However, in some cases when models were applied on the other site, the r^2 was low, and development of robust multisite models is in progress using additional sites. Such models will be used to examine the influence of environment and silviculture on *E. nitens* wood properties.

Keywords: *Eucalyptus nitens*, near-infrared spectroscopy, density, stiffness, SilviScan

Strength Grading of Scots Pine Utility Poles and Small Diameter Posts Using Acoustic Velocity

Jukka Antikainen[1], Erkki Verkasalo[1], Henrik Heräjärvi[1], Veikko Möttönen[1], Janne Monni[2]
[1] Finnish Forest Research Institute
[2] Iivari Mononen Ltd.

The aim of this study was to evaluate the usability of acoustic velocity for strength grading of Scots pine (*Pinus sylvestris*) utility poles and small-diameter fencing posts. Experiments were done using 300 untreated Scots pine utility poles length of 8 to 14 m and 35 small-diameter Scots pine fencing posts length of 2.35 m. For small posts, the effect of pressure impregnation and pine oil impregnation to bending properties were evaluated. Acoustic velocities of the poles were measured using a Fibre-Gen Hitman HM200 hand-held tool. Dynamic modulus of elasticity was calculated for each specimen using density and acoustic velocity. After the acoustic velocity measurements, static bending test was performed by using the standards EN 14229 for the utility poles and EN 408 for the fencing posts. The usability of acoustic velocity differed between the different pole sample sets. Regarding the utility poles, the coefficient of determination (r^2) was between 0.286 and 0.361 for nonstandard and standard poles, respectively. For small untreated posts, the r^2 coefficient between static MOR and dynamic MOE varied from 0.750 to 0.604 and for the impregnated posts the variation was between 0.958 (pine oil impregnation) and 0.009 (chromium-copper impregnation, CC). Although the sample size for the fencing posts was relatively low, it seems that the acoustic velocity works better for smaller posts than for larger poles and the impregnation affects dramatically to the prediction results.

Keywords: Acoustic velocity, utility poles, strength grading, modulus of rupture, dynamic modulus of elasticity, Scots pine

Experimental and numerical investigation of effect of sawn timber dimensions in ultrasonic velocity measurements of Spanish softwoods

Daniel F. Llana
ETSI Montes, Universidad Politécnica de Madrid, Madrid, Spain, d.f.llana@upm.es

Sergio J. Sanabria
Wood Physics, Institute for Building Materials, ETH Zürich, Switzerland, ssanabria@ethz.ch

Guillermo Iñiguez-Gonzalez
ETSI Montes, Universidad Politécnica de Madrid, Madrid, Spain, guillermo.iniguez@upm.es

Francisco Arriaga
ETSI Montes, Universidad Politécnica de Madrid, Madrid, Spain, francisco.arriaga@upm.es

Peter Niemz
Wood Physics, Institute for Building Materials, ETH Zürich, Switzerland, niemzp@ethz.ch

Abstract

Ultrasonic sound velocity measurements with hand-held equipment remain due to their simplicity among the most used methods for non-destructive grading of sawn woods, yet a dedicated normalization effort with respect to strength classes for Spanish species is still required.

As part of an ongoing project with the aim of definition of standard testing methods, the effect of the dimensions of commonly tested Scots pine *(Pinus sylvestris* L.) timbers and equipment testing frequency on ultrasonic velocity were investigated. A dedicated full-wave finite-difference time-domain software allowed simulation of pulse propagation through timbers of representative length and section combinations. Sound velocity measurements v_L were performed along the grain with the indirect method at 22 kHz and 45 kHz for grids of measurement points at specific distances.

For sample sections larger than the cross-sectional wavelength λ_{RT}, the simulated sound velocity v_L converges to $v_L = (C_L/\rho)^{0.5}$. For smaller square sections the sound velocity drops down to $v_L = (E_L/\rho)^{0.5}$, where C_L, E_L and ρ are the stiffness, E-modul and density, respectively. The experiments confirm a linear regression between time of flight and measurement distance even at less than two wavelength $<2\lambda_L$ distance, the fitted sound speed values increased by 15% between the two tested frequencies.

Keywords: ultrasonic wave; dimensions effect; *Pinus sylvestris*

Speckle Laser and Particle Image Velocimetry for Assessment of Deformation in Wood of *Pinus* Subjected to Compression

José Tarcísio Lima, Tomé Moreira Souza, Ellen Waleska Nascimento Da Fonseca, Lucas Tiago Silva
Universidade Federal de Lavras, Lavras, Minas Gerais, Brazil

Abstract

Mechanical tests in wood are usually performed in a destructive way, which allows verifying when the material initiates the deformation, without a map with the distributed deformation in the sample. Optical metrology can be a feasible way to achieve the information nonintrusively. Particle image velocimetry (PIV) and the sunset laser can be addressed as optical techniques with a potential application in the wood deformation monitoring. This work aimed to evaluate the stiffness of *Pinus* wood samples using the optical technique sunset laser associated to PIV in order to create a deformation map. The sunset was carried on positioning the laser in parallel to the wood surface, and the images of the fringes and artifacts obtained from the surface were used to generate the map of vectors by means of the PIV. The samples of *Pinus* were simultaneously evaluated by an Universal Testing Machine (UTM) and PIV/Sunset. Each image generated by PIV was associated to the corresponding force applied by the UTM. The results showed the deformation map of the wood, therefore in which parts the wood was subject to higher force and, consequently, suffered higher deformation. The technique also confirmed the mechanism of compression. As the technique is visual, it was possible to certify the balance of the UTM.

Keywords: Speckle laser, particle image velocimetry, deformation, wood

Evaluation of the Radial Wood Density Profile of *Pinus* (*Pinus caribaea* var. hondurensis Barr. et Golf.) by X-ray Densitometry in Brazil

Vinicius Resende de Castro, Mario Tomazello Filho, Paula Gabriella Surdi
University of São Paulo, Piracicaba, São Paulo, Brazil

Abstract

X-ray densitometry is a classic methodology to analyze tree rings and obtain the radial wood density profile as well as the intra and inter-annual tree-rings density variation. The wood densitometric analyses can be applied to wood quality of trees and genetics, management practices, and other factors. In this study, 5-mm-diameter wood samples were extracted from the trunks of 18 standing 18-year-old *Pinus* trees by increment borer. The radial wood densities of 2-mm-thick wood samples were determined by direct X-ray scanning, using the equipment QTRS-01X. The results allowed us to obtain the wood densitometric density profile of adult *Pinus* trees, which showed an increase of wood density in the radial direction, the juvenile-mature wood differentiation, and the distinctiveness of early-late wood and false tree rings. The *Pinus* trees were grouped into three classes by the variability of wood density applying the Scott–Knott test statistic. In this paper, the applicability of X-ray densitometry as a nondestructive method to characterize wood of *Pinus* trees is discussed.

Keywords: X-ray densitometry, wood quality, tree-rings

Internal Decay Image Reconstruction in Wooden Pillars Testing Using an Interpolation Method

Hailin Feng, Sheng Fu, Guanghui Li
Zhejiang Agriculture and Forestry University, Hangzhou, Zhejiang, China

Abstract

This study aimed to detect internal decay in wooden pillars and reconstruct the cross-sectional image of the wood based on an interpolation method. The mathematic relationship between the stress-wave signal and the damage inside the wood was analyzed first. Then the testing data were treated to obtain the information needed. The 2D image reconstructing algorithm of the internal decay was proposed based on an interpolation method, which achieved the information of unknown sampling point by using the pretreated parameters. The extent of damage in pillars was also investigated because the stress-wave propagating data were traditionally regarded as an indicator of the extent of damage inside the wood. We have done some experiments in the wooden pillars from Tiananmen in Beijing, where 20 wood pillars were tested by our equipment and each pillar was tested at intervals of 50 cm. The internal decay in these pillars was investigated and predicted by calculating in advance with our testing data. We reconstructed the internal decay images and compared the virtual image display with the actual situation inside the pillars by cutting the test specimen as the predetermined intervals. The results showed the area, positions, and extent of the decay in pillars can be displayed by the method using our equipment.

Keywords: Stress wave, decay image reconstruction, nondestructive testing, interpolation method

Evaluation of Wood of Standing *Pinus* Trees (*Pinus caribaea* var. hondurensis Barr. et Golf.) by Impulse Tomography in Brazil

Vinicius Resende de Castro, Mario Tomazello Filho, Paula Gabriella Surdi
University of São Paulo, Piracicaba, São Paulo, Brazil

Abstract

Impulse tomography, as a nondestructive method, constitutes an alternative to analyze standing trees and to provide information on their wood quality. The impulse tomography equipment is based on measuring the transmission of mechanical waves through the wood, evaluated by sensors attached on the tree's trunk. Some equipment allowed us to determine the speed of mechanical waves and also generate an image of wood cross section by applying a specific software. This image of the internal wood structure of standing trees can be correlated with their physical–mechanical properties (e.g., density, moisture, and modulus of elasticity). In this study, the trunks of 18 standing18-year-old *Pinus* trees from a plantation established in Piracicaba city, Brazil, were analyzed using Arbotom equipment. The results allowed us to determine the mean speed value of mechanical waves of 1,087 m/s through the *Pinus* tree trunks, decreasing toward the pith and correlated with the trunk diameter, and also internal wood defects were delineated by color differences on the tomography images. The applicability of impulse tomography as a nondestructive method to characterize wood of standing *Pinus* trees is discussed.

Keywords: Nondestructive method, wood quality, impulse tomography

X-ray Densitometry Applied in Technological Evaluation of Oriented Strandboard of *Pinus* spp. in Brazil

Paula Gabriella Surdi, Geraldo Bortoletto Júnior, Vinicius Resende de Castro
University of São Paulo, Piracicaba, São Paulo, Brazil

Abstract

The objective of this study was to evaluate the method of X-ray densitometry in determination of apparent density in the thickness direction of OSB panels of *Pinus taeda* and *P. elliottii* var. elliottii x *P. caribaea* var. hondurensis. The experiment consisted of eight treatments arranged in a factorial design at two press cycles and four mixing ratios of wood particles of *P. elliottii* var. elliottii x *P. caribaea* var. hondurensis e de *P. taeda* L. Samples (50 by 50 mm) were submitted to the technique of X-ray densitometry, using the equipment QDP-01X. The results indicated that no statistical difference exists between treatments for the variable analyzed. The OSB panels, independently of press cycle, showed higher values of density in faces and lower values in core, forming a characteristic profile, in the shape of letter M. The technique of X-ray densitometry has a great potential for evaluation of the apparent density along the thickness of OSB panels, because the method allows the measurement variables of the industrial process of production and obtains technological parameters.

Keywords: Density profile, wood panels, apparent density

Internal decay detection in standing *Picea koyamae* trees

Kana Yamashita
Department of Wood Properties, Forestry and Forest Products Research Institute, Tsukuba, Ibaraki, Japan, zaikana@ffpri.affrc.go.jp

Toshio Katsuki
Tama Forest Science Garden, Forestry and Forest Products Research Institute, Hachioji, Tokyo, Japan, katsuki@ffpri.affrc.go.jp

Masanobu Tabata
Department of Forest Microbiology, Forestry and Forest Products Research Institute, Tsukuba, Ibaraki, Japan, butter@affrc.go.jp

Yuko Ota
Department of Forest Microbiology, Forestry and Forest Products Research Institute, Tsukuba, Ibaraki, Japan, yuota@ffpri.affrc.go.jp

Toshihiro Yamada
The University of Tokyo Chiba Forest, The University of Tokyo, Kamogawa, Chiba, Japan, yamari@uf.a.u-tokyo.ac.jp

Abstract

Internal decay in standing living trees of an endangered species, *Picea koyamae*, was studied. Heartwood decay was found to progress from the outer part of the heartwood at a lower height above ground. Three methods involving the use of portable equipment, including acoustic tomography, lateral impact vibration method, and gamma radiation method, were used for the detection of internal decay in the standing living trees. These methods yielded similar diagnose and could detect intermediate to advanced decay; however, detection of incipient decay or obtaining an accurate assessment was considered to require visual assessment. Individual tree assessment by the lateral impact vibration method was conducted in a conservation forest, which revealed that internal decay had advanced in considerable numbers of trees.

Keywords: *Picea koyamae*, butt rot, stress-wave velocity, lateral impact vibration method, gamma-ray

Introduction

Picea koyamae Shiras. (*yatsugatake-tôhi* in Japanese) is a tall conifer with morphology similar to Norway spruce (*Picea abies* (L.) Karst.). Its wood quality also resembles Norway spruce and other *Picea* spp. (Kubojima et al. 2010, Yamashita et al. 2010). It is listed as a vulnerable species in the Red Data Plant Report because it is sparsely distributed across only about 70 km of Honshu Island, Japan (Katsuki et al. 2011). Although the population size is an important factor for the population structure and regeneration, there are only less than 1,000 living mature trees in the Yatsugatake and Akashi mountains.

Karamatsu-sawa (N35°56′, E138°19′) in the Nishidake national forest is designated as a genetic resource conservation forest, because it harbors about 100 mature trees that are about 120 years old. Although the trees appeared sound externally, 1 tree fell in 2007 and 11 trees fell in 2009 due to stem breaking or uprooting following strong typhoon winds, suggesting butt decay in these trees. Evaluation of the risk of further windfall of living trees in that stand requires non-destructive testing to detect internal decay.

First, the variation in internal decay within stems in radial and longitudinal directions was determined using 2 windfall trees. Second, the performance of portable devices were assessed using 3 kinds of non-destructive testing methods (acoustic tomography by stress-wave velocity, lateral impact vibration method, and gamma radiation method) in 13 living natural trees in Karamatsu-sawa and 6 plantation trees at 2 sites. Core samples collected from some trees in Karamatsu-sawa and cross sections collected from some trees in Karamatsu-sawa were visually assessed. Finally, the lateral impact vibration method was used for individual assessment of mature trees in Karamatsu-sawa.

Materials and methods

Sample trees and decay assessment

Table 1 shows the sample trees used to examine the decay distribution within stems and compare the performances of non-destructive testing equipments. From the 2 uprooted windfall trees torn up by the roots without stem breakage in Karamatsu-sawa, logs of 1 m length were obtained from the butt to a level of 4 m above ground. Acoustic tomography was performed at 10 cm or 20 cm intervals. Disk at each tested level was obtained. Decay areas were visually assessed in terms of discoloration and hollow, and their percentage was calculated. Basic density and moisture content were measured using blocks divided into 5 pieces from pith to bark in 16 cardinals (Figure 1b).

The 3 non-destructive testing methods were conducted at 1 m above ground for 19 living trees (13 in Karamatsu-sawa and 6 in the plantation forests) (Table 1). The 6 plantation trees were felled, whereupon a cross-section at the tested level was visually observed, and the density and moisture content were measured using blocks obtained diametrically and orthogonally to each other.

The 75 living trees with a diameter of 33–68 cm in Karamatsu-sawa were tested using the lateral impact vibration method at 1 m above ground. Of these, 9 trees were used for sampling increment cores in 4 cardinals at 0.3–0.5 m above ground and were visually observed.

Table 1—Sample trees of *Picea koyamae*

Site	Stand type[a]	Location	Altitude (m)	Tree type[b]	N[c]	Age	D. B. H (cm)	Height (m)
Karamatsu-sawa	N	N35°56′, E138°19′	1,700	F	2	About 120	42	22
Karamatsu-sawa	N	N35°56′, E138°19′	1,700	S	13	About 120	33–47	19–27
Nishidake	P	N35°57′, E138°17′	1,500	S	3	About 43	24–32	25
Higashimata	P	N36°06′, E138°06′	1,000	S	3	About 51	25–25	16–18

[a] N: natural forest, P: plantation forest; [b] F: fallen tree, S: standing living tree; [c] number of trees

Acoustic tomography by stress-wave velocity

Acoustic tomography was performed using an Arbotom (Rinntech, Germany). In all, 8 sensors were evenly placed around the trunk in a horizontal plane. Each sensor was fixed on a pin that was inserted into the bark and sapwood. Acoustic impulses were produced by tapping on each pin using a steel hammer. The stress-wave velocities were automatically calculated on the basis of the registered time of the impulse passage between pairs of sensors. The ratio of velocity between the sensors in diagonal positions (V_R) and the near-tangential velocity between neighboring sensors (V_T) was also calculated for each cross-section (Figure 1a) (Divos and Szalai 2002).

Lateral impact vibration method

The product of diameter (*D*) and lateral impact resonance frequency (*F*) are expressed using equation (1) (Kamaguchi et al. 2000)

$$D \bullet F = \sqrt{\frac{E}{\rho \bullet K}} \quad (1)$$

where *E* is the radial modulus of elasticity, ρ is the mass density of material, and *K* is the shape factor.

The *F* was measured (Ponta, World survey and design Co. Ltd, Shimane) in 2 cardinals for each tree. The product of *D* and *F* (*DF*) was obtained. When the results of the 2 cardinals were different, the measurement was obtained for the third cardinal.

Gamma radiation method

Low-energy gamma radiation attenuates when it passes through an object. The ratio of the transit dose passing through an object compared to that not passing through an object is related to the thickness and density of the object; this method enables the detection of internal decay in green wood (Karslovic and Morales 2002).

The stem cross-sectional shape and gamma-ray transit dose were measured coincidently (Chugai Technos Corporation, Hiroshima) (Iizuka 2007). A set of a laser oscillator and its detector for measuring the stem diameter and a radiation source set (^{137}Cs, 3.7 MBq) as well as its detector for measuring the gamma-ray transit dose were simultaneously moved horizontally on rails set in parallel. The transit dose in the case that the stem was sound was estimated from the transit dose at the outer part of the stem. The area where the measured transit dose exceeded the calculated dose was defined as the heartwood. The procedures were conducted in 2 orthogonal directions (north-south and east-west), and the heartwood area was presumed to be ellipse. The heartwood area percentage was obtained, and the sapwood and heartwood densities were estimated from the measured transit dose.

Results and Discussion

Decay distribution

Internal decay distribution within the stem

Figure 1 shows the within-stem distribution of the decay area percentage (Figure 1d), basic density (Figure 1e), and moisture content (Figure 1f) for a fallen tree caused by a typhoon. In the longitudinal direction, the heartwood decay was less severe in the upper cross-section but increased in area and degree with decreasing elevation (Figure 1c). In the radial direction, the heartwood decay was severe in the outer part of the heartwood, which is shown as block C in Figure 1b. The basic density was small and the moisture content was high in this position with advanced decay. The same trend was observed for another fallen tree.

The cross section analysis of parts at 1 m above ground of plantation trees revealed that 5 trees were sound. One tree (WA634) had an incipient decay in the outer part of the heartwood, but its density was not smaller than that of sound part because it had originally high density due to the compression wood.

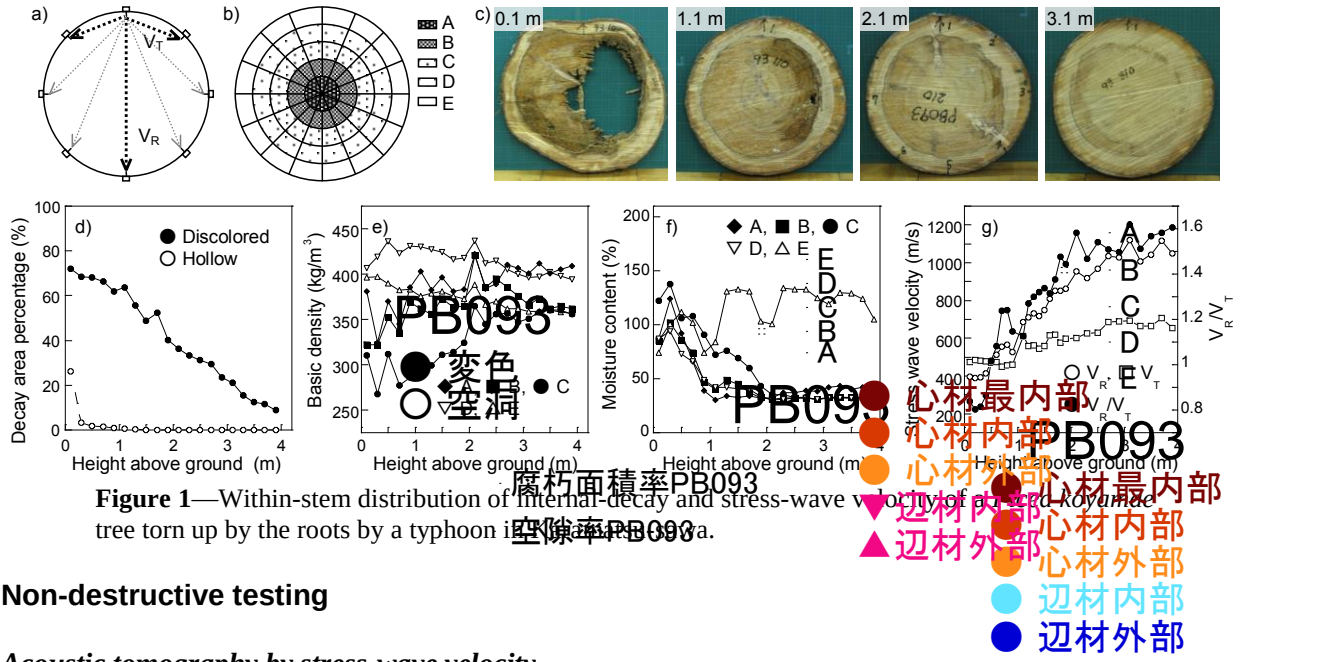

Figure 1—Within-stem distribution of internal-decay and stress-wave velocity of an *Picea koyamae* tree torn up by the roots by a typhoon in Karamatsu-sawa.

Non-destructive testing

Acoustic tomography by stress-wave velocity

The stress-wave velocity for a fallen tree stem revealed that, as the elevation dropped, V_R and V_R/V_T decreased while the decay area percentage increased (Figure 1g). The V_R/V_T was less than 1 at levels of below 0.5 m above ground, where decay was advanced and hollow existed. The other fallen tree exhibited the same trend.

The stress-wave velocity for the 19 living trees revealed that V_R ranged from 459 to 983 m/s and V_R/V_T from 0.74 to 1.53 (Figure 2a). The trees for which V_R was less than V_T were presumed to show advanced decay.

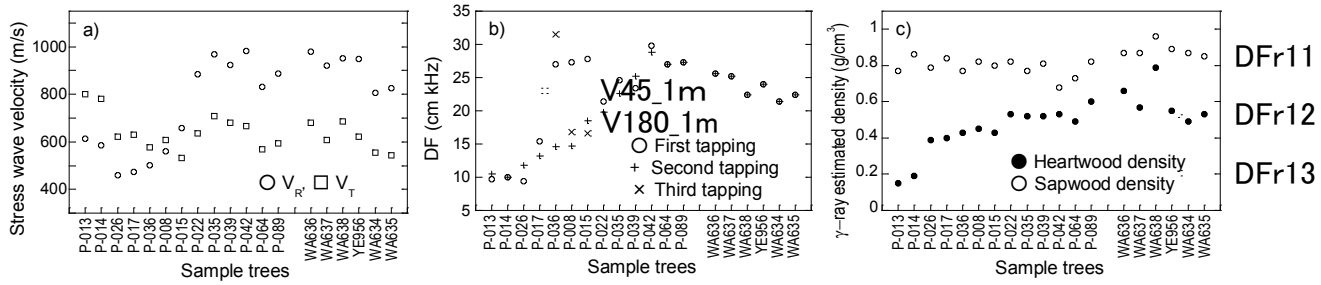

Figure 2—Stress-wave velocity, product of diameter and lateral impact vibration frequency, and estimated density by the gamma-ray transit dose for *Picea koyamae* living trees from Karamatsu-sawa (P) and plantation forests (WA, YE).

Lateral impact vibration method

The *DF* for the 19 living trees is shown in Figure 2b. For the trees that exhibited large differences between the first and second tapping, minimum *DF* was used as the representative *DF* during the third tapping. Such trees were presumed to have non-concentric internal decay. The minimum *DF* ranged from 9.7 to 28.8 cm·kHz.

The lateral impact vibration method was applied to the 75 living mature trees in Karamatsu-sawa. The *DF* ranged from 9.7 to 31.4 cm·kHz.

Gamma radiation method

The gamma radiation method for estimating density of the 19 living trees showed that the heartwood density ranged from 0.15 to 0.96 g/cm^3 (Figure 2c).

The heartwood density, sapwood density, and heartwood percentage estimated by the gamma radiation method and those measured from the plantation trees from 2 stands were compared (Table 2). The estimated and measured heartwood density and percentage were higher for Higashimata than for Nishidake.

Table 2—Gamma-ray estimated and measured density and heartwood percentage for the *Picea koyamae* living trees from plantation forests

Site	Tree No.	Heartwood density (g/cm^3)		Sapwood density (g/cm^3)		Heartwood percentage (%)	
		Estimated	Measured	Estimated	Measured	Estimated	Measured
Nishidake	WA636	0.55	0.44	0.87	1.05	36	34
	WA637	0.49	0.47	0.87	1.02	40	35
	WA635	0.53	0.48	0.96	1.07	34	21
Higashimata	YE956	0.66	0.63	0.89	1.09	60	55
	WA634	0.57	0.58	0.87	1.07	63	59
	WA635	0.79	0.62	0.85	1.07	53	57

Comparison between observation and non-destructive testing results

The comparison of decay distribution and stress-wave velocity for the fallen tree stems, revealed that the stems exhibiting V_R/V_T less than 1.3 contained decayed heartwood with density reduction (Figure 1d, 1e, 1g). The results of the 3 non-destructive testing methods for the 19 living trees were almost in agreement with these findings (Figure 2). The relationships between the results of the 3 non-destructive testing methods are shown in Figure 3. The *DF* obtained by the lateral impact vibration method exhibited a high correlation with the stress-wave velocity ratio (V_R/V_T) and gamma-ray estimated heartwood density. The trees with *DF* less than 18 cm·kHz exhibited V_R/V_T lower than 1.3 and gamma-ray estimated heartwood density lower than 0.45 g/cm^3; these trees were presumed to contain decay with density reduction. Among them, the 6 plantation trees were confirmed to be sound by visual assessment except one tree that had incipient decay. The V_R/V_T, *DF*, and gamma-ray estimated heartwood density for the 5 trees were higher than 1.4, 21 cm·kHz, and 0.49 g/cm^3, respectively. The stems exhibiting higher value than these might be considered to be sound.

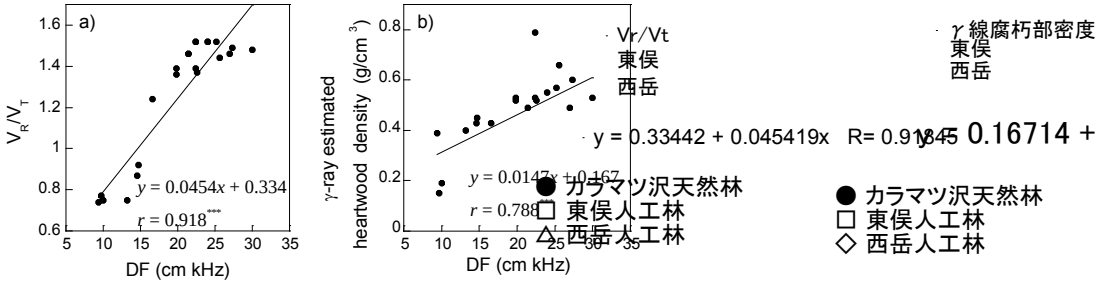

Figure 3—Relationship between stress-wave velocity ratio (V_R/V_T), lateral impact vibration method (*DF*), and gamma-ray estimated heartwood density for *Picea koyamae* living trees from Karamatsu-sawa and plantation forests.

The gamma-ray apparatus was developed to diagnose the decay level for trees (Iizuka 2007) and used for detecting inner cavity of a wooden pole (Fujii et al. 2011). The agreement of heartwood area percentage between gamma-ray estimated and measured data suggested that this is a useful method to

determine the heartwood area of trees with low moisture content. The accuracy of density estimation needs to be improved.

The incipient decay was not detected for 1 plantation tree (WA634) by the 3 testing methods in this study. Incipient decay without remarkable density reduction was considered difficult to estimate. Furthermore, density variation by compression wood or growth conditions might affect the decay estimate.

Among the 3 methods used in this study, the lateral impact vibration method was the fastest, and its results mostly coincided with those obtained using the other methods. This method is convenient, a relatively cost-effective, and stable; therefore, it can be used for the assessment of individual trees. This method has been applied for detecting not only trees with internal defects (Kodama et al. 1999, Suyama et al. 2010, Kamaguchi et al. 2001, Suyama et al. 2012) but also the Japanese cedar trees with high heartwood moisture content (Kamaguchi et al. 2000a, Kamaguchi et al. 2000b, Nakada and Tamura 2006). FEM analysis showed that the stress became larger close to the center in the radial direction, and that the stress at the center was 14 times as large as that in the outermost part (Kamaguchi et al. 2000a). The accuracy of detecting internal decay is considered better at the core part of the stem than at the outer part. For *Picea koyamae*, the heartwood decay was found to progress from the outer part of the heartwood (Figure 1c, 1e). Therefore, detecting the incipient small decay at the outer part of the heartwood, especially in the absence of certain changes in density, would be difficult. Direct observation using increment core might be required for precise diagnosing such decay.

Increment cores were obtained in the 4 cardinals at a level of 0.3–0.5 m above ground from 3 trees diagnosed as sound (*DF* > 22 cm·kHz) and 3 trees diagnosed as decayed (*DF* < 15 cm·kHz) in Karamatsu-sawa. Of the 6 trees, 1 (P-064) was diagnosed to be sound and did not show decay. The other 5 trees showed decay to a greater or lesser extent. The 2 trees (P-035, P-042) presumed to be sound by non-destructive testing methods (Figure 2) had incipient decay in their increment cores. This could be because of (1) the accuracy limit of the non-destructive testing methods used in this study, and (2) the difference of tested levels between non-destructive testing (1 m) and core-sampling (0.3–0.5 m). In this study, non-destructive testing was conducted at 1 m aboveground level, because of the limit of the impact vibration method, whereas core-sampling was conducted to detect fungal decay. Of the 75 trees that were assessed at 1 m above ground in Karamatsu-sawa, 13 exhibited *DF* less than 18 cm·kHz, which suggested the presence of intermediate or advanced decay. More numbers of trees might have internal decay at the butt of the stem.

Laboratory examination confirmed the presence of decay fungus at the butt of the fallen trees by *Onnia tomentosa*, *Sparassis crispa*, *Phaeolus schweinitzii*; in the increment core samples by *Metulodontia* sp. and *Resincium* sp.; and in the root of weakened trees by *Armillaria ostoyae* in Karamatsu-sawa. These results suggested that fungal decay causes serious damage to the seed trees in the conservation forest.

Conclusions

The lateral impact vibration method is a rapid and useful non-destructive testing method to detect intermediate to advanced internal decay in *Picea koyamae* living trees. Visual assessment is required to detect incipient decay. Individual assessment by the lateral impact vibration method revealed that internal decay was advanced in numerous trees in the conservation forest at Karamatsu-sawa.

Acknowledgments

The authors wish to thank Dr. Futoshi Ishiguri, Mr. Jun Tanabe, Mr. Kohji Akashi, and Mr. Kojiro Iwamoto for assistance with non-destructive testing, and Chubu Regional Forest Office for supporting this research.

References

Divos F. and Szalai L. 2002. In: Beall F. C. ed. Proceedings, the 13th International Symposium on Nondestructive Testing of Wood. Richimond, California: University of California, Berkeley Campus: 251–256.

Fujii,Y.; Fujiwara, Y.; Kigawa, R. [and others]. 2011. Nondestructive detection of inner cavity of wooden pole using Gamma-ray. Science for Conservation. 50: 185–189.

Iizuka Y. 2007. Wood-decay diagnosis system. Journal of Tree Health. 11(3): 135–139.

Kamaguchi, A.; Nakao, T.; Kodama, Y. 2000a. Non-destructive measurement of heartwood moisture content in sugi (*Cryptomeria japonica* D. Don) standing tree by lateral impact vibration method. Mokuzai Gakkaishi. 46(1): 13–19.

Kamaguchi, A.; Nakao, T.; Nakai, T. 2000b. Non-destructive study on heartwood moisture content of standing Japanese cedars, *Cryptomeria japonica*, by lateral impact vibration method: comparison between several cultivars of *Cryptomeria japonica* planted at Tatsunokuchi Green Shower, Okayama Prefecture. Journal of Tree Health. 4(1): 1–7.

Kamaguchi, A.; Nakao, T.; Nakai, T. 2001. Non-destructive diagnosis of internal defects of the living trees by the lateral impact vibration method. Journal of Tree Health. 5(2): 59–63.

Karsulovic J. and Morales R. 2002. Nondestructive gamma radiation methods for detection of internal decay in Lenga logs. In: Beall F. C. ed. Proceedings, the 13th International Symposium on Nondestructive Testing of Wood. Richimond, California: University of California, Berkeley Campus: 307–311.

Katsuki, T.; Shimada, K.; Yoshimaru, H. 2011. Process to extinction and genetic structure of a threatened Japanese conifer species, *Picea koyamae*. Journal of Forestry Research. 16(4): 292–301.

Kodama, Y.; Kamaguchi, A.; Nakao, T.; Harada, T. 1999. Non-destructive inspection of cavities in standing trees by lateral impact vibration method. Journal of Tree Health. 3(1): 5–9.

Kubojima, Y.; Katsuki, T.; Akashi, K. [and others]. 2010. Radial variations in wood properties of a threatened species, *Picea koyamae*. Mokuzai Gakkaishi. 56(4): 258–264.

Nakada R. and Tamura A. 2006. An application of the lateral impact vibration method to the genetic improvement of heartwood moisture content in *Cryptomeria japonica*. Mokuzai Gakkaishi. 52(3): 137–144.

Suyama, H.; Nakao, T.; Tomimatsu, Y. 2010. Non-destructive diagnosis of the butt heart rot in *Chamaecyparis obtusa* by the lateral impact vibration method. Journal of Tree Health. 14(3): 83–91.

Suyama, H.; Nagaishi, N.; Sakagoshi, K. 2012. Estimation of decay or hollow-area ratios in stems of Japanese black pines by lateral impact vibration method. Journal of the Japanese Forest Society. 94(4): 161–166.

Yamashita, K.; Katsuki, T.; Akashi, K. [and others]. 2010. Wood properties of *Picea koyamae*: within-tree variation of grain angle, tracheid length, microfibril angle, wood density and shrinkage. Bulletin of Forestry and Forest Products Research Institute. 9(2): 19–29.

Evaluation of high moisture content of Japanese cedar（*Cryptmeria Japonica*）log using the phase detector of electromagnetic wave transmitter

Kiyohiko IKEDA
Shizuoka Prefectural Research Institute of Agriculture and Forestry, Hamakita-ku, Hamamatsu, Japan, kiyohiko1_ikeda@pref.shizuoka.lg.jp

Takeshi HOSHIKAWA
Shizuoka Prefectural Research Institute of Agriculture and Forestry, Hamakita-ku, Hamamatsu, Japan, Hoshikawa.T@gmail.com

Jun WATAI
Shizuoka Prefectural Research Institute of Agriculture and Forestry, Hamakita-ku, Hamamatsu, Japan, jun1_watai@pref.shizuoka.lg.jp

Youki SUZUKI
Forestry and Forest Products Research Institute, Tsukuba, Ibaraki, Japan, youki@ffpri.affrc.go.jp

Nobuo SOBUE
Faculty of Agriculture, Shizuoka university, Suruga-ku, Shizuoka, Japan, rsf48535@nifty.com

Akihiro SUGIYAMA
Micro Measure Co., Ltd. Shimada, Shizuoka, Japan, sugia@micromes.com

Abstract
We are developing a log-grading system that sorts logs by moisture content and young's modulus. We have studied a contactless and nondestructive evaluation method that can evaluates moisture distribution by the phase difference of electromagnetic wave. Our previous study showed that appropriate frequency range for this evaluation is from 60 MHz to 2.4 GHz. To receive the electromagnetic wave with the above-mentioned frequency, we made a prototype device, which consists of a dipole transceiving antenna, and a reading equipment of phase difference related to moisture content. Some square timbers that were adjusted their moisture content artificially were used for testing the validity of the device. And the result showed that the frequencies related to moisture content of both sapwood and heartwood was in the detectable region. Furthermore, coefficient of correlation between phase difference and moisture content; and between phase difference and green density is 0.75-0.85, and 0.85-0.95, respectively, in surveyed Japanese cedar logs. Therefore, this finding demonstrates the possibility of practical use of our developing log-grading system in the future.

Keywords: Moisture content, Electromagnetic wave, Phase difference, Japanese cedar, Log-grading system.

Introduction
Several lumber-mills have been introducing grading machine for strength and drying for timber in Japan. This is for quality control. On the other hand, prototypes of strength grading machine for logs are developed by modification of that for timber. This is for classification by use. There are obstacles in kiln

drying in regard to Japanese cedar that has large variety of moisture content in heart wood. Nevertheless, none of moisture grading machine are developed.

There have been several basic research for estimating moisture content of logs using neutron radiation, cross-sectional vibration and electromagnetic wave, in particular, microwave transmission and attenuation[1-7]. However, technical application of moisture estimation to log sorting system.has not been yet. In this study, we developed moisture estimation technique in log-sorting system using electromagnetic wave. It is thought to be difficult to apply microwave water content meter to timber with a high water, because microwave scatter and attenuation. We examined moisture estimation with a prototype sensor using microwave phase as with the impedance measurement under 1 MHz range. Accordingly, We made a prototype of log water content meter using transceiving dipole antenna 100 to 320 MHz range in frequency. Using the prototype device, we examined characteristics of antenna by MC-controled lumbers and logs.

Methods and materials

1. Searching appropriate range of frequency for wood with a high moisture content and test production of antenna

Assuming lot diamètre range 18 - 60 cm, log's moisture content 50 - 300%, we searched appropriate range of frequency about depth of transmission and permittivity. The numbers of log specimens is about two hundreds. Accordingly, we made two types of antenna that have different range of frequency for transmitting and receiving. about antenna of 2.4 GHz, distance between antennas set 37 cm. We examined phase difference and attenuation when we stack eleven pieces of lumbers one by one. About antenna of 116 MHz, distance between antennas set 1meter. We examined phase difference and attenuation when we stack 55 lumbers one by one.

2. Test production of moisture grading machine for logs

We made a prototype of log-grading machine for logs to intend to high water log unless than 50 cm diameter. this instrument was consisted of transceiving antenna, 116 MHz frequency, sequencer, touch panel controller.

3. Performance assessment of antenna using MC-controlled lumbers

we made square timbers. We use 150% M.C. specimen as outer part, and use 150, 100, 50, 20% M.C. specimen as inner part respectively.

4. Performance assessment of antenna using log in actual

We used 120 logs of Japanese cedar, top diameter ranged 26 - 42 cm, length 4 m. We measured green (apparent) density(weight / volume) of specimen and phase using log grading machine above. The phase difference were measured at 1 meter from top end assuming that the distance between dipole anttenas was 1 meter. Afterwards, MC by oven drying method was obtained from total disc and separated disc into two parts(heart wood and sap wood).

Results and discussion

1. Searching appropriate range of frequency for wood with a high moisture content and test production of antenna

It was implied that appropriate range of frequency was 2.4 - 1 GHz for surface layer, 150 - 60 MHz for inner layer because of relationship between frequency and half-value depth, water saturated wood's electric behavior(permittivity and dielectric tangent) and temperature. We made two kind of transceiving dipole antenna(116MHz and 2.4GHz frequency). In 2.4 GHz antenna(0.3 m length), phase and attenuation were increased as number of veneer between antennas was increased. Especially, phase and number of veneers were highly correlated (Fig. 1). In 116 MHz antenna (1 m length), the phase was

increased linearly as number of veneer between antennas that assume moisture content of a log was increased in the same way (Fig.2).

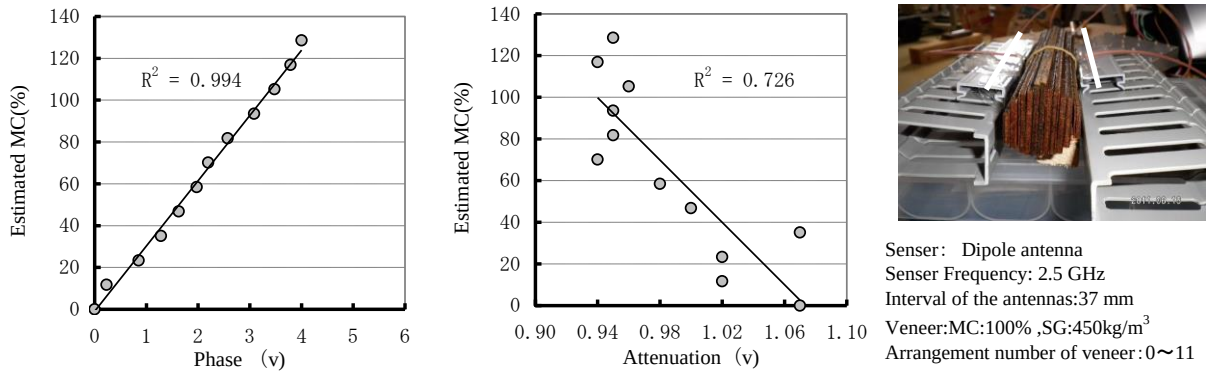

Fig.1 Change of phase and attenuation when arranging sheets of veneer of MC100% in the sensors (Frequency:2.4 GHz).

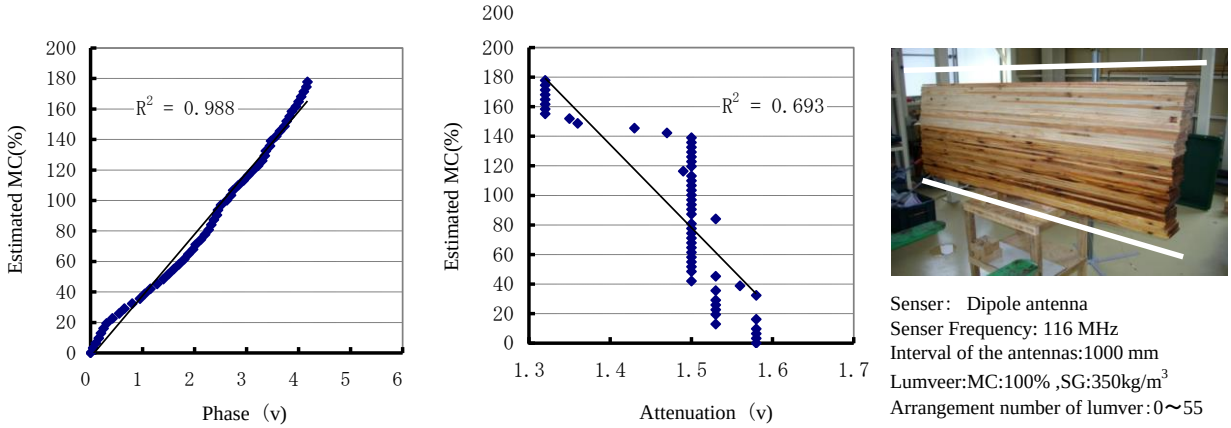

Fig.2 Change of phase and attenuation when arranging sheets of lumber of MC100% in the sensors (Frequency:116 MHz).

2. Test production of moisture content grading-machine for logs

Figure 3 gives a broad overview of moisture grading machine for logs. Sensors that are dipole antenna 1 m length and 116 MHz frequency pick up phase angle and attenuation correlated with moisture content and display the voltage calculated on a pro-rata basis from modulus on a monitor.

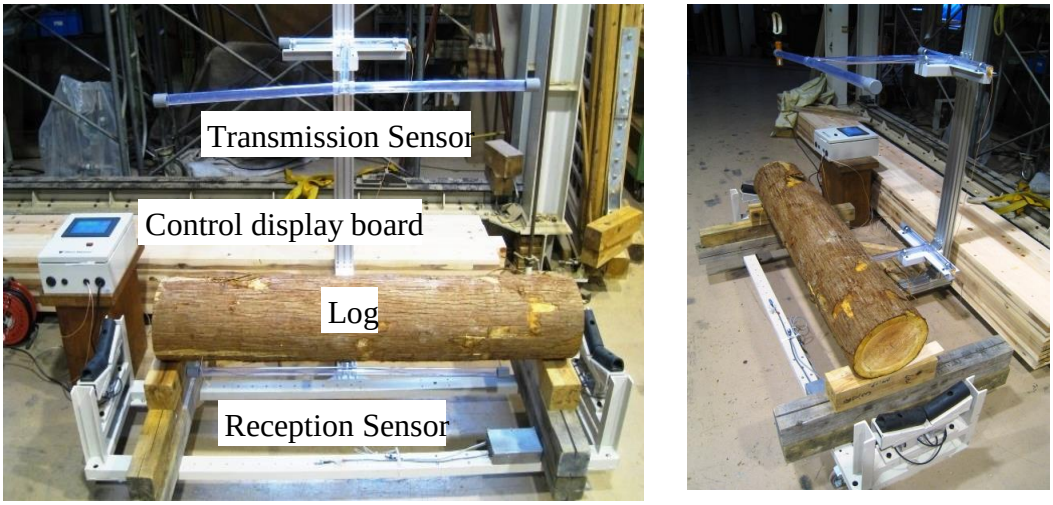

Fig.3 Survey of the log moisture quantity evaluation equipment

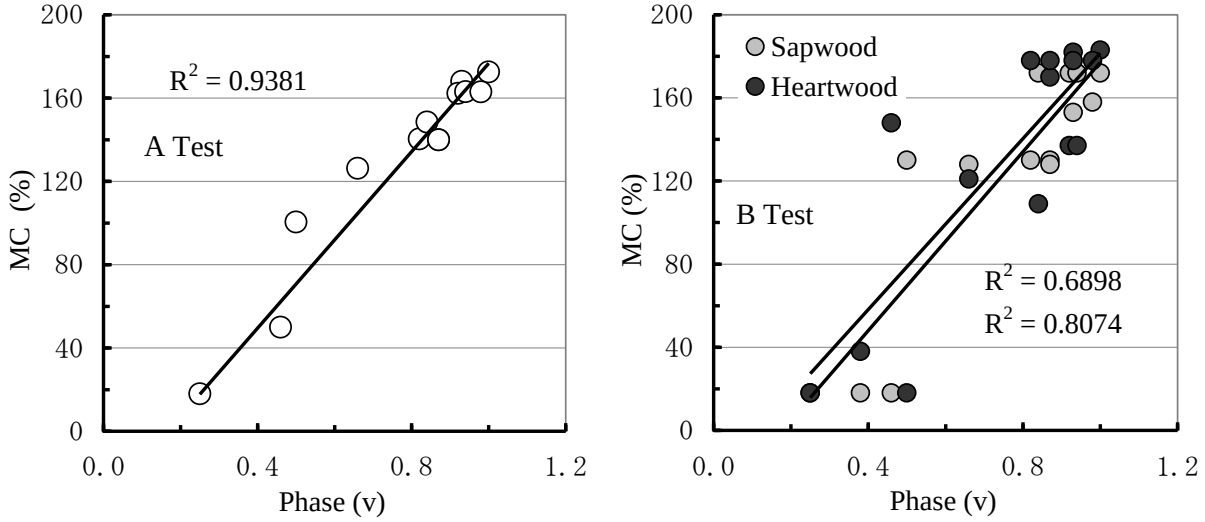

Fig.4 Relation between the MC and phase of the model examination specimen which adjusted MC

3. Performance evaluation of antenna using MC-controlled lumbers

In A test, the phase was declined as moisture content of inner parts was declined. This result implicate phase is proportional not only to outer parts (sapwood), but also inner parts (heartwood). In B test, the phase differences are highly correlated with overall moisture content(r = 0.974, Fig. 4). This result is consistent with A test. The phase differences are also correlated with moisture content of sapwood and heartwood(r = 0.831, 0.898 respectively). However, in the two moisture content pattern, one has 180% in sapwood and 18% in heartwood, another have 18% in sapwood and 180% in heartwood, these phase difference were nearly identical.

4. Performance evaluation of antenna using logs in actual

The phase differences had significant correlations with moisture content with respect to each diameter class(r: 0.75-0.88 for overall, 0.75-0.87 for heartwood, Fig. 5). The phase difference was also correlated with green density (r = 0.84-0.94, Fig. 6). Relationships between phase difference and moisture content and green density were approximated by exponential functions.

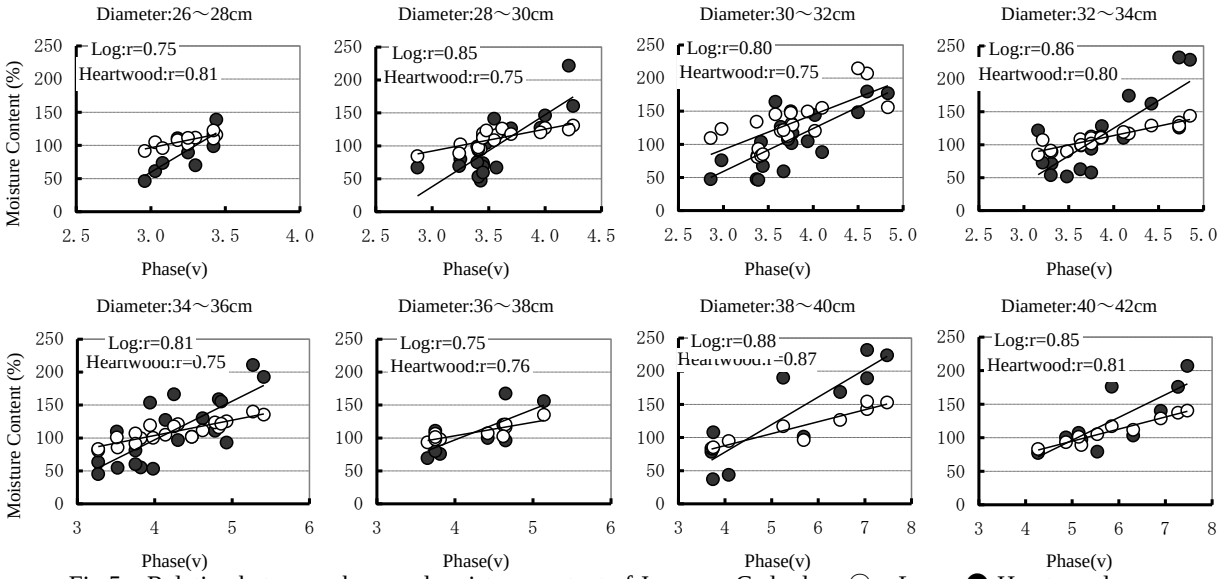

Fig.5 Relation between phase and moisture content of Japanese Cedar log. ○ : Log, ●:Heartwood

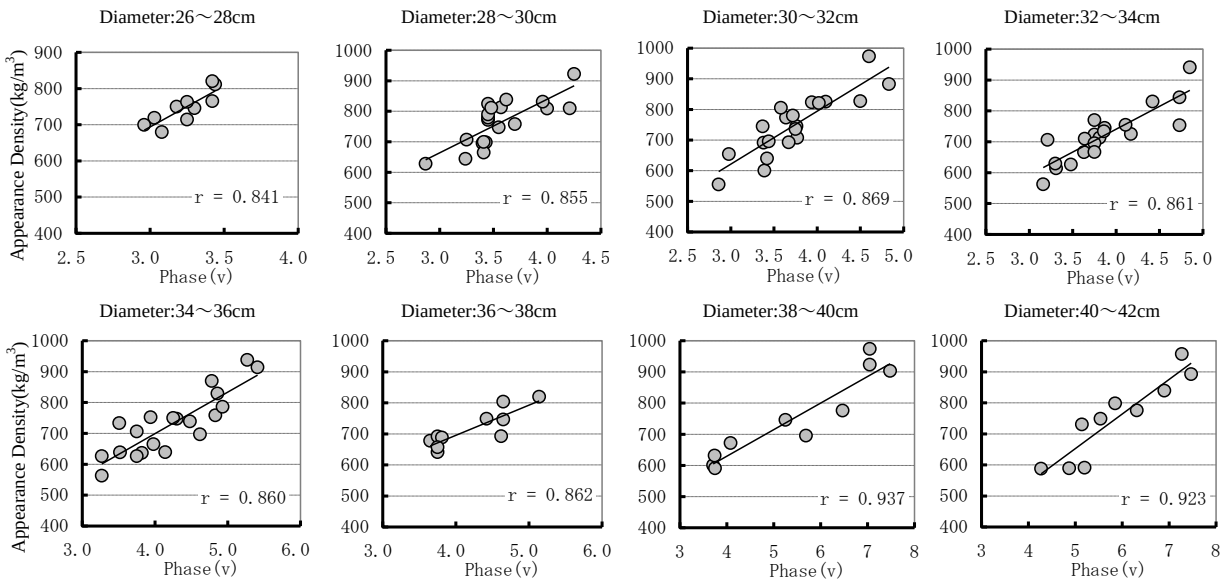

Fig.6 Relation between phase and appearance density of Japanese Cedar log.

When estimating the high moisture content of log on the sorting device, or evaluating the green density, it was necessary to measure weight of log by using loadcell after stopping once the log. Therefore, the introduction of measuring of weight of log into the sorting device from functionality and cost has been difficult until now. From the test results, by installing the antenna and transmitter of the electromagnetic pulses into sorting device, it seemed that be able evaluated the log moisture content or green density by phase difference efficiently and low cost.

Conclusions

- The appropriate frequency range of electromagnetic wave was 2.4 - 1 GHz in near the surface of a log, and 150 - 60 MHz in the inside of a log.
- The test result of the prototype device with a dipole antenna (116 MHz and 2.4 GHz frequency) showed that the phase and the attenuation were increased with the increase of moisture content between antennas.
- We made a prototype device with the dipole antenna (1 m length, 116 MHz) that picks up phase angle and attenuation correlated with moisture content, and displays the voltage calculated on a pro-rata basis from modulus on a monitor.
- In two types of model test, the phase and moisture content in overall and heartwood, implicating the phase is proportional not only to sapwood, but also to heartwood.
- Using 120-test specimen of Japanese cedar logs that top diameter ranged 26 - 42 cm, the phase differences had significant correlations with moisture content with respect to each diameter class.
- Relationships between phase difference and moisture content were approximated by exponential functions.

References

1) Suzuki, Y. 2005. Evaluation of moisture Content of wood by Electrical measurements (in Japanese). Wood Industry. 60(10): 483-488.
2) Suzuki, Y.; Kuroda, N. 2003. Dielectric properties of wood with High Moisture Content (in Japanese). Mokuzai gakkaishi. 49(3): 161-170.
3) Sobue, N.; Doi, K.; Date, M. 2011. New impedance measurement system estimating cross-sectional moisture distribution in cylindrical and electric network modeling. J wood Sci. 57(5): 395-400.

4) Johanson,J. Hagman,0 Fjellner,B.A 2003Predicting moisture content and density distribution of Scots pine by microwave scanning of sawn timber. J wood Sci. 49(5): 312-316.
5) Suzuki, Y.; Ikeda, K. 2011. Evaluation of moisture content in a log using impedance Model. ISMAE11th. 269-274.
6) Suzuki, Y.; Ikeda, K. 2009. Estimation of water distribution in sugi log using Impedance Model. ISMAE8th. 289-294
7) Sobue, N.; Inagaki, M. 2007. Estimation of cross-sectional moisture content in commercial timbers by impedance in RF ranges. ISMAE8th. 123-128.

Tomography of the internal structure of roundwood – a comparison of x-ray based computed tomography and stress wave

Franka Brüchert
Forest Research Institute Baden-Württemberg, Freiburg, Germany, franka.bruechert@forst.bwl.de

Samuel Holz
Dold Holzwerke GmbH, Germany
samuelholz@gmx.de

Tobias Biechele
Rinntech, Heidelberg, Germany
tobias.biechele@rinntech.com

Frank Rinn
Rinntech, Heidelberg, Germany
frank.rinn@rinntech.com

Udo H. Sauter
Forest Research Institute Baden-Württemberg, Freiburg, Germany, udo.sauter@forst.bwl.de
udo.sauter@forst.bwl.de

Abstract
This paper presents results on the comparison of Arbotom impulse propagation measurements with x-ray based computed tomography scans. The methods had been applied to one log of Douglas fir to analyse the variation of the stem over its length. Tomograms of 20 cross sections at 50 cm distances were interpreted on the basis of gray value variation representing either wood density (CT scan) or impulse run time (Arbotom).
The comparison of the methods clearly showed the differences in feature detection with respect to special resolution of the tomograms. CT scans showed in high resolution images allowing detailed feature detection such as knots, ring structure, and sapwood/heartwood differences due to moisture content. The Arbotom tomograms showed the homogenous cross sections of the stem, distinguishing between areas which could be identified as drier heartwood or water-containing sapwood.
The comparison showed that the methods can be used complementary for interpretation of tomograms improving their specific applications as raw data can be converted into a matching gray value system which allows matching visualisation.

Key words: Arbotom, CT.Log, internal wood structure

Introduction and objectives

The measurement of stress wave velocity is a well-tested and widely applied methodology in wood industry for non-destructive testing for MOE on sawn timber. The technology is also long time introduced to tree inspection. As an example: the Arbotom® impulse tomograph (Arbotom, 2010) is used to evaluate trees on internal defects and damage which could decrease strength and safety of urban trees. The Arbotom® uses the time of flight of a manually induced stress wave travelling between sensors attached around the tree. From these flight times apparent stress wave velocities can be calculated and displayed in a tomogram to show internal heterogeneity of the wood structure.
X-ray based computed tomography allows non-destructively a detailed view into the internal structure of a log (Lindgren 1991). Structural elements such as knots or rot cavities can be identified, precisely located and measured. Stress wave tomography on the other hand due to its method only allows to

measure the existence and location of a defect. Operators need experience to correctly interpret such defects in a tomogram.
A comparison of both methods could help to evaluate potential applications for both technologies. For the tests, softwood logs have been tested with both technologies. Analysis comprised visual assessment of the stress wave tomograms and the CT reconstruction of individual cross sections. Statistical analysis on the variation of mean sound velocity per cross section and variation along a log was compared to density level derived from CT scanning and heterogeneity due to internal structures such as knots.

Material and methods

The comparison was undertaken on one log of Douglas fir (*Pseudotsugs menziesii* (Mirb.) Franco). The log originated from tree height of 3.6m height (2nd log). It was 4.65m long with a mid-diameter of 39 cm. The log showed no defects from outside.

The log was tested with the Arbotom ver. 2.04 impulse tomograph (Rinntech, Germany). 156 sensors were attached to the log, 8 sensors per measurement plane (4 sensors at one individual plane), 20 planes at a distance of 20 cm. The sensors were attached at the following positions: 0°, 45°, 90°, 135°, 180°, 225, 170, 315° (Figure 1)

Figure 1 – Test set-up with Arbotom gauges and CT.Log scanner in the background

Each gauge was hit 5 times for replication of measurement and the run time of the impulse was measured. A 2D tomogram was derived for each of the 20 measurement plane based on the measurements of the 8 respectively 4 gauges.

For comparison of the tomograms a x-ray based computer tomogram was extracted from a computer tomographic scan for the respective measurement planes. The CT.Log (Microtec, Italy) scanner is equipped with a x-ray source working at 14 mA current and180 kV voltage. Reconstruction was calculated on the basis of 768x768 pixels, allowing a resolution of 1mm by 1 mm in the cross sectional view over a slice thickness of 5 mm.

To compare the two tomograms the grey value scale for both images was set 8 Bit (256 grey scales). For the Arbotom measurements the scale varies from 0 = black (low impulse velocity) to 255 = white (high impulse velocity). For CT scanning the scale varies from 0 = black (air) to 255 = white (density of water, high material density). As impulse velocity increases with density (eq. 1) (for constant

modulus of elasticity) the change in gray scale for the Arbotom tomogram follows the same logic in the visualization as for the CT scan.

$$C = \sqrt{\frac{E}{p}} \tag{1}$$

Where C is the impulse velocity, E the modulus of elasticity, and p is the density of the material.

Results

Figure 2 presents selected planes from the scans, on the left side the visualization of the CT scan, on the right side the visualization of the same plane in the Arbotom measurement.

Both tomograms show the variation in wood properties, though at a different resolution. In the top row of Figure 2, the CT image shows a homogeneous, partially dried cross section of the Douglas fir with even ring structure. The ring structure is visible by the strong density contrast between dark early wood (lower density) and bright latewood (higher wood density). In the remaining sapwood area the early wood areas are also brighter due to a higher moisture content which implies a higher absorption of the radiation. The heartwood core of the stem around the pith appears slightly darker with a lower x-ray absorption, which indicates drier wood. In the outer section of the cross section an area with a higher moisture content is visible between positions “2” and “4” (45°-135°) by the brighter gray values. The inner core also contains knot traces which appear brighter than the surrounding stem wood due to the higher branch wood density. The Arbotom tomogram also picks up different levels of “impulse velocity”, i.e. wood density. In the inner core, the darkest area matches in good agreement with the drier heartwood core found in the CT image. Between position 2 and 3 the Arbotom “recognizes” an area with higher impulse velocity, e.i. higher “density”. The Arbotom measurement however does not distinguish the knots in the inner core.

In the middle row in Figure 2 (left), the sapwood ring in the periphery of the log is still complete and not dried out as in the top image, and appears overall brighter than in image above. The drier heart-wood core can be identified clearly by the overall darker appearance of the early wood areas. The Arbotom also identifies the larger variation of density and moisture content in the cross section. The tomogram shows a dark central core with a slightly brighter periphery towards position 2 and 4, and distinctly brighter gray shades on the other side between position 5 and 8. Again the knot traces are overlaid by impulse velocity measured in the surrounding stem wood.

The left image in Figure 2, bottom row again show the uniform ring structure distribution of the tree. Similar to the image in the top row the cross section appears patchy due to uneven drying progress of the stem. The impulse measurement in the same plane also identifies areas of different impulse velocity, however the highest velocity does not match with the area in the CT scan where the highest moisture content in the sapwood could be found.

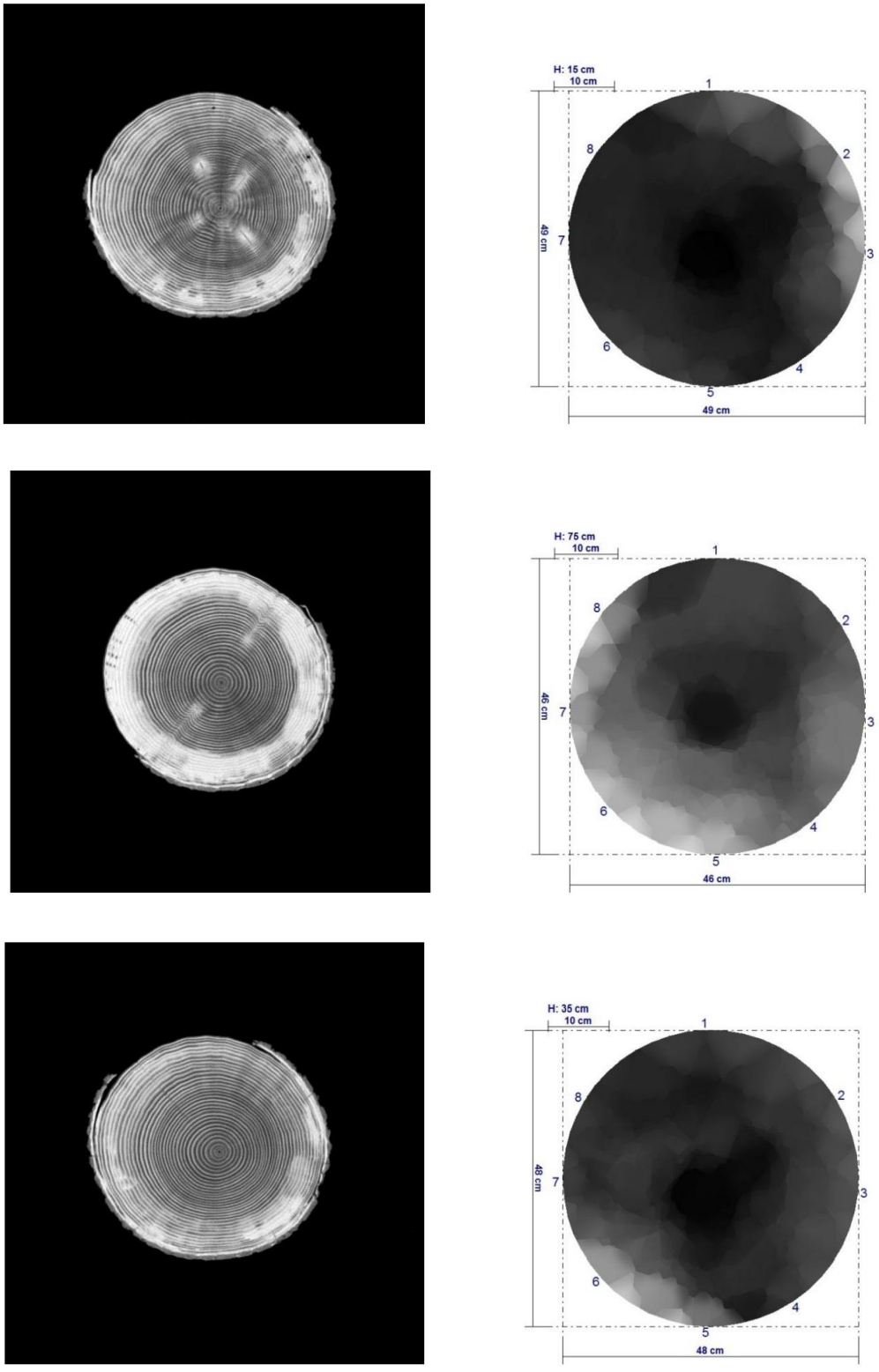

Figure 2 – Selected examples of tomograms from the log. Left: CT scan, right: Arbotom

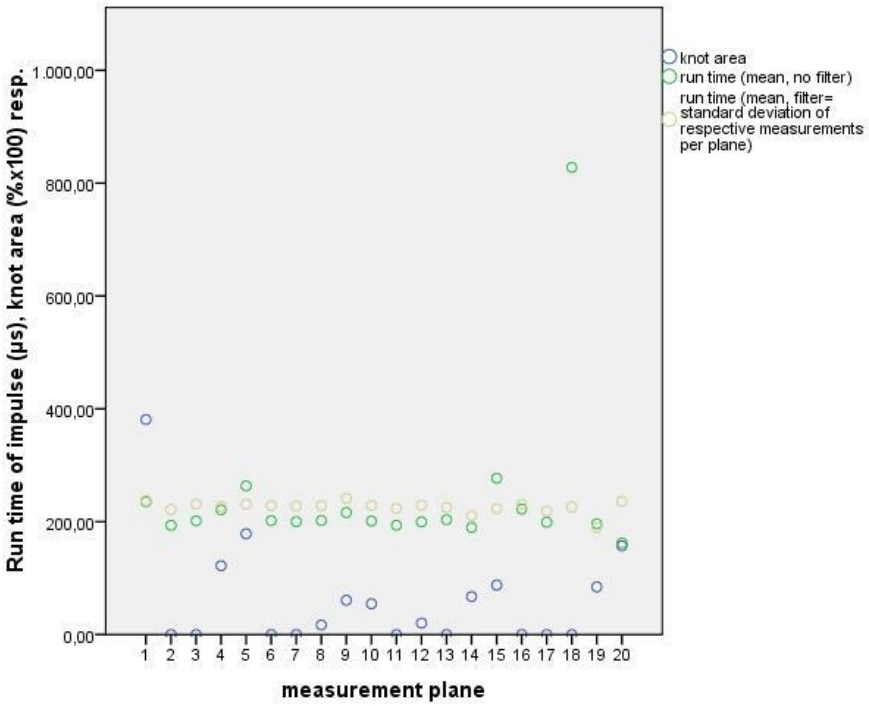

Figure 3 – Variation of run time of impulse (mean) and knot area (%) in the cross section over length of log. To equalize the scale, knot area percentage has been multiplied x 100 to match the scale of the run time.

Figure 3 shows the variation of original measurement signal of the Arbotom measurement, the impulse run time, over the length of the log. Run time means calculated from the raw data without further filtering show a large peak in plane 18 and smaller peaks in plane 5 and plane 15 (symbols on green). However the planes with these maxima in impulse run time do not match clearly with planes of specific internal structure like knots (shown as % knot area in the cross section in Figure 3, blue symboles). Further inspection of these planes did not show an obvious reason visible in the CT scans for these large deviations from the other planes.

Figure 4 and 5 show the variation of the Arbotom signals (converted to gray values) and the CT gray values (as representation of the wood density) over the length of the log. The analysis is based on the gray value frequency distribution of the tomograms as shown in Fig. 1. Impulse measurement with the Arbotom tool show a larger variation in gray value mean and standard deviation (Fig. 4) than the CT scans. The large variation in the gray values resulted in statistical significantly distinguishable planes based on univariate ANOVA ($\alpha<0.05$). 11 out of 20 planes did differ significantly from each other. The other planes were very similar to either one other plane or two planes, however not adjacent ones. ANOVA analysis of the CT gray value showed less differentiation between the different planes due to the small differences in gray value means.

Discussion and conclusion

Arbotom and CT scanning are two technologies which allow the visualization of stem cross section based on either impulse propagation measurement (Arbotom 2010; Rinn 1999) or x-ray based transmission (Buzug 2008). The underlying physical principles for both methods are mechanical material properties, in particular wood density which in turn is strongly influenced by the presence of water (Kollmann and Cote 1968). As measurements have been carried out at the same time, these influences can be neglected as irrelevant when comparing both methods.

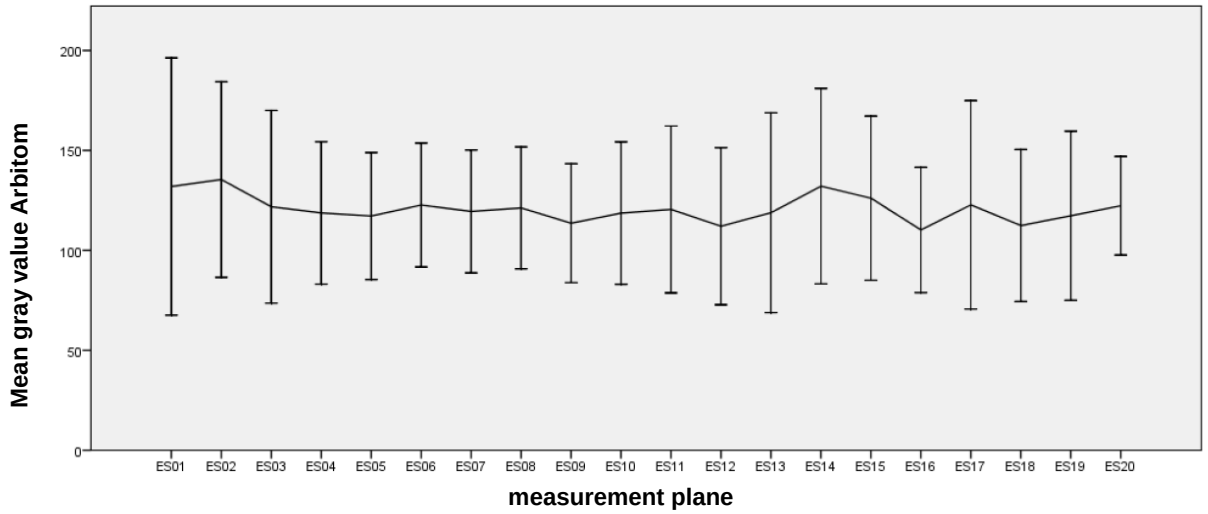

Figure 4 – Variation of gray value (Arbotom) over length of log (mean ± 2* standard deviation)

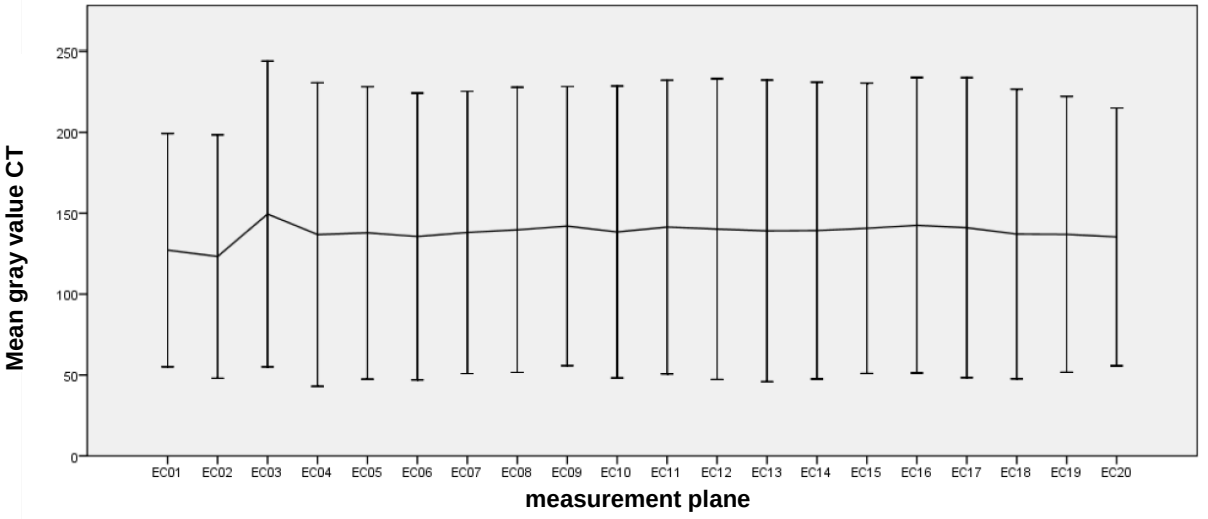

Figure 5 – Variation of gray value (CT scan) over length of log (mean ± 2* standard deviation)

The computer tomogram shows a high resolution representation of a stem cross section and allows to identify small spacial density variation (1x1 mm² resolution). The strength lays in the detailness of the tomogram as density contrast on fine spacial level can be identified. The method allows a high level of information in an image which can be used for detailed analysis of variation of internal stem structures of a tree for with a wide range of application, mainly in the sawmilling industry (Benson-Cooper et al. 1982, Taylor et al. 1984, Funt and Bryant 1987, Grundberg and Grönlund 1992, Bhandarkar et al. 1999, Oja 2000). These features are knots (Andreu and Rinnhofer 2003, Hagman and Grundberg 1995, Oja 2000, Nordmark 2003, Breinig et al. 2012, Longuetaud et al. 2012), but also splits (Wehrhausen et al. 2012), wounds from bark damage (Metzler et al. 2011) beside other features (Boukadida et al. 2012, Fromm et al. 2001, Longuetaud et al. 2004, 2007, 2009). The applications CT scans are used for require an exact location of different, distinguishable features (Nordmark 2003, Berglund 2013).

The impulse propagation measurements are usually applied for standing tree assessment (Kowohl et al. 2001, Pellerin and Ross 2002) and tree stability evaluation. Tree safety and stability is not affected by small spacial changes of the internal wood structure, but by larger losses of load bearing cross

section detectably by lower wood density and cavities (Dackermann et. al, 2013, Mattheck and Hölzl 1997). Thus detection and identification of larger areas in tomogram are sufficient. Interpretation of impulse propagation in a cross section between different measurement planes on the basis of variation of the measurements in the individual planes allowed good differentiation of the individual cross sections by simple statistical means. The results show that the detailness of CT tomograms would only be required for further interpretation of the actual change in signal.

It can be concluded that the two methodologies are not competitive as they provide different applications, but can be successfully used for complementary investigations.

Acknowledgement

This investigation was a project between Rinntec GmbH, Germany and Forest Research Institute Baden-Württemberg, Department of Forest Utilisation. The project was supported by Prof. Dr. Dr. h.c. Gero Becker, Chair for Forest Utilisation, University of Freiburg, Germany, by supervising Mr. Holz as bachelor student.

References

Andreu, J.-P., Rinnhofer, A. 2003. Modeling Knot Geometry in Norway Spruce from Industrial CT Images. Proceedings of the 13th Scandinavian Conference on Image Analysis, June 29 – July 2, Halmstad, Sweden: 786–791.

ARBOTOM® - Bedienungsanleitung, 2010

Benson-Cooper, D.M., Knowles, R.L.. Thompson, F.J, Cown, D.J. 1982. Computed tomographic scanning for the detection of defects within logs. Forest Research Institute, New Zealand Forest Service. Bulletin No. 8.

Berglund A., Broman O., Grönlund A., Fredriksson M. 2013. Optimizing log rotation with an industrial computed tomography scanner. Computers and Electronics in Agriculture 90: 152-158.

Bhandarkar, S.M., Faust, T.D., Tang, M. 1999. CATALOG: a system for detection and rendering of internal log defects using computer tomography. Machine Vision and Applications 11: 171–190.

Boukadida, H., Longuetaud, F., Colin, F., Freyburger, C., Constant, T., Leban, J.-M., Mothe, F. 2012. PithExtract: a robust algorithm for pith detection in computer tomography images of wood. Computers and Electronics in Agriculture 85: 90-98.

Breinig, L. Brüchert, F. , Baumgartner, R., Sauter, U.H. 2012. Measurement of knot width in CT images of Norway spruce (Picea abies [L.] Karst.) - Evaluating the accuracy of an image analysis method. Computers and Electronics in Agriculture 85: 149–156

Buzug, T. M. 2008. Computed Tomography: From Photon Statistics to Modern Cone-Beam CT. Springer Verlag. 536 p.

Dackermann, U., Crews, K., Kasal, B., Li, J.,Riggio, M., Rinn F., Tannert T., 2013. In situ assessment of structural timber using stress-wave measurements. Materials and Structures, 10.1617/s11527-013-0095-4.

Fromm, J.H., Sautter I., Matthies D., Kremer J., Schumacher P., Ganter C. 2001. Xylem water content and wood density in spruce and oak trees detected by high-resolution computed tomography. Plant Physiol. 127: 416–425.

Funt, B.V., Bryant, E.C. 1987. Detection of internal log defects by automatic interpretation of computer tomography images. Forest Products Journal 37 (1), 56–62.

Grundberg, S., Grönlund, A. 1992. Log scanning – extraction of knot geometry. Seminar/Workshop on Scanning Technology and Image Processing on Wood. August 30 – September 1, 1992, Skellefteå.

Hagman, P. O. G.; Grundberg, S. A. 1995. Classification of scots pine (Pinus sylvestris) knots in density images from CT scanned logs. Holz als Roh-und Werkstoff 53 (1): 75–81.

Kollmann, F.F.P., Cote, W.A.Jr. (1968): Principles of Wood Science and Technology. I. Solid wood. 592 pp. 687 figs., Springer Verlag,

Kowohl, T., Kehr, R., Wohlers, A., Dujesiefken, D. 2001 Wundreaktionen und Pilzbefall im Holzkörper nach Resistograph- und Zuwachsbohrer-Einsatz zur Baumuntersuchung im Bereich von Fäulen, Jahrbuch der Baumpflege: 203 ff.

Lindgren, L.O. 1991. Medical CAT-scanning: X-ray absorption coefficients, CT-numbers and their relation to wood density. Wood Science and Technology 25: 341–349.

Longuetaud, F., Caraglio, Y., 2009. Pith: a marker of primary growth in Picea abies (L.) Karst. Trees-Structure and Function 23(2): 325–334.

Longuetaud, F., Leban, J.-M., Mothe, F., Kerrien, E., Berger, M. O. 2004. Automatic detection of pith on CT images of spruce logs. Computers and Electronics in Agriculture 44: 107–119.

Longuetaud, F., Mothe, F., Leban, J.-M. 2007. Automatic detection of the heartwood/sapwood boundary within Norway spruce (Picea abies (L.) Karst.) logs by means of CT images. Computers and Electronics in Agriculture 58: 100–111.

Longuetaud, F., Mothe, F., Kerautret, B., Krähenbühl, A., Hory, L., Leban, J.M., Debled-Rennesson, I., 2012. Automatic knot detection and measurements from X-ray CT images of wood: A review and validation of an improved algorithm on softwood samples. Computers and Electronics in Agriculture 85: 77-89.

Mattheck, Claus; Hötzel, Hans-Joachim 1997, Baumkontrolle mit VTA. [fachliche Anleitung und rechtliche Absicherung]. 1. Aufl. Freiburg im Breisgau: Rombach.

Metzler B. , Hecht U., Nill M., Brüchert F., Fink S., Kohnle U. (2012): Comparing Norway spruce and silver fir regarding impact of bark wounds. - Forest Ecology and Management 274: 99-107.

Nordmark, U. 2003: Models of Knots and Log Geometry of Young Pinus sylvestris Sawlogs Extracted from Computed Tomographic Images. Scandinavian Journal of Forest Research 18: 168–175.

Oja, J. 2000. Evaluation of knot parameters measured automatically in CT-images of Norway spruce (Picea abies [L.] Karst.). Holz als Roh- und Werkstoff 58: 375–379.

Pellerin, R. F.; Ross, Robert J. 2002. Nondestructive evaluation of wood. Madison, WI: Forest Products Society.

Rinn, F. 1999. Method and device for 3d-tomographic investigating of materials. US-Patent. PCT/DE00/01467.

Taylor, F.W., Wagner, Jr., F.G., McMillin, C.W., Morgan, I.L., Hopkins, F.F. 1984. Locating knots by industrial tomography—A feasibility study. Forest Products Journal 34(5): 42–46.

Wehrhausen M., Laudon N., Brüchert F., Sauter U.H. 2012. Crack detection in computertomographic scans of softwood tree discs. – Forest Products Journal 62 (6): 434-442.

Evaluation of growth stress in hardwood species using non-destructive equipment's

Frederico França
Department of Forest and Wood Science, Federal University of Espírito Santo, Jerônimo Monteiro, Espírito Santo, Brazil, frederico_franca@hotmail.com

Graziela Baptista Vidaurre
Department of Forest and Wood Science, Federal University of Espírito Santo, Jerônimo Monteiro, Espírito Santo, Brazil, grazividaurre@gmail.com

Leif Nutto
Department of Forest Engineering and Technology, Federal University of Paraná, Curitiba, Paraná, Brazil, lnutto.ufpr@gmail.com

Jordão Cabral Moulin
Department of Forest and Wood Science, Federal University of Espírito Santo, Jerônimo Monteiro, Espírito Santo, Brazil,

João Gabriel Missia da Silva
Department of Forest and Wood Science, Federal University of Espírito Santo, Jerônimo Monteiro, Espírito Santo, Brazil,

Tâmara Suely Filgueira Amorim
Department of Forest and Wood Science, Federal University of Espírito Santo, Jerônimo Monteiro, Espírito Santo, Brazil, tamy.amorim@hotmail.com

Abstract

The aim of the study was to evaluate the level of growth stress detected with CIRAD Forêt method of measurement and correlate with stress wave flight time obtained by different equipment. The phenomenon of development of growth stress and its adverse effects are common to all species, and in angiosperms wood, the occurrence is quite diverse. Stress Wave Timer Metriguard (SWT) and ARBOTOM (ARB) were used in the evaluation. The SWT obtained longitudinal speeds expected for stress waves in living hardwood trees. The values obtained in the transverse direction were lower than reported in the literature. The ARB has obtained longitudinal speeds below those found in the literature, but the values obtained in the transverse direction fall within the expected for stress waves in hardwood living trees. It is necessary a better understanding of the calibration of the equipment, which despite using the same physical principle, its sensors were calibrated to perform different activities. The results were not comparable with those generated by the measuring method of growth stresses.

Keywords: Wood defects. Stress wave timer. Tomograph.

Introduction

Growth stresses are as well-known problem when using wood for higher-value uses. Warping and cracking cause serious mechanical damage and reduce the production of lumber significantly. Strong efforts are made to select genetic material with voltages lower growth or even to assess the factors that influence the levels of stress in standing trees.

The phenomenon of developing growth stresses and adverse effects are common to all species of wood, being of lesser intensity in gymnosperms (Nicholson 1973). In woods of angiosperms, the occurrence is quite diverse. Ponce (1993) reports having seen evidence of these tensions in key species of the Brazilian Amazon, as Mahogany (*Swietenia macrophylla*), Jatoba (*Hymenaea* sp.), Andiroba (*Carapa guianensis*), Cedar (*Cedrela* sp.), Cupiuba (*Goupia glabra*) and in Tatajuba (*Bagassa guianensis*).

The growth stresses are generated within the tissues of the wood, in formations of new consecutive layers of cells from the exchange during the development of the tree (Scanavaca Junior and Garcia 2003). Vidaurre (2010) found that boards Schizolobium amazonicum showed cracks that affect their use as solid and suggested studies for determination of growth stresses, still in the field, using devices such as strain gauges, which measure the DRL (longitudinal residual strain).

The methodology usually applied to measure the stress of growth is the "Growth Strain Gauge", developed by the "Centre de Coopération Internationale Recherche Agronomique pour le in Développement", Département des Forêt - CIRAD Forêt - "Growth Strain Gauge" (Meter Deformation growth), France (Gonçalves et al. 2010). This methodology is semi-destructive and not reproducible in the same measuring point. The equipment measures the longitudinal residual strain (Nutto et al. 2012).

Looking for faster methods to evaluate nondestructive and standing trees in terms of growth stresses, the analysis based on stress wave propagation can offer interesting perspectives on changes in wood. According to Morales (2006) stress wave uses low molecular motions voltage to measure two properties: the stored energy and dissipation. The stored energy is manifested by the rate at which the wave travels through the material, while the rate under which the wave is attenuated is an indication of energy dissipation.

The wave propagation is a dynamic process which is directly related to the physical and mechanical properties of wood. In general, possess greater stress wave propagation speed in high quality wood than in wood or poor quality deteriorated. By measuring the transmission time of the wave through a tree stem in the radial direction, the internal condition of the tree can be estimated fairly accurately (Wang et al. 2004).

The ARBOTOM is a device that performs internal analysis of trees from the difference between the densities of the trunk. This equipment consists of several sensors that are distributed homogeneously by the circumference of the tree, at two different heights, thereby forming two levels. All sensors are connected to a battery, connected to each other via cables and secured in the bole of the tree by means of studs that connect between the sensor and the inside of the shank.

With these small raids nails fixed in trunk, waves emitted in a sensor to propagate through other sensors shock waves, thus creating many connections between sensors. The aim of the study was to evaluate the levels of growth stress detected in the French method of measuring the DRL and corelacinar with flight times of stress waves measured with the help of ARBOTOM and Stress Wave Timer Metriguard.

Materials and Methods

The study was in Vale Nature Reserve, located in the northern state of Espírito Santo, Brazil. 19° 06' and 19° 18' south latitude 39° 45' and 40° 19' west longitude.

The soils are classified as "Yellow dystrophic Oxisol, clayey phase." The climate of this location is AW (tropical humid), with mean annual rainfall of 1,202 mm., Average temperature 22.2° C, relative humidity of 84.3% and altitude between 28 to 65 m (Jesus 2001).

Were selected representing seven trees plantations *Schizolobium amazonicum* (paricá), *Terminalia ivorensis* (peladão), *Swietenia macrophylla* (mahogany), *Cariniana legalis* (jequitibá rosa) and *Pterigota brasiliensis* (farinha seca) to be evaluated.

The method used to measure longitudinal residual strain growth (DRL) is the CIRAD Forêt. It was measured at DBH level in the cardinal directions, north, east, south and west.

Equipment used to determine the velocities of stress waves propagation in longitudinal and transverse directions were Stress Wave Timer Model 239 A from Metriguard (SWT) and ARBOTOM manufactured by Rintech (ARB). Equipment can be viewed in Figure 1.

Figure 1 - Stress Wave Timer Metriguard (left) and ARBOTOM (right).

Beats carried on the shaft, issued to shock waves by means of a sensor, spreading to the other sensor. The operation is based on the speed at which a pulse generated by a strike hammer moves to a sensor fixed at a known distance.

The devices use different methodologies of measurement. It took advantage of the open windows to determine the DRL running for measuring the time of flight. The SWT employs a hammer to generate the shock wave and an accelerometer for detecting the wave. The Metriguard and vibration testing scheme for longitudinal and transverse directions are shown in figure 2.

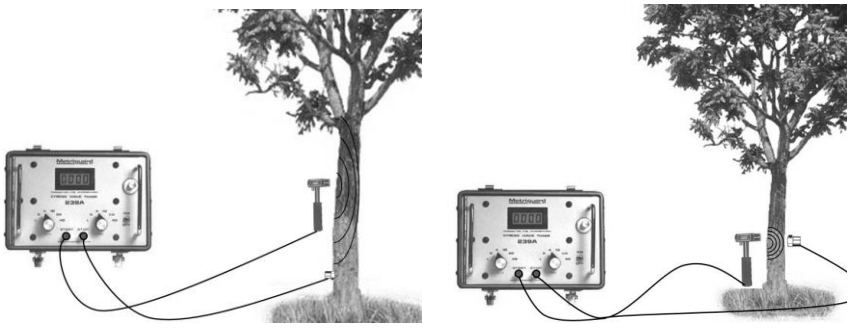

Figure 2 - Schematic of the longitudinal and transverse vibration test.

It was measured the wave propagation time with the SWT (± 1 s.) In the longitudinal direction from top to bottom, set at one meter distance and in the transverse direction from north to south considering the distance of wave propagation equal to DBH. It repeated the measurement ten times. The velocities of the shock waves were calculated using Equation 1.

$$V = \frac{d}{t} \quad (1)$$

where V is velocity of the shock wave, d is distance between generation and reception point, and t is wave transmission time.

Two sensors were used in ARB and the same points used to obtain the STW wave propagation. In the longitudinal direction was performed step towards top-down and bottom-up fixed distance of one meter. In the transverse direction, we considered the DBH as distance flight and conducted measurements in the directions North to South and South to North.

Results and Discussion

Speeds obtained for stress waves with both devices in the longitudinal and transverse directions for the species under study are shown in Table 1.

Table 1 – Velocity obtained for stress waves with both devices in the longitudinal and transverse directions for the species under study

EQUIPMENT	DIRECTION	VELOCITY (m/s)				
		Paricá	Peladão	Farinha seca	Jequitiba Rosa	Mahogany
Metriguard	Longitudinal top-down	4847,60 (5,19)[1]	3466,97 (10,14)	4729,97 (28,49)	5646,60 (23,21)	4188,91 (11,41)
	Transversal north-south	312,653 (21,17)	418,66 (10,81)	551,49 (31,65)	682,76 (32,23)	694,16 (15,61)
ARBOTOM	Longitudinal bottom-up	2084,80 (20,28)	1462,96 (25,93)	1644,124 (16,77)	1614,376 (12,57)	2038,34 (10,86)
	Longitudinal top-down	2084,80 (17,09)	1719,12 (8,52)	1712,49 (16,58)	1872,76 (27,46)	1515,00 (27,74)
	Transversal north-south	597,29 (31,04)	1332,14 (11,68)	1489,57 (8,00)	1500,43 (13,80)	1352,00 (3,83)
	Transversal south-north	590,86 (36,44)	1368,00 (2,12)	1703,00 (6,81)	1639,29 (9,88)	1459,00 (7,75)

1 – variation coefficient (%)

The SWT equipment obtained longitudinal speeds expected for strees waves in living hardwood trees. The values obtained in the transverse direction were lower than reported in the literature. Perhaps this is the largest fitness equipment for measuring propagation times in the longitudinal direction.

The ARB has obtained longitudinal speeds below those found in the literature, but the values obtained in the transverse direction fall within the expected stress wave speeds for hardwood living trees. This equipment is calibrated to detect stress wave propagation times in transverse direction.

The correlations obtained at speeds DRL and longitudinal and transverse directions for the equipment are shown in Table 2.

Table 2 – Correlation between DRL and stress wave velocities in longitudinal and transversal directions for both equipment.

EQUIPMENT	DIRECTION	CORRELATION DRL/ STRESS WAVE VELOCITY				
		Paricá	Peladão	Farinha seca	Jequitiba Rosa	Mahogany
Metriguard	Longitudinal up-down	-0,2492 (0,5900)[1]	-0,4955 (0,2582)	-0,4806 (0,2750)	-0,5142 (0,2377)	-0,6842 (0,0900)
	Transversal north-south	0,1677 (0,7193)	0,8079 (0,0279)	0,5065 (0,2461)	-0,2179 (0,6387)	-0,6625 (0,1049)
ARBOTOM	Longitudinal bottom-up	-0,0004 (0,9992)	-0,8045 (0,0291)	-0,1276 (0,7852)	0,6135 (0,1429)	-0,1000 (0,8311)
	Longitudinal up-down	-0,2069 (0,6563)	-0,1076 (0,8184)	0,2769 (0,5477)	0,2975 (0,5171)	0,8725 (0,0104)
	Transversal north-south	0,8440 (0,0169)	0,0359 (0,9390)	-0,0061 (0,9897)	-0,0505 (0,9143)	-0,5413 (0,2049)
	Transversal south-north	0,7750 (0,0407)	-0,4386 (0,3250)	0,2525 (0,5849)	-0,2061 (0,6575)	0,3222 (0,4810)

1 – variation coefficient (%)

The results show that by using the methodologies used it is not possible to evaluate the growth stresses with the use of ARB and SWT. However, a larger sample may produce results with greater consistency. To create assessment models DRL using SWT and ARB is required to create new methods of analysis.

Conclusions

It`s necessary a better understanding of the calibration of the equipment, which despite using the same physical principle, its sensors were calibrated to perform different activities.

The ARBOTOM showed capability to determinate propagation speeds in transverse direction and Stress Wave Timer Metriguard was able to measure the longitudinal speeds with greater precision.

The two devices allow repeated measurements at the same location of the tree. The results were somewhat comparable to those generated by the growth stresses measuring method CIRAD Forêt.

The ARBOTOM and Stress Wave Timer Metriguard can be applied in studies and characterization of the wood from trees, directed to sustainable forest management and wood technology, such as determining the density, existence of defects within the wood, and correlations mechanical properties.

More research is needed to generate reference values for different tree species wood densities and levels of growth stress.

Acknowledgments

The company VALE for providing the material under study.

References

GONÇALVES et al. Parâmetros dendrométricos e correlações com propriedades tecnológicas de um híbrido clonal de Eucalyptus urophylla x Eucalyptus grandis. Viçosa: Revista Árvore, vol. 34, 2010.

JESUS, R. M. Manejo florestal: impactos da exploração na estrutura da floresta e sua sustentabilidade econômica. 2001. 244 p. Tese (Doutorado) - Universidade de Campinas, 2001.

MORALES, E. A. M. Técnicas de propagação de onda na estimativa de propriedades mecânicas de painéis OSB. 2006, 210 p. Mestrado (Dissertação – Ciências e Engenharia de Materiais), Universidade de São Carlos, 2006.

NICHOLSON, J. E. Growth stress differences in Eucalypts. Bethesda: Forest Science. n. 19, 1973, p. 74-169.

NUTTO, L.; WATZLAWICK, L. F.; GAMMACHU, W. The use of Arbotom® as a non-destructive method for analyzing growth stresses in Eucalyptus benthamii trees. Curitiba: IV Congresso Florestal Paranaense, 2012.

PONCE, R. H. Eucalipto como madeira serrada. São Paulo: Instituto de Pesquisas Tecnológicas, 1993. 22p.

SCANAVACA JUNIOR, L.; GARCIA, J. N. Rendimento em madeira serrada de Eucalyptus urophylla. Scientia Forestalis. Piracicaba n. 63, p. 32-43, jun. 2003.

VIDAURRE, G. B. Caracterização anatômica, química e físico-mecânica da madeira de paricá (*Schizolobium amazonicum*) para produção de energia e polpa celulósica. Viçosa, 2010. Tese (doutorado) – Universidade Federal de Viçosa. 74f.

WANG, X.; FERENC, D.; PILON, C.; BRASHAW, B. K.; ROSS, R. J.; PELLERIN, R. F. Assessment of Decay in Standing Timber Using Stress Wave Timing Evaluation Tools. Madison: Forest Products Laboratory. United States Department of Agriculture, 2004, 14p. (Forest Products Laboratory. General Technical Report).

Evaluation Module of Elasticity of Wood Paraju (Manilkara sp.) Using Nondestructive Testing

Pedro Gutemberg de Alcântara SEGUNDINHO[1]
Lélio Caiado Abreu FRANÇA[2]
Rafael Amorim ROSA[3]
Vinicius Munaldi LUBE[4]
[1,2,3,4]Department of Forestry and Wood Sciences, Center of Agricultural Sciences, Federal University of Espírito Santo - UFES, Av. Gov. Lindemberg, 316, CEP 29550-000, Jerônimo Monteiro, ES, Brazil. E-mails: [1]p_gutemberg2001@yahoo.com.br; [1]pedro.segundinho@ufes.br; [2]leliocaf@gmail.com; [3]rafaelrosa.001@gmail.com; [4]vinicius@woodblog.com.br

Abstract

The aim of this study was to evaluate different methods to obtain the modulus of elasticity (MOE) in specimens of wood *Manilkara* sp. subjected to nondestructive testing. The specimens of dimensions 2.5 cm by 2.5 cm by 76 cm were at ambient moisture conditions and were subjected to the tests of transverse vibration, stress-wave timer, and static bending. The results were analyzed statistically to obtain the correlation between the static MOE obtained by the method in relation to nondestructive methods. We concluded that the most practical and accurate method for obtaining MOE transverse vibration was being a viable alternative to the structural classification of wood.

Keywords: *Manilkara sp.*, nondestructive methods, transverse vibration, stress-wave timer

Dynamic Investigation of a Cable-Stayed Timber Footbridge

Pedro Gutemberg de Alcântara SEGUNDINHO
Department of Forestry and Wood Sciences, Center of Agricultural Sciences, Federal University of Espírito Santo - UFES, Av. Gov. Lindemberg, 316, CEP 29550-000, Jerônimo Monteiro, ES, Brazil. E-mail: p_gutemberg2001@yahoo.com.br; pedro.segundinho@ufes.br

Antonio Alves DIAS
Wood and Timber Structures Laboratory, Department of Structural Engineering, São Carlos School of Engineering, University of São Paulo - USP, Av. Trabalhador Sãocarlense, 400, Parque Arnold Schmidt, CEP 13566-590, São Carlos, SP, Brazil. E-mail: dias@sc.usp.br

Marcelo Rodrigo CARREIRA
Coordination of Civil Engineering, Campus Campo Mourão, Federal Technological University of Paraná - UTFPR, BR 369 km 0,5, CEP 87301-006, Campo Mourão, PR, Brazil. E-mail: carreira@utfpr.edu.br

Abstract

Presented are results of a dynamic numerical analysis of a cable-stayed timber footbridge of approximately span form 35 m and width equal to 2 m located at São Carlos Engineering School, São Paulo State University, São Carlos, Brazil. The timber footbridge modular deck is fabricated from seven interconnected curved stress-laminated timber plates. The timber pylon is made from a single log of *Eucalipto citriodora* standing alone over a spatial hinge. *Pinus taeda* and *Eucalipto citriodora* were the chosen lumbers, because they met the sustainability requirements. The timber footbridge may be described as a curved bridge, supported by 12 steel bars working as stays. The study of the effects caused by human excitation on structures has gained a significant evolution during the last few years. The increased understanding that followed the first studies is difficult to codify and, therefore, is not yet clearly stated in regulatory guidance on dynamic design of a cable-stayed timber footbridge. Walking, running, and jumping on footbridges produce dynamic forces that can activate appreciable vibrations. These vibrations can cause discomfort to pedestrian and deterioration of the footbridge's structural integrity. In the course of this study, which involved the dynamic analysis of a numerical model of the three-dimensional structure developed using the SAP2000® software, vibration modes of the deck were determined. Different loading models were developed to incorporate the dynamical effects, induced by people walking and running, in the dynamical response of the cable-stayed timber footbridge. The dynamic behavior of cable-stayed timber footbridges under walking and running dynamic loads was simulated by resonant vibration caused by synchronous excitations. Completing this study, guidelines for vibration performance are shown, focusing on the definition of the pedestrian load, frequency ranges of interest, criteria that can evaluate dynamic behavior and human comfort on footbridges with acceptable limits of vibration. The results indicated that this footbridge can reach high vibration levels that could compromise the user's comfort limit state. Established measurement criteria allow designers to calculate new structures, and also evaluate the need of repairs of existing ones.

Keywords: Footbridge, cable-stayed, pedestrian, vertical and lateral vibrations, numerical analysis

Estimate of the Modulus of Elasticity of Log Wood through Transverse Vibration

Marcelo Rodrigo CARREIRA
Coordination of Civil Engineering, Campus Campo Mourão, Federal Technological University of Paraná - UTFPR, BR 369 km 0,5, CEP 87301-006, Campo Mourão, PR, Brazil. E-mail: carreira@utfpr.edu.br

Antonio Alves DIAS
Wood and Timber Structures Laboratory, Department of Structural Engineering, São Carlos School of Engineering, University of São Paulo - USP, Av. Trabalhador Sãocarlense, 400, Parque Arnold Schmidt, CEP 13566-590, São Carlos, SP, Brazil. E-mail: dias@sc.usp.br

Pedro Gutemberg de Alcântara SEGUNDINHO
Department of Forestry and Wood Sciences, Center of Agricultural Sciences, Federal University of Espírito Santo - UFES, Av. Gov. Lindemberg, 316, CEP 29550-000, Jerônimo Monteiro, ES, Brazil. E-mail: p_gutemberg2001@yahoo.com.br; pedro.segundinho@ufes.br

Abstract

The logs intended for structural applications need to go through a process of quality assessment to verify that their mechanical properties meet the design requirements. The oldest method of assessment is to visually inspect the surface of the logs. However, one of the biggest drawbacks of this method is that it is impossible to examine the internal integrity of the material. Thus, visual inspection should always be accompanied by a complementary method of nondestructive evaluation (NDE) among the most used are static bending and dynamic tests as ultrasound and transverse vibration. This paper presents an experimental study on estimating the bending modulus of elasticity of logs by transverse vibration tests. Ten Eucalyptus citriodora logs with a length of about 4.5 m and diameter of 16 cm were tested for static bending and transverse vibration. The results showed a good correlation between the static and dynamic modules of elasticity, indicating that the vibration test can be used to evaluate with good accuracy the bending stiffness of logs.

Keywords: Nondestructive evaluation, bending stiffness, wood logs

Colorimetric evaluation of *Hymenolobium petraeum* after accelerated weathering testing

Ricardo Faustino Teles
Ph.D candidate, Department of Forest Engineering, University of Brasília, Brasília, Brazil, rfteles@gmail.com

Alexandre Florian da Costa
Department of Forest Engineering, University of Brasília, Brasília, Brazil, lucate@unb.br

Joaquim Carlos Gonçalez
Department of Forest Engineering, University of Brasília, Brasília, Brazil, goncalez@unb.br

Frederico de Souza
Ph.D candidate, Department of Forest Engineering, University of Brasília, Brasília, Brazil, fredericodesouza@hotmail.com

Patrícia Gomes Ribeiro
Ph.D candidate, Department of Forest Engineering, University of Brasília, Brasília, Brazil, patriciagomesribeiro@gmail.com

Abstract

Weathering is the general term that defines the degradation of materials when exposed to the weather. In order to reduce cost and the duration of the field tests for the assessment of weathering, laboratory tests have been developed to simulate weathering and estimate and compare the natural durability of various wood species. In this context, the objective of this study was to evaluate the effect of accelerated weathering on the colorimetric properties of *Hymenolobium petraeum* wood. Thirty wood samples were produced randomly oriented in the tangential and radial directions. For the evaluation of accelerated weathering a climatic chamber machine QUV/Spray was used and the samples exposed to alternating cycles of radiation, humidity and temperature controlled in accordance with ASTM G 154/2006. The samples were evaluated according to the CIELab system in a spectrophotocolorimeter after successive periods of 24 hours until a total of 240 hours in the exposed faces. It was observed that in the first 24 hours of exposure occurred a darkening in the wood surface by decreasing the lightness variable (L*) and for the entire period of evaluation this parameter stabilized. For the others variables that were noticed an increase of red (a*) and yellow (b*) pigments with subsequent decline on the value of these variables. After 144 hours of exposure, yellow parameter equaled the value of the pattern. These results may indicate a leaching process in the wood surface, modifying the natural color of the wood specie analyzed.

Keywords: CIELab, weathering, color pigments, tropical wood.

Introduction

Weathering is the general term used to define the slow degradation of the materials when exposed to the weather (Williams 2005). The mechanism of degradation depends on the type of material, but the cause is a combination of factors found in nature such as humidity, solar radiation, heat and cold, the use of chemicals in the material surface, abrasion and biological causes. To Ishiguri et al. (2003) weathering is

considered a problem for wood consumers because of the change on texture, color and brightness, as well as affecting the performance of the products applied on its surface.

Wood when exposed to weather suffers damages that are initially observed on the variation of the natural color that can affect the chemical, physical and mechanical properties. Silva et al. (2007) analyzing the effect of weathering on the wood colors claim that this property suffers the action of weathering caused by leaching of rain or by the incidence of light.

The decomposition process due to ultraviolet radiation (UV) presents in sunlight is the most damaging because it begins the chemical modification on the main wood polymers: cellulose, hemicellulose and lignin (Feist and Hon 1984). According to the authors, the action of water leaches the extractives and the photodegraded products, exposing a new surface to weathering.

Chemically, according to Pastore (2004), lignin is taken as the first polymeric component to decompose and the process can be accompanied by the decrease of lignin content and the formation of carbonyl groups on the surface. The cellulose degradation is indicated by weight loss and reduction in degree of polymerization (Pandey 2005). Thus, the photodegradation of wood is a surface phenomenon, due to the large number of chemical groups (carbonyl, double bond, phenolic hydroxyl) or chromophores systems (quinones, biphenyl, and others) of the components distributed in the outer layer that prevents the entry of light into wood (Costa et al. 2011; Pastore 2004).

The color of the wood derives from the chemical composition of the substances present in the xylem: tannins, phenols, flavonoids, stilbenes and other quinones. These substances give the different colors to the wood (Williams 2005). The color, however, is not stable in a timber, since it tends to change with the passage of time, darkening due to oxidation caused mainly by light, which reacts with the chemical components such as lignin.

Colorimetry describes each element of the color composition numerically thru suitable devices. This approach color analysis is used in different plant production systems, such as textile, automotive and chemicals and arts. One of the most used color measurement system is the CIELAB (Commission International de L'Eclairage or International Commission of Illuminant). According to Camargos (1999) and Camargos and Gonçalez (2001), the CIELAB system is a method that defines the sense of the color and is based on three elements: lightness (L*), saturation (C) and hue (a *, b * and h *).

By this context, the objective of this study was to evaluate the effect of accelerated weathering on the colorimetric properties of *Hymenolobium petraeum* wood.

Experimental Methods

Angelim pedra wood (*Hymenolobium petraeum* Ducke) was purchased in form of boards by the dimensions 250 x 30 x 1500 mm (width x length x thickness) and kiln dried at 12% of moisture content. The samples used in the experiment were obtained by a separation of the boards in 200 x 30 x 300 mm dimensions and sawn in the tangential and radial directions. Subsequently, the samples were randomly selected and 30 samples were used in the experiment (15 sample of each direction).

Accelerated weathering

For the accelerated weathering evaluation a UV and condensation a simulating chamber QUV/Spray from Q-Lab Company was used. The chamber simulates the effect of degradation on the surfaces of products caused by sunlight, rain and dew.

The samples were exposed to alternated cycles of radiation, humidity and temperature controlled as specified in ASTM G 154 (2006), Annex I, Cycle 7. Table 1 presents the technical parameters that were applied in the test.

Table 1 - Technical parameters of the cycles applied in the accelerated weathering test.

Parameter	Characteristic
Radiation	1.35W/m²/nm using UVA 340 lamps with a wavelength of approximately 340 nm.
Light exposure	8h on UV range at 60 ± 3°C
Moisture exposure	0.25h moisture spray (no light) in non-temperature controlled
Condensation	3.75 h of condensation at 50 ± 3°C.

The samples were placed in the extension of the display area of the device. All material was previously sanded with a wood sanding (100 grain) to patter the exposed surfaces.

The samples were evaluated in spaced periods of 0, 24, 48, 72, 96, 120, 144, 168, 192, 216 and 240 hours of expose, with 12 hours per cycle, totaling 20 cycles throughout the test. In each periods interval the samples were removed from the equipment and evaluated.

Colorimetric test

The colorimetric parameters were defined by using the technique of diffuse reflectance in the visible range of electromagnetic spectrum. For this test an Eye Color - XTH - X-rite spectrophotocolorimeter was employed connected to a notebook, with a D65 illuminant and 10 ° angle, at room temperature. On each sample 15 evaluations on the exposed surface were determined.

CIELab (CIELAB 1976) was the methodology used to determine the colorimetric parameters. The L* (lightness), a* and b* coordinates (hue), C (saturation) and h* (ink angle) were determined directly from the device software. Saturation (C) was determined by Equation 1:

$$C = \left(a^{*^2} + b^{*^2}\right)^{\frac{1}{2}} \quad (1)$$

where C = saturation; a* = chromatic coordinate on the red-green axis; b* = chromatic coordinate on the blue-yellow axis.

The ink angle (h*) was determined by Equation 2:

$$h^* = tan^{-1}\left(\frac{b^*}{a^*}\right) \quad (2)$$

Additionally, the total color change was determined (Equation 3) according to ASTM D 2244/2009.

$$\Delta E = \sqrt{\Delta L^{*2} + \Delta a^{*2} + \Delta b^{*2}} \quad (3)$$

where Δ= variation between an initial and a final reading.

An analysis of outlier was performed followed by an analysis of variance (ANOVA) and a Tukey test at 5% significance to compare the mean values among the variables.

Results and discussions

Table 2 and Figure 1 show the mean results of the colorimetric parameters evaluated and the standard deviation according to the evaluation periods.

Table 2 - Colorimetric parameters results for the exposure period.

Exposure time	L*	a*	b*	C	hº
0h	58,5a (2,2)	13,5a (0,9)	26,2a (1,2)	29,5a (1,3)	62,7a (1,7)
24h	49,3b (2,1)	20,1b (1,1)	30,0b (1,3)	36,1b (1,3)	56,1b (1,8)
48h	48,8bc (2,3)	19,6c (0,9)	28,2c (1,2)	34,3c (1,0)	55,1c (1,9)
72h	48,4bc (2,4)	19,0d (0,9)	26,8d (1,2)	32,8d (1,1)	54,6c (1,9)
96h	47,7c (2,5)	17,8e (1,0)	24,4e (1,1)	30,2e (1,1)	53,9d (2,0)
120h	47,7cd (2,5)	16,7e (1,0)	22,9f (1,2)	28,4f (1,3)	53,9d (2,0)
144h	48,0cd (2,6)	16,4e (1,1)	22,4g (1,3)	27,8g (1,4)	53,7d (2,0)
168h	48,6de (2,7)	15,8f (1,2)	21,4h (1,3)	26,7h (1,5)	53,6d (1,9)
192h	49,4e (2,7)	15,1g (1,3)	20,7i (1,4)	25,6i (1,7)	54,0d (2,1)
216h	50,0f (2,9)	14,5h (1,4)	19,7j (1,5)	24,5j (1,9)	53,7d (2,0)
240h	50,2f (2,8)	14,1a (1,3)	19,1k (1,5)	23,7k (1,8)	53,6d (1,9)

Where L*=lightness, a*=chromatic coordinate on the red-green axis, b*=chromatic coordinate on the blue-yellow axis, C= chromaticity h*=ink angle. Values shown in parentheses represent the standard deviation. Means with the same letters are not significantly different at p=0.05

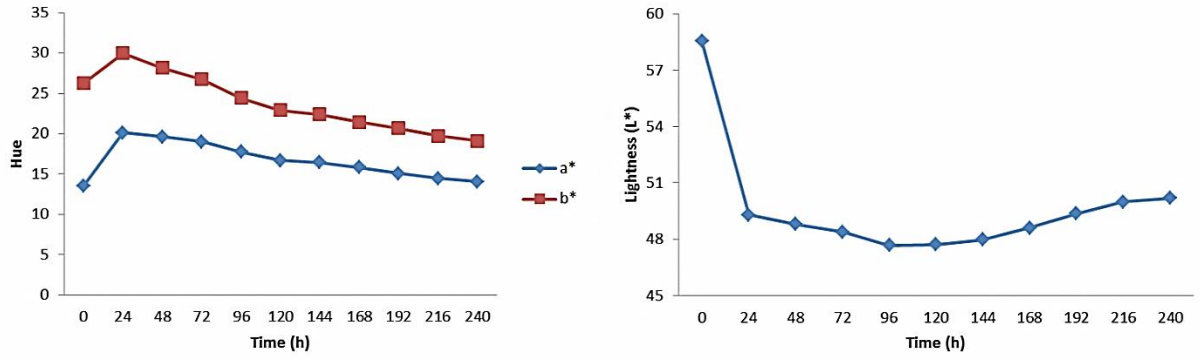

Figure 1 - Changes of hue (a* and b* coordinates) and lightness (L*) over time according to the weathering on *Hymenolobium petraeum* wood.

The hue axis (a* and b*) show the tendency of stabilization and the return of the pigmentation to the initial value, with a tendency to decrease the red and yellow pigments, as the latter being more intense. For lightness (L there was a downward trend in values between 96 and 120 hours of exposure with subsequent positive increment. For chromaticity (C*) it was observed a decrease of the values causing a

decrease in the total color saturation of the wood. This variable represents the deviation from the point corresponding to the gray axis or brightness, and the farther from the axis, the more saturated will be the color. This may be associated with leaching of the photodegraded from the wood surface, leaving the exposed face greyish depending on the depolymerization of lignin and cellulose (Evans et al. 2000).

These factors can be associated with modification of the lignin present in chromophores groups which are capable of absorbing the light radiation in the UV range between 300 and 400 nm. It has been shown that the degradation process is trigged by the formation of free radicals by UV irradiation (Moore and Owen 2001). The wood constituent polymers show different capacities with respect to absorbing UV light to form radicals (Pandey 2005). Lignin is extremely susceptible to UV irradiation, leading to the formation of aromatic free radicals (phenoxyl radicals), which further react with the oxygen to produce carbonyl and carboxyl groups, these being related to wood discoloration by occurrence of unsaturated carbonyl compounds (quinones).

Figure 2 illustrates the curves profiles of reflectance divided into periods of 48 hours of evaluation. It was observed that after the initial exposure to radiation in the region 400-590 nm presented a higher reflectance in accordance with the increase of the exposure period and after reaching the red range above 620 nm the reflectance decreased slightly. This demonstrates the influence of yellow and red pigments in the formation of wood color and the change the color is given by these pigmentations when receiving ultraviolet irradiation. The darkening of *Hymenolobium petraeum* is strongly influenced by the decrease of yellow pigmentation, but with significant activity of red pigmentation.

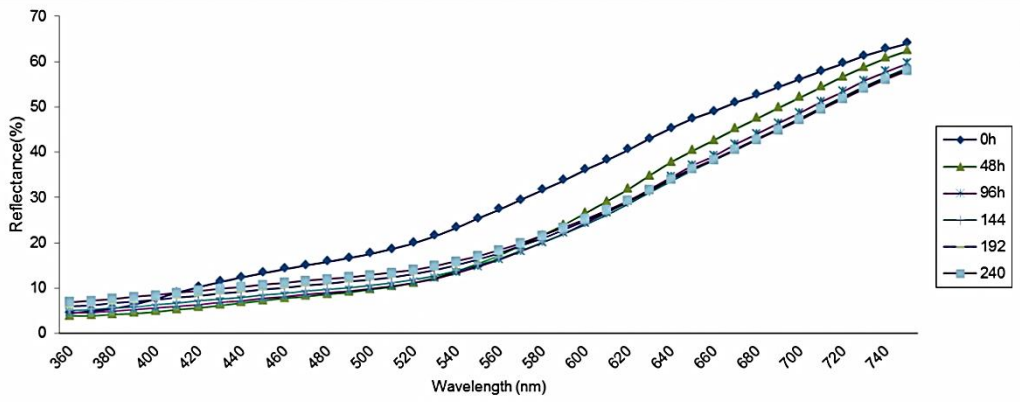

Figure 2— Reflectance curves for *Hymenolobium petraeum* after exposure to artificial weathering.

Regarding to the total change of color, it was observed that there was an appreciable change in relation to the original color of the wood (Figure 3). It was noted that while the first hours of exposure color change was high ($\Delta E = 12$), with the passing of time there was a decrease in the colorimetric change, but still significant. This may be due to the leaching from the wood surface layer, partially renewing the colorimetric profile. Tolvaj (1994) and Martins et al. (2011) observed a similar effect in the influence of ultraviolet radiation on different wood species and concluded that the changes brought about by the action of radiation were more intense during the first 20 hours of exposure, with a pronounced darkening on all species surfaces.

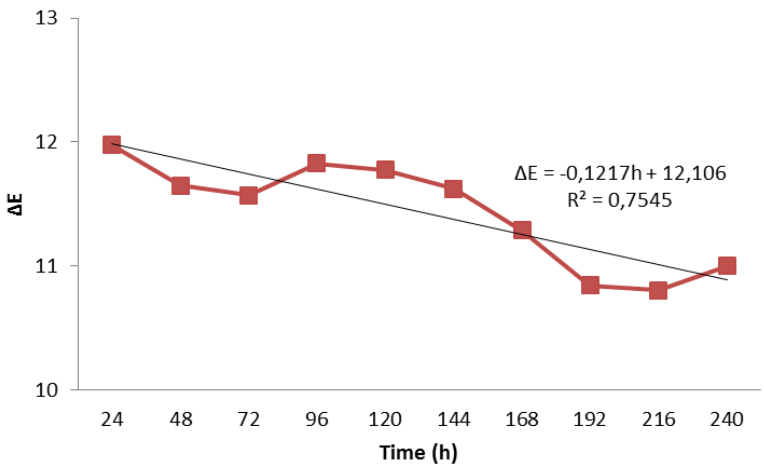

Figure 3 — Variations of total color change (ΔE) for *Hymenolobium petraeum* in different periods of accelerated weathering.

Conclusions

It was observed that in the first 24 hours of exposure occurred a darkening in the wood surface by decreasing the lightness variable (L*) and for the entire period of evaluation this parameter stabilized. For the others variables that were noticed an increase of red (a*) and yellow (b*) pigments with subsequent decline on the value of these variables. After 144 hours of exposure, yellow parameter equaled the value of the pattern. These results may indicate a leaching process in the wood surface, modifying the natural color of the wood specie analyzed.

Reference list

American Society for Testing and Materials. ASTM G 154 - Standard practice for operating fluorescent light apparatus for uv exposure of nonmetallic materials. 2006. Philadelphia, PA.

Camargos, J.A.A. 1999. Colorimetria aplicada na elaboração de uma tabela de cores para madeiras tropicais. Universidade de Brasília, Brasília. 95 p. M.S. thesis.

Camargos, J.A.A.; Gonçalez, J.C.A. 2001. Colorimetria aplicada como instrumento na elaboração de uma tabela de cores de madeira. Brasil Florestal. 71: 30-41.

Costa, J.A.; Gonçalez, J.C.; Camargos, J.A.A.; Gomes, I.A.S. 2011. Fotodegradação de duas espécies de madeiras tropicais: jatobá (*Hymenaea courbaril*) e tauari (*Couratari oblongifolia*) submetidas à radiação ultravioleta. Cerne. 17(1): 133-139.

Evans, P.D.; Beutel, P.J.; Donnelly, C.; Cunningham, R.B. Surface Checking of CCA-treated Radiata Pine Decking Timber Exposed to Natural Weathering. 2000. In: ANNUAL MEETING, 31., Kona, 2000. 12p. Proceedings. Stockholm: The International Research Group on Wood Preservation.

Feist, W.C.; Hon, D.N.S. 1984. Chemistry of weathering e protection. In: ROWELL, R.M. The chemistry of solid wood. Washington D.C.: Am. Chem. Soc.

Ishiguri, F. [and others]. 2003. Extractives relating to heartwood color changes in sugi (*Crytomeria japonica*) by a combination of smoke-heating and UV radiation exposure. J. Wood Sci. 49: 135-139.

Martins, S., Santos, C., Gonçalez, J., Camargos, J. 2011. Envelhecimento artificial acelerado por radiação ultravioleta de madeiras de *Eucalyptus benthamii* e *Pinus caribaea* var. *hondurensis*. Floresta. 41(1): 87-96.

Moore, A.K.; Owen, N.L. 2001. Infrared spectroscopic studies of solid wood. Appl. Spectrosc. Rev. 36: 65-86.

Pandey, K.K. 2005. A note on the influence of extractives on the photo-discoloration and photo-degradation of wood. Polymer Degradation and Stability. 87: 375-379.

Pastore, T.C.M. Estudos do efeito da radiação ultravioleta em madeiras por espectroscopias Raman (FTRaman), de refletância difusa no infravermelho (DRIFT) e no visível (CIE-L*a*b*). 2004. Brasília: Universidade de Brasília. 117p. Ph.D. thesis.

Silva, J.O.; Pastore, T.C.M.; Pastore Júnior, F. 2007. Resistência ao intemperismo artificial de cinco madeiras tropicais e de dois produtos de acabamento. Ciência Florestal. 17(1): 17-23.

Tolvaj, L. 1994. Discoloration and deterioration of wood surface by ultraviolet light. In: Wood Structure and Properties'94 - The 2nd International Symposium. Zvolen – Slovakia.

Williams, R.S. 2005. Weathering of wood. In: ROWELL, R. M. Handbook of wood chemistry and wood composites. Florida: CRC Press. Chapter 7.

Non-destructive evaluation of standing trees and logs in intensively managed second-growth Douglas-fir on Vancouver Island

Ross Koppenaal and Cosmin Filipescu
Canadian Wood Fibre Centre, Canadian Forest Service, Victoria BC

Second-growth plantations of Douglas-fir have become increasingly important to the forest industry in the Pacific Northwest and southwestern British Columbia; however some concerns remain regarding wood quality as a result of intensive management regimes, especially for wood destined for structural applications. In this study we assessed wood mechanical properties in 64-year-old Douglas-fir trees using non-destructive (acoustic velocity) and destructive (SilviScan analysis) techniques in response to pre-commercial thinning and fertilization on a long-term research site on Vancouver Island, British Columbia. The trees were 24 years old when treatments were applied and were assessed forty years later. Trees were sampled in plots in a 2x2 factorial design, with two levels of thinning (control and 1/3 basal area retention) and two levels of fertilization (control and 448 kg N/ha). Acoustic velocity was measured with a time-of-flight tool (ST300, Fibre-gen) on standing trees, as well as with a resonance tool (Director HM200, Fibre-gen) on logs. Wood samples were cut at breast height, 10.7 m and the merchantable top (10 cm diameter) for SilviScan analysis (detailed image analysis, X-ray densitometry, and X-ray diffractometry). Additional disc samples were obtained from multiple stem positions to determine wood density using the water-displacement method. Predictive models of destructive and non-destructive methods were compared to assess the practical implications of intensive silviculture for wood quality. Non-destructive and destructive methods confirm that pre-commercial thinning or fertilization on relatively dry and nutrient-poor sites such as this one (SI=29 m at 50 years), while increasing tree height and diameter, does not adversely affect wood mechanical properties (MOE and density) and may even yield modest gains. Factors responsible for these findings including seasonal soil moisture deficits and crown development are being investigated.

Keywords: NDT tools, acoustic velocity, wood density, MOE, Douglas-fir, thinning, fertilization.

Predicting Wood Quality of Brazilian Amazon Forest Species using a Stress-Wave Timer

Claudete Nascimento, Sámia Valéria dos Santos Barros, Rômulo Geisel Santos Medeiros
Instituto Nacional de Pesquisas da Amzônia, Manaus, Amazonas, Brasil

Abstract

The use of nondestructive techniques can help to classify wood to determine the final use of the product. It can also provide new technological information about species that are lesser known in the marketplace. The study aimed to evaluate the wood quality of the species *Marmaroxlon racemosum* (Ducke) Killlip. ex Record. and *Caraipa densiflora* Mart. through dynamic modulus of elasticity (MOEd) using a stress-wave timer device. The experiment consisted of two treatments with three repetitions. Standing trees of the selected species were evaluated nondestructively using the stress-wave technique to determine the speed and the MOEd. The data were correlated with basic density and shrinkage of the wood species. The expected result is the prediction of wood quality of trees in forest management plans. This will allow for the approximation of a value of the standing timber as well as classifying the raw materials before harvesting in order to predict the best-suited products for the raw materials and determine its resistance properties (MOEd). Emphasizing the variation between trees and species allows for the classification of wood. This method provides an efficient nondestructive technique that allows companies to predict tree quality and develop management plans for approval.

Keywords: Amazon rainforest, tropical forest, tropical woods, stress-wave timer, dynamic modulus of elasticity

Nondestructive Characterization of Tree-Ring Morphology Using the Ring Profiler

David Vahey, C. Tim Scott
USDA Forest Products Laboratory, Madison, WI, USA

Abstract

Ring Profiler is a compact, near portable instrument for characterizing the morphology of tree rings prepared from cores. Sanded specimens are placed in a specially designed microscope and illuminated from the side using the near-infrared radiation from an LED. A precision mount holds the specimen at the microscope focus as it is automatically scanned from pith to bark. Each frame contains several hundred tracheids, from which radial and tangential diameters and wall thicknesses can be determined using image analysis. Frames are characterized for latewood, early-earlywood, and late-earlywood content, and special software can be applied to measure the details of density transition across the growing season. Successive frames are easily patched together to provide a dendrochronological history of the tree, and the nominal density of cellulose, 1.5 g/cm^3, can be applied to the data to estimate the amount of stored carbon. The Ring Profiler could ultimately provide a portable, low-cost instrument for use in dendrochronology, climate change, and Forest Inventory Analysis.

Keywords: Tracheid, morphology, growth ring, latewood, earlywood, radial tangential diameter, wall thickness, density, microscopy, side illumination, dendrochronology, carbon storage, climate change, suppressed growth, Ring Profiler, U.S. Patent 7945098

Could growth competition between trees affect acoustic velocity in standing trees?

Esther Merlo
Departamento de Innovación y Tecnología. MADERA PLUS CALIDAD FORESTAL S.L. Parque Tecnológico de Galicia, Rúa de Vigo nº 2, 32901. San Cibrao dad Viñas. Ourense. Tel +34 988049360. maderaplus@maderaplus.es. www.maderaplus.es

Oscar Santaclara
Departamento de Innovación y Tecnología. MADERA PLUS CALIDAD FORESTAL S.L. Parque Tecnológico de Galicia, Rúa de Vigo nº 2, 32901. San Cibrao dad Viñas. Ourense. Tel +34 988049360. maderaplus@maderaplus.es. www.maderaplus.es

J. Gabriel Alvarez -González
Departamento de Ingeniería Agroforestal, Unidad de Gestión Forestal Sostenible. Universidad de Santiago de Compostela, Campus Universitario s/n E-27002 Lugo, Spain.

Alberto Rojo Alboreca
Departamento de Ingeniería Agroforestal, Unidad de Gestión Forestal Sostenible. Universidad de Santiago de Compostela, Campus Universitario s/n E-27002 Lugo, Spain.

Abstract

Some previous studies showed how thinning does affect growth parameters of individual tree, but can also adversely affect mechanical wood quality. However, none of these raised whether the decrease in wood quality is a side effect resulting from an increase in diameter or a direct effect of the decrease in individual competition. In this study the mechanical wood quality with nondestructive methods was evaluated on standing tree in a radiata pine thinning field trial, established in Galicia (Spain). Three thinning treatments and two social status (dominant and co-dominant) within each treatment were compared. For every tree, individual growth data was assessed and an index of individual competition (BAL) was calculated. Then, two balanced samples of dominant and co-dominant trees per thinning treatment were selected. Every selected tree within each social status were from a similar diameter class and samples covered all the variability of individual index of competition. Acoustic velocity was determined on every sampled tree with a HitmanST300 tool. Difference in acoustic velocity was no significant between thinning treatments but significant between social status, obtaining higher acoustic velocities in co-dominant trees within each thinning treatment. Initial stand density and competition effects were discussed.

Keywords: thinning, wood quality, radiata pine, ST300

Introduction

Technology using the speed of sound for assessing mechanical and physical properties of wood and wood based materials is well known and documented (Achim, et al, 2011). In recent years, research in this field developed methods to assess the acoustic velocity in standing trees to extend these predictions along the tree-to-product chain (Carter et al. 2005, Dickson et al. 2004, Santaclara et al, 2011 (a,b), Merlo et al, 2009 (a,b) , Santaclara et al, 2013). This research has led to commercial field tools for assessing acoustic velocity of trees and logs. Some of these tools (e.g., Fakopp TreeSonic, Fibre-gen ST-300) use the time-

of-flight method to measure acoustic velocity. Outerwood stress-wave velocity is a good predictor of modulus of elasticity which is a key performance criterion for structural timber.

The silvicultural decisions made by forest managers combine with site conditions and environmental factors to influence tree growth and form, and to manipulate the quality of the final crop. Spacing is one of the best tools to control stand development, and increased spacing has a positive effect on growth rate. Thinning treatments are most often implemented with the goal of manipulating tree growth to enhance vigor or crown size. Increased spacing results in less inter-tree competition which results in larger and longer living crowns leading to faster diameter growth (Hapla et al., 2000).

The significant effect of thinning has been reported by other authors (Carter et al. 2005, Wang et al. 2001), but Carter found that thinning led to an increase in acoustic velocity while Wang found a decrease. Differences in species, site conditions, and type of thinning may produce seemingly contradictory effects of thinning. We do not fully understand effects of spacing on MOE.

Radiata pine management must integrate the biological aspects of growing trees with socio-economics, management objectives, practical considerations and other constraints and opportunities. Radiata pine tends to have lower stiffness than many of its competitors in the structural wood market. Furthermore, less is known about how silvicultural practices affect acoustic velocity of trees in a stand; information that is important to managers wishing to make informed choices to enhance stiffness and value of radiata pine plantations, for management of siIvicuItural operations and potential integration with growth models.

Material and Methods

The study was carried out in radiata pine long-term thinning trial established by the Forest Sustainable Unit of the University of Santiago (Lombardero et al., 2012). The trial was located in Begonte, near Lugo, in temperate-subhumid bioclimatic gradient (Martínez-Cortizas and Pérez-Alberti, 1999). The initial stockings at de plantation was of 1670 stems per hectare, and was thinned in 2004, at 12 year old. The thinning treatments were: no thinning, light thinning (10% of basal area removed) and heavy thinning (20% of basal area removed). The time of our study was 9 years after thinning. Three thinning treatments in nine plots randomly distributed in the stand and two social status (dominant and co-dominant, see Figure 1) within each thinning treatment were compared.

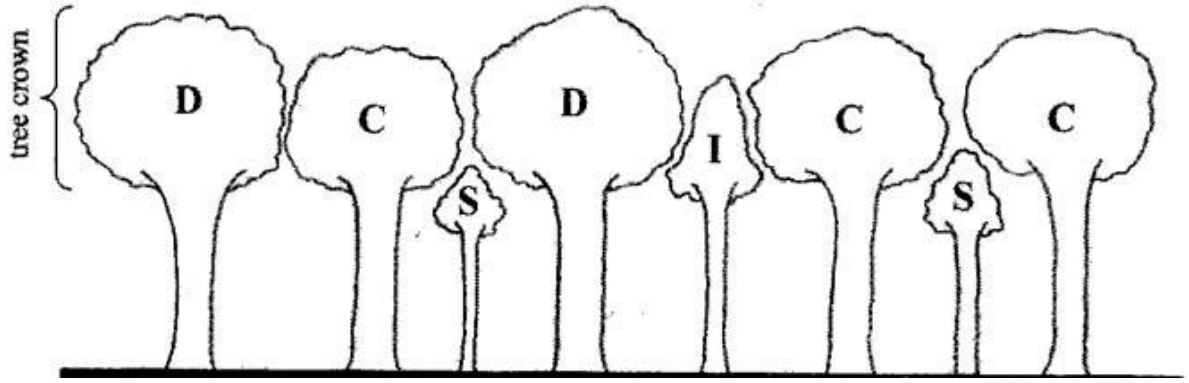

Figure 1. Social status based in tree crown position as it relates to dominance in a forest stand. D=Dominant, C=Codominant, I=Intermediate, S=Supressed (by M. Tarr adapted from Smith 1986).

Some tree variables were measured in all the trees in each plot: Diameter at breast height, (DBH,mm); Total height,(H, m); Height to crown base, (Hc, dm); Slenderness (H/DBH, cm/cm); Crown diameter, m; Spatial index based on basal area (BAL) and a stem basal area (G, m^2/ha).

Then, two balanced samples of dominant and co-dominant trees per thinning treatment were selected (25-36 trees by social status and thinning treatment). Every selected tree within each social status were from a similar diameter class and samples covered all the variability of individual index of competition. Acoustic velocity was measured with a time-of-flight method with a HitmanST300 tool over 1 m distance (Figure 2) on approximately 30 selected trees in each of nine plots (n=172 trees).

Figure 2. Acoustic velocity (m/s) assessment with a Fiber-Gen ST300 tool over 1 m distance.

The data was analyzed with a two-way ANOVA of thinning treatment (heavy, light and control), social status (dominant vs. codominant) and their interaction all treated as fixed effects. Simple linear regressions developed between acoustic velocity data and tree variables provide an overview of the correlation for the trees on each thinning treatments.

Results and discussions

The analysis of variance shows no significant differences in acoustic velocity between thinning treatments but shows significant differences between the social status (Figure 3), with no interaction between the two factors. Codominant trees have higher acoustic velocity in all treatment.

Table 1: Analysis of Variance for V - Type III Sums of Squares

Source	*Sum of Squares*	*Df*	*Mean Square*	*F-Ratio*	*P-Value*
MAIN EFFECTS					
A:Social Status	4,79715E6	1	4,79715E6	25,56	0,0000
B:Thinning treatment	98546,2	2	49273,1	0,26	0,7694
INTERACTIONS					
AB	694489,	2	347245,	1,85	0,1604
RESIDUAL	3,15284E7	168	187669,		
TOTAL (CORRECTED)	3,71428E7	173			

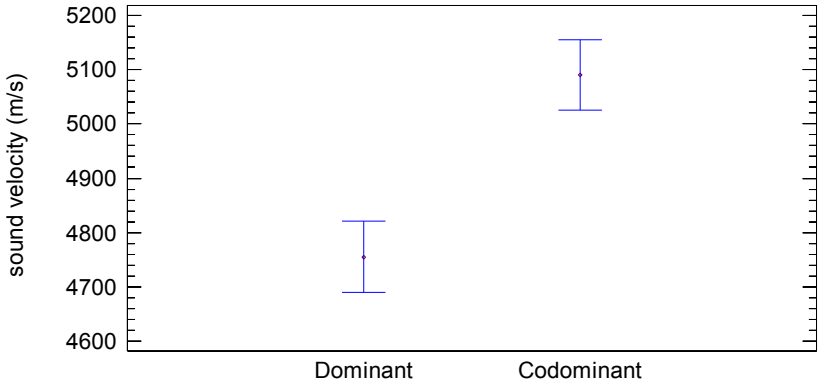

Figure 3. Effect of social status on acoustic velocity

Acoustic velocity was significantly higher in codominant vs. dominant trees (Figure 3). Differences among social status may be related with significant differences between dominant and codominant trees in dbh, crown diameter and height to crown base (data not shown). That is problably because lower acoustic velocity and lower structural quality is associated with a higher percentage of juvenile wood and the formation process of juvenile wood is related to the crown size. This implies that at the same age, probably thay are more juvenile wood section on the dominant trees, than on codominant trees.

The effects of thinning on structural quality of the wood, estimated with the acoustic velocity, have been different in the dominant trees social status versus codominant social status. Thinning causes an increased acoustic velocity of dominant trees but causes a decrease in acoustic velocity on codominant trees (Figure 4).

Coniferous tree crowns continuously change and adapt, responding to thinning factors. The changes in crown morphology in turn initiate changes in the activity of the vascular cambium and the derivation of xylary cells. The influence of the crown on the cambium is exerted through the distribution of photosynthates and the growth regulating hormones— auxins, gibberellins, abscisic acid, cytokinins and ethylene (Larson, 1969; Savidge and Wareing, 1984). It is now well accepted that growth hormones play

an important role in determining cell size and the development of earlywood and latewood, as well as the width of the juvenile wood along the length of the bole.

The differences in acoustic velocity between codominant vs. dominant trees shorten with increasing thinning intensity. This means that the structural quality of the wood can be controlled and can be homogenized within a radiata population, with good thinning management, once the trees have begun the process of formation of mature wood (estimated at 10 years for *Pinus sp.*).

Furthermore, and still higher since the acoustic velocity of the dominant versus codominats is proposed the possibility of providing the elimination of dominant trees in favor of co-dominant in the next thinning mass towards achieving a higher quality for structural use at the time of final crop.

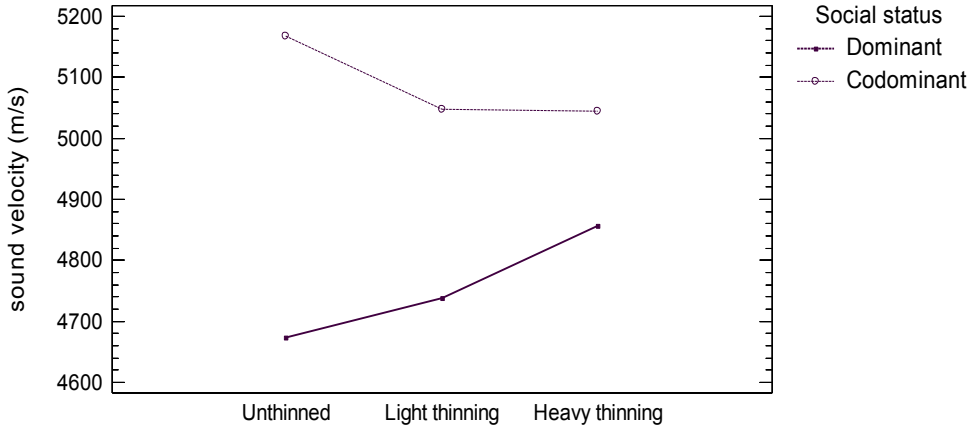

Figure 4. Social status an Thinning treatments interaction

Numerous literature shows the negative correlation between tree diameter and slenderness wtih the acoustic velocity (eg Watt et al. 2006, Laserre et al, 2008). In this paper we show that this correlation is higher in plots without thinning and disappearing nine years after you make a heavy thinning (Figure 5).

The same is observed with the slenderness ratio, with a significant and moderate correlation with the acoustic velocity in the unthinned plots, which decreases by half in the treatment of light thinning and we observed no correlation nine years after heavy thinning treatment. We observed that the crown width is inversely correlated with the acoustic velocity in unthinned plots and this correlation decreases nine years after light thinning and disapear after heavy thinning. The same is observed for the crown height.

Based on this study, in which the dominant fast-growing trees had the lowest sound velocities estimating MOE properties, thinning operations should include removal of trees in the larger dbh classes, along with the more traditional removal of smaller diameter, suppressed trees and damaged trees.

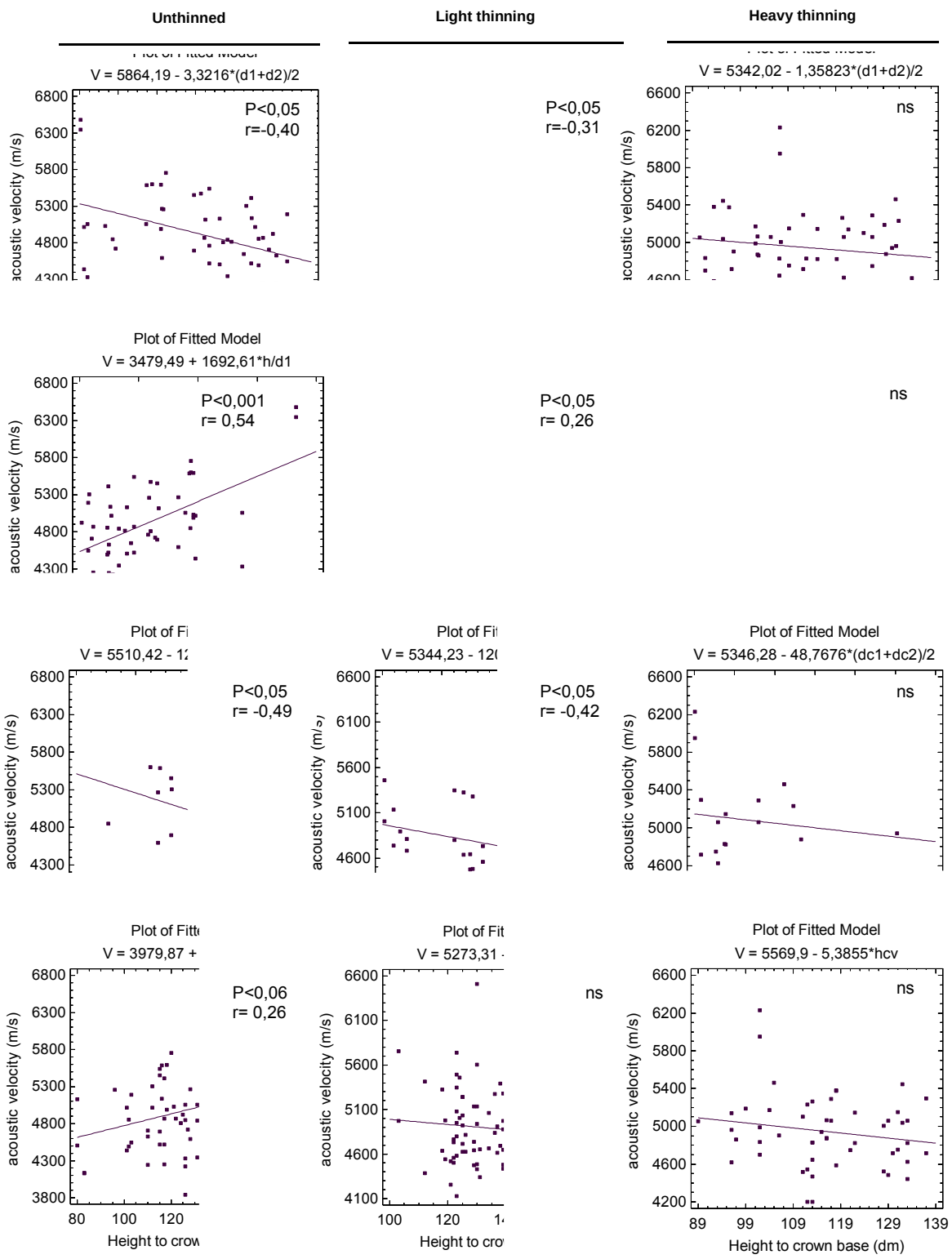

crown diameter and height to crow base variables in each thinning treatment

Conclusions

Acoustic velocity was significantly higher in codominant vs. dominant trees. Differences among social status may be related with significant differences between dominant and codominant trees in dbh, crown diameter and height to crown base.

The effects of thinning on structural quality of the wood, estimated with the acoustic velocity, have been different in the dominant trees social status versus codominant social status. Thinning causes an increased acoustic velocity of dominant trees but causes a decrease in acoustic velocity on codominant trees.

The differences in acoustic velocity between codominant vs. dominant trees shorten with increasing thinning intensity. This means that the structural quality of the wood can be controlled and can be homogenized within a radiata population, with good thinning management, once the trees have begun the process of formation of mature wood.

The tree tools provide a means by which silviculturists, forest managers, and planners can predict stiffness potential of stands prior to harvest and could assist in valuation, stumpage purchase, and harvest scheduling decisions.

Based on this study, in which the dominant fast-growing trees had the lowest sound velocities estimating MOE properties, thinning operations should include removal of trees in the larger dbh classes, along with the more traditional removal of smaller diameter, suppressed trees and damaged trees.

Acknowledgments

We thank field staff of Sustainable Forest Management Unit Research Groups of the University of Santiago de Compostela (code GI-1837-UXFS) official Research Groups of Galician RD System (code 09IDI1794) for their cooperation.

References

Achim, A.; Paradis, N.; Carter, P.; Hernández, R.E.; 2011. Using acoustic sensors to improve the efficiency of the forest value chain in Canada: a case study with laminated veneer lumber. Sensors 2011, 11, 5716-5728.

Carter, P., D.G. Briggs, R.J. Ross, and X. Wang 2005. Acoustic testing to enhance western forest values and meet customer wood quality needs. In: Productivity of Western Forests: A Forest Products Focus. Gen. Tech. Rep. PNW-GTR-642. USDA, Forest Service Pacific Northwest Research Station, Portland, OR. pp 121-129.

Dickson, RL., A.C. Mathieson, B. Joe, J. Ilic, and J.Y. Owen. 2004. Acoustic segregation of Pinus radiata logs for sawmilling. New Zealand J. of Forestry Sci. 34(2): 175-189.

Hapla, F.,Oliver-Villaneuva,J. V.,&Gonzalez-Monila,J. M. (2000). Effect of silvicultural management on wood quality and timber utilisation of *Cedrus atlantica* in the European mediterranean area. European Journal of Wood and Wood Products, 18.

Lasserre, J.P., Mason, E.G., & Watt, M.S., 2008, Influence of the main and interactive effects of site, stand stocking and clone on Pinus radiata D.Don corewood modulus of elasticity, Forest Ecology and Management 255 (8-9), 3455-3459

Lombardero MJ, Alonso-Rodríguez M, Roca-Posada, EP,2012. Tree insects and pathogens display opposite tendencies to attack native vs. non-native pines. Forest Ecology and Management 281:121-129.

Martínez-Cortizas A, Pérez-Alberti A, 1999. Atlas climático de Galicia. Consellería de Medio Ambiente, Xunta de Galicia, Santiago de Compostela, Spain.

Merlo, E.; Santaclara, O.; Pedras, X.F. 2009 (a). Relationship between stress-wave velocity of standing tree and wood quality in 27 year old Douglas-fir. 16 th International Nondestructive Testing and Evaluation of Wood Symposium. Beijing.

Merlo E.; Santaclara, O.; Alvarez, J.G. 2009 (b). Metodología no destructiva para determinación de la calidad mecánica de la madera. V Congreso Forestal Español. Ávila (Spain).

Moore, J.; Lyon, A.; Searles, G.; Ridley-Ellis, D.; 2009. The use of acoustic-based NDT to predict the wood properties of UK-grown sitka spruce at different stages in the wood supply chain. Proceedings of 16th International Symposium on Nondestructive Testing and Evaluation of Wood. 65-70.

Santaclara, O.; Álvarez, J.G.; Merlo, E.; 2011 (a). Modeling structural lumber quality for *Pinus pinaster* Ait. in northwestern Spain using standing tree acoustic assesment, tree characteristics and stand variables. Proceedings of 17th International Nondestructive Testing and Evaluation of Wood Symposium. Sep. 2011. Sopron, Hungary.

Santaclara, O.; Merlo, E.; 2011(b). Acoustic segregation of *Pinus pinaster* logs for structural lumber production according to strength classes. Proceedings of 17th International Nondestructive Testing and Evaluation of Wood Symposium. Sep. 2011. Sopron, Hungary.

Santaclara, O.; Merlo, E.; 2013 Implicaciones financieras de la evaluación de calidad estructural de la madera sobre árboles en pie y trozas de *Pinus pinaster* mediante métodos no destructivos. 6º Congreso Forestal Español. Vitoria.

Wang, X., R.J. Ross, M. McClellan, R.J. Barbour, J.R. Erickson, J.W. Forsman, and G.D. McGinnis. 2001. Nondestructive evaluation of standing trees with a stress wave method. Wood & Fiber Sci. 33(4): 522-533.

Watt, M.S., Facon, J.P., Moore, J.R., Downes, G.M., Clinton, P.W., Coker, G., Davis, M., Simcock, R., Parfitt, R., Dando, J., Mason, E.G., and Bown, H., 2006, Modelling the influence of stand structural, edaphic and climatic influences on Pinus radiata dynamic modulus of elasticity. Forest Ecology and Management, 229 (1-3): 136-144

Structural Evaluation of the Century-Old Paper Mill Building

Xiping Wang, James P. Wacker
USDA Forest Products Laboratory, Madison, WI, USA

Marko Teder
Estonian University of Life Sciences, Tartu, Estonia

Abstract

The purpose of this investigation was to assess the condition of the timber members that serve as the main framing structure of the paper mill—a century-old industrial building in Eau Claire, Wisconsin. The scope of our physical inspection was limited to the areas that were under concern and specified by the facility engineers. A combination of visual, sounding, stress-wave timing, and micro-resistance drilling (Resistograph) techniques were used to inspect the heavy timber structures in predefined areas. The specific tasks were to (1) collect the temperature and relative humidity data for inside air condition of the building; (2) collect wood core samples from representative timber members for species identification; (3) conduct moisture content measurements at various members and locations; and (4) visually inspect and nondestructively test the timber members in specified areas. The physical conditions of the heavy timber structures were determined by analyzing all the visual and NDT data. The evaluation results were presented in color-coded maps created using the Graphisoft software.

Keywords: Condition assessment, condition mapping, inspection, nondestructive testing, timber structure

Visual and Nondestructive Evaluation of Turkish Black Pine (*Pinus nigra*) Structural Lumber

Türker Dündar, H. Volkan Gorguny
Istanbul University, Dept. of Wood Technology, Istanbul, Turkey

Abstract

The objective of this study was to investigate the correlations between the visual strength grading and the mechanical strength of Turkish black pine (*Pinus nigra*) structural lumber determined by both nondestructive and destructive tests. Visual strength grading was carried out on 53 structural lumber samples with the dimensions of 6 by 8 cm (width by depth), 6 by 10 cm and 2-m length according to three different European visual strength grading standards (TS 1265, DIN 4074, and BS 4978). Following the visual evaluation, dynamic modulus of elasticity (DMOE) was determined by both longitudinal vibration and stress-wave nondestructive test methods. The static modulus of elasticity (SMOE) and the modulus of rupture (MOR) were then determined on the lumbers in structural size according to EN 408. Visual, nondestructive, and destructive evaluations were compared statistically to assess the relationships between them. The results indicated significant relationships ($p < 0.05$) between the visual grading classes of BS 4978 and both DMOE and SMOE and MOR, whereas no significant relation was found for other visual strength grading standards. Mechanical grading was more reliable and more efficient than visual grading. Strong correlations were found between the DMOE and SMOE of the lumber ($R > 0.9$). Longitudinal vibration method showed better correlation with SMOE than the stress-wave method. There were also good relationships between the DMOE and MOR but the correlations were lower than SMOE.

Keywords: Longitudinal vibration, stress wave, visual strength grading, nondestructive evaluation, Turkish black pine

A Microwave Application for the Study of Wood Properties

Erik Baradit, Roberto Aedo, Cristhian Aguilera, Marcos Avendaño, Miguel Peredo, Cristian Barria
Universidad del Bio Bio., Concepción, Chile

Abstract

Large expansions of forest plantations in Chile offer great potential to the timber industry for exploitation and export of timber resources. Important elements in optimizing use of the resource include evaluating and classifying a tree's quality, preferable by incorporating new, fast, and noninvasive technologies. In this work, a microwave technology is applied to study properties of wood from *Pinus radiata* D. Don, present in areas of southern Chile. A microwave polarized source of 15 mW power and 10.5 GHz frequency and two systems of detection, formed by a horn antenna and a diode array, were used in this study. These systems were used to evaluate microwave intensity versus moisture content, thickness of material, and grain angle. At the same time, dynamic detection of knots in solid wood was analyzed. Results are shown in graphs of induced voltage intensity of microwaves transmitted through the material versus various physical parameters and tomography images of knots.

Keywords: Microwaves, wood, grain angle, knots

Effect of annual rings on millimeter wave transmission image of wood

Soichi Tanaka
Advanced Wood-based Material Technology Group, Materials Research Institute for Sustainable Development, Advanced Industrial Science and Technology, Nagoya, Japan, sch-tanaka@aist.go.jp

Yuko Fujiwara
Laboratory of Wood Processing, Division of Forest and Biomaterials Science, Graduate School of Agriculture, Kyoto University, Kyoto, Japan, fujiwara@h3news1.kais.kyoto-u.ac.jp

Yoshihisa Fujii
Laboratory of Wood Processing, Division of Forest and Biomaterials Science, Graduate School of Agriculture, Kyoto University, Kyoto, Japan, fujii@h3news1.kais.kyoto-u.ac.jp

Shogo Okumura
Kyoto University, Kyoto, Japan, shogo.okumura.76m@st.kyoto-u.ac.jp

Hiroyoshi Togo
NTT Microsystem Integration Laboratories, Atsugi, Japan, togo@aecl.ntt.co.jp

Abstract

Annual ring structure is important in determining the dimensional stability and strength of wood. But the practical method to detect the structure has been limited to the ionizing radiation such as X-ray. A millimeter wave (MMW) technique has attracted much attention as a new technique that can detect the annual ring structure. In this paper, the effect of annual rings on the millimeter wave image was investigated. The transmission images of the MMW transmitted through 2 mm thick quarter-sawn specimens of six wood species were obtained as the distributions of phase shift and attenuation, and they were campared with the density distributions obtained by the X-ray radiography. The phase shift and attenuation distributions did not always match the density distribution. This probably resulted from the diffraction of MMW in wood.

Keywords: millimeter wave, transmission image, density distribution

Introduction

Wood density distribution due to the annual ring structure is important for the wood product, because the abrupt change of the density may cause the strength reduction and the machining defects such as raised and loosened grain. The practical method for the density distribution evaluation has been limited to the X-ray technique because of its high rectilinearity and penetrability. However, the X-ray has a risk of ionizing radiation exposure.

Millimeter wave (MMW) techniques, which deal with the electromagnetic wave in a frequency range of 30–300 GHz, non-ionizing radiation, have been applied to the non-destructive evaluation of wood (Oyama et al. 2009, Laurinavičius et al. 2010, Tanaka et al. 2011, 2013a, 2013b). It was reported that the

image from this technique showed a higher resolution than that from the conventional microwave technique (Johansson et al. 2007). Laurinavičius et al. (2010) claimed that the MMW transmission image of wood was able to capture the annual rings. However, the relation of the image to the density distribution due to the annual rings has been obscure. In our previous study (Tanaka et al. 2013b) the diffraction of MMW in wood was theoretically and experimentally examined in relation to the annual ring structure.

The purpose of this paper is to clarify the effect of annual rings on the MMW transmission image, which was measured as the distribution of phase shift and attenuation of the MMW transmitted through 2 mm thick quarter-sawn specimens of six wood species with various kinds of annual ring structure. The density distribution of specimens was obtained by the X-ray radiography and compared with the MMW transmission image.

Materials and Methods

Specimens

Quarter-sawn specimens, 100 mm square and 2 mm thick, were prepared from the sound wood of softwoods, hinoki (*Chamaecyparis obtusa*), sugi (*Cryptomeria japonica*), and akamatsu (*Pinus densiflora*); ring-porous hardwoods, kiri (*Paulownia tomentosa*) and keyaki (*Zelkova serrata*); and diffuse-porous hardwood, tochinoki (*Aesculus turbinata*).

All the specimens were stored over a saturated NaBr solution in a desiccator at 27.5 °C to be conditioned at 11% moisture content.

Density measurement with X-ray radiography

The transmission image, intensity distribution, of a specimen was obtained by an X-ray television inspection system (FI-30, Shimadzu). The Cartesian coordinate system on the image, (X, Y), was transformed into the system on the specimen, (x, y), using Shepard's method and the transmission image of a square mesh of 0.35 mm thick steel wires with 5 mm spacing. Furthermore, the X-ray transmission image was converted into the density distribution using the relation between the average density of the specimen and the average intensity of the X-ray (Tanaka et al. 2013b).

Transmission image obtained using MMW measurement system

Figure 1 shows an experimental set-up of a MMW measurement system arranged in a right-handed Cartesian coordinate system (x, y, z). A MMW signal of 100 GHz with an average output power of 10 mW was oscillated in a Gunn diode and divided into two signals, measurement and reference, by a directional coupler. The reference signal was sent to an in-phase/quadrature mixer (IQ-mixer) through a dielectric waveguide. The measurement signal was modulated using a PIN diode at a switching frequency of 100 kHz and passed through a phase shifter. The wave linearly polarized in the y direction was transmitted by a conical horn antenna towards the z direction, and collimated using a Teflon plano-parabolic lens with a diameter of 80 mm and a focal length of 33 mm. The wave that passed through the specimen was received by an open-ended rectangular waveguide with an inner cross section of 2.54 mm in the x direction and 1.27 mm in the y direction and sent to the IQ-mixer, where the in-phase (I) and quadrature (Q) components were discriminated by comparing the measurement and reference signals. The signals from the IQ-mixer were processed into the voltages, V_I and V_Q, in a lock-in amplifier. The front face of the waveguide, excluding the aperture, was covered with MMW absorbent material to prevent reflections from the waveguide and surrounding apparatuses.

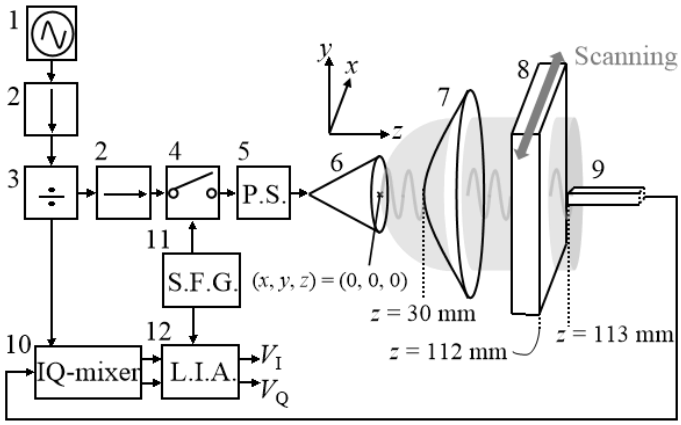

Figure 1—Experimental setup. 1. Gunn diode (100 GHz), 2. Isolator, 3. Directional coupler, 4. PIN diode, 5. Phase shifter, 6. Conical horn antenna, 7. Teflon plano-parabolic lens, 8. Specimen, 9. Open-ended rectangular waveguide (cross section: $x \times y$ = 2.54 mm × 1.27 mm) covered with absorbent of millimeter wave, 10. IQ-mixer, 11. Switching frequency generator (100 kHz), 12. Lock-in amplifier. V_I and V_Q are output voltages of in-phase and quadrature components of millimeter wave.

The phase shift and attenuation of the MMW through the specimen were determined as $\arg(V/V_0)$ and $-10\log|V/V_0|$, where V and V_0 are the complex amplitude of the MMW with and without the specimen, respectively, and they were determined by the voltages, V_I and V_Q, and some correction processes (Tanaka et al. 2013a).

The waveguide was set at (x, y, z) = (0, 0, 113 mm). The specimen was set at (y, z) = (0, 113 mm) and moved along the x-axis in steps of 1 mm within a range of $-10 \text{ mm} \leq x \leq 10$ mm of its center.

Results and discussion

Figures 2–7 show the relation of (a) density and (b) phase shift and attenuation to horizontal position of the specimen of each species.

The phase shift fluctuated with the horizontal position for sugi, akamtsu, and kiri (Figures 3**b**, 4**b**, and 5**b**), while it fluctuated little for hinoki, keyaki, and tochinoki (Figures 2**b**, 6**b**, and 7**b**). Especially for akamatsu and kiri, there was a positive correlation between the density and phase shift in the corresponding position (Figures 4 and 5).

The attenuation significantly fluctuated with the horizontal position for sugi, akamatsu, and kiri (Figures 3**a**, 4**a**, and 5**a**), while it fluctuated a little for other species (Figures 2**a**, 6**a**, and 7**a**). There was a negative correlation between the density and attenuation in the corresponding position for akamatsu and kiri (Figures 4 and 5), while such a correlation was not observed for other species.

The above findings were not entirely consistent with the dielectric properties of wood in the frequency below 10 GHz, in which the phase shift and attenuation was proportional to the density (Torgovnikov 1993). This may be caused by the diffraction of the MMW in the wood specimen (Tanaka et al. 2013b), or a MMW beam may not transmit straight through the specimen. Therefore, for the attenuation in akamatsu and kiri the deformation of the MMW was considered to be inverted by the diffraction, while

for the phase shift in these species the deformation caused by the density distribution might remain after the diffraction.

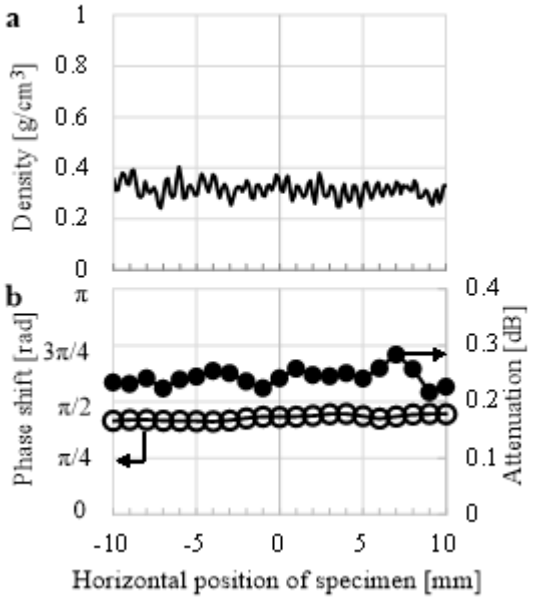

Figure 2—Relation of (a) density and (b) phase shift and attenuation to horizontal position for hinoki.

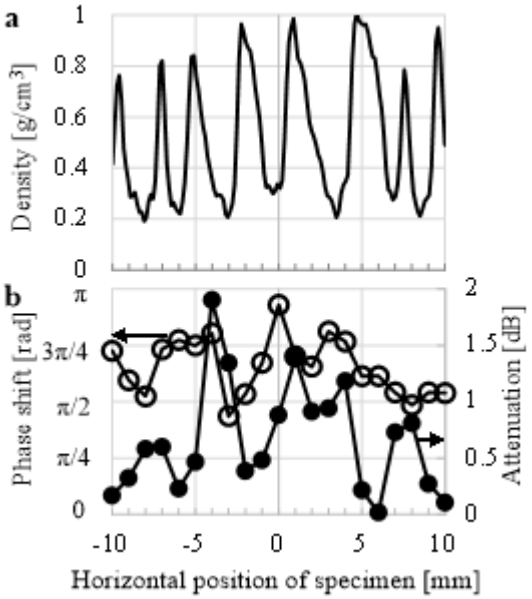

Figure 3—Relation of (a) density and (b) phase shift and attenuation to horizontal position for sugi.

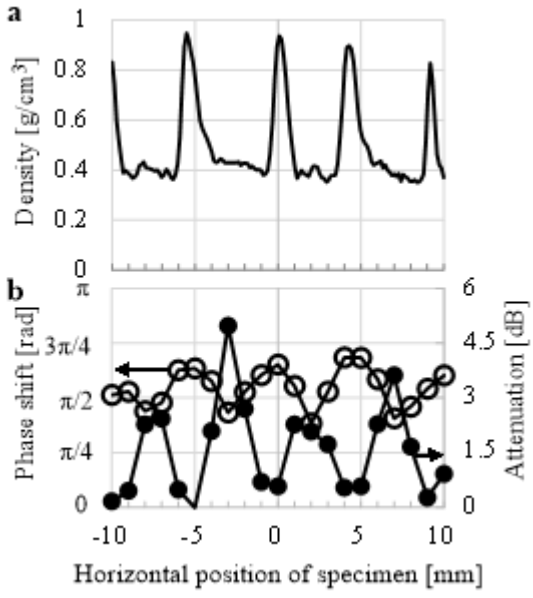

Figure 4—Relation of (a) density and (b) phase shift and attenuation to horizontal position for akamastu.

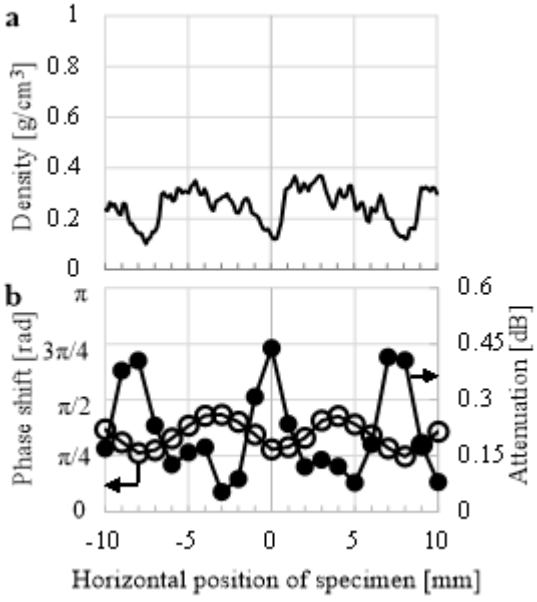

Figure 5—Relation of (a) density and (b) phase shift and attenuation to horizontal position for kiri.

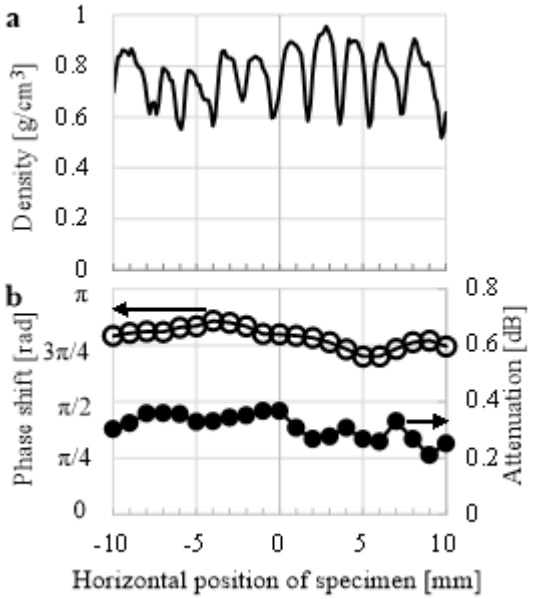

Figure 6—Relation of (a) density and (b) phase shift and attenuation to horizontal position for keyaki.

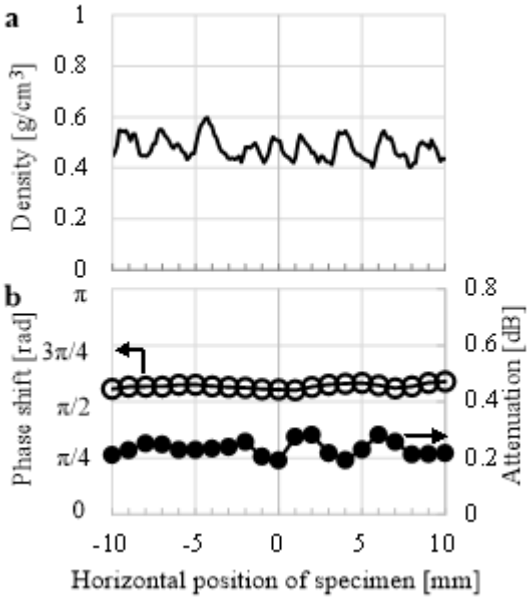

Figure 7—Relation of (a) density and (b) phase shift and attenuation to horizontal position for tochinoki.

Conclusions

To clarify the effect of annual rings on the MMW transmission image, the MMW transmission image, or phase shift and attenuation distributions, of the 2 mm thick quarter-sawn specimen for six wood species was measured using a 100 GHz MMW measurement system. The density distribution along the corresponding range in the specimen was obtained by a X-ray radiography.

The MMW transmission image was not consistent with the density distribution except for phase shift in the specimens of akamatsu and kiri. This may be caused by the diffraction of the MMW beam in the specimens. It is necessary to further examine these findings using the theoretical model or the simulation. This is the challenge to be solved.

Acknowledgments

This work was supported in part by a Grant-in-Aid from the Japan Society for the Promotion of Science for JSPS Fellows (233453) and in part by a Grant-in-Aid from the JSPS (21300329). The authors would like to express their appreciation to Professor Dr. Tadao Nagatsuma of the Graduate School of Engineering Science, Osaka University, who gave us advise on how to adjust the measurement system.

References

Johansson, J.; Hagman, O.; Fjellner, B-A. 2003. Predicting moisture content and density distribution of Scots pine by microwave scanning of sawn timber. Journal of Wood Science. 49(4):312–316

Laurinavičius, A.; Baltrušaitis, A.; Pranckevičiene, V.; Ukvalbergienė, K. 2010. Wood characterization by scanning millimeter wave beam. ISSN 1392-1320 Materials Science (Medžiagotyra). 16(1):63–66

Oyama, Y.; Zhen, L.; Tanabe, T.; Kagaya, M. 2009. Sub-terahertz imaging of defects in building blocks. NDT & E International 42:28–33

Tanaka, S.; Fujiwara, Y.; Fujii, Y.; Okumura, S.; Togo, H.; Kukutsu, N.; Nagatsuma, T. 2011. Effect of grain direction on transmittance of 100-GHz millimeter wave for hinoki (*Chamaecyparis Obtusa*). Journal of Wood Science. 57(3):189–194.

Tanaka, S.; Fujiwara, Y.; Fujii, Y.; Okumura, S.; Togo, H., Kukutsu, N.; Mochizuki, S. 2013a. Dielectric anisotropy of oven- and air-dried wood evaluated using a free space millimeter wave. Journal of Wood Science. DOI 10.1007/s10086-013-1341-7, Published April 2013

Tanaka, S.; Fujiwara, Y.; Fujii, Y.; Okumura, S.; Togo, H., Kukutsu, N.; Mochizuki, S. 2013b. Effect of annual rings on transmission of 100 GHz millimeter waves through wood. Journal of Wood Science. DOI 10.1007/s10086-013-1342-6

Torgovnikov, G.I. 1993. Dielectric properties of Wood and Wood-Based Materials. Springer-Verlag:1-76

Classification of Water Molecules in Wood by a Near-Infrared Spectroscopic Analysis and a Water Mixture Theory

Sang-Yun, Yang
Dept. of Forest Sciences, Seoul National University, Seoul, Korea, email: sly1357@snu.ac.kr
Chang-Deuk, Eom
Research Associate, Korea Forest Research Institute, Seoul, Korea, email: willyeom@gmail.com
Yeonjung, Han
Dept. of Forest Sciences, Seoul National University, Seoul, Korea, email: jack2001@snu.ac.kr
Yoonseong, Chang
Dept. of Forest Sciences, Seoul National University, Seoul, Korea, email: Jang646@snu.ac.kr
Yonggun, Park
Dept. of Forest Sciences, Seoul National University, Seoul, Korea, email: gunny007@snu.ac.kr
Jun-Jae, LEE
Research Institute for Agriculture and Life Sciences, Dept. of Forest Sciences, Seoul National University Seoul, Korea, email: junjae@snu.ac.kr
Joon-Weon, Choi
Research Institute for Agriculture and Life Sciences, Dept. of Forest Sciences, Seoul National University Seoul, Korea, email: cjw@snu.ac.kr
Hwanmyeong, Yeo*
Research Institute for Agriculture and Life Sciences, Dept. of Forest Sciences, Seoul National University Seoul, Korea, email: email: hyeo@snu.ac.kr
(* corresponding author)

Abstract

In this study, the mechanism of moisture adsorption/desorption in wood was analyzed by near-infrared (NIR) spectroscopy. NIR spectra (in the range from 1800 nm to 2100 nm) reflected from moist wood were acquired. According to the Water Mixtures theory of Buijs and Choppin, the spectra, which were sensitive to water variation, were decomposed into three different components. We assumed that the three components represent three types of bound water: water molecule without –OH groups engaged in hydrogen bonds (S0), water molecule with one –OH group engaged in a hydrogen bond (S1), and water molecule with two –OH groups engaged in hydrogen bonds (S2). The ratios of the decomposed spectra of NIR absorbed by each type of water molecule were analyzed during water adsorption/desorption states. A sorption model for predicting the structural state of each water component in wood was constructed through this analysis,. By this model, the effect of each water component on the occurrence of hysteresis could be explained as well as the transient state between bound water and free water. The model shows that the monomolecular water layer in yellow poplar wood forms below approximately 8% Moisture content (MC) during adsorption. Additionally, the model demonstrates that the phenomenon of hysteresis was occurred by the difference between the ratios of the S2 components in desorption and those in adsorption.

Keywords: Water in wood, Near-infrared spectroscopy, Water mixture theory, Buij-Choppin theory

Introduction

For the rational use of wood, which is a representative hygroscopic material, moisture control is essential. Moisture in wood is one of the most important factors that determine its physicochemical properties, such as specific gravity, size, strength, and optical and electrical properties. To analyze and

control these properties, many studies have been conducted on water in wood (Siau 1995; Jung et al. 2008).

In general, water within wood is classified as free water or bound water. Free water is liquid-state water found in lumens or intercellular spaces. Because this water exists in wood just by capillary force and is not chemically associated with cell wall, variations in free water have little effect on the physical and chemical properties of wood. On the other hand, water that is strongly associated with the cell wall in wood is classified as bound water. The bound water adsorbed by wood is held by intermolecular forces between water molecules and the major chemical components of wood, such as cellulose, hemicellulose and lignin. The fiber saturation point (FSP) occurs when the sorption sites in wood are fully filled with water molecules. Below the FSP, the physicochemical properties of wood vary significantly with changes in moisture content (Stamm 1964; Skaar 1988; Eom 2013). Many researchers have posited that the reactivity of hydroxyl groups in the cell wall and dipole interactions between water molecules play a significant role in the moisture desorption/adsorption process. However, this hypothesis has not been clearly demonstrated at the molecular level due to a lack of appropriate analytical techniques.

In this study, near-infrared (NIR) spectroscopy was employed for interpreting the states of water in wood. The NIR absorption bands of pure water are known to appear at 960 nm, 1063 nm 1450 nm, and 1912 nm (Schwanninger et al. 2011). We interpreted water states in the adsorption/desorption processes on the order of hydrogen bonding by analyzing the NIR absorption band, including the 1912 nm wavelength.

Materials and methods

Sample preparation

The yellow poplar (Liriodendron tulipifera) was used in these experiments. The specimen was cut into a small rectangular plate with dimensions of 50×50×10 mm (radial, tangential and longitudinal directions).

Isothermal adsorption/desorption experiments

To analyze water states in the adsorption/desorption process, specimens were first dried in an oven. Using the schedule in Table 1, specimens were humidified at 12 different relative humidity (RH) conditions in the adsorption (0% to 100% RH) process and in the desorption process (100% to 15% RH) until reaching an equilibrium moisture content (EMC) for each. Because it is difficult to achieve 0% MC in a thermohygrostat, specimens were dried in a desiccator.

After completing the adsorption process, the thermohygrostat maintained 100% RH to supply oversaturated moist air for several hours. During this process, the moisture in the oversaturated air condensed as liquid water on the surface of the specimens. This process could induce uniform high MC in specimens. NIR spectra of specimens were acquired 4 times until 50% MC was achieved as moisture content increased. The desorption process was performed by reversing this procedure.

Table 1 Temperature and relative humidity conditions employed in the isothermal adsorption-desorption experiment

Temperature (℃)	Relative humidity (%)											
25	0	15	30	40	50	60	70	80	90	95	99	100

Acquisition of NIR spectra

For measuring NIR spectra, an optical probe-type NIR spectrometer (NIR Quest 256-2.5, Ocean Optics, USA) was used in this study. The optical probe, connected to a tungsten-halogen lamp (20 W) light source, was composed of 7 optical fibers. The outer 6 optical fibers illuminate the surface of the specimen with NIR rays, and the central optical fiber delivers the reflected rays to spectrometer.

NIR reflectance spectra were acquired at the same position of the specimen when the specimen reached equilibrium moisture content during adsorption/desorption processes. For reducing variations in the moisture content on the surface of the specimen caused by factors such as evaporation, NIR spectra were

acquired in a thermohygrostat. To enhance the signal-to-noise ratio, 15 scans were averaged. NIR spectra were acquired at a spectral resolution of 6.3 nm.

Chemometric analysis of NIR spectra

In this study, we analyzed the states of water in wood using NIR spectra, monitoring variations in the water absorption band of wood. To analyze the dependence of the state of water in wood on MC, NIR absorption spectra at each MC were decomposed. Although the spectrometer acquired NIR spectra from 1000 nm to 2400 nm, only the water absorption combination band from 1800 nm to 2100 nm was extracted for analysis. Because the combination band showed large differences in absorbance with changing MC, it was suitable for analyzing water structure in wood.

To analyze the structure of water in wood, we had to choose a model of water structure because there has been controversy between two liquid water structure theories: the mixture and continuum models (Falk and Ford, 1966). The continuum model describes liquid water as a complete water molecule network fully hydrogen bonded with different hydrogen bond energies and geometries. This model explains that the average strength of hydrogen bonds in water is weaker than that in ice because of random distortion and elongation. In contrast, the mixture model describes liquid water as an equilibrium mixture composed of different numbers of hydrogen bonds per molecule. This model explains that the each water molecule has a different hydrogen bonding energy. Additionally, the proposion of each number of hydrogen bonds at particular temperature is maintained at an equilibrium state in this model. Although these two models still conflict with each other, we applied a water mixture model that is adjusted to the classical adsorption model of wood; this concept has been researched extensively in water structure analysis (Maeda et al. 1995; Segtnan et al. 2001).

Buijs and Choppin (1963) proposed that water molecules could be classified into three categories: water molecules without hydrogen bonds (S0), water molecules with one –OH group engaged in a hydrogen bond (S1), and molecules with two –OH groups engaged in hydrogen bonds (S2). In fact, a water molecule is able to engage in four hydrogen bonds. However, because the hydrogen bonds involving the free orbitals of oxygen merely affect the vibrational energy of the water molecule, water molecules could be defined using just three categories.

In this study, difference absorbance spectra, which are the result of subtracting the NIR absorbance of each MC specimen from that of the oven-dried specimen, were calculated to decompose the state of water molecules into three components (fig 1a, b). This computation is able to reduce the overlap of NIR spectra with wood and simplify NIR absorbance spectra so that they only contain the variations of water molecules in wood. In the NIR region, there is a characteristic increase in absorbance as wavelength increases. Therefore, NIR spectra were baselined from 1800 nm to 2100 nm (fig 1 c). The difference spectrum subjected to baseline correction is expected to show only the variation of water equilibrated with atmospheric conditions.

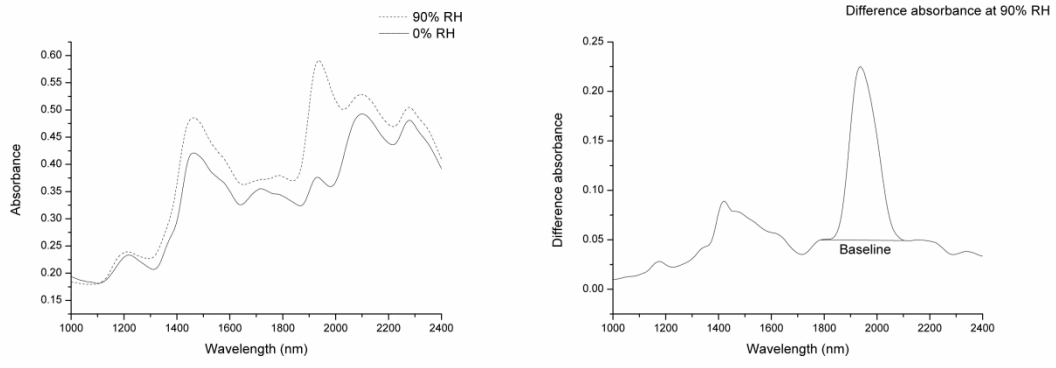

(a) (b)

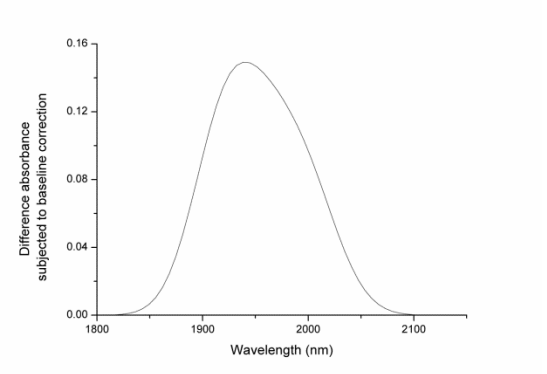

(c)

Figure 1 Procedures for calculating difference spectra. (a) original spectra(RH=90%, 0%), (b) difference absorbance spectra(subtraction from those for RH=0%), (c) difference absorbance spectra after baseline correction

Results and discussion

Categorizing water molecules by the number of hydrogen bonds

One might be able to control the hydrogen bonding state of liquid water by thermal and chemical treatments (Fornés and Chaussidon 1978). However, it is difficult to precisely manipulate the state of water in wood artificially because wood has a complex structure. The NIR absorption band relevant to water in wood could be assigned statistically according to the number of hydrogen bonds formed by each water molecule. In this study, principal component analysis (PCA) was applied to assign bands by the number of hydrogen bonds involved. PCA, which is a type of multivariate analysis, has previously been used successfully to decompose the water sorption band (Tsuchikawa and Tsutsumi 1998; Inagaki et al. 2008).

The water absorption band for each order of hydrogen bonding could be estimated from the spectral loading plot of PC2 (fig. 2). The water absorption band from 1800 nm to 2100 nm was selected to separate the S0, S1 and S2 components. PCA was carried out on all baselined difference spectra, ranging from 1% RH to 99% RH (fig. 2).

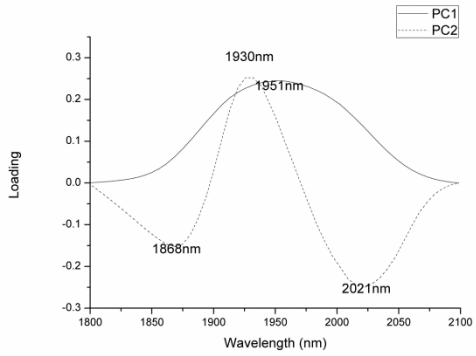

Figure 2 Loading plots of the first and second principal components for the specimen

A normal distribution with a center axis at 1951 nm was derived by PC1, and it covers 98.59% of the variance of the raw spectra. If we assume that water is composed of just one type of component, the peak at 1951 nm can represent that water component. However, because we assumed that water was composed of three types of components (S0, S1, and S2), three peaks should be derived by PC2. Thus, it is concluded that the three distinct peaks at 1868 nm, 1930 nm and 2021 nm represent the three water components S0, S1, and S2, described by Buijs-Choppin theory.

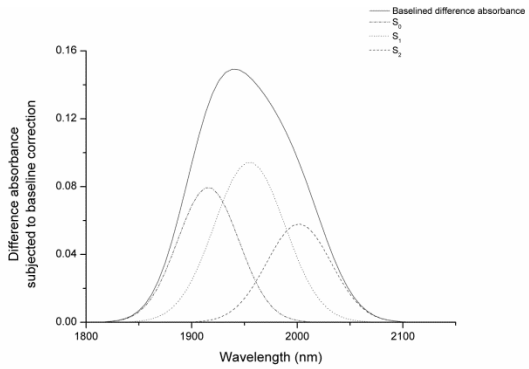

Figure 3 Baselined difference absorbance and decomposed spectra of the specimen

Although the baselined difference spectra are composed of the overlapped water absorption bands of each component, the absorption of each water component could be separated by a curve-fitting procedure using OriginPro 8 (fig. 3). If the absorbance of water molecules was assumed to be a normal distribution, the absorption of each water component could be expressed by an area-integrated method using eq. 1. In eq. 1, AI is area intensity, Sn is the name of the component delineated by the order (n = 0, 1, or 2) of hydrogen bonding, and DA(λ) is the baselined difference absorbance at a wavelength λ.

$$\mathrm{AI(Sn)} = \int DA(\lambda)\mathrm{d}\lambda \tag{1}$$

Variation of water in wood observed by spectral decomposition

Bound water in wood is known to be associated with the cell wall or with other bound water. Wood contains sorption sites, which comprise the –OH and –COOH groups in cellulose, hemicellulose and lignin. In particular, the association of water molecules with the cell wall primarily occurs at –OH groups because the –OH group is the most abundant functional group.

In the early stage of water adsorption by oven-dried wood, water vapor molecules in the air first become hydrogen bonded with sorption sites of the cell wall. The first absorbed water molecules are called mono-molecularly absorbed water. As the adsorption process continues, water molecules in the surrounding air continue to form hydrogen bonds with the absorbed water until the equilibrium moisture content is reached. The water molecules layered upon mono-molecularly absorbed water are called poly-molecularly absorbed water (Skaar 1988; Hartley et al 1992). The absorbed water layers in wood are shown in figure 4.

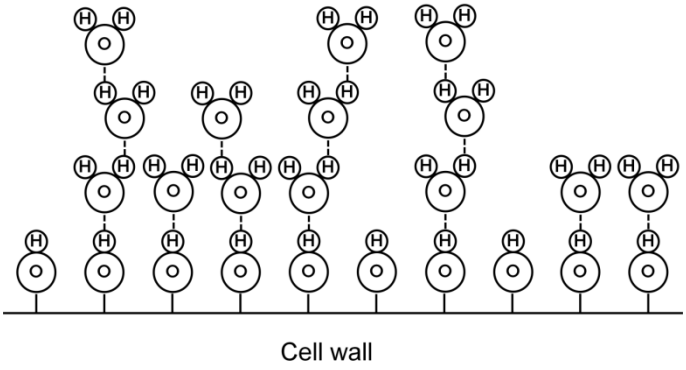

Figure 4 Adsorption model of bound water in wood

With respect to bound water in wood, each adsorbed water molecule is hydrogen bonded. Using the concept of liquid water molecule components (S0, S1, and S2) of Buij and Choppin theory, we separated the states of water in wood. We supposed that the state of water depends on the order of hydrogen bonding. In our model, the oxygen atom of the water molecule is hydrogen bonded to the hydrogen atom

of an –OH group at a sorption site of wood, and the same mechanism is assumed to take place in poly-molecular layer expansion.

The S0 component, water without –OH groups engaged in hydrogen bonds (equivalently, water with no hydrogen bond at either of its own hydrogen atoms), can exist as mono-molecularly adsorbed water or as the water molecule located at the top of the poly-molecularly adsorbed water layer (Tsuchikawa et al. 2006).

The S1 component, which consists of water molecules with one –OH group engaged in a hydrogen bond (equivalently, water with a hydrogen bond at one of its own hydrogen sites), can exist as an adsorbed water molecule in the poly-molecular layer between the sorption site and the top mono-molecular layer water molecule. In the adsorption process, the poly-molecular layer increases with the moisture content of wood. In this case, the oxygen atom of a water molecule in water vapor attaches on the hydrogen atom of mono-molecular water in a progressive process. As a result, the top water molecule in the adsorbed layer is converted from an S0 component to an S1 component.

The S2 component, which consists of water molecules with two –OH groups engaged in hydrogen bonds (equivalently, water with a hydrogen bond at each of its own hydrogen sites), can exist as an adsorbed water molecule with extra hydrogen bonds in the poly-molecular layer. The S2 component could appear at high moisture content because when the adsorption layer grows, water molecules become closer, and more opportunities to bond with other water molecule occur in the three-dimensional structure of the adsorption layer.

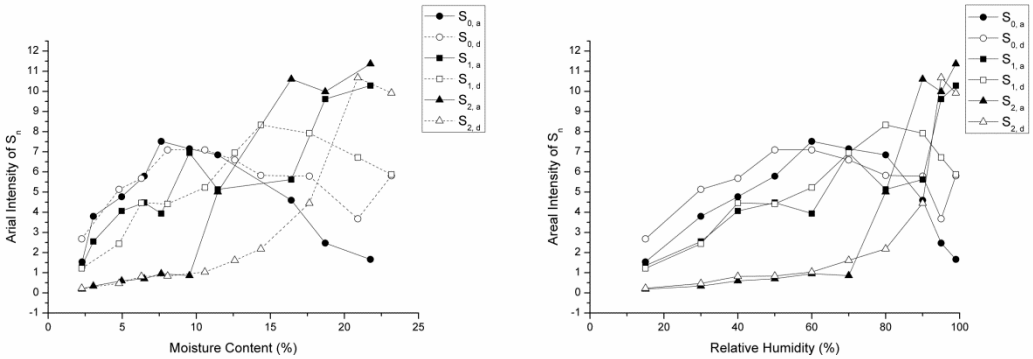

Figure 5 Variations of the S0, S1, S2 components with (a) moisture contents, (b) relative humidity of the specimen

S2 component

When analyzing the moisture adsorption/desorption process in wood, it was more effective to understand the change in the water state of wood if the S2 component was analyzed first. As shown in figure 5 (a), in the adsorption process, the AI of the S2 component was nearly zero until reaching 70% RH (9.54% MC). From 70% RH to 90% RH (16.4% MC), there was a rapid increase in the S2 component. Then, the AI of S2 showed similar values between 90% RH and 99% RH (21.75% MC).

The rapid increase in the S2 component after reaching 9.54% MC during the adsorption process could be explained by the idea that the adsorbed water in the poly-molecular layer started to engage in additional hydrogen bonding with nearby water molecules in the layer. This effect means that there is a threshold for extra bonding. When they overcame the threshold, the water molecules rapidly interacted as MC increased. However, between 90% RH and 99% RH, there was no significant change in the S2 component. This result means that most hydrogen bonding between neighboring adsorbed water molecules is complete at approximately 16.4% MC.

In the desorption process, the AI of the S2 component decreased rapidly from 95% RH (20.91% MC) to 60% RH (10.57% MC). At between 60% RH and the oven-dried state, the AI of S2 in desorption is similar to that in the adsorption process. The reason for the S2 component decrease was concluded to be that evaporation of one S2 water molecule causes the conversion of two S2 water molecules to the S1 component. Because the hydrogen bonding energy decreases as the order of hydrogen bonding increases, the evaporation of S2 water is easier and faster than that of the other types of water, S0 or S1. When one

fully hydrogen-bonded S2 water molecule evaporates, hydrogen bonding between the oxygen atom of the evaporated water molecule and a hydrogen atom of a nearby S2 water molecule, which was bonded to the evaporated water molecule, is broken.

We posited that this difference in S2 AI between adsorption and desorption could be a cause of hysteresis. The range of variation of the S2 component in the adsorption process (70% RH ~ 90% RH) is smaller than that in the desorption process (95% RH ~ 60% RH).

S1 component

In the adsorption process, the AI of the S1 component consistently increased with MC increase. This result could be explained by the amount of increase of poly-molecularly adsorbed water. In particular, the AI of S1 increased rapidly between 90% RH and 99% RH (21.75% MC). In this range, the poly-molecularly adsorbed layer might form additional hydrogen bonds with another adsorbed layer that has grown on another cell wall. Because top-layer water molecules, which are S0 components, bond with other top-layer mono water molecules grown on other cell walls in the high RH condition, the top-layer S0 water molecules are converted to S1 components.

In the desorption process, the AI of the S1 component increased as RH decreased from 99% RH to 80% RH (14.36% MC). This can be interpreted as a state-change relationship between the S2 component and the S1 component. As S2 water evaporated with the breakage of hydrogen bonds, the other S2 components remaining in the adsorption layer were converted to the S1 component. As the desorption process continued, the S1 component consistently decreased with RH decrease from 80% to 15% RH (2.27% MC). This effect was caused by the decrease in the poly-molecular layer.

S0 Component

In the adsorption process, the AI of S0 increased until reaching 60% RH (7.63% MC). This result might be the result of sorption sites in the cell wall being fully occupied with water molecules. As mentioned above, mono-molecularly adsorbed water and top-layer mono water molecules are S0 components in our model. In this range, the poly-molecular layer (S1 component) and the S0 component grew with MC. Considering the change in the S1 component in this range, it could be concluded that the poly-molecular layer growth started before the mono-molecular adsorption was completely finished. This phenomenon occurred because of steric hindrance and accessibility. From 60% RH to 99% RH, the AI of S0 decreased at the end of adsorption process. In this range, it was supposed that poly-molecularly adsorbed water was converted to the S1 or S2 component, binding to nearby water molecules. Upon reaching 99% RH, the top mono water molecule in the poly-molecular layer was converted to the S1 component by binding to other mono water molecules grown on another cell wall.

In the desorption process, the S0 component showed a high AI at 99% RH (23.17% MC). This might be due to the occurrence of capillary water above the fiber saturation point. However, this explanation is just a hypothesis, which should be further researched. The change in the S0 component proceeded as the reverse of the adsorption process. The increase in the S0 component during desorption from 99% RH to 50% RH (8.06% MC) resulted from the rebound of the decrease in the S2 component. In other words, when water molecules with many hydrogen bonds (i.e., the S2 component) evaporated, the S0 component was created. As desorption proceeded from 50% RH to the oven-dried state, the AI of S0 decreased. The reason for the decrease of the S0 component in this range could be concluded to be the evaporation of mono-molecularly adsorbed water from sorption sites. During the adsorption and desorption processes, the maximum AI of S0 appeared at approximately 8% MC. Mono-molecular water adsorption on sorption sites would be complete at approximately 8% MC

Conclusion

By principal component analysis of NIR spectra of water adsorbed to moist wood, we succeeded in extracting 3 different types of bound water molecule components (S0, S1, and S2), which are distinguished by the number of hydrogen bonds formed by the hydrogen atom of the water molecule. It is

found that the change of ratios of each water component during adsorption is different from that in desorption. The ratios of the 3 types of water molecule components in wood during adsorption and desorption were analyzed quantitatively, and we established a sorption model to explain the creation and dissolution of each water component. By our model, it is found that mono-molecular water adsorption on sorption sites would be completed at approximately 8% MC. Additionally, by our model, it is found that there is a large difference between S2 components in adsorption and in desorption; thus, among the three types of water, the S2 component plays the major role in causing hysteresis.

References

Buijs, K.; Choppin, G.; 1963. Near-infrared studies of the structure of water. I. Pure water, Journal of Chemical Physics. 39(8): 2035-2041.

Falk, M.; Ford, T. 1966. Infrared spectrum and structure of liquid water. Canadian Journal of Chemistry. 44(14): 1699-1707.

Eom, C.D.; Park, J.H.; Choi, I.G. [and others]. 2013. Determining surface emission coefficient of wood using theoretical methods and near-infrared spectroscopy. Wood Science Technology. 45(1): 76-83.

Fornes, V.; Chaussidon, J. 1978. An interpretation of the evolution with temperature of the v2+v3 combination band in water. Journal of Chemical Physics. 68(10): 4667-4671.

Hartley, I.D.; Kamke, F.A.; Peemoeller, H. 1992. Cluster theory for water sorption in wood. Wood Science Technology. 26(2): 83-99

Inagaki, T.; Yonenobu, H.; Tsuchikawa, S. 2008. Near-infrared spectroscopic monitoring of the water adsorption/desorption process in modern and archaeological wood. Applied Spectroscopy. 62(8): 860-865

Jung, H.S.; Kang, H.Y.; Park, J.H. [and others]. 2008. A new introduction to wood drying. Seoul: Seoul National University Press.

Maeda, H.; Ozaki, Y.; Tanaka, M. [and others] 1995. Near infrared spectroscopy and chemometrics studies of temperature-dependent spectral variations of water: relationship between spectral changes and hydrogen bonds. Journal of Near Infrared Spectroscopy. 3(4): 191-202.

Schwanninger, M.; Rodrigues, J.; Fackler, K. 2011. A review of band assignments in near infrared spectra of wood and wood components. Jounal of Near Infrared Spectroscopy. 19(5): 287-308.

Segtnan, V.H.; Šašić, Š.; Isaksson, T. [and others]. 2001. Studies on the structure of water using near infrared two-dimensional correlation spectroscopy and principal componant analysis. Analytical Chemistry. 73(13): 3153-3161.

Siau, J.F. 1995. Wood: influence of moisture on physical properties. Department of wood science and forest products. Virginia Polytechnic Institute and State University.

Skaar, C. 1988. Wood-water relations. Berlin: Springer-Verlag.

Stamm, A.J. 1964. Wood and cellulose science. New York: Ronald Press.

Tsuchikawa S.; Tsutsumi S. 1998. Adsorptive and capillary condensed water in biological material. Journal of Materials Science Letters. 17(8): 661-663

MC Prediction Below and Above the FSP by Regression Analysis on the NIR Absorption Spectra

Sang-Yun, Yang
Dept. of Forest Sciences, Seoul National University, Seoul, Korea, email: sly1357@snu.ac.kr
Kwang-Mo, Kim
Research Associate, Korea Forest Research Institute, Seoul, Korea, email: lovewood@forest.go.kr
Yeonjung, Han
Dept. of Forest Sciences, Seoul National University, Seoul, Korea, email: jack2001@snu.ac.kr
Jun-Ho, Park
Dept. of Forest Sciences, Seoul National University, Seoul, Korea, email: gentice7@snu.ac.kr
Yoonseong, Chang
Dept. of Forest Sciences, Seoul National University, Seoul, Korea, email: Jang646@snu.ac.kr
In-Gyu, Choi
Research Institute for Agriculture and Life Sciences, Dept. of Forest Sciences, Seoul National University Seoul, Korea, email: cingyu@snu.ac.kr
Hwanmyeong, Yeo*
Research Institute for Agriculture and Life Sciences, Dept. of Forest Sciences, Seoul National University Seoul, Korea, email: email: hyeo@snu.ac.kr
(* corresponding author)

Abstract

This study was carried out to predict the surface moisture content of Korean pine (*Pinus koraiensis*) wood containing low moisture content (approximately 0%) and high moisture content above the fiber saturation point using near infrared (NIR) spectroscopy. NIR absorbance spectra of circular specimens were acquired at various moisture contents at 25℃. Mathematical preprocessing, the 3-point moving average and Norris 2nd derivatives, were performed to enhance the precision of the regression model. After preprocessing, partial least squares (PLS) regression was carried out to establish the moisture content prediction model. The specimens were divided into two groups based on their moisture content. For the first group, which possessed moisture contents less than 30%, the squared correlation coefficient (R2) and the root mean square errors of prediction (RMSEP) of the regression model were 0.97 and 0.64, respectively. For the second group, which possessed moisture contents greater than 30%, the R2 value and RMSEP of the model were 0.90 and 5.47, respectively. For all of the moisture contents, the R2 and RMSEP were 0.94 and 6.2, respectively. As the range of moisture contents included in the prediction model was expanded, the error of the model increased. In addition, the peak position of the water absorption band (1450 nm and 1940 nm) shifted to longer wavelengths at higher moisture contents.

Keywords: moisture content prediction, near infrared spectroscopy, water absorption band, shift moisture content dependence

Introduction

Usually log that has been cut down in the forest and a freshly sawn timber contain a large amount of water. Because various defects such as cracks and warps are induced by drying stresses during the drying process, the optimization of the drying process is essential for the rational use of green wood. In addition, inappropriate management of the moisture content (MC) of wood during storage and transportation causes many problems, which can result in economic loss and reduced wood resource quality. The MC of wood-based material must be determined to control physio-chemical reactions during painting, adhesion, preservative treatment and biorefining.

To measure the MC of wood in real time, methods based on electrical resistance, electrical capacitance, microwave and ultrasound have been developed. However, for the electrical resistance method, because

the electrical pin is inserted into the measuring point to determine the electrical resistance, this procedure produces holes on the surface of the material, and the size of the holes depends on the MC and strength of the wood. The presence of holes with variable sizes leads to irreproducible signals and inaccurate MC measurements. With other prediction methods, the average MC of wood can be detected; however, the surface MC is difficult to measure, which affects the occurrence of surface defects.

In the present study, the surface MC was predicted using near infrared (NIR) spectroscopy, which can provide information on the presence of surface water and changes in other chemicals. The NIR spectra reflected from the object at wavelengths of 780 to 2500 nm were used. To achieve an objective quality evaluation without the subjective visual inspection of experts, near-infrared spectroscopy has been applied in agriculture and food-related industries. Because the characteristics of wood can be measured by near-infrared spectroscopy without pretreatment such as pelletization, various studies on the correlation between wood and near-infrared spectra have been performed.

Near infrared light penetrates deeper than visible light into wood and is easily transmitted through wood (Brown, 1957). For sitka spruce, the maximum penetration depth that sufficiently interacts with near-infrared light is different for each wavelength (Tsuchikawa et al, 1996). Moreover, longer wavelengths produce lower penetration depths. Tsuchikawa (1996) developed regression models to predict the MC below the fiber saturation point of major Japanese species using near-infrared spectroscopy. Thygesen and Lundqvist (2000) reported that the water absorption spectra of wood in the near-infrared region are shifted due to temperature changes. Due to the aforementioned phenomena, temperature compensation must be performed on absorption spectra to validate the results.

In the present study, a NIR spectroscopic wide range MC prediction model was developed using PLS analysis. Moreover, the MC dependence of the absorption spectra, which were shifted due to variations in the MC, was determined.

Materials and methods

Materials

Korean pine (Pinus koraiensis) was evaluated in the current study. To acquire accurate spectra, the sample must have a sufficient penetration depth, which is the minimum sample thickness in which light is sufficiently diffuse-reflected. Specifically, the minimum thickness for sufficient diffuse-reflection decreases with an increase in the wavelength of light. For sitka spruce, which presents an average surface roughness of 8.7 μm, the sample thickness should be more than 1 mm at 1100 nm to negate the effect of thickness (Tsuchikawa et al, 1996). To consider the effect of thickness, 15 specimens with a thickness of approximately 5 mm were prepared. The cross section was cut into a circle to minimize the presence of an MC gradient at high MCs. Because a rectangular shape tends to induce a MC gradient at the edges and vertices of the specimen, it is easier to control the MC gradient when the sample has a round shape rather than a rectangular shape.

Methods

Below the fiber saturation point

Specimens were humidified to different MCs below the fiber saturation point by changing the humidity at a constant temperature of 25℃. The hygrostat used in the present study was designed to acquire near-infrared reflectance spectra in a chamber. After the specimens reached the equilibrium moisture content (EMC) at every relative humidity (Table 1), NIR spectra of the specimens were acquired.

Table 1—Environmental conditions for humidifying wood specimens below the fiber saturation point.

Temperature (℃)	RH (%)	Average EMC* (%)	Standard deviation of EMC	Facility
25	99	25.18	1.02	Thermohygrostat
	95	18.20	0.39	

	80	15.30	0.51	
	65	12.90	0.41	
	50	9.70	0.30	
	25	7.64	0.36	
	1	0.76	0.16	

*Equilibrium moisture content

High moisture content

The MC is difficult to derive experimentally as the fiber saturation point is approached (approximately 30%). However, to construct a regression model including high MCs, a MC near the fiber saturation point must be induced because the fiber saturation point is a transition state. To induce a MC near the fiber saturation point, the thermohygrostat was controlled at 25 ℃ and 100% RH. Under these conditions, super-saturated air was supplied into the hygrostat, and moisture present in air was condensed on the surface of the specimens. Through this process, the MCs of the specimens were derived according to the results shown in Table 2.

Table 2—Environmental conditions used to achieve MCs near the fiber saturation point using super-saturated air.

Temperature (℃)	RH (%)	Time (h)	Average MC (%)	Standard deviation of MC (%)	Facility
25	100	4	28.88	1.02	Thermohygrostat
	100	10	32.66	0.39	

To obtain an MC close to that of green wood, specimens were immersed in a water bath for specified periods of time. After removing the specimens from the water bath, the samples were centrifuged for 5 minutes at 25℃ and 100% RH to prevent water evaporation from the surface and reduce the effects of gravity, which interfere with the uniform distribution of liquid water in the specimen. Table 3 shows the soaking times and corresponding MCs.

Table 3—Soaking conditions employed to prepare wet wood specimens above the fiber saturation point.

Temperature	Soaking time (h)	Average MC (%)	Standard deviation of MC (%)	Facility
25℃	0.5	38.35	2.04	Thermohygrostat
	1	49.40	2.42	
	3	57.59	2.84	
	6	68.42	2.26	
	24	88.45	3.02	

Chemometric analysis

To acquire the reflectance spectra, a NIR spectrometer (NIR QUEST 256-2.5, Ocean Optics) was used. The instrument was composed of a tungsten-halogen lamp (20 W), optical probe and spectrometer. The spectrometer was calibrated using a standard substance (WS-1-SL, Labsphere) at wavelengths ranging from 1000 nm to 2400 nm. The optical probe was maintained at 45° when the reflectance spectra were acquired. The reflectance data were converted to the corresponding absorbance, and mathematical preprocessing was performed to develop a more precise prediction model. The performed preprocessing treatments included smoothing (3-point moving average) and Norris 2nd gap derivatization (gap size=1). PLS regressions were performed using the Unscrambler

(Ver. 9.7, Camo Inc, Norway) in cross-validation mode with a maximum of 20 principal components. In the statistical analysis, several parameters were used to evaluate the reliability of the model. In the present study, the coefficient of determination (R^2) and root mean square error of prediction (RMSEP) of each model was compared.

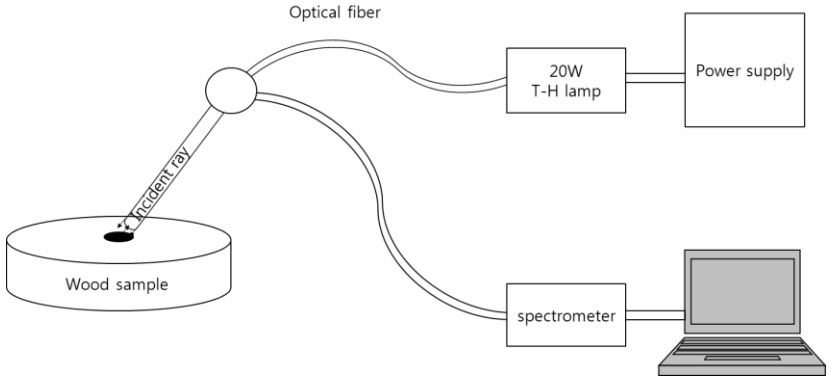

Figure 1—Schematic diagram of the experimental setup used to measure the reflectance spectra of the specimens.

Results and discussion

The dependence of water absorption bands on the moisture content

The original absorption spectra and preprocessed spectra of each moist specimen are shown in Figure 2(a) and Figure 2(b), respectively. In Figure 2 (a), the absorbance at 1440 nm and 1930 nm increased with an increase in the MC. These absorption bands were transformed into negative peaks after obtaining the 2nd derivatives, as shown as in Figure 2 (b). In the current study, PLS analysis was conducted to obtain the 2nd derivative of the absorbance spectra. Spectroscopic interpretations of preprocessed spectra must be performed. As shown in Figure 2(b), the peak at 1930 nm and 1440 nm moved to a lower wavelength as the MC increased, and the negative peak at 1440 nm in the 2nd derivative absorbance spectra moved to 1422 nm as the MC increased. Similarly, the negative peak at 1930 nm moved to 1900 nm as the MC increased. These results indicated that the peak positions of the water absorption bands shifted due to changes in the MC of wood. The observed shifts in the peak position may be due to an increase in the error of the validation model when the MC prediction range was expanded.

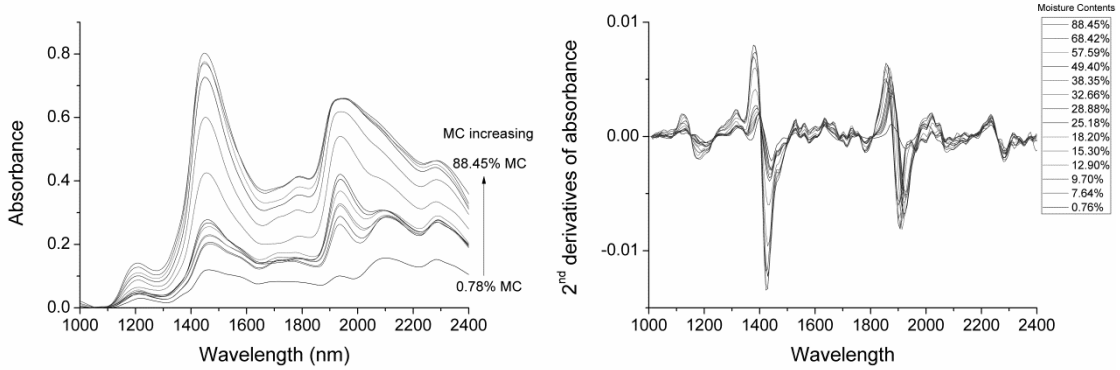

(a) (b)

Figure 2—Absorbance spectra of: (a) original absorbance spectra, (b) preprocessed (3-point moving average, Norris 2nd derivative (gap size=1)) absorbance spectra.

NIR model analysis

Figure 3 shows the validity of the MC prediction model below the fiber saturation point using preprocessed spectra (Fig. 3 (a)) and the regression coefficients of the model at each principal component (Fig. 3 (b). MCs below the fiber saturation point only included the states shown in Table 1. For the prediction of MCs below the fiber saturation point, the model showed high correlations (R2=0.96, RMSEP=1.48) and contained three PCs after optimization. However, relatively high prediction errors were observed for the 0.76% EMC group, which was conditioned at 1% RH. Because of the high prediction error, we analyzed the regression coefficients of each principal component and spectral characteristic.

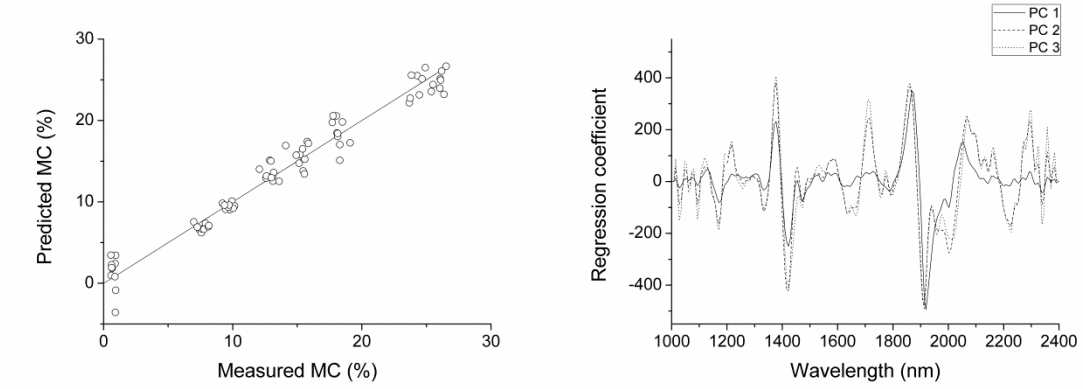

(a) (b)

Figure 3—Surface moisture content prediction model below the fiber saturation point, which was developed by PLS analysis with preprocessed NIR spectra: (a) validation result, (b) regression coefficient of each principal component.

As shown in Figure 2 (a), the absorbance of light by wood, especially light at wavelengths of 1440 nm and 1930 nm, which are the absorption bands of water, increased with an increase in the moisture content in the hygroscopic range. In contrast, dried wood humidified at 1% RH barely absorbed light. Based on the high absolute values of the regression coefficients for each component, water absorption bands can be used to predict the MC of moist specimens but not those of dried specimens humidified at 1% RH.. The aforementioned results may be attributed to the fact that the regression coefficients of each principal component appeared as negative peaks at wavelengths of 1422 nm and 1913 nm ~ 1919 nm. Additionally, the peak position moved to shorter wavelengths as the number of PCs increased.

As shown in Figure 4, the positions of the negative peaks in the 2nd derivative spectra moved from 1441 nm to 1435 nm and 1932 nm to 1919 nm when the MC increased.

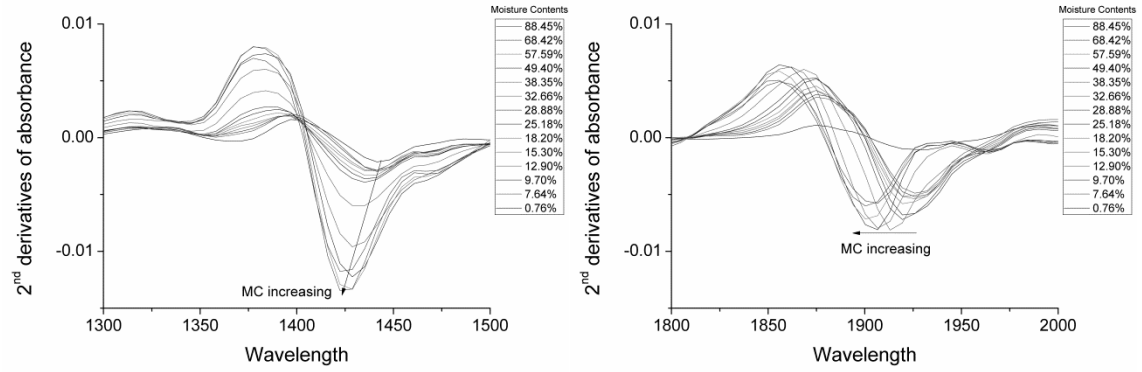

(a) (b)

Figure 4—Preprocessed (3-point moving average, Norris 2nd derivative (gap size=1)) absorbance spectra: (a) 1440 nm band, (b) 1930 nm band.

Figure 5 shows the validation results of the regression model for high MCs and the corresponding regression coefficients. The MC predicted by the model, which contained seven PCs after optimization, presented a high correlation with the actual MC, although the error was high (R2=0.94, RMSEP=4.88). The RMSEP of the prediction model for high MCs was higher than that of MCs below the fiber saturation point. The observed increase in error due to an increase in the MC was attributed to two primary causes.

First, for high MCs, the MC of the spectra acquisition point may be different from that of the average MC of the specimen. To obtain a uniform high MC, specimens were soaked in a water bath for a long period of time and were subjected to a centrifuging process to obtain a uniform MC distribution in the specimen. Nevertheless, differences between the MC of the NIR acquisition point and average MC of specimen may be inevitable. Second, as shown in Figure 5(b), gaps were observed between the peak positions of the regression coefficients at each principal component and water absorption band. Although the negative peak position at 1930 nm in the 2nd derivatives spectra moved to shorter wavelengths when the MC increased, the regression coefficients of PC1, PC2 and PC3 showed positive peaks at 1919, 1906 and 1900 nm, respectively.

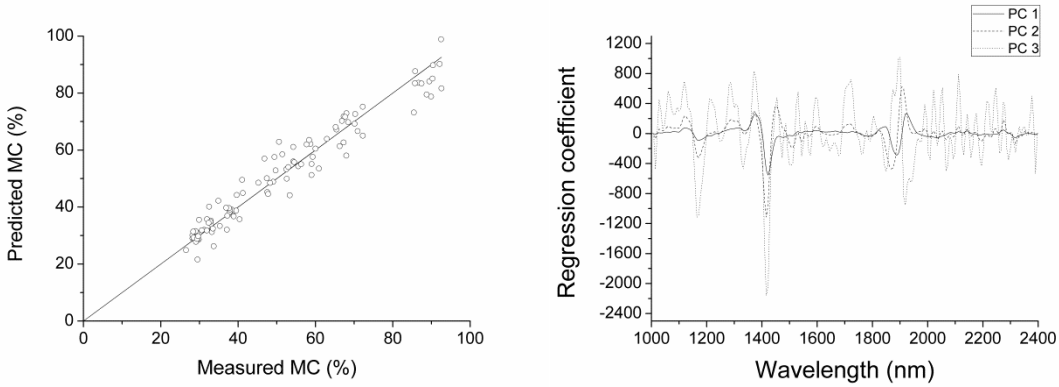

(a) (b)

Figure 5—Surface moisture content prediction model above the fiber saturation point developed by PLS analysis with preprocessed NIR spectra: (a) validation result, (b) regression coefficient.

The peak positions of the regression coefficients of each principal component showed opposite signs and displayed wider shifts compared to those of the prediction model below the fiber saturation point. For the 1420-nm absorption band, negative peaks of regression coefficients were observed at 1416 nm, which represented a 6-nm difference compared to that obtained below the fiber saturation point. The observed difference may be due to shifts in the water absorption peak in the 2nd derivatives spectra, which were attributed to changes in the MC level.

Figure 6 shows the validation results of the MC prediction model for the entire MC range of wood (Table 1, 2 and 3) using preprocessed spectra (a) and regression coefficients of the model at each principal component (b). The MC predicted by the model, which contained six PCs after optimization, presented a high correlation with the measured MC, although the error was high (R2=0.96, RMSEP=5.15). The RMSEP of the prediction model for all of the MCs was higher than that of MCs below the fiber saturation point (and high MCs???). The root cause of the high error may be similar to that of the high MC prediction model. To analyze the regression model of high MCs, we analyzed the regression coefficients of all of the MC models from PC1 to PC3

For the 1420-nm absorption band, a significant shift in the peaks of the regression coefficients was not observed. PC1, PC2 and PC3 showed negative peaks at 1422 nm, 1416 nm and 1416 nm. In contrast, the regression coefficients showed a positive peak for PC1 (1932 nm) and negative peaks for PC2 (1925 nm) and PC3 (1932 nm) in the water absorption band located at approximately 1930 nm. In the 2nd derivative spectra, the water absorption bands shifted from 1932 nm to 1900 nm and 1440 nm to 1422 nm as the MC

increased. That is, differences between the peak positions of the 2nd derivative spectra and regression coefficients of each principal component were detected, which may result in significant errors.

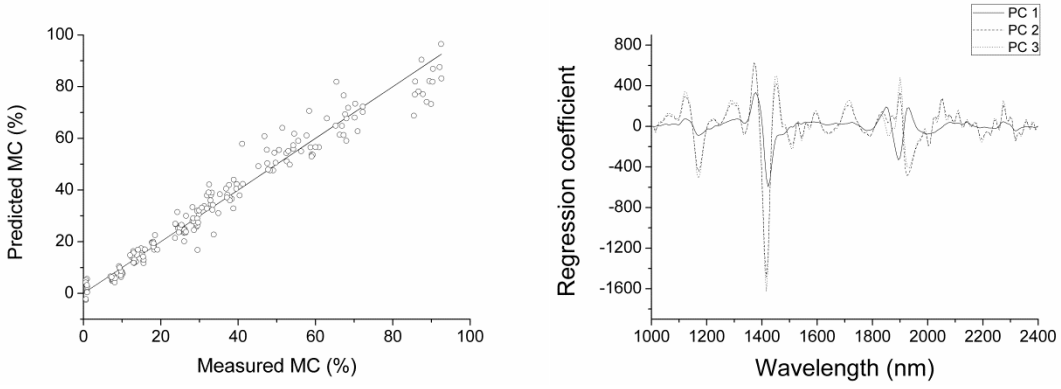

(a) (b)

Figure 6—Surface moisture content prediction model for the entire MC range, which was developed by PLS analysis with preprocessed NIR spectra: (a) validation result, (b) regression coefficient.

Conclusion

In the present study, we confirmed that surface wood MCs could be predicted using near-infrared spectra at wavelengths of 1000 nm to 2400 nm when the MC is less than 100%. The peaks of preprocessed absorbance spectra shifted as the MC increased. As a result, as the range of MCs within the prediction model was expanded, the RMSEP increased. However, the R2 values did not show the same tendency. Therefore, to develop a more concise MC prediction model, shifts in the peaks of preprocessed absorbance spectra should be considered. Calibration of the observed peak shift may improve the validity and reliability of the proposed MC prediction model.

References

Browne, F. 1957. The penetration of light into wood. Forest Product Journal. 7: 308-314.

Czarnik-Matusewicz, B.; Pilorz, S. 2006. Study of the temperature-dependent near-infrared spectra of water by two-dimensional correlation spectroscopy and principal components analysis. Vibrational spectroscopy. 40(2): 235-245.

Cho, K.C. 1998. Application to agricultural study of Near Infrared Spectroscopy. Korean Society for Agricultural Machinery. 23(2): 195-205.

Eom, C.D.; Han, Y.J.; Chang, Y.S. [and others]. 2010. Evaluation of surface moisture content of Liriodendron tulipifera wood in the hygroscopic range using NIR spectroscopy. Journal of the Korean Wood Science and Technology. Mokchae Konghak. 38(6): 526-531.

Inagaki, T.; Yonenobu, H.; Tsuchikawa, S. 2008. Near-Infrared Spectroscopic Monitoring of the Water Adsorption/Desorption Process in Modern and Archaeological Wood. Applied Spectroscopy. 62(8): 860-865.

Thygesen, L.G.; Lundqvist, S.O. 2000. NIR measurement of moisture content in wood under unstable temperature conditions. Part 1. Thermal effects in near infrared spectra of wood. Journal of Near Infrared Spectroscopy. 8(3): 183-190.

Tsuchikawa, S. 2007. A review of recent near infrared research for wood and paper. Applied Spectroscopy. 42(1): 43-71.

Tsuchikawa, S.; Hayashi, K.; Tsutsumi, S. 1996. Nondestructive measurement of the subsurface structure of biological material having cellular structure by using near-infrared spectroscopy. Applied spectroscopy. 50(9): 1117-1124

Tsuchikawa, S.; Torii, M.; TsuTsumi, S. 1996. Application of near infrared spectrophotometry to wood, 4: Calibration equations for moisture content. Journal of the Japan Wood Research Society (Japan). 42(8): 743-754

Use of Nondestructive Testing Methods for Wood Structural Inspection in a Divine Granary

Tao Zhang, Jianxin Xing, Shan Liu, Wei Zhang
Beijing Research Institute of Architectural Heritages, Beijing, China

Abstract

This paper reports a structural investigation of the wooden divine granary built during Jiajing period of the Ming Dynasty in Beijing, China. Following the traditional visual and sounding inspection of the structure, we tested the key structural elements of the granary using a Resistograph and an Impulse Tomograph technique. Small wood samples were also collected from different wood members in the granary for obtaining some basic performance information of the structure, such as natural durability and physical-mechanical properties, which can provide a basis to formulate a repair and maintenance plan. Results showed that it is necessary to use different nondestructive testing methods to assess different types of structural members in an ancient wooden structure. Compared with traditional test methods, Resistograph and Impulse Tomograph are able to provide more accurate and in-depth information in terms of internal conditions of the structure components. The true physical conditions of the wooden structure components can be better evaluated if a combination of traditional and nondestructive testing methods be applied in such a structure condition survey. The results of this investigation also indicated that cracking and decay were two major defects in the structural members of this divine granary.

Keywords: Divine granary, nondestructive testing, structural members, Resistograph, Impulse Tomograph

Correlation of Wood Anatomical Properties with Acousto-Ultrasonic Nondestructive Evaluation in Larch

Xunya Zhang
Research Institute of Wood Industry, Chinese Academy of Forestry, Beijing, China
zhangxy@caf.ac.cn

Xiaomei Jiang
Research Institute of Wood Industry, Chinese Academy of Forestry, Beijing, China
xiaomei@caf.ac.cn

Bin Luo
Research Institute of Wood Industry, Chinese Academy of Forestry, Beijing, China

Yafang Yin *
Research Institute of Wood Industry, Chinese Academy of Forestry, Beijing, China
*Corresponding author: yafang@caf.ac.cn

Abstract

Evaluation of the anatomical features of Larch wood (Larix gmelinii Rupr.), i.e., growth ring width (RW), ratio of latewood (LR), tracheid length (TL), tracheid width (TW) and microfiber angle (MFA), with the AU nondestructive (NDT) evaluation method was investigated in this study. The time domain parameters including time of flight (TOF), maximum voltage (Vmax), time at Vmax (TAV), root mean square voltage(RMS), time centroid (TC), and the parameters of frequency domain including frequency-centroid (FC) and peak frequency (PF) was correlated with anatomical features to prove the feasibility of AU technology for estimating anatomical properties of Larch wood. The results indicated that TOF and MFA gave the high correlation coefficient (r = 0.798) and the multiple regression model based on AU parameters could explain 76% of MFA variability.

Keywords: acousto-ultrasonic(AU), time of flight (TOF), Larch, microfiber angle (MFA)

Introduction

Wood Acousto-Ultrasonic (AU) technology, i.e., the acoustic emission simulation technique with an ultrasonic source has been developed as a complement to the acoustic emission technique. The AU technique is used to characterize the properties of the material between the sender and the receiver, which used for wood and wood-based composites was first developed in the 1980s at Forest Products Laboratory, University of California (Beall 2002., Bucur 2006). A number of applications consequently, ranging from knot detection in solid wood, adhesive curing, biodeterioration detection of wood structural members, and reliability of adhesive-bonded structures, to springback of compressed particleboards have been developed (Kawamoto and Williams 2002).

Growth ring features and tracheid features are classically used to select wood for the industry, and paper mills in particular because of their relationships with mechanical properties of wood and the quality of paper (Frimpong-Mensah 1987, Bendtsen and Senft 1986, Dinwoodie 1965). Microfiber angle (MFA) is recognized as an important factor in determining the mechanical properties of individual fibres (Page et al.

1972, 1977) and in conjunction with density largely determines the strength and stiffness of solid wood (Cave and Walker 1994, Megraw et al. 1999, Evans 2001).

The effect of fibre length on the ultrasonic wave transmission velocity has been studied. These studies indicated that ultrasonic wave transmission velocity increases with the fibre length increasing, but some reported a higher linear correlation and some reported a lower linear correlation (Raczkowski and Helinska-Raczkowska 2004). For example, Raczkowski (Raczkowski and Helinska-Raczkowska 2004) reported a lower linear correlation ($r < 0.50$) between the ultrasonic wave transmission velocity along the fibres and the tracheid length in the wood of 12 coniferous species, and Polge (1984) reported a high linear correlation ($r > 0.90$) in *Prunus avium* L. wood.

Kawamoto et al (2010) investigated the propagation of Acoustic Emission and Acousto-ultrasonic wave in wood materials and found that the microfiber angle in the latewood tracheid affects the attenuation of AU amplitude significantly.

In view of the above reports it seems that it is important to perform a comprehensive study to evaluate wood anatomical properties using AU technique because the published results have only advanced the problem without solving it. Thus, this study is undertaken to check the relationship between wood anatomical features and AU parameters, and to investigate the feasibility of using AU technology for estimating anatomical properties in Larch (*Larix gmelinii* Rupr.) wood.

Materials and Methods

2.1 Specimen preparation

The trees of Larch were sampled from Pangu and Cuigang Forestry Centers, Tahe county of Heilongjiang province in China. The sample trees were above 35 years old and the diameter at breast height (DBH) ranged from 16 to 34 cm.

A total of 40 small and clean specimens with the dimension of 300mm (L)× 20mm (R) ×20mm(T) were processed, and then conditioned to the equilibrium moisture content (EMC) of about 12% in a chamber at 20℃and 65% relative humidity (RH). AU test was performed on these 40 small and clean specimens Fig.1 gives the schematic diagram of specimen preparation for anatomical properties test. After finishing the AU test, a 30mm (L)× 20mm (T)×20 (R) mm block was sawn at the location of 50mm from the end of the specimen to measure RW and LR, and 30 mm (L) × 1.5mm (T) ×1.5mm (R) slice was then cut from each specimen for MFA analysis.

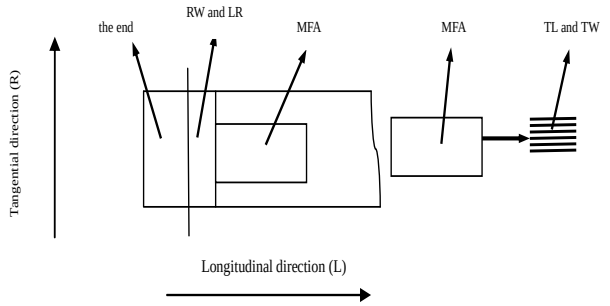

Figure 1— Schematic diagram of specimen preparation for anatomical properties test

After finishing the MFA analysis, specimens which will be subjected to maceration in order to measure tracheid length and tracheid width were then cut from MFA specimens. The MFA, TL and TW were measured in the specimens covering the growth rings located in the middle of the site at which the transducers were placed during the AU measurement.

2.2 Methods

2.2.1 Acousto-Ultrasonic Measurement

The schematic diagram of AU test system is shown in Fig.2. An ultrasonic device (CNS Farnell Limited Corporation, PUNDIT 6) sends and receives a longitudinal ultrasonic wave using two piezoelectric transducers.

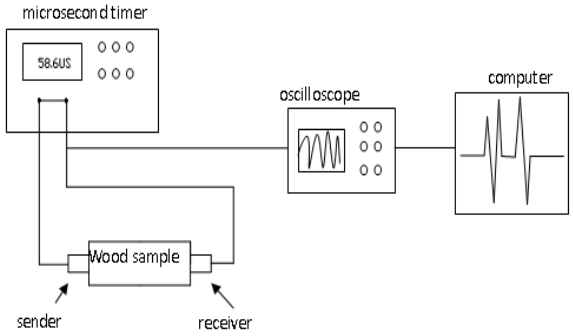

Figure 2— Schematic diagram of AU test system

The transducers (200 kHz) were placed in an assembly jig to assure a constant coupling pressure and vaseline was used as the coupling agent to avoid the disturbance of signal.

A numerical oscilloscope (Tektronix Corporation, TEK 1012B) records the signal received from the transducers, and samples the signal 2500 points at a sampling rate of 1000 kHz. A computer with the data acquisition software OpenChoice®PC was used to save signal data for calculating AU parameters. In this study, seven AU parameters were selected to characterize the wood anatomical properties of Larch. The ultrasonic wave parameters calculated by Excel and Matlab software were, in the time domain, time of flight (TOF) which represents the wave phase velocity, maximum voltage (Vmax), time at Vmax (TAV) which represents the wave group velocity, root mean square（RMS）voltage which represents the signal energy of the transmitted wave, time centroid (TC) which relates to the shape of the signal, and in the frequency domain, frequency-centroid (FC), the center frequency relative to the energy received and peak frequency (PF).

2.2.2 Measurement of growth ring width and the ratio of latewood

The specimens were polished on the cross section to reveal growth rings. The width of growth ring and latewood were measured on polished blocks by means of a scanner and Photoshop software. The ratio of latewood is the ratio between the width of latewood and growth ring width:

$$LR = LW/RW$$

Where RW is the growth ring width and LW is the latewood width.

2.2.3 Determination of micro fiber angle

MFA was measured using X-ray diffractometry (Panalytical Corporation, Philips X'Pert Pro) in a conditioned room maintained at about 50% RH and 20℃.

2.2.4 Measurement of the tracheid length and tracheid width

The wood specimens for tracheid features measurement were macerated in a mixture of H2O2:C2H4O2:H2O=5:4:21. The maceration was performed at 70℃ for 4 days and dyed by water-alcohol solution of safranine. In each specimen the length of 50 tracheids and the width of 30 tracheids were measured by a digital image analyzer (Olympus vm-60N).

2.2.5 Statistical analysis

SAS 10.0 software was used to perform correlation analysis and multiple regressions analysis. A correlation analysis is vital when sorting out suitable predictor variables for regression analysis. Stepwise regression was used to select the AU parameters to establish the multiple regression models to evaluate the sensitivity of the variables to the anatomical features. Both the accepted minimum probability of F-to-enter and F-to remove was set at 0.1.

Results and Discussion

3.1 Results of the anatomical features

Measurement results of the anatomical features of Larch are given in Table 1. RW ranged from 0.4mm to 2.9 mm. LR ranged from 23.4 % to 65.2%. TL ranged from 3311.5μm to 5025.3μm. TW ranged from 34.0μm to 43.3μm. MFA ranged from 8.8 to 29.7 degree.

Table 1—The measurement result of anatomical parameters

Anatomical properties	Min	Max	Mean	Std	*COV(%)*
RW（mm）	0.4	2.9	1.4	0. 6	42.9
LR（%）	23.4	65.2	35.1	7.5	21.4
TL（μm）	3311.5	5025.3	4281.9	460.7	10.8
TW（μm）	34.0	43.3	37.8	2.4	6.3
MFA（°）	8.8	29.7	13.3	5.2	39.1

3.2 Results of the AU parameters

The typical AU output signal is shown in Fig.3. The AU parameters are given in Table 2. The statistical variability of data expressed by the coefficient of variation (COV) in percent was large with range from 7.7% for TOF to 54.5% for Vmax. This observation indicates that more information may be contained in the parameters of Vmax, RMS and FP with larger coefficient of variation than in the parameters of TOF, TAV, TC and FC.

Table 2— The measurement result of AU parameters

AU	Min	Max	Mean	Std	*COV(%)*
TOF(μs)	41.40	58.50	46.14	3.55	7.7
TAV(μs)	48.70	99.80	75.42	12.99	17.2
Vmax(v)	0.02	0.49	0.22	0.12	54.5
RMS(v)	0.00	0.05	0.02	0.01	50.0

TC(μs)	96.58	224.44	137.00	22.30	16.3
PF (v)	1.04	11.11	5.08	2.37	46.7
FC(KHz)	49.61	70.57	61.58	4.51	7.3

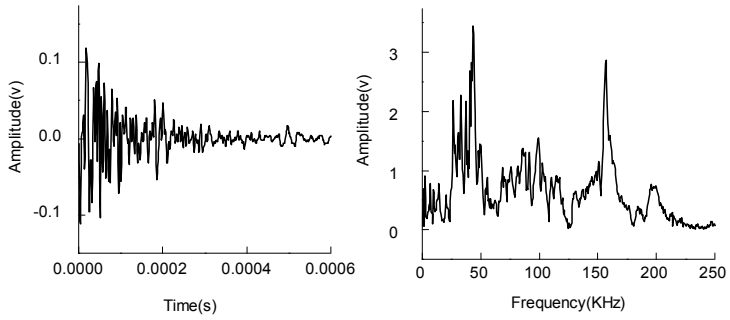

Figure 3— Ultrasonic time-domain signal (left) and frequency-domain signal (right) of Larch

3.3 AU and anatomical features

The Pearson's correlation coefficients between AU parameters and anatomical features are given in Table 3. Table 4 shows a summary of linear regression algorithms generated through the multiple regression approach, and only the regression equations significant at 0.001 level are shown in table 4.

Table 3— The relationship between AU parameters and anatomical properties

AU	RW	LR	TL	TW	MFA
TOF	-0.025	0.271	-0.433(**)	-0.232	0.798(**)
TAV	0.017	0.225	-0.109	-0.055	0.396(**)
Vmax	-0.208	-0.242	0.174	0.201	-0.325(*)
RMS	-0.128	-0.178	0.042	0.152	-0.202
TC	0.02	0.18	-0.141	-0.244	0.221
PF	0.131	-0.025	-0.203	0.052	0.016
FC	-0.054	-0.129	0.404(**)	0.179	-0.372(**)

Note: * significant at 0.05 level; ** significant at 0.01 level

Table 4— The single and multiple regression equation between anatomical features and AU parameters

Dependent	Independent	Equation model	R^2	P
TL	TOF, V_{max}, PF	TL=45482.4-21.76TOF+2764 V_{max} -1149.9PF	0.40	<0.0001
MFA	TOF	MFA=-37.41+1.10TOF	0.64	<0.0001
MFA	TOF，TAV，Vmax, RMS	MFA=-31.90+0.76TOF+0.14 TAV-43.78V_{max}+430.09RMS	0.76	<0.0001

RW, LR

It can be seen from Table 3 that the relationship of all AU parameters versus RW, LR are significantly weak, and Pearson's correlation coefficients ranged from -0.242 to 0.271. Using the stepwise method, all

the variables cannot enter into the RW and LR models. In conclusion, these AU parameters bring little information to determine RW and LR.

TL, TW

As shown in table 3, TOF and FC correlated with TL significantly at 0.01 level (r=-0.433, 0.404 respectively). On the other hand, the relationship of TAV, Vmax, RMS, TC, PF versus TL are significantly weak. It indicates that TOF and FC give a little information on the TL prediction. The correlation coefficients (r=-0.433) characterizing the relationships between time of flight and tracheid length are near to those reported by Raczkowski[12] for 12 coniferous species (r= 0.413-0.480).

Using the stepwise method, the variables of TOF, Vmax, and PF can enter into the TL model. A low level of explained variance (R2 =0.40) was obtained with the inclusion of TOF, Vmax, and PF in the regression. The results of this study showed that the use of the AU method for estimation of the tracheid length does not bring reliable values because the determination coefficient (R2 =0.40) characterizing the correlation is rather low.

It can be seen from Table 3 that the relationship of all AU parameters versus TW are significantly weak, and Pearson's correlation coefficients ranged from -0.244 to 0.201. Using the stepwise method, all the variables cannot enter into the TW model. In conclusion, these AU parameters bring little information to determine TW.

MFA

As shown in table 3, TOF, TAV and FC correlated with MFA significantly at 0.01 level (r=0.798, 0.396 and -0.372 respectively), and Vmax correlated with MFA significantly at 0.05 level (r=-0.325). On the other hand, RMS, TC, PF did not correlate with MFA significantly. So it indicates that TOF, TAV, FC and Vmax give relatively better information on the MFA prediction compared to RMS, TC and PF.

The result of the significant relationship between Vmax and MFA confirmed the findings of Kawamoto[2] that the microfiber angle in the latewood tracheid affect the attenuation of AU amplitude.

Using the stepwise method, the variables of TOF, TAV, Vmax and RMS can enter into the MFA model. A moderate level of explained variance (R2 =0.76) was obtained with the inclusion of TOF， T， Vmax and RMS in the regression. The results of this study have shown that the use of the AU method for estimation of the MFA is reliable.

Conclusions

1) In this study, RW of Larch wood ranged from 0.4mm to 2.9 mm. LR ranged from 23.4 % to 65.2%. TL ranged from 3311.5μm to 5025.3μm. TW ranged from 34.0 μm to 43.3μm. MFA ranged from 8.8 to 29.7 degree.

2) The relationships of all AU parameters versus RW, LR, TL and TW are weak, and the multiple regression model based on AU parameters can't give reliable results to estimate RW, LR, TL and TW.

3) TOF, T, FC and Vmax correlated with MFA significantly, and the correlation between TOF and MFA gave the high correlation coefficient (r = 0.798). The multiple regression model based on AU parameters can explain 76% of variability of MFA.

Acknowledgments

This work is sponsored by the National Project of State Forestry Administration (No. 2006BAD18B07).

References

Beall F.C. 2002. Overview of the use of ultrasonic technologies in research on wood properties. Wood Science and Technology. 36(3):197-212.

Bendtsen B.A.; Senft J. 1986. Mechanical and anatomical prop-erties in individual growth rings of plantation-grown eastern cot-tonwood and loblolly pine, Wood Fiber Science. 18(1):23-38.

Bucur V. 2006. Acoustics of wood. Springer Verlag.

Cave I.D.; Walker J.C.F.1994. Stiffness of wood in fast grown plantation softwoods: The influence of microfibril angle, Forest Products Journal. 44(5):43-48.

Dinwoodie J.M. 1965. The relationship between fiber morphology and paper properties: a review of literature. Tappi Journal. 48(8): 440-447.

Evans R.J.I. 2001. Rapid prediction of wood stiffness from microfibril angle and density. Forest Products Journal. 51(3):53-57.

Frimpong-Mensah K. 1987. Fiber length and basic density variation in the wood of Norway spruce (Picea abies (L.) Karst.) from northern Norway, Vol. 40,: Meddelelser fra Norsk Institutt for Skogforskning.

Kawamoto S.; Kiguchi M.; Kataoka Y.; Matsunaga M. 2010. Propagation of Acoustic Emission and Acousto-ultrasonic Waves in Wood Materials, in EWGAE 2010 Vienna, 8th to 10th September.

Kawamoto S.; Williams R.S. 2002. Acoustic emission and acousto-ultrasonic techniques for wood and wood-based composites: a review. US Department of Agriculture, Forest Service, Forest Products Laboratory.

Megraw R.; Bremer D.; Leaf G.; Roers J. 1999. Stiffness in loblolly pine as a function of ring position and height, and its relationship to microfibril angle and specific gravity. In:Proc. Third Workshop – Connection Between Silviculture and Wood Quality Through Modeling Approaches. IUFRO working party S 5.01-04, La Londe-les Maures, France.IUFRO, Vienna,Austria, 385-386.

Page D.H.; El-Hosseiny F.; Winkler K.; Bain R. 1972. The mechanical properties of single wood-pulp fibres. Part 1: A new approach. Pulp Pap. Mag. Can. 73:72-77.

Page D.H.; El-Hosseiny F.; Winkler K.; Lancaster A.P.S. 1977. Elastic modulus of single wood pulp fibres, Tappi Journal. 60:114 -117.

Polge H.; Essai de caracterisation de la veine verte du merisier. 1984. Ann. Sci. For. 41(1): 45-58.
Raczkowski J.; Helinska-Raczkowska L. 2004. Relationship Between Lengthwise Ultrasound Transmission and Tracheid Length in Wood of Selected Softwood Species. Folia. Forestalia Polonica, Seria B. 35:3-12.

Mapping the Decay Field around a Bolt Hole Using Ultrasound and Electrical Measurements and Relating It to Decreased Mechanical Properties

Douglas R. Rammer, Samuel L. Zelinka, Grant Kirker
USDA Forest Products Laboratory, Madison, Wisconsin, USA

Abstract

Bolt holes are frequently drilled on-site and often serve as an ingress point for wood decay fungi. This paper describes how fungi colonize the wood surrounding a bolt hole and the resulting effect on mechanical properties of the connection. The advancing decay field will be mapped out by taking both electrical resistance and ultrasound measurements in the region surrounding the bolt hole. One key aspect of this work was ensuring that measurements were taken at the same locations throughout the wood decay process. To address this, we designed a unique stepper motor system to position the sensors. This paper includes details about the measurement system design and preliminary results. Eventual outcomes of this research will help determine the residual capacity of bolted connections found in-service.

Keywords: Ultrasound, electrical resistance, decay, bolt bearing strength

Tension Chord Lumber: Construction and Mechanical Properties of Novel Southern Pine Composite Beams

Bonnie Z. Yang, Dan Seale, Jose Dahlen, David Jones
Mississippi State University, Starkville, Mississippi, USA

Abstract

This paper presents results of a study in which novel engineered composite lumber was developed, manufactured, and tested. Engineered composite lumber was made by edge-laminating lower grade sawn lumber and higher grade tension chord material to yield tension chord lumber (TCL). Three groups of TCL (38 mm by 235 mm by 4.9 m) were made with various combinations of southern pine lumber raw materials and tested under static third-point bending load in a universal testing machine. One group of control lumber (38 mm by 184 mm by 4.9 m) was also tested. Values of modulus of elasticity (MOE) and modulus of rupture (MOR) were estimated from each of the four groups of specimens. Values of MOE and MOR for TCL are increased over those of the control lumber. Mean MOE values of TCL ranged from 12.4 to 12.6 GPa, compared with 9.57 GPa for control lumber. Mean MOR values of TCL ranged from 39.3 to 47.6 MPa, compared with 35.9 MPa for control lumber.

Keywords: Bending strength, composite material, engineered lumber, southern yellow pine

Inspection to assessment and intervention proposal of timber roof structures by "Tekno" at gymnasium at “São Carlos Clube” in Brazil

Leandro Dussarrat Brito
Department of Structural Engineering – SET, Laboratory of Wood and Wooden Structures – LaMEM, University of São Paulo – USP, São Carlos School of Engineering – EESC, São Carlos, São Paulo, Brazil, dussarrat@sc.usp.br

Carlito Calil Junior
Department of Structural Engineering – SET, Laboratory of Wood and Wooden Structures – LaMEM, University of São Paulo – USP, São Carlos School of Engineering – EESC, São Carlos, São Paulo, Brazil, calil@sc.usp.br

Abstract

This paper presents the assessment of the current safety condition of roof timber structure type “Hauff” performed by "Tekno" at "Gymnasium São Carlos Clube" in São Carlos, São Paulo state in Brazil, inaugurated on November 4, 1952. In 2011, occurred a rupture in an inclined beam type boxed composed with pieces of wood and plywood. To identify the cause of the rupture of main beam and pathologies found throughout the timber structure of existing roof, it was held technical inspections to develop a technical report, aiming to suggest corrective measures for maintenance, reinforcement and intervention of structural elements. Thus, other steps were performed for the second phase of the inspection. The methodology used for the structural elements analysis was the nondestructive technique (NDT) by visual inspection, among others. The first study also consisted in the analysis of a coverage spatial model (3D), to estimate whether security conditions of the structural elements designed at that time, meet the safety requirements of the structure to the current condition considering the criteria of NBR 7190:1997. Recently, there were performed the interventions of the structures of the roofs of the bleachers, with the replacement of the existing beams that had excessive deformations, for glued laminated timber beams, as well the maintenance for conservation and rehabilitation with reinforcement of structural elements and replacement of fiber cement roofs for metal roofs.

“Keywords”: timber structures, inspection, assessment, intervention, pathologies, sustainability.

Introduction

The roof timber structure type “Hauff” performed by "Tekno" of "Gymnasium São Carlos Clube" in São Carlos, São Paulo state in Brazil, inaugurated on November 4, 1952.

On May 3rd, 2011 it was held the first technical visit to survey and inspection of the structural elements that compose the wooden structure of the roof of the gym with their dimensions and geometries. The objective of this first work was to perform technical visits for evaluating the current structural wood conditions of the roof by “Tekno” type “Hauff” and at the adjacent regions to concrete pillar top support of the "São Carlos Clube" Gymnasium" by using the visual inspection technique to investigate and evaluate their conditions and to propose possible corrective measures (CALIL et al 2011 & BRITO et al 2012). In the second phase of work, on October 2012, with the structure disassembled, there were other requests for inspection.

The gym is located at GPS coordinates 22º 00’28,20”S; 47º 53’ 32,60”O; 856 meters altitude. [Google Earth], as show in Fig. 1.

a) Aerial view. b) Northeast Facade: roof maintenance.

Figure 1 - GPS coordinates 22º 00'28,20"S; 47º 53' 32,60"O; 856 meters altitude. [Google Earth].

During the first technical visit the following conditions were observed by visual inspection technique: damaged tiles; pieces with symptoms of lateral buckling; regions with evidence of moisture migration from tiles (Fig. 2a), the plywood webbed structures beam V5 (north N, Fig. 2a) showed rupture at the amendment region, which shows inadequate maintenance, the exchange of existing offset plates, for plates that have no structural function, as well as insufficient nails; top of some concrete pillars, support timber beams, present cracks in the concrete (Fig. 2b) and evidence of steel corrosion (Fig. 2c), all sloping timber beams, at the grandstand roof, show arrows deformation by creep (Beam V2 south S, Fig. 2d), among others, (CALIL et al 2011 & BRITO et al 2012). Thus, other steps were performed for the second phase of the inspection. As a result of detected pathologies, recommendations for corrective maintenance, reinforcement and intervention of structural elements were made.

a) Beam V5 N: Rupture. b) Cracks (Pillar). c) Bat urine: corrosion (Steel). d) Beam V2 S: deformation by creep

Figure 2 - Main pathologies detected by visual inspection, in the first technical visit. Photos: BRITO (2011)

Restoring existing structures for reuse of the building is a major trend in the global issue of sustainability, (COIAS 2011). With this attitude you can reduce waste generation and material consumption that would result from the process of constructing a new building at the place of that existing old one.

Description of the structure

The timber roof structure consists of two distinct structural systems: the central region on the sports arrangements with arched wooden coffin (plywood webbed structures arch) with profiles offset type "I" of 1.2 meters high, and two covers on the sides of the bleachers beamed sloping wooden plywood coffin type [plywood webbed structures (STAMATO 2002)] of 0.55 meters (Fig. 3 and Fig. 4).

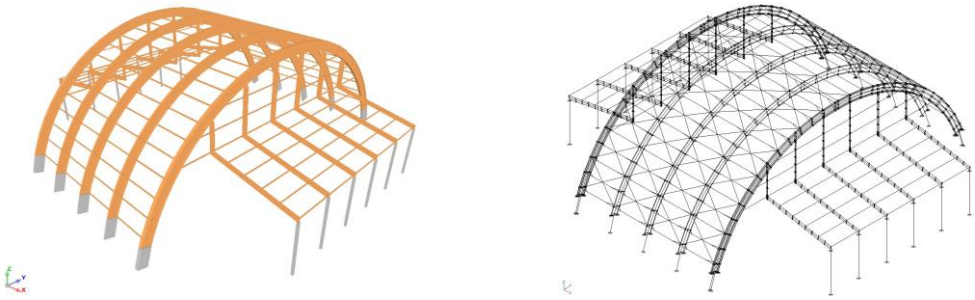

a) 3D Spatial Model (CAD) b) 3D Model unifilar (MEF)

Figure 3 - Analysis of bar 3D Spatial Model by Finite Element Method (MEF) of the roof structure. BRITO (2011)

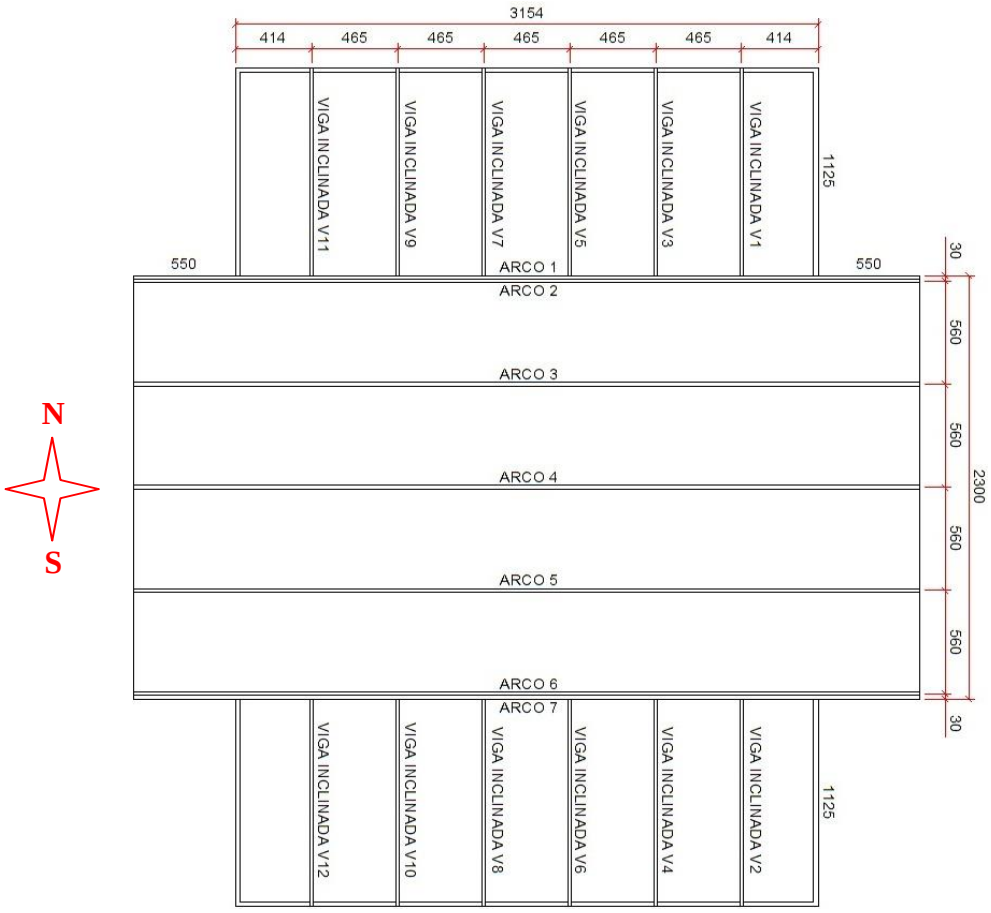

Figure 4 - Schematic plant of the roof for identification of the timber structural elements. BRITO (2011)

The first phase of study also consisted in the analysis unifilar of bar of the 3D Spatial Model (Fig. 3) (CALIL et al 2011 & BRITO et al 2012) by Finite Element Method (MEF) of the timber roof structure, to estimate whether security conditions of the structural elements designed at that time, meet the safety requirements of the timber structure to the current condition considering the criteria of NBR 7190:1997.

Inspection techniques to assess timber structures

The wood is an amazing combination that exhibits both strength and durability as a structural material used for roof structures. Nevertheless, from the time it is formed in the tree, wood is subject to deterioration by a variety of agents biotic and abiotic (HIGHLEY & SCHEFFER, 1989; RITTER & MORRELL, 1990; CALIL JR. & BRITO, 2010). Damage ranges from relatively minor discolorations caused by fungi or chemicals to more serious decay and insect attack.

Timber inspection is a learned process that requires some knowledge of wood pathology, wood technology, and timber engineering (RITTER & MORRELL 1990). This paper covers the fundamentals of timber roof structure inspection for decay and deterioration; it identifies the agents of deterioration and outlines used inspection methods.

For this, there are the main methods that can be used for inspection and evaluation of timber roofs: types and areas for deterioration; inspection techniques; equipment and tools; NDE tool; performance monitoring.

The main methods that are available for inspecting timber structures, normally do not require sophisticated tools. These methods, which include visual characteristics by visual inspection technique; sounding; probing test; pick test with mortise chisel; measuring moisture content by moisture meter; and microdrilling by Resistograph for example, may be used singly or in combination (HIGHLEY & SCHEFFER, 1989; RITTER & MORRELL, 1990; PELLERIN & ROSS, 2002; ARRIAGA et al 2002).

However timber structure inspectors have the difficult task of accurately assessing the condition of an existing structure. They must understand the biotic and abiotic factors associated with wood deterioration as well as the relative rate at which these processes occur in a given environment (RITTER & MORRELL 1990).

The visual inspection technique is used for evaluations of the visual characteristics due to the presence of defects, insects attacks, decay and other deteriorations (HIGHLEY & SCHEFFER, 1989; RITTER & MORRELL, 1990; PELLERIN & ROSS, 2002; ARRIAGA et al 2002). Camera can be used for picture a time to reflect existing damage, taking photos of the affected areas is quite important (ARRIAGA et al 2002; BRITO et al 2012). A good way to begin an inspection for decay is a visual inspection technique search for decay manifestations, emphasizing locations or conditions most conducive to prolonged wetting. The main pathological manifestations that can be observed by visual inspection technique are: signs of distress (collapsed, failed members, excessive deflections); missing members; fruiting bodies; sunken faces or localized surface depressions; staining or discoloration; insect activity; fungi, cracks; grade stamps; checks.

Decay usually results in abnormal coloration of the wood. The first indication of decay is often brown streaks or blotches; purplish streaks are sometimes present. As wood approaches advanced stages of decay, it loses luster and may exhibit pronounced changes in color. Of course, judgments based on color necessitate familiarity with the appearance of sound wood. Sound, healthy softwood has a pleasant, fresh, resinous smell, whereas decayed wood usually has a mushroom-like, stale odor. However, a musty, moldy smell, though indicative of damage conditions favorable to decay, does not necessarily indicate the presence of decay (HIGHLEY & SCHEFFER, 1989).

Nondestructive evaluation is the science of identifying the physical and mechanical properties of materials without altering its end-use capabilities and then using this information to make decisions regarding appropriate applications (PELLERIN & ROSS 2002). Nondestructive evaluation (NDE) technologies have contributed significantly toward detect structural problems. Table 1 shows the main Nondestructive techniques (by PELLERIN and ROSS 2002).

Table 1 – Nondestructive techniques (PELLERIN and ROSS 2002).

Avaliação não destrutiva da madeira (NDT)	
Evaluation of visual characteristics	Chemical tests
Color Presence of defects	Composition Presence of treatments - Preservatives - Fire retardants
Physical tests	Mechanical tests
Electrical Resistance Dielectric properties Vibrational properties Wave Propagation Acoustic emissions X-ray	Flexural stiffness Proof loading - Bending - Tension - Compression Probes/coring

Second phase of the inspection for assessment timber roof structure

In the second stage of inspection, after the timber roof structure disassembled, conditions were evaluated timber structural members of the internal wood beams, type boxed section composed with pieces of plywood, in the beams bowed and in the arches.

The nondestructive techniques (NDT) used in this work were evaluation of visual characteristics, Sounding with hammer, Probing test with chisel, and moisture meter, for related to structural problems, that is, absence of bracing, buckland members, deterioration due wood humidity and deterioration due fungi and insects attacks. The pictures Fig. 5 to Fig. 10 shows these types of structural problems inspected by visual inspection technique.

During inspections at the bases of external arcs were detected large amounts of bat excretions. This proves that the external arcs of metal bars were corroded by urine bats (Fig. 5), accumulated overtime.

a) outer arc A1 (northeast): corrosion of steel bars. b) outer arc A1 (northwest): corrosion of steel bars.

Figure 5 - External arcs of metal bars were corroded by urine bats. Photos: BRITO (2012)

The fungi begin as minute spores that germinate and grow through the wood (Fig. 7). Once enough energy has been obtained, the fungus produces a fruiting body and releases spores that spread and infect other wood (Fig. 6 e Fig. 7). The rupture in beam V5 N was caused by incorrect maintenance and decay by fungi (Fig. 6).

a) Beam V5 N (north): Overview. b) Beam V5 N: Maintenance performed worse caused rupture.

Figure 6- Rupture in Beam V5 N (north): Early stage-discoloration in surface end grain. Mail late stage– cracked and collapsed wood. Photos: BRITO (2012)

The white rot (Fig. 7) feeds upon the cellulose, hemi-cellulose, and the lignin and makes the wood white and stringy.

a) Beam V2 S disassembled (showed that creep flow).

b) Beam V2 S had decay by fungi (moisture stains).

Figure 7 – Beam V2 S (South), (Fig. 2d): showed that creep flow, moisture stains and decay of woods with white rot fungi characteristics. Photos: BRITO (2012)

The brown rot (Fig. 8 and Fig. 9) degrades the cellulose and hemi-cellulose leaving the lignin as a framework which makes the wood dark brown and crumbly.

a) Base arch A2: bat excretion, fungi and corrosion of steel.

b) Base arch A2 (northeast): brown rot fungi.

Figure 8 - Woods infected with brown rot fungi characteristics. The decayed wood has a darkened color with a cracked, brittle surface that resembles charred wood. Photos: BRITO (2012)

If it is necessary to identify the type of fungus, it is recommended biological analysis in laboratory. Soft rot in wood often appears brown and can be confused with decay caused by brown rot fungi.

a) outer arch A7 (southwest).

b) Base arch A7 (Bat excretions)

c) Bat excretions: fungi wood and corrosion of steel.

Figure 9 - Soft rot in wood often appears brown and can be confused with decay caused by brown rot fungi.
Photos: BRITO (2012)

During the inspection also were detected debris accumulations two holes of beetle larvae characteristics, at points located in wood of the Arch A6 L (east), as shown in Fig. 10.

a) Arch A6 L (east).

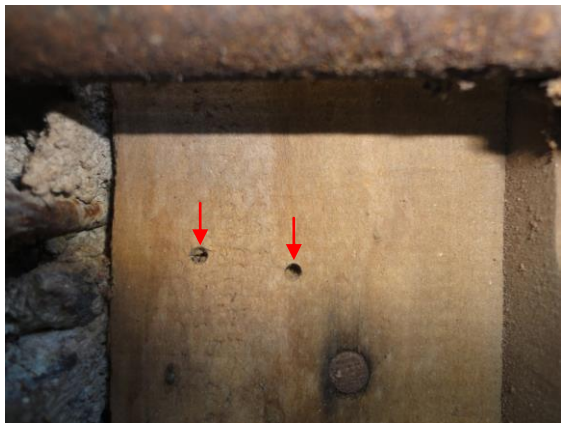

b) Zoom in base Arch A6 L (east).

Figure 10 - Two holes of beetle larvae characteristics. In this case always note the frass and debris accumulations in the tunnels. Photos: BRITO (2012)

Intervention proposal, maintenance and rehabilitation of the timber roof

After performing the necessary maintenance and rehabilitation of existing timber roof structural members, the entire structure was painted with synthetic enamel paint for surface protection.

The interventions of the timber roof structures of the bleachers, were the replacements of wooden beams type plywood coffin for glued laminated timber (MLC) beams (Fig. 11). The species of wood used for the clothing of the beams was the "Lyptus" which is a clone of Eucalyptus.

a) Rehabilitation of base Arch A7 (southwest).

b) Intervention of the bleachers roofs replacements for MLC.

Figure 11 - Maintenance, rehabilitation and intervention in the timber roof structure. Photos: BRITO (2012)

The tiles of fiber cement were replaced for tiles sandwich double galvanized steel, Fig. 12.

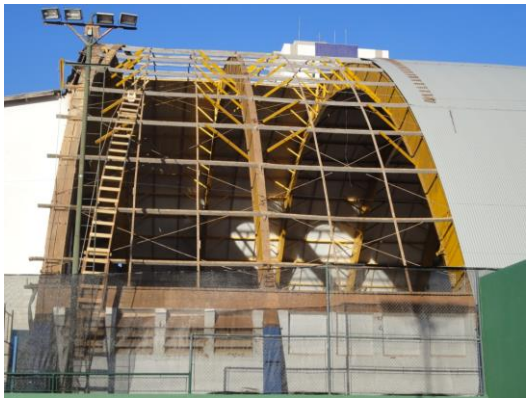

Figure 12 - Replacement of roof on tiles of galvanized steel, with double-layer sandwich. Photos: BRITO (2012)

Conclusions

The types of deterioration has been analyzed using visual technique inspections. Detailed evaluation and technical report has been carried out with the support of the "Laboratory of Wood and Wood Structures" (LaMEM), São Carlos School of Engineering (EESC), University of São Paulo (USP), Brazil, in order to propose suggestions and recommendations for maintenance, rehabilitation and intervention of this timber structure roof at gymnasium at "São Carlos Clube" in São Carlos, in São Paulo state.

In this work, it was possible to detect pathologies in various timber roof structural members, which could be avoided with regular inspections and preventive maintenance. There were finding lack of preventative maintenance and control of s and of timber roofs in Brazil. In this way the assessment, maintenance and rehabilitation of timber structures must be a important subject for the future of timber structures in Brazil.

The routine sequential for recommendation at the inspection process of timber roofs, can be used: the visual inspection technique, with records photos; the probing test; the pick test with mortise chisel; the moisture meter; the sounding technique with hammer; the microdrilling with resistograph; among others tests.

Acknowledgements

The authors thank CNPq (National Council for Scientific and Technological Development.) for its financial backing of this work.

References

ARRIAGA, F.; PEZAZA, F.; ESTEBAN, M.; BOBADILLA, I.; GARCIA, F. 2002. Intervención en estructuras de madera. ISBN 84-87381-24-3. AITIM, Madrid.

BRITO, Leandro Dussarrat; CALIL NETO, Carlito; SARTORTI, Arthur L. CALIL JUNIOR, Carlito 2012. Inspeção visual (NDT) da estrutura de cobertura tipo "Hauff" do ginásio São Carlos Clube. In: XIII EBRAMEM - Encontro Brasileiro em Madeiras e em Estruturas de Madeira. Vitória, ES, Brasil, 2012.

CALIL JR., Carlito; BRITO, Leandro Dussarrat 2010. Manual de Projeto e Construção de Estruturas com Peças Roliças de Madeira de Reflorestamento. Departamento de Engenharia de Estruturas, Escola de Engenharia de São Carlos, Universidade de São Paulo. ISBN: 978-85-8023-000-0. Editora EESC. São Carlos. Free download: <*http://www.set.eesc.usp.br/portal/pt/livros/371-manual-de-projeto-e-construcao-de-estruturas-com-pecas-rolicas-de-madeira-de-reflorestamento*>.

CALIL JUNIOR, Carlito; BRITO, Leandro Dussarrat; CALIL NETO, Carlito; SARTORTI, Arthur L. 2011. Relatório Técnico: Laudo de Verificação da Estrutura da Cobertura do "Ginásio São Carlos Clube". USP/EESC/SET/LaMEM. Brasil.

CÓIAS, V.. Qualificação dos profissionais e das empresas para a qualidade na reabilitação de estruturas de madeira. CIMAD 11 – 1º Congresso Ibero – Latino Americano da Madeira na Construção. Coimbra, Portugal, 2011.

HIGHLEY, T. L.; SCHEFFER, T. Controlling decay in waterfront structures. Evaluation, Prevention, and Remedial Treatments. Department of Agriculture, Forest Service, Forest Products Laboratory. FPL-RP-494. Madison, WI, U.S.A., 1989.

PELLERIN, Roy F.; ROSS, J.. Nondestructive Evaluation of Wood. Forest Products Society, Madison, WI, USA, 2002.

RITTER, M. A.; MORRELL, J. J. 1990. Timber bridges. Department of Forest Products, Oregon State University.

STAMATO, G. C. 2002. Ligações em estruturas de madeira compostas por chapas de madeira compensada. Tese (Doutorado) apresentada ao Departamento de Engenharia de Estruturas, da Escola de Engenharia de São Carlos, da Universidade de São. São Carlos.

UNIVERSITY OF MINNESOTA. 2011. Microorganisms causing decay in trees and wood. <*http://forestpathology.cfans.umn.edu/microbes.htm* >

Neural Network Models for the Establishment of a Structural Stress Grading Methodology Using Nondestructive Techniques

Jose L. García de Ceca, Eva Hermoso, Raquel Mateo, Guillermo Iñiguez-Gonzalez
INIA-CIFOR, Depto. Industrias Forestales, Grupo Madera y Corcho; Madrid; Spain

Abstract

The objective of this work is the development of neural network (NN) models to establish a stress grading structural classification methodology by means of nondestructive techniques. Scots pine (*Pinus sylvestris* L.) wood is the object of study. Considering the suitability of applying NN models to grade timber beam specimens, the following input variables were considered for a series of NN models: wood provenance, real and nominal dimensions, beam length, visual grade, longitudinal vibration velocity, knot proportion on a section, depth of penetration, and screw withdrawal force. Output characteristics were global density, static MOE, modulus of rupture (MOR), and the three of them together. The models show acceptable figures for correlation results (ranging from 0.552 to 0.779), and performance values are good (ranging from 0.701 to 0.887). No model shows an equivalent result for correlation vs. performance values, but except for the global density model where only one good value was found. In a nutsell, the model showing the best correlation (or performance) is not necessarily the model showing the best performance (or correlation). The observed vs. predicted plots follow a 45° pattern, meaning a good approach for prediction. Further studies will include enlarging *P. sylvestris* data set, considering other species, studying the economic feasibility of the method, in-factory control, and environmental epigenomics and structural stress changes susceptibility.

Keywords: Grading timber, *Pinus sylvestris* L., MOE, MOR